Memoria de Tesis Doctoral

Taxonomía, ecología y evolución de los rinocerontes (Rhinocerotidae, Perissodactyla) del Mioceno de la Península Ibérica

Oscar Sanisidro Morant



Departamento de Biología, Facultad de Ciencias,
Universidad Autónoma de Madrid

Departamento de Paleobiología, Museo Nacional
de Ciencias Naturales - CSIC

Memoria de Tesis Doctoral

Taxonomía, Ecología y Evolución de los rinocerontes (Rhinocerotidae, Perissodactyla) del Mioceno de la Península Ibérica

Oscar Sanisidro Morant

Tesis dirigida por los dres. María Teresa Alberdi Alonso y Jorge Morales Romero

Tutor: Dr. José Luis Sanz García

Departamento de Biología, Facultad de Ciencias, Universidad Autónoma de Madrid
Departamento de Paleobiología, Museo Nacional de Ciencias Naturales - CSIC

mncn museonacionaldecienciasnaturales

CSIC Consejo Superior de Investigaciones Científicas

UAM Universidad Autonoma de Madrid



Madrid, a 15 de Septiembre de 2015



Design & Layout: O. Sanisidro

Contents

Agradecimientos 1

Objetivos / Aim of this work 2

Introduction 7

General Methodoloy and Measurements 25

Chapter 1 45
The golden age and the demise of rhinos: untangling the fossil record of Rhinocerotidae

Chapter 2 73
A new rhinoceros (Rhinocerotidae, Perissodactyla) genus from the Middle Miocene of the Iberian Peninsula

Chapter 3 105
A Miocene Rhinocerotidae from El Bierzo Basin (Leon Province, northwestern Spain)

Chapter 4 121
The first complete skull of *Hispanotherium matritense* (Lartet *in* Prado, 1864) (Perissodactyla, Rhinocerotidae) from the Middle Miocene of the Iberian Peninsula

Chapter 5 141
Intraspecific variability of *Hispanotherium matritense* (Lartet *in* Prado, 1864)

Chapter 6 261
Nuevas técnicas paleobiogeográficas aplicadas a la familia Rhinocerotidae (Perissodactyla)

Chapter 7 269
Alicornops simorrense (Mammalia, Perissodactyla) from the middle Miocene locality of M-407 Rotonda (Madrid Province, Spain)

Chapter 8 297
New *Lartetotherium* remains from the Iberian site of M-407 Rotonda (Middle Miocene)

Chapter 9 321
Paleoecological analysis of *Alicornops simorrense* and *Lartetotherium sansaniense* (Mammalia, Perissodactyla) from the Middle Miocene of the Iberian Peninsula

Chapter 10 337
Aceratherium incisivum (Kaup, 1832) (Mammalia, Rhinocerotidae) from the Upper Miocene of Cerro de los Batallones (Madrid Basin, Spain)

Chapter 11 379
Lartetotherium sp. (Rhinocerotidae, Perissodactyla) from the Vallesian of Cerro de los Batallones area (Upper Miocene, Spain)

Chapter 12 417
Rhinocerotidae remains (Mammalia, Perissodactyla) from the Upper Miocene site of Corral de Lobato (Guadalajara, Spain)

Chapter 13 425
New data on *Dihoplus schleiermacheri* (Rhinocerotidae, Perissodactyla) from the Turolian of Venta del Moro and Crevillente-2 (Comunidad Valenciana, Spain)

Appendix: Rhinocerotidae osteology 447

Conclusiones generales / General conclusions 465

Agradecimientos

Ahora que (por fin) ha terminado este largo alumbramiento, es el momento de acordarme de todas aquellas comadronas que han estado pendientes de la parturienta durante los últimos años y han ayudado a que el pequeño haya salido sano y bastante crecidito.

Son numerosas las personas que han contribuido de una u otra forma al trabajo aquí presentado. Me gustaría mencionar a tantos de ellos como mi limitada memoria permita.

Este trabajo se ha podido llevar a cabo gracias al apoyo económico por parte del MICINN y MINECO a través de la Beca Predoctoral para la Formación del Profesorado Universitario (FPU). También agradezco el apoyo y confianza prestada por el proyecto BSCH-UCM 910607. Al Museo Nacional de Ciencias Naturales – CSIC por los medios y el espacio facilitado para el desarrollo de la tesis.

Al Dr. Plinio Montoya por los buenos consejos y apoyo mientras empezaba mi colaboración con el Departamento de Geología de la Universidad de Valencia así como de introducirme en el mundo de la Paleontología a través de los increíbles yacimientos de Venta del Moro y el Cerro de los Batallones.

Por su responsabilidad, implicación, orientación y apoyo que han proporcionado a este trabajo, estoy especialmente agradecido a mis directores y maestros, los Drs. Mª Teresa (Maite) Alberdi y Jorge Morales. Las facilidades demostradas a mi llegada al departamento, así como durante el transcurso de estos años han hecho del Departamento de Paleobiología mi segunda casa.

A los Drs. José Luis Sanz, Manuel Hernández-Fernández, Jesús Marugán y Nieves López por enseñarme algunos de los muchos caminos de la Paleontología y la motivación necesaria para explorarlos.

A los Drs. Pierre-Olivier Antoine (PierrO), Ioannis Giaourtsakis, Kurt Heissig y Esperanza Cerdeño por su colaboración con los distintos capítulos de este volumen que facilitaron en gran medida mi iniciación en el grupo de estudio. Cada conversación con ellos ha sido una clase maestra en anatomía y evolución de los rinocerontes. También quisiera agradecer a los correctores de los diferentes artículos publicados sobre el tema, los Drs. Donald Prothero y Esperanza Cerdeño.

A los distintos preparadores que, con su trabajo, han hecho posible el estudio de los ejemplares de esta tesis: Eleuterio Baeza (Museo Geológico y Minero), Paloma Gutiérrez y Blanca Gómez (Museo Nacional de Ciencias Naturales). Mi especial agradecimiento a Enrique Cantero (Museo Nacional de Ciencias Naturales) quien ha hecho posible la preparación de la mayor parte del material de Cerro de los Batallones o Molina de Aragón entre otros. Sin el gran trabajo de todos ellos, este volumen no sería posible.

A las incontables personas que han participado de algún modo en la extracción de los fósiles estudiados a lo largo de innumerables campañas de excavación. A los participantes de las campañas de Batallones, Venta del Moro, Casas de la Valenciana y Molina de Aragón por compartir sol, lluvia, polvo, fatiga y, sobre todo, risas. Del mismo modo, mi agradecimiento a las empresas ArqueoEstudio S. C., Geosfera, Paleoymás S. L. L., Argea S. L. y TOLSA ya que gracias a su intervención han podido ser recuperados muchos de los fósiles que se incluyen en el presente trabajo.

A todos los coautores de los artículos que componen esta tesis: los Drs. Laura y Soledad Domingo, Cayetana Martínez-Maza, Juan L. Cantalapiedra, Ioannis Giaourtsakis, Esperanza Cerdeño, Plinio Montoya y Pierre-Olivier Antoine. Vuestra colaboración ha sido indispensable para que el presente trabajo llegue a buen puerto.

Agradezco a Jim Martin y a Bloomsbury Publishing Plc. por el permiso para usar las excelentes ilustraciones de rinocerontes realizadas por David Quinn para el libro "Rhinos, endangered species" (publicado originalmente por Malcom Penny Eds).

Gracias a Norbert Micklich, Dr. Oliver Sandrock (Darmstadt Hessisches Landesmuseum), Dr. Wilma Wessels (Utrecht University), Yves Laurent (*Muséum* d'Histoire Naturelle de *Toulouse*) y Abel Prieur (Université Claude Bernard *Lyon* 1) por su amable asistencia y cálida acogida. Gracias también al Dr. Deng Tao por su amable invitación a visitar el IVPP. En este apartado quiero expresar mi agradecimiento a Judith Galkin, Eileen Westwig y Ana Balcárcel (American Museum of Natural History) y los Drs. Lars van den Hoek Ostende (*Naturalis* Biodiversity Center), Gertrud Rössner (Bayerische Staatssammlung für Paläontologie und Geologie), Pierre-Olivier Antoine y Maeva Orliac (Université Montpellier 2) por ser los mejores anfitriones durante mis estancia en los distintos centros de investigación. La larga lista de pruebas que lo demuestra incluye un papel manuscrito con las tiendas de Brooklyn donde comprar ingredientes para la paella, un cuaderno de dibujo con ilustraciones del mejor museo del mundo hechas después del cierre, arañazos de zarzales (indispensables para la elaboración de la mejor tarta de moras con el permiso de mi madre) o la mezcla de resignación y alegría de ver un fatídico España-Holanda entre amigos y risas lejos de casa.

Me gustaría dedicar unas palabras a los miembros del tribunal de la tesis doctoral por su valioso tiempo dedicado a la supervisión del manuscrito.

Gracias a todos aquellos que habéis ofrecido vuestra ayuda en las últimas semanas antes de su publicación y en particular a Gema, Raef, Cristina, Israel, Adriana, Kristina, Paloma, Pablo, Vero, Enrique, Susana, Blanca, Laura, Sole y María.

Me gustaría agradecer de forma especial a mis amigos, no importa cuánto camino hayan recorrido a mi lado: desde aquellos conocidos desde mi infancia en Valencia a los últimos hechos en Madrid. Os deseo lo mejor, ya sea en España o cualquier otro lugar del mundo donde la vida os lleve. Gracias de corazón por estar ahí.

A mis cuatro abuelos: José María, Salvador, María y María que no han podido ver el resultado de este trabajo. Esta tesis va dedicada a vosotros.

Nada de esto sería posible sin mi padre, Enrique, mi hermano Sergio y muy especialmente mi madre Cristina. Vuestra paciencia, amor y cariño han sido pilares fundamentales para mí.

Una vez más, gracias.

OBJETIVOS

Los objetivos generales de la presente Tesis Doctoral son la revisión de las faunas de rinocerontes del Mioceno español presentes en diversos yacimientos de las cuencas del Tajo, Bierzo y Levante, la actualización de la sistemática del grupo y finalmente obtener información acerca de la diversidad y ecología del grupo. Los capítulos del presente trabajo han sido realizados en forma de trabajos independientes ordenados por los yacimientos de estudio y desde un punto de vista cronológico, dando lugar a tres grandes bloques: Mioceno Inferior, Medio y Superior. Los principales objetivos de la presente tesis son los siguientes:

- Establecer una revisión sistemática de los rinocerontes fósiles del Mioceno Ibérico de los diferentes yacimientos de estudio. Esto incluye la descripción de nuevos taxones y su comparación con especies próximas. Cuando la cantidad de restos así lo ha permitido, se ha realizado un análisis cuantitativo de las variaciones intraespecíficas observadas, así como análisis estadísticos para testar las hipótesis planteadas. Dichos análisis han permitido conocer si existen cambios significativos en la morfología y/o talla entre las diferentes localidades.

- Plantear una nueva hipótesis filogenética tanto de los nuevos taxones como de aquellos en los que se aporta nueva información contrastando hipótesis previas.

- Identificar los patrones de reemplazo faunístico y diversificación dentro del grupo a escala global y continental como preámbulo a la parte sistemática. Este trabajo incluye todos los rinocerontes del registro fósil previa recopilación de datos bioestratigráficos y sistemáticos ya publicados.

- Realizar un estudio exploratorio de la histología del esqueleto postcraneal en rinocerontes para obtener información acerca del modo de vida y edad de madurez sexual en especies fósiles.

- Describir la morfología de los restos y contrastarla con datos obtenidos del análisis de los isótopos de carbono y oxígeno en el esmalte.

AIM OF THIS WORK

This Thesis has been devoted to the review of the rhinoceros faunas from the Spanish Miocene recorded in several localities from the Tagus, Bierzo, and Levantine Basins, update the group's systematics, and, finally, provide information about their ecology and diversity. The chapters of the current work have been grouped in the form of works that, while independent from each other, have been grouped firstly by the fossil locality and secondly by a chronological criteria in three blocks: Early, Middle, and Late Miocene.

- In first place, a systematic review of the rhinoceros remains from the studied fossil localities is intended. Some of the studied remains pertain to new taxa, which have been described, figured and compared with related species. When the number of available remains was sufficient, another objective has been the quantitative analysis of their intraspecific variations and the statistical analysis of these comparisons. These analyses allowed comparing the morphology and size among different localities.

- Another main objective is to formulate an updated phylogenetic hypothesis for the newly described taxa as well as for those which relevant information is provided and to update the available character matrix on the light of new data. To do so, the studied species have been coded according to previously published phylogenetic works, which permitted to test previous hypotheses.

- As a preamble to the systematic part, an overall work on the fossil record of Rhinocerotidae has been conducted by means of a recompilation of the biostratigraphic ranges and an updated systematic arrangement. The objectives of this work are identifying diversification and turnover patterns in the group at both global and continental scales.

- Another objective deals with the study of the histology of the postcranial skeleton in rhinoceroses. The results have provided information about the mode of life and age of the sexual maturity in rhinoceros fossil species.

- The morphological description of the fossil remains has allowed characterizing the dental and locomotor adaptations and comparing them with the carbon and oxygen isotopic data obtained from the dental enamel.

Introduction

Abstract. Perissodactyls, or "odd-toed" ungulates, are an order of hoofed mammals. The fossil record of the group spans over 55 Ma. During the Eocene, the group experienced an early evolutionary radiation with a plethora of perissodactyl Families. Small sizes and a primitive dental pattern gave way to a wide range of morphologies and dimensions, from tiny cat-sized animals (like the earliest horses and tapiroids) to the colossal hyracodontid *Paraceratherium*, the biggest land mammal ever to live on Earth. Rhinoceroses are one of the three surviving perissodactyl families together with horses and tapirs. Once an important Family distributed along Eurasia, North America, and Africa, rhinoceroses are now on the verge of extinction with only six species still stood.

THE ORDER PERISSODACTYLA

Perissodactyls are an order of hoofed mammals. The name Perissodactyla (from the greek *perissos* = "uneven" and *daktulos* = "finger/toe") was given by Sir Richard Owen from the most obvious of their shared specializations: the mesaxony. Mesaxony occurs when the symmetry plane of a hand or a foot passes through the central digit, usually the third one (Figure 1A). As a result, most of the weight is borne on it. Mesaxony contrasts with the paraxonic limbs of the cetartiodactyls or even-toed ungulates (order Cetartiodactyla), in which the axis passes between the third and fourth toes and the weight is distributed between the two digits. The reduction of the lateral digits undergone in parallel in mesaxonic and paraxonic limbs and reflects an increase in cursoriality, as limb bones became more mechanical efficient during faster strides. Other postcranial adaptations include the loss of the clavicle bone and the development of a particular ankle joint: the astragalus has a shortened neck with a 'saddle'-shaped distal navicular-facet (Figure 1B) and a restricted articulation with the cuboid. This tight joint permits the astragalus to be the primary weight-bearing tarsal and strengths the whole limb. However, it sacrifices its lateral flexibility (avoiding rapid postural changes) and jumping ability. Finally, the femur has a developed third trochanter, place of insertion of the *m. gluteus superficialis*. All these adaptations are related with an increase in mobility and size.

Aside from these locomotory adaptations, perissodactyls present lophodont teeth (more rarely bunodont). Their dental formula varies within groups, rather complete in basal species, more simplified in the modern ones. Regarding the digestive

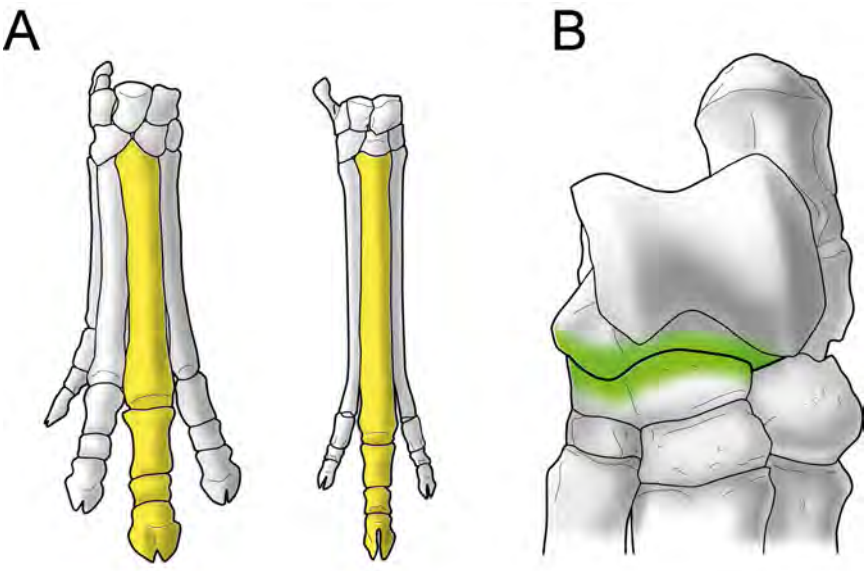


Fig. 1. Principal characters defining Perissodactyla. A, mesaxonic forelimb. Right autopodiums of *Heptodon* and *Lophialetes* in dorsal view (modified from Radinsky, 1969). B, tarsal bones of *Aceratherium* in cranial view showing the typical 'saddle'-shaped facet between astragalus and navicular (in green; modified from Hünermann, 1989). Figures not to scale.

system, perissodactyls have simpler stomachs coupled with a large and sacculated caecum. As a result, most part of the digestion takes place in the intestine, where the cellulose is processed. This type of feeding mechanism requires a superior time of foraging but makes a more efficient use of proteins and high-quality food. Hindgut fermentation is the plesiomorphic condition for mammals and contrasts with cetartiodactyls, which present a foregut system of fermentation (although they may retain a small degree of hindgut one). Foregut modality of fermentation has been proposed as one of the key feature that explains the relative evolutionary success of cetartiodactyls in general and ruminants in particular.

The position of Perissodactyla within the mammalian tree is unclear. The current concept of Perissodactyls as mesaxonic ungulates was originally noticed by de Blainville (1816). When Owen formally erected Perissodactyla in 1848, he considered hyraxes (Hyracoidea) as members of the Order Perissodactyla. Some authors have argued in this sense, with perissodactyls nesting with hyracoids or with hyracoids together with sirenians and proboscideans (Fischer, 1986, 1989; Fischer and Tassy, 1993; McKenna, 1975; Prothero et al., 1988). The second scenario presents perissodactyls related to Carnivora (Waddell et al., 1999) as well as to Pholidota. In a similar way, phylogenetic analyses resulting from ancient retroposon (L1) insertion linked Perissodactyla with Carnivora and Chiroptera in a clade named as "Pegasosferae" (Nishihara et al., 2006). A third alternative places perissodactyls with other hoofed mammals like the cetartiodactyls in Laurasitheria (e.g.: McKenna, 1975; Novacek and Wyss, 1986). This hypothesis coincides with the recent cladistic framework proposed by Spaulding et al. (2009) which included up to 12,222 morphological, behavioral and molecular characters.

The relationships of perissodactyls with other mammalian groups get more complicated if fossil taxa are considered. Leonard Radinsky (1966) proposed that perissodactyls evolved from phenacodontids, an archaic group of condylarth-like ungulates from the Paleocene and Eocene. This hypothesis was followed by subsequent studies (Fischer and Tassy, 1993; MacFadden, 1976; McKenna, 1975; Prothero et al., 1988; Thewissen and Domning, 1992). More recently, an updated phylogenetic analysis positioned the cambaytheres (a small, bunodont group of hoofed mammals with potential stem-perissodactyl affinities) as sister group of Perissodactyla and, more distantly, related to the clade Phenacodontidae + Afrotheria (Rose et al., 2014). However, the link between perissodactyls and phenacodontids remains controversial

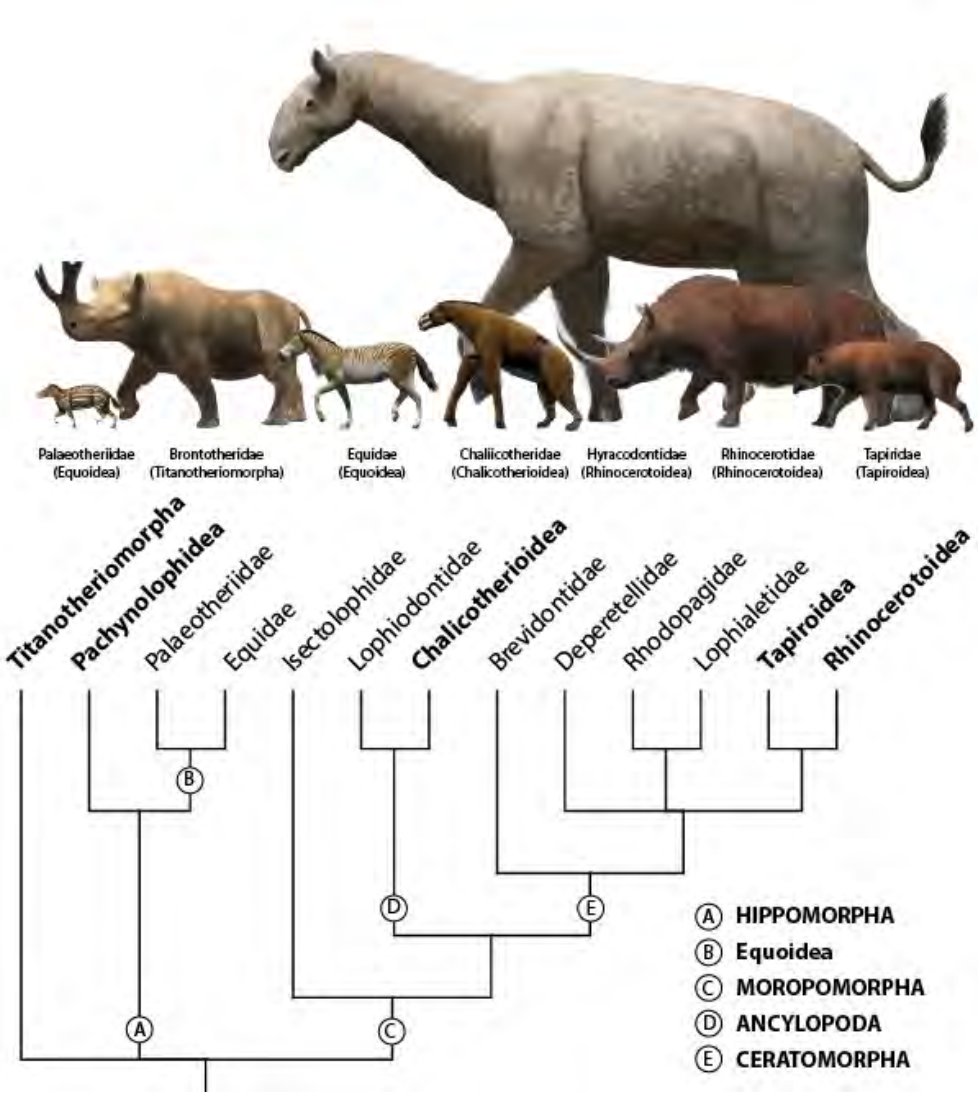


Fig. 2. Cladistic hypothesis of Perissodactyla according to Janis et al. (2008) and reconstructed appearance of various perissodactyl groups. Supra-familiar clades are represented in bold face.

(Hooker, 2005; Kondrashov and Lucas, 2012; Ladevèze et al., 2010), and has been progressively replaced by grouping Perissodactyla and Cetartiodactyla within Laurasitheria (Asher et al., 2003; Buckley, 2015; Meredith et al., 2011; Murphy et al., 2001; O'Leary et al., 2013; Springer et al., 2003). A recent study with collagen proteins mainly based on living species not only supported Laurasitheria, but found that South American 'native ungulates' (i.e. toxodonts and liptoterns) nest as sister group of Perissodactyla (Buckley, 2015). As both 'native' South American hoofed mammals and perissodactyls have considered derived from condylarths, the possibility of a clade formed by condylarths + (perissodactyls + South American 'native ungulates') sister to Cetartiodactyla (all within Laurasitheria) is feasible.

Almost every phylogenetic proposal dealing with the three living perissodactyl Families places horses as sister group of both tapirs and rhinoceros. Once again, the picture gets more complicated when looking at the fossil record. Perissodactyls experienced an early evolutionary radiation with a peak of diversity in the early Middle Eocene. As a result, around 15 different families have been recognized at that moment, a reflection of the diversity and importance of the group in ancient ecosystems. Unfortunately, many of them are only known from dental remains and their validity and phylogenetic relationships vary substantially according to each author. The Eocene genera *Arenahippus*, *Protorohippus* (both formerly included in *Hyracotherium*), and *Heptodon* are exceptions to the paucity of early perissodactyl postcranial remains and are currently consider the best proxies for the primitive perissodactyl morphotype (Holbrook et al., 2004).

A comprehensive review of the arrangement of the different perissodactyl families is summarized in Schoch (1989) and Janis et al. (2008). Radinsky published taxonomic reviews on tapiroids (Radinsky, 1963), rhinocerotoids (Radinsky, 1963), and early chalicotherioids (Radinsky, 1964), setting a valuable morphological background for posterior studies. More recently, Luke Holbrook reviewed the tapiromorphs (Holbrook, 2001) and several perissodactyl families like lophiodontids (Holbrook, 2009) or isectolophids (Holbrook et al., 2004). The present-day concept of Perissodactyla includes five superfamilies (Holbrook, 1999; Janis et al., 2008): Equoidea (horses and fossil relatives like paleotheres), Brontotherioidea (brontotheres; roughly equivalent to Brontotheriomorpha), Chalicotherioidea (chalicotheres), Tapiroidea (tapirs and related forms) and Rhinocerotoidea (rhinoceroses, amynodontids, and hyracodontids) together with several families with uncertain taxonomic affinities (Figure 2).

Both Central America and Asia were classically proposed as sources of origin of Perissodactyla. The Central American hypothesis is supported by the purported phenacodontid ancestor. As this link has been progressively abandoned, the American origin was discarded in favor of an Asian one. Indeed, Asia is nowadays considered the most feasible origin (Beard, 1998; Hooker, 2005). A particular scenario place the first perissodactyls in the Indian Sub-continent during its northwards drift during the Paleocene-Eocene. The identification of cambaytherids remains in the early Eocene of India would provide evidence in this sense (Rose et al., 2014).

THE FAMILY RHINOCEROTIDAE GILL, 1872

Rhinoceroses are one of the multiple perissodactyl lineages which have independently evolved large body sizes,

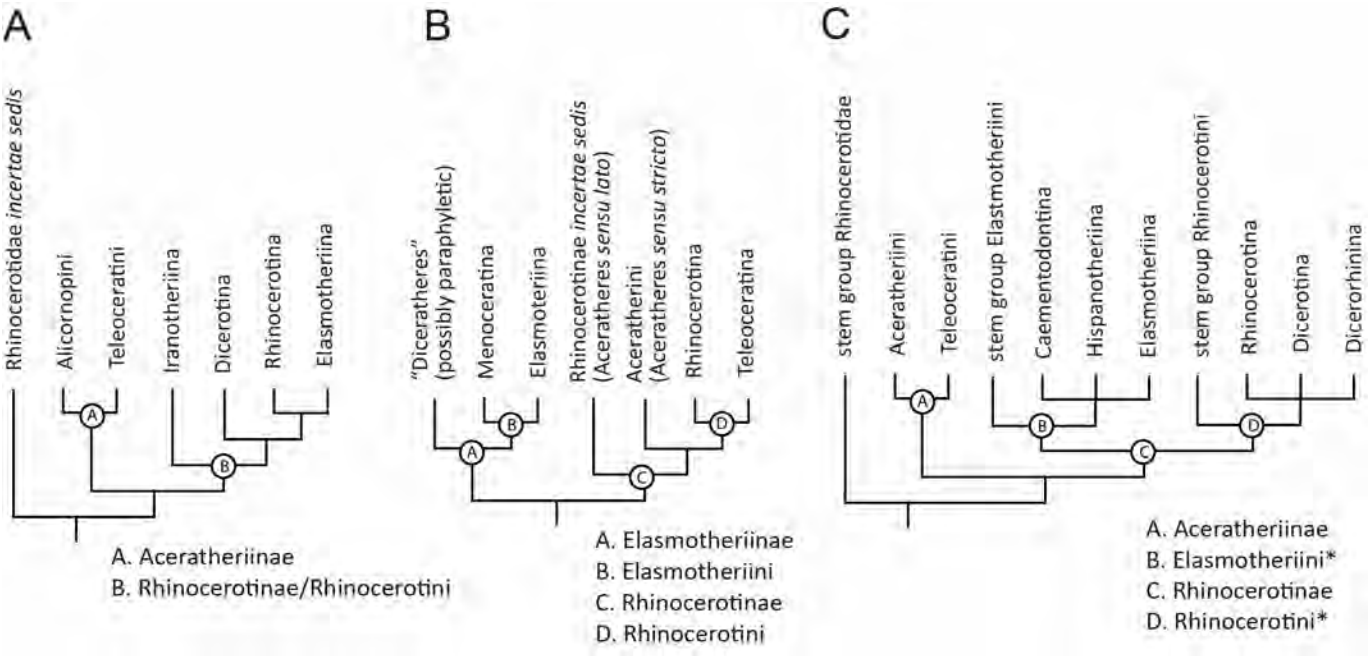


Fig. 3 Selection of cladistic hypotheses within Rhinocerotidae. A, following Cerdeño (1995); B, according to Becker et al. (2013); C, Heissig's (2012) proposal (asterisks represents groups mentioned but not solved in Heissig's work).

lophodonty and premolars similar in shape with the molars. Extant rhinos are readily distinguishable by their nasal and/or frontal horns. Present in Asia and North America since the first steps of their evolutionary life history as part of the early Perissodactyl radiation, their arrival to the European continent date back from the lower Oligocene. At that time, the Family Rhinocerotidae became widespread and reached their peak during the Miocene, starting their decline thereinafter. The group maintains its presence in Europe to the latest Pleistocene. During its evolutionary history, rhinos have been able to occupy a wide arrange of biomes, from the arctic tundra to the equatorial rainforests.

In general, four main clades are consistently recovered: Teleoceratini, Rhinocerotini, Elasmotheriina (sometimes mixed with Rhinocerotini), and Aceratheriini/ina (see chapter 10 for a synthetic description of each one). However, convergent traits and parallelisms misled the systematic arrangement and supra-generic cladistic hypotheses vary significantly among specialists (Figure 3). The early members of the Family Rhinocerotidae were small 'sheep'-sized animals with no horn insertions or a pair of submedian nasal horn bosses. They were defined according to several synapomorphies summarized by Heissig (2012). In general, the members of the family Rhinocerotidae are recognized by two synapomorphies (characters 1 and 2 in Heissig, 2012; bold face). The remaining characters cited are important but present a variable degree of homoplasy:

Dentition:

- **Enlargement of a tusk-like i2** (Figure 4A). The development of the "chisel-tusk shearing complex" (Prothero et al., 1989) has been considered the main character which defines the Family Rhinocerotidae. Such complex is formed by a developed, tusk-like, i2 and an occluding chisel-shaped I1. Noticeably, the later was not developed in the first rhinocerotid genera (*Ronzotherium* and *Amphicaenopus*) and appeared posteriorly (e.g. *Epiaceratherium* or *Trigonias*; Heissig, 2012). Therefore, this character should be restricted to the enlargement of the tusk-like i2.
- **Simplification of the M3** (Figure 4B) due to the reduction of the metacone (reduced in Elasmotherinae, absent in Rhinocerotinae) and the metastyle together with a strong shortening of the posterior cingulum.
- Posterior premolars and M1-2 with the typical 'π'-shaped pattern formed by the connection of protoloph, ectoloph, and metaloph.
- The anterior dentition is reduced early in the evolution

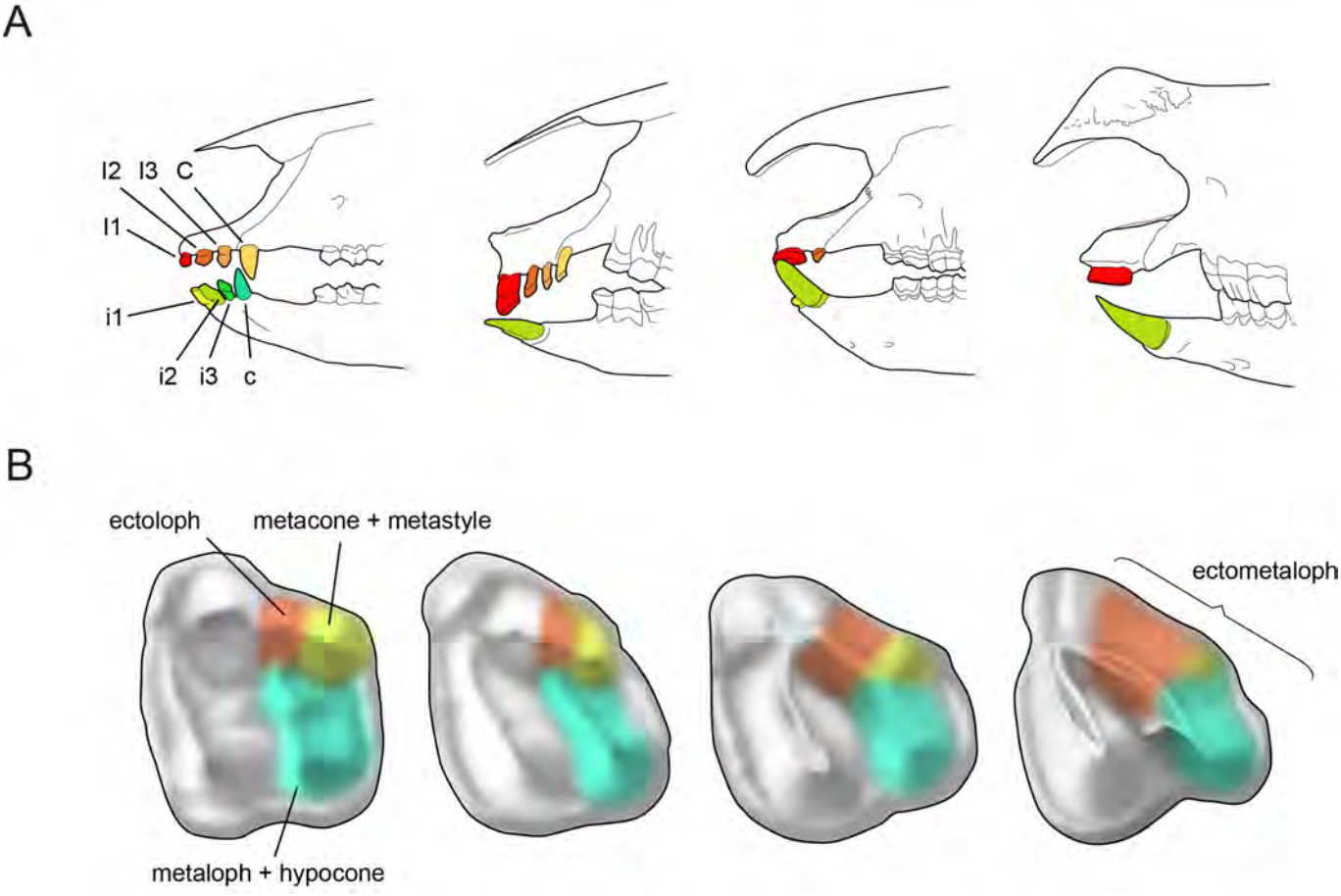


Fig. 4 Principal characters defining Rhinocerotidae. A, reduction of the anterior dentition and parallel development of the 'chisel-tusk shearing complex' (i.e. enlargement of the tusk-like i2 and its occlusion with the upper I1). From left to right: *Hyrachyus* (a tapiroid showing the basal perissodactyl condition), *Trigonias, Subhyracodon,* and *Dicerorhinus* (all rhinocerotids). The first two are modified from Radinsky (1969). B, examples of the simplification of the M3 through the reduction of the metacone and the metastyle (yellow). From left to right: *Hyracotherium* (an equoid showing the basal perissodactyl condition), *Homogalax* (tapiroid), *Teletaceras* (basal rhinocerotid) and *Dihoplus* (Pliocene rhinocerotid). The first two are modified from Radinsky (1969), the third from Radinsky (1967). Figures not to scale.

of the group (except for the I1 and the i2; Figure 4A). The second and third upper incisors are absent in most genera and, except for the most primitive representatives, the canines are lost.

- Presence of entoconid in the p4.

Skull and mandible:

- Low, 'saddle'-shaped skull (i.e. concave dorsal profile). The parasagittal crest is wide and flanked by the lamboid crests
- Premaxillary-nasal contact lost.

Postcranial bones:

- Reduction of the fifth anterior digit, resulting in a functionally-tridactyl manus (the finger is independently lost in Elasmotheriini and Rhinocerotini, reduced in Aceratheriinae).

EXTANT REPRESENTATIVES

Once a diverse family, living rhinos are represented by six species grouped into four genera (i.e. *Ceratotherium*, *Diceros*, *Rhinoceros*, and *Dicerorhinus*). They are the last representatives of the tribe Rhinocerotini. Their common ancestor dates back from 28 to 33 Ma (Willerslev et al., 2009). Their historical distribution (Figures 5-8) places them in the tropical and subtropical regions: in the African continent from the tropical boreal belt to South Africa (excluding part of the equatorial rainforests) and from India and Pakistan to Borneo and Java in the Asian continent.

White rhino – *Ceratotherium simum* (Burchell, 1817)

Evolution and taxonomy—the genus *Ceratotherium* was widespread during the middle-late Pliocene and Pleistocene of Africa. Its grazing adaptations permitted to spread together with the open grasslands expansion through Africa (Guérin, 1980). Up to now, four fossil taxa have been recognized within *Ceratotherium* (being considered as distinct species or subspecies depending on the author). These are: *Ceratotherium mauritanicum, Ceratotherium simum germanoafricanum, Ceratotherium scotti* and *Ceratotherium efficax* (Giaourtsakis et al., 2009).

Geographic distribution (Figure 5)—the historic range of the white rhino lies South of the Zambezi River. It inhabited Central-Eastern Namibia, a large part of Botswana, South Mozambique and the Northern part of South Africa (Rookmaaker and Antoine, 2012).

Description—the skull is highly dolichocephalic skull and presents a backwards-oriented occipital plate. The anterior teeth are absent. *C. simum* is the third largest land mammal and the biggest among living rhinos. The shoulder height has been reported to be 157 – 178 cm (Groves, 2010). Adult males weight 2,000 – 2,400 kg, while adult females weight 1,500 – 1,700 kg. The lips are squared, suitable for grazing. The lower lip bears a hardened pad (Van der Bergh, 1955). The shoulder height of the species is between 165 and 188 cm. They weight between 1,600 kg in adult females to 2,300 kg in adult males. However, maximum adult weights of 3,200 and 3,600 kg have been recorded (Foster, 1960). The medial nasal horn is conical, up to 166 cm long (from an outstanding specimen recorded by Heller in 1913). Females usually bear more slender horns. A second frontal horn, tandem placed, is present at the level of the orbits. The anterior dentition is absent. The morphology of the cheek teeth is very characteristic: teeth are very high-crowned hypsodont, carry abundant cementum, protoloph and metaloph contacts at early wear stages, the lingual cingulum in premolar teeth is very reduced to absent, M1-2 has strongly distolingually bended protoloph and metaloph, closed medifossete always present, deep parastyle groove, prominent mesostyle fold, subrectangular M3, the lower premolars have closed fossetids in medium wear stages and lower molars have lingually flattened lophids (Giaourtsakis et al., 2009). The mandible has a deeply convex lower margin and a backwards oriented ascending ramus.

Ecology and behavior—in South Africa is mostly found in the areas of bushveldt. It is classified as a typical grazing species. White rhinos are area-selective short-grass grazers. They favor the higher nutrient bottomlands and drainage line (Perrin and Brereton-Stiles, 1999). In Pafuri (Kruger National Park, South Africa), white rhinos fed on perennial grass species (Pedersen, 2009). Despite its robust proportions, white rhinos are able to trot at 25 km/h and gallop over short distances at 40 km/h (Van der Bergh, 1955).

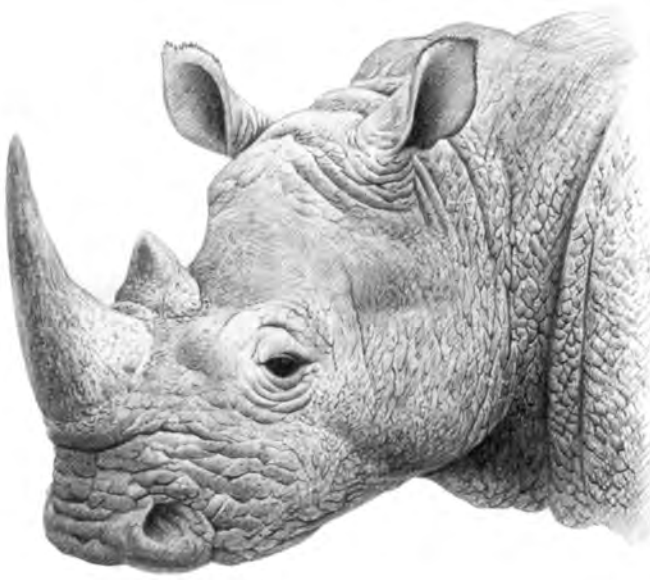
Nile rhino – *Ceratotherium cottoni* (Lydekker, 1908)

Evolution and taxonomy—both extant *Ceratotherium* species have distinguished as a subspecies level within a single species (*C. simum*). Recently, Groves et al. (2010) considered the two forms of white rhinos, Northern and Southern, as two distinct species: the Northern white rhino *Ceratotherium cottoni* and the Southern white rhino *Ceratotherium simum*. They were geographically isolated at the last glacial (Hooijer, 1969). However, genetic exchange was restricted much earlier as, according to mitochondrial DNA, both species separated 0.75 – 1.4 Ma (Groves, 2010). However, genetic analyses show that both species do not differ consistently: Nei's distance, based on 25 allozyme loci was 0.005 between Northern and Southern species (very low if compared to 0.32, the distance between *Diceros* and *Ceratotherium*; Merenlender et al., 1989). Additionally, no differences were found regarding ecology and behavior.

Geographic distribution (Figure 5)—the Nile rhino was originally distributed along Northern equatorial Africa. It ranged over parts of North-Western Uganda, Southern Chad, South-Western Sudan, the eastern part of Central African Republic and the North-Eastern Democratic Republic of Congo. Additional fossil evidence places it in Kenya around 3000 BC (Rookmaaker and Antoine, 2012).



Fig. 5 Historical (AD 1800) distribution map of the white rhino (*Ceratotherium simum*; in orange) and Nile rhino (*Ceratotherium cottoni*; green) in Africa. Crosses represent introduced populations, circles native ones (considered by country; redrawn from Antoine and Rookmaker, 2013). On the right, head portrait of a white rhino, so-called square-lipped rhino due to the broad lips adapted to graze short turf and the slit-like nostrils. Drawing by David Quinn.



Description—the Nile rhino is morphologically similar to the white rhino. However, some differences have been outlined. *C. cottoni* has a shorter upper teeth row and a deeper dorsal profile of the skull. Contrary to the white rhino, adults are hairless (Groves, 1972), limb bones are longer, the crural index (tibia expressed as percentage of femur length) is slightly lower (Groves, 2010), and the overall size smaller and shorter than the white rhino: the shoulder height is 150 – 165 cm (Groves, 2010). Males weight 1,600 – 1,400 kg and weighted females 1,400 – 1500 kg (Groves, 2010). The cranial differences include a shorter palate, an anteriorly placed incisive foramen, a flattened dorsal profile (concave in the white rhino), and a shorter tooth row length (less obvious among females of both species; (Groves, 2010). Their dentitions show some minor differences: the molars of the Nile rhino are lower-crowned and present a larger metastyle on M3.

Ecology and behavior—the Nile rhino inhabits the open forests dominated by *Combretum* trees and adjacent plains. Open prairies are not permanently inhabited; being only traversed (Guggisberg, 1966). In Uganda they go into swampy areas in the dry season (Foster, 1967).

Black rhino – *Diceros bicornis* (Linnaeus, 1758)

Evolution and taxonomy—three living subspecies of black rhino have been recognized (*Diceros bicornis bicornis, Diceros bicornis minor*, and *Diceros bicornis michaeli*). The South-central (*D. b. minor*) and South western (*D. b. bicornis*) species maintain around 2,000 individuals each, while the Eastern (*D. b. michaeli*) has an 800 population. A fourth subspecies, the Western African black rhino (*Diceros bicornis longipes*), was tentatively declared extinct in 2011.

Geographic distribution (Figure 6)—its historic range (AD 1500; Rookmaaker and Antoine, 2012) was distributed along Southern and Eastern Africa, from South Africa (except the area around Lesotho to the South East and Inhambane in Mozambique) to the horn of Africa (except two Northern areas located North West to Djibouti and around the Gulf of Aden). Additionally, the species was present along an East-West belt from Somalia to Togo and the Southern edge of Sahara.

Description—the black rhino is a medium-sized species according to extant standards. Its weight varies among subspecies. For instance, males from Hluhluwe had a mean weight of 854 kg, while females were somewhat heavier (von La Chevallerie). On the contrary, the mean values for females from Kenya (1,080 kg) were slightly lighter than males (1,124 kg; von La Chevallerie, 1970). A maximum body weight of 2,896 was reported for the species (Guggisberg, 1966). A larger South African race has been cited, but became extinct at the end of the 19th century and no weight measurements were recorded (Hillman-Smith and Groves, 1994). Regardless its light body, it is a long limbed species (height at shoulder 132 – 180 cm). They bear two tandem-placed medial horns. The nasal horn is usually larger, up to 135 cm (Hillman-Smith and Groves, 1994), the posterior frontal horn usually more modest, with a maximum recorded length of 81 cm. Some populations can develop larger frontal than nasal horns (Best et al., 1962). The upper lip is prehensile and hooked, an adaptation for its browsing diet. The skull is slightly dolichocephalic, with a concave dorsal profile. The nasal bone is short and bumpy.

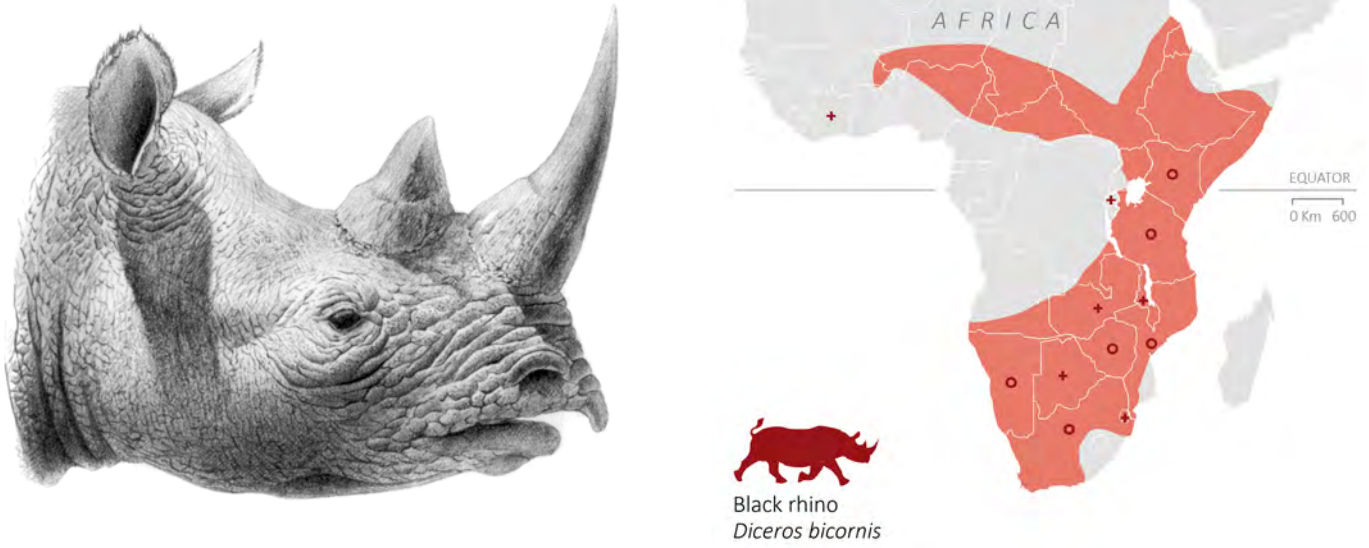


Fig. 6 Historical (AD 1500) distribution map of the black rhino (*Diceros bicornis*) in Africa and head portrait of the species. Notice the prehensile upper lip, capable to manipulate twigs and leaves during feeding. Map redrawn from Antoine and Rookmaker (2013). Crosses represent introduced populations, circles native ones (considered by country). Drawing by David Quinn.

The frontal horn boss is large and can extend over the orbits, particularly in older specimens. The occipital plate is backwards oriented, but less than in *Ceratotherium* (Hillman-Smith and Groves, 1994). As the other two African species, the black rhino is void of anterior dentition and the premaxillary area is highly reduced. Cheek teeth are brachyodont and their crowns do not present cement. The secondary folding is weak. Crista present on the premolar teeth, absent from the molars. Permanent P1 is present but can affect the eruption of the P2 (Hillman-Smith and Groves, 1994; Schaurte, 1966). The mandible is slender, has a convex ventral profile and a somewhat vertical ascending ramus. The symphiseal region is very short.

Ecology and behavior—the black rhinoceros is a very versatile species. It can be found in a very wide range of habitats: from montane forests to desert including grasslands, grasslands-woodlands ecotones, savanna woodland, and semi-desert (Hillman-Smith and Groves, 1994). The species is absent from equatorial forest. Black rhinos prefers medium to dense cover during daytime if available. Black rhinos are mixed browsers that forage on woody shrubs, small trees and forbs (Hillman-Smith and Groves, 1994). The list of consumed species is varied and often surpasses the hundred species, with a maximum of 191 species in Ngorongoro (Kenya; Goddard, 1968, 1970). Certain ones like *Acacia* and *Dichrostachys* are often preferred as well as some nitrogen-fixing legumes (Hillman-Smith and Groves, 1994). A proportion of > 95% of dicot material has been reported in its diet (Owen-Smith, 1988). In drier environments, browsing is focused on a few key plant species, with a tendency of leafy and succulent ones together some grass in the dry season (Buk, 2004; Buk and Knight, 2010; Mukinya, 1973).

Javan rhino – *Rhinoceros sondaicus* Desmarest, 1822

Evolution and taxonomy—the first records of *R. sondaicus* have been found in the middle Pleistocene of Java (Hooijer, 1964). The fossil specimens are more graceful-built (Hooijer, 1949). Three recent subspecies have been recognized: *Rhinoceros sondaicus annamiticus* (Vietnam, extinct), *Rhinoceros sondaicus inermis* (Sunderbunds, extinct) and *Rhinoceros sondaicus sondaicus* (currently West Java). At least one additional fossil subspecies, *Rhinoceros sondaicus simplisinus*, has been cited (Hooijer, 1946).

Geographic distribution (Figure 7)—the species was widespread through South-east Asia. It occurred in the Sunderbunds of India and Bangladesh, Myanmar, Thailand (Loch, 1937), Malaysia, Sumatra, Java, Laos, Cambodia in the Neolithic (Flower, 1900; Harper, 1945; Rookmaaker, 1980), Vietnam, and Laos up to the Chinese border (Rookmaaker, 1980). It have inhabited most part of India and Sri Lanka in the Pleistocene (Chauhan, 2008; Deraniyagala, 1937, 1938, 1946); (Lidekker, 1884; Lydekker, 1886a, b; Manamendra-Arachchi et al., 2005), Borneo in the late Pleistocene-late Holocene until, probably, the 10th century (Cranbrook, 1986) and a large area of southern China. Sadly it is currently restricted to the Ujung Kulong National Park (Java).

Description—(Figure 7) the Javan rhino is the rarer and smaller extant representative of the genus *Rhinoceros*. Its size is similar to the black rhino. Only three weight measurements are known. They range from 1,200 (a female) to 2,280 kg (Groves, 1982; Sody, 1959). Shoulder height spans from 120 – 170 cm. Females seem to be larger than males (Groves, 1982; Hoogerwerf, 1970), but the lower sampling impedes definitive conclusions. Its body can be covered by a sparse hair, not

as evident as in the Sumatran species (Cave, 1969; Groves, 1967), and its thick dermal armour is divided into segments. A short (up to 19 cm height; Groves and Leslie, 2011), medial nasal horn is usually present but is less developed than in the one great-horned rhino. This character is reflected in more pointed nasal bones. Significantly, some populations like the Sunderbuns or Sumatra lacked it, presenting a convex nasal area instead (De Poncins, 1935; Fraser, 1875; Sclater, 1876; Vageler, 1927). The dorsal profile of the skull is clearly concave and the orientation of the occipital plate is forward oriented. It presents a greater orbitoaural length than orbitonasal. The mandible retains both lower incisors, a typical character of *Rhinoceros*. More brachyodont than the Indian rhinoceros, teeth are low crowned, show a strong paracone style, a straight protoloph (only widened at its basalmost extent and void of protocone fold). The secondary enamel folding is restricted to a small crista (when present). There is a rudimentary tubercle on the entrance of the median valley on the molar teeth of some specimens.

Ecology and behavior—*R. sondaicus* is a generalist browser (Groves and Leslie, 2011). Its diet is shifted to leaves, shoots, and twigs of woody species (Ammann, 1985; Hoogerwerf, 1970; Pratiknyo, 1991; Santiapillai et al., 1993a, b; Schenkel and Schenkel-Hulliger, 1969a; Sody, 1959). Only a few herbaceous species or fruits are consumed and little to no grass (Groves and Leslie, 2011). These plants are mainly found in "thick scrub jungle or heavy secondary forest", but riverine and coastal areas are also frequented in Ujung Kulon NP (Hoogerwerf, 1970). Isotopic analyses made on *R. sondaicus* remains from the Middle Pleistocene Snake Cave (Thailand) demonstrated a similar use of the environment, with Javan rhinos feeding on closed-canopy forests despite the presence of more open C^3 and C^4 habitats (Pushkina et al., 2010). Even though more than 190 species have been included in its diet so far, only four (*Spondia spinnata*, *Amomum*, *Leea sambucina* and *Dillenia excelsa*) made up 44% of its diet (Ammann, 1985). Studies made on the recently extinct Southeastern Asian subspecies, revealed consumption of woody genera *Acacia*, *Calamus*, *Bambusia*, and minor contributions of tree ferns and poisonous *Strychnos* species (Santiapillai et al., 1993a). The Javan rhino uses its neck and chin together with its prehensile upper lip to reach the foliage, with some marks produced exceeding 250 cm height.

Today a solitary species (Schenkel and Schenkel-Hulliger,



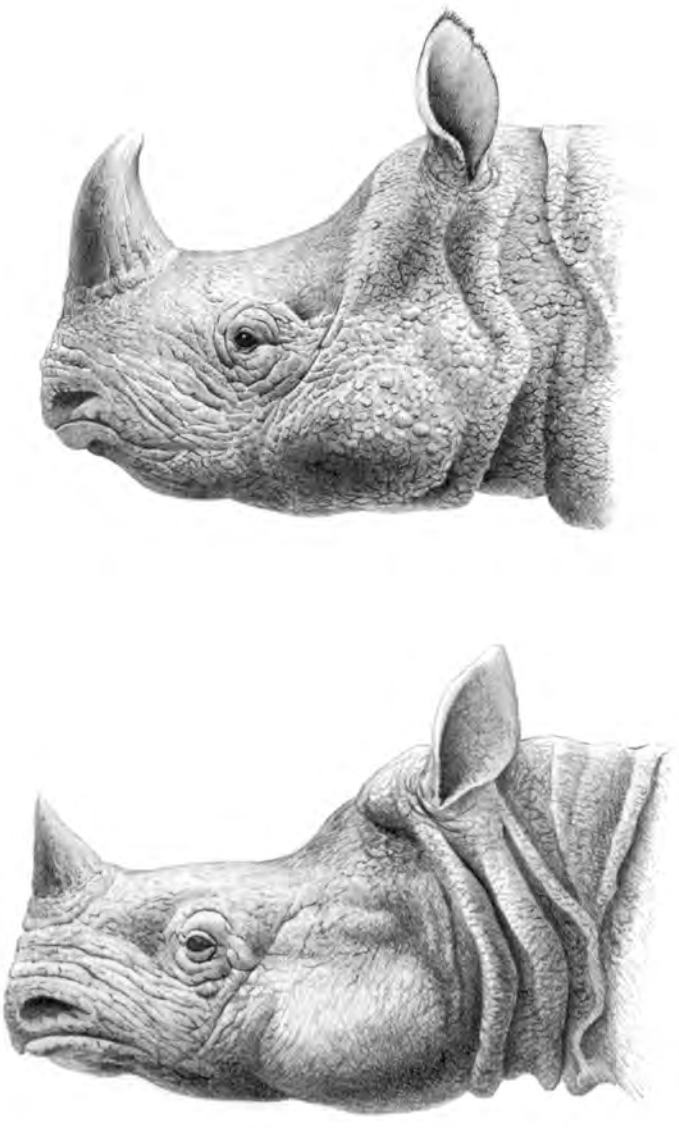


Fig. 7. Maximum distribution map (Holocene) of the great one-horned rhinoceros (*Rhinoceros unicornis*; light blue) and Javan rhino (*Rhinoceros sondaicus*; dark blue) in Asia. Redrawn from Antoine (2011). Circles in the map represent living populations. On the right, head portrait of a great-horned rhino (upper figure) and the Javan rhino (lower one). The upper lip is shorter than that of the black rhino, permitting a wider diet range typical of a mixed-feeder herbivore. Drawing by David Quinn.

1969a, b), the Javan rhino should have presented some grouping behavior when more abundant, as accounted by early descriptions (Horsfield, 1824).

Indian or Greater one-horned rhino – *Rhinoceros unicornis* (Linnaeus, 1758)

Evolution and taxonomy—the first fossil evidence of the great one-horned rhino date from the Middle Pleistocene (Laurie et al., 1983). The historical populations are enough homogeneous to differentiate subspecies, but fossil remains are usually larger (Laurie et al., 1983). At least two Pleistocene forms, *Rhinoceros unicornis jamrachii* and *Rhinoceros unicornis kendengindicus,* should be considered as subspecies according to Laurie et al. (1983). However, Antoine et al. (2011) included all large *Rhinoceros* remains from South Asia in *R. unicornis*, including *R. kendengindicus*, *R. jamrachii*, or some widely-used species like *Rhinoceros sinensis* or *Rhinoceros sivalensis*. The subspecific validity of these should be reviewed on the light of a thorough review of this material.

Geographic distribution (Figure 7)—Its historical distribution ranged along a large part of India, Bangladesh, and Myanmar extending west to the Punjab foothills, Pakistan (Barnejee and Chakraborty, 1973; Laurie et al., 1983; Rookmaaker, 1980). Its occurrence in China and Indochina are controversial (Rookmaaker, 1980). The species is nowadays confined to the Chitawan valley (Nepal) and Assam and West Bengal (India; Laurie et al., 1983).

Description (Figure 7)—*R. unicornis* is a mediportal heavy species. Females can weight around 1,600 kg, while males are heavier, around 2,100 (Laurie et al., 1983). However, the weight rank provided by Srivastav et al. (2010) is higher, between 1,800 and 2,700 kg. The species is 1,4 – 1,9 m height at the shoulders (1,75 – 2 m according to Srivastav et al., 2010) and around 3 – 3,8 m long (Srivastav et al., 2010). As its common name describes, the greater one-horned possess a single nasal medial horn. Its maximum length is 572 mm (Laurie et al., 1983). Premaxillae are short and stout. They tend to ossify at their midline and with the maxillary bone (in contrast to the Javan rhino, which remains articulated). The skull is stout and shows a concave dorsal profile. The occipital plate is slightly forward oriented. Teeths are high-crowned. The ectoloph is flattened. The crista is present and encloses a medifossete early in wear. Postfossetes are formed in advanced wear stages. There is no cingulum. As in other Asian species, the i2 are big, tusk-like and occlude with big upper I1. *R. unicornis* mantains small and peg-like i1.

Ecology and behavior—the greater one-horned rhino is an alluvial plains specialist. It is frequently found in riverine grassland plains with very tall grasses (up to 8 m; Laurie et al., 1983), swampy areas and nearby riverine woodlands. Indian rhinos feed mostly on herbs (especially tall grass) and shrubs from grasslands (Hazarika and Saikia, 2012). Rapid and seasonal changes affect large number of species consumed (e.g. 183 species in Chitwan NP; Laurie, 1978). However, grass percentage is variable through the year. Grass comprises more than the 85% during the hot season, descending to more modest values (42-70%) in the winter (Hazarika and Saikia, 2012; Laurie et al., 1983). Apart from tall grass, other foods are consumed: tender sprouts of tree species, fruits, shrubs, bark of trees, cane, sedges, aquatic plants, ferns, and crops (Konwar et al., 2009; Laurie et al., 1983). Fruits can be another seasonal contribution part to its diet. Aside from humans, adults have no regular predators. Only younger individuals less than 6 months of age are preyed by tigers (*Panthera tigris*; Laurie, 1982).

Sumatran rhino – *Dicerorhinus sumatrensis* (Fischer, 1814)

Evolution and taxonomy—three subspecies have been distinguished: the Western Sumatran rhino (*D. sumatrensis sumatrensis*), the Eastern Sumatran rhino (*D. sumatrensis harrissoni*), and the Northern Sumatran rhino (*D. sumatrensis lasiotis*; probably extinct).

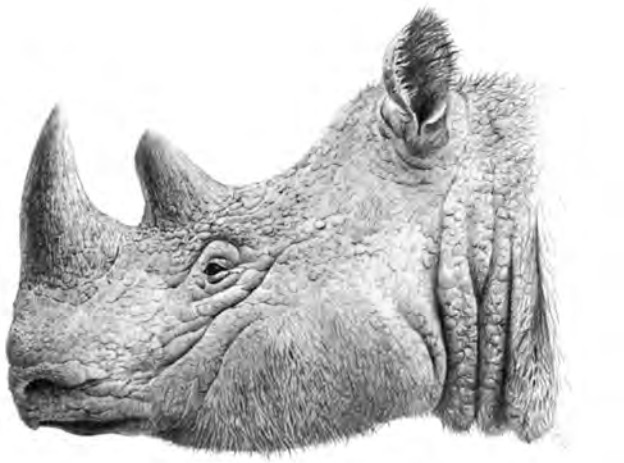
Geographic distribution (Figure 8)—*D. s. lasiotis* was distributed along the eastern border of Bangladesh, Myanmar and a small portion of West Thailand. *D. s. sumatrensis* was distributed along the lands South of the Gulf of Martaban along the whole Malay Peninsula, and Sumatra. Finally, *D. s. harrisoni* was present along the eastern half of Borneo.

Description (Figure 8)—with its 2.3 – 3.1 m length and 1 – 1.5 m height at the shoulder, the Sumatran rhino is the smallest living species. Its weight ranges between 800 and 2,000 kg (Skafte, 1961; Ullrich, 1955). The outer aspect of the Sumatran rhino is clearly distinctive from the remaining extant species. It possesses a shaggy reddish-brown fur covering its body and limbs in young calves, but bald areas usually occur with age. It has two tandem-placed horns. The medial nasal horn is robust and can attain considerable lengths, up to 69 cm long; the medial frontal horn is conspicuous and usually blunt (Groves and Kurt, 1972). As in the remaining Asian rhinos, the anterior dentition is represented by the I1 and tusk-like, lower i2. The skull has a relatively long muzzle (orbitonasal length greater than orbitoaural),

Ecology and behavior—the Sumatran rhino is commonly found on hilly areas with permanent availability of water. It inhabits tropical rain forest and mountain moss forest (Groves and Kurt, 1972), but frequents secondary growth forests and crops, where the species can found most of its food (Strickland, 1967). They can swim well and climb steep slopes with ease (Evans, 1905; Groves and Kurt, 1972). Sumatran rhinos achieve seasonal vertical migrations depending on the rainy season and, possibly, by the abundance of horse-flies in the lowlands (Skafte, 1961). Foods include fruit, leaves, twigs, and barks. Wild mangoes, figs, some bamboo species and leaves of several species are among their preferred food items (Evans, 1904; Hubback, 1939; Metcalfe, 1961; Thom, 1935). Rhinos are used to break down small trees and bushes with the horn (Groves and Kurt, 1972). As with the other two Asian species, only young and sick individuals are victims of large carnivores such as tigers.



Fig. 8 Maximum distribution map (Holocene) of the Sumatran rhino (*Dicerorhinus sumatrensis*) in Asia and head portrait of the species. Notice the characteristic hairy areas. Circles in the map represent living populations. Redrawn from Antoine (2011). Drawing by David Quinn.



RHINO CONSERVANCY AND CURRENT POPULATION STATUS

Occasionally hunted for meat, rhinos maintained considerable numbers into historical times. In the 17 and 18th centuries, several animals from the Asian colonies were shipped as gifts to the royal courts and exhibited in the European menageries (Hoage and Deiss, 1996). Rhinos started their drastic decline worldwide in the late 19th century due to sports hunting. Ever expanding human population has produced deep landscape transformations, mainly in agriculture and infrastructure development. New farmed areas entered in conflict with pre-existent wildlife. Frequently considered as pests or dangers to their crops, rhinos have been taken down by farmers and ranchers. On the other hand, new roads and settlements fragmented the once continuous habitats, increasing species risk of extinction by increasing dispersal barriers, reducing the habitat's quality, and favoring the contact with human populations. Therefore, ideal rhino habitats were rapidly transformed, driving rhino species to suboptimal areas. From the 1950s on, the continued demand on rhino horn for medicinal purposes has decimated the remaining rhino populations. On the other hand, both Asian and African populations have been intermittently threatened by civil unrest (1997). Only the recent conservation efforts have mitigated the negative trend recorded during the last century, with different results for each rhino species.

The massive killing by Europeans in the 19th century nearly wipes out both *Ceratotherium* species. Due to early conservation efforts, the white rhino recovered from a bottleneck of 20 left in the early 1895 to over 20,000 today. The species is the most populous rhino, andits survival is currently considered a conservation success. It is listed as nearly threatened by the IUCN nowadays.

The Nile rhino (*Ceratotherium cottoni*) is highly threatened. This species has never been as abundant as its southern relative (less than 1,000 by 1979/80; Hillman-Smith, 1986). Sadly, the last wild Nile rhinos from Garamba National Park were killed by poachers around 2011. Subsequently, four individuals from the eight surviving worldwide at that moment (all kept in captivity) were moved from the Dvůr Králové Zoo (Czech Republic) to Ol Pejeta (Kenya). By 2014, 7 Northern white rhinos were recorded in the latest census, an exiguous population unlikely to be viable in the longer term (IUCN).

The black rhino followed a different life history. From an estimated number of 65,000 individuals in 1970, the species bottomed out to a minimum number of 2,300 in 1993. Due to conservancy efforts in the early 1990s on, black rhino population figures have been increasing to a current population of 5,055. Their species' perspectives range from positive to declining depending on their local protection status and management, being listed as critically endangered by the IUCN. Only three subspecies persist. These are *D. b. bicornis*, *D. b. michaeli*, and *D. b. minor*. Tragically, the western black rhino (*Diceros bicornis longipes*) was poached to its extinction around 2003, but the new status was not officially declared by the IUCN until 2011.

Sumatran and Javan rhino species are critically endangered (IUCN). The world population of Sumatran rhino has dropped from over 800 in 1984 to 75 viable animals left in the wild (Nardelli, 2014). From the three subspecies of Sumatran rhino, the Northern Sumatran rhino (once distributed along India, Bangladesh and Myanmar), may have disappeared. New combined ex situ and in situ conservation plans for the next decade have been proposed to ensure the survival of this rapidly declining species (Nardelli, 2014). Once widespread along large part of Southeast Asia, the Javan rhino is now

considered the second most threatened rhino species (after the Nile rhino), with less than 50 individuals worldwide. Unfortunately, two subspecies, the Indian Javan rhino (disappeared one century ago) and the Southeastern Javan rhino (declared extinct in 2010; Brook et al., 2014), have been hunted into extinction. The only known population is located in Ujung Kulon National Park, an area that has reached its maximum carrying capacity. Conservancy effort of this critically endangered species (IUCN) are focused on relocate few individuals to more suitable areas.

The Greater one-horned rhino enjoy healthier populations than the remaining two Asian species and has been classified as vulnerable (IUCN). The historical geographic reduction was largely influenced by the disappearance of the Indian alluvial plain grasslands. Thanks to its protection, the population of the species rose from barely 100 animals in 1960 to the more than 3,000 individuals distributed along India and Nepal today (70% of them in a single site, the Indian Kaziranga National Park), becoming the most numerous of the three Asian species. However, illegal poaching and continuous habitat degradation is jeopardizing the species' recovery.

Direct conservation strategies include the protection of larger populations in the wild, intensive in situ management of smaller populations, and ex situ programs to reinforce wild populations. Unfortunately, illegal poaching is soaring last years, driving some species' perspectives back to low numbers. Even South Africa, which escaped from the rhino poaching peak prior to the mid-1990s, has witnessed a dramatic climb from 2006 on. This boost culminated in 2014 with 1,020 rhinos killed (2014), truncating the conservation histories of the Southern white and black rhino species and starting to threaten the once abundant southern white rhino. To reverse this situation, international cooperation has to be more efficient and effective than ever.

THE IMPORTANCE OF RHINOCEROS SPECIES

Ecological significance of extant rhinos

As large herbivores, rhinos are exposed to a low predation pressure, especially if compared to smaller ungulates. Nevertheless, predation sometimes occurs. In Africa, lions exceptionally predate on rhinos, particularly on young calves (Brain et al., 1999; Elliot, 1987; Goddard, 1976; Patton, 2009; Ritchie, 1963) and subadults (Western, 1982). Tigers also prey on calves of Asian species, but these interactions are nowadays difficult to record due to the scarcity of both predator and preys. Spotted hyenas have been observed to attack rhinos, but no successful attack has been ever reported (Sillero-Zubiri and Gottelli, 1991). Large herbivores have not always been immune to predators. Saber-tooth cats show an extremely specialized craniodental anatomy (summarized in; Arribas and Palmqvist, 1999) that permit them to take down big ungulate prey relative to their own size. As today with larger felines, younger rhinos were probably among the prey of saber-tooth cats, and smaller rhino species would have been part of their diet together with several large carnivores from the Oligocene and Miocene like amphycionids (as proposed in; Antunes et al., 2006). Additionally, a variable amount of flesh and bone nutrients left by specialized predators like the saber-toothed cats could have been scavenged by a plethora of fossil species, including humans (Arribas and Palmqvist, 1999; Marean, 1989).

Extant rhinos establish symbiotic relationships with several genera of birds (e.g. *Buphagus, Bubulcus, Lamprocolius, Corvus*; Owen-Smith, 1973; Player and Feely, 1960; Stutterheim, 1980; Thomson, 1971). The birds eat the insects disturbed by the rhino, whereas the rhino responds to their warning calls of the birds. In a similar way, black rhinos have been seen forming temporal associations with buffalos (*Syncerus caffer*), taking advantage of the more acute eyesight of the later (Hillman-Smith and Groves, 1994).

Rhinos play an important role as ecosystem landscapers. For example, black rhinos have been responsible for rapid local vegetation changes (i.e. loss of the 33% of the trees in Laikipia, Kenya during a 3-year period; Birkett and Stevens-Wood, 2005). Rhinos can digest a wider variety of available species than other herbivores and are able to process plants with chemical defenses (Loutit et al., 1987). Trampling and grazing by large herbivores like rhinos reduce the vegetation cover (Hagenah, 2006) and produce deep effects on their ecosystems. Grazing species creates vegetation mosaics, thus improving the food quality and vegetation structure. Additionally, they can make some vegetation resources available for other herbivores. For example, the close-crop grazing of white rhinos opens grazing patches in messic savannas for other short grass grazers like zebras (*Equus quagga*) or blue wildebeest (*Connochaetes taurinus*) and mixed-feeders like impalas (*Aepyceros melampus*; Waldram et al., 2008). However, too intense grazing pressure increases the exposure of smaller herbivores to predators and limits their food resources, thus affecting negatively to their populations (Hagenah, 2006). The tracks made to get to feeding areas or water resources are permanently used, impeding the growth of vegetation in the African savannahs (Schenkel and Schenkel-Hulliger, 1969a) or creating depressions in the ground of the jungle favoring small water courses during the rainy season.

Rhinos not only favor the development of open vegetation. They also play an important role in creating new forested ones. Tropical forests are dominated by trees that depend on animals for primary dispersal (so-called zoochorous). In extant tropical forests there is a variable but significant proportion of zoochorous species specialized on large herbivores (> 10 % in Chitwan, Nepal, 30% in the Ivory Coast; Dinerstein and Wemmer, 1988). Elephants, tapirs, and rhinoceros are examples of the short list of large, potentially frugivorous, extant species. These megafaunal remnants are of capital importance to ensure the survival of the specialized flora. Even though these interactions have been previously questioned in fossil megaherbivores such as mastodons (Howe, 1985),

living rhino species have been reported as specialized seed dispersers. For example, the great-horned rhinoceros is the only herbivore species present in Chitwan's forests (Nepal) that processes and favors the dispersion of the large and heavy *Trewia* seeds (Dinerstein and Wemmer, 1988). Javan rhino also disseminates big seeds in feces. This particularity together with an extensive use of the understory resources when feeding and trampling (Dinerstein, 1992; Dinerstein and Price, 1991), would have shaped forest structure in the past, when the species was more abundant (Groves, 1982). Additionally, rhino dung favors seed germination and the settle of a diverse associated fauna, principally dominated by insects.

Economic and cultural status

Rhino horn has been used since ancient times to make ornamental objects like carvings in distantly related cultures in Africa, Europe or Asia. The oldest preserved object made with rhino horn is a Chinese cup from the Tang dynasty (AD 618-906). Nowadays, uses of rhino horn presents two main sources of demand: the first and more important is for medicinal purposes, the second in importance is for making ceremonial 'Djambiyas' dagger handles in Yemen and Oman (Leader-Williams, 1992; Martin and Vigne, 1986).

Rhino horns have played part in traditional medicine worldwide but is in the traditional Asian medicine (mainly China, but also present in other regions like Korea, India or the Indochinese Peninsula) where they attain a higher demand. The medicinal use of rhino horn in Asia dates back several centuries and is probably that Asian rhino species provided the source of all horn. As rhinos became extinct in China, suppliers for traditional medications had to range far afield for their sources, raising their value and depleting African populations too. The imported African horn (or 'water-horn') filled the gap left by the Asian horn (often referred to as 'fire horn' and regarded as superior) at lower market prizes when both were available ('t Sas-Rolfes, 1993). In China, powdered rhino horn was used as an all-purpose health tonic, particularly as a treatment for high fever. In the last years its medicinal use has been broadened to additional pathologies, some of them without treatment. Recently, rhino horn has become popular in Vietnam as a recreational drug, thus increasing its demand. Posteriorly, Western media added to the purported stimulant surge aphrodisiac and sexual properties, in a similar way to its traditional use in the Indian region of Gujarat (Hoogerwerf, 1970). The use of rhino horn is not restricted to Asia. Along Central Europe, prehistoric fossil horns from caves were collected during the 16th century for medicinal purposes (Encyclopaedia Britannica, 11thed). In this case, horn supplies would be rare and limited by occasional findings.

Several studies tested the possible medicinal uses of rhino horn for reducing fever showed no results. A posterior research carried out by the Hong Kong University confirmed some antipyretic effect, but in very high doses (much higher than all available drugs). In 1975-77 the Convention on International Trade in Endangered Species (CITES) banned the trade of animal parts such as horns. Nowadays illegal animal poaching is part of a multibillion dollar business, only surpassed by drug trafficking. With rhino horn commanding a higher price tag than gold (more than 100,000$/Kg predicted for 2017; Msimang), conservation is challenging in most cases (Ellis, 2010).

Rhinos are magnificent creatures that link us to a wild and remote nature. Noticeably, some of the earliest cave art of wildlife comes from the Paleolithic cave of Chauvet (France) and represents two wooly rhinos and a bison. Rhinos are considered flagship and umbrella species for international conservation (Bowen-Jones and Entwistle, 2002; Emslie and Brooks, 1999). Flagship species are enough publicly charismatic to secure its economic and social support for conservation, whereas umbrella ones need large territories to ensure their survival. These large areas host many others neglected species that benefit from their protection. Consequently, conservation programs transcend beyond many other kinds of wildlife. Finally, rhinoceroses are an important source of revenue through eco-tourism and contribute in a significant way to the natural parks and game reserves revenue along Asia and Africa (Adhikari et al., 2005; Gordon et al., 2004; Minin et al., 2012). Alternative economic opportunities to game hunting and poaching using wildlife preservation as a local socioeconomic catalyst for change are necessary for ensuring the survival of the few living rhinos.

ACKNOWLEDGMENTS

Thanks to David Quinn for his gorgeous rhino illustration (originally published in "Rhinos, endangered species" by Malcom Penny) and Jim Martin (Bloomsbury Publishing Plc.) for his permission to include them in the present work. I also thank to Eileen Westwig and the staff of the AMNH for access to living species specimens in their care.

LITERATURE CITED

1911, Encyclopædia Britannica Eleventh Edition, *in* Chisholm, H., ed., Cambridge University Press.

't Sas-Rolfes, M. J., 1993, The economics of rhino conservation. An economic analysis of policy options for the management of wild rhino populations in Africa [Masters Course in Environmental and Resource Economics: UCL, 83 p.

Adhikari, B., Haider, W., Gurung, O., Poudyal, M., Beardmore, B., Knowler, D., and Van Beukering, P., 2005, Economic incentives and poaching of the one-horned Indian Rhinoceros in Nepal Poverty Reduction and Environmental Management (PREM) v. 05-12, p. 1-44.

Ammann, H., 1985, Contributions to the ecology and sociology of the Javan rhinoceros (*Rhinoceros sondaicus*

Desm.) [Inaugural dissertation: Universität Basel.

Antoine, P. O., 2011, Pleistocene and Holocene rhinocerotids (Mammalia, Perissodactyla) from the Indochinese Peninsula: Comptes Rendus Palevol.

Antunes, M. T., Balbino, A. C., and Ginsburg, L., 2006, Ichnological evidence of a Miocene rhinoceros bitten by a bear-dog (Amphicyon giganteus): Annales de Paléontologie, v. 92, no. 1, p. 31-39.

Arribas, A., and Palmqvist, P., 1999, On the ecological connection between sabre-tooths and hominids: faunal dispersal events in the lower Pleistocene and a review of the evidence for the first human arrival in Europe: Journal of Archaeological Science, v. 26, no. 5, p. 571-585.

Asher, R. J., Novacek, M. J., and Geisler, J. H., 2003, Relationships of endemic African mammals and their fossil relatives based on morphological and molecular evidence: Journal of Mammalian Evolution, v. 10, p. 131-194.

Barnejee, S., and Chakraborty, S., 1973, Remains of the great one-horned rhinoceros, *Rhinoceros unicornis* Linnaeus from Rajashtan: Science and Culture, v. 39, p. 430-431.

Beard, K. C., 1998, Dawn of the Age of Mammals in Asia, Bulletin of the Carnegie Museum of Natural History.

Becker, D., Antoine, P. O., and Maridet, O., 2013, A new genus of Rhinocerotidae (Mammalia, Perissodactyla) from the Oligocene of Europe: Journal of Systematic Palaeontology.

Birkett, A., and Stevens-Wood, B., 2005, Effect of low rainfall and browsing by large herbivores on an enclosed savannah habitat in Kenya: African Journal of Ecology, v. 43, p. 123-130.

Bowen-Jones, E., and Entwistle, A., 2002, Identifying appropriate flagship species: the importance of culture and local contexts: Oryx, v. 36, p. 189-195.

Brain, C., Forge, O., and Erb, P., 1999, Lion predation on black rhinoceros (*Diceros bicornis*) in Etosha National Park: African Journal of Ecology, v. 37, p. 107-109.

Brook, S. M., Dudley, N., Mahood, S. P., Polet, G., Williams, A. C., Duckworth, J. W., Ngoc, T. V., and Long, B., 2014, Lessons learned from the loss of a flagship: The extinction of the Javan rhinoceros *Rhinoceros sondaicus annamiticus* from Vietnam: Biological Conservation, v. 174, p. 21-29.

Buckley, M., 2015, Ancient collagen reveals evolutionary history of the endemic South American 'ungulates': Proceedings of the Royal Society B, v. 282, p. 1-9.

Buk, K. G., 2004, Diet selection and habitat suitability for black rhino for Augrabies Falls National Park, South AfricaM. Sc.Thesis]: University of Copenhagen, 128 p.

Buk, K. G., and Knight, M. H., 2010, Seasonal diet preferences in black rhinoceros in three arid Southern African National Parks: Journal of Ecology, v. 48, p. 1064-1075.

Cave, A. J. E., 1969, Hairs and vibrissae in the Rhinocerotidae: Journal of Zoology, v. 157, p. 247-257.

Cerdeño, E., 1995, Cladistic analysis of the Family Rhinocerotidae (Perissodactyla): American Museum Novitates, v. 3143, p. 1-25.

Cranbrook, E. o., 1986, A review of fossil and prehistoric remains of rhinoceroses of Borneo: Sabah Museum and Archives Journal, v. 1, p. 50-110.

Chauhan, P. R., 2008, Large mammal fossil occurrences and associated archaeological evidence in Pleistocene contexts of peninsular India and Sir Lanka: Quaternary International, v. 192, p. 20-42.

de Blainville, H. M. D., 1816, Prodrome d'une novelle distribution systématique du règne animal: Bulletin des Sciences, Societé Philomathique de Paris, Série 3, v. 3, p. 105-124.

De Poncins, V. E., 1935, A hunting trip in the Sunderbunds in 1892: Journal of the Bombay Natural History Society, v. 37, p. 844-858.

Deraniyagala, P. E. P., 1937, Some Miocene and Upper Siwalik vertebrates from Ceylon: Ceylon Journal of Science, v. B, no. 10, p. 191-200.

-, 1938, Some fossils from Ceylon. Part II.: Journal of the Ceylon Branch of the Royal Asiatic Society of Great Britain and Ireland, v. 34, p. 231-239.

-, 1946, Some mammals of the extinct Ratnapura fauna of Ceylon: Spolia Zeylanica, v. 24, p. 161-167.

Dinerstein, E., 1992, Effects of *Rhinoceros unicornis* on Riverine Forest Structure in Lowland Nepal: Ecology, v. 73, no. 2, p. 701-704.

Dinerstein, E., and Price, L., 1991, Demography and habitat use by greater one-horned rhinoceros in Nepal: Journal of Wildlife Management, v. 55, p. 401-411.

Dinerstein, E., and Wemmer, C. M., 1988, Fruits Rhinoceros Eat: Dispersal of *Trewia nudiflora* (Euphorbiaceae) in Lowland Nepal: Ecology, v. 69, no. 6, p. 1768-1774.

Elliot, W. M., 1987, Possible Predation of a Black Rhinoceros Calf by a Lion: Lammergeyer, v. 38, p. 68.

Ellis, R., 2010, Rhino horn: facts and myths: African Indaba - eNewsletter, v. 8, no. 6, p. 16-18.

Emslie, R., and Brooks, M., 1999, African Rhino: Status Survey and Action Plan: IUCN.

Evans, G. H., 1904, The Asiatic two-horned rhinoceros (Rhinoceros sumatrensis): Journal of the Bombay Natural History Society, v. 16, p. 160-161.

-, 1905, Notes on rhinoceroses in Burma, *R. sondaicus* and *sumatrensis*: Journal of Bombay Natural History Society, v. 16, p. 555-561.

Fischer, M., 1986, Die Stellung der Schliefer (Hyracoidea) im phylogenetischen System der Eutheria. Zugleich ein Beitrag zur Anpassungsgeschichte der Procaviidae: Courier Forschungsinstitut Senckenberg, v. 84, p. 1-132.

-, 1989, Hyracoids as perissodactyls, *in* Prothero, D. R., and Schoch, R. M., eds., The Evolution of Perissodactyls: New

York, Oxford University Press, p. 37-56.

Fischer, M. S., and Tassy, P., 1993, The interrelation between Proboscidea, Sirenia, Hyracoidea, and Mesaxonia: The morphological evidence, *in* Szalay, F. S., Novacek, M. J., and McKenna, M. C., eds., Mammal Phylogeny, Volume 2: New York, Springer-Verlag, p. 217-234.

Flower, S. S., 1900, On the Mammalia of Siam and the Malay Peninsula: Proceedings of the Zoological Society of London, p. 306-379.

Foose, T. J., and van Strien, N., 1997, Asian Rhinos, Gland, Switzerland and Cambridge, UK, IUCN, Status Survey and Conservation Plan. IUCN/SSC Asian Rhino Specialist Group.

Foster, J. B., 1967, The square-lipped rhinoceros (*Ceratotherium simum cottoni* (Lydekker)) in Uganda: East African Wildlife Journal, v. 1, p. 25-35.

Foster, W. E., 1960, The square-lipped rhinoceros: Lammergeyer, v. 1, p. 25-35.

Fraser, O. L., 1875, Note on a partially ossified nasal septum in *Rhinoceros sondaicus*: Journal of the Asiatic Society of Bengal, v. 44, p. 10-12.

Giaourtsakis, I., Phlevan, C., and Haile-Selassie, Y., 2009, 14. Rhinocerotidae, *in* Haile-Selassie, Y., and Woldegabriel, G., eds., *Ardipithecus kadabba*. Late Miocene Evidence from the Middle Awash, Ethiopia: Berkeley, Los Angeles, and London, University of California Press and University of California Press, Ltd., p. 429-472.

Goddard, J., 1968, Food preferences of two black rhinoceros populations.: East African Wildlife Journal, v. 6, p. 1-18.

-, 1970, Food preferences of black rhinoceros in Tsavo National Park: East African Wildlife Journal, v. 8, p. 145-161.

-, 1976, Home Range, Behaviour and Recruitment of Rhinos: East African Wildlife Journal, v. 5, p. 133-150.

Gordon, I. J., Hester, A. J., and Festa-Bianchet, M., 2004, The management of wild large herbivores to meet economic, conservation and environmental objectives: Applied Ecology, v. 41, p. 1021-1031.

Groves, C. P., 1967, On the Rhinoceroses of South-East Asia: Säugetierk. Mitteilungen, München, v. 15, p. 221-237.

-, 1972, *Ceratotherium simum*: Mammalian Species. The American Society of Mammalogists, v. 8, p. 1-6.

-, 1982, Asian rhinoceroses: down but not out.: Malayan Naturalist, v. 36, no. 1, p. 11-17.

Groves, C. P., 2010, The Sixth Rhino: A Taxonomic Re-Assessment of the Critically Endangered Northern White Rhinoceros: PLoS ONE, v. 5, no. 4, p. 1-15.

Groves, C. P., and Kurt, F., 1972, *Dicerorhinus sumatrensis*: Mammalian Species. The American Society of Mammalogists, v. 21, p. 1-6.

Groves, C. P., and Leslie, D. M. J., 2011, *Rhinoceros sondaicus*: Mammalian Species. The American Society of Mammalogists, v. 43, no. 887, p. 190-208.

Guérin, C., À propos des rhinocéros (Mammalia, Perissodactyla) néogènes et quaternaires d'Afrique : essai de synthèse sur les espèces et sur les gisements, *in* Proceedings Proceedings 8th. PanAfrican Congress Prehistory Quaternary Studies, Nairobi, Nairobi, September, 1977 1980, p. 58-63.

Guggisberg, C. A. W., 1966, SOS rhino, London, 174 p.:

Hagenah, N., 2006, Among rodents and rhinos: interplay between small mammals and large herbivores in a South African savanna [Ph.D. Dissertation: University of Wageningen, 146 p.

Harper, F., 1945, Extinct and vanishing mammals of the Old World, New York, New York Zoological Park, Special Publication 12. American Committee for International Wild Life Protection.

Hazarika, B. C., and Saikia, P. K., 2012, Food habit and feeding patterns of great Indian one-horned rhinoceros (*Rhinoceros unicornis*) in Rajiv Gandhi National Park, Assam, India: International Scholarly Research Network 2012, p. 1-11.

Heissig, K., 2012, The American genus Penetrigonias Tanner & Martin, 1976 (Mammalia: Rhinocerotidae) as a stem group elasmothere and ancestor of *Menoceras* Troxell, 1921: Zitteliana, v. A 52, p. 79-96.

Heller, E., 1913, The white rhinoceros: Smithsonian Miscelaneous Collections, v. 61, no. 1, p. 1-77.

Hillman-Smith, A. K., 1986, Notes on dentition, cranial and body measurements of the northern white rhinoceros (Ceratotherium simum cottoni): Journal of Zoology, v. 210, p. 377-379.

Hillman-Smith, A. K., and Groves, C. P., 1994, *Diceros bicornis*: Mammalian Species, v. 445, p. 1-8.

Hoage, R. J., and Deiss, W. A., 1996, New worlds, new animals: from menagerie to zoological park in the nineteenth century, Baltimore and London, The John Hopkins University Press.

Holbrook, L. T., 1999, The Phylogeny and Classification of Tapiromorph Perissodactyls (Mammalia): Cladistics, v. 15, p. 331-350.

-, 2001, Comparative osteology of early Tertiary tapiromorphs (Mammalia, Perissodactyla): Zoological Journal of the Linnean Society, v. 132, p. 1-54.

-, 2009, Osteology of *Lophiodon* Cuvier, 1822 (Mammalia, Perissodactyla) and its Phylogenetic Implications: Journal of Vertebrate Paleontology, v. 29, no. 1, p. 212-230.

Holbrook, L. T., Lucas, S. G., and Emry, R. J., 2004, Skulls of the Eocene perissodactyls (Mammalia) *Homogalax* and *Isectolophus*: Journal of Vertebrate Paleontology, v. 24, no. 4, p. 951-956.

Hoogerwerf, A., 1970, Udjung Kulon the Land of the Last Javan Rhinoceros, Brill Archive.

Hooijer, D. A., 1946, Prehistoric and Fossil Rhinoceroses

from the Malay Archipelago and India: Zoologische Mededelingen, v. 26, no. 1, p. 1-138.

-, 1949, Mammalian evolution in the Quaternary of southern and eastern Asia: Evolution, v. 3, p. 125-128.

-, 1964, New records of mammals from the Middle Pleistocene of Sangiran, Central Java: Zoologische Mededelingen, Leiden, v. 40, p. 73-87.

-, 1969, Pleistocene East African rhinoceroses: Fossil Vertebrates of Africa, v. 1, p. 71-98.

Hooker, J. J., 2005, Origins and Relationships of the Major Extant Clades, *in* Rose, K. D., and Archibald, J. D., eds., The Rise of Placental Mammals, Johns Hopkins Univ. Press, p. 199–214.

Horsfield, T., 1824, Zoological researches in Java, and the neighbouring islands, London, Kingsbury, Parbury, & Allen.

Howe, H. F., 1985, Gomphothere fruits: a critique: American Naturalist, v. 125, p. 853-865.

Hubback, T. R., 1939, The Asiatic two-horned rhinoceros: Journal of Mammalogy, v. 20, p. 1-20.

Janis, C., Colbert, M. W., Coombs, M. C., Lambert, D., MacFadden, B. J., Mader, B. J., Prothero, R., Donald, Schoch, R. M., Shoshani, J., and Wall, W. P., 2008, 35. Perissodactyla and Proboscidea, *in* Janis, C., Scott, K. M., and Jacobs, L. L., eds., Evolution of Tertiary Mammals of North America. Volume 1: Terrestrial Carnivores, Ungulates and Ungulatelike Mammals, p. 511-524.

Kondrashov, P., and Lucas, S. G., 2012, Nearly complete skeleton of Tetraclaenodon (Mammalia, Phenacodontidae) from the early Paleocene of New Mexico: morpho-functional analysis: Journal of Paleontology, v. 86, p. 25-43.

Konwar, P., Saikia, M. K., and Saikia, P. K., 2009, Abundance of food plant species and food habits of *Rhinoceros unicornis* Linn. In Pobitora Wildlife Sanctuary, Assam, India: Journal of Threatened Taxa, v. 1, no. 9, p. 457-460.

Ladevèze, S., Missiaen, P., and Smith, T., 2010, First skull of Orthaspidotherium edwardsi (Mammalia, Condylarthra) from the late Paleocene of Berru (France) and phylogenetic affinities of the enigmatic European family Pleuraspidotheriidae: Journal of Vertebrate Paleontology, v. 30, p. 1559-1578.

Laurie, W. A., 1978, The ecology and behaviour of the greater one-horned rhinoceros [Doctor of Philosophy: University of Cambridge, 450 p.

-, 1982, Behavioral ecology of the greater one-horned rhinoceros (*Rhinoceros unicornis*): Journal of Zoology, v. 196, p. 307-607.

Laurie, W. A., Lang, E. M., and Groves, C. P., 1983, *Rhinoceros unicornis*: Mammalian Species. The American Society of Mammalogists, v. 211, p. 1-6.

Leader-Williams, N., 1992, The World Trade in Rhino Horn: A Review, Cambridge, Traffic International, Traffic International.

Lidekker, R., 1884, Catalogue of Vertebrate Fossils from the Siwaliks of India in the Science and Art Museum. Dublin: Scientific Transactions of the Royan Dublin Society. Series 2, v. 3, p. 69-86.

Loch, C. H., 1937, *Rhinoceros sondaicus*. The Javan or lesser onehorned rhinoceros and its geographical distribution: Journal of Malayan Branch of the Royal Asiatic Society, Singapore, v. 15, p. 130-149.

Loutit, B. D., Louw, G. N., and Seely, M. K., 1987, First approximation of food preferences and the chemical composition of the diet of the desert-dwelling black rhinoceros, *Diceros bicornis* L.: Madoqua, v. 15, p. 35-54.

Lydekker, R., 1886a, The fauna of the Karnul Caves. Memoirs of the Geological Survey of India: Palaeontologia Indica. Series X, Indian Tertiary & Post-Tertiary Vertebrata, v. 4, no. Part II, p. 22-58.

-, 1886b, Preliminary note on the Mammalia of the Karnul Caves: Records of the Geological Survey of India, v. 19, p. 120-122.

MacFadden, B. J., 1976, Cladistic Analysis of Primitive Equids, with Notes on Other Perissodactyls: Systematic Zoology, v. 25, no. 1, p. 1-14.

Manamendra-Arachchi, K., Pethiyagoda, R., Dissanayake, R., and Meegaskumbura, M., 2005, A second extinct big cat from the late Quaternary of Sri Lanka: The Raffles Bulletin of Zoology, v. Supplement 12, p. 423-434.

Marean, C. W., 1989, Sabertooth cats and their relevance for early hominid diet and evolution: Journal of Human Evolution, v. 18, p. 559-582.

Martin, E. B., and Vigne, L., 1986, International trade in rhino products: WWF Yearbook 1985-1986, p. 46-48.

McKenna, M. C., 1975, Toward a phylogenetic classification of the Mammalia, *in* Luckett, W. P., and Szalay, F. S., eds., hylogeny of the Primates: A Multidisciplinary Radinsky: New York, Plenum Press, p. 21-46.

Meredith, R. W., Janecka, J. E., Gatesy, J., Ryder, O. A., Fisher, C. A., Teeling, E. C., Goodbla, A., Eizirik, E., Simão, T. L. L., Stadler, T., Rabosky, D. L., Honeycutt, R. L., Flynn, J. J., Ingram, C. M., Steiner, C., L.Williams, T., Robinson, T. J., Burk-Herrick, A., Westerman, M., Ayoub, N. A., Springer, M. S., and Murphy, W. J., 2011, Impacts of the Cretaceous terrestrial revolution and KPg extinction on mammal diversification: Science, v. 334, p. 521-524.

Merenlender, A. M., Woodruff, D. S., Ryder, O. A., Kock, R., and Va´hala, J., 1989, Allozyme variation and differentiation in African and Indian rhinoceroses: Journal of Heredity, v. 80, p. 377-382.

Metcalfe, G. T. C., 1961, Rhinoceros in Malasya and their future: Malayan Nature Journal, v. Special Issue 21st Anniversary, p. 103-106.

Minin, E. D., Fraser, I., Slotow, R., and MacMillan, D. C., 2012,

Understanding heterogeneous preference of touristsfor big game species: implications for conservationand management: Animal Conservation, p. 1-10.

Msimang, M., 2013, Rhino Issue Management Report 2013, *in* Africa, E. A. D. R. o. S., ed.: Pretoria, p. 34.

Mukinya, J. G., 1973, Density, distribution, population structure and social organisation of the black rhinoceros in Masai Mara Game Reserve: East African Wildlife Journal, v. 11, p. 385-400.

Murphy, W. J., Eizirik, E., Johnson, W. E., Zhang, Y. P., Ryderk, O. A., and O'Brien, S. J., 2001, Molecular phylogenetics and the origins of placental mammals: Nature, v. 409, p. 614-618.

Nardelli, F., 2014, The last chance for the Sumatran rhinoceros?: Pachyderm, v. 55, no. 43-53.

Nishihara, H., Hasegawa, M., and Okada, N., 2006, Pegasoferae, an unexpected mammalian clade revealed by tracking ancient retroposon insertions: Proceedings of the National Academy of Sciences, v. 103, no. 26, p. 9929-9934.

Novacek, M. J., and Wyss, A. R., 1986, Higher-level relationships of the Recent eutherian orders: Morphological evidence: Cladistics, v. 2, p. 257-287.

O'Leary, M. A., Bloch, J. I., Flynn, J. J., Gaudin, T. J., Giallombardo, A., Giannini, N. P., Goldberg, S. L., Kraatz, B. P., Luo, Z.-X., Meng, J., Ni, X., Novacek, M. J., Perini, F. A., Randall, Z. S., Rougier, G. W., Sargis, E. J., Silcox, M. T., Simmons, N. B., Spaulding, M., Velazco, P. M., Weksler, M., Wible, J. R., and Cirranello, A. L., 2013, The placental mammal ancestor and the post-K-Pg radiation of placentals.: Science, v. 6120, p. 662-667

Owen-Smith, N., 1988, Megaherbivores: The Influence of Very Large Body Size on Ecology, Cambridge.

Owen-Smith, R. N., 1973, The behavioural ecology of the white rhinoceros [PhD Thesis: University of Winsconsin, 1572 p.

Owen, R., 1848, Description of teeth and portions of jaws of two extinct Anthracotherioid quadrupeds (*Hyopotamys vectianus* and *Hyop. bavinus*) discovered by the Marchioness of Hastings in the Eocene deposits of the N. W. coast of the Isle of Wright: with an attempt to develop Cuvier's idea of the classification of pachyderms by the number of their toes: Quarterly Journal of the Geological Society of London, v. 4, p. 103-141.

Patton, F., 2009, Lion predation on the African Black Rhinoceros and its potential effect on management: Endangered Species UPDATE, v. 26, no. 1, p. 43-49.

Pedersen, G., 2009, Habitat use and diet selection of reintroduced white rhinoceros (Ceratotherium simum) in Pafuri, Kruger National Park [Master of Science: Stellenbosch University, 120 p.

Perrin, M. R., and Brereton-Stiles, R., 1999, Habitat use and feeding behaviour of the buffalo and the white rhinoceros in the Hluhluwe-Umfolozi Game Reserve: South African Journal of Wildlife Research, v. 29, p. 72-80.

Player, I., and Feely, J. M., 1960, A preliminary report on the square-lipped rhinoceros *Ceratotherium simum simum*: Lammergeyer, v. 1, p. 3-22.

Pratiknyo, H., 1991, The diet of the Javan rhino: Voice of Nature, v. 93, p. 12-13.

Prothero, D., Guérin, C., and Manning, E., 1989, The History of the Rhinocerotoidea, The Evolution of Perissodactyls, p. 321-340.

Prothero, D. R., Manning, E., and Fischer, M. S., 1988, The phylogeny of ungulates, *in* Benton, M. J., ed., The Phylogeny and Classification of the Tetrapods, Volume 2: Oxford, Clarendon Press, p. 201-234.

Pushkina, D., Bocherens, H., Chaimanee, Y., and Jaeger, J.-J., 2010, Stable carbon isotope reconstructions of diet and paleoenvironment from the late Middle Pleistocene Snake Cave in Northeastern Thailand: Naturwissenschaften, v. 97, p. 299-309.

Radinsky, L. B., 1966, The Adaptive Radiation of the Phenacodontid Condylarths and the Origin of the Perissodactyla: Evolution, v. 20, no. 3, p. 408-417.

Ritchie, A. T. A., 1963, The Black Rhinoceros (*Diceros bicornis* L.): East African Wildlife Journal, v. 1, p. 54-62.

Rookmaaker, L. C., 1980, The distribution of the rhinoceros in eastern India, Bangladesh, China, and the Indo-Chinese region: Zoologischer Anzeiger, v. 205, p. 253-268.

Rookmaaker, L. C., and Antoine, P. O., 2012, New maps representing the historical and recent distribution of the African species of rhinoceros: Diceros bicornis, *Ceratotherium simum* and *Ceratotherium cottoni*: Pachyderm, v. 52, p. 91-96.

Rose, K. D., Holbrook, L. T., Rana, R. S., Kumar, K., Jones, K. E., Ahrens, H. E., Missiaen, P., Sahni, A., and Smith, T., 2014, Early Eocene fossils suggest that the mammalian order Perissodactyla originated in India: Nature communications, p. 1-9.

Santiapillai, C., Giao, P. M., and Dung, V. V., 1993a, Conservation and management of Javan rhino (*Rhinoceros sondaicus annamiticus*) in Vietnam: Tiger Paper, v. 20, p. 7-15.

-, Conservation and management of Javan rhino (*Rhinoceros sondaicus*) in Vietnam, *in* Proceedings Rhinoceros biology and conservation, San Diego, 1993b, Zoological Society of San Diego, p. 248-256.

Sclater, P. L., 1876, On the rhinoceroses now or lately living in the Society's menagerie: Transactions of the Zoological Society of London, v. 9, p. 645-660.

Schaurte, W. T., 1966, Beitrage zur Kenntnis des Gebisses und Zahnbaues der afrikanischen Nashorner: Säugetierkundliche Mitteilungen, v. 14, p. 327-341.

Schenkel, R., and Schenkel-Hulliger, L., 1969a, The Javan rhinoceros (*Rh. sondaicus* Desm.) in Udjung Kulon Nature Reserve. Its ecology and behaviour. Field study 1967 and

1968: Acta Tropica, v. 26, p. 97-135.

-, 1969b, The last remnants of the Javan rhinoceros in Udjung Kulon Nature Reserve, Java.: Biological Conservation, v. 2, p. 68-70.

Schoch, R. M., 1989, A brief historical review of perissodactyl classification, *in* Prothero, D. R., and Schoch, R. M., eds., The Evolution of Perissodactyls: Oxford, Clarendon, p. 13-23.

Sillero-Zubiri, C., and Gottelli, D., 1991, Threat to Aberdares Rhinos: Predation versus Poaching: Pachyderm, v. 14, p. 37-38.

Skafte, H., 1961, A contribution to the preservation of the Sumatran rhinoceros: Acta Tropica, v. 18, p. 167-176.

Sody, H. J. V., 1959, Das Javanische Nashorn Rhincoeros sondaicus historisch und biologisch: Zeitschrift für Säugetierkunde, v. 24, p. 109-240.

Spaulding, M., O'Leary, M. A., and Gatesy, J., 2009, Relationships of Cetacea (Artiodactyla) Among Mammals: Increased Taxon Sampling Alters Interpretations of Key Fossils and Character Evolution: Plos ONE, v. 4, no. 9, p. e7062.

Springer, M. S., Murphy, W. J., Eizirik, E., and O'Brien, S. J., 2003, Placental mammal diversification and the Cretaceous-Tertiary boundary: Proceedings of the National Academy of Sciences, v. 100, p. 1056-1061.

Strickland, D. L., 1967, Ecology of the Rhinoceros in Malaya: Malayan Nature Journal, v. 20, p. 1-17.

Stutterheim, C. J., 1980, Cleaning symbioses involving crows and white rhino: Lammergeyer, v. 30, p. 61.

Thewissen, J. G. M., and Domning, D. P., 1992, The role of phenacodontids in the origin of the modern orders of ungulate mammals.: Journal of Vertebrate Paleontology, v. 12, p. 494-504.

Thom, W. S., 1935, Rhinoceros shooting in Burma: Journal of Bombay Natural History Society, v. 38, p. 138-150.

Thomson, W. R., 1971, Factors affecting the distribution and survival of Black Rhinoceros (*Diceros bicornis* L.) in Rhodesia [Certificate in Field Ecology: University of Rhodesia, 122 p.

Ullrich, W., 1955, Bemerkenswerte Aufnahmen eines junges Sumatra-Nashorns (*Dicerorhinus sumatrensis*): Zoologischer Garten, v. 22, p. 29-33.

Vageler, P., 1927, Ein neues Rhinozeros: Die Umschau, v. 31, p. 289-290.

Van der Bergh, W., 1955, Nos rhinocéros blancs (*Ceratotherium simum cottoni* Lydekker): Zoologischer Garten, v. 21, p. 129-151.

von La Chevallerie, M., 1970, Meat production from wild ungulates: Proceedings of the South African Society of Animal Production, v. 9, p. 73-87.

Waddell, P. J., Okada, N., and Hasegawa, M., 1999, Systematic Biology: 48, p. 1-5.

Waldram, M., Bond, W. J., and Stock, W. D., 2008, Ecological engineering by a mega-grazer: white rhino impacts on a South African savanna: Ecosystems, v. 11, no. 1, p. 101-112.

WESSA, 2014, http://wessa.org.za/get-involved/rhino-initiative/current-rhino-poaching-stats.htm, Volume 2014, WESSA. People caring for the Earth.

Western, D., 1982, Patterns of depletion in a Kenya rhino population and the conservation implications: Biological Conservation, v. 24, p. 147-156.

Willerslev, E., Gilbert, M. T. P., Binladen, J., Ho, S. Y. W., Campos, P. F., Ratan, A., Tomsho, L. P., Fonseca, R. R. d., Sher, A., Kuznetsova, T. V., Nowak-Kemp, M., Roth, T. L., Miller, W., and Schuster, S. C., 2009, Analysis of complete mitochondrial genomes from extinct and extant rhinoceroses reveals lack of phylogenetic resolution: BMC Evolutionary Biology, v. 9.

General Methodology and Measurements

MATERIAL OF STUDY

Temporal and Geographic context

The material studied in the present PhD Thesis is constituted by fossil rhinoceros remains from the late Early to the latest Miocene (lower Aragonian-late Turolian, MN4-MN13 Mein's Biozone; Mein, 1999) from the Tagus, Bierzo, and Levantine basins. Cranial, dental, and postcranial remains have been included. More than 2,650 elements belonging to 8 species of the genera *Lartetotherium, 'Protaceratherium', Aceratherium, Dihoplus, Alicornops*, and *Hispanotherium* have been studied. The list of localities included in the present study is detailed as follows:

- **Early Miocene**
  + Aragonian: Mesegar-1 and Mesegar-2
- **Middle Miocene**
  + Aragonian: M-407 Rotonda, Casa de Campo/Marqués de Monistrol M-30, Príncipe Pío-2, Fresno de Torote, Yunquera de Tajo, La Peineta, Embajadores-R and Fábrica Mahou.
- **Upper Miocene**
  + Vallesian: Batallones-1, Batallones-2, Batallones-3, Batallones-5, Batallones-6, Batallones-10, and Valdeinfierno.
  + Turolian: Corral de Lobato and Venta del Moro.
- Undetermined age (possibly Lower Miocene): Santalla del Bierzo.

Figure 1 shows their geographic location; Figure 2 represents their stratigraphic position. Additional remains from the localities of La Encinilla (Ramblian, Lower Miocene), and Autovía Orbital UB-40 (Vallesian, Upper Miocene) were also studied and published (Quiralte et al., 2011; Tomàs et al., 2010). Due to their scarcity of rhino remains, these were described together with their accompanying faunas and have therefore been excluded from the present work. Additional remains from both living and fossil species that have been examined for comparative purposes are stored in the following institutions:

- Spain: MNCN, Museo Nacional de Ciencias Naturales-CSIC (Madrid); IGME, Instituto Geológico Minero Español (Madrid), ICP, Institut Català de Paleontologia (Sabadell); MGUV, Museo de Geología de la Universitat de València (Valencia), Museo de Ciencias de Valencia (Valencia).
- France: MHNT, Muséum d'Histoire Naturelle de Toulouse (Toulouse); Museé de la Faculté des Sciences de Lyon.
- Germany: BSPG, Bayerische Staatssammlung für Paläontologie un Geologie (Munich); Darmstadt Hessische Landesmuseum (Darmstadt).
- Netherlands: University of Utretch-Faculty of Geosciences (Utrecht).
- United States: AMNH, American Museum of Natural History (New York).

DESCRIPTIVE METHODOLOGY

Postcranial elements of the axial skeleton have been described in cephalocaudal direction. Appendicular elements have been described from the proximal extent to the distal one. Inside each face, facets position, shape, relief and orientation have been described when necessary as well as those relevant soft-tissue insertions placed in long bones. Bone orientations when describing follow the rules given by the Nomina Anatomica Veterinaria (2005), resulting as follows: rostral in head is equivalent to cranial in stylopodium-zeugopodium and dorsal in acropodium; caudal in head is equivalent to caudal in stylopodium-zeugopodium, palmar in the anterior acropodium and plantar in the posterior acropodium; dorsal in the head is equivalent to proximal in the postcranial skeleton; ventral in the head is equivalent to distal in the postcranial skeleton; lateral (external, contrary to the symmetry plane) and medial (internal, towards the symmetry plane) are common to all the regions of the body. The position guides have been schematized in the Figure 1.

ANATOMICAL NOMENCLATURE

The general anatomical terminology follows Budras (2009) and Schaller (2007). In addition, that used by other authors has also been taken into consideration (Antoine, 2002; Antoine et al., 2010; Becker et al., 2013; Guérin, 1980; Heissig, 1972a, 1999). More detailed information of the craniodental anatomy can be found in the Appendix at the end of this volume. For more information regarding the postcranial skeleton

see Chapter 5. Capital letters are used for upper teeth (I1-3, C, D1-4, P1-4, M1-3), and lower case for lower teeth (i1-3, c, d1-4, p1-4, m1-3) as proposed by Jepsen (1996).

PHOTOGRAPHIC AND METRICAL DATA

Specimens were photographed with a Nikon D300 digital camera with a fixed-focus lens Nikkor 50mm f/1.8D. The specimen is centered on the image and the distance to the camera is adjusted in a way that a sufficient empty margin (approximately equivalent to 1/5 of the total length of the subject) is left in all sides in order to avoid barrel-distortions. When possible, pieces have been placed in a photographic platform provided with adjustable spotlights. Typically, 6 views of each one were stored in TIFF format at 300 ppp. Supplementary photographs of areas of interest were taken if required. Images were subsequently processed with Nikon View NX and Adobe Photoshop CS2 – CS5. Posterior specimen illustrations from photographic sources were accomplished using overlays in Adobe Illustrator CS2 – CS5 as well. Additionally, some specimens were sketched in a notebook as a way to understand its structures.

All metrical data up to 150 mm were made with a digital caliper Mitutoyo Digimatic Model 500-196-20 with a precision of 0.1 mm. With up to 600 mm measurements a manual caliper with a precision of 1 mm has been necessary. Million years before present is represented as Ma. All linear measure-

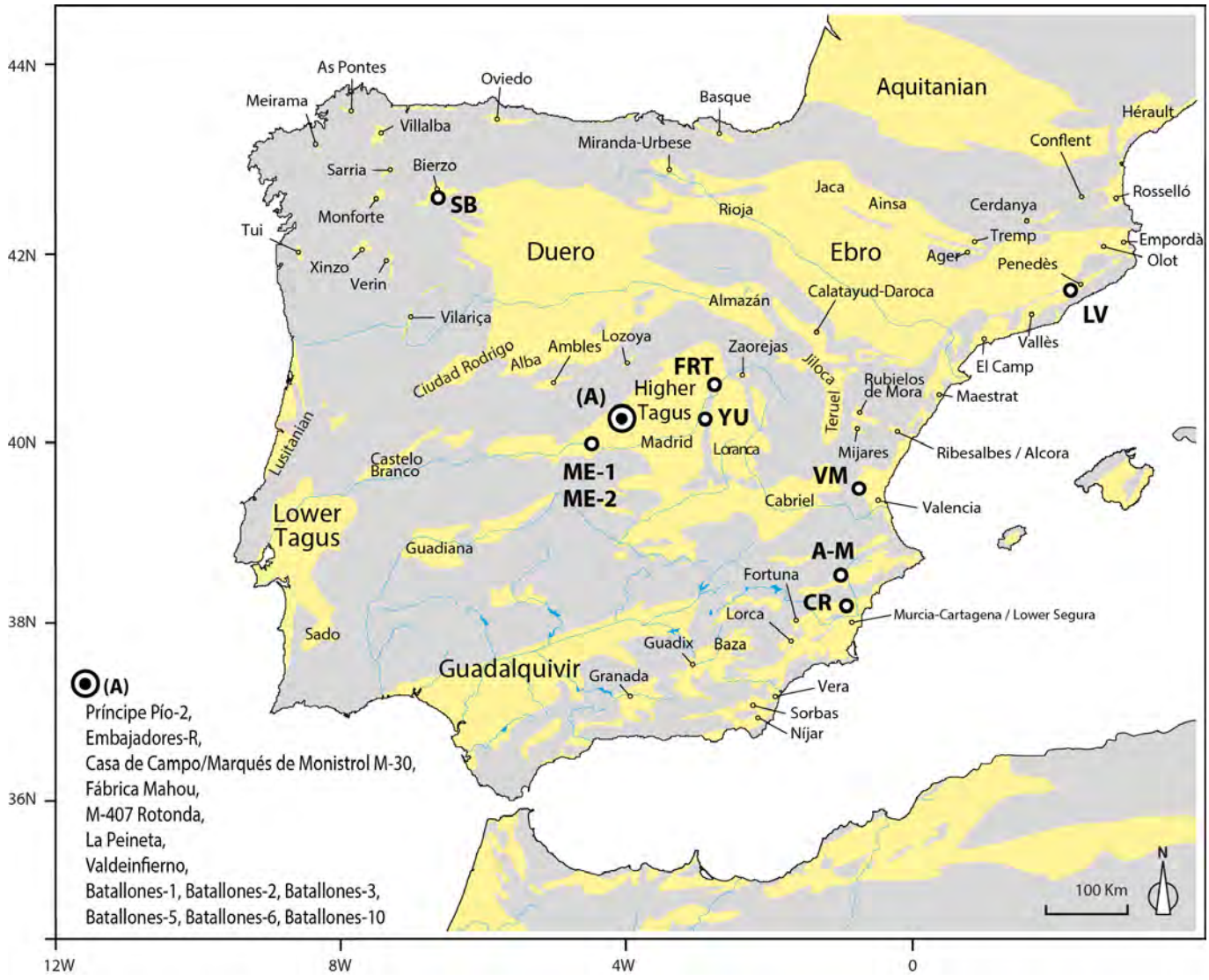
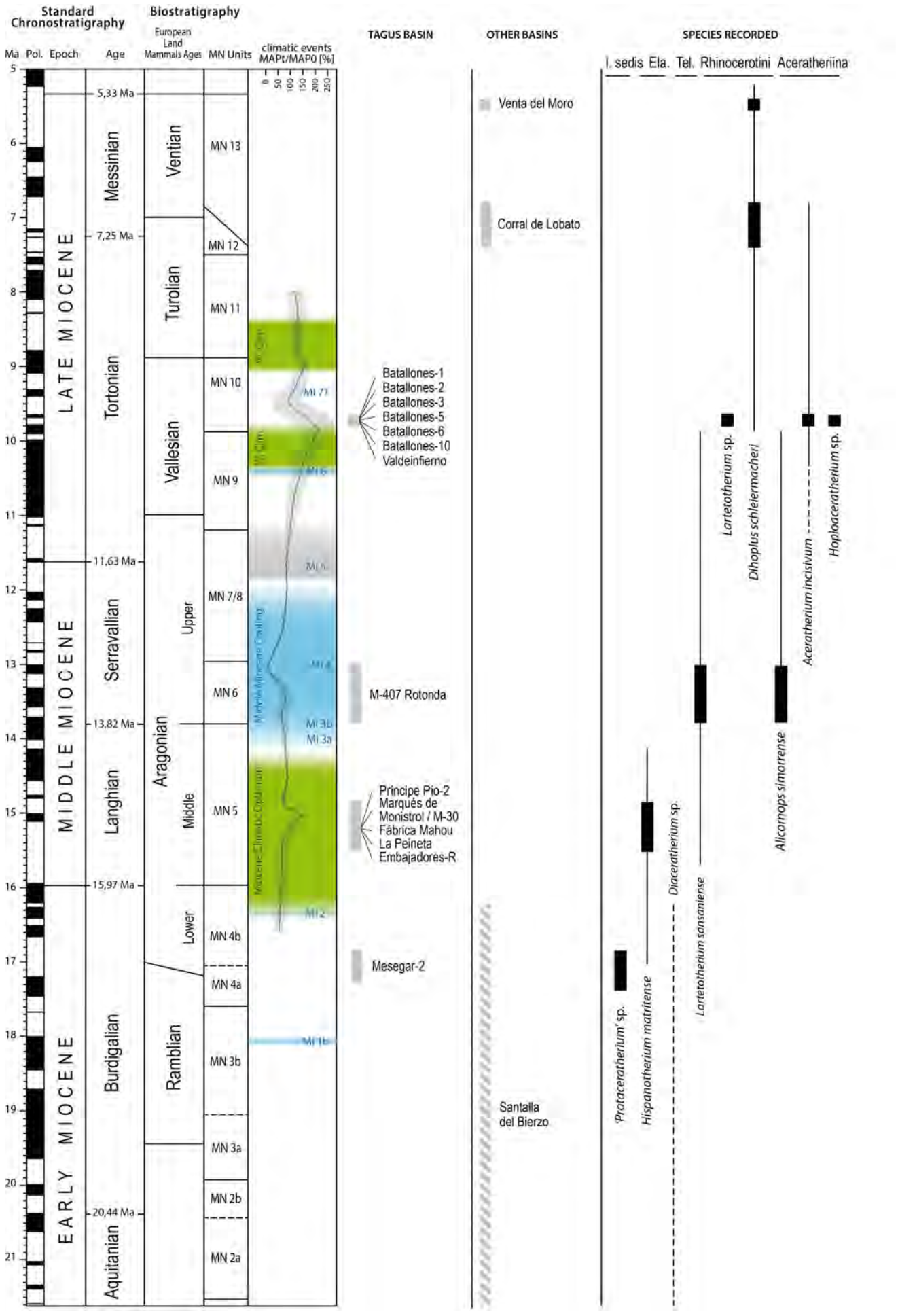


Fig. 1 General map of the Iberian Peninsula with its Cenozoic basins represented in yellow. The location of the localities included in the present work is represented with empty circles. LV, La Valenciana; VM, Venta del Moro; A-M, Alcoy-Mina; CR, Crevillente-2; ME-2, Mesegar-1 and 2; SB, Santalla del Bierzo; FRT, Fresno del Torote; YU, Yunquera de Tajo. (A) represents the localities in the Madrid city area detailed on the left. Map modified from (Andeweg, 2002).

Fig. 2 (next page) Stratigraphic position of the localities included in the present work (gray) and the biostratigraphic ranges of the studied species (as a line) together with the biostratigraphic rank of the locality where it has been recognized (in black). Stratigraphic context according to Hilgen et al. (2012) and van der Meulen et al. (2012). Climatic data according to Aiglstorfer (2014). Biostratigraphic range of rhinoceros species according to Cerdeño (1992). Discontinuous lines represents uncertain ranges.


Standard Chronostratigraphy
Biostratigraphy
Ma
Pol.
Epoch
Age
European Land Mammals Ages
MN Units
climatic events MAPt/MAP0 [%]
0
50
100
150
200
250
5,33 Ma
7,25 Ma
11,63 Ma
13,82 Ma
15,97 Ma
20,44 Ma
LATE MIOCENE
MIDDLE MIOCENE
EARLY MIOCENE
Messinian
Tortonian
Serravallian
Langhian
Burdigalian
Aquitanian
Ventian
Turolian
Vallesian
Upper
Middle
Lower
Aragonian
Ramblian
MN 13
MN 12
MN 11
MN 10
MN 9
MN 7/8
MN 6
MN 5
MN 4b
MN 4a
MN 3b
MN 3a
MN 2b
MN 2a
W. Clim.
M. Clim.
Middle Miocene Cooling
Middle Miocene Climatic Optimum
Mi 7
Mi 6
Mi 5
Mi 4
Mi 3b
Mi 3a
Mi 2
Mi 1b
TAGUS BASIN
Batallones-1
Batallones-2
Batallones-3
Batallones-5
Batallones-6
Batallones-10
Valdeinfierno
M-407 Rotonda
Príncipe Pío-2
Marqués de Monistrol / M-30
Fábrica Mahou
La Peineta
Embajadores-R
Mesegar-2
OTHER BASINS
Venta del Moro
Corral de Lobato
Santalla del Bierzo
SPECIES RECORDED
I. sedis
Ela.
Tel.
Rhinocerotini
Aceratheriina
'Prataceratherium' sp.
Hispanotherium matritense
Diaceratherium sp.
Lartetotherium sansaniense
Lartetotherium sp.
Dihoplus schleiermacheri
Alicornops simorrense
Aceratherium incisivum
Hoploaceratherium sp.

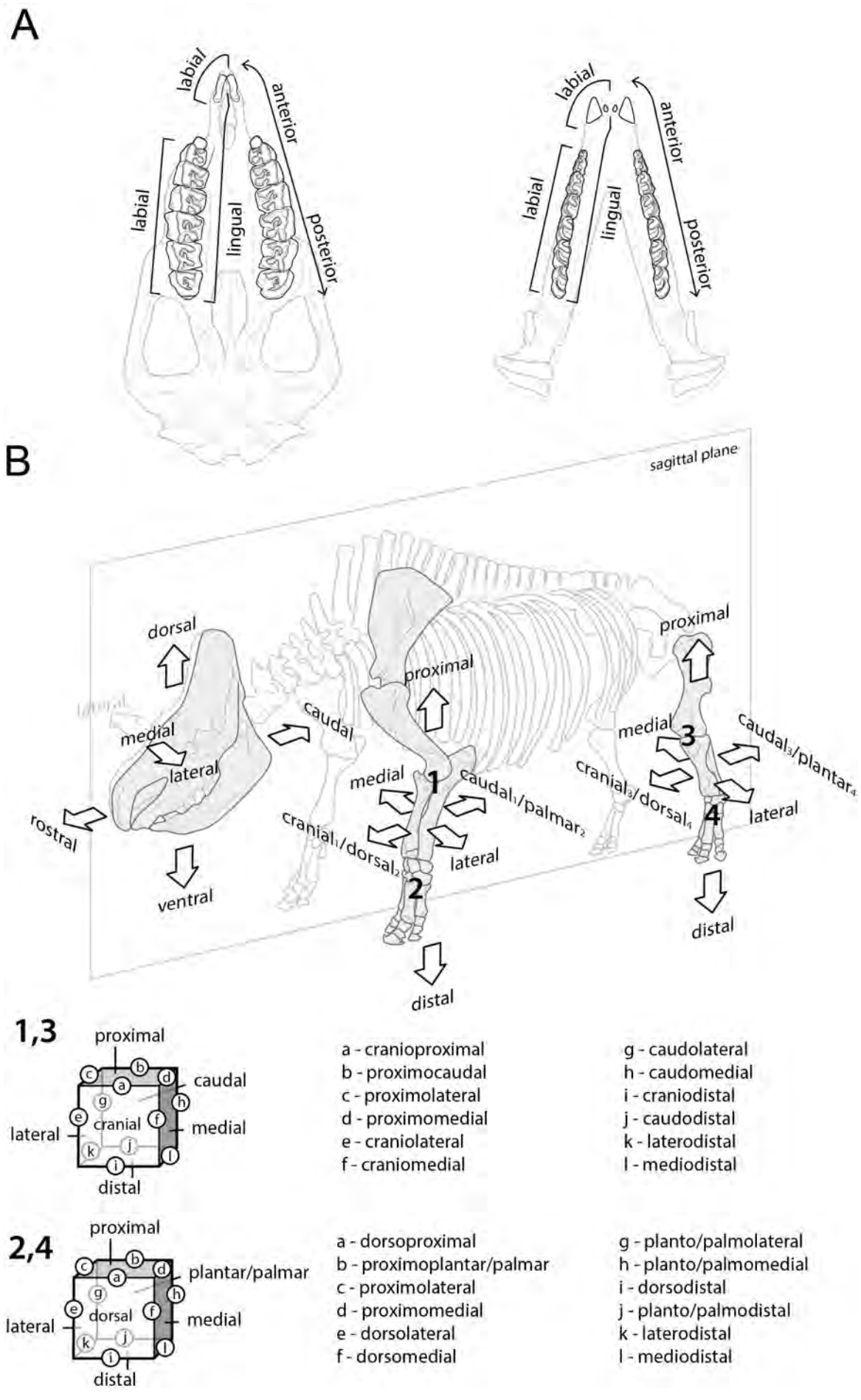


Fig. 3 Position guides used in the descriptions of the present work

ments are given in millimeters (mm), volume in cubic meters (m^3), and mass in kilograms (kg). Approximate measurements are preceded by a "~" (e.g. a missing tip of a volar process, a crushed or distorted bone, or the approximated total length of a fragmented metapodial with loose contact between its two fragments). None of the estimated or reconstructed measurements have been included in statistical analyses.

A basic set of cranial and postcranial measurements have been obtained following Guérin (1980) and Cerdeño (1989) respectively. Some additional measurements were implemented. Apart from its description, a list of synonymies is included from several sources, with the code number as follows: Guérin (1980; codified as "G"); Cerdeño (1989; "C"); Prothero (2005; "P"), Becker (2009; "B"), and Van der Made (2010, "VM") to assess the reliability of proportions comparison between different works. Approximate equivalences are preceded by a "~". Abbreviations of the measurements are as follows: ant, anterior (= dorsal); art, articular; APD, antero-posterior distance (measured along the sagittal plane of the bone); col, neck; cor, crown; dia, diaphysis; dis, distal; epi, epiphysis; f, facet; H, height; inf, inferior (= distal); int, internal (= medial); L, length; max, maximum; md, maximum distance; min, minimum; vproc, volar process; R, radius; tuberdelt, deltoid tuberosity; sus, sustentaculum; 3t, third trochanter.

Skull (Fig. 3)

The measurements of the skull follow those described in Guérin (1980). Character number 10-12 and 24 were not included in the original publication:

1: Distance between occipital condyle and premaxillary tip

2: Distance between nasal tip and occipital condyle

3: Distance between nasal tip and occipital crest

4: Distance between nasal tip and notch

5: Minimal width of the braincase

6: Distance between occipital crest and postorbital process

7: Distance between occipital crest and supraorbital tubercle

8: Distance between occipital crest and lachrymal tubercle

9: Distance between nasal notch and orbit

13: Distance between occipital condyle and M3

14: Distance between nasal tip and orbit

15: Width of occipital crest

16: Width between mastoid processes

17: Minimal width between parietal crests

18: Width between postorbital processes

19: Width between supraorbital tubercles

20: Width between lachrymal tubercles

21: Maximal width between zygomatic arches

22: Width of nasal base

23: Heigth of the occipital face

25: Cranial height in front of P2

26: Cranial height in front of M1

27: Height of skull in front of M3

28: Width of palate in front of P2

29: Width of palate in front of M1

30: Width of palate in front of M3

31: Width of foramen magnum

32: Width between exterior borders of occipital condyles

Mandible (Fig. 4)

APDart: Maximum antero-posterior distance of the facet of the condyle. VM = "21".

APDcor: Maximum antero-posterior distance measured at the base of the coronoid process.

APDdia: Maximum antero-posterior distance of the symphiseal border measured from the outer most point of the outer most incisor to the anterior most point of the first premolar measured at the level of the gingival border.

APDhr: Minimal antero-posterior distance of the ascending ramus at about half its heigth. G = "3"; VM = "22".

APDmx: Maximum antero-posterior distance of the molar series.

APDproc: Maximum antero-posterior distance between the tip of the coronoid process and the midpoint of the condylar articulation.

APDpx: Maximum antero-posterior distance of the premolar series.

Hart: Height of the facet of the condylar articulation above the lower border of the mandible. As pointed out, this measurement is subject to the orientation of the mandible and is somewhat subjective (van der Made, 2010). G = "5"; VM = "16".

Hcor: Height of the coronoid process above the lower border of the mandible. This measurement is also subject to the orientation of the mandible, and is therefore subjective (van der Made, 2010). G = "6"; VM = "15".

Hp1-Hm2 and Hm3a: height of the horizontal ramus at the anterior side of the gingival border of the tooth. G = "3" (Hp2) – "7" (Hm2); VM = "3" (Hp1) – "7" (Hm3a).

Hm3p: height of the horizontal ramus at the posterior side of the gingival border of the m3. G = "8"; VM = "8".

L: length of the mandible from the gingival border of the i2 to the caudal most side of the mandibular angle. VM = "1".

Lcor: Distance from the posterior gingival border of the m3 to the tip of the coronoid process.

Lart: Distance from the posterior gingival border of the m3 to the tip of the articular process.

Lsin: Length of the symphysis at the sagittal plane. VM = "11".

TDart: Transverse diameter of the glenoid articular surface. VM = "14".

TDart-art: Transverse diameter between the innermost point

of the condylar surface of each hemimandible.

TDcor-cor: Transverse diameter between the tip of the coronoid process of each hemimandible.

TDia: Transverse diameter between the inner borders of the outer most lower incisors. VM = "17".

TDm3: Transverse diameter between the postero lingual angle of the m3 of both hemimandibles.

TDpx: Transverse diameter of the mandible taken at the anterior gingival border of the anterior most premolar tooth.

TDsin: minimal transverse diameter of the symphysis at the place of waisting. VM = "18".

Hyoid bone (Fig. 4)

A single hyoid bone (BAT-1 w/n; Batallones-1) has been described. Its measurements are included in the text.

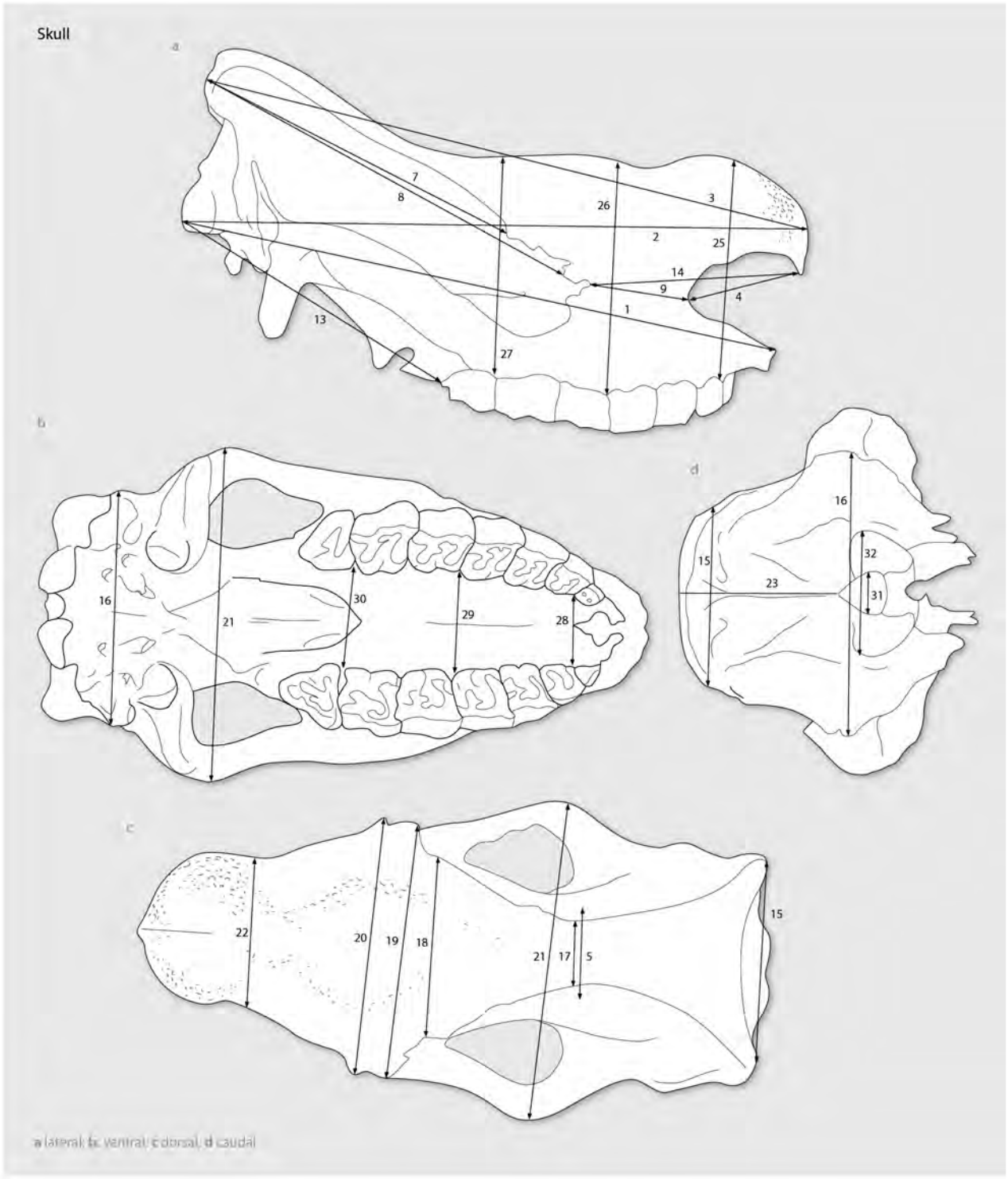


Fig. 4 Measurements of the skull used in the present work. Numbers are detailed in the text. Redrawn from Guérin (1980).

APD: Maximum antero-posterior distance of the hyoid bone measured parallel to the sagittal plane. VM = "L".

TDmax: Maximum transverse diameter of the hyoid bone. VM = "DT".

TDart: Transverse diameter antero-posterior distance. VM = "DTtch".

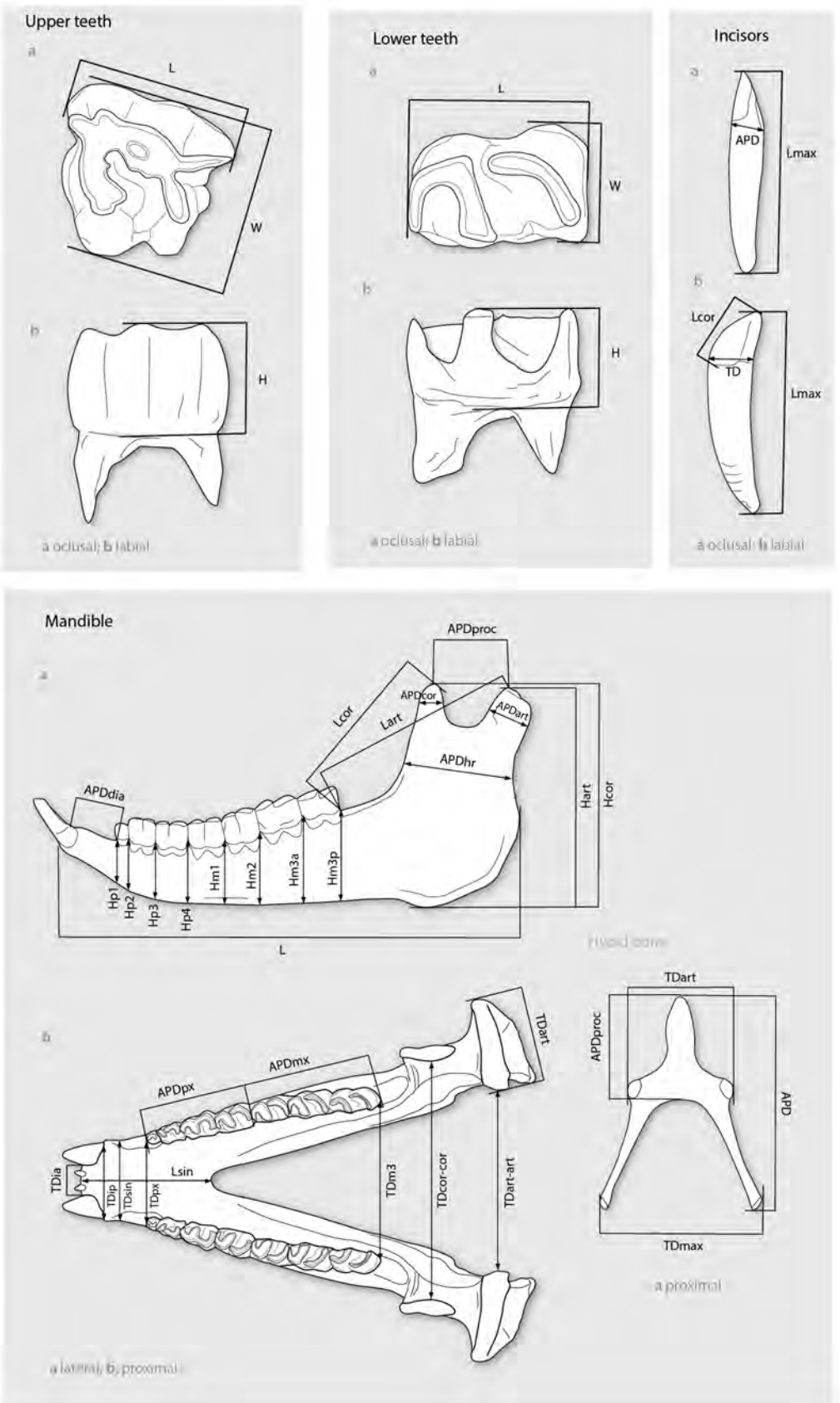


Fig. 5 Measurements of the dentition and mandible used in the present work. Abbreviations are detailed in the text. Occlusal views of upper and lower teeth redrawn from Heissig (1969), hyoid bone redrawn from van der Made (2010).

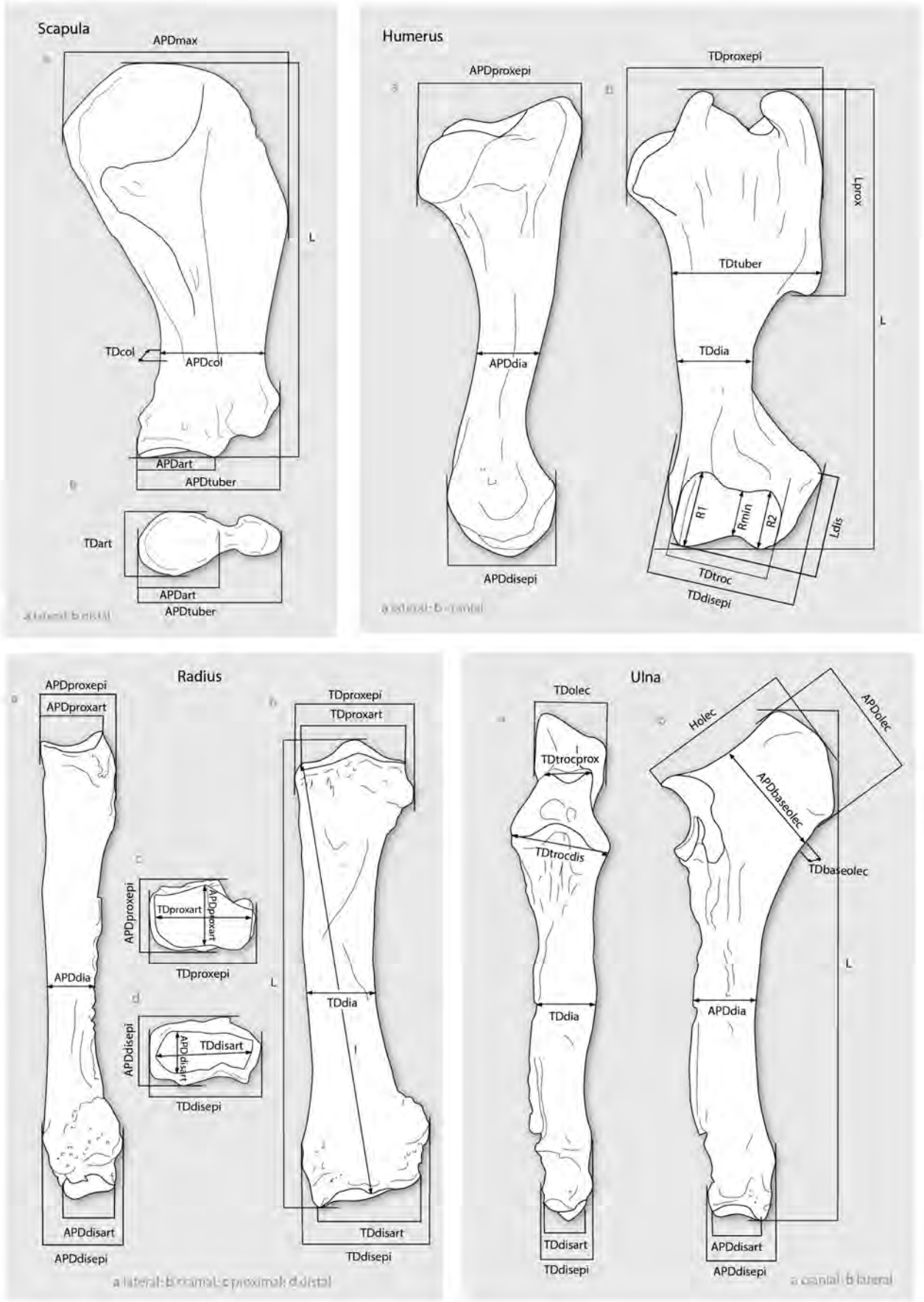


Fig. 6 Measurements of the scapula and long bones of the forelimb used in the present work. Abbreviations are detailed in the text. Long bones redrawn from Hünermann (1989).

Dentition (Fig. 4)

Three basic measurements have been obtained for the upper and lower cheek teeth. These are:

L: the maximum antero-posterior distance measured on the labial upper border of the tooth. In the case of the M3, which is nearly-triangular in occlusal view, the measurement is perpendicular to the line through the anterior most parts of the tooth in the middle and at the buccal side at the same level as the posterior measuring point. VM = "DAPpo".

W: the maximum transversal distance of the tooth, measured at the wider lobe. VM = "DTa".

H: in both upper and lower molars, the height has been measured at the point with a greater distance between the uppermost point of the labial border with the lowermost point in the gingival border one. The place of this measurement maximum height of a tooth may depend on the species, the placement of the tooth, the masticatory preferences of a certain individual, or even to pathologic conditions. In some particular studies (like the comparison between the distinct wear stages of a single species), the measurement has been obtained in a homologous point described in the text.

Incisors and canines were measured as follows:

Lmax: maximum length of the whole teeth from the tip to the

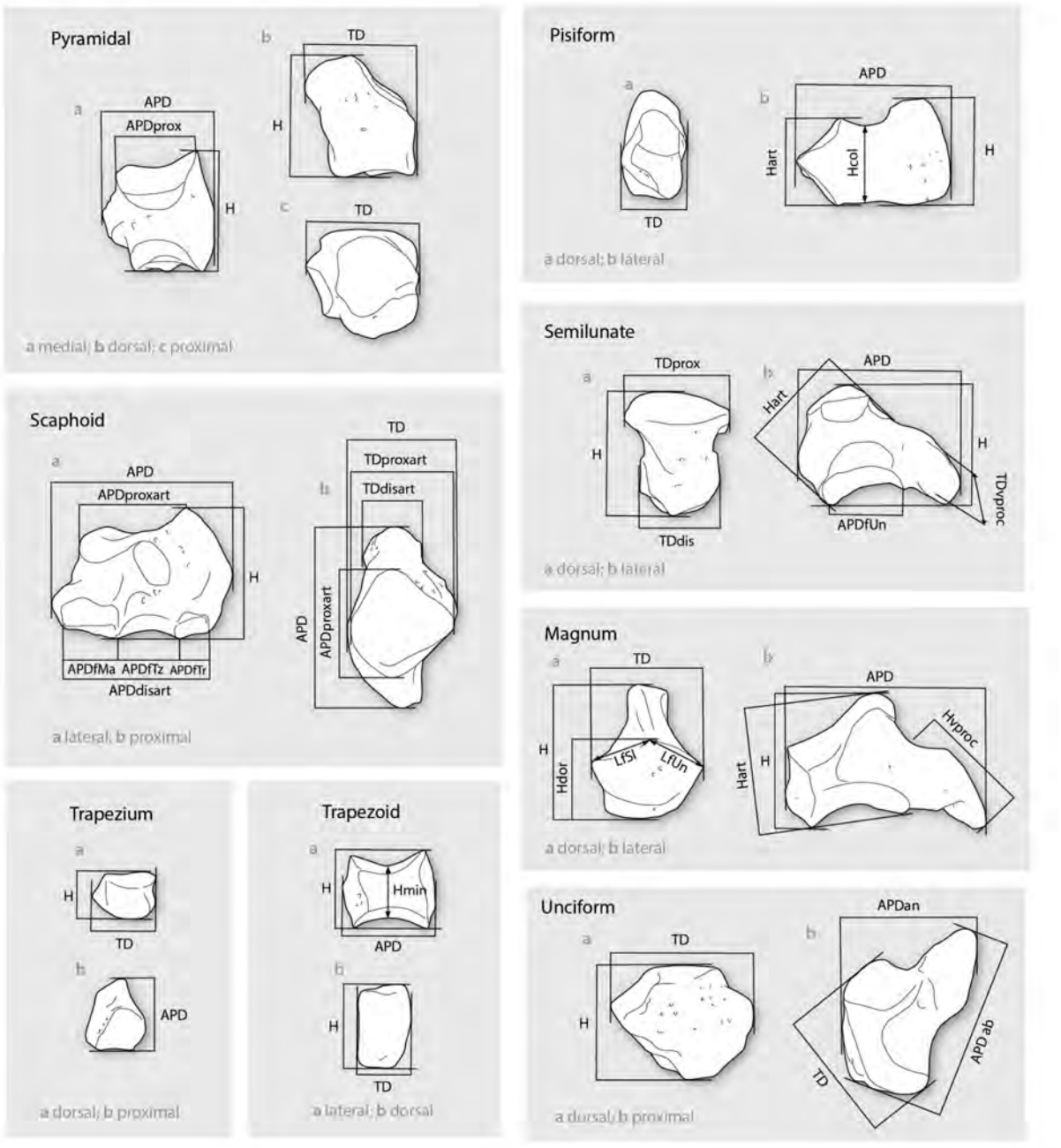


Fig. 7 Measurements of the carpal bones used in the present work. Abbreviations are detailed in the text. Figures redrawn from Hünermann (1989).

base of the root, measured only if the root is intact. This is not a real reflection of the real tooth length, as it does not follow the central path of the tooth. However, it is very useful as a scale reference for posterior digital measurements.

Lcor: maximum length of the crown of the teeth measured at its

TD: maximum transversal distance of the crown measured at the base at the basal limit of the enamel of the labial side (generally the wider part).

APD: maximum antero-posterior distance of the crown measured at the basal limit of the enamel of the labial side (generally the thicker part).

Vertebrae

Except for the articulated specimen from Batallones-1, the descriptions of most of the thoracic vertebrae have been excluded from the present work. Standard measurements of these vertebrae (which usually are restricted to the body of the vertebra) are included in the text and comprise the height, antero-posterior distance and maximum transverse distance (the latter measured at the "waist") of the body. In well-preserved specimens, the height and antero-posterior distance of the neural spine has been also measured.

Scapula (Fig. 6)

APDart: maximum antero-posterior distance of the glenoid articulation. VM = "DAPdf".

APDcol: minimal antero-posterior distance of the "neck" of the scapula. VM = "DAPn".

APDmax: maximum antero-posterior distance of the blade.

APDtuber: maximum antero-posterior distance measured at of the distal glenoid tubercle. VM = "DAPd".

L: maximum length of the scapula.

TDart: maximum transverse distance of the distal glenoid articulation. VM = "DTd".

TDcol: maximum transverse distance of the scapula measured at the "neck".

Humerus (Fig. 6)

APDdia: minimum antero-posterior distance of the diaphysis.

APDdisepi: maximum antero-posterior distance of the distal epiphysis. VM = "DAPd".

APDproxepi: maximum antero-posterior distance of the proximal epiphysis. VM = "DAPp".

L: maximum length of the humerus. This measurement is taken parallel to the major axis of the bone.

Ldis: length of the distal epiphysis of the humerus measured from the lateral most point of the epiphysis to the distal end of the radio-ulnar trochlea.

Lprox: length of the humerus from the upper most point of the proximal epiphysis to the distal most point of the deltoid tuberosity.

TDdia: minimum transversal distance of the diaphysis.

TDdisepi: maximum transversal distance of the distal epiphysis. VM = "DTd".

TDdia: minimum transversal distance of the diaphysis.

TDproxepi: maximum transversal distance of the proximal epiphysis. VM = "DTp".

TDtroc: maximum transversal distance of the whole distal trochlea. VM = "DTdf".

TDtuber: maximum transversal distance of the proximal half of the bone at the level of the deltoid tuberosity.

R1: maximum distance of the medial articular lip of the distal humeral trochlea.

Rmin: minimum distance of the distal humeral trochlea. VM = "R2".

R2: maximum distance of the lateral articular lip of the distal humeral trochlea. VM = "R3".

Radius (Fig. 6)

APDdisart: maximum antero-posterior distance of the distal articular surface. VM = "DAPp (distal epiphysis)".

APDproxart: maximum antero-posterior distance of the proximal articular surface. VM = "DAPp (proximal epiphysis)".

APDdia: minimum antero-posterior distance of the diaphysis.

APDdisepi: maximum antero-posterior distance of the distal epiphysis.

APDproxepi: maximum antero-posterior distance of the proximal epiphysis.

L: maximum length of the radius. This measurement is taken parallel to the major axis of the bone.

l: alternative measurement of the length, between the proximo-medial border of the proximal articular surface to the midpoint of the disto-cranial border of the distal articular surface.

TDdisart: maximum transversal distance of the distal articular surface. VM = "DTp (distal epiphysis)".

TDproxart: maximum transversal distance of the proximal articular surface. VM = "DTp (proximal epiphysis)".

TDdia: minimum transversal distance of the diaphysis.

TDdisepi: maximum transversal distance of the distal epiphysis.

TDproxepi: maximum transversal distance of the proximal epiphysis.

Ulna (Fig. 6)

APDbaseolec: minimum antero-posterior distance of the

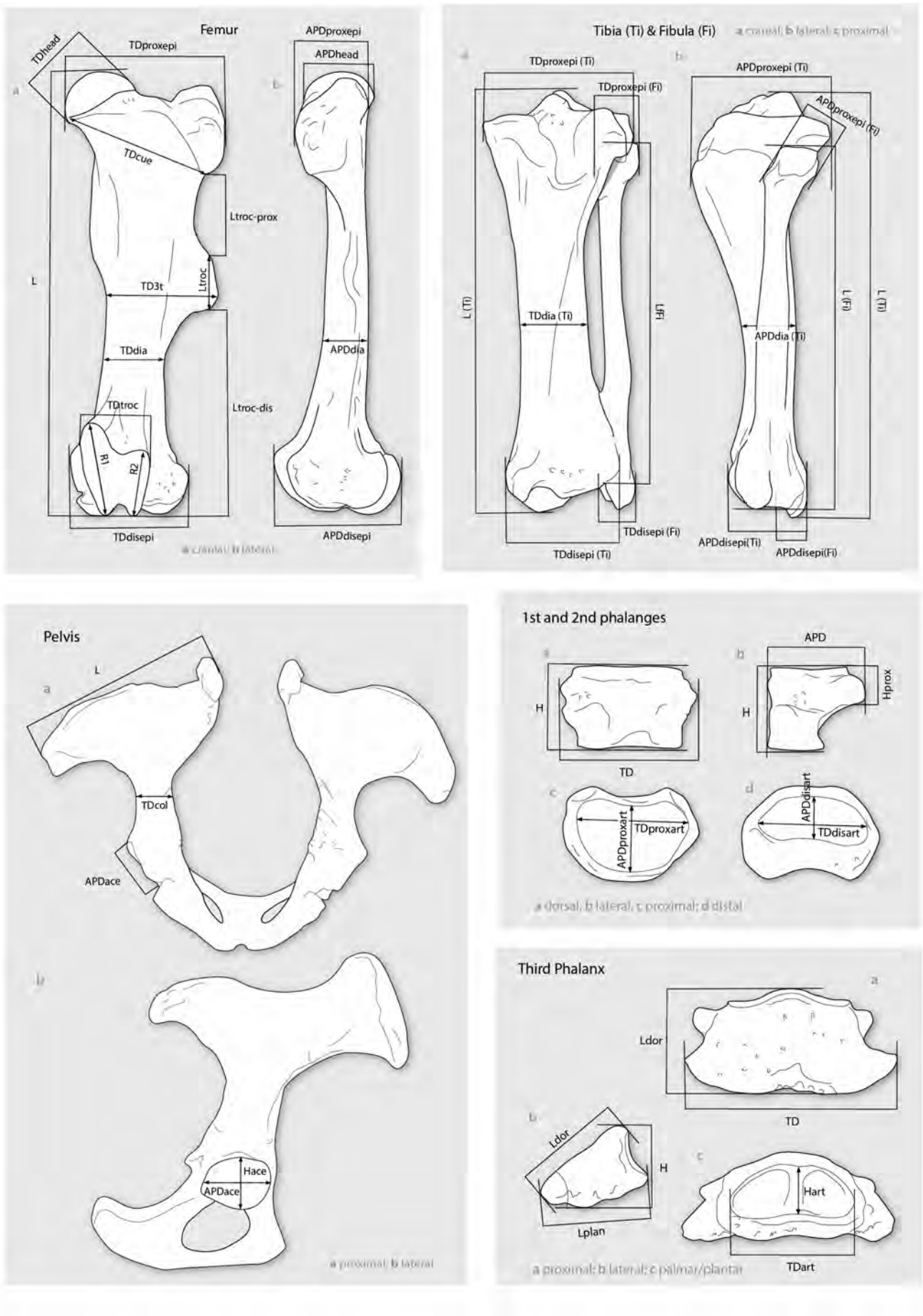


Fig. 8 Measurements of the long bones, phalanges and pelvis used in the present work. Abbreviations are detailed in the text. Figures redrawn from Hünermann (1989).

"neck" of the olecranon.

APDdia: minimum antero-posterior diameter of the diaphysis.

APDdisart: maximum antero-posterior diameter of the distal articular surface.

APDdisepi: maximum antero-posterior diameter of the distal epiphysis.

APDolec: maximum antero-posterior diameter of the olecranon.

Holec: maximum height of the olecranon, measured parallel to its proximal border.

L: maximum length of the bone, measured parallel to the cranial border of the shaft.

TDbaseolec: minimum transversal distance measured at the level of the "neck" of the olecranon.

TDdia: minimum transversal diameter of the diaphysis.

TDdisart: maximum transversal distance of the distal articular facet.

TDdisepi: maximum transversal distance of the distal epiphysis.

TDolec: maximum transversal distance of the olecranon.

TDtrocdis: maximum transversal distance of the distal lobes of the humeral trochlea.

TDtrocprox: maximum transversal distance of the proximal protuberance of the humeral trochlea.

Pyramidal (Fig. 7)

APD: maximum antero-posterior diameter. C = "DAP"

APDprox: maximum antero-posterior diameter of the proximal "neck". C = "DAP pr."

H: maximum height.

TD: maximum transverse distance. C = "DT".

Scaphoid (Fig. 7)

APD: maximum antero-posterior distance. C = "DAP"

APDproxart: maximum antero-posterior distance of the proximal articular surface. C = "DAP art.prox"

APDfMa: maximum antero-posterior distance of the magnum-facet.

APDfTz: maximum antero-posterior distance of the trapezoid-facet.

APDfTr: maximum antero-posterior distance of the trapezium-facet.

APDdisart: maximum antero-posterior distance of the distal articular surface. C = "DAP art. dis"

H: maximum height of the bone, measured at the level of its palmar protuberance.

TD: maximum transverse distance of the bone. C = "DT"

TDdisart: maximum transverse distance of the distal articular surface.

TDproxart: maximum transverse distance of the proximal articular surface.

Magnum (Fig. 7)

APD: maximum antero-posterior distance. C = "DAP".

H: maximum height of the bone.

Hart: maximum height of the bone measured according Cerdeño (1989). C = "H art."

Hdor: maximum height of bone measured dorsal to the dorsal crest.

Hvproc: maximum height of the volar process.

LfSl: maximum length of the dorsal border of the semilunate-facet in dorsal view.

LfUn: maximum length of the dorsal border of the unciform-facet in dorsal view.

TD: maximum transverse distance of the bone. C = "DT"

Semilunate (Fig. 7)

APD: maximum antero-posterior distance. C = "DAP"

APDfUn: maximum antero-posterior distance of the distal unciform-facet.

H: maximum height of the bone.

Hart: maximum height of the bone at an oblique angle, parallel to the palmar expansion of the radial-facet following Cerdeño (1989).

TDdis: maximum transverse distance of the portion of the bone distal to the radial-facet measured in dorsal view.

TDpal: maximum transverse distance of the volar process.

TDprox: maximum transverse distance of the radial-facet. C = "DT".

Trapezium (Fig. 7)

APD: maximum antero-posterior distance. C = "DAP".

H: maximum height of the bone.

TD: maximum transverse distance of the bone. C = "DT".

Pisiform (Fig. 7)

APD: maximum antero-posterior distance. C = "DAP".

H: maximum height of the bone measured at the level of the volar process.

Hcol: maximum height of the 'neck' between the volar process and the articular facets.

Hart: maximum height of the articular area of the bone.

TD: maximum transverse distance of the bone.

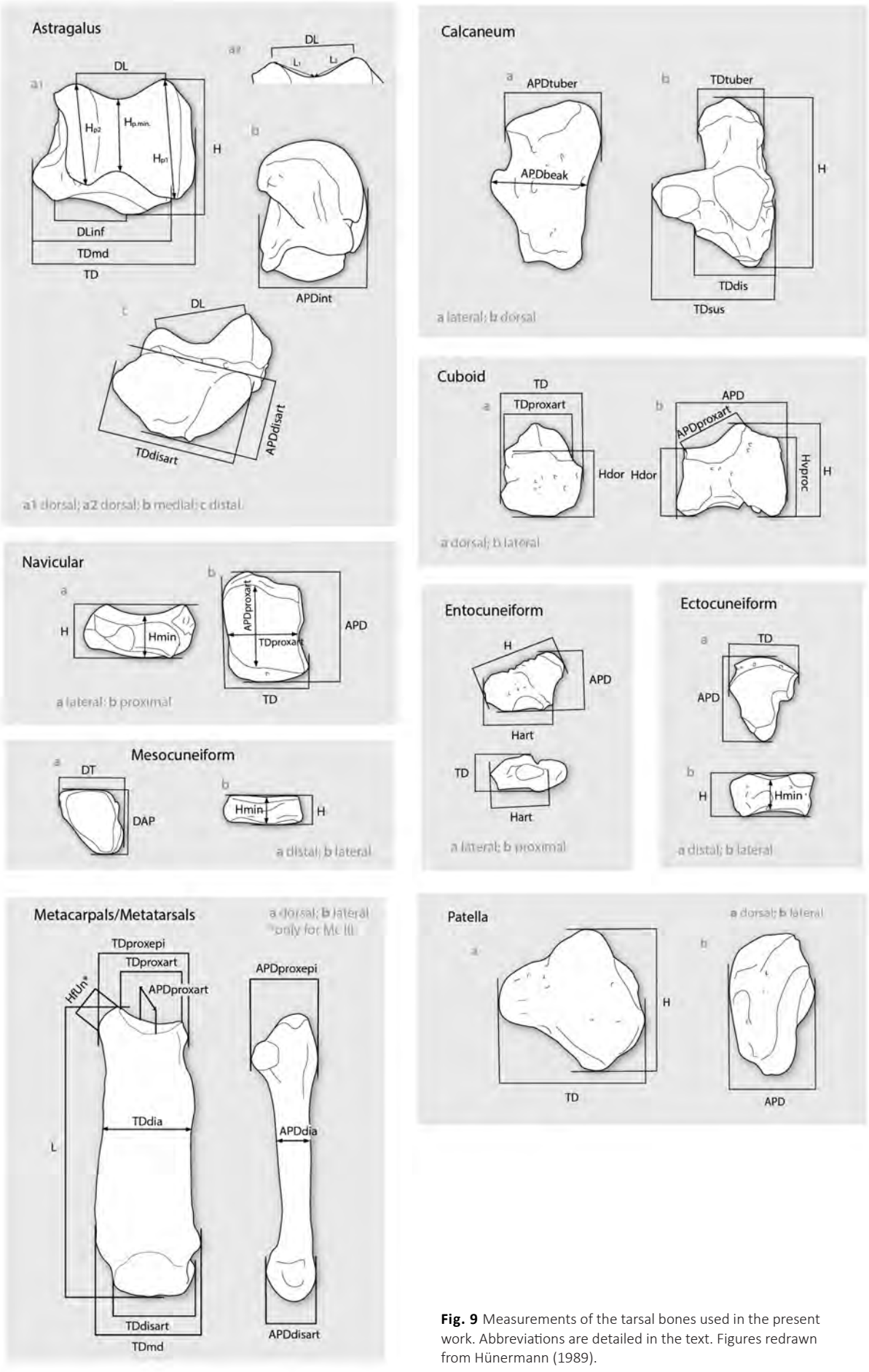


Fig. 9 Measurements of the tarsal bones used in the present work. Abbreviations are detailed in the text. Figures redrawn from Hünermann (1989).

Trapezoid (Fig. 7)

APD: maximum antero-posterior distance.

H: maximum height of the bone (typically measured at the palmar side).

Hmin: minimum height of the bone, measured at the mid-point of the bone.

TD: maximum transverse distance of the bone.

Unciform (Fig. 7)

APDab: maximum antero-posterior distance measured from the dorsal most point of the pyramidal-semilunate contact to the distal most point of the volar process. C = "L ab."

APDan: maximum antero-posterior distance measured parallel to the dorsal surface of the bone. C = "L an."

H: maximum height of the bone.

TD: maximum transverse distance of the bone. C = "DT".

Pelvis (Fig. 8)

APDace: maximum antero-posterior distance of the acetabulum.

L: maximum length of the iliac blade.

TDace: maximum transversal distance of the acetabulum.

TDcol: minimum transversal distance of the neck of the ilium.

Femur (Fig. 8)

APDdia: minimum antero-posterior distance of the diaphysis.

APDdisepi: maximum antero-posterior distance of the distal epiphysis measured on its medial side.

APDhead: maximum antero-posterior distance of the femoral head.

APDproxepi: maximum antero-posterior distance of the proximal epiphysis measured on its lateral side.

Ltroc-dis: maximum length from the distal border of the 3rd trochanter to the distal most point of the distal epiphysis.

Ltroc-prox: maximum length from the proximal border of the proximal epiphysis to the proximal border of the 3rd trochanter.

Ltroc: maximum length of the 3rd trochanter.

L: maximum length of the bone. As with the other long bones, this measurement is taken parallel to the major axis of the bone.

TD3t: maximum transversal distance of the diaphysis at the level of the third trochanter.

TDcue: maximum transversal distance of the proximal head from the disto-medial border of the femoral head in cranial view to the disto-lateral border of the proximal epiphysis.

TDdia: maximum transversal distance of the "neck" of the diaphysis from the 3rt trochanter to the distal epiphysis.

TDdisepi: maximum transversal distance of the distal articular epiphysis. VM = "DTd".

TDhead: maximum transversal distance of the femoral head.

TDproxepi: maximum transversal distance of the proximal epiphysis. VM = "DTp".

TDtroc: transversal diameter of the patellar trochlea (both lips) measured at their maximum width.

R1: height of the medial lip of the patellar trochlea of the distal epiphysis.

R2: height of the lateral lip of the patellar trochlea of the distal epiphysis.

Tibia (Fig. 8)

APDdia: minimum antero-posterior distance of the diaphysis.

APDproxepi: maximum antero-posterior distance of the proximal epiphysis.

APDdisepi: maximum antero-posterior distance of the distal epiphysis.

L: maximum length of the bone. This measurement is taken parallel to the major axis of the bone.

LfFi: maximum distance between the proximal border of the proximal fibular facet to the distal most border of the distal articular facet.

TDdisepi: maximum transversal distance of the distal epiphysis.

TDproxepi: maximum transversal distance of the proximal epiphysis.

TDdia: minimum transversal distance of the diaphysis.

Fibula (Fig. 8)

APDprox: maximum antero-posterior distance of the proximal epiphysis.

APDdis: maximum antero-posterior distance of the distal epiphysis.

L: maximum length of the bone.

TDdis: maximum transverse distance of the distal epiphyis

TDprox: maximum transverse distance of the proximal epiphysis.

Patella (Fig. 9)

In order to make comparable measurements, the patella has been oriented following the femoral articulation of its caudal side (which should be placed vertical).

APD: maximum antero-posterior distance.

H: maximum height of the bone.

TD: maximum transverse distance of the bone.

Astragalus (Fig. 9)

APDint: maximum antero-posterior diameter, typically measured on the medial side. C = "DAPint".

APDartdis: maximum antero-posterior distance of the distal articular surface, including both navicular and cuboid-facets. C = "DAP a. d.".

DL: transversal diameter of the astragalar trochlea (both lips) measured at their dorsal most side. B = "TDT".

DLinf: distance between the medial border of the navicular-facet and the boundary of the navicular/cuboid facets measured at it most distally-protruding points in dorsal view.

H: maximum height of the bone. C = "H".

Hp2: maximum height of the astragalar trochlea measured at the level of the medial lip.

Hpmin: minimum height of the astragalar trochlea.

Hp1: maximum height of the astragalar trochlea measured at the level of the lateral lip.

L1: maximum linear length of the medial lip to the inflexion point of the trochlea measured at the dorsal most border of the latter.

L2: maximum linear length of the lateral lip to the inflexion point of the trochlea measured at the dorsal most border of the latter.

TD: maximum transverse distance of the bone, typically measured between the distal most point of the navicular/cuboid boundary and the proximal most point of the lateral lip of the trochlea. C = "DT".

TDartdis: maximum transverse distance of the distal articular surface, including both navicular and cuboid-facets. C = "DT art. dis."

TDmd: maximum transverse distance of the "base" of the astragalus. C = "DT m. d.".

Calcaneus (Fig. 9)

APDtuber: maximum antero-posterior distance of the tuber calcis. C = "DAPtuber".

APDbeak: maximum antero-posterior distance measured at the level of the "beak" of the calcaneum. C = "DAPpico".

TDdis: maximum transverse distance measured in the narrowing below the medial expansion of the second astragalar facet.

TDtuber: maximum transverse distance of the tuber calcis. C = "DTtuber".

TDsus: maximum transverse distance of the sustentaculum. C = "DTsus".

H: maximum height of the bone. C = "H".

Navicular (Fig. 9)

APD: maximum antero-posterior distance. C = "DAP".

APDproxart: maximum antero-posterior distance of the proximal articular surface.

H: maximum height of the bone.

Hmin: minimum height of the bone.

TD: maximum transverse distance. C = "DT".

TDproxart: maximum transverse distance of the proximal articular surface.

Cuboid (Fig. 9)

Hdor: maximum height of the bone measured at its dorsal side.

Hvproc: maximum height of the volar process of the bone.

H: maximum height of the bone measured between the plantar side of the articular surface and the distal most point of the volar process.

APDproxart: maximum antero-posterior diameter of the proximal articular surface. C = DAP art. pr.

APD: maximum antero-posterior diameter (including the volar process).

TD: maximum transverse distance (including the volar process).

TDproxart: maximum transverse distance of the proximal articular surface.

Ectocuneiform (Fig. 9)

APD: maximum antero-posterior diameter of the bone. C = "DAP"

H: maximum height of the bone. C = "H"

Hmin: minimum height of the bone.

TD: maximum transverse distance of the bone, typically measured in the dorsal border. C = "DT"

Mesocuneiform (Fig. 9)

APD: maximum antero-posterior diameter. C = "DAP"

TD: maximum transverse distance. C = "DT"

H: maximum height of the bone.

Hmin: minimum height of the bone.

Entocuneiform (Fig. 9)

APD: maximum antero-posterior diameter. C = "H"

APDart: maximum height of the bone . C = "Hart"

H: maximum height of the bone. C = "DAP"

TD: maximum transverse distance.

Metapodials (Fig. 9)

Most metapodials share the same set of measurements. In some species with reduced Mc V (e.g. *Hispanotherium ma-*

tritense), the proportions from the diaphysis and the distal epiphysis have been omitted.

APDproxart: maximum dorso-plantar/palmar distance of the proximal articular surface in proximal view. See TDep for further information. VM = "DAPp"; C = "DAP ep. pr."

APDdia: maximum dorso-palmar/plantar distance measured at the level of TDdia. G = "5"; C = DAP dia.".

APDdist: maximum dorso-palmar/plantar distance of the distal epiphysis at the level of the trochlea in lateral/medial view. C = "DAPdist"; G = "8"; VM = "DAPdf".

APDproxepi: maximum dorso-plantar/palmar distance of the proximal epiphysis in proximal view. See TDep for further information. C = "DAPep.pr."; G = "3" only in Mc/Mt III.

HfUn: Only in the Mc III. HfUn measures the maximum distance of the unciform-facet in dorsal view measured parallel to its (flattened) surface.

L: maximum length of the bone measured parallel to the major axis of the shaft. C = "L"; G = "1".

TDproxart: maximum transversal distance of the proximal articular surface in proximal view perpendicular to APDap. See TDep for further information. VM = "DTp".

TDdia: maximum transversal distance at the midpoint of the diaphysis measured in dorsal view, at the same distance from the proximal and distal epiphyses. C = probably "TDdia", regardless not being represented in the measurement figure; G = "4".

TDdisart: maximum transversal distance of the distal epiphysis at the level of the trochlea in dorsal view. C ~ "DTa.d.", see TDmd; G = "7"; VM = "DTdf"; VM = "DTdf".

TDproxepi: maximum transversal distance of the proximal epiphysis measured perpendicular to the major axis of the shaft. Guérin (1989) measures the maximum proximal transverse diameter by aligning the proximal measurements with the distal epiphysis (Guérin, 1989; p. 113, Fig. 17C). These measurements are somewhat conflictive, as the distal epiphysis is slightly twisted and laterally/medially projected respect to the rest of the bone in the lateral metapodials. Moreover, the different degree in torsion would lead to distinct and non-homologous measurements. In its place, we have considered the "dorsal" straight side of the proximal epiphysis as an estimate of the proximal epiphysis. The same criterion has been used for the TDap/APDap. C = "DT ep.pr."; G = "2" only in Mc/Mt III.

TDmd: maximum transversal distance of the distal epiphysis at the level of the protuberances for the insertion of the m. interossei. Cerdeño (1989) measures it as perpendicular to the major axis of the bone, not to the distal epiphysis, leading to a similar but not exact measurement. The same occurs with DTa.d. C ~ "DTm.d."; G = "6"; VM = "DTd".

Phalanges (Fig. 8)

APD: maximum dorso-plantar/palmar distance typically measured at the level of the palmar/plantar shelf. VM = "DAPp".

APDdisart: maximum dorso-plantar/palmar distance with the corresponding phalanx. VM = "DAPd".

APDproxart: maximum dorso-plantar/palmar distance of the proximal articular surface with the corresponding metapodial.

H: maximum height of the bone measured at its dorsal side.

Hprox: maximum height of the palmar/plantar shelf bordering the proximal articular surface of the bone.

TD: maximum transversal distance of the phalanx, typically measured behind the proximal articular surface.

TDproxart: maximum transversal distance of the proximal articular surface with the corresponding metapodial. VM = "DTp".

TDdisart: maximum transversal distance of the distal articular surface with the corresponding phalanx. VM = "DTd".

Third Phalanges (Fig. 8)

Hart: maximum height of the articular surface.

H: maximum height of the bone. This measurement may vary depending on the orientation.

Ldor: maximum length of the dorsal side of the bone.

Lplan: maximum length of the palmar/plantar side of the bone.

TD: maximum transversal distance of the phalanx, measured at the hoof insertion.

TDart: maximum transversal distance of the articular surface.

Sesamoids (Fig. 9)

Sesamoid bones are typically excluded from descriptive analyses due to the difficulty to assign them to a certain position. However, exceptional findings such as the articulated skeleton from Batallones-1 permits to describe its overall morphology. Only three measurements have been taken: H, maximum height of the bone; APD, maximum antero-posterior distance; and TD, maximum transverse distance.

DATABASE

A dataset with the all the studied rhinoceros remains has been built with the software Microsoft Office Excel v.2007-2011. New specimens are recorded with a series of different fields which include the species, the anatomical determination, side, label (= collection number; can be divided into collection number and field number), locality, age, coordinates in the fossil site, and additional notes (where the preservation status, pathologies, particular taphonomic conditions and/or predation marks, or inmature conditions is detailed). The database is arranged by anatomic element and locality.

STATISTICAL TESTS

Mathematical data transformation and descriptive statistics were conducted with Microsoft Excel 2010 v. 14. Inferential statistical data analysis performed in the present work has been made using SPSS (Statistical Package for the Social Sciences) v. 17.

Descriptive Statistics

When large measurements with a normal distribution were available, raw data have been transformed in a series of parameters, or descriptive statistics, that describe the distribution, the central tendency, and the dispersion of the data. These data, displayed in supplementary tables, include the number of valid data (N), the minimum value (min; lower limit of the distribution), the mean (as central tendency), the maximum value (max; upper limit of the distribution), and the standard deviation (SD; as a measurement of the dispersion).

Inferential Statistics

t-Student Test: In the present work, a particular case of t-Student Test for two-samples has been performed. This test is used to compare population location parameters among two independent samples (equal variances assumed). If the null hypothesis is not supported, the means of both groups are significantly different from each other.

$$H_0: \mu_1 = \mu_2$$
$$H_A: \mu_1 \neq \mu_2$$

Jonckheere trend test (or Jonckheere-Terpstra Test): Non-parametric test used to compare population location parameters among two or more groups based on independent samples. It poses as a more powerful alternative to Kruskal-Wallis non-parametric test if the alternatives to the null hypothesis are ordered a priori (i.e. one of the groups is significantly smaller than the preceding one/s). In order to quantify the trend, a Kendall's tau test was, complementing the information provided by Jonckheere trend test (correlation coefficient). This test assumes homogeneity of variance but not assumes normality in data distribution. Letting θ be the population median for the /th population, the null hypothesis is:

$$H_0: \theta_1 = \theta_2 = \ldots = \theta_\kappa$$
$$H_A: \theta_1 \leq \theta_2 \leq \ldots \leq \theta_\kappa$$

PHYLOGENETIC ANALYSIS

This section is not pretended to be a detailed explanation of the cladistics' theory, but an overview of the main concepts and methodology used in the present work together with a critical review of the most used techniques in Paleontology. Phylogenetic analyses have been performed using TNT (Tree Analysis Using New Technology) v. 1.1. (Goloboff et al., 2008). TNT is much quicker at parsimony analysis than PAUP, particularly with larger datasets. In the datasets included in the present work, missing and inappropriate characters are represented by a question mark "?" and a dash "–" respectively.

The main goal of every cladistic analysis is to find a classification of organisms. To do so, the observed variation is discretized in a set of polymorphic characters coded in form of a matrix. From there on, a mathematical model is applied to the dataset (in this case maximum parsimony). The result is displayed in form of a tree/s with the minimum number of character-states changes preferred between its species (i.e., the shortest tree/s), that is to say, the species are arranged according to the resemblance. Ideally, the best approach to obtain the shortest tree/s is the use of exhaustive methods. These look for all the possible combination of the data included in the matrix (the total evidence) and always find the shortest tree(s). The exhaustive search is available in some cladistics packages. However, when datasets include more than 10-15 taxa, the possible combinations exceed the computational resources of current hardware (e.g.: for 20 taxa the possible number of trees exceed the 8,200 trillion of combinations). To solve this issue, alternatives of 'data exploration', or heuristic methods, have been designed. They allow getting closer the total evidence with a fraction of the computational requirements of a heuristic search. Some of the most used search methods are:

- Branch and bound: this method proceeds by constructing a tree using the Wagner method. Its length is set as the maximum number of steps. Then, two its taxa are tied with the outgroup in a separate tree. More taxa are added one by one, and placed in every possible position of the tree. Only if the length of the trees with the new taxa is lower than the original Wagner tree, a new taxon is added. Branch and bound is still time consuming and impractical for large datasets.
- Tree bisection-reconnection (TBR): detaches a subtree from an interior node of a tree and rearranges it at all the possible locations between both. This method can be repeated iteratively to improve the results.

Obtaining the consensus tree

Parsimony priorizes the cladistic hypothesis with the fewest step number. Sometimes a data set can produce various equally parsimonious trees with the same number of steps. To resolve this, several approaches have been developed. One of the most frequently used in Paleontology is the majority-rule consensus tree (MRC). It is a form of consensus that retains all the nodes found in more than a certain percentage of the shortest trees (usually 50 %). However, this method has proven to be problematic (Sharkey and Leathers, 2001). In consequence, an alternative and more conservative approach is used in the present work, using only the nodes that are consistent in all the shortest trees (i.e.: requires agreement across all the shortest trees). This method is called strict consensus and show only those relationships that are unambiguously supported by the data.

Homoplasy measurements

Once the consensus tree is obtained, its overall quality (homoplasy) can be estimated by means of several indices (normally used to compare between different trees):

- Consistency Index (CI): the CI is currently used as a measurement of the relative amount of homoplasy. It measures the number of advanced states it has the data and is calculated by means of the quotient between the total character state changes expected given the data set (i.e. theoretical total character changes without reversions) multiplied by 100 and the actual number of steps in the tree. This index is widely used and very popular in Paleontology systematics. As a result, it has been implemented in all the cladistics packages. Unfortunately, it is a poor homoplasy estimation as it is affected by the number of taxa, quality of the characters, character states, and the independent evolution of each independent character (Kluge and Farris, 1969). The consistency index of an individual character is the number of advanced states it has in the data set divided by the number of steps in the tree multiplied by 100.
- Retention Index (RI): relative measurement of homoplasy. Measures "the amount of synapomorphy expected from a data that is retained as synapomorphy on a cladogram". The retention index for an individual character is the number of taxa with its higher character state (typically 1) "take away the number of steps the character makes in the tree divided by the maximum steps for the character take away the number of state changes we expect multiplied by 100".

As cladistics developed, there was a particular emphasis on how confident a particular internal branch in tree is (its "reliability", "support" or "strength"). To measure it, several randomization methods have been designed. These are grouped in permutation, Jackknifing, Monte Carlo (bootstrapping), Decay analyses and Bayesian Posterior Probabilities methods. In the present work only Decay analyses (Bremer Support) and Monte Carlo (bootstrapping) methods have been used.

- Bootstrapping: the bootstrap method was introduced by Efron (1979) and applied to cladistics analysis by Felsensetein (1985). It consists in resampling the data set many times by taking characters out of the analysis. These pseudoreplicates are used to generate new trees and test if the same nodes of the original tree are recovered. However, its usefulness has been contested by several issues like the size of the data matrix, the cladogram topology, or the characters chosen among others (Kitching et al., 2003). Felsenstein (1985) originally proposed 95% as the cutoff for statistically significant supported clades in Bootstrapping. A posterior work by Hillis and Bull (1993) dropped it to 70%, a limit typically used in posterior studies. However, the premises required for the calculation of the Bootstrapping are not generally met by real phylogenies (Hillis and Bull, 1993). An alternative and more recommended interpretation of the bootstrap value is that proposed by Felsenstein and Kishino (1993). The result of 1 – P (being P the Bootstrap value) should be interpreted as the inverse probability of Type I error (falsely accepting a clade that is not there; Felsenstein and Kishino, 1993) and not as clade support (as many systematic studies do).
- Bremer support (or Branch support, decay analyses, length difference, or clade stability; Bremer, 1988): Bremer support assesses the number of steps required before a clade is lost from the strict consensus tree, or the number of characters that supports each node in a strict consensus cladogram. Only groups found in all most parsimonious trees have BS > 0. As with bootstrapping, Bremer support values are largely dependent on the dataset. They should be interpreted in light of branch lengths.
  + Absolute Bremer support: is the integer value of steps as defined above (ranges from 0 to N)
  + Relative Bremer support: is the percentage of steps (related to the greater Bremer support recorded in the tree).

It should be taken into account that these support estimates (Bootstrap, Jackknife, Bremer) have been typically used as confidence statements. Despite some works made supporting this point (Norén and Jondelius, 1999), this interpretation is largely controversial when working with morphological datasets (Soltis and Soltis, 2003).

LITERATURE CITED

-, 1993-2007, SPSS Statistics: Chicago, SPSS Inc.

-, 2005, Nomina Anatomica Veterinaria, Editorial Comitee Hannover, Columbia, Gent, Sapporo, 190 p.:

Andeweg, B., 2002, Cenozoic tectonic evolution of the Iberian Peninsula: effects and causes of changing stress fields [PhD thesis: University Amsterdam, 178 p.

Antoine, P. O., 2000, Origine et différenciation des Elasmotheriina parmi les Rhinocerotidae (Mammalia, Perissodactyla) : analyse cladistique et implications biostratigraphiques et paléobiogéographiquesUnpublished Ph.D. dissertation], 350 p.

Antoine, P. O., 2002, Phylogénie et évolution des Elasmotheriina: (Mammalia, Rhinocerotidae): Mémoires du Muséum National d'Histoire Naturelle, v. 188, p. 5-350.

Becker, D., Bürgin, T., Oberli, U., and Scherler, L., 2009, *Diaceratherium lemanense* (Rhinocerotidae) from Eschenbach (eastern Switzerland): systematics, palaeoecology, palaeobiogeography: Neues Jahrbuch für Geologie und Paläontologie Abhandlungen, v. 245, no. 1-2, p. 5-39.

Budras, K.-D., Sack, W. O., and Röck, S., 2009, Anatomy of the Horse, Hannover, Schlütersche Verlagsgesellschaft mbH & Co.

Cerdeño, E., 1989, Revisión de la sistemática de los rinocerontes del Neógeno de EspañaPh.D. Dissertation]: Universidad Complutense de Madrid, 429 p.

Efron, B., 1979, Bootstrap methods: Another look at the jackknife: Annalitic Statistics, v. 7, p. 1-26.

Felsestein, J., 1985, Confidence limits on phylogenies: An approach using the bootstrap: Evolution, v. 39, p. 783-791.

Felsestein, J., and Kishino, H., 1993, Is there something wrong with the bootstrap on phylogenies? A reply to Hillis and Bull: Systematic Biology, v. 42, p. 193-200.

Goloboff, P., Farris, J., and Nixon, K., 2008, TNT, a free program for phylogenetic analysis: Cladistics, v. 24, p. 774-786.

Guérin, C., 1980, Les rhinocéros (Mammalia, Perissodactyla) du Miocène terminal au Pléistocène supérieur en Europe occidentale : comparaison avec les espèces actuelles: Documents des Laboratoires de Géologie de Lyon, v. 79, p. 1-1184.

Heissig, K., 1969, Die Rhinocerotidae (Mammalia) aus der oberolizogänen Spaltenfüllung von Gaimersheim bei Ingolstadt in Bayern und ihre phylogenetische Stellung: Bayerische Akademie der Wissenschaften, Mathematisch-Naturwissenschaftliche Klasse, Abhandlungen, v. 138, p. 1-133.

-, 1972, Die obermiozäne Fossil-Lagerstätte Sandelzhausen. 5. Rhinocerotidae (Mammalia), Systematik und Okologie: Mitteilungen der Bayerischen Staatssammlung Paläontologie und historische Geologie, v. 14, p. 37.

-, 1999, 16. Family Rhinocerotidae, *in* Rössner, G. E., and Heissig, K., eds., The Miocene Land Mammals of Europe: Pfeil, Munich, p. 175-188.

Hillis, D. M., and Bull, J. J., 1993, An empirical test of bootstrapping as a method for assessing confidence in phylogenetic analysis: Systematic Biology, v. 42, p. 182-192.

Hünnerman, K. A., 1989, Die Narshornskelette (*Aceratherium incisivum* Kaup 1832) aus dem Jungtertiär vom Höwennegg im Hegau (Südwestdeutschland): Andrias, v. 6, p. 117.

Jepsen, G. L., 1996, Early Eocene bat from Wyoming: Science, v. 154, no. 3754, p. 1333-1339.

Kitching, I. J., Forey, P. L., Humphries, C. J., and Williams, D. M., 2003, Cladistics: The Theory and Practice of Parsimony Analysis, Oxford Science Publications, The Systematics Association Publication, v. 2, 228 p.:

Kluge, A. G., and Farris, J. S., 1969, Quantitative phyletics and the evolution of anurans: Systematic Zoology, v. 18, p. 1-32.

Mein, P., 1999, European Miocene mammal biochronology, *in* Rössner, G. E., and Hessig, K., eds., The Miocene Land Mammals of Europe: München, Verlag Dr. Friedrich Pfeil, p. 25-38.

Norén, M., and Jondelius, U., 1999, Phylogeny of the Proleci-thophora (Platyhelminthes) inferred from 18S rDNA sequences: Cladistics, v. 15, p. 103-112.

Prothero, D., 2005, The Evolution of North American Rhinoceroses, Cambridge, Cambridge University Press, 218 p.:

Quiralte, V., Morales, J., Sánchez, I. M., Sanisidro, O., Pozo, M., Mingo, B., Huertas, M. J., Varas, M. J., Sánchez-Muñoz, L., Crespo-Feo, E., Servert, L., Hernández-Rodero, M. F., Aparicio, A., Caballero, J., Torres, Y., Agut, D., Diéguez, C., Chicote, G., Díaz-Martínez, E., Nieto-Codina, A., Martín-Escorza, C., and Hernández-Ferreirós, P., 2011, La Fauna de Mamíferos Fósiles del Mioceno Inferior de La Encinilla (Colmenar Viejo, Madrid), *in* Fernández Hernán, M., Santos Santos, G., and García Guinea, J., eds., Geología de Colmenar Viejo y alrededores más próximos: Colmenar Viejo, Ayuntamiento de Colmenar Viejo. Concejalía de Medio Ambiente, p. 123-131.

Schaller, O., 2007, Illustrated Veterinary Anatomical Nomenclature, Sttutgart, Enke.

Sharkey, M. J., and Leathers, J. W., 2001, Majority Does Not Rule: The Trouble with Majority-Rule Consensus Trees: Cladistics, v. 17, p. 282-284.

Soltis, P. S., and Soltis, D. E., 2003, Applying the Bootstrap in Phylogeny Reconstruction: Statistical Science, v. 18, no. 2, p. 256-267.

Tomàs, M., Alba, D. M., Sanisidro, O., Bolet, A., and Checa, L., 2010, Los perisodáctilos del Mioceno Superior de la Autovía Orbital de Barcelona B-40, tramo Olesa de Montserrat - Viladecavalls (Cuenca del Vallès-Penedès): Cidaris, v. 30, p. 317-324.

van der Made, J., 2010, The rhinos from the Middle Pleistocene of Neumark-Nord (Saxony-Anhalt), p. 463-527.

1. The golden age and the demise of rhinos: untangling the fossil record of Rhinocerotidae

Oscar Sanisidro
Juan L. Cantalapiedra
and Jorge Morales

Abstract. Extant rhinoceros species represent but a vestige of the great diversity that the family Rhinocerontidae attained during the Cenozoic. Recent taxonomic reviews permit an updated compilation of the first and last appearance data in order to estimate net diversity and turnover rates. Our results show several taxonomic replacements along Seven main faunal turnovers have been described in detail, showing an episodic pattern of strong pulses. Overall net diversity rates in Rhinocerotidae differ from continental results thus outlining different ecological and regional factors.

INTRODUCTION

The six living species of rhinoceros exhibit relatively homogeneous overall morphological and taxonomic affinities, representing but a vestige of the great diversity that the family Rhinocerotidae attained in the past. Rhinoceros were amongst the most abundant, ubiquitous, and diverse terrestrial mammals during the Cenozoic, occupying all the ecological niches available to large mammalian terrestrial herbivores. The ubiquity and profusion of rhinocerotid remains in fossil localities highlight the important role that this group played within the mammalian communities in the past as medium to large-bodied herbivores. Rhinocerotids were also very diverse ecomorphologicaly. Their body sizes and proportions range from sheep-sized subcursorial to the short-limbed hippopotamus-like forms (Fig. 1A), and showed feeding habits between pure browsers to grazer hypselodont specialists. Unlike today's rhinoceros, fossil evidence suggests that some species probably used to occur in large herds. Interestingly, most of the known fossil rhinos were hornless and presented sexually-dimorphic tusk-like lower incisors that were likely used for defense and male-male competition.

The Rhinocerotidae is a perissodactyl family included in the Superfamily Rhinocerotoidea, in turn the sister group to Tapiroidea (Janis et al., 1998). The members of Rhinocerotidae are diagnosed by the development of a combined set of upper chisel-like incisors (I1) and lower tusk-like incisors (i2), known as the incisor shearing complex (I1/i2; Heissig, 1989; Prothero, 2005). In early steps of their evolution, rhinos also experienced a reduction of the anterior dentition (canines, I2, I3 and i3) concurrently with the molarization of premolars (Heissig, 1989; Prothero, 2005). Other outstanding anatomical features of the group include a reduction of the fifth digit in most major clades (Antoine, 2002) and a wide array of skull morphologies that probably reflect highly disparate ecological niches (Deng et al., 2013; Sanisidro et al., 2011).

Early rhinocerotids probably arose during the late middle Eocene, around 40 Ma, in the mid-latitudes of the Asian continent (Fig. 1B and 1C; Hanson, 1989; Holroyd et al., 2006; Prothero, 2005), from where they quickly expanded to North America (Prothero, 1998). In the early Oligocene (33 Ma) they dispersed into Europe, and by the early Miocene (19 Ma) the new climatic and geographic conditions —the establishment of the Arabian Bridge— allowed them to reach Africa, achieving an almost pan-continental distribution (Deng, 2002; Geraads, 2010; Heissig, 1989; Prothero, 2005). Along their evolutionary history, rhinos have diversified into tropical rain and deciduous forests, savannas, xeric scrublands, cold steppes and the tundra (Deng et al., 2011; Fortelius et al., 1993; Groves, 1972; Prothero, 1993).

Yet, despite having taken part in one of the most impressive examples of mammalian diversification, there has been relatively little research on macroevolutionary aspects of the rhinocerotids. As a consequence, their complex macroevolutionary history, fulfilled of faunal replacements,

evolutionary radiations and continental migrations, remains poorly understood. The scarce body of research tackling the broad-scale evolutionary patterns of the group mainly focus on raw diversity patterns, absolute originations and extinctions (not evolutionary rates e.g. speciation, extinction, turnover), being especially noteworthy the revision made by Cerdeño at both global and continental scales (Cerdeño, 1998). The results agreed on a general pattern that depicts a diversity maximum in the middle Miocene and other secondary peaks in the late Early Oligocene and the Late Miocene at both specific and generic scale. It also included a considerable diversity drop in the latest Miocene. Other analyses at a continental scale include those of Prothero of the North American rhinocerotid record (2005), Cerdeño and Nieto's of European rhinos (1995), and Deng's review of the Chinese species (2002). These studies carried at the species level, acknowledged similar patterns with some particularities at a continental scale (e.g. a maximum in the European record in the Lower Miocene previous to the Middle Miocene climax). In some cases, some of these diversity peaks have been tied with rises and falls in temperature and humidity by visual comparison (Cerdeño and Nieto, 1995; Deng, 2002).

Assessing diversity dynamics is of great importance to understand the tempo and mode of evolution (Jablonski, 1996, 2005; Valentine, 1985). However, diversity curves need to be interpreted with caution, as they can be considerably modified by geological and sampling biases (Smith and McGowan, 2011b). Moreover, geological biases are difficult to estimate at a large scale, being necessary other sampling-related proxies as the fossil collection data (Dunhill et al., 2012; McGowan and Smith, 2008). Sampling biases are generally determined by differences in sampling effort (see Smith and MacGowan, (Smith and McGowan, 2011b) and references included therein), and when they are controlled for, diversity curves can portrait very different results from the original dataset (Alroy, 2008; Alroy et al., 2001; Lloyd, 2012a; Mannion et al., 2010; Smith and McGowan, 2011b). Regarding the sampling biases in rhino diversity patterns, Prothero (2005) assessed the degree of correlation between the number of North American geographic regions (as proxy of sampling bias) and species diversity through time. The results showed a positive but considerably weak linear correlation. This is to say, the species richness pattern of North American rhinos is not fully explained by the sampling effort, suggesting that diversity trends in the fossil record likely reflect an underlying biological signal (Prothero, 2005). Nonetheless, to our knowledge, Prothero's review is the only study where diversity patterns of rhinos have controlled for sampling bias.

Deciphering the diversity curve is of great importance to understand the tempo and mode of evolution (Jablonski, 1996, 2005; Valentine, 1985). From a methodological point of view, classic diversity studies rely on taxic approaches by summing the number of taxa recorded in each time interval to describe a diversity curve (Levinton, 1988). This approach, called taxic diversity estimate (TDE), is relatively simple to calculate and includes all the available taxa. However, it excludes the singletone taxa (i.e. those taxa which appear and disappear within one of the selected time bins), avoids the phylogenetic relationships and mainly depends on the reliability of the fossil record. The second way to obtain species diversity curves starts from a phylogenetic hypothesis (PDE). Even though it is able to fill the missing lineages not observed in the fossil record, being relevant when tackling macroevolutionary analyses of fossil groups (Lloyd et al., 2008; Mannion et al., 2010), this method only reconstructs their first appearance times, leaving an asymmetrical extended range (Foote, 2000; Wagner, 1995, 2000).

Based on a reviewed taxonomic framework (Supplementary Data 1 and 3), in the present work we aim to explore the macroevolutionary patterns of the family Rhinocerotidae at the global and continental scales, the succession of its evolutionary faunas during the last 40 Ma, and to test the correlation of the appearance, diversification and extinction of such faunas with climatic change in the past. In particular, our purpose is to tackle the following questions:

1) Is our interpretation of the diversity patterns of the family Rhinocerotidae shaped by the sampling effort of paleontologists? We here assess whether the diversity peaks and troughs of the group as recovered from the fossil record have a true biological signal, falling beyond the effect of the collecting effort. To tackle this issue, for each continent, we calculated the species diversity through time and applied a recently developed modeling approach (Lloyd, 2012a) to remove the sampling bias and identify the peaks and troughs of the diversity curve depicting biological signal.

2) Can the evolutionary history of rhinocerotids be portrayed as a succession of evolutionary faunas? If so, how did the patterns of diversification and faunal replacements shape this succession? To answer these questions, we assessed net diversification and turnover rates through time (Foote, 2000), and performed a factor analysis (FA) to describe the 'evolutionary faunas' of the Cenozoic Rhinocerotid fossil record as in Sepkoski (1981).

3) Did the rise and fall of the rhinocerotid 'evolutionary faunas' track climatic shifts? Physical environmental change has been proposed as one of the main drivers of evolution (Barnosky, 2001; Benton, 2009; Janis, 1989; Janis, 1993b; Vrba, 1992), potentially affecting the capability of living beings to shift their geographic distributions (Casanovas-Vilar et al., 2010; Vrba, 1999) and even their speciation and extinction rates (Barnosky, 2005; Cantalapiedra et al., 2011; Vrba, 1987). We applied the method developed by Figueirido et al. (2012) to test the direct correlation of the diversification and extinction of these 'evolutionary faunas' with the global temperature curve as estimated from oxygen isotopic values ($\delta^{18}O$) (Zachos et al., 2008). Figuerido's study encompassed the Cenozoic terrestrial mammals of North America, while here we focus on a single mammalian family at the continental scale. Other factors such as regional climate, tectonics (continental connections), migrations and ecological exclusion may have

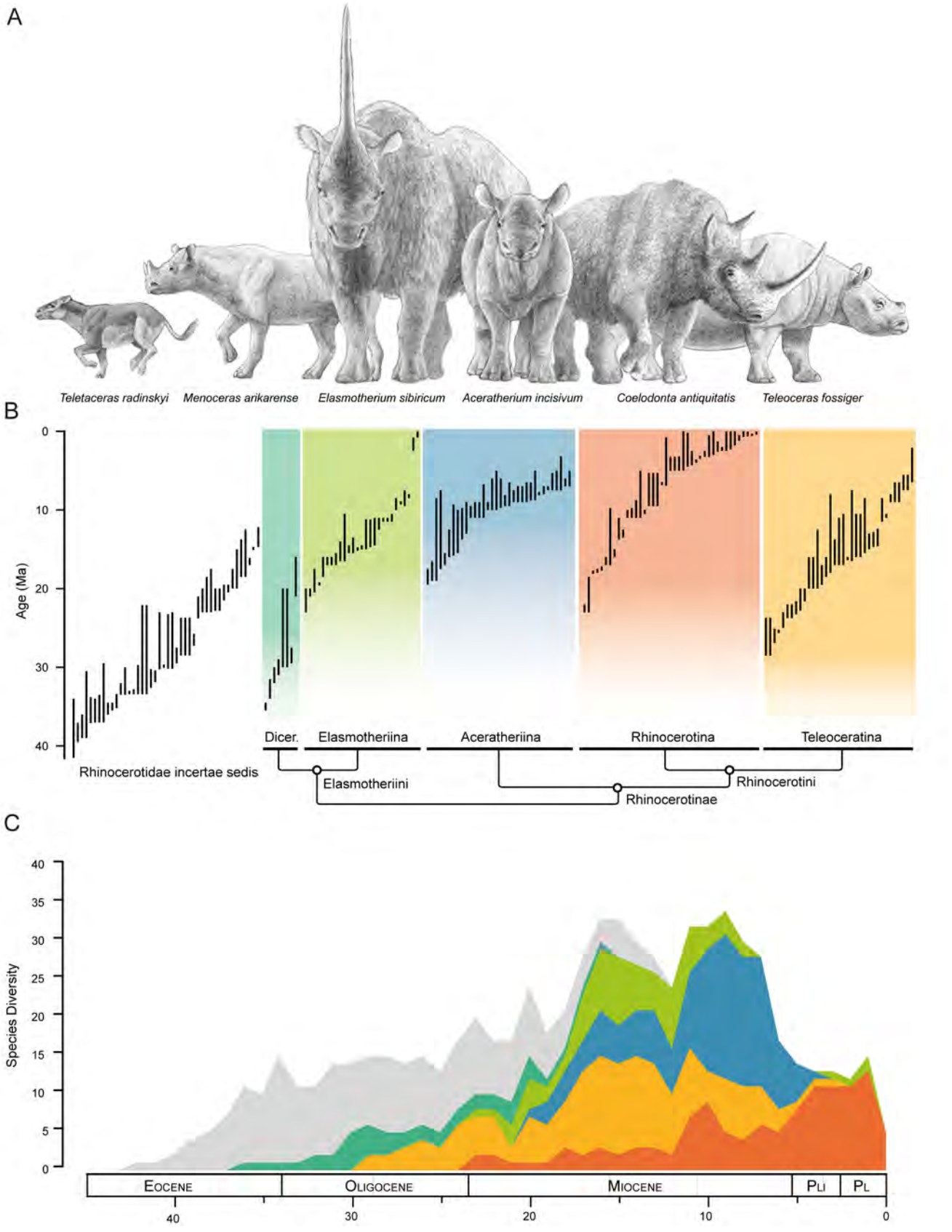


Fig. 1 A, Hypothetical life-appearance reconstructions of some representative rhinoceros species. From left to right: *Teletaceras radinskyi* from the North American Eocene, *Menoceras arikarense* from the North American Oligocene, *Elasmotherium sibiricum* from the Eurasian Pleistocene, *Chilotherium wimani* from the Asian Miocene, *Coelodonta antiquitatis* from the Eurasian Pleistocene and *Teleoceras fossiger* from the North American Miocene. Shoulder height of *E. sibiricum* 280 cm. B, Biostratigraphic range of the included species in the present work and phylogenetic affinities of the Family Rhinocerotidae according to the suprageneric level classification established by Antoine (2003). Rhinocerotidae incertae sedis include not only the basalmost species but others with doubtful phylogenetic affinities. (C) Rhinoceros taxic diversity estimate (TDE) of the major taxonomic groups. Illustration by the authors (O. S.). The reconstruction of *C. antiquitatis* was modified from an original drawing by Mauricio Antón. Abbreviations: Dicer., Diceratheriini; Pli, Pliocene; Pl, Pleistocene.

also a paramount role in shaping the evolutionary faunas at this scale.

Our results show that, generally, diversity patterns in the rhinocerotid fossil record lack effect of sampling effort, likely reflecting biological processes. Globally, the 40 million years of rhinocerotid evolution can be summarized in a succession of seven faunas, shaped by an uneven sequence of peaks of turnover, coupled with apexes and troughs in net diversification. Only two of these faunas significantly track the global temperature curve (Zachos et al., 2008), suggesting that other factors (regional climate, migrations and subsequent ecological replacement) played a main role in the rise and demise of rhinocerotid faunas.

MATERIAL AND METHODS

Systematic and biostratigraphic overview

We constructed a global database of all known taxa inside Rhinocerotidae, consisting of 189 species (in 62 genera). Some fossil remains have been considered as a separate species, even if not formal descriptions have been published (as detailed in the Supplementary Data 1). In the same way, remarks about the validity of some disputable species have been also detailed. We opted for a species-level approach to attain a higher resolution when estimating diversification dynamics and assessing the 'evolutionary faunas', as specified below. Information of stratigraphic ranges, paleobiogeographic distribution (at the continental scale), and supraspecific taxonomy (Antoine, 2002) was also included in our database. Even though we are aware that the phylogenetic approach proposed by Antoine has been recently questioned (Geraads et al., 2012), we think that it represents a reliable framework at suprageneric scale to work with (Fig. 1). All these data were gathered after an intensive review of paleontological literature (see Supplementary Data 1 and 3). As a result, a raw taxic diversity estimate was calculated.

Published cladistic hypothesis of Rhinocerontidae are fragmentary, focus on deep-supraspecific relationships and rarely depicting complete species level relationships (Antoine, 2002; Deng et al., 2011; Fortelius and Heissig, 1989; Prothero, 2005), thus avoiding a phylogenetic diversity estimate. Undoubtedly, future paleobiological and macroevolutionary studies of Rhinocerotidae (e.g. paleobiogeography, diversification dynamics, phylogenetic community structure) will largely benefit from the construction of family-wide species level calibrated trees.

Evaluating the influence of sampling in rhinocerotid diversity

Raw taxic diversity curves are usually shaped by the collecting effort of paleontologists (see Introduction). Thus, time series analyses of diversity require that sampling bias be removed (Smith and McGowan, 2011a). Here, a recently developed modeling approach for removing the sampling signal in diversity curves was applied to our data set (Lloyd, 2012b). This method requires a sampling proxy and the raw diversity values through time, and assumes that the true diversity is constant and observed diversity is a mere artifact of the sampling proxy. Therefore, it fits linear and non-linear models to the dataset and choses the 'best' model by calculating the sample size-corrected Akaike Information Criterion (AIC_c). The model is used to calculate predicted values of diversity, and residuals are estimated by subtracting the predicted diversity from the observed diversity values. By comparing the predicted and observed diversity through time, we could identify peaks and troughs of the diversity curve that fall beyond the biased-model and potentially reflect biological signal. The number of fossil localities was used as the sampling proxy. The Lloyd (2012) method was applied to the raw diversity and the sampling proxy measured per million-year for each continent separately (Cerdeño, 1998; Cerdeño and Nieto, 1995; Deng, 2002). The sources and the number of fossil sites and taxa included in the several continental sampling-models are detailed in the Supplementary Information (Table S2).

Turnover and diversification rates analyses

Evolutionary rates as recovered from the fossil record are affected by interval duration and sampling quality. Increasing sampling of a given time unit will entail that a higher number of rare taxa are known exclusively from that unit. These exclusive taxa are named *singleton* (Foote, 2000), and are particularly sensitive to variation in preservation and interval length. Hence, most metrics of taxonomic and evolutionary rates correct for the effect of the singleton or even exclude them from calculations (see Van Valen ; Van Valen). Besides the presence of *singletons*, the calculation of origination and extinction rates is affected by the total taxonomic diversity within an interval. These rates will be higher for those intervals with the higher the number of taxa and, therefore, when comparing time units containing a different total number of taxa, per-capita rates must be calculated (Foote, 2000). We calculated per-capita origination (p) and extinction (q) rates as follows:

$$p = -ln\,(N_{bt} / N_t)\,\Delta t$$
$$q = -ln\,(N_{bt} / N_b)\,\Delta t$$

where N_b and N_t are the number of taxa that cross the lower and upper limits of the time interval (*crossers*) and N_{bt} is the number of taxa known from before and after the time interval (Foote uses b and t to refer to crossing the *bottom* and *top* boundaries of the interval (2000)). The metrics are normalized by interval duration (Δt). In this work the time period of the study was divided into 1-million-year intervals (Finarelli and Badgley, 2010). Hence, since the time bins are of equal length, the interval duration (Δt) can be omitted. Other relevant rates were also assessed from Foote's metrics. The net diversification rate (d) was calculated as the balance between the speciation rate and the extinction rate ($p - q$), whereas turnover (t) was

calculated as the sum of both rates ($p + q$). In this manner, the assessment of the turnover rate accounts for the proportion of change of the faunas throughout the time interval rendered by both origination and extinction events. Thus, peaks in faunal turnovers can be produce by accelerating extinction, or origination, or both.

We also took into consideration the variance in the data by bootstrap resampling (Foote, 2003). Considering the stratigraphic range of a species the fundamental sampling unit, the dataset was bootstrapped with replacement 1000 times, each time with a different bootstrap sample. For each time bin, 1000 estimates of origination (p), extinction (q), diversification (d) and turnover (t) rates were calculated. The mean parameter estimation from the 1000 bootstraps was considered the best-fit rate estimates, and ± 1 standard deviation of the distribution around each mean was used to define the uncertainty in the corresponding rate estimate (Finarelli and Badgley, 2010).

Identifying rhinocerotid faunas

Factor analytic descriptions can be applied to the fossil record to identify evolutionary faunas composed of a characteristic association of taxa that share times of origination, diversification and demise (Figueirido et al., 2012; Sepkoski, 1981). In order to depict how the turnover and diversification dynamics shaped rhinocerotid faunas through the Cenozoic, we performed *Q*-mode factor analyses (FA) as in Sepkoski (1981). We divided the analysis interval (42 Ma) in 21 two-million-years time bins and calculate the diversity of species within each of the 62 genera in each bin. The resulting diversity matrix was constructed so that the temporal intervals were columns, and then analyzed using the function "factana"l in R (R Development Core team, 2015). The rotation "*varimax*", which maximizes the sum of the variances of the squared loadings, was used. We selected those factors with eigenvalues greater or equal to 1, or those conforming a marked slope when plotted against the rank (Supplementary Data 3, Fig. S2) (Figueirido et al., 2012; Sepkoski, 1981). The "scree graph" was analyzed using the R package *nFactors*. The genera with scores greater that 1 were retained, since they represent an important contribution to the total diversity of each evolutionary fauna (Sepkoski, 1981).

Correlating faunas' diversification to global climate

Figueirido and coauthors (2012) developed a method for directly testing the correlation between the onset, diversification and extinction of evolutionary faunas assessed from the factor analysis (FA; see above), and the climate change in the past. This approach uses the positive factor loadings (PFLs) of each fauna, which reflects the fauna's timespan, as a proxy of its paleodiversity, and the deep-sea oxygen isotopic values ($\delta^{18}O$) form Zachos et al. (2008) as a proxy of the paleoclimate for those intervals where the faunas showed positive loadings (see supporting information in Figueirido et al., 2012). Then, ordinary least square regressions are applied to the data. Alternatively, the approach also uses the species paleodiversity curve of those genera scoring > 1 in each fauna (Supplementary Data 3, Fig. S2) as a proxy of paleodiversity (genera diversity within families in the original work of Figueirido et al. (Figueirido et al., 2012)). However, we should be cautious when applying ordinary regressions to data within a time series, since the observations depend to some extent on the preceding values. Hence, before applying least square regressions to our data, their serial correlation component was removed using the method of generalized differences (GDA) developed by Wonnacott and Wonnacott (Wonnacott and Wonnacott, 1984). This method, which has been previously applied to paleobiological studies (Alroy et al., 2008; Figueirido et al., 2012; McKinney and Oyen, 1989), allows to extract the serial correlation components from both PFLs or the diversity values of species, and the $\delta^{18}O$ values of the respective time intervals. The lag 1 autocorrelation coefficient (ρ) was calculated using the *ACF* function in the package *nlme* in R (Pinheiro et al., 2005), and used to transform the values:

$$\Delta Y_t = \rho Y_{t-1}$$

where Y_t is the original value of PFL, species diversity within genus or $\delta^{18}O$, and ρ the correlation coefficient. For the first observations, which lack a previous observation, we performed the transformation as follows (Figueirido et al., 2012; Wonnacott and Wonnacott, 1984):

$$\Delta Y_t = (1-\rho^2)^{0.5} Y_1$$

RESULTS

Sampling and evolutionary faunas

Diversity and sampling

We found that diversity fluctuations in the Rhinocerotidae fossil record generally lack systematic effects of sampling efficiency and reflect biological processes (Supplementary Data 2). The diversity peaks during the Eocene generally fall inside the 95% confidence intervals of the sampling-driving model, but a first diversification increase is recovered at the Eocene-Oligocene boundary in North American and Asian rhinocerotids (Fig. S1). The diversity dynamics during the Oligocene are also particularly well recognizable in North American and Asian faunas, where all the fluctuations fall well beyond the confidence intervals. Short-term trends are also clear during the Miocene of Asia, North America and Europe. Species-level rhinocerotid data from the African Miocene shows medium-term trends, but still lack the detail of those from other continents. The African fossil record is considerably less studied than their Eurasian and North American counterparts, thus being more sensitive to future taxonomic updates (Geraads, 2010). The dramatic trough of rhinocerotid paleodiversity during the Plio-Pleistocene is well supported by the data from North America and Eurasia (Supplementary Data 2). Overall, we consider that the fossil

record of the group at the global scale is well sampled and allow to soundly studying diversity dynamics and faunal replacement as we do here.

Evolutionary faunas of the Family Rhinocerotidae

The factor analysis (FA) performed from the species within genera matrix yielded six factors with eigenvalues greater than 1 that explained the 85% of the original variance. However, based on the "scree graph" (Supplementary Data 3; Fig. S2), we included an extra factor (with an eigenvalue of 0.88) that increased the percentage of explained variation up to 90%. This rather high value reflects common synchronic faunal replacements across continents. Globally, the fossil record of the rhinocerotids can be summarized in seven 'evolutionary faunas' that share timing of origination and demise (Figueirido et al., 2012; Sepkoski, 1981): (i) middle-late Eocene, (ii) late Eocene-early Oligocene, (iii) Oligocene, (iv) early Miocene, (v) early-middle Miocene, (vi) late Miocene-early Pliocene and (vii) Plio-Pleistocene (Fig 2).

Long-term evolutionary patterns and climate correlation

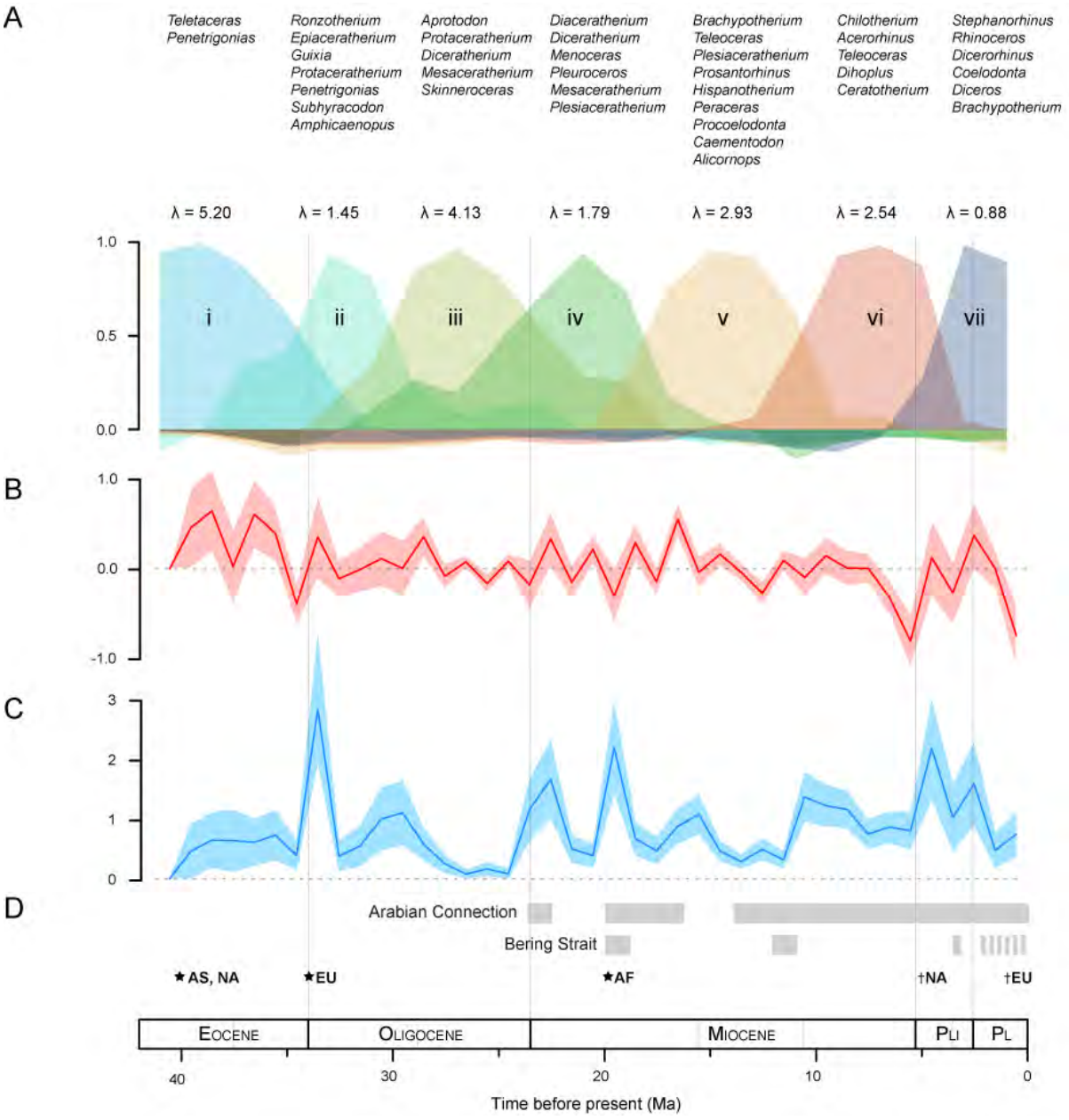


Fig. 2 Summary of the results of diverse macroevolutionary analyses performed over the global fossil record of Rhinocerotidae: A) Factor loadings within the seven factors from the Q-mode factor analysis plotted against geologic time and reordered according to the temporal sequence. B) Net diversification rate (d = p – q; red). C) Faunal turnover rate (t = p + q; blue). The shaded regions represent ± 1 SE on the basis of the bootstrap resampling. Gaps in the curve resulted from bins without crosser taxa. D) Land masses connections (grey bars), continental first (*) and last appearances (†). Abbreviations: AS, Asia; NA, North America; EU, Europe; AF, Africa; Pli, Pliocene; Pl, Pleistocene.

Turnover episodes

The succession of rhinocerotid faunas (Fig. 2A) can be paired with the temporal pattern of evolutionary rates (diversification and turnover; Fig. 2B and 2C). Transitions between evolutionary faunas are associated with major turnover pulses. For instance, marked pulses are recovered during the Eocene-Oligocene Transition, the Oligocene-Miocene, the early Miocene and the Miocene-Pliocene. Secondary episodes of faunal replacement can be observed during the early Oligocene, the early to middle Miocene and the Plio-Pleistocene transition. Turnover rates were low during late Oligocene and the middle Miocene, remaining relatively high during the late Miocene (Fig. 2C).

Interestingly, the turnover rates are usually rendered by simultaneously increasing speciation and extinction

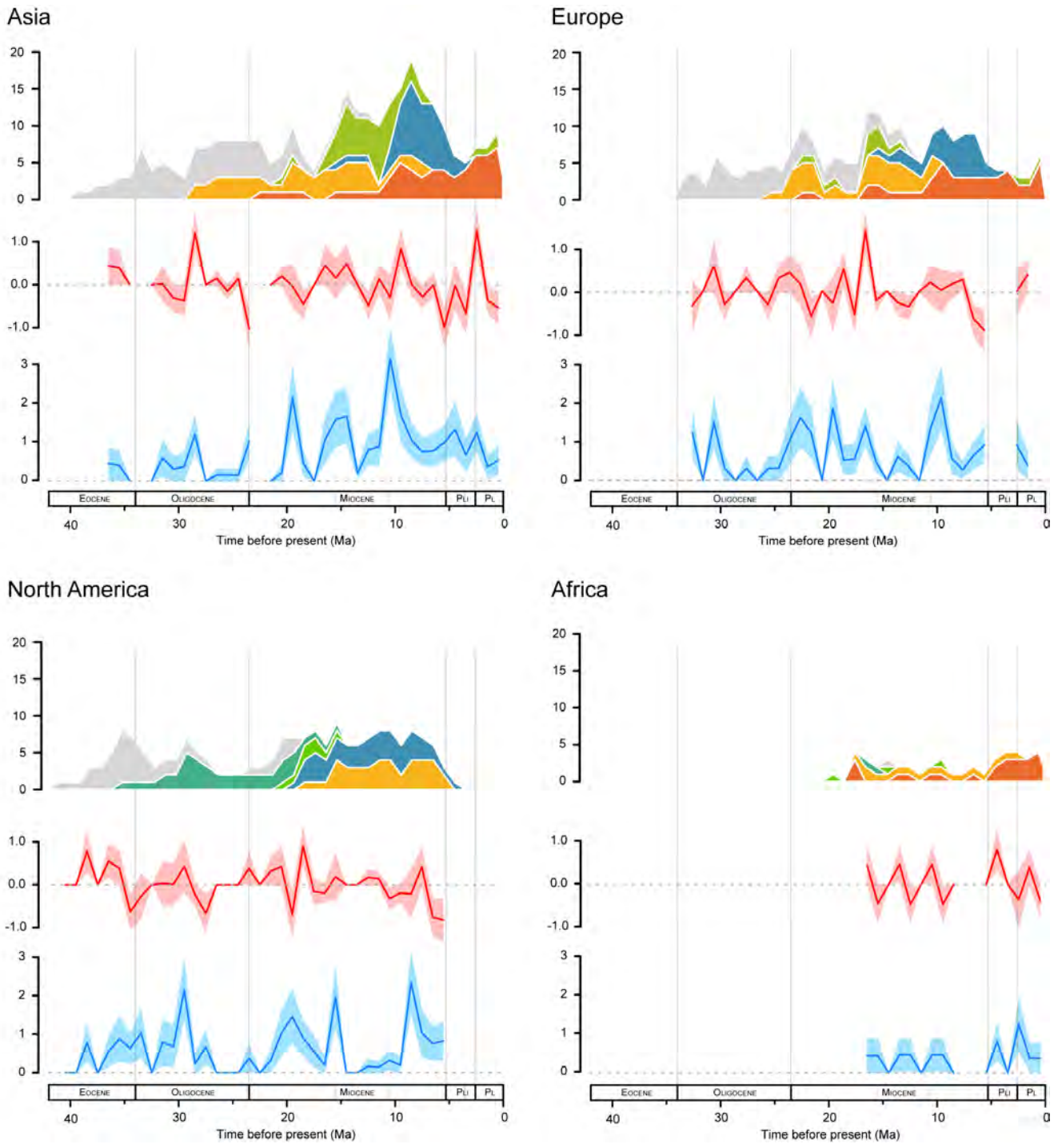


Fig. 3. Evolutionary patterns across continents. For each, the taxic diversity estimate (TDE) of the major taxonomic groups {Antoine, 2003 #155}, the net diversification rate (d = p – q; red), and the faunal turnover rate (t = p + q; blue) are shown. The shaded regions represent ± 1 SE on the basis of the bootstrap resampling. Gaps in the curve resulted from bins without crosser taxa. Colours represent the clades detailed in figure 1 . Abbreviations: Pli, Pliocene; Pl, Pleistocene.

rates. This is consistent with the notion that speciation and extinction rates are generally correlated and bunched in time forming turnover pulses. This shows that faunal replacements on the global and continental scale probably respond to external abiotic factors (e.g. climate and tectonics)(Benton, 2009; Finarelli and Badgley, 2010; Vrba, 1995). Nonetheless, we found that the periods of "stasis" between pulses are commonly characterized by a non-negligible background turnover rate (Fig. 2C).

Continental stories

Despite been summarized as a series of seven faunas at the global scale, the evolutionary history of rhinos shows disparate diversity and taxonomic dynamics in each continent (Fig. 3).

In North America, rhinocerotid faunas were dominated by diceratheriines until well into the early Miocene, around 20 Ma, when a prolonged turnover episode rendered their decline and brought about the onset of rhinocerotid faunas dominated by aceratheriines and teleoceratines (Fig. 3). These new forms emigrated from Asia, and maintained similar and constant species richness until their decline and extinction in the early Pliocene (~5 Ma), when rhinos finally disappeared from North America.

On the contrary, diceratheriines never entered Eurasia, where teleoceratines were the predominant forms since the early Oligocene (~28 Ma) until the middle Miocene (~15 Ma). The Eurasian middle Miocene was a period of marked change in the rhinocerotid evolution (Fig. 3A and 3B). In fact, the Oligocene to early Miocene transition mostly represented an evolutionary continuum, rather than a change. This is clearly shown by our representation of the factor analysis (Fig. 2A), where faunas ii, iii and iv are largely overlapped. The early to middle Miocene transition in Eurasia (Fig. 2A, fauna v), on the other hand, resulted in the radiation and domination of the elasmotheriines, which probably migrated from North America. Our climatic analyses also suggest that the onset of the middle Miocene faunas could be associated with the global high temperature of the middle Miocene Climatic Optimum (Zachos et al., 2008).

The middle Miocene of Eurasia was dominated by both teloceratines and elasmotheriines, which declined around 13 Ma. The late Miocene witnessed the demise of the teleoceratines and the decline of the elasmotheriines in Eurasia, which was concomitant with the radiation of acerathrine rhinos (see the marked diversification peak at 9 Ma, Fig. 3A). Their increase in species richness resulted in the diversity peak of the late Miocene, around 8 Ma.

The late late Miocene brought about the end of the golden age of rhinos, a dramatic trough of their diversity and a taxonomic impoverishment of their faunas (Fig. 1C and Fig. 3). However, the decline was asynchronous in different continents and, presumably, had different causes. In North America only one teleoceratine survived the Miocene-Pliocene boundary, disappearing shortly after. In Eurasia, the rhinocerothines became the dominant forms, and the acerothines disappeared along the Pliocene.

A detailed overview of the Rhinocerotidae evolution

Eocene and Oligocene

The first representatives of the family Rhinocerotidae probably arose in the mid-latitudes of the Asian continent around 40 Ma, with *Teletaceras* as the first recorded genus (Hanson, 1989; Holroyd et al., 2006; Prothero, 2005). The former steps of the rhinoceros history are characterized by an early entrance of *Teletaceras* to North America together with other Asian taxa

(Emry, 1981; Emry et al., 1987). This remarkable paleogeographic event took place around the boundary between the North American Uintan and Duchesnean (~ 42 Ma). According to our results, the high diversification rates of the initial radiation in Asia and North America were coupled with low faunal replacement (fauna i in Fig. 2). As part of these first positive diversification rates, the genus *Teletaceras* experienced a short radiation, formed by the North American consecutive species *Teletaceras radinskyi* (see reconstruction in Fig. 1) and *Teletaceras mortivallis* and the Asian *Teletaceras borissiaki*. *Penetrigonias dakotensis*, also small-sized taxa, was also recorded among the first rhinocerotids of North America.

The middle-late Eocene faunas declined as global temperature dropped (Figs. 2 and Supplementary Data 2, Fig. 3), a result of a climatic event associated with the onset of Antarctic glaciation, which transformed terrestrial ecosystems towards the latest Eocene. The transition between the Eocene and the Oligocene Epochs (EOT), about 34 Ma, is regarded as one of the most dramatic stages of climatic change of the Cenozoic (Blondel et al., 1997; Brunet, 1977; Legendre and Hartenberger, 1992). A gradual decrease in temperature during the later Eocene culminated in a sudden cooling event, favoring the permanent formation of ice-sheets in Antarctica (Zachos et al., 2008). This global climatic change was accompanied by new land bridges that favored important paleo-geographical transformations. The Turgaï Straits closure and the formation of a corridor in southeast Europe permitted the entrance of dispersing Asian taxa in Europe during the Early Oligocene (Ducrocq, 1995; Heissig, 1999; Pomerol). This faunal event was termed as the "Grande Coupure" by Stehlin in 1910, who firstly recognized it in the European fossil record. Regarding rhinos, the EOT brought about accelerating extinction rates (negative net diversification; see Fig. 2) followed by a profound faunal turnover —high speciation and extinction rates— that meant the transition towards the early Oligocene rhinocerotids (Fig. 2, fauna ii). These high turnover rates are particularly well recovered in the North American record (Fig. 3), and rendered the extinction of the genera *Trigonias*, and some species of the genera *Penetrigonias*, and *Subhyracodon*. In Asia, the impoverished late Eocene assemblages continued in the early Oligocene with the new genera *Protaceratherium*, *Epiaceratherium* and

the first teleoceratines, represented by the genus *Aprotodon*. This small-sized genus shows a particular wide symphiseal region and enormous tusk-like lower incisors (Qiu and Xie, 1997). Posterior teleoceratine species were geographically widespread, developing particularly short-limbed proportions and barrel-shaped thorax, being sometimes referred as hippo-like rhinos. At this point the first entrance of rhinocerotids into Europe is recorded (Heissig, 1999). Within these incoming genera were *Ronzotherium* and the much rarer and specialized *Epiaceratherium*. Significantly, these early Oligocene species (ii) compose the first multispecific assemblages in Eurasia, suggesting an early ecological segregation into different niches (Antoine et al., 2003).

During the early to late Oligocene transition, new turnover episodes are recorded in Europe (~ 31 Ma), North America (~ 29 Ma) and Asia (~ 28 Ma), being depicted as a single blunt peak around 30 Ma at a global scale due to their lag (Figs. 2 and 3). Such pulses configured the rhinocerotid assemblages of the late Oligocene (Fig. 2, iii). In North America, rhinoceros experienced a high diversity peak tied to a marked turnover pulse (Fig. 3C), although we did not find evidence of an increase in diversification. The two commonest Arikareean species, *Diceratherium armatum* and the smaller *Diceratherium annectens* (comprising the vast majority of the rhinoceros remains for over 10 Ma) were briefly encompassed by much rarer, endemic species in the earliest Arikareean (late Oligocene) (Prothero, 2005). These are *Skinneroceras manningi*, *Subhyracodon kewi*, *Woodoceras brachyops, Diceratherium radtkei* and the earliest member of the genus *Amphicaenopus* (Stone, 1970). Extinction rates rose in the early late Oligocene, producing the disappearance of these minority taxa and the subsequent decline of the species richness (Fig. 3C). As a consequence, during most of the late Oligocene, *Diceratherium* remained the only surviving genus in North America. In Asia, peaking origination rates were accompanied by positive but moderate turnover in the early late Oligocene (Fig. 3A). This event resulted in the extinction of the *Protaceratherium* species and the renewal of primitive forms of the genus *Aprotodon* by more derived species as *Aprotodon aralense*, *Aprotodon smithwoodwardi* and *Aprotodon lanzhouense*. Dropping diversification rates are recorded during the late Oligocene Asian rhinocerotids, forced by the extinction of most of the *Aprotodon* species and two distinct but undetermined rhinoceros (Fig. 3A). In the European scenario the firstly arrived species, established since the earliest Oligocene, were enriched with the genera *Protaceratherium*, *Mesaceratherium* and, towards the end of the Oligocene, *Diaceratherium*. While *Protaceratherium* and *Mesaceratherium* were small to medium sized hornless rhinoceros with slender limb proportions, *Diaceratherium* is the first recorded European teleoceratine, showing the typical short, brachypodial limbs and a very small horn insertion placed on the tip of the nasals. Overall, the late Oligocene is characterized by relatively low faunal replacement (globally and across continents), a trend also reported by Cerdeño (1998) for the North American rhinos.

Miocene

The late Oligocene to early Miocene boundary implied one of the most important episodes of mammalian turnover in terrestrial mammalian faunas. Globally, around the Oligocene-Miocene transition (23 Ma), turnover rates peaked. However, rhinocerotid faunas (Fig. 2, transition from iii to iv) were affected in very disparate ways by this event, depending on each continental scenario (Fig. 3). These different evolutionary patterns across continents signify that continental or even regional factors configured this faunal replacement. In North America, turnover rates and net diversification are not detectable through the Oligocene-Miocene boundary (Fig. 3C). *D. annectens*, *D. armatum* and *D. radtkei*, the survivors from the early Arikareean diverse assemblages (~27 Ma), are the only rhinoceros species up to the Hemigfordian (~18 Ma). In Asia, the faunal replacement was caused by a severe increase in extinction rates at the Oligocene-Miocene boundary. However, this remarkable diversity decrease seems to be correlated with sampling (Fig. S2). During the earliest Miocene of China three species have been recorded, *Plesiaceratherium gracile* and two teleoceratines, *A. lanzhouense* and a second species sometimes referred as *D. aginense* (Deng, 2002). The species diversity in Central Asia is represented by one species of the genus *Aprotodon*, *Aprotodon aralense*, and an undetermined *Protaceratherium* species (Antoine et al., 2003). During the Oligocene-Miocene boundary, the European rhinoceros experienced a taxonomic enrichment, with moderately positive origination and accelerating turnover rates. The teleoceratine *D. lemanense* surpassed the O-M boundary, and afterwards experienced a short radiation, giving raise to *Diaceratherium tomerdingense*, *Diaceratherium asphaltense*, as well as the later *Diaceratherium aginense*. The genus *Mesaceratherium* briefly entered the Miocene with the species *Mesaceratherium paulhiaciense*. The short-lived dicerathere *Menoceras zitteli*, poses an interesting biogeographic dilemma, as it represents the only record of a typical North American clade. This rather diverse assemblage was further enriched with *Protaceratherium minutum*, a species morphologically close to *Plesiaceratherium*, and *Pleuroceros pleuroceros* (a taxonomically uncertain taxon). All these radiations resulted in the inception of the early Miocene faunas (Fig. 2A, fauna iv).

The early Miocene marked a shift towards a climate with a weak seasonality, overall humid and warm conditions, and shallow temperature gradients (Flower and Kennett, 1994; Miller et al., 1991). Nevertheless, not direct relationship between the diversification of the early Miocene rhinoceros fauna and the global climate curve has been found (Supplementary Data 2, Fig. S3). The diceratheres *D. annectens*, *D. armatum* and *D. radtkei*, three Oligocene survivors, persisted throughout the late Arikareean of North America (24 – 19 Ma). Regarding the Asian rhinocerotids, the impoverished record of the

earliest Miocene was replaced by a richer assemblage by means of higher net diversity values, a maintained tendency that lasted until the Early Miocene diversity peak (~ 19 Ma) (Fig. 3B). These new Asian rhinoceros included some species of Oligocene origin as *Plesiaceratherium*, *Mesaceratherium* or *Protaceratherium*, and other with uncertain affinities as *Pleuroceros*. Contrary to the Asian scenario, the European record of the earliest Miocene underwent a moderate extinction event, with very high associated replacement rates (~23 to 21 Ma). At this point several European species of the genera *Diaceratherium*, *Menoceras*, *Protaceratherium,* and *Plesiaceratherium* went finally extinct.

The decline of the early Miocene rhinos appears concomitant with a pronounced turnover pulse ~19 Ma (Fig. 2). This event affected both Eurasian and North American rhinocerotids (Fig. 3). The North American core species *D. annectens* and *D. armatum* and the scarcer *D. radtkei* were replaced by several new taxa (Prothero, 2005). These include three dicerathere species (*Diceratherium niobarense*, *Menoceras arikarense* and *Menoceras barbouri*), *Teleoceras americanum* (the first American teleoceratine), an undescribed rhino species (Prothero, 2005), and a bloom of aceratherine rhinoceros (Fig. 3C). This early aceratherine radiation was roled by the species *Gulfoceras westfalli*, *Aphelops megalodus*, *Floridaceras whitei* and *Galushaceras levelorum*. Whereas *G. westfalli*, *G. levelorum* and the undetermined ´Haughton rhino´ are restricted to a single locality —and are considered as punctual endemisms (Albright, 1999; Prothero, 2005)—, *Diceratherium niobrarense* and *Aphelops megalodus* are more common species, extending their biostratigraphic range to the early Hemingfordian and the Clarendonian, respectively. In Eurasia, extensive terrestrial faunal exchanges were initiated by the intermittent closure of the Tethyan Seaway in the Early Miocene (~ 19 Ma). High turnover scores associated with increasing speciation and extinction rates took place in Asia around 19 Ma. Amid the new Asian taxa, *Bugtirhinus praecursor* represents the first recorded elasmotheriine (Fig. 3A). This group of relatively slender rhinoceros with specialized dentition was adapted to open landscapes and spread through Eurasia and Africa (Antoine, 2002). Among teleoceratines, *Brachypotherium gajense* and *Brachypotherium pugnator*, the first members of the succesful genus *Brachypotherium*, appeared. A smaller relative, *Prosantorhinus shahbazi*, was also recorded in the Asian fossil record, whereas *Diaceratherium* continued with the species *Diaceratherium askazansorense*. In Europe, another turnover peak started *circa* 20 Ma. *D. aginense* was replaced by the bigger species *Diaceratherium aurelianense*. The primitive hornless genera *Plesiaceratherium* flourished at that time, being represented by the species *Plesiaceratherium platyodon* and the subsequent *Plesiaceratherium lumiarense* and *Plesiaceratherium mirallesi*. On the other hand, several earliest Miocene taxa with Oligocene roots as *Mesaceratherium paulhaciense*, *P. pleuroceros* or *M. zitteli*, went extinct. As part of the extensive geographic changes, the African-Eurasian corridor opened, permitting the entrance of the rhinoceros into Africa for the first time. Despite showing a relatively low species richness, these early African rhino assemblages were rather diverse, including representatives of the rhinocerotines (i.e. *Rusingaceros leakeyi* and '*Diceros*' *australis*), aceratheriine-related species (*Turkanatherium acutirostratum*), aceratheriines (*Chilotheridium pattersoni*), teleoceratines (*Brachypotherium snowi*) and primitive elasmotheriines (*Ougandatherium napakense*). Significantly, *R. leakeyi* is considered the earliest rhinocerotine species of modern type and shows the tandem-placed horns of modern African rhinos. The later '*D*'. *australis* is a large and slender rhinocerotine with uncertain affinities (Geraads, 2010). Whether *Ougandatherium* comprise the first recorded species of an African elasmotheriine lineage (including the later genera *Victoriaceros* and/or *Kenyatherium*) will remain an unsolved issue until a phylogenetic hypothesis is proposed or new findings fill the gap produced by the paucity of the African fossil record.

Diversification increased between 18 – 16 Ma at a global scale, giving rise to the flourishing faunas of the middle Miocene (fauna v in Fig. 2), when the rhinocerotid diversity reached its climax (with a maximum of some 30 species; Fig. 1). After accounting for sampling biases, our results offer support to previous studies of European and Asian faunas (Cerdeño, 1998; Cerdeño and Nieto, 1995). However, our diversification analyses do not provide evidence of peaking extinction rates in the European assemblages during the middle Aragonian (Cerdeño, 1998). This burst of diversification of the middle Miocene is almost synchronic in North America, Asia and Europe (Fig. 3), and according to our generalized differences analysis (Fig. S3) is significantly correlated to the high global temperatures of the Miocene Climatic Optimum (Zachos et al., 2008), suggesting that rhinocerotid faunas probably responded similarly to climate worldwide during this period. This climate change, which has been recorded globally, caused the onset of higher seasonality, marked regional differentiation in precipitation regimes (Bruch et al., 2007; Eronen et al., 2010), and a steeper latitudinal thermal gradient (Janis, 1993a). Evidence of global warmth in the middle Miocene includes lateritic soils and thermophilic flora extending along continents of both North and South hemispheres. Around 18 to 15 Ma, rhinos underwent a profound faunal replacement in Asia, Europe and North America (Fig. 2C and Fig. 3). This turnover had been previously reported in Asian faunas of the middle Aragonian and American faunas of the late Hemingfordian (Cerdeño, 1998). Overall, while the last Diceratheriini finally disappeared from the North American fossil record, most groups bloomed worldwide (Fig. 1C). In North America, diceratherine and aceratheriine species were replaced by the long-lasting aceratheriine species *Aphelops megalodus* and *Peraceras profectum*. *Teleoceras americanum*, the only North American teleoceratine species, was substituted by *Teleoceras medicornutum*, *Teleoceras meridianum* and *Teleoceras brachyrhinum*. The Aceratheriini was another important group in the middle Miocene, represented by

numerous genera found in both North American and Asian fossil faunas. Primitive elasmotheriine rhinoceros experienced a considerable diversification (Fig. 1C), specially in the Asian register, hosting the elasmotheriine genera *Anatolitherium* in the Anatolian Peninsula and *Procoelodonta*, *Caementodon*, *Huaqingtherium* and *Hispanotherium* in the central and eastern parts of the continent. Some derived traits as the presence of cementum in their cheek teeth or the secondary enamel folding are already present in these species in an early degree (Antoine, 2002). The first Asian aceratheriines include the species *Chilotheridium pattersoni* and *Alicornops laogouense*. Despite of the substantial variety of Aceratheriini and Elasmotheriini species, the protagonists of the middle Miocene Eurasian faunas were the 'hippo-like' teleoceratines (Fig. 1C; Fig. 2A, fauna v). The *Brachypotherium* species *B. gajense* and *B. pugnator* were replaced by the species *Brachypotherium shanwangensis*, *Brachypotherium fatehjangense*, and *Brachypotherium perimense*. Additionally, the first species of the genus *Subchilotherium* was also recorded. Among the European teleoceratine guild, only represented by the species *D. aurelianense*, was replaced by a richer assemblage with the large *Brachypotherium brachypus* and two tiny *Prosantorhinus* species (i.e. *Prosantorhinus douvillei* and *Prosantorhinus germanicus*). On the other hand, elasmotheriine rhinoceros of genus *Hispanotherium* shortly radiated in Western Europe, taking advantage of the arid regional climatic conditions. In Africa, *B. snowi* was accompanied by a second smaller teleoceratine species described in Buluk, Kenya (Geraads, 2010) and elasmotheriine rhinoceros persisted with the species *Victoriaceros kenyensis*. Towards the late middle Miocene (~13 Ma), accelerating extinction rates produced a drastic diversity loss in Europe and Asia, although the impoverishment of Asian faunas seems to be correlated with sampling biases (Fig. S2). This outcome contrasts with the diversity increased reported by Cerdeño and Nieto in Europe around this time (Cerdeño and Nieto, 1995). Such impoverishment of the faunas constituted the end of the aceratheriine-dominated faunas of the middle Miocene (fauna v in Fig. 2).

Globally, during the beginning of the upper Miocene (around 11 to 9 Ma), paired high origination and extinction rates resulted in a marked turnover event, which eventually shaped the late Miocene faunas (vi). The replacement occurred asynchronously in Eurasia and North America (Fig. 3), which signifies decoupled evolutionary responses across continents. This might be the reason why the onset and establishment of these faunas did not correlate with the global climate proxy (Fig. S3). Particularly, net diversification rates increased in Asia (Fig. 3A), rendering a second species maximum (Fig. 1C and Fig. 3A). Around 9 to 8 Ma, North American rhinos underwent remarkable faunal replacement starred by teloceratine and aceratheriine species. Most *Teleoceras* species disappeared, being replaced by *Teleoceras major*, the subsequent *Teleoceras fossiger* (see reconstruction in Fig. 1) and, later on, in the lastest Miocene, *Teleoceras hicksi* and *Teleoceras guymonense*. The aceratheriine genus *Peraceras* increased its body-size range with the species *Peraceras hessei* and *Peraceras superciliosum* (Prothero, 2005). From there on, the American aceratheriines witnessed the progressive extinction of the species *P. hessei*, *P. superciliosum* and *P. profectum* as part of a marked diversity fall (Fig. 3 and Fig. S2). However, two large-sized *Aphelops* species (*Aphelops malacorhinus* and *Aphelops mutilus*) appeared close to the Mio-Pliocene boundary, replacing the abundant *A. megalodus*.

In Eurasia, if the middle Miocene rhinocerotid assemblages were dominated by teleoceratines, the late Miocene witnessed predominance of the hornless aceratheriines (Fig. 1C). In Central and Eastern Asia, the aceratherines experienced a short but high diversification peak nourished by the genera *Chilotherium* and *Acerorhinus* (~ 10 Ma). These related genera of hornless grazer specialists attained a high diversity, reaching a total number of 14 species during the upper Miocene. Asian Elasmotheriine rhinoceros expanded at this time, being common in the early late Miocene assemblages. The species within this clade, pertaining to the genera *Huaqinghterium*, *Parelasmotherium* and *Ningxiatherium*, augmented in size and progressively developed more hypsodont molars with intricate enamel patterns and a thicker cementum cover (Antoine, 2002). Such adaptations reflect that these forms were likely open-habitat dwellers. After this first pulse, later representatives of the Miocene elasmotheriines (i.e. *Sinotherium* and *Iranotherium*) spread in Central and Eastern Asia (Chapter 6).

In Western Europe, the species *Aceratherium incisivum* (see reconstruction in Fig. 1) replaced *Hoploaceratherium tetradactylum* and the species *A. simorrense* was substituted by *Alicornops alfambrense*, maintaining a constant number of aceratheriine species. Nonetheless, the Eastern European assemblages were largely influenced by Asian immigrant genera. Specifically, the genus *Chilotherium* spread in Greece and Turkey, reaching a maximum of five species (*Chilotherium kowalevskii*, *Chilotherium kiliasi*, *Chilotherium sarmaticum*, *Chilotherium samium* and *Chilotherium schlosseri*). Regarding the teloceratines, the last two European species (of the genus *Brachypotherium*) dissapeared during the late Miocene. Among the Eurasian rhinocerotine forms (the group of extant rhinoceros), three taxa are worth mentioning. Firstly, the primitive rhinocerotine *Gaindatherium browni* was replaced by the species *Gaindatherium vidali*. Secondly, *Diceros gansuensis*, the first relative of the extant black rhino lineage (*Diceros bicornis*), appeared in the Chinese record. Finally, the living genus *Ceratotherium* is firstly recorded with the species *Ceratotherium neumayri* and *Ceratotherium douariense* in the early late Miocene of the Eurasian and North African assemblages.

In the European basins at this time, rhinocerotines experienced a moderate flourishment during the early late Miocene (Fig. 1C). The European species, represented by the primitive *Lartetotherium sansaniense*, gave way to the larger genus *Dihoplus*, widespread along Eurasia. The elasmotheriines

appeared again in the African fossil record with the poorly known species *Kenyatherium bishopi* (Aguirre and Guérin, 1974). From there on, elasmotheriine rhinoceros disappeared from the fossil record until the Pleistocene (Fig. 1C), probably remaining as high latitude, hypsodont specialists.

During the latest Miocene rhinoceros faunas underwent a strong demise of a wide variety of rhinoceros species, being the aceratheriines particularly affected (Fig. 1C). In North America, peaking extinction rates starting around 8 Ma resulted in an important loss of species diversity (Fig. 3 and Fig. S2). Almost every American rhino went extinct before the end of the Miocene (Cerdeño, 1998). Only *Teleoceras hicksi* surpassed the Pliocene boundary, but disappeared from the North American record shortly after (Gustafson, 1977). During more than 30 Ma of evolution in North America, rhinoceros experienced successive dispersions from Eurasia. Intriguingly though, posterior openings of the Bering Strait did not involve newer dispersals, unlike other megafaunal species of the Plio-Pleistocene.

In Asia the extinction rate rose, and our sampling modeling analyses pointed to a significant loss of rhinocerotid diversity starting around 7 Ma (Fig. 3 and Fig. S2). The only Asian aceratheriine rhinoceros that reached Pliocene times was *Shanshirhinus ringstromi*, a genus closely related to the Miocene *Chilotherium* (Deng, 2005). Whereas most of the teleoceratines, aceratheriines and elasmotheriines disappeared in Asia before the Miocene-Pliocene boundary, the rhinocerotines became the most important group of the Plio-Pleistocene (Fig. 1C). The later Western Asian species (e.g. *Dihoplus pikermiensis, Dihoplus ringstroemi*) were substituted by the Plio-Pleistocene genus *Stephanorhinus*. The species *C. neumayri* also disappeared from the Anatolian and Greek basins, limiting the distribution of the extant genus *Ceratotherium* to the African continent. On the other hand, other rhinocerotine species emerged, as *Punjabitherium platyrhinus* in the Indian sub-continent, or the genus *Rhinoceros* in Eastern Asia. The first *Rhinoceros* species, *Rhinoceros sivalensis* and the extant *Rhinoceros unicornis* (the Indian rhinoceros), spread from the temperate forests of China to the tropical rain forests of South-east Asia. The European rhinocerotid faunas also experienced an extinction event that started around 7 Ma (Fig. 3). All the aceratheriines (i.e. *Aceratherium*, *Acerorhinus* and the diverse genus *Chilotherium*) and the genus *Dihoplus*, the only rhinocerotine representative in the latest Miocene, were severely affected, finally disappearing from the European record.

At this moment African rhinos underwent an impoverishment of their diversity too (Fig. 3D and Fig. S2). However, the rather fragmentary African record, consisting exclusively of singletons (Foote, 2000), precluded the performing of diversification and turnover rates estimates (Fig. 2, Fig. 3).

Plio-Pleistocene

Overall, the elevated extinction rates and subsequent diversity loss at the end of the Miocene, together with the posterior radiation in African lineages, and the minor recovery of Asian and European elements during the Pleistocene constituted a new evolutionary fauna (vii). The Rhinocerina experienced a quick recovery after the late Miocene extinction (Fig. 1). Consecutive *Stephanorhinus* species stepwise replaced each other (probably reflecting the constant short-term climatic oscillations from the middle Pliocene to the latest Pleistocene), becoming a common component in the Pleistocene Eurasian assemblages (Geraads, 2010; Lacombat, 2007; van der Made, 2010). The species *S. etruscus* and *S. jeanvireti* continued the *Stephanorhinus* lineage in the middle Pliocene. Both share a brachyodont dentition and overall slender proportions, even though the last attained a larger size (Guérin, 1972). Another rhinocerotine from the middle Pliocene was *Coelodonta thibetana*. It inhabited the uplifted basins of Central Asia and already displayed the essential features characteristic of the wooly rhino lineage (e.g. laterally flattened nasal horn, high tooth crowns). These traits, developed in cold, high altitude environments, favored the genus expansion into low altitude, high latitude habitats in the Pleistocene (Deng et al., 2011). In South East Asia, four distinct rhinocerotine species were recorded in the Plio-Pleistocene. These are the extant *Dicerorhinus sumatrensis* (Sumatran rhinoceros), *Rhinoceros sondaicus* (Javan rhinoceros), and *R. unicornis*, as well as the extinct *R. sivalensis* (Zin-Maung-Maung-Thein et al., 2010). The persistence of other groups apart from the Rhinocerotina in the Pliocene is merely anecdotal. Among the once widespread aceratheriines, only the Chinese genus *Shansirhinus* persists as their last representative (Fig. 1C).

Towards the end of the Pliocene, the Family Rhinocerotidae shows a significant turnover pulse in the Eurasian and African registers together with an Asian positive diversification (Cerdeño, 1998). The European assemblages held a succession of rhinocerotines up to the later Pleistocene. The last teleoceratine rhinoceros, represented by *Brachypotherium lewisi*, finally disappeared from the African early Pleistocene. Among the elasmotheriines, another relict group, only *Elasmotherium* reached the Middle Pleistocene. Its hypselodonty is an extreme feeding adaptation to a highly abrasive diet and poses it as a unique case among rhinoceros (Koenigswald et al., 2011). Regarding the Rhinocerotina, the later Pleistocene species of the genus *Stephanorhinus*, once widely distributed along North Africa, Europe and Asia, went extinct. The species of *Coelodonta* successively dispersed into Eurasia. These include *C. nihowanensis*, from the early Pleistocene of Northern China, *C. tologoijensis*, from the middle Pleistocene of Siberia and Western Europe and the Eurasian wooly rhino, *Coelodonta antiquitatis*, as the last representative of its kin (see reconstruction in Fig. 1). The most recent wooly rhinos disappeared at the end of the Pleistocene together with the remaining *Stephanorhinus*, after being common elements in the Eurasian faunas. The modern black rhinoceros (*Diceros bicornis*) remained as the surviving

species of a long-lasting genus with its older representatives dating back to the African lower Miocene. Likewise, the African white rhinoceros (*C. simum*) is the last representative of a grazing lineage that can be tracked back to the upper Miocene. On the other hand, the Asian fauna was reduced to the extant three species: the Sumatran (*D. sumatrensis*), the Indian (*R. unicornis*) and the Javan rhinoceros (*R. sondaicus*). Nowadays, anthropogenic perturbations have emphasized the declining of the remaining five rhinoceros species, challenging their preservation.

CONCLUSIONS

With nearly 200 described species, the known fossil record of the Family Rhinocerotidae allows carrying out macroevolutionary analyses as those presented here. Overall, rhinoceros diversity patterns seem to reflect genuine biological effects. However, exploring the sampling effort on a continental scale showed some poorly supported diversification patterns in the Asian Eocene and the African early Miocene and Plio-Pleistocene. Future paleontological effort should shed light on these parts of rhinocerotid evolution.

This is the first study where the succession of rhinocerotid faunas is statistically tested against a paleoclimate proxy. However, only the Eocene and middle Miocene faunas seem to be associated with global temperature changes (Fig. S3). We suggest that global temperature alone can not explain the evolutionary history of rhinocerotids across continents. Climate proxies may explain evolutionary dinamics of terrestrial ecosystems at a regional scale (e.g. continental) (Figueirido et al. 2012). However, regional climatic, macroecological and tectonic dynamics likely played a paramount role in the evolution of rhinos.

Here, we present an overview of the main macroevolutionary patterns of the rhinocerotids, while testing for potential correlation with global climate. The application of new analytical frameworks (e.g. geometric morphometrics) on broad temporal and spatial scales will be crucial to elucidate the ecological aspects after the macroevolutionary dynamics described here, as well as the evolution of niche partitioning across the 40 million years of rhinocerotid evolution.

ACKNOWLEDGMENTS

We are grateful to the reviewers whose comments on an earlier version of this manuscript have greatly improved it. We also want to thank for his/her help and collaboration. The manuscript was greatly improved by helpful advice, discussion and comments from P. Peláez-Campomanes and M. Hernández-Fernández. The two reviewers and the editor also provided useful comments. Financial support was provided by the MINECO grants CGL 2011-25754. O. S. acknowledges a predoctoral grant from the Spanish Government.

LITERATURE CITED

Aguirre, E., and Guérin, C., 1974, Première découverte d'un Iranotheriinae (Mammalia. Perissodactyla, Rhinocerotidae) en Afrique : *Kenyatherium bishopi* nov. gen. nov. sp. de la formation vallésienne (Miocène supérieur) de Nakali (Kénya): Estudios Geológicos, v. 30, p. 229-233.

Albright, L.B., 1999, Ungulates from the Toledo Bend local fauna (late Arikareean, early Miocene), Texas Coastal Plain: Bulletin of the Florida Museum of Natural History, v. 42, p. 1-80.

Alroy, J., 2008, Dynamics of origination and extinction in the marine fossil record: Proceedings of the National Academy of Sciences of the United States of America, v. 105, p. 11536–11542.

Alroy, J., Aberhan, M., Bottjer, D.J., Foote, M., Fursich, F.T., Harries, P.J., Hendy, A.J.W., Holland, S.M., Ivany, L.C., Kiessling, W., Kosnik, M.A., Marshall, C.R., McGowan, A.J., Miller, A.I., Olszewski, T.D., Patzkowsky, M.E., Peters, S.E., Villier, L.c., Wagner, P.J., Bonuso, N., Borkow, P.S., Brenneis, B., Clapham, M.E., Fall, L.M., Ferguson, C.A., Hanson, V.L., Krug, A.Z., Layou, K.M., Leckey, E.H., Nürnberg, S., Powers, C.M., Sessa, J.A., Simpson, C., Tomašových, A., and Visaggi, C.C., 2008, Phanerozoic trends in the global diversity of marine invertebrates: Science (New York, NY), v. 321, p. 97.

Alroy, J., Marshall, C.R., Bambach, R.K., Bezusko, K., Foote, M., Fürsich, F.T., Hansen, T.A., Holland, S.M., Ivany, L.C., Jablonski, D., Jacobs, D.K., Jones, D.C., Kosnik, M.A., Lidgard, S., Low, S., Miller, A.I., Novack-Gottshall, P.M., Olszewski, T.D., Patzkowsky, M.E., Raup, D.M., Roy, K., Sepkoski, J.J., Sommes, M.G., Wagner, P.J., and Webber, A., 2001, Effects of sampling standarization on estimates of Phanerozoic marine diversification.: Proceedings of the National Academy of Sciences of the United States of America, v. 98, p. 6261-6266.

Antoine, P.O., 2002, Phylogénie et évolution des Elasmotheriina: (Mammalia, Rhinocerotidae): Mémoires du Muséum National d'Histoire Naturelle, v. 188, p. 5-350.

—, 2003, Middle Miocene elasmotheriine Rhinocerotidae from China and Mongolia: taxonomic revision and phylogenetic relationships: Zoologica Scripta, v. 32, p. 95-118.

Antoine, P.O., Ducrocq, S., Marivaux, L., Chaimanee, Y., Crochet, J.Y., J.J. Jaeger, and Welcomme, J.L., 2003, Early rhinocerotids (Mammalia: Perissodactyla) from South Asia and a review of the Holarctic Paleogene rhinocerotid record: Canadian Journal of Earth Sciences, v. 40, p. 365-374.

Barnosky, A.D., 2001, Distinguishing the effects of the Red Queen and Court Jester on Meiocene mammal evolution in the northern Rocky Mountains: Journal of Vertebrate Paleontology, v. 21, p. 172-185.

—, 2005, Effects of Quaternary climatic change on speciation in mammals: Journal of Mammalian Evolution, v. 12, p. 247-264.

Benton, M.J., 2009, The Red Queen and the Court Jester: Species Diversity and the Role of Biotic and Abiotic Factors Through Time: Science, v. 323, p. 728-732.

Bernades, C., Sicuro, F.L., Avilla, L.S., and Pinheiro, A.E.P., 2012, Rostral reconstruction of South American 1 hippidiforms (Mammalia, Perissodactyla, Equidae): New anatomical and ecomorphological inferences: Acta Paleontologica Polonica, v. 58, p. 669-678.

Blondel, C., Bocherens, H., and Mariotti, A., 1997, Stable carbon and oxygen isotope ratios in ungulate teeth from French Eocene-Oligocene localities: Bulletin de la Société Géologique de France, v. 168, p. 83-89.

Bruch, A., Uhl, D., and Mosbrugger, V., 2007, Miocene climate in Europe – patterns and evolution: a first synthesis of NECLIME: Palaeogeography, Palaeoclimatology, Palaeoecology, v. 253, p. 1-7.

Brunet, M., 1977, Les Mammiféres et le probléme de la limite Eocéne-Oligocéne en Europe: Geobios Mém. Spéc., v. 1, p. 11-27.

Cantalapiedra, J.L., Hernández Fernández, M., and Morales, J., 2011, Biomic specialization and speciation rates in ruminants (Cetartiodactyla, Mammalia): a test of the resource-use hypothesis at the global scale: PLoS One, v. 6, p. e28749.

Casanovas-Vilar, I., García Paredes, I., Alba, D.M., Van Den Hoek Ostende, L.W., and Moyà- Solà, S., 2010, The European Far West: Miocene mammal isolation, diversity and turnover in the Iberian Peninsula: Journal of Biogeography, v. 37, p. 1079-1093.

Cerdeño, E., 1998, Diversity and evolutionary trends of the Family Rhinocerotidae (Perissodactyla): Palaeogeography Palaeoclimatology Palaeoecology, v. 141, p. 13-34.

Cerdeño, E., and Nieto, M., 1995, Changes in Western European Rhinocerotidae related to climatic variations: Palaeogeography, Palaeoclimatology, Palaeoecology v. 114, p. 325-338.

Deng, T., 2002, Evolution of Chinese Neogene Rhinocerotidae and Its Response to Climatic Variations: Acta Geologica Sinica, v. 76, p. 139-145.

—, 2005, New cranial material of *Shansirhinus* (Rhinocerotidae, Perissodactyla) from the Lower Pliocene of the Linxia Basin in Gansu, China: Geobios, v. 38, p. 301-313.

Deng, T., Fortelius, M., Li, Q., Wang, Y., Tseng, Z.J., Takeuchi, G.T., Saylor, J.E., Säilä, L.K., and Xie, G., 2011, Out of Tibet: Pliocene Woolly Rhino Suggests High-Plateau Origin of Ice Age Megaherbivores: Science, v. 333, p. 1285-1286.

Deng, T., Wang, S., and Hou, S., 2013, A bizarre tandem-horned elasmothere rhino from the Late Miocene of northwestern China and origin of the true elasmothere: Chinese Science Bulletin, v. 15, p. 1811-1817.

Ducrocq, S., 1995, The contribution of Paleogene anthracotheriid artiodactyls in the paleobiogeographical history of southern Europe: Neues Jahrbuch für Geologie und Paläontologie Abhadungen, v. 6, p. 355-362.

Dunhill, A.M., Benton, M.J., Twitchett, R.J., and Newell, A.J., 2012, Completeness of the fossil record and the validity of sampling proxies at outcrop level: Palaeontology, v. 55, p. 1155-1175.

Emry, R.J., 1981, Additions to the mammalian fauna of the type Duchesnean, with comments on the status of the Duchesnean "age": Journal of Paleontology, v. 55, p. 563-570.

Emry, R.J., Russell, L.S., and Bjork, P.R., 1987, Chadronian, Orellan and Whitneyan North American land mammal ages, *in* Woodburne, M.O., ed., Cenozoic mammals of North America. Geochronology and biostratigraphy: Berkeley, University of California Press, p. 118-152.

Eronen, J.T., Evans, A.R., Fortelius, M., and Jernvall, J., 2010, The impact of regional climate on the evolution of mammals: a case study using fossil horses: Evolution, v. 64, p. 398-408.

Figueirido, B., Janis, C.M., Pérez-Claros, J.A., De Renzi, M., and Palmqvist, P., 2012, Cenozoic climate change influences mammalian evolutionary dynamics: Proceedings of the National Academy of Sciences of the United States of America, v. 109, p. 722-727.

Finarelli, J.A., and Badgley, C., 2010, Diversity dynamics of Miocene mammals in relation to the history of tectonism and climate: Proceedings of the Royal Society B, v. 277, p. 2721-2726.

Flower, B., and Kennett, J., 1994, The middle Miocene climatic transition: East Antarctic ice sheet development, deep ocean circulation and global carbon cycling: Palaeogeography, Palaeoclimatology, Palaeoecology, v. 108, p. 537-555.

Foote, M., 2000, Origination and Extinction Components of Taxonomic Diversity: General Problems: Paleobiology, v. 26, p. 72-102.

—, 2003, Origination and extinction through the Phanerozoic: a new approach: The Journal of Geology, v. 111, p. 125-148.

Fortelius, M., and Heissig, K., 1989, The phylogenetic relationships of the Elasmotherini (Rhinocerotidae, Mamm.): Mitteilungen Bayerische Staatssammlung Paläontologische historische Geologie v. 29, p. 227-233.

Fortelius, M., Mazza, P., and Sala, B., 1993, *Stephanorhinus* (Mammalia: Rhinocerotidae) of the western European Pleistocene, with a revision of *S. etruscus* (Falconer, 1868): Palaeontographia italica, v. 80, p. 63-155.

Geraads, D., 2010, 34. Rhinocerotidae, *in* Werdelin, L., and Sanders, W.J., eds., Cenozoic Mammals of Africa, University of California Press, p. 669-683.

Geraads, D., McCrossin, M., and Benefit, B., 2012, A New Rhinoceros, *Victoriaceros kenyensis* gen. et sp. nov., and

Other Perissodactyla from the Middle Miocene of Maboko, Kenya: Journal of Mammalian Evolution, v. 19, p. 57-75.

Groves, C.P., 1972, *Ceratotherium simum*: Mammalian Species. The American Society of Mammalogists, v. 8, p. 1-6.

Guérin, C., 1972, Une nouvelle espèce de rhinocéros (Mammalia, Perissodactyla) à Vialette (Haute-Loire, France) et dans d'autres gisements du Villafranchien inférieure européen: *Dicerorhinus jeanvireti* n. sp.: Documents des Laboratoires de la Faculté des Sciences de Lyon, v. 49, p. 1-156.

Gustafson, E.P., 1977, First record of *Teleoceras* (Rhinocerotidae) from the Ringold Formation, Pliocene of Washington: Paleobios, v. 27.

Hanson, C.B., 1989, Teletaceras radinskyi, a new primitive rhinocerotid from the late Eocene Clarno Formation, Oregon, *in* Prothero, D.R., and Schoch, R.M., eds., Evolution of Perissodactyls: New York, Oxford University Press, p. 379-398.

Heissig, K., 1989, The Rhinocerotidae, *in* Prothero, D., and Schoch, R.M., eds., The evolution of Perissodactyls, Oxford University Press, p. 399-417.

—, 1999, 16. Family Rhinocerotidae, *in* Rössner, G.E., and Heissig, K., eds., The Miocene Land Mammals of Europe: Pfeil, Munich, p. 175-188.

Holroyd, P.A., Tsubamoto, T., Egi, N., Ciochon, R.L., Takai, M., Tun, S.T., Sein, C., and Gunnell, G.F., 2006, A Rhinocerotid Perissodactyl from the Late Middle Eocene Pondaung Formation, Myanmar: Journal of Vertebrate Paleontology, v. 26, p. 491-494.

Jablonski, D., 1996, Mass extinctions: persistent problems and new directions: Geological Society of America Special Paper, v. 307, p. 1-9.

—, 2005, Evolutionary innovations in the fossil record: The intersection of ecology, development, and macroevolution: Journal of Experimental Zoology Part B: Molecular and Developmental Evolution, v. 304, p. 504-519.

Janis, C., 1989, A climatic explanation for patterns of evolutionary diversity in ungulate mammals: Palaeontology, v. 32, p. 463-481.

Janis, C.M., 1993a, Tertiary Mammal Evolution in the Context of Changing Climates, Vegetation, and Tectonic Events: Annual review of Ecology and Systematics, v. 24, p. 467-500.

—, 1993b, Tertiary mammal evolution in the context of changing climates, vegetation, and tectonic events: Annual Review of Ecology and Systematics, v. 24, p. 467-500.

Janis, C.M., Colbert, M.W., Coombs, M.C., Lambert, W.D., MacFadden, B.J., Mader, B.J., Prothero, D., Schoch, R.M., Shoshani, J., and Wall, W.P., 1998, 35. Perissodactyla and Proboscidea, p. 511-524.

Koenigswald, W.v., Holbrook, L.T., and Rose, K.D., 2011, Diversity and evolution of Hunter-Schreger band configuration in tooth enamel of perissodactyls mammals: Acta Palaeontologica Polonica, v. 56, p. 11-32.

Lacombat, F., 2007, Phylogeny of the genus *Stephanorhinus* in the Plio-Pleistocene of Europe: Hallesches Jahrb. Geowiss., v. 23, p. 63-64.

Legendre, S., and Hartenberger, J.-L., 1992, Evolution of mammalian faunas in Europe during the Eocene and Oligocene, *in* Prothero, D.R., and Berggren, W.A., eds., Eocene-Oligocene Climatic And Biotic Evolution: Oxford, Princeton University Press, p. 516-528.

Levinton, J., 1988, Genetics, Paleontology and Macroevolution: Cambridge, Cambridge University Press.

Lloyd, G.T., 2012a, A refined modelling approach to assess the influence of sampling on palaeobiodiversity curves: new support for declining Cretaceous dinosaur richness: Biology Letters, v. 8, p. 123-126.

—, 2012b, A refined modelling approach to assess the influence of sampling on palaeobiodiversity curves: new support for declining Cretaceous dinosaur richness: Biology Letters, v. 8, p. 123-126.

Lloyd, G.T., Davis, K.E., Pisani, D., Tarver, J.E., Ruta, M., Sakamoto, M., Hone, D.W.E., Jennings, R., and Benton, M.J., 2008, Dinosaurs and the Cretaceous terrestrial revolution: Proceedings of the Royal Society B, v. 275, p. 2483-2490.

Mannion, P.D., Upchurch, P., Carrano, M.T., and Barrett, P.M., 2010, Testing the effect of the rock record on diversity: a multidisciplinary approach to elucidating the generic richness of sauropodomorph dinosaurs through time: Biological Reviews, v. 86, p. 157-181.

McGowan, A.J., and Smith, A.B., 2008, Are global Phaneorozoic marine diversity curves truly global? A study of the relationship between regional rock records and global Phanerozoic marine diversity: Paleobiology, v. 34, p. 80-103.

McKinney, M.L., and Oyen, C.W., 1989, Causation and nonrandomness in biological and geological time series: temperature as a proximal control of extinction and diversity: Palaios, v. 4, p. 3-15.

Miller, K.G., Wright, J.D., and Fairbanks, R., 1991, Unlocking the ice house: Oligocene-Miocene oxygen isotopes, eustasy, and margin erosion: Journal of Geophysical Research, v. 96, p. 6829-6848.

Pinheiro, J., Bates, D., DebRoy, S., Sarkar, D., and Team, R.D.C., 2005, nlme: linear and nonlinear mixed effects models. R package version 3.1-103.

Pomerol, C., 1967, Esquisse paléogéographique du Bassin de paris, à l'ère tertiaire et aux temps quaternaires: Revue de géographie physique et de géologie dynamique, v. IX, p. 35-85.

Prothero, D., 1993, Fifty Million Years of Rhinoceros Evolution, *in* Ryder, O.A., ed., Rhinoceros Biology and Conservation: San Diego, Zoological Society of San Diego, p. 82-91.

—, 1998, 42 Rhinocerotidae, *in* Janis, C., Scott, K.M., and Jacobs, L.L., eds., Evolution of Tertiary Mammals of North America, Cambridge University Press, p. 595-605.

—, 2005, The Evolution of North American Rhinoceroses: Cambridge, Cambridge University Press, 218 p.

Qiu, Z.X., and Xie, J.Y., 1997, A new species of *Aprotodon* (Perissodactyla, Rhinocerotidae) from Lanzhou Basin, Gansu, China: Vertebrata Palasiatica, v. 35.

R Development Core team, 2015, R: A language and environment for statistical computing.: Viena, Austria. ISBN 3-900051-07-0, URL http://www.R-project.org., R Foundation for Statistical Computing.

Sanisidro, O., Alberdi, M.T., and Morales, J., 2011, The first complete skull of *Hispanotherium matritense* (Prado, 1864) (Perissodactyla, Rhinocerotidae) from the Middle Miocene of the Iberian Peninsula: Journal of Vertebrate Paleontology, v. in press.

Sepkoski, J.J., 1981, A factor analytic description of the Phanerozoic marine fossil record: Paleobiology, v. 7, p. 36-53.

Smith, A.B., and McGowan, A.J., 2011a, The ties linking rock and fossil records and why they are important for palaeobiodiversity studies: Geological Society, London, Special Publications, v. 358, p. 1-7.

—, 2011b, The ties linking rock and fossil records and why they are important for palaeobiodiversity studies: Geological Society, Special Publications, v. 358, p. 1-7.

Stehlin, H.G., 1910, Remarques sur les faunules de Mammifères des couches eocenes et oligocenes du Bassin de Paris: Bulletin de la Société Géologique de France, v. 4, p. 488-520.

Stone, W.J., 1970, Stratigraphic significance of fossil rhinoceros remains in Slope County, North Dakota: Proceedings of the North Dakota Academy of Science, v. 24, p. 32.

Valentine, J.W., 1985, Phanerozoic diversity patterns: Profiles in macroevolution: New Jersey, Princeton University Press.

van der Made, J., 2010, The rhinos from the Middle Pleistocene of Neumark-Nord (Saxony-Anhalt), p. 463-527.

Van Valen, L.M., 1984, A resetting of Phanerozoic community evolution: Nature, v. 307, p. 50-52.

Vrba, E.S., 1987, Ecology in relation to speciation rates: some case histories of Miocene-Recent mammal clades: Evolutionary Ecology, v. 1, p. 283–300.

—, 1992, Mammals as a key to evolutionary theory: Journal of Mammalogy, v. 73, p. 1-28.

—, 1995, On the connections between paleoclimate and evolution, *in* Vrba, E.S., Denton, G.H., Patridge, T.C., and Burcke, L.H., eds., Paleoclimate and Evolution with Emphasis on Human Origins: New Haven, Yale University Press, p. 24-45.

—, 1999, Habitat theory in relation to the evolution in African Neogene biota and hominids, *in* Bromage, T.G., and Schrenk, F., eds., African Biogeography, Climate Change and Human Evolution: New York, Oxford University Press, p. 19-39.

Wagner, P.J., 1995, Stratigraphic tests of cladistic hypotheses: Paleobiology, v. 21, p. 153-178.

—, 2000, Phylogenetic analyses and the fossi record: tests and inferences, hypotheses and models: Paleobiology, v. 26, p. 341-371.

Wonnacott, T., and Wonnacott, R., 1984, Introductory Statistics for Business and Economics: New York, Wiley.

Zachos, J.C., Dickens, G.R., and Zeebe, R.E., 2008, An early Cenozoic perspective on greenhouse warming and carbon-cycle dynamics: Nature, v. 451, p. 279-283.

Zin-Maung-Maung-Thein, Takai, M., Tsubamoto, T., Egi, N., Thaung-Htike, T.N., and Maung-Maung, Z.-W., 2010, A review of fossil rhinoceroses from the Neogene of Myanmar with description of new specimens from the Irrawaddy Sediments: Journal of Asian Earth Sciences, v. 37, p. 154-165.

SUPPLEMENTARY DATA 1

Remarks on species taxonomy

Asia

The systematic of the Asian aceratheres, one of the most important groups along the Asian Miocene, is being gradually resolved. We have largely followed the systematic update proposed by Deng (2006) and Athanassiaou et al. (2014). Even though not described in detail, the *Acerorhinus* remains from Sinap Formation (Turkey) point to a different species (Fortelius et al., 2003). As rather complete remains, which include a skull and a mandible, have been found (thus providing a complete portrait of this form), it has been considered in the present analysis as a distinct species. On the other hand, other Asian rhinoceros remains with unclear systematic affinities and scattered and/or fragmentary remains have been excluded from our analysis until their taxonomic validity is proposed and/or their descriptions updated. These include the Chinese *Aceratherium* sp. from Ulantalal, *Aceratherium* sp. from Feijue, Rhinocerotidae indet of Caijiachong, Rhinocerotidae indet of Tabenbuluk and Rhinocerotidae indet of Sary-Su (Antoine et al., 2003). Rhinocerotidae remains from the Asian Late Eocene-earliest Oligocene are far from being well-known (Böhme et al., 2014). The undetermined *Plesiaceratherium* remains from Mizunami (Japan) show several differences with other members of the genus. Nevertheless, as the available material is too scarce, further remains are needed to erect a new species and thus being included in the present work. Additionally, the Rhinocerotini remains determined as "*Rhinoceros shindoi*" by Tokunaga (1931) appear to be invalid (Ogino et al., 2009). Finally, a second species of *Sanshirhinus*, *Sanshirhinus brancoi* (Schlosser, 1903), was described on the basis of several teeth acquired in a Chinese traditional drug store (Deng, 2005). Even though their morphology points to a distinctive species, biostratigraphic data is not available, thus avoiding its inclusion in the analysis.

North America

The 'Haughton Astrobleme rhino' is a formally-undescribed species represented by an incomplete skeleton found in the Haughton crater filling sediments of the Canadian Northwestern territories. The highly distinctive combination of basal and derived morphologies points to an environmental or geographic isolation (Prothero, 2005). New *Teleoceras* remains has been described from the Late Hemphillian deposits from Gray Fossil Site (Tennessee; (Short, 2013). Its morphological particularities on its dentition indicate that it represents a new, unnamed species.

Africa

The African fossil record is considerably less studied that their Eurasian or North American counterparts, thus being more sensitive to taxonomic updates. Nevertheless, some remarks have to be made, as three formally unpublished species have been included in our analysis. Their validity follows the taxonomic criteria exposed by Geraads (2010). The rhino remains from Nyakach (Kenya) were originally cited in Pickford (1986). The sample, represented by two skulls, was tentatively assigned to *Plesiaceratherium* by Geraads (2010). However, differences between the Eurasian *Plesiaceratherium* and the Nyakach skulls summarized by Geraads (2010) (i.e. the presence of terminal horns, larger premolars with strong lingual cingulum and the possible loss of upper incisors) point to a distinct genus. The undetermined *Brachypotherium* species from Buluk (Kenya) has a similar cranial morphology to the European type species, differing on its considerably smaller size thus being considered as a different species. On the other hand, a P2 from Chorora, Ethiopia (Geraads et al., 2002), attributed to an early form of *Ceratotherium* has not been listed in our analysis, as further remains are needed in order to clarify its precise affinities. Finally, the fragmentary nature of the African record leaves several species, like *Ceratotherium? primaevum*, the very large *Brachypotherium lewisi* or *Kenyatherium bishopi*, as singletons, having no reflection on the performed analysis.

Europe

Two large distinct forms of *Hoploaceratherium* and *Lartetotherium* from Cerro de los Batallones (the latter included in Chapter 13) have been included.

REFERENCES

Athanassiou, A., Roussiakis, S. J., Giaourtsakis, I. X., Theodorou, G. E., and Iliopoulos, G., 2014, A new hornless rhinoceros of the genus Acerorhinus (Perissodactyla: Rhinocerotidae) from the Upper Miocene of Kerassiá (Euboea, Greece), with a revision of related forms: Palaeontographica, Abt. A: Palaeozoology – Stratigraphy, v. 303, no. 1-3, p. 23-59.

Böhme, M., Aiglstorfer, M., Antoine, P.-O., Appel, E., Havlik, P., Métais, G., Phuc, L. T., Schneider, S., Setzer, F., Tappert, R., Tran, D. N., Uhl, D., and Prieto, J., 2014, Na Duong (northern Vietnam) – an exceptional window into Eocene ecosystems from Southeast Asia: Bayerische Staatssammlung für Paläontologie und Geologie, v. 53, p. 120-167.

Deng, T., 2006, A primitive species of *Chilotherium* (Perissodactyla, Rhinocerotidae) from the late Miocene of the Linxia Basin

(Gansu, China): Cainozoic Research, v. 5, p. 93-102.

Fortelius, M., Heissig, K., Saraç, G., and Sen, S., 2003, Rhinocerotidae (Perissodactyla), *in* Fortelius, M., Kappelman, J., Sen, S., and Bernor, R. L., eds., Geology and Paleontology of the Miocene Sinap Formation, Turkey: New York, Columbia University Press, p. 282-307.

Geraads, D., 2010, 34. Rhinocerotidae, *in* Werdelin, L., and Sanders, W. J., eds., Cenozoic Mammals of Africa, University of California Press, p. 669-683.

Geraads, D., Alemsegerd, Z., and Bellon, H., 2002, The late Miocene mammalian fauna of Chorora, Awash basin, Ethiopia: Systematics, biochronology and 40K-40Ar age of the associated volcanics: Tertiary Research, v. 21, no. 113-122.

Ogino, S., Otsuka, H., and Harunari, H., 2009, The middle Pleistocene Matsugae fauna, northern Kyushu, West Japan: Paleontological Research, v. 13, no. 4, p. 367-384.

Pickford, M., 1986, Cainozoic paleontological sites of Western Kenya: Münchner geowissenschaftliche Abhandlungen, v. A 8 p. 1-151.

Prothero, D., 2005, The Evolution of North American Rhinoceroses, Cambridge, Cambridge University Press, 218 p.:

Short, R. A., 2013, A New Species of Teleoceras from the Late Miocene Gray Fossil Site, with Comparisons to Other North American Hemphillian Species [Master of Science in Geosciences: East Tennessee State University, 284 p.

Tokunaga, S., 1931, Remains of the Pleistocene den dwellers in Honshu, Kyushu and Chosen.: Nippon Gakujyutsu Kyokai Hokoku, v. 6, p. 175-178.

SUPPLEMENTARY DATA 2

Figure S1

Continental-scale analyses of sampling correction and diversity modeling. Model detrended taxonomic richness representing the time series of residuals as a grey-filled area graph. The model assumes a constant taxonomic richness purely driven by sampling. Dashed lines limit 1.96 standard errors and dashed-dotted line 1.96 standard deviation of the model according to Lloyd {, 2012 #1598}. Geological epochs are abbreviated as follows: Pli, Pliocene; Pl, Pleistocene

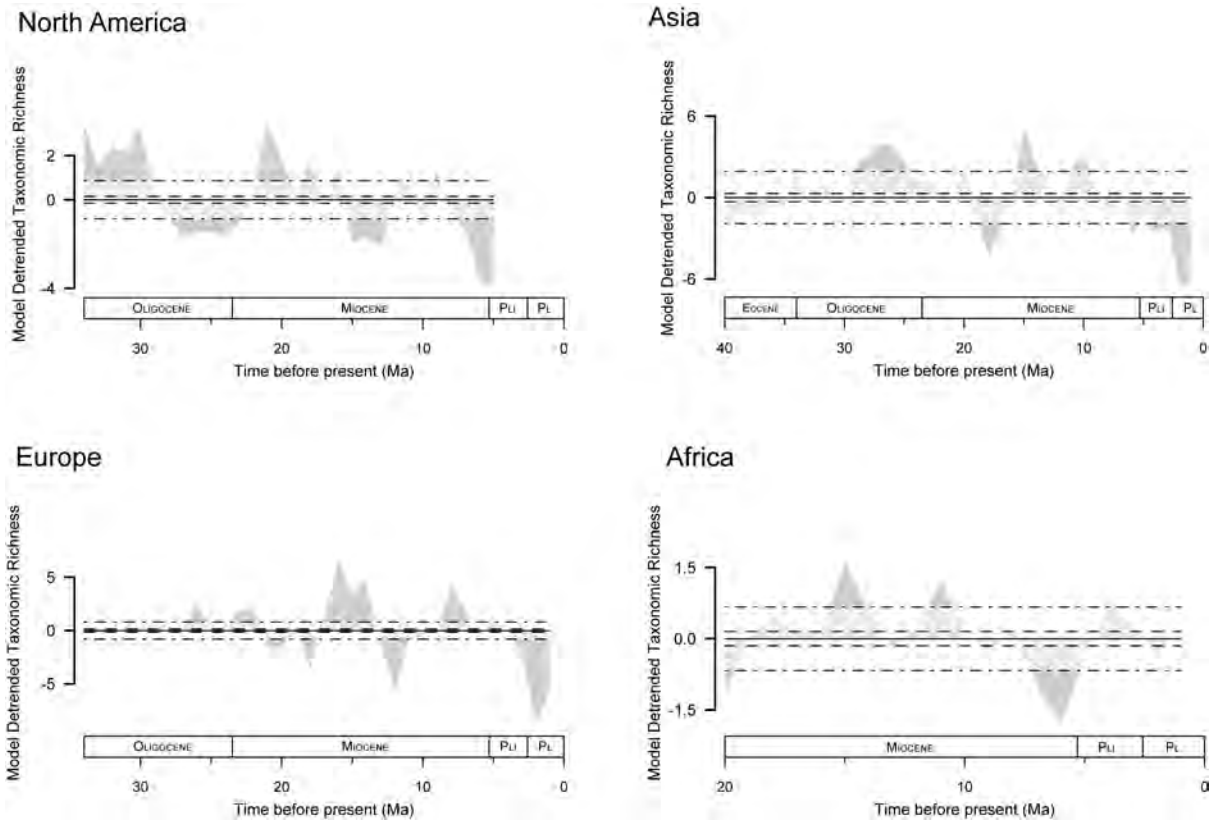


Figure S2

Bivariate plot of the eigenvalues against their rank for the first 21 factors. The faunas have been labeled according their geologic time appearance, as represented in the Figure 2A.

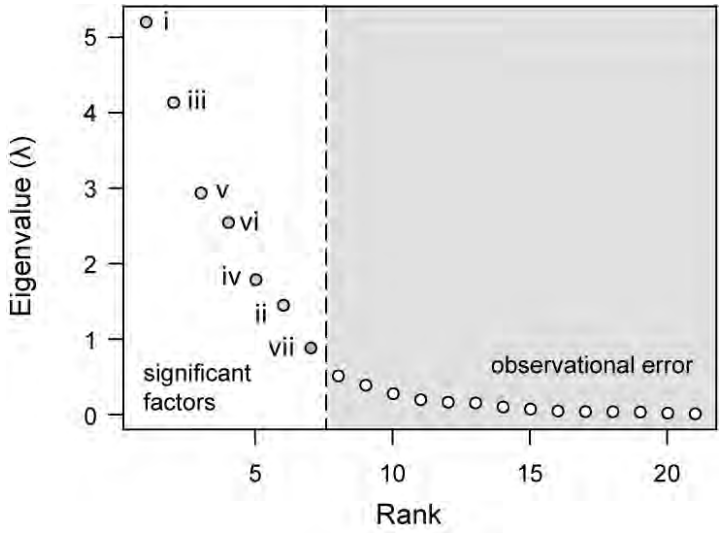
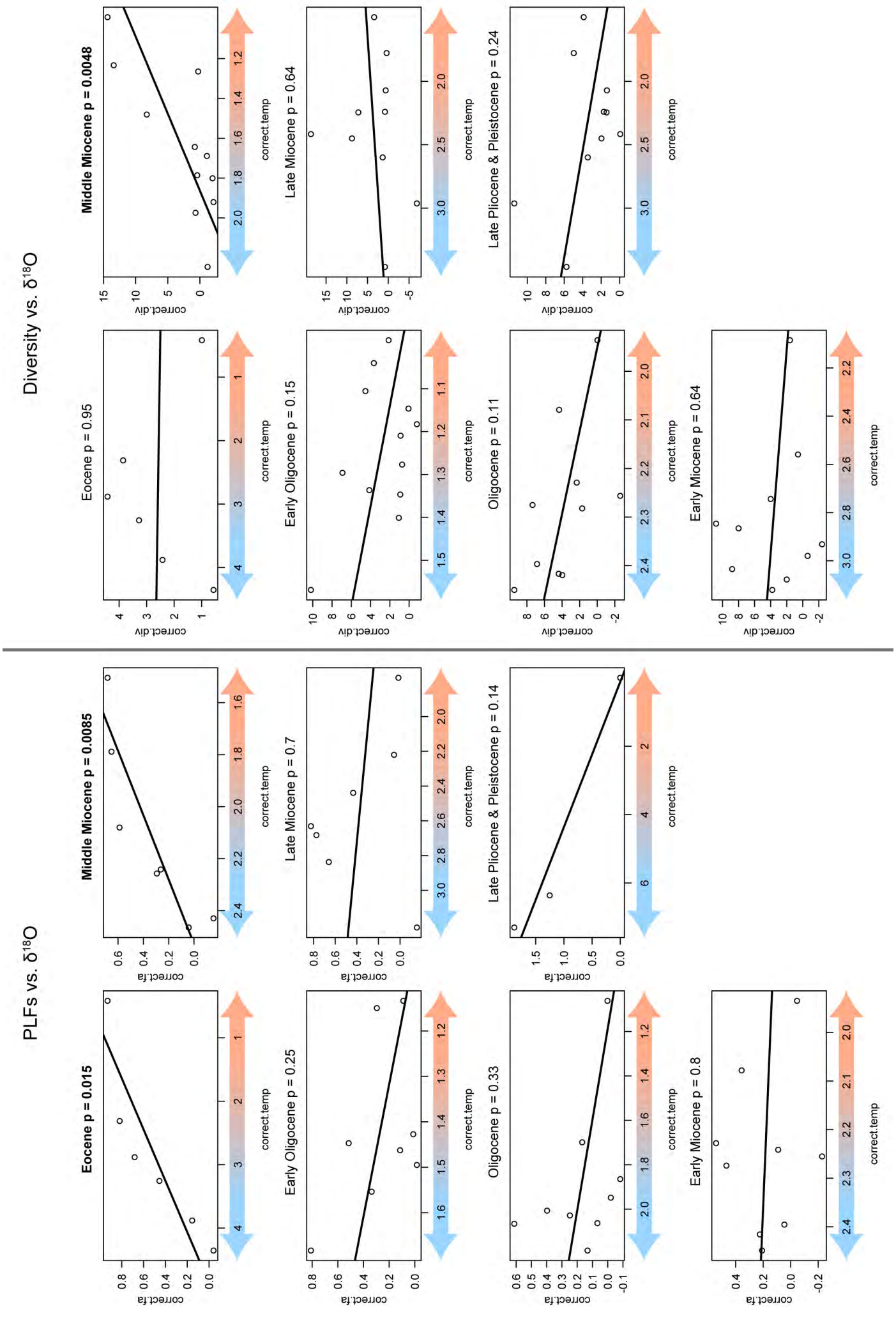


Figure S3 (Next page)

Bivariate plots of $\delta^{18}O$ isotopic values on the diversity of the seven main rhinocerotid evolutionary faunas respect the net diversity and the positive factor loadings of each fauna. Significative correlations are marked in bold face. Temporal faunas have been identified according to the specific richness of the genera with contribution scores greater than 1. Isotopic values are obtained from Zachos (2008).


PLFs vs. δ18O
Diversity vs. δ18O
Eocene p = 0.015
Middle Miocene p = 0.0085
Early Oligocene p = 0.25
Late Miocene p = 0.7
Oligocene p = 0.33
Late Pliocene & Pleistocene p = 0.14
Early Miocene p = 0.8
Eocene p = 0.95
Middle Miocene p = 0.0048
Early Oligocene p = 0.15
Late Miocene p = 0.64
Oligocene p = 0.11
Late Pliocene & Pleistocene p = 0.24
Early Miocene p = 0.64
correct.fa
correct.div
correct.temp

SUPPLEMENTARY DATA 3

First and last occurrences of the Rhinocerotidae species included in the present work with remarks on geographic data at a continental scale and the suprageneric taxonomic division stated by Antoine (2003). Abbreviations: AS, Asia; NA, North America; EU, Europe; AF, Africa. IS, Incertae sedis; DI, Diceratheriini; EL, Elasmotheriina; TE, Teleoceratina; AC, Aceratheriina; RH, Rhinocerotina.

Cont.	Subf.	Genus	Species	FAD	LAD	Species' author	Reference
EU	ACE	*Aceratherium*	*Aceratherium incisivum*	11	6.75	(Kaup, 1832-34)	Heissig, 1999
AS	ACE	*Aceratherium*	*Aceratherium porpani*	7.5	7	Deng, 2013	Deng, 2013
EU	ACE	*Acerorhinus*	*Acerorhinus alfambrense*	9.5	8.1	(Cerdeño, 1989)	Antoine et al., 2003
AS	ACE	*Acerorhinus*	*Acerorhinus fuguensis*	8	7	Deng, 2000	Deng, 2002
AS	ACE	*Acerorhinus*	*Acerorhinus hezhengensis*	10	9	(Qiu et al., 1988)	Deng, 2003
AS	ACE	*Acerorhinus*	*Acerorhinus lufengensis*	7	6	Deng & Qi, 2009	Deng & Qi, 2009
AS	ACE	*Acerorhinus*	*Acerorhinus neleus*	9	7	Athanassious et al., 2014	Athanassious et al., 2014
AS	ACE	*Acerorhinus*	*Acerorhinus palaeosinensis*	9	7	(Ringström, 1924)	Deng, 2002
AS	ACE	*Acerorhinus*	*Acerorhinus simplex*	10	8	Krokos, 1914	Krokos, 1914
AS	ACE	*Acerorhinus*	*Acerorhinus tsaidamensis*	11	9	(Bohlin, 1937)	Deng, 2002
AS	ACE	*Acerorhinus*	*Acerorhinus zernowi*	10	6	(Borissiak, 1905)	Deng, 2006
AS	ACE	*Alicornops*	*Alicornops laogouense*	16	12.5	Deng, 2004	Deng, 2004
EU	ACE	*Alicornops*	*Alicornops simorrense*	15.8	9.3	(Lartet, 1851)	Antoine et al., 2003
NA	INS	*Amphicaenopus*	*Amphicaenopus platycephalus*	37	29.5	(Osborn and Wortman, 1894)	Prothero, 2005
NA	ACE	*Aphelops*	*Aphelops malacorhinus*	9	6.5	Cope, 1878	Prothero, 2005
NA	ACE	*Aphelops*	*Aphelops megalodus*	19	8.5	(Cope, 1873)	Prothero, 2005
NA	ACE	*Aphelops*	*Aphelops mutilus*	7.5	5	(Matthew, 1923)	Prothero, 2005
AS	TEL	*Aprotodon*	*Aprotodon aralense*	28.5	23.7	(Borissiak, 1954)	Antoine et al., 2003
AS	TEL	*Aprotodon*	*Aprotodon lanzhouense*	28.5	23.7	Qiu and Xie, 1997	Antoine et al., 2003
AS	TEL	*Aprotodon*	*Aprotodon smithwoodwardi*	26.9	25.1	Forster-Cooper, 1915	Antoine et al., 2003
AS	TEL	*Brachypotherium*	*Brachypotherium gajense*	20	16	(Pilgrim, 1912)	Khan, 2010
AS	TEL	*Brachypotherium*	*Brachypotherium pugnator*	19.5	17	(Matsumoto, 1921)	Fukuchi & Kawai, 2011
AF	TEL	*Brachypotherium*	*Brachypotherium snowi*	18	8	Fourtau, 1918	Geraads, 2010
AF	TEL	*Brachypotherium*	*Brachypotherium minor*	16.5	16.5	-	Geraads, 2013
AS	TEL	*Brachypotherium*	*Brachypotherium shanwangensis*	15	13	(Matsumoto, 1821)	Qiu & Qiu, 1995
AS	TEL	*Brachypotherium*	*Brachypotherium fatehjangense*	14.7	12.8	(Pilgrim, 1910)	Maung Maung et al., 2010
AS	TEL	*Brachypotherium*	*Brachypotherium perimense*	14.6	12.4	(Falconer & Cautley, 1847)	Maung Maung et al., 2010
EU	TEL	*Brachypotherium*	*Brachypotherium brachypus*	17	10.5	(Lartet in Laurillard 1848)	Antoine et al., 2003
EU	TEL	*Brachypotherium*	*Brachypotherium goldfussi*	11	10.5	(Kaup, 1834)	Heissig, 2009
AF	TEL	*Brachypotherium*	*Brachypotherium lewisi*	6.5	2.1	Hooijer and Patterson, 1972	Geraads, 2010
AS	ELA	*Bugtirhinus*	*Bugtirhinus praecursor*	21	20	Antoine & Welcomme, 2000	Antoine, 2002
AS	ELA	*Caementodon*	*Caementodon (Begertherium) caucasicum*	17	15.5	(Borissiak, 1935)	Antoine, 2002
AS	ELA	*Caementodon*	*Caementodon (Begertherium) fangxianense*	15.5	14.5	(Yan, 1979)	Antoine, 2002
AS	ELA	*Caementodon*	*Caementodon (Caementodon) oettingenae*	16.5	10.5	Heissig, 1972	Antoine, 2002
AF	RHI	*Ceratotherium*	*Ceratotherium simum*	1.8	0	(Burchell, 1817)	Geraads, 2010
AF	RHI	*Ceratotherium*	*?Ceratotherium mauritanicum*	4.5	0.2	(Pomel, 1888)	Geraads, 2010
AS	RHI	*Ceratotherium*	*Ceratotherium neumayri*	9.5	5.3	(Osborn, 1900)	Heissig, 1999
AF	RHI	*Ceratotherium*	*?Ceratotherium primaevum*	7	7	(Arambourg, 1959)	Geraads, 2010
AF	RHI	*Ceratotherium*	*Ceratotherium douariense*	10.5	10	(Guérin, 1966)	Geraads, 2010
AF	ACE	*Chilotheridium*	*Chilotheridium pattersoni*	17	15.5	Hooijer, 1971	Geraads, 2010
AS	ACE	*Chilotherium*	*Chilotherium anderssoni*	9	7	Ringström, 1923	Deng, 2003
AS	ACE	*Chilotherium*	*Chilotherium complanatum*	9.7	6	Antoine et al., 2003	Antoine et al., 2003
AS	ACE	*Chilotherium*	*Chilotherium habereri*	10	5	Schlosser, 1903	Deng, 2002
EU	ACE	*Chilotherium*	*Chilotherium kowalevskii*	9.5	6.5	(Pavlov, 1913)	Heissig, 1996
AS	ACE	*Chilotherium*	*Chilotherium persiae*	9	7.5	(Pohlig, 1885)	Deng, 2006

AS	ACE	*Chilotherium*	*Chilotherium primigenius*	11	9.5	Deng, 2006	Deng, 2006
EU	ACE	*Chilotherium*	*Chilotherium samium*	8.75	6.5	(Weber, 1905)	Deng, 2006
EU	ACE	*Chilotherium*	*Chilotherium sarmaticum*	8.75	5	(Korotkevich, 1958a y b)	Geraads & Koufos, 1990
EU	ACE	*Chilotherium*	*Chilotherium schlosseri*	7.5	5.3	(Weber, 1905)	Heissig, 1996
AS	ACE	*Chilotherium*	*Chilotherium wimani*	11	9	Ringström, 1924	Deng, 2003
AS	ACE	*Chilotherium*	*Chilotherium xizangensis*	7	5	Ji et al., 1980	Deng, 2002
AS	RHI	*Coelodonta*	*Coelodonta antiquitatis*	0.7	0.01	(Blumenbach, 1799)	Cerdeño, 1998
AS	RHI	*Coelodonta*	*Coelodonta nihowanensis*	2.5	2	Kahlke, 1969	Deng, 2006
AS	RHI	*Coelodonta*	*Coelodonta thibetana*	3.7	3.7	Deng et al., 2011	Deng et al., 2011
AS	RHI	*Coelodonta*	*Coelodonta tologoijensis*	0.6	0.3	(Beliajeva, 1966)	Deng et al., 2011
EU	TEL	*Diaceratherium*	*Diaceratherium massiliae*	25.75	25.75	Ménouret & Guérin, 2009	Ménouret & Guérin, 2009
EU	TEL	*Diaceratherium*	*Diaceratherium asphaltense*	23.75	22	(Déperet & Douxami, 1902)	Scherler, 2011
AS	TEL	*Diaceratherium*	*Diaceratherium askazansorense*	22.8	20	Kordikova, 2001	Kordikova, 2001
EU	TEL	*Diaceratherium*	*Diaceratherium tomerdingense*	23.75	22	Dietrich, 1931	Scherler, 2011
EU	TEL	*Diaceratherium*	*Diaceratherium lemanense*	23.25	21.6	(Pomel, 1853)	Becker et al., 2011; Scherler, 2011
AS	TEL	*Diaceratherium*	*Diaceratherium lamilloquense*	25	23	Michel, 1987	Marivaux et al., 2004
EU	TEL	*Diaceratherium*	*Diaceratherium aginense*	21.6	20	(Répelin, 1917)	Becker et al., 2011
EU	TEL	*Diaceratherium*	*Diaceratherium aurelianense*	20	12.5	(Nouel, 1866)	Scherler, 2011
NA	TEL	*Diceratherium*	*Diceratherium annectens*	30	20	(Marsh, 1873)	Prothero, 2005
NA	TEL	*Diceratherium*	*Diceratherium armatum*	30	20	Marsh, 1875	Prothero, 2005
NA	TEL	*Diceratherium*	*Diceratherium niobrarense*	21	16	Peterson, 1906	Prothero, 2005
NA	TEL	*Diceratherium*	*Diceratherium tridactylum*	32	30	(Osborn, 1893)	Prothero, 2005
NA	INS	*Diceratherium*	*Diceratherium? matutinum*	20.5	19.5	-	Prothero, 2005
AS	RHI	*Dicerorhinus*	*Dicerorhinus cixianensis*	16	15	Chen & Wu, 1976	Qiu & Qiu, 1995
AS	RHI	*Dicerorhinus*	*Dicerorhinus gwebinensis*	2.6	1.3	Maung Maung et al., 2010	Maung Maung et al., 2010
AS	RHI	*Dicerorhinus*	*Dicerorhinus sumatrensis*	2.3	0	Gloger, 1841	Maung Maung et al., 2010
AF	RHI	*Diceros*	*Diceros bicornis*	2.5	0	Gray, 1821	Geraads, 2010
AF	RHI	*Diceros*	*Diceros praecox*	4.3	2.5	(Hooijer and Patterson, 1972)	Geraads, 2010
AS	RHI	*Diceros*	*Diceros gansuensis*	11	10	Deng & Qiu, 2007	Deng & Qiu, 2007
AF	RHI	*Diceros*	*Diceros australis*	18	18	Guérin, 2000	Geraads, 2010
EU	RHI	*Dihoplus*	*Dihoplus megarhinus*	5	3.25	(De Christol, 1834)	Palombo and Valli 2003
AS	RHI	*Dihoplus*	*Dihoplus pikermiensis*	9.5	5.3	(Toula, 1906)	Deng et al., 2011
AS	RHI	*Dihoplus*	*Dihoplus ringstroemi*	9.5	5.3	(Arambourg, 1959)	Deng et al., 2011
EU	RHI	*Dihoplus*	*Dihoplus schleiermacheri*	11	5	(Kaup, 1832-34)	Antoine et al., 2003
AS	ELA	*Elasmotherium*	*Elasmotherium caucasicum*	0.8	0.02	Borissiak, 1914	Antoine, 2002
AS	ELA	*Elasmotherium*	*Elasmotherium sibiricum*	2.5	0.8	Fischer 1809	Antoine, 2002
EU	INS	*Epiaceratherium*	*Epiaceratherium bolcense*	33.4	33	(Abel, 1910)	Becker, 2009
AS	INS	*Epiaceratherium*	*Epiaceratherium* cf. *magnum*	31.9	30.4	Uhlig, 1999	Antoine et al., 2003
EU	INS	*Epiaceratherium*	*Epiaceratherium magnum*	33.5	30	Uhlig, 1999	Becker , 2003; Scherler, 2011
AS	INS	*Epiaceratherium*	*Epiaceratherium naduongense*	39	35	Böhme et al., 2014	Böhme et al., 2014
NA	ACE	*Floridaceras*	*Floridaceras whitei*	19.5	17.5	Wood, 1964	Prothero, 2005
AS	RHI	*Gaindatherium*	*Gaindatherium browni*	13.75	11	Colbert, 1934	Cerdeño, 1998
AS	RHI	*Gaindatherium*	*Gaindatherium vidali*	11	8.75	Colbert, 1934	Cerdeño, 1998
NA	ACE	*Galushaceras*	*Galushaceras levellorum*	19	16.5	Prothero, 2005	Prothero, 2005
AS	INS	*Guixia*	*Guixia simplex*	37	33.5	You, 1977	Antoine et al 2003
AS	INS	*Guixia*	*Guixia youjiangensis*	33.5	32	You, 1977	Antoine et al 2003
NA	INS	*Gulfoceras*	*Gulfoceras westfali*	21.5	19.5	Albright, 1999	Prothero, 2005
EU	ELA	*Hispanotherium*	*Hispanotherium beonense*	17	16	(Antoine, 1997)	Becker, 2003
EU	ELA	*Hispanotherium*	*Hispanotherium corcolense*	17	16	Antoine et al., 2002	Sanisidro 2011
AS	ELA	*Hispanotherium*	*Hispanotherium grimmi*	14.5	11	(Heissig, 1974)	Antoine, 2002
EU	ELA	*Hispanotherium*	*Hispanotherium matritense*	16.5	14	(Prado, 1854)	Sanisidro 2011
AS	ELA	*Hispanotherium*	*Hispanotherium* sp.	12.5	11	-	Deng, 2003
EU	ACE	*Hoploaceratherium*	*Hoploaceratherium tetradactylum*	13.75	9.75	(Lartet, 1837)	Antoine et al., 2003

EU	ACE	*Hoploaceratherium*	*Hoploaceratherium* sp.	10	9	-	(this volume)
AS	ELA	*Huaqingtherium*	*Huaqingtherium lintungense*	15	11.2	(Zhai, 1978)	Antoine, 2002
AS	INS	Indet.	*?Aceratherium* sp. Feijue	28.5	23.7	-	Antoine et al., 2003
AS	INS	Indet.	*"Aceratherium* sp. Ulantatal"	33.4	29.7	-	Antoine et al., 2003
NA	INS	Indet.	Haughton astrobleme rhino	23.8	21	-	Prothero, 2005; Gomaa et al., 1987
AS	INS	Indet.	*Plesiaceratherium naricum*	14.7	12.2	-	Maung Maung et al., 2010
AS	INS	Indet.	*Rhinocerotidae* Caijiachong	35.2	33.4	-	Antoine et al., 2003
AS	INS	Indet.	*Rhinocerotidae* Sary-Su	28.5	23.7	-	Antoine et al., 2003
AS	INS	Indet.	*Rhinocerotidae* Tabenbuluk	28.5	23.7	-	Antoine et al., 2003
AS	ELA	*Iranotherium*	*Iranotherium morgani*	8.5	8	(Mecquenem, 1908)	Antoine, 2002
AF	ELA	*Kenyatherium*	*Kenyatherium bishopi*	9.5	9.5	Aguirre and Guérin, 1974	Geraads, 2010
EU	RHI	*Lartetotherium*	*Lartetotherium montesi*	17	16	(Santafé et al., 1987)	Cerdeño, 1995
EU	RHI	*Lartetotherium*	*Lartetotherium sansaniense*	17	9.75	(Lartet, 1837)	Becker, 2003
EU	RHI	*Lartetotherium*	*Lartetotherium? steinheimensis*	11	9.75	(Jäeger, 1839)	Cerdeño, 1998
EU	RHI	*Lartetotherium*	*Lartetotherium* sp.	10	9	-	(this volume)
NA	ELA	*Menoceras*	*Menoceras arikarense*	20.5	17.5	(Barbour, 1906)	Prothero, 2005
NA	ELA	*Menoceras*	*Menoceras barbouri*	18.5	16	(Wood, 1964)	Prothero, 2005
EU	ELA	*Menoceras*	*Menoceras zitteli*	23	20	(Schlosser, 1902)	Becker, 2003
EU	INS	*Mesaceratherium*	*Mesaceratherium gaimersheimense*	30.25	23	Heissig, 1969	Becker , 2003; Scherler, 2011
EU	INS	*Mesaceratherium*	*Mesaceratherium paulhiacense*	23	20	(Richard, 1937)	Scherler, 2011
EU	INS	*Mesaceratherium*	*Mesaceratherium* sp.	27.25	25.75	-	Becker , 2003
AS	INS	*Mesaceratherium*	*Mesaceratherium welcommi*	23	18.5	Antoine & Downing, 2010	Antoine et al., 2003
EU	INS	*Molassitherium*	*Molassitherium albigense*	30.2	23	(Roman, 1912)	Becker, 2009
EU	INS	*Molassitherium*	*Molassitherium delemontense*	30.2	23	(Roman, 1912)	Becker, 2009
AS	ELA	*Ningxiatherium*	*Ningxiatherium euryrhinus*	11.5	11	Deng, 2008	Deng, 2008
AS	ELA	*Ningxiatherium*	*Ningxiatherium longirhinum*	11.5	11	Chen, 1977	Deng, 2008
AF	INS	*Nyakach genus*	*Rhinocerotidae* Nyakach	15	15	-	Geraads, 2010
AF	ELA	*Ougandatherium*	*Ougandatherium napakense*	19.5	19.5	Guérin and Pickford, 2003	Geraads, 2010
AF	RHI	*Paradiceros*	*Paradiceros mukirii*	13.5	12.5	Hooijer, 1968	Geraads, 2010
AS	ELA	*Parelasmotherium*	*Parelasmotherium linxiaense*	11.5	10.5	Deng, 2001	Deng, 2001
AS	ELA	*Parelasmotherium*	*Parelasmotherium schansiense*	10	8.5	Killgus, 1923	Antoine, 2002
NA	INS	*Penetrigonias*	*Penetrigonias dakotensis*	39	30.5	(Peterson, 1920)	Prothero, 2005
NA	INS	*Penetrigonias*	*Penetrigonias sagittatus*	37	34	(Russell, 1982)	Prothero, 2005
NA	ACE	*Peraceras*	*Peraceras hessei*	15.5	10	Prothero and Manning, 1987	Prothero, 2005
NA	ACE	*Peraceras*	*Peraceras profectum*	17.5	7.5	(Matthew, 1899)	Prothero, 2005
NA	ACE	*Peraceras*	*Peraceras superciliosum*	13	9	Cope, 1880	Prothero, 2005
EU	INS	*Plesiaceratherium*	*Plesiaceratherium aquitanicum*	MN2	MN3	(Répelin, 1917)	Antoine & Becker, 2013
AS	INS	*Plesiaceratherium*	*Plesiaceratherium commune*	22.8	20	Kordikova, 2001	Kordikova, 2001
EU	INS	*Plesiaceratherium*	*Plesiaceratherium fahlbuschi*	17	16.1	(Heissig, 1972)	Heissig, 1999
AS	INS	*Plesiaceratherium*	*Plesiaceratherium gracile*	20	15	(Young, 1937)	
EU	INS	*Plesiaceratherium*	*Plesiaceratherium lumiarense*	18.5	13.75	(Antunes & Ginsburg, 1983)	Antoine et al., 1997
EU	INS	*Plesiaceratherium*	*Plesiaceratherium mirallesi*	18.5	12.5	(Crusafont, Villalta & Truyols, 1955)	Heissig, 1999
EU	INS	*Plesiaceratherium*	*Plesiaceratherium platyodon*	20	17.5	(Mermier, 1895)	Heissig, 1999
EU	INS	*Plesiaceratherium*	*"Plesiaceratherium"* sp.			-	(this volume)
AS	RHI	*Pleuroceros*	*Pleuroceros blanfordi*	23	18.5	(Lydekker, 1884)	Antoine et al., 2010
EU	RHI	*Pleuroceros*	*Pleuroceros pleuroceros*	23	22	(Duvernoy, 1852)	Scherler, 2011
AS	ELA	*Procoelodonta*	*Procoelodonta (Begertherium) borissiaki*	14.7	11.2	(Beliajeva, 1971)	Antoine, 2002
AS	ELA	*Procoelodonta*	*Procoelodonta (Pasalarhinus) tekkayai*	15	14.5	(Heissig, 1974)	Antoine, 2002
AS	ELA	*Procoelodonta*	*Procoelodonta Procoelodonta mongoliense*	15.5	13.5	(Osborn, 1924)	Antoine, 2002
EU	TEL	*Prosantorhinus*	*Prosantorhinus germanicus*	17	13.75	(Wang, 1929)	Antoine et al., 2003
EU	TEL	*Prosantorhinus*	*Prosantorhinus douvillei*	17	11	(Osborn, 1900)	Cerdeño, 1996
AS	TEL	*Prosantorhinus*	*Prosantorhinus shahbazi*	20	16	(Pilgrim, 1910)	Khan, 2010
EU	TEL	*Prosantorhinus*	*Prosantorhinus laubei*	19	18	Heissig and Fejfar, 2007	Heissig and Fejfar, 2007

AS	INS	*Protaceratherium*	*Protaceratherium askazansorense*	22.8	20	Kordikova, 2001	Kordikova, 2001
AS	INS	*Protaceratherium*	*Protaceratherium betpakdalense*	33.4	22.1	(Borissiak, 1938)	Antoine et al., 2008
AS	INS	*Protaceratherium*	*Protaceratherium* cf. *albigense*	33.4	22.1	(Roman, 1912)	Antoine et al., 2008
EU	INS	*Protaceratherium*	*Protaceratherium minutum*	23	17.5	(Cuvier, 1822)	Becker, 2009
AS	RHI	*Punjabitherium*	*Punjabitherium platyrhinus*	5	3.2	(Khan, 1971)	Cerdeño, 1998
AS	RHI	*Rhinoceros*	*Rhinoceros sivalensis*	6.9	0.75	-	Maung Maung et al., 2010
AS	RHI	*Rhinoceros*	*Rhinoceros sondaicus*	3	0	Linnaeus, 1758	Maung Maung et al., 2010
AS	RHI	*Rhinoceros*	*Rhinoceros unicornis*	5	0	Von Waldheim, 1814	Cerdeño, 1998
AS	INS	*Ronzotherium*	*Ronzotherium brevirostre*	37.1	33.8	(Beliajeva, 1954	Antoine et al., 2003
EU	INS	*Ronzotherium*	*Ronzotherium filholi*	32.6	30.25	(Osborn, 1900)	Becker, 2009; Scherler 2011
EU	INS	*Ronzotherium*	*Ronzotherium romani*	30.2	23.25	Kretzoï, 1940	Becker, 2009; Scherler 2011
EU	INS	*Ronzotherium*	*Ronzotherium velaunum*	33.4	32.8	(Aymard, 1853)	Becker, 2009
AF	RHI	*Rusingaceros*	*Rusingaceros leakeyi*	18	17.5	(Hooijer, 1966)	Geraads, 2010
AS	ACE	*Shansirhinus*	*Shansirhinus ringstromi*	7.5	3.2	Kretzoi, 1942	Deng, 2005
AS	ACE	*Shansirhinus*	*aff. Shansirhinus* sp. Sinap	8.1	8.1	-	Fortelius et al., 2003; Athanassiou et al., 2014
AS	ELA	*Sinotherium*	*Sinotherium lagrelii*	9.5	7.5	Ringström, 1923	Antoine, 2002
NA	TEL	*Skinneroceras*	*Skinneroceras manningi*	29.5	27.5	Prothero, 2005	Prothero, 2005
AF	RHI	*Stephanorhinus*	*Stephanorhinus africanus*	4	4	(Arambourg, 1970)	Geraads, 2010
EU	RHI	*Stephanorhinus*	*Stephanorhinus etruscus*	3.25	0.5	(Falconer, 1859)	Van der Made, 2010
EU	RHI	*Stephanorhinus*	*Stephanorhinus hemitoechus*	0.4	0.05	(Falconer in Murchison, 1868)	Van der Made, 2010
EU	RHI	*Stephanorhinus*	*Stephanorhinus hundsheimensis*	1.2	0.5	(Toula, 1902)	Van der Made, 2010
EU	RHI	*Stephanorhinus*	*Stephanorhinus jeanvireti*	3.25	2.5	Guérin, 1972	Lacombat, 2008
AS	RHI	*Stephanorhinus*	*Stephanorhinus kirchbergensis*	0.65	0.05	(Jäger, 1839)	Van der Made, 2010
EU	RHI	*Stephanorhinus*	*Stephanorhinus miquelcrusafonti*	5	3.25	(Guérin, 1978)	Palombo and Valli 2003
AS	TEL	*Subchilotherium*	*Subchilotherium intermedium*	16.5	7.5	(Lydekker, 1882, 1884)	Khan, 2011
AS	TEL	*Subchilotherium*	*Subchilotherium pygmaeum*	9	8	(Ringström, 1927)	Fang et al., 2005
NA	TEL	*Subhyracodon*	*Subhyracodon kewi*	31	29	Stock, 1933	Prothero, 2005
NA	TEL	*Subhyracodon*	*Subhyracodon mitis*	35.5	34.5	(Cope, 1874)	Prothero, 2005
NA	TEL	*Subhyracodon*	*Subhyracodon occidentalis*	34	31.5	(Leidy, 1850)	Prothero, 2005
NA	TEL	*Teleoceras*	Teleoceras Gray fossil site	7.5	4.8	Short, 2013	Short, 2013
NA	TEL	*Teleoceras*	*Teleoceras americanum*	18.5	16	(Yatkola and Tanner, 1979)	Prothero, 2005
NA	TEL	*Teleoceras*	*Teleoceras brachyrhinum*	15.5	8.5	Prothero, 2005	Prothero, 2005
NA	TEL	*Teleoceras*	*Teleoceras fossiger*	9	6.5	(Cope, 1878)	Prothero, 2005
NA	TEL	*Teleoceras*	*Teleoceras guymonense*	7.5	5.5	Prothero, 2005	Prothero, 2005
NA	TEL	*Teleoceras*	*Teleoceras hicksi*	7.5	5.5	Cook, 1927	Prothero, 2005
NA	TEL	*Teleoceras*	*Teleoceras major*	11.5	8.5	Hatcher, 1894	Prothero, 2005
NA	TEL	*Teleoceras*	*Teleoceras medicornutum*	16	10.5	Osborn, 1904	Prothero, 2005
NA	TEL	*Teleoceras*	*Teleoceras meridianum*	16	10.5	(Leidy, 1865)	Prothero, 2005
NA	TEL	*Teleoceras*	*Teleoceras proterum*	9	6.5	(Leidy, 1885)	Prothero, 2005
AS	INS	*Teletaceras*	*Teletaceras borissiaki*	39.5	37.1	(Beliajeva, 1959)	Antoine et al., 2003
NA	INS	*Teletaceras*	*Teletaceras mortivallis*	39	36	(Stock, 1949)	Prothero, 2005
NA	INS	*Teletaceras*	*Teletaceras radinskyi*	41.5	34	Hanson, 1989	Prothero, 2005
NA	INS	*Trigonias*	*Trigonias osborni*	36	34.5	Lucas, 1900	Prothero, 2005
NA	INS	*Trigonias*	*Trigonias wellsi*	35.5	34.5	Wood, 1927	Prothero, 2005
AF	RHI	*Turkanatherium*	*Turkanatherium acutirostratum*	17.7	17.2	Deraniyagala, 1951	Geraads, 2010
AF	ELA	*Victoriaceros*	*Victoriaceros kenyensis*	15	15	Geraads et al., 2012	Geraads et al., 2012
NA	INS	*Woodoceras*	*Woodoceras brachyops*	29.5	27.5	Prothero, 2005	Prothero, 2005

REFERENCES

Antoine, P. O. 2002. Phylogénie et évolution des Elasmotheriina: (Mammalia, Rhinocerotidae). Memoires du Museum National d'Histoire Naturelle 188:5-350.

Antoine, P. O. 2003. Middle Miocene elasmotheriine Rhinocerotidae from China and Mongolia: taxonomic revision and phylogenetic relationships. Zoologica Scripta 32:95-118.

Antoine, P. O., F. Duranthon, and P. Yassy. 1997: L'apport des grands mammiferes (Rhinocerotides, Suoides, Proboscidiens) a la connaissance des gisements du miocene d'Aquitaine (France). Actes du Congres BiochroM'97. Mémoires et Travaux del'E.P.H.E., Institut de Montpellier, 1997.

Antoine, P. O., F. Duranthon, and J. L. Welcomme. 2003a. *Alicornops* (Mammalia, Rhinocerotidae) dans le Miocène supérieur des Collines Bugti (Balouchistan, Pakistan) : implications phylogénétiques. Geodiversitas 25:575-603.

Antoine, P. O., L. Karadenizli, G. Saraç, and S. Sen. 2008. A giant rhinocerotoid (Mammalia, Perissodactyla) from the Late Oligocene of north-central Anatolia (Turkey). Zoological Journal of the Linnean Society 152:581-592.

Antoine, P. O., S. Ducrocq, L. Marivaux, Y. Chaimanee, J. Y. Crochet, J.J. Jaeger, and J. L. Welcomme. 2003b. Early rhinocerotids (Mammalia: Perissodactyla) from South Asia and a review of the Holarctic Paleogene rhinocerotid record. Canadian Journal of Earth Sciences 40:365-374.

Antoine, P. O., K. F. Downing, J.-Y. Crochet, F. Duranthon, L. J. Flynn, L. Marivaux, G. Métais, A. R. Rajpar, and G. Roohi. 2010. A revision of *Aceratherium blanfordi* Lydekker, 1884 (Mammalia: Rhinocerotidae) from the Early Miocene of Pakistan: postcranials as a key. Zoological Journal of the Linnean Society 160:139-194.

Becker, D. 2003. Paléoécologie et paléoclimats de la Molasse du Jura (Oligo-Miocène) : apport des Rhinocerotoidea (Mammalia) et des minéraux argileux. Grade de Doctor rerum naturalium thesis/dissertation, Departement de Geosciences - Geologie et Paleontologie -, Universite de Fribourg (Suisse), Zürich, 327 pp.

Becker, D. 2009. Earliest record of rhinocerotoids (Mammalia: Perissodactyla) from Switzerland: systematics and biostratigraphy. Swiss Journal of Geosciences 102:489-504.

Becker, D., T. Bürgin, U. Oberli, and L. Scherler. 2009. *Diaceratherium lemanense* (Rhinocerotidae) from Eschenbach (eastern Switzerland): systematics, palaeoecology, palaeobiogeography. Neues Jahrbuch für Geologie und Paläontologie Abhandlungen 245:5-39.

Becker, D., P. O. Antoine, B. Engesser, F. Hiard, B. Hostettler, U. Menkveld-Gfeller, B. Mennecart, L. Scherler, and J.-P. Berger. 2011. Late Aquitanian mammals from Engehalde (Molasse Basin, Canton Bern, Switzerland). Annales de Paleontologie 96:95-116.

Boada-Saña, A., S. Hervet, and P. O. Antoine. 2007. Nouvelles donnees sur les rhinoceros fossiles de Gannat (Allier, limite Oligocene-Miocene). Revue des Sciences Naturelles d'Auvergne 71:3-25.

Cerdeño, E. 1993. Étude sur Diaceratherium aurelianense et *Brachypotherium brachypus* (Rhinocerotidae, Mammalia) du Miocène moyen de France. Bulletin du Muséum national d'Histoire naturelle, Paris Section C, 1-4:25-77.

Cerdeño, E. 1996. *Prosantorhinus*, the small teleoceratine rhinocerotid from the Miocene of western Europe. Geobios 29:111-124.

Cerdeño, E. 1998. Diversity and evolutionary trends of the Family Rhinocerotidae (Perissodactyla). Palaeogeography Palaeoclimatology Palaeoecology 141:13-34.

Cerdeño, E., and M. Nieto. 1995. Changes in Western European Rhinocerotidae related to climatic variations. Palaeogeography, Palaeoclimatology, Palaeoecology 114:325-338.

Cerdeño, E., and B. Sánchez. 2000. Intraspecific variation and evolutionary trends of *Alicornops simorrense* (Rhinocerotidae) in Spain. Zoologica Scripta 29:275-305.

Deng, T. 2001. New remains of *Parelasmotherium* (Perissodactyla, Rhinocerotidae) from the late Miocene in Dongxiang, Gansu, China. Vertebrata Palasiatica 39:306-311.

Deng, T. 2002. Evolution of Chinese Neogene Rhinocerotidae and Its Response to Climatic Variations. Acta Geologica Sinica 76:139-145.

Deng, T. 2003. New material of *Hispanotherium matritense* (Rhinocerotidae, Perissodactyla) from Laogou of Hezheng County (Gansu, China), with special reference to the Chinese Middle Miocene elasmotheres. Geobios 36:141-150.

Deng, T. 2004. A new species of the Rhinoceros *Alicornops* from the Middle Miocene of the Linxia Basin, Gansu, China. Palaeontology 47:1427-1439.

Deng, T. 2005. New cranial material of *Shansirhinus* (Rhinocerotidae, Perissodactyla) from the Lower Pliocene of the Linxia Basin in Gansu, China. Geobios 38:301-313.

Deng, T. 2006a. A primitive species of *Chilotherium* (Perissodactyla, Rhinocerotidae) from the late Miocene of the Linxia Basin (Gansu, China). Cainozoic Research 5:93-102.

Deng, T. 2006b. Neogene rhinoceroses of the Linxia Basin (Gansu, China). Late Neogene and Quaternary Biodiversity and Evolution: Regional Developments and Interregional Correlations, Vol 1 256:43-56.

Deng, T. 2008. A new elasmothere (Perissodactyla, Rhinocerotidae) from the late Miocene of the Linxia Basin in Gansu, China. Geobios 41:719-728.

Deng, T., and Z.-X. Qiu. 2007. First discovery of *Diceros* (Perissodactyla, Rhinocerotidae) in China. Vertebrata Palasiatica 45:287-306.

Deng, T., and G.-J. Qi. 2009. Rhinocerotids (Mammalis, Perissodactyla) from Lufengpithecus site, Lufeng, Yunnan. Vertebrata Palasiatica 47:135-152.

Deng, T., M. Fortelius, Q. Li, Y. Wang, Z. J. Tseng, G. T. Takeuchi, J. E. Saylor, L. K. Säilä, and G. Xie. 2011. Out of Tibet: Pliocene Woolly Rhino Suggests High-Plateau Origin of Ice Age Megaherbivores. Science 333:1285-1286.

Fang, X., M. Yan, R. Van der Voo, C. Song, J. M. Parés, J. Gao, J. Nie, and S. Dai. 2005. Late Cenozoic deformation and uplift of the NE Tibetan Plateau: Evidence from high-resolution magnetostratigraphy of the Guide Basin, Qinghai Province, China. GSA Bulletin (September/October 2005) 117:1208-1225.

Fortelius, M., K. Heissig, G. Saraç, and S. Sen. 2003. Rhinocerotidae (Perissodactyla); pp. 282-307 in M. Fortelius, J. Kappelman, S. Sen, and R. L. Bernor (eds.), Geology and Paleontology of the Miocene Sinap Formation, Turkey. Columbia University Press, New York.

Fukuchi, A., and K. Kawai. 2011. Revision of Fossil Rhinoceroses from the Miocene Mizunami Group, Japan. Paleontological Research 15:247-257.

Geraads, D. 2010. Rhinocerotidae; pp. 669-683 in L. Werdelin and W. J. Sanders (eds.), Cenozoic Mammals of Africa. University of California Press.

Geraads, D., and G. Koufos. 1990. Upper Miocene Rhinocerotidae (Mammalia) from Pentaloph-1, Macedonia, Greece. Palaeontographica Abteilung A 210:151-168.

Geraads, D., M. McCrossin, and B. Benefit. 2012. A New Rhinoceros, *Victoriaceros kenyensis* gen. et sp. nov., and Other Perissodactyla from the Middle Miocene of Maboko, Kenya. Journal of Mammalian Evolution 19:57-75.

Heissig, K. 1996. The stratigraphical range of fossil rhinoceroses in the Late Neogene of Europe and the Eastern Mediterranean; pp. 339-347 in R. L. Bernor, V. Falhlbusch, and H.-W. Mittmann (eds.), The Evolution of Western Eurasian Neogene Mammal Faunas. Columbia University Press, New York.

Heissig, K. 1999. 16. Family Rhinocerotidae; pp. 175-188 in G. E. Rössner and K. Heissig (eds.), The Miocene Land Mammals of Europe, Pfeil, Munich.

Khan, A. M. 2010. Taxonomy and distribution of Rhinoceroses from the Siwaliks Hills of Pakistan. Department of Zoology, University of the Punjab Lahore, 182 pp.

Khan, A. M., E. Cerdeño, M. A. Khan, M. Akhtar, and M. Ali. 2011. *Chilotherium intermedium* (Rhinocerotidae: Mammalia) from the Siwaliks of Pakistan: systematic implications. JouPakistan Journal of Zoology 43:651-663.

Kordikova, E. G. 2001. Remarks on the Oligocene-Miocene mammal paleontology and sequence stratigraphy of South-Western Betpakdala Steppe, South Kazakhstan. Neues Jahrbuch für Geologie und Paläontologie Abhandlungen 221:35-79.

Lacombat, F. 2008. The northernmost occurrence of the rare Late Pliocene rhinoceros *Stephanorhinus jeanvireti* (Mammalia, Perissodactyla). Neues Jahrbuch für Geologie und Paläontologie Abhandlungen 249/2:157-165.

Ménouret, B., and C. Guérin. 2009. *Diaceratherium massiliae* nov. sp. des argiles oligocènes de Saint-André et Saint-Henri à Marseille et de Les Milles près d'Aix-en-Provence (SE de la France), premier grand Rhinocerotidae brachypode européen. Geobios In Press, Accepted Manuscript.

Palombo, M. R., and A. M. F. Valli. 2003-2004. Remarks on the Biochronology of Mammalian Faunal Complexes from the Pliocene to the Middle Pleistocene in France. Geologica Romana 37:145-163.

Prothero, D. 2005. The Evolution of North American Rhinoceroses. Cambridge University Press, Cambridge, 218 pp.

Prothero, D. R. 2008. New Giant Rhinoceros from the Arikareean (Oligocene-Miocene) of Montana, South Dakota and Wyoming. Neogene Mammals. New Mexico Museum of Natural History and Science Bulletin 44:323-329.

Qiu, Z., and Z. Qiu. 1995. Chronological sequence and subdivision of Chinese Neogene mammalian faunas. Palaeogeography, Palaeoclimatology, Palaeoecology 116:41-70.

Sanisidro, O., M. T. Alberdi, and J. Morales. 2011. The first complete skull of *Hispanotherium matritense* (Prado, 1864) (Perissodactyla, Rhinocerotidae) from the Middle Miocene of the Iberian Peninsula. Journal of Vertebrate Paleontology in press.

Scherler, L., D. Becker, and J.-P. Berger. 2011. Tapiridae (Perissodactyla, Mammalia) of the Swiss Molasse Basin during the Oligocene-Miocene Transition. Journal of Vertebrate Paleontology 31:479-496.

van der Made, J. 2010. The rhinos from the Middle Pleistocene of Neumark-Nord (Saxony-Anhalt).463-527.

Zin-Maung-Maung-Thein, M. Takai, T. Tsubamoto, N. Egi, T. N. Thaung-Htike, and Z.-W. Maung-Maung. 2010. A review of fossil rhinoceroses from the Neogene of Myanmar with description of new specimens from the Irrawaddy Sediments. Journal of Asian Earth Sciences 37:154-165.

SUPPLEMENTARY DATA 4

Data source of the number of fossil localities with presence of Rhinocerotidae at a continental scale used as a sampling bias. The European localities and timespans have been obtained from the references detailed in Table S3.

Continent	Sampling Proxy	Number of Taxa	Number of Fossil Sites / Collections	Source
Africa	Fossil sites	20	110	Geraads, 2010
North America	Fossil Sites	38	875	MIOMAP (Carrasco et al., 2005)
Europe	Fossil Sites	55	597	NOW (Fortelius, -)
Asia	Fossil Sites	83	565	NOW (Fortelius, -) and Antonie et al., 2003

REFERENCES

Antoine, P. O., S. Ducrocq, L. Marivaux, Y. Chaimanee, J. Y. Crochet, J.J. Jaeger, and J. L. Welcomme. 2003. Early rhinocerotids (Mammalia: Perissodactyla) from South Asia and a review of the Holarctic Paleogene rhinocerotid record. Canadian Journal of Earth Sciences 40:365-374.

Carrasco, M. A., B. P. Kraatz, E. B. Davis, and A. D. Barnosky. Miocene Mammal Mapping Project (MIOMAP).

Fortelius, M. New and Old Worlds Database of Fossil Mammals (NOW).

Geraads, D. 2010. Rhinocerotidae; pp. 669-683 in L. Werdelin and W. J. Sanders (eds.), Cenozoic Mammals of Africa. University of California Press.

2. A new rhinoceros (Rhinocerotidae, Perissodactyla) genus from the Middle Miocene of the Iberian Peninsula

Oscar Sanisidro
Pierre Oliver Antoine
María Teresa Alberdi
and Jorge Morales

Abstract. A new genus and species of rhinoceros from the lowest Aragonian of Mesegar-1 and Mesegar-2 (Toledo Province, Spain) is described from a skull and several isolated postcranial remains. This material occurs in the medial to distal parts of the alluvial fan systems formed in origin at the base of the Toledo Mounts. These sediments are dated as Lower Aragonian (late Early Miocene). A cladistic phylogeny mainly focused on early Rhinocerotinae genera (Oligocene - Middle Miocene) was constructed with 282 characters and 43 taxa. The new form from Mesegar is included in the same clade as the remains from Loranca and Valquemado, previously identified as *Protaceratherium minutum*, and apart from the type collection of *P. minutum* of Budenheim. Additionally, several misleading problems in the taxonomy of these early Rhinocerotinae are addressed: *Plesiaceratherium* is the stem group of Rhinocerotini + Aceratheriini, *Plesiaceratherium* is a potentially paraphyletic genus and *Protaceratherium tagicum* is nested within Elasmotheriinae.

INTRODUCTION

Mesegar-1 and Mesegar-2 fossil sites are placed in a roadside bank, south of the city of Mesegar del Tajo (Toledo, Spain), as represented in the Figure 1. Both sites were found during the cartographic survey of the vicinity of Torrijos (Díaz de Neira, 2009). From a stratigraphic view, they are included in the "*Arcosas con cantos y conglomerados del Embalse de Castrejón*" Stratigraphic Unit, inside the Madrid area of the Tagus Basin. (more data about the geological setting of the locality can be found in; López Olmedo et al., 2004). Both localities are of great relevance due the scarcity of early Aragonian localities in the Iberian Peninsula and the exceptional preservation degree. The faunal list of of Mesegar-1 includes the glirids *Simplomys simplicidens* (de Bruijn, 1966) and *Peridyromys murinus* (Pomel, 1853), and undetermined remains of bovids, cervids and palaeomerycids (López Olmedo *et al*., 2004). These taxa are compatible with a Local biozone C. However, a B biozone cannot be ruled out, as its macromammal fossil assemblage is poorly represented. The faunal assemblage of Mesegar-2 includes the rodent *Praearmantomys crusafonti*, the suid *Listriodon splendens*, a large unidentified ruminant referred to Paleomerycidae indet., the three-toed equid *Anchitherium* sp. and an unidentified bovid. Rhinoceros remains have been found in both Mesegar-1 and 2.

Rhinoceros comprise one of the most important herbivore mammalian groups of the Miocene, characterized by unique dental and postcranial features. The group appeared in the late middle Eocene and became major elements of Miocene mammalian faunas of the Northern Hemisphere. The taxonomy of the Family Rhinocerotidae is still under debate, even at high-ranked levels. Nevertheless, efforts have been made in recent times to settle a sound phylogenetic framework (Antoine et al., 2010; Antoine et al., 2003; Becker et al., 2013; Cerdeño, 1995; Fortelius and Heissig, 1989; Heissig, 2012). The last hypotheses divide the Family Rhinocerotidae in two SubFamilies: the Elasmotheriinae and the Rhinocerotinae. Rhinocerotinae are, in turn, divided into Rhinocerotini and Aceratheriina. Aceratheriina are hornless rhinos with (usually) mediportal proportions. On the other hand, Rhinocerotini are formed by the short-limbed Teleoceratina and the Rhinocerotina (where the living species belong). Each of these three groups is firmly established and clearly-outlined in the literature. In contrast to their widely-accepted status, there is an array of conflictive genera typical from the Oligocene to Middle Miocene of Eurasia. These taxa, which include the genera *Protaceratherium*, *Plesiaceratherium*, *Mesaceratherium*, *Epiaceratherium*, *Pleuroceros* and (more recently described) *Molassitherium* have in common their small size, slender limb proportions, slim nasal bones and brachyodont dentition. Their significance not only relies on the understanding of the diversification patterns in the Oligocene and Early Miocene but the rooting of Aceratheriina + Rhinocerotini and the early evolution of the main rhinoceros clades.

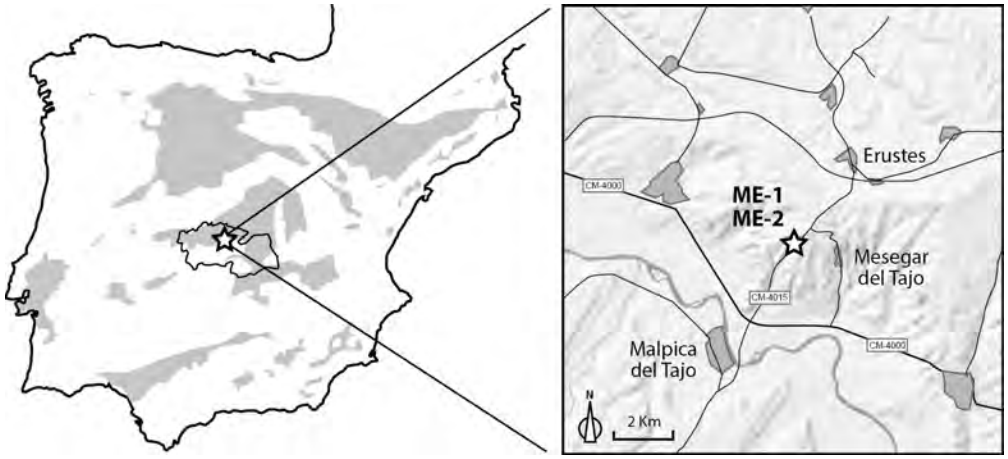


Fig. 1 Simplified general map of the Iberian Peninsula with the Tertiary basins represented as shaded outlines and a detail map showing the Toledo Province and the location of Mesegar-1 and Mesegar-2 sites (ME-1 and ME-2 respectively), represented as a star.

The Iberian fossil record of the mentioned genera is scarce. *Plesiaceratherium* is represented by the species *Plesiaceratherium platyodon* and *Plesiaceratherium mirallesi*, whereas the only *Protaceratherium* species recorded are *Protaceratherium minutum* and *Protaceratherium tagicum*. Some remains from Cetina de Aragón (MN 2) and Artesilla (MN 4) may represent additional taxa, possibly *Pleuroceros*, but are in need of revision (Cerdeño, 1992).

In the present study, we report new cranial and postcranial rhinocerotid remains from Mesegar-1 and 2. The biostratigraphic position of these sites, included in the MN4 biozone, increase the rhinoceros diversity of the late Lower Miocene in the Iberian Peninsula, thus completing the evolutionary scenario of several along most of its European biostratigraphic range.

MATERIAL AND METHODS

Institutional and locality abbreviations—GPIT, Paläontologische Sammlung der Universität (Tübingen, Germany); **MHN-Mon**, Muséum d'Histoire Naturelle de Montauban (Tarn-et-Garonne, France); **MNCN**, Museo Nacional de Ciencias Naturales (Madrid, Spain).

Measurements—all measurements are given in millimeters. Approximate measurements are given in parentheses. Measurements were made with a digital caliper and a measuring tape for elements larger than 150 mm.

Anatomical nomenclature and characters—capital letters are used for upper teeth (D, P, M), and lower case letters for lower teeth (d, p, m); m. muscle. The morphological features described correspond basically to cladistic characters used and listed by Antoine (2002) and Antoine et al. (2010), and then refined by Becker et al. (2013). Additionally, anatomical terminology follows Budras (2009) and Schaller (2007), but that used by other authors has also been taken into consideration (Antoine, 2002; Antoine et al., 2010; Becker et al., 2013; Guérin, 1980; Heissig, 1972, 1999). These are summarized in the Supplementary Data 6 from the Chapter 5 (postcranial skeleton) and the Appendix Chapter (craniodental terminology).

Phylogenetic analysis—the character list and character states derive from those of Antoine (2002, 2003) and Antoine et al. (2003b, 2010). The character list appears in the Supplementary Data 2 and 3.

Forty-three terminal taxa were included in the phylogenetic analysis. The character coding sources (either direct observation and/or literature) are provided in the Table 1. Three terminals were selected as outgroups: the extant tapirid *Tapirus terrestris* Linnaeus, 1758, the Eocene hyrachyid rhinocerotoid *Hyrachyus eximius* Leidy, 1871, and the Eocene stem rhinocerotid *Trigonias osborni* (Lucas, 1900) from North America. As detailed in Becker et al. (2013), the in-group *sensu lato* consists of both taxa of interest (in-group *sensu stricto*) and selected terminals forming a "branching group", sensu Antoine (2002) and Orliac *et al.* (2010). We have chosen to consider a wide array of Oligocene and Miocene hornless rhinocerotids within the phylogenetic analysis. The in-group *sensu stricto* includes the rhinocerotid sample from Mesegar-2 (Early Miocene) as a terminal taxon. Given its general morphology, showing close affinities with coeval Loranca and Valquemado remains, and their previous assignment to *Protaceratherium minutum* (Cuvier, 1822) by Cerdeño (1989), we have also amalgamated the corresponding samples within a single terminal taxon ("*P. minutum* from Spain"). *Protaceratherium minutum* sensu stricto was scored separately. The puzzling "*Rhinoceros* (*Ceratorhinus*?) *tagicus* Roman, 1907" from the early Burdigalian of Portugal, was also scored as a distinct terminal, under the name "*Protaceratherium tagicum* (Roman, 1907)", according to Antunes and Ginsburg's (1983) opinion. We have included an exhaustive sampling at species level for *Plesiaceratherium* Young, 1937, from the Early and Middle Miocene of Eurasia: *P. gracile* Young, 1937 (type species), *P. platyodon* (Mermier, 1895), *P. naricum* (Pilgrim, 1910), *P. aquitanicum* (Répelin, 1917), *P. mirallesi* (Crusafont, Villalta & Truyols, 1955), *P. fahlbuschi* Heissig, 1972, and *P. lumiarense* Antunes & Ginsburg, 1983. Other hornless rhinocerotids included within the analysis are *Epiaceratherium*

Abel, 1910 (with *E. bolcense* Abel, 1910 and *E. magnum* Uhlig, 1999, from the Early Oligocene of Western Europe; *E. naduongense* Böhme et al., 2014 from the ?Late Eocene of Vietnam), *Molassitherium* Becker and Antoine, 2013 (with *M. albigense* (Roman, 1912), from the late Early-Late Oligocene of Europe and *M. delemontense* Becker and Antoine, 2013 from the Early Oligocene of Europe) and *Mesaceratherium* Heissig, 1969 (with *M. paulhiacense* (Richard, 1937) and *M. gaimersheimense* Heissig, 1969, from around the Oligocene-Miocene transition in Europe, as well as *M. welcommi* Antoine & Downing, 2010, from the Early Miocene of Pakistan). The type species of *Protaceratherium* Abel, 1910, *Protaceratherium minutum* (Cuvier, 1822), from the Early Miocene of Western Europe, and, were also considered in the analysis in order to test the monophyly of the concerned genus, recently challenged in the phylogeny proposed by Antoine *et al.* (2010). The ingroup also includes the aceratheriines *Aceratherium incisivum* Kaup, 1832, *Alicornops simorrense* (Lartet, 1851), *Hoploaceratherium tetradactylum* (Lartet, 1851), and *Acerorhinus zernowi* (Borissiak, 1914) from the middle and/or late Miocene of Eurasia. The small rhinocerotine *Pleuroceros* Roger, 1898 complements the ingroup, with *P. pleuroceros* (Duvernoy, 1853) and *P. blanfordi* (Lydekker, 1884) from the Early Miocene of Europe and Pakistan, respectively (see Antoine et al., 2010).

As a concept originally defined by Antoine (2002, 2003), the "branching group" includes i) type species or well represented species of type genera of suprageneric groups

Terminal taxon	Character coding (source)	
	Direct observation	Literature
Aceratherium incisivum Kaup, 1832	MHNT; MNHN; UCBL	Kaup, 1832; Guérin, 1980; Hünermann, 1989
Acerorhinus zernowi (Borissiak, 1914)	–	Borissiak 1914, 1915
Alicornops simorrense (Lartet, 1851)	MHNT; MNHN; NHM; UCBL	Guérin, 1980; Cerdeño & Sánchez, 2000; Heissig, 2012
Brachypotherium brachypus (Lartet, 1837)	MHNT; MNHN; UCBL	Roman & Viret, 1930, 1934; Guérin, 1980; Ginsburg & Bulot, 1984; Cerdeño, 1993
Bugtirhinus praecursor Antoine & Welcomme, 2000	MHNT; pers. obs. (POA)	Antoine & Welcomme, 2000
Diaceratherium aginense (Répelin, 1917)	MHNT; MHNH; UCBL; Rhinopolis	Répelin, 1917; de Bonis, 1973; Boada-Saña *et al*., 2008
Diceratherium armatum Marsh, 1875	AMNH	Prothero, 2005
Dicerorhinus sumatrensis (Fischer Von Waldheim , 1814)	MNHN	Cuvier, 1822; Guérin, 1980
Diceros bicornis (Linnaeus, 1758)	MNHN	Guérin, 1980
Epiaceratherium bolcense (Dal Piaz, 1930)	-	Dal Piaz, 1930; Becker et al., 2013
Epiaceratherium magnum Uhlig, 1999	MHN-Mon	Uhlig, 1999;
Epiaceratherium naduongense Böhme et al., 2014	GBIT	Böhme et al., 2014
Hispanotherium beonense (Antoine, 1997)	MHNT	Antoine, 1997, 2002, 2003; Antoine, Bulot & Ginsburg, 2000
Hoploaceratherium tetradactylum (Lartet, 1851)	MHNT; MNHN; UCBL	Klaits 1973; Guérin 1980; Ginsburg & Heissig 1989; Heissig, 2012
Huaqingtherium lintungense (Zhai, 1978)	IVPP; AMNH	Zhai, 1978; Cerdeño, 1995
Hyrachyus eximius Leidy, 1871	AMNH	Leidy, 1871
Lartetotherium sansaniense (Lartet, 1837)	MHNT; MNHN; NHM	Klaits, 1973; Guérin, 1980; Heissig, 2012
Menoceras arikarense (Barbour, 1906)	AMNH	Tanner, 1969; Prothero, 2005
Mesaceratherium paulhiacense (Richard, 1937)	MHNT; Rhinopolis	Richard, 1937; de Bonis, 1973
Mesaceratherium gaimersheimense Heissig, 1969	MHNT; MHN-Mon	Heissig, 1969; Laudet & Antoine, 2004; Antoine *et al.*, 2006
Mesaceratherium welcommi Antoine & Downing, 2010	MHNT; HUPM	Falconer & Cautley, 1846; Pilgrim, 1912; Forster-Cooper, 1934; Lindsay, 2005; Antoine *et al*., 2010
Molassitherium albigense (Roman, 1912)	MHNT; FSL; MHN-Mon; UM2; Coll. Rafaÿ	Duvernoy, 1853; Roman, 1912; Antoine *et al*., 2008; Lihoreau *et al.*, 2009 ; Becker et al., 2013
Molassitherium delemontense Becker, Antoine & Maridet, 2013	MJSN	Becker et al., 2013
Plesiaceratherium aquitanicum (Répelin, 1917)	MHNT	Répelin, 1917 ; Ginsburg et al., 1991
Plesiaceratherium fahlbuschi Heissig, 1972	BSP	Heissig, 1972; Yan & Heissig, 1986; Peter, 2002
Plesiaceratherium gracile Young, 1937	BSP	Yan, 1983; Yan & Heissig, 1986; Lu Xiaokang, 2013
Plesiaceratherium lumiarense Antunes & Ginsburg, 1983	MNHN	Antunes & Ginsburg, 1983

Table. 1 Character coding sources (direct observation and/or literature) for each terminal taxon included within the present phylogenetic analysis. Taxa are arranged in alphabetic order. See Material and Methods section for detail on institutional abbreviations

recognized as having closer affinities with the in-group sensu stricto than classical outgroups and ii) early representatives of these suprageneric groups, in order to branch the taxa of interest within a wider taxonomic sample than usual, to define more accurately their generic and suprageneric affinities, and to avoid long-branch attraction artifacts due to parallelism (Antoine, 2002; Becker et al., 2013: 950). The present branching group comprises the earliest European rhinocerotid *Ronzotherium filholi* (Osborn, 1900), but also well known early Elasmotheriinae, such as the Miocene Elasmotheriina *Hispanotherium beonense* (Antoine, 1997), *Bugtirhinus praecursor* Antoine & Welcomme, 2000), and *Huaqingtherium lintungense* (Zhai, 1978), the menoceratine *Menoceras arikarense* (Barbour, 1906), from the Early Miocene of North America, and the "diceratheres" *Diceratherium armatum* Marsh, 1875 and *Subhyracodon occidentalis* (Leidy, 1851), from the Oligocene of North America). Rhinocerotinae are represented by the living Rhinocerotina *Rhinoceros sondaicus* Desmarest, 1822, *Diceros bicornis* (Linnaeus, 1758), and *Dicerorhinus sumatrensis* (Fischer Von Waldheim, 1814), and the Miocene rhinocerotine *Lartetotherium sansaniense* (Lartet, 1837) from Europe, and by Teleoceratina, with *Teleoceras fossiger* (Cope, 1873) from the Late Miocene of North America, *Brachypotherium brachypus* (Lartet, 1837), *Diaceratherium aginense* (Répelin, 1917), and *Prosantorhinus douvillei* (Osborn, 1900), from the Miocene of Europe.

CT Scanning and Reconstruction—in order to describe the morphology of the adult dentition, a digital 3D model was built for the maxilla MNCN 72812 using Micro-CT data. The maxilla was scanned in three series using a Nikon XT H-160 computed tomographic scanner (scan parameters: 141 Kv, 50 mA, 0.125 mm copper filter, 1008 x 1008 matrix, 1583 projections, 4 frame averaging per projection, 720 lines per translation, and 5 translations). Pixel dimensions and slice thickness between reconstructed serial images were isometric with resolutions of 127 microns (mm) (i.e., 127 mm x 127 mm x 127 mm). A single-iteration median filter has been applied. Finally, the enamel from the unworn teeth series has been emphasized from the superimposed DP4, dentine and bone surrounding tissues for a better observation and description of the premolar morphology by means of the computer 2D graphics software VG Studio Max 2.2 and Adobe Photoshop CS5.

Studied material—All the referred specimens are stored in the Museo Nacional de Ciencias Naturales de Madrid, MNCN. These are:

Mesegar-1: MNCN 72813, right P4.

Mesegar-2: MNCN 72811, fragmented skull and associated maxilla (MNCN 72812) with left and right DP2, DP4, M1, and a right incipient M3; MNCN 72843, fragmentary right humerus; MNCN 72842, left ulna; MNCN 72834, right unciform; MNCN 72831, right semilunate; MNCN 72835, right magnum; MNCN 72829, right scaphoid; MNCN 72830, left scaphoid; MNCN 72839, left ectocuneiform; MNCN 72836, right trapezium; MNCN 72837, left trapezium; MNCN 72832, right pyramidal; MNCN 72828, left Mc II; MNCN 72827, right Mc III; MNCN 72855 left and MNCN 72856 right hemipelvis of a single individual, MNCN 72840 and MNCN 27841, distal fragments of a right juvenile tibia; MNCN 72838, left cuboid; MNCN 72839, left ectocuneiform; MNCN 72815, first central phalanx; MNCN 72816; MNCN 72817; MNCN 72818 and MNCN 72819, first lateral phalanges; MNCN 72820 and MNCN 72821 second central phalanges; MNCN 72822, MNCN 72823 and MNCN 72846, second lateral phalanges; MNCN 72824 third right central phalanx; MNCN 72825, MNCN 72826 and MNCN 72847, third lateral phalanges.

SYSTEMATIC PALEONTOLOGY

Family Rhinocerotidae Owen, 1845

Subfamily Rhinocerotinae Owen, 1845

Genus *Protaceratherium* Abel, 1910

'*Protaceratherium*' sp.

Generic diagnosis: Small and slender stem Rhinocerotinae with a crochet usually present on P3-4, protocone and hypocone separate on P3-4, a crista usually present on P3, a short metaloph on M1-2, without a postero-proximal semilunate facet on the scaphoid, with a low collum tali, a nearly straight caudo-proximal border on the astragalus, a non-twisted astragalus, and a wide and low expansion of the astragalus/calcanear facet 1.

Holotype: Partial skull and associated maxilla (MNCN 72811 and 72812) with both DP1, DP4 and M1 series stored at the Museo Nacional de Ciencias Naturales-CSIC (Madrid, Spain).

Hypodigm: All the referred material listed in material and methods. All of them are stored at the Museo Nacional de Ciencias Naturales-CSIC (Madrid, Spain).

Locus typicus: Mesegar (Toledo, Spain)

Stratum typicum: Early Miocene, Lower Aragonian, Local Zone B or C and MN4.

Geographical and Stratigraphical range: restricted to the type locality.

Diagnosis: Differs from all other species of *Protaceratherium* by always having a crochet and a metaloph constriction on P2-4 but no antecrochet on P4, in having an antecrochet on upper molars, a trigonid forming an acute dihedron in occlusal view on lower cheek teeth, a continuous lingual cingulum on lower premolars but no lingual cingulum on lower molars, a posterior valley usually closed on p2, calcaneus-facets 2 and 3 always separate on the astragalus, and a massive tuber calcanei. Further differs from *P. minutum* by having a concave dorsal profile, a partly closed auditory pseudo-meatus, the occipital side inclined up-and backward, a dolichocephalic skull, a processus tympanicus little developed, a corpus mandibulae with a straight ventral profile, wrinkled enamel, separate roots on upper teeth, a protoloph joined to the ectoloph on P2, a posterior part of the ectoloph straight and a long metaloph

on M2, a constriction of the protocone always present on M3, vertical external rugosities on lower premolars, an external groove marked and a metalophid without constriction on lower cheek teeth, a hypolohid transverse on lower molars, a mesostyle on D3-4, a large trapezium-facet on the scaphoid, a semilunate with a keeled anterior side, a shallow indentation on the medial side of the magnum, a posterior McIII-facet always present on the McII, and the presence of an antero-distal groove on the tibia. Diverges from *P. naricum* in having a multiple crochet on P2-4 and protocone and hypocone separate on P2, in having always a crista on P3, a crochet on upper molars, a short metaloph on M1-2, a quadrangular M3, an angular trigonid on lower cheek teeth, a labial cingulum usually present but reduced on lower molars, a flat insertion of the m. extensor carpalis on metacarpals, a shallow medio-distal gutter on the tibia, a subvertical fibula-facet on the astragalus, and a distal widening of the diaphysis on the MtIII.

The craniodental and postcranial remains from Mesegar-2 closely resemble the specimens from Loranca and Valquemado (early Miocene of Spain), previously referred to as *Protaceratherium minutum* (Cuvier, 1822) by Cerdeño (1989). Yet, some minor discrepancies exist between those samples. They are known to document infraspecific variation in other rhinocerotid species (e.g., Antoine, 2002) and mostly visible on upper permanent teeth, due to the small size of the concerned sample in Mesegar-2 (only one merging germ of P2, two M1s, and one isolated P4). They concern the preservation of a thin layer of cement (present in Mesegar-2/absent in Loranca and Valquemado), the frequency of a labial cingulum on upper cheek teeth (always present/usually present), the medifossette (present/absent), and the relationships between the protocone and hypocone in P4 (separate/sometimes joined). As a consequence, we consider these differences to be insufficient to justify a distinction at species level between these three samples. Based on the concerned hypodigm, we define a new genus, still unnamed, so far restricted to Loranca, Valquemado, and Mesegar-2 localities in Spain. Due to the large samples available from the two first localities, their specific equivalence with the rhinoceros from Mesegar-1 and 2 and detailed description will be discussed in a future paper.

DESCRIPTION

Craniodental morphology

Skull (Fig. 2; Table S1)—MNCN 72811 and MNCN 72812 are two fragments of a single skull. The bigger fragment has broken zygomatic arches. The naso-frontal part and the basicranium are lacking, but it can be assumed that there was no frontal horn (no frontal rugosity). The presence of left and right DP1, DP4, and M1 series together with incipient P2 and M3 on the right maxilla suggest that the specimen belonged to a juvenile individual. The nasal notch and the anterorbital foramina reach the P4 level. A wide longitudinal groove runs along the anterior side of the nasal notch from the posteriormost edge to the P1 level. The anterior border of the orbit is above the middle of the M1. The lachrymal tubercle is poorly developed, extending as a short ridge in the antero-dorsal side of the orbit and ending with a small lump. The lachrymal foramen is single, oval, and placed behind the lachrymal tubercle. The orbit is large and rounded. The base of the zygomatic process of the maxilla begins one centimeter above the neck of the M1, with no antero-lateral projection in ventral view. The dorsal profile of the posterior half of the skull is somewhat concave. Two temporal crests are well-separated by a flat surface >20 mm-wide. The area between the temporal and nuchal crests is flat. The occipital face is inclined backwards, but the original orientation is difficult to address due to the preservation of this area. The occipital crest is forked, and narrow. In ventral view, the pterygoidean crests are trapezoidal and laterally bent, with a posterior margin close to the horizontal line. They have an outer oblique ridge and a flat tip. The articular tubercle on the squamosal is smooth and straight transversally. Only the postglenoidalis and posttympanic processes are preserved. They have the same length and almost enclose the external auditory pseudomeatus. The postglenoidalis processes are bent forward, with an oval cross section (convex articulation; Antoine, 2002). They are topped by a smooth sagittal ridge. Posttympanic processes are also bent forward, with their tip almost reaching the postglenoidalis processes, with a sub-square section and a blunt rough tip. The basioccipital is not preserved.

Upper dentition (Fig. 3; Table S2)—teeth are brachydont. The enamel is thin and thinly crenulated vertically. The DP1 is subtriangular in occlusal view and birradiculated. The ectoloph is wide, attaining its maximum width at the level of the paracone. The protocone and hypocone contact by a narrow bridge, enclosing a rounded medifossette. The protocone, tear-like, contacts the ectoloph by a weak and narrow protoloph. On the other hand, the hypocone is rounded and bigger than the protocone. Both are connected by a narrow bridge. There is a small sagittal crochet. The parastyle is well developed and ends anteriorly in a flattened surface. The anterofossette is triangular and narrow, the postfossette subtriangular and wide. The anterior, lingual, and posterior cingula are restricted to three independent low walls at both sides of the protocone and at the posterior side of the hypocone. The anterior end of the lingual cingulum contacts the parastyle, forming a postero-lingual hooked expansion. The DP4 are fan-shaped (i.e., with a lingual side much shorter than the labial side), with protoloph and ectoloph wider than the metaloph. The labial wall of the ectoloph is long and has a protruding anterior border and a lingually inclined posterior half. The protocone is constricted anteriorly and expanded posteriorly, with a strong antecrochet. The paracone rib and the parastyle groove are marked, posterior to the long and sagittal parastyle. The crochet is short and simple. Anterior and posterior cingula are low and continuous, the latter reaching the antero-lingual angle of the protocone. The postfossette is triangular, wide and

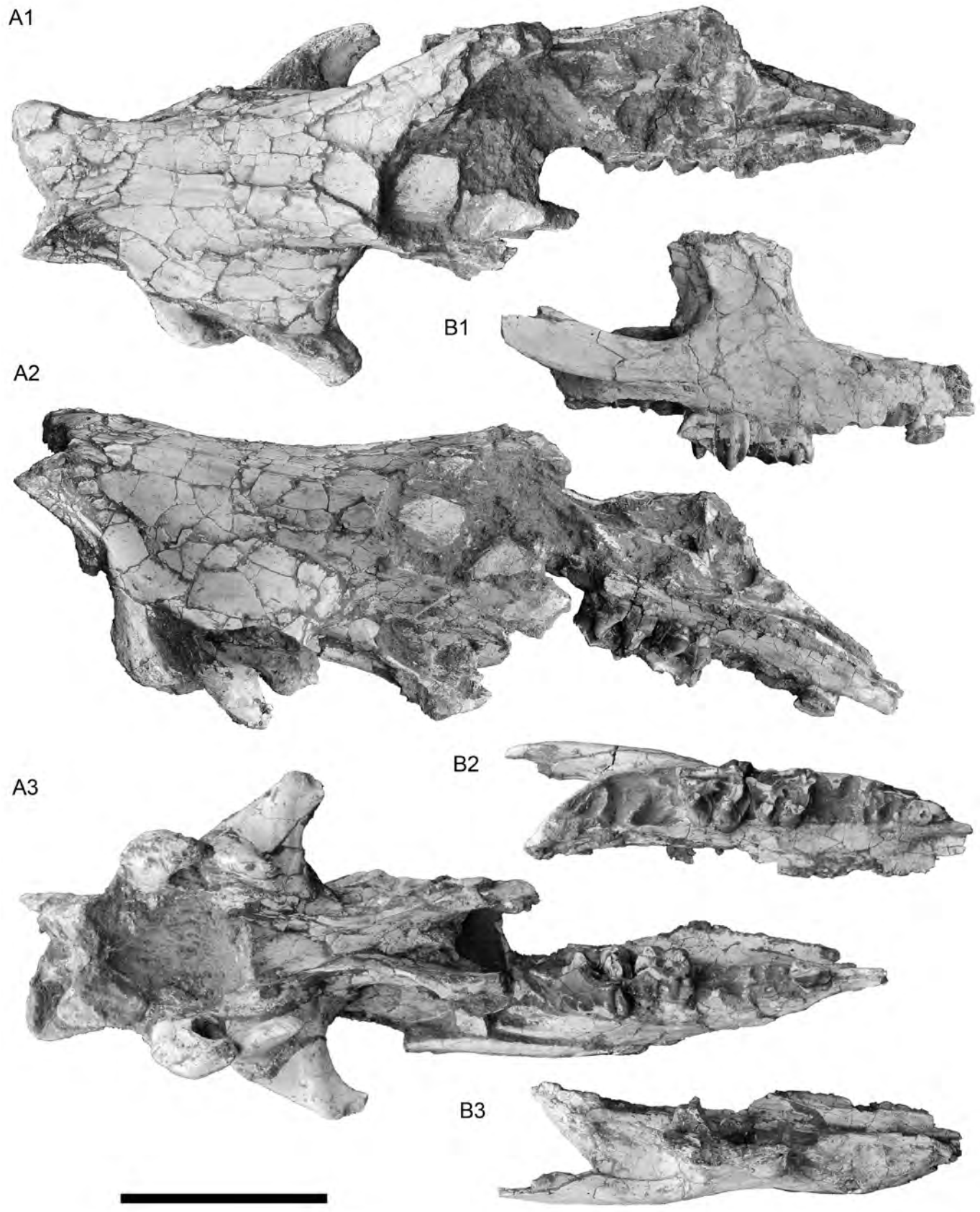


Fig. 2 '*Protaceratherium*' sp. MNCN 72811 from Mesegar-2. A Partial skull in dorsal (A1), lateral (A2) and ventral (A3) views. B maxilar bone MNCN 72812 in lateral (B1), ventral (B2) and dorsal (B3) views. Both fragments pertain to the same individual. Scale bar equals 100 mm.

very shallow. Lingual and labial cingula are absent. The unworn P2 is 'fan'-shaped. The ectoloph is flattened to slightly convex. Protoloph and metaloph are curved, run parallel and about the same length (the hypocone is bigger than the protocone in the P3). There is no evident protocone or hypocone folding. The parastyle is short, pointed and placed at the level of the crista, leaving a wide and shallow paracone fold. There is a narrow crista and three crochets of the same length and width.

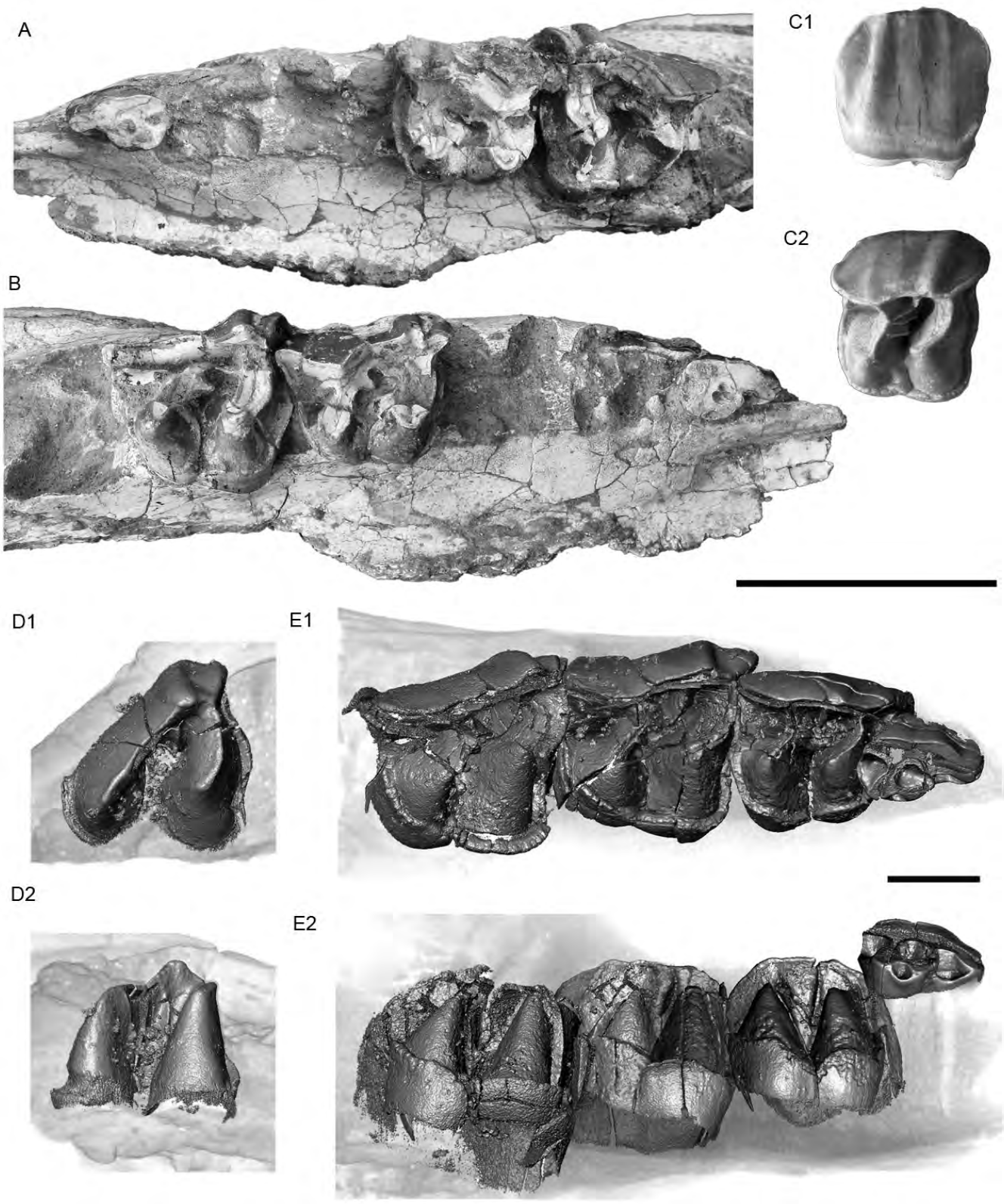


Fig. 3 Upper dentition of '*Protaceratherium*' sp. from Mesegar-1 (MNCN 72812) and Mesegar-2 (MNCN 72811). A, left DP1, DP4 and M1 (MNCN 72811) in occlusal view; B, right DP1, DP4 and M1 (MNCN 72812) in occlusal view; C, right P4 (MNCN 72813) in C1, labial and C2 occusal views; D, unworn right M3 (from the same maxilla figured in B) in D1, occlusal and D2, lingual views; E, right DP1 and unworn right P2-P4 series (from the same maxilla figured in B) in E1, occlusal and E2, lingual views. Upper scale bar (A-C) equals 50 mm; lower scale bar (D- E) equals 10 mm.

A continuous cingulum runs along the anterior, lingual and posterior sides of the tooth. It is higher on the lingual-most sides of protocone and hypocone. The unworn P3 has a slightly concave ectoloph. In this tooth, the contact between protoloph and ectoloph is placed almost contacting the anterior end of the later, delimiting a very short parastyle. The only protocone folding is a shallow concavity on its postero-lingual side. As in the P3, there is a continuous anterior, lingual and posterior cingulum, stronger at the anterolingual angle of the tooth. The crochet is thin and contacts the crista at a very low level, pointing to a closed and rounded medifossete in very advanced wear stages. Additional intermittent enamel ridges protrude from the median side of the metaloph. As in the P2, the postfossette is subtriangular and big, due to a long metastyle. In the P4 the paracone fold is more concave. The P4 MNCN 72813 is rectangular in occlusal view, while the unworn P4 MNCN 72812 has a more 'fan'-like contour. The ectoloph is convex in the first individual (with paracone and metacone ribs visible), almost straight in the second. As in the P3, it has a continuous cingulum surrounding the anterior, lingual, and posterior sides of the tooth. The labial cingulum is subtle in MNCN 72813, represented by two small ridges on the anterior and posterior ends and a smooth ridge between them. In MNCN 72812 the incomplete amelogenesis of the ectoloph prevents the description of its basal part. The lingual cingulum of MNCN 72813 has a smooth tubercle in the lingual end of the median valley (also present in MNCN 72812). In MNCN 72813, the posterior cingulum has a central incision in front of the postfossette, which is rounded and deep. A triple crochet and one crista are present. They consist of small and sharp ridges attached to the median valley. The median valley of MNCN 72812 is badly preserved and, even though fragmentary, a triple crochet is also present. The crista seems thinner than in MNCN 72813. The M1 has a trapezoidal contour, with long protoloph/ectoloph and a short metaloph. It presents a single, narrow and pointed crochet. The protocone is wide, concave posteriorly, and constricted both anteriorly and posteriorly (antecrochet well-developed). Both parastyle and paracone folds are well developed, with a strong paracone groove between them. The mesostyle is smooth. The metastyle is broad and elongate. The lingual cingulum is low, irregular and contacts with the anterior cingulum. It is interrupted on the hypocone. The metaloph is not constricted. The posfossette is narrow and elongate sagittally. As in the P4 from the same maxilla (MNCN 72812), the amelogenesis of the M3 is incomplete. This is evident along the basilar portion of the tooth crown, which presents an indentation of poorly mineralized tissue. Other areas with incomplete amelogenesis are found in the median valley and, particularly, on the lingual side of the protocone. The ectoloph and the metaloph are fused into an ectometaloph. It is nearly straight and smooth, the protoloph is curved. The paracone is protrudes from the ectometaloph wall. The paracone fold is wide and smooth. The parastyle is smaller and sharper than the paracone. The protocone is big, rounded and has a faint indentation on the base of its anterior side. The crochet is represented as a small enamel ridge on the labial-most part of the median valley. The posterior cingulum starts abruptly on the posterior side of the hypocone. While the posterior arrangement is visible, its mineralization fades out anteriorly towards the median valley. The carving around base of the hypocone (produced by poorly mineralized enamel and possibly related to the cingular attachment) continues in this area, pointing at its continuation. In a similar way, the anterior cingulum, which runs from the parastyle to the anterior side of the protocone, fades out lingually. However, in this case, it seems to continue only to the lingualmost side of the protocone, not reaching the median valley.

Postcranial skeleton

Ulna (Fig. 4; Table S3)—MNCN 72842 is the only ulna recovered. It is slender and has the distal end broken. The olecranon is also long, slender, and has a flange topping a depressed area on its lateral side. In medial view, it has a flat area with a sharp edge flanking its proximal border. The humerus-facet is typically lambda-shaped, with no constriction between the proximal overhanging side and the distal expansions. A straight and thin flange protrudes from the lateral side of the humerus-facet, extending as a sinuous ridge to the shaft. Radius-facets are distinct. In proximal view, they form an obtuse angle. The lateral one is comma-shaped, flat and elongate transversally. The medial radius-facet is triangular, concave, very large and strikingly developed proximo-distally. The radius and ulna were not fused but in contact along the proximal third of the diaphysis.

Scaphoid (Fig. 5A; Table S6)—the scaphoid is documented by two specimens. It is as high as wide in medial view, and quite narrow transversely. The posterior border is rounded and considerably higher than the anterior one. The proximal radius-facet is semicircular, concave-convex in lateral view. The anterior edge of the radius-facet is straight and contacts with the semilunate-facet. In lateral view, the scaphoid has a massive postero-proximal smoothed, surrounded by a shallow but well marked groove that widens anteriorly. The proximal semilunate-facet is rhomboidal, elongate transversely and has a squared posterior end. There is no postero-proximal semilunate-facet. The distal semilunate-facet is semicircular and divided into two small flat surfaces, with a diagonal slope change between them. On the distal side, the magnum-facet is crescentiform, concave in lateral view and convex in anterior view. The trapezoid-facet is saddle-shaped and well developed, with a large rounded expansion on the medial side and a triangular projection on the lateral one. The tear-like trapezium-facet is large, concave, and subhorizontal, with a pointed extent on the distal side of the piece.

Semilunate (Fig. 5B; Table S7)—The semilunate is quite robust with respect to other carpals. The anterior side has a smooth tubercle with a flat surface, slightly displaced to the lateral side. The medial border of the anterior tubercle is straight and obliquely oriented. The distal border of the anterior face is slightly curved and keeled. The radius-facet occupies the

entire anterior half of the proximal side. It is transversely flat and sagittally convex, with a shallow depression separating it from its elongated posterior end favoring a 'humbacked' dorsal bone profile. The anterior side has an evident, wide and tendinous scar edging its distal border. There is no ulnar-facet. The radius-facet expands posteriorly with a semicircular flat surface. The scaphoid-facets are semicircular, flat and similar in size. The proximal pyramidal-facet is much smaller than the distal one. Distally, the unciform-facet is squared and faintly concave in lateral view. Its anterior border is rounded and the posterior one straight. The magnum-facet is elongated, oval, concave and flanked by a medial sharp ridge. The volar process is long and wide, with a straight proximal outline.

Pyramidal (Fig. 5; Table S9)—the pyramidal is high and slender. The anterior face is smooth, with a narrow neck and a low base. The proximal ulnar-facet is square in proximal view, with a hooked expansion in the posterior border of the lateral face. On the medial side, the proximal semilunate-facet is small, low, and flat. The distal semilunate-facet is considerably larger, comma-shaped (higher posteriorly), and flat, whereas the distal unciform-facet is transversally concave and triangular with an acute angle on its antero-lateral vertex.



Fig. 4 Right ulnae (MNCN 72842) of '*Protaceratherium*' sp. from Mesegar-2 in A, lateral and B, anterior views. Scale bar equals 50 mm.

Pisiform (Fig. 5; Table S10)—the pyramidal-facet is narrow, flat and comma-like, while the ulna-facet is concave, high and semicircular. Both comprise an acute angle. The neck is well marked and has a semicircular incision on the distal border. The posterior tuberosity is high and rounded, with a straight distal border and a curved upper one.

Magnum (Fig. 5; Table S8)—the anterior side has two lateral pointed angles, a rounded distal border and a developed central tubercle, coinciding with the insertion for the *m. interossei dorsales*. The scaphoid-facet is transversely flat in its anterior part. Its posterior tip reaches the top of the proximal process. The semilunate-facet is transversally convex and laterally flat to slightly concave. The unciform-facet is flat, rectangular on its anterior half and it has a straight anterior border. The proximal process is high, narrow and regularly rounded. The anterior indentation between the scaphoid- and the McII-facet is small, triangular and very shallow. The volar process is robust, straight, and pointed postero-distally. It bears a rough ridge skirting its distal end. In distal view, the Mc III facet is triangular, with rounded anterior angles. It is saddle-shaped, concave sagittally and convex transversally.

Unciform (Fig. 5E; Table S11)—the unciform is as wide as high. The volar process is straight and thin, positioned at an angle of about 50º relative to the anterior side of the bone in proximal view. It has an overhanging distal end, with a subcircular cross section. The anterior side is flat and smooth. On its distal border, a smooth oblique ridge flanks the distal facet without reaching the lateral edge. The ridge and the flat surface of the anterior side are separated by a well-marked step, more evident on the medial half. The insertion of the *m. interosseus dorsalis* in the medial corner is small, triangular in anterior view, blunt and distally oriented. The pyramidal-facet is triangular, convex sagittally and flat laterally and displaced towards the medial border. Its postero-lateral expansion is badly preserved. It does not look like joining the Mc V-facet. The semilunate-facet is flat, vaguely pentagonal and has a very short border facing the anterior side of the bone. Both facets are separated by an obtuse angle. The distal facets are separate by faint and smooth ridges. The Mc V-facet has not been totally preserved either, but a partial wide round concavity is visible. Its distal orientation, 45° from the horizontal line, points to a functional McV, and thus to a tetradactyl manus (see Antoine, 2002).

Mc II (Fig. 5I; Table S13)—the Mc II is slender. The proximal facet for the trapezoid is semicircular, convex antero-posteriorly and slightly concave laterally. There is no trapezium-facet. The lateral articular area is formed by both

the magnum- and McIII-facets. The magnum-facet forms a ~100° angle with the proximal trapezoid-facet. The former is flat sagittally with a distally concave kidney-shaped outline. It does not extend over the dorsal and blunt ridge which prolongs the facet in MNCN 72828. The McIII-facet is low and restricted to the anterior half of the bone. A subtle bone expansion is present on the medial side of the proximal epiphysis. The diaphysis is slender, slightly curved and antero-posteriorly flattened. A smooth tendinous insertion for the *m. interossei* protrudes from the lateral border, surpassing its midshaft. The distal trochlea is subtriangular in distal view (wider posteriorly). Its lateral lip is flat and horizontal transversely while the medial lip is slightly concave and oblique transversely. No keel separates them.

Mc III (Fig. 5H; Table S14)—the bone is as slender as the McII. The magnum-facet is triangular in proximal view, with parallel borders for the McII-facet and the unciform-facet, slightly concave transversely and regularly convex sagittally. This facet is widely visible in anterior view. The unciform-facet is flat, semicircular and contacts the anterior McIV-facet through a smooth boundary. The later is narrow and obliquely oriented. The posterior McIV-facet is oval and flat, located distally with respect to the unciform-facet. The area between both McIV-facets is slightly depressed. In anterior view, the limit between the proximal facets for the magnum and the unciform is high and sharp, forming a 100º angle between them. The medial angle is almost aligned with the diaphysis, thus being little projected. The insertion for the *m. extensor carpii* is well developed; it has a straight upper limit and is placed in the center of the epiphysis. The diaphysis widens distally. The bone is void of postero-distal diaphyseal tubercle. The intermediate relieves are high and pointed. The insertion

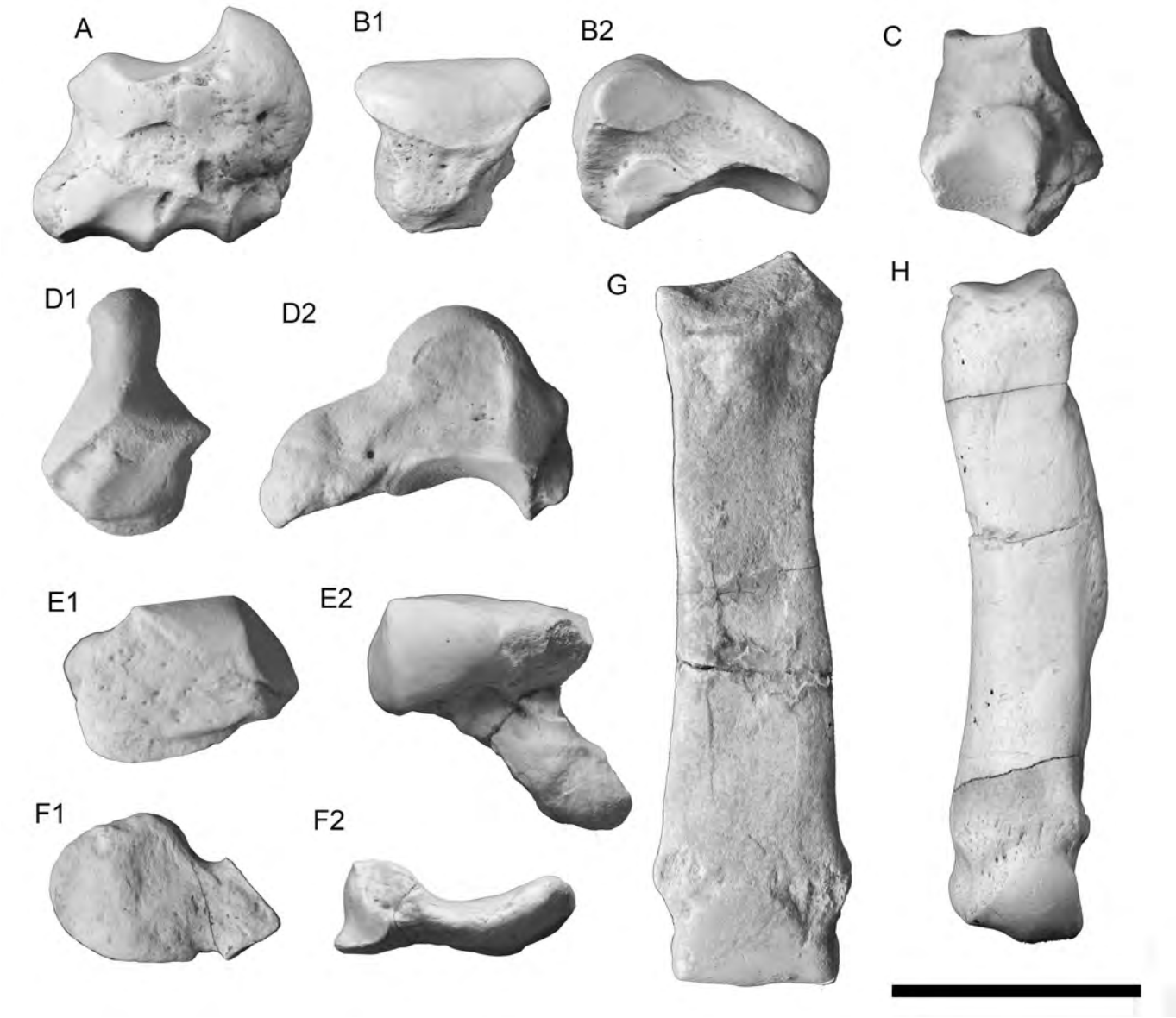


Fig. 5 Carpal and metacarpal bones of '*Protaceratherium*' sp. from Mesegar-2. A, left scaphoid (MNCN 72830); B, right semilunate (MNCN 72831) in B1 anterior and B2 views; C, right pyramidal (MNCN 72832) in medial view; D right magnum (MNCN 72835) in D1 anterior and D2 views; E, right unciform (MNCN 72834) in E1 anterior and E2 proximal views; F, left pisiform (MNCN 72833) in F1 lateral and F2 proximal views; H, left Mc III (MNCN 72827) in anterior view; I, right Mc II (MNCN 72828) in anterior view. Scale bar equals 50 mm.

area for the *m interossei* is long, almost exceeding two thirds of the shaft's total length. The distal border of the distal trochlea is almost straight in proximal view, with a well-marked keel dividing it into two symmetrical halves.

Pelvis—an almost complete pelvis has been recovered from Mesegar-2 (MNCN 7285-72856). The crista of the ilium lacks its lateral half. The medial border of the iliac blade is almost straight, finishing in a sharp and rough tip. The neck of the ilium is broad and short. The outline of the acetabulum is subtriangular. The cotyloid notch is deep (almost reaching the center of the acetabulum), wide, and with straight borders. The obturator foramen is big and ovate in outline, being flanked by a blade-like tuberosity of the ischium.

Tibia (Fig. 6A; Table S4)—a juvenile fragmented specimen (LM-64) is preserved from Mesegar-2. The bone was slender, long, and narrow. The proximal epiphysis has a smooth anterior ridge on the tibial tuberosity. The tuberosity is small but well-marked. The lateral articular facet of LM-64 is incomplete. The medial articular facet has an inner flat area, rising towards the intercondylar prominence. The distal articulation is trapezoid in distal view, with wider anterior and medial sides. The medio-distal groove is marked, in median position on the medial side. The fibula-facet is flat and vertical. The postero-medial process is high and sharp.

Cuboid (Fig. 6B; Table S13)—the cuboid MNCN from Mesegar-2 is high, with an asymmetrical anterior side (pinched medio-distally). The proximal articulation is oval and sagittally elongate, with equally developed astragalus- and calcaneum-facets. The latter are slightly biconcave and separate one another by a smooth ridge. On the medial side, the posterior navicular-facet widely contacts the tibia-facet. Other articular facets are eroded or destroyed on that side. The posterior process is high and narrow, ovoid and symmetrical in posterior view. It widely overhangs the subtriangular and horizontal distal facet (for the MtIV).

Ectocuneiform (Fig. 6C; Table S12)—the preserved specimen has a considerable height with respect to what is observed in other rhinocerotids. The proximal navicular-facet is kidney-shaped and concave, with a central funnel next to the lateral incision. The anterior side is very thick compared to the posterior side, which is reduced and finishes in a squared end. In lateral view, the bone has a biconcave outline. The anterior pyramidal-facet is square whereas the posterior one is triangular. Both facets have flat surfaces and are separate by the lateral incision. The postero-lateral process is weak. The mesocuneiform-facet is badly preserved, represented as a very narrow broken border. Both Mt II-facets are flat and rounded, being the anterior one higher than wide and the posterior one elongate sagittally. The distal Mt III-facet is faintly laterally convex, with a lower posterior end. The posterior pyramidal-facet is hardly visible in this view.

Mt IV—MNCN 59275 from Mesegar-1 is badly preserved. However, the proximal cuboid-facet is nearly complete. It is subtriangular, saddle-shaped, and with a strong plantar protuberance.

Phalanges—first, second and third phalanges, both central and lateral, have been found. Their overall proportions are slender. The central phalanges have a small antero-posterior diameter. The groove for the central metapodial keel is shallow. The paired mucular insertions are salient and located laterally.

DISCUSSION

Biostratigraphic context of Mesegar fossil sites

The age of Mesegar-1 and 2 has not been precisely determined. Micromammal remains are scarce, but enough to make some inferences. The species *S. simplicidens* and *P. murinus* have been recorded in Mesegar-1. *S. simplicidens* ranges throughout the MN 2-5 interval (García-Paredes et al., 2012). The small size of the available teeth from Mesegar-1 fits with remains prior to the Dc Local Zone, considering that from that moment on, the species shows a considerable size increase (Olmedo et al., 2004). *P. murinus*, the second species from Mesegar-1, spans to the Dc Local Zone, being particularly abundant in the B and C Zones (Olmedo et al.,

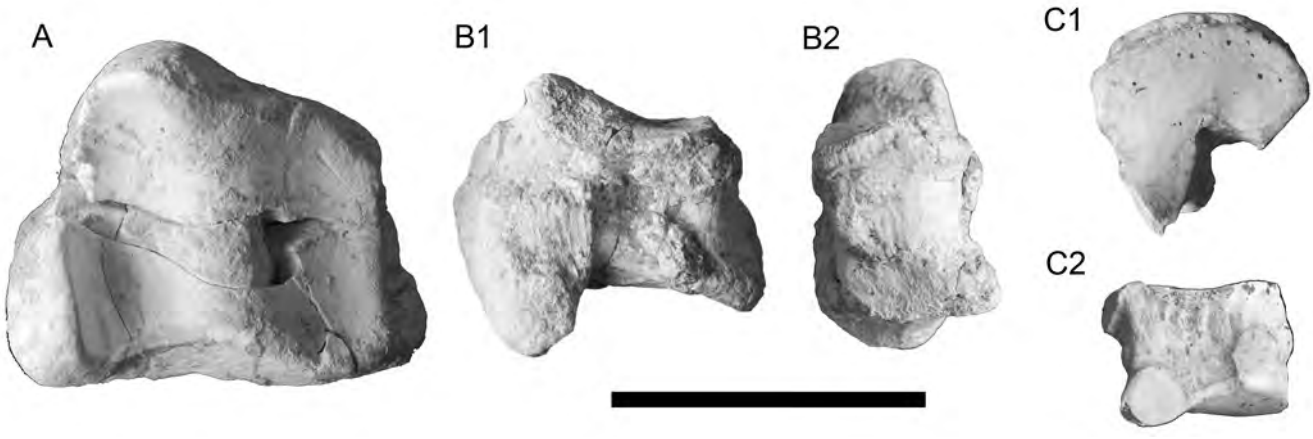


Fig. 6 Fragmentary tibia and tarsal bones of '*Protaceratherium*' sp. from Mesegar-2. A, right tibia (MNCN 72840) in distal view; B, left cuboid (MNCN 72838) in B1 lateral and B2 anterior views; C, left ectocuneiform (MNCN 72839) in C1 proximal and C2 medial views. Scale bar equals 50 mm.

2004). Mesegar-2 has yielded several remains from the glirid *P. crusafonti* (Olmedo et al., 2004). The species has been recorded from the MN2 up to the MN4, being particularly abundant in the Local Zone B (early MN4; Daams, 1991). The remaining mammalian assemblage of Mesegar-1 includes a horn cone from a small, undetermined bovid. The first bovid remains in the Iberian Peninsula dates from the Local Zone C (MN 4). Nevertheless, macromammals have not been recorded during the Local Zone B (early MN 4) in the Iberian Peninsula, thus an older dating (early MN 4) is possible (Olmedo et al., 2004). The macromammals recorded in Mesegar-2 comprise anchitheriine and paleomerycid remains comparable to other lower MN 4 remains. The dental paleomerycid remains are brachyodont and shows small proportions, far from *Triceromeryx pachecoi*, the first palaeomerycid from the Iberian Peninsula, but close to *Palaeomeryx kaupi* from Artenay (MN 4). Both paleomerycid and equid remains (a small undetermined anchitheriine) are currently under study. In other words, the Mesegar-2 assemblage points to a MN 4 age, possibly documenting the Local Zone B (early MN4), which is an extremely poorly sampled interval in the Iberian Peninsula. Other Iberian localities referred to the MN4 include Buñol, Can Mas, Córcoles, and Lisboa.

Morphological comparison

The rhinoceros remains from Mesegar-2 were originally identified as *Hispanotherium matritense* (Lartet in Prado, 1864) by López Olmedo et al. (2004). We consider that they pertain to a new distinct species. *H. matritense* show overall bigger proportions, larger and more hypsodont teeth with greater enamel folding, valleys and fossae filled with abundant cementum and no cingula. Other differences found in the skull MNCN 72811 from Mesegar-2 like the greater distance between the parietal crests and the flattened surface left between them (also typical from *Protaceratherium* and *Plesiaceratherium*), the placement of the orbit over the level of the M1 boundary (above M3 in H. matritense; Sanisidro et al., 2011), the shorter distance between nasal notch and the anterior rim of the orbit (considerably longer in *H. matritense*) or the bigger size of the orbits in may vary depending on sexual dimorphism and/or ontogenetic status in rhinoceros. Regarding the postcranial skeleton, the postcranial remains from Mesegar-2 are smaller and more slender than *H. matritense* and morphologically distinct (see Cerdeño, 1982 for an overall description of the postcranial skeleton of *H. matritense*).

Other related cranial remains from the Iberian fossil record include a posterior fragment from Loranca (MNCN 65901) and a partial juvenile skull (MNCN 45560) from Valquemado. The posterior fragment MNCN 65901, mentioned in Cerdeño (1992), has a high and narrow occiput. The dorsal part of the occipital crest is narrow and deeply emarginated. The occipital face attains its maximum width at the level of the posttympanic processes, which are wide and independent from the postglenoid processes. The paroccipital processes are damaged but separated from the posttympanic ones. The middle occipital crest is smooth except for the area next of the nuchal tubercle. The lateral occipital crests are very close to the lateral borders. The occipital condyles are small and the foramen magnum is slightly oval. The parietal bones are little domed over the temporal bones and the parietal crests are well separated, as in the juvenile individual from Mesegar-2. The basal portion preserves the basilar half of the occipital condyle, the basilar part of the occipital bone, the origin of the basisphenoid and the area for the oval and lacerum foramina. The fragmentary skull from Valquemado (MNCN 45560) lacks the posterior half of the skull, so no information about the presence of M1 is provided. Nevertheless, its overall proportions and the presence of the right DP4 and the left DP2-4 series point to a neonate individual. The right DP4 is practically unworn but morphologically comparable with those of the skull from Mesegar-2. The orbits are large, rounded and the anterior rim is placed over the anterior border of the DP4. The nasal suture is clearly visible and the nasal bones are very small. The foramen infraorbitalis is placed close to the nasal incision, above the anterior half of the DP3.

Despite their different ontogenetic stages, those cranial remains permits to establish some ontogenetic comparisons with the Iberian sample from Loranca, Valquemado and Mesegar-2. The neonate morphology shows a relatively big, rounded orbit, a small lachrymal tubercle and a well-developed postorbital process. During its ontogeny, some regions of the splachnocranium remain constant. The size and shape of the orbit, as well as the relative position of the lachrymal tubercle are remarkably constant. The main rostral changes rely on the maxillary and premaxillary bones, which experience a considerable elongation. The relative position of the P4 is progressively displaced farther from the orbit as the new molar series appear, increasing the shearing surface. Therefore, this rostral enlargement involves a greatly enlarged dental battery contained within the maxillary bone in the adult stage. In a parallel way, the maxillary bone enclosing the posterior side of the nasal incision expands bucally. As a result, the posterior rim of the nasal incision becomes longer and more squared-shaped respect to the triangular and little-carved morphology of the neonate stage. An increasing size of the rostral part of the maxilla together with the elongation of the nasal bones makes the whole incision widens and expanding rostrally.

As previously commented, rhinoceros remains from Loranca and Valquemado were tied to the species *P. minutum*. Therefore, some comparisons are compulsory between those and the main source of information about the cranial morphology in *P. minutum*, restricted to the German locality of Budenheim (Roman, 1924). The first individual from Bundenheim figured in Roman (1924), and labeled as Crâne 2, is heavily laterally distorted. Nonetheless, its completeness poses it as the main source of information about the adult morphology of *P. minutum*. The second one is a highly fragmented individual with largely reconstructed areas according to the Crâne 2. If compared with the German skulls

from Budenheim, the distance between the parietal crests of the skull from Mesegar-2 is fairly wider and the whole skull narrower.

The DP4 from Mesegar-1 closely resembles that from Loranca (MNCN 59551) and is similar to the DP4 of *P. minutum* from Pechbonieu (1968 XIV 127). All of them share multiple crochets, continuous labial cingula and a thin antecrochets. The M1 teeth from Mesegar-2 present a low and irregular lingual cingulum which contacts with the anterior cingulum but do not reach the posterior one. The same cingular configuration can be observed in BSPG 1968 XIV 126 from La Chaux assigned to *P. minutum*. Conversely, most M1 and M2 from Loranca are void of lingual and labial cingula. The same occurs in other species as *P. minutum* (e.g. Cintegabelle, Ulm or Laugnac). The M3 from Mesegar-2 is equivalent to the remains of *P. platyodon* from Estrepouy (Sanisidro et al. 2011).

The ulna from Mesegar-2 (MNCN 72842) shares with *P. minutum* a very long medial radius-facet. However, the lateral flange, well developed and rugous in MNCN 72842, is stronger in the individual from Mesegar-2. In general, carpal bones from Mesegar-2 are more robust (lower H and higher APD values) and present longer volar processes than the specimens from Valquemado and Loranca. The scaphoid from Mesegar-2 is short (lower H) respect to the scaphoid from Loranca. The crest between the magnum and trapezoid-facets is shorter than the trapezoid-trapezium one, in contrast to the remaining European sample where clearly protrudes from the distal side of the bone. The dorsal border is rounder in lateral view and shorter (differing from the genus *Plesiaceratherium*, which present a straighter and higher dorsal border). The lunate from Mesegar-2 is stouter, has a lower dorsal side (low H) and presents a radius-facet posterior expansion as a semicircular flat surface, not present in Valquemado nor Loranca. The anterior face of the bone is wider than in the sample from Valquemado and, specially, in that from Loranca. The anterodistal rim is wider in the individuals from Loranca. The volar process of the lunate is longer, wider, less curved and presents a straighter dorsal profile than those from Valquemado and Loranca. If compared with other species, the lunates of *P. fahlbuschi* from Sandelzhausen and *P. minutum* from Budenheim have a shorter volar process and a higher anterior side. On the pyramidal, the distal lunate-facet from Mesegar-2 is wider and bigger than that from Loranca (MNCN 32574). The pisiform from Mesegar-2 is shorter (low H) and presents a narrower lower constriction and a rounder upper one than that from Budenheim (i.e. 1968 XIV 106, replica). The Mc III is more robust, wider (higher TD value) and presents a straighter magnum-facet in dorsal view. The shaft has diverging margins, being the lateral one slightly convex at its midpoint. The boundary between magnum and unciform-facets is less protruding than other specimens from Budenheim, Loranca and Valquemado. The distal epiphysis of the tibia from Mesegar-2 stands out for its long medial astragalar-facet, surpassing the lateral one (the same morphology can be found in the tibiae from Budenheim). It contrasts with the sample from Valquemado (MNCN 94520/1 and MNCN 95420/2) where both grooves are equally developed or the tibia MNCN 60285 from Loranca which shows a slightly longer lateral facet. The cuboid is shorter (low H) and presents a pointed volar process, similar to some Loranca individuals. Finally, the ectocuneiform from Mesegar-2 has a wider dorsal side (higher APD value) and a shorter plantar extension (lower APD value) in proximal view.

A detailed comparison of the rhinoceros from Mesegar-1 and 2 with "*P. tagicum*" show some similarities, as the presence of multiple crochets on P3-4 or the overall molar morphology, but also differences: "*P. tagicum*" show a strong hypocone constriction on the P2, strong cristae along the dental series which partially encircles big, rounded medifossetes, both absent in Mesegar. Further remains of "*P. tagicum*" are therefore required to assess the phylogenetic placement of the species.

Phylogenetic relationships

Twelve most parsimonious trees (1650 steps; Consistency Index (CI)=0.22; Retention Index (RI)=0.48) were obtained by using the heuristic search of PAUP 4.0v10 (unweighted parsimony; branchswapping TBR, 1000 replications with random taxa addition, 100 treeholds by replication; Swofford, 2002). The strict consensus tree is shown in Fig. 6. Only four alternative topologies occur (two polytomies), with three distinct sets of optimized characters. The branch support, assessed by calculating the Bremer indices (Bremer 1994), is indicated below the branches in Fig. 6 (italicized, left to the corresponding node); the number of unambiguous synapomorphies, detailed in Supplementary Data 4, appears above the branches. The nodes discussed in the text are designated by a circled number in the same figure (Fig. 6, Nodes 1-11).

Suprageneric relationships within Rhinocerotidae are much consistent with recent morphology-based phylogenies, such as those proposed by Antoine (2002), Antoine et al. (2003a), Antoine et al. (2010), and especially Becker et al. (2013). Rhinocerotidae are monophyletic, with *Trigonias osborni* as the first offshoot (Fig. 6). The next node coincides with a basal split within Rhinocerotidae, i.e. with the divergence of Elasmotheriinae and Rhinocerotinae clades (Fig. 6).

The Elasmotheriinae consist of [*Ronzotherium filholi* [*Subhyracodon occidentalis* [*Diceratherium armatum* [[*Menoceras arikarense*, "*Protaceratherium tagicum*"] [*Bugtirhinus praecursor* [*Hispanotherium beonense*, *Huaqingtherium lintungense*]]]]], in a way similar to the results proposed by Antoine *et al.* (2010) and Becker et al. (2013), where "*P. tagicum*" and *H. lintungense* were not included, though. Most nodes are well-supported, with a number of unambiguous synapomorphies comprised between 8 and 23 (Fig. 6), except for the clade [*Menoceras arikarense*, "*Protaceratherium tagicum*"], only supported by four unambiguous synapomorphies (protocone and hypocone

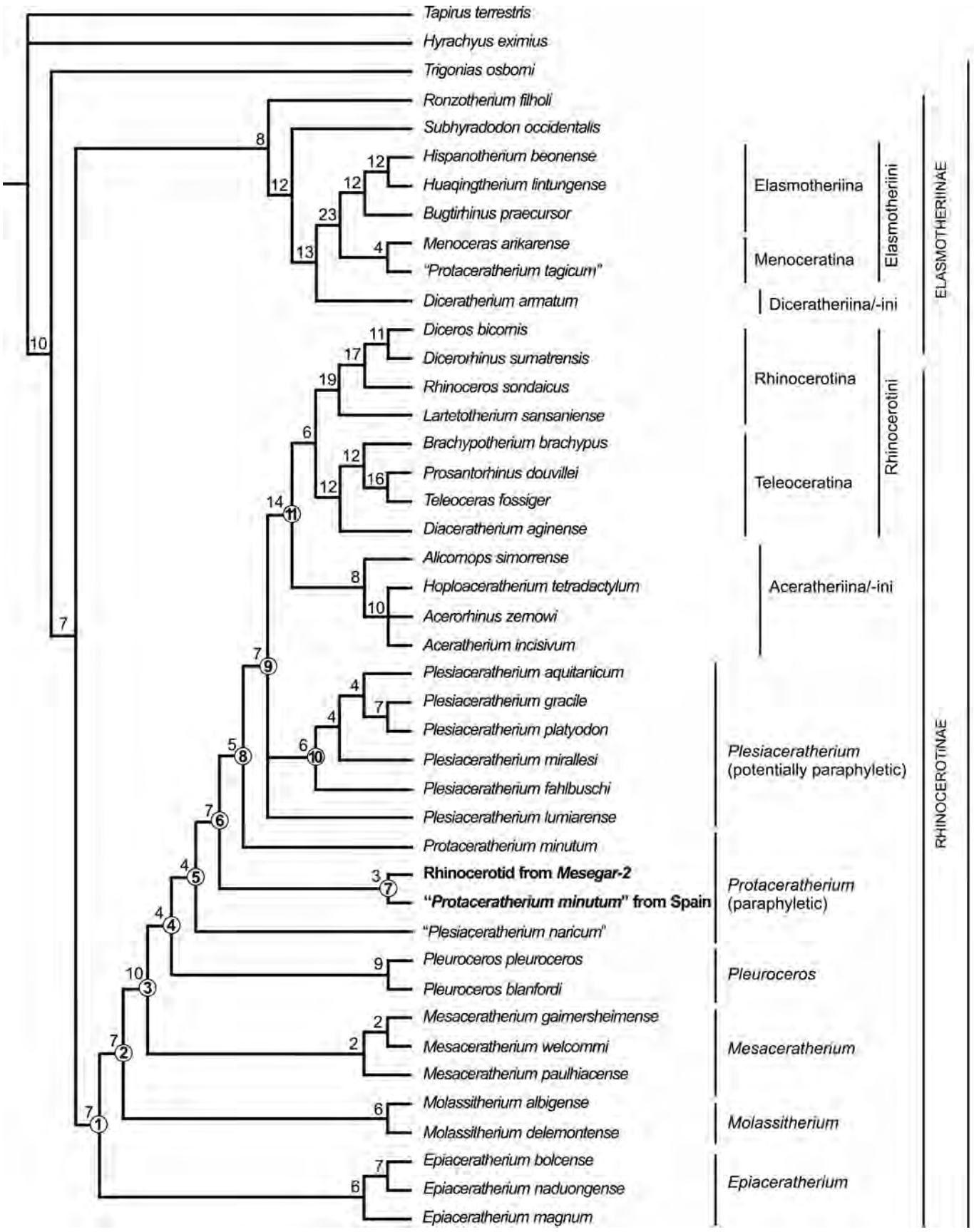


Fig. 7 Strict consensus tree of twelve most parsimonious trees (1650 steps; CI=0.22; RI=0.48) obtained using PAUP 4.0 10 (Swofford, 1998), based on 282 morphological characters, and performed on 43 rhinocerotid, rhinocerotoid, and tapirid taxa, with *Tapirus terrestris, Hyrachyus eximius*, and *Trigonias osborni* as outgroups. Suprageneric group names are based on current phylogenetic relationships and match those proposed by Antoine et al. (2010) and Becker et al. (2013). The number of unambiguous synapomorphies for each node appears above the internal branches left to the corresponding node. The nodes are designated by a number. Taxa of interest are bold-typed.

separate, and medifossette usually present on P3-4; crista always present on P3, and usually present on upper molars). "*P. tagicum*" is only known by two upper tooth rows from a single individual, which might explain such a weak support. Nevertheless, the node uniting that clade with Elasmotheriina is supported by 23 unambiguous synapomorphies, among which six are observed in "*P. tagicum*" (i.e., not optimized): crochet usually present and lingual cingulum always reduced on P2-4; crochet and constriction of the protocone always present on upper molars; metaloph short on M1-2; mesostyle present on M2).

Rhinocerotinae are monophyletic. Their first offshoot (Fig. 6, Node 1) encompasses the monophyletic genus *Epiaceratherium*, with *E. magnum* being sister taxon to the clade [*E. bolcense*, *E. naduongense*], as assumed by Böhme et al. (2014) without formal phylogenetic analysis. The Node 1 is supported by seven dental and postcranial unambiguous synapomorphies (see Supplementary Data 4 for more details). The next offshoot (Fig. 6, Node 2) is the *Molassitherium* clade formed by *M. albigense* and *M. delemontense*, as in Becker et al. (2013), and supported by seven cranio-dentaland postcranial unambiguous synapomorphies (see Supplementary Data 4 for more details). The Node 3, supported by 10 unambiguous dental and postcranial synapomorphies, individualizes *Mesaceratherium* as a monophyletic genus, under the sequence [*M. paulhiacense* [*M. gaimersheimense*, *M. welcommi*]], in agreement with Antoine et al.'s (2010) conclusions (see Supplementary Data 4 for more details). Accordingly, *Pleuroceros* is the next monophyletic offshoot (Node 4: four dental synapomorphies), with the clade [*P. pleuroceros*, *P. blanfordi*] supported by nine mandibular, dental, and postcranial synapomorphies (Fig. 6; Supplementary Data 4). The next node (Node 5) places *Plesiaceratherium naricum* as sister taxon to more apical Rhinocerotinae (Node 6), notably due to three talar synapomorphies (see Supplementary Data 4 for more details), quite remote from the type species of *Plesiaceratherium*, *P. gracile* (see below). "*Protaceratherium minutum* from Spain" and the rhinocerotid from Mesegar-2 form a clade (Node 7) sharing a common ancestor with the Node 8 ([*Protaceratherium minutum* [*Plesiaceratherium*, *Rhinocerotini*, *Aceratheriini*]]]). This Spanish clade is supported by three unambiguous synapomorphies (crochet and metaloph constriction always present on P2-4; loss of the antecrochet on P4 -- reversal). *Protaceratherium minutum* diverges then (Node 8), as in Antoine et al. (2010) and Becker et al. (2013). This node is supported by four dental and postcranial unambiguous synapomorphies (labial cingulum usually absent on upper premolars; metacone fold present on M1-2; mesostyle absent on D3-4; expansion of the calcanear facet-1 wide and low on the astragalus). The next node (Node 9) is a polytomy encompassing *Plesiaceratherium lumiarense*, a clade formed by all other species of *Plesiaceratherium* (including the type species *P. gracile*), and the clade [Rhinocerotini, Aceratheriini]. Seven unambiguous dental and postcranial synapomorphies support the Node 9 (M3 triangular; labial cingulum reduced and lingual cingulum usually present on lower molars; secondary folds present on D2; condylar facets kidney-like on the atlas; glenoid fossa with a straight medial border on the scapula; tibia-facet always present on the calcaneus). The topology of the *Plesiaceratherium* clade sensu stricto (Node 10) is [*P. fahlbuschi* [*P. mirallesi* [*P. aquitanicum* [*P. gracile*, *P. platyodon*]]]]. This clade is supported by six unambiguous cranial and dental synapomorphies, such as the presence of a flat area between the temporal and the nuchal crests, of a much developed nuchal tubercle, of very long nasal bones, of a d1 usually one-rooted, and of vertical rugosities on the ectolophid of lower milk molars, as well as the absence of an antecrochet on P2-3. Fourteen unambiguous cranio-dental and postcranial synapomorphies support the clade encompassing [Aceratheriini, Rhinocerotini] (Node 11; see Supplementary Data 4 for more details). The monophyly of Aceratheriini is supported by eight unambiguous cranio-mandibular, dental, and postcranial synapomorphies (see Supplementary Data 4 for more details). This tribe includes [*Alicornops simorrense* [*Hoploaceratherium tetradactylum*, *Acerorhinus zernowi*, *Aceratherium incisivum*]]. Their sister taxon (Rhinocerotini) consists of Rhinocerotina and Teleoceratina, the branching sequences of which are [*Lartetotherium sansaniense* [*Rhinoceros sondaicus* [*Diceros bicornis* [*Dicerorhinus sumatrensis*]]] and [*Diaceratherium aginense* [*Brachypotherium brachypus* [*Teleoceras fossiger*, *Prosantorhinus douvillei*]]], respectively.

Taxonomic implications

The genera *Epiaceratherium* (Eocene-Oligocene; monophyletic), *Molassitherium* (Oligocene; monophyletic), *Mesaceratherium* (Oligocene-Early Miocene; monophyletic), *Pleuroceros* (Late Oligocene-Early Miocene; monophyletic), *Protaceratherium* (Early Miocene; paraphyletic), and *Plesiaceratherium* (Early-Middle Miocene; potentially paraphyletic) are here considered as Rhinocerotinae *incertae sedis*, in good agreement with Antoine et al. (2010) and/or Becker et al. (2013).

The rhinocerotid from Mesegar-2 and "*Protaceratherium minutum* from Spain" form a clade the sister group to which has *Protaceratherium minutum* as a first offshoot (Fig. 6, Nodes 7 and 8, respectively). As already explained in the previous section (Systematic Palaeontology), we consider both Spanish terminals as documenting a single taxon, in spite of several discrepancies, such as the presence/absence of cement (possible taphonomic bias), the constant/usual presence of a labial cingulum on upper premolars and molars, the presence/absence of a medifossette and the junction/separation of lingual cusps on P3-4. All these features are considered as potentially variable among species within Rhinocerotidae (see Antoine, 2002). Together with its original morphology (crochet and metaloph constriction always present on P2-4; loss of the antecrochet on P4), the close affinities of the Spanish clade with the type species of *Protaceratherium* (*P. minutum*)

lead us to consider it as a new genus and species, provisionally included in '*Protaceratherium*'.

Likewise, "*Diceratherium naricum* Pilgrim, 1910" shall be removed from *Plesiaceratherium*, contra Antoine et al. (2010), and be provisionally referred to as "*Protaceratherium naricum* (Pilgrim, 1910)". Be as it may, this species from the earliest Miocene of the Bugti Hills is documented by very few dental and postcranial remains (Pilgrim, 1910; Forster-Cooper, 1934; Antoine et al., 2010; pers. obs. by POA) and as such, the phylogenetic relationships as proposed in the current work might be somewhat modified with supplemental material.

Moreover, "*Rhinoceros* (*Ceratorhinus*?) *tagicus* Roman, 1907" from the Burdigalian site of Horta das Tripas (Lisbon Basin, Portugal), here considered *a priori* as "*Protaceratherium tagicum* (Roman, 1907)", has no close affinities with either *Protaceratherium minutum* (hypothesis of Antunes and Ginsburg, 1983), the teleoceratine *Prosantorhinus* (hypothesis of Heissig, 1972; Antunes and Ginsburg, 1979) or any other representative of Rhinocerotinae (Fig. 6). Conversely, it appears as closely related to the small pair-horned North American menoceratine *Menoceras arikarense* within Elasmotheriini/-inae.

The current analysis confirms the a priori assignment of *Plesiaceratherium platyodon*, *P. aquitanicum*, *P. mirallesi*, and *P. fahlbuschi* to *Plesiaceratherium*, instead of *Protaceratherium*, contra Iñigo (1994) and/or Cerdeño (1995), due to their close phylogenetic affinities to the type species, *P. gracile* (Fig. 6). At last, the position of *P. lumiarense* potentially outside the *Plesiaceratherium* clade sensu stricto (Fig. 6, Node 9) might be biased by the lack of significant cranial remains attributed to the former species (see Antunes and Ginsburg, 1983). Pending new findings, we propose to maintain the generic assignment of *P. lumiarense*.

CONCLUSIONS

Basal rhinoceros taxonomy was classically regarded as being in need of revision. However, our phylogenetic research shows that these forms attained a certain diversity that extended up to the Early Miocene. The rhinoceros from Mesegar-1 and 2 shows a combination of dental, cranial and postcranial morphology that groups it with the forms from Valquemado and Loranca, previously considered as *Protaceratherium minutum*. This clade is defined by . This group (confined to the Iberian Peninsula) nests it between the clades Rhinocerotini+Aceratheriina/-ini and more primitive taxa such as *Pleuroceros*, *Mesaceratherium* or *Molassitherium*.

'*Protaceratherium*' *tagicum* from Horta das Tripas (Lisbon, Portugal) does not seem to fall into the *Plesiaceratherium* nor *Protaceratherium* lineages but with menoceratina, thus discarding its synonymy with *P. minutum*. However, due to the scarce remains, this taxon is in need of supplementary material.

The species *P. minutum* should therefore be excluded from the Iberian fossil record. On the other hand, the genus *Plesiaceratherium* is shown here as potentially paraphyletic, as the species *P. naricum* and *P. lumiarense* are set apart from the remaining core species.

ACKNOWLEDGEMENTS

We are very grateful to all the members of the digging campaign of Mesegar 2008. Thanks to P. Peláez-Campomanes and I. Paredes for their advice regarding the micromammal assemblage of Mesegar-1 and 2. We specially thank P. Pérez Dios (Museo Nacional de Ciencias Naturales de Madrid) for the funding necessary for the CT-Scan, A. Prieur (Collections of the Université Claude Bernard Lyon-1), G. Rössner (Paleontologisches Museum, Munich), J. Galkin (American Museum of Natural History, New York), Yves Laurent and Pierre Dalous (MNHT, Tolouse), Christine Argot, Claire Sagne, and Pascal Tassy (MNHN, Paris), Aude Bergeret (MHN, Montauban), and Madelaine Böhme (GBIT, Tübingen) for having granted access to the collections they are in charge of. This study is part of the Spanish Government MICINN research project CGL2008-05813-CO2-01, and is included in the research Group BSCH-UCM 910607.

LITERATURE CITED

Alcalá, L., Cerdeño, E., Montoya, P., Morales, J., Pérez, B., and Soria, D., 1990, Composición Taxonómica y Anatómica de los Restos de Macrovertebrados del Mioceno Inferior Contintental de Loranca del Campo (Cuenca), *in* Fernández López, S., ed., Comunicaciones de la Reunión de Tafonomía y Fosilización: Madrid, Universidad Complutense de Madrid/CSIC, p. 7-12.

Antoine, P.O., 2002, Phylogénie et évolution des Elasmotheriina: (Mammalia, Rhinocerotidae): Mémoires du Muséum National d'Histoire Naturelle, v. 188, p. 5-350.

Antoine, P.O., Downing, K.F., Crochet, J.-Y., Duranthon, F., Flynn, L.J., Marivaux, L., Métais, G., Rajpar, A.R., and Roohi, G., 2010, A revision of *Aceratherium blanfordi* Lydekker, 1884 (Mammalia: Rhinocerotidae) from the Early Miocene of Pakistan: postcranials as a key: Zoological Journal of the Linnean Society, v. 160, p. 139-194.

Antoine, P.O., Duranthon, F., and Welcomme, J.L., 2003, *Alicornops* (Mammalia, Rhinocerotidae) dans le Miocène supérieur des Collines Bugti (Balouchistan, Pakistan) : implications phylogénétiques: Geodiversitas, v. 25, p. 575-603.

Antunes, M.T., and Ginsburg, L., 1983, Les Rhinocérotidés du Miocène de Lisbonne. Systématique, écologie, paléobiogéographie, valeur stratigraphique: Ciências da Terra (UNL), v. 7, p. 17-98.

Becker, D., Antoine, P.O., and Maridet, O., 2013, A new genus of Rhinocerotidae (Mammalia, Perissodactyla) from the

Oligocene of Europe: Journal of Systematic Palaeontology.

Budras, K.-D., Sack, W.O., and Röck, S., 2009, Anatomy of the Horse: Hannover, Schlütersche Verlagsgesellschaft mbH & Co.

Cerdeño, E., 1992, Spanish Neogene Rhinoceroses: Palaeontology, v. 35, p. 297-308.

—, 1995, Cladistic analysis of the Family Rhinocerotidae (Perissodactyla): American Museum Novitates, v. 3143, p. 1-25.

Díaz de Neira, A.L.O., F., 2009, Mapa Geológico de España 1:50.000. Hoja nº 628 (Torrijos), MAGNA 50 (2ª Serie): Madrid, IGME.

Fortelius, M., and Heissig, K., 1989, The phylogenetic relationships of the Elasmotherini (Rhinocerotidae, Mamm.): Mitteilungen Bayerische Staatssammlung Paläontologische historische Geologie v. 29, p. 227-233.

Ginsburg, L., 1974, Les Rhinocerotides du Miocene de Sansan (Gers): Compte Rendus des Seances de l'Academie des Sciences, Paris, v. 278, p. 597-600.

Guérin, C., 1980, Les rhinocéros (Mammalia, Perissodactyla) du Miocène terminal au Pléistocène supérieur en Europe occidentale : comparaison avec les espèces actuelles: Documents des Laboratoires de Géologie de Lyon, v. 79, p. 1-1184.

Heissig, K., 1972, Die obermiozäne Fossil-Lagerstätte Sandelzhausen. 5. Rhinocerotidae (Mammalia), Systematik und Okologie: Mitteilungen der Bayerischen Staatssammlung Paläontologie und historische Geologie, v. 14, p. 37.

—, 1989, The Rhinocerotidae, *in* Prothero, D., and Schoch, R.M., eds., The evolution of Perissodactyls, Oxford University Press, p. 399-417.

—, 1999, 16. Family Rhinocerotidae, *in* Rössner, G.E., and Heissig, K., eds., The Miocene Land Mammals of Europe: Pfeil, Munich, p. 175-188.

—, 2012, The American genus Penetrigonias Tanner & Martin, 1976 (Mammalia: Rhinocerotidae) as a stem group elasmothere and ancestor of *Menoceras* Troxell, 1921: Zitteliana, v. A 52, p. 79-96.

Kordikova, E.G., De Bonis, K., and Brunet, M., 1998, Miocene Rinoceroses of Southern-Western Betpakdala Steppe, South Kazakhstan: Journal of Vertebrate Paleontology, v. 18, p. 56A.

López Olmedo, F., Díaz de Neira, A., Martín Serrano, A., Calvo, J.P., Morales, J., and Peláez-Campomanes, P., 2004, Unidades Estratigráficas en el Registro Sedimentario Neógeno del Sector Occidental de la Cuenca de Madrid: Revista de la Sociedad Geológica de España, v. 17, p. 87-101.

Olmedo, F.L., Neira, A.D.d., Serrano, A.M., Calvo, J.P., Morales, J., and Peláez-Campomanes, P., 2004, Unidades Estratigráficas en el Registro Sedimentario Neógeno del Sector Occidental de la Cuenca de Madrid: Revista de la Sociedad Geológica de España, v. 17, p. 87-101.

Quiralte, V., Morales, J., Sánchez, I.M., Sanisidro, O., Pozo, M., Mingo, B., Huertas, M.J., Varas, M.J., Sánchez-Muñoz, L., Crespo-Feo, E., Servert, L., Hernández-Rodero, M.F., Aparicio, A., Caballero, J., Torres, Y., Agut, D., Diéguez, C., Chicote, G., Díaz-Martínez, E., Nieto-Codina, A., Martín-Escorza, C., and Hernández-Ferreirós, P., 2011, La Fauna de Mamíferos Fósiles del Mioceno Inferior de La Encinilla (Colmenar Viejo, Madrid), *in* Fernández Hernán, M., Santos Santos, G., and García Guinea, J., eds., Geología de Colmenar Viejo y alrededores más próximos: Colmenar Viejo, Ayuntamiento de Colmenar Viejo. Concejalía de Medio Ambiente, p. 123-131.

Roman, F., 1924, Contribution a l'Étude de la Faune de Mammifères des Littorinenkalk (Oligocène Supérieur) du Bassin de Mayence. Les Rhinocéros: Travaux du Laboratoire de Géologie de la Faculté des Sciences de Lyon, v. 7.

Sanisidro, O., Alberdi, M.T., and Morales, J., 2011, The first complete skull of *Hispanotherium matritense* (Prado, 1864) (Perissodactyla, Rhinocerotidae) from the Middle Miocene of the Iberian Peninsula: Journal of Vertebrate Paleontology, v. in press.

Schaller, O., 2007, Illustrated Veterinary Anatomical Nomenclature: Sttutgart, Enke.

SUPPLEMENTARY DATA 1

Measurements (mm) of the skull (Table S1), mandible (Table S2), ulna (Table S3), tibia (Table S4), and pelvis (Table S5) of the rhinocerotid remains from Mesegar-2 (Toledo Province, Spain). Side is detailed as follows: l, left; r, right.

Table S1	MNCN 72811
5. Minimal width of braincase	90?
9. Distance between nasal notch and orbit	40.7
15. Width of occipital crest	74.4
16. Width between mastoid processes	153.8
17. Minimal width between parietal crests	25.1

Table S2		MNCN 72813	MNCN 72811 / MNCN 72812	
Upper teeth		r	l	r
	L		20.5	20.6
(D)P1	W		12.6	12.8
	H		10.1	9.97
	L			34.3
P2	W			35.0
	H			34.4
	L			30.9
P3	W			27.3
	H			30.6
	L	28.9	(D) 34.4	(D) 34.2 / 37.4
P4	W	33.0	(D) 29.1	(D) 31.4 / 33.4
	H	31.2	(D) 19.5	(D) 20.8 / 34.7
	L		36.0	38.5
M1	W		35.5	38.0
	H		29.1	33.3
	L			32.7
M3	W			34.6
	H			27.4

Table S3		olecranon							TDart		APDart		dia.		dis. art.		dis. epi.	
Ulna	L	TD	APD	H	TDbase	APDbase	APDart1	DAP artinf	prox1	dist	med	lat	TD	APD	TD	APD	TD	APD
MNCN 72842 (l)	—	36.8	66.8	100.9	15.1	61.5	—	—	25.9	52.8	56.2	46.1	31.9	20.4	—	—	—	—

Table S4			prox. dia.		dis. art.		dia.		dis. epi.	
Tibia	L	Lfib	TD	APD	TD	APD	TD	APD	TD	APD
MNCN 72841 (r)	—	—	—	—	—	—	—	—	71.7	56.7

Table S5				acetabulum	
Pelvis	L	l	TDcol	TD	APD
MNCN 72855 (l hemipelvis)	65.0	53.2	61.5	—	—
MNCN 72856 (r hemipelvis)	70.4	56.9	62.7	—	—

SUPPLEMENTARY DATA 1 (CONT.)

Measurements (mm) of the scaphoid (Table S6), semilunate (Table S7), magnum (Table S8), pyramidal (Table S9), pisiform (Table S10), and unciform (Table S11), ectocuneiform (Table S12), cuboid (Table S13, Mc II (Table S14), and Mc III (Table S15) of the rhinocerotid remains from Mesegar-2 (Toledo Province, Spain). Side is detailed as follows: l, left; r, right.

Table S6

	prox. art.			dis. art.					
Scaphoid	TD	APD	H	TD	APD	APD-fMa	APDfTz	APDfTr	TD	APD
MNCN 72829 (r)	30.4	55.8	45.1	29.8	34.2	16.2	18.7	13.0	18.3	41.7
MNCN 72830 (l)	30.2	55.8	44.6	28.6	33.5	16.3	17.2	14.2	19.0	42.0

Table S8

		prox. epi.		prox. art.			dia.	
Magnum	L	TD	APD	TD	APD	HfUn	TD	APD
MNCN 72835 (r)	32.1	17.2	20.0	67.3	46.1	25.7	40.9	41.5

Table S9

Pyramidal	TD	H	APD	APD prox
MNCN 72832 (r)	33.5	37.2	37.5	19.2

Table S10

Pisiform	APD	DT	H	Hcol	Hart
MNCN 72833 (r)	49.9	19.0	32.3	—	21.5

Table S11

Unciform	TD	APD	APDan	APDab
MNCN 72834 (r)	48.3	33.1	45.3	65.6

Table S12

	art. prox.			
Ectocuneiform	TD	APD	H	Hmin
MNCN 72839 (l)	35.4	37.1	22.0	19.8

Table S13

						art. prox.	
Cuboid	TD	APD	H	Hant	Hproc	TD	APD
MNCN 72838 (l)	26.5	53.6	46.0	31.3	37.7	26.2	31.9

Table S14

		prox. epi.		prox. art.		dia.			dis. art.	
Mc II	L	TD	APD	TD	APD	TD	APD	TDmd	TD	APD
MNCN 72828 (l)	131.0	20.8	28.5	16.5	23.2	26.5	13.0	33.3	25.5	26.9

Table S15

		prox. epi.		prox. art.			dia.			dis. art.	
Mc III	L	TD	APD	TD	APD	HfUn	TD	APD	TDmd	TD	APD
MNCN 72827 (l)	154.0	37.5	33.3	29.2	31.8	15.7	31.2	11.7	39.7	33.7	29.0

SUPPLEMENTARY DATA 2

Cranial, dental and postcranial characters and character states used for the cladistic analysis from Antoine et al., 2003.

SKULL

1 Nasal: lateral apophysis = 0, absent; 1, present
2 Maxillary: *foramen infraorbitalis*= 0 above premolars; 1, above molars
3 Nasal notch = 0, very short (in front of P1); 1, short (above P1-3); 2, long (above P4-M1)
4 Nasal septum = 0, never ossified; 1, ossified even sometimes
5 Nasal septum: ossified = 0, partially; 1, totally
6 Nasal/lacrymal: contact = 0, long; 1, punctual or absent
7 Orbit: anterior border = 0, above P4-M2; 1, above M3; 2, behind M3
8 Lacrymal: *processus lacrymalis*= 0, present; 1, absent
9 Frontal: *processus postorbitalis*= 0, present; 1, absent
10 Maxillary: anterior base of the *processus zygomaticus maxillari*= 0, high; 1, low
11 Zygomatic arch = 0, low; 1, high; 2, very high
12 Zygomatic arch: *processus postorbitalis*= 0, present; 1, absent
13 Zygomatic arch: *processus postorbitalis*= 0, on jugal; 1, on squamosal
14 Jugal/squamosal: suture = 0, smooth; 1, rough
15 Skull: dorsal profile = 0, flat; 1, concave; 2, very concave
16 Sphenoid: *foramen sphenorbitale* and *f. rotundum*= 0, distinct; 1, fused
17 Squamosal: area between temporal and nuchal crests = 0, flat; 1, depression
18 External auditory pseudo-meatus = 0, open; 1, partly closed; 2, totally closed (circular)
19 Occipital side = 0, inclined forward; 1, vertical; 2, inclined backward
20 Occipital: nuchal tubercle = 0, little developed; 1, developed; 2, very developed
21 Skull: back of teeth row = 0, in the posterior half; 1, restricted to the anterior half
22 Pterygoid: posterior margin = 0 nearly horizontal; 1, nearly vertical
23 Skull = 0, dolichocephalic; 1, brachycephalic
24 Nasal bones: rostral end = 0, narrow; 1, broad; 2, very broad
25 Nasal bones = 0, totally separate; 1, anteriorly separate; 2, fused
26 Nasal bones = 0, long; 1, short; 2, very long
27 Median nasal horn = 0, absent; 1, present
28 Median nasal horn = 0, small; 1, developed
29 Paired nasal horns = 0, absent; 1, present
30 Paired nasal horns = 0, terminal bumps; 1, lateral crests
31 Frontal horn = 0, absent; 1, present
32 Frontal horn = 0, small; 1, huge
33 Orbit: lateral projection = 0, absent; 1, present
34 Zygomatic width/frontal width = 0, less than 1.5; 1, more than 1.5
35 Frontal-parietal = 0, sagittal crest; 1, close frontoparietal crests; 2, distant crests
36 Occipital crest = 0, concave; 1, straight; 2, forked
37 Maxillary: *processus zygomaticus maxillari*, anterior tip = 0, progressive; 1, brutal
38 Vomer = 0, acute; 1, rounded
39 Squamosal: articular tubercle = 0, smooth; 1 high
40 Squamosal: transversal profile of articular tubercle = 0, straight; 1, concave
41 Squamosal: *foramen postglenoideum*= 0, distant from the *processus postglenoidalis*; 1, close to it.
42 Squamosal: *processus postglenoidalis*= 0, flat; 1, convex; 2, dihedron
43 Basioccipital: *foramen nervi hypoglossi*= 0, in the middle of the fossa; 1 shift antero-externally
44 Basioccipital: sagittal crest on the basilar process = 0, absent; 1, present
45 Squamosal: posterior groove on the *processus zygomaticus*= 0, absent; 1, present
46 Squamosal-occipital: *processus posttympanicus* and *processus paraoccipitalis*= 0, fused; 1, distant
47 Squamosal: *processus posttympanicus*= 0, well developed; 1, little developed; 2, huge

48 Occipital: *processus paraoccipitalis*= 0, well developed; 1, little developed
49 Occipital: *foramen magnum*= 0, circular; 1, subtriangular
50 Basioccipital: median ridge on the condyle = 0, absent; 1, present
51 Basioccipital: medial truncation on the condyle = 0, absent; 1, present
52 Basioccipital: medial truncation on the condyle = 0, present at juvenile stage; 1, still present at adult stage

MANDIBLE

53 Symphysis (orientation) = 0, very upraised; 1, upraised; 2, nearly horizontal; 3, sloping down
54 Symphysis = 0, spindly; 1, massive; 2, very massive
55 Symphysis: posterior margin = 0, in front of p2; 1, level of p2-4
56 *Foramen mentale*= 0, in front of p2; 1, level of p2-4
57 *Corpus mandibulae*: lingual groove = 0, present; 1, absent
58 *Corpus mandibulae*: lingual groove = 0, still present at adult stage; 1, present at juvenile stage only
59 *Corpus mandibulae*: base = 0, straight; 1, convex; 2, very convex
60 Ramus = 0, vertical; 1, inclined forward; 2, inclined backward
61 Ramus: *processus coronoideus*= 0, well developed; 1, little developed
62 *Foramen mandibulare*= 0, below the teeth neck; 1, above the teeth neck

TEETH

63 Compared length of the premolars/molars rows = 0, $100 \times L_{P3-4}/L_{M1-3} > 50$; 1, $42 < 100 \times L_{P3-4}/L_{M1-3} < 50$; 2, $100 \times L_{P3-4}/L_{M1-3} < 42$
64 Cheekteeth: enamel foldings = 0, absent; 1, weak; 2, developed; 3, intense
65 Cheekteeth: cement = 0, absent; 1, present
66 Cheekteeth: cement = 0, weak or variable; 1, abundant
67 Cheekteeth: shape of enamel = 0, wrinkled; 1, wrinkled and corrugated; 2, corrugated and arborescent
68 Cheekteeth: crown = 0, low; 1, high
69 Cheek teeth: crown = 0, high; 1, partial hypsodonty; 2, hypsodonty; 3, hypselodonty
70 Cheekteeth: roots = 0, distinct; 1, joined; 2, fused
71 I1 = 0, present; 1, absent
72 I1: shape of the crown cross section = 0, almond; 1, oval; 2, halfmoon NA
73 I2 = 0, present; 1, absent
74 I3 = 0, present; 1, absent
75 C1 = 0, present; 1, absent
76 i1 = 0, present; 1, absent
77 i1: crown = 0, developed, with a pronounced neck; 1, reduced
78 i2 = 0, present; 1, absent
79 i2: shape = 0, incisor-like; 1, tusk-like
80 i2: orientation = 0, parallel; 1, divergent
81 i3 = 0, present; 1, absent
82 c1 = 0, present; 1, absent
83 Upper premolars: labial cingulum = 0, always present; 1, usually present; 2, usually absent; 3, always absent
84 P2-4: crochet = 0, always absent; 1, usually present; 2, always present
85 P2-4: crochet = 0, always simple; 1, usually simple; 2, usually multiple
86 P2-4: metaloph constriction = 0, absent; 1, present
87 P2-4: lingual cingulum = 0, always present; 1, usually present; 2, usually absent; 3, always absent
88 P2-4: lingual cingulum = 0, continuous; 1, usually reduced; 2, always reduced
89 P2-4: postfossette = 0, narrow; 1, wide; 2, posterior wall
90 P2-3: antecrochet = 0, always absent; 1, usually absent; 2, usually present; 3, always present
91 P1 (in adults) = 0, always present; 1, usually present; 2, usually absent
92 P1: antero-lingual cingulum = 0, present; 1, absent
93 P2 = 0, present; 1, absent
94 P2: protocone and hypocone = 0, fused; 1, lingual bridge; 2, separated; 3, lingual wall NA
95 P2: metaloph = 0, hypocone posterior to metacone; 1, transverse; hypocone anterior to metacone

P2: lingual groove = 0, present; 1, absent

P2: protocone = 0, equal or stronger than the hypocone; 1, less strong than the hypocone

P2: protoloph = 0, present; 1, absent

P2: protoloph = 0, joined to the ectoloph; 1, sometimes interrupted; 2, always interrupted

P3-4: medifossette = 0, always absent; 1, usually absent; 2, usually present; 3, always present

P3-4: constriction of the protocone = 0, always absent; 1, usually absent; 2, usually present; 3, always present

P3-4: protocone and hypocone = 0, fused; 1, lingual bridge; 2, separate; 3, lingual wall NA

P3-4: metaloph = 0, transverse; 1, hypocone posterior to metacone; 2, hypocone anterior to metacone

P3: protoloph = 0, joined to the ectoloph; 1, interrupted

P3: crista = 0, always absent; 1, usually absent; 2, usually present; 3, always present

P3: pseudometaloph = 0, always absent; 1, sometimes present

P4: antecrochet = 0, always absent; 1, usually absent; 2, usually present; 3, always present

P4: hypocone and metacone = 0, joined; 1, separate

Upper molars: labial cingulum = 0, always present; 1, usually present; 2, usually absent; 3, always absent

Upper molars: antecrochet = 0, always absent; 1, usually absent; 2, usually present; 3, always present

Upper molars: crochet = 0, always absent; 1, usually absent; 2, usually present; 3, always present

Upper molars: crista = 0, always absent; 1, usually absent; 2, usually present; 3, always present

Upper molars: medifossette = 0, always absent; 1, usually absent; 2, usually present

Upper molars: lingual cingulum = 0, always present; 1, usually present; 2, usually absent; 3, always absent

M1-2: constriction of the protocone = 0, always absent; 1, usually absent; 2, usually present; 3, always present

M1-2: constriction of the protocone = 0, weak; 1, strong

M1-2: paracone fold = 0, present; 1, absent

M1-2: paracone fold = 0, strong; 1, weak

M1-2: metacone fold = 0, present; 1, absent

M1-2: metastyle = 0, short; 1, long

M1-2: metaloph = 0, long; 1, short

M1-2: posterior part of the ectoloph = 0, straight; 1, concave

M1-2: cristella = 0, always absent; 1, usually present; 2, always present

M1-2: posterior cingulum = 0, continuous; 1, low and reduced

M1: metaloph = 0, continuous; 1, hypocone isolated

M1: antecrochet-hypocone = 0, always separate; 1, sometimes joined; 2, always joined

M1: postfossette = 0, present; 1, usually absent

M2: protocone, lingual groove = 0, always absent; 1, usually absent; 2, always present

M2: metaloph = 0, continuous; 1, hypocone isolated

M2: mesostyle = 0, absent; 1, present

M2: mesostyle = 0, weak; 1, strong

M2: antecrochet and hypocone = 0, separate; 1, joined

M3: ectoloph and metaloph = 0, distinct; 1, fused ectometaloph

M3: shape = 0, quadrangular; 1, triangular

M3: constriction of the protocone = 0, always absent; 1, usually absent; 2, always present

M3: protocone = 0, trefoil-shape; 1, indented

M3: protoloph = 0, transverse; 1, lingually elongated

M3: posterior groove on the ectometaloph = 0, present; 1, absent

p2-3: vertical external roughnesses = 0, absent; 1, present

Lower cheekteeth: external groove = 0, developed; 1, smooth, U-shaped; 2, angular, V-shaped (NA)

Lower cheekteeth: external groove = 0, vanishing before the neck; 1, developed until the neck

Lower cheekteeth: trigonid = 0, angular; 1, rounded

Lower cheekteeth: trigonid = 0, obtuse or right dihedron; 1, acute dihedron

Lower cheek teeth: metaconid = 0, joined to the metalophid; 1, constricted

Lower cheekteeth: entoconid = 0, joined to the hypolophid; 1, constricted

Lower premolars: lingual opening of the posterior valley = 0, U-shape; 1, narrow, V-shape

147 Lower premolars: lingual cingulum = 0, always present; 1, usually present; 2, usually absent; 3, always absent
148 Lower premolars: lingual cingulum = 0, reduced; 1, continuous
149 Lower premolars: labial cingulum = 0, present; 1, usually absent; 2, absent
150 Lower premolars: labial cingulum = 0, continuous; 1, reduced
151 d1/p1 in adults = 0, always present; 1, usually present; 2, usually absent; 3, always absent
152 d1: 0, always two-rooted; 1, usually two-rooted; 2, always one-rooted
153 p2 = 0, always present; 1, usually present; 2, always absent
154 p2: paralophid = 0, isolated, spur-like; 1, curved, without constriction
155 p2: paraconid = 0, developed; 1, reduced
156 p2: posterior valley = 0, lingually open; 1, usually closed; 2, always closed
157 Lower molars: lingual cingulum = 0, always present; 1, usually present; 2, usually absent; 3, always absent
158 Lower molars: lingual cingulum = 0, reduced; 1, continuous
159 Lower molars: labial cingulum = 0, always present; 1, usually present; 2, usually absent; 3, always absent
160 Lower molars: labial cingulum = 0, continuous; 1, reduced
161 Lower molars: hypolophid = 0, transverse; 1, oblique; 2, almost sagittal
162 m2-3: lingual groove of the entoconid = 0, absent; 1, present
163 dI1 = 0, present; 1, absent
164 dI2 = 0, present; 1, absent
165 D2: mesostyle = 0, present; 1, absent
166 D3-4: mesostyle = 0, absent; 1, present
167 D2: lingual wall = 0, absent; 1, present
168 D2: secondary folds = 0, absent; 1, present
169 D2: mesoloph = 0, absent; 1, present
170 di1 = 0, present; 1, absent
171 di2 = 0, present; 1, absent
172 Lower milk teeth: constriction of the metaconid = 0, present; 1, absent
173 Lower milk teeth: constriction of the entoconid = 0, absent; 1, present
174 Lower milk teeth: protoconid fold = 0, present; 1, absent
175 d1 (in juveniles) = 0, present; 1, absent
176 d2-3: vertical external roughnesses = 0, absent; 1, present
177 d2-3: ectolophid fold = 0, present; 1, absent
178 d2: anterior groove on the ectolophid = 0, absent; 1, present
179 d2: paralophid = 0, simple; 1, double
180 d2: posterior valley = 0, always open; 1, usually open; 2, usually closed; 3, always closed
181 d3: paralophid = 0, double; 1, simple
182 d3: lingual groove on the entoconid = 0, always absent; 1, usually absent; 2, always present

POSTCRANIAL SKELETON

183 Atlas: outline of the rachidian canal = 0, bulb; 1, mushroom
184 Atlas: alar notch = 0, absent; 1, present
185 Atlas: *foramen vertebrale lateralis*= 0, absent; 1, present
186 Atlas: condyle-facets = 0, comma-like; 1, kidney-like
187 Atlas: axis-facets = 0, straight; 1, sigmoid; 2, transversally concave NA
188 Atlas: *foramen transversarium*= 0, present; 1, absent
189 Atlas: *foramen transversarium*= beside the axis-facet; 1, hidden by the axis-facet
190 Scapula = 0, elongated ($1.5 < H/APD \leq 2$); 1, very elongated ($H/APD > 2$); 2, spatula-shaped ($H/APD \leq 1.5$)
191 Scapula: glenoid fossa = 0, oval; 1, medial border straight
192 Humerus: greater trochiter = 0, high; 1, low
193 Humerus: *fossa olecrani*= 0, high; 1, low
194 Humerus: distal articulation = 0, egg cup (shallow median constriction); 1, diabolo (deep median constriction)
195 Humerus: scar on the trochlea = 0, absent; 1, present

196 Humerus: distal gutter on the epicondyle = 0, absent; 1, present
197 Radius: anterior border of the proximal articulation = 0, straight; 1, M-shaped
198 Radius: medial border of the diaphysis = 0, straight; 1, concave
199 Radius: proximal ulna-facets = 0, always separated; 1, usually separated; 2, usually fused; 3, always fused
200 Radius: insertion of the *m. biceps brachii*= 0, shallow; 1, deep
201 Radius/ulna = 0, independent; 1, in contact or fused
202 Radius: gutter for the *m. extensor carpi*= 0, deep and wide; 1, weak
203 Radius/ulna: second distal articulation = 0, absent; 1, present
204 Radius: posterior expansion of the scaphoid-facet = 0, low; 1, high
205 Ulna: angle between diaphysis and olecranon = 0, open; 1, closed
206 Ulna: anterior tubercle on the distal end = 0, absent; 1, present
207 Scaphoid: postero-proximal facet with semilunate = 0, present; 1, absent or contact
208 Scaphoid: trapezium-facet = 0, large; 1, small
209 Scaphoid: magnum-facet in lateral view = 0, concave; 1, straight
210 Scaphoid: comparison between anterior and posterior heights = 0, equal; 1, Hant < H post
211 Semilunate: ulna-facet = 0, absent; 1, present
212 Semilunate: distal border of anterior side = 0, acute; 1, rounded
213 Semilunate: anterior side = 0, keeled; 1, smooth
214 Pyramidal: distal facet for semilunate = 0, symmetric; 1, asymmetric; 2, L-shaped
215 Pyramidal: distal side = 0, triangular; 1, elliptic
216 Trapezoid: proximal border in anterior view = 0, symmetric; 1, asymmetric
217 Magnum: proximal border of the anterior side = 0, nearly straight; 1, concave
218 Magnum: indentation on the medial side = 0, absent; 1, present
219 Magnum: indentation on the medial side = 0, always shallow; 1, usually shallow; 2, always deep
220 Magnum: posterior tuberosity = 0, short; 1, long
221 Magnum: posterior tuberosity = 0, curved; 1, straight
222 Unciform: pyramidal-facet and McV-facet = 0, always separate; 1, usually separate; 2, always in contact
223 Unciform: posterior expansion of the pyramidal-facet = 0, always absent; 1, usually absent; 2, usually present; 3, always present
224 McII: magnum-facet = 0, curved; 1, straight
225 McII: anterior McIII-facet = 0, present; 1, sometimes absent
226 McII: posterior McIII-facet = 0, always absent; 1, usually absent; 2, always present
227 McII: anterior and posterior McIII-facets = 0, separated; 1, fused
228 McII: trapezium-facet = 0, always present; 1, usually present; 2, always absent
229 McIII: magnum-facet in anterior view = 0, visible; 1, invisible
230 McIV: proximal facet, outline = 0, trapezoid; 1, pentagonal; 2, triangular
231 McV: 0, functional; 1, vestigial
232 Metacarpals: insertion of the *m. extensor carpalis*= 0, flat; 1, salient
233 Coxal: *acetabulum*= 0, oval or circular; 1, subtriangular
234 Femur: trochanter major = 0, high; 1, low
235 Femur: head = 0, hemispheric; 1, medially stiff
236 Femur: surface of epiphysis of the head = 0, flat; 1, crescent-shaped
237 Femur: *fovea capitis*= 0, present; 1, absent
238 Femur: *fovea capitis*= 0, high and narrow; 1, low and wide
239 Femur: third trochanter = 0, developed; 1, very developed
240 Femur: relations between the medial lip of the trochlea and the diaphysis = 0, rupture; 1, ramp
241 Femur: proximal border of the patellar trochlea = 0, curved; 1, straight
242 Tibia: antero-distal groove = 0, present; 1, absent
243 Tibia: medio-distal gutter (tendon *m. tibialis posterior*) = 0, always present; 1, usually present; 2, always absent
244 Tibia: medio-distal gutter = 0, shallow; 1, deep
245 Tibia-fibula = 0, independent; 1, in contact or fused
246 Tibia: posterior apophysis = 0, high; 1, low

247 Tibia: posterior apophysis = 0, acute; 1, rounded
248 Fibula: proximal articulation = 0, low; 1, high
249 Fibula: distal end = 0, slender; 1, robust
250 Fibula: latero-distal gutter (tendon *peronaeus* muscles) = 0, shallow; 1, deep
251 Fibula: position of the latero-distal gutter = 0, posterior; 1, median
252 Astragalus: (Transverse Diameter/Height) ratio = 0, TD/H < 1; 1, 1 ≤ TD/H < 1.2; 2, 1.2 ≤ TD/H
253 Astragalus: (Antero-Posterior Diameter/Height) ratio = 0, APD/H < 0.65; 1, 0.65 ≤ APD/H
254 Astragalus: orientation of the fibula-facet = 0, subvertical; 1, oblique
255 Astragalus: fibula-facet = 0, flat; 1, concave
256 Astragalus: *collum tali*= 0, high; 1, low
257 Astragalus: posterior stop on the cuboid-facet = 0, present; 1, absent
258 Astragalus: caudal border of the trochlea, in proximal view = 0, sinuous; 1, nearly straight
259 Astragalus: orientation trochlea/distal articulation = 0, very oblique; 1, same axis
260 Astragalus: expansion of the calcaneus-facet 1 = 0, always present; 1, usually present
261 Astragalus: expansion of the calcaneus-facet 1 = 0, always wide and low; 1, usually wide and low; 2, always high and narrow
262 Astragalus: calcaneus-facet 1 = 0, very concave; 1, nearly flat
263 Astragalus: calcaneus-facets 2 and 3 = 0, always independent; 1, usually independent; 2, usually fused; 3, always fused
264 Calcaneus: fibula-facet = 0, always absent; 1, usually absent; 2, usually present; 3, always present
265 Calcaneus: tibia-facet = 0, always absent; 1, usually absent; 2, always present
266 Calcaneus: tuber calcanei = 0, massive; 1, slender
267 Calcaneus: insertion of the *m. fibularis longus*= 0, salient; 1, invisible
268 Navicular: cross section = 0, lozenge; 1, rectangle
269 Cuboid: proximal side = 0, oval; 1, triangular
270 Ectocuneiform: postero-lateral process = 0, weak; 1, developed
271 MtIII: proximal border of the anterior side = 0, straight; 1, concave; 2, sigmoid
272 MtIII: posterior MtII-facet = 0, present; 1, absent
273 MtIII: MtIV-facets = 0, distinct; 1, sometimes joined
274 MtIII: distal widening of the diaphysis (in adults) = 0, absent; 1, present
275 MtIII: cuboid-facet = 0, absent; 1, usually absent; 2, present
276 MtIII: cuboid-facet = 0, small; 1, large
277 MtIV: postero-proximal tuberosity = 0, isolated; 1, pad-shaped and continuous
278 Phalanx I for MtIII: symmetric insertions = 0, lateral; 1, nearly anterior
279 Limbs = 0, slender; 1, robust (brachypod)
280 Metapodials: intermediate relief = 0, high and acute; 1, low and smooth
281 Central metapodials: postero-distal tubercle on the diaphysis = 0, absent; 1, present
282 Lateral metapodials: insertion of the *m. interossei*= 0, long; 1, short (does not reach distal half of the shaft)

SUPPLEMENTARY DATA 3

Data matrix including 282 cranial, dental, and postcranial characters recorded for terminal taxa (after Antoine, 2002, 2003b, 2010). It contains four outgroup taxa (one used as real outgroup, *Tapirus terrestris*), plus 15 elasmotheres and 12 non–elasmothere rhinocerotids. Characters and character states are described in Antoine (2003, Appendix 1). Missing observations and non-applicable characters are coded '?' and '–', respectively.

Taxa	1	2	3	4	5	6	7	8	9	10	11	12	13	14	15	16	17	18	19	20	21	22	23	24	25	26	27	28	29	30	31	32	33	34	35	36	37	38	39	40	41	42	43	44	45	46	47	48	49	50	51	52	53	54	55	56	57	58	59	60
Tapirus terrestris	0	0	1	0	-	1	0	0	0	0	0	0	0	0	0	0	0	0	1	0	0	1	0	0	0	1	0	-	0	-	0	-	0	1	0	0	0	0	0	1	0	0	0	0	0	0	0	0	0	0	-	0	0	1	0	0	0	0	0
Hyrachyus eximius	0	0	0	0	-	0	0	?	0	1	1	0	0	0	0	0	0	1	0	2	0	0	0	0	0	0	0	0	-	0	-	0	-	0	0	0	0	0	?	0	0	0	0	0	0	0	0	0	0	0	0	-	0	0	0	1	0	0	0	1
Trigonias osborni	1	0	0	0	-	1	0	0	0	0	1	0	0	0	0	?	0	1	0	2	0	0	1	0	0	0	0	0	-	0	-	0	-	0	0	0	0	0	?	0	0	0	0	0	1	0	0	1	0	1	0	0	-	2	0	1	1	0	0	0	0
Ronzotherium filholi	0	1	0	0	-	?	0	0	0	0	0	1	-	0	1	1	0	0	0	0	0	0	0	1	0	0	0	0	-	0	-	0	-	0	0	1	1	1	1	0	0	0	1	0	1	0	0	0	0	0	0	0	-	0	0	0	0	0	1	0	0
Plesiaceratherium mirallesi	0	?	1	0	-	?	0	?	?	0	0	?	?	0	0	?	1	1	0	0	?	?	?	0	0	0	0	-	0	-	0	-	0	?	0	1	0	?	1	0	1	2	0	0	1	0	0	0	0	1	1	0	1	1	1	1	0	0	0	?
Protaceratherium minutum	0	0	1	0	-	?	0	?	?	0	1	?	?	?	0	?	?	0	1	0	0	?	1	0	0	0	0	-	0	-	0	-	0	?	?	?	0	?	0	?	?	?	?	?	?	?	?	?	0	?	0	?	?	?	?	?	0	1	0	?	0	1	0
Diceratherium armatum	0	0	0	0	-	?	0	1	0	1	1	0	0	0	1	?	1	2	0	2	0	1	0	0	0	0	0	-	1	1	0	-	0	0	0	0	0	1	1	0	0	1	0	1	0	?	?	?	0	0	0	?	2	0	1	0	0	0	0	0
Menoceras arikarense	0	0	0	0	-	?	0	0	0	1	1	0	0	0	1	1	0	0	1	2	0	1	?	0	0	0	0	-	1	0	0	-	0	0	?	0	0	1	0	1	0	2	0	1	1	1	0	1	1	0	0	?	1	0	1	1	1	-	1	0
Kenyatherium bishopi	?	?	?	?	?	?	?	?	?	?	?	?	?	?	?	?	?	?	?	?	?	?	?	?	?	?	?	?	?	?	?	?	?	?	?	?	?	?	?	?	?	?	?	?	?	?	?	?	?	?	?	?	?	?	?	?	?	?	?	?
Bugtirhinus praecursor	?	0	?	?	?	?	?	?	?	?	?	?	?	?	?	?	?	?	?	?	?	?	?	?	?	?	?	?	?	?	?	?	?	?	?	?	?	?	?	?	?	?	?	?	?	?	?	?	?	?	?	?	?	?	?	?	?	?	?	?
`Caementodon´caucasicum	1	?	0	0	-	?	0	?	?	0	1	?	?	?	?	?	?	?	?	?	?	?	?	0	0	0	1	0	0	-	0	-	?	?	?	?	0	?	?	?	?	?	?	?	?	?	?	?	?	?	0	1	1	1	-	1	0
Caementodon oettingenae	?	?	?	?	?	?	?	?	?	?	?	?	?	?	?	?	?	?	?	?	?	?	?	?	?	?	?	?	?	?	?	?	?	?	?	?	?	?	?	?	?	?	?	?	?	?	?	?	?	?	?	?	?	?	?	?	?	?	?	?
`Hispanotherium´ grimmi	?	0	?	0	-	?	?	?	?	?	?	?	?	?	?	?	?	?	?	?	?	?	?	0	0	?	1	0	0	-	?	?	?	?	2	0	?	?	?	?	?	?	?	?	?	?	?	?	?	?	1	0	1	1	1	-	1	0
Hispanotherium beonense	0	0	0	0	-	?	0	0	0	1	1	0	1	0	1	1	1	0	2	2	0	0	0	0	0	0	1	0	0	-	0	-	0	0	1	0	1	?	0	?	0	1	0	1	1	0	0	0	1	0	1	1	1	0	0	0	0	1	1	0
Hispanotherium corcolense	?	?	?	?	?	?	?	?	?	?	?	?	?	?	?	?	?	?	?	?	?	?	?	?	?	?	?	?	?	?	?	?	?	?	?	?	?	?	?	?	?	?	?	?	?	?	?	?	?	?	?	?	?	?	?	?	?	?	?	?
Hispanotherium matritense	0	0	0	0	-	?	0	?	?	1	1	0	-	0	?	?	0	0	?	?	1	?	?	0	0	0	0	-	0	-	0	-	0	?	1	?	1	0	1	1	0	1	0	1	1	0	0	0	1	?	?	?	1	0	1	1	0	1	1	0
`Procoelodonta´ tekkayai	?	0	1	?	?	?	?	?	?	1	?	?	?	?	?	?	?	?	?	?	?	?	?	?	?	?	?	?	?	?	?	?	?	?	?	?	0	?	?	?	?	?	?	?	?	?	?	?	?	?	?	?	?	?	?	?	?	?	?	?
Procoelodonta mongoliense	1	0	0	0	-	?	0	0	0	1	2	0	0	0	?	?	?	?	?	?	?	?	?	0	0	2	1	0	0	-	0	-	0	0	2	?	0	?	1	?	?	?	?	?	1	?	?	?	?	?	?	?	?	?	?	?	?	?	?	?	?
Huaqingtherium lintungense	0	0	0	0	-	0	0	0	0	0	1	0	-	0	1	1	1	0	2	2	0	0	0	1	0	0	1	1	0	-	0	-	1	0	2	0	0	1	0	1	0	1	0	1	1	0	0	0	1	0	0	-	1	0	1	1	0	1	1	0
`Hispanotherium´ tungurense	0	0	0	0	-	?	0	0	0	0	1	0	1	0	1	?	1	0	2	2	0	0	0	1	0	0	1	1	0	-	0	-	1	0	2	0	0	?	0	1	0	1	0	1	1	0	0	0	1	0	0	-	1	0	1	1	0	1	1	0
Iranotherium morgani	0	0	0	0	-	?	1	0	0	1	2	1	-	?	1	1	1	0	2	2	1	0	0	1	1	0	1	1	0	-	0	-	1	1	2	?	0	?	0	1	?	1	0	1	1	0	2	0	1	0	1	1	1	1	1	1	-	1	?
Parelasmotherium schansiense	0	1	1	1	0	?	2	1	0	0	1	0	1	?	1	?	1	0	2	2	1	0	0	2	2	0	1	1	0	-	0	-	1	0	2	0	0	1	0	0	0	1	?	1	0	1	2	1	0	0	1	1	?	?	?	?	?	?	?	?
Sinotherium lagrelii	?	1	1	?	?	?	2	?	?	0	?	?	?	?	?	?	?	?	?	?	?	?	?	?	?	?	?	?	?	?	?	?	?	?	?	?	?	?	?	?	?	?	?	?	?	?	?	?	?	?	?	?	?	?	?	?	?	?	1	?
Elasmotherium caucasicum	?	?	?	?	?	?	?	?	?	?	?	?	?	?	?	?	?	?	?	?	?	?	?	?	?	?	?	?	?	?	?	?	?	?	?	?	?	?	?	?	?	?	?	?	?	?	?	?	?	?	?	?	?	?	?	?	?	2	?	1	?	?	2	2
Elasmotherium sibiricum	0	1	1	1	1	?	1	-	0	0	0	1	-	?	1	1	0	0	2	2	1	0	0	0	2	0	0	-	0	-	1	1	1	0	2	2	1	1	0	0	0	2	1	1	0	1	2	1	0	0	1	1	1	2	1	1	1	-	2	2

SUPPLEMENTARY DATA 3 (CONT.)

Taxa	661	662	663	664	665	666	667	668	669	670	671	672	673	674	675	676	677	678	679	680	681	682	683	684	685	686	687	688	689	690	691	692	693	694	695	696	697	698	699	6100	6101	6102	6103	6104	6105	6106	6107	6108	6109	6110	6111	6112	6113	6114	6115	6116	6117	6118	6119	6120
Tapirus terrestris	0	0	0	0	0	-	-	0	-	0	0	0	0	0	0	0	0	0	0	0	0	0	0	0	0	0	-	0	0	0	0	0	0	0	2	0	-	1	0	0	0	0	2	0	0	0	0	0	0	0	0	0	0	0	0	0	-	0	0	0	0
Hyrachyus eximius	0	0	1	0	0	-	0	0	-	0	0	0	0	0	0	0	0	0	0	0	0	0	0	1	0	-	0	0	0	0	0	0	0	0	0	-	-	-	1	-	0	0	0	0	1	0	0	0	1	2	0	0	0	0	0	0	-	0	0	0	0
Trigonias osborni	0	?	1	0	0	-	0	0	-	?	0	1	0	0	0	0	0	0	0	1	0	1	1	0	0	-	0	0	0	0	0	0	0	0	2	0	-	0	0	1	0	0	2	0	0	0	0	0	1	0	1	0	0	0	0	0	-	0	1	0	0
Ronzotherium filholi	1	0	0	0	0	-	0	0	-	0	0	0	0	1	1	0	?	0	1	0	1	1	0	0	-	0	0	0	1	0	0	0	0	1	0	-	0	0	1	0	0	3	0	0	2	0	1	0	1	2	2	2	0	0	0	-	0	0	1	1
Plesiaceratherium mirallesi	?	?	0	0	0	-	0	0	-	0	0	1	?	?	1	0	0	0	1	0	1	1	2	2	1	0	0	0	0	1	0	0	0	1	0	-	0	0	1	2	0	2	1	0	1	0	1	0	2	2	3	0	0	1	3	0	0	0	0	1
Protaceratherium minutum	0	?	0	0	0	-	1	0	-	1	0	1	?	?	1	0	1	0	1	0	1	1	3	2	2	0	0	0	0	0	0	0	0	0	2	0	-	0	0	1	1	0	2	1	0	2	0	2	0	2	2	3	0	0	0	3	0	0	0	0	1
Diceratherium armatum	0	0	0	0	1	0	1	0	-	1	0	1	0	1	1	0	0	0	1	0	1	1	3	0	-	0	0	0	0	0	0	0	0	1	0	-	0	0	1	0	0	1	1	0	0	0	0	0	0	3	1	0	0	0	2	0	0	1	0	0
Menoceras arikarense	0	0	0	0	1	0	1	0	-	2	0	2	1	1	0	1	-	0	1	0	1	1	3	2	2	0	0	1	0	0	0	0	0	1	0	-	0	0	1	2	3	2	1	0	3	0	0	0	0	3	3	2	0	0	3	0	0	0	0	1
Kenyatherium bishopi	?	?	?	0	1	1	1	1	0	?	?	?	?	?	?	?	?	?	?	?	?	?	?	3	2	2	0	0	1	1	0	?	?	?	?	?	?	?	?	?	0	3	3	0	0	0	0	?	?	?	3	3	0	0	0	3	1	?	?	?	1
Bugtirhinus praecursor	?	?	1	0	1	0	1	0	-	1	0	2	?	?	?	?	?	?	0	1	?	?	?	0	2	0	0	3	-	1	0	0	?	0	3	1	0	0	0	1	0	1	3	1	0	0	0	0	0	0	0	3	3	0	0	1	3	1	0	1	?	?
`Caementodon´caucasicum	?	?	1	0	1	0	1	1	0	?	?	?	?	?	?	?	0	0	0	1	0	1	1	2	2	0	0	3	-	1	0	0	0	0	3	2	0	1	0	1	0	1	3	1	0	0	0	0	1	3	3	3	0	0	3	3	0	0	0	0	1
Caementodon oettingenae	?	?	?	0	1	0	1	1	0	1	0	1	?	?	?	?	?	?	0	1	?	?	?	2	2	1	0	0	1	1	0	0	?	0	3	1	0	0	0	1	0	2	3	1	0	0	0	0	0	0	3	3	0	0	2	3	1	0	1	0	1
`Hispanotherium´grimmi	?	0	1	0	1	0	1	1	0	2	?	?	?	?	?	?	0	1	1	-	-	1	1	2	2	1	0	2	1	1	0	0	0	0	3	1	0	1	0	1	1	3	3	1	0	3	0	0	0	1	3	3	0	0	3	3	1	0	1	0	1
Hispanotherium beonense	?	1	1	0	1	0	1	1	0	2	0	2	1	1	1	0	1	0	1	0	1	1	2	2	1	0	1	1	1	0	0	0	0	3	1	0	0	1	-	0	3	3	1	1	0	0	0	0	1	3	3	0	0	2	3	1	0	0	0	1
Hispanotherium corcolense	?	?	1	0	1	0	1	1	0	2	?	?	?	?	?	?	0	0	0	1	0	1	1	1	2	1	0	1	1	1	0	0	0	0	3	1	0	1	0	1	0	3	3	1	0	0	0	2	0	1	3	3	1	0	2	3	1	0	0	0	1
Hispanotherium matritense	0	1	1	0	1	0	1	1	0	2	0	?	?	?	?	?	0	0	0	1	0	1	1	2	2	2	0	2	1	1	0	0	0	0	0	3	1	0	1	0	1	0	3	3	1	0	1	0	0	0	1	3	3	1	0	2	3	1	0	0	0	1
`Procoelodonta´tekkayai	?	?	?	0	1	0	1	1	0	?	?	?	?	?	?	?	?	?	?	?	?	?	?	1	2	0	0	0	0	1	0	?	?	0	3	1	0	0	0	1	0	3	3	0	0	?	?	0	0	1	3	3	0	0	3	3	1	0	0	0	1
Procoelodonta mongoliense	?	?	?	0	1	0	2	1	0	?	?	?	?	?	?	?	?	?	?	?	?	?	?	?	0	2	0	0	3	-	1	?	?	?	?	?	?	?	?	?	?	0	3	3	1	?	?	?	0	0	1	3	3	2	0	3	3	1	0	1	0	?
Huaqingtherium lintungense	0	1	1	0	1	1	2	1	0	2	?	?	?	?	?	1	0	1	1	-	-	1	1	3	2	1	0	2	1	1	0	0	0	0	3	1	0	1	0	0	0	3	3	0	0	2	0	0	1	2	3	3	1	0	3	3	1	0	0	0	1
`Hispanotherium´tungurense	0	1	1	0	1	1	2	1	0	2	?	?	?	?	?	1	0	1	1	-	-	1	1	3	2	1	0	2	1	1	0	0	0	0	3	1	0	1	0	0	0	3	3	0	0	2	0	0	1	2	3	3	1	0	3	3	1	0	0	0	1
Iranotherium morgani	?	1	2	1	1	1	2	1	1	2	?	?	?	?	?	1	1	-	1	-	-	1	1	3	2	0	0	3	-	1	0	?	?	0	?	?	?	?	?	?	?	0	3	3	1	0	3	0	0	0	3	3	3	2	0	3	3	1	0	1	1	1
Parelasmotherium schansiense	?	?	2	1	1	1	2	1	1	2	1	-	1	1	1	?	?	?	?	?	?	?	?	3	0	-	0	3	?	1	?	2	-	0	?	?	?	?	?	?	?	0	3	3	1	?	?	?	0	0	3	3	2	2	0	3	3	1	0	1	1	0
Sinotherium lagrelii	?	?	1	2	1	1	2	1	2	2	?	?	?	?	?	?	?	?	?	?	?	?	?	3	1	0	0	3	-	1	2	2	-	0	3	0	1	0	0	1	0	3	2	1	0	2	1	3	0	3	3	1	3	0	3	3	1	0	1	1	1
Elasmotherium caucasicum	?	?	2	3	1	1	2	1	3	-	?	?	?	?	?	?	1	-	1	-	-	1	1	3	0	-	0	3	-	2	3	?	-	1	-	-	-	-	-	-	-	1	3	2	1	0	3	1	3	0	3	3	0	3	0	3	3	1	1	-	1	1
Elasmotherium sibiricum	0	0	2	3	1	1	2	1	3	-	1	-	1	1	1	1	-	1	-	-	-	1	1	3	0	-	0	3	-	2	3	2	-	-	-	-	-	-	-	-	-	1	0	3	2	1	0	2	0	3	0	3	3	0	3	0	3	3	1	1	-	1	0

| Taxa | 6 1 | 6 2 | 6 3 | 6 4 | 6 5 | 6 6 | 6 7 | 6 8 | 6 9 | 7 0 | 7 1 | 7 2 | 7 3 | 7 4 | 7 5 | 7 6 | 7 7 | 7 8 | 7 9 | 8 0 | 8 1 | 8 2 | 8 3 | 8 4 | 8 5 | 8 6 | 8 7 | 8 8 | 8 9 | 9 0 | 9 1 | 9 2 | 9 3 | 9 4 | 9 5 | 9 6 | 9 7 | 9 8 | 9 9 | 1 0 0 | 1 0 1 | 1 0 2 | 1 0 3 | 1 0 4 | 1 0 5 | 1 0 6 | 1 0 7 | 1 0 8 | 1 0 9 | 1 1 0 | 1 1 1 | 1 1 2 | 1 1 3 | 1 1 4 | 1 1 5 | 1 1 6 | 1 1 7 | 1 1 8 | 1 1 9 | 1 2 0 |
|---|---|---

SUPPLEMENTARY DATA 3 (CONT.)

| Taxa | 6 1 | 6 2 | 6 3 | 6 4 | 6 5 | 6 6 | 6 7 | 6 8 | 6 9 | 7 0 | 7 1 | 7 2 | 7 3 | 7 4 | 7 5 | 7 6 | 7 7 | 7 8 | 7 9 | 8 0 | 8 1 | 8 2 | 8 3 | 8 4 | 8 5 | 8 6 | 8 7 | 8 8 | 8 9 | 9 0 | 9 1 | 9 2 | 9 3 | 9 4 | 9 5 | 9 6 | 9 7 | 9 8 | 9 9 | 1 0 0 | 1 0 1 | 1 0 2 | 1 0 3 | 1 0 4 | 1 0 5 | 1 0 6 | 1 0 7 | 1 0 8 | 1 0 9 | 1 1 0 | 1 1 1 | 1 1 2 | 1 1 3 | 1 1 4 | 1 1 5 | 1 1 6 | 1 1 7 | 1 1 8 | 1 1 9 | 1 2 0 |
|---|---|---

Taxa	241	242	243	244	245	246	247	248	249	250	251	252	253	254	255	256	257	258	259	260	261	262	263	264	265	266	267	268	269	270	271	272	273	274	275	276	277	278	279	280	281	282
Tapirus terrestris	0	1	0	1	0	0	0	0	0	1	0	0	0	1	0	0	0	0	0	0	0	0	0	0	0	0	0	0	0	2	0	0	0	0	-	0	0	0	0	0	0	0
Hyrachyus eximius	0	0	0	0	0	0	0	0	0	0	0	0	0	0	0	0	0	0	0	0	0	0	3	0	0	0	0	0	0	0	2	1	-	0	1	0	0	0	0	0	0	0
Trigonias osborni	1	0	1	-	0	0	0	?	0	0	0	1	1	0	0	0	0	0	0	0	0	0	0	?	?	1	?	0	0	?	0	0	0	0	?	?	?	?	0	0	0	1
Ronzotherium filholi	0	0	0	0	0	0	0	0	0	0	0	1	?	0	0	0	0	1	0	0	2	0	1	0	1	0	0	1	?	0	0	0	0	0	0	-	0	?	0	0	0	0
Plesiaceratherium mirallesi	0	1	0	0	0	0	0	0	1	0	1	1	1	0	0	1	0	0	1	0	1	0	3	1	2	0	0	0	0	0	1	1	-	0	0	-	0	0	0	0	1	0
Protaceratherium minutum	0	0	?	?	0	0	0	?	?	?	?	1	1	0	0	1	0	0	1	0	0	0	1	1	0	0	0	0	0	0	2	?	?	1	0	-	?	1	0	0	0	0
Diceratherium armatum	0	0	0	0	0	0	1	1	0	0	0	1	0	0	0	0	1	0	0	0	0	0	3	1	2	0	0	1	0	0	2	0	0	1	0	-	0	0	0	0	0	1
Menoceras arikarense	0	0	0	1	0	0	1	1	0	0	0	1	1	1	0	1	0	0	1	0	1	0	3	3	2	1	0	1	1	0	1	0	0	1	1	0	0	1	0	0	0	0
Kenyatherium bishopi	?	?	?	?	?	?	?	?	?	?	?	?	?	?	?	?	?	?	?	?	?	?	?	?	?	?	?	?	?	?	?	?	?	?	?	?	?	?	?	?	?	?
Bugtirhinus praecursor	?	?	?	?	?	?	?	?	0	1	1	1	1	1	0	1	?	?	1	0	0	0	3	?	?	1	?	1	?	0	2	0	0	1	1	0	1	1	0	0	?	0
`Caementodon´caucasicum	?	?	?	?	?	?	?	?	?	?	?	1	1	1	0	1	0	0	1	0	0	0	3	?	?	?	?	?	?	?	?	?	?	?	?	?	?	1	?	0	?	?	?
Caementodon oettingenae	0	1	?	?	1	?	?	?	?	?	?	1	1	1	0	1	0	0	1	0	0	0	3	0	2	1	0	1	1	0	1	0	0	0	1	0	1	?	0	0	0	0
`Hispanotherium´ grimmi	?	1	0	1	?	1	1	?	?	?	?	1	1	1	1	1	0	?	1	0	1	0	3	1	2	1	0	1	0	0	2	0	0	1	1	0	1	1	0	1	0	0
Hispanotherium beonense	?	1	0	1	1	1	1	?	?	?	?	1	1	1	0	1	0	1	1	0	1	0	3	0	2	?	0	1	0	?	?	?	?	?	?	?	1	?	0	1	0	0
Hispanotherium corcolense	0	1	0	1	1	1	1	1	0	1	1	2	1	1	1	1	0	1	1	0	2	0	3	3	2	1	1	1	0	1	2	0	0	1	1	0	1	1	0	1	0	0
Hispanotherium matritense	?	1	0	1	1	1	1	1	0	1	1	1	1	1	0	1	0	0	1	0	1	0	3	1	2	1	0	1	0	0	1	0	0	0	0	-	1	1	0	1	0	0
`Procoelodonta´ tekkayai	?	?	?	?	?	?	?	?	?	?	?	?	?	?	?	?	?	?	?	?	?	?	?	?	?	?	?	?	?	?	?	?	?	?	?	?	?	?	?	?	?	?
Procoelodonta mongoliense	?	?	?	?	?	?	?	?	?	?	?	?	?	?	?	?	?	?	?	?	?	?	?	?	?	?	?	?	?	?	?	?	?	?	?	?	?	?	?	?	?	?
Huaqingtherium lintungense	0	1	0	1	1	1	1	?	0	1	1	1	1	1	0	1	0	?	1	0	2	0	3	?	2	1	0	1	0	0	2	?	?	?	?	?	?	1	0	1	0	0
`Hispanotherium´ tungurense	0	1	0	1	1	1	1	?	0	1	1	1	1	1	0	1	0	?	1	0	2	0	3	?	2	1	0	1	0	0	2	?	?	?	?	?	?	1	0	1	0	0
Iranotherium morgani	?	1	0	1	1	1	1	?	?	?	?	2	1	1	0	1	?	1	1	0	2	0	0	?	?	?	?	1	?	?	?	?	?	?	?	?	?	?	0	1	?	0
Parelasmotherium schansiense	?	?	?	?	?	?	?	?	?	?	?	1	1	1	0	1	0	1	1	0	2	0	0	?	?	?	?	1	?	?	?	?	?	?	?	?	?	?	0	?	?	?
Sinotherium lagrelii	?	?	?	?	?	?	?	?	?	?	?	?	?	?	?	?	?	?	?	?	?	?	?	?	?	?	?	?	?	?	?	?	?	?	?	?	?	?	?	?	?	?
Elasmotherium caucasicum	?	?	?	?	?	?	?	?	?	?	?	?	?	?	?	?	?	?	?	?	?	?	?	?	?	?	?	?	?	2	0	0	?	1	0	1	?	0	1	?	0
Elasmotherium sibiricum	?	1	2	-	1	1	1	1	0	1	1	?	?	1	0	1	?	?	1	0	2	1	0	3	2	0	1	?	?	?	?	?	?	?	?	?	?	?	0	1	0	0

SUPPLEMENTARY DATA 4

Distribution of nonambiguous apomorphies at each node of the consensus tree (as labeled in Fig. 6). Reversions are preceded by the sign '–'.

Node 1: 40^{1}, 49^{1}, 57^{1}, 72^{2}, 73^{1}, 88^{1}, 101^{3}, 130^{1}, 154^{1}, 159^{2}, 176^{1}, 235^{1}, 244^{1}, 254^{1}, 266^{1}, 275^{1}

Node 2: 27^{1}, 63^{1}, 68^{1}, 83^{2}, 89^{1}, 94^{3}, 95^{1}, 102^{3}, 116^{3}, 135^{2}, 147^{3}, 149^{1}, 157^{2}, 192^{1}, 197^{1}, 200^{1}, 205^{1}, 211^{1}, 216^{1}, 240^{1}, 242^{1}, 245^{1}, 250^{1}, 251^{1}, 277^{1}

Node 3: -35^{1}, 37^{1}, -57^{0}, 87^{1}, -114^{2}, 124^{1}

Node 4: -77^{0}, 97^{1}, 112^{1}, -122^{0}

Node 5e: 70^{2}, 77^{1}, 109^{1}, 125^{1}. 193^{1}, 198^{1}, 199^{3}, 208^{1}, 209^{1}, 221^{1}, 258^{1}, 261^{1}, 280^{1}

Node 6: -122^{0}, 167^{1}, 173^{1}

Node 7: 67^{2}, 87^{3}, 112^{2}, 126^{2}

Node 8: -57^{0}, 85^{1}, -87^{2}, 97^{1}, 99^{0}, -103^{0}, 108^{1}, -112^{1}, 124^{1}, 191^{1}, 223^{3}

Node 9: 28^{1}, 33^{1}, 66^{1}

Node 10: 21^{1}, 47^{2}, 63^{2}, 64^{1}, 68^{1}, 76^{1}, 119^{1}, 123^{1}, 127^{1}, -263^{0}

Node 11: 2^{1}, 3^{1}, 4^{1}, -40^{0}, -45^{0}, 46^{1}, 48^{1}, -49^{0}, -84^{0}, -130^{0}, 136^{1}, 137^{1}

3. A Miocene Rhinocerotidae from El Bierzo Basin (Leon Province, northwestern Spain)

Oscar Sanisidro
and Juan Carlos Gutiérrez-Marco

Abstract. We describe a rhinoceros partial rostrum with its associated mandible from the locality of Santalla del Bierzo (El Bierzo Basin, Leon Province). The rhinoceros from Santalla del Bierzo represents not only the first ones reported from the El Bierzo Cenozoic Basin, but the most Northwestern record of Miocene rhinocerotids in the Iberian Peninsula, filling a geographic gap in the fossil record of the group in the Iberian Peninsula. The craniomandibular and dental morphologies present a very distinctive morphology, characterized by is robust nasal bones with an upwards oriented tip, a bulky surface over the orbits, and a long premaxilla. On the other hand, the dentition shows continuous lingual cingula, large antecrochets, and lingually-pierced hypocones on M1-2. If compared with the European rhinocerotid record, the studied remains fall closer to the primitive forms of the genus *Diaceratherium* like that from Gannat or Saulcet, thus being determined as *Diaceratherium* sp.

INTRODUCTION

The abandoned quarry that provided the paleontological remains studied in the present work is situated right south of the N-536 road, about 50 m to the east of "El Balcón del Bierzo" regional landscape viewpoint, in the northeastern termination of the village of Santalla del Bierzo (geographic coordinates: lat. 42º30'23.5" N; long. 6º41'10,9" W; Figure 1). The village of Santalla del Bierzo is in turn located 8.5 Km southwest from Ponferrada city (Castilla y León Province, Spain; Figure 1). From the geological perspective, the fossiliferous bed lies in the upper part of the Santalla Formation at their homonymous locality, were it comprises less than 150 m of pale sandstones, gravels with polygenic pebbles (quartzite, sandstones, schists and shales) and reddish lutites, that overlie an older sequence, ca. 200 m-thick, of clays, lacustrine limestones and arkosic sandstones belonging to the Toral Formation. The latter was dated recently as Oligocene by means of two late Rupelian assemblages of fossil rodents recorded in the northern Bierzo Basin, belonging to the MP biozones 24 and 25 (Freudenthal et al., 2010; Martín-González et al., 2013).

El Bierzo Basin is the biggest in extension among the North-Western continental Cenozoic basins. Its detrital sediments of continental origin span over a 150 m stratigraphic interval fed by a system of arid and semi-arid systems of alluvial fans (Martín-González and Heredia, 2011a). These deposits were deposited unconformably overlying the altered and eroded Paleozoic basement. The present-day El Bierzo Basin of NW Spain is considered as the western prolongation of a more extensive Duero foreland basin (Figure 1), which was divided during the Alpine uplift of the Galician-Leonesian Mountains through high to moderate-dipping reverse faults (De Vicente et al., 2011; Martín-González et al., 2013; Martín-González and Heredia, 2011a, b; Rodríguez Fernández et al., 2015). Three formations have been distinguished throughout the distribution of these deposits: Toral Fm., Santalla Fm. and Médulas Fm. According with the stratigraphical superposition of the Santalla Formation over the early Oligocene Toral Formation, the Santalla Formation was considered tentatively as deposited along the Miocene epoch, in absence of biostratigraphic or chronostratigraphic data.

One of the main problems of these NW Tertiary basins is the lack of a precise dating of their sedimentary continental infillings. The only exceptions are the basins of As Pontes, which revealed an Oligocene-lower Miocene age according to micro and macromammal remains (Huerta et al., 1997; López-Martínez et al., 1993; Santanach, 1994; Santanach et al., 2005) and the Oviedo basin, dated as Eocene (Truyols et al., 1991). Recently, the study of the micromammal assemblage from Toral Fm. has attributed a lower Oligocene (MP24-MP25) age (Freudenthal et al., 2010). The remaining Santalla and Médulas Formations are considered Mio-Pliocene according to sedimentary correlations (Brell and Doval, 1974; Hérail, 1981; Martín-Serrano, 1982; Martín-Serrano et al., 1996; Vergnolle, 1990). Both Formations are considered the medial and proximal sides of a common alluvial fan system established from the South (Martín-González and Heredia, 2011a). Conversely, an older Paleogene age for the Médulas Fm. (older than the Toral Fm.) has been proposed (Freudenthal et al., 2010; Gutiérrez-Marco, 2006; Hacar et al., 1999), leaving the Santalla Fm. as the recent-most of the basin. According to

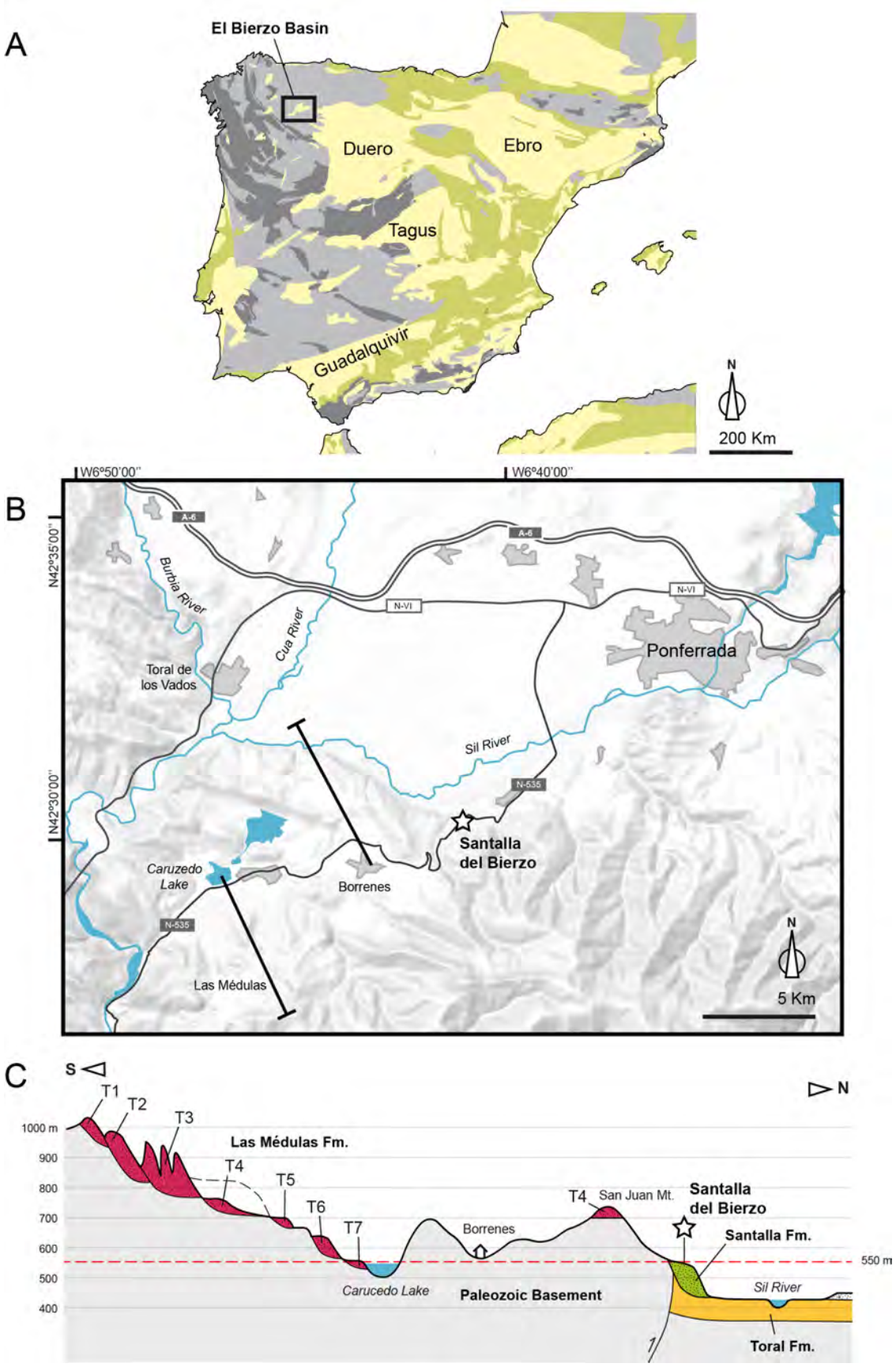


Fig. 1 A, Simplified map of the Iberian Peninsula with the main Cenozoic basins represented as yellow outlines; B, simplified map showing the fossil locality of Santalla del Bierzo (represented as a star), about 8,5 Km southwest of the Ponferrada city. C, Simplified cross section of the SW margin of the El Bierzo Basin (bar to the right of A) showing the depositional relationships of the Cenozoic Las Médulas, Santalla and Toral formations and the Quaternary terraces (T5–T7) above Lake Carucedo (sketch after M. Hacar, partly based on Hacar et al. 1999, fig. 3). Rhinocerotid remains (represented as a star) were found at an altitude of 545 m, within the upper part of the Santalla Formation at the Santalla del Bierzo section. Variscan tectonic structures have been omitted.

some authors, the Santalla Formation of El Bierzo Basin can be correlated with the Candanedo Formation of the northern Duero Basin, which ranges from the Oligocene (Colmenero et al., 1982; Corrochano, 1989) to the late Miocene (Herrero et al., 2004) in age.

Fossil vertebrates are scarcely represented in the Cenozoic basins of NW Spain, where single records of large mammals were only reported from some Eocene deposits of the Oviedo Basin (Truyols et al., 1991) and in the Oligocene coal basin of As Pontes (López-Martínez et al., 1993). The occurrence of few rodent faunas was briefly indicated in the late Eocene-early Oligocene of Asturias (Álvarez-Sierra and Daams in De Vicente et al., 2007) and lately studied by several Oligocene discoveries /samples from the El Bierzo and Sarria basins (Freudenthal et al., 2010; Martín-González et al., 2013). Scarcity of paleontological data difficult correlation among the diverse Alpine Cenozoic basins of NW Iberia, which are a relict of the complex tectonic and tectonostratigraphic evolution enhanced by the western termination of the Pyrenean-Cantabrian Orogen (De Vicente et al., 2011; Martín-González and Heredia, 2011a, b; Rodríguez Fernández et al., 2015).

The studied material consists in a large skull fragment with mandibles that was collected in 1970 in an ephemerous quarry for the search of plastic mud lenses intercalated in sandstones, placed just eastwards of the village of Santalla del Bierzo (El Bierzo region, west of the León province). The scientific author of the discovery, Mr. Ignacio Fidalgo Piensos, an historian and scholar living in Ponferrada, noticed the presence of fragments of large bones and some other post-craneal remains belonging to a partially preserved, single skeleton. Unfortunately, after this finding, only skull and mandible were recovered, embedded in a single argillaceous block. These were posteriorly donated through his daughter to the Museo Geominero of Madrid and recently prepared for the present study.

The studied specimen represents the first rhinocerotid remain from the El Bierzo Basin. Moreover, it involves interesting implications for the regional geology of the Cenozoic basins. Up to now, vertebrate remains were unknown in the Santalla Fm. The studied fossil, whose evolutive characters suggest an early Miocene age, represents the first and unique rhinoceros remains from the Neogene found in NW Iberia. The closest rhinoceros-bearing localities known to date from the nearby main Duero Basin come from the middle Miocene sediments in the vicinity of Palencia city (Leon Province). They include two skulls, originally mentioned by Dantín (1914) and Hernández-Pacheco (1915) respectively and subsequently reviewed as *Alicornops simorrense* and *Lartetotherium sansaniense* by Cerdeño (1989). In the present work we describe the cranial, associated mandible and both upper and lower dental series found in Santalla del Bierzo area and compare them with several Miocene species in order to discern their taxonomic affinities.

MATERIAL & METHODS

Institutional and locality abbreviations—The abbreviations of additional localities used for comparative purposes are detailed as follows: MNHN, Museum national d'Histoire naturelle de Paris; MHNT, Museum d'Histoire naturelle de Toulouse.

Measurements—All measurements are given in millimeters. Approximate measurements are given in parentheses. Measurements were made with a digital caliper and a measuring tape for elements larger than 150 mm.

Anatomical nomenclature and characters—Capital letters are used for upper teeth (D, P, M) and lower case letters for lower teeth (d, p, m); m. muscle. The dental terminology follows Heissig (1969), Uhlig (1999) and Antoine (2002). The cranio-dental and osteological features described correspond basically to cladistic characters used and listed by Antoine (2002) and Antoine et al. (2010) and then refined by Becker et al. (2013).

Studied material—A fragmentary rostrum (which includes the nasal and premaxilary bones; Fig. 1; Table 1) together with a palate with the two upper dental series (left P1-M3 and right M1-3; Fig. 3, Table 2) and an incomplete mandible with part of the lower series with the right p3-m3 (the left m3 incomplete) and roots of the right p2 and left p3-m2 series (both p3 and m2 incomplete) have been found (Fig. 3, Table 3). All the fragments pertain to a single individual, void of collection number. The advanced wear points to an adult, IDAS 3 stage according to Anders (2011). The referred specimen is stored in the collections of the Instituto Geológico y Minero de España (IGME).

SISTEMATIC PALEONTOLOGY

Family Rhinocerotidae Owen, 1845

Subfamily Rhinocerotinae Owen, 1845

Tribe Rhinocerotini Owen, 1845

Subtribe Teleoceratina Hay, 1902

Genus *Diaceratherium* Dietrich, 1931

Type species—*Diaceratherium tomerdingense* (Dietrich, 1931)

Included species—*Diaceratherium lamilloquense,* Michel 1983; *Diaceratherium lemanense* (Pomel, 1853); *Diaceratherium asphaltense* (Depéret and Douxami 1902); *Diaceratherium tomerdingense* Dietrich, 1931; *Diaceratherium aginense* (Répelin, 1917); *Diaceratherium askazansorense* Kordikova, 2001 and *Diaceratherium aurelianense* (Nouel, 1866).

Diaceratherium sp. (Figs. 1-3; Tables 1-3)

DESCRIPTION

Skull (Figure 2; Table 1)

The preserved rostrum is laterally compressed, has a partially broken premaxilla. They are long, almost reaching the length of the nasal bones. The rostral end is raised, possibly due to a deformation of the rostral-most part of the whole specimen (also observable in the tip of the nasal bones). Moreover, this area is deteriorated and the total length of the bone would be at the same level, if not exceed, the nasal bones. The nasal bones have a moderate length (approximately 149 mm long from the point at the level of the caudal-most point of the nasal notch), has a straight ventral profile and a slightly concave dorsal one. The section of the nasal bones at their base is 'C'-shaped, due to the partial lateral collapse of their lateral borders. The nasal notch is profound and has parallel dorso-ventral borders.

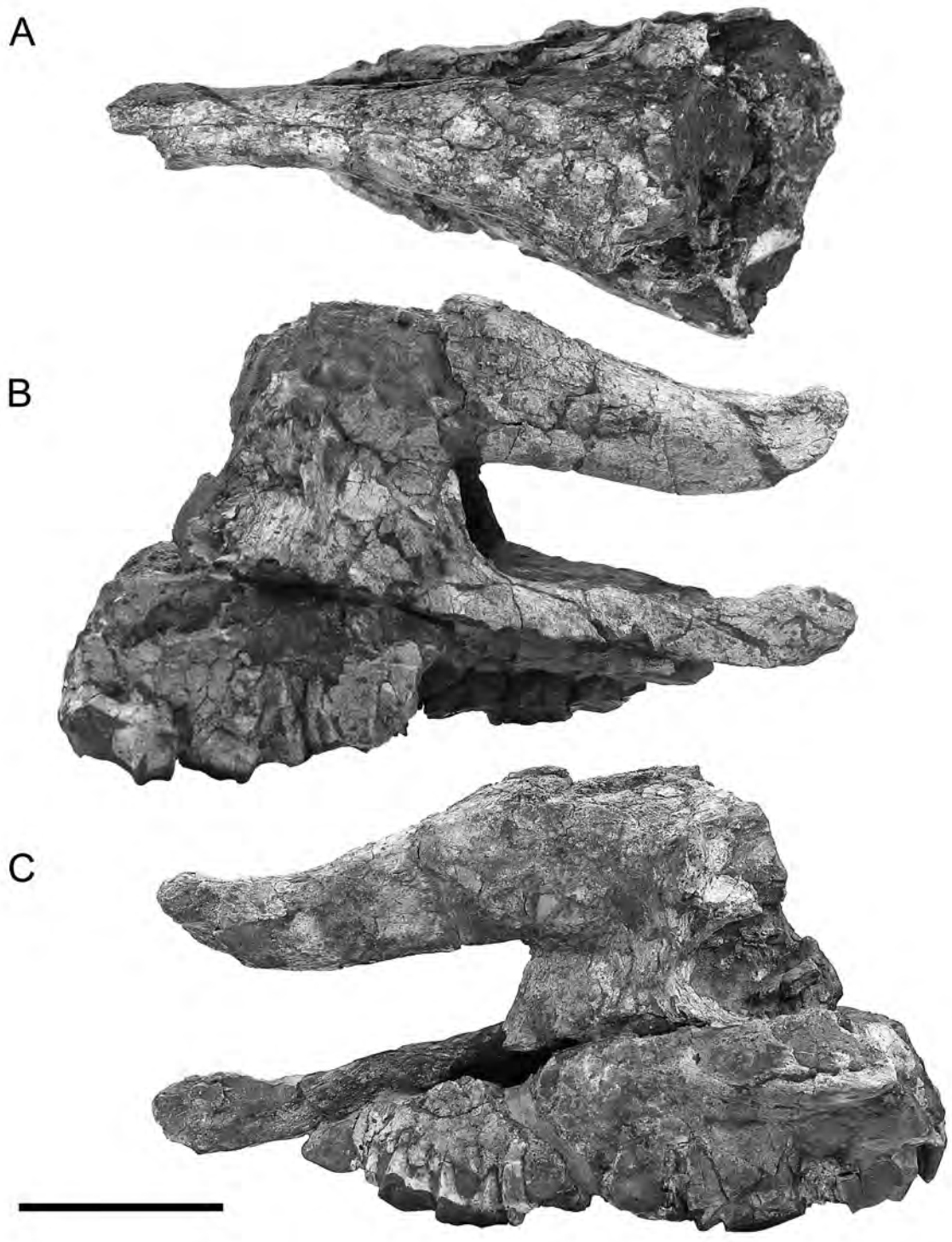


Fig. 2 Partial rostrum IGME-w/n from Santalla del Bierzo (Ponferrada, Spain) in A, proximal; B, right, and C, left views. Scale bar equals 50 mm.

The caudal border of the notch is straight and forms an acute angle with the dorsal one. The nasal tip is dorsally raised (even though probably not as much as observed on the right side, which has a fracture which increases its elevation). Its tip has a rugous surface (preserved on the right side) that does not spread through the dorso-rostral side of the tip but not to the lateral extent. The nasal suture reaches the level of the caudal-most side of the nasal notch, fading thereinafter due to the cracked surface. The base of the nasal bone is robust, high and slightly widens above the orbits. There rostral rim of the orbit is flattened, has no trace of lachrymal tubercle and is placed at the level of the M1-2 boundary. The lachrymal foramen is oval, around 95 mm high and placed over the level of the infraorbital foramen. Such foramen, more evident on the right side, is separated 18 mm from the nasal notch wall, aligned with the dorsal border of the premaxilla and placed at the level of the P4.

Mandible (Figure 2)

The mandible lacks the symphiseal region and the posterior half, including the ascending ramus. Furthermore, the cranial part of the left side is fractured and displaced. Only the anterior part of the mandible is preserved. Its lower border curves upwards. Both horizontal rami seem to be laterally compressed.

Upper series (Figure 3; Table 2)

The crowns are low, partially due to the advanced wear, pointing to an adult specimen. There is no trace of cement on the dental series. The shape of the enamel is slightly wrinkled and presents evident horizontal striations (as a result of the Hunter-Schreger bands).

The hypocone appears to be fused with the hypocone on this heavily worn P1, leaving a sinusoid lingual border. Its fragmentary condition impedes a detailed description. The P2 has a wide ectoloph (about 16 mm width), with an even and convex labial border. The parastyle is constricted by a paracone fold on the labial side and a small notch in the anterior valley on the lingual one. The latter is triangular. The protocone is smaller than the hypocone. Both are 'tear'-shaped, present loose connections with the ectoloph and contact through a lingual bridge (sensu Antoine, 1997), leaving a small, subtriangular closed median valley. The advanced wear stage has favored the contact of the hypocone with the posterior cingulum as a hooked posterior expansion of the former, almost enclosing a small and oval postfossette. There is a low and continuous labial cingulum following the shape of the gum contact. The lingual cingulum is only evident on the entrance of the (closed) median valley in form of a blunt tubercle.

The P3 has a rectangular outline. The ectoloph is very wide (18.4 mm), has a very smoothly undulated border. Both paracone style and parastyle are faint and barely protrudes from its labial border. The paracone fold left in between is very shallow. The crochet seems to be well-developed but fused to the ectoloph due to the advanced wear. Protocone and hypocone are about the same size. Both contact by means of a wide area. The protocone presents a big antecrochet delimited by a not very marked posterior protocone fold. The tooth lacks an anterior protocone fold. The anterior cingulum continues lingually. The lingual cingulum reaches the lingual midpoint of the hypocone (could be continuous and more elevated on its postero-lingual side, but the advanced wear fades out its morphology). The labial cingulum is continuous and low.

The P4 has lost part of the ectoloph. As in the P3, the antecrochet is large and rounded. The median valley of the

	IGME-w/n l / r
4. Distance between the nasal tip and notch	153.8
9. Distance between nasal notch and orbit	74.5 / 74.9
14. Distance between the nasal tip and the orbit	215.0 / 240.0
19. Width between supraorbital tuberosities	~ 105
20. Width between lachrimal tubercles	~ 110
22. Width of nasal base	55.1
25. Cranial height in front of P2	132.0
26. Cranial height in front of M1	174.0

Table 1 Cranial measurements of the rhinoceros remains from Santalla del Bierzo (Ponferrada, Spain).

Upper teeth		IGME-w/n l	r
P2	L	26.4	
	W	33.2	
	H	18.3	
P3	L	30.7	
	W	42.1	
	H	14.3	
P4	L	~ 33	
	W	~ 48	
	H	—	
M1	L	~ 41	
	W	~ 57	
	H	—	
M2	L	~ 54	~ 55
	W	~ 52	~ 50
	H	—	—
M3	L	—	51.6
	W	54.3	47.2
	H	—	—

Table 2 Upper teeth measurements from Santalla del Bierzo (Ponferrada, Spain).

P4 is not closed but very narrow (with the enamel of both antecrochet and hypocone almost in contact), sinuous and forked at its inner side. The hypocone has a narrow connection with the ectoloph through a sigmoid bridge. The closed posterior valley left posteriorly is 'pear'-shaped. As in P3, the advanced wear stage has fused the crochet with the ectoloph. The lingual cingulum is continuous, reaching the level of the hypocone and contacts the anterior and the posterior cingula.

M1 and M2 are morphologically similar. Both M1 lack the whole ectoloph (as in the left P4) and both M2 lack the anterior side of the paracone style and parastyle. Nevertheless, the ectoloph of the M2 and the maximum width of the M1 point a rectangular outline in the M1. The M2, on the other hand, present a more squared outline. The antecrochet is smaller than the P4 but better defined by a marked posterior protocone fold. The anterior protocone fold is also present and well-marked. In the M1 the anterior side of the protoloph is swollen, nearly straight in the M2. The protocone is rounded (with a slightly more flattened lingual side in the M2). The median valley is curved in the M1 and closed by the contact of the enamel between antecrochet and metaloph (while remaining unfused). In the M2 the median valley is sigmoid and wider. Antecrochet and metaloph do not contact in these teeth. There is a blunt crochet attached to the contact between metaloph and ectoloph of the M2. In the M1 the crochet is restricted to a small and pointed salient on the right side, with no trace of it on the left one. The hypocone presents a well-marked anterior folding, leaving an anterior convex area. The posterior is not as evident. The advanced wear favors the contact between hypocone and the posterior cingulum, producing a big squared area of dentine with an angulous postero-lingual side. There is a continuous cingulum from

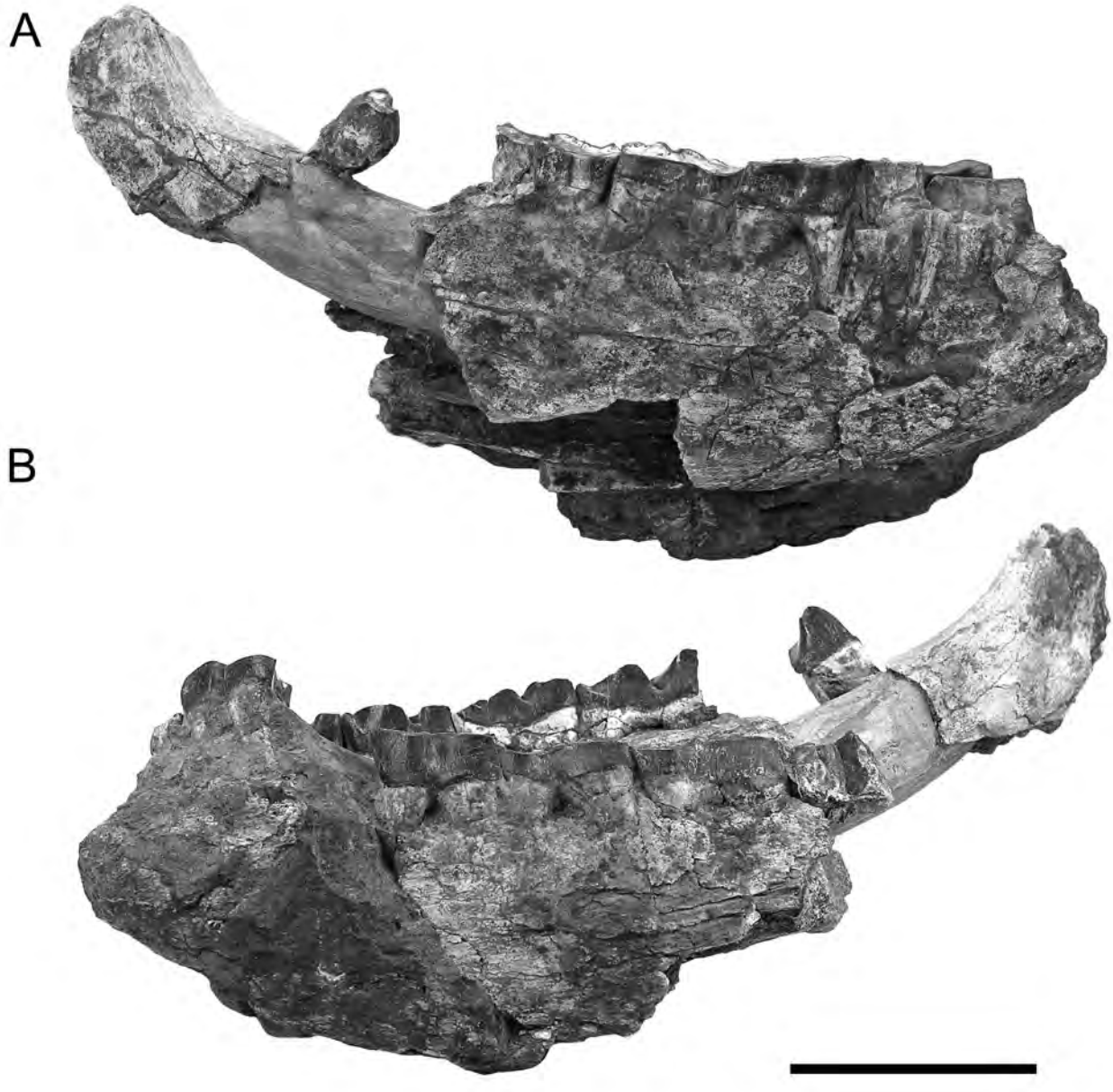


Fig. 3 Incomplete mandible IGME-w/n from Santalla del Bierzo (Ponferrada, Spain) in A, right and B, left views. Scale bar equals 50 mm.

the anterior through the entrance of the median valley on the labial one, where a big, blunt enamel bump is present (in both M1 and M2). The lingual-most extent of the hypocone is devoid of lingual cingulum. The labial side of the M2 ectoloph (the only preserved) is straight and presents a short labial cingulum attached to its posterior side.

The M3 has a characteristic quadrangular outline, giving the protoloph and ectometaloph a 'horseshoe' appearance. The ectometaloph presents a constant width and a protruding lingual border at the level of the hypocone. Its labial surface is covered with a thin layer of tartar (*sensu* Heissig, 2011). Both paracone style and parastyle are about the same size, short, blunt and separated by a wide and smooth paracone fold. The median valley is wide. A small enamel fold is present attached to the anterior side of the metaloph, possibly the remains of a worn out crochet. Likewise, in the remaining molar teeth the antecrochet is well-developed and individualized from the protocone by a marked posterior protocone fold. The anterior protocone fold is also present but weaker. The protocone has a flattened lingual side. The anterior cingulum continues on the lingual side with the lingual one. It is bumpy, low and encircles the total lingual perimeter of the tooth up to its posterior side (getting somewhat weaker in the posterior half, being almost imperceptible on the postero-lingual side of the hypocone). In the entrance of the median valley the lingual cingulum is strengthened by 3-4 bumps. It continues as a faint ridge on the posterior side and a small tubercle at the level of the interior-most border of the median valley.

Lower series (Figure 3; Table 3)

Lower teeth are represented by a left p3-m3 and roots of the missing right p2 (the m3 fragmentary) series and a right p3-m2 (both p3 and m2 incomplete).

The left p3 is anteriorly displaced from its original position in the lower series. As in the remaining teeth, the posterior valley is 'V'-shaped, deep and shows a small ridge on its anterior side. The lingual side of the metalophid is concave.

The p4 shows a narrower anterior side. The anterior labial groove is narrow and triangular. The posterior valley is similar

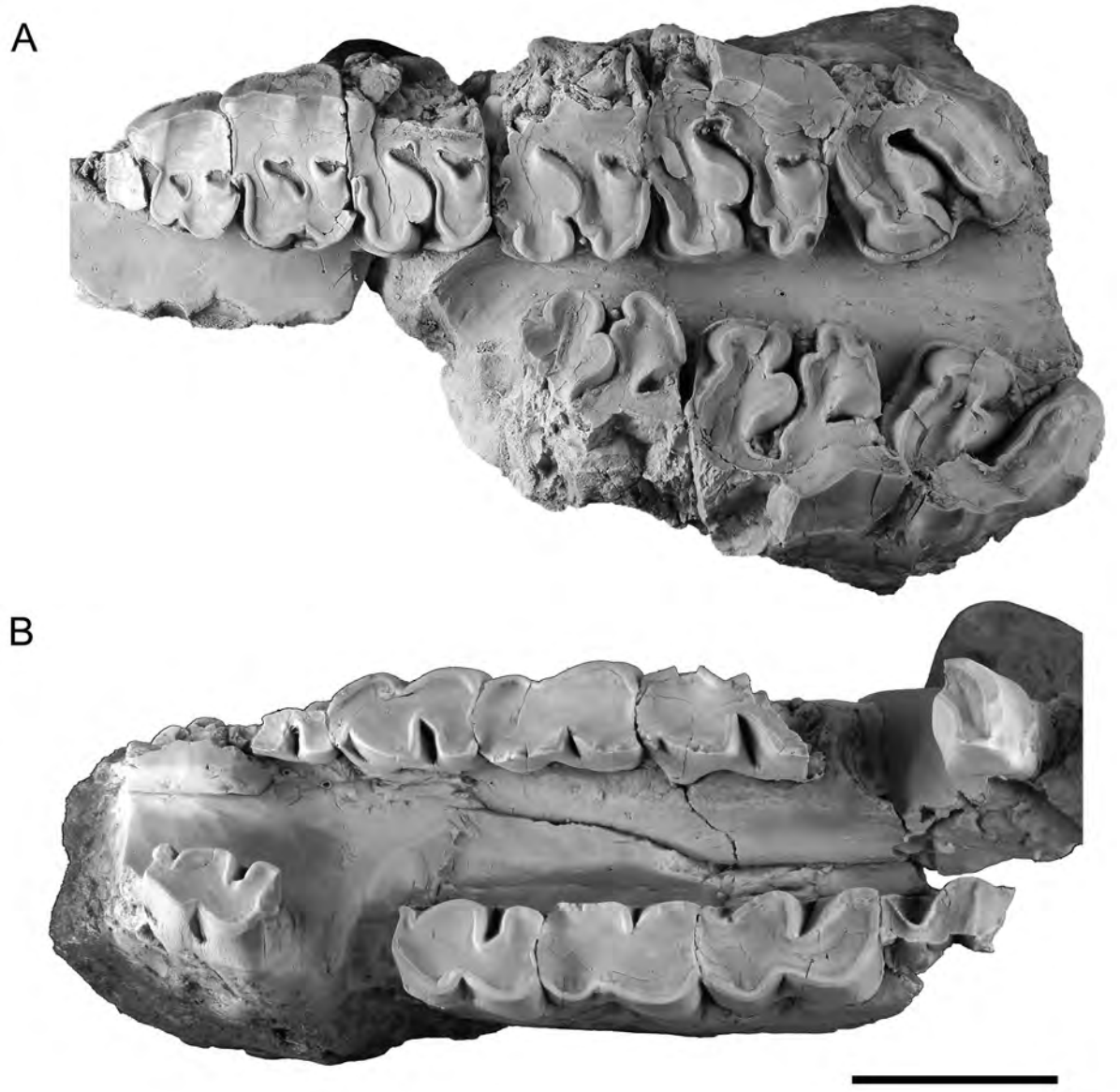


Fig. 4 Dental Rhinocerotid remains from Santalla del Bierzo (Ponferrada, Spain). A, upper teeth IGME-w/n with P1 (fragmentary)-P4 and M1-3 in occlusal view; B, partial mandible with both p3-m3 in B1, occlusal and B2, right labial views. Scale bar represents 50 mm.

Lower teeth		IGME-w/n l	r
p3	L	31.9	
	W	—	
	H	—	
p4	L	36.8	37.0
	W	26.0	26.8
	H	16.4	12.3
m1	L	39.4	39.0
	W	26.6	27.7
	H	9.3	9.1
m2	L	44.3	—
	W	25.3	25.4
	H	8.9	10.2

Table 3 Lower teeth measurements from Santalla del Bierzo (Ponferrada, Spain).

to that of the p3 but more profound. The labial groove is present but smoothed (forming an obtuse angle). It does not reach the gingival border, vanishing before the neck (which presents some bumps). The lingual side of the metalophid is concave. Its lingual border on the occlusal surface is convex. The anterior valley is 'V'-shaped too (but wider) and flanked by a faint cingulid on its anterior border. Such cingulid is present in the m1-2 too (and seems stronger as more posteriorly placed the tooth is).

The m1 are heavily worn. As a result, the ectolophid have a straight lingual border in occlusal view and the anterior valleys have almost disappeared. The posterior ones are 'V'-shaped. As in the p4, the lingual surface of the ectolophid is concave. An important feature distinguish premolar and molar teeth: the labial grooves are slightly oblique and displaced over the trigonid (clearly noticeable in the m1, not as much in the m2).

The m2 is similar to the m1 but less worn. It presents a strong antero-lingual cingulid. The hypolophid is rounded, the protoconid angulous. The lingual side of the entoconid is flat. In occlusal view, the posterior valley is triangular and anteriorly curved, the anterior is rounded and shallower. The m3 is only represented by a partial posterior side. The lingual border of the entoconid is flat and there is a short posterior cingulum that gets stronger towards the lingual side of the tooth.

DISCUSSION

Rhinoceroses are common representatives of the Iberian faunas from the early Miocene to the Late Pleistocene. All the main rhinoceros groups that diversified during the Miocene in Eurasia (i.e. Elasmotheriina, Teleoceratina, Aceratheriina and Rhinocerotini) have been recorded in the Iberian Peninsula. Its particular geographic position as an cul-de-sac in the European West end emphasizes its importance to establish the number and extension of the main Asian migrations of the group at a continental scale. Due to the controversial stratigraphic information of the locality of Santalla del Bierzo, all these major recorded in the Miocene of Western Europe (particularly the Iberian Peninsula) have been taken into account to establish a reliable taxonomic determination.

The Western European record of the Elasmotheriine rhinoceroses is restricted to the Aragonian. By far, *Hispanotherium matritense* is the commonest middle Aragonian species in the Iberian central Basins. It shows very distinctive dental characters related with a highly hypsodont dentition which differ from with the individual from Santalla del Bierzo. These include abundant cementum covering the ectoloph wall and filling the inner valleys, absence of lingual cingula, deeper enamel folding and bigger overall proportions (all typical of most Miocene elasmotheriine species and absent in Santalla del Bierzo's specimen). Additionally, the rostrum of *H. matritense* differs from the described specimen in its more slender nasal bone void of rugosities at their tips (Sanisidro et al., 2012). Other Western European elasmotheriines like *Hispanotherium beonense* or *Hispanotherium corcolense* show more plesiomorphic characters and smaller proportions but still lack the lingual cingula, the strong hypocone folding, or the antecrochet on the M3 of the studied specimen.

Rhinocerotine rhinoceroses are firstly recorded in the Iberian early Aragonian, persisting until the last glacial maximum (Álvarez-Lao and García, 2011). The strong constriction of the lingual cusps in the P4-M2 of the specimen from Santalla del Bierzo discards the ascription of several genera (i.e. *Lartetotherium*, *Dihoplus*, or *Stephanorhinus*) that display much simpler teeth morphology and a completely distinct rostral morphology dominated by its most prominent feature: a dome-like dorsal surface of the nasal bones topped with a insertion for the nasal horn together with a more elongated rostrum.

Therefore, the shortened rostrum, absence of nasal horn insertion, presence of constricted lingual cusps and the protocone/hypocone proportion in the P2-3 would point to an Aceratheriini or Teleoceratini rhinoceros.

Regarding the Aceratheres sensu lato (according to Becker et al., 2013), a small form was cited in the lower Miocene sites of Loranca and Valquemado (Cerdeño, 1989). These remains, previously identified as *Protaceratherium minutum,* share a similar cingular pattern with the specimen from Santalla del Bierzo (i.e. continuous in the premolars, incomplete in the molars and faint labial ones restricted to the anterior and posterior borders in some individuals). However, the teeth of *P. minutum* have smaller proportions and simpler enamel folding (e.g. they lack the lingual expansion of the hypocone or the deep anterior and posterior protocone constrictions).

The genus *Plesiaceratherium* is characterized by the presence of upper cheek teeth with clumsy paracone and faint constrictions on their inner cusps. Lower premolars are long and narrow, with shallow outer groove and flattened outer edge of the protoconid (together with common rugosities on the outer wall; Yan & Heissig, 1986). Premolar series of some *Plesiaceratherium* (i.e. *P. gracile* or *P. fahlbuschi*) species present always separated protocone and hypocone (Yan and Heissig, 1989; Fig. 3). All the '*Plesiaceratherium*' species share a continuous cingulum on premolars. However, the presence of a cingulum among molar teeth is variable within the genus. *P. gracile* presents a developed anterior cingulum (which continues to the anterior side of the protocone) and a strong posterior cingulum (Yan and Heissig, 1986, p. 88). On the other hand, *P. fahlbuschi* share the anterior

cingulum but lacks the tubercle on the entrance of the median valley. In this sense, the remains from Santalla del Bierzo are closer to those of *P. gracile*. The type series of *P. mirallesi* consists of the lower dentition and some limb-bones (mainly carpal bones) of a single individual (Crusafont and Truyols, 1955). Additional dental remains have been cited in the French localities of Pellecahus and Montréal-du-Gers (Béon 1) by Antoine (Antoine) and Antoine et al. (2000). If compared with the dental remains from Santalla del Bierzo, *P. mirallesi* (MHNT Béon 1040), the specimen from Santalla del Bierzo shares a similar cingular pattern (at both lingual and labial sides) and the presence of lingual bridges on premolar teeth. Alternatively, it lacks the deeply-constricted hypocone on M1-2 (probably a result of different wear degree), the large antecrochets, the inflated ectometaloph and the continuous lingual cingulum on the M3, or the presence of an anterior hypocone fold on the P4 (together with a large antecrochet). The proportions of the teeth from Santalla del Bierzo have some particularities. Premolars are shorter than *P. fahlbuschi* and *P. mirallesi* from Georgensmund and molars longer, reflecting some similarities with *Plesiaceratherium lumiarense* (Supplementary Data). Regarding the skull, the nasal bone morphology (shorter with an upraised tip with rugosities at their lateral sides) is distinct from the *Plesiaceratherium* species with known cranial remains (i.e. *Plesiaceratherium fahlbuschi*, *Plesiaceratherium naricum*, *Plesiaceratherium gracile* and *Plesiaceratherium mirallesi*), which present straight and longer nasal bones (Figure 5). All this leads to discard its inclusion in *Plesiaceratherium*.

Among Aceratheriina, Yan and Heissig (1986) listed the evolutionary changes between *Plesiaceratherium* towards later 'true' aceratheriines like *Hoploaceratherium* on several characters. The paracone is narrow (and sometimes flattened) in *Plesiaceratherium*, becoming large and obtuse in *Hoploaceratherium*. On the other hand, the parastyle fold is sharp in *Plesiaceratherium* and turns faint in the later (Yan and Heissig, 1986); finally, the lingual cingula of the upper premolars are continuous and reduced respectively. Other dental characters like the presence of the upper I1 (present in *Plesiaceratherium*, absent or vestigial in Hoploaceratherium) cannot be checked. With respect to the skull, the nasal tip of the nasals are pointed and void of rugosities in *Plesiaceratherium*, more robust and with some rugosities in *Hoploaceratherium*.

The genus *Hoploaceratherium* was created by Ginsburg and Heissig (1989) to distinguish the species *Hoploaceratherium tetradactylum* and *Hoploaceratherium bavaricum* from other European aceratheres. Out of the diagnosal characters proposed, only one, the presence of a "faint horn boss at the tip of the unfused nasals" is preserved in Santalla del Bierzo. However and as cited by the authors, this character is shared by primitive Teleoceratine species. *H. tetradactylum* has been cited in the Central Iberian localities of Andurriales, Coca and, possibly, Cerro del la Plata and Henares-1 (Cerdeño, 1992). On the other hand, is in France and Germany were the species is more abundant. The comprehensive review of the remains of *H. tetradactylum* from Sansan (Heissig, 2012) serves as a reference for our comparative purposes. The upper dental series of *H. tetradactylum* somewhat

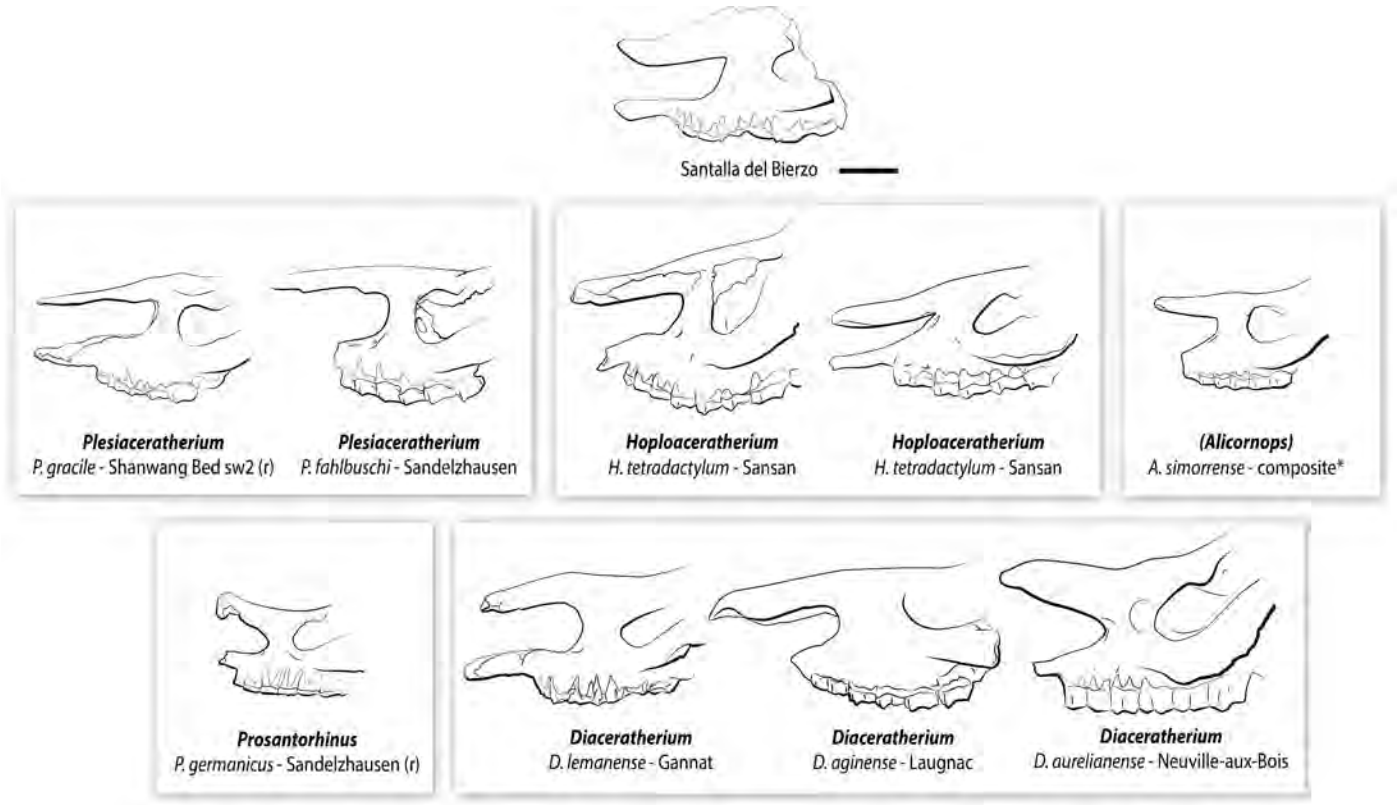


Fig. 5 Rostra comparison of several rhinoceros species from the Lower and Middle Miocene from Western Europe discussed in the text (except for *P. gracile*; China). *P. gracile*, redrawn from Defa and Heissig (1983); both *H. tetradactylum* skulls redrawn from Heissig (2012); ***D. aurelianense*** redrawn from Nouel (1866); (*A*). *simorrense* skull figured according the reconstruction published in this volume. Reversed skulls from the original publication are represented with a (r). Scale bar represents 50 mm.

resembles those from Santalla del Bierzo: both have roughly similar lingual cingular configuration (with both premolar and molar series and in the lingual and labial sides), shape and disposition of the lingual cones in the P3, folded protocone in P4-M3 and 'U'-shaped M3. However, some differences can be stressed: for a similar wear stage than the specimens from Sansan (Heissig, 2012), the rhino from Santalla del Bierzo has deeper protocone and hypocone folding, together with the mentioned small, rounded, lingual expansion of the hypocone (MNHN Sa 10170-1, Fig. 9 in Heissig, 2012) and continuous lingual cingula on both premolar and molar teeth (interrupted at the level of the cusps in the premolars of *Hoploaceratherium* and never continuous on the molar series; Heissig, 2012, p. 336). On the other hand, the proportions of the premolar teeth fall below the observed variability (shorter and narrower P2; shorter P3 and narrower P4; Figure A1). The same can be detected in the lower series (Figure A2). The presence of additional folds in the crista and crochet are highly homoplastic and must be taken with caution. The skull of *H. tetradactylum* has a relatively longer and straighter nasal bone and higher orbit, but coincides in the swollen dorsal region of the skull behind the nasal incision, the nasal notch outline and the configuration of the premaxilla. In summary, while vaguely similar, its distinct proportions and cited craniodental particularities exclude the specimen from Santalla del Bierzo from *Hoploaceratherium*.

The Teleoceratine rhinoceroses in the Iberian Peninsula are restricted to the Ramblian and lower and middle Aragonian (Cerdeño, 1992). Four species have been cited: *Brachypotherium brachypus*, *Diaceratherium aurelianense* and *Prosantorhinus douvillei*. The specimen from Santalla del Bierzo, despite similar to *Brachypotherium* in the short and broad premolar teeth and the shallow labial groove on the lower molars, differs on its deeper constriction of the protocone in the M3, the considerable smaller size (in both skull and dentition) and distinct rostrum (particularly on the longer nasal bones). *Prosantorhinus* is one of the smallest teleoceratine genera (Cerdeño, 1996). It shows a similar P4-M2 series. However, differs from Santalla del Bierzo sample on the morphology of the P2 (clearly distinct), the M3, which lacks the crochet and the deep protocone constriction and the shorter and raised nasal bone together with a shallower nasal notch (Figure 5). *Diaceratherium*, is another highly variable European teleoceratine genus. In the Iberian Peninsula the genus is represented by the species *Diaceratherium aurelianense*, which has been solely cited in the Iberian localities of Rubielos de Mora, La Artesilla, Molí Calopa and Somosaguas Norte (Cerdeño, 1992; Hernández Fernández et al., 2006). It can be distinguished from other Western European teleoceratine rhinoceroses by its moderate size, upper premolars void of crista, short M3, lower cheek teeth with not-so straight labial wall and labial cingulid rarely present (Cerdeño, 1993). The left upper row of *D. aurelianense* from Artenay MNHN Ar-2160 (lower Aragonian, MN 4a Mein's Biozone; Figured in Cerdeño, 1993) is very similar to the upper row from Santalla del Bierzo: from the distribution and development of the labial and lingual cingula to the 'horseshoe'-like M3 (including the faint crochet and the marked posterior protocone constriction). Secondly, the hypocones of the M1-2 from MNHN Ar-2160 seem to be entangled at their bases, thus they are expected to produce the lingual rounded expansion of the hypocone at more advanced wear stages (like those observed in Santalla del Bierzo). As in MNHN Ar-2160, the crista on the premolar teeth is faint. Apart from some minor differences in their dentition (i.e. the stronger lingual cingulum on molar teeth and the weaker antero-posterior constriction of the hypocone, a characteristic partially explained by the smaller wear degree in MNHN Ar-2160), their rostral morphology clearly differ, as shown in Figure 5. Interestingly, the more primitive species *Diaceratherium lemanense* can be linked with the rostrum from Santalla del Bierzo through its similar cranial proportions, inflated and stout nasal insertion, downwards nasal bones and small orbit accompanied by a relatively narrow zygomatic arch and a long premaxilla (Figure 5). Differences between them are restricted to the outline of the nasal incision, more acute in Santalla del Bierzo and a convex proximal profile of the premaxilla. Unfortunately, Gannat's *D. lemanense* pertains to a senile specimen (IDAS 5) and dental morphology cannot be compared. In addition, while premolar proportions would fit within the boundaries of *D. lemanense*, molars from Santalla del Bierzo are smaller. Significantly, other species of similar dental size to Santalla del Bierzo specimen, *Diaceratherium asphaltense* (Figure A1) figured in Becker et al., (2009; Fig. 4d) also matches the observed morphology: from the cingular pattern to the constriction of the hypocone in M1. In this case, no cranial remains have been cited for the species. In conclusion and according to the cited particularities, the studied rhinoceros remains would be ascribed to an undetermined *Diaceratherium* species.

CONCLUSIONS

The new rhinoceros remains from Santalla del Bierzo represent the first macromammal remains from El Bierzo Basin, expanding the presence of fossil rhinoceros to the North-Western basins of the Iberian Peninsula. Both skull and mandible pertain to a single, adult individual. The upper dentition is morphologically and metrically comparable with medium-sized early Miocene teleoceratines like *D. asphaltense*, *D. lamilloquense*, or *D. aginense*. In contrast, the skull displays a unique combination of characters (i.e. upwards-oriented nasal tip and angulous nasal notch together with an inflated nasal base and long premaxilla) unique among Teleoceratina. Consequently, these remains have been determined as pertaining to an undetermined form similar to the earliest forms of *Diaceratherium* described in the Lowest Miocene of Gannat or Saulcet (both MN 1, Aquitanian). These early *Diaceratherium* species are part of a described regional radiation together with a geographic expansion through Germany, Switzerland, up to Western France during

the earliest Miocene (MN 1-2) named as phase 2 (Becker et al., 2009). Our data expand the geographic boundaries of the cited diversification peak of the Lowest Miocene to the Northern Iberian Peninsula. However, the absence of further stratigraphic context impedes determining if the presence of the genus in the North Western extent of the Iberian Peninsula is really part of the diversification phase 2 or a possible persistence of the primitive forms of *Diaceratherium* posterior to the MN 1-2 in El Bierzo Basin.

The record of a large rhinocerotid from El Bierzo Basin follows the recent finding of Oligocene micromammals in two localities of the same basin (Freudenthal et al. 2010, Martín-González et al. 2013). Although the Santalla Formation are being traditionally assigned to the Miocene epoch, this is the first paleontological confirmation of such dating. The Bierzo basin represents a westwards small remnant of the Duero Basin, but the stratigraphy of its continental infill, mainly developed under the direct influx of the Alpine tectonics, is still imperfectly known. The three stratigraphic formations currently considered from the 1980's (from base to top: the Toral, Santalla and Las Médulas formations) have been changing its definition and even its stratigraphic order in the last years. First, when Hacar et al. (1999) suggested an older age for the Las Médulas Formation relative to the remaining two and second when the Las Médulas Formation was modified to integrate the Santalla Formation as a lateral equivalent of the typical gold-bearing red conglomerates and sandstones (Heredia et al., 2015).

In the present work we agree with Rodríguez-Fernández et al. (in press) in to maintain the Santalla Formation as a separate unit with a typical syntectonic character and whose stratigraphic precedence below Las Médulas Formation still rest to be unambiguously demonstrated. The main disappointing data of the work exposed by Hacar et al. (1999) and Pagés et al. (1998, 2001) with regard to the traditional geology of the area have non been solved by Heredia et al. (2015), in a work where excessive interpretation predominates over important field evidences. Some of the conclusions in the same paper also disagree with the more accurate tectonosedimentary and geotectonic model of Rodríguez Fernández et al. (in press) for El Bierzo Basin.

ACKNOWLEDGMENTS

We thank Helena Fidalgo Robleda (Ponferrada), daughter of the fossils' discoverer, for make the specimen available for study, E. Baeza Chico (Museo Geominero, Madrid) for his careful preparation of same and Carlos Alonso (Universidad Complutense de Madrid) for his photographic assistance. The regional geologist Manuel P. Hacar (deceased on December, 2014) provided us with the schematic section of the Figute 1B; he is helped for his guidance in the field and by its eternal friendship, so we want to dedicate this paper to his memory. Comments by the referees improved the manuscript.

LITERATURE CITED

Álvarez-Lao, D. J., and García, N., 2011, Southern dispersal and Palaeoecological implications of woolly rhinoceros (*Coelodonta antiquitatis*): review of the Iberian occurrences: Quaternary Science Reviews, v. 30, p. 2002-2017.

Anders, U., Koenigswald, W. v., Ruf, I., and Smith, B. H., 2011, Generalized individual dental age stages for fossil and extant placental mammals: Paläontologische Zeitschrift, v. 85, p. 321-339.

Antoine, P. O., 2000, Origine et différenciation des Elasmotheriina parmi les Rhinocerotidae (Mammalia, Perissodactyla) : analyse cladistique et implications biostratigraphiques et paléobiogéographiquesUnpublished Ph.D. dissertation], 350 p.

Antoine, P. O., 2002, Phylogénie et évolution des Elasmotheriina: (Mammalia, Rhinocerotidae): Mémoires du Muséum National d'Histoire Naturelle, v. 188, p. 5-350.

Antoine, P. O., Bulot, C., and Ginsburg, L., 2000, Une Faune rare de Rhinocérotidés (Mammalia, Perissodactyla) dans le Miocène Inférieur de Pellecahus (Gers, France): Geobios, v. 33, no. 2, p. 249-255.

Antoine, P. O., Downing, K. F., Crochet, J.-Y., Duranthon, F., Flynn, L. J., Marivaux, L., Métais, G., Rajpar, A. R., and Roohi, G., 2010, A revision of *Aceratherium blanfordi* Lydekker, 1884 (Mammalia: Rhinocerotidae) from the Early Miocene of Pakistan: postcranials as a key: Zoological Journal of the Linnean Society, v. 160, p. 139-194.

Becker, D., Antoine, P. O., and Maridet, O., 2013, A new genus of Rhinocerotidae (Mammalia, Perissodactyla) from the Oligocene of Europe: Journal of Systematic Palaeontology.

Becker, D., Bürgin, T., Oberli, U., and Scherler, L., 2009, *Diaceratherium lemanense* (Rhinocerotidae) from Eschenbach (eastern Switzerland): systematics, palaeoecology, palaeobiogeography: Neues Jahrbuch für Geologie und Paläontologie Abhandlungen, v. 245, no. 1-2, p. 5-39.

Brell, J., and Doval, M., 1974, Un ejemplo de correlación litoestratigráfica aplicado a las cuencas terciarias del NW de la Península: Estudios Geológicos, v. 30, p. 631-638.

Cerdeño, E., 1989, Revisión de la sistemática de los rinocerontes del Neógeno de EspañaPh.D. Dissertation]: Universidad Complutense de Madrid, 429 p.

-, 1992, Spanish Neogene Rhinoceroses: Palaeontology, v. 35, p. 297-308.

-, 1993, Étude sur *Diaceratherium aurelianense* et *Brachypotherium brachypus* (Rhinocerotidae, Mammalia) du Miocène moyen de France: Bulletin du Muséum national d'Histoire naturelle, Paris. Section C, v. 1-4, p. 25-77.

-, 1996, *Prosantorhinus*, the small teleoceratine rhinocerotid from the Miocene of western Europe: Geobios, v. 29, no.

1, p. 111-124.

Colmenero, J. R., García-Ramos, J. C., Manjón, M., and Vargas, I., Evolución de la sedimentación terciaria en el borde N. de la Cuenca del Duero entre los valles del Torío y Pisuerga (León-Palencia), *in* Proceedings I Reunión sobre la Geología de la Cuenca del Duero, Salamanca 1979, 1982, Volume 6, Instituto Geológico y Minero de España, p. 171-181.

Corrochano, A., 1989, Facies del Cretácico terminal y arquitectura secuencial de los abanicos terciarios del borde norte de la Depresión del Duero (Valle de las Arrimadas, León): Stvdia Geologica Salmanticensia, v. 5, p. 89-106.

Crusafont, M., and Truyols, J., 1955, El Burdigaliense Continental de la Cuenca del Vallés-Penedés, Barcelona, Consejo Superior de Investigaciones Científicas, Memorias y Comunicaciones del Instituto Geológico.

Dantin, J., 1914, Acerca de un nuevo "*Rhinoceros*" mioceno "*Rhinoceros austriacus*" PETERS, mutación "*hispanicus*": Boletín de la Sociedad Española de Historia Natural. Madrid, v. XIV, p. 391-397.

De Vicente, G., Cloetingh, S., Van Wees, J. D., and Cunha, P. P., 2011, Tectonic classification of Cenozoic Iberian foreland basins: Tectonophysics, v. 502, p. 38-61.

De Vicente, G., González-Nistral, S., Muñoz Martín, A., Vegas, R., Olaiz, A., Fernández Lozano, J., and De Vicente, R., 2007, El cabalgamiento cenozoico de Boinás (Cordillera Cantábrica, España): Geogaceta, v. 42, p. 7-10.

Defa, Y., and Heissig, K., 1983, On classification and morphology of rhinocerotid genus *Plesiaceratherium*: Vertebrata Palasiatica, v. 21, no. 2, p. 134-143.

Freudenthal, M., Martin-Suarez, E., Heredia, N., Rodriguez-Fernandez, l. R., and Martín-González, F., 2010, Rodents from the Lower Oligocene of the Bierzo Basin (Leon, Spain): Neues Jahrbuch für Geologie und Paläontologie Abhdanlungen, v. 257, p. 317-340.

Ginsburg, L., and Heissig, K., 1989, *Hoploaceratherium* n. gen., a new generic name for "*Aceratherium*" *tetradactylum* (Lartet, 1837), *in* Prothero, D., and Schoch, R. M., eds., The Evolution of Perissodactyls: New York, Oxford University Press, p. 418-421.

Guérin, C., 1980, Les rhinocéros (Mammalia, Perissodactyla) du Miocène terminal au Pléistocène supérieur en Europe occidentale : comparaison avec les espèces actuelles: Documents des Laboratoires de Géologie de Lyon, v. 79, p. 1-1184.

Gutiérrez-Marco, J. C., 2006, Hallazgo de un fósil silúrico en los depósitos auríferos cenozoicos de la mina romana de Las Médulas (León, NO de España): Geogaceta, v. 40, p. 179-182.

Hacar, M., Pagés, J. L., and Alonso, A., 1999, Nueva interpretación geológica de la mina romana de Las Médulas. El Bierzo, León: Geogaceta, v. 25, p. 83-86.

Heissig, K., 1969, Die Rhinocerotidae (Mammalia) aus der oberolizogänen Spaltenfüllung von Gaimersheim bei Ingolstadt in Bayern und ihre phylogenetische Stellung: Bayerische Akademie der Wissenschaften, Mathematisch-Naturwissenschaftliche Klasse, Abhandlungen, v. 138, p. 1-133.

-, 2012a, The American genus Penetrigonias Tanner & Martin, 1976 (Mammalia: Rhinocerotidae) as a stem group elasmothere and ancestor of *Menoceras* Troxell, 1921: Zitteliana, v. A 52, p. 79-96.

-, 2012b, Les Rhinocerotidae (Perissodactyla) de Sansan, *in* Peigné, S., and Sen, S., eds., Mammifères de Sansan, Volume 203: Paris, Muséum national d'Histoire naturelle, p. 317-485.

Hérail, G., 1981, Le Bierzo: géomorphogénese fini-tertiaire d'un bassin intramontagneux (Espagne): Revue Geographique des Pyrénées et du Sud-Ouest, v. 52, p. 217-232.

Heredia, N., Fernández, L. P., Martín-González, F., and Bahamonde, J. R., 2015, Depositional style and tectonostratigraphic evolution of El Bierzo Tertiary sub-basin (Pyrenean orogen, NW Spain): Geologica Acta, v. 13, no. 1, p. 1-23.

Hernández-Pacheco, F., and Dantín Cereceda, J., 1915, Geologia y Paleontologia del Mioceno de Palencia, Madrid, Museo Nacional de Ciencias Naturales, 295 p.:

Hernández Fernández, M., Cárdaba, J. A., Cuevas González, J., Fesharaki, O., Salesa, M. J., Corrales, B., Domingo, L., Elez Villar, J., López-Guerrero, P., Sala-Burgos, N., Morales, J., and López-Martínez, N., 2006, Los yacimientos de vertebrados del Mioceno medio de Somosaguas (Pozuelo de Alarcón, Madrid): implicaciones paleoambientales y paleoclimáticas: Estudios Geológicos, v. 62, no. 1, p. 263-294.

Herrero, A., Alonso Gavilán, G., and Colmenero, J. R., 2004, Estratigrafía del subsuelo en el sector noroeste de la cuenca del Duero (Provincia de León):: Revista de la Sociedad Geológica de España, v. 17, p. 199-216.

Huerta, A., Pares, J. M., Cabrera, L., Ferrus, B., and Saez, A., 1997, Magnetocronología de las sucesiones cenozoicas de la cuenca de As Pontes (La Coruña, noroeste de España): Acta Geológica Hispánica, v. 32, p. 127-145.

López-Martínez, N., Fernández Marrón, M., Peláez-Campomanes, P., and de la Peña Zarzuelo, A., 1993, Estudio paleontológico en las cuencas terciarias de Galicia: Revista de la Sociedad Geológica de España, v. 6, p. 19-28.

Martín-González, F., Freudenthal, M., Heredia, N., Martín-Suárez, E., and Rodríguez-Fernández, R., 2013, Palaeontological age and correlations of the Tertiary deposits of the NW Iberian Peninsula: the tectonic evolution of a broken foreland basin: Geological Journal, v. 49, no. 1, p. 15-27.

Martín-González, F., and Heredia, N., 2011a, Complex tectonic and tectonostratigraphic evolution of an alpine foreland basin: the western Duero Basin and the related Tertiary

depressions of the NW Iberian Peninsula: Tectonophysics, v. 502, p. 75-89.

-, 2011b, Geometry, structures and evolution of the western termination of the Alpine-Pyrenean Orogen reliefs (NW Iberian Peninsula): Journal of Iberian Geology, v. 37, p. 103-120.

Martín-Serrano, A., 1982, El Terciario de Galicia; Significado y posición cronoestratigrafica de sus yacimientos de lignito: Tecniterrae, v. 48, p. 19-41.

Martín-Serrano, A., Mediavilla, R., and Santisteban, J. I., 1996, North-western Cainozoic record: present knowledge and the correlation problem, *in* Friend, P. F., and J., D. C., eds., Tertiary basins of Spain: Cambridge, Cambridge University Press, p. 237-246.

Nouel, A., 1866, Mémoire sur un nouveau Rhinocéros fossile: Mémoires de la Société Agricole et Scientifique, Orléans, v. 7, p. 1-13.

Pagés, J. L., Alonso, A., and Hacar, M. P., 1998, Explotaciones romanas y mineralizaciones de oro en el sector de San Pedro de Olleros (El Bierzo, León): Cuadernos do Laboratorio Xeolóxico de Laxe, v. 23, p. 7-25.

Pagés, J. L., Hacar, M. P., and Alonso, A., 2001, Problemática de la Formacion Las Médulas y sus implicaciones morfotectónicas (El Bierzo y SE de Galicia): Geogaceta, v. 30, p. 99-102.

Peter, K., 2002, Odontologie der Nashornverwandten (Rhinocerotidae) aus dem Miozän (MN 5) von Sandelzhausen (Bayern): Zitteliana. Abhandlungen der Bayerischen Staatssammlung für Paläontologie und Geologie, v. 22, p. 3-168.

Rodríguez Fernández, L. R., Pedrera, A., Pous, J., Ayala, C., González Menéndez, L., Ibarra, P., Martín-González, F., González Cuadra, P., and H., S., 2015, Crustal structure of the south-western termination of the Alpine Pyrenean-Cantabrian Orogen (NW Iberian Peninsula): Tectonophysics, v. pre-print online 17.

Sanisidro, O., Alberdi, M. T., and Morales, J., 2011, The first complete skull of *Hispanotherium matritense* (Prado, 1864) (Perissodactyla, Rhinocerotidae) from the Middle Miocene of the Iberian Peninsula: Journal of Vertebrate Paleontology, v. in press.

Santanach, P., 1994, Las cuencas terciarias gallegas en la terminación occidental de los relieves pirenaicos: Cuadernos del Laboratorio Xeológico de Laxe, v. 19, p. 57-71.

Santanach, P., Ferrús, B., Cabrera, L., and Sáez, A., 2005, Origin of a restraining bend in an evolving strike-slip system: The Cenozoic As Pontes basin (NW Spain): Geológica Acta, v. 3, p. 225-239.

Truyols, J., Garcia Ramos, J. C., Casanovas-Cladellas, M. L., and Santafé-Llopis, J. V., 1991, El Terciario de los alrededores de Oviedo: Acta Geológica Hispánica, v. 26, p. 229-233.

Uhlig, v. U., 1999, Die Rhinocerotoidea (Mammalia) aus der unteroligozänen Spaltenfüllung Möhren 13 bei Treuchtlingen in Bayern, Abhandlungen der Bayerische Akademie der Wissenschaften, Mathematisch-Naturwissenschaftliche Klasse, Neue Folge, 254 p.:

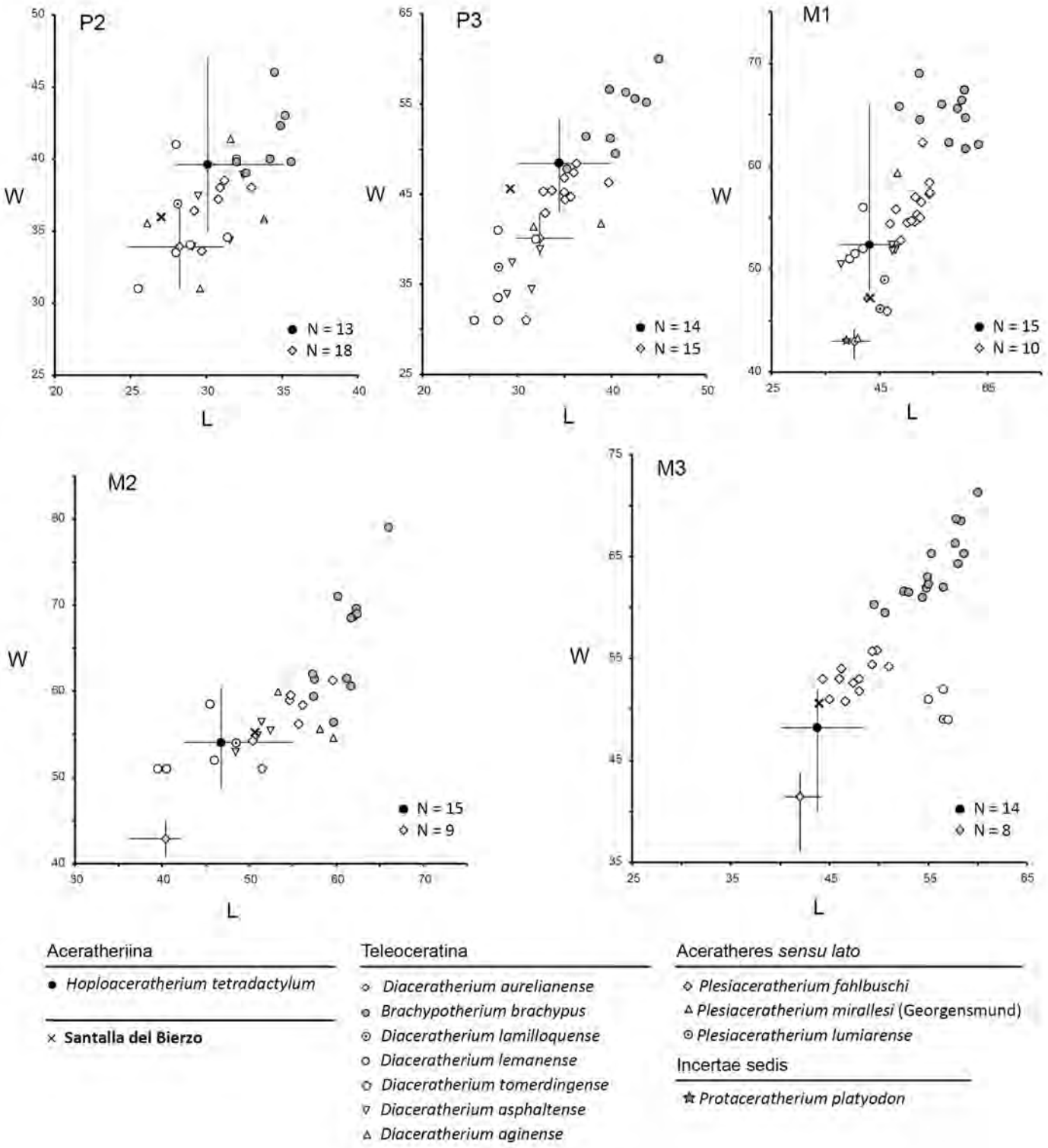
Vergnolle, C., 1990, Morfogenese des reliefs cotieres associes a la marge continentale nordespagnole. L'example du nord-est de la Galice, Laboratorio Xeolóxico de Laxe, O Castro, Serie Nova Terra 1, 315 p.:

Yan, D., and Heissig, K., 1986, Revision and Autopodial Morphology of the Chinese-European Rhinocerotid Genus *Plesiaceratherium* Young 1937: Zitteliana, v. 14, p. 81-94.

SUPPLEMENTARY DATA

FIGURE A1

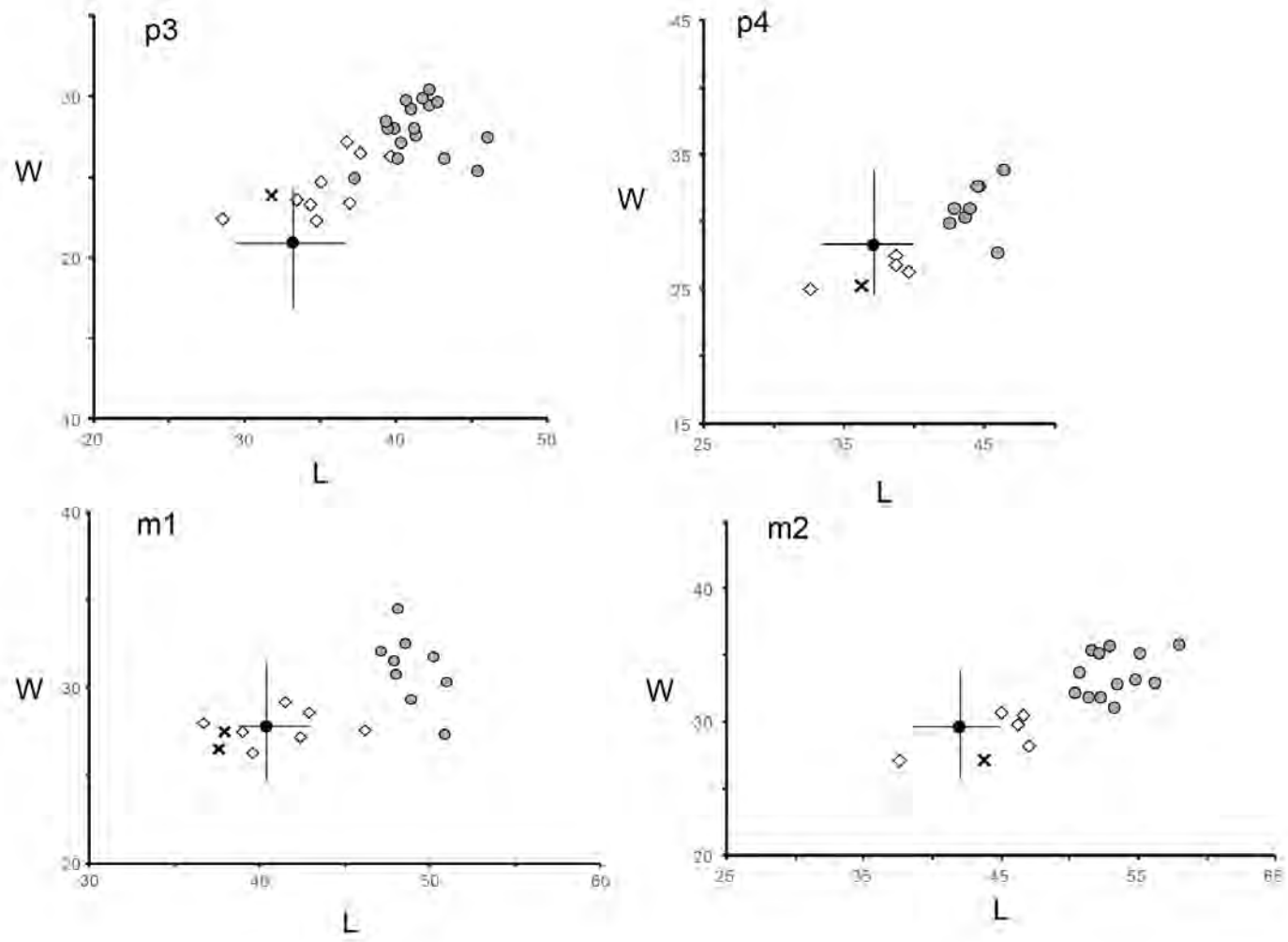
Scatter plots of the upper teeth of several rhinoceros species discussed in the text together with the sample from Santalla del Bierzo (Ponferrada, Leon Province, Spain). Measurements taken from Peter (2002), Defa and Heissig (1986), Cerdeño (1993), and Becker et al. (2009). Measurements are given in mm.



SUPPLEMENTARY DATA (CONT.)

FIGURE A2

Scatter plots of the lower teeth of several rhinoceros species discussed in the text together with the sample from Santalla del Bierzo (Ponferrada, Leon Province, Spain). Measurements taken from Peter (2002), Defa and Heissig (1986), and Cerdeño (1993). Measurements are given in mm.



4. The first complete skull of *Hispanotherium matritense* (Lartet *in* Prado, 1864) (Perissodactyla, Rhinocerotidae) from the Middle Miocene of the Iberian Peninsula

Oscar Sanisidro
María Teresa Alberdi
and Jorge Morales

Abstract. New rhinocerotid remains from the Early Middle Miocene site of Príncipe Pío-2, Madrid Basin (Madrid, Spain) are described and identified as belonging to *Hispanotherium matritense*. They constitute the first complete cranial remains recorded for this species, permitting the description of its cranial morphology and updating the species diagnosis. New remains show *H. matritense* as a Middle-sized hornless elasmotheriine rhinoceros, contrary to previous studies. Phylogenetic analysis places the Western European *Hispanotherium matritense* close to the coeval Spanish species *Hispanotherium corcolense* and more distantly related to the French species *Hispanotherium beonense*. The late Middle Miocene '*H.*' *tungurense* from Inner Mongolia is placed near more derived elasmotheres, and its belonging to the genus *Hispanotherium* is questioned.

INTRODUCTION

Hispanotherium matritense is a medium-sized rhinoceros species known from the Early Aragonian (MN4) of Western Europe to the MN6 of Asia. It was firstly defined by Prado in 1864 as *Rhinoceros matritensis* based on a few dental remains from the locality of Puente de Toledo in Madrid (Spain). Almost a century later, Crusafont and Villalta (1947) found enough differences to place this species in its own genus, naming it *Hispanotherium*. Thereafter many Iberian remains of *H. matritense* have been described (Hernández-Pacheco and Crusafont, 1960; Antunes, 1979; Aguirre et al., 1982; Antunes and Ginsburg, 1983; Cerdeño and Alberdi, 1983; Ginsburg et al., 1987; Cerdeño, 1992; Cerdeño and Iñigo, 1997). Its appearance in the Iberian central basins was interpreted as being related to an aridity increase (Cerdeño and Nieto, 1995). *H. matritense* was so abundant in these basins that lead M. T. Antunes to refer their typical Aragonian species assemblage as "*Hispanotherium* faunas" (Antunes, 1979). In addition to the Iberian specimens, remains attributed to *H. matritense* have been reported from the French locality of Faluns d'Anjou (Ginsburg et al., 1987) and the Chinese site of Laogou (Deng, 2003), extending its paleobiogeographic range beyond the Iberian Peninsula

The material described in this paper was recovered in 2007 during the construction of the Príncipe Pío transport interchange inside the city of Madrid (figure 1). The site is next to Príncipe Pío-1, where several giant tortoise remains were previously found (unpublished data). Príncipe Pío-2 site (formerly known as Intercambiador Príncipe Pío; Roca et al., 2009) revealed a rich accumulation of over a thousand remains of *H. matritense*, comprising the bulk of the fossil association. Príncipe Pío-2 is stratigraphically and geographically close to Puente de Toledo, the type locality of *H. matritense*. The fossil beds pertain to the geological Intermediate Unit of the Madrid Basin. The available data indicate a Middle Aragonian age (MN5), local zone Dc, 15 Ma (Roca et al., 2009).

The taxonomic status of some species attributed to the genus *Hispanotherium* has been a cause of debate. Our phylogenetic hypothesis is based on the data matrix made by Antoine (2000; 2003), but we are aware that other previous phylogenies have provided very different scenarios depending on the taxonomic samples used, so phylogenetic relationships within Elasmotheriina are still far from been completely settled.

The first well preserved skulls of *H. matritense* provide not only the first cranial information on the type species, but more importantly shed light on our understanding of the genus diversification during the first half of the Miocene.

MATERIAL AND METHODS

The Príncipe Pío-2 faunal assemblage contains a vast array of vertebrate remains ranging from articulated limbs

to undetermined fragments. Most of them show several taphonomical modifications like abrasion (eroded articular angles), pitting surfaces, and weathering (superficial cracking in long bone diaphysis). The material includes cranial remains, mandibles, isolated dentition, numerous limb-bone elements, vertebrae, and ribs. The great amount of recovered postcranial remains of *H. matritense* is currently under study, falling beyond the scope of the present work. The fossils studied in this paper are housed at the Museo Nacional de Ciencias Naturales (MNCN), Madrid. Measurements were taken with a digital caliper and a measuring tape for elements larger than 150 mm. They are given in millimeters with an accuracy of one decimal digit. Approximate measurements are given in parentheses. The terminology applied in the description of the anatomical characters generally follows Guérin (1980), but that used by other authors has also been taken into consideration (Heissig, 1972, 1999; Antoine, 2002).

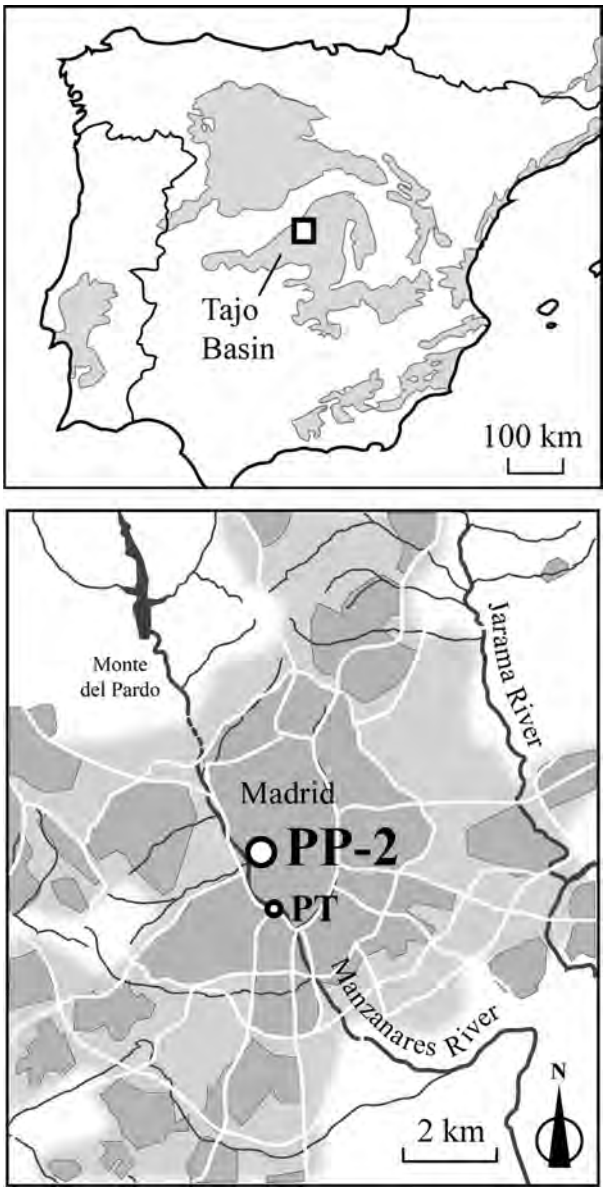


Fig. 1 Geographic location of the Miocene Iberian continental basins and the Príncipe Pío-2 site (PPio-2) and the type locality of *Hispanotherium matritense* Puente de Toledo (PTO).

Phylogenetic analyses were carried out with the software TNT: Tree Analysis Using New Technology (Goloboff et al., 2008). The character-taxon matrix has been obtained from bibliographic sources (Antoine, 2002; Antoine, 2003; Deng, 2008), completed with *H. matritense* remains from the Príncipe Pío-2 site and included the absence of nasal horn in *H. grimmi* as discussed ahead (detailed in the Supplementary Data 1 and 2 and Supplementary Data 1 of the Chapter 2). 24 terminal taxa were included. The outgroup is *Tapirus terrestris* (Linnaeus, 1758). All the characters were equally weighted and unordered. Parsimony analysis was performed with 1000 starting addition sequences and a tree-bisection-reconnection swapping algorithm (TBR). No more than ten trees from each replication were retained.

Anatomical Abbreviations—**H**, height; **L**, length; **P**, upper premolar; **M**, upper molar; **W**, width.

SYSTEMATIC PALEONTOLOGY

Order PERISSODACTYLA Owen, 1848

Family RHINOCEROTIDAE Owen, 1845

SubFamily ELASMOTHERIINAE Bonaparte, 1845

Tribe ELASMOTHERIINI Dollo, 1885

Genus *Hipanotherium* Crusafont & Villalta, 1947

Type Species—*Hispanotherium matritense* (Prado, 1864)

Emended Diagnosis—As for the type species

Hispanotherium matritense (Lartet *in* Prado, 1864)

Holotype—right M2 (unlabeled) figured in Prado (1864; fig. 5) and Crusafont and Villalta (1947; fig. 1). The type series include a left m1 figured in Prado (1864; fig. 6) and Crusafont and Villalta (1947; fig. 3). They are stored in the Museo del Instituto Geológico y Minero de España (IGME), Madrid, Spain.

Emended Diagnosis—Small sized elasmothere without nasal or frontal horns on the available sample. Nasals elongate, with the nasal notch reaching the level of the P4, a straight upper border and a concave lower profile. Anterior orbital margin above M3. Subhypsodont cheek teeth with very thick cement cover, deeply constricted protocone and slightly constricted metaconid. Upper premolars with closed median valley. Secondary folds of the enamel developed. The i2 like small tusks, with sexual dimorphism in shape and size. Postcranial skeleton slender, with a reduced non-functional McV.

Referred Material—MNCN-05/101/2/7000, MNCN-05/101/2/7001, and MNCN-05/101/2/7002. Museo Nacional de Ciencias Naturales from Madrid, Spain.

Studied Locality—Príncipe Pío-2, Madrid city, Madrid Province, Spain; Early Middle Miocene (Middle Aragonian, MN5 zone, local zone D, 14-16 Ma).

DESCRIPTION

MNCN-05/101/2/7000 is a dorsoventrally compressed skull with an incomplete left zygomatic arch, both P4-M3 series, a damaged premaxillary bone, and nasals displaced inside the nasal incision (figure 2). MNCN-05/101/2/7001 and MNCN-05/101/2/7002 are two partial skulls, laterally twisted and compressed, broken off behind the orbit and not preserving the premaxillary bone (figure 3). MNCN-05/101/2/7001 has both P1-M1 series and MNCN-05/101/2/7002 has both P3-M1. The nasal bones are laterally rotated and have their anterior tips broken. Descriptions are mainly based on MNCN-05/101/2/7000, though comparisons with the other two specimens are detailed when necessary.

Skull—The dorsal profile of the skull is almost flat, partially due to its strong dorsoventral compression. The postorbital region is slightly raised, indicating a probable original dolichocephalic skull roof. The frontal bone is flat. The braincase is wide and low, with the maximum width located between the posterior half of the zygomatic arches. The nasals are long and unfused, anteriorly pointed. Their dorsal surface is smooth and has a soft concave profile, lacking any signal of horn boss. Their ventral surface is concave, with a soft ridge flanking the internasal suture. The anterior half of the nasals is narrow, expanding at about the Middle of their total length. The nasal incision reaches the level of P4, but has been displaced because of the general backward slanting suffered by the skull. Its profile is dorsally straight and ventrally concave. Fragments of the posterior part of the premaxilla are preserved, but badly crushed. Orbits are situated just under the skull roof, with their anterior borders reaching the level of the M3; they are not laterally projected. Badly preserved oval infraorbital foramina can be observed on each side of the skull at the level of the anterior border of the P4 in MNCN-05/101/2/7000 and above the P3 level in MNCN-05/101/2/7001 and MNCN-05/101/2/7002. The supraorbital apophyses are triangular, small, pointed, laterally projected, and individualized from the orbital margins. The anterior part of each zygomatic arch constitutes a laterally developed facial crest, beginning above the anterior border of the M3. Zygomatic arches are high and fairly developed, becoming narrower posteriorly, and bending upwards at their final extreme. Frontoparietal crests are sharp and converge backward, without forming a single sagittal crest. The minimal distance between them is 11.6 mm. The occipital face is damaged, preventing its description.

The posterior border of the palate is rounded and their pterygoidean crests are straight, partially broken and diverge forming an acute angle. The basicranium has the postglenoid and posttympanic processes clEarly separated. The postglenoid process is short, oval in section, and anteriorly curved at the tip. The posttympanic process is short, oblique, and anteriorly curved. The paraoccipital process is also oblique and oriented forwards, having the same length as the posttympanic one. Paraoccipital and posttympanic processes are basally fused and placed forming a "C". The external auditory meatus is partially closed by a lateral flange of the posttympanic process, and is placed at the level of the dorsal border of the occipital condyles. The occipital foramen is oval and has the same width as each occipital condyle. These are subtriangular, with the wider surface flat and oriented downward.

Upper Dentition—The fragmented 05/101/2/7001 and MNCN-05/101/2/7002 (figure 4B), remains of cement cover the ectoloph of the premolars and fill the valleys. Cheek teeth are subhypsodont, with a softly undulated ectoloph. The protocones of M2-M3 are more constricted than that of M1; the parastyle is short and wide except on the M3, where it is very narrow and sharp; cement is present in their median valley and the postfossette of the M2. All of them belong to adult individuals, as judged from their wear degree.

P1 is oval in occlusal view. The protoloph is absent. Anterior and posterior cingula are present. The ectoloph is wide. Protocone and hypocone are connected by a wide lingual bridge. Crochet and crista are small and narrow.

	MNCN 05/101/2/7000	MNCN 05/101/2/7001
5. Minimal width of braincase	~ 105	
9. Distance between nasal notch and orbit	113.0	~ 107
13. Distance between occipital condyle and M3	~ 397	
16. Width between mastoid processes	190.0	
17. Minimal width between parietal crests	11.0	
18. Width between postorbital processes	~ 151	
20. Width between lachrimal tubercles	~ 165	
21. Maximal width between zygomatic arches	~ 284	
22. Width of nasal base	~ 65	~ 67
25. Cranial height in front of P2		~ 150
26. Cranial height in front of M1		~ 189
31. Width of foramen magnum	40.0	
32. Width between exterior borders of occipital condyles	118.0	

Table 1 Comparative measurements (mm) of the skulls of *Hispanotherium matritense* from the middle Miocene of Intercambiador Príncipe Pío (Madrid Basin, Spain).

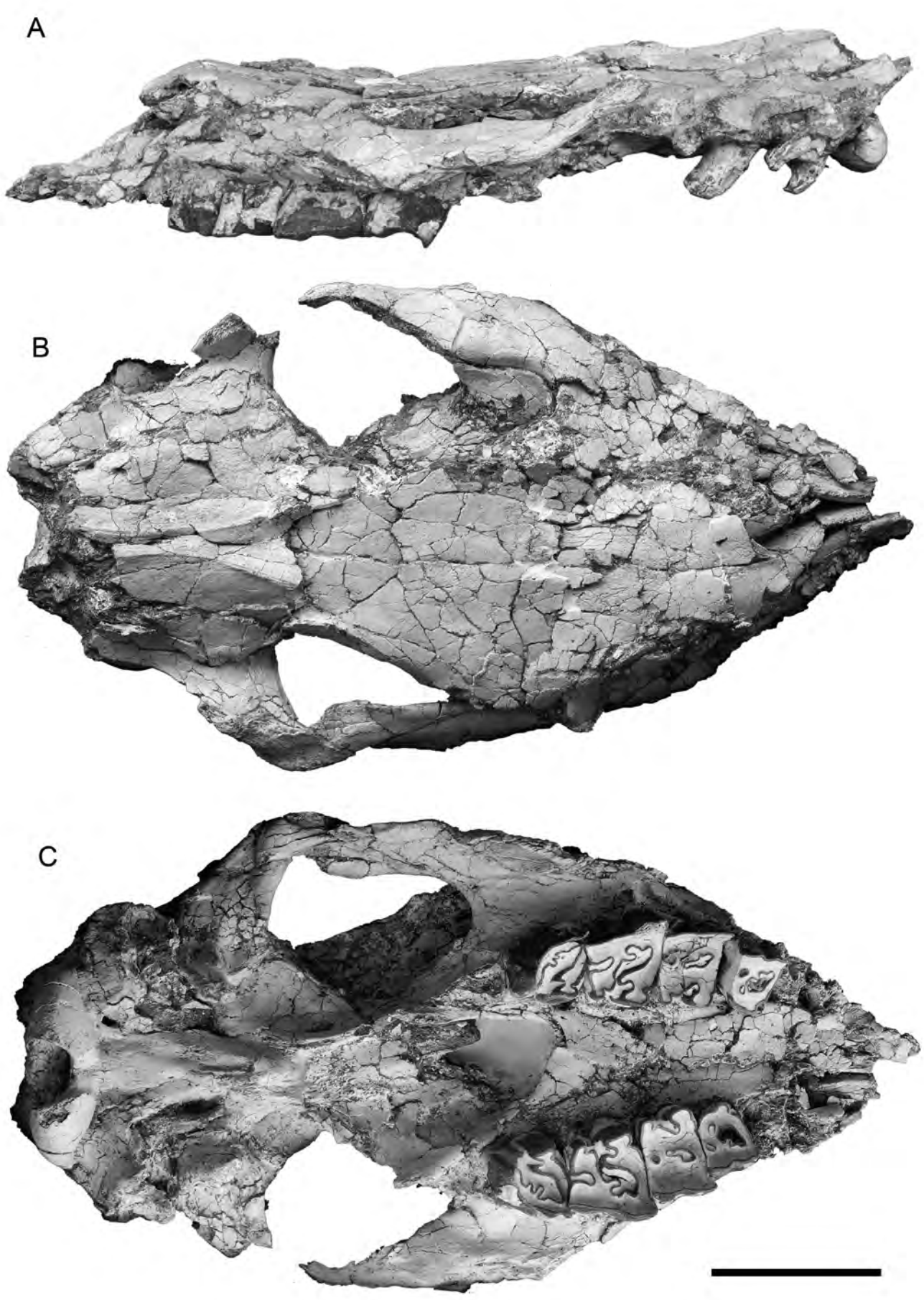


Fig. 2 Skull of the elasmotheriine rhinocerotid *Hispanotherium matritense* from the Early Middle Miocene of Príncipe Pío-2 (Madrid Basin, Spain), MNCN-05/101/2/7000. A, left view; B, dorsal view; C, occlusal view. Scale bar equals 100 mm.

P2 is square in occlusal view, the protocone is rounded. The hypocone is lingually expanded in the lingual side and is smaller than the protocone. The posterior cingulum is well developed, and encloses a small posterior valley. The anterior and lingual cingulum are absent. Crochet and crista are fused, forming a rounded small medifossete.

The protocone of P3 is rounded, has a flat lingual side, and both anterior and posterior protocone folds well developed. The ectoloph and the lingual bridge are broad and have the same width. The protoloph has a pointed fold on its lingual side that contacts with the base of the protocone. As in P2, crista and crochet are united, forming a rounded median valley, filled with cementum.

In P4, the protocone is smooth and rounded, with the anterior fold slightly more developed than the posterior one; hypocone and protocone are fused, delimiting a close median valley; the ectoloph is much wider than protoloph and metaloph; double crochet present; the labial crochet is blunt and short, the lingual crochet is narrow, very long, lingually oriented, and contacts with the lingual bridge, closing a small oval fossette; the crista is short and smooth; the parastyle is narrow and the mestastyle is wide; there is a shallow, oval postfossette; the lingual cingulum is a low smooth ridge extending posteriorly from the protocone, more developed in the right P4. In MNCN-05/101/2/7001, crista and crochet are rounded and separated.

M1 is squared in oclusal view and heavily worn; protocone is rounded and constricted at both sides. Due to its advanced wear, metaloph and protoloph are fused, delimiting a closed median valley. The postfossette is reduced and rounded. The anterior cingulum is absent. The metastyle is wide. The hypocone has a small lingual rounded expansion limited by an anterior groove.

M2 is larger than M1 and has a longer ectoloph that gives a

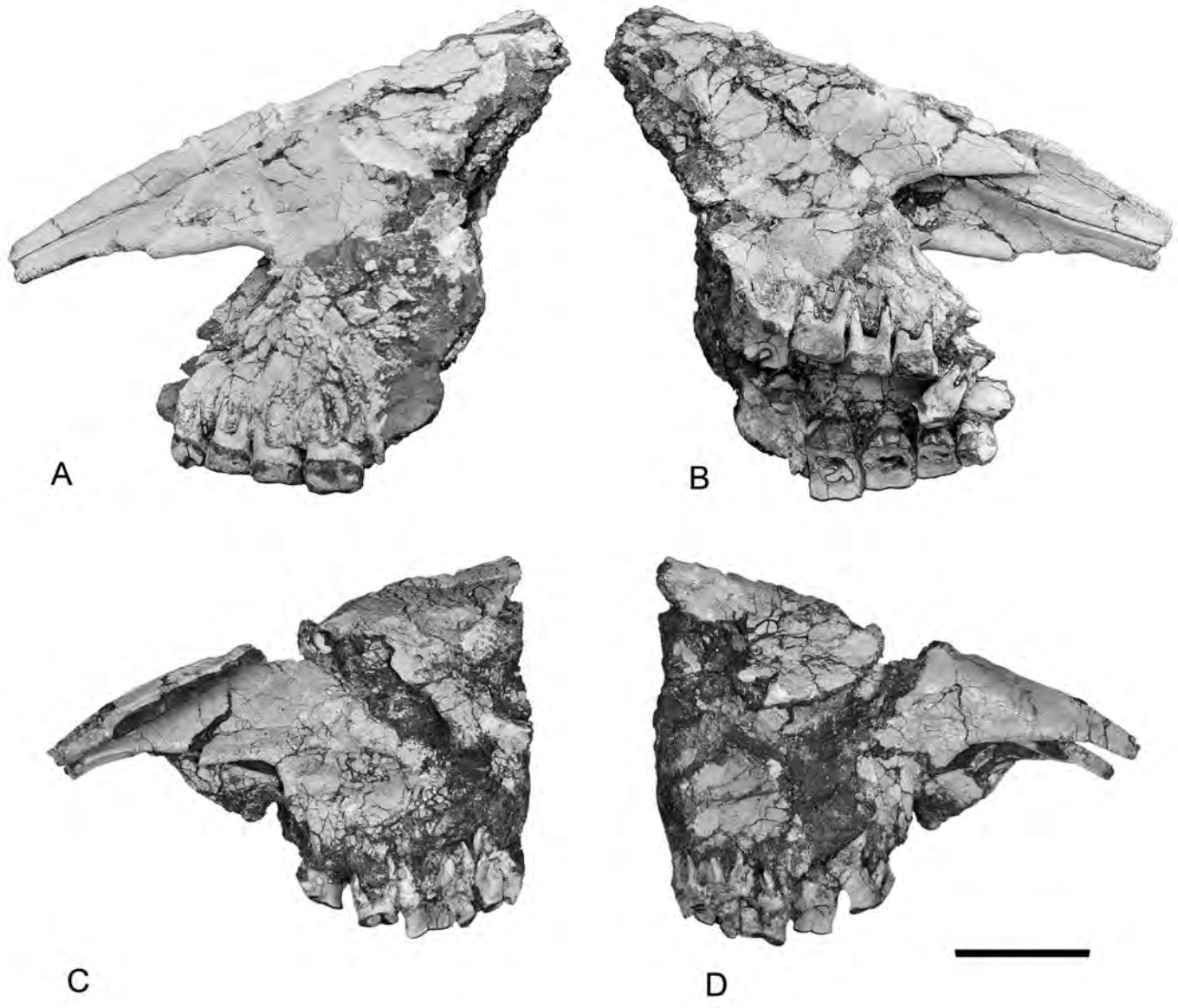


Fig. 3 Fragmentary skulls of the elasmotheriine rhinocerotid *Hispanotherium matritense* from the Early Middle Miocene of Príncipe Pío-2 (Madrid Basin, Spain) in lateral view. A, B, MNCN-05/101/2/7001; C, D, MNCN-05/101/2/7002. Scale bar equals 100 mm.

more 'fan'-like shape in occlusal view. The protocone is wide, strongly constricted, and lingually flattened. The antecrochet is strong, extending posteriorly as a hanging expansion into the median valley, but it does not reaches the metaloph at the present stage of wear, leaving a narrow opening of the median valley. The crochet is thick and short; the crista is present but poorly developed. The metastyle is wide and long. The protocone is well developed, expanded, square and has an expansion similar to that of M1. The posterior cingulum is present, closing a narrow and curved posterior valley filled with cement. Cement also fills the median valley. No anterior cingulum has been observed.

M3 has a typical triangular occlusal surface; the protocone has a flat to slightly concave lingual border, is wider and more constricted than the M2. The hypocone is less developed than the protocone. Antecrochet and crista are absent. There are two crochets and a third incipient expansion. A tiny fossette is present in the median valley of the right M3, in front of the labialmost crochet. Protoloph is oblique, oriented posteriorly and has a triangular expansion, less developed than the M2. The protoloph-ectometaloph connection is narrow. The ectometaloph is labially convex, it has a constant width and

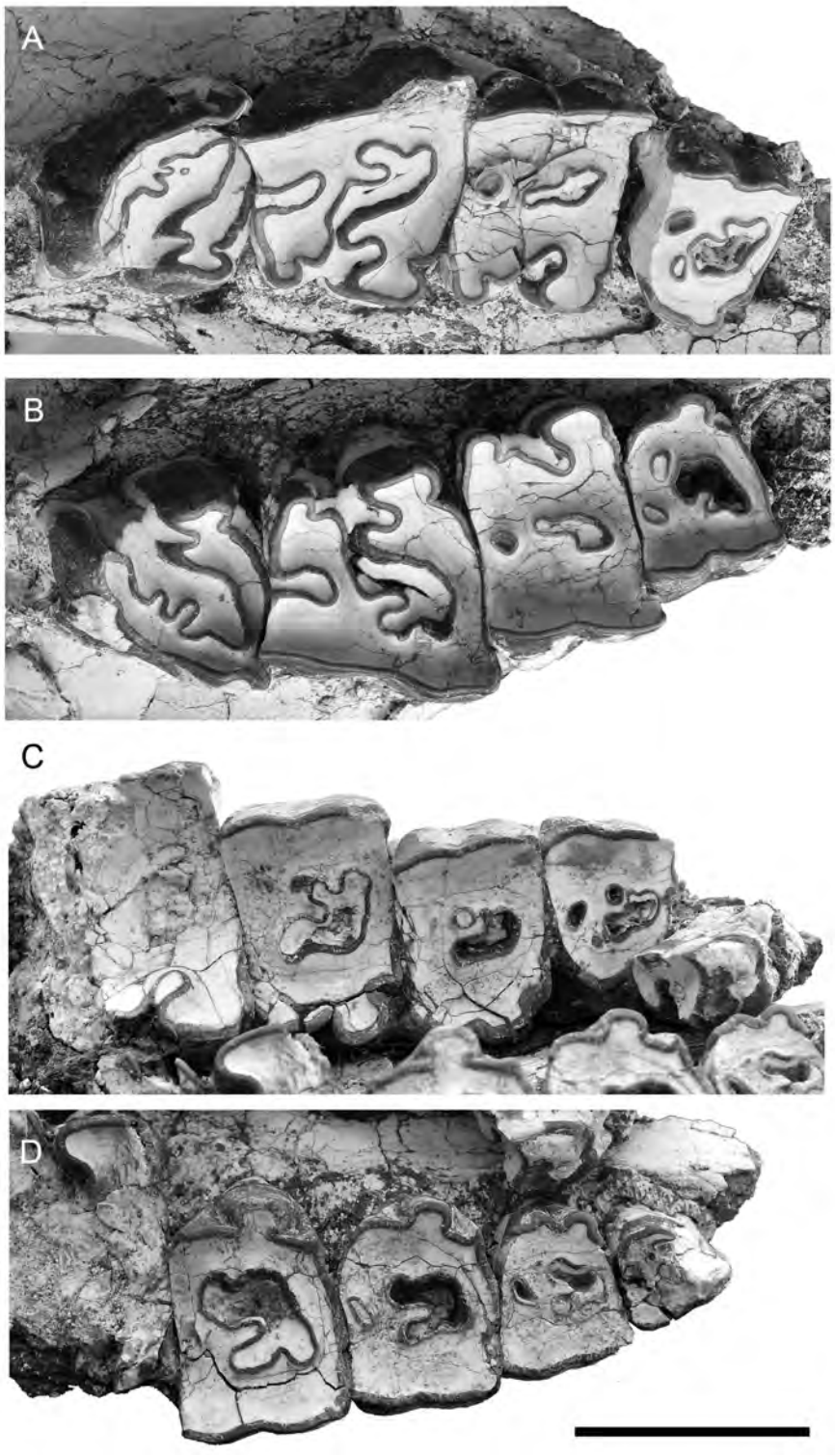


Fig. 4 Upper teeth of the elasmotheriine rhinocerotid *Hispanotherium matritense* from the Early Middle Miocene of Príncipe Pío-2 (Madrid Basin, Spain) in occlusal view. MNCN-05/101/2/7000 A, right P4-M3; B, left P4-M3. MNCN-05/101/2/7001 C, right P1-M1; D, left P1-M1. Scale bar equals 50 mm

Upper teeth		Príncipe Pío-2 MNCN 05/101/2/7000 l	MNCN 05/101/2/7000 r	MNCN 05/101/2/7001 l	MNCN 05/101/2/7001 r	Hommes (France)[1] l	Laogou (China)[2]
	L			20.9	—		22.5 - 24.0
P1	W			21.2	20.4		23.0
	H			19.4	18.7		25.0
	L			25.8	25.4		
P2	W			29.7	30.4		
	H			16.0	14.6		
	L			27.5	27.2	26.0	30.0
P3	W			35.0	37.1	38.9	41.0
	H			15.1	13.1	—	38.0
	L	29.6	30.4	30.4	30.4		33.5
P4	W	40.8	40.9	41.0	43.0		45.5
	H	18.7	18.2	19.1	18.2		44.5
	L	37.7	37.8				44.5
M1	W	51.7	53.4	—	51.0		52.5
	H	13.4	12.3				44.0
	L	51.9	52.1				49.0 - 56.0
M2	W	57.5	59.4				55.0 - 57.0
	H	23.9	23.4				44.0 - 63.6
	L	56.0	57.7				47.0 - 49.5
M3	W	37.5	41.8				49.5 - 50.5
	H	27.7	28.4				30 - 70*

Table 2 Measurements (mm) of upper teeth of *Hispanotherium matritense* (05/101/2/7000, 05/101/2/7001 and 05/101/2/7002) from the middle Miocene of Intercambiador Príncipe Pío in the Madrid Basin (Madrid, Spain). *Unworn teeth. Measurements from Laogou (China) and Hommes (France) were obtained from Deng (2003)[1] and Ginsburg et al. (1987)[2] respectively.

finishes in a sharp hypocone. The parastyle is short, very narrow, sharp and projected forwards. The paracone fold is not very developed. The posterior cingulum is reduced to a prominent tubercle partially covered by cement. Cement fills completely the median valley and covers the anterolingual side of the tooth.

MORPHOLOGICAL COMPARISON

The dental morphology of the rhinoceros material from Príncipe Pío-2 fits with that of the type series of *Hispanotherium matritense* from Puente de Toledo (Madrid), showing a closed median valley on the premolars and developed secondary enamel folds. Their enamel folding in the median valley and ectoloph undulation fall within the observed variability in the Iberian specimens, being simpler and smoother, respectively, than Asian specimens referred to *H. matritense* by Deng (2003). A preliminary study of the abundant postcranial remains confirms its determination. Postcranial differences between *H. matritense* and some related species are carefully detailed in Antoine (2002), so we will mainly focus on cranial characters in light of the new remains from Príncipe Pío-2.

The last diagnosis for *H. matritense* was given by Deng as a "small rhinocerotid with one nasal horn, maybe with sexual dimorphism" (Deng, 2003:142). The inclusion of '*H.*' *tungurense* within the genus *Hispanotherium* lead to consider the horn presence as a sexually dimorphic character (Cerdeño, 1995, 1996). If we focus on *H. matritense*, only one nasal bone has been published. The piece, labeled as MNCN-Ac-17, is a well preserved nasal fragment from the Spanish locality of Paseo de las Acacias (Madrid). It is long, straight, narrow and does not exhibit any signal of nasal horn boss (Cerdeño and Iñigo, 1997). Its general morphology matches with that of the three nasal bones studied from Príncipe Pío-2 site, pointing to a hornless condition for *H. matritense*.

The Spanish site of Córcoles represents the earliest record of the genus *Hispanotherium* (Iñigo, 1993). Firstly recognized as *H. matritense* (Íñigo, 1993; Íñigo and Cerdeño, 1997), their remains were later identified as *Hispanotherium corcolense* (Antoine et al., 2002). An unpublished braincase fragment (IGME 1174M) stored in the Museo del Instituto Geológico y Minero de España is the only known cranial material from Córcoles. Even though it coincides with MNCN-05/101/2/7000 from Príncipe Pío-2 in the rather flat skull roof and their low, sharp, and converging, but separated, frontoparietal crests, these traits are also shared with '*Plesiaceratherium*' *platyodon*, the second rhinoceros identified at Córcoles.

A new species of *Hispanotherium* from the Tung-gur Formation (late Miocene) from Inner Mongolia was described based on both cranial and postcranial remains and erected as *Hispanotherium tungurense* (Cerdeño, 1996). Broadly, *H. tungurense* is larger and has a developed nasal horn boss, contrary to *H. matritense*. It has also stronger enamel

folding, more constricted protocone and more undulated ectoloph. Both have the same nasal incision shape and an elevated posterior end of the zygomatic arch (even though is much more developed in '*H.*' *tungurense*). It is important to mention that other shared characters as infraorbitalis foramen reaching the level of P4, anterior part of the orbit at the level of the M3, and a flat skull profile, can be easily distorted by general slanting and ontogeny (Borsuk-Bialynicka, 1973) and should be compared with caution. The same occurs with some cranial differences as a deeper nasal incision (above P4) in *H. matritense*, a linking characteristic with more modern elasmotheriines as *Ningxiatherium*. Dental morphology of both *H. matritense* and '*H.*' *tungurense* are not far from each other. H. tungurense show a more undulated ectoloph. This fact is shared by most Miocene elasmotheriines, as they show a rather similar dental pattern quite different from the enamel folding complexity of the derived hypsodont species as *Sinotherium*, *Elasmotherium* or even *Iranotherium*.

Heissig (1974) described the species *Hispanotherium grimmi* according to several remains from the Turkish locality of Sofça 4. The species was synonimized with *H. matritense* by Cerdeño (1989) and posteriorly retained as a distinct species of the genus *Hispanotherium* by several authors (Cerdeño, 1995; Antoine et al., 2002). Our phylogenetic analysis places '*H.*' *grimmi* apart from the genus *Hispanotherium*. 1968 VI 43, the only known nasal bone lacks any nasal roughness, albeit horn insertion was included as a diagnostic character for the species (Heissig, 1974). The nasal is short, robust and triangular in lateral view, resembling the nasals of *Hispanotherium beonense* to some degree. Even though we have not directly observed it, Heissig describes some kind of shallow rugosities present on its posterior half (Heissig, 1976). We think that the simple nasal suture and the position of this scars suggests the absence of nasal horn, instead of being a juvenile stage of development as proposed (Heissig, 1974). If horn presence in '*H.*' *grimmi* is not proven to be dimorphic, it could be a linking character with *H. matritense*.

H. beonense was discovered in the late Early Miocene (MN4-5) of France and originally named as *Aegyrcitherium beonense* (Antoine, 1997). Shortly after *Aegyrcitherium* was considered a subgenus of *Hispanotherium* (Antoine et al., 2002; Guérin and Pickford, 2003). Posteriorly, the species was directly included in the genus *Hispanotherium*, even though phylogenetic analysis set it as a distinct taxa (Antoine, 2003). Both *H. matritense* and *H. beonense* share a low anterior end, a high posterior end of the zygomatic arch and a flat skull profile. In contrast to *H. matritense*, *H. beonense* has a small triangular nasal bone, rostrally broadened nasals, a processus postorbitalis on the zygomatic arch, laterally projected orbits, labial cingulum on upper premolars, and stronger zygomatic arches. Several nasal bones from *H. beonense* have been recorded. Some of them have nasal rugosities confined to the nasal tip (MNHN Béon 1998 E3 3060 and MHNT Béon 1991 G4 64), likewise placed as those found in some Teleoceratina rhinoceroses as *Brachypotherium* or *Teleoceras*. Others

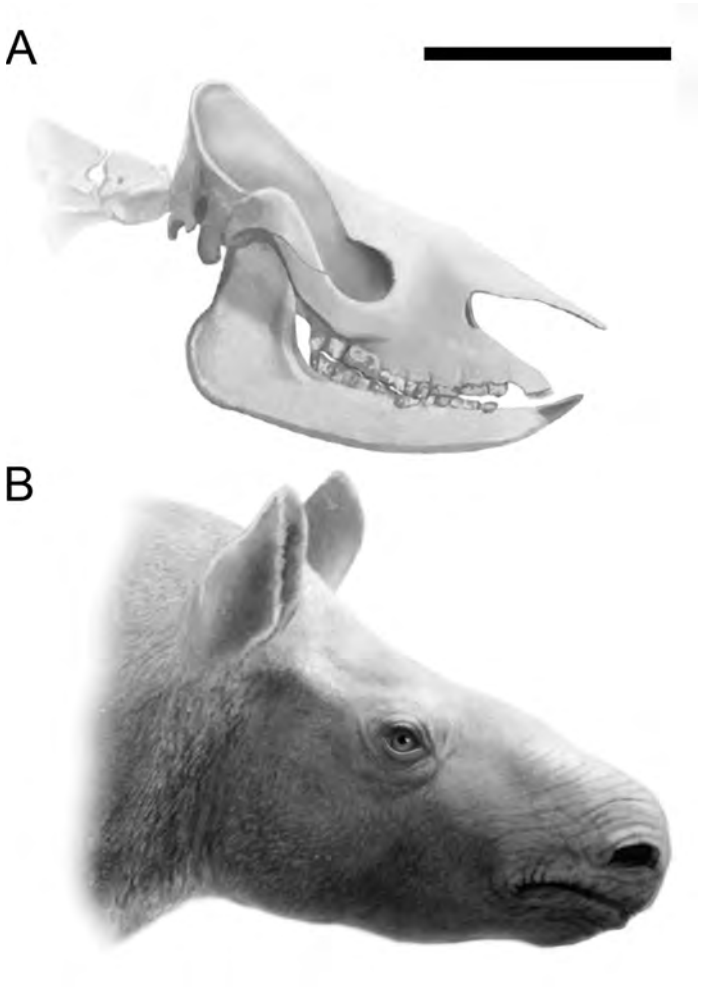


Fig. 5 Reconstructed life appearance of *Hispanotherium matritene* based on the cranial remains from Príncipe Pío-2. The occiput and the shape of the zigomatic arches have been reconstructed according to the skull MHNT.PAL.2004.0.58 of *Hispanotherium beonense* from Béone. The premaxilary bone is hypotetical and has been reconstructed with the basic morphology of early elasmotheres (e.g. *Menoceras*). Scale bars represent 200 mm

are narrower and have a smooth dorsal surface, so sexual dimorphism could be feasible in this species (Antoine, 2002), a main cranial difference with *H. matritense*. The peculiar horn rugosities of *H. beonense* or the horn absence in *H. matritense*, '*H.*' *grimmi* and more distantly *Ougandatherium napakense* (Guérin and Pickford, 2003) suggests a diverse nasal horn development within Early Elasmotheriini, characterized by a hornless basal condition and a rapid diversification towards well developed nasal or frontal horns. These data contrasts with previous works, which proposed the presence of a nasofrontal horn as a synapomorphy of the whole elasmotheriine group (Fortelius and Heissig, 1989).

CLADISTIC ANALYSIS

The taxonomic status of some species attributed to the genus *Hispanotherium* has been a cause of debate. This

problem, widespread among Elasmotheriina, is mainly caused by a limited knowledge of several basal taxa together with common dental morphologies at an intergeneric level. Íñigo and Cerdeño (1997) revisited the Asian *Caementodon oettingenae, Beliajevina caucasica* and *Begertherium borissiaki* and considered them as synonymous with *H. matritense*. Posterior analyses on Elasmotheriina made by Antoine (2002; 2003) kept some of them in their own genus: placing *Caementodon oettingenae* basal to '*Caementodon*' (*Beliajevina*) *caucasicum*, transferring *Begertherium borissiaki* close to the more derived species *Procoelodonta mongoliense*, and finally considering *Hispanotherium* as a paraphyletic group composed by '*H.*' *grimmi*, *H. matritense*, *H. corcolense,* and '*H.*' *beonense* (Antoine, 2002; Antoine, 2003). In addition, Deng (2003) assumed a wider intraspecific variability partially coinciding with Íñigo and Cerdeño (1997) and referred some of the elasmotheriine remains from the Chinese locality of Laogou to the type species *H. matritense*. The same analyses considered '*H.*' *tungurense* basal to the more derived Elasmotheriina, separating it from other *Hispanotherium* species (Antoine et al., 2002; Deng, 2003).

Our phylogenetic analysis produced three most parsimonious trees with a length of 646 steps long (CI=0.52; RI=0.66). Consistency index are similar to those of previously published phylogenies (Antoine et al., 2002). The strict consensus tree is represented in figure 5. The tree topology generated in our analysis is broadly consistent with that forwarded by Deng (2008) except for the unsolved politomy of *Ningxiatherium euryrhinus*, *Ningxiatherium longirhinus* and the genus *Elasmotherium*. The branching sequence of Elasmotheriina is (*K. bishopi, B. praecursor, 'C.' caucasicum, C. oettingenae* ('*H.*' *grimmi* (*H. beonense* (*H. matritense, H. corcolense*)) ('*P.*' *tekkayai* (*P. mongoliense* ((*H. lintungense*, '*H.*' *tungurense*) (*I. morgani* (*P. schansiense* (*S. lagrelii* (*E. sibiricum, E. caucasicum*))))))))). Cranial data provided for *H. matritense* clarify the phylogenetic relationships of the genus *Hispanotherium*. Monophyly for a *H. matritense*, *H. corcolense* and *H. beonense* clade (node c) is weakly supported by the following synapomorphies: close frontoparietal crests, abrupt anterior tip of the *processus zygomaticus maxillary*, lingual groove of the *corpus mandibulae* present, lingual cingulum usually present on P2-P4 and usually absent on M1-M3, and posterior cingulum low and reduced on the M1-M2. The monophyly of the Iberian *Hispanotherium* species, comprised by *H. matritense* and *H. corcolense* (node d), has been previously proposed as a feasible alternative for the paraphyletic status of the French and Iberian species (Antoine et al., 2002). In our analysis is supported by five synapomorphies: developed crown of the i1, weaker protocone than hypocone on the P2, usually present crista on the upper molars, straight posterior part of the ectoloph on the M1-2 and usually absent calcaneus fibula-facet. On the other hand, '*H.*' *tungurense* appears as a more derived representative of the Elasmotheriina. This clade, labeled as node h, strongly sets apart '*H.*' *tungurense* and *H. lintungense* relying on following synapomorphies: usually simple crochet and usually absent lingual cingulum on P2-P4, protocone less strong than the hypocone and protoloph joined to the ectoloph on the P2, transverse metaloph on the P3-4, separated hypocone and metacone on the P4, crista usually absent on the upper molars, glenoid fossa of the scapula with a straight medial border and always present posterior expansion of the pyramidal-facet of the unciform. The presence of a lingual groove in the *corpus mandibulae* and the low and reduced posterior cingulum on M1-M2 appear also in the genus *Hispanotherium* and are considered as convergent characters. '*H.*' *grimmi* is also excluded and placed as the sister-group of the genus *Hispanotherium* and the more evolved Elasmotheriina clade.

Three elasmotheriine species have been recorded from the European Early to Middle Miocene: *H. corcolense*, *H. beonense* and *H. matritense*. *H. corcolense* is restricted to the lower Miocene of Córcoles (MN4a, zone C), being the first occurrence of the group in the Iberian Peninsula (Antoine et al., 2002). At the same time, *H. beonense* appeared in the lower Miocene of Pellecahus, France (MN4a, zone C; Antoine et al., 2000), extending its chronostratigraphic range up to the MN5 of the Aquitaine and Loire Basins (Antoine, 1997). Finally, *H. matritense* appeared in the Western European fossil record, becoming a key species in the Iberian Middle Miocene macromammal assemblages (from the MN4b to the MN5, zones D-E; Antoine et al., 2002). At least some French assemblages had the greatest diversity of Western European Elasmotheriines, as *H. matritense* and *H. beonense* were sympatric on the Loire Basin (Ginsburg et al., 1987; Antoine et al., 2002).

The evolutionary history of the Elasmotheriina is marked by a rapid lower Miocene radiation. This was probably favored by a wide early paleobiogeographic distribution and a global polar cooling that progressively substituted moist subtropical forests by open landscapes characterized by drought-adapted vegetation (Axelrod, 1975). The new geographic and climatic conditions favored a major dispersal event between Asia and Europe (named as 'Proboscidean Datum Event'; Madden and Van Couvering, 1976). *H. corcolense* and *H. beonense* appeared in the Early Miocene (MN4a, Zone C), being the earliest known elasmotheriine species in the European fossil record. Their common ancestor would have been differentiated in Asia, passed through the Anatolian plate and dispersed westwards ,into southwestern Europe (Antoine et al., 2002; Deng, 2003). Our novel phylogenetic hypothesis suggests that the European climatic conditions during the Middle Miocene favored a short-termed evolutionary radiation independent from the main Asian elasmotheriine lineage. This diversification has been also observed in other contemporary macromammal groups as anchitheriine equids (Sánchez et al., 1998; Salesa et al., 2004) and boselaphine bovids (Gentry et al., 1999).

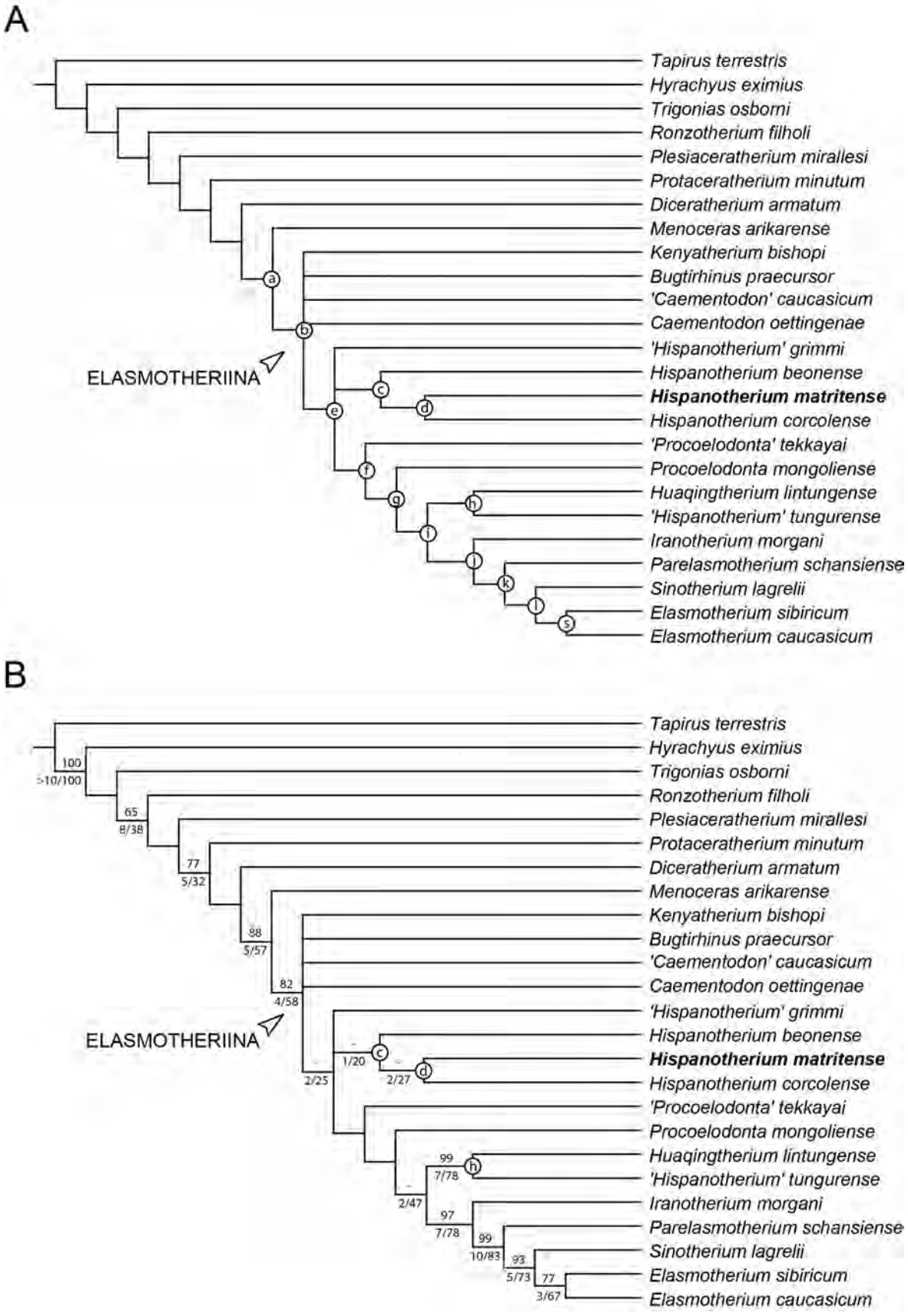


Fig. 6 Phylogenetic relationships of *Hispanotherium matritense* within Elasmotheriina (Rhinocerotidae). A, single strict consensus tree (646 steps; CI = 0.52; RI= 0.66) obtained from three most parsimonious trees by means of TnT v. 1.1. (Goloboff et al., 2008). Synapomorphies of each node are defined in Supplementary Data 3. B, same tree with the support values of each node. The value above each branch represents the Bootstrap proportions for clades found in more than 50% of 1000 replicates. The pair of numbers below a branch represents, from left to right, absolute and relative Bremer values respectively (according to Goloboff, 2008). Character/taxa matrix is basically that of Antoine (2002; 2003) and Deng (2008), as detailed in Supplementary data 1-2.

CONCLUSIONS

The analysis of new specimens of *H. matritense* from the Middle Miocene of Príncipe Pío-2 (Madrid Basin, Spain) gives a full picture of the species and supplements the previously known material. The probable horn absence in *H. matritense* is shared with other primitive elasmotheriines (as *O. napakense*) whereas its dental configuration is closer to other derived species as *Procoelodonta mongoliense*. The hornless nasals of *H. matritense* point out that the presence and shape of nasal horns are homoplastic characters above genus level in Elasmotheriina. Our phylogenetic analysis, places *H. matritense* close to *H. corcolense* and *H. beonense* (*H. beonense* (*H. corcolense*, *H. matritense*)), pointing to a monophyletic *Hispanotherium* genus. The exclusion of '*H. tungurense* and '*H. grimmi*, clarifies the previously paraphyletic status of the genus. In addition, the cladistic topology of the genus *Hispanotherium* produced by our analysis results in a satisfactory alternative hypothesis to those previously proposed (Antoine, 2002; Antoine et al., 2002; Antoine, 2003) by both geographical and chronostratigraphical points of view.

ACKNOWLEDGMENTS

Thanks to the reviewers D. R. Prothero and P. O. Antoine and the editor B. Van Valkenburgh for their useful comments and suggestions whose have greatly improved the original manuscript. We are also indebted to E. Cerdeño for her critical reading of the preliminary draft and all people who allowed O.S. to study material under their care: Y. Laurent (Muséum d'Histoire Naturelle de Toulouse), A. Arribas, S. Menéndez (Museo Geominero-IGME) and P. Pérez Dios (Museo Nacional de Ciencias Naturales de Madrid). Thanks to S. Fraile and ArqueoEstudio for their support with the fieldwork and E. Cantero for the excellent preparation of the specimens. We also thank A.R. Gómez-Cano for sharing with us the Neogene map modified in figure 1. O.S. acknowledges a predoctoral grant from the Spanish Government MICINN. This study is part of the Spanish Government MICINN research project CGL2008-05813-CO2-01, and is included in the research Group BSCH-UCM 910607.

LITERATURE CITED

Aguirre, E., M. T. Alberdi, C. Martín-Escorza, T. Torres, J. Morales, C. Sesé, and D. Soria. 1982. Torrijos: nueva fauna con *Hispanotherium* de la cuenca media del Tajo. Acta Geologica Hispanica 1-2:39-61.

Antoine, P. O. 1997. *Aegyrcitherium beonensis* nov. gen. nov. sp., nouvel élasmothère (Mammalia, Rhinocerotidae) du gisement miocène (MN 4b) de Montréal-du-Gers (Gers, France). Position phylogénétique au sein des Elasmotheriini. Neues Jahrbuch für Geologie und Paläontologie Abhandlungen 204:399-414.

Antoine, P. O. 2000. Origine et différenciation des Elasmotheriina parmi les Rhinocerotidae (Mammalia, Perissodactyla) : analyse cladistique et implications biostratigraphiques et paléobiogéographiques. Unpublished Ph.D. dissertation thesis/dissertation, Muséum National d'Histoire Naturelle, Paris, 350 pp.

Antoine, P. O. 2002. Phylogénie et évolution des Elasmotheriina: (Mammalia, Rhinocerotidae). Mémoires du Muséum National d'Histoire Naturelle 188:5-350.

Antoine, P. O. 2003. Middle Miocene elasmotheriine Rhinocerotidae from China and Mongolia: taxonomic revision and phylogenetic relationships. Zoologica Scripta 32:95-118.

Antoine, P. O., C. Bulot, and L. Ginsburg. 2000. Une Faune rare de Rhinocérotidés (Mammalia, Perissodactyla) dans le Miocène Inférieur de Pellecahus (Gers, France). Geobios 33:249-255.

Antoine, P. O., F. Alférez, and C. Iñigo. 2002. A new elasmotheriine (Mammalia, Rhinocerotidae) from the Early Miocene of Spain. Comptes Rendus Palevol 1:19-26.

Antunes, M. T. 1960. Notes sur la géologie et la paléontologie du Miocène de Lisbonne - 1. Stratigraphie et faunes de mammifères terrestres. Boletim da Sociedade Geológica de Portugal 13:257-267.

Antunes, M. T. 1979: *Hispanotherium* fauna in Iberian Middle Miocene; its importance and paleogeographical meaning. Annales Geologiques Pays. Hellèn. VII International Congress on Mediterranean Neogene, 1979.

Antunes, M. T., and L. Ginsburg. 1983. Les Rhinocérotidés du Miocène de Lisbonne. Systématique, écologie, paléobiogéographie, valeur stratigraphique. Ciências da Terra (UNL) 7:17-98.

Axelrod, D. I. 1975. Evolution and biogeography of Madrean-Tethyan sclerophyll vegetation. Annals of the Missouri Botanical Garden 62:280-334.

Boné, E., M. T. Alberdi, M. Hoyos, and N. López. 1980. Prospection paléontologique de la région de Torralba de Ribota (Burdigalien du Bassin de Calatayud, Zaragoza, España). Paleovertebrata Mem. juv. R. Lavocat:233-247.

Borsuk-Bialynicka, M. 1973. Studies on the Pleistocene rhinoceros *Coelodonta antiquitatis* (Blumenbach). Acta Palaeontologica Polonica 29:1-94.

Cerdeño, E. 1989. Revisión de la sistemática de los rinocerontes del Neógeno de España. Universidad Complutense de Madrid, Madrid, 429 pp.

Cerdeño, E. 1992. Spanish Neogene Rhinoceroses. Palaeontology 35:297-308.

Cerdeño, E. 1995. Cladistic analysis of the Family Rhinocerotidae (Perissodactyla). American Museum Novitates 3143:1-25.

Cerdeño, E. 1996. Rhinocerotidae from the Middle Miocene of the Tung-gur Formation, Inner Mongolia (China). American Museum Novitates 3184:1-43.

Cerdeño, E., and M. T. Alberdi. 1983. Estudio descriptivo del esqueleto postcraneal de *Hispanotherium matritense* del yacimiento Mioceno de Torrijos (Toledo). Estudios Geológicos 39:225-235.

Cerdeño, E., and M. Nieto. 1995. Changes in Western European Rhinocerotidae related to climatic variations. Palaeogeography, Palaeoclimatology, Palaeoecology 114:325-338.

Cerdeño, E., and C. Iñigo. 1997. *Hispanotherium matritense* (Rhinocerotidae) de la ciudad de Madrid (España) y su relación con el paleoambiente del Aragoniense medio (Mioceno Medio). Revista Española de Paleontología 12:80-90.

Crusafont, M., and J. F. Villalta. 1947. Sobre un interesante rinoceronte (*Hispanotherium*) del Mioceno del Valle de Manzanares. Las Ciencias 12:869-883.

Deng, T. 2003. New material of *Hispanotherium matritense* (Rhinocerotidae, Perissodactyla) from Laogou of Hezheng County (Gansu, China), with special reference to the Chinese Middle Miocene elasmotheres. Geobios 36:141-150.

Deng, T. 2008. A new elasmothere (Perissodactyla, Rhinocerotidae) from the late Miocene of the Linxia Basin in Gansu, China. Geobios 41:719-728.

Fortelius, M., and K. Heissig. 1989. The phylogenetic relationships of the Elasmotherini (Rhinocerotidae, Mamm.). Mitteilungen Bayerische Staatssammlung Paläontologische historische Geologie 29:227-233.

Gentry, A. W., G. E. Rössner, and E. P. J. Heizmann. 1999. Suborder Ruminantia; pp. 225-253 in G. E. Rössner and K. Heissig (eds.), The Miocene Land Mammals of Europe. Verlag Dr. Friedrich Pfeil, München.

Ginsburg, L., F. Maubert, and M. T. Antunes. 1987. Discovery of *Hispanotherium* and *Gaindatherium* (Rhinocerotidae, Mammalia) in the Miocene of France. Bulletin du Muséum national d'histoire naturelle. Section C, Sciences de la terre, paléontologie, géologie, minéralogie 9:303-311.

Goloboff, P., J. Farris, and K. Nixon. 2008. TNT, a free program for phylogenetic analysis. Cladistics 24:774-786.

Guérin, C. 1980. Les rhinocéros (Mammalia, Perissodactyla) du Miocène terminal au Pléistocène supérieur en Europe occidentale : comparaison avec les espèces actuelles. Documents des Laboratoires de Géologie de Lyon 79:1-1184.

Guérin, C., and M. Pickford. 2003. *Ougandatherium napakense* nov. gen. nov. sp., le plus ancien Rhinocerotidae Iranotheriinae d'Afrique. Annales de paléontologie 89:1-35.

Heissig, K. 1972. Die obermiozäne Fossil-Lagerstätte Sandelzhausen. 5. Rhinocerotidae (Mammalia), Systematik und Okologie. Mitteilungen der Bayerischen Staatssammlung Paläontologie und historische Geologie 14:37.

Heissig, K. 1974. Neue Elasmotherini (Rhinocerotidae, Mammalia) aus dem Obermiozän Anatoliens. Mitteilungen der Bayerischen Staatssammlung Paläontologie und historische Geologie 14:21-35.

Heissig, K. 1999. 16. Family Rhinocerotidae; pp. 175-188 in G. E. Rössner and K. Heissig (eds.), The Miocene Land Mammals of Europe, Pfeil, Munich.

Hernández-Pacheco, F., and M. Crusafont. 1960. Primera caracterización paleontológica del Terciario de Extremadura. Boletín de la Real Sociedad Española de Historia Natural (Geol.) 58:275-282.

Iñigo, C. 1993. Estudio de los Perisodáctilos del yacimiento Mioceno de Córcoles (Guadalajara). Tesis Doctoral (Unpublished) thesis/dissertation, Facultad de Ciencias Biológicas, Universidad Complutense Madrid Madrid, 559 pp.

Iñigo, C., and E. Cerdeño. 1997. The *Hispanotherium matritense* (Rhinocerotidae) from Córcoles (Guadalajara, Spain): Its contribution to the systematics of the Miocene Iranotheriina. Geobios 30:243-266.

Madden, C. T., and J. A. Van Couvering. 1976: The Proboscidean Datum Event: Early Miocene migration from Africa. Geological Society of America. Abstracts with Program, 1976.

Prado, C. d. 1864. Descripción Física y Geológica de la Provincia de Madrid. Junta General de Estadística. Imprenta Nacional, Madrid.

Roca, L. P., S. Fraile, G. Bernal, M. Dumas, A. Alonso, L. Galindo, and V. Marcos Sánchez. 2009. Nuevos hallazgos Paleontológicos y Arqueológicos en el "Intercambiador de transportes de Príncipe Pío", Madrid.; pp. 172-187. Consorcio Regional de Transportes de Madrid. Consejería de Transportes e Infraestructuras de la Comunidad de Madrid.

Salesa, M. J., I. M. Sánchez, and J. Morales. 2004. Presence of the Miocene Asian genus Sinohippus (Perissodactyla, Equidae) in Spain. Acta Palaeontologica Polonica 49:189-196.

Sánchez, I. M., M. J. Salesa, and J. Morales. 1998. Revisión Sistemática del Género Anchitherium MEYER 1834 (Equidae; Perissodactyla) en España. Estudios Geológicos 54:39-63.

Saraç, G. 1978. A new *Hispanotherium* species (Mammalia, Rhinocerotidae): *Hispanotherium alpani* n. sp. from the Upper Miocene of Southwest Anatolia. Bulletin of the Mineral Research and Exploration Institute of Turkey 89:90-95.

Zbyszewsky, G. 1952. Les mammifères miocènes de Quintanelas (Sabugo). Comunicaçóes Serviço Géologico Portugal 33:22.

SUPPLEMENTARY DATA 1

Cranial, dental and postcranial characters and character states used for the cladistic analysis from Antoine et al. (2003) and Deng (2008). The character matrix basically follows that detailed in the Supplementary Data 1 of the Chapter 2 except for the following characters:

SKULL

3	Nasal notch = 0, above P1-3; 1, above P4-M1
18	External auditory *pseudo-meatus*= 0, open; 1, partially closed; 2, closed
48	Occipital: *processus paraoccipitalis*= 0, well developed; 1, little developed
49	Occipital: *foramen magnum*= 0, circular; 1, subtriangular
50	Basioccipital: median ridge on the condyle = 0, absent; 1, present
51	Basioccipital: medial truncation on the condyle = 0, absent; 1, present
52	Basioccipital: medial truncation on the condyle = 0, present at juvenile stage; 1, still present at adult stage

MANDIBLE

53	Symphysis = 0, very upraised; 1, upraised; 2, nearly horizontal

TEETH

65	Cheekteeth: cement = 0, absent; 1, present
69	Cheekteeth: crown = 0, high; 1, partial hypsodonty; 2, subhypsodonty; 3, hypsodonty
88	P2-4: lingual cingulum = 0, continuous; 1, reduced
91	P1 in adults = 0, always present; 1, usually present; 2, always absent
99	P2: protoloph = 0, joined to the ectoloph; 1, interrupted
149	Lower premolars: labial cingulum = 0, present; 1, absent

POSTCRANIAL SKELETON

275	MtIII: cuboid-facet = 0, absent; 1, present

SUPPLEMENTARY DATA 2

Data matrix including 282 cranial, dental, and postcranial characters recorded for terminal taxa (after Antoine, 2002 and Deng, 2008). It contains four outgroup taxa (one used as real outgroup, *Tapirus terrestris*), plus 15 elasmotheres and 12 non–elasmothere rhinocerotids. Characters and character states are described in Antoine (2003, Appendix 1). Missing observations and non-applicable characters are coded '?' and '–', respectively.

Taxa	1	2	3	4	5	6	7	8	9	10	11	12	13	14	15	16	17	18	19	20	21	22	23	24	25	26	27	28	29	30	31	32	33	34	35	36	37	38	39	40	41	42	43	44	45	46	47	48	49	50	51	52	53	54	55	56	57	58	59	60
Tapirus terrestris	0	0	1	0	-	1	0	0	0	0	0	0	0	0	0	0	0	0	1	0	0	1	0	0	0	1	0	-	0	-	0	-	0	1	0	0	0	0	0	1	0	0	0	0	0	0	0	0	0	0	0	-	0	0	1	0	0	0	0	0
Hyrachyus eximius	0	0	0	0	-	0	0	?	0	1	1	0	0	0	0	0	0	1	0	2	0	0	0	0	0	0	0	-	0	-	0	-	0	0	0	0	0	?	0	0	0	0	0	0	0	0	0	0	0	0	0	-	0	0	0	1	0	0	0	1
Trigonias osborni	1	0	0	0	-	1	0	0	0	0	1	0	0	0	0	?	0	1	0	2	0	0	1	0	0	0	0	-	0	-	0	-	0	0	0	0	0	?	0	0	0	0	0	1	0	0	1	0	1	0	0	-	2	0	1	1	0	0	0	0
Ronzotherium filholi	0	1	0	0	-	?	0	0	0	0	0	1	-	0	1	1	0	0	0	0	0	0	0	1	0	0	0	0	-	0	-	0	-	0	0	1	1	1	1	0	0	0	1	0	1	0	0	0	0	0	0	0	-	0	0	0	0	0	1	0	0
Plesiaceratherium mirallesi	0	?	1	0	-	?	0	?	?	0	0	?	?	0	0	?	1	1	0	0	?	?	?	0	0	0	0	-	0	-	0	-	0	?	0	1	0	?	1	0	1	2	0	0	1	0	0	0	0	1	1	0	1	1	1	1	0	0	0	?
Protaceratherium minutum	0	0	1	0	-	?	0	?	?	0	1	?	?	?	0	?	?	0	1	0	0	?	1	0	0	0	0	-	0	-	0	-	0	?	?	?	0	?	0	?	?	?	?	?	?	?	?	0	?	0	?	?	?	?	?	0	1	0	?	0	1	0
Diceratherium armatum	0	0	0	0	-	?	0	1	0	1	1	0	0	0	1	?	1	2	0	2	0	1	0	0	0	0	0	-	1	1	0	-	0	0	0	0	0	1	1	0	0	1	0	1	0	?	?	?	0	0	0	?	2	0	1	0	0	0	0	0
Menoceras arikarense	0	0	0	0	-	?	0	0	0	1	1	0	0	0	1	1	0	0	1	2	0	1	?	0	0	0	0	-	1	0	0	-	0	0	?	0	0	1	0	1	0	2	0	1	1	1	0	1	1	0	0	?	1	0	1	1	1	-	1	0
Kenyatherium bishopi	?	?	?	?	?	?	?	?	?	?	?	?	?	?	?	?	?	?	?	?	?	?	?	?	?	?	?	?	?	?	?	?	?	?	?	?	?	?	?	?	?	?	?	?	?	?	?	?	?	?	?	?	?	?	?	?	?	?	?	?
Bugtirhinus praecursor	?	0	?	?	?	?	?	?	?	?	?	?	?	?	?	?	?	?	?	?	?	?	?	?	?	?	?	?	?	?	?	?	?	?	?	?	?	?	?	?	?	?	?	?	?	?	?	?	?	?	?	?	?	?	?	?	?	?	?	?
`Caementodon´caucasicum	1	?	0	0	-	?	0	?	?	0	1	?	?	?	?	?	?	?	?	?	?	?	?	0	0	0	1	0	0	-	0	-	?	?	?	?	0	?	?	?	?	?	?	?	?	?	?	?	?	?	?	?	0	1	1	1	-	1	0
Caementodon oettingenae	?	?	?	?	?	?	?	?	?	?	?	?	?	?	?	?	?	?	?	?	?	?	?	?	?	?	?	?	?	?	?	?	?	?	?	?	?	?	?	?	?	?	?	?	?	?	?	?	?	?	?	?	?	?	?	?	?	?	?	?
`Hispanotherium´grimmi	?	0	?	0	-	?	?	?	?	?	?	?	?	?	?	?	?	?	?	?	?	?	?	0	0	?	1	0	0	-	?	?	?	?	2	0	?	?	?	?	?	?	?	?	?	?	?	?	?	?	?	?	1	0	1	1	1	-	1	0
Hispanotherium beonense	0	0	0	0	-	?	0	0	0	1	1	0	1	0	1	1	1	0	2	2	0	0	0	0	0	0	1	0	0	-	0	-	0	0	1	0	1	?	0	?	0	1	0	1	1	0	0	0	1	0	1	1	1	0	0	0	0	1	1	0
Hispanotherium corcolense	?	?	?	?	?	?	?	?	?	?	?	?	?	?	?	?	?	?	?	?	?	?	?	?	?	?	?	?	?	?	?	?	?	?	?	?	?	?	?	?	?	?	?	?	?	?	?	?	?	?	?	?	?	?	?	?	?	?	?	?
Hispanotherium matritense	0	0	0	0	-	?	0	?	?	1	1	0	-	0	?	?	0	0	?	?	1	?	?	0	0	0	0	-	0	-	0	-	0	?	1	?	1	0	1	1	0	1	0	1	1	0	0	0	1	?	?	?	1	0	1	1	0	1	1	0
`Procoelodonta´tekkayai	?	0	1	?	?	?	?	?	?	1	?	?	?	?	?	?	?	?	?	?	?	?	?	?	?	?	?	?	?	?	?	?	?	?	?	0	?	?	?	?	?	?	?	?	?	?	?	?	?	?	?	?	?	?	?	?	?	?	?	?
Procoelodonta mongoliense	1	0	0	0	-	?	0	0	0	1	2	0	0	0	?	?	?	?	?	?	?	?	?	0	0	2	1	0	0	-	0	-	0	0	2	?	0	?	1	?	?	?	?	?	1	?	?	?	?	?	?	?	?	?	?	?	?	?	?	?	?
Huaqingtherium lintungense	0	0	0	0	-	0	0	0	0	0	1	0	-	0	1	1	1	0	2	2	0	0	0	1	0	0	1	1	0	-	0	-	1	0	2	0	0	1	0	1	0	1	0	1	1	0	0	0	1	0	0	-	1	0	1	1	0	1	1	0
`Hispanotherium´tungurense	0	0	0	0	-	?	0	0	0	0	1	0	1	0	1	?	1	0	2	2	0	0	0	1	0	0	1	1	0	-	0	-	1	0	2	0	0	?	0	1	0	1	0	1	1	0	0	0	1	0	0	-	1	0	1	1	0	1	1	0
Iranotherium morgani	0	0	0	0	-	?	1	0	0	1	2	1	-	?	1	1	1	0	2	2	1	0	0	1	1	0	1	1	0	-	0	-	1	1	2	?	0	?	0	1	?	1	0	1	1	0	2	0	1	0	1	1	1	1	1	1	-	1	?
Parelasmotherium schansiense	0	1	1	1	0	?	2	1	0	0	1	0	1	?	1	?	1	0	2	2	1	0	0	2	2	0	1	1	0	-	0	-	1	0	2	0	0	1	0	0	0	1	?	1	0	1	2	1	0	0	1	1	?	?	?	?	?	?	?	?
Sinotherium lagrelii	?	1	1	?	?	?	2	?	?	0	?	?	?	?	?	?	?	?	?	?	?	?	?	?	?	?	?	?	?	?	?	?	?	?	?	1	?	?	?	?	?	?	?	?	?	?	?	?	?	?	?	?	?	?	?	?	?	1	?
Elasmotherium caucasicum	?	?	?	?	?	?	?	?	?	?	?	?	?	?	?	?	?	?	?	?	?	?	?	?	?	?	?	?	?	?	?	?	?	?	?	?	?	?	?	?	?	?	?	?	?	?	?	?	?	?	?	?	?	?	?	?	?	?	2	2
Elasmotherium sibiricum	0	1	1	1	1	?	1	-	0	0	0	1	-	?	1	1	0	0	2	2	1	0	0	0	2	0	0	-	0	-	1	1	1	0	2	2	1	1	0	0	0	2	1	1	0	1	2	1	0	0	1	1	1	2	1	1	1	-	2	2

SUPPLEMENTARY DATA 2 (CONT.)

| Taxa | 6 1 | 6 2 | 6 3 | 6 4 | 6 5 | 6 6 | 6 7 | 6 8 | 6 9 | 7 0 | 7 1 | 7 2 | 7 3 | 7 4 | 7 5 | 7 6 | 7 7 | 7 8 | 7 9 | 8 0 | 8 1 | 8 2 | 8 3 | 8 4 | 8 5 | 8 6 | 8 7 | 8 8 | 8 9 | 9 0 | 9 1 | 9 2 | 9 3 | 9 4 | 9 5 | 9 6 | 9 7 | 9 8 | 9 9 | 1 0 0 | 1 0 1 | 1 0 2 | 1 0 3 | 1 0 4 | 1 0 5 | 1 0 6 | 1 0 7 | 1 0 8 | 1 0 9 | 1 1 0 | 1 1 1 | 1 1 2 | 1 1 3 | 1 1 4 | 1 1 5 | 1 1 6 | 1 1 7 | 1 1 8 | 1 1 9 | 1 2 0 |
|---|---|---

Taxa	1 2 1	1 2 2	1 2 3	1 2 4	1 2 5	1 2 6	1 2 7	1 2 8	1 2 9	1 3 0	1 3 1	1 3 2	1 3 3	1 3 4	1 3 5	1 3 6	1 3 7	1 3 8	1 3 9	1 4 0	1 4 1	1 4 2	1 4 3	1 4 4	1 4 5	1 4 6	1 4 7	1 4 8	1 4 9	1 5 0	1 5 1	1 5 2	1 5 3	1 5 4	1 5 5	1 5 6	1 5 7	1 5 8	1 5 9	1 6 0	1 6 1	1 6 2	1 6 3	1 6 4	1 6 5	1 6 6	1 6 7	1 6 8	1 6 9	1 7 0	1 7 1	1 7 2	1 7 3	1 7 4	1 7 5	1 7 6	1 7 7	1 7 8	1 7 9	1 8 0
Tapirus terrestris	0	0	0	0	0	-	0	0	0	0	-	0	0	0	0	-	0	-	0	-	-	1	1	0	0	0	0	0	0	1	3	-	0	1	0	0	0	0	0	1	0	0	0	0	1	0	0	0	0	0	0	0	0	0	0	0	0	0	0	0
Hyrachyus eximius	1	0	0	0	0	-	0	0	0	0	-	0	0	0	0	-	0	-	0	0	0	0	0	1	0	0	3	-	0	0	0	0	0	1	0	0	2	-	0	0	0	0	?	?	0	0	0	0	0	?	?	?	?	?	?	?	?	?	?	?
Trigonias osborni	0	0	0	0	0	0	0	0	0	0	-	0	0	0	0	-	0	0	0	0	0	0	0	1	0	0	2	0	1	-	0	0	0	0	0	0	2	-	2	-	0	0	?	?	0	0	0	0	0	0	0	0	0	1	0	0	?	0	?	?
Ronzotherium filholi	0	0	0	0	0	0	0	0	0	0	-	0	0	0	0	-	0	0	0	0	0	0	0	0	0	0	1	0	0	0	0	0	0	0	0	0	0	0	0	0	0	0	?	?	0	0	0	0	0	0	?	0	0	0	0	?	0	0	1	0
Plesiaceratherium mirallesi	1	1	0	0	0	0	0	0	0	0	-	0	1	1	0	-	0	1	1	0	0	1	0	0	0	1	0	0	0	1	1	1	0	0	0	0	0	0	0	1	0	0	?	?	0	0	0	1	0	0	0	0	0	0	0	1	0	0	0	0
Protaceratherium minutum	1	1	0	0	0	0	0	0	1	0	-	0	1	0	0	-	0	1	0	2	0	0	0	1	0	1	0	0	0	0	0	2	0	0	0	0	0	0	1	1	1	0	?	?	0	0	0	0	0	?	?	0	0	0	0	0	0	0	?	?
Diceratherium armatum	0	1	0	0	0	0	0	0	1	0	-	0	1	0	0	-	0	1	0	0	0	0	1	0	0	0	0	1	0	0	3	?	0	0	0	0	0	1	0	0	1	0	?	?	0	0	0	?	0	?	?	1	0	0	0	0	0	1	2
Menoceras arikarense	1	1	0	1	0	0	0	0	0	1	0	0	1	0	0	-	0	0	0	2	0	0	1	0	0	1	0	1	0	0	3	?	0	1	0	0	0	0	2	-	1	0	?	?	1	0	0	0	1	0	0	1	0	0	0	1	0	0	1	0
Kenyatherium bishopi	0	?	0	0	0	0	0	?	?	?	?	?	?	?	?	?	?	?	?	?	?	?	?	?	?	?	?	?	?	?	?	?	?	?	?	?	?	?	?	?	?	?	?	?	?	?	?	?	?	?	?	?	?	?	?	?	?	?	?
Bugtirhinus praecursor	1	1	0	0	?	?	?	0	1	1	0	0	1	0	2	0	0	?	0	2	0	0	1	0	0	1	2	0	1	-	3	?	0	?	?	?	1	0	1	1	1	0	?	?	0	0	0	0	0	?	?	?	?	?	?	?	?	?	?	?
`Caementodon´caucasicum	1	1	0	1	0	0	0	0	?	1	0	0	1	0	2	0	0	?	0	2	0	0	1	1	0	1	3	-	1	-	3	?	0	1	0	0	2	-	2	-	1	0	?	?	?	?	?	?	?	?	?	?	?	?	?	?	?	?	?	?	?	?
Caementodon oettingenae	1	1	0	1	0	0	0	2	1	0	-	0	1	0	2	0	0	1	0	2	0	0	?	0	0	?	?	?	?	?	3	?	0	1	0	0	2	-	2	-	1	0	?	?	0	0	0	0	0	?	?	?	?	?	?	?	?	?	?	?	?	?
`Hispanotherium´ grimmi	1	1	0	0	1	0	0	0	1	1	0	0	1	0	2	0	0	0	0	2	0	0	1	0	0	1	3	-	1	-	3	0	0	?	?	?	2	-	2	-	1	0	?	?	0	0	?	?	?	?	0	1	0	0	0	1	1	1	1	0
Hispanotherium beonense	1	1	0	1	1	0	0	2	1	1	0	0	1	0	2	0	0	0	0	2	0	0	1	1	0	1	3	-	1	-	3	0	0	1	0	0	2	-	2	-	1	0	?	?	0	0	0	0	0	0	0	0	0	0	1	1	1	1	0
Hispanotherium corcolense	1	0	0	1	1	0	0	0	1	1	0	0	1	0	2	0	0	0	0	2	0	0	1	1	0	1	3	-	1	-	3	0	0	1	0	0	2	-	2	-	1	0	?	?	0	0	0	0	0	0	?	0	0	0	0	1	1	1	1	1
Hispanotherium matritense	1	0	0	1	1	0	0	1	1	1	0	0	1	0	2	0	0	0	0	2	0	0	1	1	0	1	3	-	1	-	3	?	0	1	0	0	2	-	2	-	1	0	?	?	0	0	1	0	0	?	?	0	0	0	0	1	1	1	1	0
`Procoelodonta´ tekkayai	1	0	0	0	1	0	0	?	?	1	0	0	1	0	2	0	0	0	0	2	0	0	1	1	0	1	2	0	1	-	?	0	0	1	0	2	2	-	2	-	1	0	?	?	0	0	1	0	0	?	0	0	1	0	0	1	1	1	1	0
Procoelodonta mongoliense	?	0	0	0	1	2	0	0	?	1	1	0	?	0	2	0	0	?	?	?	?	?	?	?	?	?	?	?	?	?	?	?	?	?	?	?	?	?	?	?	?	?	?	?	?	?	?	?	?	?	?	?	?	?	?	?	?	?	?	?	?	?	?
Huaqingtherium lintungense	1	0	0	1	1	2	0	0	1	1	1	0	1	0	2	0	0	0	0	2	1	1	1	1	1	1	3	-	1	-	3	1	0	1	0	0	2	-	2	-	1	0	?	?	0	1	1	0	0	0	1	0	1	1	0	1	1	1	1	0
`Hispanotherium´ tungurense	1	0	0	1	1	2	0	0	1	1	1	0	1	0	2	0	0	0	0	2	1	1	1	1	1	1	3	-	1	-	3	1	0	1	0	0	2	-	2	-	1	0	?	?	0	1	1	0	0	0	1	0	1	1	0	1	1	1	1	0
Iranotherium morgani	1	0	1	0	1	2	1	2	1	1	0	0	1	0	2	0	0	0	0	2	1	1	1	1	1	1	3	-	1	-	3	?	0	1	0	?	2	-	2	-	1	0	?	?	?	?	?	?	?	?	?	?	?	?	?	?	?	?	?	?	?	?
Parelasmotherium schansiense	1	0	2	0	1	2	1	0	1	0	-	1	1	0	2	1	1	?	?	?	?	?	?	?	?	?	?	?	?	?	?	?	?	?	?	?	?	?	?	?	?	?	?	?	?	?	?	?	?	?	?	?	?	?	?	?	?	?	?	?	?	?	?
Sinotherium lagrelii	0	0	1	0	1	0	0	0	1	0	-	0	1	0	2	1	1	0	?	2	1	1	0	1	1	?	3	-	1	-	3	?	0	?	?	?	2	-	2	-	0	0	?	?	?	?	?	?	?	?	?	?	?	?	?	?	?	?	?	?	?	?
Elasmotherium caucasicum	0	0	1	0	1	0	1	?	1	0	-	0	1	0	2	0	0	1	0	2	0	0	0	1	1	?	3	-	1	-	3	?	2	-	-	-	2	-	2	-	2	0	?	?	?	1	?	?	?	?	?	?	?	?	?	?	?	?	?	?	?	?	?
Elasmotherium sibiricum	0	0	1	-	1	0	1	?	1	0	-	0	1	0	2	1	1	0	0	1	-	1	0	1	1	?	3	-	1	-	3	?	2	-	-	-	2	-	2	-	2	0	?	?	?	1	?	?	?	?	?	?	?	?	?	?	?	?	?	?	?	?	?

SUPPLEMENTARY DATA 2 (CONT.)

| Taxa | 1 | 1 | 1 | 1 | 1 | 1 | 1 | 1 | 1 | 1 | 1 | 1 | 1 | 1 | 1 | 1 | 1 | 1 | 1 | 2 | 2 | 2

SUPPLEMENTARY DATA 2 (CONT.)

Taxa	241	242	243	244	245	246	247	248	249	250	251	252	253	254	255	256	257	258	259	260	261	262	263	264	265	266	267	268	269	270	271	272	273	274	275	276	277	278	279	280	281	282
Tapirus terrestris	0	1	0	1	0	0	0	0	0	0	1	0	0	0	1	0	0	0	0	0	0	0	0	0	0	0	0	0	0	0	2	0	0	0	0	-	0	0	0	0	0	0
Hyrachyus eximius	0	0	0	0	0	0	0	0	0	0	0	0	0	0	0	0	0	0	0	0	0	0	3	0	0	0	0	0	0	0	2	1	-	0	1	0	0	0	0	0	0	0
Trigonias osborni	1	0	1	-	0	0	0	?	0	0	0	1	1	0	0	0	0	0	0	0	0	0	0	?	?	1	?	0	0	?	0	0	0	0	?	?	?	?	0	0	0	1
Ronzotherium filholi	0	0	0	0	0	0	0	0	0	0	0	0	1	?	0	0	0	0	1	0	0	2	0	1	0	1	0	0	1	?	0	0	0	0	0	0	-	0	?	0	0	0	0
Plesiaceratherium mirallesi	0	1	0	0	0	0	0	0	1	0	1	1	1	0	0	1	0	0	1	0	1	0	3	1	2	0	0	0	0	0	1	1	-	0	0	-	0	0	0	0	1	0
Protaceratherium minutum	0	0	?	?	0	0	0	?	?	?	?	1	1	0	0	1	0	0	1	0	0	0	1	1	0	0	0	0	0	0	2	?	?	1	0	-	?	1	0	0	0	0
Diceratherium armatum	0	0	0	0	0	0	1	1	0	0	0	1	0	0	0	0	1	0	0	0	0	0	3	1	2	0	0	1	0	0	2	0	0	1	0	-	0	0	0	0	0	1
Menoceras arikarense	0	0	0	1	0	0	1	1	0	0	0	1	1	1	0	1	0	0	1	0	1	0	3	3	2	1	0	1	1	0	1	0	0	1	1	0	0	1	0	0	0	0
Kenyatherium bishopi	?	?	?	?	?	?	?	?	?	?	?	?	?	?	?	?	?	?	?	?	?	?	?	?	?	?	?	?	?	?	?	?	?	?	?	?	?	?	?	?	?	?
Bugtirhinus praecursor	?	?	?	?	?	?	?	?	0	1	1	1	1	1	0	1	?	?	1	0	0	0	3	?	?	1	?	1	?	0	2	0	0	1	1	0	1	1	0	0	?	0
`Caementodon´caucasicum	?	?	?	?	?	?	?	?	?	?	?	1	1	1	0	1	0	0	1	0	0	0	3	?	?	?	?	?	?	?	?	?	?	?	?	?	?	1	?	0	?	?	?
Caementodon oettingenae	0	1	?	?	1	?	?	?	?	?	?	1	1	1	0	1	0	0	1	0	0	0	3	0	2	1	0	1	1	0	1	0	0	0	1	0	1	?	0	0	0	0
`Hispanotherium´ grimmi	?	1	0	1	?	1	1	?	?	?	?	1	1	1	1	1	0	?	1	0	1	0	3	1	2	1	0	1	0	0	2	0	0	1	1	0	1	1	0	1	0	0
Hispanotherium beonense	?	1	0	1	1	1	1	?	?	?	?	1	1	1	0	1	0	1	1	0	1	0	3	0	2	?	0	1	0	?	?	?	?	?	?	?	?	1	?	0	1	0	0
Hispanotherium corcolense	0	1	0	1	1	1	1	1	0	1	1	2	1	1	1	1	0	1	1	0	2	0	3	3	2	1	1	1	0	1	2	0	0	1	1	0	1	1	0	1	0	0
Hispanotherium matritense	?	1	0	1	1	1	1	1	0	1	1	1	1	1	0	1	0	0	1	0	1	0	3	1	2	1	0	1	0	0	1	0	0	0	0	-	1	1	0	1	0	0
`Procoelodonta´ tekkayai	?	?	?	?	?	?	?	?	?	?	?	?	?	?	?	?	?	?	?	?	?	?	?	?	?	?	?	?	?	?	?	?	?	?	?	?	?	?	?	?	?	?
Procoelodonta mongoliense	?	?	?	?	?	?	?	?	?	?	?	?	?	?	?	?	?	?	?	?	?	?	?	?	?	?	?	?	?	?	?	?	?	?	?	?	?	?	?	?	?	?
Huaqingtherium lintungense	0	1	0	1	1	1	1	?	0	1	1	1	1	1	0	1	0	?	1	0	2	0	3	?	2	1	0	1	0	0	2	?	?	?	?	?	?	1	0	1	0	0
`Hispanotherium´ tungurense	0	1	0	1	1	1	1	?	0	1	1	1	1	1	0	1	0	?	1	0	2	0	3	?	2	1	0	1	0	0	2	?	?	?	?	?	?	1	0	1	0	0
Iranotherium morgani	?	1	0	1	1	1	1	?	?	?	?	2	1	1	0	1	?	1	1	0	2	0	0	?	?	?	?	1	?	?	?	?	?	?	?	?	?	?	?	0	1	?	0
Parelasmotherium schansiense	?	?	?	?	?	?	?	?	?	?	?	1	1	1	0	1	0	1	1	0	2	0	0	?	?	?	?	1	?	?	?	?	?	?	?	?	?	?	?	0	?	?	?
Sinotherium lagrelii	?	?	?	?	?	?	?	?	?	?	?	?	?	?	?	?	?	?	?	?	?	?	?	?	?	?	?	?	?	?	?	?	?	?	?	?	?	?	?	?	?	?
Elasmotherium caucasicum	?	?	?	?	?	?	?	?	?	?	?	?	?	?	?	?	?	?	?	?	?	?	?	?	?	?	?	?	?	?	2	0	0	?	1	0	1	?	0	1	?	0
Elasmotherium sibiricum	?	1	2	-	1	1	1	1	0	1	1	?	?	1	0	1	?	?	1	0	2	1	0	3	2	0	1	?	?	?	?	?	?	?	?	?	?	?	?	0	1	0	0

SUPPLEMENTARY DATA 3

Distribution of nonambiguous apomorphies of Elasmotheriini at each node of the consensus tree (as labeled in Fig. 6A). The reversions are preceded by the sign '–'.

Node a: 40^{1}, 49^{1}, 57^{1}, 72^{2}, 73^{1}, 88^{1}, 101^{3}, 130^{1}, 154^{1}, 159^{2}, 176^{1}, 235^{1}, 244^{1}, 254^{1}, 266^{1}, 275^{1}

Node b: 27^{1}, 63^{1}, 68^{1}, 83^{2}, 89^{1}, 94^{3}, 95^{1}, 102^{3}, 116^{3}, 135^{2}, 147^{3}, 149^{1}, 157^{2}, 192^{1}, 197^{1}, 200^{1}, 205^{1}, 211^{1}, 216^{1}, 240^{1}, 242^{1}, 245^{1}, 250^{1}, 251^{1}, 277^{1}

Node c: -35^{1}, 37^{1}, -57^{0}, 87^{1}, -114^{2}, 124^{1}

Node d: -77^{0}, 97^{1}, 112^{1}, -122^{0}

Node e: 70^{2}, 77^{1}, 109^{1}, 125^{1}. 193^{1}, 198^{1}, 199^{3}, 208^{1}, 209^{1}, 221^{1}, 258^{1}, 261^{1}, 280^{1}

Node f: -122^{0}, 167^{1}, 173^{1}

Node g: 67^{2}, 87^{3}, 112^{2}, 126^{2}

Node h: -57^{0}, 85^{1}, -87^{2}, 97^{1}, 99^{0}, -103^{0}, 108^{1}, -112^{1}, 124^{1}, 191^{1}, 223^{3}

Node i: 28^{1}, 33^{1}, 66^{1}

Node j: 21^{1}, 47^{2}, 63^{2}, 64^{1}, 68^{1}, 76^{1}, 119^{1}, 123^{1}, 127^{1}, -263^{0}

Node k: 2^{1}, 3^{1}, 4^{1}, -40^{0}, -45^{0}, 46^{1}, 48^{1}, -49^{0}, -84^{0}, -130^{0}, 136^{1}, 137^{1}

Node l: 37^{1}, -102^{2}, 107^{3}, 112^{3}, -121^{0}, -126^{0}

Node m: 59^{2}, 89^{2}, 117^{1}, 153^{2}

5. Intraspecific variability of *Hispanotherium matritense* (Lartet *in* Prado, 1864)

Oscar Sanisidro
Cayetana Martínez-Maza
María Teresa Alberdi
and Jorge Morales

Abstract. *Hispanotherium matritense* is one of the most abundant fossil mammals of the middle Aragonian of the Iberian Peninsula, spanning over the Local Zone D. Its particular subhypsodont dental morphology and slender postcranial proportions among the Miocene rhinoceroses have been suggested as indicators of dry and warm climatic conditions. The discovery of several localities scattered along the Madrid and Guadalajara Provinces and the supervision of several public works underwent during the last years in Madrid City provided a large collection of *H. matritense* remains. These new sites with presence of the species are Casa de Campo / Marqués de Monistrol M-30, Fábrica Mahou, Embajadores-R, Fresno del Torote, Las Ventas, and Yunquera del Tajo. The sites of Casa de Campo / Marqués de Monistrol M-30, Mahou, and Príncipe Pío-2 have provided a great amount of fossil remains, some of them geographically and stratigraphically close to the type locality of Puente de Toledo. This, together with the comprehensive review of the Iberian published material, provides an exhaustive and complete overview of the postcranial variation of the species, permitting to confidently outline its external appearance. We present a size estimation based on a sub-complete associated specimen. Several intraspecific variations have been detected within the postcranial remains within well-sampled localities. Our data help to make an overall review of the characters that define the species and outline their morphologic boundaries with purported Eurasian material.

INTRODUCTION

In 1864, C. del Prado and M. de la Paz Graells were commissioned to update the Geological charts of the Iberian Peninsula. The resulting work, published two years prior to the death of del Prado, includes a monographic volume describing the geology and paleontology of the Madrid Province. Among the cited paleontological localities, they describe some vertebrate remains (including several rhinoceros teeth) from Puente de Toledo collected by von Meyer and Gervais. As del Prado comments, rhinoceros fossils from Puente de Toledo were previously assigned by M. Lartet to a new species, named as '*Rhinoceros Matritensis*'. Even though Lartet did not leave any formal mention, it is currently considered the species' author. Subsequently, E. Hernández-Pacheco discarded the validity of the species based solely on the cement (quoting the opinion of N. G. Stehlin; Hernández-Pacheco, 1914), an opinion followed by posterior authors (Pérez de Barradas, 1926; Schlosser, 1921). At the end of the 40's, M. Crusafont and J. F. de Villalta brought renewed interest to the rhinoceros from Madrid. They linked the hypsodont dentition and cementum fillings in the valleys with *Iranotherium morgani* from Maragha and the Chinese *Sinotherium lagrelii*, the only two elasmotheres known at the time. Besides recognizing its elasmothere affinities, they noted enough differences to erect a new genus, naming it *Hispanotherium* (Crusafont and Villalta, 1947). Posteriorly, in 1952, Zbyszewski reported some teeth of a new species, *Chilotherium quintanelensis* from Quintanelas, Portugal (currently considered as pertaining to *H. matritense*; Aguirre et al., 1982; Villalta and Crusafont, 1955). The species was found in additional Portuguese localities as Casul Chitaz (posteriorly known as Casal das Chitas; Antunes and Ginsburg, 1983) and Areneiro do Jose da Graça (Antunes, 1965, 1972; Antunes and Ginsburg, 1983). In the late 70's numerous new fossil sites with presence of *H. matritense* were reported along the central basins of the Iberian Peninsula. Their macrofaunal associations were called "*Hispanotherium* faunas" due to the abundance of this rhinoceros species and its importance as a biostratigraphic indicator of the Middle Aragonian (Antunes, 1979; Antunes and Ginsburg, 1983; Cerdeño, 1987, 1992a; Cerdeño and Alberdi, 1983). Summarizing, *H. matritense* has been recorded at the sites listed below from the Tertiary basins of the Iberian Peninsula and France (see Appendix 1 for a updated list of *H. matritense* remains):

- **Calatayud-Montalbán Basin**: Valdemoros 1A (Aragonian type area; Cerdeño, 1989; Ginsburg and Antunes, 1979), Valdemoros 2, Valdemoros 3C, Valdemoros 4A, Munébrega-1, and Munébrega-3 (Calatayud Area; Antunes, 1979; Cerdeño, 1989),

Villafeliche-4 (Cerdeño, 1989), Torralba de Ribota I-III and Torralba de Ribota V (Zaragoza; Boné et al., 1980).

- **Ebro Basin**: Tarazona de Aragón (Zaragoza; Astibia, 1985; Cerdeño, 1989).

-**Loranca Basin** (or Altomira Basin): La Retama (Cuenca; Cerdeño, 1992a; Morales et al., 1993).

- **Tagus Basin**, Lisboa Area: several localities grouped in Chelas (or Chelas-1, Lisboa; Antunes, 1965), Charneca do Lumiar (Lisboa; Antunes, 1965) and Quintanelas (Sabugo; Zbyszewsky, 1952). Middle Tagus: Dehesa de los Caballos (Cáceres; Hernández-Pacheco and Crusafont, 1960; Olivares and Rebollada, 2011). Torrijos (Toledo; Aguirre et al., 1982; Cerdeño, 1982; Cerdeño and Alberdi, 1983) and numerous localities within the city of Madrid (Madrid area, higher Tagus basin) detailed below.

The presence of *H. matritense* in the Madrid Area is restricted to the Local Zone D, Middle Aragonian (Middle Miocene), between 17,5 and 14,1 Ma. The Local Zone D is divided into four subunits according to their micromammal assemblages, of which, only Dc contains *H. matritense* remains in the Madrid region. The Local Zone Dc is represented by the "Facies Peñuela". These are formed by green clays exposed along the riverbank of the Manzanares River, from the Cerro de San Isidro and the Puente de Toledo to the Cerro de la Plata. The sediments of this subunit are distributed along a densely populated area and were originally deposited in shallow lacustrine environments located on the distal part of wide alluvial fan systems. In addition to the classic sites of Puente de Toledo and La Hidroeléctrica, the continuous expansion of the city of Madrid from 1980 onwards favored the finding of additional localities. These are (in chronological order) Moratines (Alberdi et al., 1981), Estación Imperial (1991), the new excavations in the classic site of La Hidroeléctrica,the

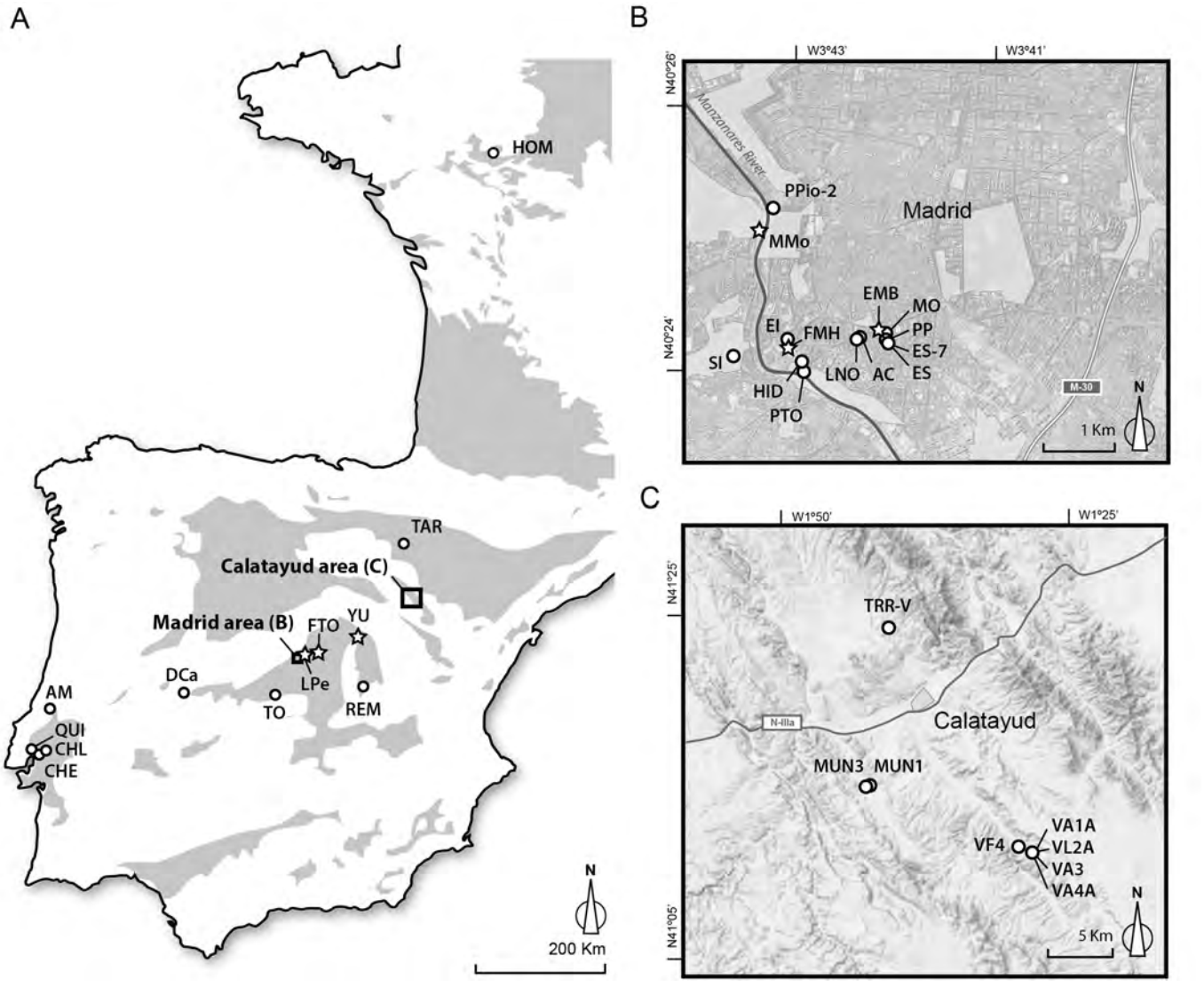


Fig. 1 Geographic position of the localities with presence of *Hispanotherium matritense* (abbreviations detailed in Material and Methods). A, simplified geographic map of the Iberian Peninsula and Western France with the Tertiary basins shaded. B, aerial photo showing the position of the localities within the Madrid City boundaries (Madrid Province). C, detailed map of the localities grouped around Calatayud (Zaragoza Province). Localities with presence of *H. matritense* firstly reported in the present work are represented with a star.

expansion of the railway green belt (1992-1993), the construction of the third airstrip of Madrid-Barajas Adolfo Suárez airport (1997-1998), the public works along the fluvial terraces of the Manzanares river, and the extensive urban works around Puerta de Toledo, which includes the fossil sites of PAR-Peñuelas (Cerdeño and Iñigo, 1997), Paseo de las Acacias (Cerdeño and Iñigo, 1997), Paseo de la Esperanza, Paseo de la Esperanza 7, Embajadores (Cerdeño and Iñigo, 1997), and Los Nogales (Herráez et al., 2006). More recently, large infrastructural works in the metropolitan area along Manzanares River during the last decade area have unearthed additional locations from Madrid and Guadalajara Provinces with presence of *H. matritense*, detailed below:

- **Casa de Campo / Marqués de Monistrol M-30**. The fossil complex of Casa de Campo / Marqués de Monistrol M-30 was discovered during the public works of the M-30 ring road section between Marqués de Monistrol Street and the bridge of Puente del Rey, close to the type locality of Puente de Toledo. Four fossiliferous spots were found: Ramal 4.1, Ramal 4.2, Colector, and Túnel A-5. Three different levels (T1, T2, and T3) have been identified along the first three spots. They lie between 573 and 575 m above the sea level. This altitudinal range makes them among the older Middle Aragonian sites within Madrid City together with Príncipe Pío-2 (base of the local zone Dc). The nature of the sediments consists on brownish silty-clay (Ramal 4.1), brownish silty-sands with interspersed carbonate layers (Ramal 4.2), or both (Colector and Túnel A-5). Sediments were deposited in a variable ambient with occasional fluvial currents and shallow lacustrine areas. As a result, fossils are often disarticulated and suffer from some degree of transport.

- **Embajadores-R**: Four different fossiliferous levels in Embajadores were discovered during the public works of the subway station of Embajadores in 2005. *H. matritense* has been recorded in three of them, named as PG-1, PG-2 and PG-4. The site, placed between 593 and 602 m above the sea level (slightly lower than Fábrica Mahou), can be preliminarily assigned to the Local Zone Dc.

- **Fábrica Mahou**: The site, found during the demolition of the Mahou brewery placed between the Paseo de Pontones and Paseo Imperial streets, has yielded an approximate amount of 1,100 remains of *H. matritense*. The altitude of the site, around 590 m, places it at a similar level than other neighboring Middle Aragonian localities like Estación Imperial (Dc Local Zone). Fossils are embedded in a fine-grained micaceous sandy matrix. Rhinocerotid remains from Fábrica Mahou are excellently preserved and show little sign of crushing or compression (more frequent in long bones). Such exceptional preservation degree together with a large number of both dental and postcranial remains, and the variety of bones (all the tarsus and carpus is represented) poses Fábrica Mahou as the most important source of information for the anatomy of the species together with Príncipe Pío-2.

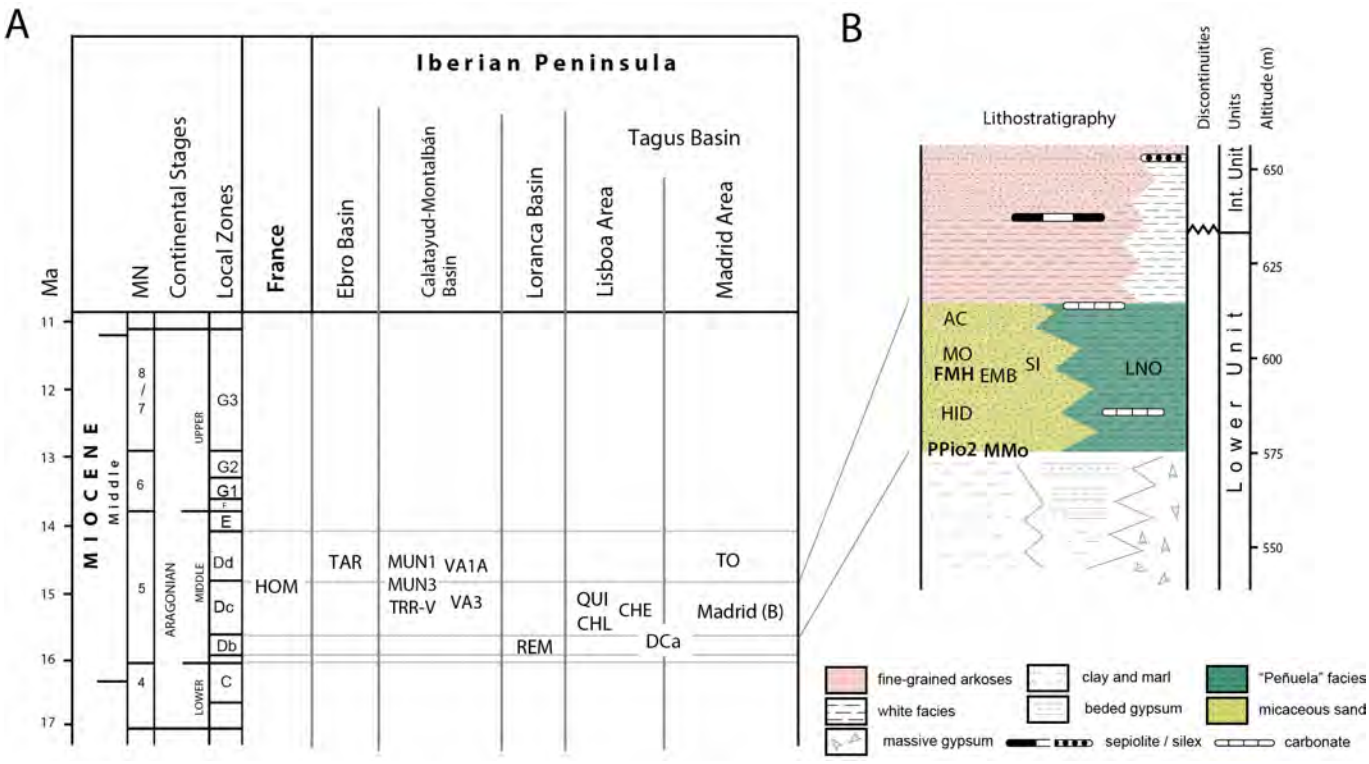


Fig. 2 A, general biostratrigraphic position of *Hispanotherium matritense* based upon the literature and the new data of study (see Introduction and Supplementary Data 2 for complete references; see material and methods for locality abbreviations). B, local stratigraphy of the Madrid City area with some localities with presence of *H. matritense* and new locality data represented in bold face.

- **Príncipe Pío-2**: The presence of *H. matritense* in Príncipe Pío-2 was firstly published in Sanisidro et al. (2011) on the basis of the first cranial material described for the species. Apart from the cited skulls, the construction of Príncipe Pío transport interchange in 2007 revealed a rich accumulation of over a thousand remains of *H. matritense*, comprising the bulk of the recovered fossil vertebrates. Apart from the cranial remains, the fossil list includes mandibles, dentition, numerous limb-bone elements, vertebrae and ribs. This vast array of remains, range from partially articulated skeletons to isolated and fragments. Fossils commonly show several taphonomical modifications like abrasion (eroded articular angles), pitting surfaces and weathering (superficial cracking in long bones diaphysis). Most fossils were found embedded in highly-compacted brown clay layer (the top of which turns more carbonated) of variable thickness (0,25 – 1 m) and a maximum altitude ranging between 574,4-575,9 m.

- **Yunquera de Tajo**, **Fresno del Torote**, and **La Peineta** (= Las Ventas): A small number of *H. matritense*'s remains have been recovered from each of these localities, for which there is no currently available stratigraphic information. Nevertheless, the site of La Peineta is geographically closer to the site of O'Donnell (Dd Local Zone) than the bulk of localities with *Hispanotherium* next to the Manzanares River (Dc Local Zone). If La Peineta pertains to the Dd Local Zone, it would be the last record of *H. matritense* in the Madrid City area.

H. matritense is here recorded for the first time in Barajas-17, Fábrica Mahou, Embajadores-R, Casa de Campo / Marqués de Monistrol M-30, La Peineta (= Las Ventas; all located in Madrid City), Fresno del Torote (Madrid Province), and Yunquera del Tajo (Guadalajara Province). Príncipe Pío-2 has been also included as a result of the overwhelming new data. The first goal of the present work is to make a comprehensive description of the new remains of *H. matritense*. These have been figured in the form of an osteological atlas for posterior studies and field works. As a result, a skeletal restoration of the species is here firstly proposed.

Two alternative approaches have been used when dealing with intraspecific variation of *H. matritense*. The first one assumes a wide range of morphologies (Antunes and Ginsburg, 1983; Cerdeño, 1989, 1995; Iñigo and Cerdeño, 1997). As a consequence, Asian remains from Anatolia, Beger-Nur (Mongolia), Chinji (Pakistan), and Bielometchetskaya (Caucasus) have been eventually assigned to *H. matritense* (Cerdeño, 1989, 1995). Other studies held a completely different view, with a more constrained intraspecific variation, splitting each one of these localities into different taxa. Only a detailed and broad study of the species would shed light on the intraspecific boundaries within the genus *Hispanotherium* and related forms (Cerdeño, 1987). The new remains described in the present work pretends to clarify this question. To do so, our second objective is to quantitatively address the instrapecific variability of *H. matritense* by means of a broad study of the well-sampled localities of Casa de Campo / Marqués de Monistrol M-30, Príncipe Pío-2, and Fábrica Mahou. The morphological variation of these localities has been registered and shown by diagrams.

Bone histological studies have been proven to provide valuable information about biological features of large mammals (e.g.Klevezal, 1996; Köhler and Moyà-Solà, 2009; Martinez-Maza et al., 2014). We have carried out a histological study of the bone microstructure of the *Hispanotherium matritense* limb bones in order to obtain more information about its biology and life history. The large postcranial sample from the locality of Príncipe Pío-2 has a significant proportion of fragmentary and/or incomplete remains, put it in an ideal position for histological studies. Hitherto, only the work by Sander and Andrassy (2006) has addressed the bone histology of Rhinocerotidae, specifically from four tibiae of *Coelodonta antiquitatis*. According to that work, the woolly rhino tibiae are characterized by small areas of primary bone with a plexiform vascular system whereas most of the tissue is replaced by secondary osteons. In spite of strong bone remodeling obscured the microscopic identification of growth marks, Sander and Andrassy (2006) suggested the presence of possible LAGs from macroscopic indications. The third objective of the present work is to provide a first description of the bone histology in rhinoceros with some remarks on the life-history of *H. matritense*.

MATERIALS AND METHODS

A total of 1320 bones of *H.matritense* from the localities of Fábrica Mahou, Embajadores-R, Casa de Campo / Marqués de Monistrol M-30, La Peineta, Fresno del Torote, Yunquera del Tajo, Príncipe Pío-2, and Los Nogales (listed in the Appendix 1) have been studied. Some of the bones (i.e. trapezium, Mc V, i1, the femur, the fibula, the tibia, the entocuneiform, and the mesocuneiform) are here firstly described. Measurements are given in millimeters with an accuracy of one decimal digit. Approximate measurements are given in parentheses. Measurements were made with a digital caliper and a measuring tape for elements larger than 150 mm. Anatomical terminology follows Guérin (1980), but that used by other authors has also been taken into consideration (Antoine, 2002; Heissig, 1972a, 1999). Measurements are detailed in the Material and Methods Chapter. In order to test the increase in robustness through time among the postcranial bones of *H. matritense,* gracility indices (*GI*) have been calculated for the six main metapodials (i.e. Mc II, Mc III, Mc IV, Mt II, Mt III, and Mt IV) according to the following formula:

$$GI = (DTdia/L)\cdot 100$$

Being TDdia the transversal diameter of the midshaft of the metapodial and L its maximum length (Cerdeño, 1989).

Anatomical Abbreviations—ant, anterior; art, articulation; dia, diaphysis; dis, distal; int, interior; epi, epiphysis; m. muscle;max, maximum; Mc, metacarpal; min, minimum; Mt, metatarsal; prox, proximal; 3tr, third trochanter. Capital letters are used for upper teeth (D, P, M; upper decidual, premolar and molar respectively), and lower case for lower teeth (d, p, m). In describing the dental elements, we follow the terminology proposed by Van Valen (1966). I, M and P designate incisors, molar and premolar respectively. Lower-case letters designate teeth from lower jaws and upper-case letters teeth from upper jaws. A preceding 'D' indicates decidual teeth (e.g., Dp2: lower second decidual premolar). The dental terminology follows Heissig (1969), Uhlig (1999), and Antoine (2002). Some of the cranio-dental and osteological features described correspond basically to cladistic characters used and listed by Antoine (2002) and Antoine et al. (2010), and subsequently refined by Becker et al. (2003).

Measurements abbreviations—APD, antero-posterior diameter; DL, distal length; H, height; L, length; TD, transverse diameter.

Institutional abbreviations—MNCN, Museo Nacional de Ciencias Naturales (Madrid, Spain), MHNT, Muséum d'histoire naturelle de Toulouse (Toulouse, France); AMNH, American Museum of Natural History (New York, USA).

Localities abbreviations—All abbreviations are given as follows: Locality abbreviation in the graphs and tables / Specimen label abbreviation of the same locality (when different). AC, Paseo de las Acacias; AM, Amor; CHE, Chelas; ChL, Charneca do Lumiar; CO2, Córcoles-2; DCa, Dehesa de los caballos; EI, Estación Imperial; EMB, Embajadores-R; ES, Paseo de la Esperanza; ES7, Paseo de la Esperanza 7; FMH, Fábrica Mahou; FT, Fresno de Torote; HID, La Hidroeléctrica; HOM, Hommes; LNO, Los Nogales; MMo, Marqués de Monistrol; MO, Moratines; MUN1, Munébrega 1; MUN3, Munébrega 3; PTO, Puente de Toledo; PP, PAR-Peñuelas; PPio-2; Príncipe Pío; QUI, Quintanelas; REM, La Retama; SI, Cerro de San Isidro; TAR, Tarazona; TO, Torrijos; TRR-V, Torralba V, VA1A, Valdemoros 1A; VA2A, Valdemoros 2A; VA3, Valdemoros 3; VA4, Villafeliche 4; VE, Las Ventas; YU, Yunquera de Henares; w/n, without field or collection number.

Biostratigraphic temporal ordination—The absolute altitude has been widely used as a reliable proxy for correlating localities from the same stratigraphic context within the Madrid City area (López-Martínez et al., 1987). This approach does not represent an absolute temporal dating but a relative temporal ordination. In the present work, it has been used to arrange temporally the nearby fossil localities of Marqués de Monistrol M-30 (574-575 m; mean = 574,5 m), Príncipe Pío-2 (574-575 m; mean = 574,5 m), Fábrica Mahou (~590 m), and Embajadores-R (593-602 m; mean = 597,5 m), PAR-Peñuelas (~598 m), and Paseo de las Acacias (~597 m), all within the Dc Biozone.

Histological study—For the histological study, we have selected a sample of 12 limb bones fragmented at the midshaft level to avoid damaging the most valuable and complete specimens (Figures 17-19). Bone histological sections were obtained following standard procedures (Lamm, 2013; Padian et al., 2013). First, a 1.5 cm-thick block taken from the midshaft region was embedded in epoxy resin EpoFix (Struers). The cutting surface was ground and polished with a Buehler low-speed Isomet with SiC grinding papers (SiC-800, SiC-1200; Struers) and fixed to a plexiglass slide using a cyanoacrylate adhesive. Subsequently, 200 µm-thick sections were cut using a Struers Discoplan TS diamond saw, and finally ground and polished to a final thickness of 100µm with the use of different SiC grinding papers (SiC-800, SiC-1200; Struers). All necessary permits were obtained for the described study, which complied with all relevant regulations (Vertebrate Paleontology Collection Department, Museo Nacional de Ciencias Naturales – CSIC, Madrid, Spain). All histological sections employed in the present paper are deposited in the Vertebrate Paleontology Collection of the MNCN and are available to researchers.

Analysis and high-resolution imaging of the thin sections were performed using an Olympus BX61 transmitted light microscope equipped with an Olympus DP71 digital camera (Grupo de Neuroprotección Molecular, Hospital Nacional de Parapléjicos, Toledo, Spain). The required images were merged and processed with Adobe Photoshop CS5 (Adobe Systems Inc). The histological description of the cortical bone microstructure follows the terminology established by Francillon-Vieillot *et al.* (1990), de Ricqlès *et al.* (1991), and Padian and Lamm (2013). For the skeletochronological analysis, we distinguished two types of growth marks within the primary cortical bone (Castanet, 2006; Castanet et al., 1993; Woodward et al., 2013). First, the lines of arrested growth (LAG) results from a cessation of bone growth followed by a sudden resumption of growth. And second, the external fundamental systems (EFS) described as aset of avascular lamellar bone and several lines close to the periosteal surface. To be considered as growth marks, lines should surround the entire section (Woodward et al., 2013).We assume that LAGs are annual growth marks from which we could infer the age of the specimen (e.g. Castanet, 2006; Klevezal, 1996; Sander and Andrässy, 2006; Woodward et al., 2013). We estimate the age of skeletal maturity as the number of LAGs until EFS following Chinsamy-Turan (2005) and Chinsamy and Valenzuela (2008).

Referred material—See Appendix 1.

SYSTEMATIC PALEONTOLOGY

Family Rhinocerotidae Gray, 1821

Subtribe Elasmotheriina Bonaparte, 1947

Genus *Hispanotherium* Crusafont and Villalta, 1947

Type species—*Hispanotherium matritense* (Lartet *in* Prado, 1864)

Other species—*Hispanotherium corcolense* Antoine, Alférez and Iñigo, 2002, *Hispanotherium beonense* Antoine, 1997.

Diagnosis—elasmotheriine rhinoceros with a constricted hypocone on the M1, and constricted protocone on the P3-4; straight medial border of the radius; proximal ulnar-facets of the radius generally independent; scaphoid with a small trapezium-facet; straight volar process of the magnum; calcaneum-facet 1 of the astragalus low and long and the intermediate relieves of the central metapodials low (Antoine et al., 2002).

Hispanotherium matritense (Lartet *in* Prado, 1864)

Lectotype—Right M3 (without label) figured in Prado (1864; Fig. 5) and Crusafont and Villalta (1947; Fig. 1).The specimen, formerly hosted in the Museo Don Felipe de Borbón y Grecia – ETSI (Madrid), is currently inaccessible and possibly missing.

Paralectotypes—left m1 (without label) figured in Prado (1864; Fig. 6) and Crusafont and Villalta (1947; Fig. 3). A decidual tooth DPx (without label; figured in Prado, 1864, Fig. 9) and a lower second incisor (without label; figured in Prado, 1864, Fig. 7) are currently inaccessible together with the lectotype (and apparently missing). The m1 is hosted in the Museo Don Felipe de Borbón y Grecia – ETSI (Madrid).

Prado (1864) did not design a holotype in its original description, being necessary the selection of a lectotype. Crusafont and Villalta (1947) designed the right M3 (w/n) as lectotype and the right M2 (w/n) as holotype. This has been followed by subsequent authors (Antoine, 1997; Cerdeño, 1989; Cerdeño and Alberdi, 1983; Deng, 2003; Olivares and Rebollada, 2011; Sanisidro et al., 2011), who considered the M2 without number as the type-bearing specimen of the species and, from a practical point of view, adopted it as a lectotype. However, the right M2 (w/n) is not suitable as lectotype as it was not included in the original publication and, therefore, is excluded from the syntype (according to the article 74.2 of the ICZN). Hence, the right M3 (w/n; Fig. 5 in Prado, 1864) should be considered the lectotype for the species in agreement with Cerdeño (1989). The right M2 (w/n), firstly figured by Crusafont and Villalta (1947), should be included in the hypotype series described by Crusafont and Villalta (1947). These include a right M2 (w/n), a left mandibular fragment with an incomplete m1, m2 and m3 (w/n); left p4 (w/n); left m1 (w/n); left m2 (w/n); right m2 (w/n), and an incomplete right m3 (w/n). Unfortunately, the collection from Puente de Toledo stored in the Museo Don Felipe de Borbón y Grecia – ETSI (Madrid) was misplaced during the Spanish Civil War and is currently inaccessible (or possibly lost). Future curational research will shed light into the type series of *H. matritense*.

Type locality—Puente de Toledo (Madrid).

Biostratigraphic and Geographic range—Western Europe (Iberian Peninsula and France), Middle Miocene (middle Aragonian); MN5 Mein's Biozone.

Diagnosis (modified from Sanisidro, 2011)—Small sized elasmothere without nasal or frontal horns. Orbit over the M3. Nasal notch reaches the level of the P4, straight upper border and a concave lower profile. Subhypsodont check teeth with very thick cement cover, deeply constricted protocone and lightly constricted metaconid. Upper premolars with closed median valley. Secondary folds of the enamel developed. i2 like small tusks, with sexual dimorphism in shape and size. Slender postcranial skeleton with a reduced, non-functional Mc V.

Differential diagnosis—*H. matritense* differs from other *Hispanotherium* species in the generally multiple crochet on the premolar teeth, presence of lingual wall on the DP2, rounded paralophid on the dp3, curved volar process of the magnum and Mt III void of cuboid-facet and a concave proximal border in dorsal view (see Antoine et al., 2003, p. 24 for a comprehensive comparison between different species).

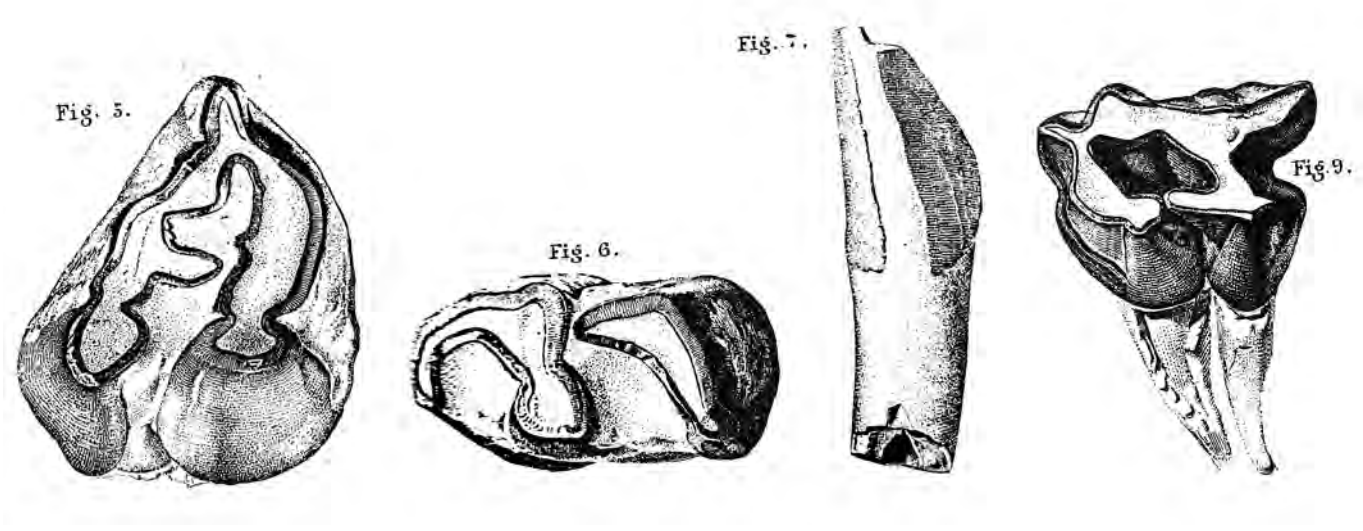


Fig. 3 Original type series of *Hispanotherium matritense* from Puente de Toledo as figured in Prado (1864). From left to right: left M3 (holotype; w/n), left m1 (w/n), right i2 (w/n), decidual tooth (DP3/4; w/n).

MORPHOLOGICAL DESCRIPTION AND INSTRASPECIFIC VARIABILITY IN *H. MATRITENSE*

Skull—The cranial morphology of *H. matritense* has been described in Sanisidro et al., 2012. The preservation degree of the three skulls from Príncipe-Pío 2 (i.e. highly crushed and distorted specimens) prevents further intraspecific comparisons except for the nasal region, which present a long and pointed nasal bone with a flattened and smooth dorsal surface.

Mandible (Figure 4)—the mandible is slender, has a vaguely-convex lower border in juvenile specimens, straight in adults. No attached hemimandibles have been preserved and the sagittal symphiseal part is usually badly preserved, so is difficult to assess if the species had foramina for the i1's. The mandibular symphisis is short, reaching the level of the (d)p1/(d)p2 boundary (e.g. FMH'14-3375). In labial view, the labial surface of the mandible is smooth and flat. The ventral border of the horizontal ramus changes from slightly convex to straight through a small angle at the level of the caudal border of the symphiseal suture. The diastema is short and rugous. In lingual view, the lingual surface of the horizontal ramus is flat and smooth except for a very faint depression that runs parallel to the distal border. The mental foramina are typically double and oval, the cranial bigger and more distally placed. The distance between both foramina and their relative position along the mandible varies between individuals (Figure 4). The ascending ramus has a concave rostral border and a slightly sigmoid caudal one. It is wide at its base and narrows proximally. The labial side is flat and occupied by two large muscular attachment areas. The m. masseter occupies the masseteric fossa. It goes from the mandibular angle (as a blunt ridge that faintly protrudes labially) to a smooth oblique crest that divides the proximal half of the ascending ramus. The rostral limit of the fossa falls behind the dental series, but is nearly imperceptible in inmature individuals. This limit is rounded to vertical and typically aligned with that of the m. temporalis. The insertion of the m. temporalis has a 'tear'-like outline, spreading over the rostro-proximal side of the ascending ramus, from the level of the gingival border to the coronoid process (e.g. 05/101/2/1698). Contrary to the m. masseter, the insertion for the m. temporalis is well-marked in, at least, IDAS 1 (e.g. 05/101/2/1694). A progressive change in the relative surface of the m. masseter and m. temporalis takes place during ontogeny. Younger specimens have a greater surface commited to the m. temporalis (with a proportion close to 1:1; Figure 4D) whereas older ones have a larger m. masseter proportion (Figure 4B). The caudal border of the mandible has a widened, flattened surface at the level of the neck of the ascending ramus. It is the place of attachment for the m. digastricus. In lingual view, the ascending ramus has a large, concave pterygoid fossa for the m. pterygoideus. Slightly rostral to its midpoint opens the mandibular foramen. It is rounded and proximo-caudally continued by a shallow oval depression. A ventral notch (Incisure vasorum facialium) roughtly divides the horizontal from the ascending rami.

Dentition

The dentition of *H. matritense* had already been described elsewhere (Aguirre et al., 1982; Cerdeño, 1989, 1992a; Olivares and Rebollada, 2011; Sanisidro et al., 2011). However, there is paucity of intraspecific variation studies and part of the teeth series (DPx, i1 have not been described yet).

Anterior dentition (Figure 5)—the i1 are small, have a spatulated crown, vaguely oval in mesial view (with a slightly bigger mesial side). The root is simple and gently proximally-curved towards the apex. Among the preserved i1's, the anterior dentition set 05/101/2/1743 from Príncipe Pío-2 (Figure 5) shows the size proportions between first and second lower incissors. The lower anterior dentition of *H. matritense* stands out for the tusk-like i2. There two main types of i2 depending on both size and morphology. Both have a straight distal border and a curved and sharp mesial one. The larger forms of i2 show a thicker root, a larger crown, a more vertically-oriented distal side followed by a more acute transition to the mesial one, and a concave-convex occlusal surface (Group I; see discussion). Additionally, larger i2 are usually void of distal constriction at the base of the crown. The typical morphology of an i2 of the "smaller group" (Group II) includes a blunt apex, a thinner and straighter root and a flat occlusal surface (with a slightly convex mesio-rostral border in the bigger specimens of the small group). See discussion for further information regarding sexual dimorphism in *H. martritense*'s i2.

Upper dentition (Figures 6 and 7)—The upper deciduals are described in the present work for the first time. They morphology of the upper deciduals is plesiomorphic, as they resemble the adult one of more brachyodont species (i.e. open median valley, moderate inner enamel folding, and parallel metaloph and protoloph). Apart from their general configuration, they share a thinner enamel wall and patchy cementum on the ectoloph and sometimes filling the bottom of the fossetes.

The DP1 is triangular in occlusal view. The ectoloph is undulated, with strong metacone and paracone pillars. The parastyle is long, thin, and straight (e.g. FMH'14-4096) or curved (e.g. 05/101/2/3620). The metastyle is short and blunt. The metaloph is perpendicular to the ectoloph. It has some small enamel folds at both anterior and posterior sides (being the posterios less important). The anterior ones, probably crochets, are usually double. Its development and placement varies among individuals. On the posterior side of the metaloph, a single enamel folding can be sometimes present (e.g. 05/101/2/3620). Protocone and hypocone are rounded and usually fuse with moderate wear. The protocone has a 'tear'-like protoloph that points to the tip of the parastyle. The protoloph is separated from the ectoloph by a gap. Instead this connection, the protoloph continues anteriorly through a low lingual cingulum that encloses an 'hourglass'-shaped median

valley+prefossete.

The DP2 is square in occlusal view and, in contrast to the DP3, its cones and lophs are nearly symmetrical. The ectoloph is undulated due to the paracone, mesostyle, and metacone pillars. From the three, the mesostyle (centered in the ectoloph and limited by a sharp posterior fold in the ectoloph) is more developed, and typically protrudes from the labial wall. Both parastyle and metastyle are similar in size and thickness in

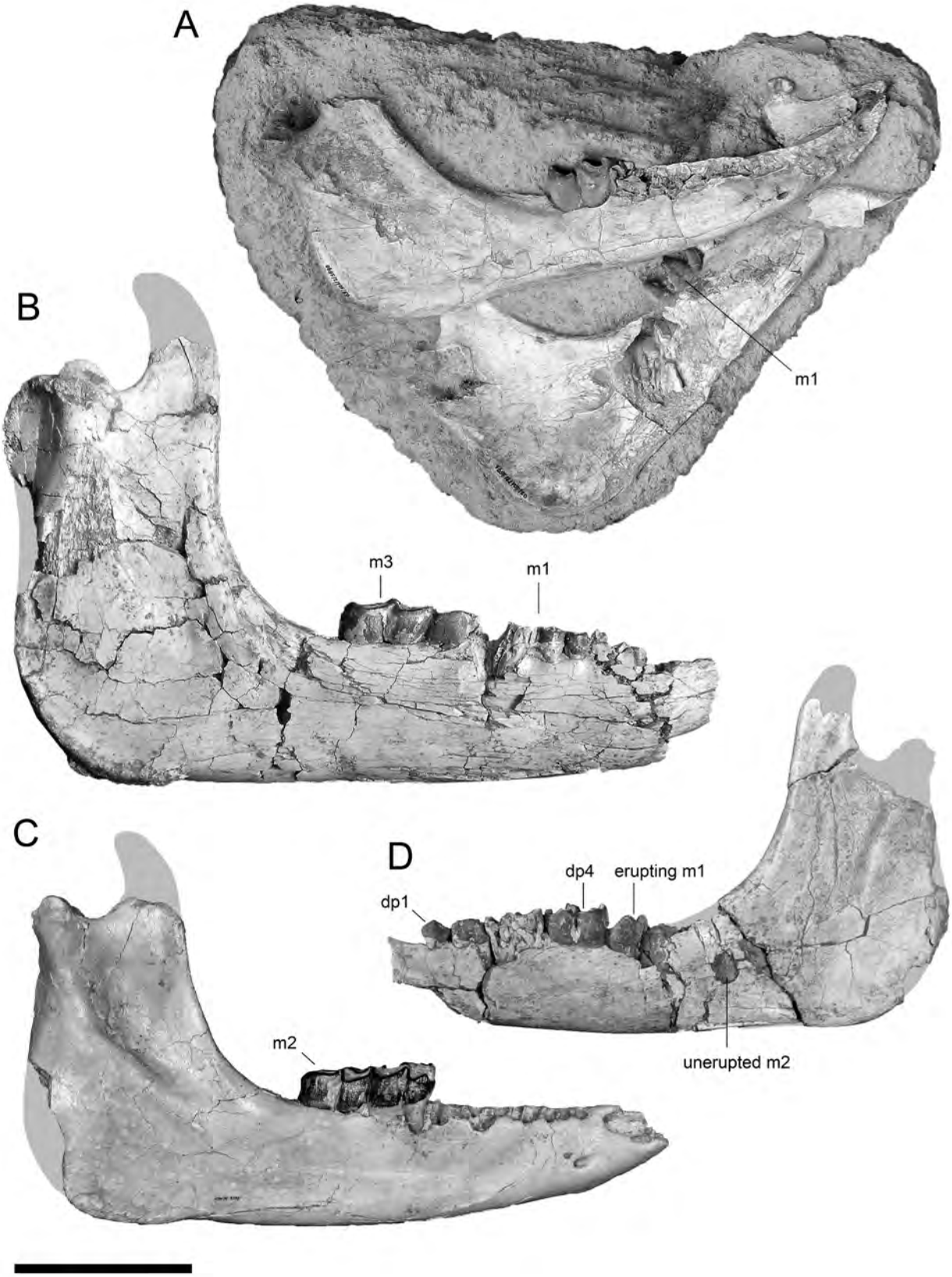


Fig. 4 Mandibles of *Hispanotherium matritense* from Príncipe Pío-2 (A-C) and Fábrica Mahou (D). A, mandible 05/101/2/1691 with both m1, dp4 (the left detached), and left dp1; B, right hemimandible 05/101/2/1743 with p4 (partially broken)- m3; C, left hemimandible 05/101/2/1694 with dp1-dp4 and erupting m1; D, right hemimandible FMH'14-3375 with m1-2 in All specimens depicted in lateral view. Gray outlines represent reconstructed missing parts. Scale bar represents 100 mm.

some individuals (e.g. FMH'14-3685), while others show a slightly more thickened metastyle (e.g. 05/101/2/3620). Both protoloph and metaloph are parallel. The metaloph contacts the ectoloph through a narrow bridge, the contact of the protoloph is somewhat wider. Both protocone and hypocone are equivalent in size. In some individuals (e.g. FMH'14-3685) they show antero-posterior constrictions, leaving rounded lingual projections (absent in others; e.g. 05/101/2/3620). Both lingual cones are usually connected through an 'inverted V'-like enamel ridge at the entrance of the median valley (absent in FMH'14-131). This ridge encloses a bilobed closure of the median valley. Its outline is interrupted by a small and pointed crochet. In FMH'14-131 the 'inverted V' enamel bridge is replaced by an irregular enamel projection (which somewhat resembles the mentioned bridge). Both DP1 and DP2 available individuals are equivalent in wear, so little can be outlined about its enamel changes with use of the tooth.

The DP3 is vaguely 'fan'-like in occlusal view but with variable proportions on the available sample (probably due to different crushing orientation). Likewise the other DP series, the ectoloph is undulated and the mesostyle is the most prominent labial pillar (and has an anterior fold next to the paracone). However, and in contrast to the DP2, the mesostyle is not centered but more anteriorly placed, paracone and metacone are weaker (resulting in slightly, not markedly, convex ectoloph surfaces). The metastyle is very long and thick. The parastyle is double (only observable at early wear stageS), short and blunt. There is no lingual bridge between protocone and hypocone. Both have anterior and posterior folds, delimiting constricted lingual cones (the one from the hypocone considerably smaller). The posterior fold of the protocone forms a rounded antecrochet. The median valley is sinuous and always open (unlike in the DP2). The crochet is tipically well-developed, pointed, and has a somewhat constricted base. As with DP1 and 2, the studied DP3's have analogous wear degrees. Even though, some differences can be outlined. In FMH'14-131 the crochet is simple, in 05/101/2/3620 and FMH'14-2669 there is an additional smaller crochet placed labial to the main one, and in 05/101/2/1741 is forked.

The DP4 has nearly-flattened ectoloph except for the mesostyle, which is very anteriorly displaced and is asymmetrical. Both mesostyle and parastyle are divided by a curved enamel fold. The metastyle is nearly straight. The parastyle is short and double at early wear. Protocone and hypocone have marked anterior and posterior folds, more developed than in the DP3. A long crista is present. A blunt tubercle encloses the entrance of the median valley. The DP4 w/n from Puente de Toledo (part of the type series and figured in del Prado, 1864) is morphologically close to FMH'14-3739 except for the crochet, which is more lingually displaced and the concavity of the ectoloph between paracone style and parastyle, less profound.

As far as the adult dentition is concerned, the P1 has an 'almond'-shaped (unworn) to trapezoidal (worn specimens) outline in occlusal view. The ectoloph starts with two symmetric labial pillars for paracone and metacone. The metastyle widens with wear, leading to a wide and straight posterior border of the tooth. The paracone maintains a similar size with wear, and only widens in advanced wear stages (e.g. FMH'14-5215). Both protocone and hypocone start connected through a thin bridge since earlier wear stages but isolated from transverse lophs (e.g. PG1-4). This lingual is thicker in older individuals. A metaloph starts as a very thin crest perpendicular to the ectoloph. With age, this loph does not contacts the hypocone but the protocone. This

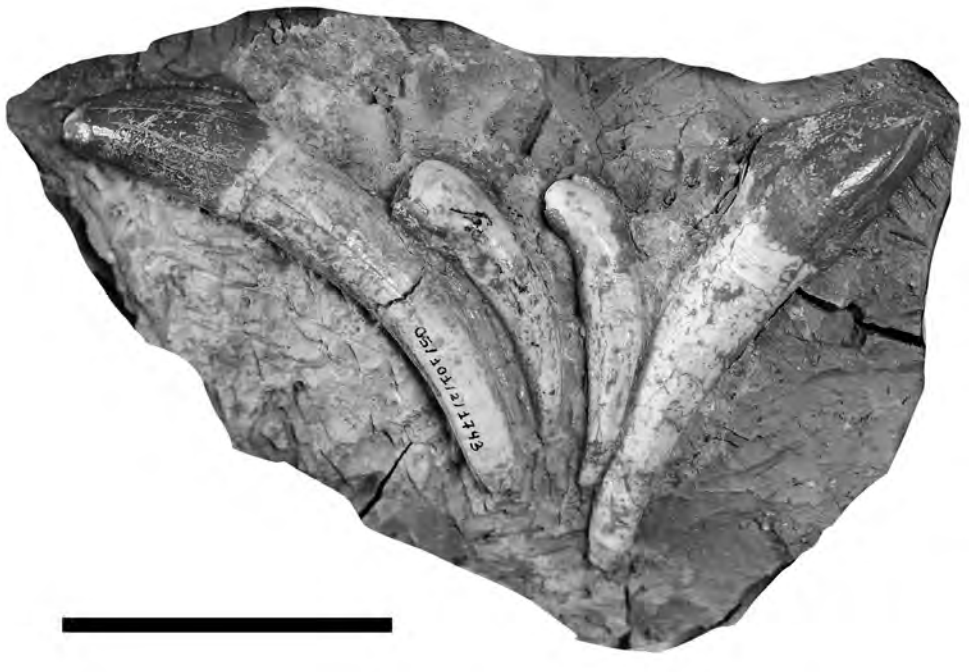


Fig. 5 Anterior dentition (right and left i1 and i2 respectively in rostral view) 05/101/2/1743 of *Hispanotherium matritense* from Príncipe Pío-2. Scale bar represents 50 mm.

path configures a distinct type of 'pseudometaloph' from that defined by Antoine (2000). The postfossete left posteriorly from the 'pseudometaloph' starts wide and oval and reduces into a 'comma'-like depression, filled with cementum. The depression formed by the median valley+prefossete is big and rounded. In FMH'14-5397, two short and thin crista and crochet that nearly-encircles a mediofosette. In a single specimen (FMH'14-5215), the advanced wear makes the lingual cingulum enclose a small closed median valley. The whole ectoloph wall and the different fossae are covered/filled with cementum.

The P2 has an oval outline in occlusal view. The ectoloph is undulated and widens posteriorly. The labial pillars of paracone, mesostyle, and metacone are similar in size. The protoloph is straight and attached to the anterior border. The metaloph is very narrow and perpendicular to the ectoloph. Procone and hypocone are connected through a lingual wall with a rounded lingual border. As the DP2, the median position of the metaloph makes tooth look vaguely symmetric. Except for a few unworn specimens, most of the sample is formed by moderately-worn specimens. The protoloph has a straight anterior border. The metaloph is sinuous and has a enamel expansion pointing posteriorly. Protocone and hypocone form a wide lingual wall that continues with a very developed posterior cingulum (as wide as the protoloph). This cingulum encloses a 'kidney'-shaped postfossete. The inner relieves are variable: the crista can be blunt (e.g. 05/101/2/3457) or pointed (05/101/2/1723). The crochet, always present, is thin parallel to the ectoloph (typically simple, forked in some specimens; e.g. 05/101/2/3457). A smaller second crochet may be present. Crista and crochet can enclose a small and rounded mediofossete.

The P3 is rectangular in occlusal view. The ectoloph is wide and undulated, with two (metacone and mesostyle), or three (plus paracone, fades out with wear) labial pillars, the more prominent of which is the paracone. The protoloph is straight or curved due a small prefosette next to the ectoloph. The metaloph is curved and sinuous. In specimens with little wear, it does not contact the hypocone. In contrast, during early wear, protocone and hypocone looks like a curved, lingual extension of the metaloph and are little differenced (e.g. 05/101/2/21790). Both protocone and hypocone share a strong lingual wall that can attain the same width as the ectoloph in worn specimens (e.g. FMH'14-2579). The protocone is rounder and has very weak anterior and posterior constrictions). The hypocone is more acute and, in contrast to the P4, gets larger with wear, surpassing the level of the protocone. The lingual wall encircles a large and closed median valley. This feature is variable in shape, depending on the inner enamel folds, which are rather variable. In FMH'14-5425 there are two long and thin crochets (one of them enclosing a smaller secondary mediofossete) and a barely-perceptible crista. In FMH'14-2579, the latter is the one long and thin, whereas the labial crochet is very short and pointed (a lingual one should have been present, but swept away by wear). The postfossete is rounded, appears early and maintains constant in size with wear.

The P4 is rectangular in occlusal view. Is by far the most

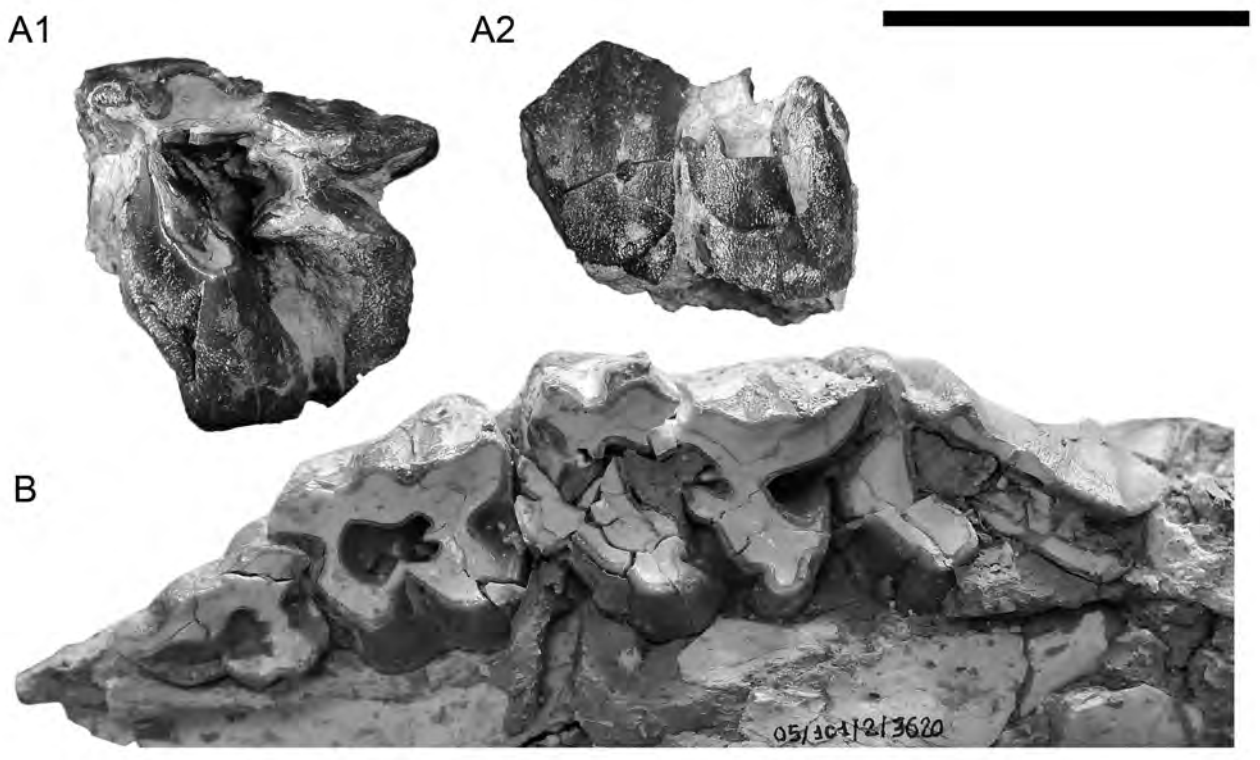


Fig. 6 Upper decidual dentition of *Hispanotherium matritense* from the Madrid Area. A, left DP4 FMH'14-3739 in A1, occlusal, and A2, labial views; B, left maxilla with DP1-4 05/101/2/3620 in occlusal view and A2, lateral views. Adult dentition is figured in the previous chapter. Scale bar represents 50 mm.

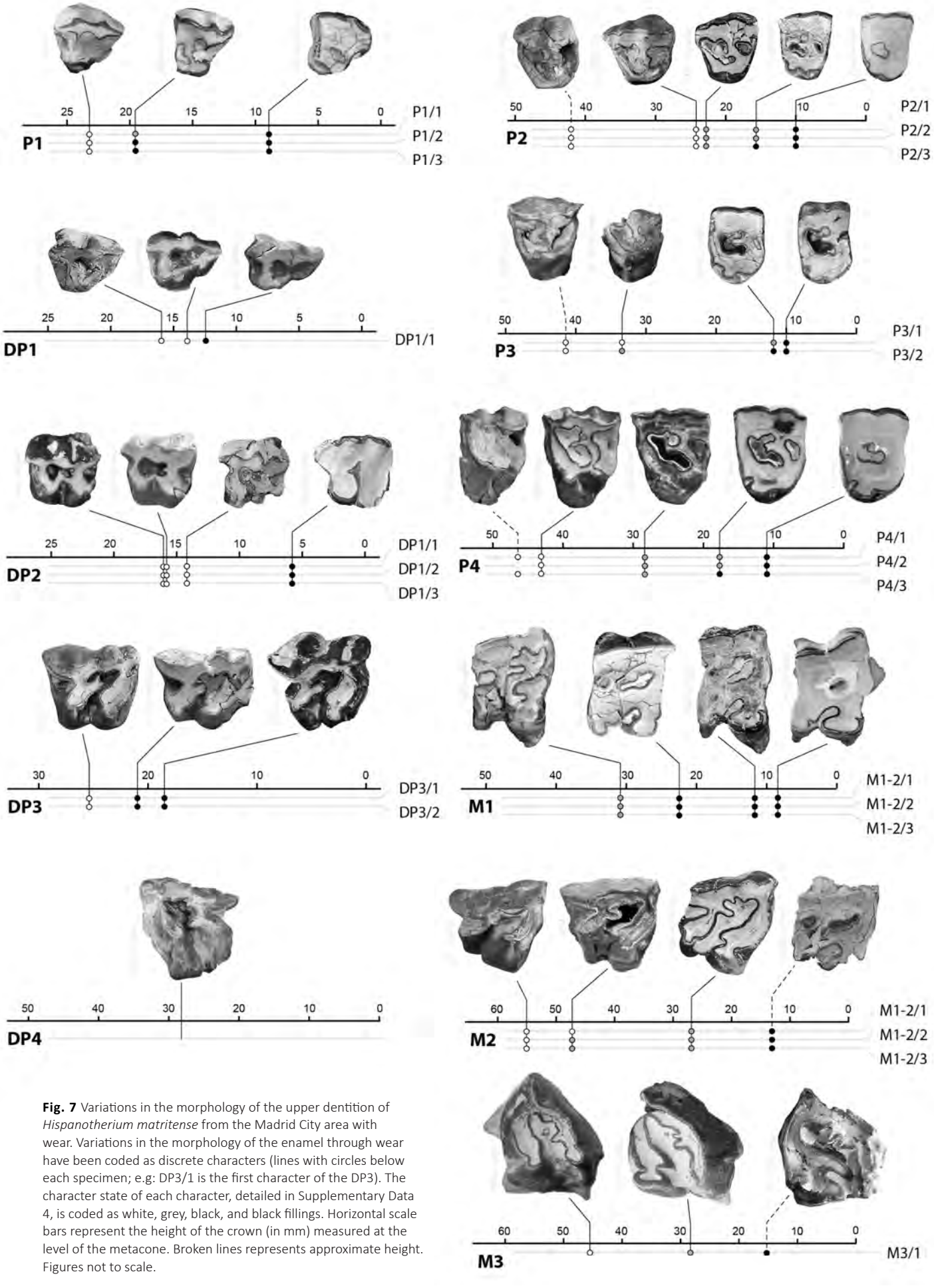


Fig. 7 Variations in the morphology of the upper dentition of *Hispanotherium matritense* from the Madrid City area with wear. Variations in the morphology of the enamel through wear have been coded as discrete characters (lines with circles below each specimen; e.g: DP3/1 is the first character of the DP3). The character state of each character, detailed in Supplementary Data 4, is coded as white, grey, black, and black fillings. Horizontal scale bars represent the height of the crown (in mm) measured at the level of the metacone. Broken lines represents approximate height. Figures not to scale.

abundant tooth in the Madrid City sample and nearly-all the wear stages are represented. The ectoloph is undulated (due to the mesostyle and metacone), particularly with little wear. The mesostyle is displaced to the anterior side and has the same size as the metacone. The protoloph is little curved with early wear, getting straighter at later wear stages. The metaloph is sinusoid and very variable in secondary enamel folding. The crochet is very variable: straight and single in some individuals (e.g: FMH'14-4857), forked (FMH'14-3755), forming a 'δ'-like structure, or double, enclosing an additional mediofossete (e.g. FMH'14-3679). A crista is also present, typically pointed and single. The postfossete remains open with early wear, closing thereinafter. The closed median valley is highly variable as a consequence of the different inner enamel configurations. Both protocone and metacone forms a high lingual wall that widens upon more advanced wear. The protocone is constricted by a profound and marked anterior fold (still noticeable in late wear) and a weaker (but marked though) posterior one. The hypocone starts as a lingually protruding structure (e.g. FMH'14-4857) that erodes quickly with wear, leading to a somewhat rounded postero-lingual border in most P4's.

In occlusal view, the M1 is nearly square but turns rectangular with early wear. Most of the studied M1's are of medium to advanced wear, and the unworn morphology has not been described. The ectoloph is nearly straight (in FMH'14-3233 it shows a median inflexion point). Protoloph and metaloph run parallel. Protocone and metacone show deep anterior and posterior folding. In the case of the protocone, unworn molars have a moderate antecrochet; upon more advanced wear the antecrochet comes out more strongly. Finally (and as with the M2), in heavily worn specimens the antecrochet is fused with the hypocone, enclosing the median valley (e.g. 05/101/2/7001). The outline of this closed median valley depends on wear and the number and disposition of the inner enamel ridges. The crochet is well-developed, blunt, and variable in orientation. One or two crista may be present, but do use to persist into advanced wear stages.

The M2 has a 'fan'-like contour in occlusal view. The ectoloph is nearly flat and has some cementum patches. The metastyle is long and pointed in unworn specimens, shorter and with a straight posterior border with moderate wear on. The parastyle is short and narrow in early worn specimens (e.g. 1429M), triangular and blunt in worn ones. The paracone fold is very weak and shallow, and the paracone style smooth and wide. Metaloph and protoloph and curved (in unworn specimens, slightly straighter with wear) and run parallel. The latter is clearly longer. Protocone and hypocone have anterior and posterior folds. The hypocone is rounded and simple with moderate wear (e.g. 1429M), constricted from there on (e.g. FMH'14-3330). The protocone starts with the same simple pattern and generates a large antecrochet with wear. The median valley is full of cementum and open except for the extensively worn specimens (e.g. 05/101/2/1747), where the antecrochet contacts the hypocone. The crochet is simple, rounded, and anteriorly oriented. Two cristae are typically found. They range from smoothed and wide to small and narrow.

The M3 is triangular in occlusal view. Protoloph and ectometaloph are convex, in a 'horseshoe'-like loph configuration. The ectometaloph has intermittent cement patches. The paracone style is pointed and long, the parastyle is absent. The protocone shows anterior and posterior folds. At early wear, these protocone folds are weak. However, upon more advanced wear, the fold gets much stronger and pronounced (particularly the posterior one). As a result, the antecrochet comes out more strongly in form of a long posterior expansion and the protocone gets longer (with a straight lingual side). The hypocone has weaker anterior and posterior folds. While the anterior hypocone fold gets deeper upon more advanced wear (e.g. FMH'14-5455), the posterior loses strength with wear. The whole median valley is completely filled with cementum. The inner enamel relieves are highly variable. Regarding the crochet, can be single and short (FMH-14'4257), single, long and curved (FMH'14-5455), or short and double (05/101/2/7000). A smooth crista is always present. It is generally simple (except for some cases like FMH'14-5455, which is double and has a small, protruding tip). Additionally, a small enamel cusp is sometimes present in the middle of the median valley (e.g. FMH'14-4257). The M3 (w/n; holotype) resembles that of FMH'14-4257 except for the enamel cusp in the median valley.

Lower dentition (Figures 8 and 9)—Due to the high number of inmature individuals in Príncipe Pío-2, the decidual series are well-represented in the studied sample. In contrast, well-present adult dentition is scarcer to the point that no complete m3 have been found.

The dp1 is 'almond'-shaped in occlusal view. The paralophid is simple and curved, partially encircling a shallow and open anterior valley. The protoconid is inflated. The metalophid is oblique and very short. The disto-labial groove is shallow. The hypolophid partially encircles the posterior valley.

The dp2 is rectangular in occlusal view and slightly narrows anteriorly. The talonid is much shorter than the trigonid. The paralophid is bifurcated. The paraconid is precluded by a labiolingually-constriction in the ectolophid (i.e. anterior groove of the ectolophid on the labial side and the anterior valley on the lingual one). The anterior valley is 'V'-shaped in occlusal view and aligned with the anterior groove of the ectolophid, which is very shallow. Both favor a considerable constriction of the ectolophid. The posterior valley is open and rounded. The disto-labial groove is also 'V'-shaped. The protoconid is inflated and contacts the metaconid through a short and anteriorly-constricted metalophid. The posterior valley is wide and rounded during early wear, being narrow and curved thereinafter. The labial groove is shallow (early wear) to slightly acute (moderate wear).

The dp3 is long and rectangular in occlusal view. The trigonid is slightly longer than the talonid (both have rounded

labial walls in the same view). The paralophid is simple, rounded, and has a posterior constriction that separates it from the paraconid. The groove of the ectolophid is acute along the whole wall. The protoconid is rounded and as large as the hypoconid. The metaconid is rounded and has an antero-posterior constriction. The anterior valley is pentagonal and sharp (e.g. 1502 M). The entoconid has a posterior indentation, that fades out with wear. The posterior valley is very wide and 'D'-shaped.

The dp4 is rectangular in occlusal view. Both lingual valleys are wide, somewhat semicircular in occlusal view, and 'U'-shaped in lingual one. The paralophid is simple and curved and parallel to the hypolophid. The protoconid is rounded and big. The metaconid is limited by means of antero-posterior constrictions. The labial groove is well-marked and deep, but

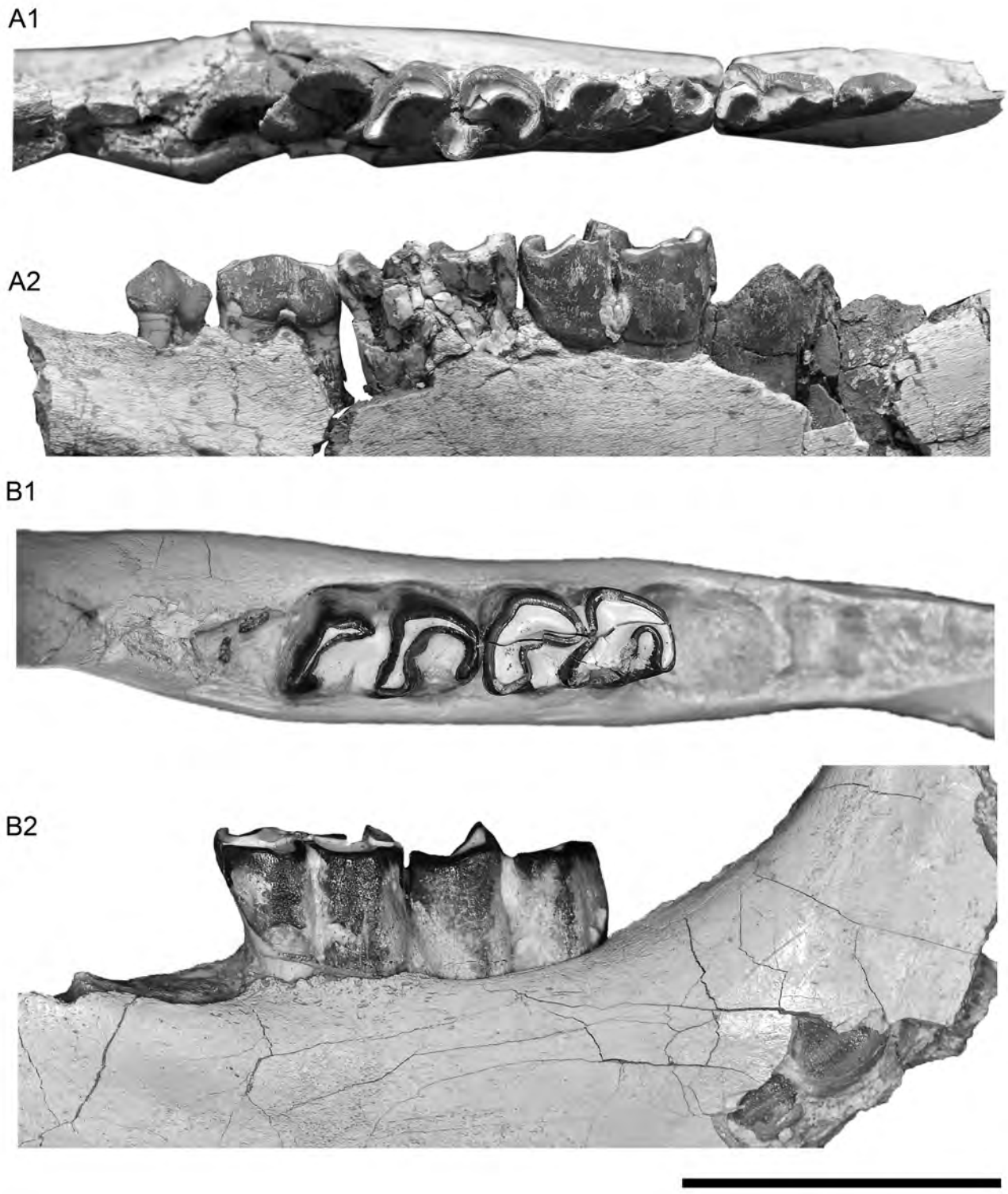


Fig. 8 Lower dentition of *Hispanotherium matritense* from Fábrica Mahou. A, left hemimandible with dp1-4 and m1 05/101/2/ in A1, occlusal, and A2, lateral views; B, left hemimandible with m1-2 and unworn m3 in B1, occlusal, and B2, labial views. Scale bar represents 50 mm.

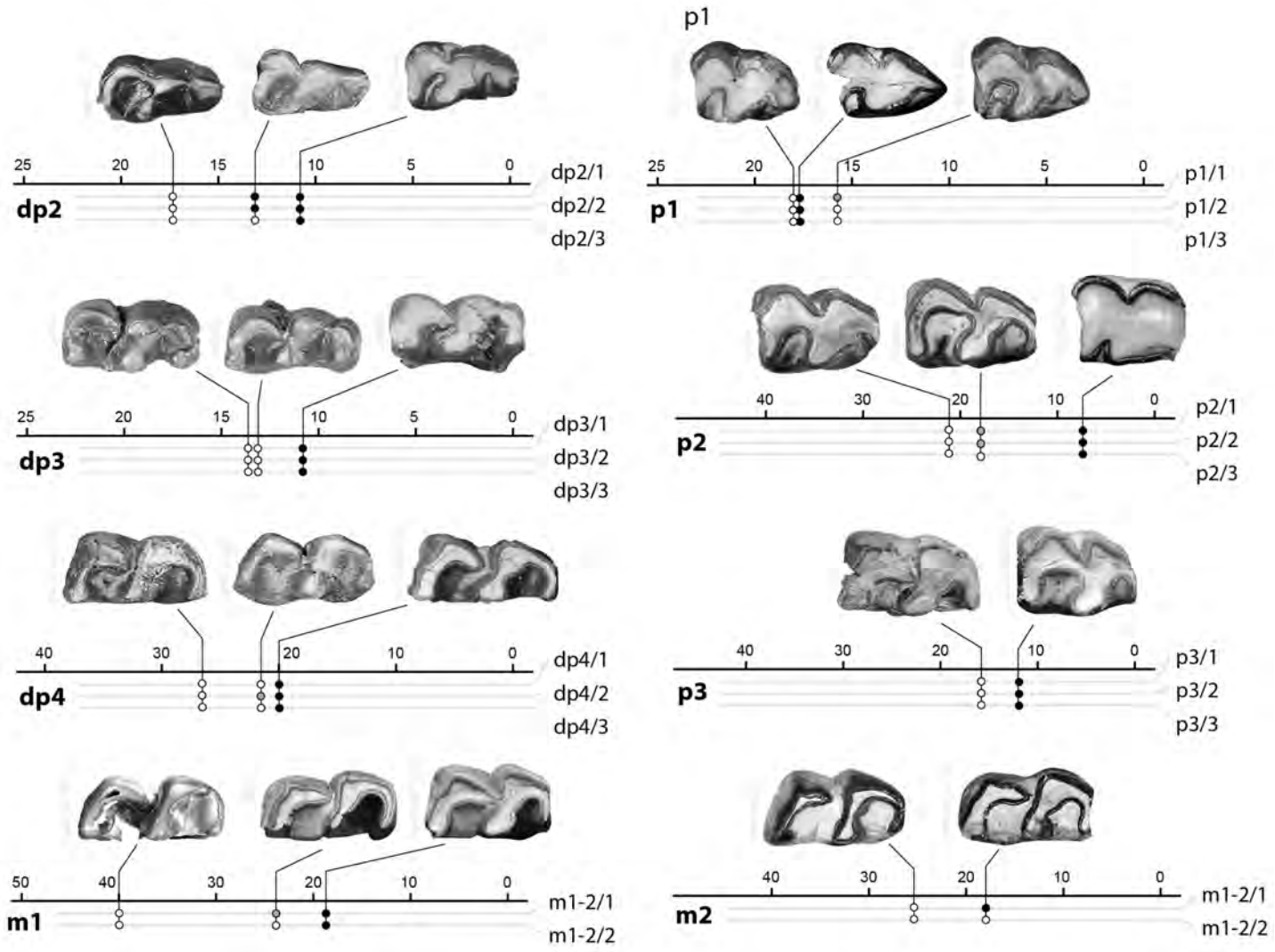


Fig. 9 Variations in the morphology of the lower dentition of *Hispanotherium matritense* from the Madrid City area with wear. Variations in the morphology of the enamel through wear have been coded as discrete characters (lines with circles below each specimen; e.g: dP3/1 is the first character of the dP3). The character state of each character, detailed in Supplementary Data 4, is coded as white, grey, black, and black fillings. Horizontal scale bars represent the height of the crown (in mm) measured at the level of the hypoconid. Characters of the dentition are detailed in the Supplementary Data 4. Figures not to scale.

the presence of cementum impedes to see if it reaches the gingival border. The hypoconid is acute and the hypolophid slightly curved. The entoconid has a straight lingual wall with advanced wear (e.g. 05/101/2/1783).

The p1 is triangular in occlusal view. The paralophid is simple and short. The protoconid is big, about the same size as the hypoconid, and has a rounded lingual expansion in the anterior valley. The anterior valley is pointed up to moderate wear stages and fades out in much worn specimens (e.g. FMH'14-3085). Both anterior and posterior valleys (together with the labial groove and part of the labial wall) are filled with cementum. The hypoconid varies from rounded to angulous. The posterior valley is curved and blunt.

The p2 is rectangular in occlusal view, with a little narrower anterior side. The paralophid is very short and lingually oriented. The protoconid is angulous, the hypoconid rounder, particularly at more advanced wear stages. The anterior valley is pointed and very small, the posterior one is wider and blunt. In heavily-worn specimens the lingual wall is straight, only interrupted by an acute posterior valley (e.g. FMH'14-2607).

The p3 and p4 have very similar morphologies. The paralophid is simple, short, narrow, and perpendicular to the major axis of the tooth. Both protoconid and hypoconid are angulous (but become rounded at late wear stages). The metaconid is antero-posteriorly constricted. The anterior valley is smaller and more pointed, the posterior one is wide and rounder.

The m1 has angulous protoconid and metaconid. The m1 is rectangular in occlusal view. The labial groove is profound and opens until the gingival border. The anterior valley is 'V'-shaped in occlusal view and shallow, the posterior is vaguely pentagonal. Metalophid and protolophid contacts at moderate wear stages. Both metalophid and hypolophid are somewhat curved (straighter in the m2). The labial wall is rugous. The

molars have a considerable amount of cement filling the labial groove and the posterior valley but, in the m1, is sometimes absent from the posterior valley.

The m2 is rectangular in occlusal view. All the m2 are heavily coated with cementum, particularly the anterior and posterior valleys and the labial groove. The paralophid is narrow, posterolingually-oriented, and parallel to metalophid and hypolophid. The protoconid is angulous and shows the shallow expansion into the anterior valley. The metalophid is straight and the metaconid is anteriorly constricted. The hypoconid is angulous too. The talonid forms an obtuse angle with little wear and closes progressively into a straight one. The entoconid is about the same size of the metaconid and slightly wider than the hypolophid. None complete m3 were available in the studied sample.

Postcranial skeleton

Scapula (Figure 10; Supplementary Table 3.2)—The scapulae are slender. The blade has an oval proximal border in lateral view, a slightly sinuous cranial one, and a convex caudal one. The neck is slender too. The supraglenoidean spine is topped with a protuberance on its apex which houses the insertion area for m. trapezius. The supraglenoidean tubercle is wide, rounded, and blunt. In medial view the blade is flat, with a smooth groove crossing it longitudinally. In distal view, the olecranion fossa has an ovate contourn. Other distal fragments present a scapular spine fading out at the level of the neck, a robust supraglenoidean tubercle, and a well-developed coracoid apophysis.

Humerus (Figure 11A; Supplementary Table 3.1)—The distal border of the deltoid tuberosity almost reaches the midshaft of the bone and is topped with a distally-oriented protuberance. The coronoid fossa is shallow. The distal epiphysis shows a wide, deep and subtriangular olecranon fossa. The articular trochlea occupies almost the whole part of this epiphysis and presents a caudal much more developed tan the cranial one. Most of the humeri recovered from Príncipe Pío-2 are distal fragments, being rare in the remaining sites with remains of *H. matritense* thus preventing a variability analysis. Some fragmentary proximal epiphyses have a well-developed TD of the trochanter of the proximal epiphysis.

Radius (Figure 11B; Supplementary Table 3.4)—The radius is slender. In cranial view, the proximal epiphysis has a long, oblique, and blunt proximal tuberosity for the ligamentum colateralle laterale. Its medial border is occupied by the proximal tuberosity for the ligamentum colateralle mediale. It is smaller, rounder and blunt. The anterior face of the proximal epiphysis has a marked fossa for the m. biceps brachii. It is subtriangular, rounded and deep. A flat and smooth insertion area for the m. brachialis occupies the medial side of the proximal third of the radius. The proximal half of the diaphysis has an oval section; the distal one has a lateral keel for the m. extensor ossis metacarpi pollicis (with rugosities in 05/101/2/300). The cranial side of the distal epiphysis has a blunt, wide and ovoid tuberosity. In caudal view, the epiphysis proximal presents the proximal ulnar-facets connected by a very narrow bridge (being clearly separated in other individuals like 05/101/2/771). The medial ulnar-facet is narrow, long, flat and spreads along the caudal edge of the humeral articular facet. The lateral ulnar-facet is big, concave and 'tear'-shaped. In proximal view, the humeral-articulation is formed by two concave assymetric surfaces, being the one for the humerus lateral keel one more developed.In proximal view the humeral

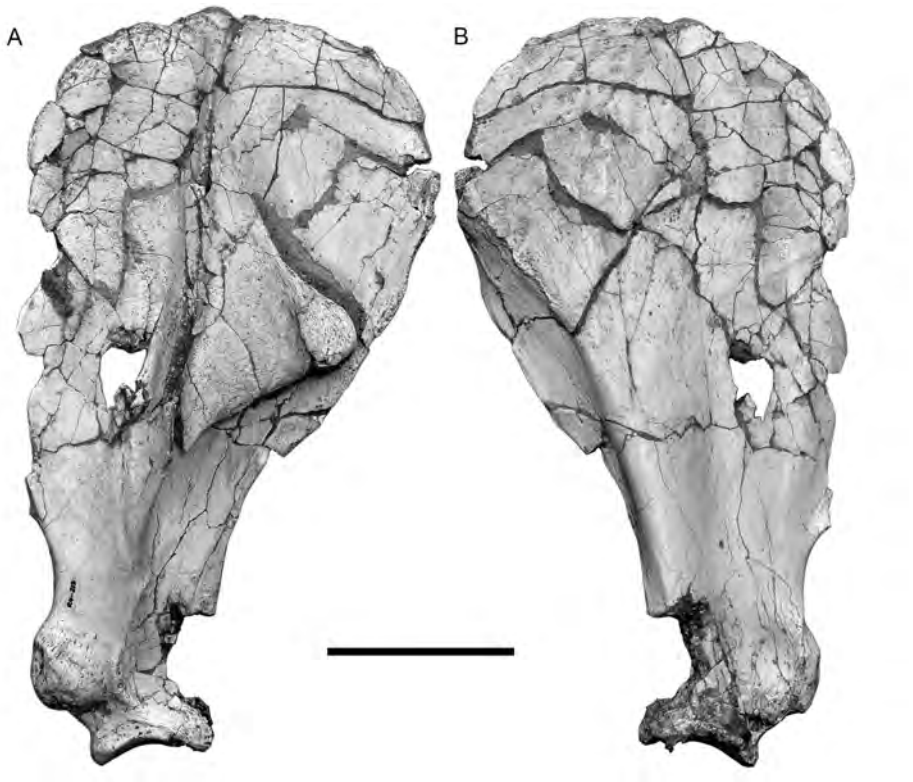


Fig. 10 A, left scapulae R4-213 of *Hispanotherium matritense* from Casa de Campo / Marqués de Monistrol M-30 in B1, lateral and B2, medial views. Scale bar represents 150 mm.

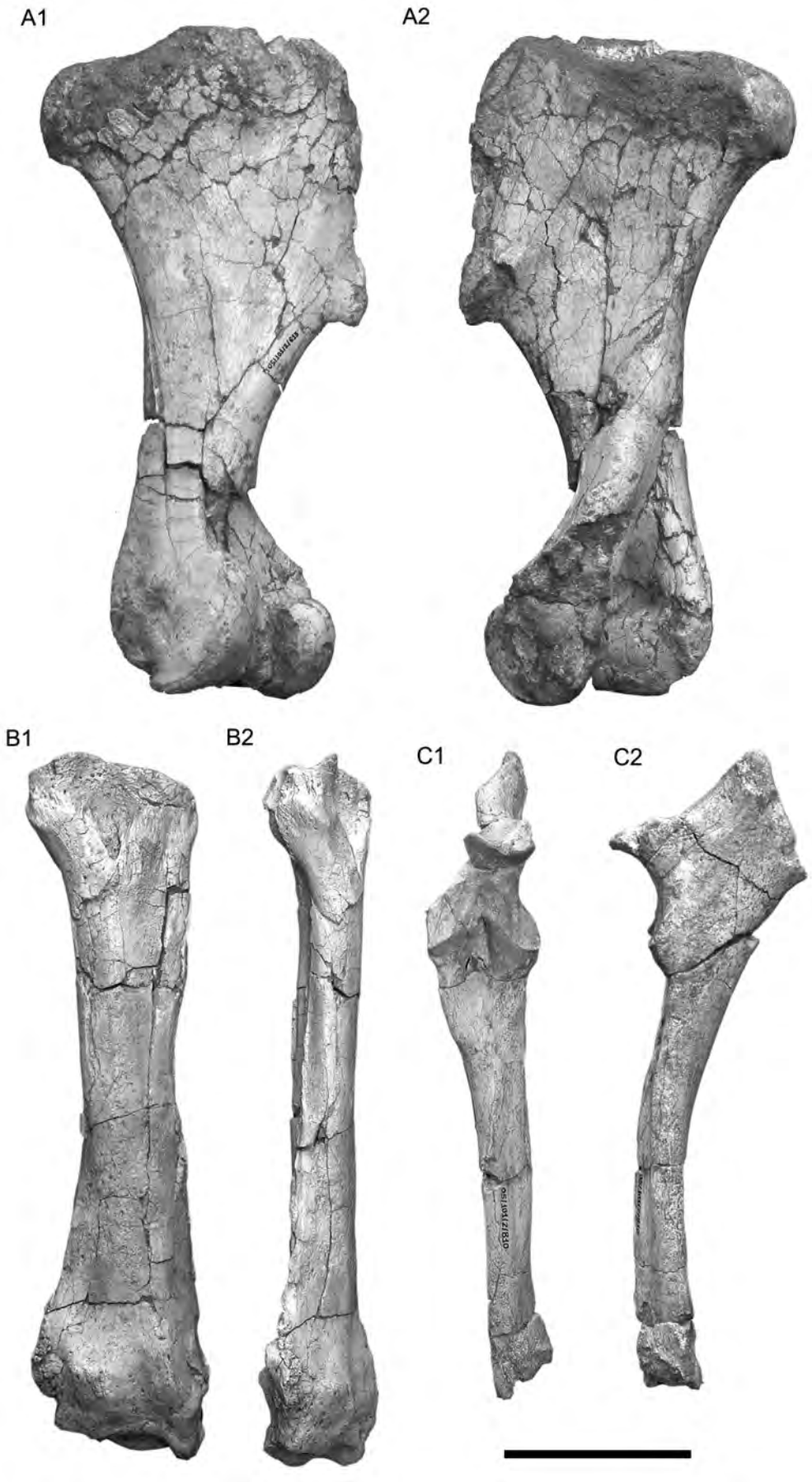


Fig. 11 Anterior stilopodium and zeugopodium of *Hispanotherium matritense*. A, left humerus 05/101/2/613 in A1, medial and A2, lateral views; B, right radius 05/101/2/323 in B1, cranial and B2 lateral views; C, right ulnae 05/101/2/810 in C1, cranial and C2, medial views. Scale bar represents 150 mm.

articulation is formed by two concave assymetrical surfaces, the lateral one ore developed. Both have a straight caudal border and a convex caudal one. In distal view the the lunate-facet is trapezoidal, craniocaudally concave, lateromedially convex and less profound than the scaphoid-facet. The latter is circular and concave, becoming convex towards its caudal border. The distal ulnar articulation has a faint lateral side. The right radius from Casa de Campo/Marques de Monistrol M-30 CMD-635 is smaller than the sample from Príncipe-Pío 2. The fossae for the m. biceps brachii is less developed, the ulnar facets are independent and the lateral border has a strong sulcus flanked by two ridges for the insertion of the m. extensor metacarpi pollicis.

Ulna (Figure 11C; Supplementary Table 3.3)—In lateral view the olecranon forms an obtuse angle with the shaft and presents a clearly convex caudal border. The proximo-caudal vertex of the olecranon houses a shallow insertion for the m. caput longum m. tricipitis. The lateral side of the olecranon is flat. The distal articular side presents a marked step on the cranial border. In medial side the olecranon has an irregular proximal border, topped by a caudo-distally oriented crest. The posterior side of the shaft is clearly convex on its proximal half. There is an crest running parallel to the major axis of the olecranon, more marked towards the border. This crest divides the insertion for the caput mediale m. tricipitis (running along the cranial border of the crest) from the m. digitalis profundus (which occupies the caudal portion of the medial side of the olecranon). In the individual 05/225/60/446 from Casa de Campo/Marqués de Monistrol M-30 this crest is very developed. The distal articulation presents a narrow articular surface for the radius which narrows caudally. On the distal side there is a rectangular pyramidal-facet, latero-medially convex and feebly craneo-caudally concave. On its lateral border has a triangular, convex and blunt projection, place of attachment for the pisiform.

Scaphoid (Figure 12A; Supplementary Table 3.5)—The scaphoid of *H. matritense* has a square outline. The radial-facet is subtriangular in proximal view. It is dorso-palmarly. concave on its dorsal half, convex on its palmar one and slightly convex latero-medially. The distal magnum-facet is oval and flat. The trapezium-facet is very reduced, semicircular, flat and medially-oriented. The dorsal surface is irregular and smoothed and shows a carved area rimming the dorsal side of the trapezoid-facet that continues as a smoothly depressed border on its dorsal half. The palmar view presents the proximal, medial and distal lunate-facets. The medial lunate-facet is oval, flat and somewhat palmarly-oriented. The distal lunate-facet is big, wide and flat. The radial-facet is wide and not very dorso-palmarly elongated.

Semilunate (Figure 12C; Supplementary Table 3.10)—The bone is stout. In dorsal view the lunate is 'mushroom'-shaped, with the radial-facet placed on the proximal side. The whole facet is latero-medially convex and inclined, presenting a higher medial side. In a dorso-palmar orientation, the facet the facet is flat (in most of the individuals from Príncipe Pío-2) to swollen (like in CMD 559 from Casa de Campo/Marqués de Monistrol M-30). The dorsal border of the radial-facet is rounded (only one piece from Príncipe Pío-2, 05/151/2/105, shows an irregular dorsal border). The palmar border expands over the proximal surface up to the midpoint of the bone. It is rounded and slightly dorsoplantarly-concave. The dorsal surface of the lunate presents a rectangular protruding area well-delimited by two sharp edges. The lateral is nearly vertical, the medial oblique. A platform of smoothed borders encircles the medial and distal edges of the dorsal side of the bone. The two medial scaphoid-facets are big and semicircular. The proximal one is flat and palmarly-oriented, the distal slightly concave and dorsally oriented. The lateral pyramidal facets are both laterally-oriented. The proximal one is attached to the radial facet through a smooth transition. The distal is semicircular, flat and bigger. On the distal side of the bone, there are two main facets. The unciform-facet is dorsally placed and varies in shape, from subsquare to trapezoidal and rounded. The dorsal, lateral and medial sides are always convex. The palmar is straight to convex and shorter than the dorsal one. In some individuals the angles of the unciform-facet are sharp (e.g. 05/101/2/105), remaining smooth in others (e.g. 05/101/2/102). The distal magnum-facet has a 'tear'-like outline, islong, reaching the palmarmost side of the volar process, concave and presents a shallow medial indentation. The volar process is wide (reaching the anterior width of the bone) and stout. The medially expanded palmar extent of the magnum-facet gives an asymmetrical contour to the process in proximal view.

Pisiform (Figure 12F; Supplementary Table 3.11)—In dorsal view, both ulnar and pyramidal-facets form a vaguely triangular surface. The ulnar-facet is triangular (05/101/2/220) to semicircular (05/101/2/222), has a straight medial border and is slightly latero-medially concave and proximally-oriented. The pyramidal-facet is flat, subtriangular (05/101/2/215) to semicircular (05/101/2/221) with a medial rounded expansion and is distally oriented. The transition between both facets is smooth in the lateral half and sharp towards the medial one. In dorsal view this boundary is sigmoid. Both form a nearly-straight angle. There is a developed and blunt tubercle running parallel to the lateral edge of the pyramidal-facet. The neck is both dorso-palmarly and latero-medially constricted. The volar process is flat in lateral view and medially bended. It varies in shape, from roughly squared (05/101/2/222; 05/101/2/219) to semicircular (05/101/2/221, 05/101/2/215) but always with a concave distal border.

Pyramidal (Figure 12G; Supplementary Table 3.7)— The body of the pyramidal has an 'L'-shaped contour in dorsal view, with the border for the ulnar-facet proximally projected and little latero-medially expanded. The ulnar-facet is placed on the proximal side. It is square, strongly latero-medially concave, dorso-palmarly convex and shows a triangular and asymmetrical expansion along the lateral side of the bone. This expansion varies in extension and contour (character Py1 in supp. table 1). In dorsal view,the pyramidal presents

a smoothed surface, only interrupted by a proximal rugous area (sometimes carved, as in CMD 92) running parallel to the ulnar-facet. On the posterior side, there is a strong protuberance attached to the pisiform-facet. There is a shallow and depressed area between this protuberance and the distal border. The postero-medial pisiform-facet is attached to the ulnar one. It is long (reaching the distal extent of the ulnar-facet), semicircular to oval in shape and flattened. There are two flattened lunate-facets in the medial side. The proximal lunate-facet is attached to the ulnar-facet, is long and narrow. The distal one is crescent-shaped and symmetric. In plantar view there is a crested protuberance on the lateral border. Its medial border contacts with the proximal lunate-facet, forming an obtuse angle between them. As in the remaining carpal bones, there is some overall size variability. However, the most variable area is focused on the development of the lateral process of the unciform-facet (05/101/2/15, pyramidal izq.; 05/101/2/904, pyramidal dcho.; 05/101/2/3, pyramidal dcho. ó 05/101/2/11 piramidal izq.).

Trapezium (Figure 12H; Supplementary Table 3.9)—This bone is here documented for the first time. Pyramidal in shape, its dorsal surface is covered by the scaphoid and trapezoid-facets. These are semicircular and form a straight angle, being the later bigger.

Trapezoid (Figure 12E; Supplementary Table 3.8)—The scaphoid-facet has saddle-like surface, narrowing on its palmar half. This facet continues with the trapezium-facet, which covers the medial side. The Mc II-facet is placed on the distal side of the bone. This is concave and has a 'tear'-shaped outline. The magnum-facet surface is concave-convex and relies on the external side. The dorsal extent of the bone presents a rugous swollen area.

Magnum (Figure 12D; Supplementary Table 3.6)—the dorsal side of the magnum is swollen and smooth and has a blunt tubercle on the lateral half, parallel to the unciform-facet. This tubercle is elongated in most specimens from Príncipe Pío, rounded in those from Casa de Campo/Marqués de Monstriol M-30 and absent in young specimens, which present a flattened dorsal surface. A small scar is sometimes present near the dorso-distal border of the dorsal side (present in all the specimens from Casa de Campo/Marqués de Monistrol M-30; e.g. 05/60/225a-124). The dorsal side of the bone is topped by the lunate and unciform-facets. Both are triangular in proximal view, flat and present a widened anterior border. Additionally, they form a straight angle and have concave outlines in dorsal view, being the lunate considerably larger. The distal border of the dorsal side is convex. The whole dorsal side of the bone is distally projected and little distally oriented. In distal view, the Mc III-facet covers the wholedistal side of the body of the magnum. The facet is subrectangular, strongly concave in latero-medial view. Its dorsal side is straight to feebly concave, the lateral concave, the medial nearly straight and the palmar shorter and obliquely-oriented but variable, being frequently convex (Supp. Data S2). Both dorso-lateral and palmo-lateral edges are rounded. The scaphoid-facet runs along the dorsal crest. In some adult individualsthis facet is well-developed, presenting a narrow salient along the lateral side of the dorsal crest (i.e. 05/60/225/196). The dorsal crest is semicircular in lateral view and well plantarly-delimited (in some individuals from Príncipe Pío-2 even by a shallow notch; e.g. 05/101/2/203). In medial view, the medial indentation is triangular and presents a variable proximal edge: from retracted to in contact with the lunate-facet (Supp. Data 2A). The medial trapezium-facet has an 'hourglass'-like outline, is dorso-palmarly elongated, has a higher dorso-proximal side and a strongly concave distal border. The volar process is high, big and oval has a rounded tip and is latero-medially flattened. Despite the conservative shape of the volar process, its orientation varies from an oblique placement (e.g. 05/60/225/198) to a sagittal one (e.g. 05/60/225/204). The thickness also varies. These characters can be influenced by mechanical distortion during fossilization and have not being included in our observations.

Unciform (Figure 12B; Supplementary Table 3.12)—In dorsal view, the bone has a hexagonal outline, with the three distal edges forming a smooth curve. The pyramidal-facet occupies the proximal side, whereas the proximo-medial side is occupied by the lunate-facet. The distal half of the dorsal side has a blunt protuberance that expands towards the medial border. In proximal view the bone has a squared outline, with the volar process projecting palmarly. The later is high, robust and laterally curved. The pyramidal-facet issubquadrangular, dorso-palmarly flat and strongly latero-medially convex. It has a straight medial border and is dorsally expanded. The lunate-facet is oval to subtriangular, flat and forms an straight angle with the pyramidal-facet. The Mc IV-facet is placed in the distal side of the bone. It continues laterally with the Mc V-facet and thereinafter through the lateral side of the volar process. The individual R4-94 from Casa de Campo/Marqués de Monistrol M-30 lacks this crest, presenting a blunt and long protuberance instead.

Mc II (Figure 12J; Supplementary Table 3.14)—the metapodials of *H. matritense* are slender. In proximal view, the trapezoid-facet of the proximal epiphysis has a semicircular outline, is narrow (low TD), dorso-palmarly convex and slightly latero-medially concave. Its palmar border is sometimes prolonged over the palmo-medial tubercle. In lateral view, the magnum-facet conforms a flat, laterally-oriented, and 'kidney'-shaped articular surface. In the individual from Paseo de las Acacias Ac-5 the magnum facet is more distally prolonged. A dorsal Mc III-facet is attached to the dorso-distal angle of the magnum-facet. It is flat and small and variable in shape: semicircular and long or triangular and asymmetric (Supplementary Data 2; Character McII1). The Mc II sample from Casa de Campo/Marqués de Monistrol M-30 shows a characteristic sigmoid lower border of the magnum facet (Supplementary Data 2; Character McIII2). This can be either a palmo-distal expansion of the magnum-facet or the presence of a palmar Mc III-facet (which seems more probable). If present, the palmar Mc III-facet is

aligned with the magnum one and their boundary extremely faded. Under the magnum/Mc III-articular surface, there is a roughly depressed area. The configuration of the pits varies among specimens (Supplementary Data 2; Character McIII4). In palmar view, the proximal epiphysis has two tubercles separated by a short and deep groove ~ 2 mm wide. The lateral one is more developed. The medial tubercle is flattened in form of an 'almond'-shaped articular surface (Supplementary Data 2; Character McIII3). However, its attaching structure is not easy to infer, as the trapezoid bone does not contacts this area. In dorsal view, the proximal epiphysis has a short (low H) rugous area for the insertion of the m. extensor carpi. This insertion has a discrete distal boundary and spans over the medial side of the shaft. The remaining shaft has a smooth and flattened dorsal surface. It is gently medially curved. In palmar view, the shaft has a smoothed central surface which starts in the palmo-lateral tubercle of the proximal epiphysis as a narrow flattened "lane" (flanked by both m. interossei) that abruptly widens from the first third of the shaft onwards. The medial one is shorter (barely surpassing the midpoint of the shaft). The lateral m. interossei occupies the whole lateral side of the bone, which is irregular and narrows distally. The diaphysis has a semicircular outline, with a marked angulous dorso-lateral angle. The distal trochlea has a globous lateral halve and a very shallowly concave medial one. In palmar view the medial is stronger, deeper, and is attached to a short medial flange that runs along the medial border of the shaft.

Mc III (Figure 12K; Supplementary Table 3.15)—the magnum-facet covers the major part of the proximal surface. In proximal view, it has a trapezoidal to semicircular outline, is dorso-palmarly convex, and latero-medially concave. Its medial border is rounded and the lateral flat except for a smooth semicircular indentation in the base of the processus for the unciform-facet. Its posterior side extends over the palmar protuberance and part of the palmar side of the proximal epiphysis. Its surface is 'saddle'-like. In lateral view, the The unciform-facet forms a straight angle with the magnum-facet. It is trapezoidal, slightly dorso-palmarly convex, and latero-proximally oriented. In lateral view, the two Mc IV-facets are separated but a shallowly-depressed and irregular space with an 'hourglass' contour. In some specimens with a particularly delicate preservation (e.g. FMH'14-3383), a synovial pouch can be observed in the proximal end of this gap. The proximal Mc IV-facet is attached to the distal border of the unciform one. It is variable, from semicircular to rectangular (Supplementary Data 2; Character McIII2), obliquely placed, flat, and latero-palmarly oriented. The distal Mc IV-facet is bigger, placed in the lateral side of the palmar projection of the proximal epiphysis, oval to rounded, flat, and laterally-oriented. Both form an obtuse angle. In medial view, the Mc II-facet is attached to the proximal articular surface. It is a protruding, blunt area in juvenile specimens. In adults is 'comma'-like and separated from the remaining medial surface of the bone by a short but marked shelf. It has a flat, oval part, medially-oriented, followed by a thin and curved palmar expansion running parallel to the proximal articular surface. In dorsal view, the diaphysis is smooth and flat, except for the area of insertion for the m. extensor carpalis. This area is asymmetric (has an oblique distal limit and a longer medial border) and gets rougher with age. It is located in the proximal third of the dorsal surface of the bone, attached to the proximal epiphysis, and presents a variable indentation (Supplementary Data 2; Character McIII1). Fábrica Mahou show somewhat stronger attachments than those from Marqués de Monistrol / M-30. The palmar surface of the shaft is smooth and flattened in younger specimens, but its attachment surfaces increase their strength with ontogeny. In adult specimens, there are two rugous areas below the expansion of the distal Mc IV-facet. The lateral protrudes and the medial is slightly concave. In the same view, the diaphyses of adult specimens show a flattened and smooth central area along the shaft flanked by the rough insertions for the lateral and medial m. interossei. These are flattened, rough textured, and have latero/medio-palmarly oriented borders extending up to ~ 10 mm above the intermediary relieves. At this point (above the intermediary relieves), one or two small tubercles can be observed between both distal ends of the m. interossei insertions in specimens with greatly developed attachments. The diaphysis is slender, has nearly-parallel borders (slightly distally diverging) and a trapezoidal to oval section. The distal articulation presents a well-marked keel on its palmar side. The Mc III is a rather conservative bone. Apart from the cited variation, other minor differences include the outline of the gap between both Mc IV-facets or the development of the intermediate relieves of the distal trochlea.

Mc IV (Figure 12L; Supplementary Table 3.16)—like the remaining long bones of *H. matritense*, the Mc IV is a slender bone. In proximal view the unciform-facet is subtriangular, latero-medially concave and slightly dorso-palmarly convex. Its proportions strongly vary from one individual to another (Supplementary Data 2; Character McIV1), and some localities, like Fábrica Mahou, have a high percentage of "deep" (high APD/TD ratio) individuals. The lateral edge of the proximal epiphysis presents a pronounced and elevated lateral prominence. In lateral view, a Mc V-facet runs along the lateral side attached to the proximal articular surface, from the lateral side of the lateral prominence to the proximo-dorsal side of the palmar tubercle. The two Mc III-facets are placed on the medial side of the proximal epiphysis. They are separated by a narrow gutter (APD ~ 5 mm), sometimes interrupted by a very thin ridge. The proximal one is more dorso-proximally placed, attached to the proximal edge. It is semicircular, small, flat and medially-oriented. The palmar Mc III-facet is subtriangular to oval (Supplementary Data 2; Character McIV3), slightly dorso-palmarly concave, and medially oriented. This facet is separated from the medial surface thorough a short shelf along its whole border (except for a small palmo-proximal contact point with the proximal unciform-facet) and its palmar side is palmarly-projected. On the medial side of the mentioned palmar projection of the palmar Mc III-facet,

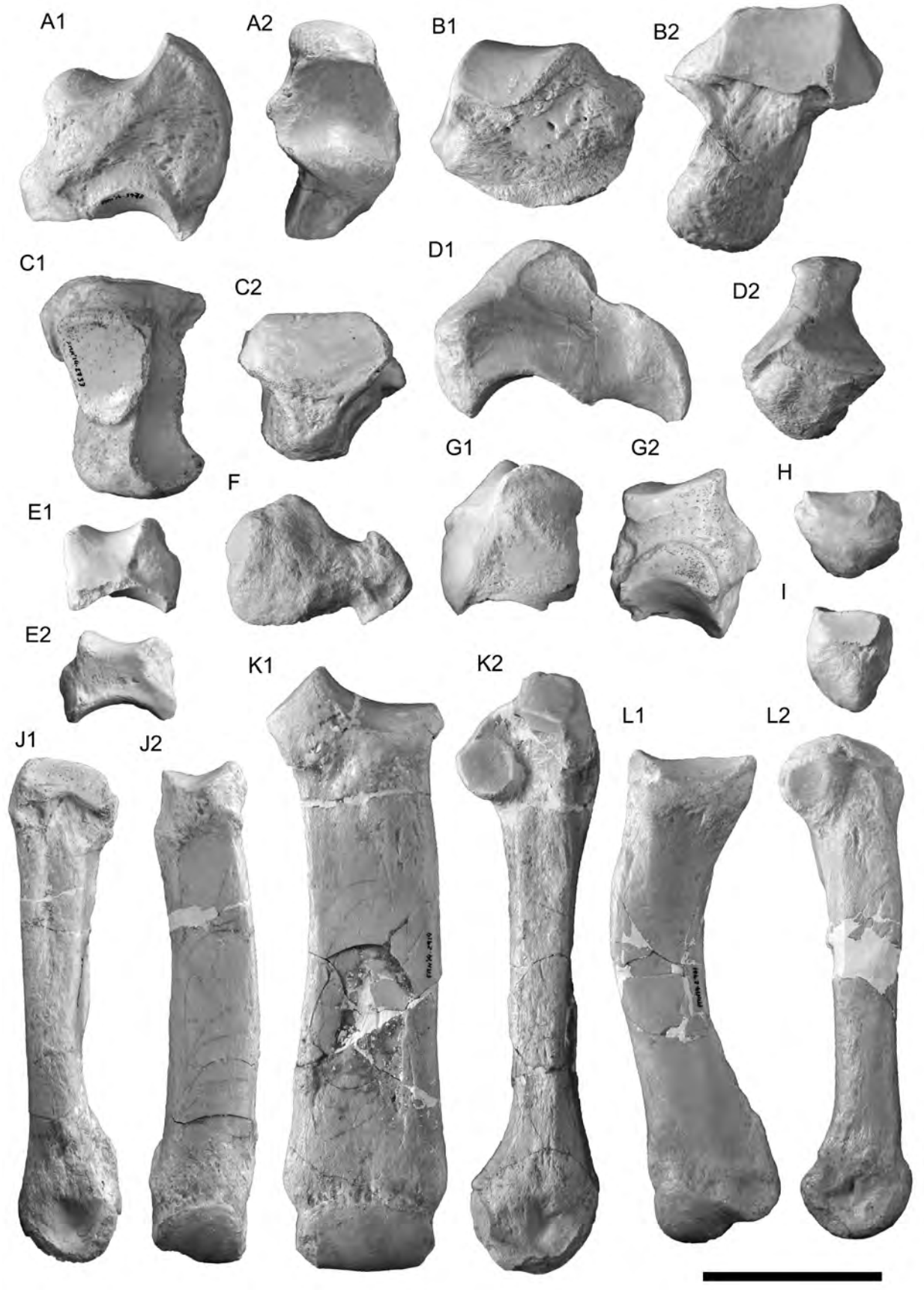


Fig. 12 Carpus and metacarpus of *Hispanotherium matritense*. A, right scaphoid FMH'14-3978 in A1, medial, and A2, proximal views; B, left unciform FMH'14- in B1, dorsal, and B2, distal views; C, right lunate FMH'14-2733 in C1, distal, and C2, dorsal views; D, right magnum FMH'14-2475 in D1, medial, and D2, dorsal views; E, left trapezoid FMH'14-4036 in E1, medial, and E2, lateral views; F, left pisiform FMH'14-3641 in lateral view; G, right pyramidal FMH'14-3042 in G1, lateral, and G2, medial views; H, right trapezium FMH'14-3199 in proximal view; I, right Mc V FMH'14- in medial view; J, right Mc II FMH'14-2698 in J1, lateral, and J2, dorsal views; K, right Mc III FMH'14-2914 in K1, dorsal, and K2, lateral views; L, left Mc IV FMH'14-2901 in L1, dorsal, and L2, medial views. Scale bar equals 50 mm.

there is a small isolated palmar tubercle. The shaft comprises two nearly-straight segments divided by an strong inflexion above the midshaft, giving the bone a characteristic curved appearance. In dorsal view, the attachment for the m. extensor carpalis are restricted to a short rim (H = ~ 10 - 15 mm) of rugous appearance attached to the proximal articular border. In some bones, like those from Casa de Campo / Marqués de Monistrol M-30, this insertion is distally interrupted by a shallow and smoothed depression (Supplementary Data 2; Character McIV2). The remaining dorsal surface of the diaphysis is smooth up to the distal epiphysis. In palmar view, distal to the palmar tubercle of the proximal epiphysis there is a flattened surface flanked by shallow ridges that starts as a triangular shallow depression, narrows up to the first third of the shaft and then widens along the shaft. Apart from the mentioned traits, here is little additional variation within the observed sample. The m. extensor carpalis are restricted to the medial side. In medial view, its attachment surface is rough and proximally widened. It extends to just above the medial intermediary relief. The distal trochlea is highly assymetrical, with a globous medial halve and a small and flattened lateral one. While the lateral one continues into a very shallow groove on its palmar side, the medial is deeper, wider, and has a short but protruding rugous flange that runs over the lateral edge of the bone.

Mc V (Figure 12I; Supplementary Table 3.13)—The Mc V has a flattened and trapezoidal unciform-facet in proximal view. This facet has a semicircular expansion over the palmar side of the bone. In medial view, the Mc IV-facet is rectangular, flat, and medially-oriented. Both diaphysis and distal epiphysis are reduced into a blunt and short distal process.

Femur (Figure 13A; Supplementary Table 3.17)— The bone is slender. The proximal epiphysis is wide; the femoral head, placed over the great trochanter, is hemispherical, slightly transversally pressed, and a slightly expanded lateral side. Its cranial border has a profound notch with a vascularized area in the bottom. The great trochanter is cranially curved. Is robust and rugous, hosting the insertions for the m. scansorius and both external and internal m. vaste. The third trochanter is placed at the same distance of both epiphyses. It is short and has a parallel and straight border, parallel to the major axis of the shaft. The distal caudal tibial-facet is narrower than the cranial one. Over the lips there is a semicircular and rugous depression for the m. vaste externe. In the cranial side of the lateral protuberance of the distal epiphysis there is a semicircular incision for the ligamentum femoro-patello mediale. In caudal view the head of the femur has a smoother notch than the cranial one. The tibial-articulation is placed on the distal epiphysis. It is formed by two differenced lips, being the medial larger. The basal part of the distal epiphysis has a medial protuberance, place of insertion for the m. ligamentum collateral mediale on its distal side and the m. semimembranaceus in the proximal one. There insertion for the m. adductor femoris runs parallel to the major axis of the shaft. In the caudal half of the distal epiphysis there is a shallow depression, place of attachment of the medial patellar ligament. Between the cranial border and the articular caudal border of the articulation there is a faint and long scar where the ligamentumcollateralelaterale attaches.

Patella (Figure 13B; Supplementary Table 3.19)—the patella has a subtriangular to oval cranial contour. In cranial view, the patella has a subtriangular to oval contour. The cranial side has an irregular surface, sometimes finely-vascularized. The caudal side is occupied by two femoral articulation areas. Between them there is a smooth and wide ridge which divides the bone into two articular surfaces. The medial femoral articular surface occupies 2/3 of the side, is triangular and concave. The lateral one is smaller, flattened and subrectangular.

Tibia (Figure 13C; Supplementary Table 3.18)—The femoral-facets are placed on the proximal side, forming a strong tibial spine with a marked central sulcus. The medial femoral-facet is semicircular, flat and smaller than the lateral one. The medial tubercle of the femoral spine is caudally displaced respect to the tubercle of the lateral side. The lateral facet is oval and cranio-caudally convex. In distal view, the astraglar-facet is rectangular, with the major lip fossete of the astragalus oval and deeper than the minor one. The cranio-medial border of the articular facet bears a long and sharp protuberance. The groove between the both astragalar lips is wide, blunt and presents a long ridge along the caudal border. The lateral astragalar-facet is rectangular and concave with a raised lateral side. The insertion for the ligamentum patellare mediale is close to the proximal epiphysis. The later is oval, wide and shallow. A small tubercle for the ligamentum collaterale mediale can be found in the medial border of the distal epiphysis. Close to it, there is a small and rugous groove parallel to the major axis of the bone where the m. flexor digitalis longus is attached. The insertion of the m. tibialis anterior is placed on the lateral side, under the proximal epiphysis. In caudal view the shaft is flat, with a wide and shallow depressed area next to the proximal epiphysis. Over this area, a deep groove is the place of attachment for the m. extensor digitalis longus. In caudal view the surface is flat, with another shallow and wide depressed area close to the proximal epyphysis, place of insertion for the m. popliteus. In the medio-distal edge of the proximal epiphysis is occupied by the insertion of the m. tibialis posterior. It is rugous, slightly carved and runs into the distal articular area. The lateral border of the bone has two articular facets for the fibula. They are big, triangular and rugous. The contact area between the tibia and fibula leaves a scare along the lateral border.

Astragalus (figure 14A; Supplementary Table 3.21)—in dorsal view the bone has a square outline. A short neck separates the trochlea from the distal articular area. The plantar side presents the three cuboid-facets. The first cuboid-facet, placed on the posterior side of the external lip, is concave and has a rounded outline with a latero-distal triangular expansion. The second calcaneum-facet is placed on the medial edge of the plantar side. It is flat, oval, vertically oriented and delimited



Fig. 13 Posterior stilopodium and zeugopodium of *Hispanotherium matritense* from Príncipe Pío-2. A1, right femur FMH'14-4247 in A1, cranial and A2, caudal views; B, right tibia 05/101/2/393 in B1, caudal and B2, cranial views; C, left patella 05/101/2/239 in C1, cranial, and C2, caudal views. Scale bar for A and B is placed on top and equals 150 mm; scale bar for C on the bottom and equals 50 mm.

by a wide and deep groove on its proximo-medial border. The first calcaneum-facet is slightly bigger than the second one. The third calcaneum facet is oval, horizontally oriented and placed along the medio-distal border of the palmar side. The fibular-facet is straight in proximal view. The navicular-facet of the distal side is 'tear'-shaped with a laterally pointed vertex and slightly latero-medially concave. The cuboid-facet is flat, long and forms and 45º angle with the anterior border. The contact between them is smoothed. The profile of the fibular-facet is straight in proximal view. In medial view there is a thin semicircular ridge in the medial boundary of the trochlea.

Calcaneum (figure 14B; Supplementary Table 3.22)—The beak of the calcaneum has a little convex and semicircular tibial-facet.The latero-proximal astragalar-facet forms a straight angle. The remaining astragalar-facets are in contact. The latero-distal one is slightly concave and partially encloses the cuboid-facet. The medial is elliptical to subtriangular and concave. The cuboid-facet is triangular and concave-convex.

Navicular (figure 14F; Supplementary Table 3.20)—The astragalar-facet is practically rectangular, dorso-plantarly concave and latero-medially convex. There is small salient on the dorso-lateral angle. The lateral side has two cuboid-facets. The posterior one is concave and covers a third of this side, the anterior is semicircular and contacts the anterior in some individuals (EJEMPLO). The distal side has the three cuneiform-facets with smoothed and raised contact edges. The ectocuneiform-facet is subtriangular, with a lateral notch. It is dorso-plantarly convex and latero-medially concave. The entocuneiform articular surface is oval and flat.

Cuboid (figure 14B; Supplementary Table 3.27)—In dorsal view the bone is subrectangular, higher than wider and constrained at the level of the neck. The proximal border is straight in dorsal view, whereas the distal one is convex. The proximal side is divided between the calcaneum-facet (lateral half) and the astragalus-facet (medial one). Both compose a big, subrectangular facetlatero-medially concave and dorso-plantarly convex. Between them there is a smooth crest, raised on its plantar extent. The Mt IV-facet covers the dorsal half of the bone. It is wide, subtriangular, latero-medially convex and continues laterally with the ectocuneiform-facet, which is smaller, triangular and dorso-plantarly long. The medial process is placed on the palmar half of the medial side. It is distally curved, the distal hanging from border of the bone. In medial view there are three ectocuneiform-facets. The navicular-facet is on the lateral side, forming a narrow area which covers the proximal border. This facet has an expanded plantar side with a subrectangular vertical surface with a concave anterior border and a convex posterior one. This portion of the navicular-facet continues with the plantar ectocuneiform-facet, which is semicircular, flat, is laterally projected and slightly distally oriented. The cuboids CMD-634 and CMD-615 are considerably smaller than R4-407. The volar process is another highly variable area, meanwhile in R4-407, CMD-615 and 05/60/225a-283 is well developed, in CMD-634 is smaller. The navicular-facet is another variable area. Its posterior border is rounded (CMD-634) to sigmoid (05/60/225a-283, R4-407).

Mesocuneiform (figure 14E; Supplementary Table 3.24)—a single mesocuneiform has been found in the studied collections. It has a semicircular contourn in proximal view. The slightly concave navicular-facet occupies the whole proximal face. In dorsal view there is a single entocuneiform-facet. It is evident and has an oval outline. The medial face is smooth. The Mt II-facet is placed on the distal side. It is semicircular and flat.

Ectocuneiform (figure 14G; Supplementary Table 3.25)—the proximal navicular-facet is concave and presents a subtriangular outline, with a marked lateral notch.The Mt III-facet covers the complete distal side. As the proximal one, it is concave and has a subtriangularcontourn, with a marked lateral notch. The medial face presents three articular surfaces and a smooth depressed area in the center. The mesocuneiform-facet is triangular, flat, centered and attached to the proximal border. The Mt II-facets are place to both sides of the former but closet to the distal border. Al igual que la cara proximal, es cóncava y de contorno subtriangular con una marcada escotadura lateral. They usually present a semicircular profile and are flat. In lateral view there are two cuboid facets. They are flat and divided by a faint groove.

The morphology within fossil localities is very conservative. The specimen CMD-394 has a very weak dorsal Mt II-facet.

Mt II (figure 14H; Supplementary Table 3.27)—the mesocuneiform-facet is situated in the proximal side of the bone. In proximal view, the facet has a semicircular outline (rounded medial border, undulated lateral one), and a slightly dorso-plantarly convex and transversally concave surface. In lateral view, there are two articular complexes formed by an ectocuneiform (proximal) and a Mt III-facet (distal) each separated by a smooth transition. They are separated by an 'hourglass'-shaped, shallow groove (~ 7 mm long (APD). The dorsal articular complex is more proximally located. It is rounded, laterally-oriented (nearly aligned), and has two flat facets similar in size. While the dorsal (ectocuneiform) is semicircular, the distal one (Mt III) varies from semicircular to triangular (Supplementary Data 2; Character MtII2). The plantar articular complex is subtriangular. The proximal plantar ectocuneiform-facet is proximo-laterally oriented and oval to rectangular. The plantar Mt III-facet is semicircular, flat, and more laterally-oriented and smaller than the former. The plantar complex is located on a plantarly-protrusion of the proximal epiphysis. In plantar view, the bone shows a long entocuneiform facet. It is separated by ~ 5-8 mm from the proximal articular surface. It is flat, proximo-plantarly oriented, and its outline ranges from semicircular to 'tear'-shaped (Supplementary Data 2; Character MtII1). It is triangular, transversally concave and dorso-plantarly convex. The dorsal surface of the shaft is smooth. The insertion for the m. extensor carpalis is generally weak, except for some adult specimens (e.g. FMH'14-3523), and restricted to the dorsal area next to the proximal articular surface and a small part

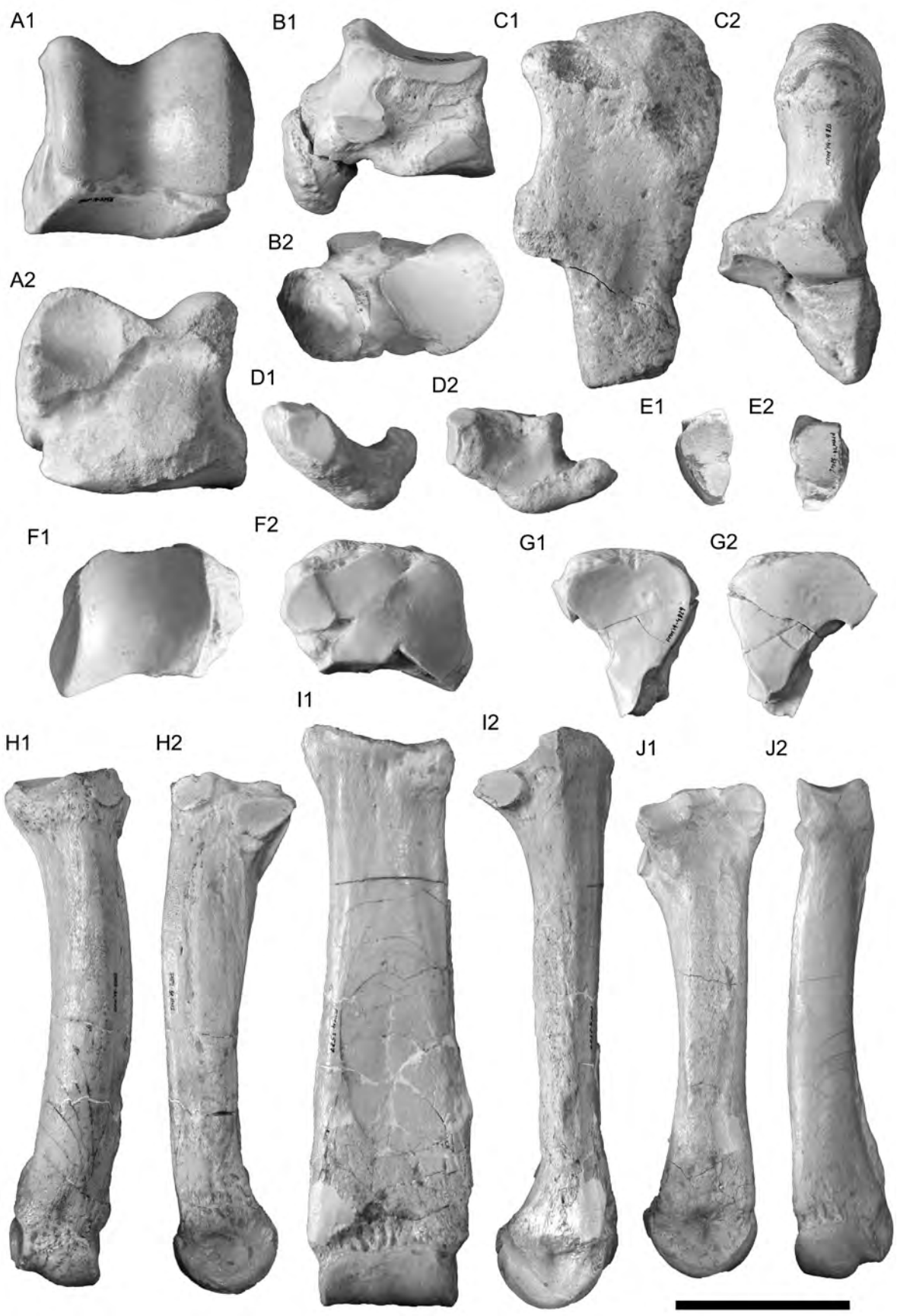


Fig. 14 Tarsus and metatarsus of *Hispanotherium matritense*. A, left astrágalus FMH'14-3356 in A1, dorsal, and A2, plantar views; B, left cuboid R4-407 in B1, medial, and B2, distal views; C, left calcaneus FMH'14-4833 in C1, lateral, and C2, dorsal views; D, right encocuneiform FMH'14-3199 in D1, dorsal, and D2, proximal views; E, right mesocuneiform FMH'14-3346 in E1, distal, and E2, proximal views; F, left navicular FMH'14-2914 in F1, proximal, and F2, distal views; G, left ectocuneiform FMH'14-4829 in G1, proximal, and G2, distal views; H, right Mt IV in H1, dorsal, and H2, medial views; I, right Mt III in I1, dorsal, and I2, lateral views; J, right Mt II in J1, dorsal, and J2, lateral views; Scale bar equals 50 mm.

of the lateral side of the bone. The section of the diaphysis is 'D'-like, with a flattened lateral side. In lateral view, the lateral m. interossei occupies the whole shaft up to the intermediate relieve. In medial view, the medial flange is sharp, rough in adult specimens (Supplementary Data 2; Character MtII3). The diaphysis is neary straight in lateral view (faintly medially divergent in dorsal one). The intermediate relieves are small and weak, and the trochlea narrow.

Mt III (figure 14I; Supplementary Table 3.29)—the bone is high and slender in dorsal view. In proximal view, the ectocuneiform-facet has a subtriangular to semicircular outline, is slightly dorso-plantarly concave and transversally flat. It is flat and 'D'-shaped. In plantar view, the distal articular area has a smoothed articular keel. In CMD-630 from Marqués de Monistrol, the dorsal border of the ectocuneiform-facet is curved, whereas in R4-223 from Príncipe Pío is straight. In lateral view, there are two Mt IV-facets. The proximal Mt IV-facet is attached to the proximo-lateral salient of the proximal epiphysis. It is rounded to 'kidney'-like (Supplementary Data 2; Character MtIII1), flat, and planto-laterally oriented. The distal Mt IV-facet is relatively lower (lower TD/APD ratio), oval to squared, laterally oriented, and protrudes from the plantar border of the proximal epiphysis. Contrary to the proximal Mt IV-facet, the distal Mt IV-facet is separated from the proximal articular surface by a small groove and from the diaphysis by a short shelf, higher in adult specimens. In medial view, the dorsal Mt II-facet is small, flat, and triangular (FHM'14-3117) to semicircular (FHM'14-877) in shape. The plantar Mt II-facet is larger, subtriangular and flat. Only a single individual in our sample, FMH'14-3117 lacks this facet (but maintains the triangular tubercle that serves as basis for the facet in other individuals). Both Mt II-facets are attached to the proximal edge and similarly oriented to the medial side. The shaft of the bone has a dorsal smoothed surface, only interrupted by a dorsal tendinous insertion, variable in shape and orientation and barely detectable in young specimens (Supplementary Data 2; Character MtIII1). The diaphysis has an oval section, with a straight lateral border. Its borders are slightly divergent from the midshaft on. The intermediate relieves are small and blunt (except for one specimen, FHM'14-877). The distal trochlea is proximally-bordered by a vascularized area. Its trochlea is flat in dorsal view, and both halves are equivalent in size. Their intermediate relief is weak, only visible in plantar view.

Mt IV (figure 14J; Supplementary Table 3.28)—In proximal view, the cuboid-facet is semicircular to subtriangular (Supplementary Data 2; Character MtIV1) and slightly concave. Its dorsal border is rounded, the plantar straight and flanked by a deep groove (which can attain a width of ~ 8 mm in adult specimens) and a ridge. In medial view, there are two Mt III-facets. The proximal Mt III-facet is smaller, semicircular, flat, dorso-medially oriented and attached to the proximal border. The distal Mt III-facet is wider (longer APD), subtriangular (with a straight proximal border), flat, medially oriented, and separated from the proximal border through a small surface (which, in turn, can be concave, flat, irregular, or convex). Both facets form an obtuse angle and are separated by a gap of swollen surface ~ 6 mm wide. In lateral view, the proximal epiphysis shows a swollen and rugous area. The dorsal surface of the shaft is smooth except for the rough proximal area below the proximal articular surface for the m. extensor carpalis. In plantar view, the proximal epiphysis has a shallow tendinous insertion of variable development (Supplementary Data 2; Character MtIV2). The diaphysis is gently laterally curved. Its section is nearly circular, with a small angle on the lateral border. The distal ridges are well-developed and reach the midshaft. In dorsal view, the medial halve of the distal articular surface is globous, the lateral concave and smooth. Between both there is a faint keel that gets stronger in the plantar side of the bone.

RESULTS AND DISCUSSION

Systematic affinities with other Elasmotheriina

Crusafont and Villalta were the first to consider the species "*Rhinoceros matritensis*" as an elasmothere by linking its dental morphology with the elasmotheriine genera *Iranotherium* (Upper Miocene) and *Elasmotherium* (Plio-Pleistocene). These Asian species show highly hypsodont dentition and very long and low braincases. In addition, the insertion for the nasofrontal horn migrates backwards in the successive late elasmothere genera, resulting in a huge bony dome in the last ones (e.g. *Sinotherium* or *Elasmotherium;* (Deng et al., 2013). In contrast, more basal species (including *Hispanotherium*) while still largely hypsodont show a more moderate degree of enamel folding and lower crown heights. During the second half of the 20th century, the knowledge of the group was progressively completed with additional elasmotheriine remains.

The Middle to early Late Miocene beds from Anatolia and the Caucasus were shown to be particularly fruitful in elasmothere forms, as evidenced by the distinct genera erected at the region during the 70's. These include *Begertherium* (Beliaeva, 1971), *Caementodon* (Heissig, 1972b), and *Beliajevina* (Heissig, 1974). However, Antunes and Ginsburg (1983) considered their diagnostic characters as insufficient to discriminate them from *Hispanotherium* and, therefore, implicitly include them in the latter. Similarly, Cerdeño and Iñigo considered that, not only these genera should be considered as synonyms, but equivalent to *H. matritense* at a specific level together with other Asian elasmothere species (Cerdeño, 1989, 1992b, 1995, 1996; Cerdeño and Iñigo, 1997; Iñigo, 1993; Iñigo and Cerdeño, 1997). Oppositely, subsequent phylogenetic analyses splitted the Anatolian and Caucasus remains to the genera *Caementodon* and *Procoelodonta*, thus restricting the generic variation of *Hispanotherium* (Antoine, 2000; Antoine, 2002; Antoine, 2003; Antoine et al., 2002; Antoine and Welcomme, 2000). The new findings found in the Iberian localities around Madrid City and their variability study gives us an excellent

opportunity to review the phylogenetic affinities of these elasmotheriine forms that has been related to *H. matritense* or included into *Hispanotherium* at some point.

The elasmothere dental remains from Çandir (MN 6) were originally described as *Hispanotherium grimmi* (Heissig, 1974). The presence of a new *Hispanotherium* species in the Upper Miocene of Anatolia (only *H. matritense* was known at that time) implied interesting paleobiogeographic consequences to explain their disjunct distributions. However, posterior studies found several characters that link it together with the rhino from Paşalar in a new genus named as *Begertherium* (Fortelius, 1990; Fortelius and Heissig, 1989; Heissig, 1989). In a posterior review of the topic made by Geraads and Saraç (2003), the characters used to include the Çandir's elasmothere in *Begertherium* were found to be controversial. Curiously, the alternative used by these authors (the use of *Beliajevina* instead of *Begertherium* for the elasmothere from Çandir) is made without morphological or cladistic justifications. More recent phylogenetic proposals for the group showed that '*H'. grimmi* from Çandir is an independent lineage from both *H. matritense* and the Paşalar's elasmothere (Antoine, 2003; Antoine et al., 2002; Sanisidro et al., 2011). Apart from the different characters that separates these taxa (summarized in Antoine et al., 2002), the discovered remains from the Madrid City area permits to make some additional remarks. The only cranial remain of '*H'. grimmi* published up to date is an isolated nasal bone (Heissig, 1976). As commented in Sanisidro et al. (2011), whereas the Anatolian species presents a stout nasal bone with little height and width variation towards the tip and a slightly rugous area on both sides, *H. matritense* has a long, narrow, and very pointed nasal bone without any trace of nasal horn insertion. The type dental remains of '*H'. grimmi* described by Heissig present some differences from those of *H. matritense*. The P2 is more symmetrical and has a less globous paracone for a similar wear stage. In the P4, the protocone is less lingually protruding and the crochet sometimes triple (a condition not observed in any P4 from the Madrid Area, despite the wide range of morphologies observed). The morphology of the M2 figured in the type series is homologous to those found in our study (e.g. 1429M from Puente de Toledo). Saraç (1978) erected a new species of *Hispanotherium*, *Hispanotherium alpani* from a single P4 (MYYE. 3) found in the Upper Miocene site of Yeni Eskihisar (Yatagan, Turkey). The species was comprehensively refuted by Cerdeño based on the observed variation of the upper dentition (Cerdeño, 1987). We agree that MYYE. 3 is ascribable to '*H'. grimmi*. In addition to these craniodental differences, the overall postcranial proportions of '*H'. grimmi* are roughly equivalent to the studied sample of *H. matritense*. Among the postcranial morphology, apart from the differences described by Cerdeño and Alberdi (1982) and Antoine et al. (2002) we have detected the following ones: the volar process of the magnum is more pointed, has a concave distal profile and is distally displaced in '*H'. grimmi*; the dorsal crest of the magnum is smaller and more slender in *H. matritense;* finally, the articular facets between Mt III/Mt IV are in different planes in *H. matritense* (nearly parallel in '*H'. grimmi*; Geraads and Saraç, 2003). *H. matritense* and '*H'. grimmi* are phylogenetically close to the basal elasmothere split posterior to *Caementodon* (including the subgenus *Beliajevina*) and retain several common plesiomorphic characters. Howver, we think that their differences are enough to separate them in different genera.

The Elasmotheriine rhino from Paşalar was identified as a new genus and species since its description, being named as *Beliajevina tekkayai* (Heissig, 1974). Posteriorly, the species was grouped together with other Anatolian remains within *Begertherium* (Fortelius and Heissig, 1989). However, the clustering of the Anatolian remains in a single genus has proven to be controversial. Recent cladistics hypotheses considered the elasmothere from Paşalar well apart from '*H'. grimmi* (the other species included in *Begertherium*) in a particular subgenus within '*Procoelodonta*', [i.e. *'Procoeolodonta*' *(Pasalarhinus) tekkayai* (Antoine, 2003)]. The differences between '*Procoelodonta*' *(Pasalarhinus)* and *H. matritense* include a gradual reduction in the constriction of protocone and hypocone on M1-2 and a progressive loss of lingual cingulum on upper molars and premolars (Nodes "S"-"t" according to Antoine, 2003). Apart from these characters, used in the character matrix, and the bigger size of the remains from Paşalar (Cerdeño, 1989), we can cite the following ones:. Finally, if the affinities of the Paşalar's remains to '*Procoelodonta*'-like taxa is confirmed by further remains, the cranial remains of *H. matritense* differs from tose of '*Procoelodonta*' *(Procoelodonta) mongoliense* in its straighter, shorter, and void of lateral apophyses (Character 1 according to Antoine, 2002) nasal bones.

The elasmothere remains from Belometchetskaya (Caucasus) were synonymized with *H. matritense* by Cerdeño (1989). These, together with the rhino from Erlanggang (Hubei, China; Yan, 1979), are morphologically close to *Beliajevina* sensu Antoine (2003). The genus *Beliajevina*, originally erected by Heissig (1974) for the rhino from Paşalar, was posteriorly restricted to a subgeneric rank for the species '*Caementodon*' *Beliajevina caucasicum* under the genus '*Caementodon*' (Antoine, 2003). Both Belometchetskaya and Erlanggang remains were related to this subgenus. From the characters that defines the subgenus *Beliajevina* (defined in Antoine, 2003), like the weak constriction of the protocone on the M2 have not observed in our sample from the Madrid City Area, which confirms previous phylogenetic results. Additional differences with the dentition of '*Caementodon*' (*Beliajevina*) *fangxianense* (Antoine, 2003; Fig. 6C) and '*Caementodon*' (*Beliajevina*) *caucasica* (Heissig, 1974; Plate 2) like the connection of the protoloph and ectoloph only in worn P2 (observable even in unworn specimens of *H. matritense*; Figure 7) and the presence of a more rectangular outline in the P4 (regardless the wear stage) are firstly presented in the present study. The other *Caementodon* subgenus in Antoine's proposal, *Caementodon Caementodon*, was also synomyzed

with *H. matritense*. This subgenus is formed solely by the species *Caementodon oettingenae*. Its remains come from the Siwalik's sediments of Chinji (Pakistan; Heissig, 1972). The same differences with the studied sample of *H. matritense* outlined for the subgenus *Beliajevina* can be applied for *Caementodon*. In conclusion, the possibility that *Caementodon* and *Beliajevina* (considered as either a genus or a subgenus within *Caementodon*) should be synonymized with *H. matritense* is therefore discarded by our data in agreement with previous phylogenetic studies.

One of the best examples of mosaic evolution in Rhinocerotidae can be found in the elasmothere remains from the locality of Tung-Gur (Inner Mongolia, China). These were described by Cerdeño (1996) as *Hispanotherium tungurense* and posteriorly synonymized with *Huaqingtherium lintungense* (Antoine, 2003). Previously, Zhai (1978) separated the type collection of *H. lintungense* from Lengshuigou from *H. matritense* at a specific level based on the weaker development of the crochet and adjacent enamel folding. Our direct observation of the remains from Tung-Gur revealed a remarkable similarity of the adult cheek teeth and part of the postcranial skeleton (i.e. astragalus, pyramidal, or metapodials) with those of *H. matritense*. A clear evidence of the resemblance is that, in the last review of the evolutionary changes of the group, *Hispanotherium tungurense* is still considered as valid (Deng et al., 2013). While we think that the few dental and postcranial differences detected would be enough to separate both taxa at a specific level, the newly recovered cranial remains from Príncipe Pío-2 (Sanisidro et al., 2011) reveals that much of the differences between both are focused on the cranio-mandibular anatomy and justify a generic separation. They include a longer rostrum, shorter and domed nasal bones, slightly laterally-projected orbits, and a narrower mandibular symphisis. *H. tungurense* is an excellent example of mosaic evolution in the group: whereas part of the postcranial skeleton and dentition retained their plesiomorphic condition closer to *H. matritense*, the skull already show traits that distinguish later elasmotheriine species (i.e. rostral elongation, presence of a developed median nasal horn, and a relative elongation and lowering of the braincase) in an incipient stage. Therefore, we support the assignation of the Elasmotheriini remains from Tung-Gur apart from *Hispanotherium* and its inclusion in *Huaqingtherium*. A deeper discussion about its synonymy with the type species *H. lintungense* falls, however, out of this topic.

'H'. beonense was described by Antoine in 1997. The species was originally considered as more derived than *H. matritense* and *H. corcolense* (Antoine, 2003; Antoine et al., 2002). However, a single clade of Western European elasmotheres that includes *H. matritense*, *H. corcolense*, and '*H'. beonense* is also possible (Sanisidro et al., 2011). On the contrary, the cranial remains of '*H'. beonense* present a nasal horn insertion (absent in *H. matritense*). Apart from the nasal bone, '*H'. beonense* differs in the following dental characters from *H. matritense*: stronger paracone style in the M1-3 (almost absent in *H. matritense*), absence of contact between ectoloph and protoloph in premolar series (connected in *H. matritense* even in unworn teeth), and a double paralophid on the dp3 (not simple) together with a reduced paralophid. In general, the dentition of *H. matritense* shows a higher enamel folding and a more abundant cementum cover. Regarding the postcranial skeleton, the ulna has narrower radial-facets, and the scaphoid a straighter proximal border and a less proximally-protruding palmar side of the radial-facet in lateral view.

Several dental remains from Laogou (China) were ascribed to *H. matritense* (Deng, 2003). Some of the characters of the Laogou's remains like the more developed protoloph in the P1 (closing the median valley at moderate wear stages); more zigzagging ectoloph on the P3-M2, the squared-shaped (while moderately-worn) M1, the more complicated enamel folding, and the presence of folded metaloph and metacone on the M3 would point to a distinct species of slightly more hypsodont dentition. These small differences would place this dental remains closer to '*H'. grimmi* (Heissig, 1974); Pl. 2) than to more hypsodont elasmotheriini like *Procoelodonta*.

H. corcolense is the second elasmothere species described from the Iberian Peninsula. The morphological differences that separate both species have been previously summarized in several works (Antoine et al., 2002; Iñigo, 1993; Iñigo and Cerdeño, 1997). Prior to its recognition as a distinct species, the remains from Corcoles were compared with the Iberian populations of *H. matritense* (Iñigo, 1993). The main dental particularities of the rhino from Corcoles were the deeper labial groove on the premolars, the more anteriorly placed hypocone, the paralophid of the dp3 was double, the premolars narrower, and the molars wider. Other minor differences included the presence of a simple crochet (always), an even hypocone (not constricted) in the M2, and the double paralophid in the dp3. The only morphological difference of the postcranial bones cited concerns the semilunate, which has a less marked limit between the radial and ulnar-facets, and the distal pyramidal-facet is not constricted by a lateral groove and expands palmarly beyond the level of the unciform-facet. In a posterior study (Iñigo and Cerdeño, 1997), the main difference highlighted was the simpler and less variable inner folds of the median valley (apart from others commented in the original work of Iñigo, 1993).

The direct study of the dental and postcranial remains from both Córcoles and the current collection of *H. matritense* from Madrid City permit to establish additional differences. We agree with Iñigo and Cerdeño (1997) in that the much simpler dentition with little cementum is clearly the most characteristic part of *H. corcolense*. For example, the molars show a smaller and always simple crochet (as noticed previously; Iñigo, 1993; Iñigo and Cerdeño 1997), very shallow crista if present, even hypocone and much weaker anticrochet). In the M3, both protocone and hypocone are only slightly constricted, resembling the early wear stages of *H. matritense*. However, in worn individuals of the latter, the anticrochet can be enormously developed, a character never

reported in *H. corcolense*. The hypocone and protocone on the remaining premolars are less connected (probably separated in early wear stages), resulting in a narrower lingual groove. This contrasts with the strong lingual wall observed since the eruption in *H. matritense* (Fig. 7). The P1 of *H. corcolense* is much simpler (i.e. void of crochet and the rudimentary protoloph). The postcranial skeleton shows additional differences from that of the Madrid City Area. The carpal bones are generally more slender than those of *H. matritense*, have shallower articular surfaces, and more slender volar processes. The scaphoid of *H. corcolense* is narrower (shorter APD), has a straighter palmar border, and a shorter (lower APD) and rounder dorso-proximal lunate-facet. The magnum shows a more slender volar process and a less concave Mc III-facet in lateral view. In dorsal view, the lunate has a straighter lateral border, a less concave medial one, and a shorter (lower APD) and narrower (lower TD) volar process (in *H. matritense* can be as wide as the radial-facet, a feature never observed in the individuals from Córcoles). The radius is proportionally stouter (i.e. the diaphysal region does not narrows so abruptly as in *H. matritense*) and the distal ulnar attachment area does not protrudes from the medial side. The tarsal bones present also some particularities: the astragalus is more compact, has a larger articular surface for the calcaneum and a shorter neck. The cuboid has a shorter volar process and a squared-shaped Mt IV-facet (not 'tear' or 'fan'-like). The first astragalar-facet of the calcaneum lacks the distal expansion (a feature observed only in the 12% of the Madrid sample of *H. matritense*). We think that the traits found in the species from Córcoles (i.e. simpler dentition, and more slender carpals) are plesimorphic and place it as a more primitive elasmothere within the Iberian lineage of *H. matritense*. This was phylogenetically supported using an updated codification of *H. matritense* based on the new findings of the present work (Sanisidro et al., 2011), and contradicts previous placements as a more derived taxa (Antoine, 2003; Antoine et al., 2002). Their synonymy is therefore totally discarded.

H. matritense has been also cited in Hommes (France) on the basis of a single dental element (Ginsburg et al., 1987). Nevertheless, nº3393 shows some particularities. The proportions of nº3393 (L = 26,5 mm; W = 38,9 mm) fall beyond the observed variation of the Iberian P4 (L= 28,3 – 32,5 mm; W = 38,9 – 48,3 mm; data obtained from Cerdeño, 1989). According to the studied sample from the Madrid City area (summarized in the Figure 7), the morphology of the tooth nº3393 shows some particularities respect to the studied sample of *H. matritense*: the metaloph runs perpendicular to the ectoloph (not oblique like the whole studied sample) and contacts an anteriorly displaced hypocone (which shapes a straight lingual border parallel to the ectoloph, not rounded and asymmetric as the Iberian ones), the protocone does not protrudes lingually as much as those studied, and is somewhat more anteriorly placed. If compared with the remaining *Hispanotherium* species, the presence of a strong lingual wall and the absence of both lingual cingulum and antecrochet discards *H. corcolense* and '*H*'. *beonense*. Contrariwise to the previous localities discussed, we consider that the tooth from Hommes indeed pertain to *Hispanotherium* but somewhat differs from the type species of the genus. We therefore consider the tooth from Hommes as *Hispanotherium* aff. *Hispanotherium matritense*.

Hence, the spatial distribution of the species *H. matritense* is restricted to Southwestern Europe as part of a regional radiation of elasmotheres in the MN 4-5 (Middle Miocene) together with *Hispanotherium corcolense* and *Hispanotherium beonense*. The putative ancestor of these elasmotheres would have arrived from Asia through the peri-Tethyan region at the early middle Miocene. The presence of the closely related '*H*'. *grimmi* in the Anatolian Peninsula at the MN 6 set out two possibilities: the persistence or a pull of elasmothere species in the Anatolian Peninsula morphologically close to the *Hispanotherium* emigrants of Western Europe or a second westwards emigration event from Asia to Anatolia (Middle Miocene) from Asia (Sanisidro et al., 2011). An eastwards migration of the group from Western Europe back to Eastern Asia, even possible, seems unlikely, and the presence of an undetermined (but apparently more derived) elasmotheriine species in the Late Miocene of China is likely to a remnant of the Elasmotheriine radiation that took place in Central Asia during the middle/late Miocene (Sanisidro et al., Chapter 13). In summary, our results confirms the more restricted variation previously proposed for the species, which excludes all the Eurasian elasmothere remains outside from the Iberian Peninsula linked with *H. matritense* at some point (except for Hommes, France).

Intraspecific variability of *H. matritense*

Two of the main problems when making systematic assessments within Elasmotheriina was the lack of cranial remains and comparable dental wear stages (Iñigo and Cerdeño, 1997). The remains of *H. matritense* from the Lisbon Area published in Antunes and Ginsburg (1983) have been classically used as a reference for morphological comparisons (Geraads and Saraç, 2003; Ginsburg et al., 1987; Saraç, 1978). However, despite the large number of dental remains figured, nearly all elements figured show a moderate wear degree. As commented, the dentition of the Asian genera grouped at some point into *Hispanotherium*, is rather homogeneous, and many distinguishing characters are wear-dependent. For example, the contact between antecrochet and hypocone of the M1, always present in the more derived genera *Procoelodonta* (even at unworn stages), is not seen in the Lisbon's specimens. However, our sample shows that this contact is present in more primitive species like *H. matritense*, but is only observable in moderate to advanced wear stages (Figure 7). On the other hand, other teeth present rather different outlines in occlusal view depending on wear (e.g. M1, square at early wear to rectangular or the changes in the length of the ectoloph in the P2; Fig. 7). The present work quantitatively links the enamel

morphology with the crown height. An augment in the enamel folding has been observed with wear, with a maximum of linear exposed enamel on the occlusal surface around 20-40 mm high in the premolars and lower values the more backwards on the molar series (around 20 mm in the M3). Antoine et al. (2002) resumed in a table the differences among the between Western European elasmotheres based on their cladistics results, and part of them are related with dentition. However, the crochet on the premolar series is generally simple (not double), and is a common character of all species of the genus *Hispanotherium*. While the shape of the crochet is a variable character, it is usually simple. Only two P4 (out of 13 recorded) show double crochets.

The dentition of the remaining Iberian localities is rather variable. A heavily worn P2 from Tarazona de Aragón (Astibia, 1985) shows a rounded lingual border (with no trace of differenced protocone and hypocone like in the worn specimens from the Madrid City Area) while maintaining a closed median valley and postfosette. Aditionally, its ectoloph is oblique respect to the lingual border. However, its height is not provided and it is difficult to compare it with the studied sample. The first upper molar figured points to an M1 while the second is equivalent to an M2 (Astibia, 1985; Fig. 6b and 6c respectively). The M2 MNCN 31135 (probably collected in Cerro de San Isidro) is similar to those studied except for a slightly longer crochet and small anticrochet. The dental remains from La Retama show a double crochet in the M1 (RET-473) and a poorly developed anticrochet caused by its moderate wear (Cerdeño, 1991).

The characters that distinguish between different *Hispanotherium* species detailed in Antoine et al. (2002) have been checked in the available sample to test their intraspecific variations. Apart from the dorso-distal border of the semilunate (coded as "rounded" for *H. matritense* but variable in our sample), the selected characters are considerably stable. The studied sample of postcranial bones analyzed from the Madrid City area is morphologically homogeneous. The few differences detected, have been quantified (Supplementary Table 5) and summarized in the Supplementary Table 4. No temporal trend has been detected in the proportions of the different character states between localities. Some of the characters achieve similar proportions between sites when a sufficient number of measurements are available (e.g.: Ma1, Lu2, As4, Ca1, McII1, Pi2, or Tz1). On the contrary, others keep distinct proportions depending on the locality as a part of intraspecific variation at a population and/or temporal level (e.g.: Na1, As2, or McII2). Unfortunately, the *H. matritense* remains from the Madrid City area limited and temporal trends are difficult to assess. The astragalus from PAR Peñuelas (PP-2; Cerdeño and Iñigo, 1997) shows an equivalent morphology to those of Príncipe Pío-2 or Fábrica Mahou, including the same neck incision observed in half of the specimens (Character As3 in Supplementary Data 4). The Mc III Ac-1 from Paseo de las Acacias has an inflated area proximal to its latero-distal border, practically imperceptible in the remaining studied sample (e.g.: FMH'14-2914; Fig 12K). This is probably and artifact resulting by the central crushing of the piece.

Concerning the remaining Iberian postcranial, main differences have been previously made in the papers devoted for each locality, many of them compared with Torrijos and La Retama, the largest collections available at that time (Astibia, 1985; Cerdeño, 1992a; Cerdeño and Iñigo, 1997; Morales et al., 1993). The postcranial remains from La Retama are widely similar to those from the Madrid Area except for the carpal bones, which are slightly lower (lower H). This is also reflected in the somewhat robust proportions of the metapodials. In contrast, the astragalus RET-701 has a well-formed neck and normal proportions. The astragalus figured in Antunes and Ginsburg (a composite drawing made from the individuals nº244 from Olival da Suzanna and nº249 from Quinta da Farinheira) shows the distal expansion of the first calcaneum-facet and the neck incision, both traits recognized in the Madrid Area. However, the third calcanear-facet has a sigmoid proximal outline, a state of character firstly reported from this reconstruction (we have not viewed the original specimens and this may be a restored area). The postcranial remains from Tarazona de Aragón (Astibia, 1985), are equivalent in shape to the studied sample from the Madrid Area. The only minor differences are the shorter neck of the calcaneum, the straighter dorso-medial border of the semilunate in dorsal view (not slightly concave), the slightly narrower (lower TD) of the Mt IV-facet of the cuboid, and the more squared-shaped outline of the entocuneiform-facet of the navicular.

An increase in size and relative width (TD) of the postcranial skeleton together with an augment in the enamel folding has been proposed for the populations of *H. matritense* (Iñigo, 1993). However, their conclusions relied on datasets which included *H. corcolense*, now considered a distinct species of *Hispanotherium*. The *H. matritense* remains from Puente de Toledo (the type locality; MN 4a) are equivalent in size to those from La Retama (MN 4a) and Quintanelas (MN 5). On the contrary, those from Torrijos (MN 4b), the Calatayud-Montalbán Basin (MN 5), and the Lisbon Area (MN 4-5) are smaller (Supplementary Tables 3.1-3.29). Fábrica Mahou and the slightly younger Casa de Campo / Marqués de Monistrol-M 30 show equivalent proportions to other localities from the Madrid City Area (i.e. Puente de Toledo, Paseo de las Acacias, and PAR Peñuelas, all from the MN 5). Significantly, Príncipe Pío-2 (contemporary of the Casa de Campo / Marqués de Monistrol M-30) is the locality with a wider measurement rank and the higher proportions for the species recorded for nearly all measurements (probably due to the presence of numerous subadult individuals and/or the larger sample available). As with the morphological comparison, no significant differences in size have been found between the successive localities of the Madrid City Area. At first sight, the gracility of the recorded localities of *H. matritense* seems to increase in the manus through time (Fig. 15). The gracility indices from Fábrica Mahou are slightly lower (higher gracility) than those from Príncipe Pío-2 (and those in turn more slender

than Tarazona de Aragón). However, there is not statistical significant increase, as the large samples from Fábrica Mahou and Príncipe Pío-2 largely overlaps the observed variation of the remaining localities. In the metatarsus this trend is even weaker and values seem more stable. Mc III and Mt III show very homogeneous values between the studied localities from the Madrid City Area (around 22 in Mc III; 21 in Mt III).

Ontogeny is another source of variation within a fossil population. In the fossil site of Príncipe Pío-2, there is a high proportion of inmature individuals, a valuable opportunity to describe the ontogenetic variation of the species. Some postcranial characters like the development of the medial crest in the olecranon (e.g. 05/225/60/446), the size of the volar process in the unciform and cuboid bones, the trochlear relieves of metapodials, or the distally projected dorso-palmar angle of the pyramidal can either be related to sex (i.e. the presence of dominant males in a given sample) or age, as very old individuals in both living and fossil rhinos frequently undergo hyperostosis (Westerveld, 2011). Hyperostosis can be easily linked to a very old age in long bones. This is more frequently observed in tendinous areas, like the extensor ligaments of the Mc III (Supplementary Material 2; Character Mc III2), or the interosseous tendoms of the metapodials, Supplementary Material 2; Character Mt II3) or bony epiphyseal sutures of metapodials or calcanei. These differences in the development of the muscle and tendinous insertions can be also be a reflect of interpopulational variations independent from the ontogenetic stage (e.g. Supplementary Material 2; Character Mc IV2). Carpals and tarsals have a single growth center that ossifies early during ontogeny and are more complicated to categorize. Nevertheless, immature bones are generally smaller, have lower APD proportions, have rounded and spongy edges and pitted surface. These later two can be produced by taphonomic alterations (i.e. fungal and/or microbial alterations, subaerial exposure, or transport) and should be taken with caution. For example, the surfaces of juvenile astragali show a porous texture. In long bones, sutures in the epiphyses of young individuals remain unfused.

Other characters, while variable during growth, seem intrinsic at an individual level as a fingerprint. Examples of these are the development of the volar processes of carpal and tarsal bones (Figure 16B), or differences in the vascularization in, for example, the lateral side of the scaphoid, the dorsal side of the unciform, or the cranial side of the patella (Figure 16A).

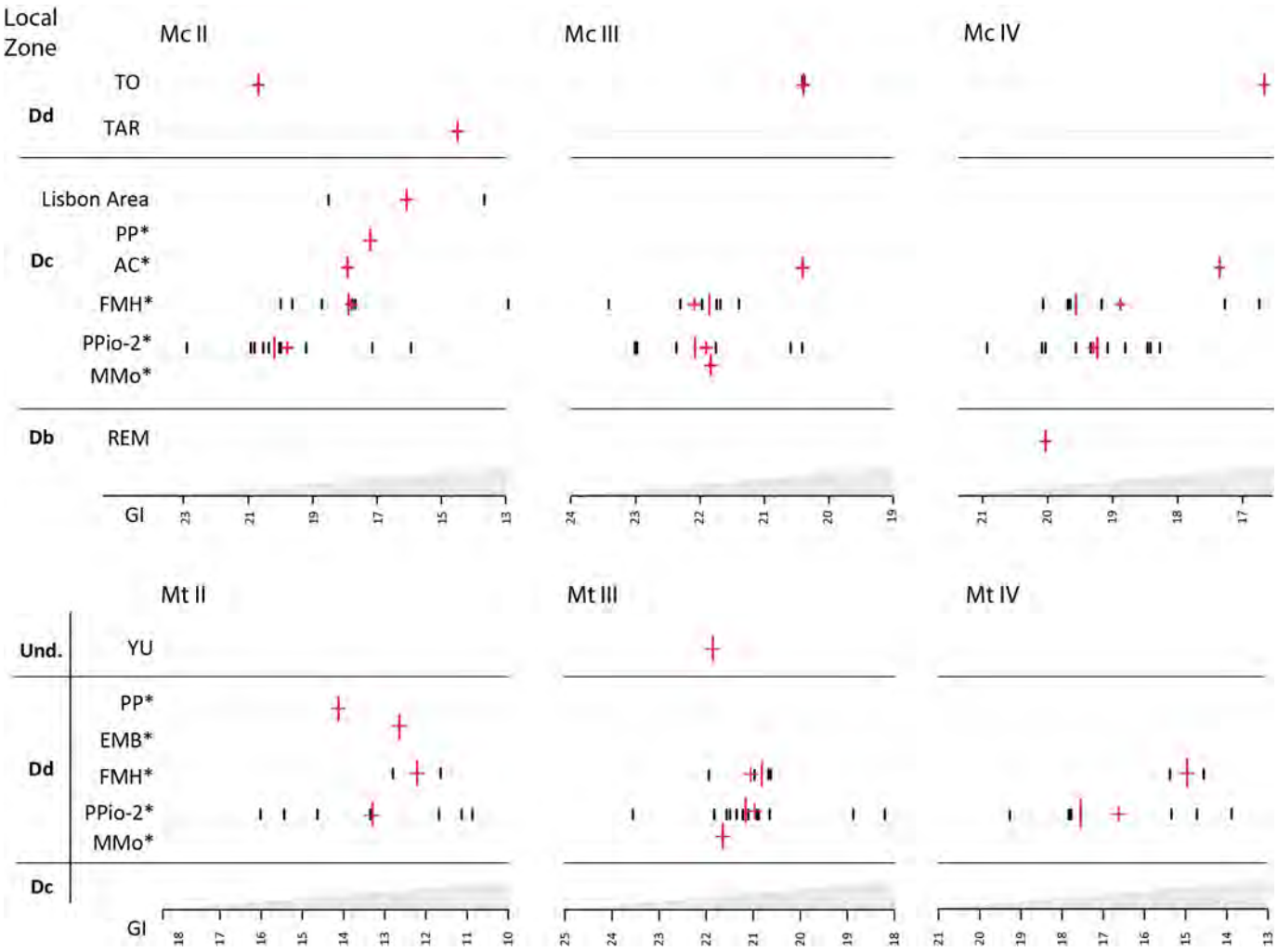


Fig. 15 Gracility indices of the localities of study compared with other Iberian localities. Localities from the Madrid CIty area with asterisk have been arranged according its altitude (see Material and Methods). Crosses represent the mean, lines the median values. Und.: Undetermined age.

Curiously, the Mc III FMH'14-3383 from Fábrica Mahou shows an aberrant vascularization pattern, with two large foramina (TD = 8.4 mm; H = 12.6 mm for the lateral; TD = 6.5 mm; H = 8.6 mm for the medial one) possibly produced by a pathology experience during the early ontogenetic stage (due to the extensive reconstruction of the bony tissues around).

Finally, metrical differences between fossil sites are frequently affected by local taphonomic processes. For instance, the high humidity and compactation of the fossil remains within plastic materials like clay in Príncipe Pío-2 have produced a variable degree of deformation mainly in the long bones to the point of drastically modify their original proportions. The plain strain of this mechanic compactation is typically parallel to the face of the bone with a larger surface and affects different bones independently from its position in the skeleton (e.g. the dorso-plantar compression of the astragali, the proximo-distal compression of the navicular bone or the latero-medial one of magnum or semilunate). Regarding the studied sample, the specimens from Príncipe Pío-2 show a higher deformation caused by compactation than those from Fábrica Mahou or Casa de Campo/Marqués de Monistrol M-30.

The postcranial skeleton of living rhino species exhibits all the possible combinations of sexual dimorphism: larger females, larger males, and monomorphic size of both genders. The study of the sexual dimorphism in fossil species is regularly associated to quarries of articulated individuals with evident dimorphic traits like the presence of the horn bosses (e.g. *Menoceras arikarense*), 'tusk'-like i2, and/or pregnant individuals (*Teleoceras* spp.). Mead (2000) cited some size differences in the postcranial bones of *Teleoceras major* related to sexual dimorphism. Deng (2001) points that males of *C. wimani* are larger than females. Mihlbachler (2005) concluded that males and females of *Teleoceras proterum* and *Aphelops malacorhinus* differed in body size and tusk proportions. Subsequently, dimorphic size differences were reported in the skull and mandible of the *Menoceras arikarense* population from Agathe Springs National Monument (Mihlbachler, 2007). Regarding Elasmotheriini, some cranial differences in males and females of *Iranotherium morgani* were cited by Deng (2005), whereas Petrova (2010) pointed likewise with *Elasmotherium sibiricum*. Most of the sexual dimorphic traits in derived elasmotheres are the greater robustness / width of particular parts of the skull together with a stronger horn insertion in males. Among more basal Elasmotheriini, Antoine (1997, 2000) show that males of *Hispanotherium beonense* have small rugosities on their nasal tips and 'tusk'-like i2, while females not.

In general, sexually dimorphic structures like antlers, horns, or tusks, serve as weapons for intragender competition for mating territories and females and/or to signal information about health to potential mates and male competitors in polygynous species. 'Tusk'-like i2 vary in size depending on the species. Among the living ones, only the Asian taxa retain 'tusk'-like i2. As many rhino species with developed anterior dentition, males of *H. matritense* exhibit longer and pointed 'tusk'-like i2 slightly diverging from the sagittal plane whereas those from females are shorter and blunter (Cerdeño, 1989; Cerdeño and Iñigo, 1997). In a preceding review of *H. matritense* remains from Madrid city, an isolated i2 from PAR-Peñuelas (PP-104) was assigned to a male individual based on its size using the individuals from Córcoles as a reference (Cerdeño and Iñigo, 1997). As mentioned, the remains from Córcoles (white squares in Figure 15) are currently considered as *H. corcolense*, a smaller elasmothere species. The i2 from Córcoles were divided into 5 females and 2 males. However, when compared with the individuals from the Madrid City Area studied in the present work, the variation observed

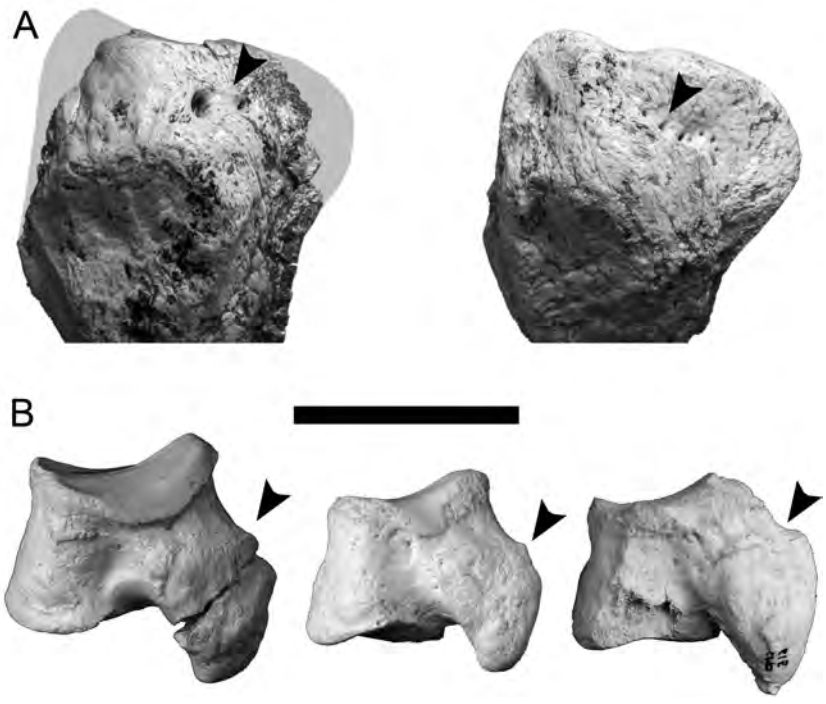


Fig. 16 Two examples of individual variations within a single population of *Hispanotherium matritense*. A, variability in the number and arrangement of vascular canals in the cranial side of two patellas from Príncipe Pío-2. The gray outline represents the reconstructed area. B, variation in the development and morphology of the volar process in the cuboids R4-407, CMD-634, and CMD-615 from Casa de Campo / Marqués de Monistrol M-30. Scale bar equals 25 mm.

between both sex groups from Córcoles can be assumed by the "Group II", and a new cluster of considerably longer crown height appears (significant differences in length between them have been found; Mann-Whitney U test p-value < 0,05). This new group, named as "Group I", bears much longer crowns, clustered around 55 mm long. The proportions of the 'tusks' assigned to the Group I is similar to the Javan rhino (*Rhinoceros sondaicus*) and we assume that they would be generally hidden by the lips. If some signaling for females / competing males was performed by males of *H. matritense*, it would be preceded by an eversion of the upper and lower lips through the contraction of the m. levator nasolabialis, the m. levator labii superioris, and the depressor labial muscles of the mandible. The very large size of the i2 reported from males of several aceratheriine species (e.g. *Chilotherium wimani*) show highly modified symphiseal morphology and may indeed have protruded from the lower lip in resting position. The second group, Group II, is more heterogeneous and ranks between 12 and 35 mm. While the specimens from Group I can be linked with adult males, Group II is not so easily interpretable, as different genders, ages, and temporal factors can be interacting. This group could be formed by females, young males and/or senescent males with largely-worn tusks. Independently, all the studied localities with more than one individual show low Group I / Group II ratios: 0,18 for Fábrica Mahou, 0,25 for Príncipe Pío-2, and 0,25 for Puente de Toledo. A female-biased adult sex ratio and a skewed age distribution of adult males toward young are frequently found in polygynous species (Wade, 1979). This biased proportion has further implications. The placement of *'H'. tungurense* (a elasmotheriine with a developed nasal horn boss) within *Hispanotherium* has led some authors to consider *H. matritense* as a sexually dimorphic species for both i2 and nasal horn insertion. The new cranial findings from the Madrid city area discarded this alternative in favor of a hornless condition (Sanisidro et al., 2011). However, the low ratio between Group I (assigned to males) and Group II indicates that adult males are scarce. If males are poorly represented, all the discovered nasal fragments (4 up to date) could be assigned to females (their ascription to possible young male calves seems unlikely as those from Príncipe Pío-2 show fully-adult dentition, IDAS 4, and the remaining isolated nasal bone from Paseo de las Acacias 7 is morphologically and metrically equivalent to the formers, pointing to an adult stage), so sexual dimorphism could not be totally discarded. Even so, the presence of a sexually-dimorphic nasal horn insertion in *H. matritense* seems unlikely and the hornless condition for the species should be maintained as a diagnostic character.

Apart from variations in length between the two groups, Fábrica Mahou i2's look somewhat wider (higher W) than those from Puente de Toledo and Príncipe Pío-2. However, there is no statistical evidence to suggest that they show temporal variations between these localities (Mann-Whitney U test p-values = 0,22 between Fábrica Mahou and Puente de Toledo, and 0,387 between Fábrica Mahou and Príncipe Pío-2). The same occurs if the W of the i2's of *H. corcolense* are compared with those of *H. matritense* (Mann-Whitney U test p-value = 0,2).

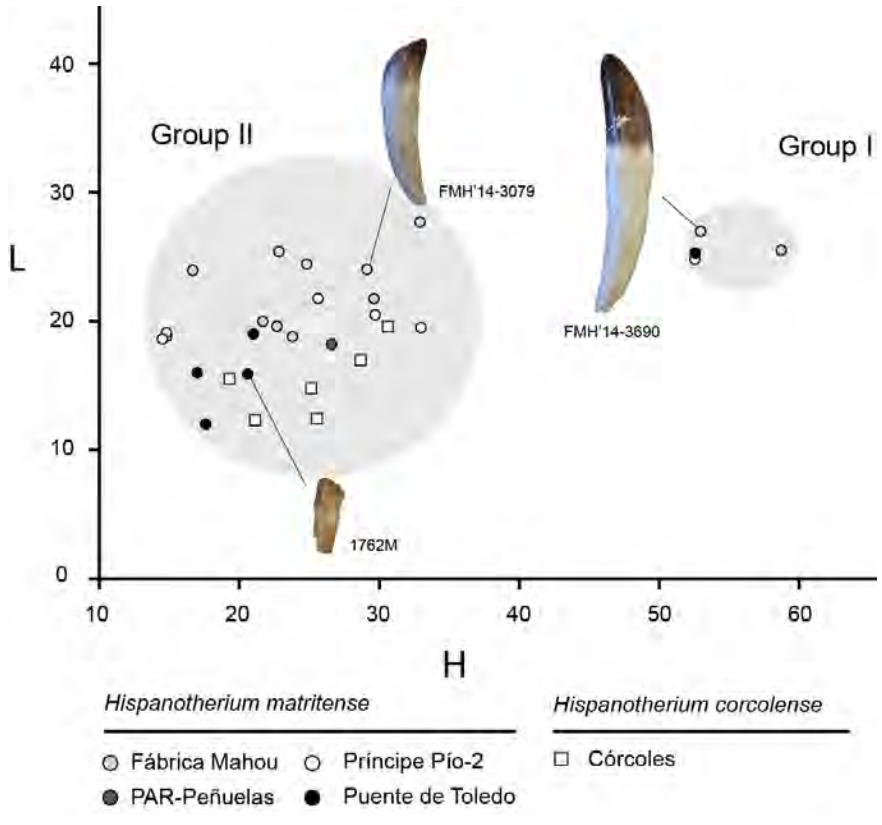


Fig. 17 Bivariate plot (length vs. wiTDh) of i2's of *Hispanotherium matritense* from various localities. The sample of *Hispanotherium corcolense* from Córcoles has been included for comparative purposes. Measurements are given in mm.

Regarding the postcranial skeleton, our sample is formed by isolated remains, and the only articulated skeleton of *H. matritense* lacked the mandible (and, therefore, the i2's), so its postcranial skeleton cannot be linked to a particular gender.

Bone histological analysis

Most of the specimens showed a highly damaged cortical bone that mainly affects the endosteal and medial regions, whereas periosteal region preserves histological features. The preserved cortical bone reveals that primary bone tissue is characterized by fibrolamellar bone tissue with differences in the vascular pattern. Humeri and femora show a laminar bone tissue with vascular canals arranged circumferentially throughout the cortical bone (Figure 17). The tibiae are characterized by a laminar vascular pattern (circumferential canals) and longitudinal primary osteons randomly distributed mainly in the ventral/plantar region. Metapodials show longitudinal primary osteons with a random distribution. Finally, the vascular pattern in radii could not be identified due to the characteristic high bone remodeling in this element.

Secondary osteons have been observed in all specimens except in the juvenile specimen 05/101/2/782 (tibia). Comparison among different elements shows that density of secondary osteons is higher in adults than in juveniles, which indicates an increase of bone remodeling during ontogeny. Interestingly, among juveniles, the third metatarsal 05/101/2/446 is highly remodeled as occur in adult specimens,

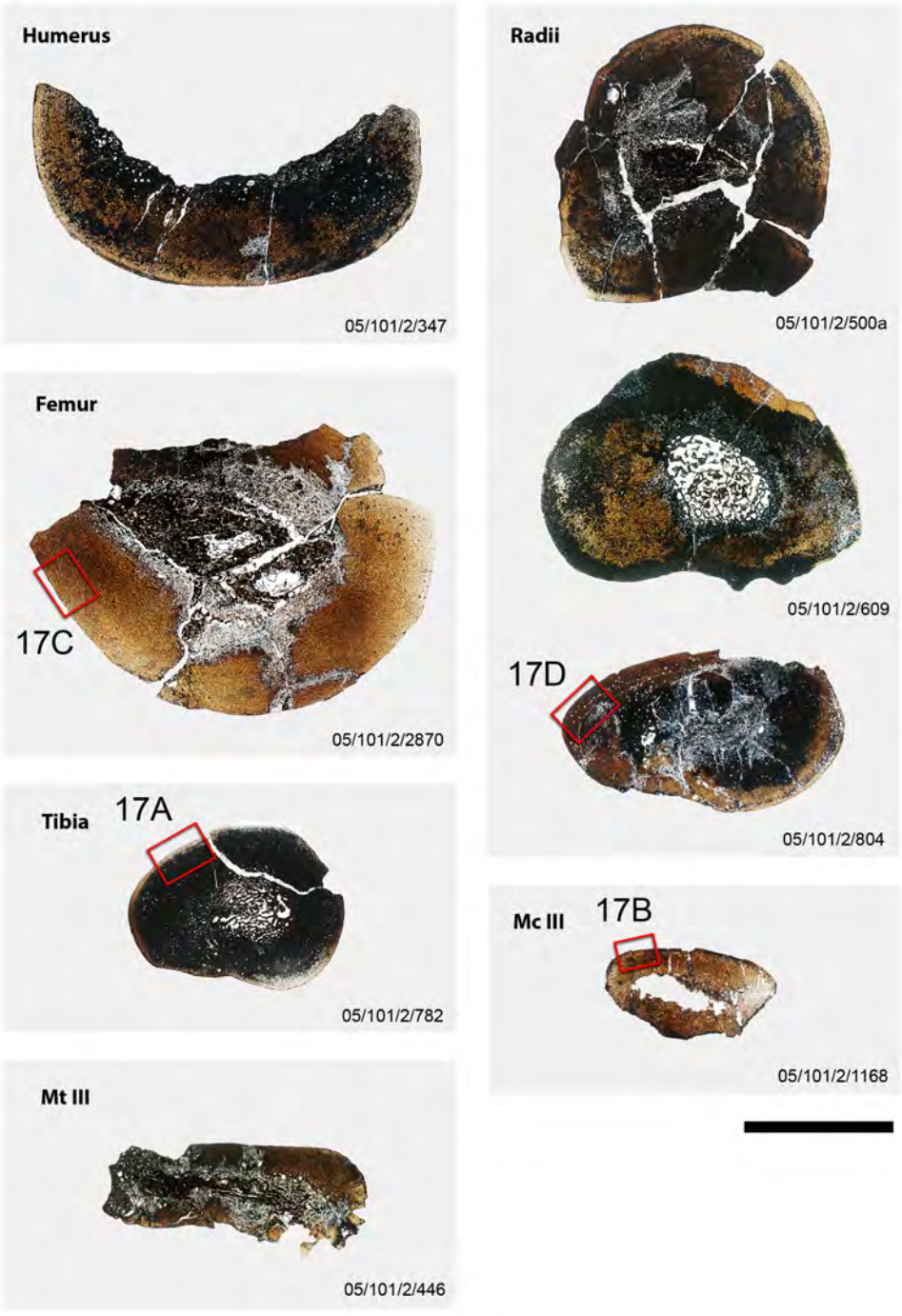


Fig. 18 Transversal sections from the sample analysed for the histological study of *Hispanotherium matritense* from the Iberian locality of Príncipe Pío-2 (Tagus Basin, Spain). This figure shows different degrees of alteration of the cortical bone. In general, periosteal region preserves the histological structure; specimens 05/101/2/2870 and 05/101/2/1168 are the best preserved sections. Squares in sections indicate the areas from where we have taken pictures used in the Figure 18. Scale bar equals 25 mm.

suggesting a main role of metatarsal in the biomechanic of *H. matritense* from an early age. Alexander and Pond (1992) suggest that skeletons of living rhinos may be able to resist higher factors of safety than other large mammals (i.e. lower stresses running while sacrificing the performance for more strenuous activities such as jumping). However, this result relies on the assumption that rhinoceros bone is as resistant as the other animals which it is being compared with in Alexander's work (buffalo, *Syncerus caffer*, and African elephant, *Loxodonta africana*). In the same paper, the authors quote the results of J. D. Currey, which found that humeri from rhinoceros carcasses were more porous than long bone from cattle. This particularity is reflected in about 20% less mechanical strength. If high remodeling from an early age is restricted to *H. matritense*, this particularity may represent a feasible strategy to keep a high safety factor while running and dealing at the same time if bone architecture is less resistant to mechanical stress. The high damaged of the cortical bone avoid us to observe a pattern of distribution of bone remodeling areas that could provide information about the biomechanic role of each element.

In spite of the high occurrence of bone remodeling, we have observed that few specimens display lines of arrested growth (LAGs) and most of the specimens show external fundamental

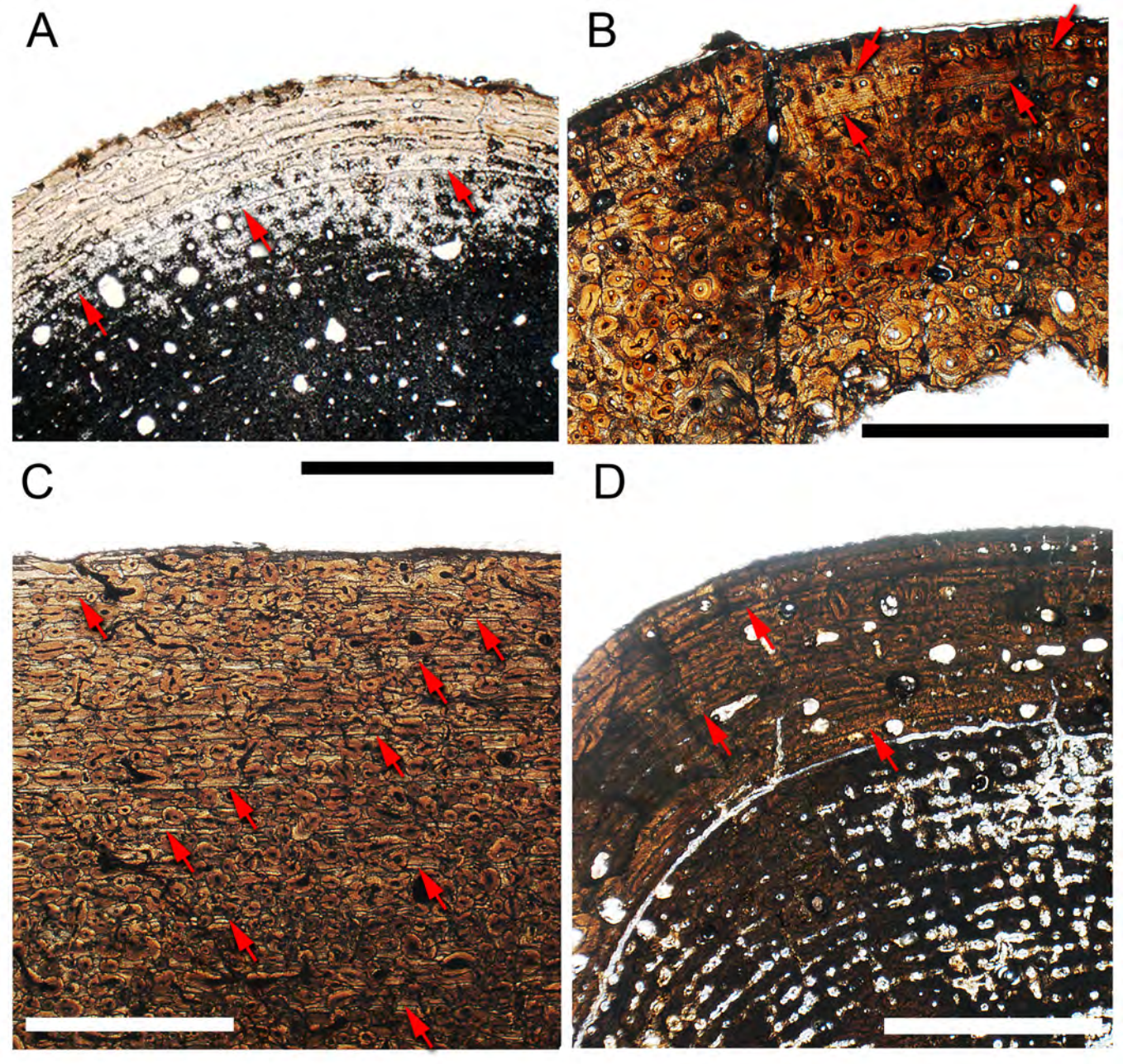


Fig. 19 Detail of the cortical bone from four *Hispanotherium matritense* from the Iberian locality of Príncipe Pío-2 (Tagus Basin, Spain). This figure shows the lines of arrested growth (red arrows) identified within the cortical bone. A, tibia 05/101/2/782; B, metatarsal 05/101/2/1168; C, femur 05/101/2/3870; D radius 05/101/2/804. Scale bar equals 2500 µm.

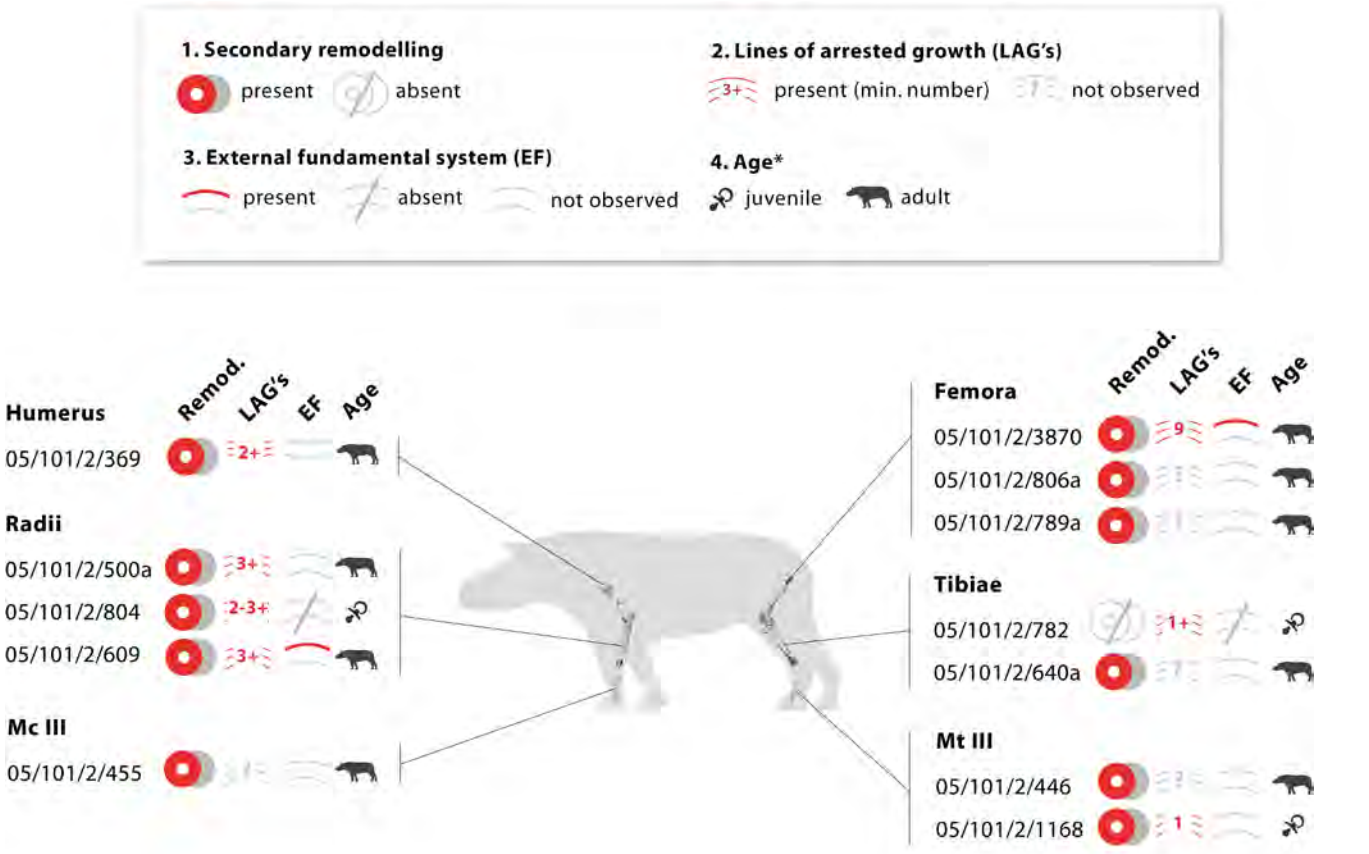


Fig. 20 Resume of the histological results of the studied sample *Hispanotherium matritense* from Príncipe Pío-2. *estimated age according to the external morphology and proportions.

system (EFS). Four specimens show LAGs within the cortical bone (Table 15 and Figure 18): one LAG (05/101/2/782), two LAGs (05/101/2/369), three LAGs (05/101/2/804), and nine LAGs (05/101/2/3870). Among these specimens, the femur 05/101/2/3870 also displays an EFS with three growth marks (Figures 17 and 18). The remaining specimens included in the sample show EFS with three or two growth lines in the periosteal region but LAGs could not be identified because of the bone remodeling or taphonomic alteration (Figures 16 and 18).

As we commented in material and methods, to be considered as a growth mark, lines should surround the entire cross section. However, the high alteration and bone remodeling of the specimens obscure part of these lines within the primary cortical bone. Therefore, the analysis of the bone histology to infer data about the biology and life history of the *H. matritense* specimens is limited by this lack of histological data. Nevertheless, and considering this limitation, we have assessed our results as a first approach to the biology of this species, which should be validated in future studies. Interpretation of growth marks allowed us to identify one-year-old specimens (tibia: 05/101/2/782), two-years-old specimen (05/101/2/1168), three-years-old specimen (05/101/2/804) and a specimen of more than nine years old (05/101/2/3870). The tibia 05/101/2/782 also shows vascular canals open to the periosteal surface and no bone remodeling, which indicate that this specimen of one-year-old is the younger in our sample. There are three specimens with EFS indicating that they are skeletally mature but we cannot infer how old they were when reached this maturity. The femur 05/101/2/3870 is the only specimen showing LAGs and EF suggesting that *H. matritense* reach the skeletal maturity at ten years old. The sexual maturity in rhinos varies among living species. Males reach the sexual maturity from 7 to 10 years, whereas females achieve it earlier, from 4 to 7 years (depending on the species; Rookmaaker, 2015). If we assume similar differences between males and females of *H. matritense*, the isolated femur 05/101/2/3870 can be assigned to an adult male individual.

Restoration of the skeleton and paleoecological remarks

A partial skeleton was found in the middle of the quarry (grid number 5B) of Príncipe Pío-2 (Fig. 20A). This specimen has served as a basis for our reconstruction of the skeletal morphology of *H. matritense*. The articulated specimen included a dorso-ventraly distorted skull (Sanisidro et al., 2011), which served as the basis for the reconstructed head model, figured in the previous chapter (Fig. 5). The proportions of the skull are based on skull MNCN-05/101/2/7000. The first skeletal restoration of *H. matritense* is proposed in the present work. The skeleton has been represented in lateral view. Missing parts have been completed as follows: The orientation of the occipital plate has been reconstructed according to the skull

MHNT.PAL.2004.0.58 of *Hispanotherium beonense*. Caudally-oriented occipital plates can be found in other mixed-feeder (e.g. Sumatran rhino) and grazer (Nile and White rhinos) rhinoceros species. The thoracic cage, vertebral column, and pelvis have been reconstructed following the complete skeleton of *Menoceras arikarense*, a Elasmotheriini of slightly more slender proportions and smaller size, originally figured by O. A. Peterson (1911) and scaled respect to the relative length of the skull and the limbs. Compared with modern species, the skeleton of *H. matritense* (Fig. 20B) displays more slender postcranial proportions. Its gracility indices fall in between modern rhino species and tapirs. However, the tapir manus work in a different way, as it retains the Mc V, a finger required for its displacement. This digit is highly reduced in

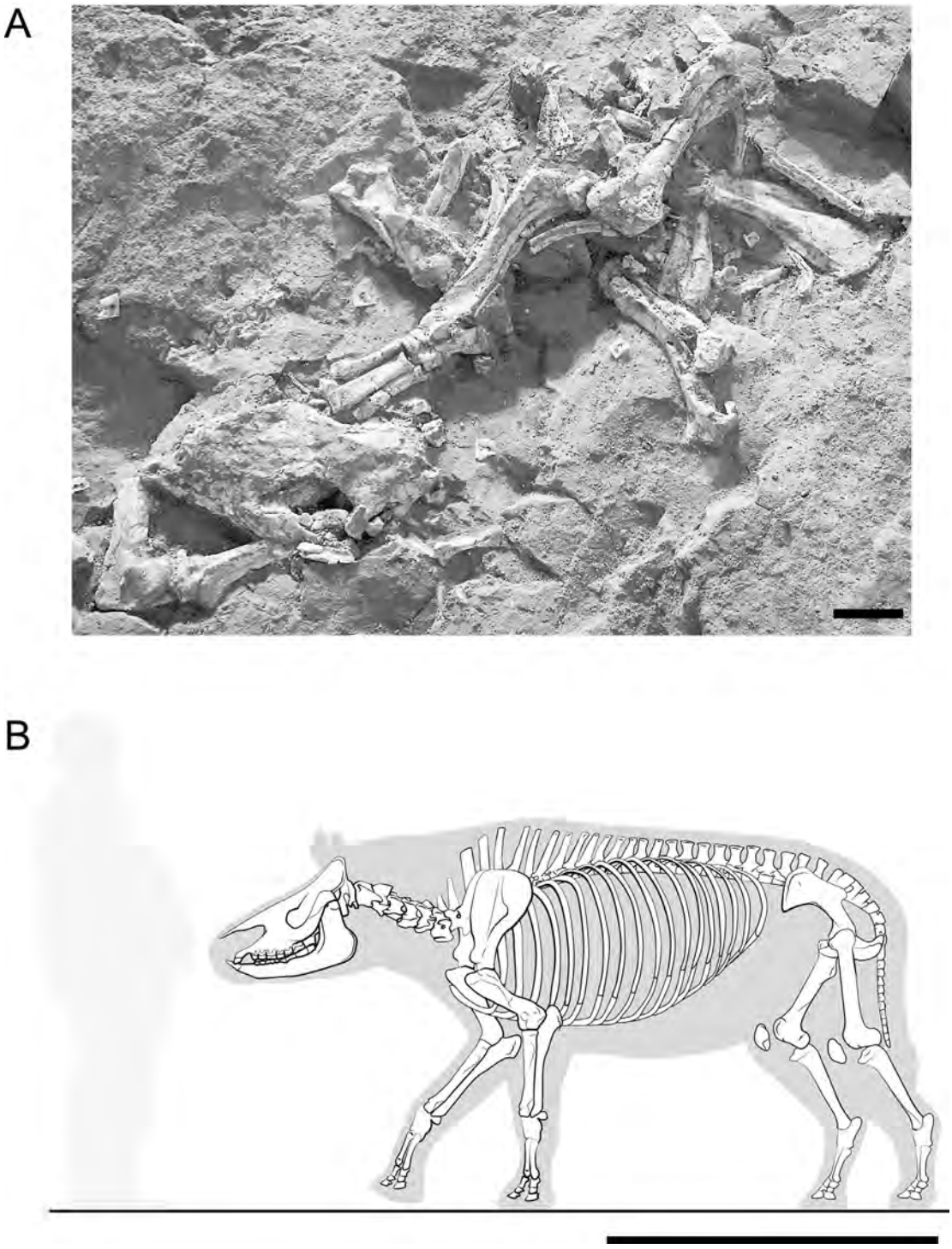


Fig. 20 A, partially articulated skeleton of *Hispanotherium matritense* from Príncipe Pío-2. B, reconstruction of the skeleton of *H. matritense* largely based on the specimen figured in A. The cranial anatomy is based on the reconstruction figured in the previous Chapter. Scale bars represent 100 mm and 500 mm respectively. Photograph by ArqueoStudio.

most elasmotheres and *H. matritense* is not an exception. As detailed in the description, the Mc V is embedded in the distal articular surface of the unciform. Both are in turn tightly attached to the Mc IV, with which form a single functional unit (Klaits, 1972).

The high hypsodonty and slender postcranial proportions led most authors to tie *H. matritense* with open environments (Cerdeño and Nieto, 1995). Recent carbon isotope analyses recorded in the Madrid Area (localities of Paseo de las Acacias, Estación Imperial, PAR Peñuelas, Puente de Toledo, and Casa de Campo/Marqués de Monistrol M-30) confirms this point, pointing to the consumption of a higher porportion of C_3 grasses and the occupancy of open areas by *H. matritense* (Domingo et al., 2012). In the localities from the Aragonian of the Madrid Basin, several species of the tridactyl equid *Anchitherium* coexisted with *Hispanotherium* (i.e. *Anchitherium matritense*, *Anchitherium alberdiae* and an undetermined *Anchitherium* species; Domingo et al., 2012). In those localities with abundance of *Anchitherium*, *Hispanotherium* is poorly represented and vice versa. Such biased proportions of both mammals have been repeatedly addressed in the literature. These differences were firstly explained as a result of distinct sedimentary conditions related to local variations of their paleogeographic environments (Morales et al., 1993). Other works found that these differences were a reflect of different paleoecological and/or climatic requirements (Cerdeño and Iñigo, 1997; Cerdeño and Nieto, 1995; Soria et al., 2000): In those localities in which *Anchitherium* predominates (e.g.: La Retama, Puente de Toledo, PAR Peñuelas and Estación Imperial) were linked to depositional ambients with ponds and/or temporal wet spots, whereas those with prevalence of *Hispanotherium* (e.g.: Torrijos and Paseo de las Acacias) were related to drier paleoambients with less humid conditions. Alternatively, an ecological competence between *Hispanotherium* and *Anchitherium* has been also proposed (Cerdeño and Alberdi, 1983). However, isotopic analysis conducted by Domingo et al. (2012), found that *H. matritense* and its accompanying *Anchitherium* species (*A. alberdiae* or *A. matritense*) have largely overlapped carbon isotope signals, which results in the occupation of similar habitats. These results are unexpected as *A. alberdiae* and, particularly, *A. matritense*, are regarded as brachyodont browsers and dependent on high humidity levels (Hernández Fernández et al., 2003), contrary to what is alleged for *Hispanotherium*. If we take a deeper look, when *A. alberdiae* is present, *Hispanotherium* is testimonial in one locality (PAR Peñuelas) and predominant in the other (Paseo de las Acacias). In the case of *A. matritense*, *Hispanotherium* is the predominant taxa in both localities (Puente de Toledo and Estación Imperial). As mentioned, the different trophic strategies of both anchitheriine horses (browsers) and *Hispanotherium* (grazer) are well-established. This ecological segregation, combined with the dry particular local paleogeographic conditions of some localities, may explain the scarcity of *A. matritense* (which relies more on humid conditions) and, if particularly dry and distant from water bodies, the low numbers of *A. alberdiae*. In conclusion, *H. matritense* inhabited dry open grasslands whose water bodies (lacking in closed vegetation, as shown by the carbon isotope data) were also frequented by anchiitherine equids. This habitat was very similar to that reconstructed in the Anatolian Peninsula and Central Asia during the Middle to Late Miocene, places where elasmothere rhinos thrived. *H. matritense* was the last elasmothere of the Iberian fossil record. Its disappearance at the end of the Middle Aragonian (~ 14,8-14,1 Ma) coincides with an enhacement in humidity and the disappearance of the dry savanna-like environments in the Iberian Peninsula.

ACKNOWLEDGMENTS

We thank Geosfera, ArqueoEstudio S. C., Paleoconsult S. L., Paleoymás S. L. L., and, especially, D. M. D. Pesquero, L. P. Roca Pacheco, G. M. Bernal Barreiro, S. Fraile, C. Rubio Bueno, S. Pozas Requejo, H. Burbano, and their field assitants for an invaluable and tireless field work unearthing a large part of the fossil remains included in the present work. Many thanks to E. Cantero, (Museo Nacional de Ciencias Naturales – CSIC) for the beautiful preparation of the specimens from Príncipe Pío-2 and Fábrica Mahou. Our deep gratitude to P. Pérez Dios, S. Fraile (Museo Nacional de Ciencias Naturales – CSIC), D. G. Rößner (Bayerische Staatssammlung für Paläontologie un Geologie), J. Galkin (American Museum of Natural History), D. W. Wessels (University of Utretch-Faculty of Geosciences), Y. Laurent (Muséum d'Histoire Naturelle de Toulouse), M. Marín (Museo Paleontológico de Elche), and S. Menéndez (Instituto Geológico y Minero Español) for their curational work and the access to the fossil specimens under their care.

sample *Hispanotherium matritense* from Príncipe Pío-2. *estimated age according to the external morphology and proportions.

LITERATURE CITED

Aguirre, E., Alberdi, M. T., Martín-Escorza, C., Torres, T., Morales, J., C. Sesé, and Soria, D., 1982, Torrijos: nueva fauna con *Hispanotherium* de la cuenca media del Tajo: Acta Geológica Hispánica, v. 1-2, p. 39-61.

Alberdi, M. T., Ginsburg, L., and Morales, J., 1981, Rhinocerotidae del Yacimiento de los Valles de Fuentidueña (Segovia): Estudios Geológicos, v. 37, p. 439-465.

Alexander, A., and Pond, C. M., 1992, Locomotion and bone strength of the white rhinoceros, *Ceratotherium simum*: Journal of Zoology, v. 227, p. 63-69.

Antoine, P. O., 1997, *Aegyrcitherium beonensis* nov. gen. nov. sp., nouvel élasmothère (Mammalia, Rhinocerotidae) du gisement miocène (MN 4b) de Montréal-du-Gers (Gers, France). Position phylogénétique au sein des

Elasmotheriini: Neues Jahrbuch für Geologie und Paläontologie Abhandlungen, v. 204, no. 3, p. 399-414.

-, 2000, Origine et différenciation des Elasmotheriina parmi les Rhinocerotidae (Mammalia, Perissodactyla) : analyse cladistique et implications biostratigraphiques et paléobiogéographiquesUnpublished Ph.D. dissertation], 350 p.

Antoine, P. O., 2002, Phylogénie et évolution des Elasmotheriina: (Mammalia, Rhinocerotidae): Mémoires du Muséum National d'Histoire Naturelle, v. 188, p. 5-350.

Antoine, P. O., 2003, Middle Miocene elasmotheriine Rhinocerotidae from China and Mongolia: taxonomic revision and phylogenetic relationships: Zoologica Scripta, v. 32, no. 2, p. 95-118.

Antoine, P. O., Alférez, F., and Iñigo, C., 2002, A new elasmotheriine (Mammalia, Rhinocerotidae) from the Early Miocene of Spain: Comptes Rendus Palevol, v. 1, no. 1, p. 19-26.

Antoine, P. O., Downing, K. F., Crochet, J.-Y., Duranthon, F., Flynn, L. J., Marivaux, L., Métais, G., Rajpar, A. R., and Roohi, G., 2010, A revision of *Aceratherium blanfordi* Lydekker, 1884 (Mammalia: Rhinocerotidae) from the Early Miocene of Pakistan: postcranials as a key: Zoological Journal of the Linnean Society, v. 160, p. 139-194.

Antoine, P. O., and Welcomme, J. L., 2000, A new rhinoceros from the lower Miocene of the Bugti Hills, Baluchistan, Pakistan: The earliest Elasmotheriine: Palaeontology, v. 43, p. 795-816.

Antunes, M. T., 1965, Un Schizotheriiné du genre *Phylotillon* (Chalicotheriidae, Perissodactyla) dans l'Helvétien Vb de Charneca do Lumiar. Remarques écologiques sur la faune de Mammifères: Bull. Soc. géol. Portugal, v. 16, p. 159-178.

-, 1972, Notes sur la géologie et la paléontologie du Miocène de Lisbonne : un nouveau rhinocerotidé, *Chilotherium ibericus* n. sp: Boletim do Museu e Laboratório Mineralógico e Geológico da Faculdade de Ciências, v. 13, no. 1, p. 25-33.

-, *Hispanotherium* fauna in Iberian Middle Miocene; its importance and paleogeographical meaning, *in* Proceedings Annales Geologiques Pays. Hellèn. VII International Congress on Mediterranean Neogene1979, p. 25-33.

Antunes, M. T., and Ginsburg, L., 1983, Les Rhinocérotidés du Miocène de Lisbonne. Systématique, écologie, paléobiogéographie, valeur stratigraphique: Ciências da Terra (UNL), v. 7, p. 17-98.

Astibia, H., 1985, Los macromamíferos del Mioceno medio de Tarazona (Depresión del Ebro, Prov. de Aragón) Tesis Doctoral]: Universidad del País Vasco, Facultad de Ciencias, 265 p.

Becker, D., 2003, Paléoécologie et paléoclimats de la Molasse du Jura (Oligo-Miocène) : apport des Rhinocerotoidea (Mammalia) et des minéraux argileuxGrade de Doctor rerum naturalium]: Universite de Fribourg (Suisse), 327 p.

Beliaeva, E. I., 1971, O nekotori nosoroga semeistva Rhinocerotidae iz Neogena zapadnoij Mongolij ("On certain rhinoceroses, family Rhinocerotidae, from the Neogene of western Mongolia"): Kajnozoja zapadnoj Mongolii, v. 3, p. 78-97.

Boné, E., Alberdi, M. T., Hoyos, M., and López, N., 1980, Prospection paléontologique de la région de Torralba de Ribota (Burdigalien du Bassin de Calatayud, Zaragoza, España): Paleovertebrata, v. Mem. juv. R. Lavocat, p. 233-247.

Burbano, H., 2009, Yacimientos de la Casa de Campo, Monistrol M-30 Sur del Aragoniense medio: Madrid, p. 72.

Castanet, J., 2006, Time recording in bone microstructures of endothermic animals; functional relationships: Comptes Rendus Palevol, v. 5, p. 629-636.

Castanet, J., Francillon-Vieillot, H., Meunier, F. J., and de Ricqlès, A., 1993, Bone and individual aging, Boca Raton, Florida, CRC Press, Bone, 245-283 p.:

Cerdeño, E., 1982, Estudio descriptivo del esqueleto postcraneal de *Hispanotherium matritense* del yacimiento de Torrijos (Toledo)Tesis de Licenciatura]: Universidad Complutense de Madrid, 117 p.

-, 1987, Consideraciones sobre la validez de la especie *Hispanotherium alpani* Saraç 1978 (Rhinocerotidae): Estudios Geológicos, v. 43, p. 531-533.

-, 1989, Revisión de la sistemática de los rinocerontes del Neógeno de EspañaPh.D. Dissertation]: Universidad Complutense de Madrid, 429 p.

-, 1992a, New Remains of the Rhinocerotid *Hispanotherium matritense* at La Retama Site: Tagus Basin, Cuenca, Spain: Geobios, v. 25, no. 5, p. 671-679.

-, 1992b, Spanish Neogene Rhinoceroses: Palaeontology, v. 35, p. 297-308.

-, 1995, Cladistic analysis of the Family Rhinocerotidae (Perissodactyla): American Museum Novitates, v. 3143, p. 1-25.

-, 1996, Rhinocerotidae from the Middle Miocene of the Tung-gur Formation, Inner Mongolia (China): American Museum Novitates, v. 3184, p. 1-43.

Cerdeño, E., and Alberdi, M. T., 1983, Estudio descriptivo del esqueleto postcraneal de *Hispanotherium matritense* del yacimiento Mioceno de Torrijos (Toledo): Estudios Geológicos, v. 39, p. 225-235.

Cerdeño, E., and Iñigo, C., 1997, *Hispanotherium matritense* (Rhinocerotidae) de la ciudad de Madrid (España) y su relación con el paleoambiente del Aragoniense medio (Mioceno Medio): Revista Española de Paleontología, v. 12, no. 1, p. 80-90.

Cerdeño, E., and Nieto, M., 1995, Changes in Western European Rhinocerotidae related to climatic variations:

Palaeogeography, Palaeoclimatology, Palaeoecology v. 114, p. 325-338.

Crusafont, M., and Villalta, J. F., 1947, Sobre un interesante rinoceronte (*Hispanotherium*) del Mioceno del Valle de Manzanares: Las Ciencias, v. 12, p. 869-883.

Chinsamy-Turan, A., 2005, The microstructure of Dinosaur bone: deciphering biology with fine-scale techniques, Baltimore and London, Johns Hopkins University Press, 216 p.:

Chinsamy, A., and Valenzuela, N., 2008, Skeletochronology of the endangered side-neck turtle, *Podocnemis expansa*: South African Journal of Science, v. 104, p. 311-314.

De Ricqlés, A., Meunier, F. J., Castanet, J., and Francillon-Vieillot, H., 1991, Comparative microstructure of bone: Bone, v. 3, p. 1-78.

Deng, T., 2001, Cranial ontogenesis of *Chilotherium wimani* (Perissodactyla, Rhinocerotidae, *in* Deng, T., and Wang, Y., eds., Proceedings of the Eighth Annual Meeting of the Chinese Society of Vertebrate Paleontology: Beijing, China Ocean Press, p. 101-112.

-, 2003, New material of *Hispanotherium matritense* (Rhinocerotidae, Perissodactyla) from Laogou of Hezheng County (Gansu, China), with special reference to the Chinese Middle Miocene elasmotheres: Geobios, v. 36, p. 141-150.

-, 2005, New discovery of *Iranotherium morgani* (Perissodactyla, Rhinocerotidae) from the Late Miocene of the Linxia Basin in Gansu, China, and its sexual dimorphism: Journal of Vertebrate Paleontology, v. 25, no. 2, p. 442-450.

Deng, T., Wang, S., and Hou, S., 2013, A bizarre tandem-horned elasmothere rhino from the Late Miocene of northwestern China and origin of the true elasmothere: Chinese Science Bulletin, v. 15, p. 1811-1817.

Domingo, L., Koch, P. L., Grimes, S. T., Morales, J., and López-Martínez, N., 2012, Isotopic paleoecology of mammals and the Middle Miocene Cooling event in the Madrid Basin (Spain): Palaeogeography, Palaeoclimatology, Palaeoecology, v. 339-341, p. 98-113.

Elliott, A. C., and Woodward, W. A., 2007, Statistical analysis quick reference guidebook with SPSS examples. 1st ed., London, Sage Publications.

Fortelius, M., 1990, Rhinocerotidae from Pasalar, middle Miocene of Anatolia (Turkey): Journal of Human Evolution, v. 19, p. 489-508.

Fortelius, M., and Heissig, K., 1989, The phylogenetic relationships of the Elasmotherini (Rhinocerotidae, Mamm.): Mitteilungen Bayerische Staatssammlung Paläontologische historische Geologie v. 29, p. 227-233.

Francillon-Vieillot, H., Buffrénil, V., Castanet, J., Géraudie, J., and Meunier, F. J., 1990, Microstructure and mineralization of vertebrate skeletal tissues, New York, Van Nostrand Reinhold, Skeletal biomineralization: Patterns, processes and evolutionary trends

Geraads, D., and Saraç, G., 2003, Rhinocerotidae from the Middle Miocene Hominoid Locality of Çandir (Turkey): Cour. Forsch.-Inst. Senckenberg, v. 240, p. 217-231.

Ginsburg, L., 1974, Les Rhinocerotides du Miocene de Sansan (Gers): Compte Rendus des Seances de l'Academie des Sciences, Paris, v. 278, no. 5, p. 597-600.

Ginsburg, L., and Antunes, M. T., 1979, Les Rhinocérotidés du Miocène inférieur et moyen de Lisbonne (Portugal). Succesion stratigraphique et incidences paléogéographiques: C. R. Acad. Sc. Paris, v. t. 288, p. 493-495.

Ginsburg, L., Maubert, F., and Antunes, M. T., 1987, Discovery of *Hispanotherium* and *Gaindatherium* (Rhinocerotidae, Mammalia) in the Miocene of France: Bulletin du Muséum national d'histoire naturelle. Section C, Sciences de la terre, paléontologie, géologie, minéralogie, v. 9, no. 3, p. 303-311.

Guérin, C., 1980, Les rhinocéros (Mammalia, Perissodactyla) du Miocène terminal au Pléistocène supérieur en Europe occidentale : comparaison avec les espèces actuelles: Documents des Laboratoires de Géologie de Lyon, v. 79, p. 1-1184.

Heissig, K., 1972a, Die obermiozäne Fossil-Lagerstätte Sandelzhausen. 5. Rhinocerotidae (Mammalia), Systematik und Okologie: Mitteilungen der Bayerischen Staatssammlung Paläontologie und historische Geologie, v. 14, p. 37.

-, 1972b, Paläontologische und geologische Untersuchungen im Tertiär von Pakistan. 5. Rhinocerotidae (Mamm.) aus den unteren und mittleren Siwalik-Schichten.: Bayerische Akademie der Wisseschaften, Mathematisch-Naturwissenschaftliche Klasse Abhandlungen, v. 152, p. 1-112.

-, 1974, Neue Elasmotherini (Rhinocerotidae, Mammalia) aus dem Obermiozän Anatoliens: Mitteilungen der Bayerischen Staatssammlung Paläontologie und historische Geologie, v. 14, p. 21-35.

-, 1989, The Rhinocerotidae, *in* Prothero, D., and Schoch, R. M., eds., The evolution of Perissodactyls, Oxford University Press, p. 399-417.

-, 1999, 16. Family Rhinocerotidae, *in* Rössner, G. E., and Heissig, K., eds., The Miocene Land Mammals of Europe: Pfeil, Munich, p. 175-188.

Hernández-Pacheco, F., 1914, Los vertebrados Miocenos de la Península Ibérica: Memorias de la Real Sociedad Española de Historia Natural, v. IX, no. Memoria 4a, p. 443-485.

Hernández-Pacheco, F., and Crusafont, M., 1960, Primera caracterización paleontológica del Terciario de Extremadura: Boletín de la Real Sociedad Española de Historia Natural (Geol.), v. 58, p. 275-282.

Hernández Fernández, M., Salesa, M. J., Sánchez, I. M., and Morales, J., 2003, Paleoecología del género

Anchitherium Von Meyer, 1834 (Equidae, Perissodactyla, Mammalia) en España: evidencias a partir de las faunas de macromamíferos.: Coloquios de Paleontología, v. Vol. Extr. 1, p. 253-280.

Herráez, E., Paredes, I. G., Peláez-Campomanes, P., and Morales, J., 2006, Los Nogales, nueva fauna de vertebrados del Mioceno medio de Madrid: Estudios Geológicos, v. 62, no. 1, p. 257-262.

Iñigo, C., 1993, Estudio de los Perisodáctilos del yacimiento Mioceno de Córcoles (Guadalajara)Tesis Doctoral (Unpublished)]: Universidad Complutense Madrid 559 p.

Iñigo, C., and Cerdeño, E., 1997, The *Hispanotherium matritense* (Rhinocerotidae) from Córcoles (Guadalajara, Spain): Its contribution to the systematics of the Miocene Iranotheriina: Geobios, v. 30, no. 2, p. 243-266.

Klaits, B. G., 1972, The moving mesaxonic manus: A comparison of tapirs and rhinoceroses: Mammalia, v. 36, no. 1, p. 126-145.

Klevezal, G. A., 1996, Recording Structures of Mammals: Determination of Age and Reconstruction of Life History, Netherlands, A. A. Balkema Publishers, 274 p.:

Köhler, M., and Moyà-Solà, S., 2009, Physiological and life history strategies of a fossillarge mammal in a resource-limited environment: PNAS, v. 106.

Lamm, E. T., 2013, Preparation and Sectioning of Specimens, Berkeley, University of California Press, Bone histology of fossil tetrapods: advancing methods, analysis, and interpretation.

López-Martínez, N., Sesé, C., and Herráez, E., 1987, Los yacimientos con Micromamíferos del área de Madrid: Boletín Geológico y Minero, v. 98, p. 159-176.

Martinez-Maza, C., Alberdi, M. T., Nieto-Diaz, M., and Prado, J. L., 2014, Life-History Traits of the Miocene Hipparion concudense (Spain) Inferred from Bone Histological Structure: PloS ONE, v. 9, no. 8.

Mead, A. J., 2000, Sexual dimorphism and paleoecology in *Teleoceras*, a North American Miocene rhinoceros: Paleobiology, v. 26, no. 4, p. 689-706.

Mihlbachler, M., 2007, Sexual Dimorphism and Mortality Bias in a Small Miocene North American Rhino, *Menoceras arikarense* : Insights into the Coevolution of Sexual Dimorphism and Sociality in Rhinos: Journal of Mammalian Evolution, v. 14, no. 4, p. 217-238.

Mihlbachler, M. C., 2005, Linking sexual dimorphism and sociality in rhinoceroses: insights from *Teleoceras proterum* and *Aphelops malacorhinus* from the late miocene of Florida: Bulletin of the Florida Museum of Natural History, v. 45, no. 4, p. 495-520.

Morales, J., Alcalá, L., Hoyos, M., Nieto, N., Pérez, B., and Soria, D., 1993, El yacimiento del Aragoniense medio de La Retama (Depresión Intermedia, Provincia de Cuenca, España): significado de las faunas con *Hispanotherium*: Scripta Geologica, v. 103, p. 23-39.

Olivares, C., and Rebollada, E., 2011, Revisión histórica, localización y actualización de los restos fósiles de Hispanotherium matritense del yacimiento Mioceno de Plasencia "Dehesa de los Caballos" (Cáceres, Extremadura), p. 1-23.

Olmedo, F. L., Neira, A. D. d., Serrano, A. M., Calvo, J. P., Morales, J., and Peláez-Campomanes, P., 2004, Unidades Estratigráficas en el Registro Sedimentario Neógeno del Sector Occidental de la Cuenca de Madrid: Revista de la Sociedad Geológica de España, v. 17, no. 1-2, p. 87-101.

Padian, K., Lamm, E.-T., and Werning, S., 2013, Selection of specimens, Berkeley, University of California Press, Bone histology of fossil tetrapods: advancing methods, analysis, and interpretation.

Pérez de Barradas, J., 1926, Algunos datos para el estudio de la climatología cuaternaria del Valle del Tajo: Boletín de la Sociedad Ibérica de Ciencias Naturales, v. 22, p. 125-145.

Peterson, O. A., 1911, A mounted skeleton of *Diceratherium cooki* Peterson: Memoirs of the Carnegie Museum, v. 7, no. 14, p. 274-279.

Petrova, E., New data about the skull of the Elasmotherium sibiricum. Quaternary Stratigraphy and Paleontology of the Southern Russia: connections between Europe, Africa and asia2010, p. 121-122.

Pozas Requejo, S., 2009, Ampliación, andenes y vestíbulos de Línea 3 de metro. Tramo II (Lavapiés-Delicias). Estación de Embajadores: Madrid, Paleoconsult S.L.

Prado, C. d., 1864, Descripción Física y Geológica de la Provincia de Madrid, Madrid, Junta General de Estadística. Imprenta Nacional.

Rookmaaker, L. C., 2015, Rhino Resource Center, Volume 2015, p. http://www.rhinoresourcecenter.com/.

Sander, P. M., and Andrässy, P., 2006, Lines of arrested growth and long bone histology in Pleistocene large mammals from Germany: What do they tell us about dinosaur physiology? : Palaeontographica, Abt. A: Palaeozoology – Stratigraphy, v. 277, p. 143-159.

Sanisidro, O., Alberdi, M. T., and Morales, J., 2011, The first complete skull of *Hispanotherium matritense* (Prado, 1864) (Perissodactyla, Rhinocerotidae) from the Middle Miocene of the Iberian Peninsula: Journal of Vertebrate Paleontology, v. in press.

Saraç, G., 1978, A new *Hispanotherium* species (Mammalia, Rhinocerotidae): *Hispanotherium alpani* n. sp. from the Upper Miocene of Southwest Anatolia: Bulletin of the Mineral Research and Exploration Institute of Turkey, v. 89, p. 90-95.

Schlosser, M., 1921, Neuere funde von Wirbelthieren, besonders Säugetieren im Tertiär und Pleistocän der Iberischen Halbinsel: Centralblatt f. Min. Gol. und Paleont., v. 14-15.

Soria, D., Amezua, L., Daams, R., Fraile, S., Herráez, E., Morales, J., Nieto, M., Peláez-Campomanes, P., Salesa,

M. J., and Sánchez, I. M., 2000, Faunas del Mioceno, *in* Morales, J., ed., Patrimonio Paleontológico de la Comunidad de Madrid: Madrid, Consejería de Educación de la Comunidad de Madrid, p. 110-177.

Uhlig, v. U., 1999, Die Rhinocerotoidea (Mammalia) aus der unteroligozänen Spaltenfüllung Möhren 13 bei Treuchtlingen in Bayern, Abhandlungen der Bayerische Akademie der Wissenschaften, Mathematisch-Naturwissenschaftliche Klasse, Neue Folge, 254 p.

Van Valen, L., 1966, Deltatheridia, a new order of mammals: Bulletin of the American Museum of Natural History, v. 132, p. 1-126.

Villalta, J. F. d., and Crusafont, M., 1955, *Chilotherium quintanelensis* Zebysz. sinonimo de *Hispanotherium matritensis* (Prado): Nota Comunicaciones del Instituto Geológico y Minero de España, v. 37, p. 1-9.

Wade, M. J., 1979, Sexual selection and variance in reproductive success: American Naturalist, v. 114, p. 742-747.

Westerveld, L. A., 2011, Diffuse idiopathic skeletal hyperostosis (DISH). The impact of spinal ankylosis on trauma patients: Utrecht University, 136 p.

Woodward, H., Padian, K., and Lee, A. H., 2013, Skeletochronology, Berkeley, University of California Press, Bone histology of fossil tetrapods: advancing methods, analysis, and interpretation.

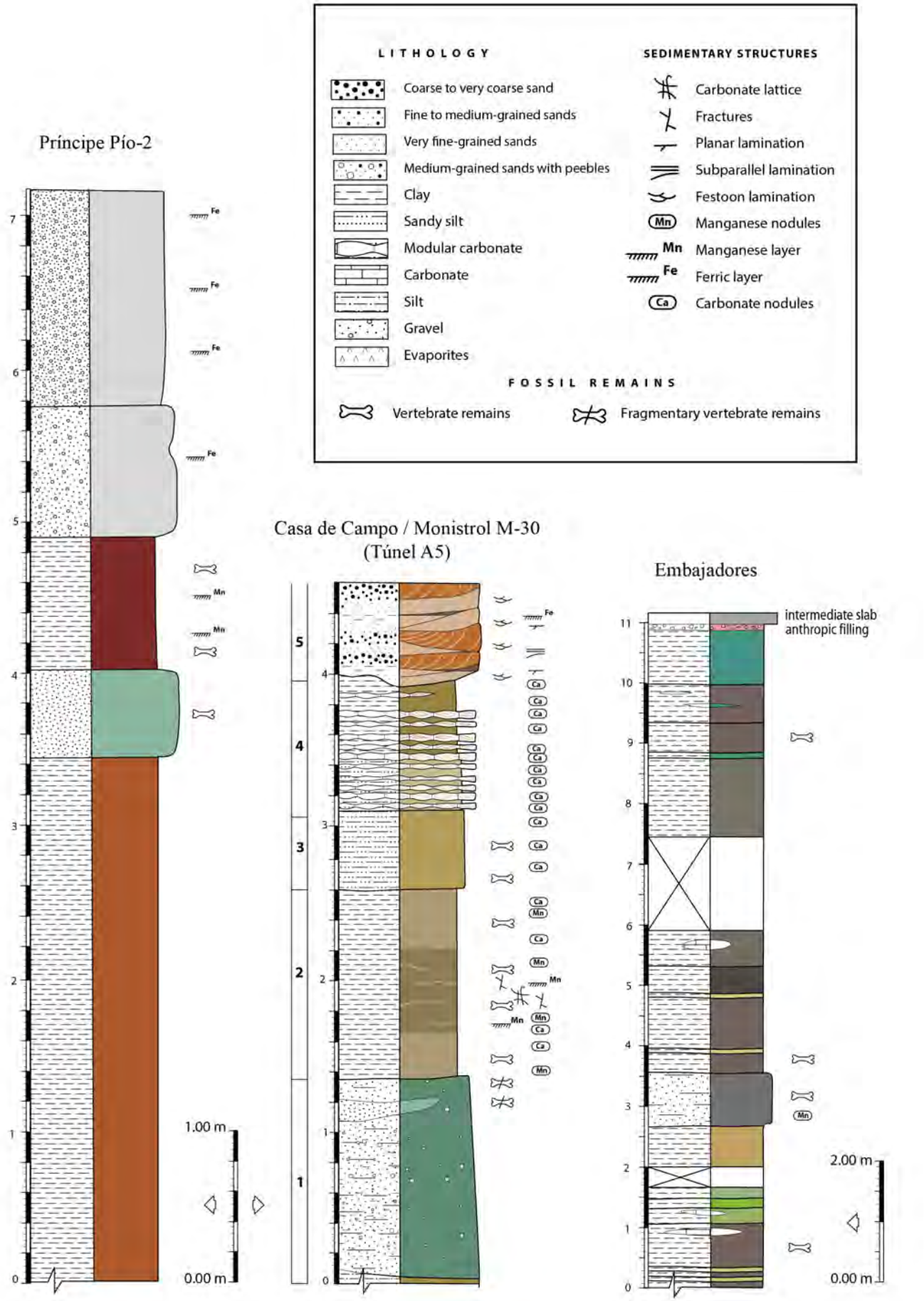
Yan, D., 1979, Einige der Fossilen Miozänen Säugetiere der Kreis von Fangxian in Der Provinz Hupei: Vertebrata Palasiatica, v. 17, p. 189-199.

Zbyszewsky, G., 1952, Les mammifères miocènes de Quintanelas (Sabugo): Comunicaçóes Serviço Géologico Portugal, v. 33, p. 22.

Zhai, R. J., 1978, A primitive elasmothere from the Miocene of Lintung, Shenshi: Professional Papers of Stratigraphy and Palaeontology, v. 7, p. 122-126.

SUPPLEMENTARY DATA 1

Stratigraphic columns of three of the studied localities with presence of *Hispanotherium matritense* firstly reported in the present work.



SUPPLEMENTARY DATA 2

Updated list of the all the stored remains of *Hispanotherium matritense*. The collection number of several published specimens has changed since their original publication. In these cases it has been updated with the current collection number. w/n: without collection number.

Loranca Basin

La Retama (REM). Published in Cerdeño (1992) and stored in the Museo Nacional de Ciencias Naturales-CSIC (Madrid, Spain). The 40 fossil remains pertain to a minimum number of three individuals, one of them juvenile: left juvenile mandible with erupting i2, dp1-dp4, m1 and erupting m2 and right mandibular fragments of the same individual with m1 and incomplete p2 and m2, RET-1; left mandibular fragment with p4-m3, RET-242; right mandibular fragment of the same individual with p3-m1, RET-99; right mandibular fragment with p4-m3, RET-243; left mandibular fragment with p2-m2, RET-6; right P1, RET-218; right M1, RET-473; fragmentary right M1, RET-474; fragmentary right M2, RET-92; i1, RET-351; left p2, RET-48; fragment of lower molar, RET-54; right humerus, RET-705; left radius, RET-310; proximal fragment of a left radius, w/n; left femur without the distal epiphysis, RET-700 and RET-704; left scaphoid, RET-713; left semilunar, RET-107; left pyramidals, RET-702; RET-703; right trapezoid, RET-402; right astragalus, RET-701; proximal fragment of a left calcaneus, RET-w/n; left mesocuneiform, RET-507; right ectocuneiform, RET-188; distal fragment of Mt III, RET-393; right Mc IV, RET-105; first central phalanxes, RET-21; RET-120; RET-121; RET-497; second central phalanxes, RET-189; first lateral phalanxes, RET-116; RET-153; RET-492; second lateral phalanxes, RET-17; RET-517.

Calatayud-Montalbán Basin

Munébrega-1 (MUN1). Stored in Utrecht University (Utrecht, Netherlands) and collected by Dr. de Bruijn (Cerdeño, 1989). Left fragmentary Mx, 55/1109; undetermined tooth fragment, 55/1110; Fragmentary glenoid area of a right? scapula, 55/1097; fragmentary vertebra, 55/1100; proximal fragment of a left radius, 55/1111; diaphysal fragment of a right? radius, 55/1098; incomplete left magnum, 55/1101; right pyramidal, 55/1102; right trapezium, 55/1151; proximal half of a right Mc IV, 55/1112; fragment of a right? epiphysis of a Mc IV, 55/1104; distal fragment of a left tibia, 55/1107; incomplete right navicular, 55/1106; first phalanx III, 55/1128; second phalanx III, 55/1129.

Torralba de Ribota V (or Torralba V; TRR-V). These fossils were originally published in Boné et al. (1980) and subsequently identified as *H. matritense* by Alberdi et al. (1983). The collection, stored in the Museo Nacional de Ciencias Naturales-CSIC (Madrid, Spain), comprises the following specimens: DP2, MNCN 56113; fragmentary M1, MNCN 56112; incomplete M3, MNCN 56114; fragmentary axis, MNCN 56127, two lumbar vertebrae, MNCN 56123 and MNCN 56121; radius, MNCN 56124; pyramidal, MNCN 56116; Mc III, MNCN 56118; patella, MNCN 56120; first central phalanx, MNCN 56115 and a sesamoid, MNCN 56122.

Valdemoros 1A (VA1A). Part of the remains were collected by Dr. de Bruijn and stored in the Utrecht University. These are represented by an astragalus, a cuboid, a patella, and a first lateral phalanx without collection numbers (Cerdeño, 1989). This collection is not available at the present moment, impeding further comparisons.

Valdemoros 2 (VA2A). Stored in the Utrecht University. Medial epicondyle of a right humerus, VAII-500; proximal fragment of a right Mc III, VAII-501; proximal fragment of a right Mt II, VAIIIC-502.

Valdemoros 3C (VA3). Stored in the Utrecht University. Left scaphoid, VAIIIC-502 and a distal fragment of a right tibia, VAIIIC-507.

Valdemoros 4A (VA4A). Stored in the Museo Nacional de Ciencias Naturales-CSIC of Madrid. Fragmentary teeth, VM4A 16, 21, 30, 34 and 35 / MNCN 36138; VM4A 31; 65 / MNCN 36136) and a humerus VM4A 76 / MNCN 36139.

Ebro Basin

Tarazona de Aragon (TAR), published in Astibia (1940) and stored in the Departamento de Geología (Laboratorio de Paleontología) of the Facultad de Ciencias of the Universidad del País Vasco (Spain): Left upper incisor, T2.92; left P2, T2.325; left M1/2, T2.221; T2.222; right M1/2, T2.256; fragmentary left M3, T5.8; left p2, T2.50; left p3, T5.55; right p4, T2.99; fragmentary m1?, T6.11; anterior half of a px or mx, T2.326; right scaphoid, T2.137; left lunate, T2.327; left pyramidal, T2.253; right calcaneum, T2.172; right astragalus, T5.57; left naviculars, T2.64; left ectocuneiform, T2.257; left cuboid, TS.11; undetermined and eroded metapodial (probably a Mc II), T2.238; first central phalanxes, T2.259; T2.305; second central phalanxes, T2.260; T2.258; first lateral phalanx, T2.91; second lateral phalanxes, T4.1; T2.41.

Tagus Basin

Amor (AM). Some isolated teeth fragments and a proximal fragment of a right tibia without collection number were originally collected from the locality of Amor (Dd / E Local zone, near Leiría) and ascribed to an undetermined rhinoceros. In a posterior review of the Miocene mammals from the Lisbon Area, these were assigned to *H. matritense* (Antunes, 2000), but no further information is provided.

Lisbon Area

These remains are scattered along several spots being classically grouped into two minor areas named as **Charneca do Lumiar** (**CHL**; nowadays surrounding the Lisbon Airport) and **Chelas 1 (CHE)**, also within Lisbon municipality (Antunes and Ginsburg, 1983). Within the localities of Charneca do Lumiar, *H. matritense* has been found in Areeiro do José da Graça, Casal das Chitas, Courelas do Covão, Quinta da Musgueira, Quinta Grande, Quinta das Pedreiras, Quinta da Raposa, Quinta da Silvéria, Quinta do Conçeição, Sabliére de Quinta das Mantegais, Olival da Suzana, and a set of unnamed localities near the areas of Musgueira and Charneca do Lumiar. On the other hand, Quinta da Farinheira and Quinta das Flamengas forms the area classically known as Chelas or Chelas 1. All of these fossil sites are currently located within the metropolitan boundaries. They are currently stored in the Museo Geológico.

Areeiro do José da Graça (Antunes and Ginsburg, 1983): left P3, Nº178 (probable origin); incomplete right P4, Nº182 (probable origin); Nº183 (probable origin); left incomplete lunate, Nº224; incomplete right unciform, Nº223; incomplete right Mc IV, Nº238; right incomplete calcaneum, Nº251;

Casal das Chitas (named as Casul Chitaz by Viret & Sbyszewsky, 1958)(Antunes and Ginsburg, 1983): right hemimandible with p2-m3, Nº170; right hemimandible with p3-m2, Nº169; left incomplete scaphoid, Nº287; incomplete right Mc IV, Nº237;

Courelas do Covão (Antunes and Ginsburg, 1983): right M2, Nº191; right m2, Nº210; right radius, Nº221; left lunate, Nº226; left incomplete lunate, Nº225; left astragalus, Nº248.

Quinta da Musgueira (Antunes and Ginsburg, 1983): right M3, Nº196; right m1, Nº208.

Quinta Grande: right DP4, Nº218; right M3, Nº195; right p4, Nº203; left p4, Nº206; fragmentary left Mc III, Nº233; fragmentary right Mc III, Nº232; incomplete right femur, Nº239; right astragalus, Nº242; Nº241.

Quinta da Raposa (Antunes and Ginsburg, 1983): left M2, Nº190; fragmentary right hemimandible with p4, Nº200; left p3, Nº199; left m3, Nº215; right left Mc II, Nº229; left fragmentary Mc III, Nº234; distal half of a left tibia, Nº240; Mt III, Nº259; right Mt III, Nº259.

Quinta da Silvéria (Antunes and Ginsburg, 1983): left P2, Nº176; right M2, Nº192; left M3, Nº197.

Quinta do Conceição (Antunes and Ginsburg, 1983): right M1, Nº188; right astragalus, Nº243.

Sabliére de Quinta das Mantegais (Antunes and Ginsburg, 1983): rightfibula, Nº262.

Unnamed localitie/s (350-500m SE from the town's church of Charneca do Lumiar)(Antunes and Ginsburg, 1983): incomplete left P4, Nº180; right m2, Nº209; left astragalus, Nº247.

Unnamed locality from Musgueira "200m SE from Torre da Musgueira, Airport" (Antunes and Ginsburg, 1983): right m3, Nº211.

Unnamed locality from Musgueira "120m SE from the Musgueira's house" (Antunes and Ginsburg, 1983): left scaphoid, Nº222.

Olival da Suzana (Antunes and Ginsburg, 1983), also known as Olival da Susana (Legoinha, 2001): left P2,Nº177; Nº175; Nº176;right M1, Nº 185; right M2, Nº193; right p4, Nº204; fragmentary right hemimandible with m3, Nº217; right m3, Nº213; left m3, Nº212; left Mc III, Nº230; left incomplete Mc IV, Nº236; right astragalus, Nº246; right astragalus, Nº244; right Mt II, Nº258; distal half of a Mt III, Nº 260.

Quinta da Farinheira and Quinta das Flamengas have been subsequently grouped together as Chelas 1 (or only Chelas; **CHE**). They all pertain to the MN5 Mein's Biozone (Mein, 2002).

Quinta da Farinheira (Antunes and Ginsburg, 1983): left maxilla with P4-M3 and a partial zygomatic arch, Nº166; right maxilla with M1-3 from the same individual, Nº165; fragmentary right DP4, Nº219; incomplete left P2, Nº174; right P3, Nº179; left P4, Nº181; right M1, Nº189; left M1, Nº186; incomplete left M1, Nº184;left M2, Nº187; incomplete left M3, Nº198; right hemimandible with p2-4 and m3, Nº172; left hemimandible with p2-4 and m2 from the same individidual, Nº171; left hemimandible with p4-m1 and m3, Nº168; left fragmentary hemimandible with m3 and ascending ramus, Nº167;right p4, Nº205; Nº202; left p4, Nº201; left m1, Nº207;right m3, Nº214; left m3, Nº216; right dp4, Nº220; right unciform, Nº228; left Mc IV, Nº235;left calcaneum, Nº252; incomplete left calcaneum, Nº250; right astragalus, Nº249; left cuboid, Nº255; Nº253.

Quinta das Flamengas (Antunes and Ginsburg, 1983): left pyramidal Nº227; incomplete left Mc III, Nº231.

Quintanelas (QUI). All the bones pertain to a single individual according to Antunes and Ginsburg (1983) and are stored in the Museo Geologico (Lisbon). These are: right P3-M3 series, Nº263; left P3-M3 series, Nº266; right P1, Nº265; incomplete left P1, Nº288; incomplete right P2, Nº287; left P2, Nº264; right i2, Nº270; left i2, Nº269; right hemimandible with p4-m3, Nº268; left hemimandible with a broken p2, p3-m3, Nº267; left scapula, Nº285; proximal epiphysis of a left radius, Nº271; fragmentary right scaphoid, Nº272; right lunate, Nº273; left lunate, Nº274; fragmentary left pyramidal, Nº276; right pyramidal, Nº275; right trapezoid, Nº277; pelvic fragment, Nº286; first central phalanx, Nº278; Nº283; Nº282; Nº280; first lateral phalanx, Nº281; second lateral phalanx, Nº279, sesamoid, Nº284.

Madrid Area

Barajas-17 (BAR-17): remains from the locality of Barajas-17 have been checked and assigned to *Hispanotherium matritense*. However, these remains are still under curational work and have not been studied.

Casa de Campo/ Marqués de Monistrol M-30 (MMo): The fossil complex of Casa de Campo/Marqués de Monistrol M-30 includes four fossiliferous spots: Ramal 4.1, Ramal 4.2 (both with the field number of R4), Colector (CMD), and Túnel A-5 (fossil label preceded by 05/60/225a). A total of 184 fossils pertaining to a minimum number of 5 individuals have been studied. Left astragalus, R4-76; left calcanei, 05/60/225a-12; 05/60/225a-15; left cuboid, 05/60/225a-283; CMD-615; right cuboids, 05/60/225a-87; CMD-634; R4-407; left ectocuneiform, CMD-394; right scaphoid, 05/60/225a-168; second phalanx II/IV, 05/60/225a-265; glenoid articular fragment of a right hemimandible, R4-190; distal epiphysis of a Mc/Mt II, R4-217; tibial fragment, 05/60/225a-234a; 05/60/225a-16; right hemimandible, 05/60/225a-3; 05/60/225a-139; 05/60/225a-234b; condylar articulation of a right hemimandible, mandible, hemimandible, 05/60/225a-474; left maxilla with P4-M1, 05/60/225a-32; fragmentary lower px/mx, 05/60/225a-207; unworn M3, 05/60/225a-425; right magnums, 05/60/225a-124; CMD-37/38; dorsal part of a right magnum, R4-420; right Mc II, 05/60/225a-100; CMD-419; CMD-637; left Mc II's. 05/60/225a-340; 05/60/225a-502; proximal fragment of a left Mc II, 05/60/225a-294; right Mc III., 05/60/225a-386; distal fragment of a right Mc III, 05/60/225a-185; 05/60/225a-65; distal fragment of a left Mc III, 05/60/225a-211; 05/60/225a-387; proximal fragment of a right Mc III, 05/60/225a-252; 05/60/225a-294; left Mc IV's., 05/60/225a-5; CMD-264; Mc IV dchos., CMD-340; CMD-398; distal fragment of a left Mc IV., 05/60/225a-366; distal fragment of an undetermined Mc/Mt III, 05/60/225a-511; distal fragment of an undetermined lateral metapodial, 05/60/225a-391; fragment of a central metapodial, R4-179; fragment of a lateral metapodial, R4-336; 05/60/225a-160; right Mt III's., 05/60/225a-223; 05/60/225a-382; left Mt III's., CMD-630(2); R4-223; proximal fragment of a right Mt III, 05/60/225a-250; proximal fragment of a left Mt III, 05/60/225a-95; lower px/mx, 05/60/225a-8; navicular, 05/60/225a-249; 05/60/225a-251; 05/60/225a-365; 05/60/225a-399; CMD-19; petrosal, R4-125B; pyramidal, 05/60/225a-166; 05/60/225a-210; 05/60/225a-468; CMD-92; proximal fragment of a right radius, 05/60/225a-21; proximal fragment of a left radius, 05/60/225a-68; patella, 05/60/225a-28; 05/60/225a-464; right semilunates, 05/60/225a-398; left semilunates, 05/60/225a-476; CMD-559; R4-220a, sesamoids, CMD-664; CMD-413; CMD-411; tibia, 05/60/225a-30; left trapezoid, 05/60/225a-152; right trapezoid, R4-173; left unciforms, 05/60/225a-43; CMD-648a; R4-191; R4-204; R4-397; right unciforms, R4-94; left scapula, R4-213; distal fragment of left femora, 05/60/225a-212; CMD-350; proximal fragment of a femur,05/60/225a-393; proximal fragment of a left femur, w/n; right humerus, R4-236; left humerus, CMD-532; fragmentary humerus, CMD-205; distal fragment of a right humerus, CMD-22; distal fragment of left humeri, 05/60/225a-445; R4-203; right McIII, 05/60/225a-446; right radii, 05/60/225a-315; 05/60/225a-34; 05/60/225a-493; CMD-533; CMD-635; left radii, 05/60/225a-446; R4-29; distal fragment of left radii, 05/60/225a-469; R4-207; proximal epiphyses of right radii, 05/60/225a-227; 05/60/225a-283; R4-263; proximal epiphyses of left radii, 05/60/225a-127; 05/60/225a-326; 05/60/225a-492; 05/60/225a-68; R4-264; left tibia, 05/60/225a-450; fragmentary left tibia, 05/60/225a-487; distal epiphysis of a left tibia, 05/60/225a-486; proximal epiphysis of a right tibia, 05/60/225a-384; right ulnae, CMD-578; R4-324; right fragmentary ulna, 05/60/225a-452; left right fragmentary ulna, 05/60/225a-215

Cerro de San Isidro (SI). The presence of *H. matritense* in Cerro de San Isidro is doubtful. The presence of rhinoceros fossils in the locality has been previously discarded (Cerdeño and Iñigo, 1997). However, a fragmentary M2, MNCN 31135, stored in the Museo Nacional de Ciencias Naturales of Madrid without collection or field number (erroneously labeled as "CanshaTD, Carboniferous") probably pertains to this classical locality.

Embajadores-R (EMB): A total of 14 fossil remains pertaining to a minimum of one individual have been studied: Mx o Px, 05/73-PG1-2; upper premolar, 05/73-PG4-01; fragments of mx/px, 05/73-PG1-71; upper molar, 05/73-PG4-285; fragment of an upper molar, 05/73-PG2-50; lower molar, 05/73-PG1-39; right trapezium, 05/73-PG1-193; left astragalus, 05/73-PG1-015; 05/73-PG1-4; patella?, 05/73-PG4-173; left Mt II, 05/73-PG4-030; distal epiphysis of a Mc/Mt III, 05/73-PG1-010; Mt III fragment, 05/73-PG1-57; central sesamoid, 05/73-PG2-3.

Estación Imperial (EI) is one of the classic localities within Madrid city. M2, MNCN 61711; Tooth fragments, MNCN 61531; MNCN 61532; MNCN 61533; MNCN 61534; proximal epiphysis of a radius, MNCN 61693; MNCN 61707; fragmentary left lunate, MNCN 61710; incomplete unciform, MNCN 61713; proximal epiphysis of a left Mc II, MNCN 61721; proximal epiphysis of a left Mc III, MNCN 61708; distal epiphysis of a central metapodial, MNCN 61709; cotyloid cavity of a pelvis, MNCN 61706; distal epiphysis of a femur, fragmentary calcaneum, MNCN 61694; MNCN 61712.

Fábrica Mahou (FMH). This is one of the last fossil sites discovered with presence of *H. matritense* and part of the same cluster of localities within the metropolitan boundary of the Manzanares River, Madrid City. It yields the better preserved fossil remains of *H. matritense*, a large fraction of which are currently under preparation process. The preliminary list is as follows: right i2, FMH'14-2859; FMH'14-3158; FMH'14-3428; FMH'14-3688 (male); FMH'14-3690 (male); FMH'14-5185; FMH'14-5208; FMH'14-5335; FMH'14-785; left i2, FMH'14-2882 (male); FMH'14-3079; FMH'14-3714; FMH'14-5324; FMH'14-786; left DP1, FMH'14-4969; right P1, FMH'14-3835; left P1's, FMH'14-5215; FMH'14-5397; 4836; right P2, FMH'14-5425; right P3's, FMH'14-3441; FMH'14-5250; left P4's, FMH'14-4840; FMH'14-4857; right M1, FMH'14-3732; FMH'14-4898; left M1-2, FMH'14-5211; undetermined fragmentary upper teeth, FMH'14-1044; FMH'14-1015; FMH'14-1108; FMH'14-1173; FMH'14-1176; undetermined lower premolars, FMH'14-2401; FMH'14-3943; right p3's, FMH'14-4025; FMH'14-5212; FMH'14-5373; FMH'14-5416; FMH'14-5468; left p3, FMH'14-5323; righ m1-2, FMH'14-4003; left m1-2, FMH'14-3954; FMH'14-4898; FMH'14-5341b; undetermined fragmentary lower teeth, FMH'14-1084; FMH'14-4841; right radius, FMH'14-4876; right semilunate, FMH'14-3997; left semilunates, FMH'14-

3454; FMH'14-3473; right trapezoid, FMH'14-5230; left trapezoid, FMH'14-3838; FMH'14-4077; right unciform, FMH'14-5197; FMH'14-3199; right trapezium, FMH'14-5485; righ magnums, FMH'14-2475; FMH'14-5419; left magnum, FMH'14-5100; right pyramidal, FMH'14-4042; right pisiform, FMH'14-5347; left pisiform, FMH'14-3953; right Mc II's, FMH'14-1975; FMH'14-3097; FMH'14-3830; FMH'14-4941; FMH'14-5269; FMH'14-5279; FMH'14-4431; proximal fragments of right Mc II's, FMH'14-2621; FMH'14-4073; left Mc II's, FMH'14-2698; FMH'14-3098; FMH'14-5288; FMH'14-754; proximal fragments of a left Mc II, FMH'14-4128; right Mc III, FMH'14-1690; FMH'14-2306; FMH'14-2914; FMH'14-2937; FMH'14-2961; FMH'14-3410; fragmentary right Mc III, FMH'14-4060; FMH'14-5441; left Mc III, FMH'14-2534; FMH'14-2910; FMH'14-3383; FMH'14-3806; FMH'14-5297; FMH'14-5311; fragmentary left Mc III, FMH'14-2094; FMH'14-2095; FMH'14-3134; FMH'14-4144; FMH'14-527; FMH'14-3673; left astragali, FMH'14-3853; FMH'14-3980; FMH'14-4068; FMH'14-4914; right astragalus, FMH'14-3981; left calcaneum, FMH'14-4833; right calcaneum, FMH'14-4928; fragmentary right calcaneum, FMH'14-3611; right cuboids, FMH'14-3490; FMH'14-3538; FMH'14-4881; right mesocuneiforms, FMH'14-5140; FMH'14-5257. right Mt II's, FMH'14-3523; FMH'14-419; fragmentary right Mt II, FMH'14-2953; fragmentary left Mt II, FMH'14-2861; right Mt III's, FMH'14-3527; FMH'14-3753; FMH'14-5394; fragmentary right Mt III's, FMH'14-1689; FMH'14-2115; FMH'14-3563; FMH'14-5123; left Mt III's, FMH'14-2977; FMH'14-3117; FMH'14-5266; FMH'14-5432; fragmentary left Mt III's, FMH'14-2585; FMH'14-3779; FMH'14-4449; right Mt IV's, FMH'14-2313; FMH'14-5272; fragmentary right Mt IV's, FMH'14-3041; left Mt IV's, FMH'14-2212; FMH'14-2696; FMH'14-3106; FMH'14-5223; fragmentary left Mt IV's, FMH'14-2915; FMH'14-2941; right naviculars, FMH'14-2301; FMH'14-3819; FMH'14-4932; left naviculars, FMH'14-3883; FMH'14-4041;

Fresno del Torote (FT): This new locality is in need of study to determine its particular stratigraphic context. A single left lunate, FRT-1, has been recovered.

La Peineta (VE): some remains from *H. matritense* were found during the field campaing of 2013, including dental and postcranial remains without field number. These are: right P2, w/n; right piramidals, w/n; w/n; right trapezoid, w/n; second phalanx II/IV, w/n; left incomplete astragalus, w/n; left incomplete calcaneum, w/n.

Los Nogales (LNO): discovered in 2003 and firstly cited in Herráez et al. (2006), Los Nogales is another fossil site located in the urban area of Madrid City. The remains of *H. matritense* are currently under curational work and have not been included in the present work.

PAR-Peñuelas (PP): The remains from Par-Peñuelas were published in Cerdeño (1997): left hemimandible with p3-m3, PP-340; right hemimandible with p3-m3, PP-384; a male i2, PP-104; fragmentary P3, PP-351; fragmentary P4, PP-170; unciform, PP-275; magnum, PP-266; pyramidal, PP-348; Mc II, PP-333; astragali, PP-2; PP-151; naviculars, PP-37; PP-175; PP-347; ectocuneiform, PP-65; Mt II, PP-376; second lateral phalanx, PP-190.

Paseo de la Esperanza (ES): w/n molar teeth, MNCN 37520; MNCN 37521; w/n calcaneum, MNCN 37525.

Paseo de las Acacias (AC): published in Cerdeño (1997) has provided the following remains: nasal fragment, Ac-17 / MNCN 37632; mandibular symphisis, Ac-3 / MNCN 37634; p2, Ac-12 / MNCN 37637; Ac-14 / MNCN 37638; undetermined lower molar teeth, Ac-11 / MNCN 37640; Ac-13 / MNCN 37639; unciform, Ac-8 / MNCN 37644; pyramidal, Ac-7 / MNCN 37647; Mc II, Ac-5 / MNCN 37631; Mc III, Ac-1 / MNCN 37635; Mc IV, Ac-4 / MNCN 37633; astragalus, Ac-10 / MNCN 37636; cuboid, Ac-2 / MNCN 37646; ectocuneiform, Ac-6 / MNCN 37645; proximal fragment of a Mt III, Ac-9 / MNCN 37643.

Príncipe Pío-2 (PPio-2): A total of 742 fossil remains have been studied. These represent only the fraction determined *in situ* during the field campaigns, so additional *H. matritense* remains are expected to increase the present list during future preparation works. They pertain to a minimum number of 20 individuals. Left scapulae, 05/101/2/738a and 05/101/2/738ab; escápula, 05/101/2/2630a and b; 05/101/2/730a y b; 05/101/2/737; 05/101/2/738a-b; acetabular area of a scapula, 05/101/2/2630a-e; 05/101/2/2746; 05/101/2/2940a-g; 05/101/2/3448; 05/101/2/3448; 05/101/2/4B-132; 05/101/2/733; 05/101/2/735; 05/101/2/744a-d; 05/101/2/748; 05/101/2/748; 05/101/2/751; 05/101/2/752; right humeri, 05/101/2/301; 05/101/2/610; 05/101/2/779; left humeri, 05/101/2/324a-c; 05/101/2/613; 05/101/2/643; 05/101/2/798; diaphysis fragment of an humerus, 05/101/2/831a-e; 05/101/2/369; diaphysis fragments of right humeri, 05/101/2/387a; 05/101/2/387b; 05/101/2/832;05/101/2/362a-c; 05/101/2/773; fragmented diaphyses of left humeri, 05/101/2/322a-e; 05/101/2/347; 05/101/2/807; 05/101/2/285a; 05/101/2/285b; distal epiphyses of left humeri; 05/101/2/288; 05/101/2/309; 05/101/2/374; 05/101/2/608; distal fragment of an left humerus,05/101/2/289a-c; 05/101/2/3155a-e; 05/101/2/352; 05/101/2/355; 05/101/2/624; humeral distal epiphysis, 05/101/2/624; right radii, 05/101/2/283; 05/101/2/300; 05/101/2/323; 05/101/2/778; 05/101/2/800a-c; 05/101/2/816 a y b; left radii, 05/101/2/633; 05/101/2/792; 05/101/2/794a and b; 05/101/2/802; 05/101/2/912; right fragmented radius, 05/101/2/364a-c; distal epiphysis of right radius, 05/101/2/292; 05/101/2/312; 05/101/2/398a-c; 05/101/2/606; 05/101/2/809; distal epiphysis of left radius, 05/101/2/373a-e; 05/101/2/801; 05/101/2/830; 05/101/2/589; proximal epiphysis of left radii, 05/101/2/310; 05/101/2/600a and b; 05/101/2/609; proximal epiphysis of right radii, 05/101/2/286; 05/101/2/628; 05/101/2/771; 05/101/2/792; 05/101/2/804; ulnae, 05/101/2/1139; 05/101/2/291a and b; 05/101/2/3610; 05/101/2/368; 05/101/2/618; right ulnae, 05/101/2/290; 05/101/2/337; 05/101/2/395; 05/101/2/613; 05/101/2/642; 05/101/2/810; left ulnae, 05/101/2/299a and b; 05/101/2/326a and b; 05/101/2/396; 05/101/2/597; 05/101/2/769; right scaphoids, 05/101/2/100; 05/101/2/101; 05/101/2/1176; 05/101/2/1587; 05/101/2/88; 05/101/2/90; 05/101/2/91; 05/101/2/92; 05/101/2/93; 05/101/2/95; 05/101/2/96; 05/101/2/97; 05/101/2/98; left scaphoids, 05/101/2/1186; 05/101/2/2792; 05/101/2/3471; 05/101/2/840; 05/101/2/863; 05/101/2/89; 05/101/2/94; 05/101/2/941; 05/101/2/99; right pyramidals, 05/101/2/1; 05/101/2/11; 05/101/2/1177; 05/101/2/2; 05/101/2/3; 05/101/2/4; 05/101/2/842; 05/101/2/904; right lunates, 05/101/2/103; 05/101/2/104; 05/101/2/105; 05/101/2/106; 05/101/2/107; 05/101/2/1175; 05/101/2/1183; 05/101/2/847; left lunates, 05/101/2/102; 05/101/2/108; 05/101/2/1189; 05/101/2/190; 05/101/2/191; 05/101/2/2635; 05/101/2/2751; 05/101/2/2938; 05/101/2/846; 05/101/2/848; 05/101/2/864; 05/101/2/902; left pyramidals, 05/101/2/10; 05/101/2/11;

05/101/2/1188; 05/101/2/12; 05/101/2/13; 05/101/2/14; 05/101/2/15; 05/101/2/17; 05/101/2/2634; 05/101/2/3173; 05/101/2/5; 05/101/2/6; 05/101/2/7; 05/101/2/8; 05/101/2/843; 05/101/2/862; 05/101/2/9; possible left pyramidal, 05/101/2/16; right pisiforms, 05/101/2/1179; 05/101/2/1394; 05/101/2/1588; 05/101/2/219; 05/101/2/220; 05/101/2/222; 05/101/2/223a; 05/101/2/225; left pisiforms, 05/101/2/1187; 05/101/2/213; 05/101/2/215; 05/101/2/216; 05/101/2/217; 05/101/2/221; 05/101/2/226; 05/101/2/2376; 05/101/2/4; right trapezoids, 05/101/2/3200; 05/101/2/41; 05/101/2/42; 05/101/2/45; 05/101/2/109; 05/101/2/114; 05/101/2/115; 05/101/2/117; 05/101/2/1180; 05/101/2/3645; 05/101/2/841; 05/101/2/905; left trapezoids, 05/101/2/1193; 05/101/2/43; 05/101/2/44; 05/101/2/46; 05/101/2/47; 05/101/2/110; 05/101/2/111; 05/101/2/112; 05/101/2/113; 05/101/2/116; 05/101/2/1190; 05/101/2/839; right magnums, 05/101/12/212; 05/101/2/1178; 05/101/2/189; 05/101/2/192; 05/101/2/193; 05/101/2/196; 05/101/2/199; 05/101/2/203; 05/101/2/204; 05/101/2/207; 05/101/2/208; 05/101/2/210; left magnums, 05/101/12/198; 05/101/12/201; 05/101/2/1191; 05/101/2/194; 05/101/2/195; 05/101/2/197; 05/101/2/200; 05/101/2/202; 05/101/2/205; 05/101/2/206; 05/101/2/209; 05/101/2/211; 05/101/2/218; 05/101/2/3141; 05/101/2/3270; 05/101/2/845; right unciforms, 05/101/2/119; 05/101/2/120; 05/101/2/123; 05/101/2/124; 05/101/2/127; 05/101/2/130; 05/101/2/131; 05/101/2/134; 05/101/2/138; 05/101/2/140; 05/101/2/2841; 05/101/2/384; 05/101/2/39; fragmented right unciform, 05/101/2/897; left unciforms, 05/101/2/118; 05/101/2/1192; 05/101/2/122; 05/101/2/125; 05/101/2/126; 05/101/2/128; 05/101/2/129; 05/101/2/132; 05/101/2/133; 05/101/2/136; 05/101/2/2273; 05/101/2/37; 05/101/2/895; right Mc II's, 05/101/2/2441; 05/101/2/399; 05/101/2/411; 05/101/2/413; 05/101/2/452; 05/101/2/458; 05/101/2/497; 05/101/2/498; 05/101/2/499; 05/101/2/516; 05/101/2/527; left Mc II's, 05/101/2/1210a; 05/101/2/1151; 05/101/2/1165; 05/101/2/1194; 05/101/2/2939; 05/101/2/401; 05/101/2/426; 05/101/2/430; 05/101/2/444; 05/101/2/518; 05/101/2/536; right Mc III's, 05/101/2/1155; 05/101/2/417; 05/101/2/450; 05/101/2/479; 05/101/2/480; 05/101/2/872; left Mc III's, 05/101/2/1210b; 05/101/2/1161; 05/101/2/1163; 05/101/2/403; 05/101/2/405; 05/101/2/428; 05/101/2/455; 05/101/2/482; 05/101/2/513; 05/101/2/514; right Mc IV's, 05/101/2/1159; 05/101/2/1169; 05/101/2/412; 05/101/2/423; 05/101/2/425; 05/101/2/448; 05/101/2/459; 05/101/2/519; left Mc IV's, 05/101/2/1210c; 05/101/2/1152; 05/101/2/1195a-b; 05/101/2/400; 05/101/2/419; 05/101/2/442; 05/101/2/457; 05/101/2/483a-b; 05/101/2/489; 05/101/2/53; possible Mc IV, 05/101/2/1036; right femora, 05/101/2/3075; 05/101/2/781; 05/101/2/819a-c; left femur, 05/101/2/282a-b; femoral diaphysis, 05/101/2/339; distal fragments of a femur, 05/101/2/2186; 05/101/2/2405; 05/101/2/287; 05/101/2/325; 05/101/2/343; 05/101/2/349; 05/101/2/353a-c; 05/101/2/386; 05/101/2/641; 05/101/2/784; 05/101/2/818; right distal fragments of right femora, 05/101/2/295; 05/101/2/826; left distal fragment of left femora, 05/101/2/280; 05/101/2/293; 05/101/2/3227a-c; 05/101/2/345a-c; 05/101/2/3870; 05/101/2/607; 05/101/2/617; 05/101/2/806a y b; proximal femoral fragments, 05/101/2/2586; 05/101/2/348; 05/101/2/350; 05/101/2/356; 05/101/2/358; 05/101/2/785; right proximal femoral fragments, 05/101/2/320a-c; 05/101/2/357; 05/101/2/789a; left proximal femoral fragment, 05/101/2/789b; right patellas, 05/101/2/1237; 05/101/2/1242; left patellas, 05/101/2/1238; 05/101/2/1239; patellas, 05/101/2/; 05/101/2/; 05/101/2/; 05/101/2/; 05/101/2/; 05/101/2/; 05/101/2/; tibia, 05/101/2/540; right tibiae,05/101/2/313a-b; 05/101/2/393; 05/101/2/685; 05/101/2/790; 05/101/2/805; right fragmentary tibia, 05/101/2/341; 05/101/2/372; 05/101/2/397a-b; 05/101/2/397a; right distal fragments of a tibia, 05/101/2/383a-c; 05/101/2/394a-c; 05/101/2/599; right proximal tibial fragment, 05/101/2/622; left proximal tibial fragment, 05/101/2/640; left tibiae, 05/101/2/3016; 05/101/2/336; 05/101/2/3868; 05/101/2/829; left distal epiphyses of a tibia, 05/101/2/625; 05/101/2/811; left proximal epiphysis of a tibia, 05/101/2/803; fragmentary tibiae, 05/101/2/366a-c; 05/101/2/782; left fragmentary tibiae, 05/101/2/335a-d; 05/101/2/601; distal tibial fragments, 05/101/2/3536; 05/101/2/821a-c; left distal fragments of a tibia, 05/101/2/3100a-b; 05/101/2/329a-c; 05/101/2/781a-c; 05/101/2/811; 05/101/2/824a-c; proximal tibial fragment, 05/101/2/939; right fragmentary fibulae, 05/101/2/341; 05/101/2/372; right proximal fibular fragment, 05/101/2/822; left fibula, 05/101/2/3869; left fragmentary fibulae,05/101/2/822; right astragali, 05/101/2/143; 05/101/2/144; 05/101/2/146; 05/101/2/148; 05/101/2/151; 05/101/2/152; 05/101/2/155; 05/101/2/156; 05/101/2/160; 05/101/2/162; 05/101/2/164; 05/101/2/166; 05/101/2/167; 05/101/2/3634; 05/101/2/887; left astragali, 05/101/2/1219; 05/101/2/142; 05/101/2/145; 05/101/2/147; 05/101/2/149; 05/101/2/150; 05/101/2/153; 05/101/2/154; 05/101/2/157; 05/101/2/158; 05/101/2/159; 05/101/2/163; 05/101/2/165; 05/101/2/169; 05/101/2/170; 05/101/2/329a-c; 05/101/2/346; 05/101/2/3647; 05/101/2/884;05/101/2/885; right calcanei,05/101/2/168; 05/101/2/176; 05/101/2/181; 05/101/2/183; 05/101/2/3228a; 05/101/2/834; left calcanei,05/101/2/171; 05/101/2/172; 05/101/2/173; 05/101/2/174; 05/101/2/175; 05/101/2/177; 05/101/2/178; 05/101/2/180; 05/101/2/182a y b; 05/101/2/184; 05/101/2/185; 05/101/2/693; fragment of a calcaneum, 05/101/2/3000; right naviculars, 05/101/2/20; 05/101/2/21; 05/101/2/22; 05/101/2/2218; 05/101/2/27; 05/101/2/29; 05/101/2/30; 05/101/2/31; 05/101/2/34; 05/101/2/35; 05/101/2/36; 05/101/2/873; left naviculars, 05/101/2/18; 05/101/2/19; 05/101/2/23; 05/101/2/24; 05/101/2/26; 05/101/2/28; 05/101/2/37; 05/101/2/39; 05/101/2/880; navicular fragment, 05/101/2/38; right right cuboids, 05/101/2/121; 05/101/2/2090; 05/101/2/2444; 05/101/2/64; 05/101/2/66; 05/101/2/67; 05/101/2/68; 05/101/2/71; 05/101/2/72; 05/101/2/76; 05/101/2/77; 05/101/2/78; 05/101/2/896; 05/101/2/903; left cuboids, 05/101/2/1059; 05/101/2/224; 05/101/2/62; 05/101/2/63; 05/101/2/65; 05/101/2/69; 05/101/2/70; 05/101/2/73; 05/101/2/74; 05/101/2/75; 05/101/2/865; cuboid fragment, 05/101/2/2323; ectocuneiform fragment, 05/101/2/2254; right ectocuneiforms, 05/101/2/2419; 05/101/2/2844; 05/101/2/32; 05/101/2/48; 05/101/2/49; 05/101/2/50; 05/101/2/52; 05/101/2/53; 05/101/2/54; 05/101/2/55; 05/101/2/57; 05/101/2/898; 05/101/2/899; left ectocuneiforms, 05/101/2/1215; 05/101/2/1713; 05/101/2/3098; 05/101/2/33; 05/101/2/40; 05/101/2/51; 05/101/2/56; right mesocuneiform, 05/101/2/2840; right entocuneiforms, 05/101/2/2089; 05/101/2/245a; 05/101/2/3236; 05/101/2/58; 05/101/2/60; 05/101/2/874; left entocuneiforms, 05/101/2/2786; 05/101/2/59; 05/101/2/61; Mt II's, 05/101/2/432; 05/101/2/3235 a-b; 05/101/2/408; 05/101/2/421; 05/101/2/447; 05/101/2/520; right proximal fragments of a Mt II, 05/101/2/415; 05/101/2/875; left Mt II's, 05/101/2/465; 05/101/2/1153; 05/101/2/420 a y b; 05/101/2/424; 05/101/2/443; 05/101/2/487 a y b; 05/101/2/491; 05/101/2/493; left proximal fragments of a Mt II, 05/101/2/2336?; 05/101/2/476; Mt III fragments, 05/101/2/1168; 05/101/2/1223 a-b; 05/101/2/445 a-b; 05/101/2/492; right Mt III's, 05/101/2/433; 05/101/2/1156; 05/101/2/11600; 05/101/2/2663; 05/101/2/2742; 05/101/2/2758; 05/101/2/404; 05/101/2/406; 05/101/2/416; 05/101/2/454;

05/101/2/456; 05/101/2/490; 05/101/2/526; left Mt III's, 05/101/2/467; 05/101/2/473; 05/101/2/1154; 05/101/2/1167; 05/101/2/1224; 05/101/2/1521; 05/101/2/431; 05/101/2/446; 05/101/2/449; 05/101/2/478; 05/101/2/494; 05/101/2/506; 05/101/2/508; 05/101/2/515; 05/101/2/522; s/s; proximal fragment of a Mt III, 05/101/2/488; right proximal fragment of a Mt III, 05/101/2/2808; 05/101/2/460; right Mt IV's, 05/101/2/434; 05/101/2/414; 05/101/2/427; 05/101/2/481; 05/101/2/495; 05/101/2/524; left Mt IV's, 05/101/2/470; 05/101/2/461; 05/101/2/473bis; 05/101/2/2599; 05/101/2/523; right proximal fragment of a Mt IV, 05/101/2/2596; distal fragment of undetermined metapodials, 05/101/2/474; 05/101/2/475; first central phalanxes, 05/101/2/1102; 05/101/2/1262; 05/101/2/1272; 05/101/2/1279; 05/101/2/1286; 05/101/2/1287; 05/101/2/1296; 05/101/2/1297; 05/101/2/1303; 05/101/2/1304; 05/101/2/2773; 05/101/2/3644; 05/101/2/636 first lateral phalanxes, 05/101/2/;05/101/2/;05/101/2/;05/101/2/;05/101/2/;05/101/2/;05/101/2/;05/101/2/1256; 05/101/2/1259; 05/101/2/1261; 05/101/2/1263; 05/101/2/1266; 05/101/2/1267; 05/101/2/1270; 05/101/2/1271; 05/101/2/1274; 05/101/2/1277; 05/101/2/1288; 05/101/2/1290; 05/101/2/1291; 05/101/2/1295; 05/101/2/1300; 05/101/2/1310; 05/101/2/1387; 05/101/2/1388; 05/101/2/2049; 05/101/2/2968; 05/101/2/637; second central phalanxes., 05/101/2/1258; 05/101/2/1282; 05/101/2/1285; second lateral phalanxes,05/101/2/1106; 05/101/2/1165;05/101/2/466; forelimb's second lateral phalanxes, 05/101/2/1211; hindlimb's second lateral phalanxes, 05/101/2/435; 05/101/2/436; third central phalanxes, 05/101/2/1317; 05/101/2/1318; 05/101/2/1314; 05/101/2/1315; 05/101/2/1316; 05/101/2/1319; 05/101/2/1320; 05/101/2/1321; 05/101/2/1322; 05/101/2/1324; 05/101/2/699; 05/101/2/879; sesamoids, 05/101/2/1102; 05/101/2/468; 05/101/2/469; 05/101/2/471; 05/101/2/472; forelimb sesamoids, 05/101/2/1212; 05/101/2/1213; hindlimb sesamoids, 05/101/2/432; 05/101/2/438; fragments of undetermined metapodials, 05/101/2/409; 05/101/2/1157; 05/101/2/1158; 05/101/2/189; 05/101/2/2174; 05/101/2/2282; 05/101/2/2340; 05/101/2/2455; 05/101/2/2457; 05/101/2/2561; 05/101/2/2594; 05/101/2/2601; 05/101/2/463; 05/101/2/464; 05/101/2/501; 05/101/2/502; 05/101/2/502; 05/101/2/504; 05/101/2/510; 05/101/2/528 a y b; 05/101/2/537; 05/101/2/741; 05/101/2/809; 05/101/2/930; 05/101/2/932; 05/101/2/422; 05/101/2/2379; 05/101/2/2735; 05/101/2/2749; 05/101/2/496; 05/101/2/440a-b; 05/101/2/1164; 05/101/2/2288; 05/101/2/3040; 05/101/2/410; 05/101/2/429; 05/101/2/505; 05/101/2/525; 05/101/2/929; 05/101/2/2699 a-b; 05/101/2/407; 05/101/2/50; 05/101/2/517.

Puente de Toledo (PT): this is the type locality of the species *H. matritense*. The type collection is hosted in the Escuela de Minas Museum. It comprises the following specimens: right M3 (w/n; considered as the lectotype of *H. matritense*), right m1 (w/n), i2 (w/n) and a left DP4 (w/n; probably lost according to Crusafont and Villalta, 1947). Additional material hosted in this institution was posteriorly described by Crusafont and Villalta (1947). It includes: right M2 (w/n); right M3 (w/n); fragmentary left hemimandible with an incomplete m1 and m2-3 (w/n); left p4 (w/n); left m1 (w/n); right m2 (w/n); left m2 (w/n) and an incomplete right m3 (w/n). Unfortunately, the previously mentioned remains from Puente de Toledo arecurrently inaccessible. Other remains from this locality can be found in the InstitutoGeológico y MineroEspañol (IGME). These are: P4, 1501M;i1, 813M; male i2, 1161M, female i2, 2128M; 1762M; left dp3's, 1547M; 2168M; 1502M; 2041M; 1849M; p3's, 378M, 1552M; lower fragmentary tooth, 1503M; lower m1/2, 1160M. Additionally, a P1 (w/n), hosted in the Paleobiology Department of the Lisbon University (Antunes and Ginsburg, 1983) and a P2 (w/n), hosted in the Museo Nacional de Ciencias Naturales of Madrid have been also cited (Cerdeño, 1989).

Torrijos (TO), published in Aguirre et al. (1982) and reviewed by Cerdeño (1989): right DP1, w/n; right DP2, w/n; w/n; right DP3, w/n; right P1, w/n; left P1, w/n; right P2, w/n; left P2, w/n; w/n; left P3, w/n; left P4, w/n; right M3, w/n; left i2, w/n; left dp1, w/n; left dp2, w/n; right dp4, w/n; w/n; right p3, w/n; right Mc III, w/n; w/n; w/n; w/n; w/n; w/n; left Mc III, w/n; w/n; w/n; right Mt IV, w/n; proximal fragments of right Mt III, w/n; w/n; right calcanei, w/n; w/n; w/n; w/n; left calcanei, w/n; w/n; right astragali, w/n; left astragali, w/n; first central phalanxes, w/n; w/n; w/n; w/n; second central phalanxes, w/n; w/n; w/n; w/n; w/n; third central phalanx, w/n; first lateral phalanxes, w/n; w/n; w/n; w/n; second lateral phalanxes, w/n; w/n; pyramidal, w/n; w/n; w/n; w/n; w/n; ectocuneiforms, w/n; w/n; w/n; patella; w/n; cuboids, w/n; w/n; w/n; trapezoids, w/n; w/n; w/n; left lunate, w/n; left unciform, w/n; magnum, w/n; pyramidals, w/n; w/n; w/n; left scaphoid, w/n.

Yunquera de Henares (YU). This site, currently under study, was recently discovered during the cartography campaign of the MAGNA 200. It yielded a left Mt III, labeled as YU-2, and a metacarpo-phalangeal sesamoid III, labeled as YU-1.

Other sites from the Tagus Basin

Dehesa de los Caballos (**DCa**; Cáceres, Spain), originally described in Hernández-Pacheco and Crusafont (1960) and posteriorly reviewed in Olivares and Rebollada (1993) comprises the following *H. matritense* remains: fragmentary P4, IPS-31288; right M1, IPS-31289; left M1, IPS-31289; left fragmentary M2, IPS-31288; right M3, IPS-31287; left M3, IPS/31289; left pyramidal, IPS-31288; fragment of a radius diaphysis, IPS-31288. All of them are hosted in the Institut Català de Paleontologia (ICP).

Indre-et-Loire Basin (France)

Hommes (HOM), published in Ginsburg et al. (1987): left P3, Coll. Huin, nº3393.

REFERENCES

Aguirre, E., Alberdi, M. T., Martín-Escorza, C., Torres, T., Morales, J., C. Sesé, and Soria, D., 1982, Torrijos: nueva fauna con *Hispanotherium* de la cuenca media del Tajo: Acta Geológica Hispánica, v. 1-2, p. 39-61.

Alberdi, M. T., Cerdeño, E., and Herráez, E., 1983, Perissodactyla de la Provincia de Madrid, Geología y Paleontología del Terciario Continental de la Provincia de Madrid, Servicio de publicaciones del CSIC, p. 61-79.

Antunes, M. T., 2000, Miocene mammals from Lisbon and geologic age. A showcase for marine-continental correlations: Ciencias da Terra, v. 14, p. 343-348.

Antunes, M. T., and Ginsburg, L., 1983, Les Rhinocérotidés du Miocène de Lisbonne. Systématique, écologie, paléobiogéographie, valeur stratigraphique: Ciências da Terra (UNL), v. 7, p. 17-98.

Boné, E., Alberdi, M. T., Hoyos, M., and López, N., 1980, Prospection paléontologique de la région de Torralba de Ribota (Burdigalien du Bassin de Calatayud, Zaragoza, España): Paleovertebrata, v. Mem. juv. R. Lavocat, p. 233-247.

Cerdeño, E., 1989, Revisión de la sistemática de los rinocerontes del Neógeno de EspañaPh.D. Dissertation]: Universidad Complutense de Madrid, 429 p.

-, 1992, New Remains of the Rhinocerotid *Hispanotherium matritense* at La Retama Site: Tagus Basin, Cuenca, Spain: Geobios, v. 25, no. 5, p. 671-679.

Cerdeño, E., and Iñigo, C., 1997, *Hispanotherium matritense* (Rhinocerotidae) de la ciudad de Madrid (España) y su relación con el paleoambiente del Aragoniense medio (Mioceno Medio): Revista Española de Paleontología, v. 12, no. 1, p. 80-90.

Crusafont, M., and Villalta, J. F., 1947, Sobre un interesante rinoceronte (*Hispanotherium*) del Mioceno del Valle de Manzanares: Las Ciencias, v. 12, p. 869-883.

Ehleringer, J. R., and Monson, R. K., 1993, Evolutionary and ecological aspects of photosynthetic pathway variation: Annual Review of Ecology and Systematics, v. 24, p. 411-439.

Ginsburg, L., Maubert, F., and Antunes, M. T., 1987, Discovery of *Hispanotherium* and *Gaindatherium* (Rhinocerotidae, Mammalia) in the Miocene of France: Bulletin du Muséum national d'histoire naturelle. Section C, Sciences de la terre, paléontologie, géologie, minéralogie, v. 9, no. 3, p. 303-311.

Hernández-Pacheco, F., and Crusafont, M., 1960, Primera caracterización paleontológica del Terciario de Extremadura: Boletín de la Real Sociedad Española de Historia Natural (Geol.), v. 58, p. 275-282.

Herráez, E., Paredes, I. G., Peláez-Campomanes, P., and Morales, J., 2006, Los Nogales, nueva fauna de vertebrados del Mioceno medio de Madrid: Estudios Geológicos, v. 62, no. 1, p. 257-262.

Simionescu, I., 1940, Mamiferele Pliocene dela Cimislia (România) – IV. Rhinocerotidae: Academia Româna, Publicatiunile Fondului Vasile Adamachi, Monitorul Oficial si Imprimeriile Statului, Imprimeria Nationala, Bucuresti, v. IX, no. 3, p. 1-50.

SUPPLEMENTARY DATA 3

Tables with measurements (in mm) of *Hispanotherium matritense*. Samples firstly studied in the present work include Príncipe Pío-2 (PPio-2), Casa de Campo / Marqués de Monistrol M-30 (MMo), Fábrica Mahou (FMH), Ventas (VE), Yunquera de Tajo (YU), and Fresno de Torote (FRT). Abbreviations and bibliographic sources from the remaining localities are detailed in Material and Methods.

Table 3.1

Humerus		MMo	PPio-2	REM
L	max	339.0	338.0	~ 297
	mean	339.0	331.0	~ 297
	min	339.0	324.0	~ 297
	SD	—	7.00	—
	N	1	2	1
L prox	max	159.0	135.0	—
	mean	159.0	134.0	—
	min	159.0	133.0	—
	SD	—	1.00	—
	N	1	2	—
TD tuber	max	117.7	120.5	~ 86
	mean	108.6	116.3	~ 86
	min	99.5	113.0	~ 86
	SD	9.14	2.72	—
	N	2	4	1
TD prox epi	max	129.9	165.0	132.0
	mean	129.9	150.2	132.0
	min	129.9	142.7	132.0
	SD	—	10.49	—
	N	1	3	1
APD prox epi	max	—	64.3	116.0
	mean	—	58.8	116.0
	min	—	52.1	116.0
	SD	—	5.04	—
	N	—	3	1
TD dia	max	53.7	65.2	52.5
	mean	50.4	55.1	52.5
	min	47.1	47.2	52.5
	SD	3.30	5.24	—
	N	2	12	1
APD dia	max	49.4	51.8	57.0
	mean	46.4	46.7	57.0
	min	43.4	42.5	57.0
	SD	2.98	3.37	—
	N	2	9	1
TD dis epi	max	116.0	97.8	—
	mean	108.3	76.2	—
	min	102.3	62.5	—
	SD	5.71	10.67	—
	N	3	7	—
TD troc	max	74.5	83.2	—
	mean	72.8	72.4	—
	min	70.5	59.5	—
	SD	1.45	9.20	—
	N	4	10	—
R1	max	72.7	88.0	—
	mean	67.2	74.9	—
	min	60.9	65.3	—
	SD	4.87	7.11	—
	N	3	10	—

Table 3.1 (cont.)

Humerus		MMo	PPio-2	REM
Rmin	max	72.7	42.5	—
	mean	67.2	36.8	—
	min	60.9	30.6	—
	SD	4.87	4.27	—
	N	3	8	—
R2	max	39.3	83.2	—
	mean	34.5	64.8	—
	min	30.1	44.9	—
	SD	3.35	15.23	—
	N	4	7	—
APD dis epi	max	50.4	88.0	~ 96
	mean	48.2	75.3	~ 96
	min	46.7	65.0	~ 96
	SD	1.57	8.08	—
	N	3	9	1

Table 3.2

Scapula		MMo	FMH	PPio-2	*H. corcolense*
L	max	392.0	—	—	—
	mean	392.0	—	—	—
	min	392.0	—	—	—
	SD	—	—	—	—
	N	1	—	—	—
APD max	max	217.0	—	202.0	—
	mean	217.0	—	202.0	—
	min	217.0	—	202.0	—
	SD	—	—	—	—
	N	1	—	1	—
TD col	max	22.2	—	30.9	32.4
	mean	22.2	—	23.4	29.0
	min	22.2	—	15.4	25.5
	SD	—	—	5.44	—
	N	1	—	5	2
APD col	max	86.5	—	92.3	88.7
	mean	86.5	—	76.1	85.9
	min	86.5	—	59.8	83.1
	SD	—	—	10.45	—
	N	1	—	9	2
APD tuber	max	—	—	106.6	98.9
	mean	—	—	97.7	98.0
	min	—	—	86.6	97.1
	SD	—	—	7.14	—
	N	—	—	7	2
APD art	max	64.5	68.4	83.9	72.1
	mean	64.5	68.4	68.7	67.5
	min	64.5	68.4	57.0	62.9
	SD	—	—	7.58	—
	N	1	1	10	2
TD art	max	39.8	—	55.9	53.4
	mean	39.8	—	41.9	53.2
	min	39.8	—	33.8	53.0
	SD	—	—	6.70	—
	N	1	—	9	2

Table 3.3

Ulna		PPio-2	FMH	MMo
L	max	—	—	417.0
	mean	—	—	417.0
	min	—	—	417.0
	SD	—	—	—
	N	—	—	1
TD olec	max	31.0	—	28.0
	mean	26.2	—	28.0
	min	21.4	—	28.0
	SD	4.79	—	—
	N	2	—	1
APD olec	max	75.4	—	92.8
	mean	68.8	—	92.8
	min	62.1	—	92.8
	SD	6.67	—	—
	N	2	—	1
H olec	max	113.7	—	99.5
	mean	111.4	—	99.5
	min	109.0	—	99.5
	SD	2.38	—	—
	N	2	—	1
TD base olec	max	27.8	—	21.5
	mean	19.5	—	18.9
	min	16.1	—	16.3
	SD	3.18	—	1.84
	N	12	—	4
APD base olec	max	78.1	—	73.0
	mean	70.4	—	68.2
	min	60.3	—	61.9
	SD	4.76	—	4.62
	N	9	—	3
TD troc prox	max	34.8	26.4	33.1
	mean	32.1	26.4	32.5
	min	28.6	26.4	30.9
	SD	2.15	—	0.92
	N	6	1	4
TD troc dis	max	55.4	—	58.7
	mean	54.8	—	58.7
	min	54.3	—	58.6
	SD	0.46	—	0.03
	N	3	—	2
APD art med	max	71.5	—	57.8
	mean	61.0	—	57.1
	min	55.2	—	55.7
	SD	5.01	—	0.97
	N	8	—	3

SUPPLEMENTARY DATA 3 (CONT.)

Table 3.3 (cont.)

Ulna		PPio-2	FMH	MMo
APD art lat	max	65.2	—	59.7
	mean	60.1	—	58.7
	min	55.5	—	57.7
	SD	3.98	—	0.81
	N	3	—	3
TD dia.	max	33.2	22.4	29.9
	mean	28.3	22.4	25.5
	min	22.5	22.4	19.7
	SD	3.49	—	4.32
	N	12	1	3
APD dia	max	41.8	—	40.4
	mean	30.9	—	35.4
	min	13.8	—	31.8
	SD	8.55	—	3.64
	N	12	—	3
TD dis art	max	23.1	—	27.0
	mean	23.1	—	35.4
	min	23.1	—	23.0
	SD	—	—	3.65
	N	1	—	2
APD dis art	max	44.4	—	49.9
	mean	44.4	—	49.3
	min	44.4	—	48.7
	SD	—	—	0.62
	N	1	—	2
TD dis epi	max	38.6	39.3	28.4
	mean	29.9	37.1	26.0
	min	21.3	39.3	23.7
	SD	8.64	3.14	2.36
	N	2	2	2
APD dis epi	max	38.6	34.0	37.9
	mean	29.2	32.3	37.7
	min	19.8	34.0	37.5
	SD	9.40	2.38	0.18
	N	2	2	2

Table 34

Radius		PPio-2	FMH	REM	Dca	QUI	*H corcolense*	*B grimmi*	*B caucasica*	*C oettingenae*
L	max	342.0	—	303.2	—	—	298.1	330.0	330.0	—
	mean	330.0	—	303.2	—	—	298.1	317.5	325.0	—
	min	321.0	—	303.2	—	—	298.1	305.0	320.0	—
	SD	7.82	—	—	—	—	—	—	—	—
	N	5	—	1	—	—	1	2	2	—
I	max	312.0	—	—	—	—	—	—	—	—
	mean	307.0	—	—	—	—	—	—	—	—
	min	302.0	—	—	—	—	—	—	—	—
	SD	4.12	—	—	—	—	—	—	—	—
	N	4	—	—	—	—	—	—	—	—
TD prox epi	max	82.6	70.0	80.3	—	82.0	84.1	96.0	81.0	—
	mean	76.8	70.0	80.3	—	82.0	78.6	86.0	80.5	—
	min	70.7	70.0	80.3	—	82.0	69.7	79.0	80.0	—
	SD	3.39	—	—	—	—	4.78	—	—	—
	N	11	1	1	—	1	9	6	2	—
APD prox epi	max	60.7	46.1	55.5	—	47.0	59.3	63.0	—	—
	mean	50.8	46.1	55.5	—	47.0	56.5	59.4	—	—
	min	43.4	46.1	55.5	—	47.0	54.0	57.0	—	—
	SD	6.12	—	—	—	—	2.36	—	—	—
	N	8	1	1	—	1	5	5	—	—
TD prox art	max	82.4	67.3	—	—	—	—	—	—	—
	mean	75.5	67.3	—	—	—	—	—	—	—
	min	69.1	67.3	—	—	—	—	—	—	—
	SD	4.30	—	—	—	—	—	—	—	—
	N	10	1	—	—	—	—	—	—	—
APD prox art	max	46.3	43.1	—	—	—	—	—	—	—
	mean	40.9	43.1	—	—	—	—	—	—	—
	min	37.2	43.1	—	—	—	—	—	—	—
	SD	3.42	—	—	—	—	—	—	—	—
	N	8	1	—	—	—	—	—	—	—
TD dia	max	48.7	34.8	44.8	—	—	47.2	—	46.0	—
	mean	44.5	31.6	44.8	—	—	43.8	—	45.0	—
	min	38.4	34.8	44.8	—	—	38.7	—	44.0	—
	SD	2.88	4.57	—	—	—	3.83	—	—	—
	N	14	2	1	—	—	5	—	2	—
APD dia	max	34.0	27.1	31.5	—	—	37.1	~ 45	37.0	—
	mean	29.4	24.9	31.5	—	—	33.6	41.0	34.5	—
	min	24.9	27.1	31.5	—	—	31.0	36.0	32.0	—
	SD	3.01	3.05	—	—	—	3.11	—	—	—
	N	12	2	1	—	—	4	3	2	—
TD dis art	max	88.6	61.2	73.5	70.0	—	68.9	93.0	80.0	80.0
	mean	82.4	61.2	73.5	70.0	—	66.5	88.0	78.0	80.0
	min	78.2	61.2	73.5	70.0	—	64.0	83.0	76.0	80.0
	SD	3.77	—	—	—	—	2.21	—	—	—
	N	7	1	1	1	—	4	2	2	1
APD dis art	max	51.7	43.6	53.6	—	—	38.3	~ 58	—	78.0
	mean	42.6	43.6	53.6	—	—	36.7	53.3	—	78.0
	min	34.1	43.6	53.6	—	—	33.9	52.0	—	78.0
	SD	5.32	—	—	—	—	2.06	—	—	—
	N	6	1	1	—	—	4	3	—	1
TD dis epi	max	66.7	—	73.5	—	—	77.2	—	69.0	—
	mean	64.5	—	73.5	—	—	74.8	—	68.5	—
	min	62.6	—	73.5	—	—	71.3	—	68.0	—
	SD	1.53	—	—	—	—	2.62	—	—	—
	N	6	—	1	—	—	4	—	2	—
APD dis epi	max	40.5	—	53.6	—	—	57.2	~ 45	41.0	—
	mean	35.8	—	53.6	—	—	52.0	41.0	41.0	—
	min	31.9	—	53.6	—	—	54.6	36.0	41.0	—
	SD	2.73	—	—	—	—	1.30	—	—	—
	N	7	—	1	—	—	2	3	2	—

SUPPLEMENTARY DATA 3 (CONT.)

Table 3.5

Scaphoid

		MMo	FMH	PPio-2	TAR	REM	TO	*H. corcolense*	*B. grimmi*	*B. caucasica*	*C. oettingenae*
TD	max	33.2	37.9	37.5	—	39.0	34.2	55.6	50.0	—	36.0
	mean	33.2	31.7	35.1	—	39.0	34.2	46.1	50.0	—	36.0
	min	33.2	27.4	32.9	—	39.0	34.2	39.7	50.0	—	36.0
	SD	—	5.51	2.16	—	39.00	—	6.02	—	—	—
	N	1	3	5	—	1	1	6	1	—	1
APD	max	66.5	65.9	75.6	60.7	56.6	57.0	60.7	71.0	63.0	57.0
	mean	66.5	61.4	65.7	60.7	56.6	57.0	56.3	71.0	63.0	57.0
	min	66.5	54.2	52.3	60.7	56.6	57.0	56.0	71.0	63.0	57.0
	SD	—	4.45	6.30	—	—	—	2.89	—	—	—
	N	1	6	10	1	1	1	7	1	1	1
H	max	47.9	59.0	64.2	52.0	54.6	38.6	57.0	67.0	54.0	44.0
	mean	47.9	55.5	55.8	52.0	54.6	38.6	52.4	67.0	54.0	44.0
	min	47.9	50.8	49.0	52.0	54.6	38.6	46.8	67.0	54.0	44.0
	SD	—	3.10	4.46	—	—	—	3.65	—	—	—
	N	1	6	11	1	1	1	9	1	1	1
TD prox art	max	32.2	37.1	39.6	—	38.7	32.8	41.5	51.0	—	—
	mean	32.2	34.2	34.2	—	38.7	32.8	40.1	51.0	—	—
	min	32.2	29.9	29.8	—	38.7	32.8	38.8	51.0	—	—
	SD	—	3.82	2.75	—	—	—	1.09	—	—	—
	N	1	3	9	—	1	1	1	1	—	—
APD prox art	max	44.0	46.4	46.3	39.9	32.4	35.1	42.4	45.0	—	—
	mean	44.0	41.5	41.1	39.9	32.4	35.1	39.3	45.0	—	—
	min	44.0	36.6	37.4	39.9	32.4	35.1	33.5	45.0	—	—
	SD	—	3.47	2.65	—	—	—	2.51	—	—	—
	N	1	8	21	1	1	1	9	1	—	—
APD fMa	max	22.7	28.4	29.7	—	—	—	—	—	—	—
	mean	22.7	24.9	24.6	—	—	—	—	—	—	—
	min	22.7	21.3	20.6	—	—	—	—	—	—	—
	SD	—	2.98	2.90	—	—	—	—	—	—	—
	N	1	5	11	—	—	—	—	—	—	—
APD fTz	max	—	21.4	24.6	—	—	—	—	—	—	—
	mean	—	18.4	21.6	—	—	—	—	—	—	—
	min	—	15.0	18.6	—	—	—	—	—	—	—
	SD	—	2.44	1.98	—	—	—	—	—	—	—
	N	—	5	14	—	—	—	—	—	—	—
APD fTr	max	—	9.9	21.9	—	—	—	—	—	—	—
	mean	—	8.3	12.2	—	—	—	—	—	—	—
	min	—	6.2	6.1	—	—	—	—	—	—	—
	SD	—	1.54	4.67	—	—	—	—	—	—	—
	N	—	6	9	—	—	—	—	—	—	—
TD dis art	max	23.7	26.3	28.1	—	26.1	—	38.0	30.0	—	—
	mean	23.7	23.7	22.9	—	26.1	—	34.8	30.0	—	—
	min	23.7	21.7	19.3	—	26.1	—	28.7	30.0	—	—
	SD	—	1.89	2.56	—	—	—	3.66	—	—	—
	N	1	7	8	—	1	—	4	1	—	—
APD dis art	max	—	54.1	55.8	54.4	50.6	—	45.4	—	—	—
	mean	—	47.5	52.4	54.4	50.6	—	44.6	—	—	—
	min	—	43.1	48.9	54.4	50.6	—	44.1	—	—	—
	SD	—	4.65	2.37	—	—	—	0.48	—	—	—
	N	—	4	7	1	1	—	4	—	—	—

SUPPLEMENTARY DATA 3 (CONT.)

Table 3.6

Magnum

		MMo	FMH	PPio-2	MUN-1	PP	TO	*H. corcolense*	*B. grimmi*	*B. caucasica*	*C. oettingenae*
	max	36.4	43.8	41.6	31.9	35.0	—	37.1	42.0	28.0	28.0
	mean	34.9	36.8	36.7	31.9	35.0	—	33.9	42.0	28.0	28.0
TD	min	32.8	32.7	32.0	31.9	35.0	—	29.9	42.0	28.0	28.0
	SD	1.51	3.62	2.84	—	—	—	3.18	—	—	—
	N	3	9	22	1	1	—	11	1	1	1
	max	—	31.9	21.6	—	—	—	—	—	—	—
	mean	—	27.5	18.9	—	—	—	—	—	—	—
LfUn	min	—	23.1	13.5	—	—	—	—	—	—	—
	SD	—	2.58	2.14	—	—	—	—	—	—	—
	N	—	10	24	—	—	—	—	—	—	—
	max	25.7	21.7	29.6	—	—	—	—	—	—	—
	mean	25.7	18.9	25.7	—	—	—	—	—	—	—
LfSl	min	25.7	17.2	20.4	—	—	—	—	—	—	—
	SD	—	1.64	2.69	—	—	—	—	—	—	—
	N	1	9	25	—	—	—	—	—	—	—
	max	77.5	75.4	81.0	—	67.4	69.2	79.7	82.0	76.0	—
	mean	77.5	73.3	74.9	—	67.4	69.2	32.5	82.0	76.0	—
APD	min	77.5	70.7	69.0	—	67.4	69.2	67.6	82.0	76.0	—
	SD	—	2.12	3.79	—	—	—	5.30	—	—	—
	N	1	5	13	—	1	1	4	1	1	—
	max	52.7	51.9	53.3	40.8	50.5	47.6	48.2	58.0	42.0	41.0
	mean	52.1	46.2	48.5	40.8	50.5	47.6	47.6	58.0	42.0	41.0
H	min	51.4	43.0	43.8	40.8	50.5	47.6	46.5	58.0	42.0	41.0
	SD	0.50	2.91	2.67	—	—	—	0.71	—	—	—
	N	3	8	17	1	1	1	5	1	1	1
	max	30.3	34.8	35.8	—	—	—	—	—	—	—
	mean	29.9	30.5	30.6	—	—	—	—	—	—	—
Hdor	min	29.2	25.3	26.1	—	—	—	—	—	—	—
	SD	0.50	2.83	2.36	—	—	—	—	—	—	—
	N	3	10	25	—	—	—	—	—	—	—
	max	41.4	33.0	47.9	—	—	—	—	—	—	—
	mean	41.4	28.4	41.6	—	—	—	—	—	—	—
H vproc	min	41.4	24.6	36.1	—	—	—	—	—	—	—
	SD	—	2.74	4.01	—	—	—	—	—	—	—
	N	1	7	12	—	—	—	—	—	—	—
	max	52.1	40.2	45.1	—	47.6	46.2	48.5	37.0	25?	—
	mean	48.7	34.4	41.1	—	47.6	46.2	45.7	37.0	25?	—
H art	min	44.1	26.1	34.4	—	47.6	46.2	44.0	37.0	25?	—
	SD	3.40	6.38	3.00	—	—	—	1.58	—	—	—
	N	3	6	14	—	1	1	7	1	1	—

SUPPLEMENTARY DATA 3 (CONT.)

Table 3.7
Pyramidal

		MMo	FMH	PPio-2	TAR	REM	PPio-2	TRR-V	LI	QUI	PP	Ac	Dca	*H. corcolense*	*B. grimmi*	*B. caucasica*	*C. oettingenae*
	max	—	44.4	56.4	—	38.2	56.4	33.2	38.0	34.0	34.1	34.2	45.0	38.7	34.0	42.0	36.0
	mean	—	39.6	40.0	—	38.2	38.2	33.2	38.0	34.0	34.1	34.2	45.0	35.3	34.0	42.0	35.0
TD	min	—	33.5	30.0	—	38.2	30.0	33.2	38.0	34.0	34.0	34.2	45.0	33.1	34.0	42.0	34.0
	SD	—	3.39	5.85	—	—	4.97	—	—	—	—	—	—	1.80	—	—	1.00
	N	—	13	18	—	1	42	1	1	2	1	1	1	10	1	1	2
	max	47.5	52.2	56.3	40.5	40.8	56.3	39.1	46.3	51.0	44.2	—	45.0	45.8	39.0	45.0	39.0
	mean	43.6	50.2	46.1	40.5	40.8	43.0	39.1	46.3	50.5	44.2	—	45.0	41.9	39.0	45.0	38.0
H	min	39.8	44.9	35.0	40.5	40.8	29.1	39.1	46.3	50.0	44.2	—	45.0	—	39.0	45.0	37.0
	SD	3.88	2.37	5.40	—	—	5.91	—	—	0.50	—	—	—	2.64	—	—	1.00
	N	2	11	19	1	1	49	1	1	2	1	—	1	11	1	1	2
	max	40.3	40.4	45.8	33.5	33.9	45.8	34.6	39.0	38.0	37.9	38.0	—	40.4	37.0	37.0	27.0
	mean	34.2	37.3	38.6	33.5	33.5	36.0	34.6	39.0	36.0	37.9	38.0	—	35.7	37.0	37.0	25.5
APD	min	28.0	33.2	34.0	33.5	33.1	24.0	34.6	39.0	34.0	37.9	38.0	—	32.1	37.0	37.0	24.0
	SD	6.15	2.12	3.35	—	0.40	4.05	—	—	2.00	—	—	—	2.06	—	—	1.50
	N	2	12	19	1	2	53	1	1	2	1	1	—	15	1	1	2
	max	22.2	30.5	29.1	—	—	29.1	—	—	—	27.0	~ 29.5	—	—	—	—	—
	mean	22.2	27.1	25.7	—	—	25.2	—	—	—	27.0	~ 29.5	—	—	—	—	—
APD prox	min	22.2	24.3	22.5	—	—	19.2	—	—	—	27.0	~ 29.5	—	—	—	—	—
	SD	—	1.90	1.83	—	—	2.31	—	—	—	—	—	—	—	—	—	—
	N	1	13	17	—	—	20	—	—	—	1	1	—	—	—	—	—

Table 3.8
Trapezoid

		MMo	FMH	PPio-2	REM	TO	*H. corcolense*	*B. caucasica*	*C. oettingenae*
	max	20.1	39.7	23.2	22.1	20.4	24.4	22.0	18.0
	mean	19.7	35.7	19.5	22.1	19.6	21.6	22.0	18.0
TD	min	19.3	32.5	14.7	22.1	18.7	18.5	22.0	18.0
	SD	0.41	2.31	2.77	—	—	1.82	—	—
	N	2	8	13	1	2	13	1	1
	max	38.3	23.7	38.8	27.3	23.2	39.9	26.0	24.0
	mean	33.7	19.7	36.5	27.3	22.9	25.5	26.0	24.0
APD	min	29.2	17.8	33.8	27.3	22.5	21.4	26.0	24.0
	SD	4.55	1.86	1.30	—	—	2.91	—	—
	N	2	8	14	1	2	14	1	1
	max	30.4	32.0	32.1	34.8	34.8	37.6	37.0	26.0
	mean	27.6	28.5	28.3	34.8	32.5	33.9	37.0	26.0
H	min	24.8	25.0	25.7	34.8	30.1	29.2	37.0	26.0
	SD	2.81	2.56	1.66	—	—	2.80	—	—
	N	2	8	14	1	2	10	1	1
	max	18.6	20.2	21.4	—	—	—	—	—
	mean	18.3	19.1	18.9	—	—	—	—	—
H min	min	18.0	17.8	16.4	—	—	—	—	—
	SD	0.29	0.71	1.48	—	—	—	—	—
	N	2	8	15	—	—	—	—	—

Table 3.9
Trapezium

		FMH	PPio-2
	max	29.5	29.4
	mean	28.3	29.2
TD	min	27.2	29.1
	SD	1.65	0.23
	N	2	2
	max	24.2	23.4
	mean	20.3	23.4
APD	min	16.4	23.4
	SD	5.49	—
	N	2	1
	max	20.3	18.9
	mean	19.5	18.9
H	min	18.7	18.9
	SD	1.07	—
	N	2	1

SUPPLEMENTARY DATA 3 (CONT.)

Table 3.10

Semilunate		MMo	FMH	PPio-2	TAR	REM	TO	LI	QUI	*H. corcolense*	*B. caucasica*	*C. oettingenae*
	max	41.7	43.5	49.3	38.8	41.0	—	40.7	40.7	40.6	43.0	~ 35
	mean	41.7	42.1	41.2	38.8	41.0	—	34.9	34.9	37.2	43.0	32.5
TD prox	min	41.7	39.8	35.2	38.8	41.0	—	~ 31	~ 31	33.1	43.0	~ 30
	SD	—	1.52	4.08	—	—	—	—	—	2.69	—	—
	N	1	6	12	1	1	—	?	?	10	1	2
	max	25.7	28.4	29.5	—	—	—	—	—	—	—	—
	mean	23.4	25.8	25.5	—	—	—	—	—	—	—	—
TD dis	min	20.7	22.8	21.0	—	—	—	—	—	—	—	—
	SD	2.06	2.15	2.16	—	—	—	—	—	—	—	—
	N	3	10	16	—	—	—	—	—	—	—	—
	max	35.0	35.1	37.4	—	—	—	—	—	—	—	—
	mean	34.8	33.2	32.5	—	—	—	—	—	—	—	—
TD pal	min	34.6	31.5	23.3	—	—	—	—	—	—	—	—
	SD	0.19	1.45	4.06	—	—	—	—	—	—	—	—
	N	2	5	10	—	—	—	—	—	—	—	—
	max	56.3	59.1	64.9	51.1	55.8	50.6	—	—	58.3	60.0	49.0
	mean	56.3	57.3	57.4	51.1	55.8	50.6	—	—	56.4	60.0	48.5
APD	min	56.3	56.5	49.9	51.1	55.8	50.6	—	—	52.8	60.0	48.0
	SD	—	0.96	4.03	—	—	—	—	—	1.72	—	—
	N	1	6	11	1	1	1	—	—	10	1	2
	max	46.3	45.0	47.4	34.4	38.9	35.3	—	—	41.7	—	38.0
	mean	43.1	40.8	40.3	34.4	38.9	35.3	—	—	39.3	—	38.0
H	min	39.9	35.5	33.9	34.4	38.9	35.3	—	—	35.1	—	38.0
	SD	3.23	3.40	3.48	—	—	—	—	—	2.13	—	—
	N	2	10	19	1	1	1	—	—	8	—	2
	max	27.5	30.4	34.3	—	—	—	—	—	—	—	—
	mean	27.5	28.6	29.0	—	—	—	—	—	—	—	—
APD fUn	min	27.5	26.9	26.1	—	—	—	—	—	—	—	—
	SD	—	1.34	2.06	—	—	—	—	—	—	—	—
	N	1	6	16	—	—	—	—	—	—	—	—
	max	43.7	39.4	46.7	37.0	41.2	37.2	—	—	46.0	43.0	—
	mean	40.7	34.0	39.8	37.0	41.2	37.2	—	—	41.1	43.0	—
Hart	min	37.7	19.4	33.8	37.0	41.2	37.2	—	—	35.0	43.0	—
	SD	2.99	6.94	3.29	—	—	—	—	—	3.07	—	—
	N	2	8	18	1	1	1	—	—	17	1	—

Table 3.11

Pisiform		FMH	PPio-2	*H. corcolense*
	max	58.9	52.9	55.7
	mean	53.8	51.8	55.7
APD	min	47.2	51.2	55.7
	SD	4.54	0.95	—
	N	6	3	1
	max	29.6	24.1	22.8
	mean	23.8	21.2	22.8
TD	min	19.9	17.6	22.8
	SD	3.28	2.78	—
	N	6	4	1
	max	43.0	35.8	40.0
	mean	38.0	34.4	40.0
H	min	34.0	32.3	40.0
	SD	3.23	1.87	—
	N	5	3	1
	max	27.4	23.6	—
	mean	21.8	19.9	—
H col	min	19.2	16.5	—
	SD	3.01	2.58	—
	N	6	5	—
	max	32.8	25.3	—
	mean	25.9	23.1	—
H art	min	22.3	20.1	—
	SD	3.76	1.95	—
	N	6	5	—

SUPPLEMENTARY DATA 3 (CONT.)

Table 3.12
Unciform

		MMo	FMH	PPio-2	PP	Ac	TO	LI	*H. corcolense*	*B. grimmi*	*B. caucasica*	*C. oettingenae*
	max	58.6	60.5	60.6	55.2	51.4	40.8?	46.2	59.1	56.0	57.0	—
	mean	55.9	55.0	54.1	55.2	51.4	40.8?	46.2	50.5	56.0	57.0	—
TD	min	54.4	49.5	46.6	55.2	51.4	40.8?	46.2	42.8	56.0	57.0	—
	SD	1.90	3.81	3.66	—	—	—	—	3.52	—	—	—
	N	3	7	22	1	1	1	1	17	1	1	—
	max	41.7	44.1	42.7	40.0	40.3	35.3	38.7	45.2	43.0	40.0	44.0
	mean	40.9	40.9	37.3	40.0	40.3	33.9	38.7	39.8	43.0	40.0	44.0
H	min	39.9	38.1	32.5	40.0	40.3	33.4	38.7	33.3	43.0	40.0	44.0
	SD	0.78	2.23	2.54	—	—	—	—	2.74	—	—	—
	N	3	9	25	1	1	2	1	22	1	1	1
	max	68.1	66.5	60.4	50.0	68.5	49.4	—	60.4	60.0	—	—
	mean	64.7	58.7	54.1	50.0	68.5	49.4	—	54.1	60.0	—	—
APD an	min	61.4	46.4	47.9	50.0	68.5	49.4	—	43.6	60.0	—	—
	SD	3.33	6.94	3.79	—	—	—	—	5.18	—	—	—
	N	2	6	14	1	1	1	—	7	1	—	—
	max	77.4	76.3	79.9	70.6	56.2	59.6	—	78.9	76.0	63.0	—
	mean	75.4	71.0	69.9	70.6	56.2	59.6	—	69.0	76.0	63.0	—
APD ab	min	73.4	62.0	60.1	70.6	56.2	59.6	—	52.5	76.0	63.0	—
	SD	2.03	5.39	5.57	—	—	—	—	8.26	—	—	—
	N	2	6	15	1	1	1	—	7	1	1	—

Table 3.13
Mc V

		FMH	PPio-2	TO
	max	33.4	29.7	25.0
	mean	29.8	28.2	25.0
L	min	26.5	26.6	25.0
	SD	3.22	2.19	—
	N	4	2	1
	max	25.4	24.0	22.5
	mean	23.1	24.0	22.5
TD prox epi	min	20.2	24.0	22.5
	SD	2.25	—	—
	N	4	1	1
	max	24.3	21.0	18.8
	mean	23.0	19.3	18.8
APD prox epi	min	20.4	17.5	18.8
	SD	1.73	2.47	—
	N	4	2	1

SUPPLEMENTARY DATA 3 (CONT.)

Table 3.14

Mc II

		MMo	FMH	PPio-2	TO	PP	Ac	LI	*H. corcolense*	*B. grimmi*	*B. caucasica*
L	max	150.1	155.0	178.0	129.7	145.5	142.0	124.0	138.7	162.0	148.0
	mean	145.0	148.3	146.7	129.7	145.5	142.0	123.0	138.7	151.3	148.0
	min	138.5	145.0	117.7	129.7	145.5	142.0	122.0	138.7	144.0	148.0
	SD	4.18	3.26	14.78	—	—	—	—	—	—	—
	N	4	7	10	1	1	1	2	1	3	1
TD prox epi	max	38.3	27.2	38.2	—	22.4	22.7	—	23.8	33.0	—
	mean	28.2	22.2	20.5	—	22.4	22.7	—	21.2	30.3	—
	min	22.4	19.4	14.8	—	22.4	22.7	—	19.3	28.0	—
	SD	7.19	3.67	5.05	—	—	—	—	1.41	—	—
	N	3	4	17	—	1	1		11	3	—
APD prox epi	max	37.3	35.0	43.4	—	~ 33	33.9	—	—	—	—
	mean	31.3	30.9	32.7	—	~ 33	33.9	—	—	—	—
	min	20.6	27.1	20.3	—	~ 33	33.9	—	—	—	—
	SD	7.65	3.95	5.33	—	—	—	—	—	—	—
	N	3	3	17	—	1	1	—	—	—	—
TD prox art	max	32.2	19.8	35.3	~ 26	18.6	—	~ 29	31.4	40.0	23.0
	mean	24.3	18.2	18.9	~ 26	18.6	—	~ 29	27.8	38.3	23.0
	min	19.7	16.6	13.0	~ 26	18.6	—	~ 29	25.3	37.0	23.0
	SD	5.57	1.34	4.99	—	—	—	—	2.26	—	—
	N	3	4	15	1	1	—	1	7	3	1
APD prox art	max	29.1	34.7	34.3	29.7	—	—	~ 27	40.3	38.0	36.0
	mean	25.0	30.8	29.5	29.7	—	—	~ 27	37.8	33.0	36.0
	min	18.5	28.0	19.0	29.7	—	—	~ 27	33.9	28.0	36.0
	SD	4.66	3.52	4.33	—	—	—	—	2.36	—	—
	N	3	3	13	1	—	—	1	5	4	1
TD dia	max	40.5	28.2	33.4	24.1	25.1	25.5	~ 23	27.5	34.0	32.0
	mean	30.1	22.5	23.9	24.1	25.1	25.5	19.9	26.0	30.3	32.0
	min	24.9	18.3	9.8	24.1	25.1	25.5	16.7	23.3	28.0	32.0
	SD	5.03	4.77	8.28	—	—	—	—	1.63	—	—
	N	6	4	15	1	1	1	2	5	3	1
APD dia	max	17.8	17.7	23.9	18.0	14.1	14.5	~ 16	24.1	17.0	18.0
	mean	15.0	15.2	17.8	18.0	14.1	14.5	15.1	21.6	17.0	18.0
	min	13.8	12.6	12.8	18.0	14.1	14.5	13.6	19.1	17.0	18.0
	SD	1.35	2.49	3.99	—	—	—	—	2.12	—	—
	N	6	4	13	1	1	1	2	5	3	1
TD md	max	38.3	35.4	39.5	—	31.2	30.4	~ 29	33.0	43.0	—
	mean	36.1	30.9	32.7	—	31.2	30.4	26.8	31.7	36.3	—
	min	33.0	26.4	22.9	—	31.2	30.4	24.0	30.3	32.0	—
	SD	2.12	6.37	5.95	—	—	—	—	—	—	—
	N	6	2	7	—	1	1	2	2	3	—
TD dis art	max	32.9	35.4	31.6	—	27.6	28.4	—	31.6	36.0	35.0
	mean	24.4	32.0	26.2	—	27.6	28.4	—	30.2	31.7	35.0
	min	21.3	28.6	22.8	—	27.6	28.4	—	28.5	29.0	35.0
	SD	4.10	4.82	3.20	—	—	—	—	1.02	—	—
	N	6	2	7	—	1	1	—	6	3	1
APD dis art	max	30.2	34.7	34.1	32.1	31.2	31.0	23.0	33.0	41.0	30.0
	mean	28.2	31.8	30.0	32.1	31.2	31.0	23.0	30.1	36.7	30.0
	min	26.4	28.9	23.4	32.1	31.2	31.0	23.0	28.0	34.0	30.0
	SD	1.43	4.08	3.54	—	—	—	—	1.72	—	—
	N	6	2	7	1	1	1	1	7	3	1

SUPPLEMENTARY DATA 3 (CONT.)

Table 3.15

Mc III

		MMo	FMH	PPio-2	Ac	TO	LI	*H. corcolense*	*B. grimmi*	*B. caucasica*
L	max	174.0	176.0	180.0	168.0	156.2	—	171.5	170.0	168.0
	mean	174.0	171.6	174.0	168.0	154.3	—	171.5	169.0	168.0
	min	174.0	168.0	164.0	168.0	152.3	—	171.5	168.0	168.0
	SD	—	3.60	5.02	—	—	—	—	—	—
	N	1	7	9	1	2	—	1	2	1
TD prox epi	max	53.9	50.7	50.4	46.4	41.9	45.5	53.2	46.0	46.0
	mean	44.1	44.1	46.0	46.4	40.1	40.5	46.6	45.6	46.0
	min	34.5	34.6	30.6	46.4	38.8	~ 36	46.0	45.0	46.0
	SD	8.74	5.14	5.43	—	—	—	3.80	—	—
	N	4	14	11	1	3	4	14	5	1
APD prox epi	max	39.8	40.7	37.3	~ 34	32.2	36.0	43.0	40.0	38.0
	mean	34.4	34.6	33.0	~ 34	30.9	32.7	38.2	39.0	38.0
	min	28.7	28.3	26.5	~ 34	29.6	30.0	32.6	36.0	38.0
	SD	5.19	3.93	3.65	—	—	—	3.53	—	—
	N	4	12	12	1	2	4	6	5	1
TD prox art	max	40.7	37.8	36.3	—	—	—	—	—	—
	mean	33.1	33.0	33.8	—	—	—	—	—	—
	min	27.9	28.0	29.7	—	—	—	—	—	—
	SD	5.50	2.94	1.88	—	—	—	—	—	—
	N	4	18	11	—	—	—	—	—	—
APD prox art	max	39.2	39.9	35.7	—	—	—	—	—	—
	mean	33.3	33.9	31.4	—	—	—	—	—	—
	min	27.7	27.4	26.2	—	—	—	—	—	—
	SD	5.89	4.32	3.37	—	—	—	—	—	—
	N	4	11	9	—	—	—	—	—	—
TD dia	max	22.6	24.0	22.6	34.3	32.3	32.5	42.1	37.0	38.0
	mean	17.1	20.8	20.4	34.3	31.6	30.8	37.0	36.6	38.0
	min	11.4	17.5	18.8	34.3	31.1	~ 29	33.4	~ 36	38.0
	SD	4.89	2.03	1.37	—	—	—	3.63	—	—
	N	4	16	10	1	4	2	6	5	1
APD dia	max	38.5	39.4	41.4	17.2	15.7	15.5	19.7	19.0	21.0
	mean	36.3	35.3	33.6	17.2	14.2	14.6	18.3	18.0	21.0
	min	33.6	26.1	18.1	17.2	13.1	~ 13	17.5	17.0	21.0
	SD	2.00	4.16	6.58	—	—	—	0.83	—	—
	N	5	15	18	1	4	2	5	3	1
TD md	max	20.8	19.9	21.6	45.0	~ 40	—	54.2	51.0	49.0
	mean	17.6	16.7	16.1	45.0	~ 40	—	49.3	50.5	49.0
	min	15.9	14.1	12.4	45.0	~ 40	—	44.6	50.0	49.0
	SD	1.96	1.56	2.25	—	—	—	3.77	—	—
	N	5	15	15	1	1	—	8	2	1
TD dis art	max	46.7	50.1	53.3	40.2	~ 34	—	46.6	42.0	—
	mean	45.9	47.4	46.9	40.2	~ 34	—	41.9	41.5	—
	min	45.1	45.8	35.6	40.2	~ 34	—	38.1	41.0	—
	SD	1.14	1.69	4.66	—	—	—	3.29	—	—
	N	2	6	11	1	1	—	8	2	—
APD dis art	max	39.6	41.9	43.0	34.8	—	—	42.2	37.0	38.0
	mean	37.5	40.4	38.3	34.8	—	—	35.6	36.5	38.0
	min	35.1	38.0	31.6	34.8	—	—	32.0	36.0	38.0
	SD	2.13	1.39	3.05	—	—	—	3.08	—	—
	N	4	8	15	1	—	—	8	2	1

SUPPLEMENTARY DATA 3 (CONT.)

Table 3.16

Mc IV

		MMo	FMH	PPio-2	Ac	TO	MUN-1	*H. corcolense*	*B. grimmi*	*B. caucasica*
L	max	140.5	145.0	149.0	136.1	120.3	—	138.4	144.0	137.0
	mean	139.3	139.8	139.1	136.1	120.3	—	134.2	142.0	137.0
	min	138.0	136.0	111.3	136.1	120.3	—	129.9	140.0	137.0
	SD	1.25	3.71	10.80	—	—	—	—	—	—
	N	2	7	10	1	1	—	2	2	1
TD prox epi	max	37.1	41.0	38.5	38.9	33.4	31.0	40.0	36.0	33.0
	mean	36.8	37.9	31.5	38.9	33.4	31.0	37.3	34.3	33.0
	min	36.3	34.7	25.6	38.9	33.4	31.0	33.0	33.0	33.0
	SD	0.38	4.45	5.26	—	—	—	2.87	—	—
	N	3	2	10	1	1	1	6	3	1
APD prox epi	max	32.7	37.0	40.9	32.8	29.5	28.7	35.7	36.0	35.0
	mean	32.4	36.7	34.4	32.8	29.5	28.7	34.0	35.3	35.0
	min	31.8	36.5	24.7	32.8	29.5	28.7	31.8	34.0	35.0
	SD	0.34	0.37	5.50	—	—	—	1.68	—	—
	N	4	2	12	1	1	1	8	3	1
TD prox art	max	34.2	34.7	34.7	—	—	—	—	—	—
	mean	33.7	34.0	28.2	—	—	—	—	—	—
	min	33.2	33.3	21.0	—	—	—	—	—	—
	SD	0.54	0.98	5.16	—	—	—	—	—	—
	N	2	2	8	—	—	—	—	—	—
APD prox art	max	30.5	33.7	38.0	—	—	—	—	—	—
	mean	28.5	32.3	31.8	—	—	—	—	—	—
	min	27.3	30.9	26.8	—	—	—	—	—	—
	SD	1.23	2.03	3.71	—	—	—	—	—	—
	N	4	2	10	—	—	—	—	—	—
TD dia	max	27.9	28.2	29.0	23.6	20.0	24.0	28.0	27.0	28.0
	mean	25.0	25.9	26.2	23.6	20.0	24.0	26.8	27.0	28.0
	min	22.4	19.8	21.5	23.6	20.0	24.0	25.3	27.0	28.0
	SD	2.00	4.03	1.78	—	—	—	1.24	—	—
	N	5	4	17	1	1	1	4	2	1
APD dia	max	21.2	19.8	18.9	19.2	15.7	17.8	21.0	17.0	20.0
	mean	17.6	18.7	16.7	19.2	15.7	17.8	18.8	16.5	20.0
	min	15.4	16.9	14.3	19.2	15.7	17.8	16.9	16.0	20.0
	SD	2.32	1.29	1.35	—	—	—	2.04	—	—
	N	5	4	16	1	1	1	4	2	1
TD md	max	37.5	37.0	40.0	32.0	25.7	—	40.0	36.0	35.0
	mean	37.2	28.4	38.0	32.0	25.7	—	35.7	36.0	35.0
	min	36.8	14.7	33.6	32.0	25.7	—	33.8	36.0	35.0
	SD	0.34	12.04	1.83	—	—	—	2.16	—	—
	N	2	3	10	1	1	—	8	2	1
TD dis art	max	32.4	33.9	38.8	28.1	22.9	—	36.2	30.0	35.0
	mean	29.5	31.6	30.7	28.1	22.9	—	32.4	30.0	35.0
	min	25.2	29.4	26.9	28.1	22.9	—	30.3	30.0	35.0
	SD	3.12	3.16	3.61	—	—	—	1.79	—	—
	N	3	2	9	1	1	—	8	2	1
APD dis art	max	29.5	33.6	30.1	31.6	24.2	—	35.8	31.0	20.4
	mean	26.9	32.6	28.1	31.6	24.2	—	32.3	31.0	20.4
	min	21.7	31.5	25.3	31.6	24.2	—	30.0	31.0	20.4
	SD	3.67	1.46	1.71	—	—	—	2.02	—	—
	N	3	2	10	1	1	—	7	2	1

SUPPLEMENTARY DATA 3 (CONT.)

Table 3.17

Femur		MMo	FMH	PPio-2
L	max	—	459.0	455.0
	mean	—	459.0	446.5
	min	—	459.0	438.0
	SD	—	—	12.02
	N	—	1	2
L troc-prox	max	—	~ 125	203.0
	mean	—	~ 125	198.0
	min	—	~ 125	193.0
	SD	—	—	7.07
	N	—	1	2
L troc	max	56.4	67.0	65.0
	mean	56.4	67.0	55.6
	min	56.4	67.0	50.5
	SD	—	—	5.98
	N	1	1	5
L troc-dis	max	218.0	222.0	215.0
	mean	218.0	222.0	215.0
	min	218.0	222.0	215.0
	SD	—	—	—
	N	1	1	1
TD head	max	69.3	82.0	89.3
	mean	69.3	82.0	83.0
	min	69.3	82.0	73.5
	SD	—	—	5.16
	N	1	1	7
APD head	max	45.4	61.0	66.9
	mean	45.4	61.0	61.3
	min	45.4	61.0	55.7
	SD	—	—	7.89
	N	—	1	2
TDprox	max	—	163.0	183.0
	mean	—	163.0	175.8
	min	—	163.0	168.0
	SD	—	—	6.18
	N	—	1	4
APDprox	max	—	—	60.0
	mean	—	—	56.4
	min	—	—	52.7
	SD	—	—	5.17
	N	—	—	2
TDcue	max	—	—	144.1
	mean	—	—	144.1
	min	—	—	144.1
	SD	—	—	—
	N	—	—	1

Table 3.17 (cont.)

Femur		MMo	FMH	PPio-2
TD 3t	max	99.8	102.0	112.1
	mean	99.8	—	100.6
	min	99.8	—	82.2
	SD	—	—	14.18
	N	1	1	4
TD dia	max	64.8	51.0	68.5
	mean	64.8	51.0	58.2
	min	64.8	51.0	33.7
	SD	—	—	16.50
	N	1	1	4
APD dia	max	34.6	47.0	38.5
	mean	34.6	47.0	38.5
	min	34.6	47.0	38.5
	SD	—	—	—
	N	1	1	1
R1	max	69.2	105.0	81.7
	mean	68.3	105.0	74.6
	min	67.4	105.0	68.8
	SD	1.28	—	3.60
	N	2	1	9
R2	max	66.2	65.0	74.6
	mean	65.0	65.0	71.7
	min	63.9	65.0	69.8
	SD	1.65	—	1.68
	N	2	1	7
TD troc	max	74.0	82.0	118.8
	mean	74.0	82.0	77.1
	min	74.0	82.0	57.8
	SD	—	—	17.74
	N	1	1	9
TD dis	max	—	120.0	97.7
	mean	—	120.0	91.2
	min	—	120.0	84.7
	SD	—	—	9.19
	N	—	1	2
APD dis	max	—	148.0	158.0
	mean	—	148.0	158.0
	min	—	148.0	158.0
	SD	—	—	—
	N	—	1	1

Table 3.18

Tibia		MMo	FMH	PPio-2	*H. corcolense*
L	max	—	364.0	386.0	—
	mean	—	364.0	370.5	—
	min	—	364.0	354.0	—
	SD	—	—	12.50	—
	N	—	1	8	—
LfFi	max	205.0	305.0	322.0	—
	mean	205.0	305.0	310.5	—
	min	205.0	305.0	305.0	—
	SD	—	—	5.68	—
	N	1	1	8	—
APD prox epi	max	85.3	96.5	91.5	97.2
	mean	85.3	96.5	76.4	97.2
	min	85.3	96.5	52.5	97.2
	SD	—	—	15.91	—
	N	1	1	4	1
TD prox epi	max	60.1	88.3	115.0	96.0
	mean	60.1	88.3	102.1	96.0
	min	60.1	88.3	81.5	96.0
	SD	—	—	14.45	—
	N	1	1	6	1
TD dia	max	45.5	43.0	100.6	49.6
	mean	44.9	43.0	53.1	49.6
	min	44.4	43.0	36.7	49.6
	SD	0.80	—	15.36	—
	N	2	1	14	1
APD dia	max	39.4	44.2	52.9	41.4
	mean	36.7	44.2	41.1	41.4
	min	34.0	44.2	35.6	41.4
	SD	3.80	—	4.75	—
	N	2	1	11	1
TD dis epi	max	77.9	80.1	97.4	92.5
	mean	77.9	72.7	85.9	90.0
	min	77.9	62.2	66.7	87.5
	SD	—	9.34	9.68	—
	N	1	3	11	2
APD dis epi	max	46.6	62.4	50.0	64.0
	mean	46.6	53.9	45.4	58.8
	min	46.6	44.9	40.5	51.7
	SD	—	8.75	2.48	—
	N	1	3	12	5

SUPPLEMENTARY DATA 3 (CONT.)

Table 3.19

Patella		PPio-2	FMH	TOR	*H. corcolense*
TD	max	84.7	76.6	~ 68	76.5
	mean	78.7	73.2	~ 68	73.5
	min	75.7	66.9	~ 68	71.0
	SD	4.26	3.60	—	1.46
	N	4	6	1	4
APD	max	35.0	45.2	43.3	39.5
	mean	30.2	37.8	43.3	36.9
	min	25.7	30.3	43.3	~ 31
	SD	3.52	4.49	—	2.58
	N	9	11	1	10
H	max	85.7	82.7	77.5	70.1
	mean	81.5	77.7	77.5	69.1
	min	76.5	71.6	77.5	67.7
	SD	3.95	3.54	—	—
	N	4	10	1	3

Table 3.20

Navicular		MMo	FMH	PPio-2	TO	TAR	PP	MUN-1	*H. corcolense*	*B. grimmi*	*B. caucasica*
APD	max	51.3	53.6	59.8	50.5	49.6	25.8	53.2	58.2	~ 55	57.0
	mean	49.9	49.0	52.7	48.4	49.6	—	53.2	50.6	50.5	55.5
	min	48.6	35.1	44.5	45.6	49.6	25.5	53.2	41.4	46.0	54.0
	SD	1.97	4.66	3.88	—	—	—	—	3.83	—	—
	N	2	13	18	3	1	2	1	26	2	2
TD	max	48.4	42.4	45.5	38.5	35.9	45.5	35.0	43.0	51?	55?
	mean	45.8	37.0	38.2	35.9	35.9	—	35.0	38.1	45.5	50.5
	min	43.2	23.3	33.7	34.2	35.9	43.8	35.0	32.3	40.0	46.0
	SD	3.72	4.66	3.16	—	—	—	—	2.95	—	—
	N	2	15	18	3	1	2	1	24	2	2
H	max	32.5	25.9	27.3	22.6	23.0	25.8	21.5	26.6	29.0	—
	mean	27.8	22.3	21.9	22.4	23.0	25.7	21.5	24.7	24.7	—
	min	23.0	18.2	17.7	22.2	23.0	25.5	21.5	20.0	19.0	—
	SD	6.72	2.21	2.44	—	—	—	—	1.71	—	—
	N	2	13	25	3	1	2	1	26	3	—
H min	max	19.0	19.0	20.7	—	—	—	—	—	—	—
	mean	18.3	17.6	18.1	—	—	—	—	—	—	—
	min	17.5	13.9	14.7	—	—	—	—	—	—	—
	SD	1.11	1.28	1.71	—	—	—	—	—	—	—
	N	2	15	22	—	—	—	—	—	—	—
TD prox art	max	32.9	40.1	42.9	—	—	—	—	—	—	—
	mean	32.9	36.6	35.3	—	—	—	—	—	—	—
	min	32.9	31.2	32.1	—	—	—	—	—	—	—
	SD	—	2.60	2.74	—	—	—	—	—	—	—
	N	1	15	19	—	—	—	—	—	—	—
APD prox art	max	32.9	41.8	40.7	—	—	—	—	—	—	—
	mean	32.9	37.6	36.8	—	—	—	—	—	—	—
	min	32.9	34.2	30.1	—	—	—	—	—	—	—
	SD	—	2.11	2.50	—	—	—	—	—	—	—
	N	1	11	17	—	—	—	—	—	—	—

SUPPLEMENTARY DATA 3 (CONT.)

Table 3.21
Astragalus

		MMo	FMH	PPio-2	TO	VA1A	Ac	PP	REM	Lisboa	*H. corcolense*	*B. grimmi*	*B. caucasica*	*C. oettingenae*
	max	76.6	79.8	83.6	71.3	—	—	~ 71	—	65.8	75.0	86.0	79.0	62.0
	mean	70.8	70.4	74.6	66.4	—	—	~ 71	—	63.5	70.4	79.5	79.0	60.5
TD	min	67.1	62.9	58.1	61.5	—	—	~ 71	—	61.6	63.5	72.0	79.0	59.0
	SD	3.71	5.83	6.19	—	—	—	—	—	—	2.11	—	—	—
	N	5	19	28	3	—	—	1	—	3	17	8	1	2
	max	65.4	71.9	77.6	68.3	~ 58	—	68.0	—	60.0	69.0	77.0	58.0	57.0
	mean	63.3	61.8	64.1	64.0	~ 58	—	67.6	—	56.0	66.3	73.0	58.0	55.5
H	min	61.9	55.8	56.7	68.3	~ 58	—	67.1	—	~ 51	63.4	65.0	58.0	54.0
	SD	1.84	4.44	5.04	—	—	—	—	—	—	2.11	—	—	—
	N	3	18	31	4	1	—	2	—	3	11	7	1	2
	max	63.3	70.7	71.4	60.1	—	70.7	~ 71	—	59.4	69.3	—	—	—
	mean	58.0	60.1	65.0	58.7	—	70.7	~ 71	—	58.2	64.2	—	—	—
TD md	min	44.0	48.0	50.5	56.1	—	70.7	~ 71	—	~ 56	58.0	—	—	—
	SD	7.95	6.29	5.06	—	—	—	—	—	—	3.25	—	—	—
	N	5	18	28	3	—	1	1	—	3	16	—	—	—
	max	37.3	51.2	48.9	—	—	—	—	—	—	—	—	—	—
	mean	34.8	37.2	38.9	—	—	—	—	—	—	—	—	—	—
DL inf	min	32.8	30.3	33.6	—	—	—	—	—	—	—	—	—	—
	SD	1.62	4.77	3.50	—	—	—	—	—	—	—	—	—	—
	N	5	18	29	—	—	—	—	—	—	—	—	—	—
	max	59.9	62.9	70.7	—	—	—	—	—	—	—	—	—	—
	mean	57.5	53.8	57.7	—	—	—	—	—	—	—	—	—	—
H1	min	55.7	45.0	47.4	—	—	—	—	—	—	—	—	—	—
	SD	2.18	5.24	4.98	—	—	—	—	—	—	—	—	—	—
	N	3	17	21	—	—	—	—	—	—	—	—	—	—
	max	41.8	47.3	49.2	—	—	—	—	—	—	—	—	—	—
	mean	39.9	39.9	41.1	—	—	—	—	—	—	—	—	—	—
H min	min	37.3	34.5	31.1	—	—	—	—	—	—	—	—	—	—
	SD	1.98	3.55	4.26	—	—	—	—	—	—	—	—	—	—
	N	5	18	25	—	—	—	—	—	—	—	—	—	—
	max	55.1	58.7	64.6	—	—	—	—	—	—	—	—	—	—
	mean	51.2	51.2	55.2	—	—	—	—	—	—	—	—	—	—
H2	min	47.3	35.1	43.9	—	—	—	—	—	—	—	—	—	—
	SD	3.61	6.41	4.13	—	—	—	—	—	—	—	—	—	—
	N	4	18	24	—	—	—	—	—	—	—	—	—	—
	max	50.2	55.4	61.9	46.5	—	45.1	50.0	—	46.0	49.6	59.4	57.4	—
	mean	45.6	47.4	50.2	44.7	—	45.1	48.7	—	45.3	46.9	58.2	55.5	—
DL	min	41.6	40.3	42.1	43.0	—	45.1	48.4	—	45.0	42.3	~ 56	~ 53	—
	SD	4.08	3.84	4.68	—	—	—	—	—	—	2.53	—	—	—
	N	4	19	28	4	—	1	2	—	3	19	3	3	—
	max	66.2	57.8	70.8	58.1	—	61.5	64.2	—	57.4	66.8	76.0	69.0	56.0
	mean	58.6	49.9	62.4	55.0	—	61.5	64.2	—	55.5	61.4	70.8	69.0	55.5
TD dis art	min	54.6	42.0	48.1	51.7?	—	61.5	64.2	—	~ 53	57.3	62.0	69.0	55.0
	SD	4.07	3.97	6.16	—	—	—	—	—	—	2.80	—	—	—
	N	6	17	31	3	—	1	1	—	3	17	8	1	2
	max	40.8	42.1	44.2	—	—	—	~ 41	—	—	45.1	46.0	43.0	35.0
	mean	38.5	37.1	38.4	—	—	—	~ 41	—	—	40.5	43.1	43.0	32.5
APD dis art	min	37.3	30.3	29.4	—	—	—	~ 41	—	—	37.0	38.0	43.0	30.0
	SD	1.38	4.17	4.02	—	—	—	—	—	—	2.15	—	—	—
	N	5	15	28	—	—	—	1	—	—	16	7	1	2

SUPPLEMENTARY DATA 3 (CONT.)

Table 3.21 (cont.)

Astragalus		MMo	FMH	PPio-2	TO	VA1A	Ac	PP	REM	Lisboa	*H. corcolense*	*B. grimmi*	*B. caucasica*	*C. oettingenae*
	max	45.6	53.8	53.6	43.3	39?	—	—	—	—	58.4	—	—	—
	mean	42.5	45.6	46.3	41.6	39?	—	—	—	—	48.7	—	—	—
APD int	min	39.6	36.4	36.1	39.9	39?	—	—	—	—	43.3	—	—	—
	SD	2.86	5.07	4.79	—	—	—	—	—	—	3.74	—	—	—
	N	5	14	28	3	1	—	—	—	—	14	—	—	—
	max	21.6	34.6	39.0	—	—	—	—	—	—	—	—	—	—
	mean	18.3	29.2	31.8	—	—	—	—	—	—	—	—	—	—
L1	min	15.4	24.7	24.1	—	—	—	—	—	—	—	—	—	—
	SD	2.36	2.17	3.03	—	—	—	—	—	—	—	—	—	—
	N	6	18	29	—	—	—	—	—	—	—	—	—	—
	max	32.4	23.8	23.9	—	—	—	—	—	—	—	—	—	—
	mean	28.4	18.7	20.5	—	—	—	—	—	—	—	—	—	—
L2	min	24.2	14.8	14.4	—	—	—	—	—	—	—	—	—	—
	SD	4.11	2.31	2.21	—	—	—	—	—	—	—	—	—	—
	N	3	18	28	—	—	—	—	—	—	—	—	—	—

Table 3.22

Calcaneum		PPio-2	FMH	PPio-2	TAR	VE	REM	*H. corcolense*	*B. grimmi*	*B. caucasica*
	max	126.6	117.5	126.6	106.7	—	—	109.7	125.0	112.0
	mean	113.6	111.6	113.3	106.7	—	—	104.7	118.0	112.0
H	min	91.2	105.0	91.2	106.7	—	—	98.2	111.0	112.0
	SD	8.65	4.52	9.63	—	—	—	4.22	—	—
	N	10	6	9	1	—	—	6	3	1
	max	39.8	42.3	39.8	37.7	—	40.3	41.6	53.0	39.0
	mean	32.6	36.0	32.6	37.7	—	40.3	39.6	44.0	39.0
TD tuber	min	23.2	23.3	23.2	37.7	—	40.3	36.5	35.0	39.0
	SD	3.85	5.79	3.97	—	—	—	1.63	—	—
	N	16	11	16	1	—	1	7	2	1
	max	66.3	64.3	66.3	58.9	—	56.3	65.0	48.0	63.0
	mean	60.7	55.6	60.7	58.9	—	56.3	60.6	48.0	63.0
APD tuber	min	53.3	36.3	53.3	58.9	—	56.3	56.4	48.0	63.0
	SD	3.51	9.24	3.64	—	—	—	3.34	—	—
	N	15	12	15	1	—	1	8	1	1
	max	59.2	57.9	59.2	—	—	—	64.1	66.0	67.0
	mean	50.1	48.8	50.1	—	—	—	63.3	66.0	67.0
TD sus	min	42.4	39.5	42.4	—	—	—	62.0	66.0	67.0
	SD	6.10	5.55	6.82	—	—	—	0.98	—	—
	N	5	11	5	—	—	—	4	1	1
	max	64.9	60.8	64.9	56.2	—	—	55.0	—	—
	mean	56.3	53.7	56.3	56.2	—	—	52.4	—	—
APD beak	min	51.2	45.0	51.2	56.2	—	—	47.5	—	—
	SD	4.02	4.06	4.22	—	—	—	2.55	—	—
	N	11	11	11	1	—	—	14	—	—
	max	33.9	36.3	33.9	~ 31	32.3	30.9	29.8	38.0	27.0
	mean	27.9	33.7	27.9	~ 31	32.3	30.9	26.7	30.7	27.0
TD dis	min	23.0	24.7	23.0	~ 31	32.3	30.9	23.5	27.0	27.0
	SD	3.21	3.75	3.39	—	—	—	2.06	—	—
	N	10	9	10	1	1	1	12	3	1

SUPPLEMENTARY DATA 3 (CONT.)

Table 3.23

Ectocuneiform		MMo	FMH	PPio-2	PP	Ac	REM	TO	*H, corcolense*	*B, caucasica*
TD prox art	max	33.3	42.2	42.2	36.3	38.3	41.2	39.2	43.3	44.0
	mean	33.3	37.2	38.9	36.3	38.3	41.2	37.3	41.3	44.0
	min	33.3	32.3	34.8	36.3	38.3	41.2	35.3	37.8	44.0
	SD	—	3.03	2.06	—	—	—	—	1.65	—
	N	1	14	19	1	1	1	2	12	1
APD prox art	max	42.7	50.1	49.5	—	44.4	43.5	39.8	47.6	47.0
	mean	42.7	44.7	46.5	—	44.4	43.5	39.7	44.1	47.0
	min	42.7	37.8	43.4	—	44.4	43.5	39.6	41.9	47.0
	SD	—	3.65	1.94	—	—	—	—	1.75	—
	N	1	14	11	—	1	1	2	7	1
H	max	18.6	23.1	22.8	—	23.1	23.0	19.8	25.7	22.0
	mean	18.6	20.2	21.1	—	23.1	23.0	19.8	24.4	22.0
	min	18.6	16.9	19.8	—	23.1	23.0	19.8	23.1	22.0
	SD	—	2.01	0.89	—	—	—	—	0.83	—
	N	1	14	20	—	1	1	1	10	1
H min	max	15.4	20.0	19.3	—	—	—	—	—	—
	mean	15.4	17.3	17.5	—	—	—	—	—	—
	min	15.4	14.9	15.4	—	—	—	—	—	—
	SD	—	1.56	1.21	—	—	—	—	—	—
	N	1	14	17	—	—	—	—	—	—

Table 3.24

Entocuneiform		FMH	PPio-2
TD	max	17.6	20.8
	mean	17.6	15.9
	min	17.6	12.3
	SD	—	2.52
	N	1	7
APD	max	47.3	36.0
	mean	47.3	32.8
	min	47.3	29.6
	SD	—	2.22
	N	1	6
H art	max	33.1	39.9
	mean	33.1	36.3
	min	33.1	33.2
	SD	—	2.16
	N	1	7
H	max	47.3	59.2
	mean	47.3	53.6
	min	47.3	47.2
	SD	—	3.62
	N	1	6

Table 3.25

Mesocuneiform		FMH	TO	*H. corcolense*
TD	max	19.7	22.3	18.2
	mean	17.1	22.3	16.0
	min	15.8	22.3	14.2
	SD	1.52	—	1.28
	N	5	1	12
APD	max	30.7	—	33.1
	mean	29.0	—	29.1
	min	27.3	—	25.1
	SD	1.53	—	2.60
	N	4	—	10
H	max	14.3	13.9	18.1
	mean	13.0	13.1	15.1
	min	11.3	12.4	12.8
	SD	1.16	1.06	1.72
	N	5	2	12
H min	max	12.3	—	—
	mean	11.1	—	—
	min	10.0	—	—
	SD	0.94	—	—
	N	5	—	—

SUPPLEMENTARY DATA 3 (CONT.)

Table 3.26 *Cuboid*		MMo	FMH	PPio-2	TAR	Ac	Lisboa	*H. corcolense*	*B. grimmi*	*B. caucasica*	*C. oettingenae*
TD	max	34.3	30.1	36.3	—	27.5	28.0	33.7	33.0	44.0	29.0
	mean	30.0	26.8	30.9	—	27.5	27.3	30.7	33.0	44.0	29.0
	min	26.1	25.4	25.5	—	27.5	26.5	26.1	33.0	44.0	29.0
	SD	3.24	1.94	2.76	—	—	—	2.05	—	—	—
	N	5	6	23	—	1	2	17	1	1	1
APD	max	60.4	56.6	60.8	—	55.5	~ 51	65.9	65.0	47.0	47.0
	mean	55.5	54.2	57.1	—	55.5	49.9	56.4	65.0	47.0	47.0
	min	51.5	51.8	51.4	—	55.5	~ 48	50.8	65.0	47.0	47.0
	SD	4.51	2.12	2.33	—	—	—	3.39	—	—	—
	N	3	7	17	—	1	2	14	1	1	1
H	max	56.9	53.5	59.1	—	52.6	—	52.5	52.0	22.0	44.0
	mean	52.1	52.7	51.9	—	52.6	—	46.3	52.0	22.0	44.0
	min	47.2	51.0	31.8	—	52.6	—	40.0	52.0	22.0	44.0
	SD	6.88	1.17	6.25	—	—	—	4.08	—	—	—
	N	2	4	16	—	1	—	11	1	1	1
H dor	max	37.5	37.0	40.7	33.3	36.4	33.1	38.8	36.0	—	—
	mean	34.8	33.7	34.6	33.3	36.4	32.6	34.7	36.0	—	—
	min	32.8	31.0	30.9	33.3	36.4	32.0	32.2	36.0	—	—
	SD	1.86	2.13	2.38	—	—	—	1.94	—	—	—
	N	5	7	26	1	1	2	20	1	—	—
H vproc	max	37.1	40.7	43.9	—	—	—	—	—	—	—
	mean	34.4	36.3	36.4	—	—	—	—	—	—	—
	min	29.0	29.1	31.6	—	—	—	—	—	—	—
	SD	4.61	3.72	2.89	—	—	—	—	—	—	—
	N	3	7	19	—	—	—	—	—	—	—
TD prox art	max	31.4	29.6	34.0	29.5	28.3	—	34.0	—	—	—
	mean	26.7	26.1	29.6	29.5	28.3	—	30.8	—	—	—
	min	23.4	24.1	25.1	29.5	28.3	—	28.0	—	—	—
	SD	3.12	2.00	2.14	—	—	—	1.57	—	—	—
	N	5	6	20	1	1	—	15	—	—	—
APD prox art	max	38.6	38.2	43.3	37.2?	36.3	—	46.3	—	—	—
	mean	34.4	36.4	37.2	37.2?	36.3	—	39.1	—	—	—
	min	31.3	34.3	34.3	37.2?	36.3	—	35.3	—	—	—
	SD	2.67	1.40	1.96	—	—	—	3.49	—	—	—
	N	5	6	20	1	1	—	15	—	—	—

SUPPLEMENTARY DATA 3 (CONT.)

Table 3.27

Mt II		MMo	FMH	PPio-2	PP	*H. corcolense*	*B. grimmi*	*B. caucasica*
	max	—	154.8	153.0	139.0	134.0	—	—
	mean	—	152.9	146.0	139.0	132.5	—	—
L	min	—	151.0	141.6	139.0	131.0	—	—
	SD	—	2.70	3.93	—	—	—	—
	N	—	2	9	1	2	—	—
	max	—	37.8	29.6	22.8	23.5	31.0	22.0
	mean	—	34.2	22.8	22.8	20.6	31.0	22.0
TD prox epi	min	—	30.2	16.2	22.8	~ 16	31.0	22.0
	SD	—	3.31	3.65	—	1.90	—	—
	N	—	5	13	1	13	2	1
	max	—	26.7	35.8	36.6	37.7	33.0	36.0
	mean	—	21.0	34.0	36.6	33.9	33.0	36.0
APD prox epi	min	—	13.9	23.9	36.6	29.3	33.0	36.0
	SD	—	4.73	3.29	—	2.77	—	—
	N	—	5	12	1	12	1	1
	max	—	37.4	29.9	16.6	20.5	31.0	—
	mean	—	33.1	20.8	16.6	16.1	29.5	—
TD prox art	min	—	28.0	16.1	16.6	13.9	28.0	—
	SD	—	4.38	3.71	—	1.86	—	—
	N	—	5	11	1	12	2	—
	max	—	21.3	35.6	—	—	—	—
	mean	—	18.9	30.5	—	—	—	—
APD prox art	min	—	13.0	21.9	—	—	—	—
	SD	—	3.34	4.47	—	—	—	—
	N	—	5	10	—	—	—	—
	max	23.7	19.3	24.5	19.7	22.5	22.0	22.0
	mean	23.7	18.1	18.8	19.7	20.9	20.5	22.0
TD dia	min	23.7	16.5	15.8	19.7	19.5	19.0	22.0
	SD	—	1.04	2.72	—	1.12	—	—
	N	1	5	14	1	6	2	1
	max	16.7	22.1	27.3	20.8	21.0	22.0	20.0
	mean	16.7	19.7	21.4	20.8	19.4	21.0	20.0
APD dia	min	16.7	16.7	15.9	20.8	18.0	20.0	20.0
	SD	—	2.32	3.54	—	1.23	—	—
	N	1	4	14	1	6	2	1
	max	21.7	28.6	40.2	29.2	28.2	—	—
	mean	21.7	28.6	31.8	29.2	27.2	—	—
TD md	min	21.7	28.6	27.2	29.2	26.0	—	—
	SD	—	—	4.59	—	0.96	—	—
	N	1	1	7	1	5	—	—
	max	—	26.1	32.7	26.8	28.0	—	—
	mean	—	26.1	24.8	26.8	26.7	—	—
TD dis art	min	—	26.1	19.2	26.8	25.6	—	—
	SD	—	—	3.57	—	0.80	—	—
	N	—	1	11	1	10	—	—
	max	—	30.3	34.0	30.1	30.0	—	—
	mean	—	30.3	30.1	30.1	28.1	—	—
APD dis art	min	—	30.3	18.9	30.1	25.5	—	—
	SD	—	—	4.08	—	1.27	—	—
	N	—	1	13	1	10	—	—

Table 3.28

Mt IV		FMH	PPio-2	TO	*H. corcolense*	*B. grimmi*	*B. caucasica*	*C. oettingenae*
	max	152.0	155.0	—	143.3	147.0	144.0	145.0
	mean	148.0	142.4	—	140.2	147.0	144.0	145.0
L	min	142.0	115.6	—	137.0	147.0	144.0	145.0
	SD	5.29	13.18	—	—	—	—	—
	N	3	7	—	2	1	1	1
	max	37.8	39.2	35.1	42.0	40.0	37.0	34.0
	mean	34.3	33.4	35.1	37.7	39.4	37.0	34.0
TD prox epi	min	31.7	23.2	35.1	31.5	37.0	37.0	34.0
	SD	2.44	4.82	—	2.74	—	—	—
	N	9	10	1	10	5	1	1
	max	37.5	36.5	29.8	41.2	45.0	42.0	31.0
	mean	33.5	32.5	29.8	36.1	40.0	42.0	31.0
APD prox epi	min	29.9	28.7	29.8	30.3	35.0	42.0	31.0
	SD	2.76	2.57	—	2.97	—	—	—
	N	10	11	1	9	5	1	1
	max	33.1	35.0	—	—	—	—	—
	mean	29.3	30.1	—	—	—	—	—
TD prox art	min	23.2	21.4	—	—	—	—	—
	SD	3.20	3.95	—	—	—	—	—
	N	9	9	—	—	—	—	—
	max	31.0	31.0	—	—	—	—	—
	mean	28.7	27.3	—	—	—	—	—
APD prox art	min	25.7	22.9	—	—	—	—	—
	SD	1.97	2.66	—	—	—	—	—
	N	10	9	—	—	—	—	—
	max	26.2	27.2	—	25.2	27.0	25.0	24.0
	mean	22.1	23.8	—	23.2	24.7	25.0	24.0
TD dia	min	18.5	16.0	—	21.9	23.0	25.0	24.0
	SD	2.21	4.11	—	1.16	—	—	—
	N	9	7	—	7	3	1	1
	max	22.8	19.6	—	25.0	21.0	23.0	20.0
	mean	20.0	17.6	—	22.0	20.5	23.0	20.0
APD dia	min	17.7	14.2	—	20.6	20.0	23.0	20.0
	SD	1.79	1.85	—	1.43	—	—	—
	N	9	7	—	7	2	1	1
	max	28.0	31.4	—	31.9	30.0	—	29.0
	mean	25.9	25.9	—	30.8	30.0	—	29.0
TD md	min	23.8	19.9	—	29.6	30.0	—	29.0
	SD	2.96	4.83	—	—	—	—	—
	N	2	4	—	2	1	—	1
	max	27.2	27.7	—	31.6	28.0	30.0	28.0
	mean	25.5	25.7	—	28.7	28.0	30.0	28.0
TD dis art	min	24.1	23.0	—	27.1	28.0	30.0	28.0
	SD	1.59	1.72	—	1.69	—	—	—
	N	3	5	—	5	1	1	1
	max	30.2	32.2	—	29.7	34.0	30.0	32.0
	mean	29.6	26.8	—	28.3	34.0	30.0	32.0
APD dis art	min	28.9	19.9	—	27.0	34.0	30.0	32.0
	SD	0.69	4.38	—	0.96	—	—	—
	N	3	6	—	5	1	1	1

SUPPLEMENTARY DATA 3 (CONT.)

Table 3.29 *Mt III*		MMo	FMH	PPio-2	JU	REM	Lisboa	*H. corcolense*	*B. caucasica*
L	max	166.0	171.0	179.0	169.0	—	147.0	150.3	—
	mean	166.0	165.6	167.5	169.0	—	147.0	147.7	—
	min	166.0	161.0	159.0	169.0	—	147.0	145.0	—
	SD	—	3.97	5.81	—	—	—	—	—
	N	1	5	12	1	—	1	2	—
TD prox epi	max	46.5	47.5	49.2	42.6	—	~ 32	49.2	47.0
	mean	41.3	41.0	43.8	42.6	—	~ 32	43.4	47.0
	min	38.6	34.6	39.4	42.6	—	~ 32	38.8	47.0
	SD	3.63	3.51	2.81	—	—	—	3.20	—
	N	4	14	25	1	—	1	21	1
APD prox epi	max	32.3	43.5	43.2	46.2	—	~ 28	41.0	43.0
	mean	30.3	36.7	36.3	46.2	—	~ 28	36.9	43.0
	min	28.2	28.1	28.8	46.2	—	~ 28	33.0	43.0
	SD	2.88	5.00	4.14	—	—	—	3.27	—
	N	2	10	14	1	—	1	8	—
TD prox art	max	44.0	42.7	46.8	39.5	—	—	—	—
	mean	38.2	37.6	40.1	39.5	—	—	—	—
	min	34.0	30.9	34.9	39.5	—	—	—	—
	SD	5.15	2.87	2.92	—	—	—	—	—
	N	3	15	24	1	—	—	—	—
APD prox art	max	30.1	38.4	39.4	41.9	—	—	—	—
	mean	28.5	34.1	33.6	41.9	—	—	—	—
	min	27.0	28.7	25.1	41.9	—	—	—	—
	SD	2.16	3.45	3.73	—	—	—	—	—
	N	2	10	14	1	—	—	—	—
TD dia	max	35.9	37.8	39.8	36.9	—	31.7	36.0	41.0
	mean	33.4	31.5	32.4	36.9	—	31.7	35.5	41.0
	min	30.9	23.4	22.5	36.9	—	31.7	35.0	41.0
	SD	3.55	4.20	4.25	—	—	—	—	—
	N	2	14	27	1	—	1	2	1
APD dia	max	19.1	19.9	22.0	22.3	—	16.6	19.8	20.0
	mean	18.0	17.5	16.8	22.3	—	16.6	19.3	20.0
	min	16.3	12.6	11.8	22.3	—	16.6	18.3	20.0
	SD	1.45	1.98	2.66	—	—	—	—	—
	N	3	14	26	1	—	1	3	1
TD md	max	45.2	47.6	49.8	50.4	41.9	~ 39	52.4	—
	mean	45.2	43.0	44.6	50.4	41.9	~ 39	48.5	—
	min	45.2	31.9	38.7	50.4	41.9	~ 39	45.8	—
	SD	—	5.73	2.99	—	—	—	2.82	—
	N	1	6	11	1	1	1	5	—
TD dis art	max	39.2	40.4	41.8	41.1	39.1	33.0	45.8	—
	mean	36.9	38.0	38.6	41.1	39.1	33.0	42.2	—
	min	34.5	36.0	34.0	41.1	39.1	33.0	39.5	—
	SD	3.30	1.93	2.65	—	—	—	2.64	—
	N	2	5	10	1	1	1	4	—
APD dis art	max	31.0	37.7	33.6	33.3	33.3	—	37.1	—
	mean	30.5	34.0	29.4	33.3	33.3	—	33.9	—
	min	30.1	28.4	24.7	33.3	33.3	—	30.8	—
	SD	0.64	3.98	3.32	—	—	—	2.31	—
	N	2	5	11	1	1	—	7	—

SUPPLEMENTARY DATA 4

Detailed list of intraspecific characters used in the present study. Some character morphologies represent the extremes of a continuous range of variation, while others are recognizable shapes predominant within the available sample. Additionally, dentition has been coded as follows: white (W), gray (G), black (B), and black with a white dot (D); Figures 7 and 9 of the manuscript. Results are provided in the Supplementary Tables 1-10. Figures not to scale.

Character of the dentition

DP1: Character DP1/1, shape of the parastyle: W, narrow and straight; B, labially curved and thick.

DP2: Character P2/1, lingual bridge: W, angulous and narrow; B, absent. **Character DP2/2**, closed median valley: W, 'diabolo'-shaped; G, narrow and triangular; **Character DP2/3**, development of the postfotsette: W: oval, small; B, absent due to wear.

DP3: Character DP3/1, posterior expansion of the metaloph: W, even metaloph; B, metaloph expanded along the posterior cingulum (without closing a postfosette). **Character DP3/2**, metastyle: W, narrow; B, as wide as the metacone.

P1: Character P1/1, development of the protoloph: W, no protoloph; G, short and narrow protoloph, without contact with the protocone; B, short and narrow protoloph, contacting the protocone; **Character P1/2**, postofosette: W, wide, open to the "median valley"; G, closed; B, absent due to wear; **Character P1/3**: W, metastyle: slightly lingually curved, giving a rounded look to the ectoloph; B, very short, wide, and square.

P2: Character P2/1, lingual bridge: W, same wiTDh as the protocone and hypocone; G, narrower than both lingual cusps; B, as wide as the protocone and smaller than the hypocone. **Character P2/2**, development of the postfosette: W, open; G, closed; B, absent due to advanced wear. **Character P2/3**, development of the closed median valley: W, two big fossae separated by the crochet, equivalent in size; G: two fossae separated by the crochet, one of them considerably narrow; B, only one fossa lingual to the crochet.

P3: Character P3/1, development of the postfosette: W, open; G, closed; B, absent due to advanced wear. **Character P3/2**, development of the lingual wall: W, restricted to the hypocone, posterior cingulum and part of the entrance of the median valley; G, narrow and continuous from the anterior to the posterior cingula; B, continuous and wide.

P4: Character P4/1, development of the postfosette: W, open; G, closed; B, absent due to advanced wear. **Character P4/2**, development of the closed median valley: W, two big fossae separated by the crochet, equivalent in size; G, two fossae separated by the crochet, the lingual narrower; B: only one narrow fossa lingual to the crochet. **Character P4/3**, outline of the ectoloph in occlusal view: W, strongly undulated; G, undulated, with the paracone style pointed; B, smoothed.

M1-2: Character M1-2/1, development of the metastyle: W, pointed and narrow; G, wide and rectangular; B, very wide, enclosing a postfossette; D, postfossette fade out by wear. **Character M1-2/2**, development of the antecrochet: W, weakly constricted; G, rounded to oval and posteriorly expanded; B, very posteriorly expanded, fused with the hypocone, closing the median valley. **Character M1-2/3**, inner enamel folding: W, only crochet present; G, crista/s and/or crochet/s observable; B, weak or no crochet/s and/or crista/s because of wear.

M3: Character M3/1: development of the protocone fold: W, little folded; G, moderately folded, with a developed antecrochet; B, deep and wide fold, very long antecrochet almost reaching the hypocone.

dp2: **Character dp2/1**, shape of the anterior valley in occlusal view: W, rounded; B, pointed. **Character dp2/2**, shape of the labial groove: W, weakly folded; B, acute. **Character dp2/3**, anterior groove of the ectolophid: W, weakly marked; B, absent.

dp3: Character dp3/1, posterior border of the hypolophid in occlusal view: W, concave, B, flat. **Character dp3/2**, anterior border of the paralophid in occlusal view: W, somewhat concave; B, flat. **Character dp3/3**, lingual border of the protoconid: W, straight; B, convex.

dp4: Character dp4/1, cementum: W, no cementum; G, on the posterior valley; B, on the posterior valley and the labial groove. **Character dp4/2**: hypolophid in occlusal view: W, narrow; G: with some wear and a rounded entoconid; B, with some wear and a squared entoconid. **Character dp4/2**: posterior border of the metalophid in occlusal view: W, straight; B, concave.

p1: Character p1/1, anterior valley in occlusal view: W, narrow, acute, and simple; G, double, acute and narrow; B, rounded and shallow. **Character p1/2**, shape of the paralophid in occlusal view: W, blunt; B, pointed. **Character p1/3**, development of the metaconid in occlusal view: W, metaconid expanded, reaching the lingual border; B, rounder and somewhat retracted metaconid.

p2 Character p2/1, posterior valley in occlusal view: W, rounded; G, wide and rounded; B; restricted to a small and pointed notch. **p2 Character p2/2**, anterior valley in occlusal view: W, rounded and small; G: rounded and wide; B, absent. **p2 Character p2/3**, outline of the labial cusps and the labial groove in occlusal view: W, acute cusps with an asymmetric groove; B, rounded with the groove centered in the labial side.

p3: Character p3/1, connection between hypoconid and metalophid: W, connected; B, not connected. **Character p3/2**, lingual border of the encotonid in occlusal view: W, straight; B, rounded. **Character p3/3**, shape of the paralophid in occlusal view: W, rounded and long; B, narrow and acute.

m1-2: Character m1-2/1, shape of the paralophid in occlusal view: W, unworn, narrow; G, narrow paralophid with a rounded anterior border; B, narrow paralophid with a straight anterior border. **Character m1-2/2**, connection between hypoconid and

metalophid: W, connected; B, not connected. **Character m1-2/3**,

Characters of the postcranial skeleton

Detailed list of intraspecific characters used in the present study. Some character morphologies represent the extremes of a continuous range of variation, while others are recognizable shapes predominant within the available sample.

Unciform: Character Un1, fold in the palmar border of the Mc III/Mc IV boundary: 0, rounded (continuing with the distal articular surface); 1, angulous. Figures in distal view, from left to right: FMH'14-2564 and FMH'14-3059 (reversed). **Character Un2**, palmar border of the pyramidal-facet: 0, nearly straight and asymmetrical; 1, slightly sigmoid. Figures from left to right: FMH'14-2564 and FMH'14-3059 (reversed).

Trapezoid: Character Tz1, dorsal border of the medial notch: 0, square; 1, pointed. Figures in medial view, from left to right: FMH'14-2824 and FMH'14-3838 (reversed).

Magnum: Character Ma1, palmar border of the Mc III-facet: 0, rounded; 1, forming an acute angle; 2, sigmoid. Figures of the body of the magnum distal view, from left to right: 05/101/2/189 (reversed), 05/101/2/192 and 05/101/2/203. **Character Ma2**: contact between the medial indentation and the proximal lunate-facet: 0, isolated from the lunate-facet; 1, small contact with the lunate-facet; 2, wide contact with the lunate-facet. Figures in distal view, from left to right: 05/101/2/210, 05/101/2/203 and 05/101/2/193.

Pisiform: Character Pi1, outline of the dorsal borders of the neck and the volar process: 0, straight neck and pointed border, 1, concave neck and rounded volar process; 2, concave neck and square dorsal volar process. Figures in medial view, from left to right: 05/101/2/219, 05/101/2/222 and 05/101/2/217 (reversed). **Character Pi2**, outline of the plantar border of the pyramidal-facet: 0, straight; 1, sigmoid; 2, straight with a small pointed expansion. Figures in distal view, from left to right: 05/101/2/222, 05/101/2/220 and 05/101/2/213 (reversed).

Semilunate: Character Lu1, dorsal side of the magnum-facet: 0, pointed; 1, blunt but narrow; 2, wide. Figures in distal view, from left to right: FMH'14-3170 (reversed), CMD559 and R4-220a. **Character Lu2**, medial side of the magnum-facet: 0, straight; 1, concave. Figures in distal view, from left to right: CMD559 and FRT-1.

Pyramidal: Character Py1, proximal border of the distal lunate-facet: 0, indented; 1, straight to concave; 2, with a small projection. Figures in postero-medial view, from left to right: 05/101/2/7 (reversed), 05/101/2/3 and 05/101/2/1. **Character Py2**, plantar expansion of the ulnar-facet: 0, straight; 1, slightly sigmoid; 2, strongly sigmoid. Figures in plantar view, from left to right: 05/101/2/1, 05/101/2/7 (reversed) and 05/101/2/3.

Scaphoid: **Character Sc1**, lateral border of the magnum-facet: 0, rounded and short; 1, long and palmo-laterally expanded. Figures in lateral view, from left to right: FMH'14-2740 and FMH'14-3978.

Mc II: **Character McII1**, distal outline of the Mc III-facet: 0, triangular and assymetrical (with the higher part closer to the dorsal border); 1, narrow and semicircular/rectangular. Figures in lateral view, from left to right: FMH'14-2698 and CMD-419 (reversed). **Character McII2**, disto-plantar border of the magnum-facet: 0, straight; 1, sigmoid (probably as a result of the presence of a dorsal palmar Mc III-facet, see description in the text). Figures in lateral view, from left to right: CMD-419 (reversed) and FHM'14-2698. **Character McII3**, shape of the palmar tendinous? facet of the proximal epiphysis: 0, slightly convex, 'tear'-shaped, and distally well-delimited by a short shelf; 1, swollen tubercle with an evident planto-medial expansion. Figures in medial view, from left to right: FHM'14-3097 and CMD-419. **Character McII4**, development of the proximo-dorsal fossa of the proximal epiphysis: 0, absent; 1, small; 2, large. Figures in lateral view, from left to right: FMH'14-1975, CMD-419, and FMH'14-3097.

Mc III: **Character McIII1**, lateral side of the insertion of the m. extensor carpalis in dorsal view: 0, very shallow/absent; 1, single and marked; 2, bilobulated and marked; 3, indented and marked. Figures in dorsal view, from left to right: FMH'14-527, R4-255, FMH'14-2914 (reversed), and 05/60/225a-386 (reversed). **Character McIII2**, palmo-distal angle of the dorsal Mc IV-facet: 0, rounded (sometimes associated with a straight distal border of the facet); 1, angulous (sometimes accompanied by a small pillar). FMH'14-2961 and R4-255 (reversed).

Mc IV: **Character McIV1**, aspect of the proximal unciform-facet, TD/APD: 0, narrow (TD/APD < 0,9); 1, deep (TD/APD > 0,9). Even though this character can be somewhat affected by taphonomic alterations, the character state 0 is sometimes accompanied by an independent palmar shelf (pl.sh.) in the proximal epiphysis, whereas in the state 1 the unciform-facet covers the whole proximal surface. Therefore, and according to the overall preservation and proportions of these (deeper) bones, this character seems genuine and independent from the distortion during fossilization. Figures in proximal view, from left to right: CMD-340 and FMH'14-3130. **Character McIV2**, development of the depression for the extensor ligament of the metacarpus: 0, no depression (no difference with the remaining distal surface of the diaphysis); 1, shallow/moderate. Figures in dorsal view, from left to right: FHM'14-3130 and CMD-398. **Character McIV3**, distal border of the medial Mc III-facet: 0, rounded/flat; 1, triangular. Figures in medial view, from left to right: FHM'14-2901; CMD-398 (reversed).

Astragalus: Character As1, latero-distal expansion of the first calcanear-facet in plantar view: 0, short and triangular (barely surpassing the inflexion point of the articular surface); 1, triangular and big; 2, rounded and long. Figures in plantar view, from left to right: FMH'14-3512 (reversed) and FMH'14-3203. **Character As2**, wiTDh of the groove between the first and second calcanear facets: 0, wide (≥ 3,5 mm); 1, narrow (< 3,5 mm). Figures in plantar view, from left to right: FMH'14-3171 and FMH'14-3203. **Character As3**, notch in the neck at the level of the trochlear inflexion: 0, absent; 1, present. Figures in dorsal view, from left to right:

FMH'14-3757 and FMH'14-4914. **Character As4**, proximal border of the third calcanear-facet: 0, straight; 1, convex. Figures in plantar view, from left to right: FMH'14-4914 (reversed) and FMH'14-3723.

Calcaneus: **Character Ca1**, distal border of the second astrgalar-facet: 0, absent (retracted to the distal surface of the beak), 1, asymmetric, triangular: 2, square. Figures in dorsal-distal view, from left to right: FMH'14-4928, FMH'14-2661, and FMH'14-2286. **Character Ca2**, tibial lateral facet of the beak: 0, absent or very weak; 1, defined but small and attached to the dorsal border; 2, variable in size but partially separated from the dorsal border; 3, big and attached to the dorsal border. Figures in lateral view, from left to right: FMH'14-4833 (reversed), FMH'14-2286, FMH'14-2756, and FMH'14-2661. **Character Ca3**, tendinous scar of the lateral side: 0, straight; 1, sigmoid, well-developed. Figures in lateral view, from left to right: FMH'14-2661 and FMH'14-4833 (reversed).

Cuboid: **Character Cb1**, plantar border of the plantar portion of the navicular-facet in medial view: 0, curved or nearly straight; 1, sigmoid. Figures in medial view, from left to right: FMH'14-3490 (reversed) and R4-407.

Navicular: **Character Na1**, proximal connection between both cuboid-facets in lateral view: 0, separated; 1, in contact trough a narrow connection; 2, well-connected (connection as high as the dorsal cuboid-facet). Figures in lateral view, from left to right: FMH'14-2714, FMH'14-3630 (reversed), and FMH'14-2722. **Character Na2**, dorso-lateral expansion of the ectocuneiform-facet in distal view: 0, short, leaving a gap with the dorso-lateral angle of the bone; 1, long, covering most of the angle Figures in distal view, from left to right: 05/101/225a-399 and FMH'14-2722.

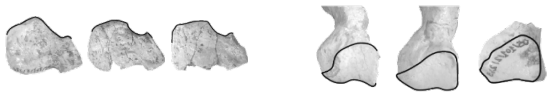
Mt II: **Character MtII1**, shape of the proximal side of the entocuneiform-facet: 0, rounded; 1, pointed. Figures in latero-plantar view, from left to right: 05/73-PG2-50 and FMH'14-2861. **Character MtII2**, outline of the Mt III(dor)-facet: 0, semicircular (usually accompanied by a smoother transition between Mt III(dor) and Ec(dor)); 1, triangular and pointed. Figures in lateral view, from left to right: FMH'14-3523 and FMH'14-2861 (reversed). **Character MtII3**, medial relieves of the diaphysis (this character can be observed along the whole diaphysis, but is particularly developed towards the epiphyseal regions): 0, faint; 1, rough. Figures in medial view, from left to right: FMH'14-419 and FMH'14-3523.

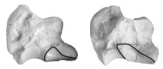
Mt III: Character MtIII1, development of the dorsal tendinous insertion in the proximal half of the diaphysis: 0, very developed and oblique, sometimes as a faint, double groove; 1, narrow and faint, sometimes restricted to the medial border; 2, absent. Figures in dorsal view, from left to right: FMH'14-877; FMH'14-3753 (reversed), and CMD-630. **Character MtIII2**, distal border of the distal Mt IV-facet: 0, straight to rouded; 1, concave. Figures in lateral view, from left to right: FMH'14-3117 and FMH'14-877.

Mt IV: **Character MtIV1**, medial border of the proximal cuboid-facet in proximal view . Figures in proximal view, from left to right: FMH'14-2915 (reversed) and FMH'14-2313. **Character MtIV2**, plantar tendinous insertion attached to the proximal epiphysis: 0, unique and wide; 2, multiple, tipically bifurcated; 3, unique and asymmetrical, displaced to the medial border. Figures in plantar view, from left to right: FMH'14-2313 (reversed) , FMH'14-2696, FMH'14-2915.

SUPPLEMENTARY DATA 4 (CONT.)

Intraspecific variability of *Hispanotherium matritense* in the localities of Fábrica Mahou, Príncipe Pío-2, Fresno del Torote, Yunquera del Tajo, Embajadores-R, and Casa de Campo / Marqués de Monistrol M-30. Each character is represented as number of individuals displaying the character / proportion of individuals displaying the character. Both are calculated from the whole sample.

	Magnum								Semilunate							Pisiform							
																							
Character code (Supp. Data 3)	Ma1-0	Ma1-1	Ma1-2	n	Ma2-0	Ma2-1	Ma2-2	n	Lu1-0	Lu1-1	Lu1-2	n	Lu2-0	Lu2-1	n	Pi1-0	Pi1-1	Pi1-2	n	Pi2-0	Pi2-1	Pi2-2	n
C. de Campo/M. de Monistrol M-30	1 / 50%	1 / 50%	0 / 00%	2	0 / 00%	2 / 67%	1 / 33%	3	1 / 33%	1 / 33%	1 / 33%	3	1 / 100%	0 / 00%	1	-	-	-	-	-	-	-	-
Embajadores-R	-	-	-	-	-	-	-	-	-	-	-	-	-	-	-	-	-	-	-	-	-	-	-
Fresno del Torote	-	-	-	-	-	-	-	-	0 / 00%	1 / 100%	0 / 00%	1	1 / 100%	0 / 00%	1	-	-	-	-	-	-	-	-
Fábrica Mahou	3 / 50%	2 / 33%	1 / 17%	6	4 / 57%	3 / 43%	0 / 00%	7	2 / 29%	5 / 71%	0 / 00%	7	4 / 80%	1 / 20%	5	4 / 80%	0 / 00%	1 / 20%	5	1 / 17%	3 / 50%	2 / 33%	6
Príncipe Pío-2	5 / 56%	4 / 44%	0 / 00%	9	11 / 55%	7 / 35%	2 / 10%	20	7 / 37%	10 / 53%	2 / 11%	19	5 / 83%	1 / 17%	6	7 / 70%	2 / 20%	1 / 10%	10	3 / 21%	9 / 64%	2 / 14%	14
Yunquera de Tajo	-	-	-	-	-	-	-	-	-	-	-	-	-	-	-	-	-	-	-	-	-	-	-
TOTAL individuals	9 / 53%	7 / 41%	1 / 6%	17	15 / 50%	12 / 40%	3 / 10%	30	10 / 34%	16 / 55%	3 / 10%	29	10 / 83%	2 / 17%	13	11 / 73%	2 / 13%	2 / 13%	15	4 / 20%	12 / 60%	4 / 20%	20

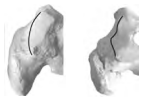
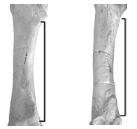
	Pyramidal								Trapezoid			Scaphoid			Unciform					
																				
Character code (Supp. Data 3)	Py1-0	Py1-1	Py1-2	n	Py2-0	Pi2-1	Pi2-2	n	Tz1-0	Tz1-1	n	Sc1-0	Sc1-1	n	Un1-0	Un1-1	n	Un2-0	Un2-1	n
C. de Campo/M. de Monistrol M-30	0 / 00%	2 / 100%	0 / 00%	2	-	-	-	-	0 / 00%	2 / 100%	2	1 / 100%	0 / 00%	1	3 / 75%	1 / 25%	4	1 / 100%	0 / 00%	1
Embajadores-R	-	-	-	-	-	-	-	-	-	-	-	-	-	-	-	-	-	-	-	-
Fresno del Torote	-	-	-	-	-	-	-	-	-	-	-	-	-	-	-	-	-	-	-	-
Fábrica Mahou	0 / 00%	11 / 92%	1 / 08%	12	5 / 56%	4 / 44%	0 / 00%	9	3 / 43%	4 / 57%	7	2 / 67%	1 / 33%	3	4 / 67%	2 / 33%	6	2 / 50%	2 / 50%	4
Príncipe Pío-2	4 / 27%	9 / 60%	2 / 13%	15	13 / 68%	5 / 26%	1 / 05%	19	6 / 46%	7 / 54%	13	7 / 54%	6 / 46%	13	3 / 20%	12 / 80%	15	6 / 46%	7 / 54%	13
Yunquera de Tajo	-	-	-	-	-	-	-	-	-	-	-	-	-	-	-	-	-	-	-	-
TOTAL individuals	4 / 14%	22 / 76%	3 / 10%	29	19 / 66%	9 / 31%	1 / 03%	29	9 / 41%	13 / 59%	22	10 / 59%	7 / 41%	17	10 / 40%	15 / 60%	25	9 / 50%	9 / 50%	18

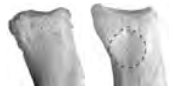
SUPPLEMENTARY DATA 4 (CONT.)

	Mc II													Mc III								
																					
Character code (Supp. Data 3)	McII1-0	McII1-1	n	Mc II2-0	Mc II2-1	n	Mc II3-0	Mc II3-1	n	Mc II4-0	Mc II4-1	Mc II4-2	n	McIII1-0	McIII1-1	McIII1-2	McIII1-3	n	McIII2-0	McIII2-1	n
C. de Campo/M. de Monistrol M-30	2 / 67%	1 / 33%	3	4 / 100%	0 / 00%	4	0 / 00%	2 / 100%	2	0 / 00%	3 / 75%	1 / 25%	4	1 / 20%	2 / 40%	0 / 00%	2 / 40%	5	1 / 33%	2 / 67%	3
Embajadores-R	-	-	-	-	-	-	-	-	-	-	-	-	-	-	-	-	-	-	-	-	-
Fresno del Torote	-	-	-	-	-	-	-	-	-	-	-	-	-	-	-	-	-	-	-	-	-
Fábrica Mahou	2 / 20%	8 / 80%	10	2 / 18%	9 / 82%	11	5 / 83%	1 / 17%	6	2 / 17%	6 / 50%	4 / 33%	12	7 / 41%	6 / 35%	3 / 18%	1 / 06%	17	7 / 54%	6 / 46%	13
Príncipe Pío-2	3 / 30%	7 / 70%	10	6 / 55%	5 / 45%	11	7 / 78%	2 / 22%	9	4 / 44%	1 / 11%	4 / 44%	9	1 / 09%	8 / 73%	0 / 00%	2 / 18%	11	5 / 63%	3 / 38%	8
Yunquera de Tajo	-	-	-	-	-	-	-	-	-	-	-	-	-	-	-	-	-	-	-	-	-
TOTAL individuals	7 / 30%	16 / 70%	23	12 / 46%	14 / 54%	26	12 / 71%	5 / 29%	17	6 / 67%	10 / 40%	9 / 36%	25	9 / 27%	16 / 48%	3 / 9%	5 / 15%	33	13 / 54%	11 / 46%	24

	Astragalus												Calcaneum												
																								
Character code (Supp. Data 3)	As1-0	As1-1	n	As2-0	As2-1	n	As3-0	As3-1	n	As4-0	As4-1	n	Ca1-0	Ca1-1	Ca1-2	n	Ca2-0	Ca2-1	Ca2-2	Ca2-3	n	Ca3-0	Ca3-1	n
C. de Campo/M. de Monistrol M-30	3 / 50%	3 / 50%	6	4 / 67%	2 / 33%	6	1 / 20%	4 / 80%	5	2 / 50%	2 / 50%	4	-	-	-	-	-	-	-	-	-	-	-	-
Embajadores-R	0 / 00%	1 / 100%	1	1 / 100%	0 / 00%	1	1 / 100%	0 / 00%	1	0 / 00%	1 / 100%	1	-	-	-	-	-	-	-	-	-	-	-	-
Fresno del Torote	-	-	-	-	-	-	-	-	-	-	-	-	-	-	-	-	-	-	-	-	-	-	-	-
Fábrica Mahou	11 / 65%	6 / 35%	17	3 / 17%	15 / 83%	18	7 / 44%	9 / 56%	16	11 / 65%	6 / 35%	17	3 / 25%	6 / 50%	3 / 25%	12	6 / 50%	2 / 17%	3 / 25%	1 / 08%	12	6 / 50%	6 / 50%	12
Príncipe Pío-2	4 / 14%	24 / 86%	28	10 / 34%	19 / 66%	29	17 / 57%	13 / 43%	30	19 / 66%	10 / 34%	29	0 / 00%	11 / 79%	3 / 21%	14	4 / 40%	1 / 10%	1 / 10%	4 / 40%	10	10 / 91%	1 / 09%	11
Yunquera de Tajo	-	-	-	-	-	-	-	-	-	-	-	-	-	-	-	-	-	-	-	-	-	-	-	-
TOTAL individuals	18 / 35%	34 / 65%	52	18 / 33%	36 / 67%	54	26 / 50%	26 / 50%	52	32 / 63%	19 / 37%	51	3 / 12%	17 / 65%	6 / 23%	26	10 / 45%	3 / 14%	4 / 18%	5 / 23%	22	16 / 36%	7 / 16%	45

SUPPLEMENTARY DATA 4 (CONT.)

	Cuboid			Navicular							Mt II								
																			
Character code (Supp. Data 3)	Cb1-0	Cb1-1	n	Na1-0	Na1-1	Na1-2	n	Na2-0	Na2-1	n	MtII1-0	MtII1-1	n	MtII2-0	MtII2-1	n	MtII3-0	MtII3-1	n
C. de Campo/M. de Monistrol M-30	2 / 40%	3 / 60%	5	0 / 00%	1 / 100%	0 / 00%	1	2 / 100%	0 / 00%	2	-	-	-	-	-	-	1 / 100%	0 / 00%	0
Embajadores-R	-	-	-	-	-	-	-	-	-	-	-	-	-	-	-	-	-	-	-
Fresno del Torote	-	-	-	-	-	-	-	-	-	-	-	-	-	-	-	-	-	-	-
Fábrica Mahou	4 / 100%	0 / 00%	4	2 / 17%	6 / 50%	4 / 33%	12	6 / 46%	7 / 54%	13	2 / 50%	2 / 50%	4	2 / 50%	2 / 50%	4	3 / 75%	1 / 25%	4
Príncipe Pío-2	6 / 46%	7 / 54%	13	3 / 17%	3 / 17%	12 / 67%	18	18 / 95%	1 / 05%	19	6 / 67%	3 / 33%	9	5 / 63%	3 / 38%	8	7 / 88%	1 / 13%	8
Yunquera de Tajo	-	-	-	-	-	-	-	-	-	-	-	-	-	-	-	-	-	-	-
TOTAL individuals	12 / 55%	10 / 45%	22	5 / 16%	10 / 32%	16 / 52%	31	26 / 76%	8 / 24%	34	9 / 64%	5 / 36%	14	8 / 62%	5 / 38%	13	12 / 86%	2 / 14%	14

	Mt III							Mt IV							Mc IV									
																								
Character code (Supp. Data 3)	MtIII1-0	MtIII1-1	MtIII1-2	n	MtIII2-0	MtIII2-1	n	MtIV1-0	MtIV1-1	n	MtIV2-0	MtIV-1	MtIV2-2	n	McIV1-0	McIV1-1	n	McIV2-0	McIV2-1	n	McIV3-0	McIV3-1	n
C. de Campo/M. de Monistrol M-30	0 / 00%	2 / 50%	2 / 50%	4	1 / 50%	1 / 50%	2	0 / 00%	1 / 100%	1	1 / 100%	0 / 00%	0 / 00%	1	2 / 100%	0 / 00%	2	0 / 00%	2 / 100%	2	0 / 00%	2 / 100%	2
Embajadores-R	-	-	-	-	-	-	-	-	-	-	-	-	-	-	-	-	-	-	-	-	-	-	-
Fresno del Torote	-	-	-	-	-	-	-	-	-	-	-	-	-	-	-	-	-	-	-	-	-	-	-
Fábrica Mahou	3 / 21%	5 / 36%	6 / 43%	14	4 / 57%	3 / 43%	7	6 / 67%	3 / 33%	9	3 / 38%	3 / 38%	2 / 25%	8	0 / 00%	6 / 100%	6	7 / 100%	0 / 00%	7	3 / 50%	3 / 50%	6
Príncipe Pío-2	1 / 08%	3 / 23%	9 / 69%	13	7 / 88%	1 / 13%	8	2 / 22%	7 / 78%	9	4 / 44%	4 / 44%	1 / 11%	9	4 / 67%	2 / 33%	6	5 / 50%	5 / 50%	10	5 / 50%	5 / 50%	10
Yunquera de Tajo	0 / 00%	0 / 00%	1 / 100%	1	-	-	-	-	-	-	-	-	-	-	-	-	-	-	-	-	-	-	-
TOTAL individuals	4 / 13%	10 / 31%	18 / 56%	32	12 / 71%	5 / 29%	17	8 / 42%	11 / 58%	19	8 / 53%	7 / 47%	3 / 20%	15	6 / 43%	8 / 57%	14	12 / 63%	7 / 37%	19	8 / 44%	10 / 56%	18

SUPPLEMENTARY DATA 5

Individual table with the variations of *Hispanotherium matritense* in the localities of Fábrica Mahou, Príncipe Pío-2, Fresno del Torote, Yunquera del Tajo, Embajadores-R, and Casa de Campo / Marqués de Monistrol M-30. Each character (1, present / - not preserved)is represented as number of individuals displaying the character / proportion of individuals displaying the character. The first is calculated from the whole sample.

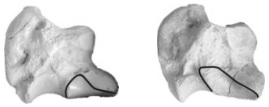
Magnum



Locality	Specimen	Ma1-0	Ma1-1	Ma1-2	n	Ma2-0	Ma2-1	Ma2-2	n
Príncipe Pío-2	PERCENTAGE (%)	55.56	44.44	0.00		55.00	35.00	10.00	
	n	5	4	0	9	11	7	2	20
	05/101/2/189	-	-	-			1		
	05/101/2/192		1			1			
	05/101/2/193	1						1	
	05/101/2/194	-	-	-		1			
	05/101/2/195	-	-	-		1			
	05/101/2/196	-	-	-		1			
	05/101/2/198	1						1	
	05/101/2/199		1			1			
	05/101/2/201		1				1		
	05/101/2/202	-	-	-			1		
	05/101/2/203	1					1		
	05/101/2/205	-	-	-		1			
	05/101/2/208	-	-	-		1			
	05/101/2/209	1				-	-	-	
	05/101/2/210	-	-	-		1			
	05/101/2/211	-	-	-			1		
	05/101/2/212	-	-	-		1			
	05/101/2/218	-	-	-			1		
	05/101/2/845	1				1			
	05/101/2/1191		1				1		
	05/101/2/3141	-	-	-		1			
C. de Campo/M. de Monistrol M-30	PERCENTAGE (%)	50.00	50.00	0.00		0.00	66.67	33.33	
	n	1	1	0	2	0	2	1	3
	R4-240	-	-	-			1		
	CMD-38	1						1	
	05/60/225A-124		1				1		
Fábrica Mahou	PERCENTAGE (%)	50.00	33.33	16.67		57.14	42.86	0.00	
	n	3	2	1	6	4	3	0	7
	FMH'14-2475	-	-	-			1		
	FMH'14-2634	1				1			
	FMH'14-2665	-	-	-			1		
	FMH'14-3104	1				1			
	FMH'14-4165		1			1			
	FMH'14-5021		1			-	-	-	
	FMH'14-5100	1				1			
	FMH'14-5419			1			1		
TOTALfos	PERCENTAGE (%)	52.94	41.18	5.88		50.00	40.00	10.00	
	N	9	7	1		15	12	3	
TOTALyac	PERCENTAGE (%)	51.85	42.59	5.56		37.38	48.17	14.44	

SUPPLEMENTARY DATA 5 (CONT.)

Scaphoid



Locality	Specimen	Sc1-0	Sc1-1	n
C. de Campo/M. de Monistrol M-30	PERCENTAGE (%)	100.00	0.00	
	n	1	0	1
	05/101/225a-168	1		
Príncipe Pío-2	PERCENTAGE (%)	53.85	46.15	
	n	7	6	13
	05/101/2/100	1		
	05/101/2/101		1	
	05/101/2/1587		1	
	05/101/2/197		1	
	05/101/2/7019		1	
	05/101/2/792	1		
	05/101/2/863		1	
	05/101/2/90	1		
	05/101/2/91	1		
	05/101/2/92		1	
	05/101/2/94	1		
	05/101/2/98	1		
	05/101/2/99	1		
Fábrica Mahou	PERCENTAGE (%)	66.67	33.33	
	n	2	1	3
	FMH'14-2740	1		
	FMH'14-3761	1		
	FMH'14-3978		1	
TOTALfos	PERCENTAGE (%)	58.82	41.18	
	N	10	7	17
TOTALyac	PERCENTAGE (%)	73.50	26.50	

SUPPLEMENTARY DATA 5 (CONT.)

Semilunate



Locality	Specimen	Lu1-0	Lu1-1	Lu1-2	n	Lu2-0	Lu2-1	n
Príncipe Pío-2	PERCENTAGE (%)	36.84	52.63	10.53		83.33	16.67	
	n	7	10	2	19	5	1	6
	05/101/2/102		1			-	-	
	05/101/2/103	1				-	-	
	05/101/2/104	1				1		
	05/101/2/105		1			-	-	
	05/101/2/106	1				-	-	
	05/101/2/107		1			-	-	
	05/101/2/108	1				-	-	
	05/101/2/1175	1				1		
	05/101/2/1183		1			-	-	
	05/101/2/191			1		-	-	
	05/101/2/2635		1			-	-	
	05/101/2/2751		1			-	-	
	05/101/2/2938		1			-	-	
	05/101/2/846	1				1		
	05/101/2/847		1				1	
	05/101/2/848		1			-	-	
	05/101/2/864			1		1		
	05/101/2/89	1				1		
	05/101/2/902		1			-	-	
Fresno del Torote	PERCENTAGE (%)	0.00	100.00	0.00		100.00	0.00	
	n	0	1	0	1	1	0	1
	FRT-1		1			1		
C. de Campo/M. de Monistrol M-30	PERCENTAGE (%)	33.33	33.33	33.33		100.00	0.00	
	n	1	1	1	3	1	0	1
	R4-220a			1		-	-	
	01/60/225a-398	1				-	-	
	CMD-559		1			1		
Fábrica Mahou	PERCENTAGE (%)	28.57	71.43	0.00		80.00	20.00	
	n	2	5	0	7	4	1	5
	FMH'14-2733		1			1		
	FMH'14-3071		1			-	-	
	FMH'14-3170	1				1		
	FMH'14-3173		1			1		
	FMH'14-3473		1				1	
	FMH'14-3629		1			1		
	FMH'14-3997	1				-	-	
TOTALfos	PERCENTAGE (%)	34.48	55.17	10.34		83.33	16.67	
	N	10	16	3	29	10	2	12
TOTALyac	PERCENTAGE (%)	32.92	52.46	14.62		87.78	12.22	

SUPPLEMENTARY DATA 5 (CONT.)

Pisiform



Locality	Specimen	Pi1-0	Pi1-1	Pi1-2	n	Pi2-0	Pi2-1	Pi2-2	n
Príncipe Pío-2	PERCENTAGE (%)	70.00	20.00	10.00		21.43	64.29	14.29	
	n	7	2	1	10	3	9	2	14
	05/101/2/220	1				1			
	05/101/2/223a		1				1		
	05/101/2/217			1		1			
	05/101/2/222	1					1		
	05/101/2/215	1					1		
	05/101/2/219	1						1	
	05/101/2/1588	-	-	-			1		
	05/101/2/1187		1				1		
	05/101/2/1179	1					1		
	05/101/2/216	-	-	-				1	
	05/101/2/7016	-	-	-			1		
	05/101/2/221	1					1		
	05/101/2/213	-	-	-		1			
	05/101/2/4	1					1		
Fábrica Mahou	PERCENTAGE (%)	80.00	0.00	20.00		16.67	50.00	33.33	
	n	4	0	1	5	1	3	2	6
	FMH'14-3045			1		1			
	FMH'14-3641	1						1	
	FMH'14-3720	1					1		
	FMH'14-3953	-	-	-			1		
	FMH'14-5347	1					1		
	FMH'14-2077	1						1	
TOTALfos	PERCENTAGE (%)	73.33	13.33	13.33		20.00	60.00	20.00	
	N	11	2	2	15	4	12	4	20
TOTALyac	PERCENTAGE (%)	75	10	15		19	57	24	

SUPPLEMENTARY DATA 5 (CONT.)

Pyramidal



Locality	Specimen	Py1-0	Py1-1	Py1-2	n	Py2-0	Py2-1	Py2-2	n
Príncipe Pío-2	PERCENTAGE (%)	26.67	60.00	13.33		68.42	26.32	5.26	
	n	4	9	2	15	13	5	1	19
	05/101/2/228								
	05/101/2/8	-	-	-		1			
	05/101/2/5			1		1			
	05/101/2/6		1			1			
	05/101/2/7017		1			1			
	05/101/2/17	-	-	-			1		
	05/101/2/842		1					1	
	05/101/2/15		1				1		
	05/101/2/11	1				1			
	05/101/2/4		1				1		
	05/101/2/7	1					1		
	05/101/862		1				1		
	05/101/2/14	1				1			
	05/101/2/118		1			1			
	05/101/2/1	1				1			
	05/101/2/2634		1			1			
	05/101/2/1177		1			1			
	05/101/2/904	-	-	-		1			
	05/101/2/2	-	-	-		1			
	05/101/2/3			1		1			
C. de Campo/M. de Monistrol M-30	PERCENTAGE (%)	0.00	100.00	0.00		100.00	0.00	0.00	
	n	0	2	0	2	1	0	0	1
	Seguimiento-468		1			-	-	-	
	CMD-92		1			1			
Fábrica Mahou	PERCENTAGE (%)	0.00	91.67	8.33		55.56	44.44	0.00	
	n	0	11	1	12	5	4	0	9
	FMH'14-2693		1			1			
	FMH'14-4181		1			1			
	FMH'14-3829		1			-	-	-	
	FMH'14-4228		1				1		
	FMH'14-3748		1				1		
	FMH'14-3080		1			1			
	FMH'14-3306	-	-	-		1			
	FMH'14-2989		1			1			
	FMH'14-2550		1			-	-	-	
	FMH'14-4042		1			-	-	-	
	FMH'14-4148		1				1		
	FMH'14-4145		1			-	-	-	
	FMH'14-3042			1			1		
TOTALfos	PERCENTAGE (%)	13.79	75.86	10.34		65.52	31.03	3.45	
	N	4	22	3	29	19	9	1	29
TOTALyac	PERCENTAGE (%)	8.89	83.89	7.22		74.66	23.59	1.75	

SUPPLEMENTARY DATA 5 (CONT.)

Unciform



Locality	Specimen	Un1-0	Un1-1	n	Un2-0	Un2-1	n
Príncipe Pío-2	PERCENTAGE (%)	20.00	80.00		46.15	53.85	
	n	3	12	15	6	7	13
	05/101/2/126						
	05/101/2/120		1		1		
	05/101/2/125		1			1	
	05/101/2/119		1			1	
	05/101/2/126		1		1		
	05/101/2/129		1		1		
	05/101/2/124		1		1		
	05/101/2/39		1			1	
	05/101/2/2841		1			1	
	05/101/2/w/n	1				1	
	05/101/2/130		1		-	-	
	05/101/2/123		1			1	
	05/101/2/137	1			-	-	
	05/101/2/133	1				1	
	05/101/2/118		1		1		
	05/101/2/127		1		1		
C. de Campo/M. de Monistrol M-30	PERCENTAGE (%)	75.00	25.00		100.00	0.00	
	n	3	1	4	1	0	1
	R4-94		1		1		
	CMD-648A	1			-	-	
	R4-204	1			-	-	
	R4-377	1			-	-	
Fábrica Mahou	PERCENTAGE (%)	66.67	33.33		50.00	50.00	
	n	4	2	6	2	2	4
	FMH'14-3059		1			1	
	FMH'14-2564	1			1		
	FMH'14-2675	1			-	-	
	FMH'14-2660	1			1		
	FMH'14-2307	-	-			1	
	FMH'14-3426	1			-	-	
	FMH'14-5197		1		-	-	
TOTALfos	PERCENTAGE (%)	40.00	60.00		50.00	50.00	
	N	10	15	25	9	9	18
TOTALyac	PERCENTAGE (%)	53.89	46.11		65.38	34.62	

SUPPLEMENTARY DATA 5 (CONT.)

Trapezoid



Locality	Specimen	Tz1-0	Tz1-1	n
Príncipe Pío-2	PERCENTAGE (%)	46.15	53.85	
	n	6	7	13
	05/101/2/110	1		
	05/101/2/841		1	
	05/101/2/114		1	
	05/101/2/109		1	
	05/101/2/905		1	
	05/101/2/839	1		
	05/101/2/113	1		
	05/101/2/3645	1		
	05/101/2/117	1		
	05/101/2/1190		1	
	05/101/2/111		1	
	05/101/2/116		1	
	05/101/2/112	1		
C. de Campo/M. de Monistrol M-30	PERCENTAGE (%)	0.00	100.00	
	n	0	2	2
	R4-173		1	
	05/60/225a-152		1	
Fábrica Mahou	PERCENTAGE (%)	42.86	57.14	
	n	3	4	7
	FMH'14-3838		1	
	FMH'14-2824	1		
	FMH'14-4030	1		
	FMH'14-3684		1	
	FMH'14-5230		1	
	FMH'14-2089	1		
	FMH'14-4077		1	
TOTALfos	PERCENTAGE	40.91	59.09	
	TODOS	9	13	22
TOTALyac	PERCENTAGE	29.67	70.33	

SUPPLEMENTARY DATA 5 (CONT.)

Cuboid



Locality	Specimen	Cb1-0	Cb1-1	n
Príncipe Pío-2	PERCENTAGE (%)	46.15	53.85	
	n	6	7	13
	05/101/2/63	1		
	05/101/2/72		1	
	05/101/2/77		1	
	05/101/2/69	1		
	05/101/2/67		1	
	05/101/2/865		1	
	05/101/2/71		1	
	05/101/2/64	1		
	05/101/2/2090	1		
	05/101/2/78		1	
	05/101/2/66	1		
	05/101/2/73	1		
	05/101/2/70		1	
C. de Campo/M. de Monistrol M-30	PERCENTAGE (%)	40.00	60.00	
	n	2	3	5
	CMD-634		1	
	CMD-615	1		
	R4-407	1		
	05/60/225a-87		1	
	05/60/225a-283		1	
Fábrica Mahou	PERCENTAGE (%)	100.00	0.00	
	n	4	0	4
	FMH'14-3538	1		
	FMH'14-3231	1		
	FMH'14-3250	1		
	FMH'14-3490	1		
TOTALfos	PERCENTAGE (%)	54.55	45.45	
	N	12	10	22
TOTALyac	PERCENTAGE (%)	62.05	37.95	

SUPPLEMENTARY DATA 5 (CONT.)

Navicular





Locality	Specimen	Na1-0	Na1-2	Na1-3	n	Na2-0	Na2-1	n
Príncipe Pío-2	PERCENTAGE (%)	16.67	16.67	66.67		94.74	5.26	
	n	3	3	12	18	18	1	19
	05/101/2/30			1		1		
	05/101/2/18			1		1		
	05/101/2/35			1		1		
	05/101/2/28			1		1		
	05/101/2/25		1				1	
	05/101/2/34			1		1		
	05/101/2/23			1		1		
	05/101/2/31		1			1		
	05/101/2/21			1		1		
	05/101/2/20	1				1		
	05/101/2/24	1				1		
	05/101/2/7018	1				1		
	05/101/2/39			1		1		
	05/101/2/873			1		-	-	
	05/101/2/26			1		1		
	05/101/2/22	-	-	-		1		
	05/101/2/37		1			1		
	05/101/2/19			1		1		
	05/101/2/27			1		1		
	05/101/2/35	-	-	-		1		
C. de Campo/M. de Monistrol M-30	PERCENTAGE (%)	0.00	100.00	0.00		100.00	0.00	
	n	0	1	0	1	2	0	2
	CMD-19		1			1		
	05/101/225a-399	-	-	-		1		
Fábrica Mahou	PERCENTAGE (%)	16.67	50.00	33.33		46.15	53.85	
	n	2	6	4	12	6	7	13
	FMH'14-4041	-	-	-		1		
	FMH'14-4932			1			1	
	FMH'14-2301			1		1		
	FMH'14-3883		1				1	
	FMH'14-3819		1				1	
	FMH'14-2722			1			1	
	FMH'14-4401		1			1		
	FMH'14-5121			1			1	
	FMH'14-3710		1			1		
	FMH'14-3053		1				1	
	FMH'14-3630	1				1		
	FMH'14-3072		1				1	
	FMH'14-2714	1				1		
TOTALfos	PERCENTAGE (%)	16.13	32.26	51.61		76.47	23.53	
	N	5	10	16	31	26	8	34
TOTALyac	PERCENTAGE (%)	11.11	55.56	33.33		80.30	19.70	

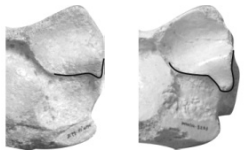
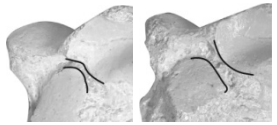
SUPPLEMENTARY DATA 5 (CONT.)

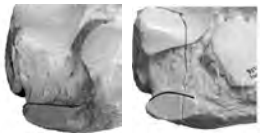
Mc III



Locality	Specimen	McIII1-0	McIII1-1	McIII1-2	McIII1-3	n	McIII2-0	McIII2-1	n
Príncipe Pío-2	PERCENTAGE (%)	9.09	72.73	0.00	18.18		62.50	37.50	
	n	1	8	0	2	11	5	3	8
	05/101/2/7015				1		-	-	
	05/101/2/480		1					1	
	05/101/2/428		1					1	
	05/101/2/1163		1				1		
	05/101/2/479		1					1	
	05/101/2/514	1					-	-	
	05/101/2/513		1				1		
	05/101/2/403		1				-	-	
	05/101/2/210b		1				1		
	05/101/2/450				1		1		
	05/101/2/482		1				1		
C. de Campo/M. de Monistrol M-30	PERCENTAGE (%)	20.00	40.00	0.00	40.00		33.33	66.67	
	n	1	2	0	2	5	1	2	3
	R4-255		1					1	
	05/60/255a/252				1		-	-	
	05/60/225a-309	1					1		
	05/60/225a-386				1			1	
	05/60/225a-446		1				-	-	
Fábrica Mahou	PERCENTAGE (%)	41.18	35.29	17.65	5.88		53.85	46.15	
	n	7	6	3	1	17	7	6	13
	FMH'14-527	1					1		
	FMH'14-1690			1			1		
	FMH'14-2094	1						1	
	FMH'14-2095	1					1		
	FMH'14-2306		1					1	
	FMH'14-2534		1				-	-	
	FMH'14-2910		1				1		
	FMH'14-2914				1		1		
	FMH'14-2937		1					1	
	FMH'14-2961		1				1		
	FMH'14-3134			1				1	
	FMH'14-3383		1					1	
	FMH'14-3410	1					-	-	
	FMH'14-3673	-	-	-	-		-	-	
	FMH'14-5297	1					1		
	FMH'14-5311	-	-	-	-		-	-	
	FMH'14-3806	-	-	-	-		-	-	
	FMH'14-4060			1				1	
	FMH'14-4414	1					-	-	
	FMH'14-5451	1					-	-	
TOTALfos	PERCENTAGE (%)	27.27	48.48	9.09	15.15		54.17	45.83	
	N	9	16	3	5	33	13	11	24
TOTALyac	PERCENTAGE (%)	30.59	37.65	8.82	22.94		43.59	56.41	

Astragalus



Locality	Specimen	As1-0	As1-1	n	As2-0	As2-1	n	As3-0	As3-1	n	As4-0	As4-1	n
Embajadores-R	PERCENTAGE (%)	0.00	100.00		100.00	0.00		100.00	0.00		0.00	100.00	
	n	0	1	1	1	0	1	1	0	1	0	1	1
	PG1-15		1		1			1				1	
Príncipe Pío-2	PERCENTAGE (%)	14.29	85.71		34.48	65.52		56.67	43.33		65.52	34.48	
	n	4	24	28	10	19	29	17	13	30	19	10	29
	05/101/2/2840		1		1			1			1		
	05/101/2/876		1			1		1			1		
	05/101/2/147		1			1			1		1		
	05/101/2/157		1			1		1			1		
	05/101/2/167		1		-	-		1			1		
	05/101/2/164		1			1		-	-		1		
	05/101/2/160	-	-			1		1			-	-	
	05/101/2/885	-	-		-	-		1			-	-	
	05/101/2/156		1		1			-	-		-	-	
	05/101/2/165		1		-	-			1		-	-	
	05/101/2/153		1			1			1			1	
	05/101/2/154	1				1		-	-			1	
	05/101/2/149		1			1		1				1	
	05/101/2/169	1			1			1			1		
	05/101/2/3647	-	-			1			1		1		
	05/101/2/158	-	-			1			1		1		
	05/101/2/159		1		1				1		-	-	
	05/101/2/163		1			1			1			1	
	05/101/2/146		1			1		1			1		
	05/101/2/143	-	-		1			1			-	-	
	05/101/2/3634	-	-		1				1			1	
	05/101/2/152		1		-	-		1			1		
	05/101/2/145		1		1			1			1		
	05/101/2/148	1				1		1			1		
	05/101/2/166	1				1		1			1		
	05/101/2/155	-	-		-	-		-	-			1	
	05/101/2/144		1			1			1		1		

	05/101/2/150		1			1		1			1		
	05/101/2/1219		1			1		1				1	
	05/101/2/884		1			1		-	-			1	
	05/101/2/170		1			1			1		1		
	05/101/2/151		1		1				1			1	
	05/101/2/142		1		1				1		1		
	05/101/2/346		1		-	-		1			1		
	05/101/2/162		1		1				1			1	
C. de Campo/M. de Monistrol M-30	PERCENTAGE (%)	50.00	50.00		66.67	33.33		20.00	80.00		50.00	50.00	
	n	3	3	6	4	2	6	1	4	5	2	2	4
	CMD-580	1				1			1		-	-	
	CMD-682		1		1				1		-	-	
	R4-7		1			1		-	-		1		
	R4-76		1		1			1			1		
	Seguimiento Monistrol-509	1			1				1			1	
	05/60/225a-123	1			1				1			1	
Fábrica Mahou	PERCENTAGE (%)	64.71	35.29		16.67	83.33		43.75	56.25		64.71	35.29	
	n	11	6	17	3	15	18	7	9	16	11	6	17
	FMH'14-646	1				1		1			1		
	FMH'14-2067		1		1				1			1	
	FMH'14-2109		1			1		-	-		1		
	FMH'14-2650		1			1		1			1		
	FMH'14-2871	-	-			1		-	-		1		
	FMH'14-3171	1				1		1				1	
	FMH'14-3203		1		1				1		1		
	FMH'14-3356		1			1		1			-	-	
	FMH'14-3512	1				1			1		1		
	FMH'14-3549	1			1				1		1		
	FMH'14-3717	1				1			1		1		
	FMH'14-3723	1				1			1			1	
	FMH'14-3757	1				1			1			1	
	FMH'14-3980	1				1			1		1		
	FMH'14-3981		1			1		1				1	
	FMH'14-4068	1				1			1		1		
	FMH'14-4482	1				1		1				1	
	FMH'14-4914	1				1		1			1		
TOTALfos	PERCENTAGE (%)	34.62	65.38		33.33	66.67		50.00	50.00		62.75	37.25	
	N	18	34	52	18	36	54	26	26	52	32	19	51
TOTALyac	PERCENTAGE (%)	32.25	67.75		54.45	45.55		55.10	44.90		45.06	54.94	

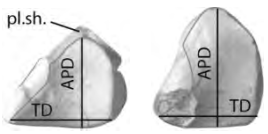
Mc II



Locality	Specimen	McII1-0	McII1-1	n	McII2-0	McII2-1	n	McII3-0	McII3-1	n	McII4-0	McII4-1	McII4-2	n
Príncipe Pío-2	PERCENTAGE (%)	30.00	70.00		54.55	45.45		77.78	22.22		44.44	11.11	44.44	
	n	3	7	10	6	5	11	7	2	9	4	1	4	9
	05/101/2/1194		1			1			1		1			
	05/101/2/7014	1			-	-		-	-		-	-	-	
	05/101/2/426	1				1			1				1	
	05/101/2/452		1		1			1					1	
	05/101/2/536	-	-		1			1			-	-	-	
	05/101/2/430	1				1		1			1			
	05/101/2/498		1		1			-	-		-	-	-	
	05/101/2/444		1			1		1				1		
	05/101/2/401		1		1			-	-		1			
	05/101/2/1151		1			1		1					1	
	05/101/2/1165	-	-		1			1					1	
	05/101/2/458		1		1			1			1			
C. de Campo/M. de Monistrol M-30	PERCENTAGE (%)	66.67	33.33		100.00	0.00		0.00	100.00		0.00	75.00	25.00	
	n	2	1	3	4	0	4	0	2	2	0	3	1	4
	50/60/225a-100	-	-		1			-	-			1		
	CMD-419		1		1				1			1		
	CMD-537	1			1			-	-			1		
	CMD-637	1			1				1				1	

Fábrica Mahou	PERCENTAGE (%)	20.00	80.00		18.18	81.82		83.33	16.67		16.67	50.00	33.33	
	n	2	8	10	2	9	11	5	1	6	2	6	4	12
	FMH'14-754	1				1		-	-		1			
	FMH'14-1975		1			1		1			1			
	FMH'14-2621	-	-		-	-		-	-				1	
	FMH'14-2698		1			1			1			1		
	FMH'14-3097	1				1		1					1	
	FMH'14-3098		1			1		1				1		
	FMH'14-4073		1			1		1				1		
	FMH'14-4941	-	-			1		-	-				1	
	FMH'14-5288		1		1			-	-			1		
	FMH'14-5269		1			1		-	-			1		
	FMH'14-5299		1		1			-	-				1	
	FMH'14-3830		1			1		1				1		
TOTALfos	PERCENTAGE (%)	30.43	69.57		46.15	53.85		70.59	29.41		66.67	40.00	36.00	
	N	7	16	23	12	14	26	12	5	17	6	10	9	25
TOTALyac	PERCENTAGE (%)	38.89	61.11		57.58	42.42		53.70	46.30		20.37	45.37	34.26	

Mc IV





Locality	Specimen	McIV1-0	McIV1-1	n	McIV2-0	McIV2-1	n	McIV3-0	McIV3-1	n
Príncipe Pío-2	PERCENTAGE (%)	66.67	33.33		50.00	50.00		50.00	50.00	
	n	4	2	6	5	5	10	5	5	10
	05/101/2/1195a	1				1			1	
	05/101/2/7013	-	-		1				1	
	05/101/2/7012	-	-			1		-	-	
	05/101/2/442	-	-		-	-		1		
	05/101/2/425	-	-		1			-	-	
	05/101/2/448		1		1			1		
	05/101/2/400	-	-			1		-	-	
	05/101/2/210a	1			-	-		1		
	05/101/2/453	1			1				1	
	05/101/2/457		1		1				1	
	05/101/2/414	-	-		-	-		1		
	05/101/2/1152	-	-			1		1		
	05/101/2/429	1				1			1	
C. de Campo/M. de Monistrol M-30	PERCENTAGE (%)	100.00	0.00		0.00	100.00		0.00	100.00	
	n	2	0	2	0	2	2	0	2	2
	05/60/225a-5	-	-		1			1		
	CMD-398	1				1			1	
	CMD-340	1				1			1	
Fábrica Mahou	PERCENTAGE (%)	0.00	100.00		100.00	0.00		50.00	50.00	
	n	0	6	6	7	0	7	3	3	6
	FMH'14-3130		1		1			1		
	FMH'14-1063	33.47	1		1				1	
	FMH'14-2901		1		1			1		
	FMH'14-3061		1		1			1		
	FMH'14-3633		1		1				1	
	FMH'14-4538	-	-		1			-	-	
	FMH'14-5444		1		1				1	
TOTALfos	PERCENTAGE (%)	42.86	57.14		63.16	36.84		44.44	55.56	
	N	6	8	14	12	7	19	8	10	18
TOTALyac	PERCENTAGE (%)	55.56	44.44		50.00	50.00		33.33	66.67	

Mt II



Locality	Specimen	MtII1-0	MtII1-1	n	MtII2-0	MtII2-1	n	MtII3-0	MtII3-1	n
Embajadores-R	PERCENTAGE (%)	100.00	0.00		100.00	0.00		100.00	0.00	
	n	1	0	1	1	0	1	1	0	1
	05/73-PG4-030	1			1			1		
Príncipe Pío-2	PERCENTAGE (%)	66.67	33.33		62.50	37.50		87.50	12.50	
	n	6	3	9	5	3	8	7	1	8
	05/101/2/7025		1		-	-			1	
	05/101/2/411	-	-		1			1		
	05/101/2/443	1				1		1		
	05/101/2432	1			1			1		
	05/101/2/424	1			1			1		
	05/101/2/1155	1			1			1		
	05/101/2/465	1			1			1		
	05/101/2/447		1			1		1		
	05/101/2/520	1			-	-		-	-	
	05/101/2/421		1			1		-	-	
C. de Campo/M. de Monistrol M-30	PERCENTAGE (%)	-	-		-	-		100.00	0.00	
	n	0	0	0	0	0	0	1	0	1
	CMD-33	-	-		-	-		1		
Fábrica Mahou	PERCENTAGE (%)	50.00	50.00		50.00	50.00		75.00	25.00	
	n	2	2	4	2	2	4	3	1	4
	FMH'14-419		1		1			1		
	FMH'14-2861		1		1			1		
	FMH'14-2953	1				1		1		
	FMH'14-3523	1				1			1	
TOTALfos	PERCENTAGE (%)	64.29	35.71		61.54	38.46		85.71	14.29	
	N	9	5	14	8	5	13	12	2	14
TOTALyac	PERCENTAGE (%)	75.00	25.00		75.00	25.00		87.50	12.50	

SUPPLEMENTARY DATA 5 (CONT.)

Mt III



Locality	Specimen	MtIII1-0	MtIII1-1	MtIII1-2	n	MtIII2-0	MtIII2-1	n
Yunquera de Tajo	PERCENTAGE (%)	0.00	0.00	100.00	1	-	-	
	n	0	0	1		0	0	0
	YU-1			1		-	-	
Príncipe Pío-2	PERCENTAGE (%)	7.69	23.08	69.23		87.50	12.50	
	n	1	3	9	13	7	1	8
	05/101/2/7024			1		1		
	05/101/2/1154		1			1		
	05/101/2/2258			1		-	-	
	05/101/2/467	1					1	
	05/101/2/490		1			1		
	05/101/2/478			1		1		
	05/101/2/456		1			-	-	
	05/101/2/416			1		-	-	
	05/101/2/433			1		-	-	
	05/101/2/406			1		1		
	05/101/2/431			1		1		
	05/101/2/404			1		1		
	05/101/2/500			1		-	-	
C. de Campo/M. de Monistrol M-30	PERCENTAGE (%)	0.00	50.00	50.00		50.00	50.00	
	n	0	2	2	4	1	1	2
	05/101/225a-95			1		-	-	
	05/101/225a-382		1			-	-	
	R4-223		1			1		
	CMD-630			1			1	
Fábrica Mahou	PERCENTAGE (%)	21.43	35.71	42.86		57.14	42.86	
	n	3	5	6	14	4	3	7
	FMH'14-877	1					1	
	FMH'14-689	1				-	-	
	FMH'14-2115			1		-	-	
	FMH'14-2585			1		-	-	
	FMH'14-2977	1					1	
	FMH'14-3117		1			1		
	FMH'14-3527		1			1		
	FMH'14-3753		1				1	
	FMH'14-3779		1			1		
	FMH'14-4078			1		-	-	
	FMH'14-4449			1		-	-	
	FMH'14-5266		1			1		
	FMH'14-5394			1		-	-	
	FMH'14-5432			1		-	-	
TOTALfos	PERCENTAGE (%)	12.50	31.25	56.25		70.59	29.41	
	N	4	10	18	32	12	5	17
TOTALyac	PERCENTAGE (%)	7.28	27.20	65.52		64.88	35.12	

SUPPLEMENTARY DATA 5 (CONT.)

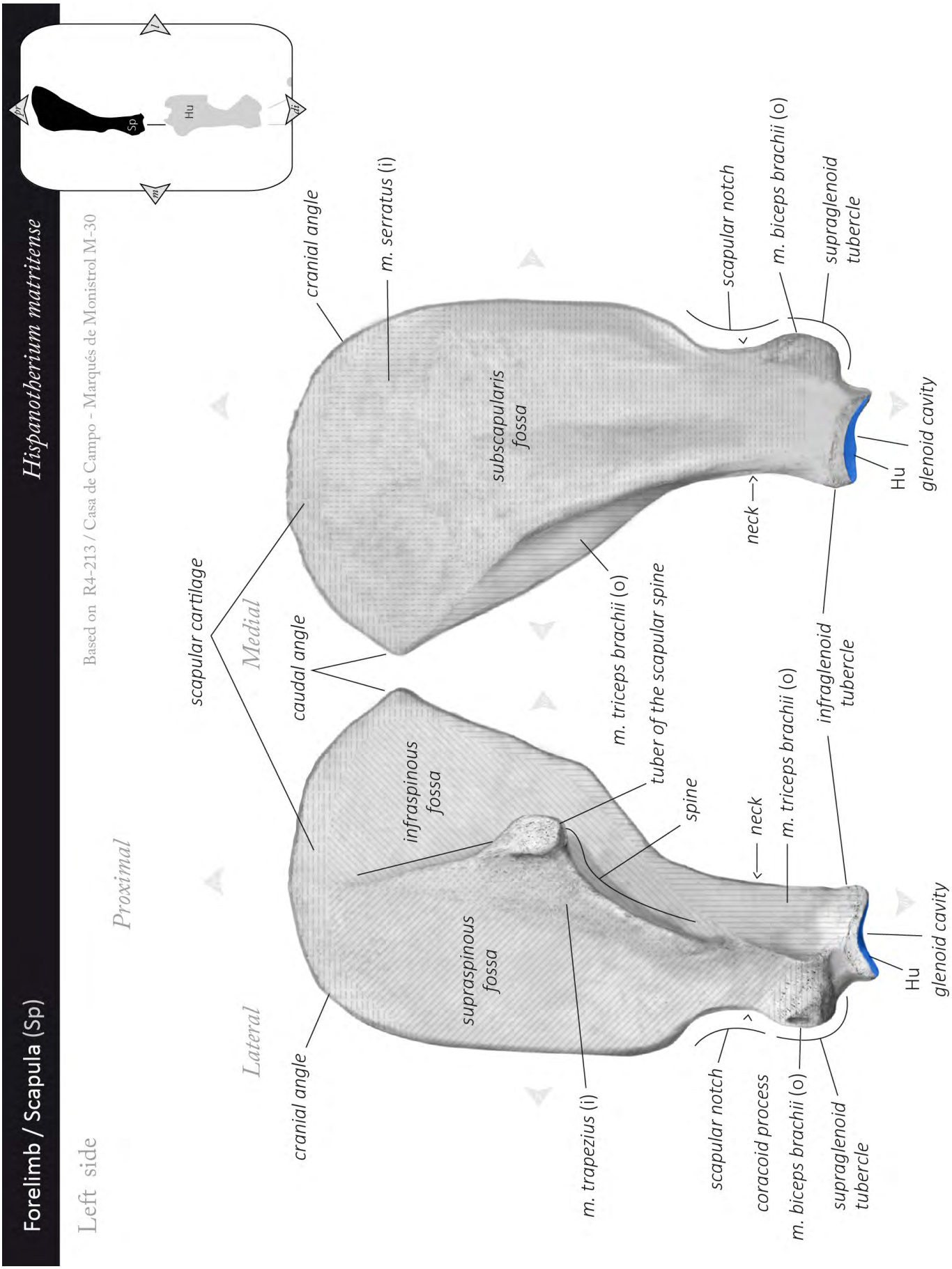
Mt IV

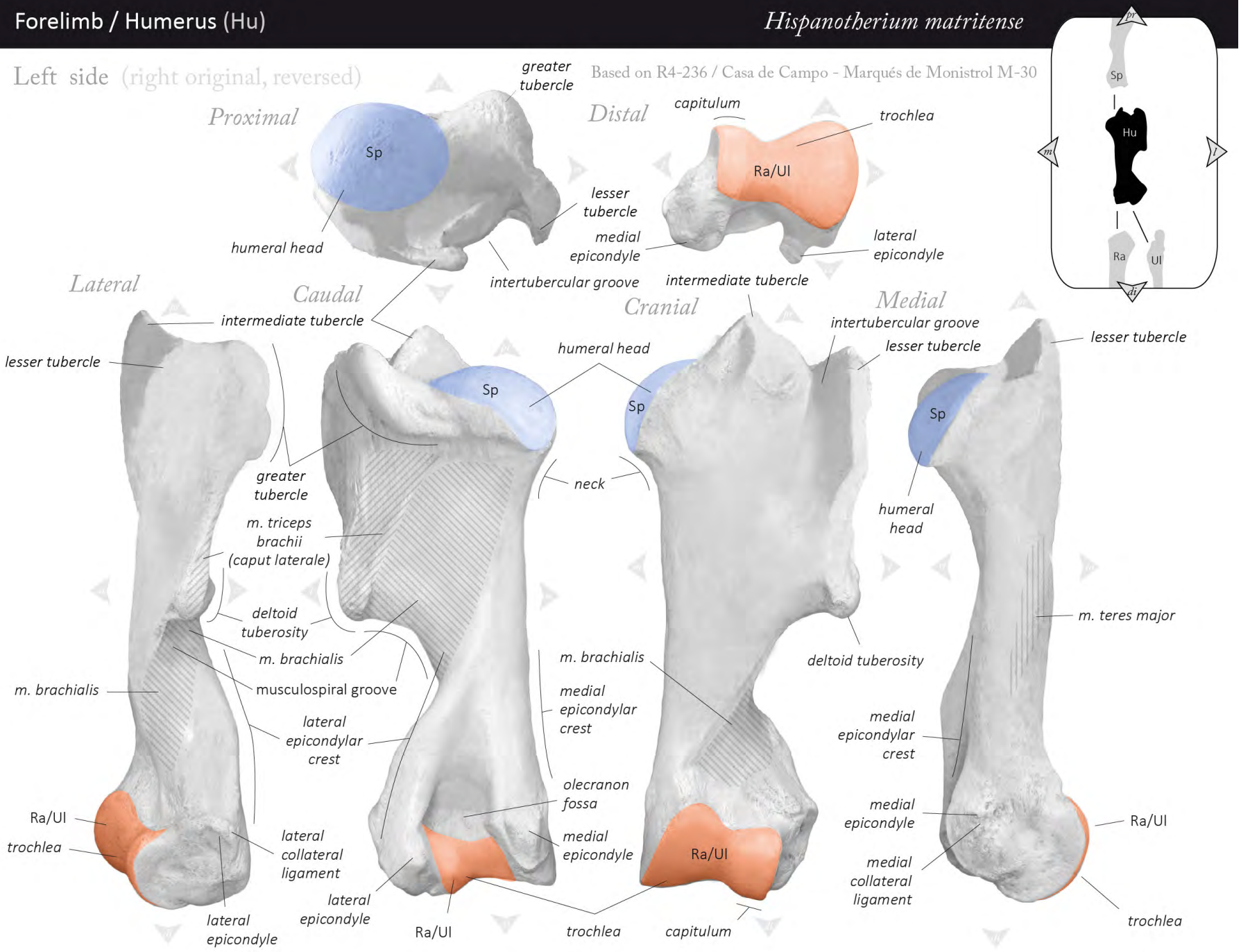


Locality	Specimen	MtIV1-0	MtIV1-1	n	MtIV2-0	MtIV2-1	MtIV2-2	n
Príncipe Pío-2	PERCENTAGE (%)	22.22	77.78		44.44	44.44	11.11	
	n	2	7	9	4	4	1	9
	05/101/2/3235a		1		1			
	05/101/2/875		1		1			
	05/101/2/7023		1			1		
	05/101/2/481	1				1		
	05/101/2/434		1		1			
	05/101/2/470		1			1		
	05/101/2/524	1			1			
	05/101/2/523		1			1		
	05/101/2/461		1				1	
C. de Campo/M. de Monistrol M-30	PERCENTAGE (%)	0.00	100.00		100.00	0.00	0.00	
	n	0	1	1	1	0	0	1
	CMD-264		1		1			
Fábrica Mahou	PERCENTAGE (%)	66.67	33.33		37.50	37.50	25.00	
	n	6	3	9	3	3	2	8
	FMH'14-2941	1					1	
	FMH'14-2212		1		1			
	FMH'14-2313		1		1			
	FMH'14-2696	1				1		
	FMH'14-2915	1			1			
	FMH'14-3106	1				1		
	FMH'14-3041	1			-	-	-	
	FMH'14-5223	1			-	-	-	
	FMH'14-5272		1			1		
	FMH'14-5407	-	-				1	
TOTALfos	PERCENTAGE (%)	42.11	57.89		53.33	46.67	20.00	
	N	8	11	19	8	7	3	15
TOTALyac	PERCENTAGE (%)	29.63	70.37		60.65	27.31	12.04	

SUPPLEMENTARY DATA 6

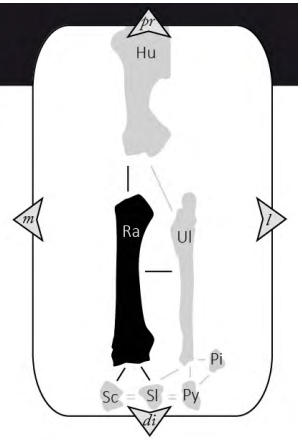
Osteology of *Hispanotherium matritense*




Left side (right original, reversed)
Based on R4-236 / Casa de Campo - Marqués de Monistrol M-30
Proximal
Distal
Lateral
Caudal
Cranial
Medial
Sp
Hu
Ra
Ul
pr
di
l
m
humeral head
greater tubercle
lesser tubercle
intertubercular groove
capitulum
trochlea
Ra/Ul
medial epicondyle
lateral epicondyle
intermediate tubercle
neck
m. triceps brachii (caput laterale)
deltoid tuberosity
m. brachialis
musculospiral groove
lateral epicondylar crest
olecranon fossa
medial epicondylar crest
m. teres major
medial collateral ligament
lateral collateral ligament
trochlea
capitulum

Left side (right original, reversed)

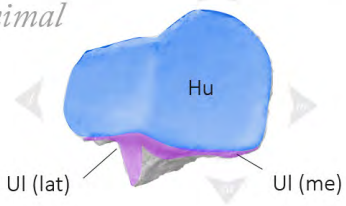
Based on CMD-635 / Casa de Campo - Marqués de Monistrol M-30



Distal



Proximal



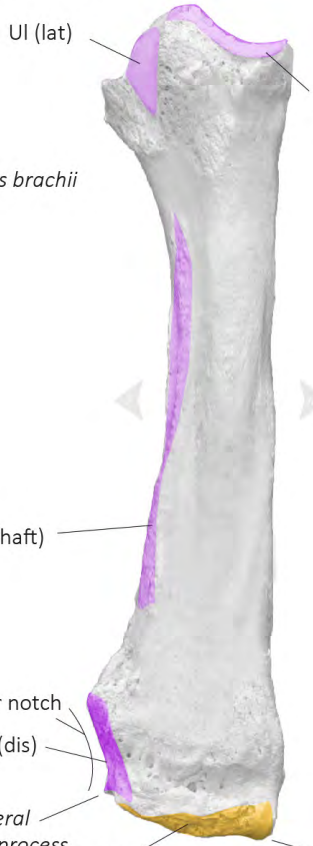
Lateral



Cranial



Caudal



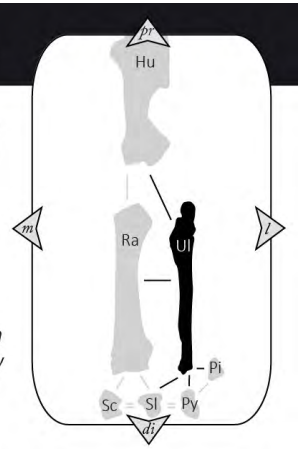
Medial

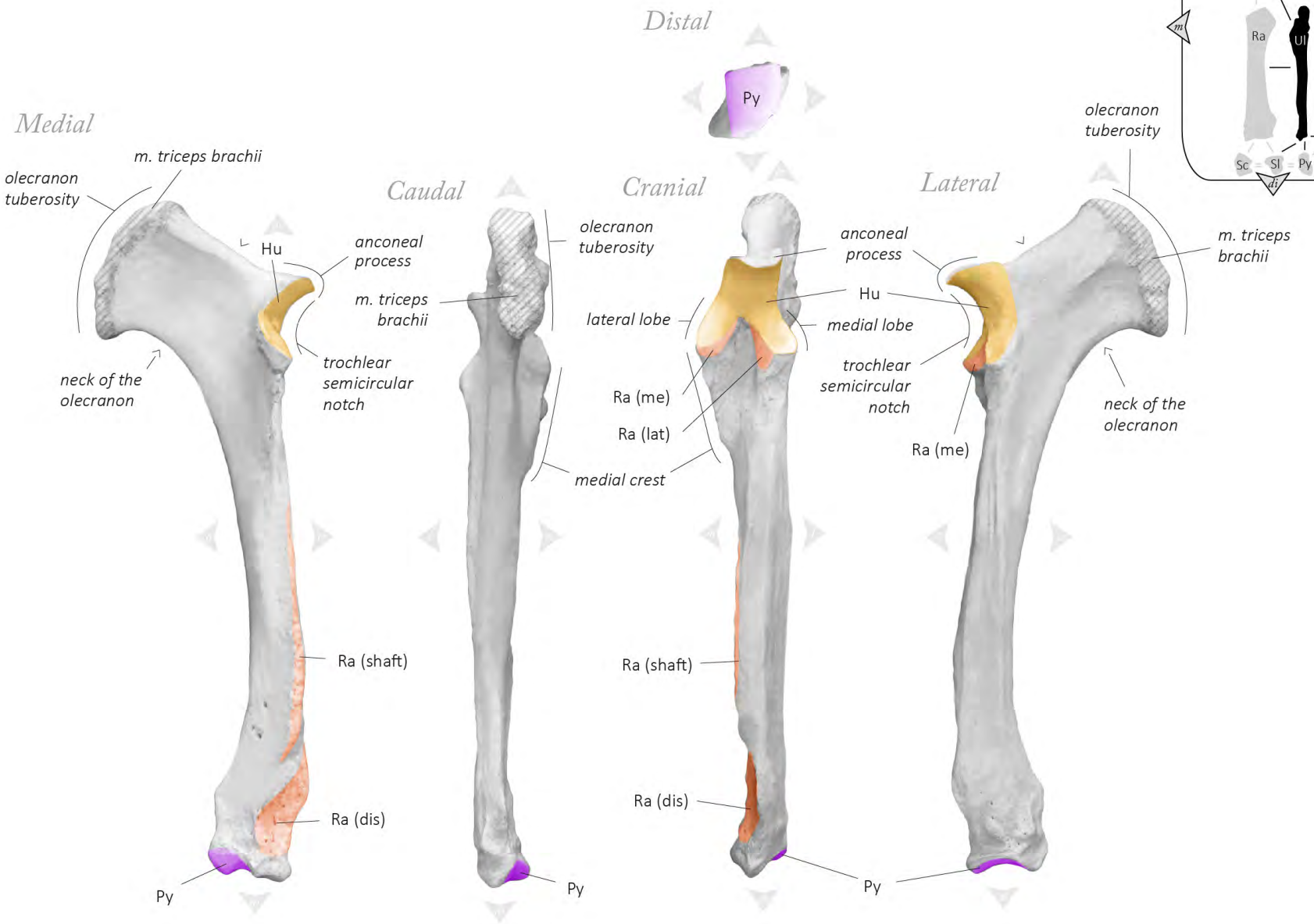


Hispanotherium matritense

Left side (right original, reversed)

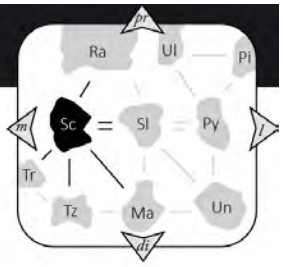
Based on R4-324 / Casa de Campo - Marqués de Monistrol M-30





Manus / Scaphoid (Sc)

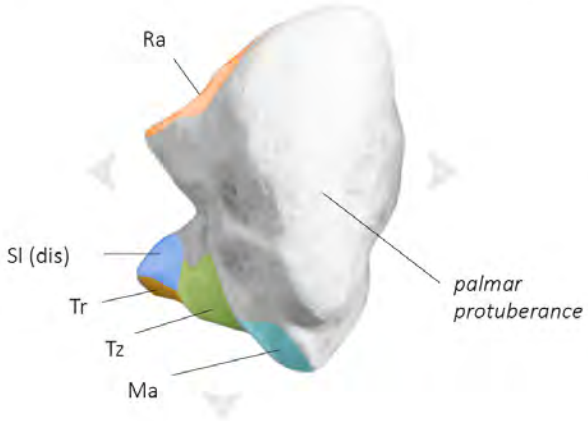
Hispanotherium matritense



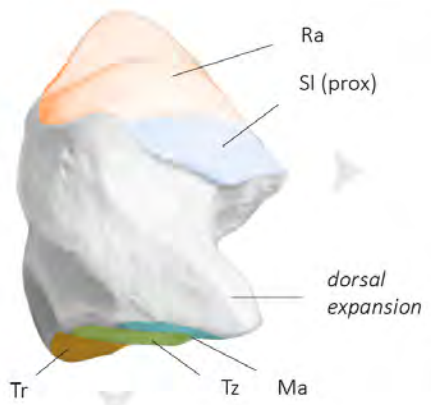
Left side (right original, reversed)

Based on FMH'14-3740 / Fábrica Mahou

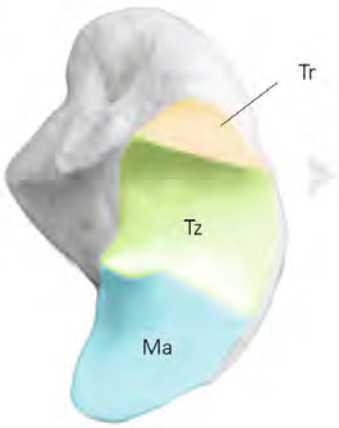
Palmar



Dorsal



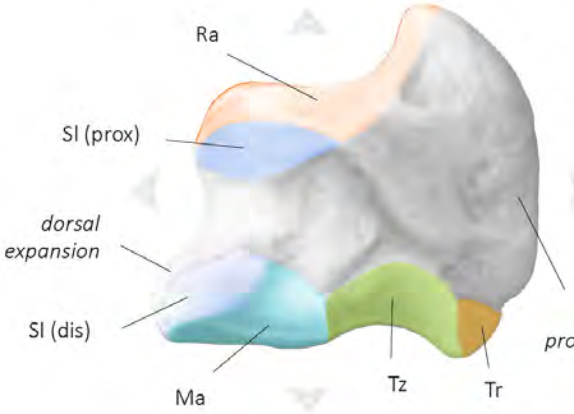
Distal



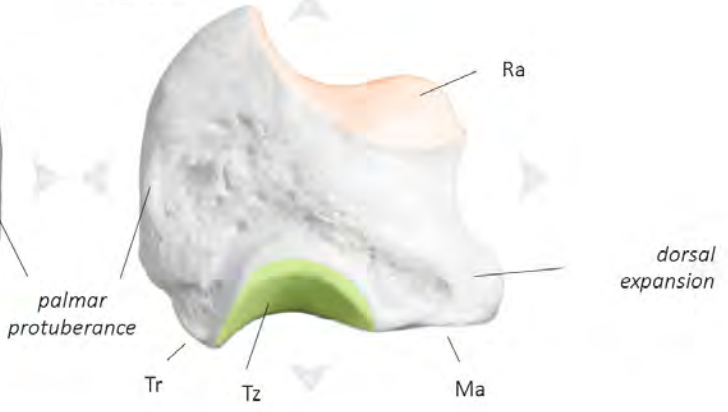
Proximal



Lateral

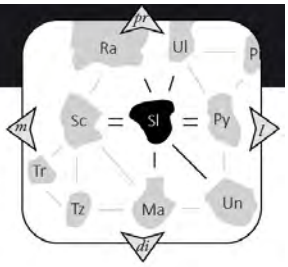


Medial



Manus / Semilunate (Sl)

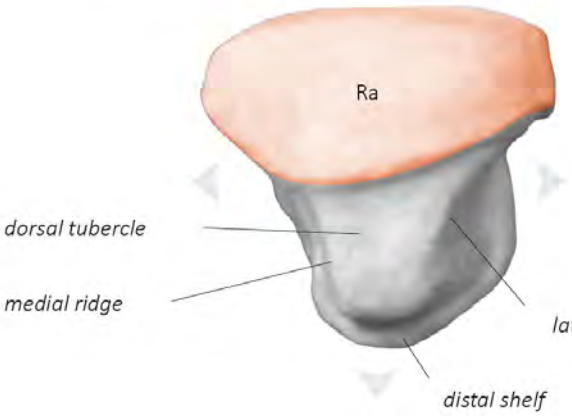
Hispanotherium matritense



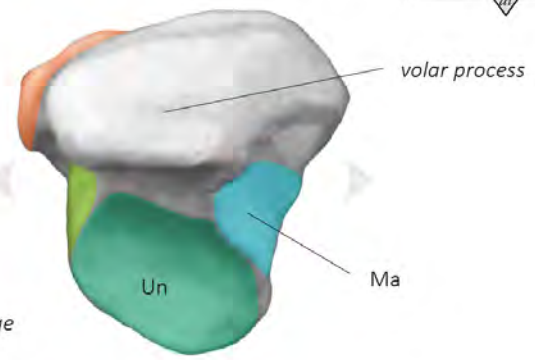
Left side

Based on / Casa de Campo - Marqués de Monistrol M-30

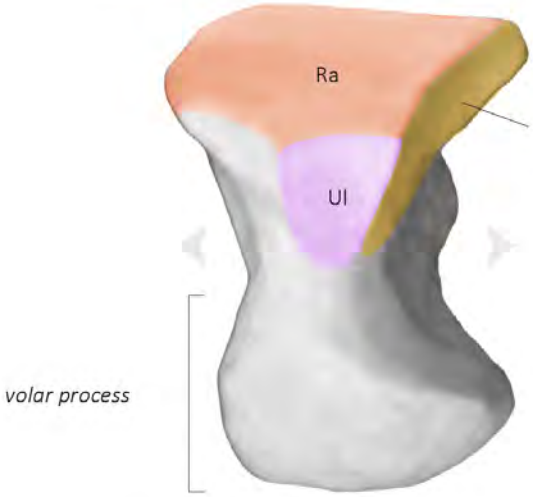
Dorsal



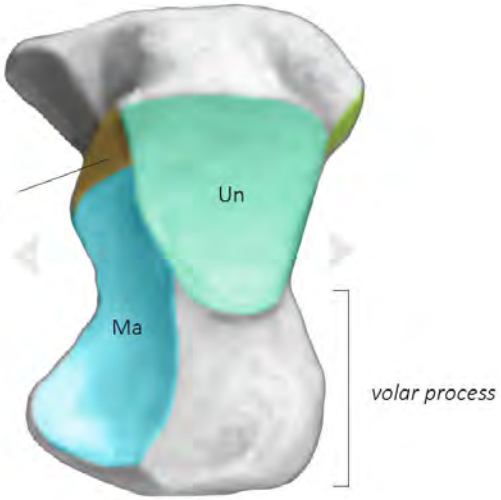
Palmar



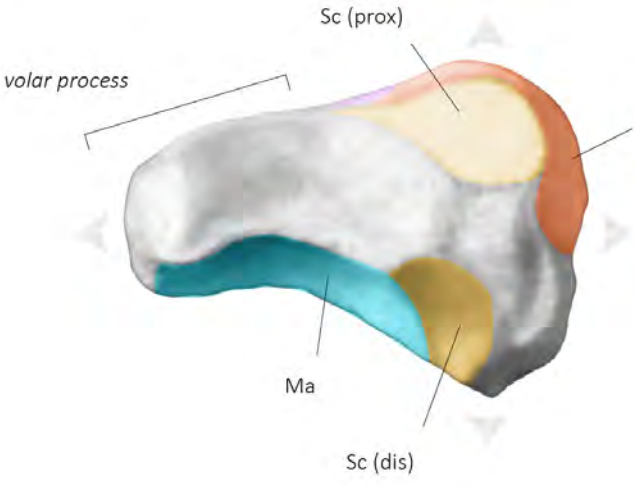
Proximal



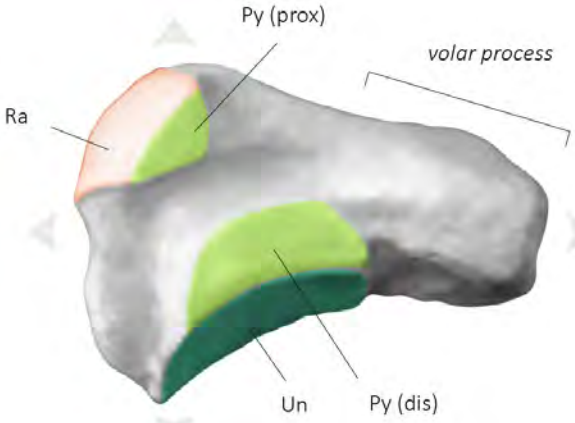
Distal



Medial

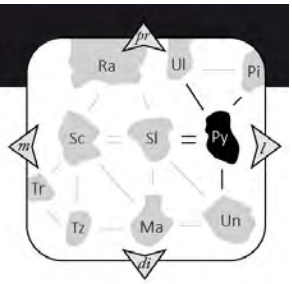


Lateral



Manus / Pyramidal (Py)

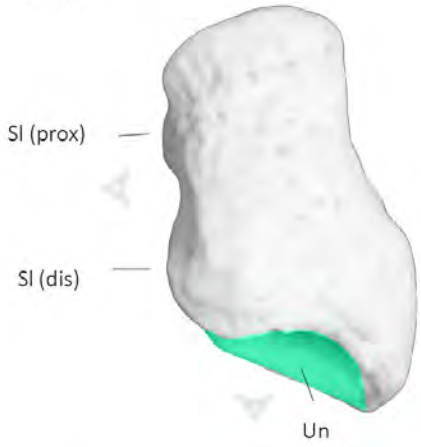
Hispanotherium matritense



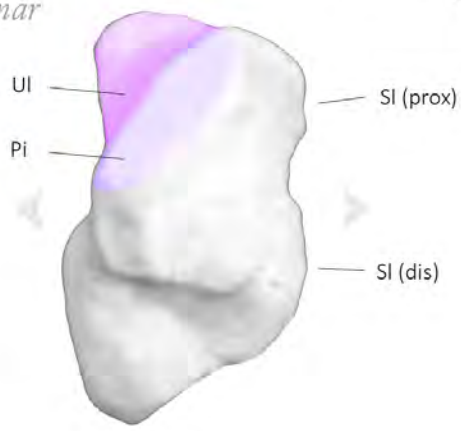
Left side
(right original, reversed)

Based on / Casa de Campo - Marqués de Monistrol M-30

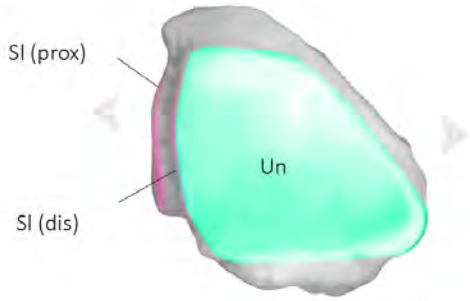
Dorsal



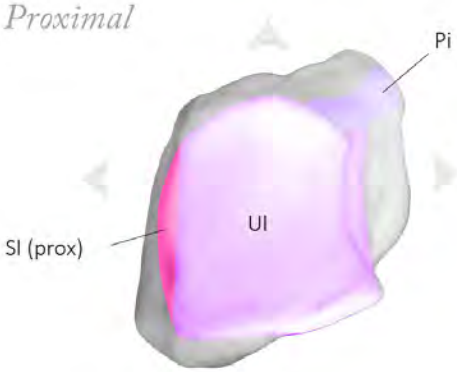
Palmar



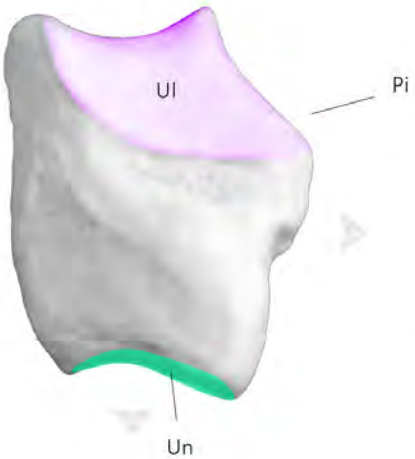
Distal



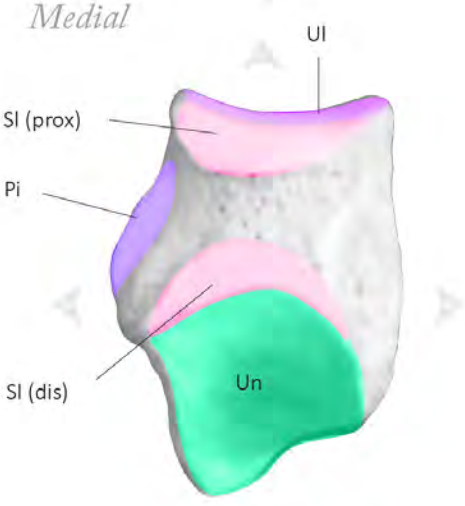
Proximal



Lateral



Medial

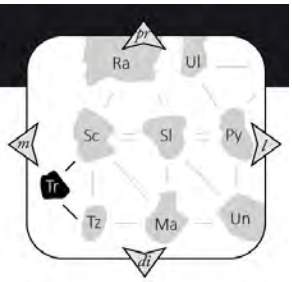


Manus / Trapezium (Tz)

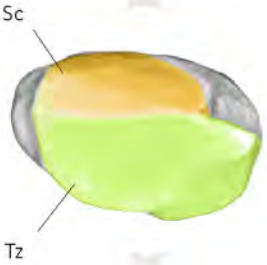
Hispanotherium matritense

Left side (right original, reversed)

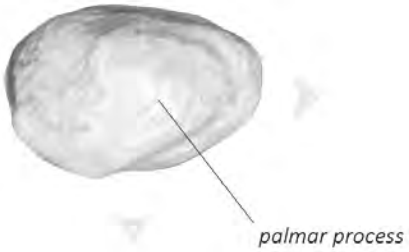
Based on FMH'14-3199 / Fábrica Mahou



Dorsal



Palmar



Proximal



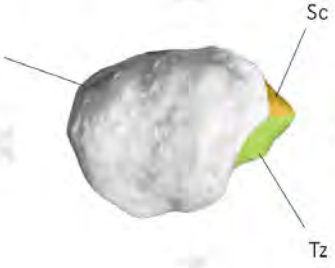
Distal



Lateral



Medial

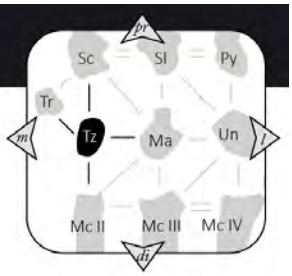


Manus / Trapezoid (Tz)

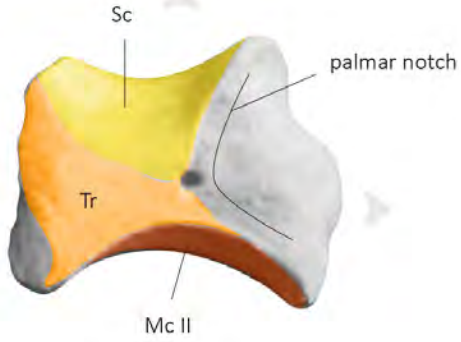
Hispanotherium matritense

Left side

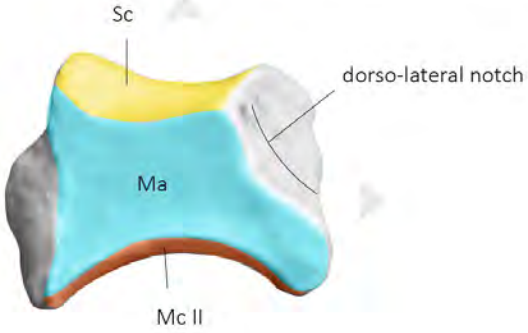
Based on FMH'14-4036 / Fábrica Mahou



Palmar



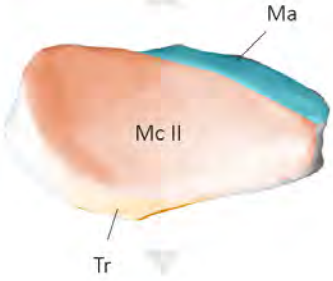
Dorsal



Proximal



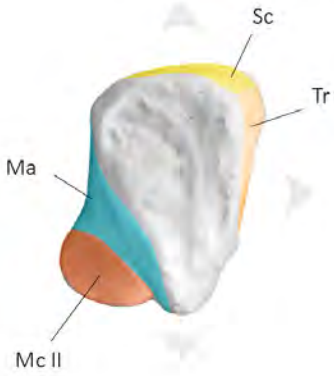
Distal



Medial



Lateral

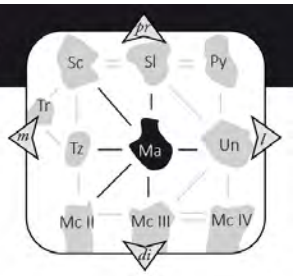


Manus / Magnum (Ma)

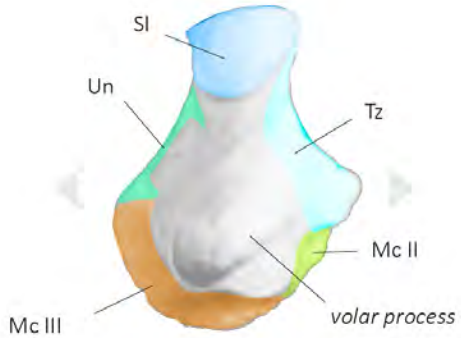
Hispanotherium matritense

Left side (right original, reversed)

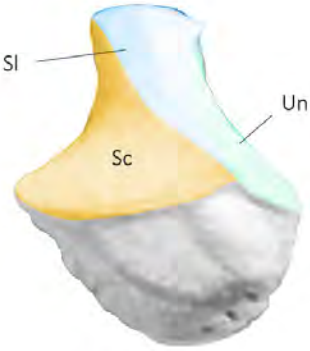
Based on FMH'14-4165 / Fábrica Mahou



Palmar



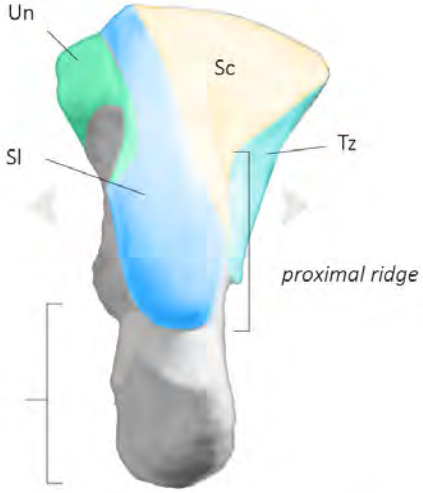
Dorsal



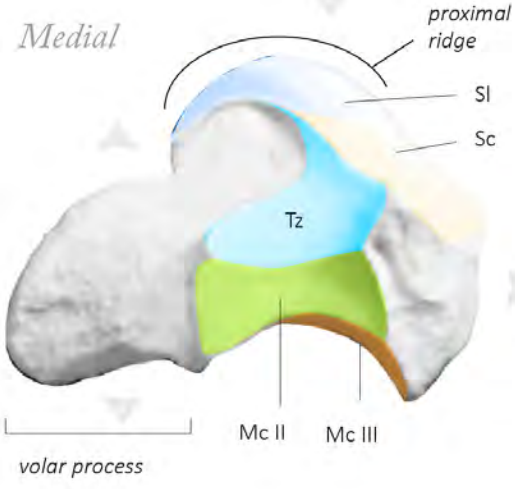
Distal



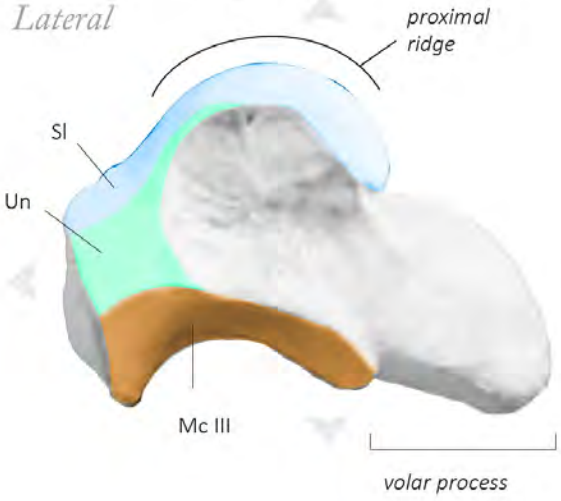
Proximal



Medial

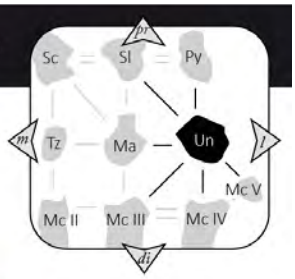


Lateral



Manus / Unciform (Un)

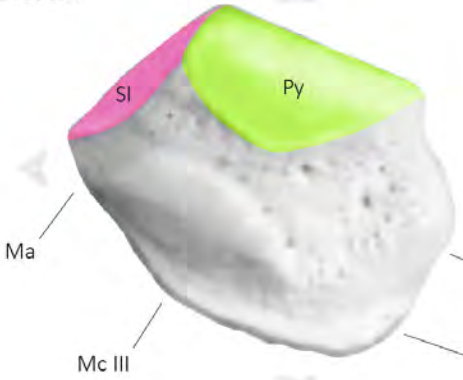
Hispanotherium matritense



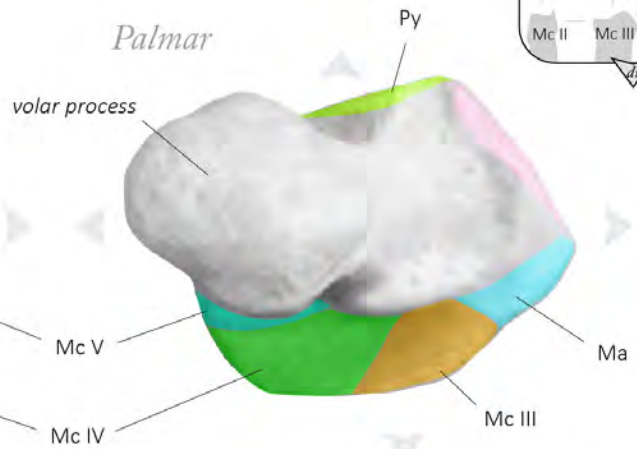
Left side
(right original, reversed)

Based on / Casa de Campo - Marqués de Monistrol M-30

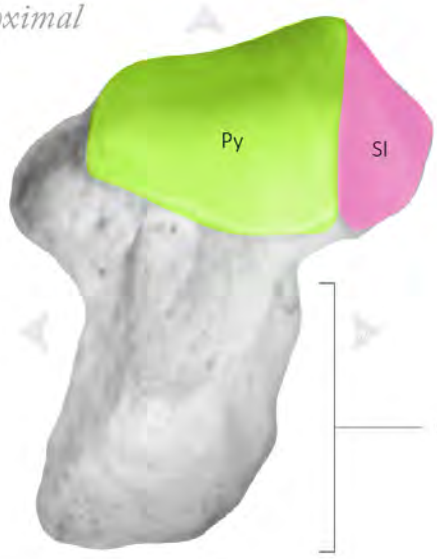
Dorsal



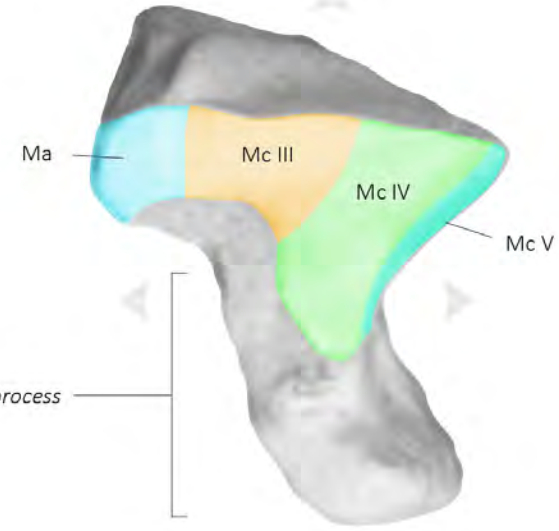
Palmar



Proximal

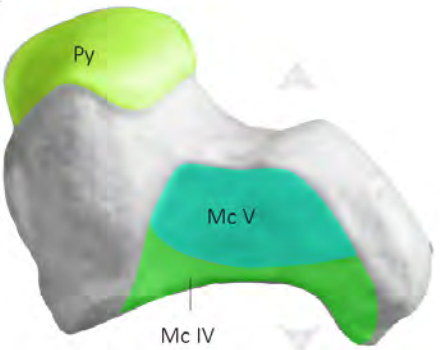


Distal



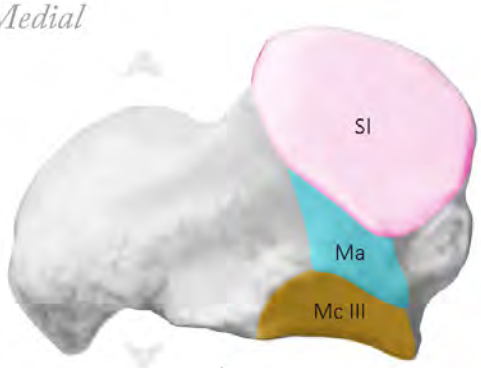
volar process

Lateral



volar process

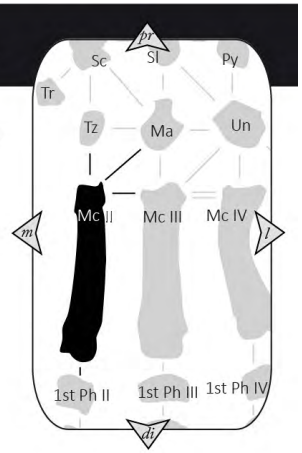
Medial



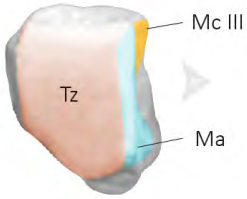
volar process

Left side (right original, reversed)

Based on CMD-398 / Casa de Campo - Marqués de Monistrol M-30



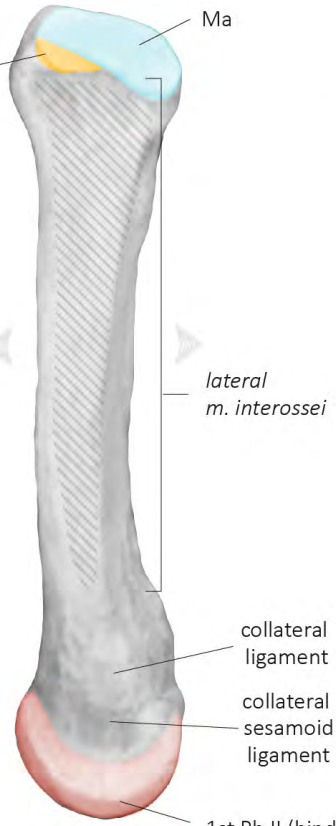
Proximal



Distal



Lateral



Dorsal



Palmar

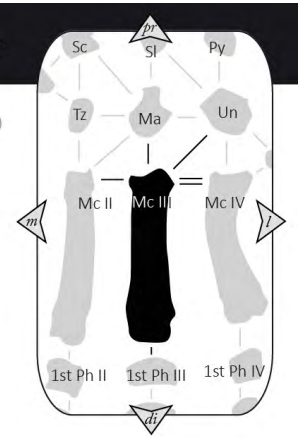


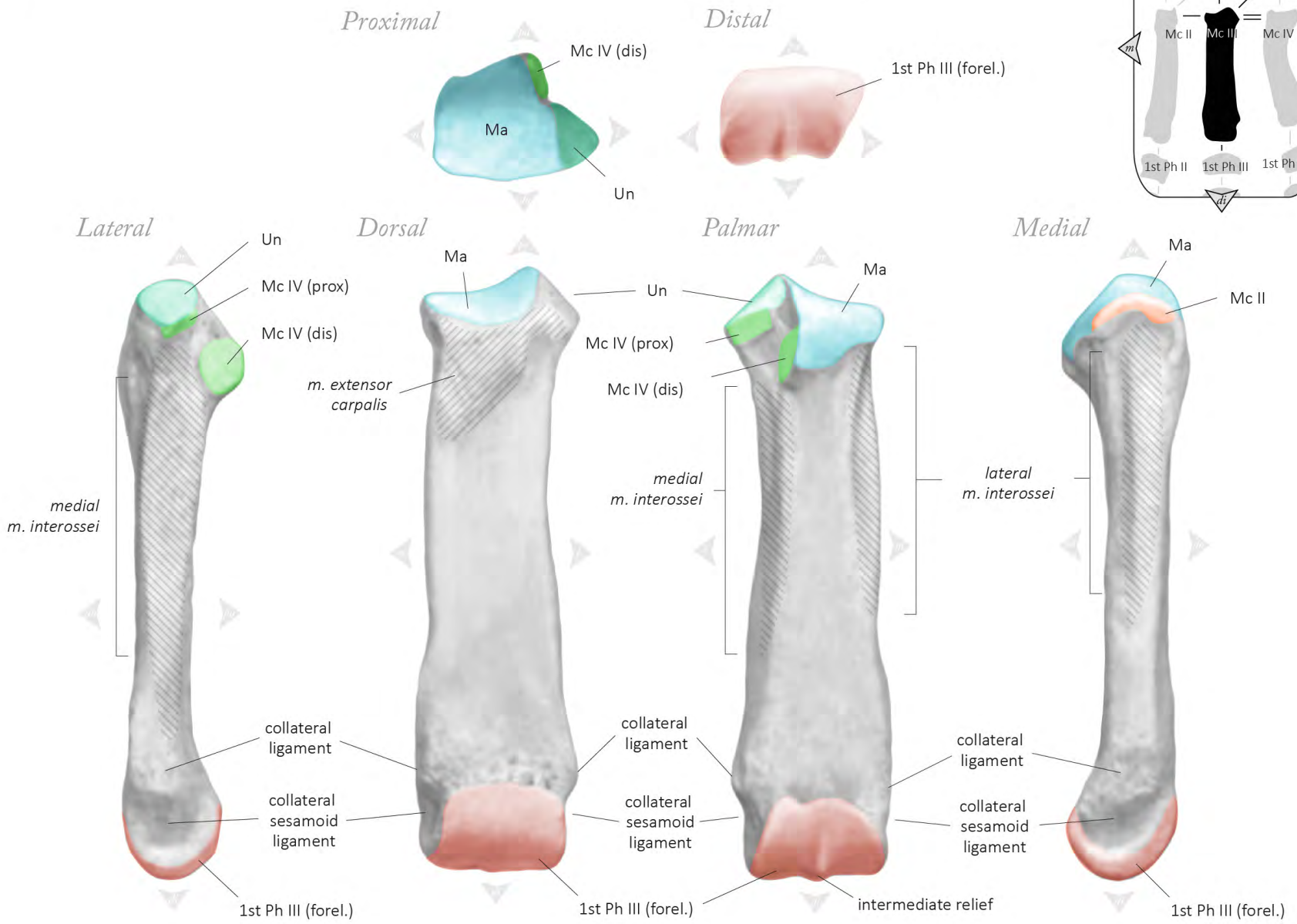
Medial



Left side

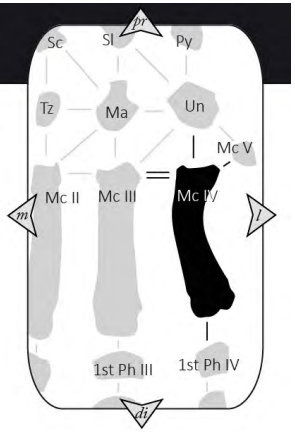
Based on R4-255 / Casa de Campo - Marqués de Monistrol M-30



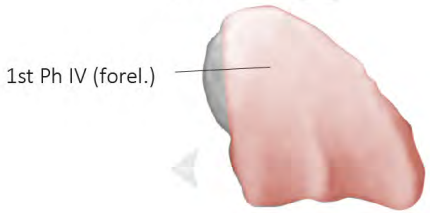


Left side (right original, reversed)

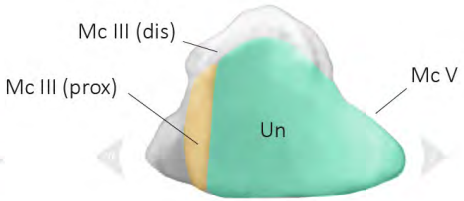
Based on CMD-398 / Casa de Campo - Marqués de Monistrol M-30



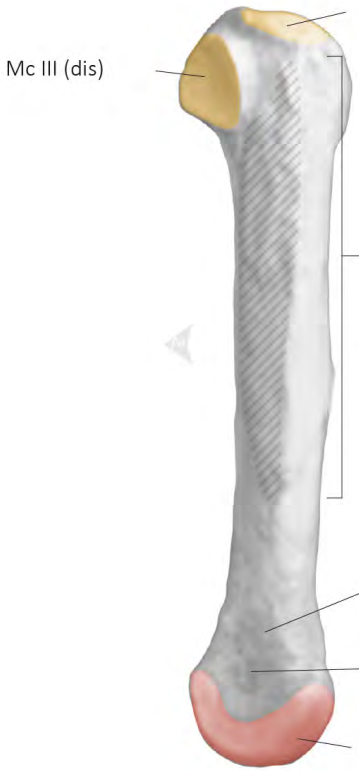
Distal



Proximal



Medial



Palmar



Dorsal



Lateral

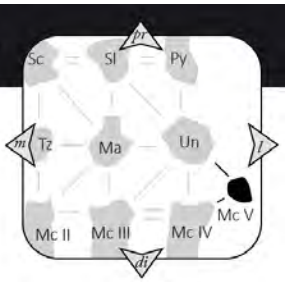


Manus / Mc V (Mc V)

Hispanotherium matritense

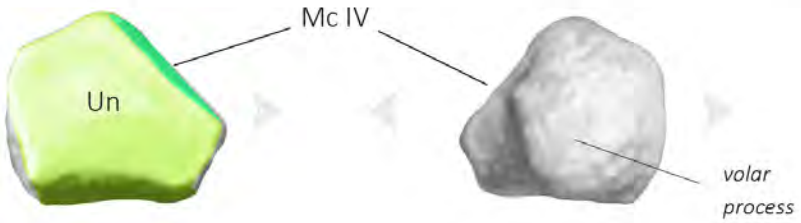
Left side

Based on FMH'14-2514 and FMH'14-3180 / Fábrica Mahou



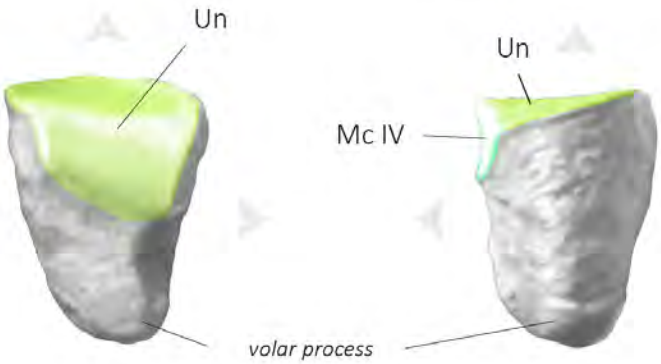
Proximal

Distal



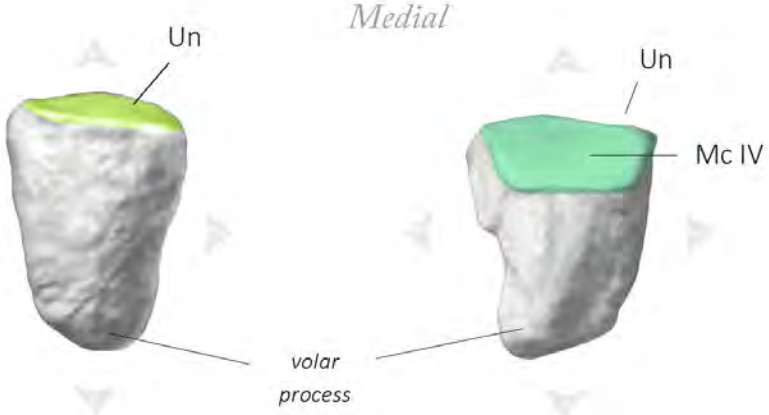
Palmar

Dorsal



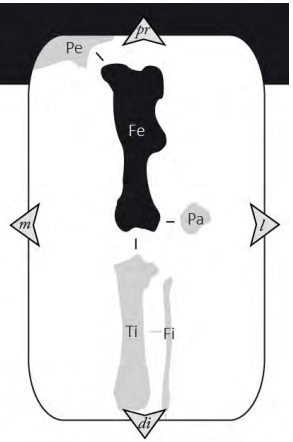
Lateral

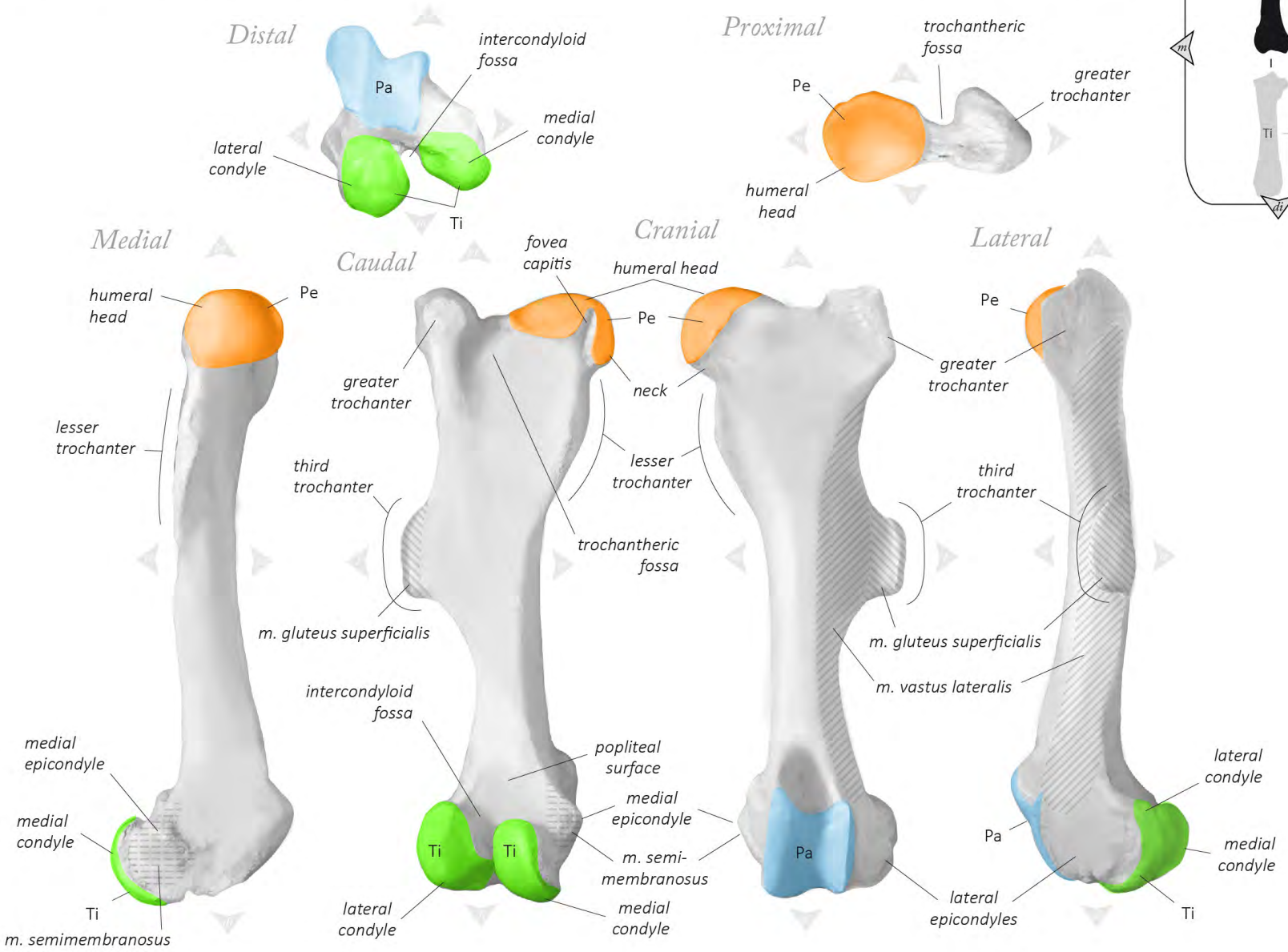
Medial



Left side (right original, reversed)

Based on 05/101/2/282B / Príncipe Pío-2



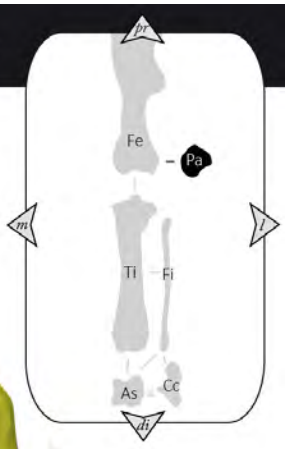


Forelimb / Patella (Pa)

Hispanotherium matritense

Left side (right original, reversed)

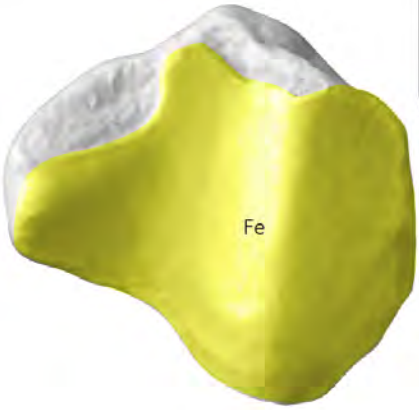
Based on FMH'14-4036 / Fábrica Mahou



Cranial



Caudal



Distal



Proximal



Medial

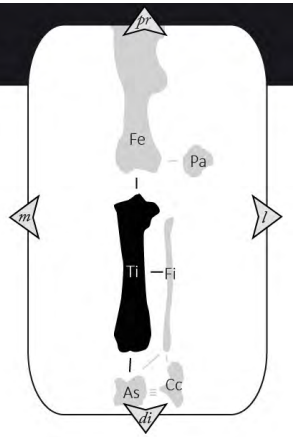


Lateral



Left side

Based on 05/101/2/393 / Príncipe Pío-2 and FMH'14-454 / Fábrica Mahou (right original, reversed)



Proximal

tibial tuberosity
groove of the middle patellar ligament
Fe (lat)
lateral condyle
Fe (me)
medial condyle
extensor groove

Distal

medial malleolus
Fi (dis)
As
cranial malleolus

intercondylar eminence
Fe (lat)
Fi (prox)
Fi (dis)
As
Lateral

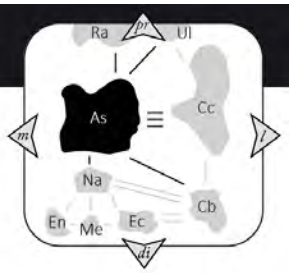
intercondylar eminence
medial condyle
Fe (me)
m. popliteus
popliteal line
popliteal notch
Fi (dis)
medial malleolus
As
Caudal

Fe (med)
Fe (lat)
groove of the middle patellar ligament
tibial tuberosity
Fi (prox)
patellar ligaments
m. tibialis cranialis
Fi (dis)
cranial malleolus
As
Cranial

groove of the middle patellar ligament
m. tibialis cranialis
As
Medial

Pes / Astragalus (As)

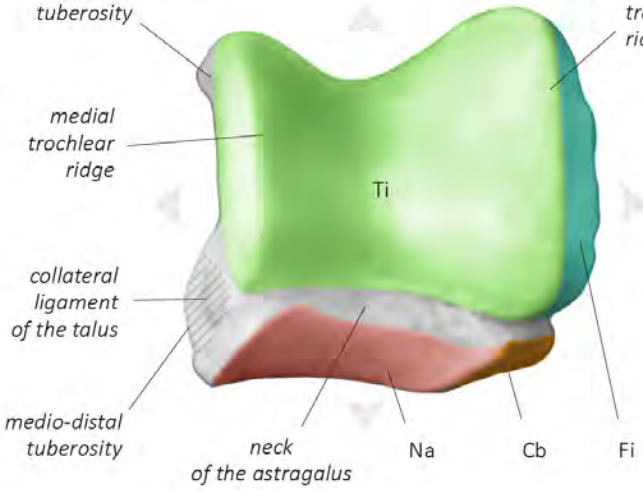
Hispanotherium matritense



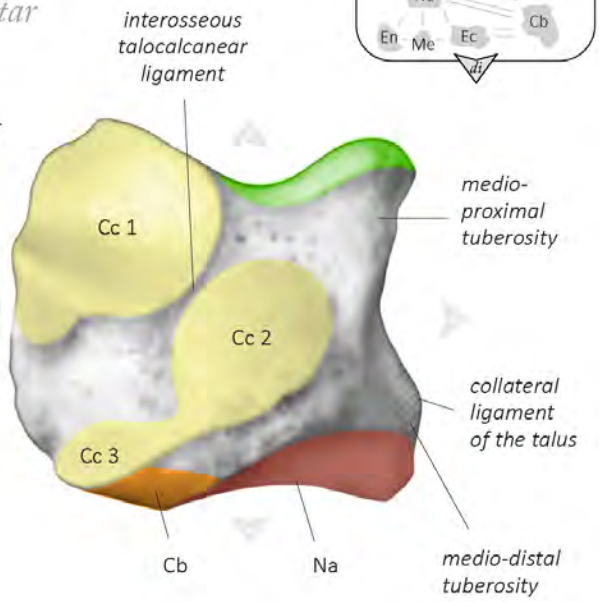
Left side

Based on CMD-682 / Casa de Campo - Marqués de Monistrol M-30

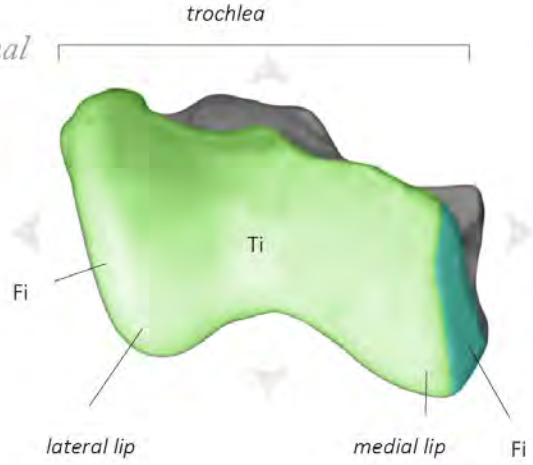
Dorsal



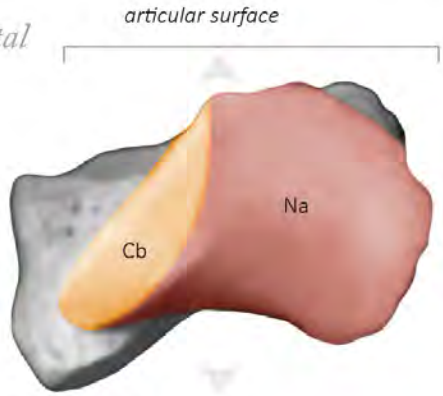
Plantar



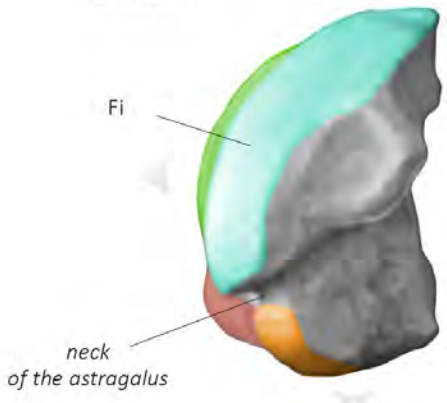
Proximal



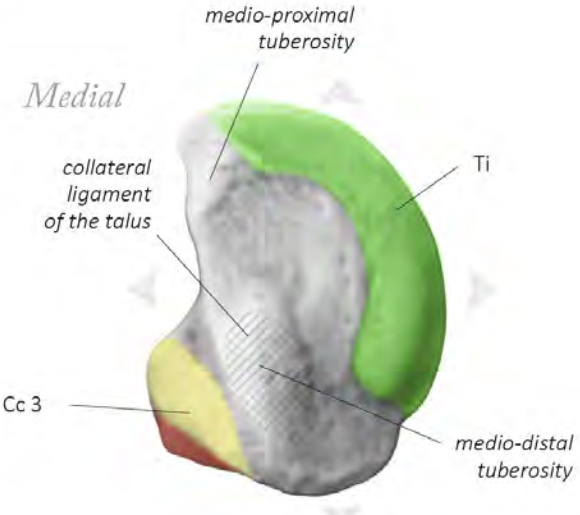
Distal



Lateral

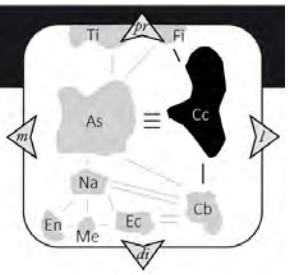


Medial



Pes / Calcaneum (Ca)

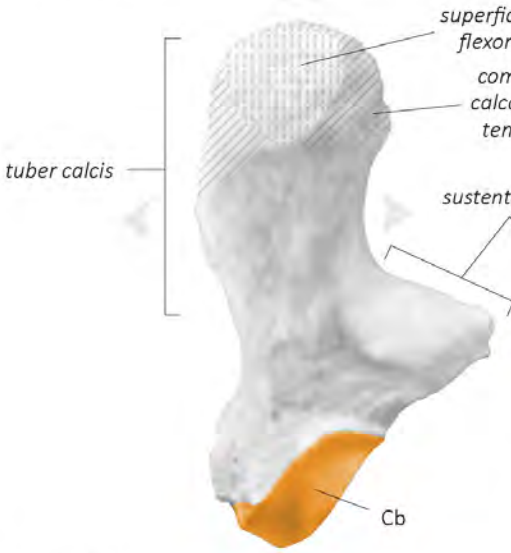
Hispanotherium matritense



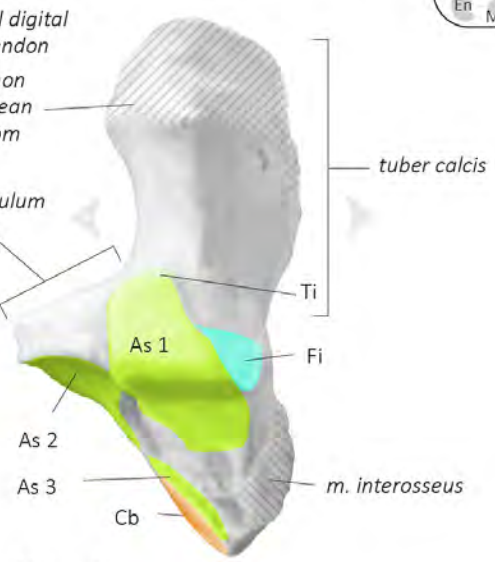
Left side (right original, reversed)

Based on FMH'14-2661 / Fábrica Mahou

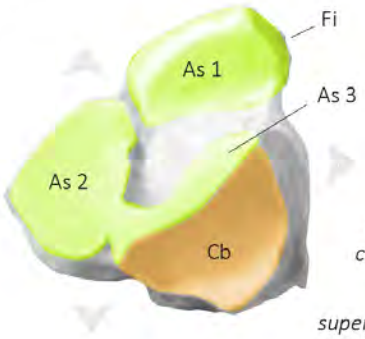
Plantar



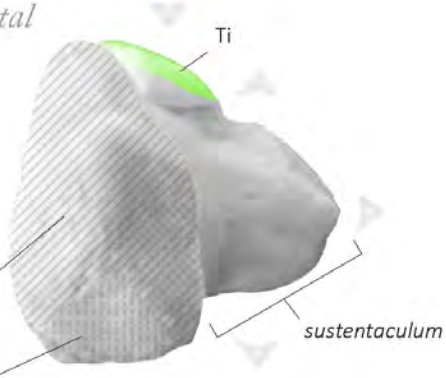
Dorsal

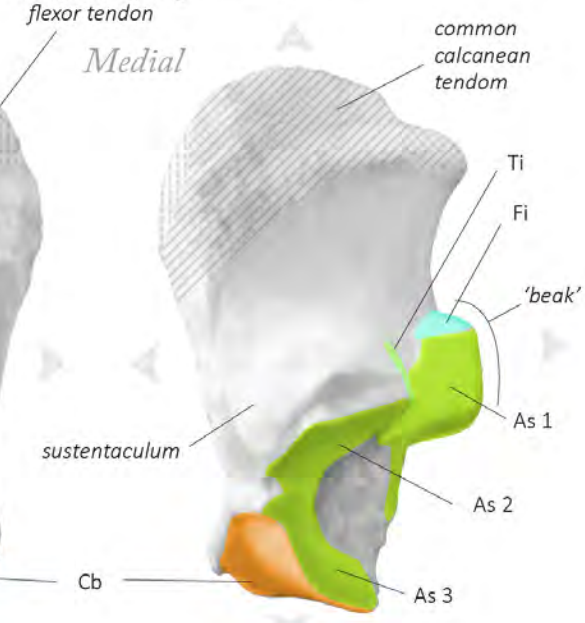


Proximal

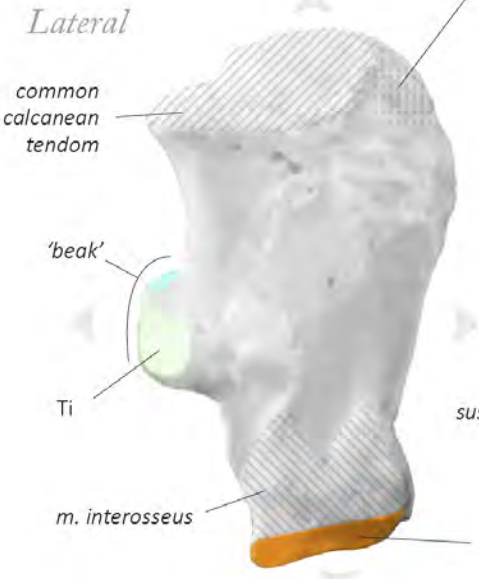


Distal





Lateral

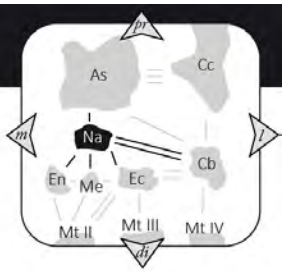


Pes / Navicular (Na)

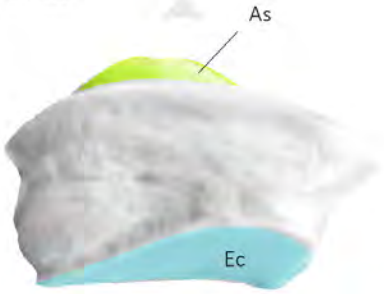
Hispanotherium matritense

Left side

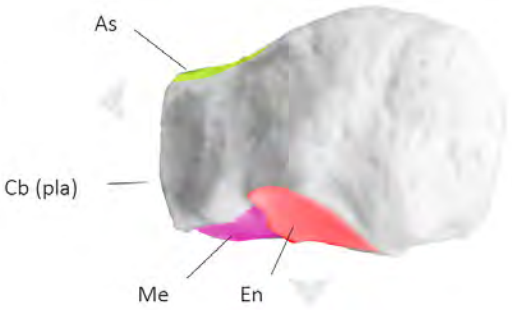
Based on FMH-14-2714 / Fábrica Mahou



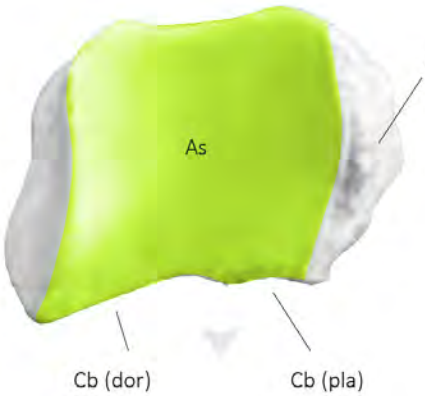
Dorsal



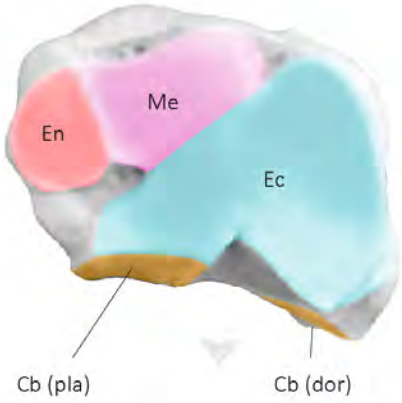
Plantar



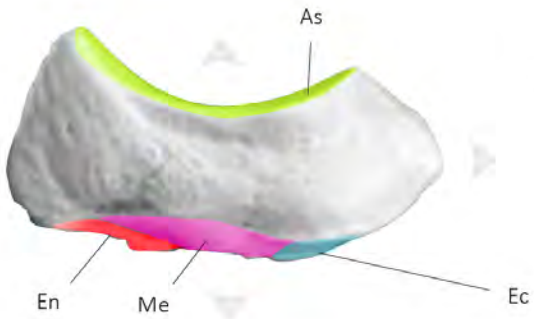
Proximal



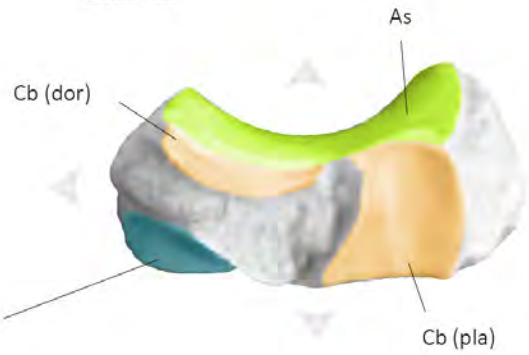
Distal



Medial

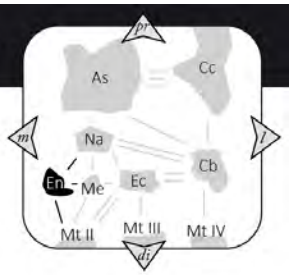


Lateral



Pes / Entocuneiform (En)

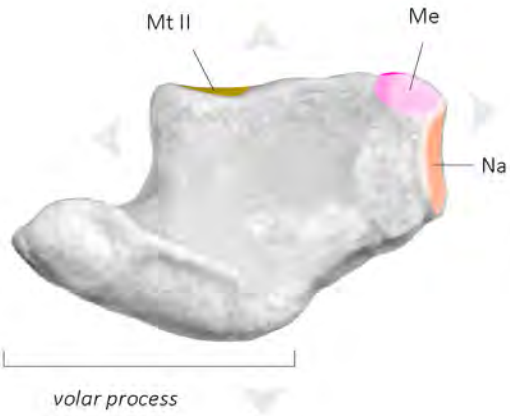
Hispanotherium matritense



Left side (right original, reversed)

Based on FMH'14-3345 / Fábrica Mahou

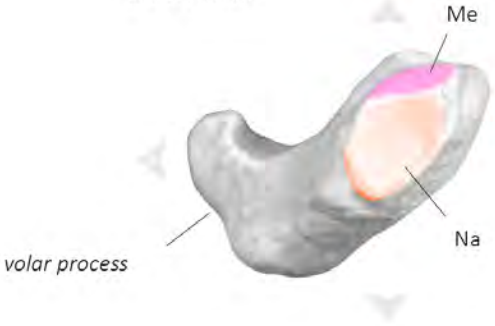
Dorsal



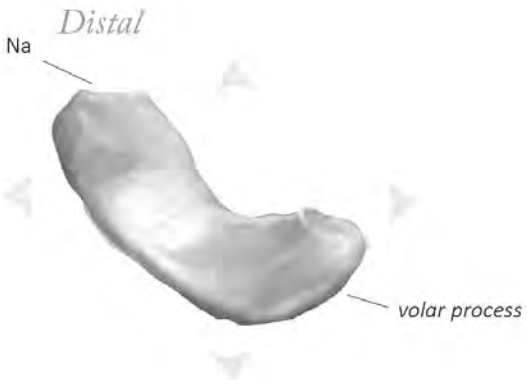
Plantar



Proximal



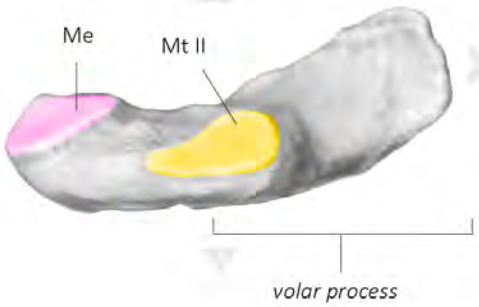
Distal



Lateral

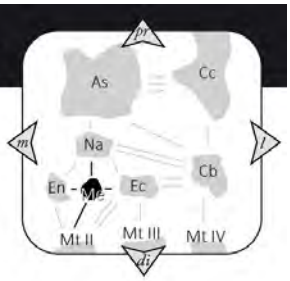


Medial



Pes / Mesocuneiform (Me)

Hispanotherium matritense



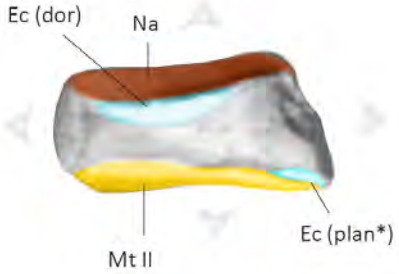
Left side

Based on FMH'14-3346 / Fábrica Mahou

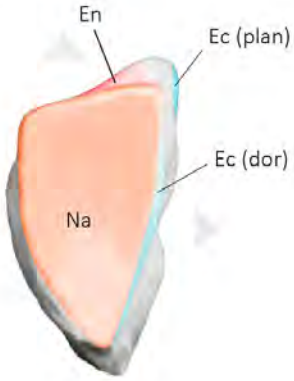
Medial



Lateral



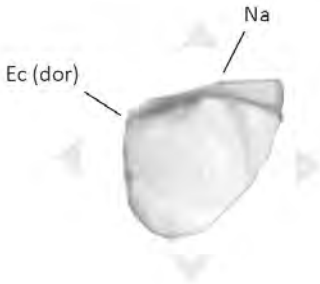
Proximal



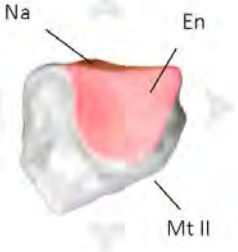
Distal



Dorsal



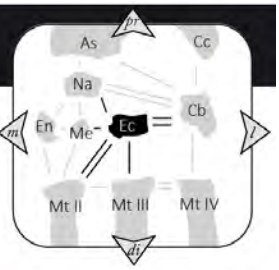
Plantar



*sometimes absent

Pes / Ectocuneiform (Ec)

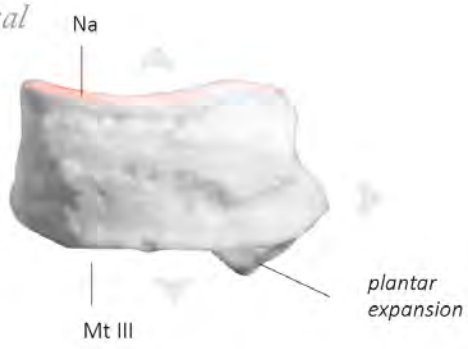
Hispanotherium matritense



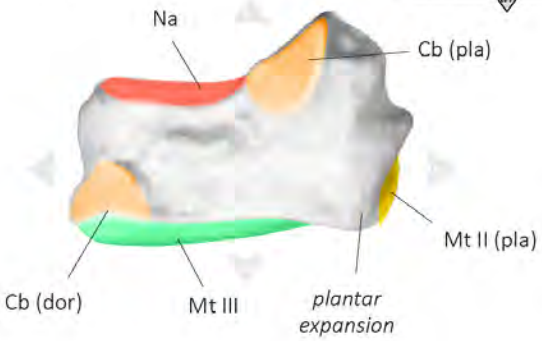
Left side (right original, reversed)

Based on FMH'14-5431 / Fábrica Mahou

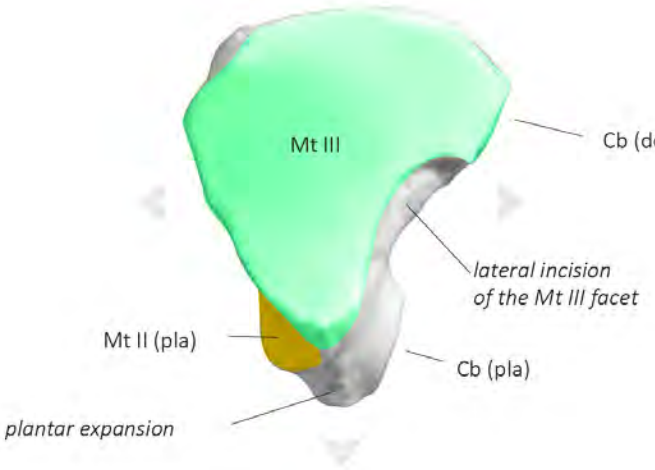
Dorsal



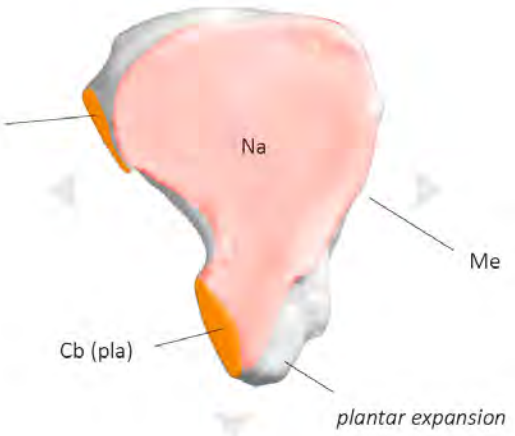
Plantar



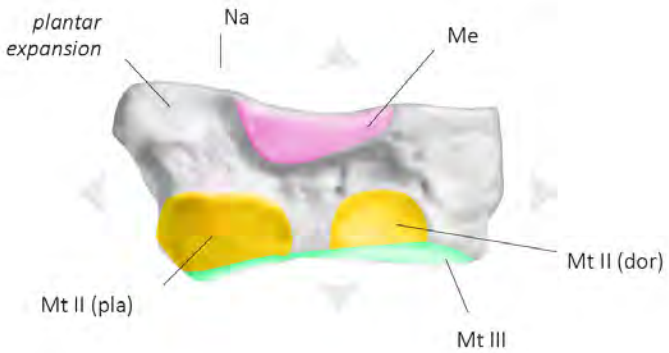
Distal



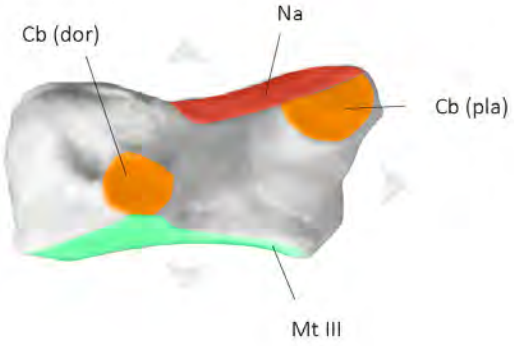
Proximal



Medial

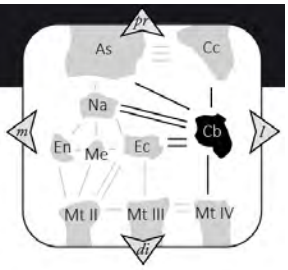


Lateral



Pes / Cuboid (Cb)

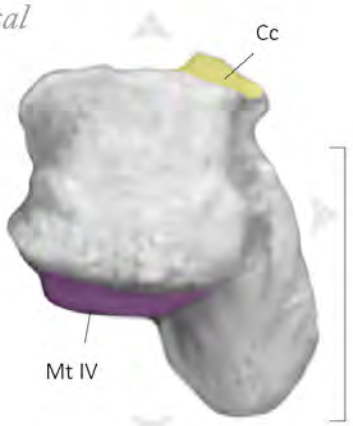
Hispanotherium matritense



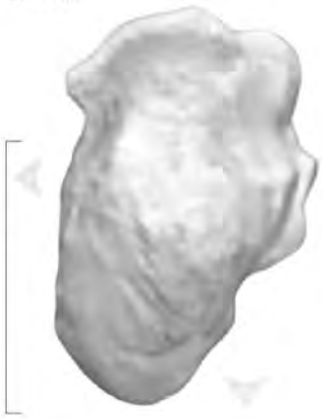
Left side

Based on / Casa de Campo - Marqués de Monistrol M-30

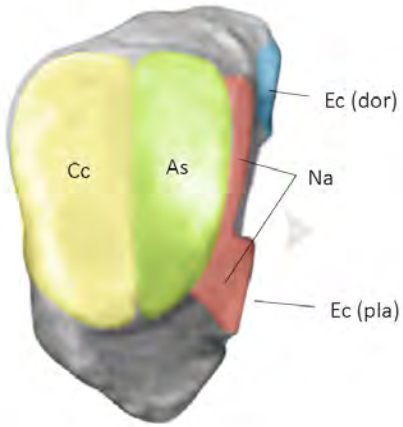
Dorsal



Plantar



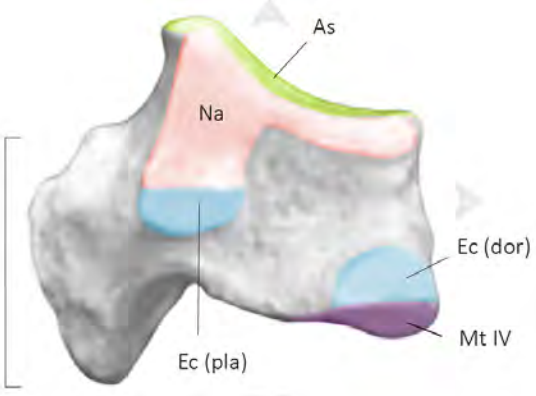
Proximal



Distal



Medial



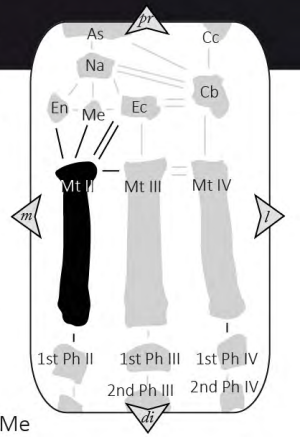
Lateral



Hispanotherium matritense

Left side (right original, reversed)

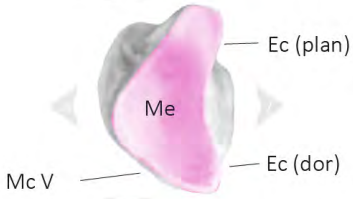
Based on FMH'14-3523 / Fábrica Mahou



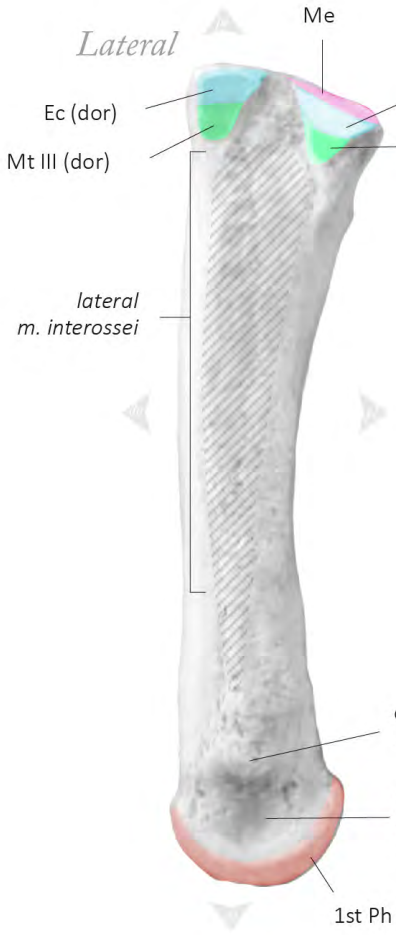
Distal



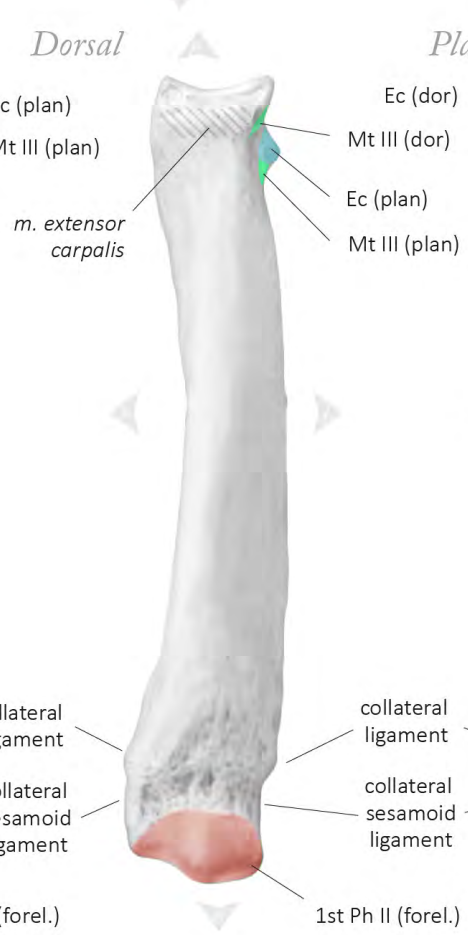
Proximal



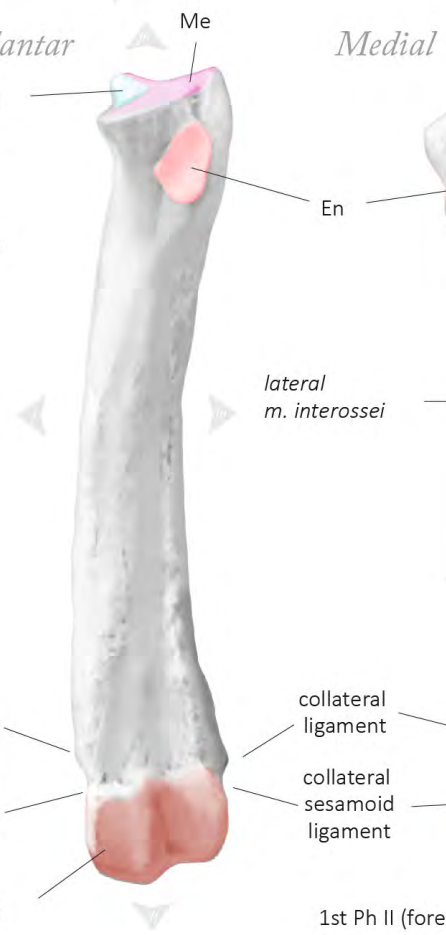
Lateral



Dorsal



Plantar

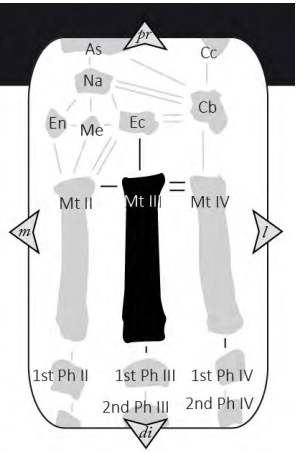


Medial

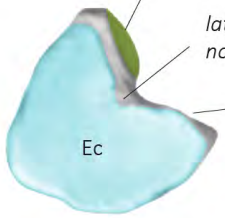


Left side

Based on 05/101/2/431 / Príncipe Pío-2



Proximal



Distal



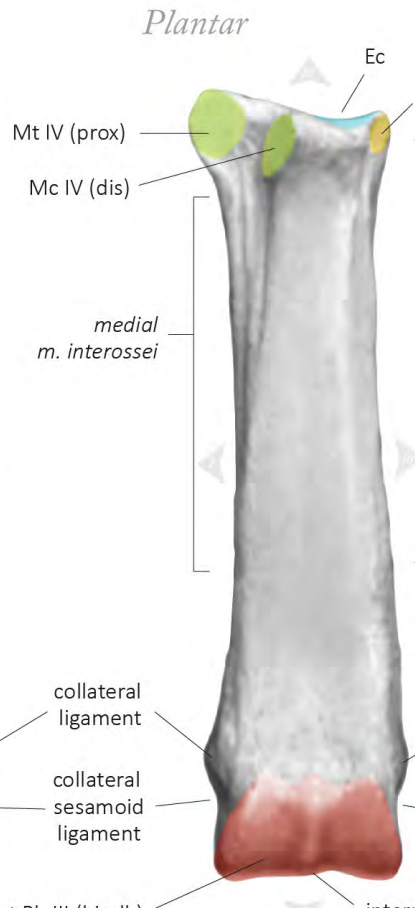
Lateral



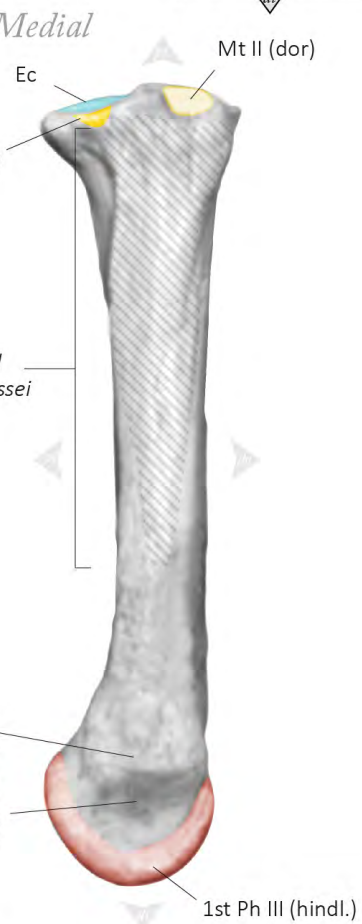
Dorsal



Plantar

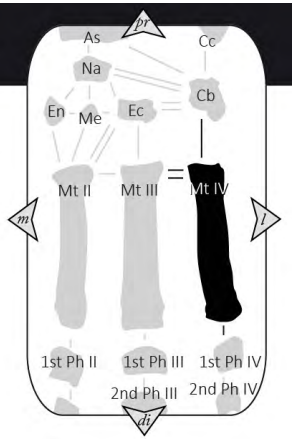


Medial



Left side (right original, reversed)

Based on CMD-398 / Casa de Campo - Marqués de Monistrol M-30



Distal

1st Ph IV (hindl.)

Proximal

Mt III (dis)

plantar shelf of the proximal epiphysis

Cb

Mt III (prox)

Lateral

Cb

collateral ligament

collateral sesamoid ligament

1st Ph IV (hindl.)

Plantar

Cb

Mt III (dis)

collateral ligament

collateral sesamoid ligament

1st Ph IV (hindl.)

Dorsal

Cb

Mt III (prox)

m. extensor carpalis

Mt III (dis)

collateral ligament

collateral sesamoid ligament

1st Ph IV (hindl.)

Medial

Cb

Mt III (prox)

Mt III (dis)

medial m. interossei

collateral ligament

collateral sesamoid ligament

1st Ph IV (hindl.)

6. Nuevas técnicas paleobiogeográficas aplicadas a la Familia Rhinocerotidae (Perissodactyla)

Oscar Sanisidro
Juan L. Cantalapiedra

Abstract. Even though phylogenetic relationships within Rhinocerotidae (Perissodactyla) have been controversial for many years, some taxa have been recently reviewed. One of the best known is the subtribe Elasmotheriina, a specialized group of Neogene rhinoceroses with a widespread distribution throughout Eurasia and Africa. Its paleobiogeographic history is complex and not easy to explain. Here we show the phylogenetic tree of this group of rhinoceroses combining both a cladistic hypothesis and published paleobiostratigraphic data, which points out to a maximum diversification event during the early late Miocene. This fact could reflect the expanding savannah-like terrestrial environment along Central Asia during the Vallesian and the vicariance due to climatic forcing. Furthermore, we conduct a biogeographic reconstruction using the recently developed Likelihood Analysis of Geographic Range Evolution (LAGRANGE) in order to examine the diversification of these fossil "running rhinoceroses" through their ancestral geographic ranges.

La filogenia de Rhinocerotidae (Perissodactyla) ha sido tema de debate durante años. Sin embargo, algunos taxones han sido revisados recientemente. Uno de los grupos mejor conocidos es la subtribu Elasmotheriina, un grupo especializado de rinocerontes extendido a lo largo de Eurasia y África. Su historia paleobiogeográfica es compleja y no fácilmente explicable. En este trabajo presentamos el árbol filogenético del grupo, basado en una hipótesis cladística y los rangos paleobioestratigráficos publicados, que apunta hacia un pico de diversidad del grupo a principios del Mioceno superior. Este hecho está posiblemente relacionado con la expansión de la continentalización del clima a lo largo de Asia Central durante el Vallesiense y la vicarianza provocada por estos cambios. Además, se ha realizado una reconstrucción biogeográfica utilizando el Análisis de Evolución de Rangos Geográficos por Máxima Probabilidad (LAGRANGE) recientemente desarrollado, para examinar los patrones de diversificación de estos "rinocerontes corredores" a través de sus rangos geográficos ancestrales.

INTRODUCCIÓN

Linneo estableció en 1758 el género *Rhinoceros* Linneo, 1758 para clasificar a todos los rinocerontes actuales. Más tarde Fischer von Valdgeim describió los restos del primer género de rinoceronte fósil, bautizándolo como *Elasmotherium* (Fischer, 1808). Las grandes diferencias morfológicas entre *E. sibiricum* (Fischer, 1808) y el resto de los rinocerontes descritos hasta el momento hicieron que Bonaparte (1845) lo incluyera dentro de un grupo propio, la subfamilia Elasmotheriina Bonaparte, 1945. Desde entonces se han descrito numerosas especies y géneros de rinocerontes elasmoterios, revelando una enorme diversidad de formas y tamaños. Posteriormente, el grupo de los elasmoterios ha ido cambiando sucesivamente de rango: desde familia (Kretzoi, 1943) a subtribu (Prothero, 2005; Antoine, 2000; 2002). En el presente trabajo seguiremos esta última asignación. De manera general, los elasmoterinos son considerados rinocerontes gráciles con dentición hipsodonta. Las formas más derivadas presentan molares de crecimiento continuo y complejos pliegues del esmalte (Heissig, 1989). De forma más detallada, Antoine (2002) define la subfamilia Elasmotheriinae como miembros de la subtribu Elasmotheriini, diagnosticados por tres caracteres dentales (sinapomorfías del análisis cladístico): presencia de cíngulo lingual, postfoseta desarrollada en los premolares superiores tercero y cuarto y fuerte constricción del protocono los molares superiores primero y segundo.

A pesar de que se han realizado varios intentos de abordar el estudio de las relaciones filogenéticas de los Rhinocerotidae fósiles, sus conclusiones divergen considerablemente entre sí. La aparición de filogenias moleculares no ha solucionado el conflicto, ya que todos los rinocerontes actuales pertenecen a un pequeño grupo relicto de entre toda la variedad de formas fósiles. Cerdeño (1995) realizó el primer análisis cladístico de

toda la familia Rhinocerotidae. En él plantea los Elasmotheriina como un grupo parafilético, por una parte emparentado con las especies más derivadas de Rhinocerotini *Coelodonta* Bronn, 1831+*Stephanorhinus* Kretzoi, 1942 y por otra como un grupo especializado de Rhinocerotinae. Sin embargo, actualmente se acepta el planteamiento realizado previamente por Heissig (1989), en el que se considera Elasmotheriina como un grupo monofilético. Finalmente, Antoine (2000, 2002, 2003) y Deng (2008) apoyan la monofilia de la tribu Elasmotheriini.

M. T. Antunes propone las primeras hipótesis biogeográficas para algunos grupos de elasmoterinos (Antunes, 1979; Antunes y Ginsburg, 1983), pero el análisis paleobiogeográfico de Elasmotheriina en conjunto no fue abordado hasta los estudios realizados por Antoine (2000, 2002). Éste plantea un origen asiático para el grupo, del que proceden las diversas especies que se distribuyen a lo largo de Eurasia. También plantea la posibilidad de un linaje africano de elasmoterinos primitivos, que persiste hasta el Mioceno superior.

En este trabajo presentamos una hipótesis paleobiogeográfica basada en una hipótesis filogenética, los datos paleontológicos publicados de Elasmotheriina y la reconstrucción de las áreas geográficas ancestrales utilizando un programa de análisis basado en modelos de máxima probabilidad.

MATERIAL Y MÉTODOS

Hipótesis filogenética

En este artículo se ha empleado la hipótesis filogenética de Elasmotheriina propuesta recientemente por Deng (2008) (ver figura 1), a partir de un análisis cladístico en el que se revisa algunas incorrecciones en la codificación de caracteres cometidas en trabajos anteriores y posee un bajo número de politomías. En total, el grupo de estudio incluye 15 especies y 20 Ma de intervalo temporal. La posición filogenética de *Diceratherium* Marsh, 1875 y *Menoceras* (Troxell, 1921) ha sido discutida: mientras los estudios clásicos los sitúan dentro de la tribu Menoceratini (Cerdeño, 1995, otros más recientes lo emplazan como tribu Elasmotheriini (Antoine, 2002; Deng, 2008). Deng (2008) excluye a *Diceratherium* y *Menoceras* de la tribu Elasmotheriini, mientras que Antoine (2002) incluye a *Menoceras* (incluyéndolo en la subtribu hermana de Elasmotheriina). Nosotros consideramos a ambos como *stem* Elasmotheriina. El resto de especies están incluidas dentro de Elasmotheriina *sensu* Antoine (2002).

Inferencia de rangos biogeográficos

Empleamos un modelo de reconstrucción biogeográfica basado en máxima probabilidad denominado DEC (Dispersal-Extinction-Cladogénesis) incluido en el paquete informático LAGRANGE (Likelihood Analysis of Geographic Range Evolution) desarrollado por Ree y Smith (2008; ver también Ree *et al.* 2005). El modelo permite fijar la configuración de las conexiones entre áreas a lo largo de la escala temporal y admite dos o más áreas como posibilidad para una sola especie. Asume tasas de dispersión y extinción constantes a lo largo de todo el árbol y trabaja con una matriz de tasas instantáneas de transición, vicarianza y extinción que funciona en pasos temporales infinitesimales, dando a la reconstrucción una dinámica mucho más real (Ree y Smith, 2008; Maguire y Matzke, 2009).

El análisis requiere que el árbol filogenético esté completamente resuelto, es decir, que no presente politomías. Sin embargo, el cladograma propuesto por Deng tiene una (fig. 1), de manera que se repitió el análisis para las tres topologías

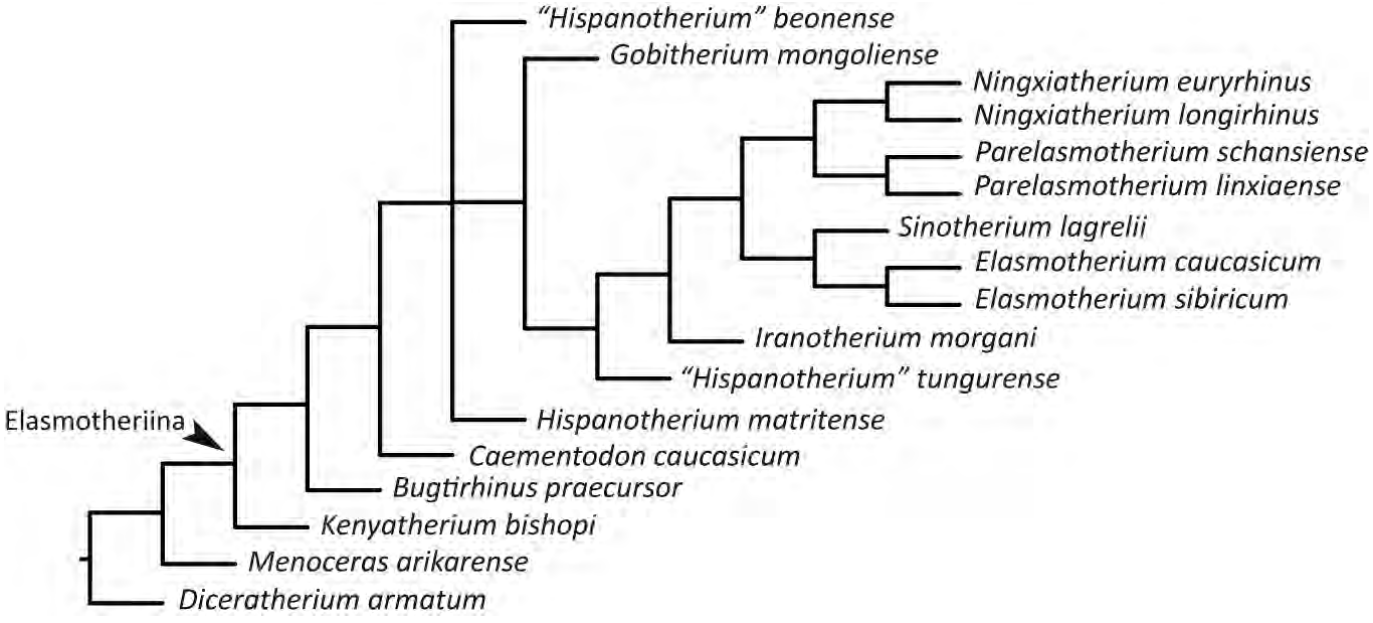


Fig. 1 Hipótesis filogenética de Elasmotheriina propuesta por Deng (2008) empleada como base del presente estudio. *Menoceras* y *Diceratherium* se consideran *stem group* del grupo.

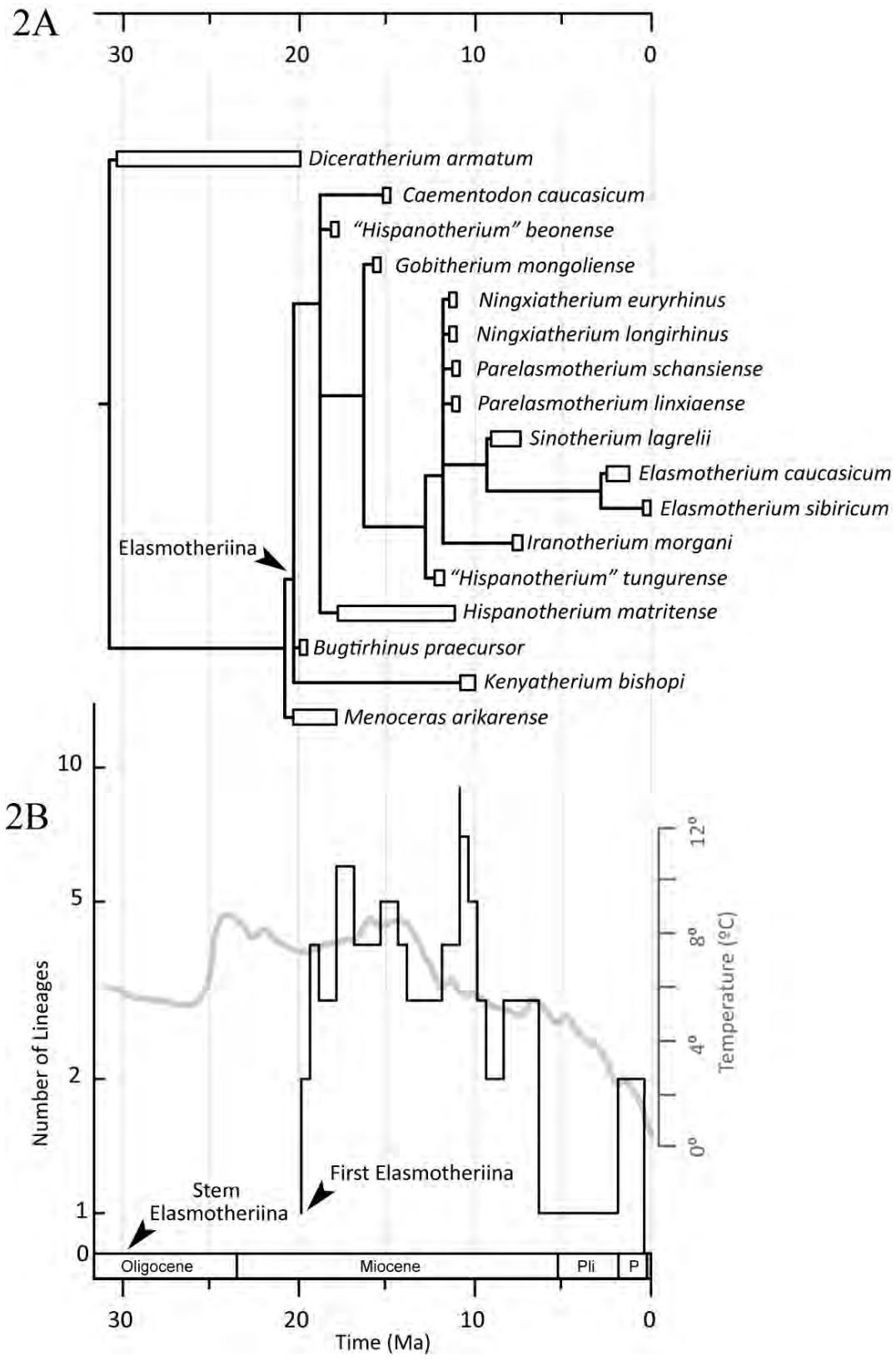


Fig. 2 A, hipótesis filogenética calibrada de Elasmotheriina en base a las relaciones cladísticas propuestas por Deng (2008) y dataciones publicadas en las descripciones de las distintas especies (detalladas en la tabla 1). Dichas dataciones han sido realizadas siguiendo métodos radiométricos y de correlación faunística. Las líneas horizontales representan linajes fantasma y extensiones de rango (Smith, 1994) que hay que añadir a los rangos estratigráficos, representados por barras, para que coincidan con la hipótesis cladística. Se señala con una flecha el nodo que contiene Elasmotheriina. 2B, curva de diversificación de los Elasmotheriina incluidos en el presente estudio en base a las relaciones filogenéticas propuestas en la figura 2A. A principios del Mioceno inferior aparecen los primeros representantes del grupo, representados por la especie Bugtirhinus praecursor del yacimiento de Bugti-Hills, Pakistán, hace alrededor de 20 Ma. A continuación, el grupo experimenta un aumento en su diversidad que alcanza un máximo hace unos 17 Ma compuesto principalmente por especies procedentes de Europa y Asia menor. El grupo alcanza su apogeo a finales del Mioceno superior gracias a la aparición de varias especies en China y Mongolia. Tras este momento, el grupo entra en declive, siendo Elasmotherium el último género del grupo. Se ha superpuesto la curva de temperatura de Zachos et al. (2001).

resueltas posibles, cotejándose luego las tres inferencias obtenidas para cada una.

Distribución paleobiogeográfica

La división en regiones corológicas se ha realizado atendiendo a la distribución biogeográfica del grupo, fruto de la recopilación bibliográfica detallada en la tabla 1. La reconstrucción paleogeográfica se basa fundamentalmente en los trabajos de Popov *et al.* (2004) y Rögl (1998).

Los cálculos de máxima probabilidad requieren el cómputo de todas las combinaciones de todos los parámetros en juego (tasas de vicarianza, extinción local y dispersión) y con el aumento del número de áreas los cálculos necesarios crecen exponencialmente. Para realizar el análisis dentro de un tiempo razonable, hemos limitado el número de intervalos temporales a 10 y el de áreas a siete. La distribución geográfica de todas las especies de Elasmotheriina ha sido dividida en los siguientes territorios: África, Oeste de Europa, Europa Central y del Este, Norte de Eurasia, Asia menor y Sudoeste asiático, y Centro de Asia y Mongolia. Además, se ha incluido América del Norte para incluir la distribución de los géneros *Diceratherium* y *Menoceras*. Las divisiones se han trazado atendiendo a barreras geográficas, por lo que se ha obviado el efecto producido por otras barreras como las climáticas, mucho más difíciles de establecer por la escala temporal y geográfica del modelo. Éstas deberán ser testadas en análisis posteriores para comprobar sus efectos junto con las anteriores.

Como se ha mencionado en el apartado anterior, LAGRANGE permite introducir información sobre disponibilidad temporal de puentes terrestres entre las áreas de estudio. Los eventos que marcan las diferentes configuraciones temporales de los puentes terrestres entre áreas se muestran en la figura 3.

RESULTADOS

Hipótesis filogenética

El árbol filogenético de Elasmoteriina y su s*tem group* (*Diceratherium* y *Menoceras*) se muestra en la figura 2.

Reconstrucción biogeográfica

La reconstrucción detallada de la biogeografía del grupo, que incluye la de las tres resoluciones de la politomía presente en el cladograma original (Deng, 2008), se muestra con detalle en la figura 3. Para una interpretación detallada ver la discusión.

DISCUSIÓN

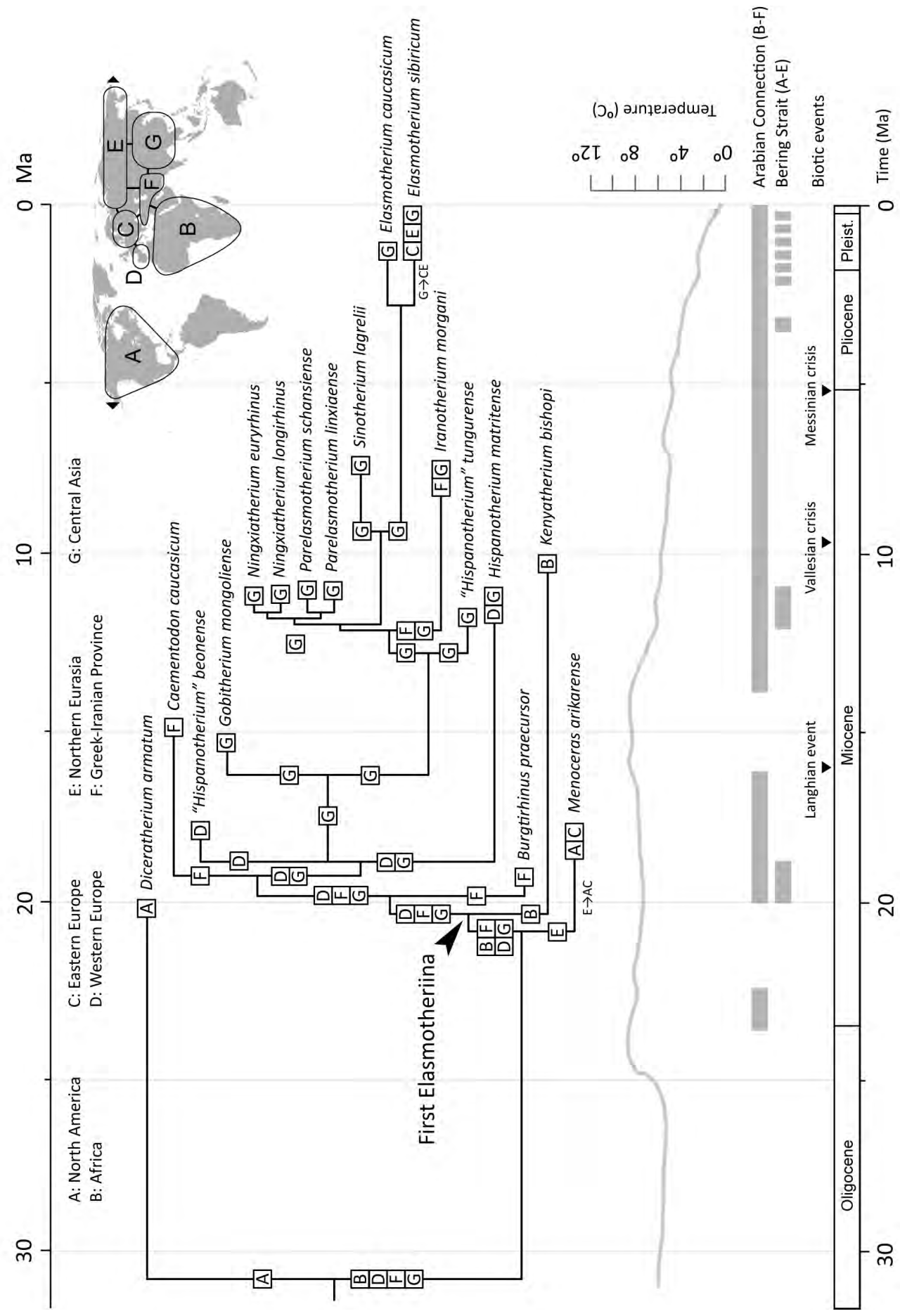
La distribución y taxonomía de las faunas de mamíferos están directamente influenciadas por la evolución paleogeográfica de su entorno (Vrba, 1992; Barnosky, 2001; Benton, 2009). La síntesis de la extensa historia paleogeográfica del Hemisferio Norte presentada puede parecer una sobresimplificación de un proceso extremadamente complejo, pero se trata de un paso necesario para la modelización de la corología de un grupo animal dado.

La distribución de los restos fósiles, base de nuestro estudio, no permite una reconstrucción precisa del nodo basal, pero apunta claramente hacia un origen del grupo y una distribución del grueso del *stem group* claramente circum-Tethys. Los resultados del análisis LAGRANGE muestran a Elasmotheriina ampliamente distribuido poco después de su primera aparición, próxima al límite Oligoceno-Mioceno (figura 3). Los resultados de las tres topologías, una vez resuelta la politomía, muestran resultados muy similares.

A diferencia de *Diceratherium*, una forma típica norteamericana, los restos de *Menoceras* han sido encontrados en yacimientos del Mioceno inferior de América del Norte y Europa occidental (Prothero, 2005, Becker, 2003). Ambos géneros cuentan con varias especies de cuernos pares lateralmente enfrentados, adaptadas a espacios abiertos. *Menoceras* aparece en el registro fósil de Estados Unidos sin haberse descrito ningún pariente próximo en el continente norteamericano. El gran número de yacimientos de este momento ubicados en las *badlands* del Medio-Oeste permiten descartar la falta de registro fósil. La reconstrucción paleobiogeográfica planteada confirma la hipótesis previa en que la presencia de *Menoceras* en América del Norte es considerada fruto de una migración desde Eurasia (Prothero, 2005; Becker, 2003). El paso de un clima cálido y húmedo del Eoceno a un clima seco y árido acompañado por una estacionalidad marcada del Oligoceno de América del Norte favoreció la expansión de esta forma próxima a Elasmotheriina (Prothero, 2005).

Kenyatherium bishopi es un elasmoterino de 9 Ma de antigüedad encontrado en el yacimiento de Nakali, Kenia (Aguirre & Guérin, 1974). Su posición filogenética basal implica que forma parte de un linaje primitivo de elasmoterinos que emigró a África desde Asia (Antoine, 2002; Guérin y Pickford, 2003). *Ougandatherium napakense* (Guérin y Pickford, 2003), procedente del yacimiento de Napak-1 en Uganda, no ha sido incluido hasta la fecha en ningún análisis filogenético del

Fig. 3 Reconstrucción biogeográfica de Elasmotheriina representada sobre el árbol filogenético del grupo. La topología del árbol está ligeramente modificada con el fin de poder incluir los símbolos de las áreas reconstruidas. Se indican las áreas ocupadas por cada linaje hijo descendiente de cada nodo. En el mapa se representan las diferentes regiones geográficas empleadas de forma esquemática y todas las conexiones posibles (los triángulos representan la conexión del estrecho de Bering), así como la leyenda. Se ha representado la curva de Zachos et al. (2001), que representa la temperatura oceánica media en el Hemisferio Norte. Debajo, las barras sombreadas representan los momentos de presencia de las conexiones Arábiga (entre África y la provincia Grecoiraní, B-F) y del Estrecho de Bering (entre América del Norte y Asia, A-E). Sobre la escala se muestran eventos importantes del Neógeno. Un asterisco (*): acompaña los nodos para los que hay otras opciones de reconstrucción cuyos valores de probabilidad caen dentro de las dos unidades logarítmicas. Ma: millones de años antes del presente.


A: North America
B: Africa
C: Eastern Europe
D: Western Europe
E: Northern Eurasia
F: Greek-Iranian Province
G: Central Asia
0 Ma
10
20
30
Dicerathetium armatum
Caementodon caucasicum
"Hispanotherium" beonense
Gobitherium mongoliense
Ningxiatherium euryrhinus
Ningxiatherium longirhinus
Parelasmotherium schansiense
Parelasmotherium linxiaense
Sinotherium lagrelii
Elasmotherium caucasicum
Elasmotherium sibiricum
G→CE
Iranotherium morgani
"Hispanotherium" tungurense
Hispanotherium matritense
Burgtirhinus praecursor
Kenyatherium bishopi
Menoceras arikarense
E→AC
First Elasmotheriina
Temperature (°C)
0° 4° 8° 12°
Arabian Connection (B-F)
Bering Strait (A-E)
Biotic events
Langhian event
Vallesian crisis
Messinian crisis
Oligocene
Miocene
Pliocene
Pleist.
Time (Ma)

grupo. Dicho yacimiento data de hace unos 19 Ma, lo que lo sitúa próximo al origen de los Elasmotheriina. Dado que no se ha realizado hasta la fecha ningún análisis filogenético de *O. napakense,* no podemos saber con certeza si se encuentra emparentado con *K. bishopi*, como plantean Guérin y Pickford (2003). Sin embargo, las características primitivas de *K. bishopi*, la presencia de *O. napakense* hace unos 20 Ma y la extensión de rango que sitúa el linaje de *K. bishopi* en África hacia ese momento parecen indicar el desarrollo de un linaje propio de elasmoterinos africanos diez millones de años antes de la aparición de *Kenyatherium*. Esto corroboraría las hipótesis propuestas por Antoine (2000) y Guérin y Pickford (2003), en las que se plantea la permanencia de un posible linaje de elasmoterinos basales africanos de los cuales no se tiene registro intermedio entre los 19 a los 9 Ma. La revisión de las dos especies africanas y el esclarecimiento de la posición filogenética de *O. napakense* permitirán contribuir a esclarecer las relaciones filogenéticas del grupo durante el Mioceno inferior, añadiendo más resolución a sus patrones de diversificación.

Los elasmoterinos se dispersan por Eurasia en diversas oleadas de forma temprana. Durante el Mioceno inferior la diversificación del grupo es gradual, ocupando las zonas periféricas de África, Europa y el Sur y Oeste de Asia. La reconstrucción paleogeográfica realizada por LAGRANGE muestra un origen asiático común a todas las formas a partir del Mioceno medio. A finales del Mioceno medio el grupo sufre una desaparición masiva de formas cursoriales típicas de latitudes ecuatoriales (como *Hispanotherium* (Crusafont y Villalta, 1947) o *Caementodon* Heissig, 1972) y son sustituidas por formas pesadas y de gran tamaño típicas de latitudes más altas a partir del Plioceno (como *Elasmotherium* o *Iranotherium* Ringström, 1924). Durante el Plio-Pleistoceno el grupo se vio drásticamente reducido en géneros y morfologías. Las diferentes especies de *Elasmotherium* eran formas muy hipsodontas, mediportales y de gran tamaño adaptadas a alimentarse de pastos pobres en nutrientes y abrasivos, vegetación típica de los biomas continentales fríos. Su especialización a hábitats propios de los intervalos glaciares del Pleistoceno los relegó a las llanuras del Norte de Eurasia. A pesar de la conexión intermitente entre Asia y América del Norte, nuestro análisis sugiere que este linaje fue incapaz de atravesar el estrecho de Bering en los momentos de máximo glaciar. Su extinción se produjo en un momento donde los elasmoterinos ya se encontraban en declive y coincidió con la de otros muchos macromamíferos.

CONCLUSIONES

El rango bioestratigráfico de Elasmotheriina se extiende desde principios del Mioceno al Pleistoceno. Su historia paleobiogeográfica comienza a escribirse en Asia hace alrededor de 20 Ma. Desde allí se extienden a Europa y África. Tras un máximo en el número de linajes del grupo, su diversidad desciende, quedando un único género tras el Plioceno inferior que sobrevive hasta el Pleistoceno medio. El análisis de la historia paleobiogeográfica de los elasmoterinos supondrá una pieza fundamental a la hora de la reconstrucción corológica de los miembros fósiles de la Familia Rhinocerotidae.

AGRADECIMIENTOS

Agradecemos a la Dra. Esperanza Cerdeño y al revisor anónimo sus útiles comentarios, que han ayudado a mejorar considerablemente el manuscrito original. A María Teresa Alberdi, Israel M. Sánchez y Jorge Morales (MNCN-CSIC) la ayuda prestada durante la preparación inicial del manuscrito. A Kaitlin Maguire y Nick Matzke (University of California Berkeley) los consejos y disquisiciones sobre LAGRANGE y códigos Python. Finalmente agradecer a Rafael Guerrero (University of Texas) la ayuda prestada con el software R! Ambos autores se benefician de dos becas predoctorales FPU dependientes del Ministerio de Educación y trabajan en el marco del proyecto CGL2008-05813-C02-01/BTE del Ministerio de Ciencia e Innovación. Este estudio está incluido en el grupo de investigación CAM-UCM 910607.

BIBLIOGRAFÍA

Aguirre, E. y Guérin, C. (1974): Première découverte d'un Iranotheriinae (Mammalia. Perissodactyla, Rhinocerotidae) en Afrique : *Kenyatherium bishopi* nov. gen. nov. sp. de la formation vallésienne (Miocène supérieur) de Nakali (Kénya). Estudios Geológicos, 30, 229-233.

Antoine, P. O. (2000): Origine et différenciation des Elasmotheriina parmi les Rhinocerotidae (Mammalia, Perissodactyla): analyse cladistique et implications biostratigraphiques et paléobiogéographiques. Tesis doctoral inédita, 360 pp.

Antoine, P. O. (2002): Phylogeny and Elasmotheriina evolution (Mammalia, rhinocerotidae). Mémoires du Muséum national d'Histoire naturelle, 188, 1-359.

Antoine, P. O. (2003): Middle Miocene elasmotheriine Rhinocerotidae from China and Mongolia: taxonomic revision and phylogenetic relationships. Zoologica Scripta, 32, 2, 95-118.

Antunes, M. T. (1979): *Hispanotherium* fauna in Iberian Middle Miocene; its importance and paleogeographical meaning. Annales Geologiques Pays Hellen, VIIth International Congress on Mediterranean Neogene.

Antunes, M. T. y Ginsburg, L. (1983): Les Rhinocérotidés du Miocène de Lisbonne. Systématique, écologie, paléobiogéographie, valeur stratigraphique. Ciências da Terra (UNL), 7, 17-98.

Barnosky, A. D. (2001): Distinguishing the effects of the Red Queen and Court Jester on Meiocene mammal evolution in the northern Rocky Mountains. Journal of Vertebrate Paleontology, 21, 1, 172-185.

Becker, D. (2003): Paléoécologie et paléoclimats de la Molasse du Jura (Oligo-Miocène): apport des Rhinocerotoidea (Mammalia) et des minéraux argileux. Tesis doctoral, 327 pp.

Benton, M. J. (2009): The Red Queen and the Court Jester: Species Diversity and the Role of Biotic and Abiotic Factors Through Time. Science, 323(5915):728-732.

Grade de Doctor rerum naturalium, Universite de Fribourg (Suisse), 327 pp.

Bonaparte, C. L. (1845): Systema Vertebratorum. Transactions of the Linnean Society of London, 18, 31-41.

Borissiak, A. (1914): Mammifères fossiles de Sebastopol, I. Trudy Geolegicheskago Komiteta. Novaja Seria, 87, 1-154.

Bronn, H. G. (1831): Ueber die fossilen Zahne eines neuen Geschlechtes aus der Dickhauter-Ordnung, Coelodonta, Hoehlenzahn. Jahrbuch fur Mineralogie, Geognosie, Geologie und Petrefaktenkunde, 2, 51-61.

Cerdeño, E. (1995): Cladistic analysis of the Family Rhinocerotidae (Perissodactyla). American Museum Novitates, 3143, 1-25.

Cerdeño, E. (1996): Rhinocerotidae from the Middle Miocene of the Tung-gur Formation, Inner Mongolia (China). American Museum Novitates, 3184, 1-43.

Cerdeño, E. (1998): Diversity and evolutionary trends of the Family Rhinocerotidae (Perissodactyla). Palaeogeography, Palaeoclimatology, Palaeoecology, 141, 13-34.

Cerdeño, E. e Iñigo, C. (1997): *Hispanotherium matritense* (Rhinocerotidae) de la ciudad de Madrid (España) y su relación con el paleoambiente del Aragoniense medio (Mioceno Medio). Revista Española de Paleontología, 12, 1, 80-90.

Chen, G. F. (1977): A new genus of Iranotheriinae of Ningxia. Vertebrata Palasiatica, 15, 143-147.

Crusafont, M. y Villalta, J. F. (1947): Sobre un interesante rinoceronte (*Hispanotherium*) del Mioceno del Valle de Manzanares. Las Ciencias, 12, 869-883.

Deng, T. (2001): New remains of *Parelasmotherium* (Perissodactyla, Rhinocerotidae) from the late Miocene in Dongxiang, Gansu, China. Vertebrata Palasiatica, 39, 306-311.

Deng, T. (2003): New material of *Hispanotherium matritense* (Rhinocerotidae, Perissodactyla) from Laogou of Hezheng County (Gansu, China), with special reference to the Chinese Middle Miocene elasmotheres. Geobios, 36, 141-150.

Deng, T. (2005): New discovery of *Iranotherium morgani* (Perissodactyla, Rhinocerotidae) from the Late Miocene of the Linxia Basin in Gansu, China, and its sexual dimorphism. Journal of Vertebrate Paleontology, 25, 2, 442-450.

Deng, T. (2008): A new elasmothere (Perissodactyla, Rhinocerotidae) from the late Miocene of the Linxia Basin in Gansu, China. Geobios, 41, 719-728.

Fischer G. F. v. W. (1808): Notice d'un animal fossile de Sibérie inconnu aux naturalistes. Programme d'Invitation aux Séances Publiques de la Societé Impériale des Naturalistes de Moscou, 4, 19-20.

Guérin, C. (1980): Les rhinocéros (Mammalia, Perissodactyla) du Miocène terminal au Pléistocène supérieur en Europe occidentale : comparaison avec les espèces actuelles. Documents des Laboratoires de Géologie de Lyon, 79, 1-1184.

Guérin, C. y Pickford, M. (2003): *Ougandatherium napakense* nov. gen. nov. sp., le plus ancien Rhinocerotidae Iranotheriinae d'Afrique. Annales de Paléontologie, 89, 1, 1-35.

Heissig, K. (1972): Die obermiozäne Fossil-Lagerstätte Sandelzhausen, 5. Rhinocerotidae (Mammalia), Systematik und Okologie. Mitteilungen der Bayerischen Staatssammlung Paläontologie und historische Geologie, 14, 37.

Heissig, K. (1989): The Rhinocerotidae. En: The evolution of Perissodactyls (Prothero, D. y R. M. Schoch ed.). Oxford University Press, 399-417.

Heissig, K. (2007): Oligocene-Miocene Vertebrates from the Valley of Lakes (Central Mongolia): Morphology, phylogenetic and stratigraphic implications. Ann. Naturhist. Mus. Wien, 108, A, 233-269.

Killgus, H. (1923): Unterpliozäne Säuger aus China. Paläontologische Zeitschrift, 5, 3, 251-257.

Kretzoi, M. (1942): Präokkupierte und durch ältere zu ersetzende Säugetiernamen. Földtany Közlöny, 72, 345-349.

Kretzoi, M. (1943): *Gobitherium* n. g. (Mammalia, Rhinocerotidae). Földtany Közlony, 73, 268-271.

Linneo, C. (1758): Tomus I. Systema naturae per regna tria naturae, secundum classes, ordines, genera, species, cum characteribus, differentiis, synonymis, locis. Editio decima, reformata. Holmiae (Laurentii Salvii), 1-4, 1-824.

Maguire, K.C. y Matzke, N. (2009): Maximum Likelihood estimation of biostratigraphic histories using the fossil record. Journal of Vertebrate Paleontology, 29, 3A, 140,

Marsh, O. C. (1875): Notice of new early Tertiary mammals. American Journal of Science, 3, 407-410, 485-488.

Popov, S. V., Rögl, S., Rozanov, A. Y., Steininger, F. F., Shcherba, I. G. y Kovac, M. (2004): Lithological-paleogeographical maps of the Paratethys. Courier Forschung-Institut Senckenberg, 250, 1-46.

Prothero, D. (2005): The Evolution of North American Rhinoceroses. Cambridge University Press, 218 pp.

Ree, R. H., Moore, B. R., Webb, C. O. y Donoghue, M. J. (2005): A likelihood framework for inferring the evolution of geographic range on phylogenetic trees. Evolution, 59, 2299-2311.

Ree, R. H. y Smith, S. A. (2008): Maximum likelihood inference of geographic range evolution by dispersal, local extinction, and cladogenesis. Systematic Biology, 57, 1, 4-14.

Ringström, T. J. (1924): Nashörner der Hipparion Fauna Nord-Chinas. Palaeontologia Sinica, Series C, 1, 1-156.

Rögl, F. (1998): Palaeogeographic considerations for Mediterranean and Paratethys seaways (Oligocene to Miocene). Annales Naturhistorisches Museum Wien, 99, 279-310.

Smith, A. B. (1994). Systematics and the fossil record. Backwell Scientific Publications, 232 pp.

Troxell, E. L. (1921). A study of Diceratherium and the diceratheres. American Journal of Science, 5, 41-51.

Vrba, E. S. (1992): Mammals as a Key to Evolutionary Theory. Journal of Mammalogy, 73, 1, 1-28.

Zachos, J., Pagani, M., Sloan, L., Thomas, E. y Billups, K. (2001): Trends, Rythms, and Aberrations in Global Climate 65 Ma to Present. Science, 292, 686-693.

7. *Alicornops simorrense* (Mammalia, Perissodactyla) from the middle Miocene M-407 Rotonda (Madrid Province, Spain)

Oscar Sanisidro
Maria Teresa Alberdi
and Jorge Morales

Abstract. Rhinocerotid remains from the species *Alicornops simorrense* from the middle Miocene locality M–407 Rotonda (Madrid Basin, Spain) are described. The studied remains include a partial skull, mandibles, teeth, vertebrae and postcranial bones. They are homologous from previously described variation of *A. simorrense* except for the proportions of several postcranial bones. In a parallel way, a review of the characters used in the literature to define the species is reviewed as well as its two systematic consequences: the placement of *Alicornops* as a subgenus of *Aceratherium* or as a genus by its own.

INTRODUCTION

Alicornops simorrense (Lartet *in* Laurillard, 1848) is a small, short-limbed aceratheriine rhinoceros. The biostratigraphic distribution of the species ranges from the early Aragonian —MN 6 Biozone (Mein, 1999), Middle Miocene— up to the late Vallesian —MN 10, Late Miocene—. Its taxonomic attribution has been controversial since the original description made by Lartet in 1851 with the name of "*Rhinoceros simorrensis*". Its assignation to *Rhinoceros* (the genus where some of the Asian living species belong) is explained by the superficial resemblance of its dentition with *Lartetotherium sansaniense*, a horned rhino species originally included in *Rhinoceros* also found in Simorre (one of the earliest localities were *A. simorrense* was recorded). After its recognition as an aceratheriine rhinoceros (Roger, 1887), the species have been repeatedly switched its generic assignation among the genera *Aceratherium* (Hooijer, 1966), *Dromoceratherium* (Ginsburg, 1974) and *Mesaceratherium* (Heissig, 1976). Ginsburg and Guérin (1979) were the first to recognize its distinctiveness by creating its own subgenus, *Alicornops*, including it into *Aceratherium*. Posteriorly, *Alicornops* was raised to a generic rank by Yan and Heissig (1986), being widely adopted thereinafter (Antoine et al., 2003; Cerdeño, 1992; Deng, 2004; Guérin, 1989; Heissig, 1989; Prothero et al., 1989). A recent reassessment of the topic leaded to different results. Meanwhile some authors opted for restoring the subgeneric rank of *Alicornops* within *Aceratherium* (Heissig, 2012). Others like remarked several differences between *A. simorrense* and *Aceratherium incisivum* outlining the boundary between both genera (Antoine et al., 2010; Becker et al., 2013).

A. simorrense is best represented in the Iberian Peninsula, where is well-known from the Vallès-Penedès, Duero, Tagus and Calatayud-Daroca Basins (Cerdeño, 1992; Cerdeño and Sánchez, 2000). The species spans from late Aragonian to Lower Vallesian in the Western and Central Basins, remaining as a relict species in the Upper Vallesian locality of Can Jofresa (Vallès-Penedès Basin; Santafé and Casanovas-Cladellas, 1978). The exhaustive study of the intraspecific variation of the species showed two "evolutionary trends" from the late Aragonian to early Vallesian (Cerdeño and Sánchez, 2000): while the populations of the Central Basins became progressively more robust through time, those from el Vallés-Penedés increased in size while maintaining their proportions (Cerdeño and Sánchez, 2000).

M–407 Rotonda site is located in the city of Fuenlabrada, South of Madrid (Spain; Fig. 1). The site was discovered as a result of the supervision of recent public works related with road construction in the area. Excavations, conducted by Argea S. A. and UTE-Recomba, revealed a rich bone assemblage from the Upper Aragonian (MN 6 Mein's Biozone, Middle Miocene; ~ 13.5 Ma), included in the Cenozoic Madrid Basin. More information about the geological setting of the site can be found in the Chapter 9. The recovered material includes abundant giant tortoise and rhinoceros remains.

MATERIAL AND METHODS

Measurements are given in millimeters with an accuracy of one decimal digit. Approximate measurements are given in parentheses. Measurements were made with a digital caliper and a measuring tape was used for elements larger than 150 mm. The general anatomical terminology follows Budras (2009) and Schaller (2007). In addition, that used by other authors has also been taken into consideration (Antoine, 2002; Antoine et al., 2010; Becker et al., 2013; Guérin, 1980; Heissig, 1972a, 1999). More detailed information of the craniodental anatomy can be found in the Appendix at the end of this volume. For more information regarding the postcranial skeleton see Chapter 5.

Anatomical Abbreviations—ant, anterior; art, articulation; dia, diaphysis; dis, distal; int, interior; epi, epiphysis; max, maximum; min, minimum; prox, proximal; 3tr, third trochanter. In describing the dental elements, we follow the terminology proposed by Jepsen (1996). Capital letters are used for upper teeth and lower case for lower teeth. I, M and P designate incisors, molar and premolar respectively. A preceding 'D' or 'd' indicate decidual teeth (e.g., DP4 or dp2).

Measurements abbreviations—APD, antero-posterior diameter; DL, distal length; H, height; L, length; TD, transverse diameter.

Institutional abbreviations—**MNCN**, Museo Nacional de Ciencias Naturales; **w/n**, without field number.

Species gracility—In order to test the increase in robustness through time among the postcranial bones of *A. simorrense*, gracility indices (*GI*) have been calculated for the six main metapodials (i.e. Mc II, Mc III, Mc IV, Mt II, Mt III and Mt IV) according to the following formula:

$$GI = (DTdia/L)\cdot 100$$

Being TDdia the transversal diameter of the midshaft of the metapodial and L its maximum length (Cerdeño, 1989).

Referred material— All the studied specimens from M–407 Rotonda are stored in the Museo Nacional de Ciencias Naturales-CSIC (Madrid, Spain). The complete list is detailed in the Supplementary Data 1.

SYSTEMATIC PALEONTOLOGY

Subfamily ACERATHERIINAE Dollo, 1885

Tribe ACERATHERINI Gray, 1821

Genus *Alicornops* Ginsburg and Guérin, 1979

Type species—*Alicornops simorrense* (Lartet, 1851)

Other referred species—*Alicornops complanatum* (Heissig, 1972b) and *Alicornops laogouense* Deng, 2004.

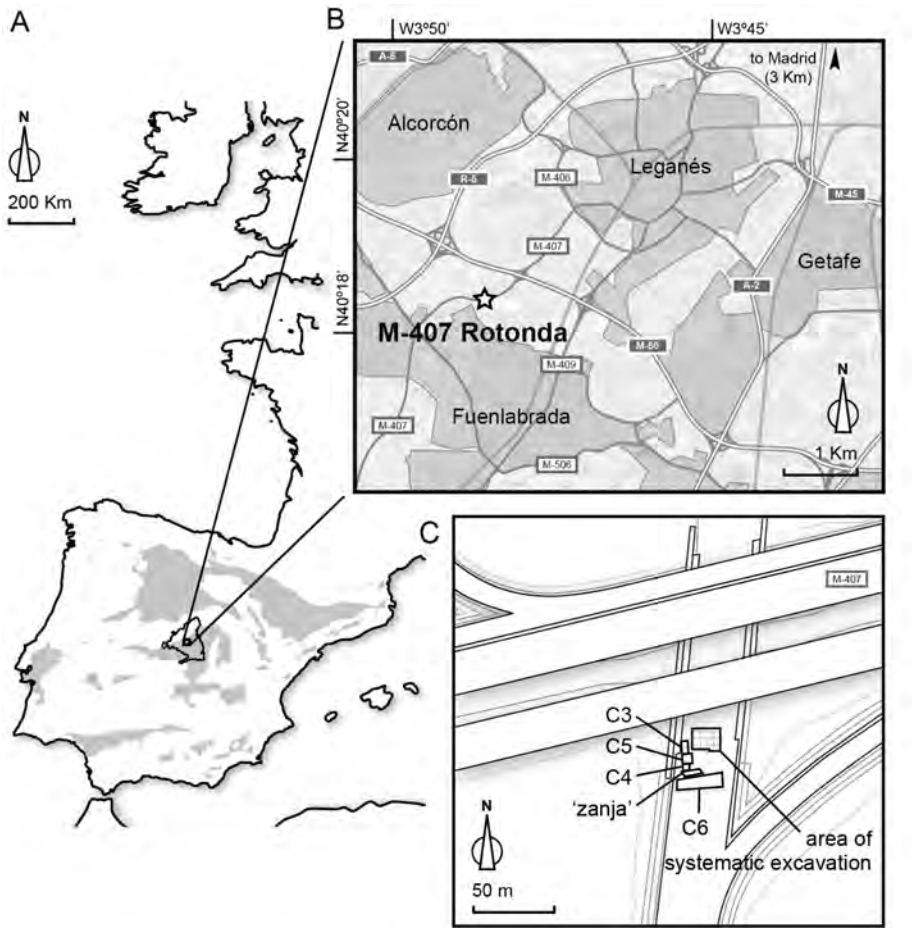


Fig. 1 Simplified general map of the Iberian Peninsula with its Cenozoic basins represented as shaded contourns. B, detailed map showing the location of M–407 Rotonda site, represented as a star. C, map with the detailed excavation area.

Diagnosis (after Ginsburg and Guérin, 1979 and Cerdeño, 1989)—"Small aceratheriine. Skull with postglenoid apophysis very developed in contact with the post-tympanic one, both slightly oblique anteriorly. Anterior dentition with I1 and i2 developed (the latter as a large tusk, greater in males). Upper cheek teeth with paracone fold strong and little projected. Crochet well developed; sometimes crista also developed. Upper premolars usually with continuous lingual cingula. Lower premolars with lingual and labial cingula. Postcranial skeleton with shortened legs, fore foot tetradactyl".

Antoine et al. (2003) emend the previous diagnosis according to the following characters included in their phylogenetic analysis: "Small Aceratheriina with a convex mandibular corpus, presence of some cement in the cheek teeth; protocone slightly smaller than the hypocone on the P2; antecrochet often present in the M2; angulous trigonid and talonid forming an acute dihedron in the lower cheek teeth; lower molars devoid of lingual cingulids; insertion of the *m. biceps brachii* forming a profound depression in the radius".

Species *Alicornops simorrense* (Lartet, 1851)

Holotype—fragmented skull with P2-M3 and lower p2-m3 from Simore, France, stored in the Museé Nationelle d'Histoire Naturelle of Paris (France).

Type locality—Villefranche-d'Astarac (Gers), France, MN 7.

Diagnosis—As for genus.

Differential diagnosis—*A. simorrense* differs from *A. laogouense* on the following characters (Deng, 2004): "nasals 1.7 times as long as wide and present a narrower nasal base; higher and bigger skull; skull roof lozenge-shaped, with a narrower maximal frontal width; frontal bone less narrowed posteriorly; wider interparietal space between the occipital crests (with a minimum of 25 mm); nasal notch placed at the level of the middle of P3; weaker postorbital process; anterior margin of the orbit at the level of the M1. It differs from *A. complanatum* on the following characters (Antoine et al., 2003): presence of a crochet (sometimes double) in the premolar series; presence of a mesostyle in the DP2; presence of a simple paralophid on the dp2; absence of I1; absence of antecrochet in the P2-3; absence of medifossete in the P3-4; absence of crista in the P3 and the upper molar series; reduced labial cingulid in the lower premolars; absence of antecrochet in the P4; lingual cingulum almost always present in the upper molars and weak p2 and dp1".

DESCRIPTION

Craniomandibular and Dental Morphology (TABLES 1-3)

Skull (Fig. 2; Table S1)—A1-1 is an adult individual (IDAS stage 3-4, adult/late adult; according to Anders et al., 2011). The occipital part of the skull is not preserved. The maxillary bone is high and broad (a typical aceratheriine feature). The nasal bones are long and robust. Their upper border is straight and smooth and shows a slightly inflated area in the nasal bone base. The section of the nasal bones at their midpoint has a concave ventral surface, with a smooth ridge along the nasal suture. Its dorsal surface is straight in lateral view, clearly marked and generates a longitudinal smooth groove, more evident towards the nasal bone base. The nasal tip is small, rounded and has a faintly rough extent, being the only possible signal of horn attachment. The nasal notch has a straight lower border, that becomes convex on its rostral half and a concave lower one, with a straight angle between them. Their walls are divergent on the upper side in frontal view. The only infraorbital foramen is oval and obliquely placed, parallel to the nasal notch concave lower border and falling above P3-P4 boundary. The space between the nasal notch and the orbit is a little depressed. The orbits are oval and well differenced by the postorbital process. Their anterior margin is situated at the level of the boundary between M1 and M2. The lachrymal process is small, blunt and positioned in the upper half of the anterior rim of the orbit. Supraorbital tubercle is small, pointed and posteriorly placed in the middle of a thick and blunt lateral projection. The postorbital process is preserved on the right side as a badly deteriorated small tubercle. The facial crest is little laterally projected, overhanging as a rounded crest. It starts higher as a wide bar attached to the lower border of the orbit, falling abruptly and changing the orientation thereinafter in an obtuse angle when the facial crest begins. The skull roof is rhomboidal, wide, flat and slightly depressed above the orbits. The broadest width is located at the level of the supraorbital tubercles. Most of the basicranium is not preserved. Even though, the palatine fossa are partially visible, small and oval-shaped with divergent borders. Two isolated occipital fragments (B2-62 and CA6-127) show short paroccipital processes little differentiated from the posttympanic ones. The paroccipital tips are blunt. The posterior surface of the paroccipital area is flattened and smooth, with a shallow condylar fossa.

Upper teeth (Fig. 3; Table S3)—in the decidual series (DES-49; Fig. 3D), the ectoloph is covered with a thin layer of cementum. DP1 outline is triangular, has a protoloph limited to a faint ridge and shows a small crochet. DP2 is trapezoidal, with a depressed anterior surface formed by an expanded parastyle and the anterior cingulum. In DP2, the mediofossete is encircled by a developed crochet and crista. The pointed expansion of the paracone and the loose connection between protoloph and ectoloph encloses a second anterior mediofossete. Whereas, only DP1 and DP2 show lingual cingula, the labial cingula are present in the posterior half of all the decidual pieces. The paracone fold is well marked in DP2-4. DP3 and DP4 are very similar in morphology and proportions, being the DP4 slightly bigger. Both share posterior protocone and anterior hypocone folding, labial cingula placed at the basal most border of the crown, strong anterior and posterior cingula and well-developed crochets. The permanent premolar teeth are rectangular in occlusal view; M1 and M2 are squared and `fan´-like respectively; the ectoloph is little undulated and

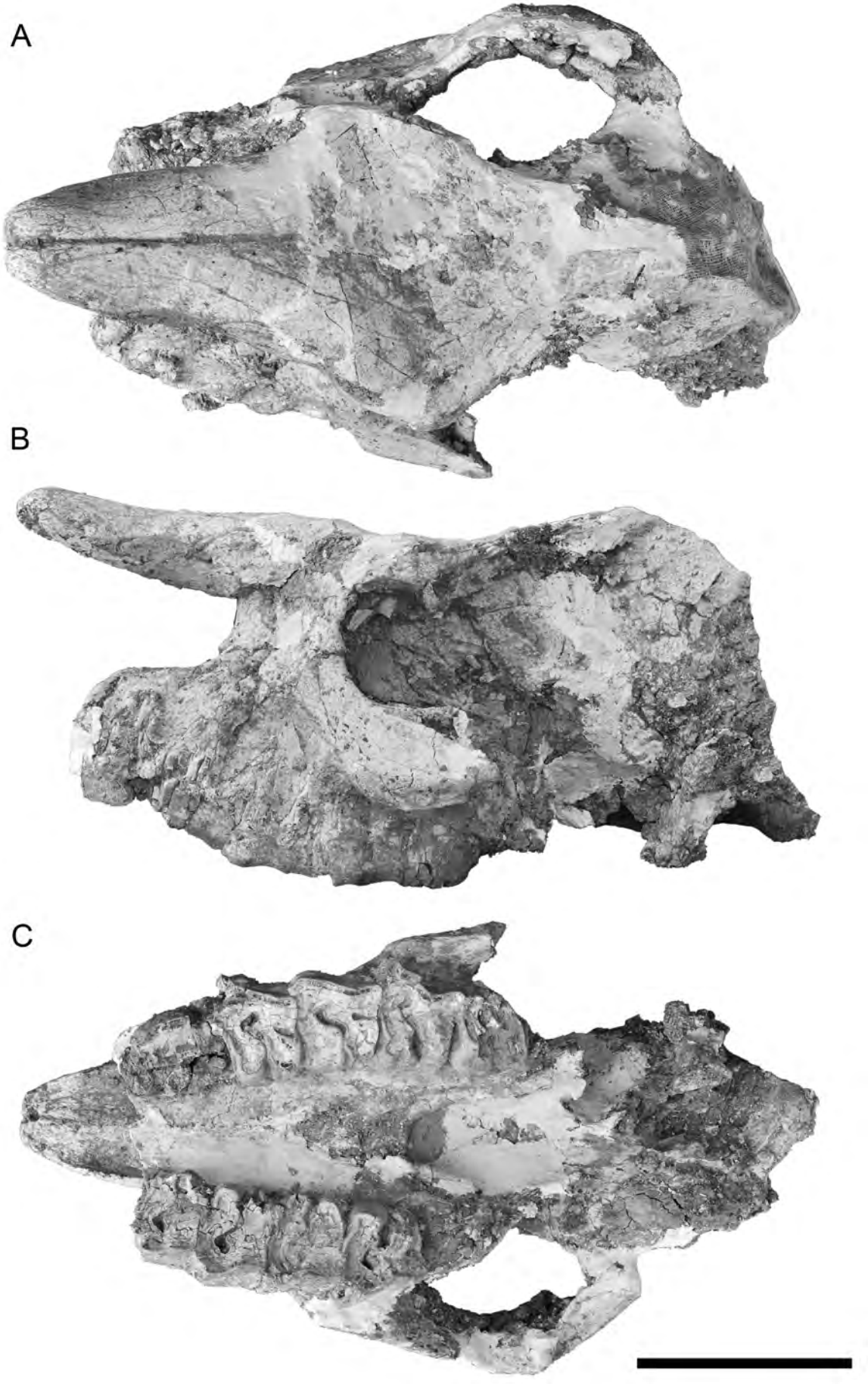


Fig. 2 Skull of *Alicornops simorrense* M407 A1-1 from M–407 Rotonda in A, dorsal, B, lateral left, and C, ventral views. Scale bar equals 100 mm.

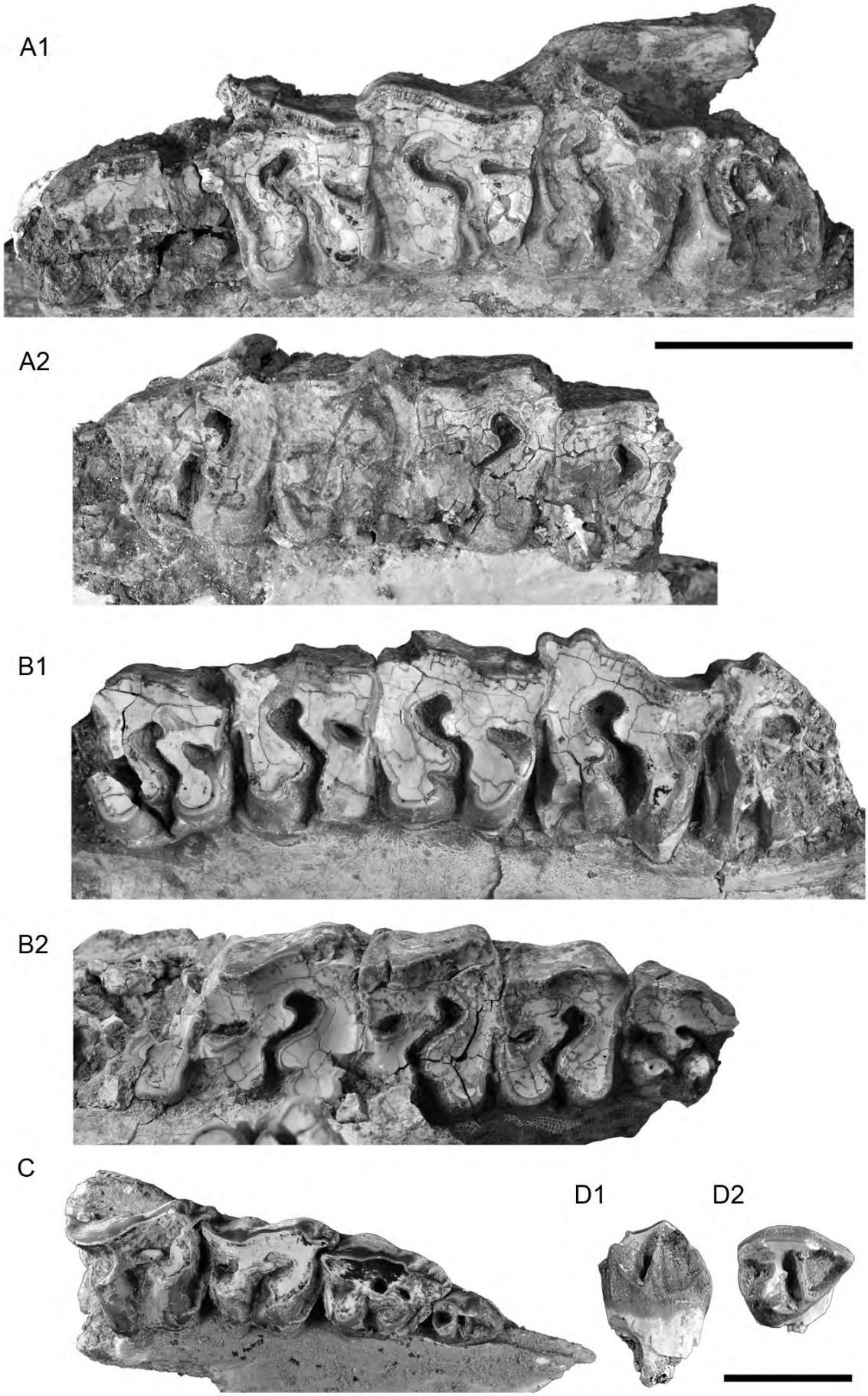


Fig. 3 Upper teeth of *Alicornops simorrense* from M–407 Rotonda in occlusal view. A1, left row P4-M3 A1-1; A2, right row P3-M2 of the same specimen; B1, left row P3-M3 H-11; B2 right row P2-M2 from the same specimen; C, right decidual series DP1-DP4 DES-49; D, right P1 C2-68. Scale bar for A, B and C, is placed on the top right and equals 50 mm. Scale bar for D, placed on the bottom right, equals 20 mm

wider in molars than premolars. Parastyle and paracone style are blunt, loosing strength with wear; hypocone is rounded and loosely connected to the metacone, being more evident in molar series; a subtle anterior hypocone fold is present in M1; posterior protocone fold marked in P4-M2, defining a rounded antecrochet; anterior protocone fold only evident in M1; crochet present in both molar and premolar series, is well developed and rounded; protocone and hypocone remain independent, even in very worn premolars; in P2, protocone and hypocone are two isolated cusps; its protoloph is distally bifurcated and oriented towards the hypocone but without contacting it; premolars have anterior, lingual and posterior cingula; the anterior cingulum is low, continuous and weak; the lingual cingulum is variable. A1-1 (Fig. 3.1A) is formed by two ridges in both sides of the median valley, while M407 H-11 (Fig. 3.1B-C) has a well-developed continuous wall; anterior and lingual cingula are continuous in the P4 of M407 H-11 but they do not contact in M407 A1-1; the posterior cingulum encloses a narrow and shallow posterior valley; median valley sigmoidal and narrow; the labial cingulum is present at the premolar series, being represented as a small posterior ridge; M3 triangular in occlusal view, with anterior cingulum, represented as a low weak ridge and posterior cingulum as a short and faint crest placed lingually.

Mandible (Fig. 4; Table S2)—the mandibles found in M-407 Rotonda are mostly incomplete. The position of the mandibular foramen varies from the p2-3 boundary (DES-48) to the level of the hypoconid of the p3 (without field number). The posterior limit of the symphisis reaches the p3. The mandibular angle is smooth, rounded and not protrudes from the vertical ramus. Its convexity is ventrally delimited by a marked depression, limit of the area of insertion for the M. masseter.

Lower teeth (Fig. 4; Table S4)—on the labial wall of the

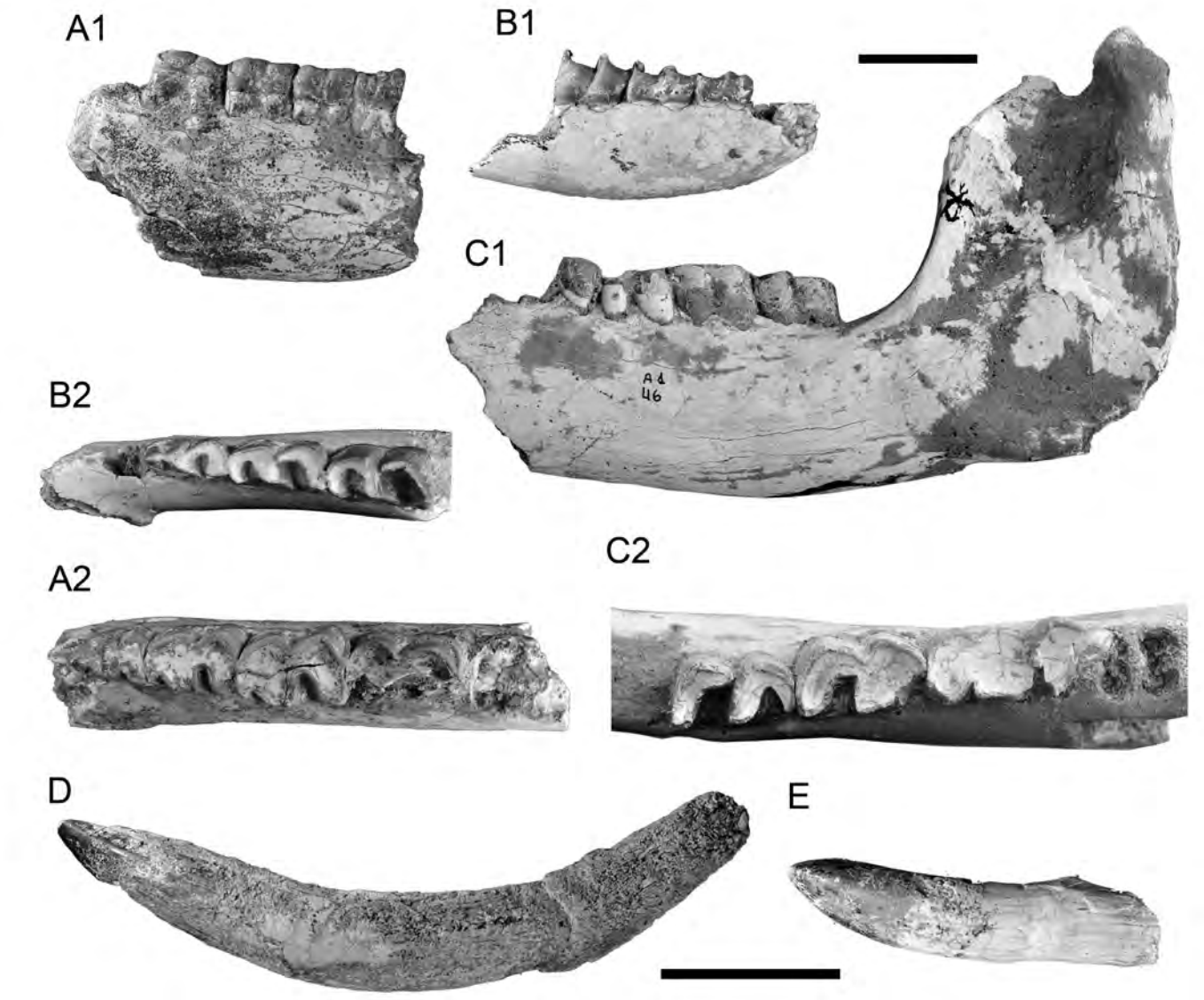


Fig. 4 Mandibles and lower teeth of *Alicornops simorrense* from M–407 Rotonda. A1, left hemimandible DES-48 with p2-p4; A2, same piece in occlusal view; B1, right juvenile hemimandible CA3-24 with dp2-dp4 in lateral view; B2, same piece in occlusal view; C1, left hemimandible A1-46 with p4-m3 in lateral view; C2, same piece in occlusal view; D, male tusk-like i2 C2-85 in anterior view; E, female tusk-like i2 CA6-209 in anterior view. Scale for A1, B1 and C1 is placed on top right corner, scale form the rest on the bottom. Both scale bars equals 50 mm.

lower teeth of *A. simorrense*, the enamel texture is corrugated and there are some cementum patches adhered to the ectoloph. The p2 has an irregular rim as labial cingulid, more developed in the third and fourth premolars (as it is formed by a discontinuous and bumpy rim). On the lingual side, there is a faint ridge anterior to the anterior valley. On the labial side, only the anterior cingulid is present, although little developed. The posterior cingulid is sometimes present (CA2-18).

Postcranial skeleton

The postcranial bones of *A. simorrense* are robust, showing remarkably shortened metapodials (Cerdeño and Sánchez, 2000). This contrasts with the relatively slender stylopodium. In M–407 Rotonda several individuals have been found, including several juvenile ones that have been excluded from the morphological description.

Atlas (Fig. 5A)—the vertebral body is short and wide, with two developed oval (A1-56) to 'D'-shaped (CA4-205) transverse processes. The condylar facets are semicircular and very concave. The rachidian canal is small and has a 'mushroom'-like outline in anterior view. The dorsal side of the vertebral body has a bumpy origin area for the *m. rectus capitis dorsalis*, divided by a longitudinal and shallow groove. On the dorsal surface, the inner *foramina vertebrale laterale* are rounded and totally individualized from the alar fossa, which is also rounded. The ventral surface has two little foramina in the base of each transverse process. The axis facets have a subsquare to semicircular outline. The atlas of *A. simorrense*

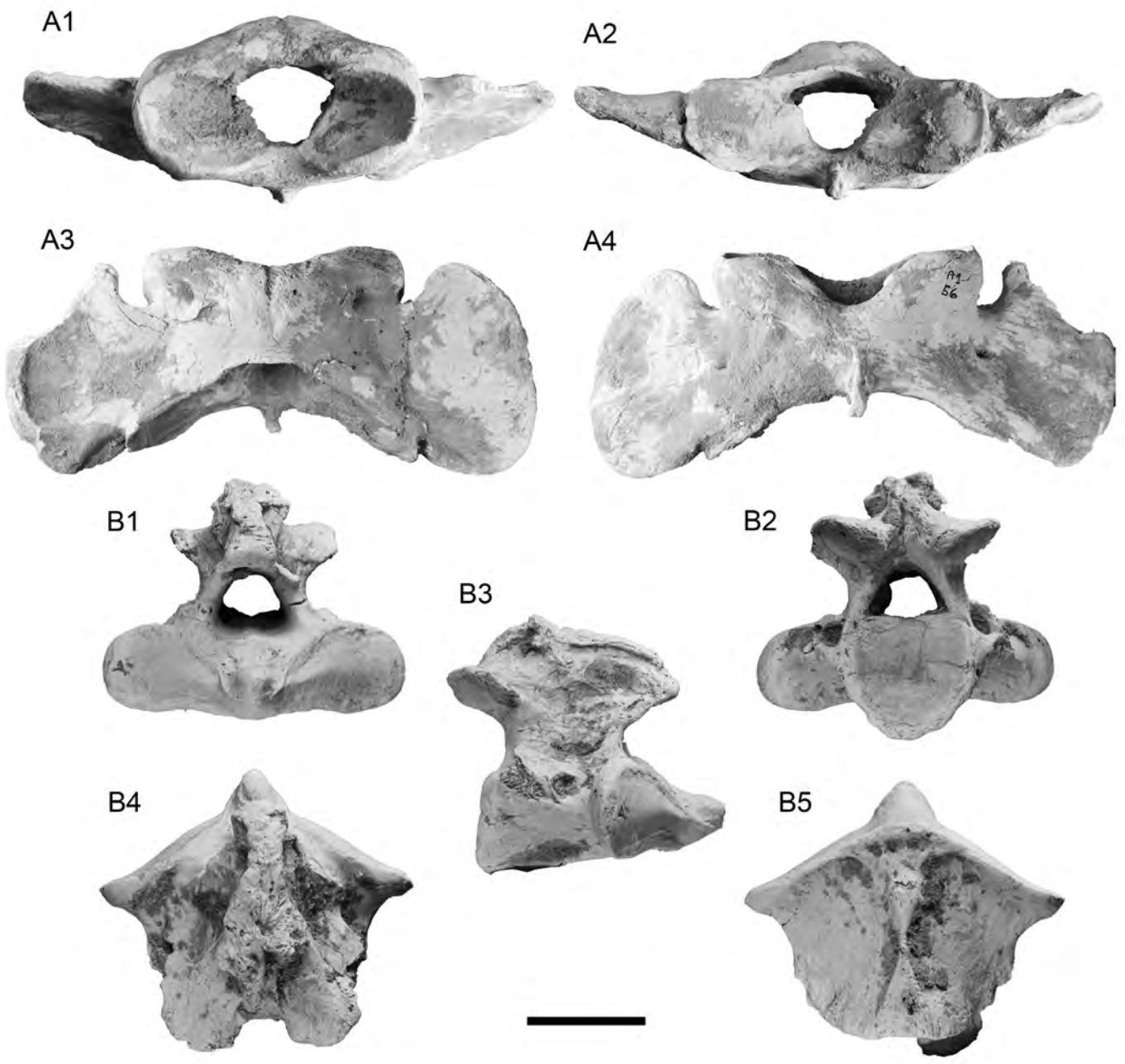


Fig. 5 Cervical vertebrae of *Alicornops simorrense* from M–407 Rotonda. A, Atlas A1-56 in A1, cranial view; A2, caudal view; A3, dorsal view and A4, ventral view. B, Axis CA4-400 in B1, cranial view; B2, caudal view; B3, right lateral view; B4, dorsal view and B5, ventral view. Scale bar equals 50 mm.

has two small *foramina transversarium*, but partially concealed behind the lateral border of the axis facets.

Axis (Fig. 5B)—the dorsal spine is sharp and shows a narrowed central part. Its anterior side is occupied by a rough and irregular area anteriorly oriented, place of attachment for the *ligamentum interspinale*. The anterior articular facets are narrow and slightly convex. Their outline is 'tear'-shaped, with a straight ventral border and an expanded dorsal one. They extend through the ventral side of the odontoid process. The transverse foramen has a rounded anterior rim and an oval to 'tear'-like posterior one. The ventral keel fades out towards the anterior side of the bone, being very smooth in the base of the odontoid process.

Scapula (Fig. 6A)—two scapulae have been found (one of them, CA3-67) badly damaged. The neck is noticeably long and slender. The distal part of the scapular spine starts at the midpoint of the neck (the remaining spine is broken in both specimens). The cranial scapular notch is extremely shallow and high. The supraglenoid tubercle is robust and rounded and the caudal border gently concave. Despite part of the blade of CA3-67 (the best preserved specimen) is somewhat broken, a caudal triangular expansion typical of Aceratherini rhinoceroses is present on its caudal border.

Humerus (Fig. 6B; Table S5)—Only distal epiphyses (e.g. DES-10 and DES-45) have been recovered. Their olecranian fossa is wide but short. The trochlea has a shallow gutter and a well-defined *capitulum* with a flattened articular surface. Due to their badly-preserved status, no reliable morphological characters have been observed.

Ulna (Fig. 6C; Table S7)—even though no ulnae with fully-preserved olecranon have been found, it seems robust and with a wide base. The angle between diaphysis and olecranon is nearly straight (Character 205 in Antoine, 2002). The humeral trochlea is asymmetric and concave in lateral view. The lateral and medial borders of the humeral articular surface of the anconeal process are divergent. The medial lobe is short and finishes in a straight distal extent. The lateral radius facet is asymmetrical and subtriangular. The medial crest is short, rounded and poorly-developed. The section of the diaphysis is triangular and presents flat surfaces.

Radius (Fig. 6D; Table S6)—the proximal epiphysis is narrow. On the proximal articular surface, the lateral portion of the humeral-facet is subtriangular and has a straight cranio-lateral border. The medial one is considerably bigger, semicircular, concave and shows a slightly concave caudal border. On the dorsal side, the insertion for the *m. biceps brachii* is strong, deep and 'tear'-shaped. The ulnar facets of the caudal side of the proximal epiphysis are independent, have a semicircular outline and form an obtuse angle. The most laterally placed is longer than the medial one (which is narrower in younger specimens as C1-21). The lateral ridge for the *ligamentum collaterale mediale* is strongly developed. The diaphysis is cranio-caudally flattened and has a subtriangular section, with marked scars for the ulnar attachment along the last two-thirds of the lateral border of the shaft. The distal epiphysis is swollen. On the cranial side, the gutter for the *m. extensor carpi* is slightly marked. The lateral side is excavated by two articular facets for the ulna. The proximal one is irregular and 'kidney'-shaped, the distal flat and oval. All the distal epiphyses found are eroded, preventing their description.

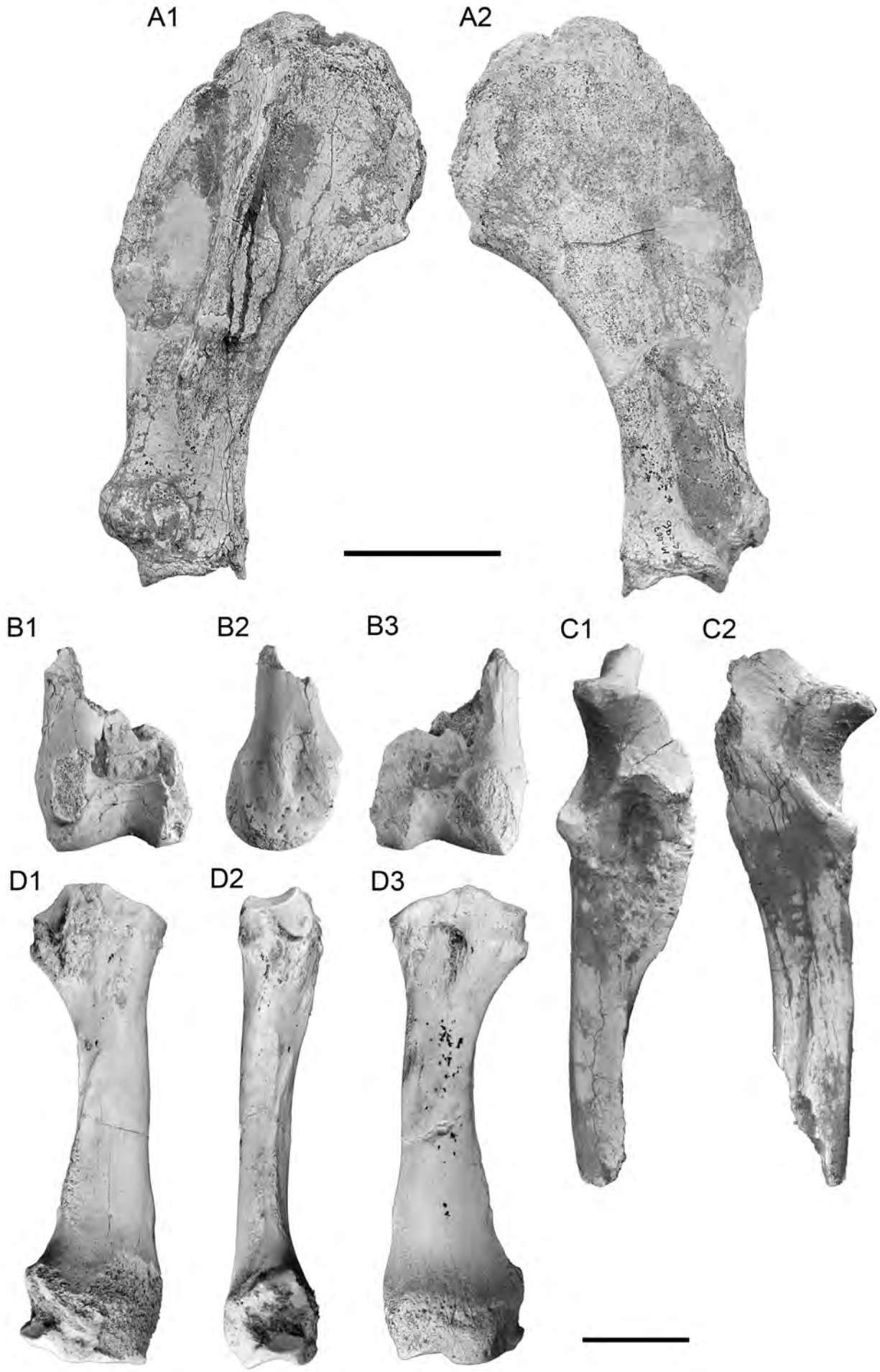
Scaphoid (Fig. 7A; Table S11)—the bone is robust and wide (high TD). The proximal radial facet is rhomboidal, wide, and has a pointed lateral expansion supported by a protruding and rough expansion. The radial facet has a typical 'saddle'-like surface, with a more elevated caudal side than the dorsal one (which has an rounded surface). On the lateral side, both semilunate facets are clearly marked. The proximal one is long and obliquely oriented, the distal rectangular and flattened. The distal side of the bone is mainly occupied by the trapezoid and magnum facets, being the trapezium one reduced to an almond-shaped small articular surface.

Semilunate (Fig. 7B; Table S12)—the semilunate is high in dorsal view. The dorsal surface of the bone shows a blunt and slightly dorsally-protruding central area. The radial-facet is prolonged palmarly, ending in a short and concave expansion for the ulna. The volar process is short and stout. The medial side of the bone hosts the scaphoid-facets. The proximal one is tapered and very long, reaching the base of the volar process; the distal scaphoid-facet is semicircular and flat. Two pyramidal-facets are placed on the lateral side of the bone. The proximal facet is narrow, smooth, and attached to the radial-facet; the distal one is semicircular and flat. On the distal side, the magnum-facet is elongated and goes from the dorsal border of the bone (by means of a narrow extension) to the palmar side of the volar process. The unciform-facet is oval and somewhat concave.

Pyramidal (Fig. 7C; Table S13)—the bone is deep (high APD). In medial view the bone shows a developed and pointed palmar extent and a gently sigmoid dorsal one. The proximal articular facet for the ulna is somewhat concave, extending through the posterior side through a triangular projection. In medial view, both semilunate facets are crescent-like, flat and similar in size.

Trapezoid (Fig. 7D)—the two trapezoids found are narrow (low TD). Both proximal and distal articular surfaces are roughly equivalent in size. In addition, if observed in dorsal view, the lateral and medial borders of the bone are somewhat convex, giving a symmetric appearance.The proximal scaphoid facet has a square outline. The distal Mc II facet is triangular.

Fig. 6 (next page) Scapula and anterior limb bones of *Alicornops simorrense* from M–407 Rotonda. A, left scapula C2-296 in A1, lateral and A2, medial views; B, distal epiphysis of a right humerus CA2-46 in B1, cranial, B2, lateral and B3 caudal views. C, right ulnae A2-35 in C1, cranial and C2, lateral views; D, right radius C1-21 in D1, caudal, D2, lateral, and D3, cranial views. Scale bar for A (center) equals 100 mm; scale bar for B-D (bottom right) equals 50 mm.


A1
A2
B1
B2
B3
C1
C2
D1
D2
D3

Both dorsal and palmar sides are flat. The dorso-lateral notch is sigmoid and shallow. The palmar notch is not preserved in the available sample.

Magnum (Fig. 7E; Table S14)—a single fragmentary magnum has been found (C1-16). It is a small bone with a low (low H) dorsal face. In dorsal view, both scaphoid and unciform-facets form a straight angle. The distal border of the dorsal surface is rounded. In lateral view, the Mc III facet is concave and short. The proximal ridge is thick and short (low APD).

Unciform (Fig. 7F; Table S15)—a single dorsal fragment has been recovered. In proximal view, the dorsal surface is gently curved, shows a very short (low APD) pyramidal facet of square outline, and a triangular and flattened semilunate one. Both form an obtuse angle in dorsal view. In the same view, a well-defined rounded tubercle protrudes from its lateral side. While not preserved, the broken insertion for the volar process is narrow, pointing to a short process.

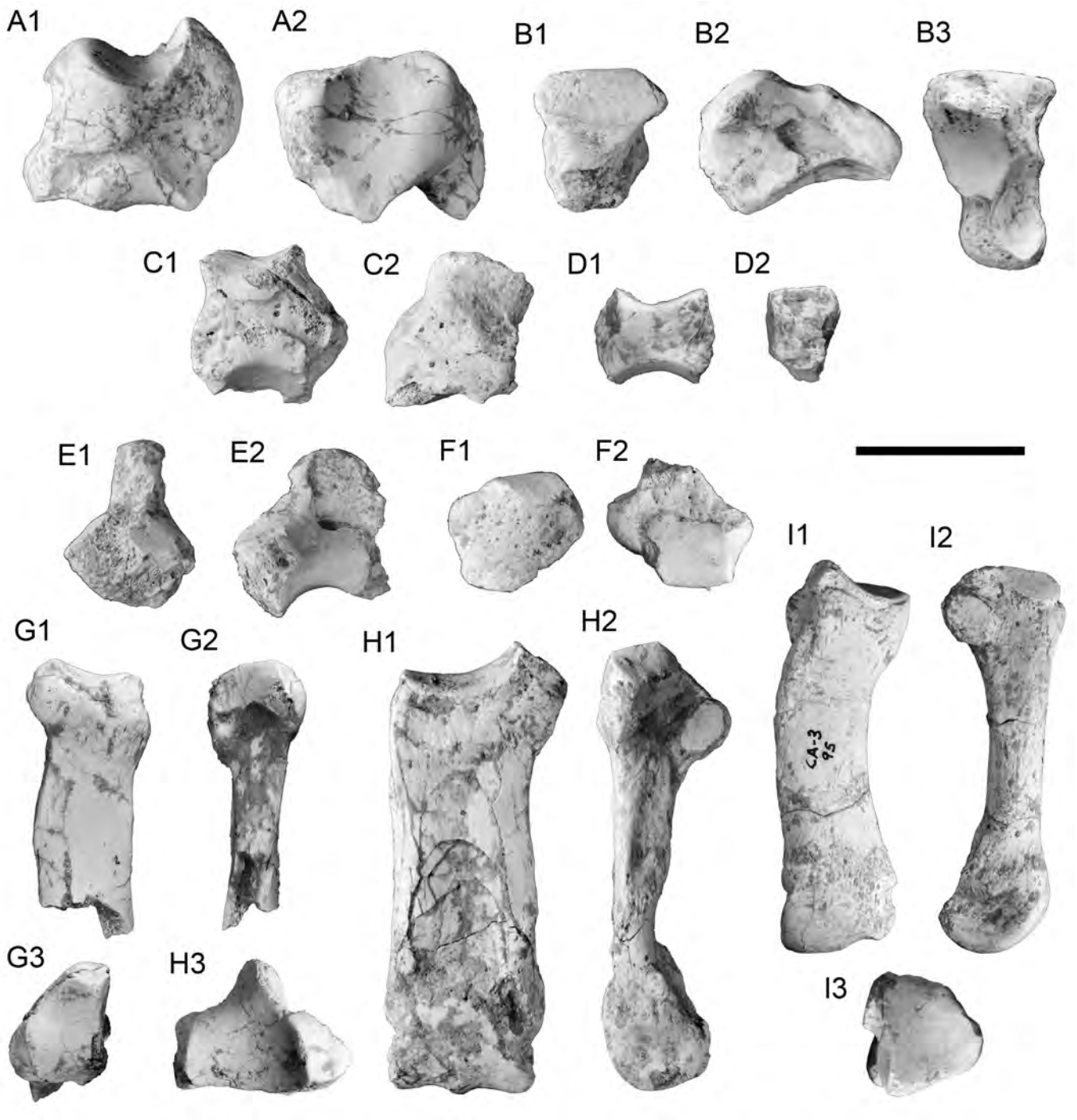


Fig. 7 Carpal and metacarpal bones of *Alicornops simorrense* from M–407 Rotonda. A, right scaphoid C2-86 in A1, lateral and A2, proximal views; B, right semilunate CA4-54 in B1, dorsal, B2, medial, and B3, distal views; C, right pyramidal CA4-36 in C1, medial and C2, dorsal views; D, right trapezoid CA4-362 in D1, dorsal and D2, lateral views; E, right magnum C1-16 in E1, dorsal and E2, lateral views; F, right unciform CA4-9 in F1, dorsal and F2, proximal views; G, right Mc II A1-23 in dorsal and G2, medial views; H, left Mc III CA6-91 in H1, dorsal and H2, lateral views; I, left Mc IV CA3-95 in I1, dorsal and I2, medial views. Scale bar equals 50 mm.

Mc II (Fig. 7G; Table S18)—only one proximal half of a Mc II (A1-23) has been found. The proximal trapezoid facet is 'D'-shaped and slightly concave in dorsal view. In dorsal view, the lateral tubercle for the *m. extensor carpalis* of the proximal epiphysis is square-shaped and clearly delimited from the shaft. On the palmo-lateral side, the magnum facet is 'kidney'-shaped and has a shallow indentation. Its lateral border presents a very small dorsal Mc III-facet. It is semicircular and distally oriented.

Mc III (Fig. 7H; Table S19)—the anterior central metacarpal is short. The proximal magnum facet, visible in dorsal view, is subtriangular, has a straight dorsal border and a pointed palmar tip. The unciform facet is very protruding, proximally oriented, trapezoidal in shape and flat. Both form a straight angle, with a sharp boundary between them. On the medial side, the Mc II facet is small and has a 'kidney'-shaped outline. Both Mc IV facets form an obtuse angle between them. The dorsal is semicircular, the palmar oval. Both are separated by a shallow and wide groove. The diaphysis is flattened and has parallel borders. The insertions for the *m. interossei* are very developed, surpassing the midshaft in extension. The distal articular surface is dorsally-oriented, leaving a short palmar surface. The central keel is present but smoothed.

Mc IV (Fig. 7I; Table S20)—a single Mc IV has been recovered from M–407 Rotonda (CA3-95). It is a short bone, with a patent curvature limited to its first third of the shaft. The proximal unciform facet is wide and subtriangular in shape, slightly convex both laterally and dorso-palmarly. The lateral border of the unciform-facet is eroded and no Mc V facet has been detected. The medial Mc III facets are independent. The dorsal one is ovoid, flattened and separated by short neck from the proximal epiphysis. The palmar facet is 'tear'-shaped and attached to the proximal articular surface. The palmar facet is more posteriorly oriented respect to the dorsal one.

Femur (Fig. 8A; Table S8)—the femoral overall proportions are slender. The head of the femur is asymmetrical and occupies more than a half of the proximal surface. It is big and rounded, with a deep and oval *fovea capitis*. The greater trochanter is low (low H), narrow and has a square profile in proximal view. Its lateral surface is narrow, flat and slightly medially inclined. The ridge of the greater trochanter is at the same level than the head of the femur. Both flank a short (low H) but deep trochanteric fossa. The lesser trochanter, on the medial side, is restricted to a long and narrow vertical ridge with a straight medial border. The distal limit of the third trochanter is well-differentiated from the shaft. Its tip is rounded and short (as observed in CA6-89). The diaphysis is narrow, with a straight medial outline. In medial view, the transition between the medial lip of the trochlea and the diaphysis results in a convex border and a distal sulcus. On the distal epiphysis, the lateral attachment scar for the *m. flexor superficialis* for the phalanxes is big and oval. In medial view, the attachment for the *m. gastrocnemius* starts at the same level as the former, is wide and expands as a depressed popliteal surface. The lateral condyle of the trochlea is more distally projected than the medial one.

Patella (Fig. 8B; Table S9)—the recovered patellae of *A. simorrense* from M-407 Rotonda are stout, deep and have rough cranial surface. The lateral flange of the bone is well developed and shows a subtriangular outline, limited from the rest of the bone by a vertical and vascularized shallow groove. The considerable expansion of the lateral flange fact makes the bone as high as wide. The caudal femoral facet partially covers the distal half of the lateral flange. Its proximal extent reaches the proximal tip of the bone, which is very short and pointed. The medial side of the femoral facet has a concave medial border. On the other hand, the lateral one shows the typical trapezoidal profile.

Tibia (Fig. 8C; Table S10)—Their overall size is small and stand out for their proportionally profound (high APD) proximal epiphyses and widened (high TD) distal one. The proximal femoral articular plate is very asymmetrical, with a larger and oval medial surface and a smaller and vaguely 'mushroom'-like lateral one. The proximal tibial tuberosity is small, narrow and placed in the cranio-lateral side of the bone. In caudal view, the popliteal notch is wide and shallow. The proximal fibular facet is triangular and narrow (low APD). The distal one is low (low H). The diaphysis is oval except for a narrow lateral keel. The astragalar articular surface has a straight lateral border, parallel to the lip of the trochlea. The medial malleolus is big has a sharp border and an outer flattened surface.

Astragalus (Fig. 9A; Table S16)—the astragalus is wide (high TD), has a deep and very asymmetrical trochlea with an overhanging lateral lip distally-projected. The neck is short and narrow. The groove between the trochlea and the distal articulation is profound and well-delimited. The distal articular facet is medially-displaced, showing a square-shaped medial protuberance. On the plantar side, the first calcanear facet is rounded to subsquare, has a concave surface and shows a well-marked distal projection. The second calcanear facet is rounded and centered on the plantar side of the bone. The third calcanear facet has an oval outline and is attached to the distal border. Its degree of connection with the second calcanear facet varies in the studied sample from totally isolated (CA5-90) to partially fused (C1-72). The distal navicular-facet is very narrow and has a rounded medial border. The cuboid-facet is thin and 'tear'-shaped.

Navicular (Fig. 9B; Table S17)—The bone's dorsal outline is rhomboidal. The astragalar facet has a concave lateral border (except in CA4-65, which is straighter) and a sigmoid plantar one. Its medial side is distally inclined, causing the central part to be thin. The plantar tuberosity is plantarly projected and rounded, leaving a laterally-placed shallow notch. On the distal side, the ectocuneiform-facet is 'heart'-shaped and the mesocuneiform one is semicircular and flat. Finally, the entocuneiform facet is small and forms an obtuse angle with the mesocuneiform one.

Cuboid (Fig. 9C; Table S18)—the only cuboid attributed to *A. simorrense* (CA2-11) from M-407 Rotonda is a small bone, maybe pertaining to a young individual. The proximal

articular area is square and flattened, with a pointed plantar expansion. The volar process is poorly developed and does not surpass the distal side of the body. On the lateral side, the proximal navicular facet is small, concave and proximally oriented. The dorsal ectocuneiform facet is semicircular and flat. The plantar ectocuneiform facet distally oriented but badly preserved. The distal Mt IV facet is triangular and has blunt edges.

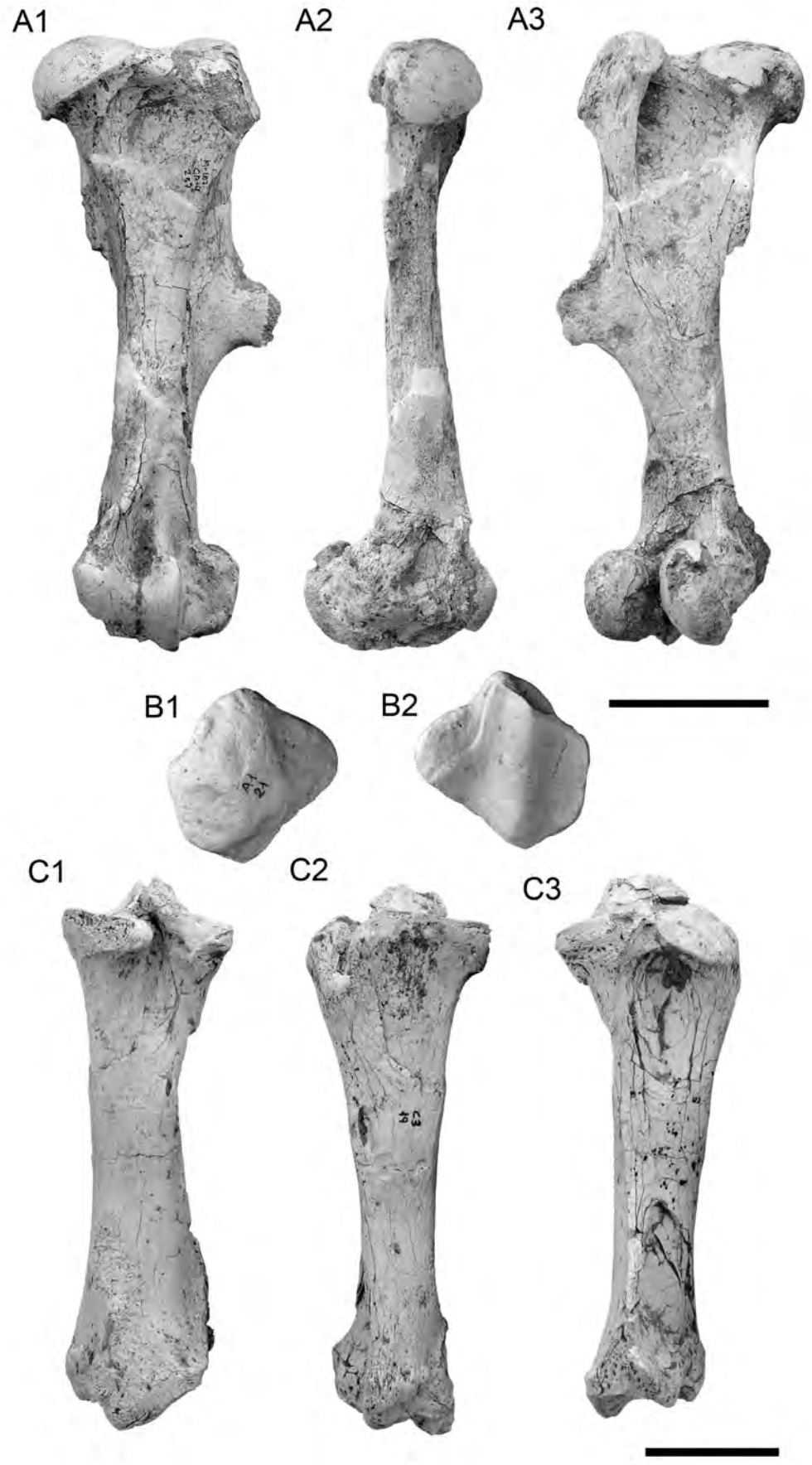


Fig. 8 Posterior limb bones of *Alicornops simorrense* from M–407 Rotonda. A, left femur CA4-287 in A1, cranial, A2, medial and A3, caudal views; B, left patella A1-21 in B1, cranial and B2, caudal views; C, right tibia C3-19 in C1, cranial, C2, medial and C3 caudal views. Scale bar equals 50 mm.

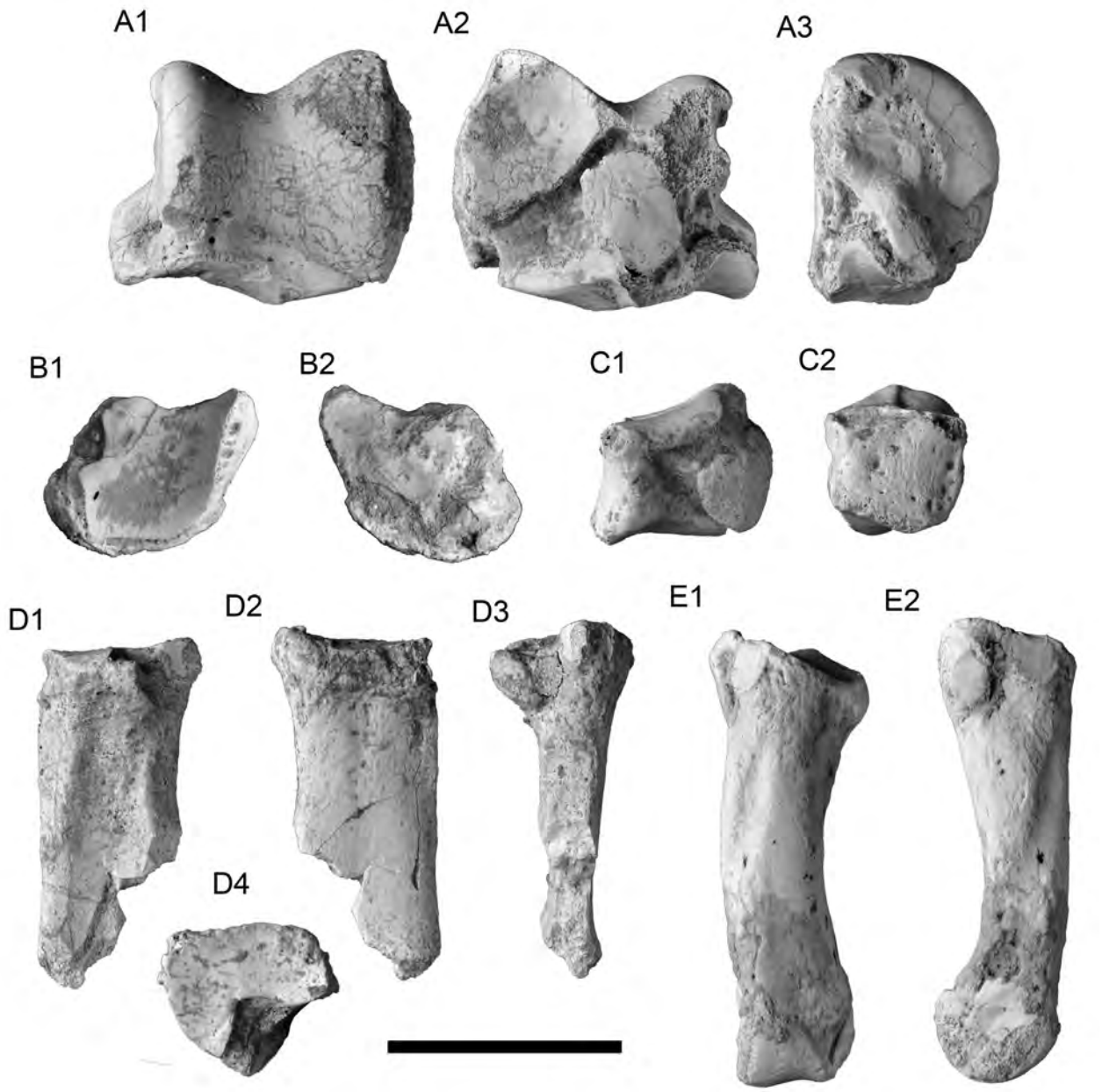


Fig. 9 Tarsal and metatarsal bones of *Alicornops simorrense* from M–407 Rotonda. A, left astragalus C1-72 in A1, dorsal, A2, plantar and A3, medial views; B, left navicular CA3-73 in B1, proximal and B2, distal views; C, right cuboid CA2-11 in C1, lateral and C2, dorsal views; D, proximal epiphysis of a right Mt III A6-232 in plantar, D2, dorsal, D3, lateral and D4, proximal views; E, left Mt IV CA4-6 in E1, dorsal and E2, medial views. Scale bar equals 50 mm

Mt III (Fig. 9D; Table S21)—two proximal epiphyses have been recovered from the area. Both are damaged and lack their posterior half. In proximal view, the proximal ectocuneiform facet has a convex dorsal border. The groove between both Mt IV facets is deep and rounded, leaving a narrow dorsal side. In dorsal view, the dorsal border of the ectocuneiform facet is somewhat concave-convex. The section of the diaphysis is oval and wide (low APD).

Mt IV (Fig. 9E; Table S22)—the bone is short, stout and bended to its midshaft. The proximal cuboid-facet is subtriangular to oval and occupies the entire proximal surface. The medial Mt III facets are individualized through a narrow groove. The dorsal one is semicircular, flattened and attached to the proximal articular facet. The plantar facet is oval, vertically placed and separated from the proximal articular surface by a swollen area. A wide but shallow groove for the *m. interossei* embraces the medial side of the midshaft. The distal articular surface is narrow and close to the medial border in dorsal view. The lateral lip is well developed and the medial one flattened.

RESULTS AND DISCUSSION

Morphological comparison with other remains of *A. simorrense*

A. simorrense is a frequent rhinoceros species in the Upper Aragonian basins from the Iberian Peninsula and Western

France, being scarcer in Central Europe. In Madrid City area, the species was previously recognized in the localities of Moraleja de Enmedio and Paracuellos-3 (Cerdeño and Sánchez, 2000). Both localities pertain to the Upper Aragonian (MN 6). The abundance of *A. simorrense* in the fossil site of M–407 Rotonda permits to establish some general comparisons with both Iberian and European remains. Up to now, cranial remains of *A. simorrense* were restricted to the localities of Simorre, Villefranche d'Astarac, Moraleja de Enmedio, Toril-3 and Arévalo (Cerdeño and Sánchez, 2000; Guérin, 1980). The type collection from Villefranche d'Astarac has been never figured nor described, being only cited in the original description made by Lartet. Simorre, another classic locality with presence of the species, has provided a palate with both teeth series figured in Guérin (1980), but the rest of the skull is missing. Lartet (1851) makes allusion to an additional skull, but not description or illustration is provided. The skull MNCN 30768 found in Moraleja de Enmedio (described in Cerdeño and Sánchez, 2000) comprises the most complete skull found for the species. It lacks the nasal bone and is slightly dorso-ventrally pressed, but the overall preservation is good, serving for morphological comparisons with the individual A1-1 from M-407 Rotonda. Additionally, the skulls recovered from Toril-3, despite their dorso-ventrally or laterally crushing, are an additional source of information of particular characters. The rostrum of A1-1 shares equivalent maxillary bones with MNCN 30768 from Moraleja de Enmedio, point of origin of the zygomatic crest (at the level of the M1) and orbit position (at the level of the M1). Both skulls share a slightly inflated area in the dorsal side of the frontal bone at the level of the orbits and the same nasal notch shape in lateral view. In dorsal view, the rhomboidal shape of the frontal bone and the nasal suture reaching the level of the anterior rim of the orbit are coincident in Toril-3 (MNCN 33420) and M-407 Rotonda. In contrast, the skull A1-1 is higher than MNCN 30768 from Moraleja de Enmedio and presents a slightly shorter distance between the nasal notch and the anterior rim of the orbit (60.5 mm in A1-1; 71.4 mm in MNCN 30768). Both specimens share an oval orbit (vertically placed in A1-1, oblique in MNCN 30768). We believe that the greater height of the skull A1-1 and the different orientation of the orbits are caused by the dorso-ventral compression and the backwards-inclined dorsal half of the skull seen in Moraleja de Enmedio. Unfortunately, it is difficult to address if such deformation has affected the orbitoaural portion of the skull producing a secondary elongation of the neurocraneum, thus modifying the occipital plate orientation. If so, the original occipital plate could be little more vertically oriented. Regarding the basicraneum, the post-palatine opening reaches the level of the M2 in A1-1. This condition is shared by the palate MNHN Sa-6431 from Sansan, in which reaches the M2 hypocone (Heissig, 2012). According to the discussed characters, we propose a reconstruction of the overall cranial morphology of *A. simorrense* and its life appearance (Figure 10). The vertical rami of the sample M-407 Rotonda presents a strong ventral notch behind the level of the m3. The articular process is also lower in contrast to the sample from Toril-3.

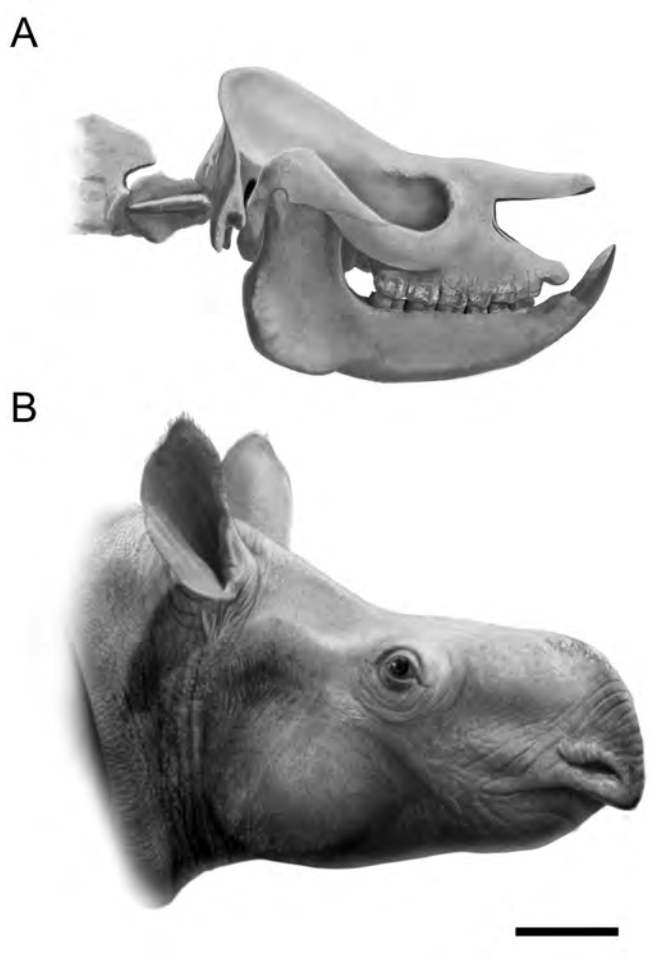


Fig. 10 A, idealized skull and B, reconstructed life appearance of *Alicornops simorrense* based on the skulls A1-1 from M-407 Rotonda and MNCN 30768 from Moraleja de Enmedio. Mandible is reconstructed according to the adult male hemimandible from Toril-3 (MNCN 31856). The placement of the lower tooth row follows the partial mandible from M-407 Rotonda A1-46. Scale bar equals 100 mm.

The teeth are very homogeneous among the Iberian samples and can be easily separated from those of *L. sansaniense*. The M1 from M-407 Rotonda —as MNHN Sa-6431 from Sansan (Heissig, 2012) or the fragmentary one figured in Stromer (1902)— have a marked anterior protocone fold, absent in the individuals from M-407 Rotonda. Teeth proportions of M-407 Rotonda fall within the observed species' variability (Supplementary Data 3). Both upper and lower rows are very similar in size to those of La Cistérniga and Toril-3 (also from the MN 7/8). If the samples from the Aragonian and the Vallesian are compared, some temporal variations can be observed (e.g. P3, P4, M1 and M2 and all the lower teeth except the p3). However, others do not follow the same pattern. The P2 and M3 from Nombrevilla show a wide size range that largely overlaps the Aragonian range. On the other hand, the p2-3 from Los Valles de Fuentidueña have particularly reduced proportions that contrast with those of Nombrevilla. Noticeably, some localities from the Middle Aragonian (i.e. Arroyo del Val-3 and 4, Armantes-3 and 6

and Montejo de la Serrezuela) present long but narrow teeth, markedly distinct from the bulk of the species. A future study of their morphology is needed to assess their specific validity.

An increase of the body size from the late Aragonian to the last Vallesian was identified among the Spanish populations of *A. simorrense* (Cerdeño & Sánchez, 2000). While in the Iberian central basins the species underwent an increase in robustness together with size, those from el Vallès Penedès Basin maintained similar proportions while augmenting in size (Cerdeño & Sánchez, 2000). The gracility indices recorded from the metapodials of M-407 Rotonda (Mc III = 30.4; Mc IV = 23.2 Mt IV = 21.6) are in agreement with the previously recorded for the species in the Iberian Peninsula (Supplementary Data 4). The Mc III CA6-91 is the most robust recorded (GI = 30.4), similar to those of La Cistérniga and Toril-3 (MN 7/8). Such elevated robustness is favored by the dorsopalmar crushing of the midshaft of CA6-91, confirmed by the very low value APD of the diaphysis (13.5 mm, in comparison with the remaining Iberian sample, which is 14 – 18.5 mm; n = 6). The gracility indices of the two Mc IV from M-407 Rotonda (GI = 96.7 and 102.3) are close to Los Valles de Fuentidueña (MN 9) and Toril-3 (MN 7/8) or la Cistérniga (MN 7/8). The gracility of the metacarpal bones are higher to previously recorded MN 6 populations, being closer to those of the MN 7/8 and MN 9. On the other hand, the gracility index of the Mt IV (22.1) is low (other Mt IV spans between 21 and 27.4). In this case, the recorded gracility are high, but compatible with those of Paracuellos-3 (20.4 and 21.7; MN 6). The scant sample

Most of the dimensions of the carpal and tarsal bones fall within the observed variability in the Iberian populations (Figure S1). The scaphoid presents a high H, close to the higher values recorded (Los Valles de Fuentidueña). The semilunate is short (low APD) and has a low anterior side (low Hart). On the contrary, the pyramidal is big (show high TD and the highest APD values among the Iberian samples). The trapezoid is narrow (short TD) and the unciform low (lowest Hant). Tarsal bones fall within the reported variation (Cerdeño and Sánchez, 2000). Only the distal articular transversal distance of the astragali is lower in M407-Rotonda.

Current status of *Alicornops*

A. simorrense was firstly described by Lartet (1851) as a rhino form with upper and lower incisors, nasal bones with a small horn insertion and slender limbs with elongated long bones. This early description was made using the remains from the localities of Villefranche-d'Astarac and Simorre (the latter figured in Guérin, 1980, p. 417). The palate with both upper series found in the latter has served as a reference for the dentition of the species from a practical point of view. As formerly mentioned, *A. simorrense* was related with the genera *Mesaceratherium*, *Dromoaceratherium* and *Aceratherium*. While the first two alternatives were posteriorly discarded (Ginsburg and Guérin, 1979; Heissig and Fejfar, 2007), its relation with *Aceratherium* persisted. The subgeneric rank of *Alicornops* within *Aceratherium* was originally proposed by Ginsburg and Guérin (1979). Thereinafter, the generic or subgenerinc rank of *Alicornops* has varied among specialists.

Heissig (2012) exposed that the common traits shared by *A. simorrense* and *A. incisivum* justify its arrangement of *Alicornops* to a subgeneric level. These are the primitive configuration of the chisel-tusk incisor complex with i2 in contact with I1, shallow proximal articular surfaces of the metapodials (lower APD) and the flattened diaphyseal sections. On the contrary, the author cites the presence of a nasal rugosity in *A. simorrense* as the main difference between both. Geraads and Saraç (2003; p. 218) suggested that Middle Miocene *Aceratherium*-like genera (like *Alicornops, Hoploaceratherium, Mesaceratherium, Plesiaceratherium,* or *Acerorhinus*) are part of poorly-defined different 'grades' within a lineage rather than different clades. As a result, they stated that their differences (which are not detailed) can be considered as intraspecific variability instead of intrageneric, thus including *Alicornops* as a subgenus in *Aceratherium* (in agreement with the original placement of *Alicornops* made by Ginsburg and Guérin).

In contrast, the phylogenetic analysis conducted by Antoine et al. (2003) provides eight synapomorphies, mostly based on dental characters, defining the genus *Alicornops.* These can be resumed as follows: convex ventral profile of the corpus mandibulae; presence of some cementum on the upper cheek teeth; weaker protocone than hypocone on the P2; presence of antecrochet on the upper molars; angulous trigonid; the talonid forms an acute dihedron in the lower teeth and lower molar teeth are void of lingual cingulum. On the postcranial side, the insertion for the *m. biceps brachii* forms a profound insertion in the radius. Deng (2013) remarks two particularities present in *Aceratherium porpani* from Tha Chang (Thailand) and absent from the Chinese *Alicornops laogouense*: the parietal crests maintain a considerable and constant distance behind the orbits and the zygomatic arches are more laterally expanded. As the author comments, the morphology of the *A. porpani* is very close to the specimen of Yulafli. However, the second is currently included in *Acerorhinus* (Athanassiou et al., 2014). The comparison of the skulls of *A. simorrense* from the Iberian Peninsula and the type collection of *A. incisivum* from Eppelsheim shows that these differences are not transferable to *Aceratherium*, as both species have a rhomboidal skull roof that narrows posteriorly in an occipital crest.

If restricted to the type series, the skull (OR 33525) from Villefranche d'Astarac, holotype of *A. simorrense*, preserves the palate (with both upper series), part of the basicranium and the left zygomatic arch (Figure 11A). Its comparison with the palate of the holotype of *A. incisivum* (HLMD 1932) shows some differences. The proportional width of the palate of *A. incisivum* respect to its dentition is narrower than that of *A. simorrense*. In addition, the dental series and the pterygoid crests are arranged parallel in *A. incisivum* (not slightly divergent as in *A. simorrense*). If the remaining cranial

remains of both species are included, further differences can be stressed. In both taxa, the nasal bones are raised and maintain a constant width up to the tip. However and according to Heissig (2012), the distal rugosity of the nasal bones of *A. simorrense* is one of the differences that separate *A. simorrense* from *A. incisivum*. This difference was originally noticed by Lartet (1851). Alternatively, the nasal bones of *A. simorrense* have a thick and blunt end and have a rugous appearance. These rugosities could be a possible place of insertion for a small distal nasal horn or a keratinized knob. On the other hand, nasal bones from *A. incisivum* have a more pointed anterior extent and a smoothed dorsal surface. The remaining shape of their rostra is remarkably similar. However, additional cranial differences can be stressed between both (using the type material from Eppelsheim for *A. incisivum* as a reference). The dorsal profile of the skull is straighter and aligned with the occiput in *A. incisivum* (elevated in *A. simorrense*, with an inflexion point behind the postorbital tubercle). However, a slightly raised occiput is present in the individuals from Höwenegg and Charmoille, so this character might be somewhat variable. In *A. incisivum*, the anterior end of the zygomatic arch is stronger and higher, lower and thinner in *A. simorrense*. The infraorbital foramen is much larger and closer to the orbit in *A. simorrense*, leaving a narrow column between them. The paraoccipital process is shorter in *A. incisivum* than *A. simorrense* (as recorded in Eppelsheim's DIN 1930 and the skull from Moraleja de Enmedio respectively). The external auditory pseudomeatus is larger and wider in *A. incisivum*. The posttympanic process would enclose the external auditory duct in *A. incisivum*. Unfortunately, the tip of the posttympanic process in DIN 1930 (the only from the type collection with this area preserved) is eroded and its

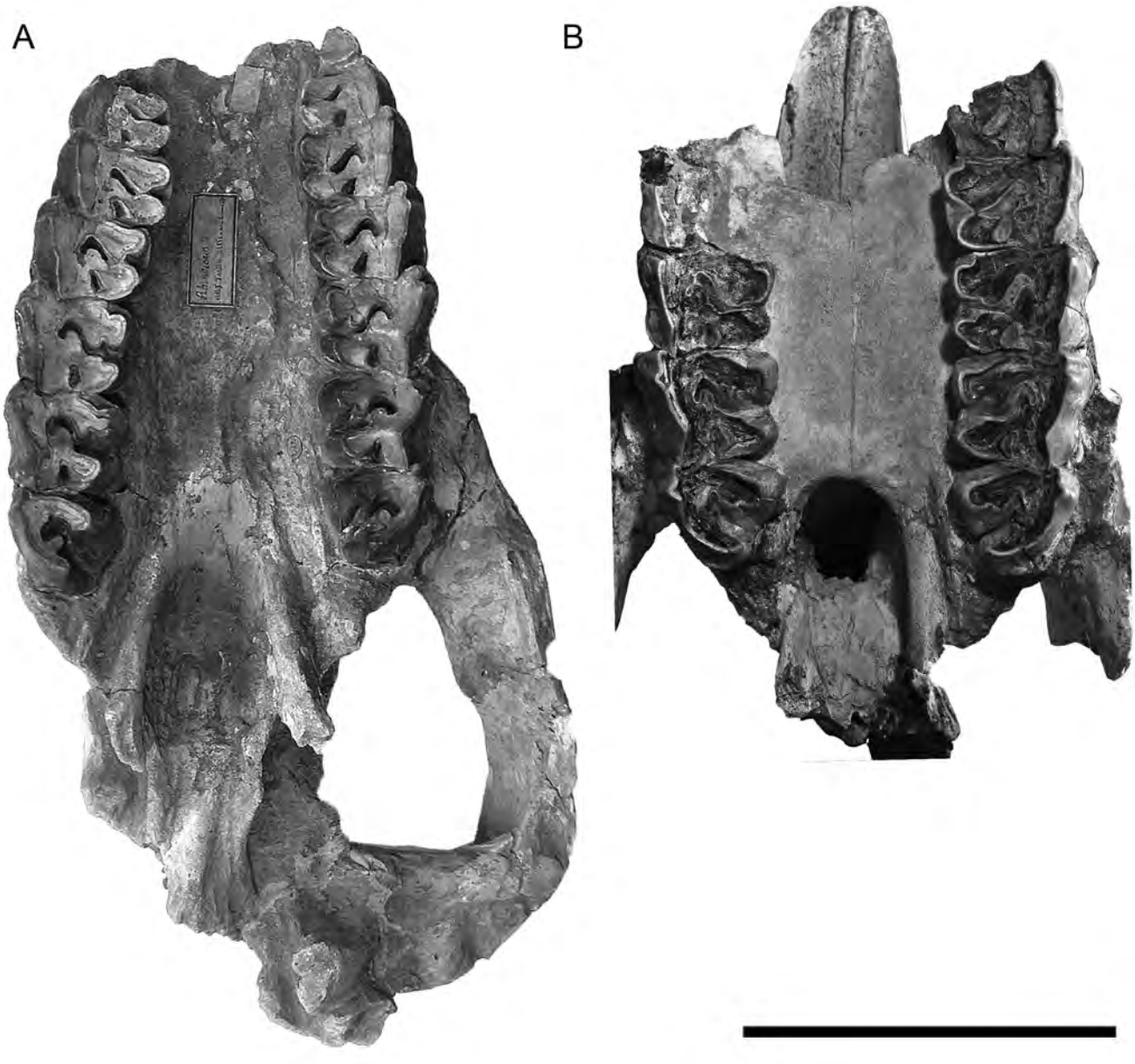


Fig. 11 Skull comparison between the holotypes of A, *Alicornops simorrense* (OR 33525 from Villefranche d'Astarac) and B, *Aceratherium incisivum* (HLMD DIN 1932 from Eppelsheim). Both are represented in ventral view. Scale bar equals 100 mm.

contact with the postglenoid one is not directly observed but feasible. The convex ventral border of the horizontal ramus of the mandible contrast with the straight ventral border observed in Eppelsheim and coincides with other aceratheres like *Acerorhinus*.

Regarding the dentition, both species share very similar dental patterns (Figure 11), in a parallel way to their cranial morphologies. The presence of cementum (present in *A. simorrense*) is a relatively variable feature in aceratheriine rhinoceros cheek teeth. The type collection of *A. incisivum* is void of cementum, but its presence has been reported from Los Batallones butte (Chapter 10). The retention of upper and lower incisors has been used to differentiate between *Hoploaceratherium* (lack of occlusion) and *Aceratherium* (lower incisors meeting the upper ones; Heissig, 2012). The loss of anterior dentition occurred several times on distantly related rhinoceros genera and is correlated with an increase in size of i2 (Aceratheriini and Teleoceratina; Heissig, 1989) or a complete loss of the i2 (i.e. latest Rhinocerotina and Elasmotherina). The presence of I1 has been used as a diagnostic character of both *A. simorrense* and *A. incisivum* (Cerdeño and Sánchez, 2000; Heissig, 2012). However, while no upper incisors have been found in the case of *A. incisivum* (except for some enamel fragments found in the premaxillary area of the Höwenegg's skull I 1953 of uncertain assignation; Chapter 10), a single I1 of *A. simorrense*, MNHN Sa-6380, has been found in Sansan. The fourth species found in Sansan, *Hoploaceratherium tetradactylum*, has an edentulous premaxilary bone.

As the postcranial skeleton regards, *A. simorrense* is easily distinguishable by its shorter limbs (radius: *A. simorrense* L = 229-242 mm; *A. incisivum* L = 295-305 mm; tibia: *A. simorrense* L = 267-282,5 mm; *A. incisivum* L = 297-322 mm). The shallow proximal articular surfaces of the metapodials and the flattened diaphyseal sections (equivalent to a lower gracility index according to Guérin, 1980) are cited by Heissig (2012) as common features between *A. simorrense* and *A. incisivum*. The gracility indices measured at the midpoint of the diaphysis not only vary between metapodials of *A. simorrense* but through time from the Middle Aragonian to the Lower Vallesian (Supplementary Data 4). For example, the GI of the Mc III oscillates between 24.6 (Sansan) to 30.4 (M-407 Rotonda), values that not only overlap most of the indices than can be obtained not only from *A. incisivum*, but other aceratheriine genera like *Chilotherium* (Deng, 2002). In a similar way, articular surfaces are variable within a species and the presence of flattened articular facets can be largely modified by distortion during fossilization. As postcranial remains from the type collection of Eppelsheim are scarce, those from Höwenneg and Batallones-1 have been used to complete the comparison with *A. incisivum*. The main differences with the radii of *A. simorrense* and *A. incisivum* are the narrower diaphysis of *A. simorrense* (while maintaining similar epiphyseal proportions) and, as previously noticed (Antoine et al., 2003), the insertion for the *m. biceps brachii* is deeper in *A. simorrense*. This rounded and deep insertion is clearly different from the broader and shallower one of *A. incisivum* (e.g. BAT-1'04 F6-149 from Batallones-1 or I34 from Höwenegg). In summary, we found that all these additional differences justify the segregation of both taxa, justifying the equivalence of both *Alicornops* and *Aceratherium* at a generic level.

ACKNOWLEDGMENTS

The manuscript was greatly improved by the useful comments of two anonymous reviewers. We would like to thank I. Rincón, S. Arcos and Argea S. A. for their field work. Thanks to P. Gutiérrez and B. Alonso for the specimen preparation and P. Pérez Dios (Museo Nacional de Ciencias Naturales de Madrid-CSIC) and P. Brewer (Natural History Museum) for kindly helping with the specimens in her care. Thanks to M. Ríos for the photographs and measurements of the specimens from Villefranche d'Astarac and C. Morant for the postprocessing of some of the images included in the present work. O.S. benefits from a FPU grant from the Spanish Ministry of Science and Innovation (MICINN). This work was supported by the Comunidad de Madrid (Dirección General de Patrimonio Histórico), Plan Nacional I/D projects CGL2011-257541 (Ministerio de Economía y Competitividad) and the research group BSCH-UCM 910607 have financially supported this study.

LITERATURE CITED

Anders, U., Koenigswald, W. v., Ruf, I., and Smith, B. H., 2011, Generalized individual dental age stages for fossil and extant placental mammals: Paläontologische Zeitschrift, v. 85, p. 321-339.

Antoine, P. O., 2002, Phylogénie et évolution des Elasmotheriina: (Mammalia, Rhinocerotidae): Mémoires du Muséum National d'Histoire Naturelle, v. 188, p. 5-350.

Antoine, P. O., Downing, K. F., Crochet, J.-Y., Duranthon, F., Flynn, L. J., Marivaux, L., Métais, G., Rajpar, A. R., and Roohi, G., 2010, A revision of *Aceratherium blanfordi* Lydekker, 1884 (Mammalia: Rhinocerotidae) from the Early Miocene of Pakistan: postcranials as a key: Zoological Journal of the Linnean Society, v. 160, p. 139-194.

Antoine, P. O., Duranthon, F., and Welcomme, J. L., 2003, *Alicornops* (Mammalia, Rhinocerotidae) dans le Miocène supérieur des Collines Bugti (Balouchistan, Pakistan) : implications phylogénétiques: Geodiversitas, v. 25, no. 3, p. 575-603.

Athanassiou, A., Roussiakis, S. J., Giaourtsakis, I. X., Theodorou, G. E., and Iliopoulos, G., 2014, A new hornless rhinoceros of the genus Acerorhinus (Perissodactyla: Rhinocerotidae) from the Upper Miocene of Kerassiá (Euboea, Greece), with a revision of related forms:

Palaeontographica, Abt. A: Palaeozoology – Stratigraphy, v. 303, no. 1-3, p. 23-59.

Becker, D., Antoine, P. O., and Maridet, O., 2013, A new genus of Rhinocerotidae (Mammalia, Perissodactyla) from the Oligocene of Europe: Journal of Systematic Palaeontology.

Budras, K.-D., Sack, W. O., and Röck, S., 2009, Anatomy of the Horse, Hannover, Schlütersche Verlagsgesellschaft mbH & Co.

Cerdeño, E., 1989, Revisión de la sistemática de los rinocerontes del Neógeno de EspañaPh.D. Dissertation]: Universidad Complutense de Madrid, 429 p.

-, 1992, Spanish Neogene Rhinoceroses: Palaeontology, v. 35, p. 297-308.

Cerdeño, E., and Sánchez, B., 2000, Intraspecific variation and evolutionary trends of *Alicornops simorrense* (Rhinocerotidae) in Spain.: Zoologica Scripta, v. 29, no. 4, p. 275-305.

Deng, T., 2002, Limb bones of *Chilotherium wimani* (Perissodactyla, Rhinocerotidae) from the Late Miocene of the Linxia Basin in Gansu, China: Vertebrata Palasiatica, v. 40, p. 305-316.

-, 2004, A new species of the Rhinoceros *Alicornops* from the Middle Miocene of the Linxia Basin, Gansu, China: Palaeontology, v. 47, p. 1427-1439.

Deng, T., Hantac, R., and Jintasakul, P., 2013, A new species of Aceratherium (Rhinocerotidae, Perissodactyla) from the late Miocene of Nakhon Ratchasima, northeastern Thailand: Journal of Vertebrate Paleontology, v. 33, no. 4, p. 977-985.

Ginsburg, L., 1974, Les Rhinocerotides du Miocene de Sansan (Gers): Compte Rendus des Seances de l'Academie des Sciences, Paris, v. 278, no. 5, p. 597-600.

Ginsburg, L., and Guérin, C., 1979, Sur l'origine et l'extension stratigraphique du petit rhinocerotide miocene *Aceratherium (Alicornops) simorrense* (Lartet, 1851), nov. subgen.: Compte Rendu Sommaire des Seances de la Societe de Geologie de France 1979, v. fasc. 3, p. 114-116.

Guérin, C., 1980, Les rhinocéros (Mammalia, Perissodactyla) du Miocène terminal au Pléistocène supérieur en Europe occidentale : comparaison avec les espèces actuelles: Documents des Laboratoires de Géologie de Lyon, v. 79, p. 1-1184.

-, 1989, La famille des Rhinocerotidae (Mammalia, Perissodactyla): Systématique, histoire, évolution, paléoécologie: Cranium, v. 6, no. 2, p. 3-14.

Heissig, K., 1972a, Die obermiozäne Fossil-Lagerstätte Sandelzhausen. 5. Rhinocerotidae (Mammalia), Systematik und Okologie: Mitteilungen der Bayerischen Staatssammlung Paläontologie und historische Geologie, v. 14, p. 37.

-, 1972b, Paläontologische und geologische Untersuchungen im Tertiär von Pakistan. 5. Rhinocerotidae (Mamm.) aus den unteren und mittleren Siwalik-Schichten.: Bayerische Akademie der Wisseschaften, Mathematisch-Naturwissenschaftliche Klasse Abhandlungen, v. 152, p. 1-112.

-, 1976, Rhinocerotidae (Mammalia) aus der *Anchitherium* Fauna Anatoliens: Geologisches Jahrbuch, v. 19, p. 3-121.

-, 1989, The Rhinocerotidae, *in* Prothero, D., and Schoch, R. M., eds., The evolution of Perissodactyls, Oxford University Press, p. 399-417.

-, 1999, 16. Family Rhinocerotidae, *in* Rössner, G. E., and Heissig, K., eds., The Miocene Land Mammals of Europe: Pfeil, Munich, p. 175-188.

-, 2012, Les Rhinocerotidae (Perissodactyla) de Sansan, *in* Peigné, S., and Sen, S., eds., Mammifères de Sansan, Volume 203: Paris, Muséum national d'Histoire naturelle, p. 317-485.

Heissig, K., and Fejfar, O., 2007, Die fossilen Nashörner (Mammalia, Rhinocerotidae) aus dem Untermiozän von Tuchořice in Nordwestböhmen.: Acta Musei Nationalis Pragae. Series B - Natural History, v. 63, no. 1, p. 17-64.

Hooijer, D. A., 1966, Fossil Mammals of Africa nº. 21: Miocene rhinoceroses of East Africa: Bulletin of British Museum (Natural History), Geology, v. 13, no. 2, p. 117-190.

Jepsen, G. L., 1996, Early Eocene bat from Wyoming: Science, v. 154, no. 3754, p. 1333-1339.

Lartet, E., 1851, Notice sur la Colline de Sansan.

Mein, P., 1999, European Miocene mammal biochronology, *in* Rössner, G. E., and Hessig, K., eds., The Miocene Land Mammals of Europe: München, Verlag Dr. Friedrich Pfeil, p. 25-38.

Prothero, D., Guérin, C., and Manning, E., 1989, The History of the Rhinocerotoidea, The Evolution of Perissodactyls, p. 321-340.

Roger, O., 1887, Verzeichniss der bisher bekannten fossilen Säugethiere.: Jahresbericht des naturwissenschaftlichen Vereins für Schwaben und Neuburg in Augsburg, v. 26, p. 1-162.

Santafé, J. V., and Casanovas-Cladellas, M. L., 1978, Los rinocerótidos de Can Perellada y Can Jofresa (Vallesiense terminal de los alrededores de Terrassa, Barcelona, España): Acta Geologica Hispanica, v. 13, no. 4, p. 105-112.

Schaller, O., 2007, Illustrated Veterinary Anatomical Nomenclature, Sttutgart, Enke.

Yan, D., and Heissig, K., 1986, Revision and Autopodial Morphology of the Chinese-European Rhinocerotid Genus *Plesiaceratherium* Young 1937: Zitteliana, v. 14, p. 81-94.

SUPPLEMENTARY DATA 1

Remains of *A. simorrense* from M-407 Rotonda studied in the present work.

A1-1, skull with right P3-M2 and left P4-M3; CA4-256, right occipital fragment; PUL11 w/n, rostral fragment; PUL11-2, nasal bone; H-11, palate with right P2-M2 and left P3-M3; DES-49, juvenile maxilar with right DP1-4; CA4-3, left P4-M3; C2-68, right DP1; CA3-191, right DP2; B2-58, C2-95, B2-57, left DP2; CA4-66, right DP3; CA6-291a, CA6-291b, left DP4; CA6-280, right P3; B1-87, left P3; CA3-83; CA4-45, right P4; B1-46, DES-51, H2-14, left P4; B1-65, D5-5, fragmentary molars; CA4-3, left M2; CA5-30, CA3-148, right M3; w/n, left M3; right hemimandible with dp3-4; DES-48, right hemimandible with p2-m1; w/n, left hemimandible with p3-m1; CA2-18, left hemimandible with p3-m2; A1-46, left hemimandible with m1-m3; D3-394, left edentate hemimandible; CA4-194, right hemimandible with dp3-4; CA2-18, right hemimandible with p3-m2; CA6-154, right hemimandible with dp2-4; CA4-333, right hemimandible with dp2-4; DES-48, right hemimandible with p2-m1; A1-46, left hemimandible with p4-m3; CA4-44, left hemimandible with dp2-3; CA3-24, CA6-154, right hemimandibles with dp2-4; w/n, left hemimandible with p3-m1; B1-95, right hemimandible with p3-4; A2-46, CA6-209; CA5-158a; CA5-158b, i2; CA3-24, right dp2-4; C4-52, CA6-243, B1-93, left dp2; C1-73, right dp2; CA4-52, right dp3; B3-10, CA5-7, left dp3; CA3-82, C2-94, right dp4; CA4-33, PUL11-4, right p3; CA6-274, left p3; CA6-293, CA6-294, right p4; B4-76, left p4; B1-85, right p4; B1-82, CA3-188, right m1; CA4-200, left m1; CA4-242, left m2; DES-71, left m3; A1-56, CA4-205, atlas; CA4-205, C4-53, D2-7, w/n, axis; DES-10, distal fragment of a right humerus; DES-45, distal fragment of a left humerus; DES-39, CA4-141, left radius; C1-21, DES-4 sec-5, right radius; DES-40, distal fragment of a left radius; CA4-51, left ulnae; A1-47, articular fragment of a left ulnae, B1-52, CA6-295, articular fragment of a right ulnae; CA6-266, C2-86, C2-62, right scaphoids; C1-16, right magnum; CA4-54, right semilunate; CA4-196, left semilunate; CA4-9, right unciform; CA4-36, right pyramidal; C1-9, left trapezoid; CA4-362, right trapezoid; A1-23, left Mc II; CA6-91, left Mc III; DES-34, proximal fragment of a left Mc III; CA6-254, CA3-95, left Mc IV; CA4-244, B4-58, A1-21, left patellae; CA6-296, left patellae; CA4-287, left femur; CA6-89, distal epiphysis of a left femur; B4-61, CA6-273, right femora; DES-14, right tibia; D5-12, CA4-385, left tibiae; B1-82, CA4-221; CA4-336, distal fragment of a left tibia; CA5-101 distal fragment of a right tibia; CA3-26, CA1-72, CA4-349, CA3-127, left astragali; CA4-327, B3-27, CA5-90, right astragali; CA3-73, CA6-122, left naviculars; CA4-65, CA6-152, right naviculars; CA2-11, right cuboid; CA5-26, CA5-118, proximal epiphyses of left Mt III; CA4-6, left Mt IV; B3-26, right Mt IV.

SUPPLEMENTARY DATA 2

Measurements (mm) of the skull (Table S1) and mandible (Table S2) of *Alicornops simorrense* from M-407 Rotonda (Madrid Province, Spain). Side is detailed as follows: l, left; r, right.

Table S1	A1-1
9. Distance between nasal notch and orbit	60.5
14. Distance between nasal tip and orbit	177.8
22. Width of nasal base	96.2
26. Cranial height in front of M1	178.0
27. Height of skull in front of M3	163.0
29. Width of palate in front of M1	67.0
30. Width of palate in front of M3	69.0

Table S2	DES-20a	CATA2-18a	CATA6-154a	DES-48a	A1-46a	CA3-24a	CA4-333a	CA4-44a
	l	l	r	r	l	r	r	l
L	~ 380	—	—	—	—	—	—	—
DAPdia	~ 28	—	19.1	—	—	—	—	—
HP1	—	—	44.8	—	—	—	—	—
HP2	60.0	—	47.8	63.0	—	37.1	40.9	28.0
HP3	58.0	—	51.3	74.0	—	42.6	48.6	37.3
HP4	59.0	75.6	55.3	73.0	72.0	46.2	51.5	35.5
HM1	62.0	74.6	49.1	77.0	74.3	—	49.0	—
HM2	60.0	74.8	—	—	80.2	—	—	—
HM3a	64.0	—	—	—	77.2	—	—	—
HM3p	66.0	—	—	—	70.3	—	—	—
DAPdent	190.0	—	—	—	—	—	—	—
Lcor	—	—	—	—	—	—	—	—
Lart	—	—	115.7	—	141.0	—	—	—
Hcor	—	—	—	—	—	—	—	—
Hart	—	—	123.2	—	149.0	—	—	—
DAPhr	—	—	79.2	—	103.0	—	—	—
DAPproc	—	—	—	—	—	—	—	—
DAPcor	—	—	34.9	—	—	—	—	—
DAPart	—	—	20.0	—	18.9	—	—	—
DTia	—	—	—	—	—	—	—	—
DTip	—	—	—	—	—	—	—	—
Lsin	159.0	—	50.6	—	—	—	—	—
DTpx	60.0	—	40.3	—	—	22.3	—	—
DTm3p	—	—	—	—	32.9	—	—	—
DTcor-cor	—	—	—	—	—	—	—	—
DTart-art	—	—	—	—	—	—	—	—
DTart	—	—	52.2	—	84.1	—	—	—

SUPPLEMENTARY DATA 2 (CONT.)

Measurements (mm) of the upper dentition (Table S3) and lower dentition (Table S4) of *Alicornops simorrense* from M-407 Rotonda (Madrid Province, Spain). Side is detailed as follows: l, left; r, right.

Table S3		A1-1		H-11		C2-68	DES-49	B2-57	C2-95	CAT3-191	CA4-66	CATA6-291	B1-46	CA4-3	CA4-45	CA5-30	w/n
Upper teeth		**l**	**r**	**l**	**r**	**r**	**r**	**l**	**l**	**r**	**r**	**l**	**l**	**l**	**r**	**r**	**l**
	L					(D) 19.1	(D) 18.4										
P1	W					(D) 15.3	(D) 14.6										
	H					(D) 19.0	(D) 20.2										
	L				27.7		(D) 33.0	(D) 34.9	(D) 33.9	—							
P2	W				32.6		(D) 27.1	—	(D) 29.4	(D) 26.7							
	H				22.9		(D) 19.7	(D) 16.8	(D) 18.4	—							
	L	—	—	—	30.7		(D) 33.9				—		—		32.9		
P3	W	—	48.1	42.3	39.9		(D) 30.4				(D) 31.8		39.3		41.3		
	H	21.6	23.2	—	23.9		(D) 23.4				—		10.7		14.2		
	L	—	—	—	—		(D) 38.3					—		36.3			
P4	W	52.7	50.7	45.8	46.2		(D) 34.0					(D) 36.9		47.2			
	H	25.1	26.1	24.6	22.7		(D) 33.0					—		10.3			
	L	44.4	—	40.1													
M1	W	—	—	45.9													
	H	—	22.2	20.8													
	L	—	—	46.3													
M2	W	52.4	51.8	46.9													
	H	24.6	24.3	28.1													
	L	43.3														—	—
M3	W	45.0														—	—
	H	24.9														16.7	14.6

Table S4		C1-73	CA3-24	CA4-333	CATA6-154	B1-93	CA4-44	CA5-13	CA6-243	CA4-194	DESUB-27	B3-10	CA5-7	C2-94	CA3-82	C4-52
Lower teeth		**r**	**r**	**r**	**r**	**l**	**l**	**l**	**l**	**r**	**r**	**l**	**l**	**r**	**r**	**r**
	L	24.0	24.7		22.2	26.0	27.8	25.8	23.6							
dp2	W	13.0	12.4		12.8	13.9	14.5	12.2	15.5							
	H	15.1	11.2		9.6	13.5	13.6	12.5	14.8							
	L		28.1	30.2	30.3		31.4			30.8	30.4	33.0	31.4			
dp3	W		14.8	17.1	15.7		16.7			17.6	18.4	17.6	17.9			
	H		12.3	11.7	11.6		16.6			5.3	23.5	16.6	21.6			
	L		31.9	34.6	—					—				36.6	35.5	34.2
dp4	W		18.7	19.6	17.7					20.3				18.4	17.5	16.0
	H		18.6	18.6	18.7					16.0				35.8	16.4	14.7

SUPPLEMENTARY DATA 2 (CONT-)

Measurements (mm) of the lower dentition (Table S4 cont.) of *Alicornops simorrense* from M-407 Rotonda (Madrid Province, Spain). Side is detailed as follows: l, left; r, right.

Table S4 (cont.)

Lower teeth		B1-82 r	CA4-200 l	CAT3-188 r	DES-20 l	DES-48 r	A1-46 l	C3-44 l	CA4-242 l	CATA2-18 l	CA-200 l	CA6-283 r	DESUB-71 l	B2-23 l	B1-95 r	C4-33 r	PUL-11-4 r	CA6-274 l	w/n l	B1-85 r	CA6-293 r	CA6-294 r	B4-76 l	DES-71 l	A3-9 l
	L				23.5	22.6																			
p2	W				20.6	16.7																			
	H				17.9	21.3																			
	L				28.7	25.9				29.7					31.6	—	30.2	29.8	28.5						
p3	W				22.6	21.3				24.3					18.3	21.0	22.2	22.8	22.5						
	H				15.2	17.7				11.2					6.7	19.6	17.1	9.1	17.2						
	L				31.7	31.3				31.2					—				33.0	—	31.2	31.7	31.5	—	33.6
p4	W				24.0	23.1				24.3					~ 20				23.5	22.4	22.7	22.4	21.8	~ 15	~ 10
	H				17.9	16.4				14.0					15.5				20.3	17.2	15.7	19.3	—	19.9	—
	L	—	33.3	32.7	33.1	32.9	29.3			32.8	34.4			34.4					35.5						
m1	W	24.5	23.0	26.0	22.7	—	22.9			24.2	22.8			20.1					24.4						
	H	13.2	14.6	16.3	17.9	12.0	11.7			11.3	15.2			32.1					18.3						
	L				38.0		37.2		37.8	37.2			36.8												
m2	W				24.9		24.7		26.1	24.7			20.9												
	H				20.1		21.3		7.0	16.2			14.6												
	L				40.2		35.9	35.9				36.6													
m3	W				23.9		21.9	22.1				23.0													
	H				26.8		20.3	26.0				21.9													

SUPPLEMENTARY DATA 2 (CONT.)

Measurements (mm) of the humeri (Table S5), radii (Table S6), ulnae (Table S7), femora (Table S8), patellae (Table S9), and tibiae (Table S10) of *Alicornops simorrense* from M-407 Rotonda (Madrid Province, Spain). Side is detailed as follows: l, left; r, right.

Table S5				prox epi		dia			dis epi					
Humerus	L	Lprox	TDtu-ber	TD	APD	TD	APD	Ldis	TD	TDtroc	R1	Rmin	R2	APD
DES-10 (r)	—	—	—	—	—	—	—	—	74.4	66.0	52.2	35.0	41.6	—
DES-45 (r)	—	—	—	—	—	—	—	—	—	—	50.9	34.0	—	—
CA6-260 (l)	—	—	—	—	—	51.0	44.3	—	—	74.6	~ 58	30.8	40.0	—
DES-45 (r)	—	—	—	—	—	—	—	—	—	66.2	53.0	33.5	39.9	—

Table S6			prox epi		prox art		dia		dis epi		dis art	
Radius	L	l	TD	APD	TD	APD	TD	APD	TD	APD	TD	APD
CA4-141 (l)	229.0	235.0	—	46.7	62.4	34.0	35.3	26.8	65.5	35.9	66.1	39.6
DES-40 (l)	—	—	—	—	—	—	36.4	25.1	67.5	33.6	67.3	—
DESUB-4 SECTOR 5 (r)	—	—	—	—	—	—	—	—	—	—	—	—
CA4-141 (l)	237.0	238.0	68.1	41.4	66.7	39.5	36.5	26.5	67.7	45.2	—	35.2
C1-21 (r)	—	—	—	—	—	—	36.7	22.4	—	—	64.0	—
DES-39 (l)	—	—	—	—	—	—	29.2	18.8	—	—	—	—

Table S7		olec					TDtroc		dia		dis epi		dis art	
Ulna	L	TD	APD	H	TD base	APD base	prox	dis	TD	APD	TD	APD	TD	APD
CA4-51 (l)	—	—	—	—	15.5	74.3	—	55.5	30.9	28.8	—	—	—	—
B1-52 (r)	—	—	—	—	—	—	40.7	—	—	—	—	—	—	—
CA6-295 (r)	—	—	—	—	16.2	53.8	—	40.9	19.4	21.4	—	—	—	—
A1-47 (l)	—	—	—	—	—	—	46.0	55.1	31.6	29.5	—	—	—	—

Table S8					head		prox epi				dia					dis epi	
Femur	L	Ltroc-prox	Ltroc	Ltroc-dis	TD	APD	TD	APD	TD-cue	TD3t	TD	APD	R1	R2	TDtroc	TD	APD
CA4-11 (l)	349.0	75.3	40.8	169.0	79.7	79.7	161.0	83.8	132.7	115.6	115.6	59.4	40.0	103.3	74.4	61.4	110.6
CA6-89 (l)	—	—	42.56	—	—	—	—	—	—	104.9	—	—	—	—	—	—	—
CA6-273 (r)	—	—	—	—	—	59.9	135.5	69.9	120.6	78.5	44.2	43.7	—	—	—	—	—

Table S9			
Patella	TD	APD	H
CA4-244 (l)	26.8	35.5	70.2
B4-58 (l)	70.5	34.0	—
A1-21 (l)	66.1	36.2	67.8

Table S10			prox epi		prox art		dia		dis epi	
Tibia	L	LfFi	TD	APD	TD	APD	TD	APD	TD	APD
CATA4-221 (l)	—	—	—	—	—	—	36.1	31.0	—	—
CATA4-336 (l)	—	—	—	—	—	—	—	—	46.5	63.1
A1-28 (r)	—	—	—	—	—	—	—	—	—	—
DES-14 (r)	—	—	—	—	—	—	—	29.0	—	20.9
CATA5-101 (l)	—	—	—	—	—	—	—	—	50.2	61.8
D5-12 (l)	—	—	—	—	—	29.0	21.8	—	—	—
CATA4-385 (l)	—	—	—	—	—	29.0	15.6	—	—	—
B1-82 (l)	—	—	—	—	—	—	47.9	33.4	47.1	60.5

SUPPLEMENTARY DATA 2 (CONT.)

Measurements (mm) of the scaphoids (Table S11), lunates (Table S12), pyramidals (Table S13), magnums (Table S14), unciforms (Table S15), astragali (Table S16), naviculars (Table S17), and cuboid (table S18) of *Alicornops simorrense* from M-407 Rotonda (Madrid Province, Spain). Side is detailed as follows: l, left; r, right.

Table S11

				prox art		dis art				
Scaphoid	TD	APD	H	TD	APD	APD-fMa	APDfTz	APDfTr	TD	APD
C2-62 (r)	—	57.0	44.2	—	35.5	23.5	18.8	10.4	45.2	21.3
C2-86 (r)	43.2	60.8	51.3	41.5	41.1	25.8	18.0	7.3	49.0	24.2

Table S12

Semilunate	TD-prox	TDdist	TDpal	DAP	H	APD fUn	Hart
CA4-54 (r)	31.9	20.7	20.3	47.5	34.8	25.6	16.7
CA4-196 (l)	31.1	19.5	—	31.9	26.5	—	27.4

Table S13

Pyramidal	TD	H	APD	APD prox
CA4-36 (r)	33.9	38.9	38.5	24.2

Table S14

Magnum	TD	LfUn	LfSl	APD	H	Hdor	Hvproc	Hart
C1-16 (r)	32.3	—	—	—	37.3	20.5	—	—

Table S15

Unciform	TD	H	APDan	APDab
CA4-9 (r)	41.9	32.8	—	—

Table S16

					(trochlea)						dis art		
Astragalus	TD	H	TDmd	DLinf	H1	Hmin	H2	L1	L2	DL	TD	APD	APD int
CA4-327	63.8	57.8	52.5	30.2	49.7	33.6	—	—	41.7	—	—	29.4	—
CA3-127	63.7	50.3	55.3	—	45.2	26.8	37.2	41.8	43.2	—	—	24.0	15.4
CA4-349	56.0	48.5	46.9	27.3	—	—	39.8	33.8	34.0	22.5	32.1	20.5	14.1
B3-27	67.8	56.4	57.8	30.1	—	—	—	47.5	47.2	37.2	—	—	—
C1-72	68.1	56.6	57.8	33.3	52.1	34.4	43.3	42.9	43.3	30.5	38.5	26.5	18.5
CA3-26	62.9	51.1	56.0	32.9	48.3	—	46.7	45.4	40.0	23.9	39.9	27.9	15.8
CATA5-90	65.5	51.4	56.7	29.6	47.8	32.9	46.2	43.1	43.8	28.8	43.9	27.9	18.1

Table S17

					prox art	
Navicular	APD	TD	H	Hmin	TD	APD
CA3-73 (l)	35.2	41.5	21.4	14.4	29.7	31.6
CA6-122 (l)	33.5	32.1	16.9	14.4	28.7	30.8
C4-65 (r)	34.4	40.6	16.8	15.4	29.0	33.7
CA6-152 (r)	28.8	36.3	13.7	11.7	28.0	29.3

Table S18

						prox art	
Cuboid	TD	APD	H	Hdor	Hvproc	TD	APD
CATA2-11 (r)	28.6	35.1	31.6	25.2	22.5	28.7	31.6

SUPPLEMENTARY DATA 2 (CONT.)

Measurements (mm) of the Mc II (Table S18), Mc III (Table S19), Mc IV (Table S20), Mt III (Table S21), and Mt IV (Tale S22) of *Alicornops simorrense* from M-407 Rotonda (Madrid Province, Spain). Side is detailed as follows: l, left; r, right.

Table S18		prox epi		prox art		dia			dis art	
Mc II	L	TD	APD	TD	APD	TD	APD	TDmd	TD	APD
A1-23 (l)	—	25.4	30.5	19.2	25.3	20.7	21.5	—	—	—

Table S19		prox epi		prox art			dia			dis art	
Mc III	L	TD	APD	TD	APD	HfUn	TD	APD	TDmd	TD	APD
CA6-91 (l)	118.0	45.6	33.9	32.7	34.3	15.9	35.9	13.5	41.3	36.6	27.4
DESUB-34 (l)	—	42.0	30.9	35.8	31.1	—	—	—	—	—	—

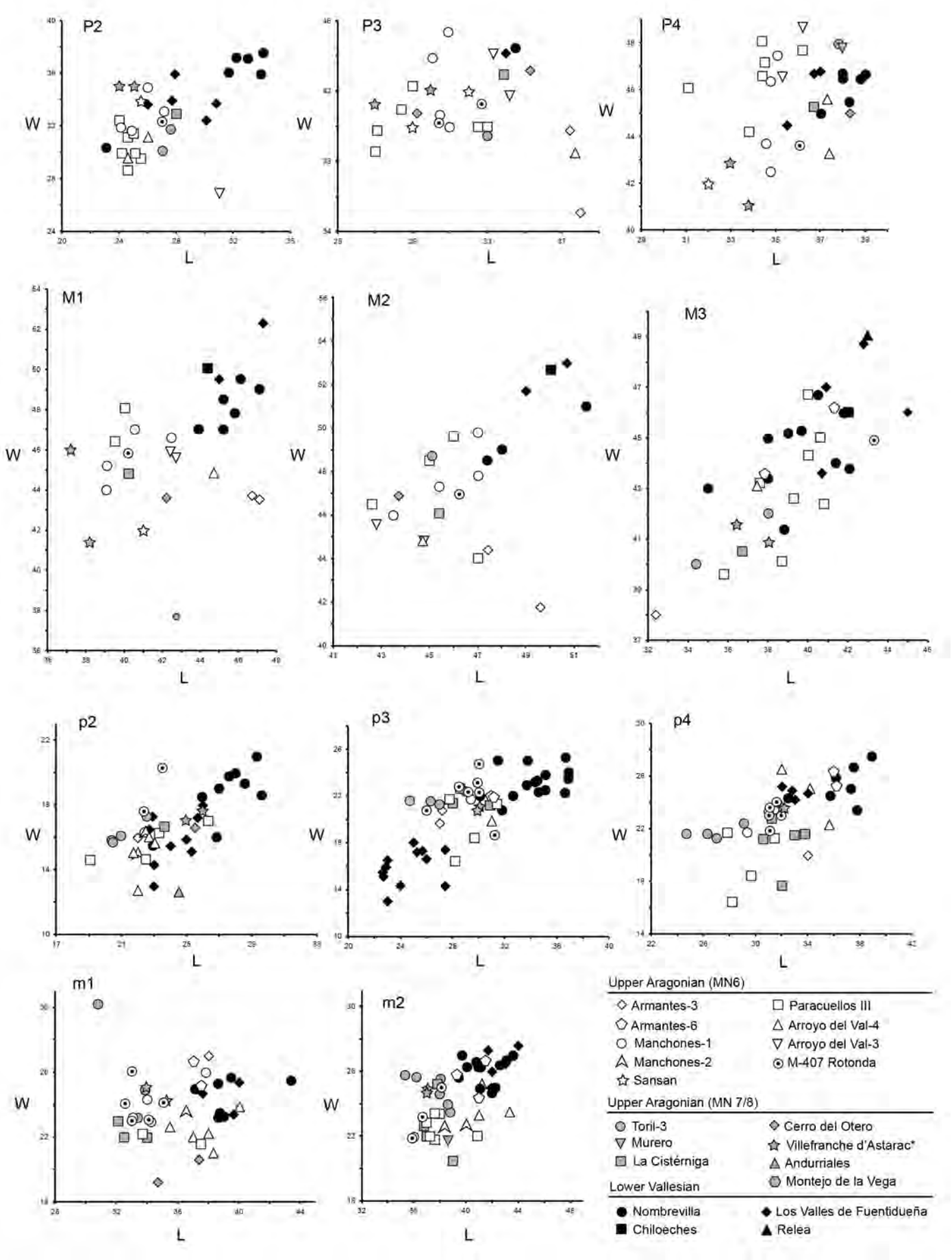
Table S20		prox epi		prox art		dia			dis art	
Mc IV	L	TD	APD	TD	APD	TD	APD	TDmd	TD	APD
CA3-95 (l)	96.7	30.8	26.5	22.6	27.8	22.5	14.3	28.0	26.3	29.5
CA6-254 (l)	102.4	30.5	—	23.6	—	~ 27	~ 11	32.7	24.2	32.5

Table S21		prox epi		prox art		dia			dis art	
Mt III	L	TD	APD	TD	APD	TD	APD	TDmd	TD	APD
CA5-26 (l)	—	35.1	30.8	34.4	24.2	32.0	14.0	—	—	—
CATA5-118 (l)	—	38.7	—	37.7	—	28.5	—	—	—	—

Table S22		prox epi		prox art		dia			dis art	
Mt IV	L	TD	APD	TD	APD	TD	APD	TDmd	TD	APD
CA4-6 (r)	102.5	31.4	30.3	26.1	30.5	22.1	18.5	25.2	25.9	29.5
B3-26 (l)	—	37.6	36.8	33.3	32.1	25.6	20.7	—	—	—

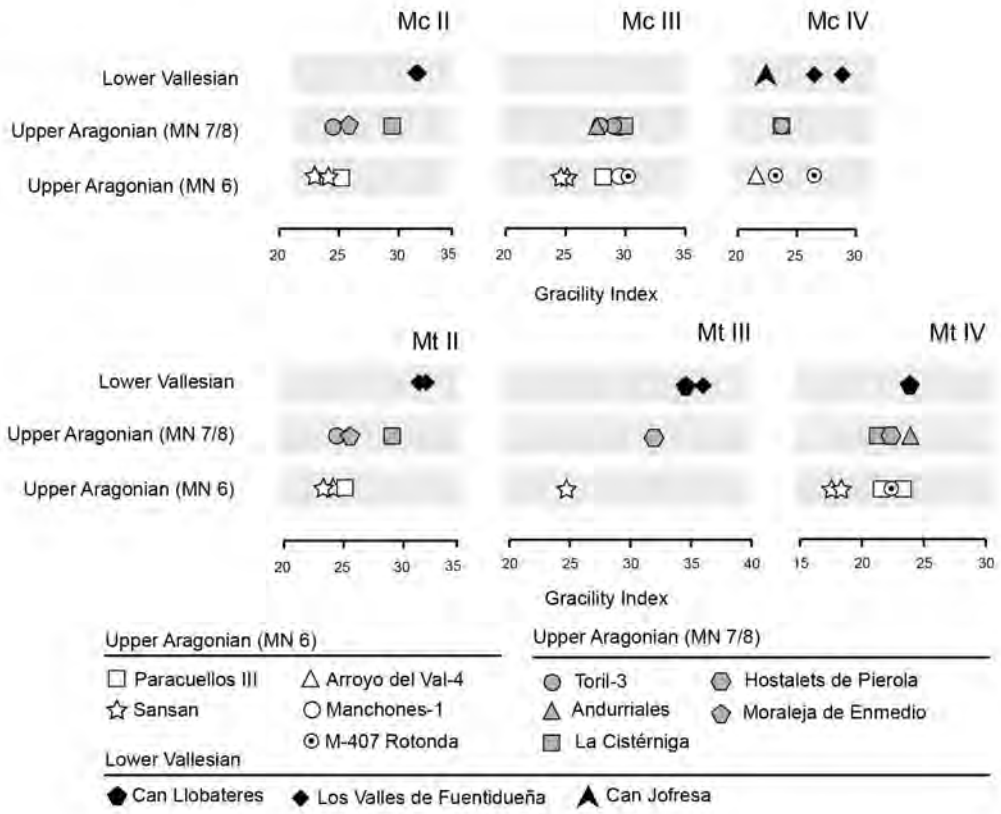
SUPPLEMENTARY DATA 3

Scatter diagram (in mm) of the upper dentition of *Alicornops simorrense* from M-407 Rotonda (dotted white circles) compared with other Iberian sites and the French localities of Sansan (white stars) and Villefranche d'Astarac (type locality; gray stars). Additional data obtained from Cerdeño (1989), Cerdeño and Sánchez (2000) and Heissig (2012).



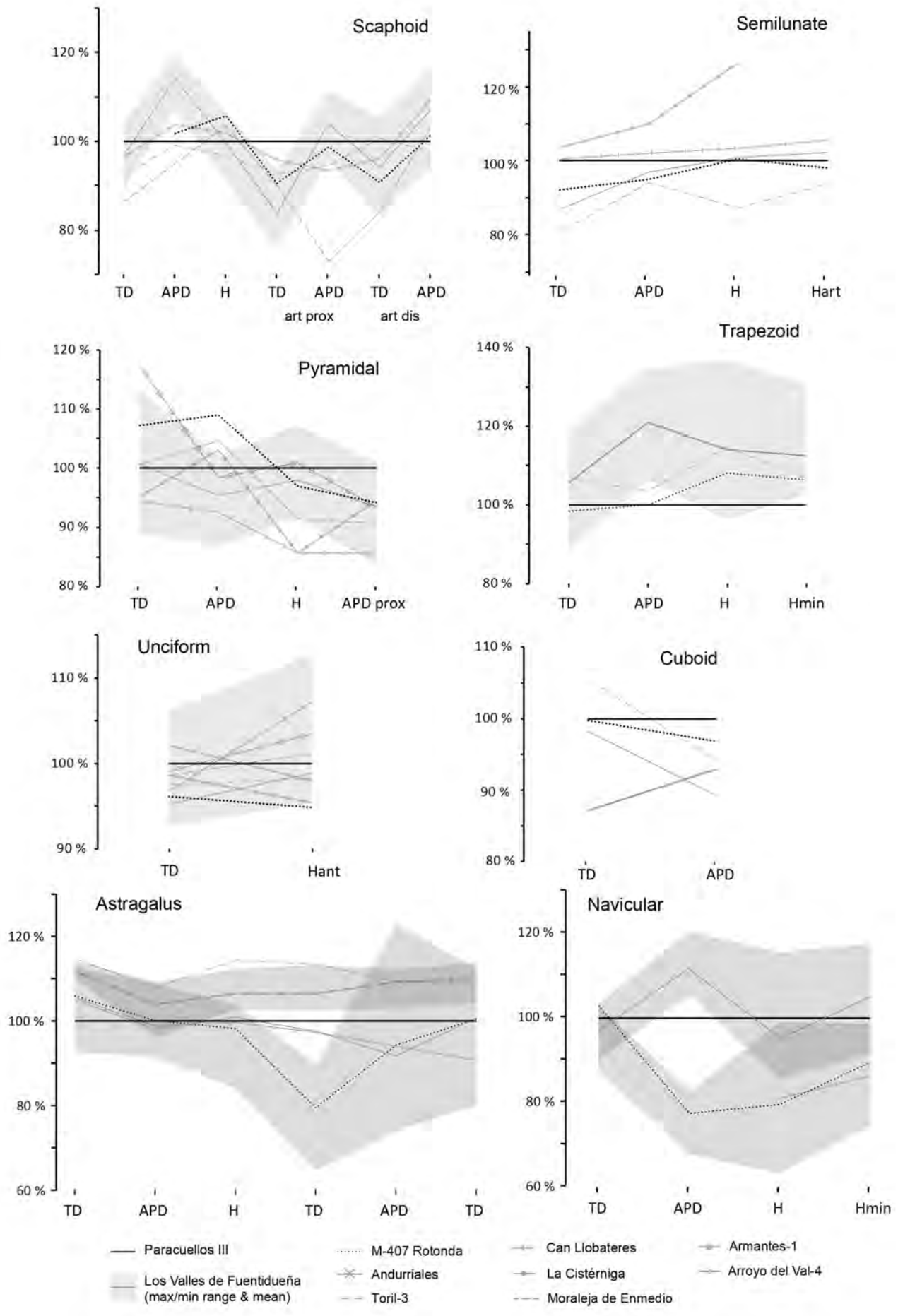
SUPPLEMENTARY DATA 4

Gracility indices of the metapodials of *Alicornops simorrense* from M-407 Rotonda (dotted white circles) compared with other Iberian sites and the French locality of Sansan (white stars). Additional data obtained from Cerdeño (1989), Cerdeño and Sánchez (2000) and Heissig (2012).



SUPPLEMENTARY DATA 5

Comparative proportions of some postcranial bones of *A. simorrense*. Value 100 corresponds to Paracuellos III. Data obtained from Cerdeño (1989) and Cerdeño and Sánchez (2000).



8. New *Lartetotherium* remains from the Iberian site of M-407 Rotonda (Middle Miocene)

Oscar Sanisidro
María Teresa Alberdi
and Jorge Morales

Abstract. We describe new remains assigned to *Lartetotherium* cf. *Lartetotherium sansaniense* from the Aragonian (middle Miocene) locality of M-407 Rotonda (Province of Madrid, Spain). The faunal assemblage of M-407 Rotonda can be preliminarily correlated with Moraleja de Enmedio (MN 6 Mein's Biozone) on the base of fossil mammal fauna and altitudinal data. New cranial and postcranial remains of *L. sansaniense* from M-407 Rotonda are described and compared with other European localities. The skull CA4-73 from M-407 Rotonda is of special interest, as it largely preserves the original three-dimensional proportions of the species cranial anatomy, linking together the morphologies of the type specimen from Sansan and the cranial remains from Sandelzhausen. Additionally, it provides new data about the intraspecific variation in *L. sansaniense*, showing particularly widened upper molars and very robust femur. Finally, a reliable cranial reconstruction of the species has been proposed.

INTRODUCTION

In 1851 Edouard Lartet reported the occurrence of a "great quantity of fossil bones" from a hill close to the French locality of Sansan (Lartet, 1851; p. 3). The fossil site, discovered two decades before, was carefully dug and is nowadays considered one of the first systematic excavations (Crouzel, 2000). Among the recovered fossil remains, currently dated as Astaracian (middle Miocene; Ginsburg and Bulot, 2000), Lartet described a medium-sized horned rhinoceros, naming it as "*Rhinoceros sansaniensis*" (Lartet, 1851). Due to their morphological affinities, both *L. sansaniense* and the extant Sumatran rhinoceros (*Dicerorhinus sumatrensis*) have configured hand in hand nomenclatural histories at a generic level. Osborn (1900) included both species in the subfamily Ceratorhinae, a waste basket for the firstly described horned forms with developed anterior dentition and relatively slender limbs. Such classification was subsequently followed by several authors as is (Roman and Torres, 1907), or considering *Ceratorhinus* as a subgenus of *Rhinoceros* (Roger, 1902). Well into the 20th century, the Sumatran rhino and, by extension, *L. sansaniense*, were assigned to *Didermocerus* (Heissig, 1972), or more frequently to *Dicerorhinus* (Pavlovic, 1963). Ginsburg (1974) reviewed the skull from Sansan, recognizing enough differences to separate it in a new genus, naming it as *Lartetotherium*. The same author used subsequently *Lartetotherium* as a subgenus of *Dicerorhinus* (Antunes and Ginsburg, 1983), coinciding with Guérin (1980). Finally, Groves (1983) restored the generic status of *Lartetotherium*.

L. sansaniense is the first Rhinocerotina (*sensu* Becker et al., 2013) of the European fossil record. Its stratigraphic range spans from the Middle Aragonian (MN4 Mein's Biozone; Mein, 1990) to the Lower Vallesian (Upper Miocene, MN9). *L. sansaniense* has been cited in more than twenty localities only in the Iberian Peninsula (Figure 1). Despite this significant number of records, *L. sansaniense* is usually poorly represented. In contrast to the scarcity of *L. sansaniense* remains in the Iberian Peninsula, the localities of Sandelzhausen (Mainburg, Germany; MN 5) and Sansan (Gers, France; MN 6) have provided a complete portrait of the species, with abundant cranial and postcranial remains (Heissig, 1972, 2012; Peter, 2002).

Previous studies of the postcranial bones among the Iberian populations of *L. sansaniense* found two size groups (Cerdeño, 1986): the Lower Aragonian sites (i.e. Buñol and Can Mas) showed postcranial proportions comparable to the type collection of Sansan whereas the Upper Aragonian and Lower Vallesian samples have smaller proportions while maintaining their morphology. These results were interpreted as two distinct evolutionary stages for the species: the greater size of the postcranial skeleton in the Lower Aragonian populations was followed by a decrease towards the Upper Aragonian (Cerdeño, 1986). Interestingly, no size differences were found among their dentitions (Cerdeño, 1986, 1989).

M-407 Rotonda fossil site was discovered during the excavations of the North road accesses of Fuenlabrada city (South of Madrid, Spain; Fig. 2). The site is included in the Miocene Intermediate Unit of the Madrid Area, within the Tagus Basin. Among the diverse Middle Miocene vertebrate association (MN 6; Sanisidro et al., this volume), land tortoises of the species *Cheirogaster bolivari* and rhinoceros stand out because of their abundance. The latter are represented by *Alicornops simorrense* and *L. sansaniense*. The remains of *L.* cf.

L. sansaniense in M-407 Rotonda comprise the larger collection of the species in a single fossil site in the Iberian Peninsula. The objective of the present contribution is the systematic description of these remains and the reassessment of these two questions: Can postcranial remains of *L. sansaniense* in the Iberian Peninsula be divided into two size groups? and, if so, do they follow a decrease in size through time?.

MATERIAL AND METHODS

All the studied specimens from M-407 Rotonda are stored in the Museo Nacional de Ciencias Naturales, Madrid. Other Iberian and European localities (particularly the type collection from Sansan; measurements published in Heissig, 2012) have been used for comparison. Measurements are given in millimeters with an accuracy of one decimal digit. Approximate measurements are given in parentheses. Measurements were made with a digital caliper and a measuring tape for elements larger than 150 mm. Ontogenetic classification follows Anders et al. (2011). The general anatomical terminology follows Budras (2009) and Schaller (2007). In addition, that used by other authors has also been taken into consideration (Antoine, 2002; Antoine et al., 2010; Becker et al., 2013; Guérin, 1980; Heissig, 1972, 1999). The cranio-dental and osteological features described are detailed in the Annex Chapter [craniodental morphology] and the Supplementary data 6 of the Chapter 5 [postcranial skeleton]).

Anatomical Abbreviations—ant, anterior; art, articulation;



Localities with presence of *Lartetotherium sansaniense*

Age	Continental stages	Zones MN (Mein, 1975; 1990)	Portugal	Spain	France	Switzerland	Germany & Austria	other localities
UPPER MIOC.	VALLESIAN	MN 9	Aveiras de Baixo	Can Llobateres/Can Ponsic/Nombrevilla/ Relea/Benavente/ Coca			Wissberg (DE) Gratkorn (AUT)	Rudabánya (HUN)
MIDDLE MIOCENE	UPPER ARAGONIAN	MN 7/8	Povoa de Santarem Pero Filho	Hostalets de Pierola Brihuega Cerro del Otero La Cisterniga Bolaños de Campos	La Grive	Place du Marché	Stenheim (DE)	
		MN 6		Paracuellos-3 **M-407 Rotonda (cf.)** Paracuellos-5	Simorre Sansan* Collet-Redon	Charmoille	Kirrberg-Tongrube (DE)	Çandir (sp.; TUR) Tăşad-Stracoş (sp.; ROM)
	MIDDLE ARAGONIAN	MN 5	Quinta Flamengas Quinta Farinheira	La Retama (cf.)	Faluns Castelnau-d'Arbieu		Weinsteig (DE) Sandelzhausen (DE) Georgensgmünd (DE)	
		MN 4	Charneca do Lumiar	Buñol/Can Mas/ Mas Antolino-3	Anjou/ La Romieu-Bézian/ Baigneaux/Pellecahus			

Fig. 1 Biostratigraphic distribution of *Lartetotherium sansaniense.* Other Spanish localities with presence of *L. sansaniense* and an uncertain stratigraphic position are Can Gabarró, Cendejas de la Torre, Poble Nou, Trinchera del Ferrocarril, San Pere de Ribes, Can Almirall, Arroyo del Val-4, Manchones and Fuensaldaña in the Iberian Peninsula; Schönegg, Steierreg, Löffelbach, Hochegger and Köflach-Voitsberg in Austria; Pozlata (Provaliski Potok; aff.) in Serbia (Pavlovic, 1963) and Çandir (Turkey). The type locality of Sansan is represented with an asterisk. M-407 Rotonda, the locality of study in the present work, with bold face. AUT, Austria; DE, Germay; HUN: Hungary; ROM: Romania. Data based upon Santafé (1978), Agustí et al. (1988), Cerdeño (1986, 1989), Antoine et al. (1997), Codrea (2000), Ménouret and Guérin (2015), Peter (2002), Becker (2003), Heissig (2005), Seehuber (2008) and Cuesta (2006). Illustration of *L. sansaniense* by Mauricio Antón.

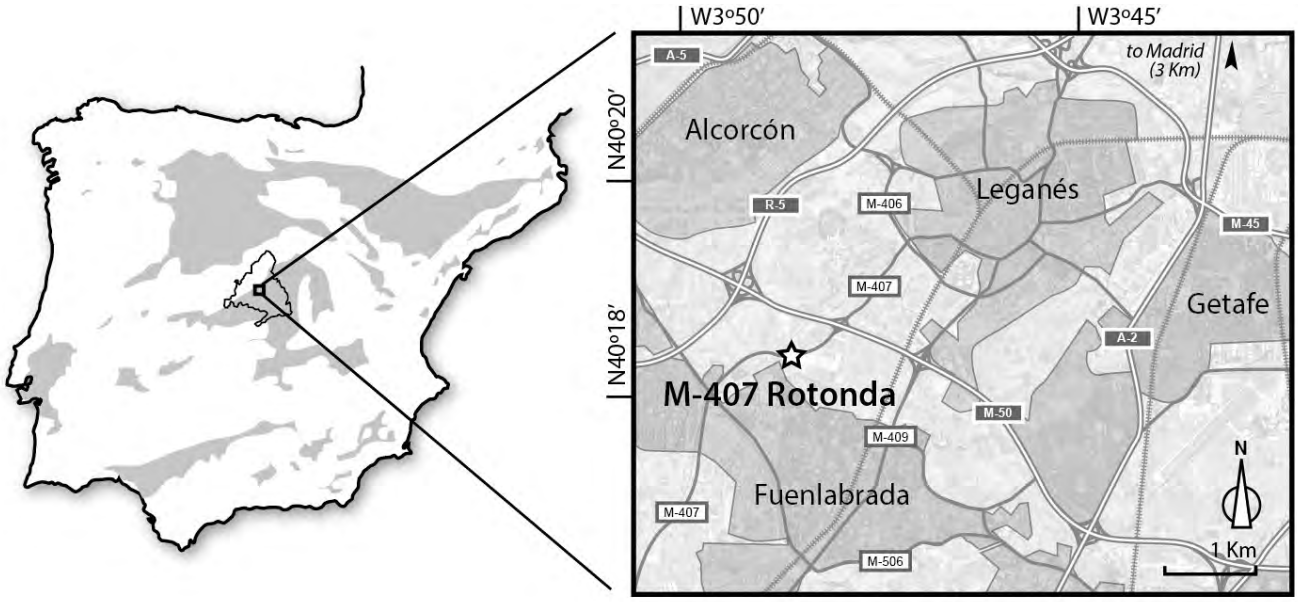


Fig. 2 Simplified general map of the Iberian Peninsula with the Tertiary basins represented as shaded contourns and a detail map showing the location of M-407 Rotonda site, represented as a star.

dia, diaphysis; dis, distal; int, interior; epi, epiphysis; max, maximum; Mc, metacarpal; min, minimum; Mt, metatarsal; prox, proximal. In describing the dental elements, we follow the terminology proposed by Jepsen (1996). I, M and P designate incisors, molar and premolar respectively. Lower-case letters designate teeth from lower series and upper-case letters teeth from upper series. A preceding 'D' or 'd' indicate decidual teeth (e.g., DP4 or dp2).

Measurements abbreviations—APD, antero-posterior diameter; DL, distal length; H, height; L, length; TD, transverse diameter.

Institutional abbreviations—**MNCN**, Museo Nacional de Ciencias Naturales (Madrid, Spain); **AMNH**, American Museum of Natural History (New York, USA); **w/n**, without field number; **NMB**, Naturhistorisches museum Basel; **BSPG**, Bayerische Staatssammlung für Paläontologie und historische Geologie, (Munich, Germany).

Measurement comparison—Astragali are by far the more abundant postcranial bones for the species in the Iberian Peninsula and have been previously used as an estimate of the body size, understood as the relative size of the animal or shoulder height, among Rhinocerotidae (Becker et al., 2009; Cerdeño, 1998; Cerdeño and Nieto, 1995). In order to test the decrease in size through time previously reported in the postcranial bones of *L. sansaniense* in the Iberian Peninsula, the transversal diameter of the astragalar trochlea or DL (see Material and Methods for a list of measurement equivalences with other authors), DT (maximum transversal distance of the bone) and H (height) measurements were used. A Jonckheere Trend test (or Jonckheere–Terpstra test) was performed to assess a possible decrease in size. This test is a non-parametric adjustment test for directionally ordered samples. In order to check the correlation coefficient, an additional Kendall's tau test has been performed. More information of both tests can be found in Material and Methods Chapter. Statistical analysis was carried out using the Statistical Package for the Social Sciences (SPSS v. 17). $p < 0.05$ results were considered statistically significant.

Referred material—See appendix 1, figures 3-9 and Supplementary tables S1-S19.

SYSTEMATIC PALEONTOLOGY

Family Rhinocerotidae Owen, 1845

Subfamily Rhinocerotinae Owen, 1845

Tribe Rhinocerotini Owen, 1845

Subtribe Rhinocerotina Gray, 1825

Genus *Lartetotherium* Ginsburg, 1974

Type species—*Lartetotherium sansaniense* (Lartet in Laurillard, 1848)

Other species—Heissig (2012) cites *L. sansaniense* is the only species by monotypy. However, the species *Lartetotherium montesi* and *Lartetotherium steinheimensis* have been also ascribed to the genus.

Diagnosis—(Heissig, 2012) "Medium-sized one-horned rhinoceros with a skull of medium length with a strongly concave dorsal profile. Anterior dentition with two pairs of lower incisors in each hemimandible, the mesial ones being sometimes lost in older individuals. Jugal teeth unirradicular, with a deep groove along the root. Strong metacone fold on the premolar teeth, weaker but present in the molars. Limbs with the primitive characters of the Tribu".

Differential diagnosis—(modified from Ginsburg, 1974, p. 597) "Rhinocerotid close to *Dicerorhinus* but with a higher occiput, pterigoidean crests posteriorly extended to almost the level of the paraoccipital apophysis, upper incisors more

developed, retained lower p1 and shortened upper P2-M3, with narrow transversal valleys. Nearly straight postglenoid processes (curved in *D. sumatrensis*), posttympanic ones short and anteriorly oriented (long and curved in the extant species). The nasal bone is longer and wider".

Lartetotherium cf. *Lartetotherium sansaniense* (Lartet in Laurillard, 1848)

Holotype—Skull with mandible NHN Sa 6478, firstly described by Lartet (1851, p.29) and not figured until Filhol (1891, plates XIII-XIV).

Type Locality—Sansan, France, ca. 15 Ma.

Diagnosis—As for genus.

Biostratigraphic and Geographic range—From lower Miocene (MN 4) to upper Miocene (MN 9) of Europe.

DESCRIPTION

Skull (Fig. 3; Table S1)—CA4-73 is relatively complete, as only lacks the premaxilla, part of the left zygomatic arch and the top of the occipital crest. Partly owing to numerous cracks on its surface, the bone sutures are not visible. The dental series are represented by the left P2-M3 and the right P4-M3. The teeth row is worn, characteristic of a mature individual (IDAS age class 4, late adult; Anders et al., 2011). The skull is short and has a concave dorsal profile with an elevated occipital end. The nasal bones are well developed, long (about a third of the total skull length) and have a convex and coarse dorsal profile and a straight, concave one. The nasal dome is conical (around 100 mm in diameter, 30 mm high) and points at the presence of a well-developed subterminal, medial, nasal horn. The tips are blunt and ventrally curved. The inner wall of the nasal bone presents a smooth developed longitudinal crest. The nasals' central suture remains unfused. There is no nasal septum. The infraorbital foramen is placed above the P3. The nasal notch reaches the P2/P3 limit, while the anterior border of the orbit is above the M1/M2 boundary. The orbit is rounded and has the rostral border laterally expanded. The lachrymal process is rough and placed in the middle of the rostral rim of the orbit. The postorbitary process is coarse and well developed, slightly protruding from the skull roof in lateral view. The rostral area of the zygomatic process is high, starting 33 mm above the M2 neck (right side). The zygomatic arch is high and thin, reaching the widest maximum behind the M3. The frontal bone is flat and lacks a horn boss insertion. The fronto-parietal crests are badly preserved, but their caudal end reaches the rostral border of the articular facets. In ventral view, the palatine fossae are long and rounded, with parallel lateral borders. The postglenoid processes are well developed, flattened, straight, rounded at their caudal end and show a rostral flat facet (bulkier in C4-315). The paroccipital processes are straight, triangular, pointed at the tip, flat and presents a rostrally projected, short and irregular posttympanic process. The external auditory pseudomeatus is partially closed, forming a deep and sinuous groove. Both posttympanic and paraoccipital processes are at the same level and lower than the occipital condyle. The space of the squamosal, left between both processes, is depressed. In caudal view, the foramen magnum is big and rounded. The occipital condyles are also big sized and subtriangular.

Mandible (Fig. 5; Table S2)—three fragmentary horizontal rami of *L. sansaniense* have been found in M-407 Rotonda. They are narrow and present a nearly straight lower profile. The symphiseal region is long, with the posterior border reaching the metaconid of the p3. The mandibular foramen is behind the limit of the p3-p4. The ascending ramus is wide and flattened. None of the mandible fragments is well-preserved.

Upper teeth (Fig. 4; Table S3)—all the upper dentition are restricted to the skull CA4-73. The upper teeth of the skull CA4-73 are considerably worn. The P2 is square in occlusal view. The ectoloph is wide and has a straight labial border. Its protoloph contacts the ectoloph weakly, enclosing a semicircular medifossete. Protocone and hypocone contact through a narrow lingual bridge. The P3-M1 have a rectangular outline in occlusal view. As the remaining premolar series, the P3 has a nearly-straight ectoloph, only interrupted by weak paracone style and parastyle. As in the P2, protocone and hypocone are fused into a lingual bridge, enclosing a roughly oval medifossete. At the advanced wear stage of CA4-73, the protocone is slightly smaller than the hypocone. A very faint crochet is present in P3-M2. The P4 is wider than the P3, shows nearly equal protocone and hypocone, with a smaller contact between them. The postfossete is narrow and long. Both protoloph and metaloph are straight and almost parallel. As the remaining teeth, there is no trace of labial or lingual cingula. In contrary, there is a developed anterior cingulum (low and bumpy) that reaches the anterolingual side of the protocone base). The M1 is rectangular in occlusal view. The ectoloph is wide and smoothly undulated. The protoloph has a rounded antecrochet. Protocone and hypocone are fused due to the advanced wear (the latter clearly bigger). The medifossete is small and 'tear'-like. The paracone fold is absent, leaving almost imperceptibles paracone style and parastyle. In contrast to the previous teeth, the M2 has a square to 'fan'-like outline in occlusal view. The ectoloph is smoothly undulated. Both protocone and hypocone (similar in size) delimit a narrow curved valley that comes out into a semicircular valley next to the ectoloph. The parastyle and paracone style are divided by a marked paracone fold. The parastyle is bigger and more anteriorly projected. The same occurs in the M3. The M3 is triangular in occlusal view. The ectometaloph is nearly straight, the protoloph curved and simple. The crochet is long, simple, well-developed and perpendicular to the ectometaloph. The posterior cingulum is formed by a short string of tubercles. The only decidual teeth found is the DP2. It is rounded in occlusal view. The mesostyle is well-defined. The protoloph is posteriorly curved, the metaloph straight and short. The crochet is short and rounded. It has anterior and posterior cingula.

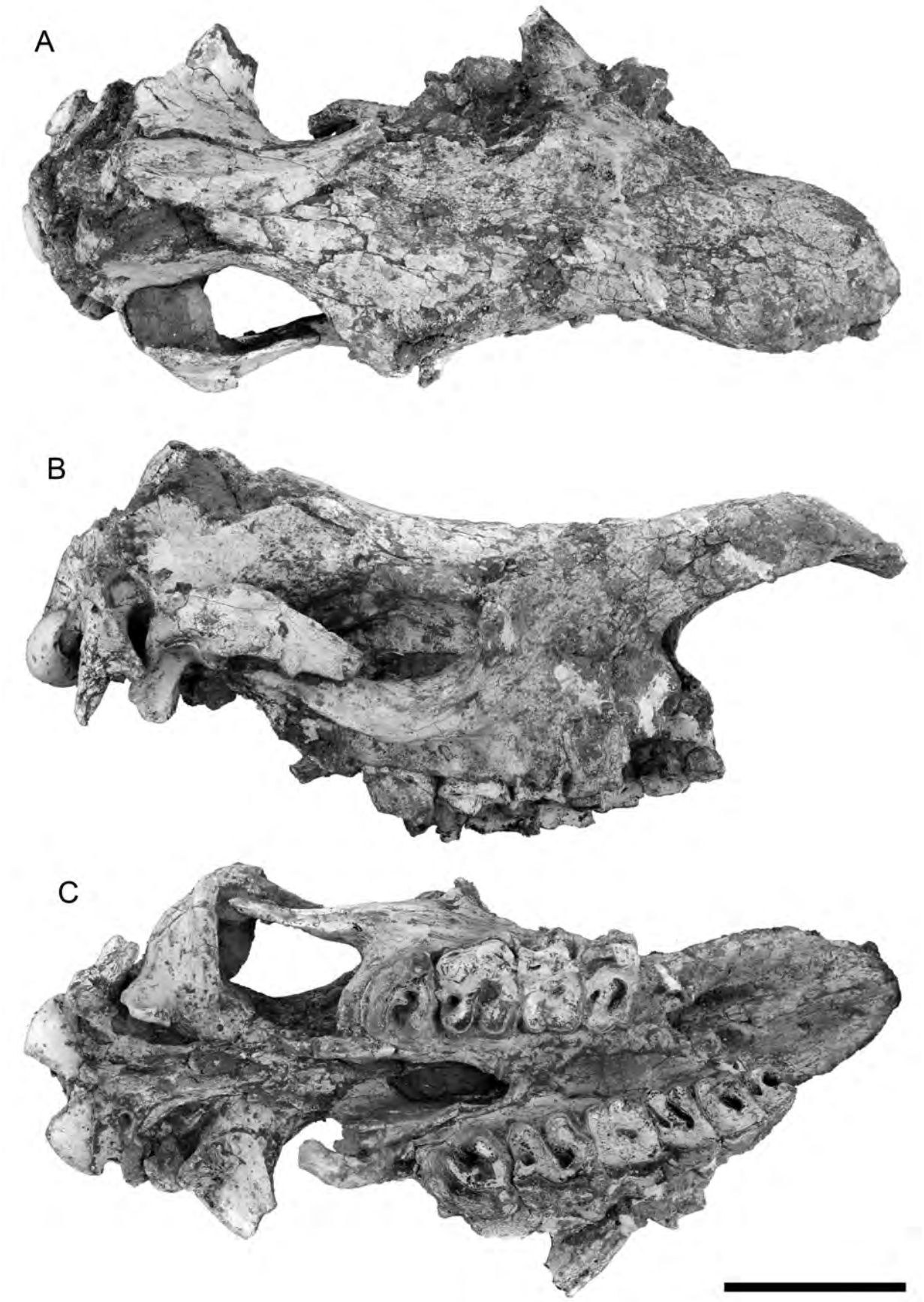


Fig. 3 Skull of *Lartetotherium* cf. *Lartetotherium sansaniense* CA4-73 from M-407 Rotonda in A, dorsal, B, lateral right and C ventral views. Scale bar equals 100 mm.

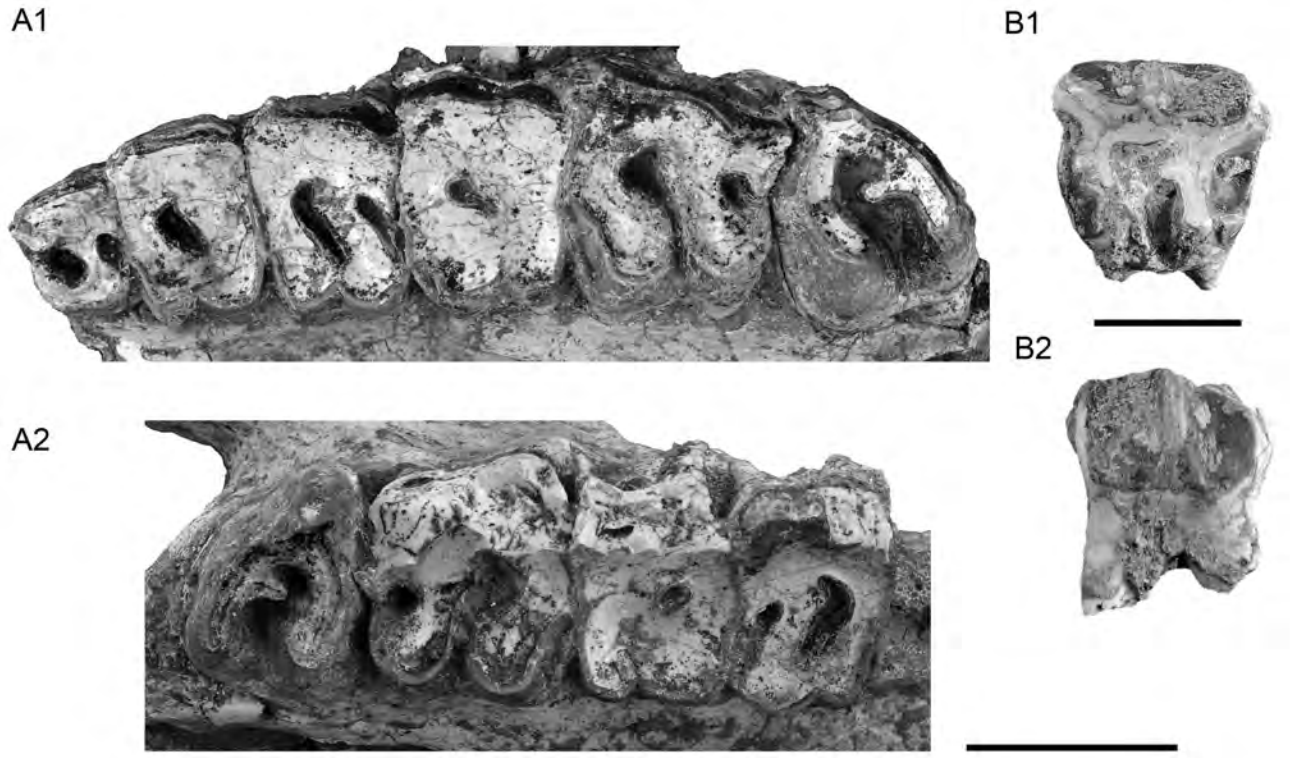


Fig. 4 Upper dentition of *Lartetotherium* cf. *Lartetotherium sansaniense* from M-407 Rotonda. A1, left P2-M3 and A2 right P4-M3 CA4-73 in occlusal views; B, left DP2 B2-55 in B1, occlusal and B2, labial views. Scale bar for A (bottom right) equals 50 mm, whereas the scale for B (upper right) equals 20 mm.

Lower teeth (Fig. 5; Table S4)—the i2 is short and triangular. The p1 is triangular in occlusal view. The labial wall has a slightly curved border, only interrupted by a very shallow labial groove. The posterior valley is small, pointed and triangular. The anterior restricted to a small and shallow notch. The paralophid is reduced to a small triangular tip. The tooth is void of labial cingulids, being the lingual one reduced to a small and weak anterior ridge. The labial cingulids of the third and fourth premolars are restricted to very small ridges in the anterior and posterior borders, more developed in the p4. Both p3 and p4 have triangular anterior valleys and wider posterior ones. Their lingual borders are flattened. The labial wall of the talonid is inflated in the premolar series, remaining at the level of the protoconid in the molars. The lower molar series also have small ridges as anterior and posterior lingual cingulids, except for the m3 which lacks the posterior lingual cingulid. The extension of the anterior lingual cingulids ranges from reaching the anterior part of the metaconid in the m1 to being limited to the paralophid in the m3. The posterior lingual cingulid is only present in the m2. The dp2 is rectangular. The posterior valley is narrow and slightly curved; the anterior one is triangular and shallow. The hypolophid is transversal. The hypoconid large and has a rounded lingual border. The labial groove is very shallow. The metaconid is blunt and the paralophid big and rounded.

Postcranial skeleton

Atlas (Fig. 6)—the first cervical vertebrae of *L. sansaniense* (D5-4) is short and wide and has short and oval wing-like transverse processes. The condyle facets are subtriangular and asymmetrical, with an expanded ventral border, flanking a spacious and mushroom-shaped rachidian canal. The dorsal face has an elevated plateau (wide and flat on the anterior side) with two small and rounded articular facets. The inner foramina vertebrale laterale of the dorsal surface are rounded and placed in a groove that expands to the alar fossa. The latter is small and oval, being almost encircled by the transverse wing. The ventral surface is smooth and has a wide posterior border. On the caudal side, the rachidian canal is expanded but preserves the globulous mushroom outline. The axis facets are long and tear-like shaped, lacking any foramen transversarium. The atlas from Sansan (Heissig, 2012) has a wider anterior border, the rachidian canal is rounded instead of mushroom-shaped (as in M-407 Rotonda).

Axis (Fig. 6)—a single axis has been found (CA4-228). The odontoid process is stout and shows a smooth transition with the axis-facets. The anterior articular facets are oval to tear-shaped and concave-convex, giving the piece a bell-like outline in dorsal view. The transverse foramen has both openings rounded, being the caudal one slightly bigger. A continuous ridge crosses the ventral surface rostrocaudally. The lamina nuchae is low and wide with an irregular surface. The process for the ligamentum interspinale is ventrally oriented. The axis from Sansan figured in Heissig (2012) differs in its convex dorsal border in lateral view, more horizontally oriented odontoid process.

Radius (Fig. 7A; Table S5)—the bone C2-46 is slender. The proximal epiphysis is laterally expanded. In proximal views, the humeral articular surface is very asymmetrical. The medial side of the humeral-facet is semicircular, has a concave surface and a caudal convex border. The lateral portion of the humeral-facet is vaguely 'tear'-shaped and has a sinusoid caudal border. On the cranial side, the surface is smooth and presents a double insertion for the *m. biceps brachii*. This insertion has two small and shallow scars, being the lateral one bigger and 'horseshoe'-shaped. Typically two ulnar facets are attached to the proximal border on the caudal side. The lateral one is big, subtriangular and has a sigmoid proximal border. The medial one is poorly-developed, being limited to a very narrow and flat surface attached to the proximal articular border. Both contact through a narrow surface. The diaphysis is long and kidney-shaped in cross-section. On the cranial side, the distal epiphysis is flattened. The gutter for the *m. extensor carpi* is wide, leaving a lateral bumpy area. No clear ulnar facets are observable on the distal extent of the bone. The medial styloid process is very protruding from the distal articular surface. The radius from M-407 Rotonda is morphologically close to the individual from Sansan Sa-6308, but with a narrower (low TD) distal epiphysis.

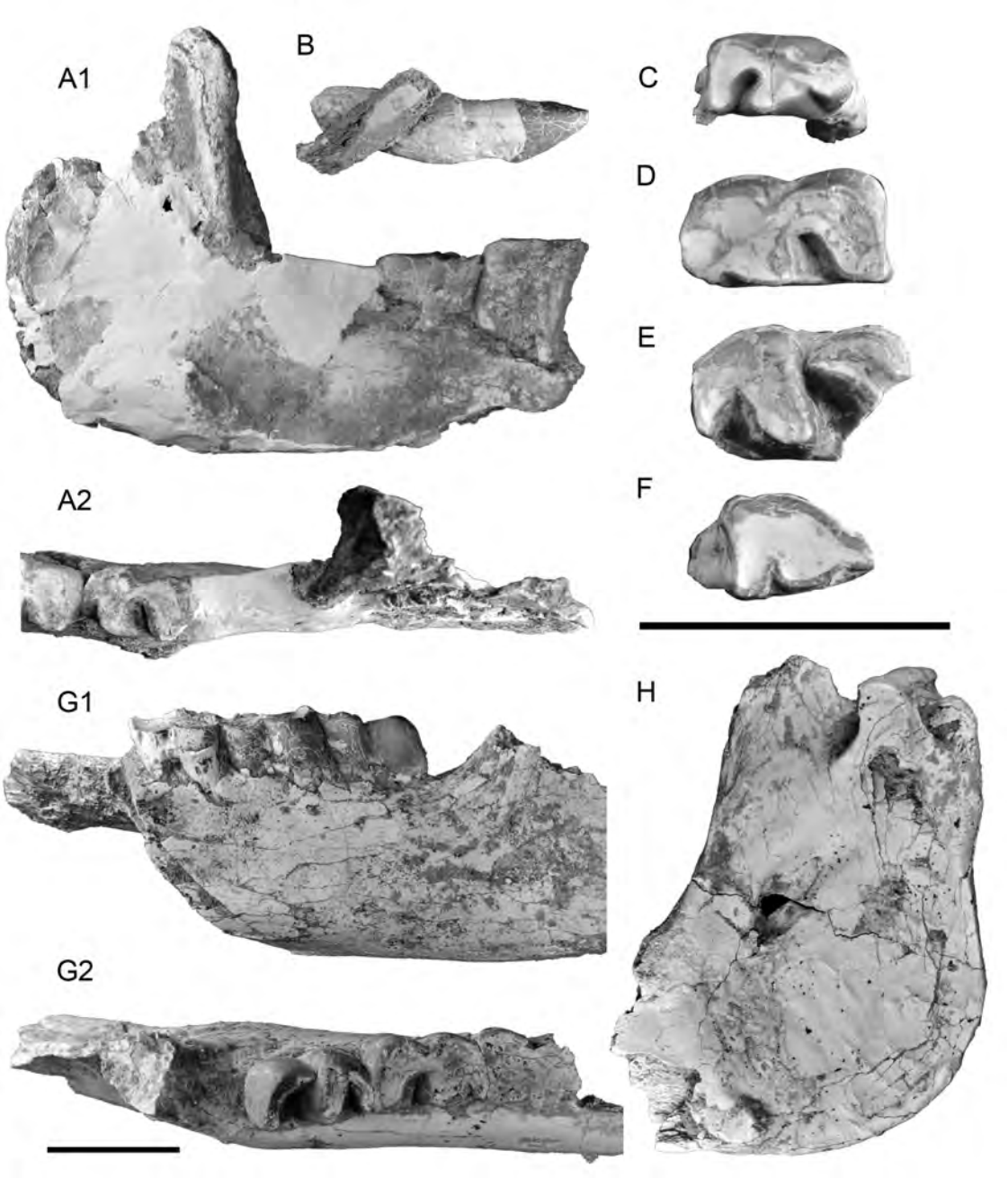


Fig. 5 Mandibles and lower teeth of *Lartetotherium* cf. *Lartetotherium sansaniense* from M-407 Rotonda. A1, fragmentary right hemimandible C2-65 with m1-2 in lateral and A2, occlusal views; B, right i2 A1-67 in labial view; C, right dp2 CA3-118 in occlusal view; D, left dp3 CA3-182 in occlusal view; E, right dp4 B1-84 in occlusal view; F, right p1 B2-73 in occlusal view; G1, fragmentary right hemimandible D5-1 with m1-3 in lateral and B2, occlusal view; C, right ascending ramus DES-3 in lateral view. Scale for A, B, F and G is placed on the botton left corner, scale form the rest on the right. Both scale bars equals 50 mm.

Ulna (Fig. 7B; Table S6)—the olecranon of CA4-51 is nearly vertically-oriented, with an almost straight caudal profile. Its medial border is irregular and vaguely convex. The anconeal process is wide, short and vaguely symmetric. The medial lobe of the humeral articular surface is shorter than the lateral one (which has a square extent, forming an obtuse angle with the lateral radial facet). The lateral radial facet is well-developed, subtriangular and flat. The medial one is only preserved in A2-35, it is narrow and small. The diaphysis has a triangular section and concave caudal sides. If compared with the proximal fragments from Sansan figured in Heissig (2012), the medial radial facet of the individuals from Sansan are somewhat shorter and the trochlear region more medially rotated.

Magnum (Fig. 7C; Table S8)—in dorsal view, the magnum from *L. sansaniense* has a nearly straight proximal border for the semilunate-facet. The distal border of the dorsal side of the bone is rounded. The volar process is delimited by a shallow rim, is flattened and is little palmarly-oriented. The proximal crest is rounded and well defined, with a concave limit with the dorsal side of the bone. In medial view, the medial indentation is shallow and triangular. The Mc III facet is highly concave in lateral view. Its outline has convex dorsal and plantar borders (the latter asymmetrical), whereas the lateral and medial and ones remains straight and little diverging. The magnum from M-407 Rotonda is morphologically similar to the individual Sa-5592 from Sansan. However some minor differences can be stressed. In lateral view, the proximal crest of Sa-5592 has smoother anterior and posterior indentations and is slightly more palmarly placed.

Unciform (Fig. 7E; Table S9)—a fragmentary dorsal fragment of a left unciform has been found. The dorsal surface is flat. The distal Mc IV-facet is subtriangular and has a concave-convex surface.

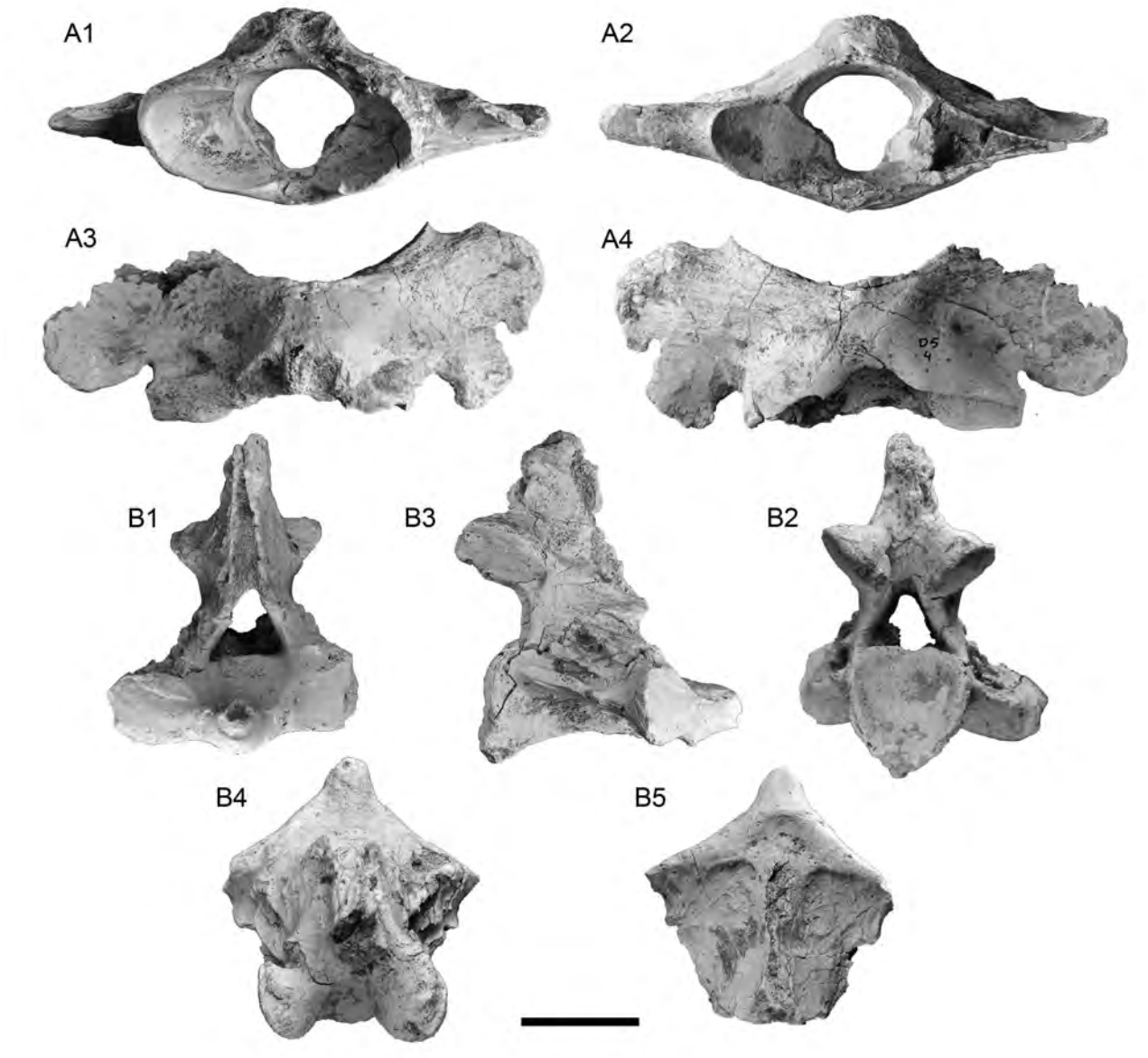


Fig. 6 Cervical vertebrae of *Lartetotherium* cf. *Lartetotherium sansaniense* from M-407 Rotonda. A, atlas D5-4 in A1 anterior, A2 posterior, A3 dorsal and A4 ventral views; B, axis (without field number) in B1 anterior, B2 posterior, B3 lateral, B4 dorsal and B5 ventral views. Scale bar equals 50 mm.

Pyramidal (Fig. 7D; Table S7)—the proximal radius-facet is concave, extending parallel to the pisiform facet along the palmar side of the bone. The palmar expansion of the pyramidal is very short and palmarly-projected. On the medial side, the proximal semilunate-facet is narrow and has a smoothed boundary with the ulnar one. The distal articular facet for the semilunate has a bilobed appearance due to a shallow proximal indentation. The distal unciform-facet is semicircular and dorso-palmarly concave.

Femur (Fig. 8A; Table S10)—the femur is short and has a wide proximal epiphysis. The head of the femur is faintly asymmetrical, with a digitated fovea capitis. The head occupies less than a half of the proximal surface. The greater trochanter is low and very wide. Its basal pillar is short and narrow and has a wide medial gutter. The caudo-medial border of the greater trochanter is wide, flattened and shows two distally-projected bony expansions. The caudal space between the greater trochanter and the head of the femur is wide and shallow. The lesser trochanter starts distal to the femoral head on the medial border and expands up to the level of the upper side of the third trochanter. It is developed in the form of an obliquely-oriented, small and blunt ridge with a short and straight border. This ridge vanishes at the level of the third trochanter. The third trochanter is long (high TD), low (low H), well delimited and has an expanded and cranially curved lateral flange. The diaphysis is short and stout. The distal epiphysis is deep and obliquely oriented. On its caudal side, the medial attachment for the *m. gastrocnemius* is very short and laterally displaced. However, the distal attachment area for the *m. flexor superficial* for the phalanxes is not preserved. The lateral condyle is more proximally placed than the medial one. The femur from Sansan Sa-15635 has a narrower (lower TD) head of the femur, a deeper and wider notch between the

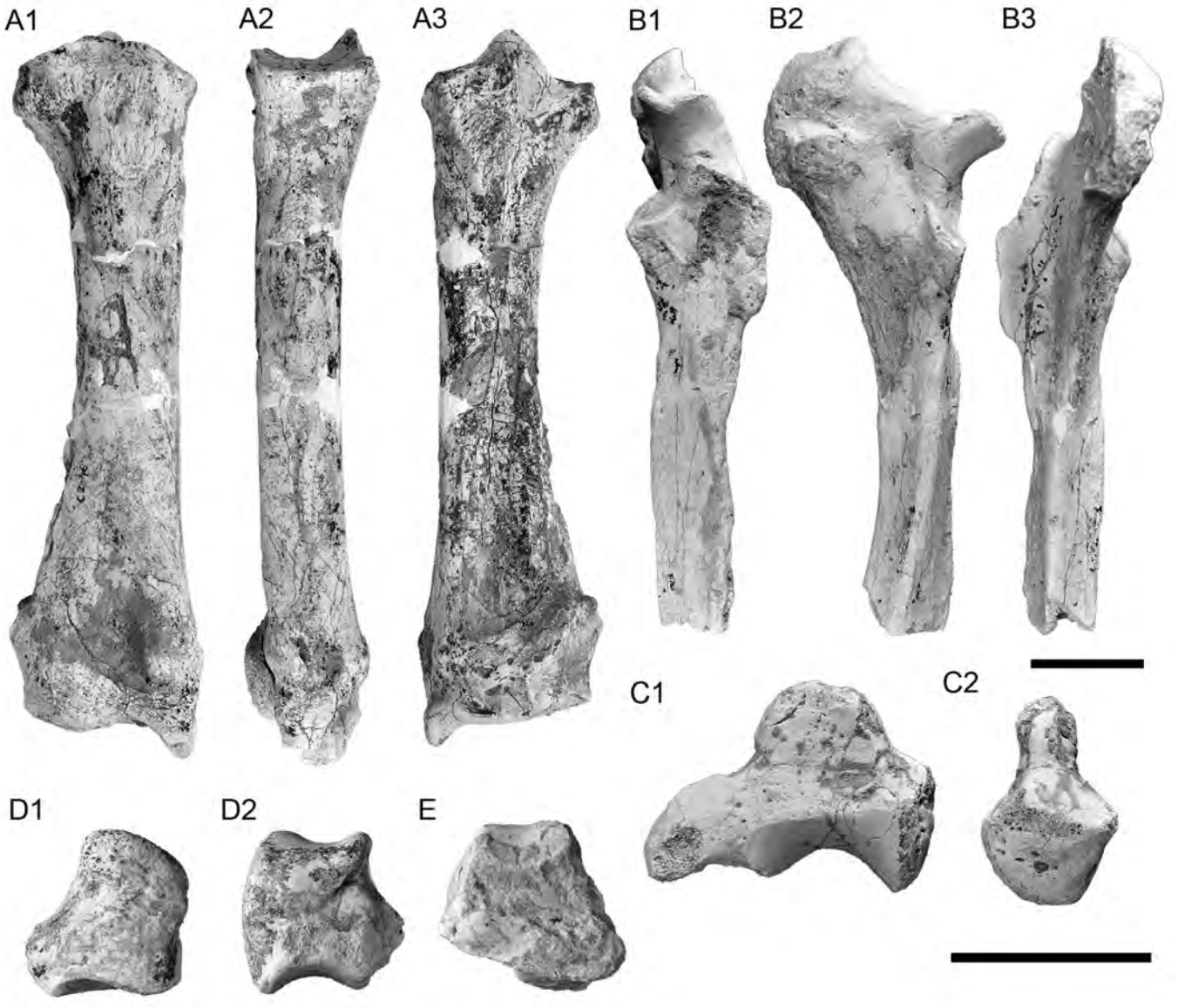


Fig. 7 Anterior limb bones and carpals of *Lartetotherium* cf. *Lartetotherium sansaniense* from M-407 Rotonda. A, right radius CA2-46 in A1 cranial, A2 medial and A3 caudal views; B, right ulna CA4-51 in B1 cranial, B2, medial and B3 caudal views; C, right magnum A2-13 in C1 lateral and C2 dorsal views; D, right pyramidal CA2-100 in D1dorsal and D2 medial views; E, left unciform CA4-5 in dorsal view. Scale for A and B is placed on the middle right, scale for the remaining bones on the bottom right. Both scale bars equal 50 mm.

head and the lesser trochanter and a less medially projected medial epicondyle. The same differences can be observed in the sample from Sandelzhausen.

Patella (Fig. 8B; Table S11)—the patella is high and oval in cranial view and has a small and symmetric lateral flange (variable in size) with a straight to modestly concave lateral border. On the proximal side there is a protruding tip. The caudal side of the bone is occupied by the femoral facets. The medial femoral facet has a vaguely rounded medial border, whereas the lateral facet is well developed and has a straight proximal border. The caudal side of the proximal tip is totally isolated from the femoral facets by a short neck. If compared with the patella from Sansan MNHN Sa 5374 (Heissig, 2012), the individual from M-407 Rotonda has a more expanded lateral expansion and a more pointed apex.

Astragalus (Fig. 9A; Table S12)—the astragalus is as high as wide. The trochlea is asymmetrical and shallow. The neck is high and has a straight lateral border. The groove of the neck is represented by a rugous and shallow area and shows a smooth separation with the trochlear border, favoring the formation of a faint ridge between the medial lip and the distal border (absent in other Iberian populations of *L. sansaniense* as MNCN-40500 from La Cistérniga). The first calcaneum-facet is big and square, the second rectangular, vertically oriented, whereas the third is oval and connects with the former through a small ridge. The bone has a considerable APD, being deeper on its distal half. The medial tubercle is small and barely surpasses the distal articular area, which has a squared navicular-facet and an oval cuboid one. If compared with the Sansan's astragalus MNHN Sa-6462, the astragali A4-8 and w/n from M-407 Rotonda present a smaller trochlea. On the plantar side, the second calcaneum-facets are wider and have a more squared profile than the individual from Sansan Sa-6462 (Heissig, 2012).

Calcaneum (Fig. 9C; Table S13)—the *tuber* is stout. In lateral view, the posterior border of the bone is straight. The

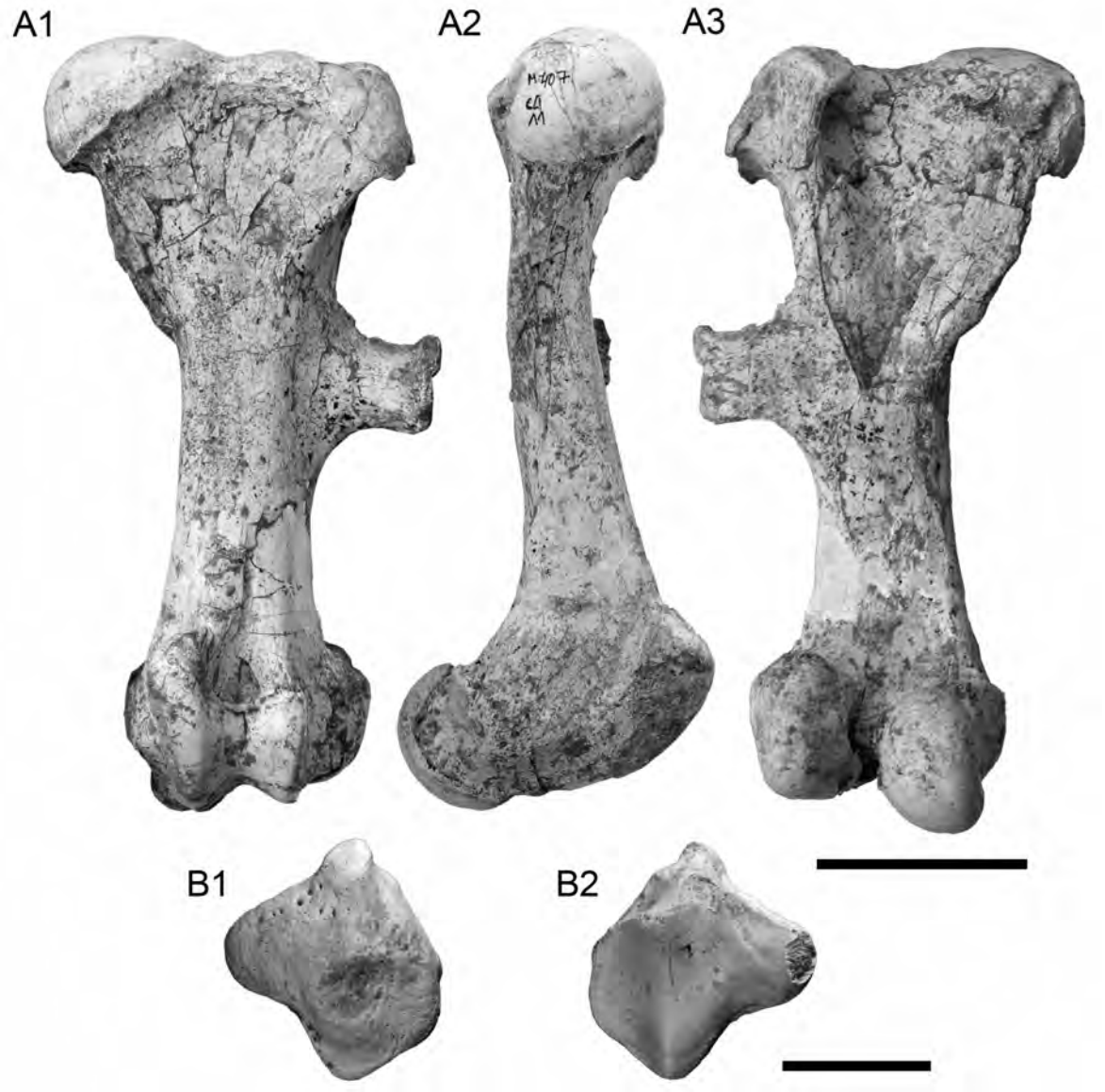


Fig. 8 Posterior limb bones of *Lartetotherium* cf. *Lartetotherium sansaniense* from M-407 Rotonda. A, CA4-11, left femur in A1 cranial, A2 medial and A3 caudal views; B, right patella CA5-226 in B1 cranial and B2 caudal views. Both scale bars equal 50 mm.

sustentaculum is horizontal (CA4-133) to slightly distally oriented (C2-91), with the dorsal outline forming a gentle slope. The first astragalar facet is rounded and bears a concave-convex surface. The second facet for the astragalus is oval, vertically oriented and almost flat. The third is narrow and has a semicircular outline. The distal tip is wide and triangular, with an almost straight distal border.

Cuboid (Fig. 9B; Table S15)—the cuboid of B3-14 is high and narrow (low TD). The volar process is well developed and stout, overhanging from the distal face of the body. The proximal articular area is concave, with a raised plantar border showing a central inlet. On the lateral side, the navicular facet is concave and 'hourglass'-shaped, forming an obtuse angle with the plantar ectocuneiform-facet, which is semicircular and laterally oriented. The dorsal ectocuneiform-facet is not preserved. The distal Mt IV-facet has straight dorsal

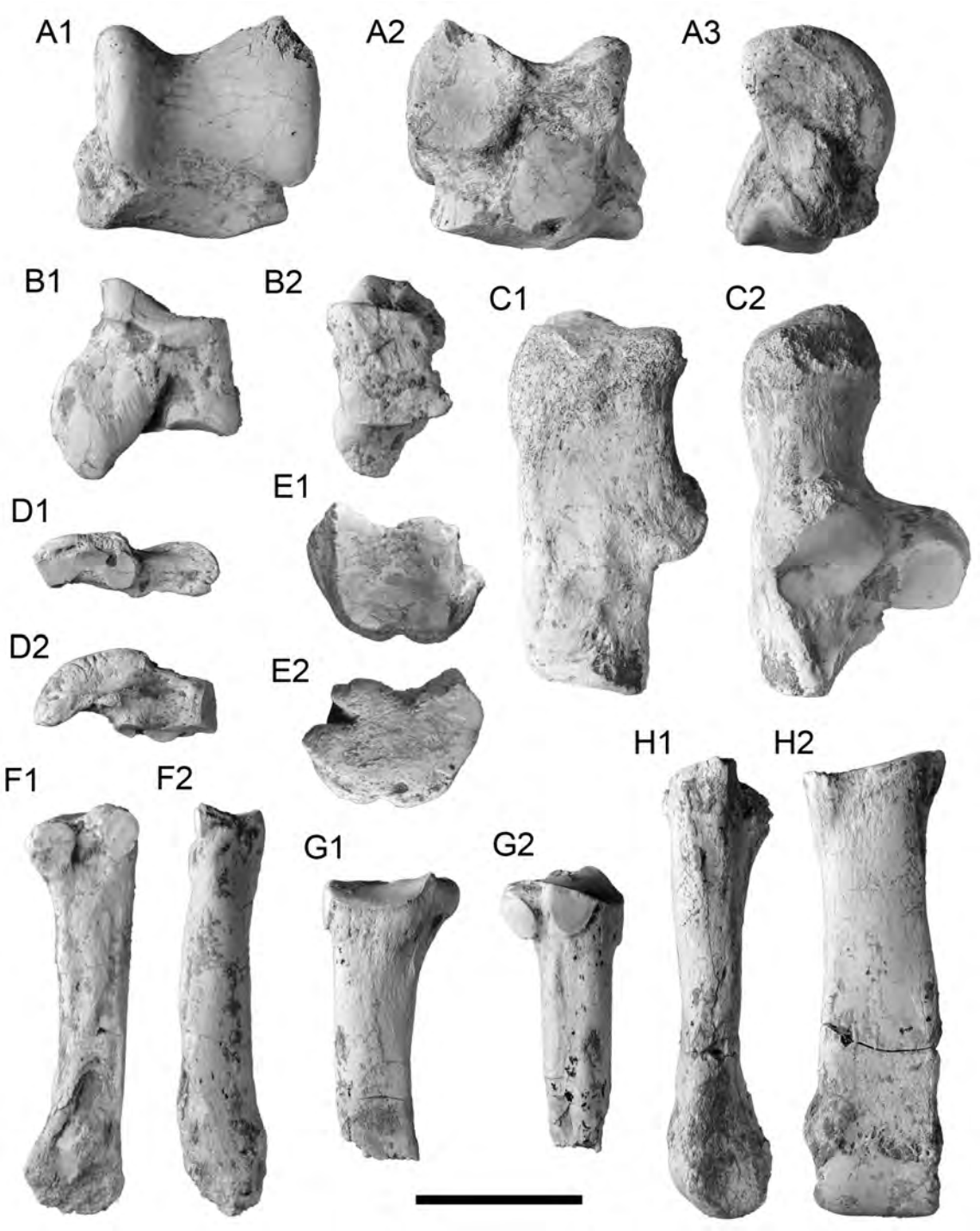


Fig. 9 Tarsal and metatarsal bones of *Lartetotherium* cf. *Lartetotherium sansaniense* from M-407 Rotonda. A, left astragalus CA-136 in A1 dorsal, A2 plantar and A3 medial views; B1, right cuboid CA2-11 in lateral view; B2, same bone in dorsal view; C, right calcaneum CA4-133 in C1 lateral and C2 anterior views; D, right entocuneiform B3-11 in D1 medial and D2 dorsal views; E, right navicular CA4-308 in E1 proximal and E2 distal views; F, right Mt II CA4-368 in F1 lateral and F2 dorsal views; G, left Mt IV CA3-42 in G1 dorsal and G2 medial views; H, left Mt III CA4-43 in H1 lateral and H2 dorsal views. Scale bar equals 50 mm.

and plantar borders, a rounded plantar expansion and lacks its plantomedial extent. The cuboid Sa-5772 from Sansan (Heissig, 2012) presents a more rounded volar process and a more dorsally projected dorso-distal border in lateral view.

Navicular (Fig. 9E; Table S14)—in proximal view, the navicular has a 'fan'-shaped outline for the astragalar facet. Its surface is dorso-plantarly concave and transversally flat. The distal articular facets are poorly delimited. Two foramina can be found in this side. The first is attached to the medial border, between the ectocuneiform and mesocuneiform-facets' limit. The second forms a deep groove on the plantar side of the bone. The same vascular pattern can be observed in Sandelzhausen (e.g. PQ 18-T 5080 20üB).

Entocuneiform (Fig. 9D; Table S16)—The volar process is flattened, elongated and sickle-shaped, being as long as the body of the bone. Its dorsal side has a blunt ridge medially curved. The dorsal navicular-facet is semicircular and flat. The mesocuneiform facet is very long, distally connecting with a kidney-shaped Mt II-facet. If compared with the specimen from Sansan Sa-5815 (Heissig, 2012) or the sample from Sandelzhausen, the individual from M-407 Rotonda has a longer and less quandrangular volar process and fused distal facets.

Mt II (Fig. 9F; Table S17)—the bone is long and slender. The proximal articular facet for the mesocuneiform is semicircular and very concave in dorsal view. On the lateral side, the dorsal ectocuneiform-facet is semicircular and attached to the Mt III-facet (which is also semicircular). The limit between both facets is smooth. The plantar Mt III-facet is oval and flat. The diaphysis is deep (high APD) and presents a straight plantar border, with a sharp planto-medial angle. The distal epiphysis is partially broken, preventing its description.

Mt III (Fig. 9H; Table S18)—in dorsal view, the ectocuneiform-facet has a sigmoid dorsal border, a straight medial one and a projected lateral border where the Mt II-facets are located. The plantar one is semicircular and flat, the dorsal reduced to a small oval facet. The dorsal Mt IV-facet is 'D'-shaped and connects with the plantar one (which is not preserved) through a narrow ridge. The diaphysis shows parallel borders up to the midshaft. Thereinafter become feebly divergent. The distal articular facet is flattened, with the medial keel only evident in its plantar side. As in the remaining metapodials, both proportions and morphology are very similar to those of Sansan (Heissig, 2012).

Mt IV (Fig. 9G; Table S19)—the Mt IV is a robust. The proximal epiphysis is 'fan'-shaped in proximal view. In the same view, the cuboid-facet has a 'mushroom'-like outline. It is dorsally concave and transversally flat. Its lateral side is raised. The posterior side of the proximal epiphysis has a swollen platform with an irregular plantar border. On the medial side, the dorsal Mt III-facet is semicircular, asymmetrical, flat, and forms a straight angle with the proximal articular surface to which is attached. This facet is slightly dorsally oriented, being visible in dorsal view. The plantar Mt III-facet has a circular outline and a marked neck, medially projected. The groove between both facets is profound. The diaphysis shows a rounded section. No distal epiphyses are preserved.

DISCUSSION

Cranial remains referred to *L. sansaniense* are hitherto limited to six (possibly seven) localities. These include the holotype from Sansan (Gers, France; Heissig, 2012), a rostrum from Cerro del Otero (Palencia, Spain; Cerdeño, 1986), a partial juvenile skull from La Retama (Cuenca, Spain; Cerdeño, 1996), four skulls from Sandelzhausen (Mainburg, Germany; Heissig, 1972), two skulls from Eibiswald (Viena, Austria; Peters, 1869) and the skull from M-407 Rotonda (Madrid, Spain; this paper). An additional skull from Tășad-Stracoș (Bihor, Romania), tentatively assigned to *Lartetotherium*, requires further study to assess a specific assignation (Codrea, 2000).

The type skull from Sansan Sa-6478 was originally described by Ginsburg (1974) and posteriorly figured and re-described by Heissig (2012). The original proportions of Sa-6478 are

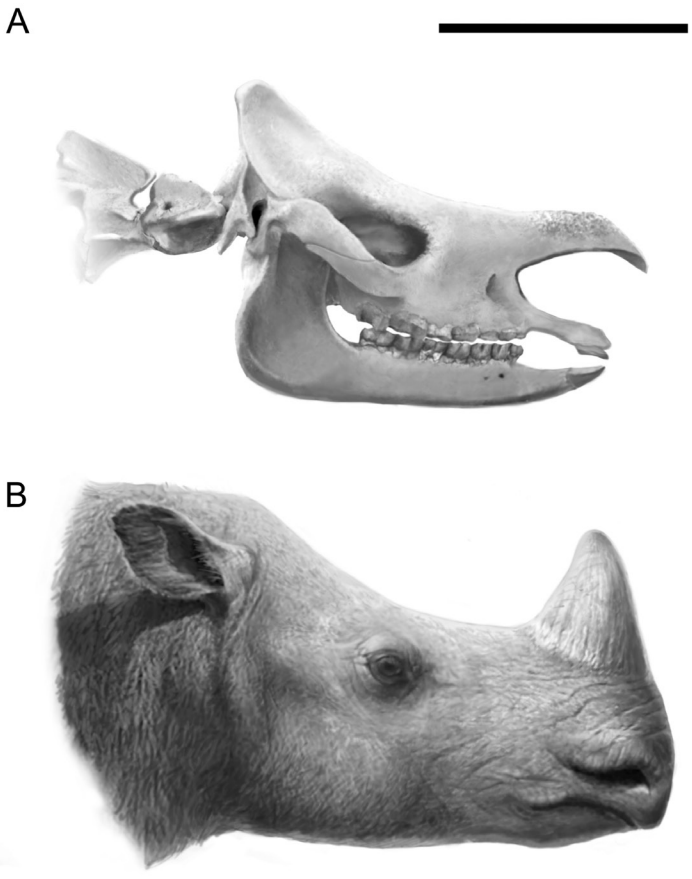


Fig. 10 A, idealized skull and B, reconstructed life appearance of *Lartetotherium sansaniense* mainly based on the skull CA4-73 from M-407 Rotonda (after the correction of the lateral bending). Occiput completed according to the specimens from Sansan Sa-6478 and the three unpublished skulls from Sandelzhausen, premaxillary bone restored according to the skulls from Sandelzhausen and Eibiswald NMW 49, and mandible completed following the holotype from Sansan Sa-6478. Scale bar equals 200 mm.

modified by its strong rostrocaudal compression, resulting in a shortened total length, a shallower nasal notch, an elevated supraorbital region and a characteristic downwards bending of the nasal tips. In addition, it emphasizes the bending of the zygomatic arches and the skull occiput elevation. The skulls from Sandelzhausen BSPG 1959II 411 (used by Groves to complete the description of the species; Groves, 1983), BSPG 1959II 16200 and BSPG 1959II 16480, are finely preserved but heavily compressed, both dorsoventrally (BSPG 1959II 16200 and BSPG 1959II 411) and laterally (BSPG 1959II 16480). Regarding the occipital morphology, both Sa-6478 from Sansan and the whole set of Sandelzhausen skulls show well separated parietal crests and a wide and bilobed occipital crest with strong muscle attachments in the occipital plate. Occipital plate orientation has been largely used in rhinoceros to determine de head position during feeding (Bales, 1996; Heissig, 1999). In *L. sansaniense*, this surface ranges from a subvertical placement in Sa-6478 from Sansan to considerably caudally inclined in the Sandelzhausen sample. The orientation of the reconstructed temporal and occipital crests of the skull from M-407 Rotonda CA4-73 points to an intermediate configuration (*po* angle of 89º following Loose, 1975 and Zeuner, 1934).

Aside from the occipital region, the overall morphology of the skull CA4-73 from M-407 Rotonda presents an intermediate configuration between the type skull from Sansan and the dorsoventrally pressed skulls from Sandelzhausen. Even though no fully complete and undistorted skulls have been found up to now, the cranial anatomy of the species can be estimated by completing missing parts (i.e. premaxillary bone and occiput) as detailed in Figure 10. As a result, the estimated orbitonasal / orbitoauralratio (the proportion between orbitonasal and orbitoaural lengths) of the specimen from M-407 Rotonda, is around 1:1. That is contrary to Groves (1983), who cites the greater orbitoaural length as a primitive character typically found in the species. This character, mainly referred to the diagnosis of the species based on the distorted Sansan's skull, is difficult to estimate from nearly all the skulls found up to date. The only skull that could present a longer postorbital region is that from Eibiswald (w/n; figured in Peters, 1869). However, it is heavily laterally compressed (as in NMW 49, also figured in Peters, 1869) and lacks part of the nasal and premaxillary bones. Moreover, their anterior rim of the orbit is not clear (above M1/M2 boundary in w/n; above M1 in NMW 49) preventing any comparison. Thus, the orbitoaural/orbitonasal ratio in the observed skulls of *L. sansaniense*is a problematic trait to define the species and may vary according to the ontogenetic stage as observed in other rhinoceros species (Hagge, 2010).

The partial adult skull from Cerro del Otero (MNCN 18085) was described by Dantín (1914). Its overall proportions are smaller than those of M-407 Rotonda (Table 1) and present a proportionally wider and more robust nasal bone and a bigger orbit while retaining the overall morphology of *L. sansaniense*. The cranial fragment MNCN 32440 (RE-927) recovered at La Retama shows the DP1-DP4 and M1, thus pertaining to a juvenile individual (IDAS 2). Noticeably, the overall morphology of the rostrum greatly resembles that of the adult individual of M-407 Rotonda, showing that most rostral changes were already present at its age. The same strategy occurs in the rostrum of *D. sumatrensis*, where cranial modifications are focused in the earlier ontogenetic steps (age classes 2-7 according to Hagge, 2010). Even though, some minor differences typical of an earlier developmental stages as the slightly shorter and narrower nasal bones (width of the nasal bones in RE-297 = 79,3 mm versus 98 mm in M-407 Rotonda) and the retracted tooth row (caudal border of the nasal notch above the DP1 in La Retama, P2/P3 in M-407 Rotonda) can be observed.

The adult upper dentition of *L. sansaniense* from M-407 Rotonda, limited to the skull CA4-73, shows some particularities if compared with the type upper series from Sansan MNHN Sa 6478 (Heissig, 2012; p. 358): the P2 from M-407 Rotonda has a narrower (lower TD) hypocone, a shorter (lower APD) protocone, a straight lingual border of the lingual bridge (lacks the lingual notch in the entrance of the median valley), a rounder posterior valley in the P2-3 (instead of triangular) remain wide and profound at advanced wear stages, and the M3 is wider, has a convex ectometaloph, a stronger crochet and is void of crista. Regardless these differences, P4-M2 series seem roughly equivalent and the differences in their occlusal surfaces can be explained by wear. Concerning its dimensions (Figure 11), P2 and P3 from CA4-73 fall within the observed width variability but are proportionally shorter than most of the remaining European sample, somewhat similar to the individuals from Sandelzhausen and Steinheim. The rest of the teeth are moderately (M1, M3) to considerably longer (P4, M2) and clearly wider than the remaining European sample (especially true of P4, M1 and M3; not as evident in P3 and M2). As a result, the M1 appears rectangular in occlusal view, the ectoloph of the M2 enlarged and the whole M3 swollen. In contrast to the extremely widened upper dentition, the lower series fall within the reported variation for the species except for the p2, which is shorter (Figure 12). Many of the teeth included in the comparative sample have an equivalent wear to CA4-73. Hence, size differences are not a reflection of dissimilar wear degrees and represent genuine differences. The widened upper molars of CA4-73 can be interpreted as a regional adaptation to local trophic requirements. A greater occlusal surface would extend the movement phase II of the power stroke (as defined by Fortelius, 1985), facing more attritional surface for food/grit processing and favoring longer horizontal grinding motions of the mandible. Another possible explanation is that CA4-73 is just an extreme example of intrapopulational variability not firstly recorded for the species. Typically, when a larger sample of the species is available from a single locality (e.g. P3 and P4 from Sandelzhausen; Fig. 11), the observed variation partially overlaps the observed range from the remaining localities. As all the measurable upper teeth of *L. sansaniense* from

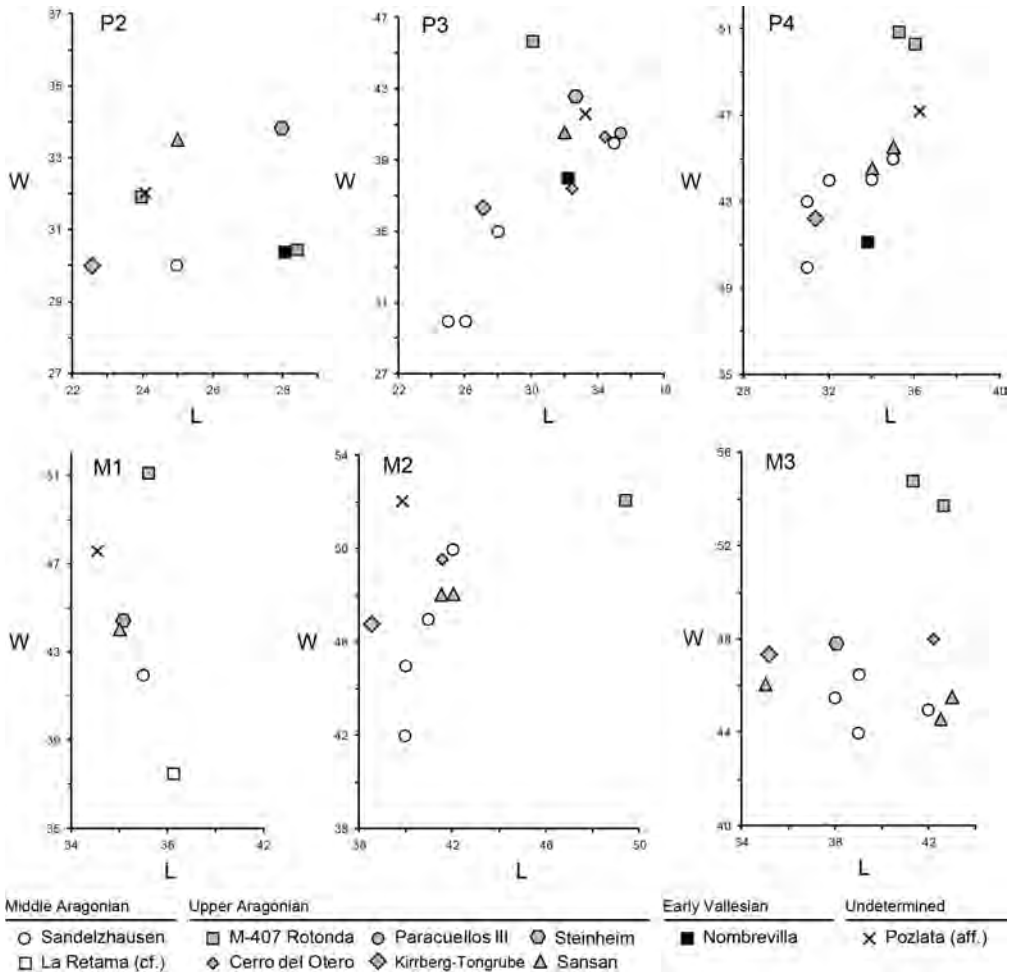


Fig. 11 Scatter diagram (in mm) of the upper dentition of *Lartetotherium* cf. *Lartetotherium sansaniense* from M-407 Rotonda (grey squares) compared with other Iberian sites and the type locality of Sansan (grey triangles). Additional data obtained from Pavlovic (1963), Cerdeño (1989), Peter (2002), Heissig (2012) and Seehuber (2008). Steineim's data obtained from the mandible AMNH 10652.

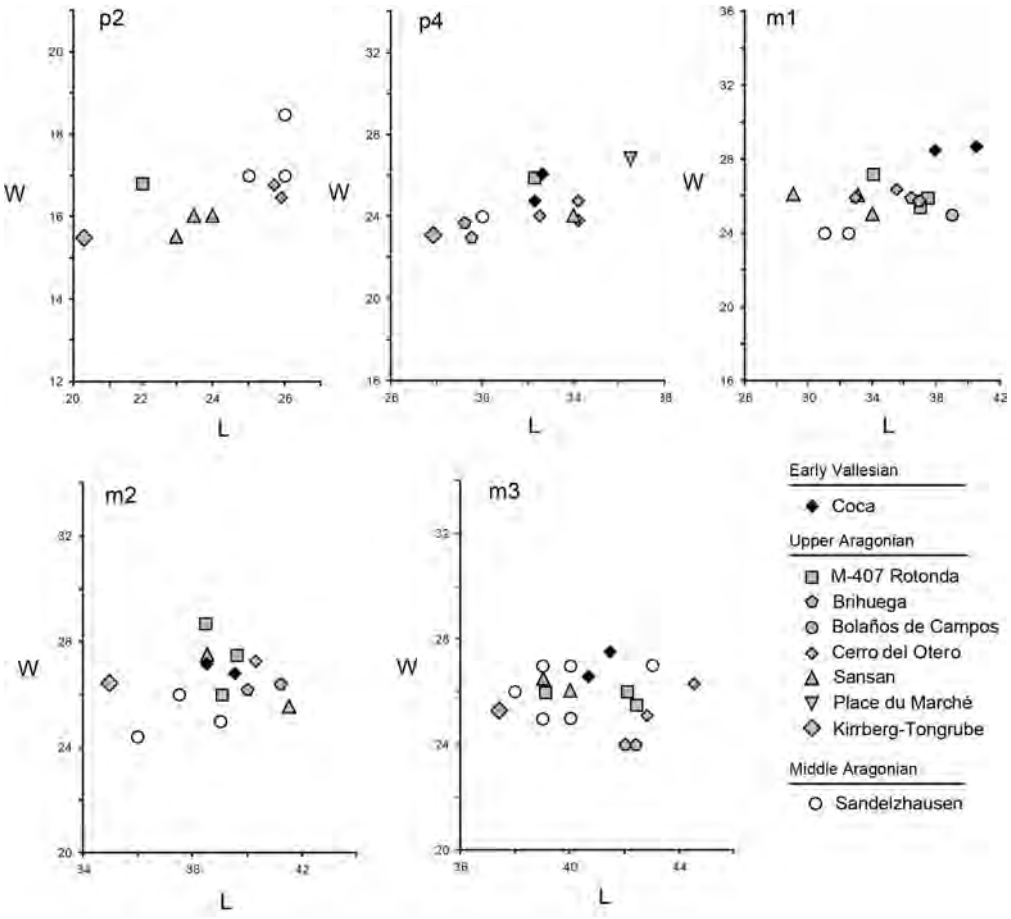


Fig. 12 Scatter diagram (in mm) of the lower dentition of *Lartetotherium* cf. *Lartetotherium sansaniense* from M-407 Rotonda (grey square) compared with other Iberian sites and the type locality of Sansan (grey triangle). Additional Iberian data obtained from Cuesta (1983), Cerdeño (1989). Data from Sandelzhausen, Sansan and Kirrberg-Tongrube obtained from Peter (2002), Heissig (2012) and Seehuber (2008) respectively.

M-407 Rotonda pertain to a single individual and further intrapopulational variation cannot be addressed, this question remains unsolved.

The Figure 11 shows some particularities in the dental proportions of other Iberian populations. The dental series of the skull MNCN 32440 from La Retama (DP1-4 and M1) are morphologically equivalent to those from Sansan but present a smaller size. Curiously, the M1 presents the smallest width recorded for *L. sansaniense*, falling opposite to M-407 Rotonda (Figure 11). It has been interpreted that the tooth is not fully erupted, thus providing a smaller width (Cerdeño, 1986). Even though MNCN 32440 is a juvenile individual and the M1 is little worn, its maximum width (measured between the paracone style of the ectoloph and the protocone) is attained at the level of the anterior and posterior cingula, slightly narrowing from there on. As both cingula are already visible, we consider that the width of the M1 from La Retama has attained its maximum possible and the resulting measurement truly represents a narrower tooth. Unfortunately, the lack of additional remains and the juvenile status of MNCN 32440 prevent further comparisons.

Apart from the differences commented in the description of each bone, the femur and the entocuneiform are the most distinctive bones if compared with other localities with *L. sansaniense*. The entocuneiform MNHN Sa-5815 from Sansan is equivalent to other Iberian *Lartetotherium*-like specimens like B791-6 from the late Miocene of Batallones-1 (Sanisidro et al., this volume). On the other hand, B3-11 from M-407 Rotonda, while retaining the overall entocuneiform morphology of Rhinocerotina, is proportionally longer, has a shorter mesocuneiform-facet and a continuous medial surface for the navicular and Mt II. The second peculiar bone is the femur CA4-11 (Figure 8). It shows different proportion from those of Sansan or Sandelzheusen in its higher robustness (i.e. higher TD of the epiphyses and shortened diaphysis). These proportions are similar to the nearly-complete individual from los Batallones butte (Vallesian / Upper Miocene, Sanisidro et al. this volume). The gracility of the remaining long bones from M-407 Rotonda is similar to the localities of Sansan and Sandelzhausen, so the limb shortening is restricted to the stylopodium (i.e.: the femur CA4-11). The femora/humeri from M-407 Rotonda and Batallones are among the only available sample in the Iberian Peninsula. If whether the mentioned long bone reduction is a characteristic trait of a single individual, the whole population from M-407 Rotonda, or represents a distinctive trait of the Iberian *Lartetotherium* lineages remains an open question.

Two size groups were recognized within the Iberian postcranial sample of *L. sansaniense* (i.e. tarsals and carpals) in the Iberian Peninsula (Cerdeño, 1986). The Middle Aragonian sites of Buñol and Can Màs presented bigger proportions, close to the type locality of Sansan (MN 6, early Upper Aragonian), whereas the Upper Aragonian and Vallesian localities of Paracuellos III, Coca, Cendejas, La Cistérniga, Relea and Can Ponsic were smaller. The Jonckheere trend test did not found significant differences (Std. J-T Statistic = 1,411; p-value = 1,58) in the DL of the Iberian astragalii (Supplementary Data 2), thus no body size differences have been found between the individuals from the Lower Aragonian and the samples from the Late Aragonian and Lower Vallesian. In contrast, TD and H measurements reported a significant decrease at that moment (Std. J-T Statistic = 2,577; p-value = 0,01 for TD; Std. J-T Statistic = 2,832; p-value < 0,01 for H). Our results do not show a body size decrease as previously described for the species in the Iberian Peninsula from the Middle to the Upper Miocene. However, an increase in the remaining general proportions of the astragali is reported. A larger astragalus can be traduced in an augment of the body mass (robusticity) for the species while maintaining a similar shoulder height. Robusticity can be calculated from the metapodials in form of "Gracility Index" (or GI; calculated according to Guérin, 1980). Unfortunately, the scarce number of metapodials recorded in the Iberian Peninsula impedes to test gracility variations through time (Supplementary data 2; Table 3). The Upper Aragonian Rhinocerotina remains from the Iberian Peninsula fit with those published of the type collection from Sansan (Heissig, 2012). However, the Lower Aragonian (Buñol and Can Màs) and part of the Vallesian (i.e. Batallones area) remains are proportionally larger, more robust and morphologically distinct not only from the type collection of *L. sansaniense* but from each other and are in need of a thorough review.

The remaining carpal and tarsal bones of *L. sansaniense* found in the Iberian Peninsula are too scarce or incomplete to statistically discriminate different size groups. Nevertheless, the remaining postcranial remains from M-407 Rotonda (Upper Aragonian, MN 6) can be roughly linked to the smaller size group defined by Cerdeño (1986). The calcaneum from M-407 Rotonda presents similar proportions to that of Cerro del Otero (close to the smaller range recorded for the species; Figure 13A). In a similar way, the proportions of the metatarsals are clearly smaller than those from Sansan and Buñol being closer to those of Coca and Relea. However, the astragali sample of *L. sansaniense* from M-407 Rotonda fall between the larger individuals from Buñol, Sansan and Can Màs and the smaller ones of Paracuellos III, La Cistérniga and Cerro del Otero (Figure 13B). The astragali of the smaller-sized group have a lower APD and a narrower trochlea (lower TD) than those of Sansan (M-407 Rotonda would match this morphology). If compared with the type remains from Sansan (MNHN Sa-6463; Heissig, 2012; p. 425), the calcanei from M-407 Rotonda are much more slender, show a narrower distal end in dorsal view (low APD) with parallel and straight dorsal and plantar borders and a more rounded first astragalar-facet in lateral view (not angulous).

In summary, while the only calcaneum found (CA4-133) nests within the smaller group (close to the calcaneum NM 18124 from Cerro del Otero or the calcaneum without collection number from Coca; Fig. 13A), the astragali scatter around the mean values for the species (Fig. 12B). These results

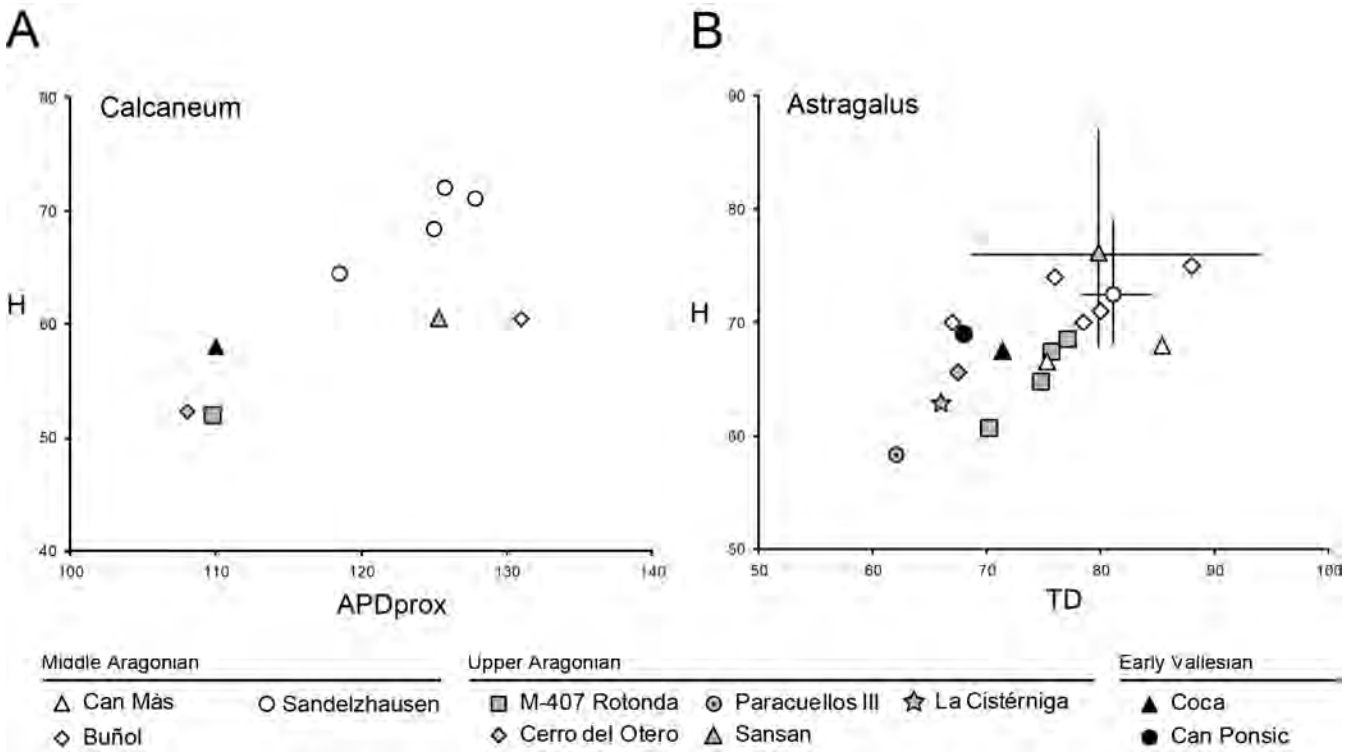


Fig. 13 Scatter diagram (in mm) of the astragali and the calcanei of *Lartetotherium* cf. *Lartetotherium sansaniense* from M-407 Rotonda (grey squares) compared with other Iberian sites and the type locality of Sansan, represented as mean (grey triangle) and minimum/maximum values (lines). Number of astragali from Sandelzhausen = 10; Sansan = 12. Iberian data obtained from Cerdeño (1986) and data from Sansan obtained from Heissig (2012).

are in need of larger samples in order to fill the gap between both groups. However, two groups with some differences in size cannot be ruled out, specially taking into account the long timespan of the species. As no articulated skeletons have been found, a possible sexual dimorphism among postcranial bones (with sexes separated according the size and morphology of the i2) cannot be tested.

Generally a scarce species, the remains of *L.* cf. *L. sansaniense* from M-407 Rotonda comprise the most complete Rhinocerotina remains from the Middle Miocene of the Iberian Peninsula. The recovered collection includes a nearly undistorted skull that has permitted to estimate the original skull appearance of the species and an updated soft-tissue reconstruction. Its comparison with other European remains reveals some particularities on its upper cheek teeth as particularly widened P4, M1 and M3 and wider and longer M2. By almost all its dimensions, the Rhinocerotina postcranial remains from M-407 Rotonda cannot be ascribed to any of the postcranial size groups described by Cerdeño (1986). Statistical analyses of the Iberian postcranial sample points to a body mass decrease (maximum height and transversal distance) in the postcranial skeleton (measured on the astragali). However, the low number of remains of *L. sansaniense* in the Iberian Peninsula limits morphological comparisons in most bones. Apart from the particularly widened molar teeth, the studied sample shows a robust and shortened femur and a distinct entocuneiform. However, the femur seem to link the species with the posterior *Lartetotherium* form Cerro de los Batallones, whereas the entocuneiform feature unique morphologies that separate them not only from latter Rhinocerotina species but from the approximately contemporary type collection from Sansan or the larger and younger sample from Sandelzhausen.

ACKNOWLEDGMENTS

Thanks to I.Rincón, S. Arcos, Argea Consultores S. L. and UTE Recomba for their field work. We also thank to P. Gutiérrez and B. Alonso for the specimen preparation. We acknowledge G. Rößner (Bayerische Staatssammlung für Paläontologie und Geologie) and P. Pérez Dios (Museo Nacional de Ciencias Naturales-CSIC de Madrid respectively) for kindly helping with the specimens from Sandelzhausen and the Iberian Peninsula respectively. Our gratitude to the Dr. Jan van der Made for the data and photographic material of the specimens from Eibiswald, the Dr. Vlad Codrea for the assistance with the specimens from Romania and the Dr. Kurt Heissig for the fruitful discussions and comments regardings the Sandelzhausen collection. The first author benefits from a FPU grant from the Spanish Ministry of Science and Innovation (MICINN). The project CGL2008-05813-CO2-01 and the research group BSCH-UCM 910607 have financially supported this work also.

LITERATURE CITED

Agustí, J., Anadón, P., Ginsburg, L., Mein, P., and Moissenet, E., 1988, Araya et Mira: nouveaux gisements de Mammifères dans le Miocène inférieur-moyen des Chaînes Ibériques orientales et méditerranéennes. Conséquences stratigraphiques et structurales: Paleontologia i Evolució, v. 22, p. 83-101.

Anders, U., Koenigswald, W. v., Ruf, I., and Smith, B. H., 2011, Generalized individual dental age stages for fossil and extant placental mammals: Paläontologische Zeitschrift, v. 85, p. 321-339.

Antoine, P. O., 2002, Phylogénie et évolution des Elasmotheriina: (Mammalia, Rhinocerotidae): Mémoires du Muséum National d'Histoire Naturelle, v. 188, p. 5-350.

Antoine, P. O., Downing, K. F., Crochet, J.-Y., Duranthon, F., Flynn, L. J., Marivaux, L., Métais, G., Rajpar, A. R., and Roohi, G., 2010, A revision of *Aceratherium blanfordi* Lydekker, 1884 (Mammalia: Rhinocerotidae) from the Early Miocene of Pakistan: postcranials as a key: Zoological Journal of the Linnean Society, v. 160, p. 139-194.

Antoine, P. O., Duranthon, F., and Yassy, P., L'apport des grands mammiferes (Rhinocerotides, Suoides, Proboscidiens) a la connaissance des gisements du miocene d'Aquitaine (France), *in* Proceedings Actes du Congres BiochroM'97. Mémoires et Travaux del'E.P.H.E., Institut de Montpellier1997, Volume 21, p. 581-590.

Antunes, M. T., and Ginsburg, L., 1983, Les Rhinocérotidés du Miocène de Lisbonne. Systématique, écologie, paléobiogéographie, valeur stratigraphique: Ciências da Terra (UNL), v. 7, p. 17-98.

Bales, G. S., 1996, Skull Evolution in the Rhinocerotidae (Mammalia, Perissodactyla): Cartesian Transformations and Functional Interpretations: Journal of Mammalian Evolution, v. 3, no. 3, p. 261-279.

Becker, D., 2003, Paléoécologie et paléoclimats de la Molasse du Jura (Oligo-Miocène) : apport des Rhinocerotoidea (Mammalia) et des minéraux argileuxGrade de Doctor rerum naturalium]: Universite de Fribourg (Suisse), 327 p.

Becker, D., Antoine, P. O., and Maridet, O., 2013, A new genus of Rhinocerotidae (Mammalia, Perissodactyla) from the Oligocene of Europe: Journal of Systematic Palaeontology.

Becker, D., Bürgin, T., Oberli, U., and Scherler, L., 2009, *Diaceratherium lemanense* (Rhinocerotidae) from Eschenbach (eastern Switzerland): systematics, palaeoecology, palaeobiogeography: Neues Jahrbuch für Geologie und Paläontologie Abhandlungen, v. 245, no. 1-2, p. 5-39.

Cerdeño, E., 1986, El Esqueleto Postcraneal de *Lartetotherium sansaniensis* (Mammalia, Rhinocerotidae): Estudios Geológicos, v. 42, p. 197-209.

-, 1989, Revisión de la sistemática de los rinocerontes del Neógeno de EspañaPh.D. Dissertation]: Universidad Complutense de Madrid, 429 p.

-, 1996, *Lartetotherium* (Rhinocerotidae) en la fauna con *Hispanotherium* del Mioceno Medio de La Retama, Cuenca, España: Revista Española de Paleontología, v. 11, no. 2, p. 193-197.

-, 1998, Diversity and evolutionary trends of the Family Rhinocerotidae (Perissodactyla): Palaeogeography Palaeoclimatology Palaeoecology, v. 141, p. 13-34.

Cerdeño, E., and Nieto, M., 1995, Changes in Western European Rhinocerotidae related to climatic variations: Palaeogeography, Palaeoclimatology, Palaeoecology v. 114, p. 325-338.

Codrea, V., 2000, Rinoceri şi tapiri terţiari din România, Presa Universitară Clujeană, Cluj Napoca, 174 p.:

Crouzel, f., 2000, Historique du gisement. Les fouilles et les hommes, *in* Ginsburg, L., ed., La faune miocène de Sansan et son environnement: Paris, p. 11-27.

Cuesta, M. A., Morales, J., and Jiménez, E., 1983, Vertebrados del Aragoniense superior de Coca (Segovia): Stvdia Geologica Salmantina, v. 19, p. 161-185.

Cuesta Ruiz-Colmenares, M. A., and Merino-Tomé, O. A., 2006, Bolaños de Campos, nuevo yacimiento de rinocerontes del Mioceno de la cuenca del Duero (provincia de Valladolid, Castilla y León, España): Studia geologica salmanticensia, v. 42, p. 33-48.

Dantín Cereda, J., 1914, Acerca de un nuevo *Rhinoceros* mioceno. *Rhinoceros austriacus* Peters, mutación *hispanicus*: Boletín de la Real Sociedad Española de Historia Natural, v. 14, p. 391-397.

Filhol, H., 1891, Études sur les Mammifères Fossiles de Sansan: Ann. Sci. Géol., v. 21, p. 1-319.

Fortelius, M., 1985, Ungulate cheeck teeth: developmental, functional and evolutionary interrelations: Acta Zoologica Fennica, v. 180, p. 1-76.

Ginsburg, L., 1974, Les Rhinocerotides du Miocene de Sansan (Gers): Compte Rendus des Seances de l'Academie des Sciences, Paris, v. 278, no. 5, p. 597-600.

Ginsburg, L., and Bulot, C., 2000, Le cadre stratigraphique du site de Sansan, *in* Ginsburg, L., ed., La faune miocène de Sansan et son environnement: Paris, p. 39-67.

Groves, C. P., 1983, Phylogeny of the living species of Rhinoceros: Zeitschrift fur Zoologische Systematik und Evolutionsforschung, v. 21, no. 4, p. 293-313.

Guérin, C., 1980, Les rhinocéros (Mammalia, Perissodactyla) du Miocène terminal au Pléistocène supérieur en Europe occidentale : comparaison avec les espèces actuelles: Documents des Laboratoires de Géologie de Lyon, v. 79, p. 1-1184.

Hagge, M. D., 2010, A functional and Ontogenetic Skull Analysis of the Extant Rhinoceroses and *Teleoceras major*, an extinct Miocene North American Rhinoceros [Master of Science: University of Wisconsin-Madison, 165 p.

Heissig, K., 1969, Die Rhinocerotidae (Mammalia) aus der oberolizogänen Spaltenfüllung von Gaimersheim bei Ingolstadt in Bayern und ihre phylogenetische Stellung: Bayerische Akademie der Wissenschaften, Mathematisch-Naturwissenschaftliche Klasse, Abhandlungen, v. 138, p. 1-133.

-, 1972, Die obermiozäne Fossil-Lagerstätte Sandelzhausen. 5. Rhinocerotidae (Mammalia), Systematik und Okologie: Mitteilungen der Bayerischen Staatssammlung Paläontologie und historische Geologie, v. 14, p. 37.

-, 1999, 16. Family Rhinocerotidae, *in* Rössner, G. E., and Heissig, K., eds., The Miocene Land Mammals of Europe: Pfeil, Munich, p. 175-188.

-, 2005, The fossil rhinoceroses of Rudabánya: Palaeontographia Italica, v. 90, p. 217-258.

-, 2012, Les Rhinocerotidae (Perissodactyla) de Sansan, *in* Peigné, S., and Sen, S., eds., Mammifères de Sansan, Volume 203: Paris, Muséum national d'Histoire naturelle, p. 317-485.

Lartet, E., 1851, Notice sur la Colline de Sansan.

Loose, H., 1975, Pleistocene Rhinocerotidae of W. Europe with reference to the recent two-horned species of Africa and S. E. Asia: Scripta Zoologica, v. 33, p. 1-59.

Mein, P., 1990, Updating of MN zones, *in* Lindsay, E., Fahlbusch, V., and Mein, P., eds., European Neogene Mammal Chronology: New York, Plenum Press, p. 73-90.

Ménouret, B., and Guérin, C., 2015, Les Périssodactyles et les Proboscidiens (Mammalia) du Miocène moyen de Collet-Redon, commune de Lambesc (Bouches-du-Rhône) : première découverte en France d'un *Metaschizotherium*: Annales de Paléontologie, v. 101, no. 2015, p. 1-19.

Osborn, H. F., 1900, Phylogeny of the Rhinoceroses of Europe: Memoirs of the American Museum of Natural History, v. 13, p. 229-267.

Pavlovic, M., 1963, *Dicerorhinus* aff. *sansaniensis* (Lart.) iz mladjeg Miocena Srbije: Geoloski Anali Balkanskoga Poluostrva, v. 30, p. 63-75.

Peter, K., 2002, Odontologie der Nashornverwandten (Rhinocerotidae) aus dem Miozän (MN 5) von Sandelzhausen (Bayern): Zitteliana. Abhandlungen der Bayerischen Staatssammlung für Paläontologie und Geologie, v. 22, p. 3-168.

Peters, K. F., 1869, Zur Kenntniss der Wirbelthiere aus den Miocänschichten von Eibiswald in Steiermark: Denkschriften der Kaiserlichen Akademie der Wissenschaften, Mathematisch-Naturwissenschaftliche Classe, v. 30, p. 29-49.

Roger, O., 1902, Uber Rhinoceros goldfussi Kaup und die anderen gleichzeitigen Rhinocerosarten, Wirbelthierreste aus dem Dinotheriensande der bayerisch-schwabischen Hochebene. Bericht des Naturwissenschaftlichen Vereins fur Schwaben und Neuberg.

Roman, F., and Torres, A., 1907, Le néogène continental dans la Vallée du Tage (rive droite). Paléontologie: Comm. des Servic. Géol. du Portugal, Lisbonne, p. 1-88.

Santafé, J. V., 1978, Revisión de los Rinocerótidos miocénicos del Vallès-Penedès: Acta Geologica Hispanica, v. 13, no. 2, p. 43-45.

Seehuber, U., 2008, Litho- und biostratigraphische Untersuchungen in der Oberen Süßwassermolasse in der Umgebung von Kirchheim in Schwaben [Inaugural-Dissertation zur Erlangung des Doktorgrades: Ludwig–Maximilians–Universität München, 162 p.

Van Valen, L., 1966, Deltatheridia, a new order of mammals: Bulletin of the American Museum of Natural History, v. 132, p. 1-126.

Zeuner, F. E., 1934, Die Beziehungen zwischen Schädelform und Lebensweisen bei den rezenten und fossilen Nashörnern: Bericht.Naturforsch. Gellesch. Freiburg in Breisgau, v. 34, no. 1, p. 21-80.

APPENDIX 1

Remains of *L. sansaniense* from M-407 Rotonda studied in the present work.

CA4-73, skull with right P4-M3 and left P2-M3; CA4-315; DES-9; CA4-255, fragmented occipitals; DES-12, B2-55, left DP2; CA5-131, right DP2; 194, DES-3, DES-46, right edentulous hemimandibles; DES-61, left hemimandible with dp3; C2-65, right hemimandible with m1-2; D5-1, left hemimandible with m1-3; CA1-18, right hemimandible with m2-3; CA3-118, left dp2; CA3-182, right dp3; B1-41, left dp3; B3-18, right, B1-84, left dp4; CA3-189, left p2; B2-73, right p2; CA3-189, left p2; CA1-26, right p4; DES-3, right m2; A1-67, A1-37, i2; A1-74, D5-4, CA4-228, atlas; w/n, axis; CA2-46, right radius; C2-46, A2-35, left ulnae; CA4-84, articular fragment of a left ulna; A2-13, right magnum; CA4-5, left unciform; C2-100, right pyramidal; B2-17, CAT45-226, right patellae; w/n, left patella; CA4-11, left femur; B4-61, right femur; CA4-136, CA4-42, CA4-374, left astragali; A4-8, right astragalus; B3-14, right cuboid; B3-11, right entocuneiform; CA4-368, right Mt II; CA4-43, left Mt III; B3-26, proximal epiphysis of a left Mt IV.

SUPPLEMENTARY DATA 1

Measurements (mm) of the skull (Table S1) and mandible (Table S2) of *Lartetotherium* cf. *Lartetotherium sansaniense* from M-407 Rotonda (Madrid Province, Spain). Side is detailed as follows: l, left; r, right.

Table S1	CA4-73
2. Distance between nasal tip and occipital condyle	~ 522.0
4. Distance between nasal tip and notch	~ 153.8
5. Minimal width of braincase	~ 69.7
9. Distance between nasal notch and orbit	133.0
13. Distance between occipital condyle and M3	190.0
14. Distance between nasal tip and orbit	~ 281.0
16. Width between mastoid processes	147.6
22. Width of nasal base	93.3
25. Cranial height in front of P2	154.0
26. Cranial height in front of M1	167.0
27. Height of skull in front of M3	152.0
29. Width of palate in front of M1	54.0
30. Width of palate in front of M3	59.6
31. Width of foramen magnum	44.6
32. Width between exterior borders of occipital condyles	106.0

Table S2	D5-1	C2-65a	CATA1-18a
	r	r	r
L	—	—	—
DAPdia	—	—	66.2
HP1	—	—	52.9
HP2	—	—	60.2
HP3	—	—	61.4
HP4	—	—	63.0
HM1	—	—	68.5
HM2	76.2	—	69.5
HM3a	76.8	—	71.6
HM3p	71.0	—	73.3
DAPdent	—	—	—
Lcor	—	—	—
Lart	—	—	—
Hcor	—	—	—
Hart	—	—	—
DAPhr	—	—	—
DAPproc	—	—	—
DAPcor	—	—	—
DAPart	—	—	—
DTia	—	—	1.9
DTip	—	—	63.1
Lsin	—	—	114.4
DTpx	—	—	57.8
DTm3p	—	—	—
DTcor-cor	—	—	—
DTart-art	—	—	—
DTart	—	—	—

SUPPLEMENTARY DATA 1

Measurements (mm) of the upper teeth (Table S3) and lower teeth (Table S4) of *Lartetotherium* cf. *Lartetotherium sansaniense* from M-407 Rotonda (Madrid Province, Spain). Side is detailed as follows: l, left; r, right.

Table S3		CA4-73		DES-12	B2-55	CA5-131	CA5-61
Upper teeth		**l**	**r**	**l**	**l**	**r**	**r**
	L	24.4		(D) ~28	(D) 30.3	(D) 30.3	28.4
P2	W	32.6		(D) 28.6	(D) 29.5	(D) 29.5	30.7
	H	17.0		(D) 17.7	(D) 19.7	(D) 19.7	—
	L	30.0					
P3	W	46.2					
	H	16.6					
	L	35.0	~ 36				
P4	W	50.3	48.9				
	H	13.9	17.5				
	L	37.1					
M1	W	49.7					
	H	11.2					
	L	49.0					
M2	W	54.0					
	H	19.7					
	L	55.4	53.2				
M3	W	43.6	38.9				
	H	31.7	32.8				

Table S4		CA3-118	CAT3-189	B2-73	B1-41	DES-61	B1-84	CAT3-182	B3-18	CA1-26	DESUB-3	D5-1	C2-65	CATA1-18
Lower teeth		**l**	**l**	**r**	**l**	**l**	**r**	**r**	**r**	**r**	**r**	**r**	**r**	**r**
	L		—	22.1										
p1	W		16.6	16.8										
	H		14.7	13.4										
	L	(d) 22.9												
p2	W	(d) 14.5												
	H	(d) 14.4												
	L				(d) 32.3	(d) 38.8	—	(d) 33.6						
p3	W				(d) 18.0	(d) 19.5	(d) 22.0	(d) 19.7						
	H				(d) 12.9	(d) 23.6	(d) 21.3	(d) 12.2						
	L								(d) 42.2	32.4				
p4	W								(d) 21.0	26.0				
	H								(d) 38.1	10.3				
	L										37.0	34.1	37.4	
m1	W										25.3	27.2	25.9	
	H										35.7	8.6	14.0	
	L											39.6	39.1	37.8
m2	W											27.5	26.0	28.5
	H											20.2	13.4	14.0
	L											42.1		42.4
m3	W											26.7		25.6
	H											24.1		18.3

SUPPLEMENTARY DATA 1

Measurements (mm) of the radius (Table S5), ulna (Table S6), pyramidal (Table S7), magnum (Table S8), unciform (Table S9), femur (Table S10), patella (Table S11), astragalus (Table S12), calcaneum (Table S13), navicular (Table S14), cuboid (Table S15), and entocuneiform (Table S16) of *Lartetotherium* cf. *Lartetotherium sansaniense* from M-407 Rotonda (Madrid Province, Spain). Side is detailed as follows: l, left; r, right.

Table S5			prox epi		prox art		dia		dis epi		dis art	
Radius	L	l	TD	APD	TD	APD	TD	APD	TD	APD	TD	APD
CA2-46 (r)	315.0	313.0	77.6	60.7	75.3	49.8	44.1	32.9	83.1	53.1	69.2	36.8

Table S6		olec					TDtroc		dia		dis epi		dis art	
Ulna	L	TD	APD	H	TD base	APD base	prox	dis	TD	APD	TD	APD	TD	APD
C2-76 (l)	—	39.2	62.7	105.4	23.5	64.8	78.8	58.58	39.4	26.2	—	—	—	—
CA4-84 (r)	—	—	—	—	—	—	—	—	39.0	31.9	—	—	—	—
A2-35 (l)	—	—	—	—	19.4	—	62.0	—	—	—	—	—	—	—

Table S7				
Pyramidal	TD	H	APD	APD prox
C2-100 (r)	40,1	40.3	41.7	26.7

Table S8								
Magnum	TD	LfUn	LfSl	APD	H	Hdor	Hvproc	Hart
A2-13 (r)	33.9	24.4	17.5	69.2	46.8	31.3	23.5	26.3

Table S9				
Unciform	TD	H	APDan	APDab
CA4-5 (l)	—	38.7	—	—

Table S10					head		prox epi				dia					dis epi	
Femur	L	Ltroc-prox	Ltroc	Ltroc-dis	TD	APD	TD	APD	TD-cue	TD3t	TD	APD	R1	R2	TDtroc	TD	APD
CA4-287 (l)	391.0	105.8	42.6	134.4	75.8	69.6	146.5	—	114.4	—	51.6	41.4	—	71.8	65.1	99.9	130.6
B4-61 (r)	404.0	—	—	110.0	—	—	—	—	—	—	—	—	—	—	—	—	—

Table S11			
Patella	TD	APD	H
s/s (l)	69.1	43.6	86.2
B4-64 (l)	71.7	42.4	82.3
B2-17 (r)	76.3	37.2	88.7
CATA5-226 (r)	73.5	45.2	80.7

Table S12					(trochlea)						dis art		
Astragalus	TD	H	TDmd	DLinf	H1	Hmin	H2	L1	L2	DL	TD	APD	APD int
CA4-136 (l)	77.1	68.5	62.8	38.1	54.7	34.4	55.6	56.5	54.4	40.7	52.8	35.2	21.2
CA4-42 (l)	75.7	67.4	65.6	35.2	55.8	35.6	53.5	49.8	57.0	37.6	45.3	30.1	19.0
A4-8 (r)	70.2	60.7	59.3	31.9	46.5	36.0	46.1	52.3	41.2	26.0	37.7	33.3	19.8
CA4-374 (l)	74.8	64.8	56.0	31.1	51.3	34.6	51.7	55.0	52.9	28.3	43.4	36.0	23.2

Table S13		tuber				
Calcaneum	H	TD	APD	TD-sus	APD-beak	TDdis
C4-59 (l)	106.7	40.9	53.6	65.4	52.0	30.3
C2-91 (r)	109.8	38.7	51.9	62.0	52.9	38.9

Table S14					prox art	
Navicular	APD	TD	H	Hmin	TD	APD
CA4-308 (r)	53.3	43.7	22.9	20.6	36.3	33.6

Table S15						prox art	
Cuboid	TD	APD	H	Hdor	Hvproc	TD	APD
CATA2-11 (r)	35.5	59.3	63.0	37.4	38.6	35.0	41.6

Table S16				
Entocuneiform	TD	APD	Hart	H
B3-11 (r)	18.9	57.7	31.5	42.0

SUPPLEMENTARY DATA 1

Measurements (mm) of the Mt II (Table S17), Mt III (Table S18), adn Mt IV (Table S19) of *Lartetotherium* cf. *Lartetotherium sansaniense* from M-407 Rotonda (Madrid Province, Spain). Side is detailed as follows: l, left; r, right.

Table S17		prox epi		prox art		dia			dis art	
Mt II	**L**	**TD**	**APD**	**TD**	**APD**	**TD**	**APD**	**TDmd**	**TD**	**APD**
CATA4-368 (r)	~128	22.1	34.9	22.1	30.8	21.8	21.9	—	—	—

Table S18		prox epi		prox art		dia			dis art	
Mt III	**L**	**TD**	**APD**	**TD**	**APD**	**TD**	**APD**	**TDmd**	**TD**	**APD**
C4-43 (l)	145.3	44.8	37.9	42.2	34.5	36.6	18.7	43.3	39.0	34.1

Table S19		prox epi		prox art		dia			dis art	
Mt IV	**L**	**TD**	**APD**	**TD**	**APD**	**TD**	**APD**	**TDmd**	**TD**	**APD**
C3-42 (l)	—	43.4	37.0	35.0	30.5	23.6	22.0	—	—	—

SUPPLEMENTARY DATA 2

Sample details (Table 1) and statistical analyses (Table 2) for the astragali of *Lartetotherium sansaniense* from several Iberian localities (data from Cerdeño, 1986 and own data) and those studied in the present work. Approximate measurements (~) were excluded from the analysis. Correl. coef.: coefficient of correlation; J-T: Jonckheere-Terpstra; juv.: juvenile. A comparative table with the Iberian metapodials have been also included for comparative purposes (Table 3).

Table 1

MN (Mein's Biozone)	Locality	Label	TD	H	DL
9	Coca	w/n	71.4	67.5	55.4
	Can Ponsic	CP 15035	68.0	69.0	51.0
7/8	Cerro del Otero	MNCN 18125	67.5	65.6	49.0
	La Cistérniga	MNCN 1357	66.0	62.9	51.0
6	Paracuellos III	PA 125	62.1	58.3	51.4
		PA 1500	~ 69	64.6	50.0
	M407	CA4-136	77.1	68.5	56.5
		CA4-42	75.7	67.4	49.8
		A4-8	70.2	60.7	52.3
		CA4-374	74.8	64.8	52.9
4a	Can Mas	CM 15125	85.4	68.0	49.2
		CM 15126	75.3	66.6	53.2
	Buñol	w/n	76.0	74.0	59.0
		FC-B 15	88.0	75.0	—
		FC-B 10	80.0	71.0	—
		FC-B 12	78.5	70.0	55.2
		BR 13	84.0	—	55.0
		FCB 88	79.0	56.5	—

Table 2

		Jonckheere Trend Test					Kendall's tau
Measurement	n	Standarized J-T Statistic	Observed J-T Statistic	Mean	SD	p-value	Correlation Coefficient
TD	18	2.577	69.0	40.0	11.255	0.01	0.524
H	17	2.832	64.0	35.0	10.241	< 0.01	0.597
DL	15	1.411	36.5	25.0	8.150	0.158	0.320

Table 3

Bone	Locality	MN (Mein's Biozone)	Label	L	TDdia	GI
Mc II	Cerro del Otero	7/8	MNCN 18122	127.6 (juv.)	25.5 (juv.)	—
	Buñol	4a	—	148.0	34.0	23.0
Mc III	Cendejas	9	—	136.4	~ 33	—
	Buñol	4a	FC-B 32	165.0	45.0	27.3
			FC-B 71	163.0	48.0	29.4
Mt II	M-407 Rotonda	6	CATA4-368	~ 128	21.8	—
Mt III	Coca	9	—	143.0	32.6	22.8
	M-407 Rotonda	6	CA4-43	145.3	36.6	25.2
	Buñol	4a	FC-B 40	158.0	38.5	24.4
			FC-B 41	171.0	41.0	24.0
Mt IV	Coca	9	—	125.4	23.7	18.9

9. Paleoecological analysis of *Alicornops simorrense* and *Lartetotherium sansaniense* (Mammalia, Perissodactyla) from the Middle Miocene of the Iberian Peninsula

Oscar Sanisidro
Laura Domingo
María Teresa Alberdi
and Jorge Morales

Abstract. *Alicornops simorrense* and *Lartetotherium sansaniense* are two sympatric rhinoceros species frequently found in the Middle Miocene ecosystems of Western Europe. Previous studies based on morphological characters linked *A. simorrense* with wet habitats whereas *L. sansaniense* was described as a habitat generalist with punctual preferences for closed areas. The present work represent an updated multi-proxy reconstruction of the ecological role of both species derived from both morphological and isotopic data. The abundance and variety of fossil remains from the new locality of M-407 Rotonda (Madrid Basin, Spain) constitutes a unique opportunity to unravel the lifestyle of both species. Isotopic results suggest that *A. simorrense* ($\delta^{13}C$ = -11.2±0.4‰, $\delta^{18}O$ = 29.3±1.3‰) and *L. sansaniense* ($\delta^{13}C$ = -9.3±0.6‰, $\delta^{18}O$ = 29.5±1.4‰) occupied a woodland, with the latter foraging on slightly more open environments, in agreement with their postcranial skeletons. In the case of *A. simorrense*,, the more developed secondary enamel folding suggests an adaptation to process tough food items, more typical related with vegetation from open spaces. This dental trait seems at odds with isotopic results that suggest a browsing diet. This apparent discrepancy shed light upon an up to now unconsidered dietary behavior for this rhinoceros pointing to the ingestion of abrasive items such as grit, dust, and/or wooden parts present in woodland areas. This adaptation may have allowed *A. simorrense* to partition resources and to avoid direct resource competition with the sympatric rhinoceros *L. sansaniense*.

INTRODUCTION

During the Late Aragonian (Middle Miocene) European rhinoceroses witnessed a rapid diversification, becoming common components of terrestrial faunas (Cerdeño and Nieto, 1995). *Alicornops simorrense* (Lartet, 1851) and *Lartetotherium sansaniense* (Lartet, 1851) are frequently found together in the Iberian Late Middle Miocene-Early Late Miocene. Although other species like *Hoploaceratherium tetradactylum*, *Aceratherium incisivum* or *Brachypotherium brachypus* can sporadically occur, *A. simorrense* is predominant (Cerdeño, 1992; Cerdeño and Sánchez, 2000). The paleoecological role of both *A. simorrense* and *L. sansaniense* has been previously outlined on the basis of morphological comparisons. Ginsburg and Guérin (1979) Guérin (1980; p. 396) linked *A. simorrense* to open woodlands with associated marshy and lacustrine areas. In a similar way, Cerdeño and Sánchez (2000) emphasized that shortened limbs and robust epiphyses are an adaptation to soft soils displacement. Finally, Heissig (2012) made some dietary inferences and considered *A. simorrense* as a folivore browser with little fibrous food intake according to its teeth morphology and head orientation. Conversely, *L. sansaniense* has been proposed as a ubiquitous generalist (Heissig, 1972, 2012), sometimes linked with more forested areas (Becker, 2003; Guérin, 1980). In order to unravel the biotic preferences of *A. simorrense* and *L. sansaniense*, a multiproxy reconstruction based on morphological comparison of both cranial and postcranial remains and tooth enamel stable isotope has been performed.

Skull, mandible, and dentition are important sources of information regarding mammalian ecology as they directly reflect species feeding habits (Butler, 1983; Hiiemae, 2000). Consequently, paleontologists usually focus on the craniodental morphology in order to infer dietary preferences in fossil taxa (e.g. Figueirido et al., 2008; Fortelius et al., 1996; Janis, 1984, 1997/98; Jernvall et al., 1996). The skull is a composite structure determined by multifactorial influences. Among rhinoceros species, traits like the orientation of the occipital plate are largely influenced by the feeding habits of a species, thus being classically used for paleoecological inferences (Bales, 1996; Heissig, 1989; Loose, 1975). Moreover, the skull hosts the masticatory apparatus, providing important clues about masticatory processes and dietary adaptations (Fortelius, 1985; Mendoza et al., 2002).

Rhinoceros tooth pattern range from brachyodont to subhypselodont (Koenigswald, 2011). Brachyodont teeth are low-crowned and show little enamel folding, while hypsodont teeth show higher crowns, thicker enamel walls, cementum fillings on the valleys and important secondary enamel folding

(Fortelius, 1982). Different strategies have been observed on the fossil record in order to avoid intense tooth wear due to abrasive diets. Damuth and Janis (2011) argued that some primitive mammals (i.e. Late Cretaceous-Early Paleocene gondwanatherian mammals and Paleocene-Early Eocene stylinodont taeniodonts) developed a hypsodont dentition linked to the ingestion of soil when foraging on roots and tubers. Specifically, Eronen et al. (2010) argued that the strategy adopted by the equid *Anchitherium* from Miocene Spanish basins consisted on increasing the tooth crown height. Another strategy consists on increasing the complexity of teeth patterns, are also observed on hypsodont taxa as a mechanism to overcome intense dental wear due to high rates of dietary abrasiveness (i.e. ingested soil while feeding; Damuth and Janis, 2011).

Analyses of the carbon isotope ($\delta^{13}C$) composition of mammalian tooth enamel have become a useful tool for paleodietary inferences (Cerling et al., 1997; Koch et al., 1992; Lee-Thorp and van der Merwe, 1987; Quade et al., 1992). Tooth enamel is the most widely used bioapatite tissue for the reconstruction of paleodiets since its structural and chemical features (e.g. larger apatite crystals, lower porosity and lower content of organic matter) make it less prone to undergo chemical alteration as a consequence of post-burial processes (Kohn and Cerling, 2002). Hence, $\delta^{13}C$ values preserved in the pristine hydroxyapatite of herbivorous mammalian tooth enamel are indicative of the type of ingested vegetation when corrected for a fractionation offset. Plants follow three main photosynthetic pathways known as C_3, C_4 and CAM (crassulacean acid metabolism; Farquhar et al., 1989; Ehleringer and Monson, 1993; Hayes, 2001). Plants following the C_3 or Calvin-Benson metabolic pathway comprise the vast majority of trees, shrubs, forbs and cool-season grasses. C_3 plants strongly discriminate against ^{13}C during CO_2 fixation, showing $\delta^{13}C$ values, which range from −36‰ to −22‰ with an average value of −27‰ (VPDB). The wide range of isotopic values observed in C_3 plants are directly related to the type of environment they occupy. C_3 plants from closed-canopy conditions show the lowest $\delta^{13}C$ values due to ^{13}C-depleted CO_2 recycling and low irradiance, whereas the highest $\delta^{13}C$ values correspond to high light, arid and/or water-stressed conditions. Plants following the C_4 or Hatch-Slack metabolic pathway comprise mainly warm-season grasses and sedges and some arid-adapted dicots and show $\delta^{13}C$ values between −17‰ to −9‰, with an average value of −13‰ (VPDB). This metabolic pathway has a competitive advantage in comparison to C_3 plants under low atmospheric CO_2, high temperature, high aridity, and high salinity. Finally, succulents and cacti follow the CAM photosynthetic pathway and show intermediate $\delta^{13}C$ values between C_3 and C_4 plants. These plants are adapted to arid environments and have limited impact on the diet of modern mammals and by extension, they are not frequently considered when inferring paleodiets. Cerling and Harris (1999) estimated a diet-to-enamel enrichment factor ($\varepsilon^*_{\text{diet-enamel}}$) of 14.4±1.6‰ for extant black rhinoceros from East Africa. However and since they only consider one species of rhinoceros from a specific area, we will use the enrichment factor of 14.1±0.5‰ estimated for a suite of extant worldwide ungulates. Since vegetation $\delta^{13}C$ values are ultimately controlled by $\delta^{13}C$ values of atmospheric CO_2, when focusing on palaeocological reconstruction it is necessary to consider the shift in the $\delta^{13}C$ value of atmospheric CO_2 due to both, natural variation and anthropogenic modification (as a consequence of fossil fuel burning since the onset of the Industrial Revolution). Using isotopic data from marine foraminifera, Tipple et al. (2010) reconstructed the $\delta^{13}C$ value of the atmospheric CO_2 for the late Aragonian (~13.8–11 Ma) as ~−6‰, a difference of 2‰ relative to the modern value, which is ~−8‰. Therefore, estimated $\delta^{13}C$ cut-off values among different environments would be: (i) closed-canopy between −20 and −14‰, (ii) woodland-mesic C_3 grassland between −14 and −9‰, (iii) open woodland-xeric C_3 grassland between −9 and −6‰, and (iv) pure C_4 feeders between −1‰ and +7‰ (see complete explanation about vegetation cut-off $\delta^{13}C$ values for the Miocene in Domingo L et al., 2012, 2013).

Mammalian tooth enamel $\delta^{18}O$ value records $\delta^{18}O$ value of body water, which is controlled by oxygen inputs (inspired O_2 and water vapor, drinking water, dietary water, oxygen in food dry matter) and outputs (excretion, expired CO_2 and water vapor) during tooth mineralization (Bryant and Froelich, 1995; Kohn, 1996). According to Levin et al. (2006), herbivore mammals can be classified into two groups depending on their isotopic sensitivity to aridity: evaporation insensitive (EI) and evaporation sensitive (ES) mammals. EI mammals drink water daily or consume nonleafy parts of plants (which contain water that has not experienced evaporation) and hence, these animals record local meteoric water $\delta^{18}O$ values. In turn, $\delta^{18}O$ values of meteoric water are positively correlated with mean annual temperature and aridity (i.e. higher temperature and higher aridity give rise to higher $\delta^{18}O$ values of meteoric water and *vice versa*). ES herbivores can survive with little or no drinking water since they obtain most of their water from leaf water, which is prone to strong evaporative ^{18}O-enrichment. Therefore, the $\delta^{18}O$ values of ES herbivores increase relative to meteoric water values (as monitored by EI herbivores) with increasing aridity. Levin et al. (2006) classified the African black rhinoceros (*Diceros bicornis*) as EI, so by analogy with extant rhinos, we will consider *A. simorrense* and *L. sansaniense* as EI mammals, thus tracking the $\delta^{18}O$ value of meteoric water.

M-407 Rotonda site (40º.18'N and 3º.48'W; between 680 and 681 m above the sea level; Fig. 1) was discovered as a result of the supervision of recent public works related with the accessibility of the North road accesses of the city of Fuenlabrada, 5 km South of Madrid City (Spain). The surrounding middle Miocene continental sediments are part of the Neogene Madrid Basin (or Higher Tagus Basin). Excavations revealed two thin fossil-bearing levels accumulated during separate debris-flow episodes. Both show

a thin level (less than 10 cm) of fine to thick, light brown colored sandy basement that grades upward into greyish green mudstones. The lower mudstone level is thicker (30 cm) and richer in fossil remains than the upper one (20 cm thick). Fossils are distributed forming clusters within each one, lack any preferential direction and are mostly horizontally-oriented. The lithology of the vertebrate-bearing strata indicates a distal facies of an alluvial fan with an arid climate. The preliminary faunal list includes the species *Heteroxerus* sp., *Amphicyon* sp., *Listriodon splendens*, Bovidae indet. 1, Bovidae indet. 2, Cervidae indet., Palaeomerycidae indet., *Anchitherium* sp., and abundant tortoise (*Cheirogaster bolivari*) and rhinoceros remains of the species *L. sansaniense* (Lartet, 1851) and *Alicornops simorrense* (Lartet, 1851). The presence of *L. splendens* —which replaced the species *Bunolistriodon lockharti* in the middle Aragonian of the Madrid area— combined with the altitudinal data, which correlates with the geographically-close locality of Moraleja de Enmedio (Peláez-Campomanes et al., 2000), permits to assign M-407 Rotonda to the early Upper Aragonian, Middle Miocene). The recovered collection of 2,154 vertebrate fossils stands out for the presence of practically undistorted both cranial and postcranial elements, most of them found isolated. This sample includes numerous remains of *L. sansaniense* and *A. simorrense* from M–407 Rotonda and provides an exceptional opportunity to characterize the paleoecological roles of these two coexisting genera.

MATERIAL AND METHODS

The studied specimens from M–407 Rotonda are housed in the Museo Nacional de Ciencias Naturales-CSIC (Madrid, Spain). Cranial and postcranial measurements provided in this study are given in millimeters with an accuracy of one decimal digit. The terminology applied in the description of the anatomical characters generally follows Guérin (1980), but that used by other authors has also been taken into consideration (Antoine, 2002; Heissig, 1972, 1999).

Anatomical nomenclature and characters—Capital letters are used for upper teeth (D, P, M), and lower case letters for lower teeth (d, p, m); m. muscle. The dental terminology follows Heissig (1969), Uhlig (1999), and Antoine (2002). The cranio-dental and osteological features described correspond

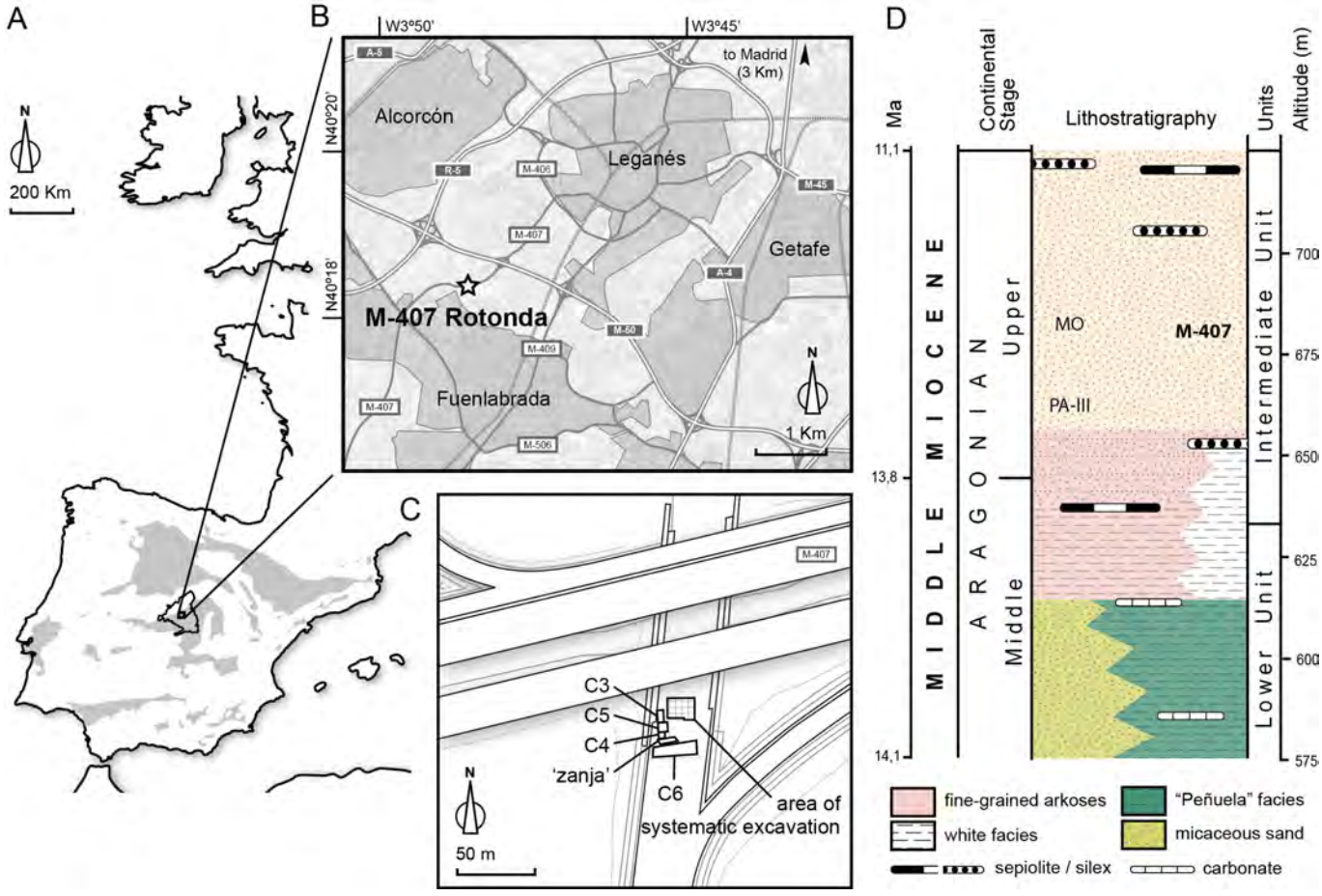


Fig. 1 A, Simplified general map of the Iberian Peninsula with its Cenozoic basins represented as shaded contours. B, detailed map showing the location of M–407 Rotonda site, represented as a star. C, map with the detailed excavation area. D, lithostratigraphy of the Madrid City area and the stratigraphic placement of the locality of M-407 Rotonda (bold) and the localities of Paracuellos III (PA-III) and Moraleja de Enmedio (MO), where fossil rhino remains have been also found.

basically to cladistic characters used and listed by Antoine (2002) and Antoine et al. (2010), and then refined by Becker et al. (2013).

Morphological descriptives—Two different measurements of the skull have been measured at the median saggital plane following Loose (1975). The occipital angle (*po*) is defined as "the angle between ophisthocranion | opisthion and palate (aborally extended)". The *m* angle is the angle between the mean plane formed by the sagittal crest and the opisthion. The sum of the main limb segments (i.e. humerus, radius, third metacarpal / femur, tibia and third metatarsal) has been used as a proxy for the shoulder height. Even though some height overestimation is expected due to the oblique orientation of the humerus in a life-like resting position, that is somewhat compensated by the absence of the tarsal/carpal bones, phalanges, and the height of the soft tissues of the plantar/palmar pad in our calculations. As some bones are missing or found incomplete in M-407 Rotonda, their total heights have been estimated (gray values in Supplementary Data 1, Table 1). In the case of *A. simorrense*, the proportions from other Iberian localities (Cerdeño and Sánchez, 2000) have been used as a proxy . For *L. sansaniense*, two alternatives have been used: the first (A in Supplementary Data 1, Table 1) infers the maximum length of each bone using the proportions of the complete individual of *Lartetotherium* from Batallones-1 as a reference. This is due to the fact that Iberian samples of *Lartetotherium* seem to differ in proportions of the stylopodium from their remaining European counterparts (Sanisidro et al., this volume). The second estimate uses the locality of Sansan as a reference (B in Supplementary Data 1, Table 1).

Isotopic Analysis—Enamel from a total of 20 rhinocerotid teeth from the M-407 Rotonda site was recovered using a rotary drill with a diamond-tipped dental burr from an area of the tooth as large as possible to avoid seasonal bias in the time of mineralization. Tooth enamel was recovered from jaw fragments with teeth in place, isolated teeth with roots and isolated enamel fragments (see Supplementary Data 2, Table 1). The carbon and oxygen isotope results are reported in the δ-notation $\delta^{H}X_{sample}=[(R_{sample}-R_{standard})/R_{standard}]$ x 1000, where X is the element, H is the mass of the rare, heavy isotope, and $R=^{13}C/^{12}C$ or $^{18}O/^{16}O$. Vienna Pee Dee Belemnite (VPDB) is the standard for $\delta^{13}C$ values and $\delta^{18}O$ values for apatite carbonate, although subsequently $\delta^{18}O$ values were calculated against Vienna Standard Mean Ocean Water (VSMOW). Rhinocerotid tooth enamel samples (11 samples for *Alicornops simorrense* and 9 samples for *Lartetotherium sansaniense*) were analyzed for the carbon and oxygen isotope composition of carbonate in bioapatite. Approximately 5 mg of enamel was soaked in 30% H_2O_2 for 24 h. After 5 rinses with Milli-Q water, enamel was soaked for 24 h in a 1 M acetic acid buffered with Ca acetate solution to ~pH 5, and again rinsed 5 times with Milli-Q water. Samples were freeze-dried at −40 °C and at a pressure of 25 x 10^{-3} Mbar for 24 h. Isotopic analyses were conducted at the Stable Isotope Laboratory at the University of California Santa Cruz (USA) using a Thermo MAT253 dual-inlet isotope-ratio mass spectrometer coupled to a Kiel IV carbonate device. The standards used were Carrara Marble (CM, $\delta^{13}C$=1.97‰ and $\delta^{18}O$=−1.61‰, both VPDB), NBS-18 ($\delta^{13}C$=−5.03‰ and $\delta^{18}O$=−23.01‰, VPDB) and NBS-19 ($\delta^{13}C$=1.95‰ and $\delta^{18}O$=−2.20‰, VPDB). The standard deviations for repeated measurements of CM (n=18) and NBS-19 (n=6) were 0.04‰ and 0.02‰, respectively for $\delta^{13}C$, and 0.06‰ and 0.07‰, respectively for $\delta^{18}O$.

RESULTS AND DISCUSSION

Morphological comparison

Extant rhino species show a close relationship between skull shape (particularly the occipital area) and dietary adaptations (Zeuner, 1934; Loose, 1975). *A. simorrense* presents a typical aceratheriine cranio-mandibular morphology: the skull has a relatively enlarged maxillary bone together with a retracted nasal incision (Cerdeño and Sánchez, 2000). As the occipital region is missing in the skull from M–407 Rotonda A1-1, the specimen from Moraleja de Enmedio (MNCN 30768) has been used as a proxy, reporting an occipital orientation of approximately *m* = 53º / *po* = 86º. The skull of *L. sansaniense* presents a long muzzle topped with a domed nasal bone (pointing to the presence of a single nasal horn). All the known complete skulls of *L. sansaniense* (i.e. Sansan and Sandelzhausen) are somewhat distorted. Albeit the occiput of the individual from M–407 Rotonda (CA4-73) is not totally preserved, parts of its occipital plate remain dorsoventrally intact, permitting an estimation of the occipital orientation by reconstructing its dorsal tip. The resulting *po* occipital angle gives an approximate value of 89º (and a *m* angle of 61), close to that of *A. simorrense*, thus pointing to comparable head orientations. Among the extant species, the extant *Ceratotherium* species (*Ceratotherium simum* and *Ceratotherium cottoni*) present a similar occipital orientation (Supplementary Data 1; table 2). The second lower incisors are a valuable source of information on the population structure of both species. *A. simorrense* presents dimorphic i2, with males carrying large (up to 60 mm long) and curved tusk-like incisors and females shorter and blunter ones. Sexual dimorphism is a common phenomenon in rhinoceros species. Contrariwise, second lower incisors of *L. sansaniense* are more homogeneous between males and females, pointing to a simpler social structure more similar to the living Asian rhinos (Heissig, 2012; Mihlbachler, 2007).

The simplified teeth of *L. sansaniense* are typical from early rhinocerotine species. They show a concave occlusal surface, low crown, nearly parallel protoloph and metaloph and lack any labial or lingual cingula on both premolar and molar teeth, all of them typical of a highly brachyodont dentition (Figure 2A). No extant species presents such configuration as even the browsers Javan (*Rhinoceros sondaicus*) and black rhinos (*Diceros bicornis*) present higher secondary folding. On the

contrary, the teeth of *A. simorrense*, while low-crowned and essentially brachyodont, show more developed secondary enamel folding (i.e. stronger antecrochet limited by a marked posterior folding, a wide and developed crista, sinuous median valley, presence of continuous anterior and posterior cingula and a low and variable labial one; Figure 2B). As a result, they face more enamel during the mastication than *L. sansaniense*, thus being able to process more abrasive food and/or to resist the wear produced by grit, dust, and/or wooden parts ingested with the diet. Despite slightly different in size, the cheek teeth morphology of *A. simorrense* basically resembles that of the Sumatran rhino, a dietary diverse browser, with fruit, twigs, bark and cultivated crops as major food items in its diet (Janis, 1990; Nowak, 1999). The presence of well-developed cingula would protect the gum against wounds during the ingestion of thorns or wood. A trait further enhanced by the presence of intermittent and thin cementum patches along the ectoloph.

L. sansaniense shows a height for their forelimbs of 798 mm (similar in length to the extant Javan rhino; *Rhinoceros sondaicus*), while hindlimbs measure 808 mm (slightly below living taxa). The segment ratios of the forelimb of *L. sansaniense*, shows a relative elongation of the zeugopodium/autopodium at the expense of the acropodium (the opposite than that observed in *A. simorrense*; Figures 3A and B). Proportionally longer distal segments of the forelimb favor a faster stroke and a rapid movement of the foot relative to the body. In our diagram (Figure 3A), *L. sansaniense* nests close to the black rhino in forelimb proportions. While white rhinos inhabit open areas (including open forests), black rhinos are found in a wide range of habitats, from montane forests through savannah woodland and grasslands to desertic regions (Groves, 1972; Hillman-Smith and Groves, 1994). On the contrary, hindlimb proportions do not show any clear pattern in living species (e.g. placing the relatively slender *Dicerorhinus sumatrensis* at a midpoint between the graviportal *Teleoceras* and the mediportal *Diceros bicornis*), so this ratio may be influenced by phylogenetic and/or body mass constraints and is in need of a deeper study.

The estimated height of *A. simorrense* is around 637 mm for the forelimbs and 854 mm for the hindlimbs (Fig. 3B). The hindlimb measurement (Cerdeño and Sánchez, 2000) points to a shoulder height of less than 1 m, a measurement below living species (Fig 3A). The total length for the forelimb exceeds that recorded in the remaining Iberian localities (mean = 712 mm). Rhinoceroses typically have slightly shorter forelimbs than hindlimbs. The large difference between both limbs in *A.*

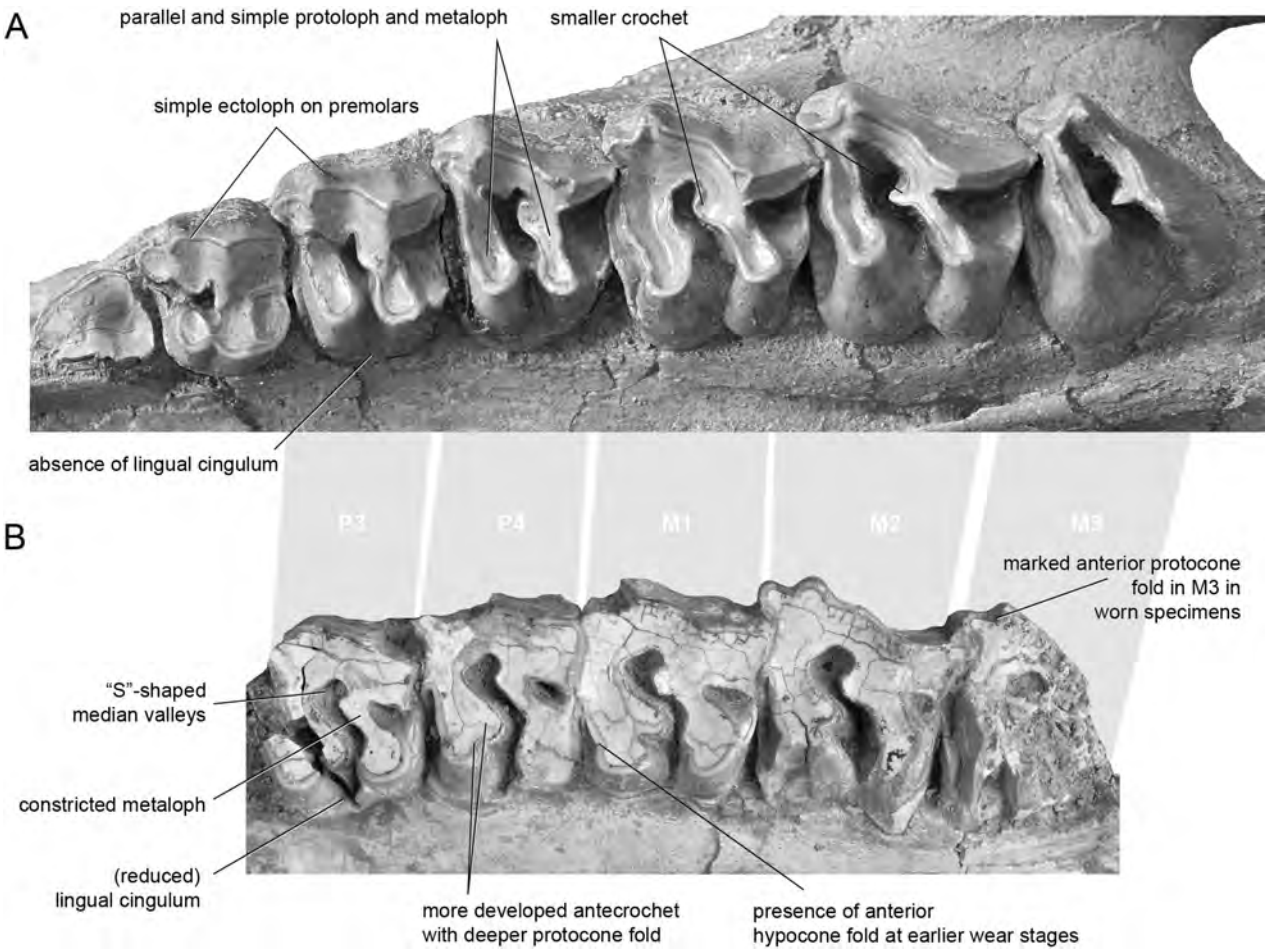


Fig. 2 Morphological comparison between the upper tooth row of A, *Lartetotherium sansaniense* (BSPG 1959 II from Sandelzhausen) and B, *Alicornops simorrense* (H1-11) from M-407 Rotonda. Scale bar equals 50 mm.

simorrense is explained by the long femur (L = 386 mm) found in M-407 Rotonda and the inferred length for the tibia and third metatarsal (Supplementary Data 1; Table 1). The robust limbs (together with a cylindrical chest) led most authors to attribute an amphibious lifestyle to teleoceratines as *Teleoceras* or *Brachypotherium* equivalent to extant hippopotamus (Geraads and Saraç, 2003; Osborn, 1898; Prothero, 1992; Scott, 1913; Webb, 1983). Hippos spend much of their time in the water or mud, foraging on land at night. Matthew (1932) linked the peculiar body form of *Teleoceras* to smooth and uniform grassy plains (Matthew, 1932; p. 435), presenting a feasible alternative to the hippo-like ecomorph. In this sense, stable isotope analyses did not support an aquatic habit for *Teleoceras* equivalent to modern hippos (Clementz et al., 2008; MacFadden, 1998). Several authors have emphasized the shortened limbs of *A. simorrense*, particularly when compared with other rhinoceros species(Cerdeño and Sánchez, 2000, p. 303; Heissig, 2012, p. 479). This peculiarity is also observed in our sample from M-407 Rotonda. Such brachypodic limbs were linked with occupation of lacustrine or marshy areas, a similar habitat to that inferred for *Teleoceras*. However, some differences can be outlined. *Teleoceras* presents whole brachypodial limbs (a general shortening of the stylopodium, zeugopodium, and autopodium), whereas the bone shortening of *A. simorrense* is restricted to the zeugopodium and autopodium (the stylopodium is not as specialized, slender and proportionally longer; Figure 2A).

The populations of *A. simorrense* and *L. sansaniense* from M-407 Rotonda have similar body masses (2492 kg for *A. simorrense* and 2243 kg for *L. sansaniense;* Supplementary Data 1, Table 3) and somewhat different total limb lengths (forelimbs: 637 mm for *A. simorrense* and 798 mm for *L. sansaniense*, and hindlimbs: 854 for *A. simorrense* and 808 mm for *L. sansaniense*; Figure 3B, Supplementary Data 1, Table 1). In order to support its body mass, radius and ulna of *A. simorrense* are shorter and closely attached to each other by means of a developed ulnar lateral scar on the radius diaphysis and the development of a second ulnar-facet on its

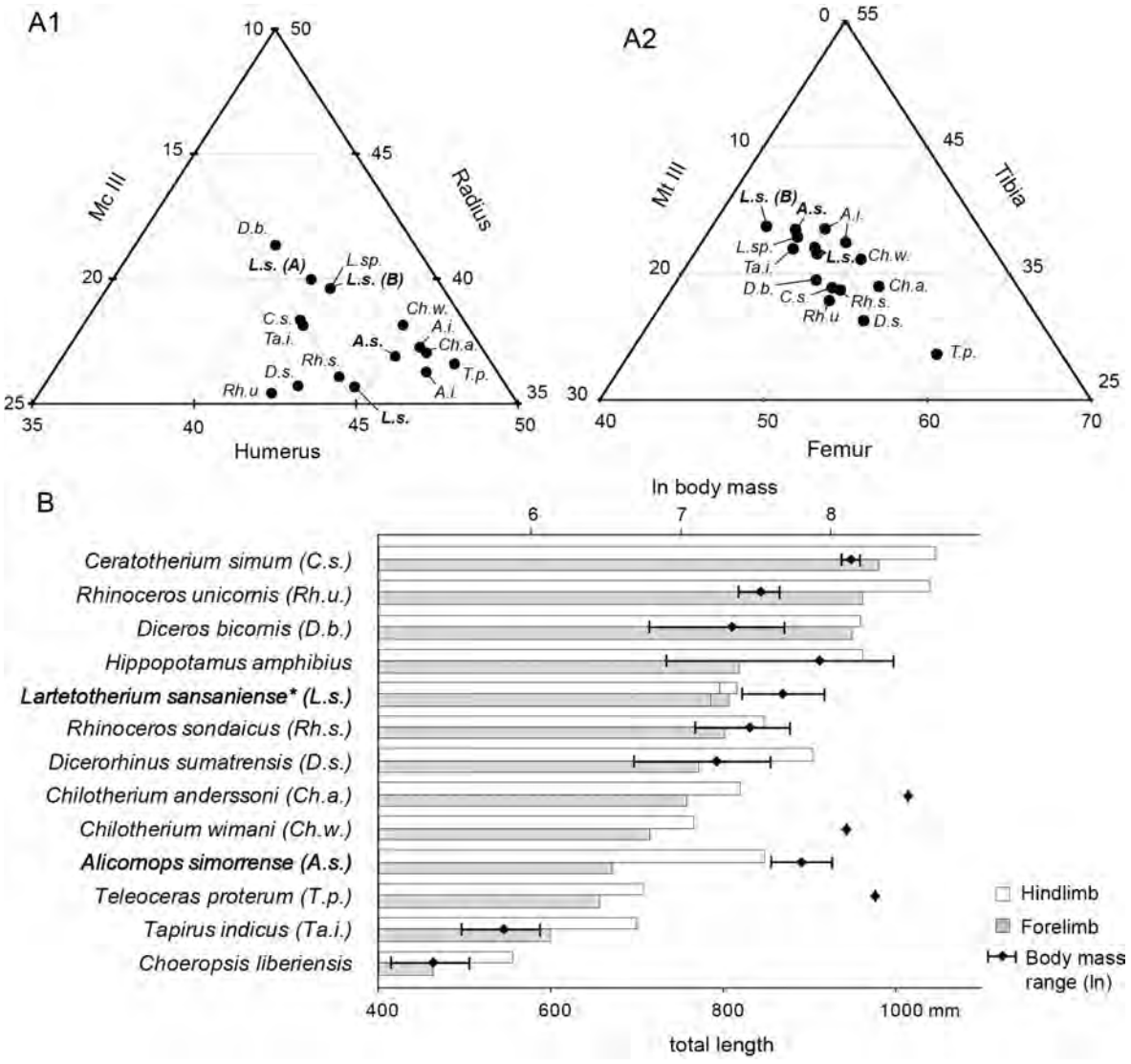


Fig. 3 Ternary diagrams displaying the limb length ratios of the forelimb (A1) and the hindlimb (A2) of several ungulate species in length percentage respect to the total limb length of some fossil and extant perissodactyl species according to the Table 1 included in Supplementary Data 1. B, Total length of the hindlimb and forelimb. Wiskers diagram represent the minimum, mean and maximum body mass expressed as a Napierian logarithm according to the Table 3 (Supplementary Data 1).

distal epiphysis. Such increase in the degree of articulation between radius and ulna, also found in proboscideans, has been related to a large body mass relative to the length of the limb (Antoine, 2002). Additionally, ulnae of *A. simorrense* show narrower, more asymmetrical lobes and a proximally displaced medial lobe. Ulnae of *L. sansaniense* are bigger and display a more vertically oriented olecranon. The main differences of the radius rely on the proximal ulnar-facets, double in *A. simorrense* and almost simple in *L. sansaniense*, being the medial one restricted to a narrow articular rim. The radius of *L. sansaniense* is longer and, on the distal epiphysis, the ulnar attachment area relatively bigger and devoid of the articular surfaces observed in *A. simorrense*.

Isotopic analysis

As expected, *A. simorrense* and *L. sansaniense* from M–407 Rotonda show $\delta^{13}C$ values indicative of C_3 vegetation since Iberian continental ecosystems during the late Aragonian (Late Miocene) were dominated by these plants (Domingo et al., 2009; Domingo et al., 2012; Domingo et al., 2013). $\delta^{13}C$ values of *A. simorrense* fluctuate between −11.8 and −10.7‰ (VPDB), yielding a mean value of −11.2±0.4‰ (Fig. 4, Supplementary Data 2, Table 2). According to these values, *A. simorrense* would have fed in woodland or mesic C_3 grassland. Our results agree well with the results of *A. simorrense* from Steinheim, Germany (−11.5‰±0.9‰ from Steinheim; Tütken et al., 2006). However, Domingo et al. (2012) reported higher isotopic values for *A. simorrense* from the nearby Late Aragonian Paracuellos-3 locality, situated also in the Madrid Basin (−9.57‰; Domingo et al., 2012). Carbon isotope values of *L. sansaniense* in M–407 Rotonda range from −10.1 to −7.9‰ (VPDB), with a mean value of −9.3±0.6‰ (Fig. 4, Supplementary Data 2, Table 2), pointing to a more open environment near the transition between woodland-mesic C_3 grassland and open woodland-xeric C_3 grassland. Previous isotopic analyses conducted on samples of *L. sansaniense* from Central Europe revealed lower carbon isotope values, indicative of occupation of more closed woodland conditions. For example, the sample from Steinheim provided values ranging from −10.5 to −12.8‰ (VPDB), suggesting a more wooded habitat inside the woodland-mesic C_3 grassland continuum (Tütken et al., 2006) —partially coinciding with the purported humid and forested environment for the species based on *L. sansaniense´*s morphology suggested by Guérin (1980)—. In a similar way, the carbon isotopic signal from Sandelzhausen ranged from −10.2 to −11.6‰ (Tütken and Vennemann, 2009). Finally, the intra-individual isotopic signal of the tooth UMJGP 203459 from Gratkorn provided results between −11.2 and −11.7‰ $\delta^{13}C$ VPDB (Aiglstorfer, 2014). Despite this forested habitat in Central Europe, when *L. sansaniense* coexists with other rhino species, is the one that attains higher $\delta^{13}C$ values (Aiglstorfer et al., 2014), suggesting more open habitat requirements within its assemblages in agreement with our data. A t-Student analysis revealed significant differences in $\delta^{13}C$ values between both genera ($t = -8.064$; p-value < 0.001), indicating some degree of resource partitioning within a woodland environment with variable portions of open conditions (Supplementary Data 2, Table 3).

$\delta^{13}C$ standard deviation in *L. sansaniense* from M-407 Rotonda is considerable if compared with that of *A. simorrense* (1.1‰ and 0.4‰ respectively) (Fig. 4). This difference in $\delta^{13}C$ standard deviation values between *A. simorrense* and *L. sansaniense* may be pointing to more restricted resource requirements in the former (lower $\delta^{13}C$ standard deviation) and wider resource flexibility for the latter (higher $\delta^{13}C$

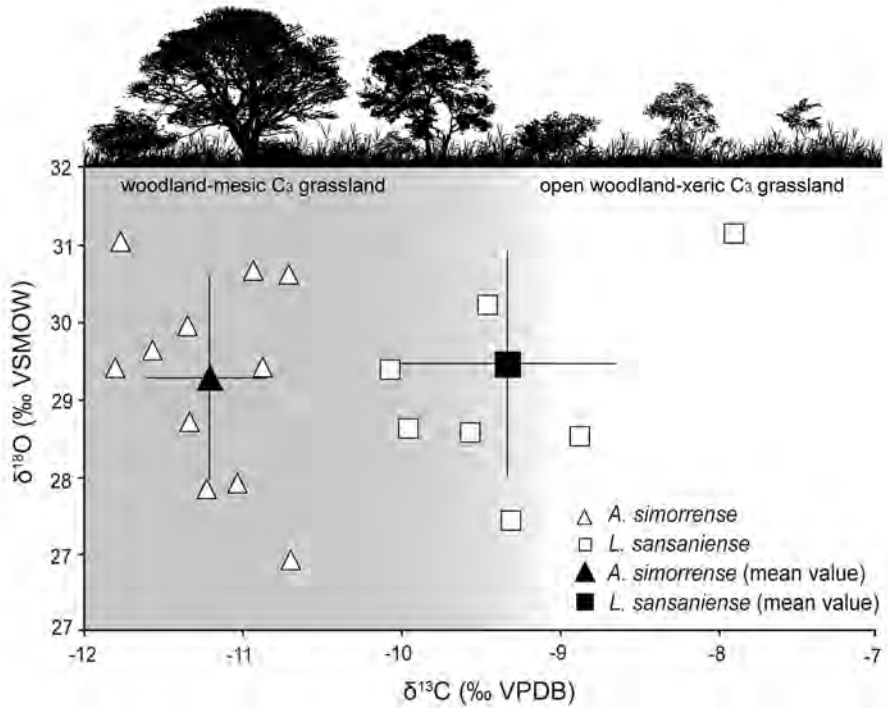


Fig. 4 Tooth enamel $\delta^{18}O$ (‰ VSMOW) and $\delta^{13}C$ (‰ VPDB) of *Alicornops simorrense* (triangles) and *Lartetotherium sansaniense* (squares) from M–407 Rotonda. Bars indicate ± 1 standard deviation.

standard deviation). This result is supported by the fact that *A. simorrense* show similar $\delta^{13}C$ values between the Iberian Peninsula and Central Europe, whereas *L. sansaniense* $\delta^{13}C$ values show more variability between these geographic areas.

In contrast to $\delta^{13}C$ values, $\delta^{18}O$ values are very similar for both genera (t = −0.259; p-value = 0.8) (Supplementary Data 2, Table 3), so that *A. simorrense* shows a mean value of 29.3±1.3‰ (VSMOW), ranging from 26.9 to 31.1‰, while *L. sansaniense* has a mean $\delta^{18}O$ value of 29.5±1.4‰, varying between 27.4 and 31.7‰ (Fig. 4, Supplementary Data 2, Table 2). Both rhinoceroses are considered evaporation insensitive (EI) taxa (like their modern counterparts), tracking the $\delta^{18}O$ value of ingested meteoric water. Hence, the lack of significant differences between both genera would be indicative of ingestion of water with a similar isotopic value. This result does not support a purported semi-aquatic behavior for *A. simorrense* since according to Clementz et al. (2008), semi-aquatic mammals should show a lower $\delta^{18}O$ mean value and a lower variance in $\delta^{18}O$ values (i.e. lower standard deviation) than the fully terrestrial associated fauna and neither of these requisites are met by the $\delta^{18}O$ values of *A. simorrense* when compared to those shown by *L. sansaniense*. Moreover, Clementz et al. (2008) calculated a linear regression relating hippopotamid (semi-aquatic) and fully terrestrial $\delta^{18}O$ values (see figure 4 in Clementz et al., 2008) in modern populations and fossil assemblages. If we consider M–407 *L. sansaniense* mean $\delta^{18}O$ value as indicative of fully terrestrial conditions, potential semi-aquatic taxa from this fossil site should have a value of 26.7‰, a value ~2.5‰ lower than the actual mean $\delta^{18}O$ value of *A. simorrense* (29.3±1.3‰) and thus, not supporting a semi-aquatic habit for this rhinoceros.

General discussion and interpretations

A. simorrense and *L. sansaniense* were sympatric species with considerably overlapped biostratigraphic and palaeobiogeographic ranges (Cerdeño, 1986, 1989; Cerdeño and Sánchez, 2000). Both species shared similar body masses and head orientations. Their forelimb lengths differ, being shorter in *A. simorrense*. As far as dentition is concerned, both *A. simorrense* and *L. sansaniense* had low-crowned (brachyodont) teeth. However, *L. sansaniense* showed a simpler dental pattern than *A. simorrense* that displayed a higher degree of complexity on its dental features, with tooth secondary enamel folding enhanced by intermittent and thin cementum patches. From a functional viewpoint, this difference in the dental pattern between both rhinoceroses points to a better adaptation to process abrasive or hard food items in the case of *A. simorrense*. Neither, $\delta^{13}C$ values observed in this study, nor previous non-isotopic studies, which have classified *A. simorrense* as a browser (Agustí and Antón, 2002; Cerdeño and Nieto, 1995; Heissig, 2012), support a high content of grass on its diet. Alternatively, this rhinoceros may have incorporated hard and/or abrasive food items from wooden parts of shrubs, as indicated by Agustí and Antón (2002) who argued that aceratheriine rhinoceroses (like *A. simorrense*), may have consumed tougher parts of woodland vegetation. Guérin (1980) stated that *A. simorrense* occupied woodlands (as supported by $\delta^{13}C$ values) with associated marshy and lacustrine areas. Feeding on these wet environments may also have enhanced the rate of abrasiveness by incorporating phytoliths and grit (Strömberg et al, 2007). *A. simorrense´*s adaptation to process this type of diet as well as its habitat occupation is illustrated by two morphological traits. Firstly, *A. simorrense* has more developed enamel folding exemplified by crochets and stronger antecrochets. Secondly, while sharing similar head orientation, *A. simorrense* presents shorter limbs than *L. sansaniense*. This feature points to an optimal feeding height closer to the ground in *A. simorrense*. Feeding closer to the ground favors the incorporation of more abrasive items to its diet (mainly based on grit, dust, wooden parts, thorns and/or soil ingestion if consuming subterranean resources), taking advantage of the aceratheriini higher tooth enamel complexity —while maintaining a brachyodont dentition—. Damuth and Janis (2011) stressed the negative consequences that an intense dental wear may exert on reproductive fitness above all on brachyodont animals. In this sense, the development of more complex enamel patterns may as well have allowed *A. simorrense* to maintain its reproductive lifespan while feeding on more abrasive items. On the other hand, *L. sansaniense*'s dental pattern and morphological traits point to consumption of softer and taller parts of the vegetation. *L. sansaniense* can be considered as a selective browser of a wider rank of habitats, particularly more open environments in the Madrid Basin and more closed environments in Central Europe, whereas *A. simorrense* may have been a more specialist taxon independently of its biogeography. Today, the only extant rhino browser that frequents open habitats is the extant black rhino (*D. bicornis*). This species is found in a very wide range of habitats, from montane forests to arid desert (Hillmann-Smith & Groves, 1994), and it is able to shift its food preferences according to the circumstances and availability. However, the black rhino shows a preference for areas with denser cover, and the relationship between density of black rhinoceroses and closed vegetation has been documented (Hitchins, 1969; Mukinya, 1973; Goddard, 1967). Therefore, the open environment preferences of *L. sansaniense* together with its browsing diet, place this species in a particular ecological role not found among extant species. The coexistence of *A. simorrense* and *L. sansaniense* during the time period of M-407 fossil assemblage may have been therefore facilitated by resource and habitat partitioning in a way that *A. simorrense* may have consumed tougher parts of woodland vegetation from more closed and wetter environments, whereas *L. sansaniense* would have fed on softer and taller parts of the vegetation from more open areas.

The apparent incongruence observed in our study between complex dental morphology and low $\delta^{13}C$ values for *A. simorrense* may not be such as previously argumented and this

support, as other studies before (Mihlbachler and Solounias, 2005; Kaiser, 2009; Eronen et al., 2010), the lack of unequivocal correspondence between brachyodonty and more closed habitats. Regarding extant rhino species, there are few studies linking the carbon isotopic signal with their ecologic role and species interactions. The historical distributions of the three Asian rhino species in the past centuries show a certain degree of geographic overlapping in Bangladesh and Eastern India (Antoine et al., 2003). Unfortunately, they are currently restricted to some small reserves with no co-occurrence between them, impeding studies dealing with niche interaction between the Javan (*Rhinoceros sondaicus*, the only living browsing rhino species) and both Sumatran and Great horned rhinos (Dicerorhinus sumatrensis and Rhinoceros unicornis, classified as mixed feeder and grazer respectively; Groves and Kurt, 1972; Laurie et al., 1983). Only the African white and black rhinos (*Ceratotherium simum* and *Diceros bicornis* respectively) can be found in the same locations. $\delta^{13}C$ data carried out on *C. simum* and *D. bicornis*'s faeces from the Kruger National Park (South Africa), support the information about resource and habitat use provided by field studies (Codron et al., 2007). *D. bicornis* showed lower $\delta^{13}C$ values (mean = −26.1‰±0.4‰ $\delta^{13}C$ VPDB) than *C. simum* (mean = −13.9‰±1.3‰ $\delta^{13}C$ VPDB), supporting different niches. In concordance, the morphology of their dentition (brachyodont and hypsodont, respectively) and occipital plate orientations (Loose, 1975) clearly differ. In our case, both species, *A. simorrense* and *L. sansaniense*, present more subtle dental differences, as both species showed brachyodont dentition (although with evident differences in dental pattern) and an analogous occipital plate angle (*po* = 85-90º).

L. sansaniense is one of the first Rhinocerotini (sensu Becker, 2013) recorded in Europe. The species span over much of the Miocene, from the Early Miocene of France (Baigneaux-en-Beauce) and Czech Republic (Ořechov) to the early Late Miocene, a time when the species had a widespread distribution (but never became abundant), across Central and Western Europe (Heissig, 2012). Classically related with the extant Sumatran rhino, the dentition of *L. sansaniense* is much simpler, closer to other early Rhinocerotini like *Gaindatherium*. Our results place *L. sansaniense* in a specific ecologic niche, browsing on plants from a variety of environments. This particularity, together with a simple social structure similar to extant rhinos (see Mihlbachler et al., 2007 for a review of the topic), would explain the scarce representation of this species along its biostratigraphic rank. At the beginning of the Late Miocene, the species was replaced by *Dihoplus schleiermacheri*, another rhinocerotini species of larger size and slightly more complicated enamel pattern.

As far the rhinoceros fossil record is concerned, the Miocene climatic optimum (MCO; 17.0–14.0 Ma), a warm and humid period, settled favorable conditions for the arrival of *A. simorrense* to the Iberian Peninsula (firstly recorded in the locality of Armantes-1, Calatayud-Daroca Basin, at 16.1 Ma). From there on, the species became a common faunal component in Central Iberia up to the earliest Late Miocene. Its high abundance contrasts with other contemporary aceratheriine species as *H. tetradactylum* or, posteriorly, *A. incisivum*. The late Middle Miocene sediments of the Madrid City area (which include the localities of M-407 Rotonda, Moraleja de Enmedio, and Paracuellos-3) were deposited in the moment of greater development of the alluvial fans coming from the Central System, pointing to a marked climatic seasonality (i.e. wide contrast between dry and wet seasons; Soria et al., 2000). These climatic conditions favored the development of woodlands patched with grasslands and gallery forests surrounding rivers and wetter spots left by abandoned meanders.

In contrast to the rather homogeneous mean annual precipitation (MAP) during the Iberian late Middle Miocene (~600 mm/yr; Van Dam, 2006), a deterioration of the climatic conditions, linked to a drop in MAP, happened during the early Late Miocene (~400-500 mm/yr). As showed by our isotopic results, *A. simorrense* inhabited more closed areas and had more restrictive resource and habitat preferences, thus making it more vulnerable to climatic and environmental perturbations. This drop in MAP may have been a crucial trigger in the extinction of *A. simorrense* in the Iberian central basins. Younger populations recorded in the Vallès- Penedès Basin persisted into the early Late Miocene. The last appearance datum of the species in the Iberian Peninsula comes from the locality of Can Jofresa (Vallès-Penedès Basin; ~9.5 Ma). Its persistence in the area up to the early Late Miocene may be related to persistence of regional humid climatic conditions. Contrariwise to the high frequency of *A. simorrense* in the Iberian Peninsula, the European populations of this species are seldom abundant and mainly restricted to the molasse sediments of the small intra-mountainous basins and karstic fissures (Heissig, 2012). In these basins *A. simorrense* is found in riparian (Simorre), lacustrine (Sansan) and karstic (Wintershof-West) formations (Ginsburg and Guérin, 1979). The scarcity of *A. simorrense* in Central Europe may be related to some ecological competence with a plethora of species like aceratheriines sensu lato (e.g. *Hoploaceratherium tetradactylum*, *Aceratherium incisivum,* or *Plesiaceratherium fahlbuschi*) and teleoceratine species (e.g. *Brachypotherium brachypus* or *Prosantorhinus germanicus*).

In Eastern Europe the last occurrence of *A. simorrense* dates from the early Late Miocene (Codrea, 2000; Lungu, 1984). At that moment, the area comprising Greece, Romania, Moldova, and Turkey, had MAP comparable to the MAP recorded during late Middle Miocene times in the Iberian Peninsula (between 500 and 800 mm/yr; Van Dam, 2006). In a similar way to the populations from Central Europe, ecological competition with Eastern rhinoceros inmigrants during the early Late Miocene (*Chilotherium* spp.), another sexually dimorphic aceratheriine with more hypsodont dentition, would explain the species demise.

CONCLUSIONS

We have carried out a multi-proxy reconstruction of the sympatric rhinocerotid species *A. simorrense* and *L. sansaniense*, discovered at the M-407 Rotonda locality (Late Aragonian, Middle Miocene, Madrid Basin). The abundance and variety of fossil rhino remains place this locality in an unparalleled position for the paleoecological characterization of both species. Morphological cranial and postcranial measurements show comparable head orientations and body masses. *A. simorrense* had shorter limbs (a shortening restricted to zeugopodium and autopodium) and a brachyodont dental pattern showed several adaptations towards a higher enamel complexity. Isotopic $\delta^{13}C$ values of *A. simorrense*, along with its dental pattern suggest preference for more closed areas and consumption of vegetation closer to the ground. The slender and longer limbs (with a reduced stylopodium) of *L. sansaniense* point to a more open habitat and more elevated feeding. Its dental pattern is characterized by simple, brachyodont teeth similar to other basal Rhinocerotini. The isotopic $\delta^{13}C$ signal of *L. sansaniense* (higher than that shown by *A. simorrense*) points to use of a more open environment and higher habitat flexibility, browsing on higher and softer vegetation parts than *A. simorrense*. $\delta^{13}C$ results place both species in a similar C_3 woodland to mesic C_3 grassland environment. The observed resource and habitat partition may have permitted the co-occurrence of both species. Finally, relative differences in $\delta^{13}C$ values of this rhino assemblage as a whole show some ecological flexibility between temporally and/or regionally separated locations.

ACKNOWLEDGMENTS

Thanks to I. Rincón, S. Arcos and Argea S. A. for their field work. Thanks to P. Gutiérrez and B. Alonso for the specimen preparation and P. Pérez Dios (Museo Nacional de Ciencias Naturales de Madrid-CSIC) for kindly helping with the specimens in her care. We acknowledge Paul L. Koch (University of California Santa Cruz) for access to his laboratory and UCSC facilities. Thanks to C. Morant for the photographic assistance. O.S. benefits from a FPU grant from the Spanish Ministry of Science and Innovation (MICINN). L.D. benefits from a Juan de la Cierva postdoctoral fellowship (MINECO, Spanish Government). This work was financially supported by the Comunidad de Madrid (Dirección General de Patrimonio Histórico), Plan Nacional I + D projects CGL2011-257541 (Ministerio de Economía y Competitividad) and the research group BSCH-UCM 910607.

LITERATURE CITED

Agustí, J., and Antón, M., 2002, Mammoths, Sabertooths and Hominids: 65 Million Years of Mammalian Evolution in Europe, California, Columbia University Press, 313 p.:

Aiglstorfer, M., Bocherens, H., and Böhme, M., 2014, Large mammal ecology in the late Middle Miocene Gratkorn locality (Austria): Palaeobiodiversity and Palaeoenvironments, v. 94, p. 189-213.

Antoine, P. O., 2002, Phylogénie et évolution des Elasmotheriina: (Mammalia, Rhinocerotidae): Mémoires du Muséum National d'Histoire Naturelle, v. 188, p. 5-350.

Antoine, P. O., Ducrocq, S., Marivaux, L., Chaimanee, Y., Crochet, J. Y., J.J. Jaeger, and Welcomme, J. L., 2003, Early rhinocerotids (Mammalia: Perissodactyla) from South Asia and a review of the Holarctic Paleogene rhinocerotid record: Canadian Journal of Earth Sciences, v. 40, p. 365-374.

Bales, G. S., 1996, Skull Evolution in the Rhinocerotidae (Mammalia, Perissodactyla): Cartesian Transformations and Functional Interpretations: Journal of Mammalian Evolution, v. 3, no. 3, p. 261-279.

Becker, D., 2003, Paléoécologie et paléoclimats de la Molasse du Jura (Oligo-Miocène) : apport des Rhinocerotoidea (Mammalia) et des minéraux argileuxGrade de Doctor rerum naturalium]: Universite de Fribourg (Suisse), 327 p.

Becker, D., Antoine, P. O., and Maridet, O., 2013, A new genus of Rhinocerotidae (Mammalia, Perissodactyla) from the Oligocene of Europe: Journal of Systematic Palaeontology.

Cerdeño, E., 1986, El Esqueleto Postcraneal de *Lartetotherium sansaniensis* (Mammalia, Rhinocerotidae): Estudios Geológicos, v. 42, p. 197-209.

-, 1989, Revisión de la sistemática de los rinocerontes del Neógeno de EspañaPh.D. Dissertation]: Universidad Complutense de Madrid, 429 p.

-, 1992, Spanish Neogene Rhinoceroses: Palaeontology, v. 35, p. 297-308.

Cerdeño, E., and Nieto, M., 1995, Changes in Western European Rhinocerotidae related to climatic variations: Palaeogeography, Palaeoclimatology, Palaeoecology v. 114, p. 325-338.

Cerdeño, E., and Sánchez, B., 2000, Intraspecific variation and evolutionary trends of *Alicornops simorrense* (Rhinocerotidae) in Spain.: Zoologica Scripta, v. 29, no. 4, p. 275-305.

Cerling, T. E., Harris, J. M., MacFadden, B. J., Leakey, M. G., J. Quade, V. Eisenmann, and Ehieringer, J. R., 1997, Global vegetation change through the Miocene/Pliocene boundary: Nature, v. 389, no. 6647, p. 153-158.

Clementz, M. T., Holroyd, P. A., and Koch, P. L., 2008, Identifying Aquatic Habits Of Herbivorous Mammals Through Stable Isotope Analysis: Palaios, v. 23, no. 9, p. 574-585.

Codrea, V., 2000, Rinoceri şi tapiri terţiari din România, Presa Universitară Clujeană, Cluj Napoca, 174 p.:

Codron, D., Codron, J., Lee-Thorp, J. A., Sponheimer, M., De Ruiter, D., Sealy, J., Grant, R., and Fourie, N., 2007, Diets of

savanna ungulates from stable carbon isotope composition of faeces: Journal of Zoology, v. 273, p. 21-29.

Damuth, J., and Janis, C. M., 2011, On the relationship between hypsodonty and feeding ecology in ungulate mammals, and its utility in palaeoecology: Biological Reviews, v. 86, p. 733-758.

Domingo, L., Grimes, S. T., Domingo, M. S., and Alberdi, M. T., 2009, Paleoenvironmental conditions in the Spanish Miocene–Pliocene boundary: isotopic analyses of *Hipparion* dental enamel: Naturwissenschaften, v. 96, p. 503-511.

Domingo, L., Koch, P. L., Grimes, S. T., Morales, J., and López-Martínez, N., 2012, Isotopic paleoecology of mammals and the Middle Miocene Cooling event in the Madrid Basin (Spain): Palaeogeography, Palaeoclimatology, Palaeoecology, v. 339-341, p. 98-113.

Domingo, L., Koch, P. L., Hernández Fernández, M., Fox, D. L., Domingo, M. S., and Alberdi, M. A., 2013, Late Neogene and Early Quaternary paleoenvironmental and paleoclimatic conditions in Southwestern Europe: isotopic analyses on mammalian taxa: Plos ONE, v. 8, no. 5, p. e63739.

Figueirido, B., Palmqvist, P., and Pérez-Claros, J. A., 2008, Ecomorphological correlates of craniodental variation in bears and paleobiological implications for extinct taxa: an approach based on geometric morphometrics: Journal of Zoology, no. 1, p. 70-80.

Fortelius, M., 1982, Ecological Aspects of Dental Functional Morphology in the Plio-Pleistocene Rhinoceroses of Europe, *in* Kurtén, B., ed., Teeth: Form, Function and Evolution: New York, Columbia University Press, p. 163-181.

-, 1985, Ungulate cheeck teeth: developmental, functional and evolutionary interrelations: Acta Zoologica Fennica, v. 180, p. 1-76.

Fortelius, M., Werdelin, L., Andrews, P., Bernor, R. L., A. Gentry, Humphrey, L., Mittmann, H.-W., and Viratana, S., 1996, Provinciality, diversity, turnover, and paleoecology in land mammal faunas of the later Miocene of western Eurasia, *in* Bernor, R. L., Fahlbusch, V., and Mittmann, H.-W., eds., The evolution of western Eurasian Neogene mammal faunas, Volume 414-448: New York, Columbia University Press.

Geraads, D., and Saraç, G., 2003, Rhinocerotidae from the Middle Miocene Hominoid Locality of Çandir (Turkey): Cour. Forsch.-Inst. Senckenberg, v. 240, p. 217-231.

Groves, C. P., 1972, *Ceratotherium simum*: Mammalian Species. The American Society of Mammalogists, v. 8, p. 1-6.

Groves, C. P., and Kurt, F., 1972, *Dicerorhinus sumatrensis*: Mammalian Species. The American Society of Mammalogists, v. 21, p. 1-6.

Guérin, C., 1980, Les rhinocéros (Mammalia, Perissodactyla) du Miocène terminal au Pléistocène supérieur en Europe occidentale : comparaison avec les espèces actuelles: Documents des Laboratoires de Géologie de Lyon, v. 79, p. 1-1184.

Heissig, K., 1972, Die obermiozäne Fossil-Lagerstätte Sandelzhausen. 5. Rhinocerotidae (Mammalia), Systematik und Okologie: Mitteilungen der Bayerischen Staatssammlung Paläontologie und historische Geologie, v. 14, p. 37.

-, 1989, The Rhinocerotidae, *in* Prothero, D., and Schoch, R. M., eds., The evolution of Perissodactyls, Oxford University Press, p. 399-417.

-, 1999, 16. Family Rhinocerotidae, *in* Rössner, G. E., and Heissig, K., eds., The Miocene Land Mammals of Europe: Pfeil, Munich, p. 175-188.

-, 2012, Les Rhinocerotidae (Perissodactyla) de Sansan, *in* Peigné, S., and Sen, S., eds., Mammifères de Sansan, Volume 203: Paris, Muséum national d'Histoire naturelle, p. 317-485.

Hillman-Smith, A. K., and Groves, C. P., 1994, *Diceros bicornis*: Mammalian Species, v. 445, p. 1-8.

Janis, C., 1984, The use of fossil ungulate communities as indicators of climate and environment, *in* Brenchley, P., ed., Fossils and climate: London, Wiley, p. 85-104.

-, 1997/98, Ungulate teeth, diets, and climatic changes at the Eocene/Oligocene boundary: Zoology—Analysis of Complex Systems, v. 100, p. 203-220.

Janis, C. M., 1990, The correlation between diet and dental wear in herbivorous mammals and its relationship to the determination of diets of extinct species, *in* Boucot, A. J., ed., Evolutionary Paleobiology of Behavior and Coevolution: Amsterdam, Elsevier, p. 241-259.

Jernvall, J., Hunter, J. P., and Fortelius, M., 1996, Molar tooth diversity, disparity and ecology in Cenozoic ungulate radiations: Science, v. 274, p. 1489-1492.

Koch, P. L., Zachos, J. C., and Gingerich, P. D., 1992, Correlation between isotope records in marine and continental carbon reservoirs near the Palaeocene/Eocene boundary: Nature, v. 358, p. 319-322.

Koenigswald, W. v., 2011, Diversity of hypsodont teeth in mammalian dentitions – construction and classification: Palaeontographica, Abt. A: Palaeozoology – Stratigraphy, v. 274, no. 1, p. 63-94.

Lartet, E., 1851, Notice sur la Colline de Sansan.

Laurie, W. A., Lang, E. M., and Groves, C. P., 1983, *Rhinoceros unicornis*: Mammalian Species. The American Society of Mammalogists, v. 211, p. 1-6.

Lee-Thorp, J., and van der Merwe, N. J., 1987, Carbon isotope analysis of fossil bone apatite: South African Journal of Science, v. 83, p. 712-715.

Levin, N. E., Cerling, T. E., Passey, B. H., Harris, J. M., and Ehleringer, J. R., 2006, A stable isotope aridity index for

terrestrial environments: PNAS, v. 103, no. 30, p. 11201-11205.

Loose, H., 1975, Pleistocene Rhinocerotidae of W. Europe with reference to the recent two-horned species of Africa and S. E. Asia: Scripta Zoologica, v. 33, p. 1-59.

Lungu, A. N., 1984, *Hipparion*-Fauna of the Middle Sarmatian in Moldavia, Kisinev, Stiinca.

MacFadden, B. J., 1998, Tale of two Rhinos: Isotopic Ecology, Paleodiet, and Niche Differentiation of Aphelops and Teloceras from the Florida Neogene: Paleobiology, v. 24, no. 2, p. 274-286.

Matthew, W. D., 1932, A review of the rhinoceroses with a description of *Aphelops* material from the pliocene of Texas: University of California Publications in Geological Sciences, v. 20, no. 12, p. 411-480.

Mendoza, M., Janis, C. M., and Palmqvist, P., 2002, Characterizing complex craniodental patterns related to feeding behaviour in ungulates: a multivariate approach: Journal of Zoology, v. 258, no. 2, p. 223-246.

Mihlbachler, M., 2007, Sexual Dimorphism and Mortality Bias in a Small Miocene North American Rhino, *Menoceras arikarense* : Insights into the Coevolution of Sexual Dimorphism and Sociality in Rhinos: Journal of Mammalian Evolution, v. 14, no. 4, p. 217-238.

Nowak, R. M., 1999, Walker's Mammals of the World, Baltimore, John Hopkins University Press, 2015 p.:

Osborn, H. F., 1898, A complete skeleton of *Teleoceras fossiger*. Notes upone the growth and sexual Characters of this species: Bulletin of the American Museum of Natural History, p. 51-59.

Peláez-Campomanes, P., Azanza, B., Calvo, J. P., Daams, R., Herráez, E., Morales, J., Nieto, N., and Soria, D., 2000, Bioestratigrafía de las faunas del Mioceno de Madrid: Datación de las unidades estratigráficas, *in* Morales, J., Nieto, N., Amezua, L., Fraile, S., Gómez, E., Herráez, E., Peláez-Campomanes, P., Salesa, M. J., Sánchez, I. M., and Soria, D., eds., Patrimonio Paleontológico de la Comunidad de Madrid, Volume 6: Madrid, Consejería de Educación Comunidad de Madrid, p. 103-109.

Prothero, D. R., 1992, Fifty million years of rhinoceros evolution, *in* Ryder, O. A., ed., Rhinoceros biology and conservation: San Diego, Zoological Society, p. 82-91.

Quade, J., Cerling, T. E., Barry, J. C., Morgan, M. E., Pilbeam, D. R., Chivas, A. R., Lee-Thorp, J. A., and van der Merwe, N. J., 1992, A 16-Ma record of paleodiet using carbon and oxygen isotopes in fossil teeth from Pakistan: Chemical Geology (Isotope Geoscience Section), v. 94, p. 183-192.

Scott, W. B., 1913, A history of land mammals in the western hemisphere, New York, The MacMillan Company, 693 p.:

Soria, D., Amezua, L., Daams, R., Fraile, S., Herráez, E., Morales, J., Nieto, M., Peláez-Campomanes, P., Salesa, M. J., and Sánchez, I. M., 2000, Faunas del Mioceno, *in* Morales, J., ed., Patrimonio Paleontológico de la Comunidad de Madrid: Madrid, Consejería de Educación de la Comunidad de Madrid, p. 110-177.

Tipple, B. J., Meyers, S. R., and Pagani, M., 2010, The carbon isotope ratio of Cenozoic CO2: a comparative evaluation of available geochemical proxies: Paleoceanography, v. PA001851.

Tütken, T., and Vennemann, T., 2009, Stable isotope ecology of Miocene large mammals from Sandelzhausen, southern Germany: Paläontologische Zeitschrift, v. 83, p. 207-226.

Tütken, T., Vennemann, T. W., and Heizmann, E. P. J., 2006, Palaeoenvironment and palaeoclimate of the Middle Miocene lake in the Steinheim basin, SW Germany: A reconstruction from C, O, and Sr isotopes of fossil remains: Palaeogeography, Palaeoclimatology, Palaeoecology, v. 241, p. 457-491.

Webb, S. D., 1983, The rise and fall of the late Miocene ungulate fauna in North America, *in* Nitecki, M. H., ed., Coevolution.: Chicago, University of Chicago Press, p. 267-306.

SUPPLEMENTARY DATA 1

Table 1. Total limb length (humerus, radius, Mc III / femur, tibia, Mt III) of several ungulate species in mm. Missing measurements of *Alicornops simorrense* and *Lartetotherium sansaniense* from M-407 Rotonda (in gray) have been estimated by interpolating information from other localities, as detailed in the Material and Methods section from the main text. References (Ref.): 1: Gregory, 1912; 2: Deng, 2002; 3: Mihlbachler et al., 2004; 4: Cerdeño and Sánchez, 2000; 5: Sanisidro et al., this volume; 6: Heissig, 2012; 7: Hünermann, 1989

Table 1	Humerus	Radius	Mc III	TOTAL	Femur	Tibia	Mt III	TOTAL	Specimen	Ref.
Tapirus indicus	250	228	120	598	320	258	120	698	not specified	1
*Chilotherium anderssoni**	349	280	127	756	430	278	110	818	composite skeleton	1
*Chilotherium wimani**	320	272	121	713	385	276	103	764	Linxia Basin sample mean	2
Teleoceras proterum	310	240	106	656	415	202	89	706	AMNH (Mixson's Bone Bed)	3
Dicerorhinus sumatrensis	330	275	165	770	478	282	142	902	NMNH 49561	3
Rhinoceros sondaicus	352	289	160	801	426	285	135	846	NMNH 269392	3
Rhinoceros unicornis	405	340	215	960	520	341	177	1038	NMNH 336953	3
Diceros bicornis	373	392	183	948	464	330	163	957	NMNH 162935	3
Ceratotherium simum	407	375	196	978	520	354	171	1045	NMNH 164635	3
Choeropsis liberiensis	219	156	88	463	277	200	78	555	NMNH 581892	3
Hippopotamus amphibius	395	270	152	817	498	332	130	960	not specified	3
Alicornops simorrense Iberian record	297	242	117	656	322	274	116	712	Iberian sample (mean)	4
***Alicornops simorrense* M-407**	286	233	118	637	386	328	139	854	M-407 sample	5
Lartetotherium sansaniense Sansan	391	380	180	951	502	386	169	1057	Sansan sample (mean)	6
Lartetotherium sansaniense Sandelzhausen	419	335	185	939	488	384	164	1036	Sandelzhausen (mean)	5
***Lartetotherium sansaniense* M-407 (A)**	334	316	147	798	350	313	145	808	M-407 sample	5
***Lartetotherium sansaniense* M-407 (B)**	325	316	149	790	350	313	145	808	M-407 sample	5
Lartetotherium sp. BAT-1 and BAT-10	365	345	161	871	424	352	153	929	Batallones-1 and 10 (mean)	5
Aceratherium incisivum BAT-1	363	295	134	792	387	297	109	793	Batallones-1 (mean)	5
Aceratherium incisivum Höwenegg	385	300	142	827	390	320	120	830	Höwenegg (mean)	7

Table 2. Occipital angles of several living and fossil rhinoceros species, including the species *Alicornops simorrense* and *Lartetotherium sansaniense* studied in the present work. *m* and *po* angles have been used following Zeuner (1934) and Loose (1975).

Table 2	*m* (mean)	*m* (min/max)	N	*po* (mean)	*po* (min/max)	N	Specimen	Reference
Rhinoceros sondaicus	90	86 / 95	4	63	56 / 73	4	Museum sample mean	Own data; AMNH
Dicerorhinus sumatrensis	55	40 / 64	12	68	54 / 107	12	Museum sample mean	Loose, 1975
Rhinoceros unicornis	78	72 / 82	5	64	60 / 69	5	Museum sample mean	Own data; AMNH
Diceros bicornis	44	35 / 54	26	67	54 / 76	25	Museum sample mean	Loose, 1975
Ceratotherium simum	46	44 / 50	5	88	85 / 90	3	Museum sample mean	Loose, 1975
Ceratotherium cottoni	42	35 / 50	7	75.5	65 / 82	6	Museum sample mean	Loose, 1975
Stephanorhinus etruscus	46	34 / 70	8	71	66 / 90	7	Museum sample mean	Loose, 1975
Stephanorhinus kirchbergensis	50	46 / 51	3	72	72 / 80	3	Museum sample mean	Loose, 1975
Stephanorhinus hemitoechus	38	28 / 44	7	—	—	—	Museum sample mean	Loose, 1975
Coelodonta antiquitatis	51	43 / 56	10	106	95 / 110	4	Museum sample mean	Loose, 1975
Alicornops simorrense	53	—	1	86	—	1	MNCN 30768 (Moraleja de Enmedio)	Own data
Lartetotherium sansaniense	61	—	1	89	—	1	CA4-73 (M-407 Rotonda)	Own data

SUPPLEMENTARY DATA 1

Table 3. Body masses estimation of the studied species. BM: body mass (Kg); TL: total length (obtained from Supplementary Data 1; Table 1). References (Ref.): 1, Lewison, 2011; 2, Medici, 2011; 3, Prothero, 2005; 4, Cerdeño and Sánchez, 2000; 5, Heissig, 2012; 6, own data; 7, Deng, 2006; 8, Ringstrom, 1924; 9, Groves and Kurt, 1972; 10, Groves and Leslie, 2011; 11, Hillman-Smith and Groves, 1994; 12, Cerdeño, 1989; 13, Laurie et al., 1983; 14, Groves, 1972.

Table 3

	M1L (min)	M1L (max)	M1W (min)	M1W (max)	BM (min)	BM (mean)	BM (max)	lnBM (min)	lnBM (mean)	lnBM (max)	Ref.
Choeropsis liberiensis	—	—	—	—	160	215	270	5.08	5.37	5.60	1
Tapirus indicus	—	—	—	—	280	340	400	5.63	5.83	5.99	2
Teleoceras proterum	47.0		55.0		3992	3992	3992	—	8.29	—	3
Alicornops simorrense	39.5	44.4	42.0	48.0	2018	2492	2967	7.61	7.82	8.00	4. 5. 6
Chilotherium wimani	38.4		59.5		3302	3302	3302	—	8.10	—	7
Chilotherium anderssoni	55.0		54.0		4942	4942	4942	—	8.51	—	8
Dicerorhinus sumatrensis	—	—	—	—	800	1400	2000	6.68	7.24	7.60	9
Rhinoceros sondaicus	—	—	—	—	1200	1740	2280	7.09	7.46	7.73	10
Hippopotamus amphibius	—	—	—	—	1000	2750	4500	6.91	7.92	8.41	1
Diceros bicornis	—	—	—	—	886	1536	2186	6.79	7.34	7.69	11
Lartetotherium sansaniense	36.0	44.0	40.5	47.0	1655	2243	2832	7.41	7.72	7.95	12. 5. 6
Rhinoceros unicornis	—	—	—	—	1600	1865	2130	7.38	7.53	7.66	13
Ceratotherium simum	—	—	—	—	3200	3400	3600	8.07	8.13	8.19	14

REFERENCES

Cerdeño, E., 1989, Revisión de la sistemática de los rinocerontes del Neógeno de España [Ph.D. Dissertation thesis]: Madrid, Universidad Complutense de Madrid.

Cerdeño, E., and Sánchez, B., 2000, Intraspecific variation and evolutionary trends of *Alicornops simorrense* (Rhinocerotidae) in Spain.: Zoologica Scripta, v. 29, p. 275-305.

Deng, T., 2002, Limb bones of *Chilotherium wimani* (Perissodactyla, Rhinocerotidae) from the Late Miocene of the Linxia Basin in Gansu, China: Vertebrata Palasiatica, v. 40, p. 305-316.

—, 2006, A primitive species of *Chilotherium* (Perissodactyla, Rhinocerotidae) from the late Miocene of the Linxia Basin (Gansu, China): Cainozoic Research, v. 5, p. 93-102.

Gregory, W.K., 1912, Notes on the principles of quadrupedal locomotion and on the mechanism of the limbs in hoofed animals: Annals of the New York Academie of Sciences, v. 22, p. 267-294.

Groves, C.P., 1972, *Ceratotherium simum*: Mammalian Species. The American Society of Mammalogists, v. 8, p. 1-6.

Groves, C.P., and Kurt, F., 1972, *Dicerorhinus sumatrensis*: Mammalian Species. The American Society of Mammalogists, v. 21, p. 1-6.

Heissig, K., 2012, Les Rhinocerotidae (Perissodactyla) de Sansan, *in* Peigné, S., and Sen, S., eds., Mammifères de Sansan, Volume 203: Paris, Muséum national d'Histoire naturelle, p. 317-485.

Hillman-Smith, A.K., and Groves, C.P., 1994, *Diceros bicornis*: Mammalian Species, v. 445, p. 1-8.

Hünnerman, K.A., 1989, Die Narshornskelette (Aceratherium incisivum Kaup [18]32) aus dem Jungtertiär vom Höwennegg im Hegau (Südwestdeutschland): Andrias, v. 6, p. 117.

Laurie, W.A., Lang, E.M., and Groves, C.P., 1983, *Rhinoceros unicornis*: Mammalian Species. The American Society of Mammalogists, v. 211, p. 1-6.

Lewison, R.L., 2011, Family Hippopotamidae (Hippopotamuses), *in* Wilson, D.E., and Mittermeier, R.A., eds., Handbook of the mammals of the world: Barcelona, Lynx Edicions, Conservation International and IUCN, p. 320-335.

Loose, H., 1975, Pleistocene Rhinocerotidae of W. Europe with reference to the recent two-horned species of Africa and S. E. Asia: Scripta Zoologica, v. 33, p. 1-59.

Medici, E.P., 2011, Family Tapiridae (Tapirs), in Wilson, D.E., and Mittermeier, R.A., eds., Handbook of the mammals of the world: Barcelona, Lynx Edicions, Conservation International and IUCN, p. [18]2-204.

SUPPLEMENTARY DATA 1

Mihlbachler, M.C., Lucas, S.G., Emry, R.J., and Bayshashov, B., 2004, A New Brontothere (Brontotheriidae, Perissodactyla, Mammalia) from the Eocene of the Ily Basin of Kazakstan and a Phylogeny of Asian "Horned" Brontotheres: American Museum Novitates, v. 3439, p. 1-43.

Prothero, D., 2005, The Evolution of North American Rhinoceroses: Cambridge, Cambridge University Press, 2^{18} p.

Ringström, T.J., 1924, Nashörner der Hipparion Fauna Nord-Chinas: Palaeontologia Sinica, Series C, v. 1, p. 1-156.

Zeuner, F.E., 1934, Die Beziehungen zwischen Schädelform und Lebensweisen bei den rezenten und fossilen Nashörnern: Bericht. Naturforsch. Gellesch. Freiburg in Breisgau, v. 34, p. 21-80.

SUPPLEMENTARY DATA 2

Table 1. Total dataset of $\delta^{13}C$ and $\delta^{18}O$ values of *Alicornops simorrense* and *Lartetotherium sansaniense* from M-407 Rotonda. $\delta^{18}O$ values are given in ‰ VPDB and ‰VSMOW.

Table 1	tooth	$\delta^{13}C_{CO3}$ (‰ VPDB)	$\delta^{18}O_{CO3}$ (‰ VPDB)	$\delta^{18}O_{CO3}$ (‰ VSMOW)
A. simorrense				
CA4-200	m1	-11.3	-2.1	28.7
B1 84	m1	-11.6	-1.2	29.6
DES-51	P4	-10.9	-0.2	30.7
H2-14	P4	-10.9	-1.4	29.4
CA6-293	p4	-11.2	-3.0	27.9
CA3-182	p3	-11.8	0.1	31.1
A2-46	i2	-11.0	-2.9	27.9
CA1-26	P4	-10.7	-0.3	30.6
w/n	M3	-11.3	-0.9	30.0
CA5-30	M3	-11.8	-1.4	29.4
CA3-148	M3	-10.7	-3.9	26.9
L. sansaniense				
SAN-1	m1-2	-7.9	0.2	31.2
C2 65	m2	-9.4	-0.7	30.2
D5 1	m3	-9.9	-2.2	28.6
A2 43	mx fragment	-9.2	-1.3	29.5
CA1-18 a	m3	-9.5	0.8	31.7
CA1-18 b	m2	-10.1	-1.5	29.4
C1-39 a	M3	-9.3	-3.4	27.4
C1-39 b	M3	-9.6	-2.3	28.6
C1-39 c	M2	-8.9	-2.3	28.5

Table 2. Mean and standard deviation $\delta^{13}C$ and $\delta^{18}O$ values of *Alicornops simorrense* and *Lartetotherium sansaniense* from M-407 Rotonda.

Table 2	n	Mean $\delta^{13}C_{CO3}$ (‰ VPDB)	SD $\delta^{13}C_{CO3}$ (‰ VPDB)	Mean $\delta^{18}O_{CO3}$ (‰ VSMOW)	SD $\delta^{18}O_{CO3}$ (‰ VSMOW)
A. simorrense	11	-11.2	0.4	29.3	1.3
L. sansaniense	9	-9.3	0.6	29.5	1.4

Table 3. T-student analyses comparing $\delta^{13}C$ and $\delta^{18}O$ values of *Alicornops simorrense* and *Lartetotherium sansaniense* from M-407 Rotonda.

Table 3		
inter-species	t-Student	p-value
$\delta^{13}C_{CO3}$ (‰ VPDB)	-8.064	< 0.001
$\delta^{18}O_{CO3}$ (‰ VSMOW)	-0.271	0.789

10. *Ceratherium incisivum* (Kaup, 1832) (Mammalia, Rhinocerotidae) from the Upper Miocene of Cerro de los Batallones (Madrid Basin, Spain)

Oscar Sanisidro
Ioannis Giaourtsakis
María Teresa Alberdi
and Jorge Morales

Abstract. We describe the new remains of *Ceratherium incisivum* from the Upper Vallesian of Cerro de los Batallones fossil complex (Batallones butte; Madrid Basin, Spain). The sample, collected in Batallones-1, 3, 5, and 6 includes a finely preserved complete skeleton. The studied material is compared to specimens from other Upper Miocene sites from the Iberian Peninsula and Western Europe. As a result, some differences mainly focused on the skull have been detected. Limb proportions and isotopic analysis indicate that *A. incisivum* was a mediportal inhabitant of the closer woodland environments of Batallones-1.

INTRODUCTION

Ceratherium incisivum (Kaup, 1832) is a middle-sized hornless rhinoceros named by Cuvier as "*Rhinoceros incisivus*" on the basis of an isolated upper incisor from Weisenau (Germany; Cuvier, 1822). It was not until a decade later when Kaup (1832) described two hornless rhino skulls from the German locality of Eppelsheim (DIN 1927 and DIN 1930), assigning them to "*R. incisivus*". Owing to the smooth and narrow nasal bones, which pointed to a hornless condition, the species was placed in a new genus named as *Ceratherium* apart from the remaining (all horned) forms known at that time, which remained in *Rhinoceros*. These two incomplete skulls from Eppelsheim have served as a reference for the species up to now. A recent review of the topic showed that not only the original incisor from Weisenau used to define the species is apparently lost but pertained to a Middle Miocene teleoceratine rhinos (Giaourtsakis and Heissig, 2004). Postcranial acerathere remains from Eppelsheim are scarce and pertain to two different species. According to Giaourtsakis and Heissig (2004), only small and robust postcranial bones from the Upper Miocene of Western and Central Europe (as those from the German locality of Höwenneg Hünnerman, 1989), should be ascribed to *A. incisivum*. Therefore, the two skulls described by Kaup should be formally considered as syntypes, the smaller acerathere postcranial remains part of the type collection and Eppelsheim the reference locality for *A. incisivum*.

The species is a common representative in the Upper Miocene European faunas (MN 9-13 (Mein's biozone; Mein, 1990, 1999). Guérin (1980) cites 23 localities with presence of *A. incisivum* in Western Europe along Spain, France, and Germany. Thereinafter, additional records have been found in Switzerland (Becker, 2003), Hungary (Heissig, 1999), Turkey (Geraads, 2005), Moldova (Macarovici, 1978; Codrea, 2000; 2014), and Romania (Codrea, 2000). However, the presence of several undetermined acerathere species in Western Europe is likely (Giaourtsakis and Heissig, 2004), and a systematic update is needed to address this question.

In the Iberian Peninsula, *A. incisivum* has a more restricted biostratigraphic range. It is firstly recorded in the Vallesian (MN 9) and last occurred in the middle Turolian (MN 12). *A incisivum* is particularly abundant in the localities of the Vallés-Penedés basin. These are the Lower Vallesian Can Llobateres (Santafé, 1978; Villalta and Crusafont, 1944), Can Ponsic (Santafé, 1978), Polinyà (Santafé and Casanovas, 1992) and Can Feu (Santafé et al., 1989-1990) and the Upper Vallesian Can Perellada (Santafé and Casanovas-Cladellas, 1978) and La Tarumba (Santafé, 1978). The species has been also found in the Vallesian site of Autovía Orbital B40, but further biostratigraphic placement remains unclear (Tomàs et al., 2010). Towards the Turolian of the Vallés-Penedés, it has been solely cited in Piera (also known as Torrentet des Traginers; Cerdeño, 1989; Fernández and Cerdeño, 1999). Oppositely, the species is scarcer among the Iberian central basins,

being present at the Lower Vallesian locality of Los Valles de Fuentidueña (Alberdi et al., 1981), the Upper Vallesian sites of La Roma 2 (Cerdeño, 1989) and the Batallones fossil complex, and the Upper Turolian sites of Concud (Cerdeño, 1989; Santafé and Casanovas-Cladellas, 1983-1984) and Masía del Barbo (Cerdeño, 1989).

In 1991, the Museo Nacional de Ciencias Naturales of Madrid started systematic excavations in Cerro de los Batallones (Los Batallones butte) fossiliferous area as a result of prospection works conducted by the Museo Nacional de Ciencias Naturales and Tolsa Mining Company. The site complex is placed between the Jarama River Valley and the Prados-Guatén Depression within the Cenozoic Madrid Basin, between the city of Valdemoro and the village of Torrejón de Velasco (30 Km South of the city of Madrid; Fig. 1A-C). Fossil remains are embedded in a sedimentary matrix discordant with the three sedimentary units of the butte (see Domingo et al., 2011 for further details of the geology of each unit). Two distinct assemblages have been recognized in the butte that differ stratigraphically, taxonomically and taphonomically (Domingo et al., 2011). Lower level assemblages (LLAs), so-called cavity-type sites, are deposited in the base of the Unit II, towards the lower-middle part of the stratigraphic sequence of the butte (Domingo et al., 2011). Examples of LLAs are the lower level of Batallones-1 and Batallones-3. Their faunas are overwhelmingly dominated by mammals of the order Carnivora. This distinctiveness is the result of particular formation conditions: ground drainage (combining a pseudokarstic process known as piping together with chambering) and posterior gypsum dissolution favored the presence of cavities that acted as natural trap caves (Pozo et al., 2004). These cavities attracted carnivores trying to scavenge entrapped preys and/or drinking collected water. Traps were filled with episodic floods which favored the rapid burial of articulated remains interspersed with long slow sedimentation periods that produced isolated bones with taphonomic marks (i.e. trampling, weathering and root and carnivore modifications; Domingo et al., 2011). Non-stratified

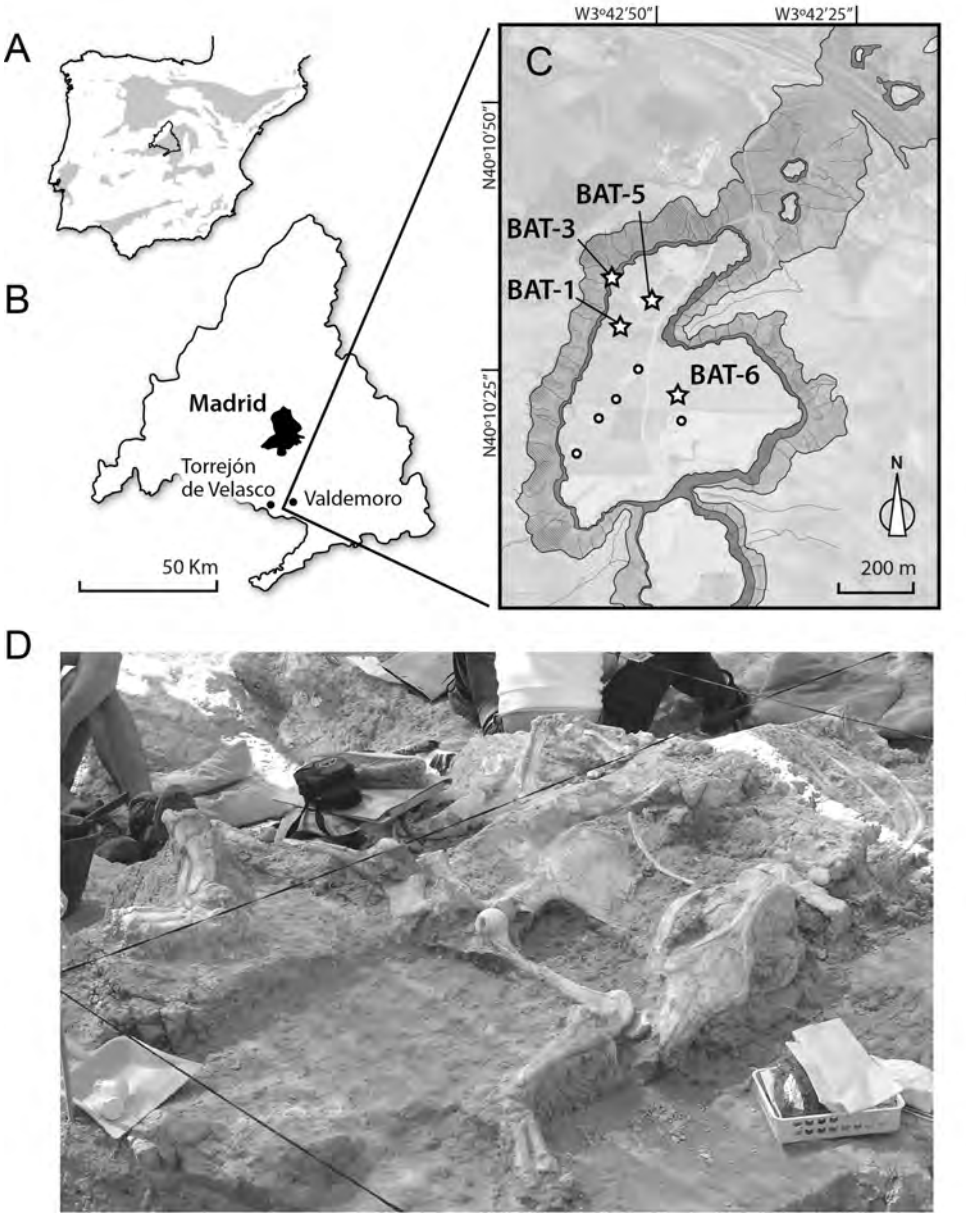


Fig. 1 A, simplified geographic map of the Iberian Peninsula with the Tertiary basins shaded and the Madrid Province outlined; B, detailed map of the Madrid Province with the situation of Cerro de los Batallones fossil complex; C, aerial photo showing the position of the areas of systematic excavations (indicated as empty circles). *Aceratherium incisivum* has been found in the fossil sites represented as stars. Medium gray, dark gray and light gray shaded areas represent the outcrops of the Unit I, II and III respectively. D, photograph of the complete ***A. incisivum*** individual in Batallones-1 during the 2004 field campaing (D; notice that the skeleton is lying on its back except for the cervical vertebrae and the skull, which are dorso-ventrally oriented). Photograph courtesy of S. Fraile.

filling sediments include green clays with carbonate and, occasionally, chert. As a consequence, LLAs have provided an extraordinary collection of carnivoran fossils (Peigné et al., 2005; Peigné et al., 2008; Salesa et al., 2005; Salesa et al., 2012; Salesa et al., 2006a; Salesa et al., 2008; Salesa et al., 2006b). Despite comprising less than 2% of the macro-mammal bones recovered from Batallones-1, herbivores were also trapped into the cavities (Domingo et al., 2013).

Upper level assemblages (ULAs, or sinkhole-type sites) comprise the remaining fossil sites of the butte and are found in uppermost part of the Unit III. They present a better-defined stratification (Domingo et al., 2011), typical of a small to medium pond or waterhole. Their specific formation processes are under study. ULAs mainly consist on mammalian herbivores like giraffes, equids, moschids, bovids and rhinos (Domingo et al., 2011; Morales et al., 2008; Sánchez et al., 2009; Sánchez et al., 2011). Up to now, six localities with upper level deposits have been found. These are Batallones-2, 3, 5, 6 and 10 (and, probably, Batallones-4). Batallones-1 and Batallones-2 contain both LLA and ULA, but other sites could have presented both levels prior to their erosion (partial loss of LLA in Batallones-1 or complete loss of LLA in Batallones-3) or present LLA in lower and still unearthed levels (Batallones-10). A narrow pipe connected the lower 'pouch'-like cavity (LLA) and the upper sediments has been detected in some sites, giving a characteristic 'hourglass' shape to the whole complex.

All the localities from Cerro de los Batallones have an Upper Vallesian age (~ 10-9 Ma, early Late Miocene; Peigné et al., 2008). Once considered coeval, the study of the micromammal assemblage of different sites of the butte revealed some temporal differences amongst them: Batallones-10 is older than Batallones-1, and Batallones-3 is the recent most of the three (López-Antoñanzas et al., 2010).

Both LLAs and ULAs yield skeletal remains that stand out for their exceptional state of preservation and completeness. Among the scarcer herbivores of Batallones-1, two rhinoceros individuals have been found. The first is represented by an almost complete *A. incisivum* skeleton found at the bottom of the trap, occupying an area of approximately two square meters (Fig. 1D). The second rhinoceros is represented by a partial skeleton of a rhinocerotini scattered along more superficial sediments (1 m above the former). The presence of *A. incisivum* in Cerro de los Batallones butte was firstly noticed by Morales et al (1992) in Batallones-1. Posteriorly, a mandible and several isolated dental remains and postcranial bones were described from the same locality and assigned to the species by Cerdeño and Sánchez (1998). From there on, additional remains of *A. incisivum* have been collected from Batallones-3, 5, and 6, comprising one of the best preserved and most complete collections of the species. Here we present a comprehensive description of the fossil remains of *A. incisivum* from Cerro de los Batallones. Additionally, we present a morphological comparison with other Iberian and European samples.

MATERIAL AND METHODS

The systematic study presented below is based on the direct examination of the specimens from Cerro de los Batallones butte stored in the collections of the Museo Nacional de Ciencias Naturales, Madrid. Measurements were made with a digital caliper and an accuracy of one decimal digit. A measuring tape was used for elements larger than 150 mm. Measurements are given in millimeters. Approximate measurements are preceded by a ~ sign and those of paired structures detailed in the text are annotated as follows: (left side / right side). 'B-' refers to fossils found in situ in Batallones-1 extracted from 1991 to 2000. The remaining fossils (extracted between 2001 and 2014, depending on the fossil site) are labeled with the abbreviation of the fossil site (e.g. Batallones-3 is labeled as BAT-3) followed by the year of extraction and the field number (e.g. BAT-1'07 E3-27 is the 27th fossil extracted from the E3 grid in 2007).

The general anatomical terminology follows Budras (2009) and Schaller (2007). In addition, that used by other authors has also been taken into consideration (Antoine, 2002; Antoine et al., 2010; Becker et al., 2013; Guérin, 1980; Heissig, 1972a, 1999). More detailed information of the craniodental anatomy can be found in the Appendix at the end of this volume. For more information regarding the postcranial skeleton see Chapter 5. Orientation guides are detailed in the Material and Methods chapter.

Cranial comparisons with the type material from Eppelsheim mainly rely on DIN 1930, whereas dental ones are focused on DIN 1927 due to its better preservation and slightly less advanced wear stage. Even though the skulls of *A. incisivum* from Eppelsheim DIN 1927 and DIN 1930 are fully accessible in the collections of the Darmstadt Hessisches Landesmuseum, its current temporal remodeling prevents any direct comparison with the postcranial bones. Alternatively, the smaller and more robust rhinocerotini postcranial casts from Eppelsheim stored in the AMNH have been used as reference for the type collection of the species. Finally, the postcranial material of *A. incisivum* from Cerro de los Batallones has been compared with the remains from Höwenegg (Hünnerman, 1989), as they pertain to the same robust and shortened morphology as that of Eppelsheim according to Giaourtsakis and Heissig (2004).

Anatomical Abbreviations—ant, anterior; art, articulation; dia, diaphysis; dis, distal; int, interior; epi, epiphysis; max, maximum; min, minimum; prox, proximal; 3tr, third trochanter. In describing the dental elements, capital letters are used for upper teeth (I1-3, C, D1-4, P1-4, M1-3), and lower case for lower teeth (i1-3, c, d1-4, p1-4, m1-3) as proposed by Jepsen (1996).

Measurements abbreviations—All measurements are given in mm. APD, antero-posterior diameter; DL, distal length; H, height; L, length; TD, transverse diameter.

Institutional abbreviations—Additional material was

used for comparison. Where this is the case, this is indicated by the following abbreviations: **AMNH**, American Museum of Natural History; **IPSCF**, Instituto Paleontológico de Sabadell Crusafont; **MNCN**, Museo Nacional de Ciencias Naturales; **w/n**, without field number.

Referred material—*A. incisivum* remains from Cerro de los Batallones are stored in the Museo Nacional de Ciencias Naturales-CSIC. The referred material included in this paper is detailed in the Appendix 1.

SYSTEMATIC PALEONTOLOGY

Family Rhinocerotidae Gray, 1821

Subfamily Rhinocerotinae Gray, 1821

Genus *Aceratherium* Kaup 1832

Type species—*Aceratherium incisivum* Kaup, 1832

Other species—*Aceratherium belbederense* (Heissig, 1999) and *Aceratherium porpani* (Deng et al., 2013).

Emended diagnosis—(modified from Deng, 2013; p 982): Small to medium sized Rhinocerotidae genus with hornless nasal bones; "elongated skull, non-projecting orbits; moderate supraorbital tuberosities, nearly vertical zygomatic arches, rounded braincase, narrow nuchal crest, wide intercondylar notch, compressed and straight postglenoid processes, thin and weakly expanded posttympanic processes, a wide U-shaped choana reaching the M2/M3 boundary, subhypsodont teeth, tusk-like i2, strong crochets, shallowly undulated labial walls, weak paracone ribs, narrow parastyles, constricted molar protocones, short and posteriorly pointed molar antecrochets, absent lingual cingulum on molars, a well-developed labial cingulum on the lower premolars, a weak or absent crista on the upper molars, a molar protocone with a rounded lingual margin, a strong molar parastyle fold, and a slightly constricted protocone on the molars".

Aceratherium incisivum Kaup 1832

Holotype—(Lectotype; see Giaourtsakis & Heissig, 2007). Incomplete adult skull (HLMD DIN 1927) with right P4-M3 and left P3-M3.

Type locality—Eppelsheim, Rheinhessen, Germany

Diagnosis—As for genus.

Stratigraphic and geographic distribution— Europe, (Spain, France, Germany, Switzerland, Romania and Austria) from the MN9 to the MN13 (Mein's biozone; Mein, 1990, 1999);

DESCRIPTION

Craniomandibular and Dental Morphology

Skull (Figure 2 and Table S1)—the skull from Batallones-1 BAT-1'05 F5-157 is almost complete, as only lacks the premaxilla. The whole skull is dorsoventrally-pressed, favoring a flattened dorsal profile of the skull and some cracking along the frontal plane. It has both P2-P3, DP4 and M1-M3 series, thus pertaining to a subadult individual. The nasals are long (137 mm length from the nasal tip to the bottom of the nasal) and wide (TD = 100 mm), narrowing abruptly at its tip. The tips are pointed, oval in section and lack any rugosity, pointing to a hornless condition. The nasal central suture is unfused, extending backwards to the level of the supraorbital tubercles. The nasals have a convex and smooth dorsal surface, a straight lower margin, concave at its tip and no trace of lateral apophysis. Their ventral surface is concave, with a smoothly convex area along the sagittal plane. The original orientation of the nasal bones was almost horizontally implanted and a little downwards inclined tip. There are two visible oval infraorbital foramina, being the inferior bigger. Both are close to the nasal notch border at the level of the P2/P3 boundary. The nasal notch is 'V'-shaped and reaches the P3 level. The maxillary bone is convex and high, with marked ridges in the roots of the teeth. It has a small and shallow depressed area in front of the orbit. There is a distance of 77.8 mm between the caudal margin of the nasal notch and the anterior rim of the orbit. The orbit does not protrude from the lateral surface. Its rostral margin is located at the level of the paracone of the M1. The supraorbital tubercles are slightly protruding, rounded, have a smooth dorsal surface and are separated from the rostral edge of the orbit by a small indentation. The postorbital processes are weak and sharp, serving as a starting point for the parietal crests. The distance between both tubercles is 184 mm, leaving a flattened surface between them. The skull roof is rhombic and is the widest between the supraorbital processes. In lateral view, the dorsal skull profile presents two straight to slightly convex areas (nasal bone and braincase) separated by a concave transition at the level of the postorbital processes. The fronto-parietal crests are faint ridges that converge 135 mm backwards from the anterior rim of the orbit, remaining parallel and independent thereinafter (1-3 mm between them) until the occipital crest. The lateral margins of the parietal crests form an obtuse angle with their dorsal surface, which are flattened and divergent. Their caudal extent is swollen and fused with a straight nuchal crest. The temporal crests link the lateral sides of the nuchal crests to the caudal extent of the zygomatic arches. They are low, sharp and laterally projected. On the caudal side, the nuchal ligament depression has ventrally collapsed, thus having a somewhat more elevated occiput. The nuchal tubercle is represented by a smooth area. The foramen magnum is subtriangular and shows a caudally projected ventral side. The occipital condyles are long and leave a minimum distance of 55.1 mm between them for the foramen magnum. The caudal side of the palate is 'U'-shaped and reaches the hypocone of the M2. There are three small palatine foramina on the left side, two on the right (as the rostral ones, at the level of the protocone of the M2, are fused). The anterior part of the zygomatic arch leaves a wide and deep area from the M1 to the M3. The pterygoidean crests are short, triangular and divergent. Their anterior border is formed by a strong straight bar, the posterior is concave and

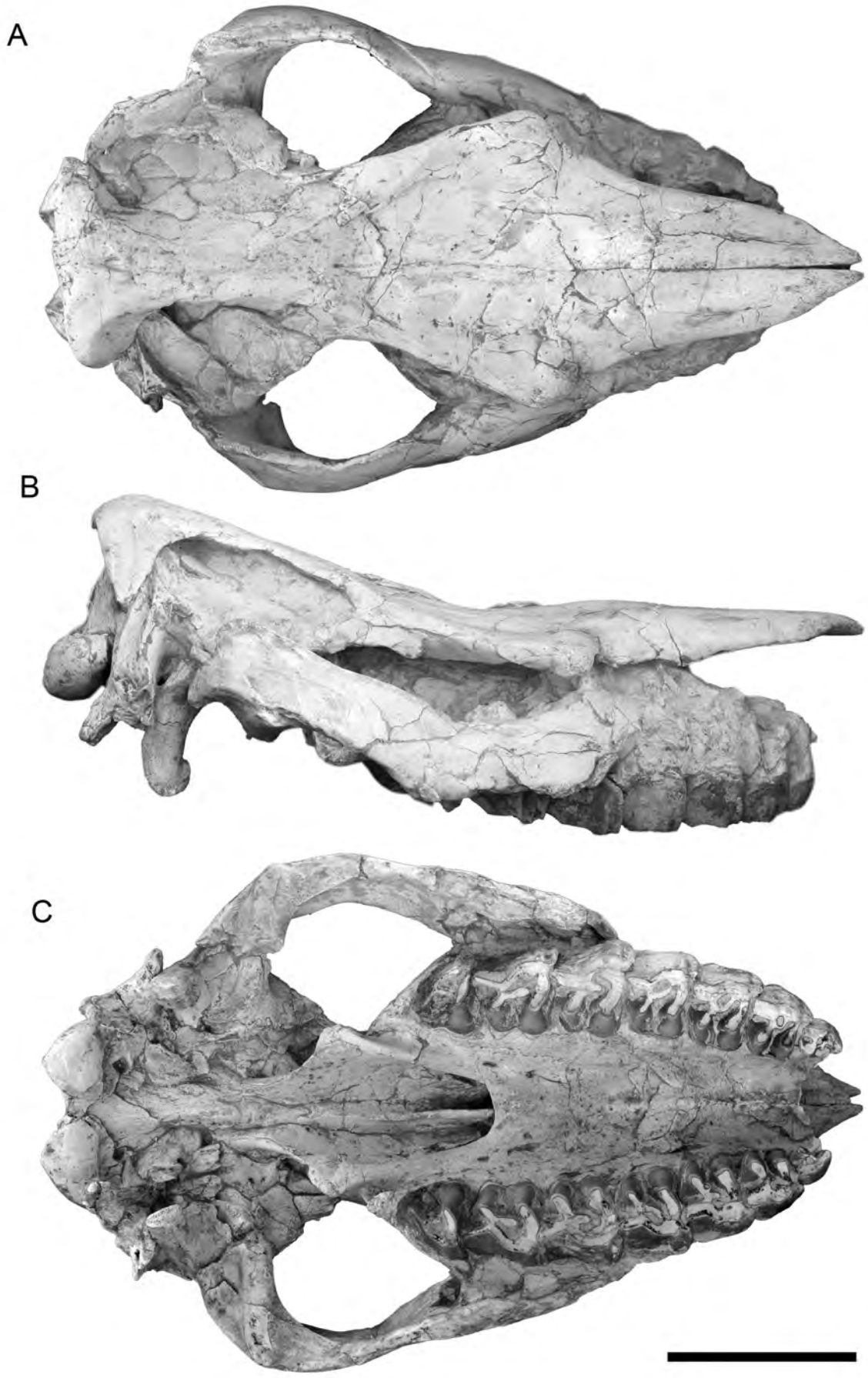


Fig. 2 Skull of *Aceratherium incisivum* BAT-1'05 F5-157 from Batallones-1 (Cerro de los Batallones, Madrid Province, Spain) in A, dorsal; B, lateral right, and C, ventral views. Scale bar represents 100 mm.

thin. The body of sphenoid is a sharp crest on the preesphenoid transforming into a blunt ridge on the basisphenoid, fading out at the level of the auditory meatus. The oval foramina are placed right after the caudal end of the pterigoidean crests. They are irregular and badly preserved. The postglenoid processes are long (~ 60-80 mm from its base) and robust (~ 15-20 mm thick at its midpoint), have a semicircular section and a rostrally projected tip. On its rostromedial base there is a small foramen postglenoideum which continues with a shallow, sinusoidal groove on the rostromedial side of the processus. The hypoglossal foramina are rounded and separated from the articular condyles by a short (~ 10 mm) neck. The posttympanic processes present an irregular lateral surface and are fused with the postglenoid ones, leaving a closed, but short, auditory pseudomeatus. The latter is very wide, deep and limited by the temporal and nuchal crests. The paroccipital process is caudally curved, has a triangular section and sticks out ~ 24 mm from the posttympanic ones. Both share a common base.

Mandible (Figure 3 and Table S2)—the mandible BAT-1'93 2788, described in Cerdeño (1998), has a long and low but considerably thick horizontal ramus. Its lower margin is curved. The premolar series protrudes from the ramus, leaving a height gap in the diastema. The symphysis has a straight upper border and a narrow diastema between both di1 alveoli. The symphyseal region has a constant width, widening at the p1 level. The posterior end, at the p3/p4 boundary, has a narrow and U-shaped valley. A marked alveolar crest departs from the paraconid of the p1 to the outer flange of the i2, fading out near its alveolus. The mental foramen is located at the level of the trigonid of the p3, close to the lower margin of the horizontal ramus. The mandibular angle has a rounded profile and has strong insertion scars as protruding rugosities on its margins, more evident on the distal margin. The ascending ramus is slightly forwards inclined and has parallel anterior and posterior borders. It has a thickened posterior border and a flattened masseteric fossa. The articular condyle is wide and robust. The coronoid apophysis is high, thin, curved inwards and backwards.

Upper dentition (Figure 4 and Table S3)—the DP3 (BAT-6'12 B1-3) has a square outline. The ectoloph is barely undulated. The paracone style is wide and rounded, the parastyle is narrow and anteriorly oriented and the metastyle has a squared posterior end. The protocone is defined by well-marked anterior and posterior folding. The hypocone is rounded and connected to the paracone through a narrow

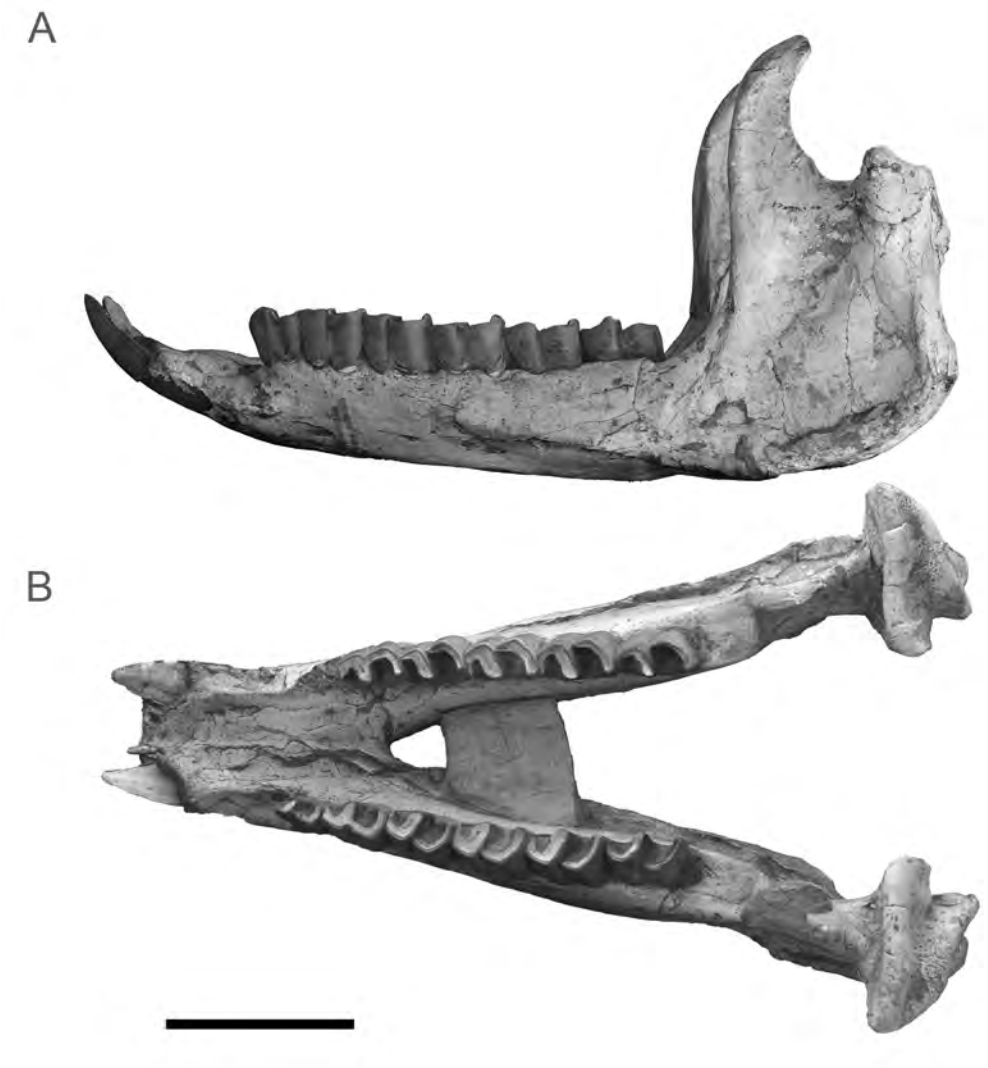


Fig. 3 Mandible of *Aceratherium incisivum* BAT-1'93 2788 from Batallones-1 (Cerro de los Batallones, Madrid Province, Spain) in A, lateral left and B, dorsal views. Scale bar represents 100 mm.

protoloph. The crochet is rounded and short. There are anterior and posterior cingula. Additionally, a small enamel tubercle is present in the entrance of the median valley. Even though the enamel of the ectoloph is much altered, a small labial cingulum is almost probable on its posterior extent. The DP4 is very similar to the DP3. However, the ectoloph is proportionally longer, the paracone style narrower, the entrance of the median valley wider and the crochet is bigger.

The enamel of the adult dentition has been described according to the dental remains from Batallones-5. The enamel of the premolar teeth is smooth (except for the P1, which is slightly wrinkled) and covered by a very thin cementum cover on the ectoloph. The secondary folding is considerably variable, even in the same individual. The P1 is subtriangular in occlusal view, with a maximum width of 21.8 mm (right side) at the metaloph level. It has a convex ectoloph, and a long rectangular parastyle. A tiny enamel projection is present on the lingual side of the parastyle of the left P1. The protoloph is very short, the metaloph is constricted. The hypocone is big and rounded. A thin crochet attached to the anterior side of the hypocone contacts the protoloph, enclosing a rounded medifossete. The lingual cingulum is low and continuous. The anterior valley is 'V'-shaped. The posterior cingulum encloses a 'tear'-like postfossete. The P2 has a subsquare outline. The ectoloph is wide, has a rectangular metastyle outline ad has a zigzagging outline in labial view, with two peaks in the paracone and the metacone. The parastyle is rather long (9.8 mm) and anteriorly oriented, leaving a faint paracone fold. Both crochet and crista are thin. Their contact encircles a rounded mediofossete on the right side, remaining separated in the left one. Protocone and hypocone are attached to the ectoloph through constricted lophs (more evident in the former). The labial cingulum is formed by two separated ridges attached to the anterior and posterior sides of the base of the ectoloph. There is a continuous cingulum along the anterior, labial and posterior sides of the tooth. The postfossette is subtriangular. The ectoloph of the P3 is also zigzagging and shows a big and squared metastyle. However, the parastyle is shorter and more labially-oriented. The secondary folding around the median valley is variable. The crochet is well developed in both sides, being attached to the crista on the right one, thus delimiting an oval mediofossete. On the left row, the crista is almost imperceptible (as a smoothly convex area) and the valley remains open. A second crochet is present in both sides. Once again, while the right metaloph presents a small and pointed secondary crochet, the left side shows a rounded and closed

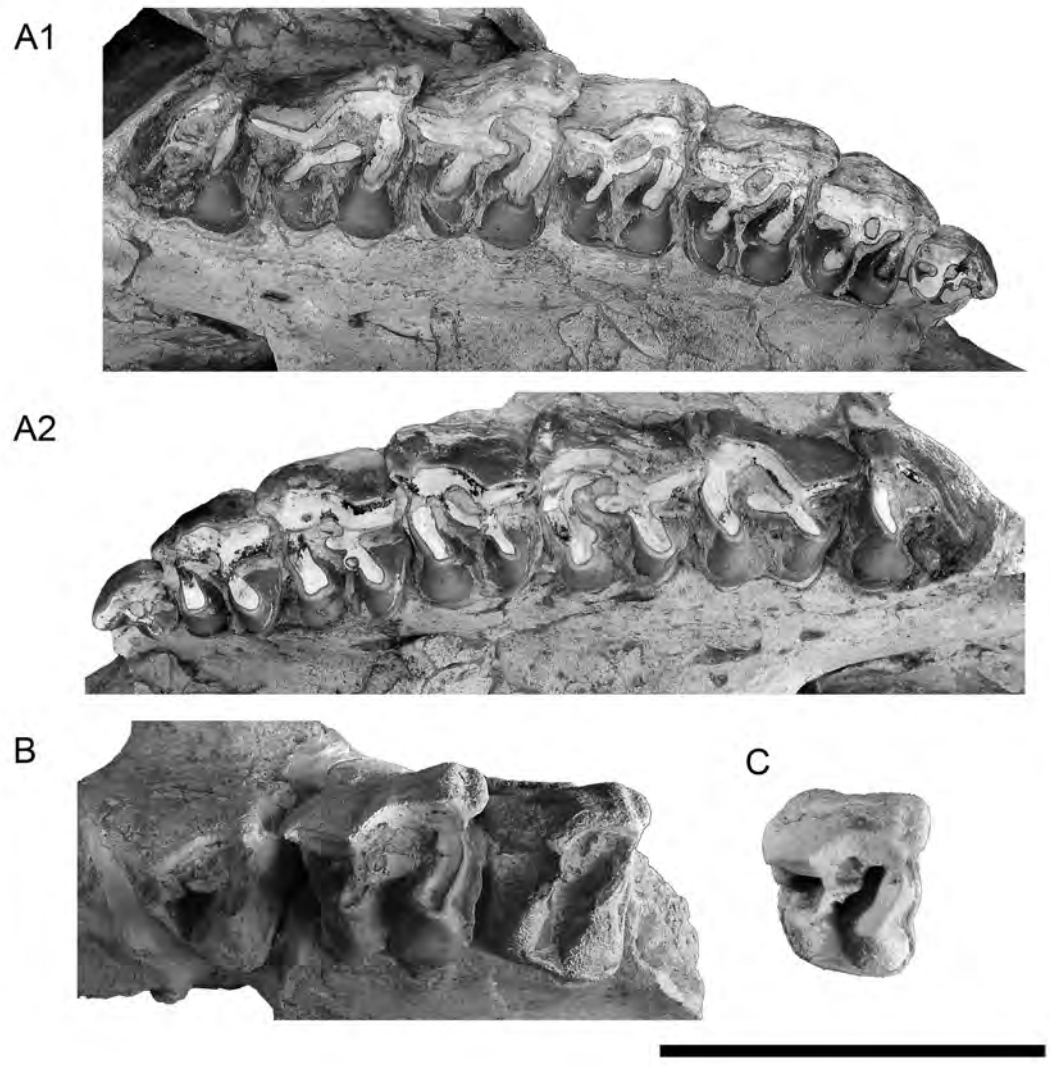


Fig. 4 Upper dentition of *Aceratherium incisivum* from Cerro de los Batallones (Madrid Province, Spain). A1, upper right, and A2, left P1-M3 series of BAT-1'05 F5-157 from Batallones-1; B, upper right series P4-M2 BAT-5'04 H11-21 from Batallones-5; C, right P3 BAT-5'05 w/n from Batallones-5. All teeth are shown in occlusal view. Scale bar represents 100 mm.

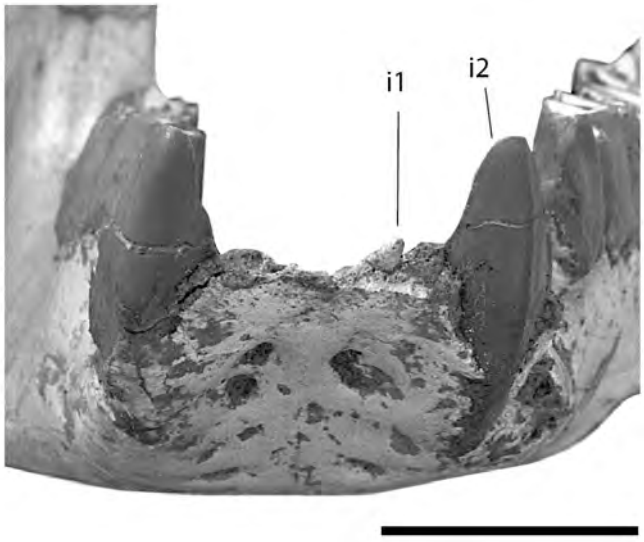


Fig. 5 Left i1 and both i2 of *Aceratherium incisivum* from the mandible BAT-1'93 2788 in cranial view. Specimen from Batallones-1 (Cerro de los Batallones, Madrid Province, Spain). Scale bar represents 50 mm.

valley attached to the metaloph formed by the contact two of these foldings. The protocone has a weak posterior fold. There is a weak and low labial cingulum restricted to the posterior side of the ectoloph. The anterior, labial and posterior cingulum is continuous. An enamel ridge between the lingual cingulum and the base of the hypocone is present at the entrance of the median valley. The P4 is very similar to the P3, but with more rectangular proportions. The ectoloph has a pointed parastyle and a slightly more marked paracone style than in the P3. The metastyle is narrower and more triangular. The main crochet becomes larger and the crista is reduced to a small tip. The mediofossete encircled by crochet and crista is oval and shows a small enamel projection attached to the metacone (pointed on the right side, blunt on the left one). The extra crochets are also small. On the right side, there is a small indentation between them. The protocone fold is deeper than that of the P3. There is a continuous anterior, lingual and posterior cingulum. The short median enamel ridge is attached to the side of the protoloph instead of the hypocone, being weaker on the left side. As in the P3, there is a short and faint posterior labial cingulum. Molar teeth are larger. The M1 has a more squared outline, whereas the M2 presents a typical 'fan'-like outline in occlusal view due to its longer ectoloph. Unlike the premolars, the ectoloph is narrower and the metacone cusp becomes higher and sharper than the paracone (more evident in the M2). The crochet is strong and rounded in the M1. In the M2 is parallel to the ectoloph, strong and longer than the metaloph, leaving a deep median valley. A secondary crochet is present in the paracone. It is faded out as a smooth convex border in the M1 and rounded in the M2. The metaloph is very constricted in the M2. The anterior paracone fold is strong in both teeth. Both teeth have continuous anterior and posterior cingula. There is no labial cingulum. The lingual cingulum is irregular and restricted to the entrance of the median valley and the anterior part of the hypocone pillar. The median enamel ridge continues with the



Fig. 6 Lower left series p2-m3 BAT-1'93 2788 of *Aceratherium incisivum* from Batallones-1 (Cerro de los Batallones, Madrid Province, Spain), in A, occlusal and B, labial views. Scale bars equal 50 mm.

lingual cingulum of the anterior side of the hypocone. The M3 is triangular in occlusal view. Protoloph and ectometaloph are narrow and separated by a shallow gap (probably due to its incipient wear). The paracone fold is smooth, the paracone style and the parastyle blunt. The crochet is long and narrow. There is an anterior cingulum (the posterior one, if present, is not visible). The lingual cingulum is restricted to a short crest in the median valley.

Lower dentition (Figure 5-6 and Table S4)—the adult dentition was described in Cerdeño (1998) according to the subadult mandible BAT-1'93 2788. A small left i1 has been preserved in the mandible BAT-1'93 2788. The tooth is small, chisel-like, blunt and a little divergent from the sagittal plane (and parallel to the i2). The i2 are big, but not fully erupted. They have a blunt tip, triangular section and are outwards curved. Their orientation is slightly divergent from the sagittal plane. The p2 is subtriangular in occlusal view. The ectolophid is elevated and presents a well-defined protoconid ridge along the labial surface of the teeth. The labial surface is flattened and presents a smooth labial groove. A short labial cingulid is present in its base. Its development is variable, in BAT-1'93 2788 is short and faint whereas B-461 shows a strong but short ridge. The p3 and p4 have a narrower anterior half. The labial groove in the p3 is double, enclosing a flattened surface along the labial side of the tooth. In the p4, the labial groove is more evident and occlusaly bifurcated. In all the premolar series, the anterior valley is shallow and V-like and the posterior widened (V-shaped in the p3 and U-shaped in the p4). All p3-m2 present low and rugous labial cingulids (which fade out along the main labial pillars) that extend in the posterior side

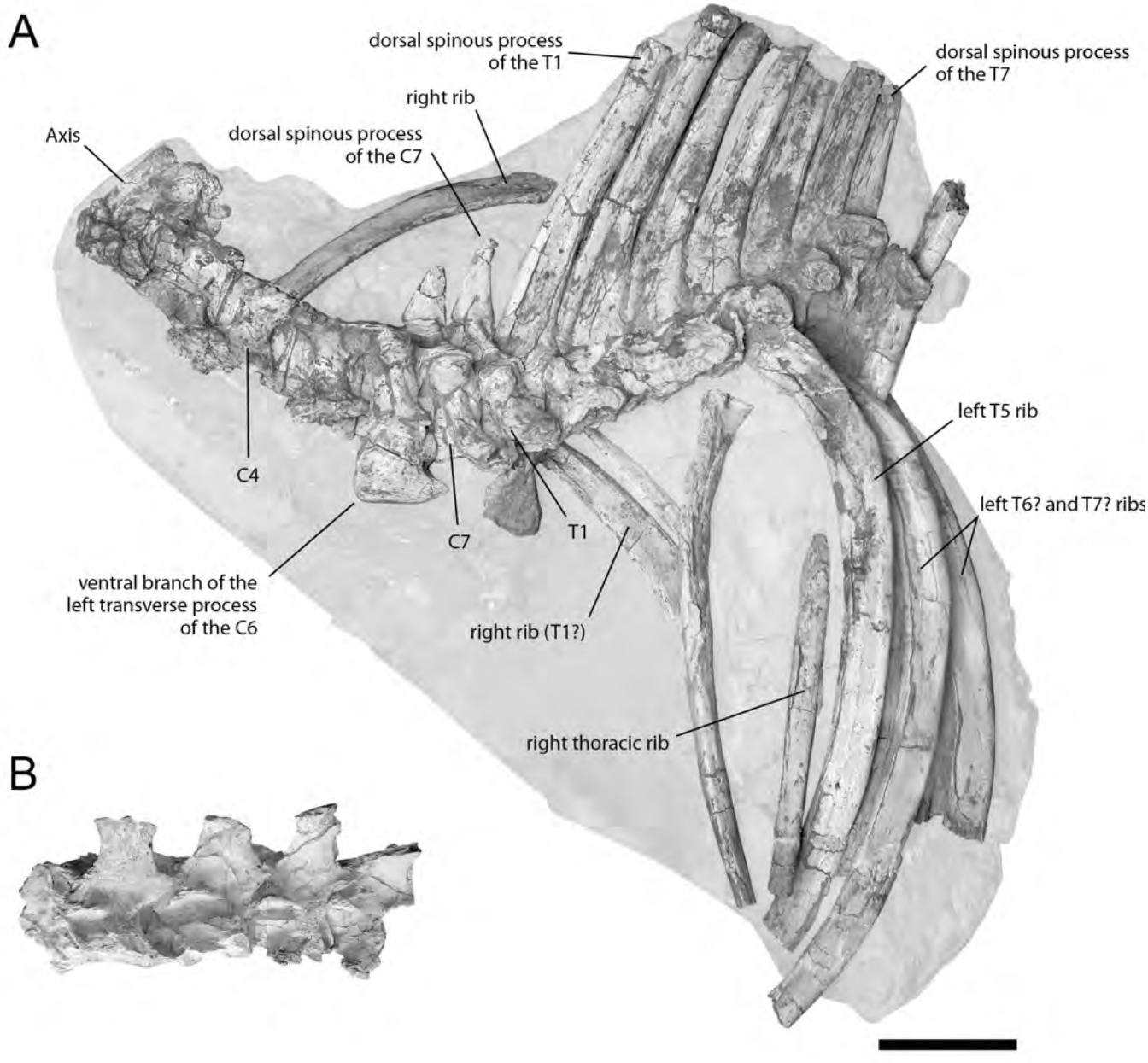


Fig. 7 A, vertebral column and partial rib cage BAT-1'04 E5/E6/F5/F6 of *Aceratherium incisivum* from Batallones-1 (Cerro de los Batallones, Madrid Province, Spain) in left lateral view and B, articulated lumbar series (probably L1-4) BAT-1'04 E5 w/n in left lateral view of the same individual. Sediment of BAT-1'04 E5/E6/F5/F6 has been digitally highlighted for a better contrast. Scale bar equals 100 mm.

of the teeth and short lingual cingulids on the anterior side of the anterior valley. The anterior valley is still V-shaped in the m1 and U-shaped in the m2-3, the posterior is wide and U-shaped. As in the premolar series, metaconid and entoconid have flattened lingual sides.

Axial skeleton and pelvic girdle

Vertebral column (Figure 7)—the vertebral column has been described according the incomplete and partially articulated thoracic cage labeled as BAT-1'04 E5/E6/F5/F6. The cervical and anterior (T1-7) thoracic vertebrae of the individual of *A.incisivum* from Batallones-1 were found in a row oriented towards the skull. Unfortunately, most of the dorsal spines, transversal processes and associated ribs were damaged, preventing most measurement. The remaining vertebral series (four undetermined lumbar and the four sacral vertebrae) were prepared in two additional blocks, the latter attached to the left iliac blade.

Atlas (Figure 8A)—three atlas fragments have been recovered from Batallones-5. However, they consist in very fragmentary remains. The complete atlas from the skeleton of Batallones-1 found in 2004 (BAT-1'04 F5-167) remains, unfortunately, unprepared.

Axis (Figure 8B)—the axis of the *A. incisivum* individual found in anatomical connection in the trap of Batallones-1 is badly damaged and most of its morphology cannot be described. On the other hand, the axis BAT-5'01 33 from Batallones-5 was found isolated and has been used for its description. The odontoid process is stout (APD = 28.7 mm; TD = 26.3 mm) and blunt. Its lower articular surface is delimited by a faint cranial rim and continues to the cranial atlas-facets. The anterior atlas facets are 'tear'-shaped (TD = 60/57 mm; H = 33/34 mm) and convex, with a change of orientation (in the cranially side) restricted to the lateral borders. The vertebral canal is semicircular and wide in cranial view (TD = 34.9 mm; H = 29.5 mm). The latter is topped

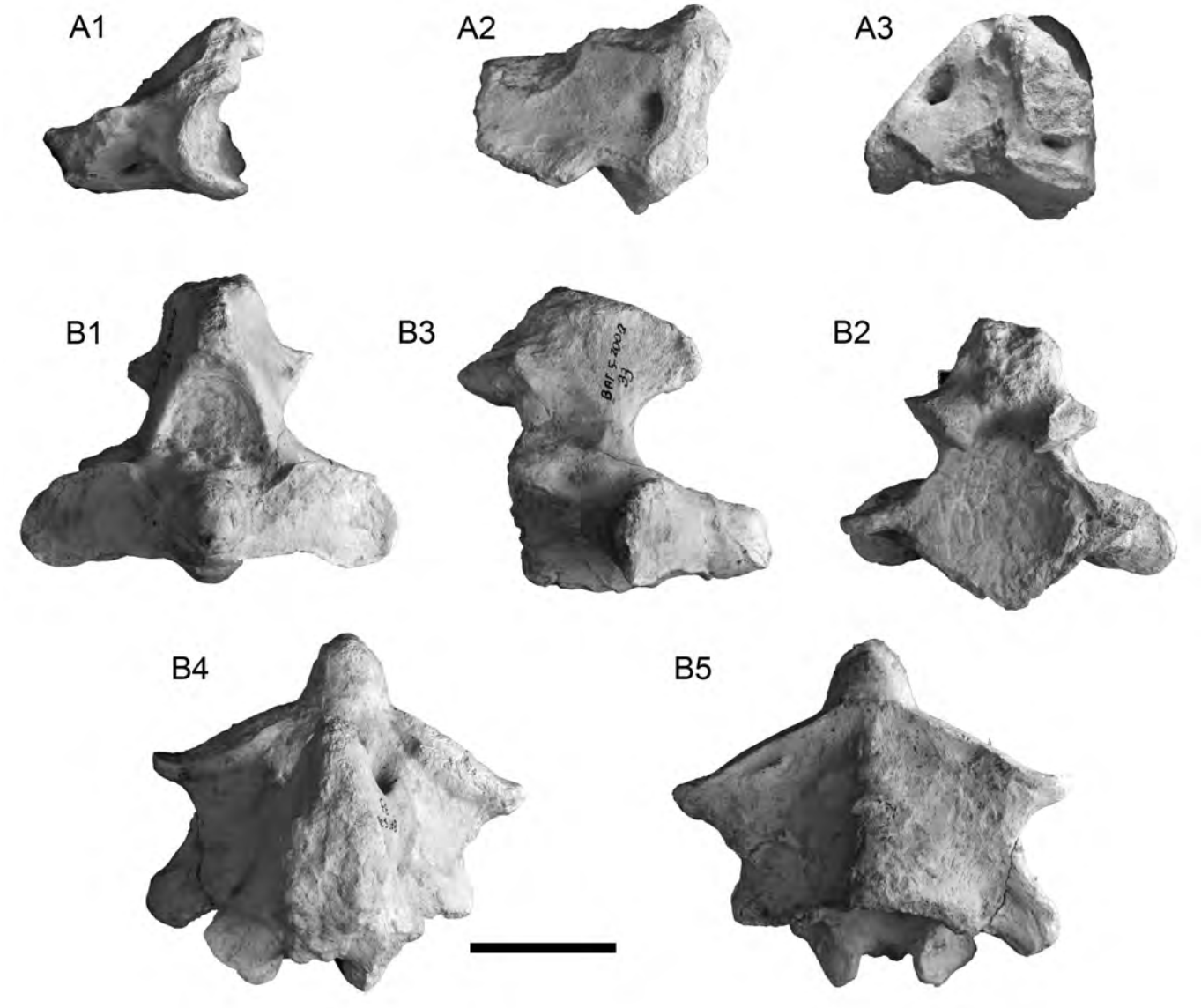


Fig. 8 Cervical vertebrae of *Aceratherium incisivum* from Batallones-5 (Cerro de los Batallones, Madrid Province, Spain). A, atlas BAT-5'10 I4-52 in A1 cranial, A2 proximal, and A3 lateral left views; B, axis BAT-5'01 33 in B1 cranial, B2 lateral right, B3 caudal, B4 proximal and B5 ventral views. Scale bar equals 50 mm.

by the cranial process for the *ligamentum interspinale*. It is cranio-ventrally oriented and triangular. The dorsal surface of the *lamina nuchae* is rough, very robust and wide (APD = 36.7 mm; TD = 77 mm). The articular surface for the main caudal facet is subtriangular (TD = 56 mm; H = 50 mm) and concave. The transverse foramina are small and placed close to the caudal border (APD from the foramina to the caudal border = 19/17 mm). The caudal articular processes protrude from the posterior side of the dorsal spine. They are circular (TD = 28/29 mm), flat, ventro-caudally oriented. The partial axis BAT-5'01 w/n presents equivalent morphology. However, the ventral keel of the odontoid process is smoother, partially due to its erosion.

Remaining cervical vertebrae (Figure 7)—the neck (C2-7) of *A. incisivum* from the individual of Batallones-1 is badly preserved. Except for the C6, none of the 'wing'-like transverse processes of the cervical vertebrae are preserved. The shape of the transverse process of the C6 is 'blade'-like, has a nearly straight ventral border, a broken anterior one, and a blunt caudal tip. The C7 has a reduced transverse process (partially broken in this specimen) and shows a caudal costal facet. The cranial process (which houses the cranial articular facet) is well preserved in most of the cervical series. It looks like as a 'tear'-like protuberance in the C3 and gets slightly smaller and rounder in the successive cervical series, finishing as a somewhat reduced and oval process in the C7 (APD = 30.4 mm; H = 33.4 mm). The vertebral body is somewhat cylindrical and reduces its antero-posterior length caudally (APD C3 = 64 mm; APD C4 = 59.7 mm; APD C5 = 57.9 mm; APD C6 = 58.8 mm; APD C7 = 55.4 mm). The dorsal spines are only preserved in C6 and C7. That of the C6 is triangular (H ~ 62 mm), low and has a blunt apex. In the C7, the dorsal spine is higher (H = 90 mm) and presents a slightly caudally bended tip.

Thoracic vertebrae (Figure 7)—the T1 shows an oval anterior costal facet (APD = 23.4 mm; H = 22.6 mm). The dorsal spinous processes are slightly caudally oriented and very long. However, it is tips are broken and their total length is unknown. As with the cervical vertebrae, their vertebral bodies get shorter as more caudally placed. Their APD's range from the 45.5 mm of the T1 to the approximately 39 mm of the T7. The T5 rib is the only in anatomical position. Like the rest of the ribs preserved, have a broken distal end. The two ribs emerging from the sediment under the T1-2 are clearly broader APD and have a shorter length, pointing to the first pair of right ribs.

Lumbar vertebrae (Figure 7B)—several lumbar vertebrae were found in a single row (BAT-1'05 E5-w/n). The vertebral bodies are 'spool'-like. They lack costal facets. All the flattened lateral 'wing'-like processes are broken. The four spinous processes lack their dorsal borders. Nonetheless, they share concave cranial and caudal borders. Their total length seems short, and the width (APD) narrows in the two caudalmost vertebrae. The anterior cranial articular processes are latero-cranially oriented and show a ridge projecting caudally and running up to the midpoint of the vertebral body (more caudally extended in the second vertebrae of the series). The caudal articular processes are short, caudo-distally oriented, and dorsally placed than the anterior cranial articular processes.

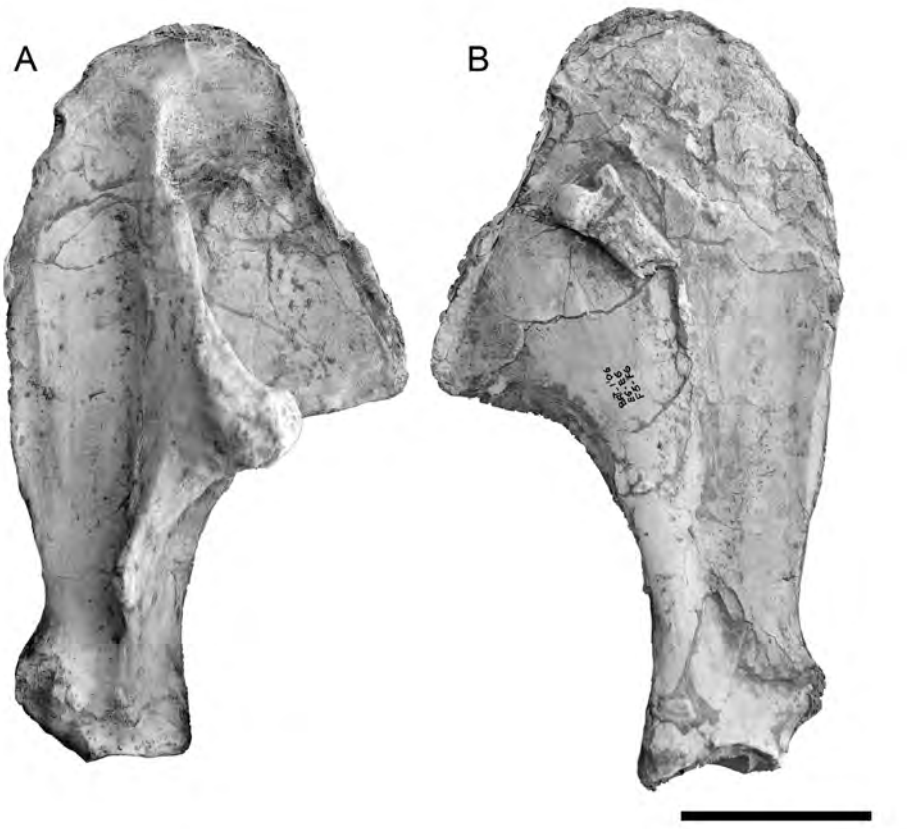


Fig. 9 Left scapula of *Aceratherium incisivum* BAT-1'04 F6-217 from Batallones-1 (Cerro de los Batallones, Madrid Province, Spain) in A, lateral and B, medial views. Scale bar equals 100 mm.



Fig. 10 Articulated left limb of *Aceratherium incisivum* from Batallones-1 (Cerro de los Batallones butte, Madrid Province, Spain) in medial view. See Appendix 2 for a detailed list of the bones included. Scale bar equals 100 mm.

Postcranial Skeleton

Scapula (Figure 9 and Table S5)—description based on the individual BAT-1'04 F6-217 from Batallones-1. The scapula from *A. incisivum* is wide and has a subtriangular, spatulated outline, a convex cranial margin, a nearly straight dorsal one (where the scapular cartilage attaches), and a strongly concave caudal border. The supraspinous fossa is long (~ 305 mm long), flat, and concave. The infraspinous fossa has a 'shark fin' outline (235 mm high; 145 mm wide at its maximum), has a rounded dorsal border, a concave ventral one. Its caudal-most extension (topped with a blunt apex) is distally projected. The glenoid cavity is oval (despite its partially broken borders), concave, and shallow. The supraglenoidean tubercle is big and blunt. It is separated from the glenoid cavity by a concave neck. The spine of the scapula is big and triangular. The caudal border of the scapula dorsal to the supraglenoidean tubercle presents an indentation. The subscapular fossa is flat and smooth. A narrow area of insertion for the *m. serratus* occupies part of the cranial border and is separated from the later by a smooth convexity.

Humerus (Figures 10 and 11A, and Table S6)—the left humerus BAT-1'04 F6-148 is almost complete but slightly cranio-caudally crushed. The humeral head is rounded to 'heart'-shaped (APD = 73.8 mm; TD = 63.1 mm) and flattened (low H). The neck transition of the humeral head is slightly marked as a narrow shelf. As with the proximal epiphysis, the distal one is partially crushed and the original latero-medial dimensions are probably underestimated. An irregular lateral ridge runs from the femoral head to the trochinter. It is concave-convex and thin. The trochinter is pointed (but not overpasses the height of the cranial flange), stout and culminates a well-delimtied lateral pillar which runs along the lateral border. Both almost enclose a rounded gutter (23.6 mm width at its proximal-most side), leaving a narrow space between them (APD = 12 mm). The deltoid tuberosity is very close to the proximal epiphysis. It is not laterally protruding but somewhat caudally folded, blunt, and rugous only on its distal area. The original section of the diaphysis is probably subtriangular. The distal trochlea is very assymetrical (H major lip = 70.4 mm; H minor one = 63 mm) and 'eggcup'-shaped (*sensu* Antoine, 1997). The lateral lip has a flattened surface and an abrupt orientation change separates it from the trochlear groove. In lateral view, the medio-distal epicondyle is restricted to two blunt bumps of equal size separated by a shallow groove 9 mm wide. The latero-distal epicondyle is very short and the lateral relief for the lateral collateral ligament is weak. In caudal view, the fossa olecrani is subtriangular and high (H = 48 mm; TD = 25 mm), partially due to the transversal distortion.

Radius (Figures 11B and Table S7)—the radii and ulnae of *A. incisivum* from Batallones-1 are of modest size. As both have been prepared attached, we have not been able to describe the radio-ulnar facets. In proximal view, the proximal humeral facet of the radius is typically biconcave, has a sinuous caudal border and a bilobed cranial one. The lateral side of the humeral facet is much smaller than the medial one, has an

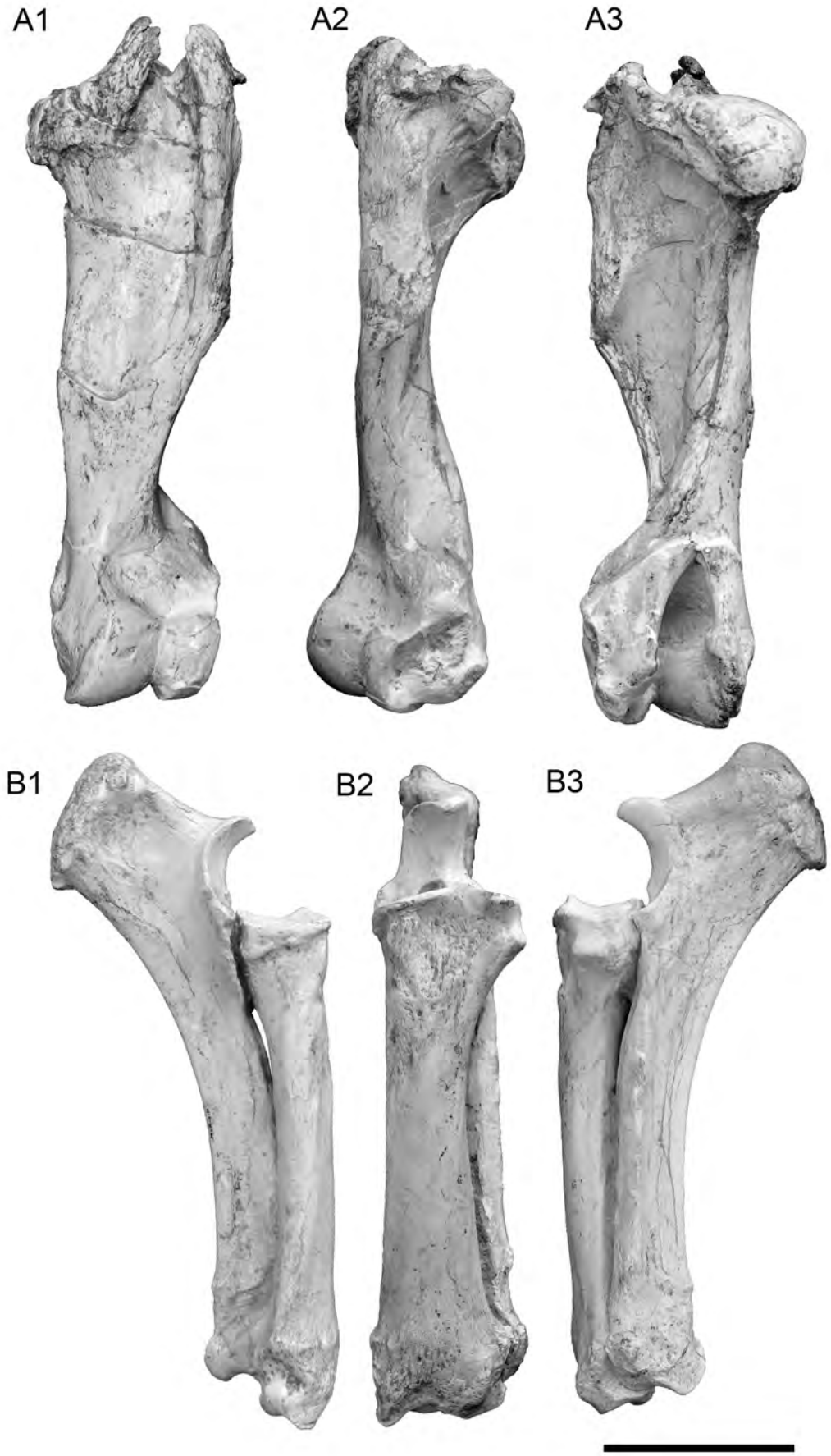


Fig. 11 Anterior limb bones of *Aceratherium incisivum* from Cerro de los Batallones (Madrid Province, Spain). A, left humerus BAT-1'04 F6-148 in A1, cranial, A2, lateral and A3, caudal views; B, left radius (BAT-1'04 F6-149) and ulna (BAT-1'04 F6-150) in B1, lateral, B2, cranial and B3 medial views. Scale bar equals 100 mm.

asymmetrical surface and a sigmoid caudal border. A small protruding rim encircles the cranial border of this articular facet. In cranial view, the cranial insertion for the *m. biceps brachii* is separated from the proximal articular surface by a smoothed space around 8 mm high. The insertion occupies a subtriangular, roughened and carved area (TD = 47 mm; H = 46.8 mm) distal to the proximal surface. In caudal view, only part of the lateral ulnar-facet is accessible in the bone BAT-1'04 F6-149. It is flat and semicircular (TD = 38.1 mm; H = 16.5 mm). In the same view, the lateral border of the proximal epiphysis has a blunt salient distal to the proximal epiphysis. The medial is narrower but not totally visible. The diaphysis has an oval section at the midshaft, becoming 'tear'-shaped towards the distal side due to the sharpening of the lateral border of the shaft. From the midshaft on, the bone slightly widens distally. Both medial and lateral expansions of the distal epiphysis are equivalent in size, as patent in cranial view. The distal articular surface for the scaphoid and semilunate is narrow, has a 'saddle'-shaped surface, and irregular caudal border and a slightly convex cranial one. In caudal view, a semicircular concave expansion spreads over the medio-caudal border of the bone. It is separated by a semicircular gap (TD = 13.1 mm) from the pyramidal-facet. The latter is placed in the lateral extent of the co-distal border of the bone, is semicircular (TD = 21.5 mm; H = 12.2 mm) and slightly concave.

Ulna (Figure 11B and Table S8)—the olecranon is narrow. The angle formed with the caudal border of the diaphysis is smoothly concave. The proximal tip of the olecranon is faintly convex and rugous. The neck of the olecranon has an inflated lateral side (which presents a craniodistally-placed smooth and shallowly depressed area) and a concave medial one. The humeral facet has a typical trilobed outline. The proximal lobe has straight and parallel borders in cranial view and is much wider (TD = 36 mm) than the distal ones. These are asymmetrical and oval. The lateral lobe is shorter and thicker, the medial longer, narrower, and slightly curved. The diaphysis is triangular, has a caudal straight border and a slightly convex cranial one. The contact with the radius starts 110 mm distal to the humeral-facet till the distal epiphysis. The distal epiphysis is narrow The lateral border of the distal epiphysis is rugous and has a 'D'-shaped notch that not reaches the distal articular surface. The distal pyramidal-facet is long, has a 'saddle'-shaped surface, a concave cranial border, a straight lateral, and convex medio-caudal ones.

Scaphoid (Figure 13A and Table S14)—the right scaphoid BAT-1'04 E5-89 is somewhat compressed latero-medially. In proximal view, the radius facet has a 'fan'-like outline, with a convex medial side, an extremely laterally protruding lateral one and raised dorsal and plantar ones (the latter higher). Its surface is 'saddle'-shaped. In lateral view, there are two big semilunate-facets. The dorso-proximal semilunate-facet is oval (APD = 31 mm; H = 12 mm), flat, and latero-dorsally oriented. The dorso-distal semilunate-facet is oval (APD = 23.8 mm; H = 12 mm) and flattened too, but more proximally oriented. Finally, a third contact area for the semilunate is present along the latero-plantar border of the lateral protuberance (with no evident facet associated). In medial view, the bone has rectangular proportions. In the same view, the palmar border is curved and narrow, has a raised proximal border but does not protrude from the distal border of the bone. The rest of the medial side is smooth except for a big, rounded tubercle between the radial and trapezoid facets. The dorsal expansion is low (H = 16.8 mm) and pointed. In distal view, there is an articular complex formed by three distinct articular facets. The magnum facet is more dorsally placed.

Magnum (Figure 13H and Table S17)—in dorsal view, the magnum has a flattened, 'fan'-like dorsal side. In medial view the Mc II facet is somewhat rectangular (APD = 29 mm; H = 16.8 mm) and flat. Its triangular dorsoproximal notch is very small and pointed. In lateral view, the unciform facet forms is dorsally rectangular (TD = 22.7 mm; APD = 13.6 mm), flat, and plantarly-expanded over the dorsal crest of the bone. In medial view, the scaphoid facet is vaguely rectangular (APD = 33.3 mm; TD = 22 mm), dorso-palmarly concave and transversally flat. Its distal boundary is elevated from the volar process through a ridge. In distal view, the Mc III facet is square (TD = 34.6 mm; APD = 37.7 mm) and presents two rounded expansions of similar size. The first, palmarly-projected, is placed on the lateropalmar angle of the facet. The second is laterally-projected and placed on the dorsolateral angle of the facet. Its surface is dorsopalmarly-flat and transversally concave. In lateral view, the proximal crest is semicircular and has an abrupt distal end, defined by a hanging distal border of the unciform-facet. The volar process has an irregular distal border and a distally curved dorsal one, it is robust (TD = 20 mm), has a narrow dorso-proximal edge, and a swollen lateral side.

Semilunate (Figure 13B and Table S15)—In dorsal view, the bone shows a 'T'-like outline. The dorsal surface is high if compared with the height of the radial facet in the same view (H = 28.5/11 mm respectively), cylindrical and blunt. The proximal radial-facet is narrow (short APD) and very convex. In distal view, the unciform-facet is 'tear'-like and very long, almost reaching the palmar end of the volar process (which is straight and 12.3 mm wide). Its surface is flat and is separated from the magnum-facet by means of a curved, sharp ridge. The magnum-facet is narrow (APD = 44.3 mm; TD = 14.6 mm), has a concave surface and runs from 7 mm behind the dorsal border of the bone to its palmar end. The volar process has a profound constriction at its base, especially noticeable on its dorsal edge. Its palmar side is widened (TD = 26 mm) and smooth. In medial view, there are two scaphoid-facets. The dorsal one is medio-palmarly oriented, flat and semicircular (APD = 28.4 mm; H = 13.8 mm). The distal scaphoid-facet is also flat and semicircular (APD = 22.8 mm; H = 14 mm) but more medially oriented. In lateral view, both pyramidal-facets are laterally oriented. The dorsal pyramidal-facet is oval (APD = 18.6 mm; H = 10.9 mm) and flat; the distal semicircular (APD = 17.3 mm; H = 7.6 mm) and attached to the magnum-

facet.

Pyramidal (Figure 13C and Table S16)—The dorsal side of the pyramidal BAT-1'04 E5-90 is flat and 'L'-shaped. In medial view, the proximal semilunate-facet is flat, rectangular, and narrows palmarly. The distal one is 'crescent'-shaped and attached to the distal unciform-facet. In medial view, the latter is concave and presents a more distally projected palmar border. The palmar process is blunt and prominent. The depression left between both facets is narrow. The proximal ulnar-facet is oval to subtriangular, the distal unciform-facet almost quadrangular. In the plantar side, the pyramidal-facet has a 'comma'-like contour, leaving a deep rounded depression on its medial side.

Unciform (Figure 13I and Table S20)—The unciform BAT-1'04 E5-82 is wider than high. The anterior side of the bone is smooth and slightly convex and smooth. The dorso-medial side of the dorsal face is pointed. The lateral tubercle is small, blunt and separated from the pyramidal-facet by a shallow depression. The proximal pyramidal-facet is subtriangular, has a convex dorsal border and straight medial and plantar ones. The semilunate-facet is 'tear'-shaped, proximally wide and flattened. Its distal end is laterally protruding. The volar process is very short, irregular and curved upwards. The lateral Mc IV-facet is wide and spreads over the lateral side of the bone, reaching its distal side.

Pisiform (Figure 13D and Table S21)—The bone has a marked neck (deeper on the proximal side) and a high and flattened volar process, almost straight in proximal view. The ulnar-facet is long, flat and 'D'-shaped. The pyramidal-facet is 'L'-shaped, with a rounder notch on its lateral side. Both dorsal facets comprise a straight angle. The volar process is oval, has rounded proximal and distal borders and a flattened palmar one. Its lateral and medial surfaces are smooth and slightly concave and convex respectively.

Trapezium (Figure 13F and Table S18)—In dorsal view, the scaphoid-facet is probably oval, but partially broken (TD = 15.4 l / r mm). In the same view, the volar process is semicircular, blunt and thin (low TD). In distal view, the trapezoid-facet is rectangular (TD = 24 mm approx l / mm r; H = 8 mm l / mm r), long, dorso-palmarly concave and transversally flat. It has a straight distal border. Attached to its disto-medial border there is a small and flattened 'tear'-shaped facet expansion (TD = 16.6 mm; TD = 8.6 mm), possible place of articulation for the Mc II. However, this is difficult to test based on the complementary facet on the Mc II, as the latter area is eroded.

Trapezoid (Figure 13E and Table S19)—In proximal view, the scaphoid-facet is rectangular (APD = 31.4 mm; TD = 24.1 mm). Its surface is 'saddle'-shaped (i.e. dorso-palmarly concave and transverselly convex). The dorsal surface is convex and smooth, the plantar is narrower (TD = 10 mm), rough, and curved. In lateral view, the magnum-facet is quadrangular (APD = 26.8 mm; H = 23.4 mm), has a plantarly expanded square area, and is flat. In medial view, the medial incision is profound, squared and covers the whole height (H = 10.2 mm) of the medial face of the bone. The distal articular surface has a 'tear'-shaped outline (APD = 31 mm; TD = 20.6 mm). Its surface is dorso-palmarly slightly convex and transversally concave.

Mc II (Figure 13J and Table S29)—The proximal trapezium-facet of the Mc II is semicircular (APD = 35.3 l / 33.9 mm; TD = 20.2 l / 22.3 mm), dorso-plantarly concave and transversally convex. The medial side of the proximal epiphysis stands above the proximal facet, it is narrow and sharp. There is a small and triangular (TD = - / 11.2 mm; H = - / 7.1 mm) trapezium-facet on the planto-medial side of the facet. The dorsal side of the proximal epiphysis is encircled by a swollen area. In lateral view, the Mc III-facet is 'kidney'-shaped (APD = 32.9 l / 33.9 mm; H = 12.9 l / 13.3 mm), flat, has a triangular dorsal expansion on its dorso-proximal angle and a small and blunt plantar one in the same side. The shaft is straight and has an oval section at its midpoint. The lateral insertion for the *m. interossei* is weak and rugous. The left Mc II has a bony ridge dorsally protruding from the dorso-medial angle of the distal epiphysis. This ridge can be explained by a possible pathologic condition or alternatively by a local distortion during diagenesis. The distal tubercles are faint and small, the medial represented as a ridge. The distal articular surface is rounded. On its plantar side, the keel is laterally shifted, leaving two asymmetrical halves of similar depth.

Mc III (Figure 13L and Table S30)—The Mc III BAT-1'04 E5-79 is of mediportal type. Both epiphysis are slightly laterally displaced, the distal also dorso-palmarly crushed. In the proximal epiphysis, the proximal magnum-facet is dorso-palmarly convex, latero-medially concave and has a vaguely triangular outline in dorsal view (TD = 37.7 mm; APD = 36.6 mm). Its dorsal border is convex in this view and has a rounded notch in the palmar angle. The unciform-facet is profound, dorso-palmarly convex and triangular-shaped (APD = 24.1 mm; TD = 18.2 mm). It forms a straight angle with the proximal magnum-facet. The Mc II-facet is small, flat, and tear-shaped (APD = 16 mm; H = 9 mm). The Mc IV-facets of the lateral side of the proximal epiphysis form an obtuse angle. The dorsal Mc IV-facet is triangular (APD = 26.7 mm; H = 16.7 mm), very elongated and flat; the plantar one is 'D'-shaped (H = 23.3 mm; APD = 12.2 mm) and about the same size. The groove between them is narrow and deep, partially due to the preparation of the fossil bone. The diaphysis widens distally, its medial border is practically straight; the lateral displays a sigmoid outline. The insertion for the *m. interossei* is only observable on the lateral side. It narrows distally up to the midshaft. The plantar half of the diaphysis is collapsed. The distal articular facet is asymmetrical and laterally shifted. The laterals and medial keels of the plantar side are sharp. The medial one is not visible in dorsal view.

Mc IV (Figure 13M and Table S31)—In proximal view, the unciform-facet is trapezoidal (APD = 40.7 mm / 38.1 mm; TD = mm 25.3 / 23.4 mm) and nearly flat. In medial view there are two big facets for the Mc III separated by a small gap approximately 6 mm width (right side, 8 mm in the left).

The dorsal Mc III-facet is best preserved on the left side. It is mainly oval (APD = 21.9 mm; H = 12.8 mm) but presents a plantar pointed and narrow expansion 10 mm long. The facet is flat, and attached to the proximal articular surface through its longer border. The plantar Mc III-facet is oval (APD = 12.2 mm / 13.3 mm; H = 19.5 mm / 22.4 mm), flat, contacts the proximal articular surface and is palmarly expanded over a palmar shelf. In lateral view, the proximal epiphysis has a longitudinal gutter dorsally flanked by a laterally projected crest and the palmar shelf for the plantar Mc III-facet. The

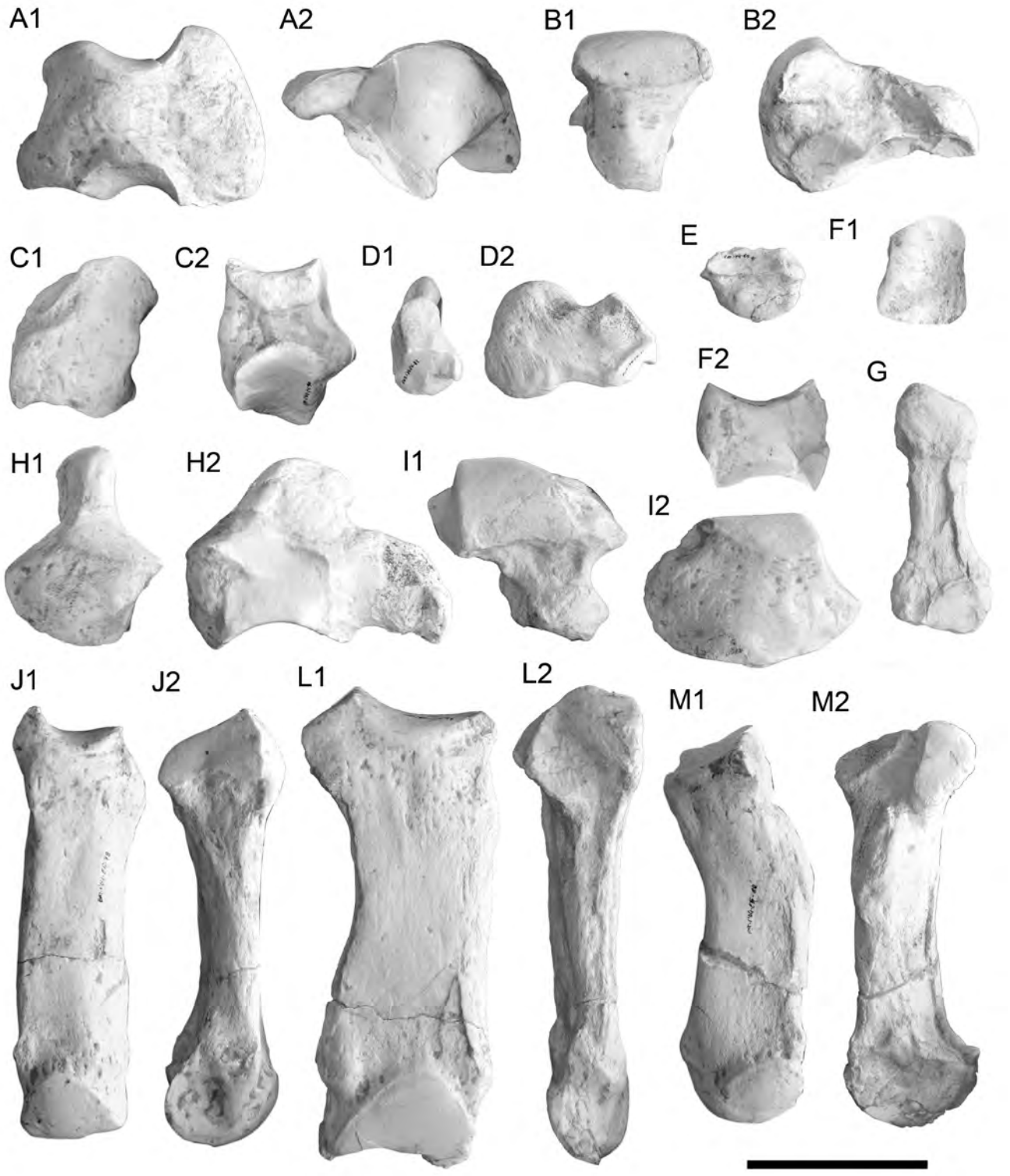


Fig. 12 Carpal and metacarpal bones of *Aceratherium incisivum* from Cerro de los Batallones (Madrid Province, Spain). A, right scaphoid BAT-1'04 E5-89 in A1 lateral and A2 proximal views; B, right lunate BAT-10'12 D6-18 in B1 dorsal and B2 lateral views; C, right pyramidal BAT'1-04 E5-90 in C1 dorsal and C2 medial views; D, right pisiform in D1 dorsal and D2 medial views; E, right trapezium BAT-1'04 E5-91 in distal view; F, right trapezoid BAT'1-04 E5-88 in F1 dorsal and F2 lateral views; G, right Mc V BAT-1'04 E5-91c in dorsal view; H, right magnum BAT-1'04 E5-86 in H1 dorsal and H2 medial views; I, right unciform BAT-1'04 E5-82 in I1 dorsal and I2 lateral views; J, right Mc II BAT-1'04 E5-78 in J1 dorsal and J2 lateral views; K right Mc III BAT-1'04 E5-79 in K1 dorsal and K2 lateral views; L right Mc IV BAT-1'04 E5-80 in L1 dorsal and L2 medial views; M right Mc V BAT-1'04 in M1 proximal and M2 dorsal views. Scale bar equals 50 mm.

medial insertion for the *m. interossei* protrudes from the medial outline of the bone in dorsal view. It is blunt and oval (H = 33.1 mm l; 32.4 mm r; APD = 15.4 mm / 14.8 mm). The diaphysis has an oval section and has very faint *m. extensor carpalis* precluding the distal epiphysis in form of small, short ridges.

Mc V (Figure 12G and Table S32)—In dorsal view, the proximal epiphysis is medially oriented. The proximal unciform-facet is deep (high APD) and oval in proximal view, very convex transversally, and longitudinally flattened. Its posterior edge is distally displaced and vertically oriented. On the medial side, the Mc IV-facet is weak and narrow, attached to the proximal surface. The distal epiphysis is wide, rounded and asymmetrical, with small insertions for the *m. extensor carpalis*.

Pelvis (Figure 13 and Table S9)—The studied pelvic material from Batallones-1 is restricted to a single iliac blade of a left hemipelvis (BAT-1'05 F5 w/n) dorso-ventrally crushed. Ischium and the pubis are lost. Four sacral vertebra have been found associated with the medial side of the blade, attached to the sacropelvic surface. Only the lateral half of the iliac blade is well-preserved. In dorsal view, its cranio-lateral border is rounded, the cranial spinous process of the ilium is triangular (APD = 65.5 mm; H = 63 mm) and flat. The shaft of the ilium (83 mm wide) has a triangular section. The caudal border of the lateral side of the blade is nearly straight.

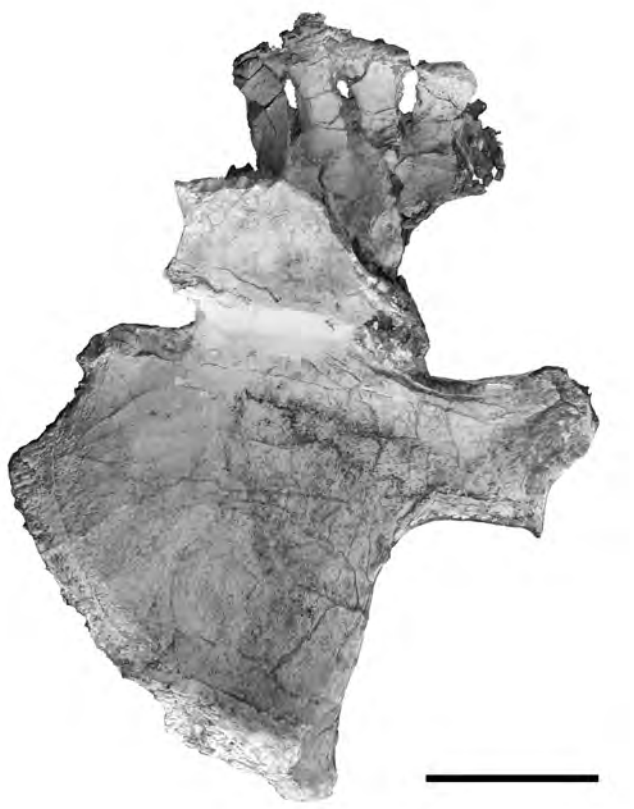


Fig. 13 Sacral vertebrae (S1-4; BAT-1'04 E5-364) and left iliac blade of the pelvis BAT-1'04 E5-365 of *Aceratherium incisivum* from Cerro de los Batallones (Madrid Province, Spain). Sacral vertebrae in lateral left view, ilium in proximal view. Scale bar equals 100 mm.

The acetabulum for the humerus is oval but partially eroded (APD = 65.2 mm; H = 46.3 mm), and has a missing ventral third (including the acetabular notch). Four sacral vertebrae were found in anatomical connection with the left iliac blade. They share short and rectangular dorsal spinous processes and fused vertebral bodies.

Femur (Figure 14A and Table S11)—The femur BAT-1'04 F5-141 (left) is very slender. The femoral head is hemispherical (with a diameter of 69 mm). Its fovea capitis, attached to its medio-caudal angle, is wide, long, and semicircular (W = 15 mm; L = 27.9 mm). In cranial view, the neck of the femoral head is slightly concave and oblique. The greater trochanter is placed at the same level of the femoral head. It is rugous and runs over the lateral side of the bone (APD = 91 mm). Its caudal extent protrudes from the caudal side of the bone as a thick ridge. The rest of the caudal side is flattened up to the distal epiphysis. Both greater trochanter and femoral head contact through a cranial irregular shelf obliquely oriented in proximal view. In lateral view the proximal epiphysis has a vertical, somewhat flattened surface. The third trochanter is damaged. However, it seems to be small (H = 40.2 mm) and not very laterally projected. In cranial view, both proximal and distal sides of the third trochanter are concave. The medial flange is nearly vertical and clearly delimited. The third trochanter together with the medial flange clearly delimits the shaft of the diaphysis, which seems to have a triangular to 'T'-shaped cross section, modified by the overall transversal distortion of the bone. The patellar trochlea is narrow (TD = 48 mm) and has a triangular and marked groove. The lateral condyle is blunt and rounded. The medial condyle is restricted to a 'comma'-like ridge close to the caudal side of the epiphysis.

Patella (Figure 14B and Table S10)—The patella (B-303) is high and has a big and rounded lateral flange. The proximal tip is triangular and rounded, slightly smaller than the lateral flange. The caudal and medial borders are rounded. The femoral facets of the caudal side are very asymmetrical. The medial one is semicircular and concave, the lateral is rhombic, with a blunt proximal border. This facet does not extends on the lateral flange.

Tibia (Figure 14C and Table S12)—The proximal articular surface is crushed and cranially sheared by a fissure. In latero-caudal view, the proximal protuberance for the fibular-facet has a 'tear'-like outline and continues distally narrowing as a short ridge, place of insertion for the inter-tendinous connection with the fibula. The fibular-facet is 'kidney'-like (inferred from the homologous facet on the fibula due to the partially broken lateral side), flat, and distally oriented. In plantar view, the popliteal notch is shallow and transversally collapsed. The diaphysis has a subtriangular section. The lateral border gets sharpener towards the distal epiphysis. The distal fibular surface is rough and triangular (H = 43.5 mm; APD = 52.8 mm). The fibular surface is not well-defined. It is rough, laterally-oriented, vaguely rectangular (APD = 47.1 mm; H = 20 mm), and cranio-caudally flanked by two protruding rugous areas, the cranial more pointed. A narrow

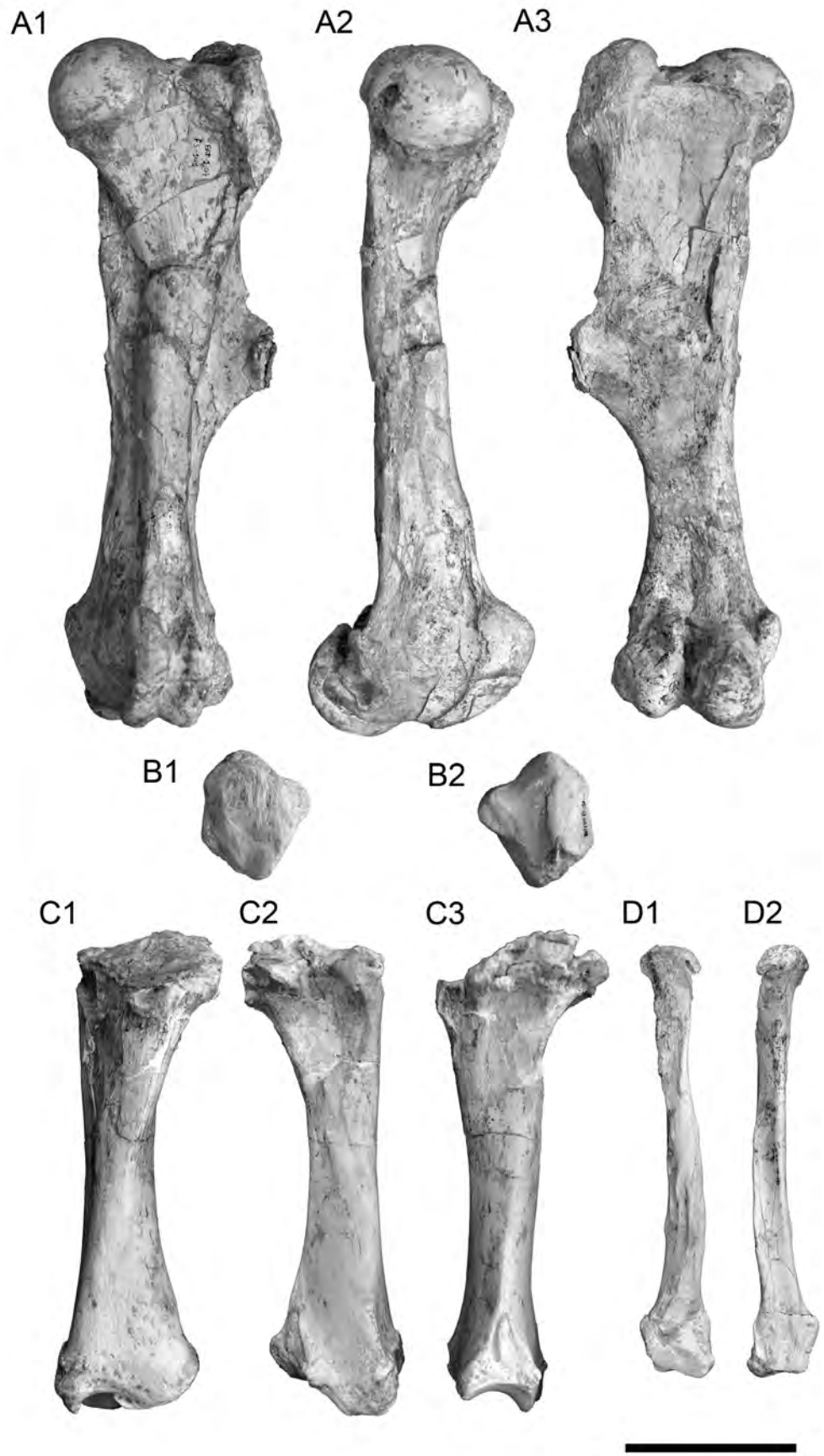


Fig. 14 Posterior limb bones of *Aceratherium incisivum* from Cerro de los Batallones (Madrid Province, Spain). A, left femur BAT-1'04 F5-141 in A1 cranial, A2 medial and A3 caudal views; B, right patella BAT-1'04 F5-158 in B1 cranial and B2 caudal views; C, left tibia BAT-1'04 F5-58 in C1 cranial, C2, caudal, and C3, lateral views; D, left fibula BAT-1'04 F5 w/n in D1 medial and D2 lateral views. Scale bar equals 100 mm.

and flattened semicircular facet (APD = 12 mm; H = 7 mm) for the fibula is present, attached to the distal astragalar border. The distal articular surface for the astragalus has a somewhat trapezoidal to 'hourglass' outline. There is no trace of medial gutter in medial view (character number 243 in Antoine, 2003). In cranial view, the caudal apophysis has a straight distal border, and is slightly more distally projected than the medial malleolus.

Fibula (Figure 14D and Table S13)—A single fibula from Batallones-1 is prepared among the MNCN collections. The proximal epiphysis is flattened and laterally projected. The proximal articular surface for the tibia is 'kidney'-like (APD = 42 mm; H = 13 mm), flat, and partially broken. The shaft of the fibula is curved, twisted, and has a subrectangular section (with a sharply-flattened medial side along the distal two thirds of the shaft). In lateral view, the latero-distal gutter is very well-defined and has a small constriction prior to the contact with the distal articular surface. Next to the distal epiphysis, the bone presents a triangular rugous surface (APD = 32 mm; H = 60.5 mm) where the tendinous contact with the tibia relies. It presents a smoother surface, attached to the medial border of the distal articular facet, which is somewhat 'hourglass'-shaped. A small semicircular facet for the tibia attached to the distal astragalar-facet is the only direct bone to bone facet. It is narrow and flat. The distal astragalar-facet is 'kidney'-shaped (APD = 33 mm; H = 12 mm), flat, and medially oriented.

Astragalus (Figure 15A and Table S22)—In dorsal view, the astragalus shows nearly rectangular proportions. The trochlea is narrow (TD = 51.6 mm) and asymmetrical. The smaller lip has a rounded distal border whereas the greater one has a straight distal one. The neck of the astragalus is high (H = 12 mm on the medial border), narrowing at the level of the medial lip of the trochlea. The lateral lip does not surpass the neck it in dorsal view. On the medial side, the medial tubercle is low, has an inclined dorsal border and is obliquely oriented in medial view. A wide and depressed area separates it from the astragalar trochlea. In plantar view, the first calcaneum facet is big and triangular. Its surface is 'saddle'-shaped, with a concave and nearly quadrangular surface (TDprox = 33 mm; H = 41.3 mm) and a long, semicircular, and somewhat flattened distal expansion (H = 14.3 mm) with a rounded tip. The second calcaneum facet is squared (TD = 23.4 mm; H = 23.8 mm), has a convex surface and is separated from the distal border through a marked furrow. The interosseus groove runs along the plantar side of the bone. It starts as a wide and shallow groove on the medial side of the bone, narrows in a very faint and shallow gutter between the second and third calcaneum facets and widens again towards the lateral side of the bone. The third calcaneum facet is attached to the distal border of the plantar side of the bone. It has a flattened 'leaf'-like outline (TD = 32.4 mm; H = 10 mm). This facet contacts the second calcaneum facet through a small contact point on its proximo-medial angle. In distal view, the outline of the distal navicular-facet is 'fan'-like, dorso-plantarly convex and transversally flat. Both dorsal and plantar borders are parallel and straight. The lateral cuboid-facet is semicircular and slightly dorso-plantarly convex. The contact with the navicular facet is curved and the lateral one (which contacts with the third calcaneum-facet of the plantar side) is straight.

Calcaneus (Figure 15B and Table S23)—The calcaneus has a short tuber. The calcaneal tuberosity is somewhat symmetrical in dorsal view. It presents two depressed areas flanking a wide and blunt central ridge. The calcaneal tuberosity is delimited from the tuber by a blunt ridge that fades out on the plantar side of the tuberosity. The sustentaculum tali is horizontally implanted, is dorsally oriented and has a pointed tip. In dorsal view the sustentaculum forms a nearly straight angle with the body of the calcaneum. Also in dorsal view, the first astragalar facet is circular (TD = 24.8 mm; H = 34.8 mm), presents a rounded distal expansion, has a concave-convex surface in lateral view and flattened in dorsal one. The second astragalar facet, located at the distal side of the sustentaculum is subsquare (TD = 29.3 mm; H = 25.4 mm), and is slightly concave. The third astragalar facet is 'leaf'-shaped (TD = 37.5 mm; H = 9.5 mm), flat and runs along the distal border of the dorsal side of the bone, reaching part of the distal side of the sustentaculum. The interosseous groove forms an 'L' around the lateral and distal sides of the second astragalar facet. The distal cuboid-facet is somewhat 'D'-shaped (TD = 43.9 mm; APD = 20.3 mm), has a straight dorsal border and an irregular plantar one.

Cuboid (Figure 15F and Table S25)—In proximal view, the proximal articular surface is divided in two articular facets. Their boundary is marked by a faint and straight line. The lateral calcaneum-facet is semicircular (APD = 41.4 mm; TD = 16.5 mm), flattened, has a raised plantar side and a semicircular and flattened expansion on the planto-lateral side (which corresponds with the planto-lateral expansion of the distal articular area of the calcaneus). This expansion leaves a narrow space (H = 3.5 mm) with the volar process. The medial astragalar facet of the proximal articular surface is trapezoidal (APD = 36.2 mm; TD = 20.3 mm), flat, and has a pointed and raised palmar angle. In dorsal view, the dorsal face of the cuboid is flattened and squared. The distal border is dorsally projected and the medio-distal angle is medially projected. On the medial side, the dorsal navicular-surface is attached to the proximal border. It is semicircular (APD = 19.5 mm; H = 6.1 mm), dorso-medially oriented, and flat. The plantar navicular-facet is large, flat, proximo-medially oriented, and has a semicircular outline (APD = 17.8 mm; H = 20.9 mm). Both navicular-facets form an obtuse angle in dorsal view and contacts through a single point attached to the proximal surface. The dorsal ectocuneiform-facet is attached to the distal border of the medial side of the bone. It is semicircular (APD = 16.5 mm; H = 7 mm) and flat. The plantar ectocuneiform-facet is attached to the distal border of the plantar navicular-facet. It is small, flat, and subtriangular (APD = 12.8 mm; H = 9 mm). The volar process is very short and blunt. It does not overhang from the distal face of the

bone. In distal view, the Mt IV-facet is 'heart'-shaped (APD = 34 mm; TD = 30.7 mm), has straight medial and dorsal borders, and a concave lateral one. Its surface is slightly dorso-plantarly and transversally concave.

Navicular (Figure 15D and Table S24)—The proximal astragalar-facet of the navicular has a 'fan'-like contour (TD = 35.5 mm; APD = 38.5 mm). Its surface is slightly dorso-palmarly convex and transversally concave. The dorsal side is smooth and curved. In lateral view, the cuboid-facet is divided in two distinct sides connected by a narrow transition. The dorsal one is semicircular (APD = 21.6; H = 7 mm), flat, and attached to the proximal border. The plantar one is 'fan'-shaped (APD = 14.7 mm; H = 21.7 mm), flat, and covers the whole plantar side. The caudal side is irregular and concave. The distal articular surface is divided between three facets with nearly straight boundaries. The ectocuneiform-facet is more dorsally placed, 'kidney'-shaped (APD = 35 mm; TD = 29.3 mm) and slightly transversally convex. The mesocuneiform is placed in the middle of the distal articular complex. It is vaguely 'fan'-shaped (APD = 24 mm; TD = 21.6 mm) and flat. Finally, the entocuneiform-facet is rounded (APD = 14.7 mm) and flat.

Ectocuneiform (Figure 15C and Table S26)—In proximal view, the proximal navicular-facet shows a 'kidney'-like outline (TD = 36 mm; APD = 35.9 mm), dorso-plantarly flat and transversally concave. The dorsal side of the bone is smoothed and shows a longitudinal and blunt ridge. In medial view, the mesocuneiform-facet is very narrow (APD = 23.1 mm; H = 4.5 mm), bilobed and attached to the proximal side of the bone. In the same side, there are two Mt II-facets attached to the distal border. The dorsal Mt II-facet is semicircular (APD = 13.4 mm; H = 8.7 mm) and flat. The plantar Mt II-facet is more plantarly oriented, subtriangular (more asymmetrical than the dorsal one; APD = 11.8; H = 6.9 mm), and flat. In lateral view, two attachment surfaces for the cuboid can be found. The dorsal one is attached to the distal border. It is semicircular (APD = 13.4 mm; H = 7 mm) and flat, the plantar one is eroded. The distal Mt III-facet has an 'L'-shaped contour (TD = 39.3 mm; APD = 33.4 mm) and is flat. Its lateral indentation forms a straight angle.

Mesocuneiform (Figure 15G and Table S27)—In proximal view, the proximal navicular-facet of the mesocuneiform is pentagonal (APD = 24.5; TD = 17.5 mm) and has parallel and straight dorsal, lateral, and plantar borders. Its surface is slightly dorso-plantarly concave and transversally flat. In dorsal view, the dorsal side is narrow and has a pointed disto-lateral angle. In medial view, there is a rounded and clearly delimited tubercle. The planto-medial side of the bone hosts the entocuneiform-facet. It is 'hourglass'-shaped, flat, and contacts both proximal and distal borders. Its plantar side is broken, but seems to be rather long (circa 11 mm according to the equivalent entocuneiform facet). In lateral view, the ectocuneiform-facet is attached to the proximal border. It is very narrow (APD = 21.3 mm; H = 3.6 mm), bilobed, and flat. In distal view, the Mt II-facet is semicircular (APD = 30.6 mm; TD = 14.4 mm), dorso-plantarly flat and transversally convex.

Entocuneiform (Figure 15E and Table S28)—The proximal ectocuneiform-facet is rounded (TD = 17 mm) and flat. Attached to its dorsal border there is a facet for the mesocuneiform. It is triangular, flat and has a small distal expansion. From there on, there is a small and narrow facet for the Mt II aligned with the former. The entocuneiform has a very short volar process. It is squared in dorsal view, has a flattened plantar border and an irregular dorsal one, crossed by an oblique blunt ridge. The lateral flange is dorsally bended.

Mt II (Figure 15H and Table S33)—In proximal view, the mesocuneiform proximal facet is semicircular (APD = 31.9 mm; TD = 20 mm). Its lateral border is straight, the medial convex. It presents a rounded dorso-lateral expansion. Its surface is dorso-palmarly flat and transversally concave. In the plantar side, the entocuneiform-facet is semicircular (TD = 9.1 mm; H = 7.7 mm), flat, and attached to the proximal border. In lateral view, the articular surfaces form two clusters (one dorsal, one plantar) separated by a distance of 7.3 mm. Each cluster has a semicircular and flat ectocuneiform-facet placed proximally and a semicircular and flat Mt III-facet placed distally. The boundaries between both pairs of facets are straight. The dorsal cluster is larger, flattened, and more proximally displaced than the plantar one. The proximal ectocuneiform-facets are larger (APD = 12.8 mm; H = 9.7 mm the dorsal; APD = 9.6 mm; H = 5.8 mm the plantar) than the distal Mt III-facets (APD = 10.6 mm; H = 4.4 mm and APD = 8.4 mm; H = 4.7 mm respectively). The insertion for the lateral *m. interossei* occupies the whole lateral side of the shaft. It is smooth and irregular. In dorsal view, the diaphysis has a faintly concave medial border and a rugous and nearly straight lateral one. The section at its midshaft is oval. In the distal epiphysis, the insertions for the *m. extensor carpalis* are follow a faintly rugous and oblique ridge on the medial side and a protruding bump on the dorso-lateral angle. In dorsal view, the lateral halve of the trochlea is concave, the medial convex. In distal view, the medial halve of the trochlea has a proximal rounded projection.

Mt III (Figure 15I and Table S34)—In proximal view, the ectocuneiform-facet has a 'L'-like contour and a flat surface (with a slightly raised lateral side). The dorsal and medial borders are straight, and the latero-plantar notch forms a straight angle. In medial view, the medial insertions for the Mt II are attached to the proximal border. They are small, narrow, semicircular (dorsal: APD = 11 mm; H = 5 mm; plantar: APD = 10 mm; H = 5 mm), and separated by a gap 6 mm wide. In lateral view, the Mt IV-facets are separated by gap 10 mm wide interrupted a narrow bony bridge. The dorsal Mt IV-facet is placed next to the dorso-proximal borders of the lateral side of the bone. It is subtriangular (APD = 16 mm; H = 11 mm) and flat. The plantar Mt IV-facet is placed on the plantar expansion of the proximal epiphysis. It is small, rounded (APD = 15 mm) and place at a lower level than the dorsal facet. A short ridge protrudes from the plantar side of the dorsal Mt IV-facet. It is sharp and plantarly-oriented. The diaphysis widens distally

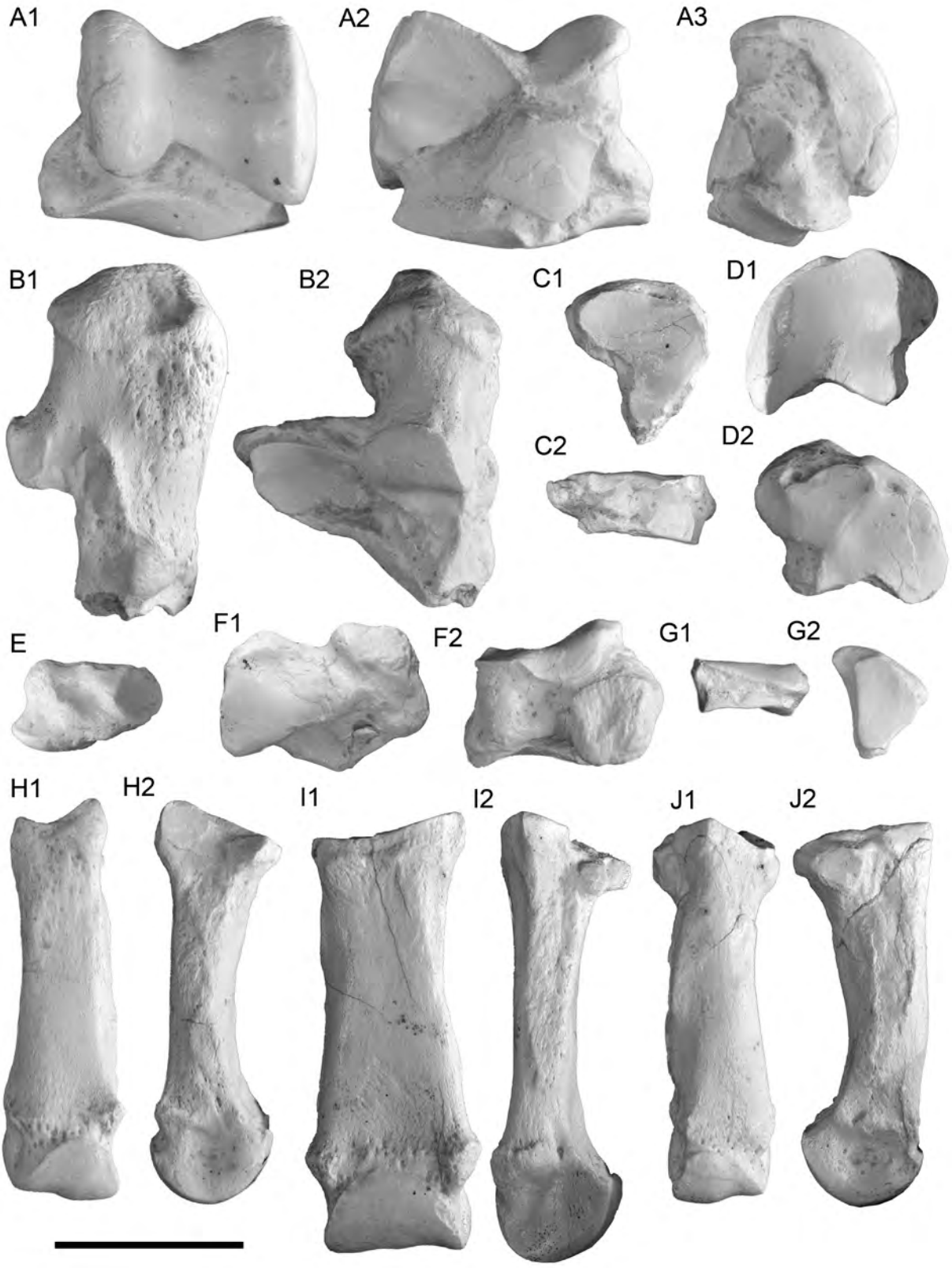


Fig. 15 Tarsal and metatarsal bones of *Aceratherium incisivum* from Batallones-1 (Cerro de los Batallones, Madrid Province, Spain) of the left articulated pes BAT-1'04 F5. A, left astragalus BAT-1'04 F5 w/n in A1 dorsal, A2 plantar, and A3 medial views; B, left calcaneum BAT-1'04 F5 w/n in B1 lateral and B2 dorsal views; C, left ectocuneiform BAT-1'04 F5 w/n in C1, distal, and C2, lateral views; D, left navicular BAT-1'04 F5 w/n in D1, proximal and D2, distal views; E, left entocuneiform BAT-1'04 F5 w/n in E1 dorsal and E2 anterior views; F, left cuboid BAT-1'04 F5 w/n in F1, distal and F2, lateral views; G, left mesocuneiform BAT-1'04 F5 w/n in G1, lateral and G2, proximal views; H, left Mt II BAT-1'04 F5 w/n in H1, dorsal and H2, lateral views; I, left Mt III BAT-1'04 F5 w/n in I1, dorsal and I2, lateral views; J, left Mt IV BAT-1'04 F5 w/n in J1, dorsal and J2, medial views. Scale bar equals 50 mm.

and has a rectangular crossection. The dorsal surface of the shaft is smooth and flattened. The insertions for the *m. intercarpalis* are dissimilar. The lateral insertion starts at the level of the Mt IV-facets, maintains a constant width (APD = 16 mm) covering the lateral side of the bone but does not reach the distal epiphysis, leaving a short smooth gap 15 mm high. The insertions for the *m. interossei* are dorso-laterally projected and triangular in dorsal view.

Mt IV (Figure 15J and Table S35)—The proximal cuboid-facet is 'heart'-shaped, dorso-plantary flat and transversally concave. The medial side of the facet is straight. The medial Mt III-facets are separated by a shallow depression 8.5 mm wide. The dorsal Mt III-facet is attached to the dorso-proximal border of the lateral side. It is semicircular (APD = 15 mm; H = 10 mm) and flat. The plantar Mt III-facet is subtriangular to rounded (APD = 15 mm; H = 11 mm) and flat. The later is placed on a medially projected base separated from the proximal articular surface. The lateral shelf of the proximal epiphysis is short and rounded, and does not encircle the whole lateral side of the cuboid-facet. The diaphysis has a rounded crossection. In dorsal view it has a concave lateral border and medial one appears smoothly undulated and irregular. The medial insertion for the *m. extensor carpalis* is rough and wide (TD = 23 mm) up to the midshaft. From there on, it is restricted to a narrow ridge on the medio-plantar border, reaching the distal epiphysis. As in the Mt II, the insertions for the *m. interossei* are weak and narrow. The medial ones are perpendicular to the major axis of the shaft and straight, the lateral somewhat oblique. The trochlea is clearly asymmetrical: while its dorsal side has a proximally projected medial border, the plantar side shows a rounded expansion on its lateral border.

Phalanges (Figure 16 and 17, and Table S36-38)—Phalanges are described independently by finger according to three parameters depending on their anatomical position: position along the finger (first, second, or third), anterior or posterior limb, and relative position among the manus or pes (i.e. lateral or central). The anterior phalanges have been described according the left articulated limb BAT-1'04 F6, the posterior set according the left articulated limb without field number BAT-1'04 F5 (both from Batallones-1).

First phalanges of the II digits (Figure 16A and 17A, and Table S36)—In proximal view, the outline of the proximal articular surface is 'D'-shaped to rounded. In the Mc II has a faint dorsomedial expansion, making its medial profile nearly straight (curved in the Mt II). In dorsal view, the proximal ridge (place of insertion for the common digital extensor tendon) is well-marked. The Mc II has a blunt bump on its dorso-medial angle (smaller and sharper, almost faded with the proximal ridge in the Mt II). In the dorsal side there is a small expansion of the distal articular facet. In the Mc II this expansion is semicircular to subtriangular (TD = 12 mm; H = 8.6 mm) and asymmetric (oriented to the lateral side). In the Mt II it is nearly symmetrical, small and semicircular (TD = 11.4 mm; H = 8.2 mm). The distal two-thirds of both lateral and medial sides are covered by oval irregular depressions in both Mc II and Mt II. The proximo-plantar/palmar shelf for the two posterior flexor tendons of the digits. These plantar prominences are small and pointed in both digits. Distal to these prominences there is a smoothed, flattened area in the Mc II and a rounded fossa in the Mt II. This may be either a pathologic condition or a individual variation of the smoothed original surface. In distal view, the distal articular surface is slightly latero-medially concave and a roughly trapezoidal outline. The main difference between Mc II and Mt II relies in the medial halve of distal surface. Its dorso-medial corner forms a straight angle in the Mc II, being obtuse in the Mt II. On the other hand, the planto-lateral border of the Mt II is shorter, slightly more curved, and separated from the body of the bone through a marked shelf (smoothed in the Mc II).

First phalanges of the III digits (Figure 16B and 17B, and Table S36)—The proximal articular surface for the Mt III is 'kidney'-shaped and latero-medially concave. The plantar expansions are pointed. The antero-posterior distance of the proximal articular surface is slightly larger on the lateral side (APDmed = 28.2 mm; APDlat = 25.7 mm). The bone has a square dorsal outline. In dorsal view, there are two protuberances for the common digital extensor tendon. They are separated by a flattened rim (approx H = 4.5 mm) from the proximal articular surface. The dorsal expansion of the distal articular surface is not smoothed as in the lateral phalanges. It is rectangular and slightly asymmetrical (TD = 11 mm; Hlat = 5.6 mm; Hmed = 7.6 mm). The plantar prominences are stout and delimit a robust and rectangular shelf with a sharp distal border. This area serves as place of attachment for the sesamoid bone. The lateral and medial depressions are rounded, about the same size, and occupy the distal half of their respective sides. The distal articular surface is semicircular, with a straight plantar border, parallel lateral and medial sides and a convex dorsal one (with a small smoothed indentation in its midpoint).

First phalanges of the IV digits (Figure 16C and 17C, and Table S36)—In proximal view, the proximal articular surface for the IV metapodial is 'D'-shaped to subtriangular in both Mc IV and Mt IV (wider in the Mc IV). This facet is clearly asymmetrical, has a curved medial and dorsal borders and a straighter lateral one. Also in proximal view, the posterior expansions of the proximal facets are more asymmetrical in the Mc IV, being the lateral bigger and wider. Their outline reflects the morphology of the plantar/palmar prominences for the posterior flexor tendons which overhang from the posterior surface. They are more symmetrical in the Mt IV. In dorsal view, the proximal ridge (place of insertion for the common digital extensor tendon) is narrow and marked and, particularly on the dorso-medial angle. A small groove delimits the insertion from the body of the bone. In the middle of the dorsal side, there is a small expansion of the distal articular facet. It is centered, small and subrectangular (TD = 12.1 mm; H = 7 mm) in the Mt IV. Even though this facet is eroded in the Mc IV, seems wider and more centered. The distal two-

thirds of both lateral and medial sides are covered by shallow irregular depressions in both phalanges. The distal articular surface is rounded (Mt II) to oval (Mc II).

First phalanx of the V digit (Figure 16I and Table S12, and Table S36)—The first phalanx of the V digit is readily recognizable by its clear smaller size and narrower proportions (low TD). In proximal view, the proximal articular surface is semicircular and slightly concave. As in the other first phalanges, has two projections on the plantar border plantar, a reflect of the plantar tubercles beneath. The dorsal surface is nearly flat and the lateral and medial relieves smoother than the remaining first set of phalanges (except for a faint ridge medial border of the dorsal side of the bone). The distal articular surface is concave (not flat or convex as other phalanges), 'D'-shaped, and more profound than wide.

Second phalanges of the II digits (Figure 16D and 17D, and Table S12, and Table S37)—Unlike the first lateral phalanges, second phalanges of the *A. incisivum* sample from Batallones-1 are more similar within manus or pes than to the equivalent phalanx of the other limb. The second phalanges of the hindlimb are narrower (lower TD), have a slightly wider dorsal furrow and a nearly straight dorsal border of the distal articular surface in distal view (not concave as in Mc II / IV). In proximal view, the proximal articular facets for the metapodials have a vaguely 'kidney'-shaped (Mc II) to subsquare (Mt II) outline. Both dorso-lateral and planto-medial angles of the proximal surface are somewhat elevated. In dorsal view, the dorsal ridge for the common digital extensor tendon is narrow, flat, but very well defined, and presents a deep furrow running parallel to its distal border (H = 5 mm in the Mt II; H = 4 mm in the Mc II). The dorsal expansion of the distal articular surface is semicircular and separated from the dorsal surface of the bone trhough a short shelf. In the Mc II is wider and more curved. The distal articular surfaces are concave in dorsal view, have a very assymetrical articular surface in distal view (with a palmarly / plantarly projected lateral side).

Second phalanges of the III digits (Figure 16B and 17B, and Table S12, and Table S37)—The bone is low and wide. The proximal articular surface with the first phalanx is semicircular and flattened. Their plantar angles are rounded, the posterior border is straight and the dorsal one slightly convex. This surface is more symmetrical than that of the first phalanx, becoming difficult to identify its side if found isolated. In the dorsal side, the rim for the common digital extensor tendon is flattened, attached to the proximal border, and does not protrude from the dorsal surface. Between this rim and the distal articular surface there is a short, depressed, and vascularized neck (approx H = 4 mm). The plantar reliefs are rectangular, short and symmetrical. The distal articular surface is 'hourglass'-shaped. In this case, the lateral side is slightly bigger than the medial one (APDlat = 21.4 mm; TDlat lip = 18.5 mm; APDmed = 18.3 mm; TDmed lip = 16.25 mm).

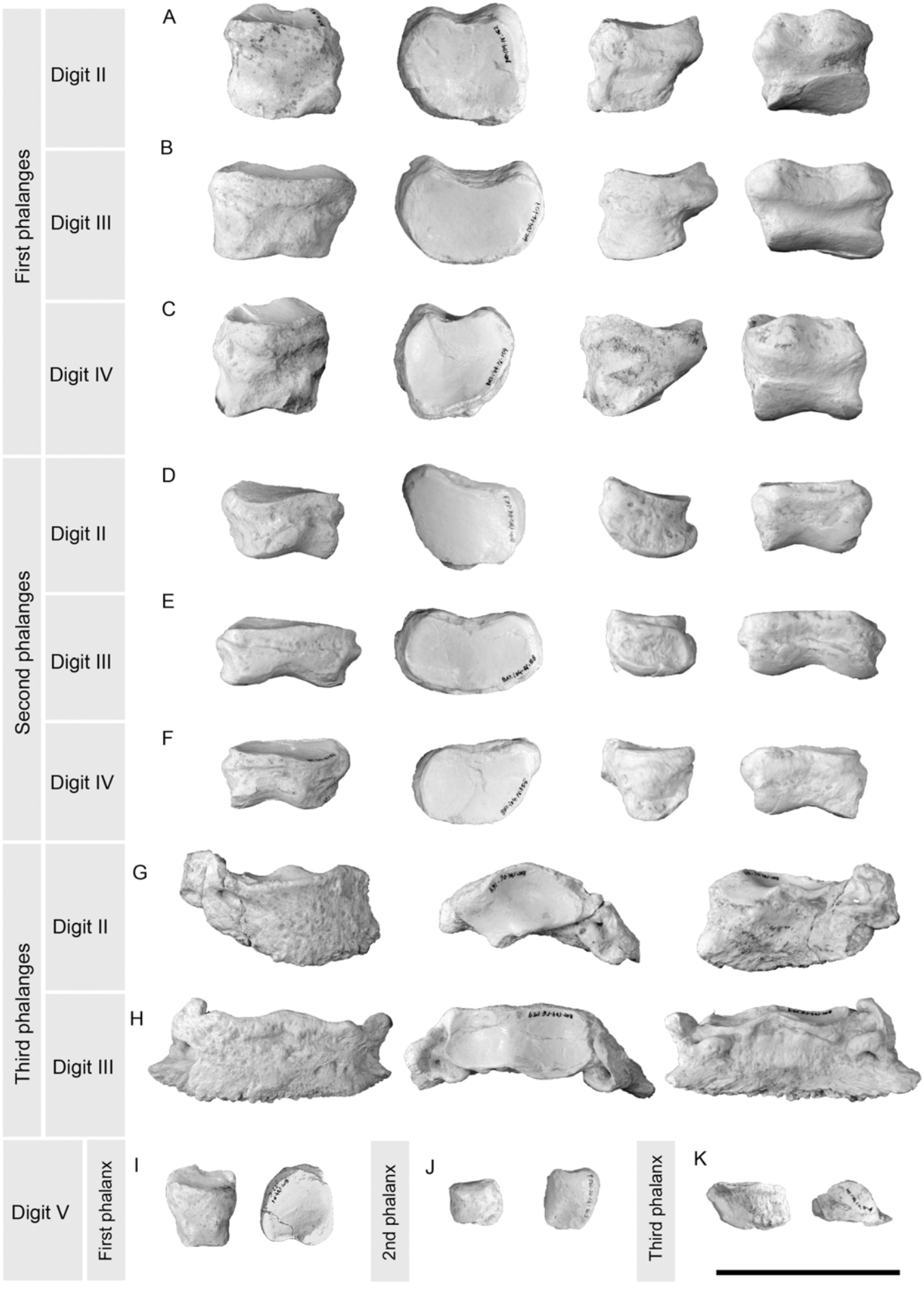
Second phalanges of the IV digits (Figure 16C and 17C, and Table S12, and Table S37)—As in the II digits, the phalanges of the hindlimbs are much wider (higher TD) and lower (low H) than the ones from the IV digit. In proximal view, the proximal articular surface has somewhat 'kidney'-shaped (proximal view) and flat. The planto-medial angle is raised respect the remaining proximal surface. In dorsal view, the proximal ridge for the common digital extensor tendon is well-marked and flat followed by a narrow furrow parallel to its distal edge (H = 2 mm in Mc IV; H = 3 mm in Mt IV). The dorsal articular expansion is semicircular in both cases, but much wider in the Mc II.

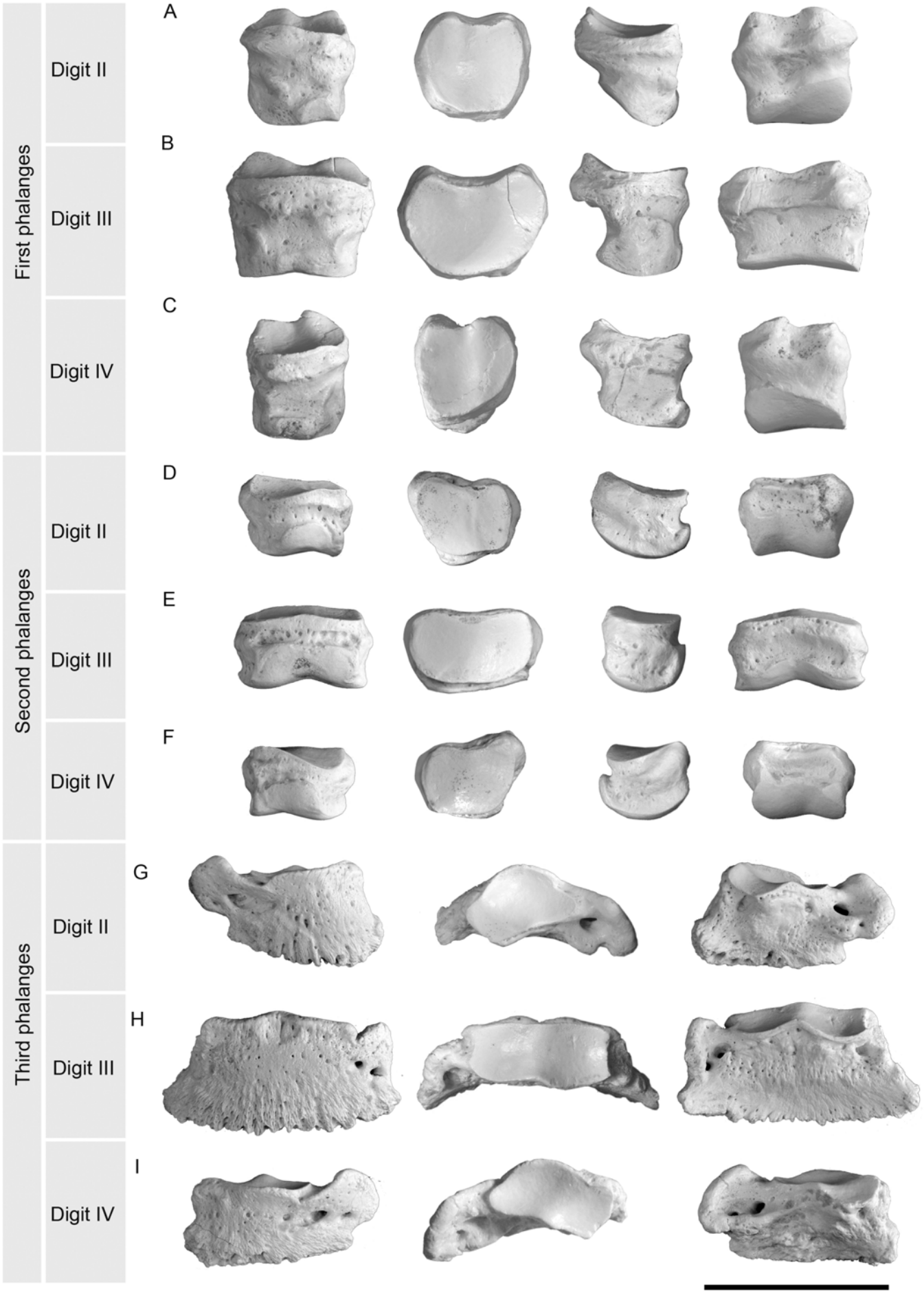
Second phalanx of the V digit (Figure 16J and Table S12, and Table S37)—The second phalanx of the Mc V is cube-shaped. In dorsal view, the proximal articular surface has a 'D'-like outline (more profound than wide). The plantar expansions of this facet are rounded and weak. In dorsal view the dorsal surface is faintly depressed. The dorsal expansion of the distal articular surface is narrow (TD = 10.6 mm l/ H = 5.2 mm l) and flat. In distal view, the distal articular surface is rectangular, transversally convex, and dorso-palmarly flat.

Third phalanges of the III digits (Figure 16H and 17H, and Table S12, and Table S38)—The bone is wide (high TD) and low (short H). The proximal articular surface is rectangular. The dorsal border is straight, the lateral is nearly straight and longer (APDlat = 13 mm) than the medial one, which is slightly concave (APDmed = 8 mm). The plantar border has a straight lateral side, a central inflexion and a slightly convex medial one. The dorsal surface is smoothed and finely vascularized. The striations are restricted to the distal half, and are stronger on the lateral side. Only the medial wing palmar process is

Fig. 16 (next page; p. 341). Phalanges of the left articulated manus BAT-1'04 F6 of *Aceratherium incisivum* from Batallones-1 (Cerro de los Batallones, Madrid Province, Spain). A, BAT-1'04 F6-162, left first anterior phalanx II; B, BAT-1'04 F6-157, left first posterior phalanx III; C, BAT-1'04 F6-154, left first posterior phalanx IV; D, 163, left second posterior phalanx II; E, BAT-1'04 F6-158, left second posterior phalanx III; F, BAT-1'04 F6-155, left second posterior phalanx IV; G, BAT-1'04 F6-164, left third posterior phalanx II; H, BAT-1'04 F6-159, left third posterior phalanx III; I, BAT-1'04 E5-w/n, left third posterior phalanx IV; J, BAT-1'04 F6-154, left first anterior phalanx V; BAT-1'04 F6-152d, left second anterior phalanx V; BAT-1'04 E5-76, right third anterior phalanx V; A, B, D and C figured in dorsal, proximal, lateral, and palmar views; D, E and F figured in dorsal, proximal, medial and palmar views; G-I, figured in dorsal, proximal, and palmar views. Scale bar equals 50 mm.

Fig. 17 (p. 342). Phalanges of the left articulated pes BAT-1'04 E5 of *Aceratherium incisivum* from Batallones-1 (Cerro de los Batallones, Madrid Province, Spain). A, BAT-1'04 E5-w/n, left first posterior phalanx II; B, BAT-1'04 E5-w/n, left first posterior phalanx III; C, BAT-1'04 E5-w/n, left first posterior phalanx IV; D, BAT-1'04 E5-w/n, left second posterior phalanx II; E, BAT-1'04 E5-w/n, left second posterior phalanx III; F, BAT-1'04 E5-w/n, left second posterior phalanx IV; G, BAT-1'04 E5-w/n, left third posterior phalanx II; H, BAT-1'04 E5-w/n, left third posterior phalanx III; I, BAT-1'04 E5-w/n, left third posterior phalanx IV; A, B, D, and E figured in dorsal, proximal, lateral, and plantar views; C and F figured in dorsal, proximal, medial, and plantar views; G-I, figured in dorsal, proximal, and plantar views. Scale bar equals 50 mm.


First phalanges
Digit II
Digit III
Digit IV
Second phalanges
Digit II
Digit III
Digit IV
Third phalanges
Digit II
Digit III
Digit V
First phalanx
2nd phalanx
Third phalanx
A
B
C
D
E
F
G
H
I
J
K


First phalanges
Second phalanges
Third phalanges
Digit II
Digit III
Digit IV
A
B
C
D
E
F
G
H
I

preserved. It is rectangular (L = 16.3 mm) and presents two big foramina in its base. Although the medial wing palmar process is not preserved, their basilar foramina seems to be absent or very weakly developed on the dorsal side (on the plantar side only the bigger one is apparent). The plantar side of the bone is flattened and smooth. The proximal articular surface presents a narrow rim encircling its plantar side distally flanked by a narrow and vascularized groove (approx H = 2 mm).

Third phalanges of the II digits (Figure 16G and 17G, and Table S12, and Table S38)—As with the second phalanges, both third lateral phalanges of the hindlimb share more similarities than with the forelimb ones. The proximal articular surface has a subrectangular outline. Its dorsal border is sinuous, the plantar one is somewhat straight (interrupted by a small notch in the Mc II) and presents a lateral rounded expansion. The dorso-proximal border is convex (straighter in the forelimb). As the IV hindlimb phalanx, the II hindlimb phalanx has a rounded notch in the same border at the level of the dorsal side of the nutritious foramen. Alternatively, the dorsal border of the third phalanx II of the forelimb is straighter and has a more smoothed notch more medially displaced. All the lateral and medial phalanges have similar wing palmar processes restricted to the lateral or medial sides. There are wing-like, semicircular processes, place of attachment for the lateral cartilage. The dorsal side of the bone is finely vascularized and grooved. The medial side of the bone is more convex than in the IV digit. The insertion of the common digital extensor tendon runs along the proximal border of the dorsal side of the bone. It shows a plate-like lateral side and rugous medial border. One (hindlimb) or two (forelimb) main lateral foramina can be found in the dorsal side. In the latter case, the lateral one is rounded and small, the medial is larger and presents a deep groove with a small foramen on its medial extent.

Third posterior phalanges of the IV digits (Figure 16I and 17I, and Table S12, and Table S38)—A single left third lateral phalanx IV of the hindlimb has been prepared. The proximal articular surface has a subrectangular outline. The borders are very similar to those of the hindlimb except for the medial one, which has an obtuse angle. The wing palmar processes are restricted to the lateral side. There are wing-like, semicircular processes, place of attachment for the lateral cartilage. These structures are morphologically similar in all second and fourth fingers. The dorsal side of the bone is finely vascularized and grooved. The medial side of the bone is smoother and higher in the Mt II (H = 29.7 mm) than the Mt IV (H = 25.5 mm). The dorsal side is more flattened in Mt IV. The insertion of the common digital extensor tendon runs along the proximal border of the dorsal side of the bone. It shows a plate-like lateral side and rugous medial border (more developed in the Mt IV). Two main lateral foramina found in the dorsal side. The lateral one is rounded and small (smaller in the Mt IV), the medial is larger and presents a deep groove with a small foramen on its medial extent. This groove is shorter and deeper in the Mt IV.

Third phalanx of the V digit (Figure 16K and Table S12, and Table S38)—A single right third phalanx has been recovered from Batallones-1. In dorsal view, the bone has a rectangular outline, with the medial side swollen. The proximal articular surface is semicircular and flat.

Sesamoid bones—Little attention has been paid to sesamoid bones of rhinoceroses in the literature. A remarkable exception is the exhaustive work describing the osteology of *A. incisivum* from Hövenegg made by Hunermann (1989). In general, forelimb sesamoids are bigger and have wider facets than those from the hindlimb. The metacarpophalangeal sesamoids of the IV digits of both forelimb and hindlimb are short and have sharper proximo-distal borders of the Mc / Mt IV articular surface. On the other hand, sesamoids from the II digits are narrower (lower TD). The metacarpophalangeal sesamoids of the III digit of the hindlimb are big and long. Both proximal and distal tips are rounded and blunt (the former is bigger and rounder). The dorsal articular surfaces with the Mt III are oval, high, have a pointed proximal tip, a straight lateral border and a faintly convex medial one. A thick crest runs along the planto-medial border of the bone. It is smoothed and medially projected (the one from the lateral sesamoid of the Mt III is laterally projected in turn). A single sesamoid complex from the V metacarpophalangeal joint has been found in situ. The bone has a particular bilobed plantar surface (probably as a result of the fusion of both metacarpophalangeal sesamoids) and a flattened and rounded Mc V articulation.

Some interphalangeal sesamoids (placed between the second and third phalanges) have been found. The left II digit of the forelimb interphalangeal sesamoid is very narrow, trapezoidal in dorsal view, and has several foramina in both dorsal and plantar sides. Both proximal and distal sides are straight. The interphalangeal sesamoid for the II digit of the hindlimb is morphologically equivalent. However, it has a more developed lateral projection. The interphalangeal sesamoid of the IV digit of the hindlimb is flattener and has a more semicircular outline, with no lateral projection nor proximo-distally flattened surfaces.The interphalangeal sesamoid of the III digit of the hindlimb is oval, very long and divided into a proximal symmetrical 'roof'-like articular surface and a flattened distal one.

Even though additional sesamoids from Batallones-1 and 5 have been recovered, they have not been described as they have not been found in anatomic connection, making difficult its correct placement.

DISCUSSION

Morphological comparison

The first prepared rhinoceros remains from Batallones-1 were referred to *A. incisivum* (Morales et al., 1992). Posterior studies of a wider sample confirmed this assignation and provided some interesting comparisons with other European localities (Cerdeño and Sánchez, 1998). However, the identity

of these early-collected bones is controversial (except for the mandible BAT-1'93 2788), as they not only show larger proportions that exceed the values recorded in the remaining European samples (a peculiarity already noticed in their original description), but show some distinctive anatomical features. The unearthing of an articulated acerathere skeleton in Batallones-1 (to which the mandible BAT-1'93 2788 belong) has clarified this situation, and we can now assign the large postcranial remains from Batallones-1 to a second partial skeleton scattered through the trap, probably pertaining to a rhinocerotini rhinoceros. A comprehensive study on the rhinocerotini remains from los Batallones butte will shed light on the morphology and taxonomic affinities of the second rhinoceros species found in the trap of Batallones-1. The main morphological differences between both individuals are as follows: the right scapula B791 lacks the triangular caudal expansion typical of acerathere rhinoceros. The left humerus B598-1 is somewhat similar to that figured in Hünermann's monography (p. 28-29; Fig. 10; see next paragraph), but clearly distinct from the in situ humeri find attached to the *A. incisivum* skeleton. Among their differences, B598-1 has a wide and shallow intertubercular groove in the proximal epiphysis (not narrow and deep) and a more robust distal epiphysis in B598-1 (including a wider and more developed lateral epicondyle). As previously noticed by Cerdeño (1998), the scaphoid B w/n lacks the posterior semilunate-facet, relating such character with *Lartetotherium*. The pisiform BAT-1 w/n figured in Cerdeño (1998 Pl. I, Fig 4), determined as a left pisiform of *A. incisivum* results in a right one of the rhinocerotini rhinoceros. Pisiforms of *A. incisivum* from Batallones-1 bear long and constricted necks, oval volar processes in lateral view. The right femur B-221 has an enlarged (high TD) proximal epiphysis, narrowing only from the level of the third trochanter level on (which is quite developed and protrudes from the anterior side). Contrariwise, the femora of *A. incisivum* presents a narrower proximal epiphysis (lower TD), the greater trochanter is shorter and has a blunt lateral edge (not overhanging), a straighter (not oval) lateral border between the greater trochanter and the third trochanter in anterior view, a longer diaphysis, and an horizontally oriented distal epiphysis (not distally inclined). As the tibiae from *A. incisivum* have damaged proximal epiphyseal regions, only the distal ones can be compared. The *A. incisivum* tibia has a more angulous, trapezoidal, and deeper (high APD) distal articular surface in distal view together with a marked caudo-medial flange of the distal epiphysis that protrudes from the bone's outline in the same view. In contrast, of the rhinocerotine species is somewhat rounder and clearly larger. Acerathere affinities can be rapidly discarded in some tarsal bones. For example, the entocuneiform B791(6) has a long and curved volar process, absent in *A. incisivum*. Similarly, the cuboid of *A. incisivum* is lower (low H) and has a short and blunt volar process (long and distally oriented in B791(5), hanging from the distal articular surface). Metatarsal bones share mediportal proportions in both species, but attain larger sizes in the rhinocerotini skeleton. In *A. incisivum* the distal half of these bones are swollen (especially noticeable in the Mt III) and the intermediate relieves stronger and more pointed. Additionally, their proximal epiphyses show some distinctive traits. The proximal view, the proximal articular surface of the Mt III is nearly semicircular in the rhinocerotine rhinoceros, with a shallow plantar indentation. In *A. incisivum*, the dorsal border is straighter and the plantar indentation is deeper and forms a straight angle. The Mt IV is straighter and more slender in the first, gently latero-plantarly curved in *A. incisivum*. The proximal articular surface is 'heart'-shaped in *A. incisivum* (not 'tear'-shaped) and lacks the palmar swollen shelf next to it.

Cranial remains of *A. incisivum* have been described from several European localities (summarized in Fig. 18). The type skulls from Eppelsheim (DIN 1927 and DIN 1930) show a straight skull roof, a small rostrum, poorly developed postorbital and lachrymal processes, a rounded cranial border of the orbits, robust but short (low APD) zygomatic arches, rounded occipital crests, and well-separated postglenoideal and posttympanic processes. The upwards-oriented nasals are shared by most of the *A. incisivum* skulls, from the dorsoventrally pressed F 1954 from Höwenegg to practically undistorted individuals like those from Eppelsheim (DIN 1930) or Charmoille (CM569 NHM Basel; Fig. 18). Upwards-oriented nasal bones are shared with other aceratheriini genera like *Alicornops* (Sanisidro et al., Chapter 7) or *Sanshirhinus* (Deng, 2005). In contrast, the nasal bones from Cerro de los Batallones are straight, slightly ventrally bent at the tip. The latter is pointed and thin (in contrast to the thick tip of Eppelsheim's specimens). The only skulls with somewhat-downwards oriented nasal bones that coincides with that from Batallones-1 are the young juvenile skull IPSCF 16034 from Can Llobateres (which shows a very small nasal bone typical of early developmental stages; Santafé, 1978), and the partially distorted nasal of the skull from Charmoille NHM CM517. Similar horizontally-oriented nasal bones can be found in aceratheres like some species of *Chilotherium* (Chen et al., 2010), *Aphelops* (Prothero, 2005) or *Hoploaceratherium* (Heissig, 2012). However, their morphologies are somewhat distinct (i.e. nasal bones laterally-narrowed from its midpoint in *Hoploaceratherium* or the whole nasal bone smoothly ventrally bended in *Aphelops*) and none of them fits accurately the observed morphology from Batallones-1. Acerathere rhinoceros possess a typical rhombic skull roof in dorsal view and *A. incisivum* is not an exception. The two adult specimens from Eppelsheim share this rhombic skull roof together with a straight dorsal profile in line with the nasal bone if observed in lateral view. On the other hand, some skulls (i.e. CM 569 from Charmoille and F 1954 from Höwenegg) show a smoothly raised neurocraneum. Between these extents, several intermediate morphologies can be observed (CM 517 from Charmoille; IPSCF 16034 from Can Feu, and 1988-ÇY/1 from Yulafli). The skull from Batallones-1 BAT-1'05 F5-157 also presents some particularities in this sense. The skull is dorsoventrally crushed, with a cracking fracture along its

frontal plane, from the caudalmost point of the nasal notch to the occiput. We think that, not only the whole skull would have been originally higher, but the occiput raised too, with an abrupt orientation change of the skull at the level of the postorbital processes. This trait would distinguish the sample from Batallones-1 from other *A. incisivum* individuals except for F 1954 from Höwenegg. The postglenoidean process and the posttympanic-paroccipital processes are separated by a small gap in the type material, defining a nearly-closed auditory meatus (observable in the right side of DIN 1930, not preserved in DIN 1927). This character appears to be rather homogeneous among the European sample, and in some of the specimens (e.g. F 1954) both processes contact each other. The skull BAT-1'05 F5-157 presents a short cranially projected flange on the posttympanic process that contacts the caudal side of the postglenoid one, defining a closed auditory meatus. Despite some variation has been previously observed in other acerathere species (Borsuk-Bialynicka, 1970), we think that the longer and straighter postglenoid process, the somewhat different arrangement of the three processes (resulting in a closed meatus), and the complete basilar fusion of the posttympanic-paroccipital complex (the suture is still visible in DIN 1930) represents a fully distinctive character of the sample from Batallones-1 from other European localities. Despite these differences, all specimens share well-developed parietal crests and robust zygomatic arches with an abrupt dorsal bending placed at the first third of the arch. Well-developed ventrally rugous anterior extents are also common to the studied sample.

In Batallones butte fossiliferous area, the dentition of *A. incisivum* remains found reveals some morphological differences with other European samples. The P3-4 show some unusual secondary folding on the anterior side of the metaloph, resulting in closed small fossetes in the left side, and small pointed salients (secondary crochets) on the right one (which has a somewhat more advanced wear). Premolar cingula of the lingual side are slightly more developed in BAT-

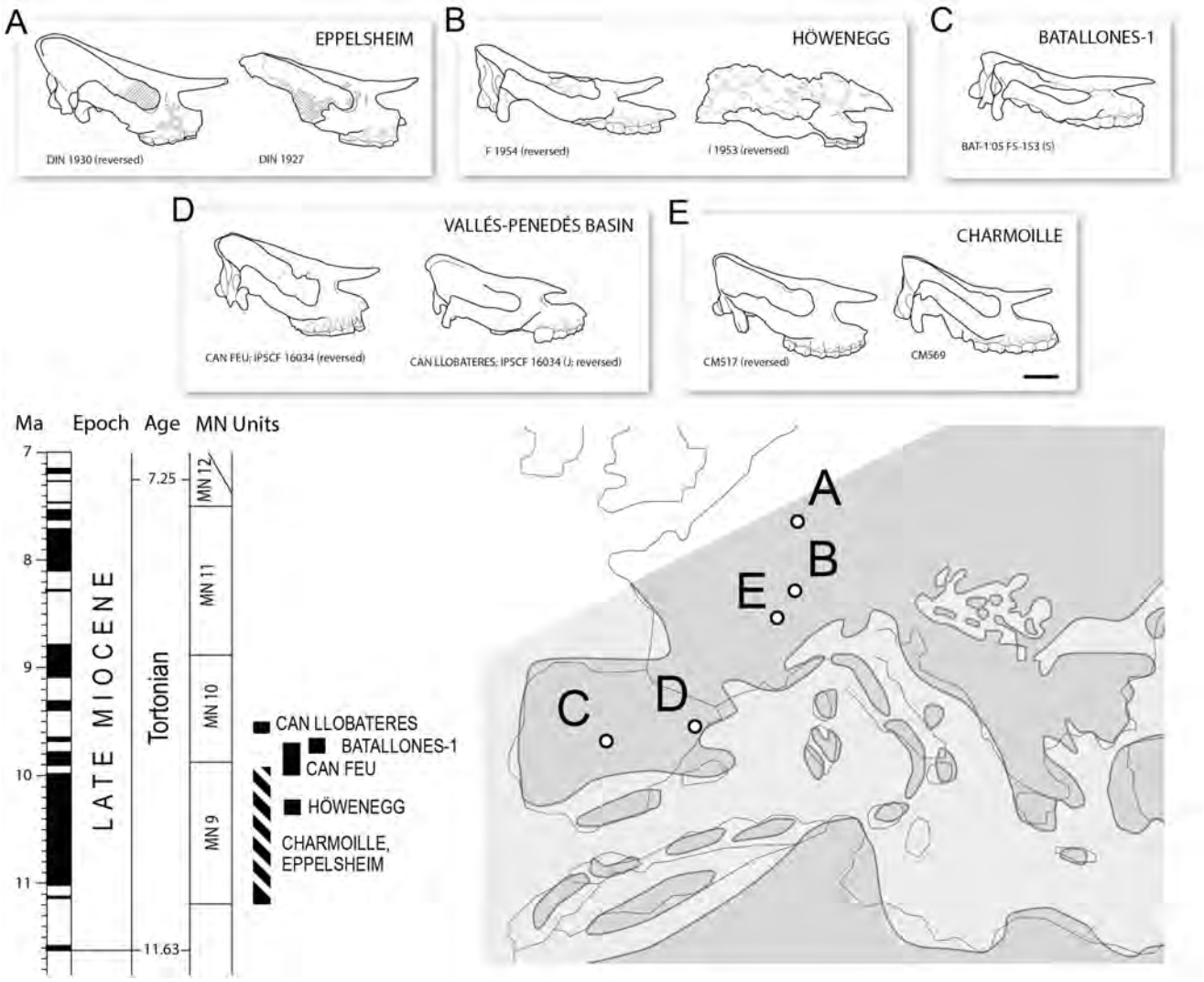


Fig. 18. Palaeobiogeographical distribution of the skulls of *Aceratherium incisivum* used for comparison in the present work. R: reversed specimen; J: juvenile; S: subadult. Black circles represent Palaeogeographic map from the Tortonian redrawn from Rögl (1999). Scale bar equals 50 mm.

1'05 F5-15 than in the Höwenegg's skull F 1957 (which has short ridges at the entrance of the median valleys in contrast to the continuous lingual cingula from Batallones-1). The presence of lingual cingula (of variable development among populations) together with the closure of medifossettes of the premolar series is widespread in the compared sample (even though not preserved in the type series). Only the premolar series from Serrat de Can Feu (P2-P4) shows a lingual bridge between both protocone and hipocone at moderate wear stages. On the M1-2, the borders of the hypocone are even (possibly due to its low wear). However, in DIN 1927, M1-2 hypocone is anteriorly constricted, leaving a rounded antecrochet. In the M1, a posterior constriction is present also (less obvious in the M2). The M3 shows a flattened ectometaloph, in contrast with the convex (nearly rounded) outline of the metaloph of DIN 1927 or F 1954. In the same tooth, the crochet is thin, very long and lingually shifted (short and blunt in DIN 1927). The mentioned increase in the secondary enamel folding can be explained as a result of regional environmental conditions. The not fully-erupted, smaller and more parallel-oriented i2's of BAT-1'93 2788 point to a subadult female. The lower series of Eppelsheim and Batallones-1 have the same cingulid configuration: discontinuous labial cingulids (more developed in p2). The different wear stage prevents further comparisons on the lower series. Despite all these morphological particularities, dental dimensions of the *A. incisivum* sample from los Batallones butte fits well with the known variation of *A. incisivum* (Appendix 3). The upper teeth are slightly bigger (less obvious in the molar series) and relatively longer than most of the European sample, being close to Can Llobateres, Montredon, Can Gonteres, Polinyà and the bigger individuals of Charmoille. However, the P1 are among the biggest recorded for the species, close to the larger specimens of Can Llobateres and Eppelsheim.

The mandible DIN 1928 has a very long horizontal ramus that forms a straight angle with the ascending ramus. The lower profile of the mandible is straight and there is a considerable diastema between the p2 and the i2. In dorsal view, i2 are slightly laterally divergent, the mandibular symphisis reaches the level of the posterior valley of the p2 and the alveolar crests are high and sharp. A tiny i2 is present on the left side of DIN 1928. The anterior morphology of the mandible BAT-1'93 2788 largely matches that of Eppelsheim. Nevertheless, the main differences are restricted to the ascending ramus, which is wider (higher APD), lower (lower H), and slightly anteriorly bended in BAT-1'93 2788. Furthermore, the angular process is lower (low H) the distal notch for the m. digastricus is more anteriorly placed and the condylar process much lower (higher and more slender in DIN 1928).

Only a few postcranial casts of *A. incisivum* from Eppelsheim are available. The astragali from Batallones-1 are morphologically equivalent to the specimen from Eppelsheim AMNH 98042 (cast). However, in dorsal view, the medial process is smoother in the astragali from Batallones butte (angulous in AMNH 98042) and the first calcaneum-facet presents a small latero-distal expansion in the samples from Batallones-1 and 5, absent in Eppelsheim. Finally, the second calcaneum-facet is wider than higher (higher TD) in Batallones, higher in Eppelsheim.

Unlike Eppelsheim's remains, both Höwenegg and Batallones-1 individuals were found articulated. If compared with the skeleton of *A. incisivum* from Höwenegg (Hünnerman, 1989), the studied sample present a considerable number of peculiarities, listed below.

The left distal humeral fragment from Höwenegg is more robust, has a bigger lateral epicondyle and a shorter diaphysis. Both radius and ulna are similar. However, as both bones have been prepared attached, comparisons regarding their articular facets are not possible. The pyramidal from Howenegg is more slender and has a more pointed palmar process. In dorsal view, the unciform from Batallones-1 lacks the straight medio-distal notch of that of Howenegg and shows a blunt and very short volar process (not pointed and straight). The dorsal ridge of the magnum from Howenegg is narrower (lower APD), the volar process is pointer and more distally projected. The pisiform (figured in Fig. 21 of Hunermann's work has a larger articular side, a narrower volar process, a wider neck and a straighter distal profile. The trapezoid (Fig. 20) has a deeper and more squared-shaped medial indentation and narrower dorso-plantar sides, particularly true in the distal half of the distal side of the bone. The oval-shaped and blunt trapezium from Batallones-1 (Fig. 19) is strikingly different from the specimen from Höwenegg, which is much higher and present a pointed tip, and has fused scaphoid and trapezoid-facets. In general, metacarpal bones are more slender in the Batallones-1 sample. The distal expansion of the Mc III-facet in the Mc II is longer, The Mc III has a concave lateral border (somewhat straight in Höwenegg's figured specimen; Hunermann, 1989). In medial view, the proximal Mc III-facet of the Mc IV is placed over the palmar one (the opposite case in the Mc IV from Howenegg). The femur from Batallones-1 BAT-1'04 F5-141 has a bigger proximal humeral head and a higher greater trochanter. The lesser trochanter is longer and has a straighter medial border whereas the third trochanter is narrower (lower H). Tibia and fibula (p. 74-75; Fig. 51; Hünermann, 1989) are equivalent to those found in Batallones-1 but slightly more robust in the case of the tibia (thicker diaphysis). The astragali from both sites are morphologically similar. The only observed differences are a more constricted trochlea in the specimens from Batallones-1 with a deeper distal notch and a more medially shifted distal expansion of the first calcanear-facet. Contrariwise to the astragali, the calcanei from Batallones-1 have a considerably different outline in lateral view: the tuber calcis is rounder (asymmetrical in Höwenegg), the distal border of the beak forms a straight angle. The second astragalar-facet is longer (nearly contacting the first one) and more distally oriented. Finally, the distal portion of the bone is narrower (lower APD). The entocuneiform lacks a clear distal articular surface for the Mt II. The cuboids of both sites are similar, only differing in a lower plantar side of the bone,

including a lower (low H) volar process. The navicular from Eppelsheim has a more rectangular outline and a straighter lateral border, which contrasts with the concave one of the Batallones-1 specimens.The metatarsals of both fossil sites show comparable proportions but more protruding proximal epiphysis (i.e. the proximolateral borders of the Mt II and the Mt III). The more profound proximal surfaces of the sample from Batallones could be related to some distortion during fossilization.

Anatomical reconstruction

The first skeletal reconstruction of the species was assembled according to the nearly complete skeleton found in Höwenegg (Hünnerman, 1989). However, some parts of this skeleton were completed according to a rhinocerotine species (probably a

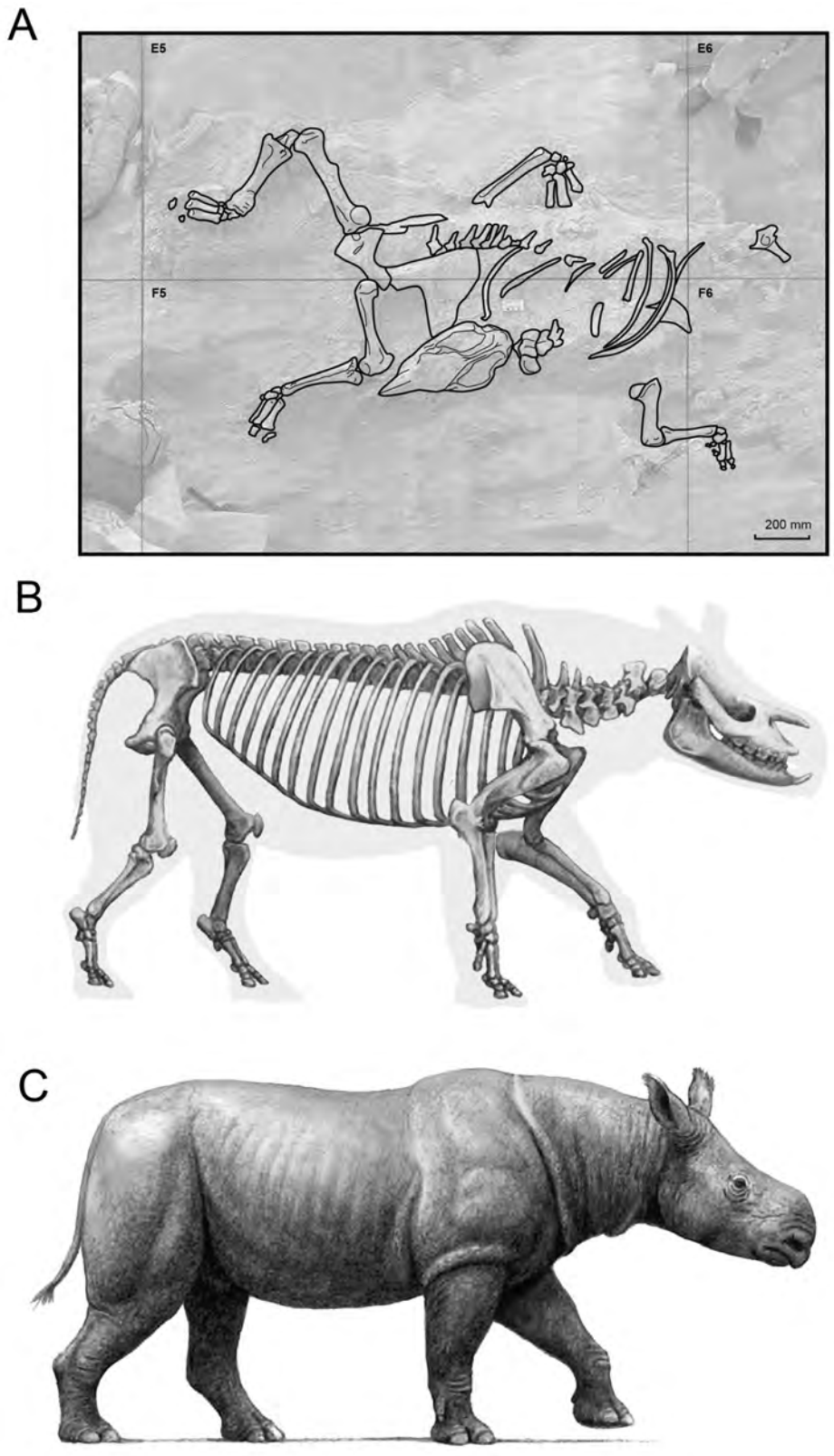


Fig. 19 A, scheme of the subadult skeleton of *Aceratherium incisivum* from the trap of Batallones-1 (Cerro de los Batallones, Madrid Province, Spain) as of 2004. B, reconstructed skeleton and C, life appearance according to the same individual. Artwork by Mauricio Antón, modified according to the skeleton from Batallones-1.

Sumatran rhino, *Dicerorhinus sumatrensis*). Here we present an updated reconstruction using the remains from Los Batallones butte as a reference (Figure 19). The resulting subadult skeleton of *A. incisivum* from Batallones-1 corresponds to an animal about 140 cm in height at the shoulders, a size comparable to the extant Sumatran rhino. Scapulae of *A. incisivum* have a caudally expanded and triangular infraspinous fossa that contrasts with the oval contour and narrower infraspinous fossa of the rhinocerotini (like the scapula reconstructed in Hünnerman's proposal, probably also reconstructed according to the Sumatran rhino; p. 110; Fig. 89). This area houses the origin of the m. infraspinatus (which inserts in the greater tubercle of the humerus) and is greatly developed in both Aceratherini and Teleoceratina and contrasts with the rounded or straight but reduced infraspinous fossa of both Elasmotheriini and Rhinocerotina. This feature, observed in other mammal Families, seen more developed in large, graviportal species (i.e. *Loxodonta, Uintatherium*, or *Brontops*). However, even the smaller acerathere rhinoceroses species (i.e. *Alicornops simorrense* or the dwarf *Peraceras* from the Texas Gulf Coastal Plains) show this feature, so it appear to be a particularity of both Teleoceratina and Aceratherini rhinos. If whether this expansion is a synapomorphy of Rhinocerotini+Aceratherini (Node K according to Becker, 2013) secondarily lost in Rhinocerotina or a convergence between Teleoceratina and Aceratherini remains open. Both Aceratherini and Teleoceratina have been recurrently linked with humid environments.

In conclusion, the nearly complete aceratherini skeleton from Batallones-1 pertains to *A. incisivum*. Isolated remains of the species have been also found in 3, 5 and 6, permitting to outline the species' appearance, as well as to expand the known intraspecific variation for the species.

ACKNOWLEDGEMENTS

We are grateful to P. Pérez Dios (Museo Nacional de Ciencias Naturales), O. Sandrock and E. Milsom (Darmstadt Hessisches Landesmuseum) who granted us access to the museum collections from Batallones and Eppelsheim respectively. We also thank all people who participated in the field campaigns at Cerro de los Batallones. Thanks to P. Gutiérrez, B. Gómez, and E. Cantero for the careful specimen preparation. O.S. acknowledges a predoctoral grant from the Spanish Government MICINN. This study is part of the Spanish Government MICINN research project CGL2008-05813-CO2-01, and is included in the research Group BSCH-UCM 910607.

LITERATURE CITED

Alberdi, M. T., Ginsburg, L., and Morales, J., 1981, Rhinocerotidae del Yacimiento de los Valles de Fuentidueña (Segovia): Estudios Geológicos, v. 37, p. 439-465.

Antoine, P. O., 2002, Phylogénie et évolution des Elasmotheriina: (Mammalia, Rhinocerotidae): Mémoires du Muséum National d'Histoire Naturelle, v. 188, p. 5-350.

Becker, D., Antoine, P. O., and Maridet, O., 2013, A new genus of Rhinocerotidae (Mammalia, Perissodactyla) from the Oligocene of Europe: Journal of Systematic Palaeontology.

Borsuk-Bialynicka, M., 1970, Lower Pliocene Rhinocerotids from Altan Teli, Western Mongolia: Acta Palaeontologica Polonica. Results of the Polish-Mongolian Palaeontological Expeditions - Part II, v. 21, p. 73-92.

Cerdeño, E., 1989, Revisión de la sistemática de los rinocerontes del Neógeno de EspañaPh.D. Dissertation]: Universidad Complutense de Madrid, 429 p.

Cerdeño, E., and Sánchez, B., 1998, *Aceratherium incisivum* (Rhinocerotidae) en el Mioceno superior de Cerro de los Batallones (Madrid): Revista Española de Paleontología, v. 13, no. 1, p. 51-60.

Cuvier, G., 1822, Recherches sur les ossements fossiles., Paris.

Chen, S., Deng, T., Hou, S., Shi, Q., and Pang, L., 2010, Sexual dimorphism in *Chilotherium wimani* (Perissodactyla, Rhinocerotidae) from the late Miocene of the Linxia Basin (Gansu, China): Acta Paleontologica Polonica, v. 55, no. 4, p. 587-597.

Deng, T., Hantac, R., and Jintasakul, P., 2013, A new species of Aceratherium (Rhinocerotidae, Perissodactyla) from the late Miocene of Nakhon Ratchasima, northeastern Thailand: Journal of Vertebrate Paleontology, v. 33, no. 4, p. 977-985.

Domingo, M. S., Domingo, L., Sánchez, I. M., Alberdi, M. T. A., B., and Morales, J., 2011, New insights on the taphonomy of the exceptional mammalian fossil sites of Cerro de los Batallones (Late Miocene, Spain) based on rare earth element geochemistry: Palaios, v. 26, p. 55-65.

Domingo, M. S., M. Teresa Alberdi, Beatriz Azanza, Pablo G. Silva, and Morales, J., 2013, Origin of an Assemblage Massively Dominated by Carnivorans from the Miocene of Spain: Plos ONE, v. 8, no. 5, p. 1-14.

Fernández, D. G., and Cerdeño, E., 1999, Nuevos datos sobre *Aceratherium incisivum* (Rhinocerotidae) del Turoliense de Piera (Barcelona) y Concud (Teruel): Butlletí del Centre d'Estudis de la Natura B-N, v. 4, no. 3, p. 279-289.

Giaourtsakis, I. X., and Heissig, K., On the nomenclatural status of *Aceratherium incisivum* (Rhinocerotidae, Mammalia), *in* Proceedings 5th International Symposium on Eastern Mediterranean Geology, Thessaloniki, Greece, 14-20 April 2004 2004.

Guérin, C., 1980, Les rhinocéros (Mammalia, Perissodactyla) du Miocène terminal au Pléistocène supérieur en Europe occidentale : comparaison avec les espèces actuelles: Documents des Laboratoires de Géologie de Lyon, v. 79,

p. 1-1184.

Heissig, K., 1972, Die obermiozäne Fossil-Lagerstätte Sandelzhausen. 5. Rhinocerotidae (Mammalia), Systematik und Okologie: Mitteilungen der Bayerischen Staatssammlung Paläontologie und historische Geologie, v. 14, p. 37.

-, 1999, 16. Family Rhinocerotidae, *in* Rössner, G. E., and Heissig, K., eds., The Miocene Land Mammals of Europe: Pfeil, Munich, p. 175-188.

Hünnerman, K. A., 1989, Die Narshornskelette (*Aceratherium incisivum* Kaup 1832) aus dem Jungtertiär vom Höwennegg im Hegau (Südwestdeutschland): Andrias, v. 6, p. 117.

Kaup, J. J., 1832, Über *Rhinoceros incisivus* Cuv. und eine neue Art *Rhinoceros schleiermacheri*: Isis, v. 8, no. 1832, p. 898-904.

López-Antoñanzas, R., Peláez-Campomanes, P., Álvarez-Sierra, M. Á., and García-Paredes, I., 2010, New species of *Hispanomys* (Rodentia, Cricetodontinae) from the Upper Miocene of Batallones (Madrid, Spain): Zoological Journal of the Linnean Society, v. 160, p. 725-747.

Mein, P., 1990, Updating of MN zones, *in* Lindsay, E., Fahlbusch, V., and Mein, P., eds., European Neogene Mammal Chronology: New York, Plenum Press, p. 73-90.

-, 1999, European Miocene mammal biochronology, *in* Rössner, G. E., and Hessig, K., eds., The Miocene Land Mammals of Europe: München, Verlag Dr. Friedrich Pfeil, p. 25-38.

Morales, J., Capitán, J., Calvo, J. P., and Sesé, C., 1992, Nuevo yacimiento de vertebrados del Mioceno Superior al Sur de Madrid (Cerro Batallones, Torrejón de Velasco): Geogaceta, v. 12, p. 77-80.

Morales, J., Pozo, M., Silva, P. G., Domingo, M. S., López-Antoñanzas, R., Sierra, M. A. Á., Antón, M., Escorza, C. M., Quiralte, V., Salesa, M. J., Sánchez, I. M., Azanza, B., Calvo, J. P., Carrasco, P., García-Paredes, I., Knoll, F., Fernández, M. H., Ostende, L. v. d. H., Merino, L., Meulen, J. v. d., Montoya, P., Peigné, S., Peláez-Campomanes, P., Sánchez-Marco, Turner, A., Abella, J., Alcalde, G. M., Andrés, M., DeMiguel, D., Cantalapiedra, J. L., Fraile, S., Yelo, B. A. G., Cano, A. R. G., Guerrero, P. L., Pérez, A. O., and Siliceo, G., El sistema de yacimientos de mamíferos miocenos del Cerro de los Batallones, Cuenca de Madrid: estado actual y perspectivas, *in* Proceedings Paleontologica Nova (VI EJIP)2008, Volume 8, p. 41-117.

Peigné, S., Salesa, M. J., Antón, M., and Morales, J., 2005, Ailurid carnivoran mammal *Simocyon* from the late Miocene of Spain and the systematics of the genus: Acta Paleontologica Polonica, v. 50, p. 219-238.

Peigné, S., Salesa, M. J., Antón, M., and Morales, J., 2008, A new amphicyonine (Carnivora: Amphicyonidae) from the Upper Miocene of Batallones-1, Madrid, Spain: Paleontology, v. 51, no. 4, p. 943-965.

Pozo, M., Calvo, J. P., Silva, P. G., Morales, J., Peláez-Campomanes, P., and Nieto, N., 2004, Geología del sistema de yacimientos de mamíferos miocenos del Cerro de los Batallones, Cuenca de Madrid: Geogaceta, v. 35, no. 143-146.

Prothero, D., 2005, The Evolution of North American Rhinoceroses, Cambridge, Cambridge University Press, 218 p.:

Rögl, F., 1999, Mediterranean and Paratethys. Facts and Hypotheses of an Oligocene to Miocene Paleogeography (short overview): Geologica Carpathica, v. 50, no. 4, p. 339-349.

Salesa, M. J., Antón, M., and Morales, J., 2005, Ailurid carnivoran mammal *Simocyon* from the Late Miocene of Spain and implications for the systematics of the genus: Acta Palaeontologica Polonica, v. 50, p. 219-238.

Salesa, M. J., Antón, M., Morales, J., and Peigné, S., 2012, Systematics and phylogeny of the small felines (Carnivora, Felidae) from the Late Miocene of Europe: a new species of Felinae from the Vallesian of Batallones (MN 10, Madrid, Spain): Journal of Systematic Palaeontology, v. 10, no. 1, p. 87-102.

Salesa, M. J., Antón, M., Peigné, S., and Morales, J., 2006a, Evidence of a false thumb in a fossil carnivore clarifies the evolution of pandas: Proceedings of the National Academy of Sciences, v. 103, p. 379-382.

Salesa, M. J., Antón, M., Peigné, S., and Morales, J., 2008, Functional anatomy and biomechanics of the postcranial skeleton of *Simocyon batalleri* (Viret, 1929) (Carnivora, Ailuridae) from the Late Miocene of Spain.: Zoological Journal of the Linnean Society, v. 152, p. 593-621.

Salesa, M. J., Antón, M., Turner, A., and Morales, J., 2006b, Inferred behaviour and ecology of the primitive sabre-toothed cat *Paramachairodus ogygia* (Felidae, Machairodontinae) from the Late Miocene of Spain: Journal of Zoology, v. 268, p. 243-254.

Sánchez, I. M., Domingo, M. S., and Morales, J., 2009, New data on the Moschidae (Mammalia, Ruminantia) from the upper Miocene of Spain (MN 10-MN 11): Journal of Vertebrate Paleontology, v. 29, p. 567-575.

Sánchez, I. M., Quiralte, V., and Morales, J., 2011, Presence of the bovid Austroportax in the upper Miocene fossil site of Batallones-1 (MN 10, Madrid Basin, Spain): Estudios Geológicos, v. 67, no. 2, p. 637-642.

Santafé, J. V., 1978, Revisión de los Rinocerótidos miocénicos del Vallès-Penedès: Acta Geologica Hispanica, v. 13, no. 2, p. 43-45.

Santafé, J. V., and Casanovas-Cladellas, M. L., 1978, Los rinocerótidos de Can Perellada y Can Jofresa (Vallesiense terminal de los alrededores de Terrassa, Barcelona, España): Acta Geologica Hispanica, v. 13, no. 4, p. 105-112.

-, 1983-1984, Elementos del esqueleto postcraneal de *Dicerorhinus schleiermacheri* y *Aceratherium incisivum*

(Perissodactyla, Rhinocerotidae) de la localidad Turoliense de Concud (Teruel): Paleontologia i Evolució, v. 18, p. 95-103.

Santafé, J. V., Casanovas-Cladellas, M. L., and Isidro Llorens, A., 1989-1990, Sobre el nuevo yacimiento de rinocerótidos (*Mammalia, Perissodactyla*) de Serrat de Can Feu (Sant Quirze del Vallès, Barcelona): Paleontologia i Evolució, v. 23, p. 187-198.

Santafé, J. V., and Casanovas, M. L., 1992, Los rinocerótidos (Mammalia, Perissodactyla) de la localidad vallesiense de Polinyá (Barcelona): Treballs del Museu de Geologia de Barcelona, v. 2, p. 45-67.

Tomàs, M., Alba, D. M., Sanisidro, O., Bolet, A., and Checa, L., 2010, Los perisodáctilos del Mioceno Superior de la Autovía Orbital de Barcelona B-40, tramo Olesa de Montserrat - Viladecavalls (Cuenca del Vallès-Penedès): Cidaris, v. 30, p. 317-324.

Villalta, J. F., and Crusafont, M., 1944, Notas para la estratigrafia de la Cuenca del Vallés-Penedés: Las Ciencias, v. 9, no. 1, p. 1-7.

APPENDIX 1

Remains of *Aceratherium incisivum* from los Batallones butte studied in the present work. Localities include Batallones-1, 3, 5, and 6.

Batallones-1

All the studied aceratheriine remains from Batallones-1 pertain to a single subadult specimen, probably a female.

BAT-1'04 F5-157, subadult skull with both P1-M3 series; BAT-1'93 2788, subadult mandible with left p2-m3 and right p3-m3 series; BAT-1'04 F5-167, atlas (associated to the skull according to field references; not prepared); BAT-1'04 E5/E6/F5/F6, large block with cervical (axis and C3-7) and thoracic vertebrae (T1-7) together with scattered ribs; BAT-1'04 E5-362; BAT-1'04 E5-371, BAT-1'04 F5-166, incomplete ribcage (not prepared); BAT-1'04 E5 w/n, associated lumbar vertebrae (probably L1-4); BAT-1'04 E5-364, sacrum associated with a left hemipelvis BAT-1'04 E5-365.

T-1'04 F6-217, left scapula; BAT-1'04 F6-148, left humerus; BAT-1'04 F6-149, left radius; BAT-1'04 F6-150, left ulna; BAT-1'04 F6-151a, left magnum; BAT-1'04 F6-151b, left scaphoid; BAT-1'04 F6-151c, left lunate; BAT-1'04 F6-151d, left pyramidal; BAT-1'04 F6-151e, left unciform; BAT-1'04 F6-151f, left pisiform; BAT-1'04 F6-151g, left trapezium; BAT-1'04 F6-151h, left trapezoid; BAT-1'04 F6-151i, left Mc II; BAT-1'04 F6-153, left Mc III; BAT-1'04 F6-152, left Mc IV; BAT-1'04 F6-152b, left Mc V; BAT-1'04 F6-162, left first anterior phalanx II; BAT-1'04 F6-163, left second anterior phalanx II; BAT-1'04 F6-164, left third anterior phalanx II; BAT-1'04 F6-157, left first anterior phalanx III; BAT-1'04 F6-158, left second anterior phalanx III; BAT-1'04 F6-159, left third anterior phalanx III; BAT-1'04 F6-154, left first anterior phalanx IV; BAT-1'04 F6-155, left second anterior phalanx IV; BAT-1'04 F6-152b, left first anterior phalanx V; BAT-1'04 F6-152d, left second anterior phalanx V; BAT-1'04 F6-162b, left interphalangeal sesamoid II of the forelimb; BAT-1'04 F6-152f, left metacarpophalangeal sesamoid II (lateral) of the forelimb; BAT-1'04 F6-152g, left metacarpophalangeal sesamoid II (medial) of the forelimb; BAT-1'04 F6-158b, left interphalangeal sesamoid III of the forelimb; BAT-1'04 F6-153b, left metacarpophalangeal sesamoid III (lateral) of the forelimb; BAT-1'04 F6-153c, left metacarpophalangeal sesamoid III (medial) of the forelimb; BAT-1'04 F6-160, left metacarpophalangeal sesamoid IV (lateral) of the forelimb; BAT-1'04 F6-161, left metacarpophalangeal sesamoid IV (medial) of the forelimb; BAT-1'04 F6-152e, left metacarpophalangeal sesamoid complex V of the forelimb.

The right anterior limb is proximally affected by a fissure, which has sharpened the edges of part of the proximal epiphyses of the humerus, radius and ulna. It comprises the following elements: BAT-1'04 E5-361, right scapula; BAT-1'04 E5-83, right humerus; BAT-1'04 E5-84, right radius; BAT-1'04 E5-84, right ulna; BAT-1'04 E5-86, right magnum; BAT-1'04 E5-89, right scaphoid; BAT-1'04 E5-81, right lunate; BAT-1'04 E5-90, right pyramidal; BAT-1'04 E5-82, right unciform; BAT-1'04 E5-87, right pisiform; BAT-1'04 E5-91, right trapezium; BAT-1'04 E5-88, right trapezoid; BAT-1'04 E5-78, right Mc II; BAT-1'04 E5-79, right Mc III; BAT-1'04 E5-80, right Mc IV; BAT-1'04 E5-91c, right Mc V; BAT-1'04 E5-77, right first anterior phalanx III; BAT-1'04 E5-76, right third anterior phalanx III; BAT-1'04 E5-91f, right first anterior phalanx V; BAT-1'04 E5-91g, right second anterior phalanx V; BAT-1'04 E5-91g, right third anterior phalanx V; BAT-1'04 E5-91a, right anterior sesamoid; BAT-1'04 E5-91b, right anterior sesamoid; BAT-1'04 E5-91d, right anterior sesamoid; BAT-1'04 E5-91e, right anterior sesamoid; BAT-1'04 E5-146, right anterior sesamoid.

The left posterior limb comprises the following bones: BAT-1'04 F5-141, left femur; BAT-1'04 F5-58, left tibia; BAT-1'04 F5-w/n, left fibula; BAT-1 F5-w/n, right calcaneum; BAT-1 F5-w/n, right astragalus; BAT-1 F5-w/n, right navicular; BAT-1 F5-w/n, right cuboid; BAT-1 F5-w/n, right ectocuneiform; BAT-1 F5-w/n, right mesocuneiform; BAT-1 F5-w/n, right entocuneiform; BAT-1 F5-w/n, right Mt II; BAT-1'04 F5- w/n, right Mt III; BAT-1 F5-w/n, right Mt IV; BAT-1'04 F5-w/n, left first posterior phalanx II; BAT-1'04 F5-w/n, left first posterior phalanx III; BAT-1'04 F5-w/n, left first posterior phalanx IV; BAT-1'04 F5-w/n, left second posterior phalanx II; BAT-1'04 F5-w/n, left second posterior phalanx III; BAT-1'04 F5-w/n, left second posterior phalanx IV; BAT-1'04 F5-w/n, left third posterior phalanx II; BAT-1'04 F5-w/n, left third posterior phalanx III; BAT-1'04 F5-w/n, left third posterior phalanx IV; BAT-1'04 F5-w/n, left posterior sesamoid IV; BAT-1'04 F5-w/n, left posterior sesamoid IV; BAT-1'04 F5-w/n, left posterior sesamoid II; BAT-1'04 F5-w/n, left posterior sesamoid II; BAT-1'04 F5-w/n, left posterior sesamoid III; BAT-1'04 F5-w/n, left posterior sesamoid III.

The right posterior limb is unprepared and no measurements have been taken except for the fragmentary right femur. This limb is formed by the following elements (most bones without field number): BAT-1'04 E5-69, proximal half of a right femur; BAT-1'05 E6-9, right patella; BAT-1'04 E5-137, left tibia; BAT-1'04 E5-138, left fibula; BAT-1'04 E5-w/n, left calcaneum; BAT-1'04 E5-139, left astragalus; BAT-1'04 E5-146, left navicular; BAT-1'04 E5-w/n, left cuboid; BAT-1'04 E5-145, left ectocuneiform; BAT-1'04 E5-144, left mesocuneiform; BAT-1'04 E5-143, left entocuneiform; BAT-1'04 E5-140, left Mt II; BAT-1'04 E5-141, left Mt III; BAT-1'04 E5-142, left Mt IV; BAT-1 E5-w/n, right first posterior phalanx II; BAT-1 E5-w/n, right first posterior phalanx III; BAT-1 E5-w/n, right first posterior phalanx IV; BAT-1 E5-w/n, right second posterior phalanx II; BAT-1 E5-w/n, right second posterior phalanx III; BAT-1 E5-w/n, right second posterior phalanx IV; BAT-1 E5-w/n, right third posterior phalanx II; BAT-1 E5-w/n, right third posterior phalanx III; BAT-1 E5-w/n, right third posterior phalanx IV; BAT-1 E5-w/n, right posterior sesamoid IV; BAT-1 E5-w/n, right posterior sesamoid IV; BAT-1 E5-w/n, right posterior sesamoid II; BAT-1 E5-w/n, right posterior sesamoid

II; BAT-1 E5-w/n, right posterior sesamoid III; BAT-1 E5-w/n, right posterior sesamoid III.

Batallones-3

A single left lunate BAT-3'10 468 has been studied.

Batallones-5

BAT-5'05 w/n, isolated nasal bones; BAT-5'10 I4-52, fragmentary atlas; BAT-5'01 33; BAT-5'10 G15-47; BAT-5'01 w/n, axis; BAT-5'05 w/n, right P3; BAT-5'04 H11-21, right maxilla with P4-M2; BAT-5'10 H12-27, right scapula; BAT-5'10 I13-80, right Mc II; BAT-5'01 5, left trapezoid; BAT-5'01 w/n, acetabular region of a left hemipelvis; BAT-5'01 2, right patella; BAT-5'01-1, left astragalus; BAT-5'01 w/n, left navicular; and BAT-5'10 I14-51, right Mt IV.

Batallones-6

BAT-*6*'12 B1-3, left DP3-4.

APPENDIX 2

Measurements (mm) of the skull (Table S1), mandible (Table S2), upper dentition (Table S3), and lower dentition (Table S4) of *Aceratherium incisivum* from Batallones-1 and 5 (Cerro de los Batallones, Madrid Province, Spain). Side is detailed as follows: l, left; r, right; (D), upper decidual teeth.

Table S1	BAT-1'04 F5-157
6. Distance between occipital crest and postorbital process	235.0
7. Distance between occipital crest and supraorbital tubercle	243.0
8. Distance between occipital crest and lacrimal tubercle	27.7
9. Distance between nasal notch and orbit	82.5
13. Distance between occipital condyle and M3	220.0
14. Distance between the nasal tip and the orbit	204.0
15. Width of occipital crest	118.0
16. Width between mastoid processes	193.0
17. Minimal width between parietal crests	34.5
18. Width between postorbital processes	146.0
19. Width between supraorbital tuberosities	173.0
20. Width between lachrimal tubercles	184.0
21. Maximal width between zygomatic arches	296.0
22. Width of nasal base	95.4
28. Width of the palate in front of P2	65.3
29. Width of the palate in front of M1	94.9
30. Width of the palate in front of M3	103.0
31. Width of foramen magnum	54.0
32. Width between exterior borders of occipital condyles	116.7

Table S3		BAT-6'12 B1-3	BAT-1'04 F5-157		BAT-5'04 H11 19-21b	BAT-5'05 bis
Upper teeth		l	l	r	r	r
	L		26.2	27		
P1	W		22.4	22.2		
	H		20.0	24.4		
	L		36.5	36.2		
P2	W		42.3	41.2		
	H		30.9	30.9		
	L	(D) 39.1	40.8	41.0		
P3	W	(D) 37.3	48.5	48.3		
	H	(D) 14.3	34.8	35.8		
	L	(D) 45.0	42.9	41.5	42.1	41.4
P4	W	(D) 41.2	49.8	51.3	50.3	47.1
	H	(D) 18.4	39.6	37.5	46.9	45.7
	L		47.0	48.0	50.2	
M1	W		54.4	51.7	50.1	
	H		—	—	41.3	
	L		48.9	49	51.4	
M2	W		49.7	49.6	48.4	
	H		—	—	43.2	
	L		45.7	45.0		
M3	W		40.0	42.0		
	H		—	—		

Table S2	BAT-1'93 2788	
	l	r
L	482.0	479.0
DAPdia	63.8	61.4
HP1	47.0	45.4
HP2	52.0	53.0
HP3	54.0	54.0
HP4	57.0	57.5
HM1	58.0	59.0
HM2	62.0	67.0
HM3a	72.0	77.0
HM3p	74.0	77.0
DAPdent	225.0	232.0
Lcor	195.0	196.0
Lart	156.0	164.0
Hcor	243.0	264.0
Hart	177.0	189.0
DAPhr	114.8	116.0
DAPproc	82.2	85.7
DAPcor	27.5	27.8
DAPart	37.9	37.4
DTia	14.3	
DTip	85.1	
Lsin	142.0	
DTpx	66.6	
DTm3p	114.8	
DTcor-cor	135.2	
DTart-art	108.0	
DTart	92.8	92.0

Table S4		BAT-1'93 2788	
Lower teeth		l	r
	L	29.5	
p2	W	19.4	
	H	26.3	
	L	35.4	36.5
p3	W	26.1	26.7
	H	29.1	27.7
	L	36.3	35.9
p4	W	28.0	28.2
	H	29.9	27.8
	L	40.8	40.6
m1	W	27.6	28.2
	H	27.9	27.8
	L	41.8	40.6
m2	W	27.5	27.6
	H	28.3	29.1
	L	42.9	42.3
m3	W	25.5	28.5
	H	27.7	32.2

APPENDIX 2 (CONT.)

Measurements (mm) of the scapulae (Table S5), humeri (Table S6), radii (Table S7), ulnae (Table S8), pelvis (Table S9), patellae (Table S10), femora (Table S11), tibia (Table S12), and fibula (Table S13) of *Aceratherium incisivum* from Batallones-1 and 5 (Cerro de los Batallones, Madrid Province, Spain). Side is detailed as follows: l, left; r, right.

Table S5			col			art	
Scapula	L	APD max	TD	APD	APD tuber	APD	TD
BAT-5'10 H12-27 (l)	391.0	253.0	36.7	90.9	99.2	74.0	61.8
BAT-1'06 F6-127 (l)	400.0	222.0	32.5	80.5	97.3	70.2	58.3

Table S6				prox epi		dia			dis epi					
Humerus	L	Lprox	TDtuber	TD	APD	TD	APD	Ldis	TD	TDtroc	R1	Rmin	R2	APD
BAT-1'04 E5-83 (r)	—	—	—	—	—	46.8	49.1	57.0	110.9	68.6	71.6	35.8	50.9	92.3
BAT-1'04 F6-148 (l)	363.0	157.0	~ 93	140.9	~ 73	54.3	41.8	71.5	86.6	67.0	72.4	~ 40	60.0	94.8

Table S7			prox epi		prox art		dia		dis epi		dis art	
Radius	L	l	TD	APD	TD	APD	TD	APD	TD	APD	TD	APD
BAT-1'04 E5-84 (r)	295.0	278.0	78.0	48.0	72.0	39.0	45.0	31.0	71.9	40.0	67.0	37.0
BAT-1'04 F6-149 (l)	287.0	265.0	82.6	47.8	78.6	~ 51	42.9	30.6	74.9	46.4	69.4	34.3

Table S8		olec					TDtroc		dia		dis epi		dis art	
Ulna	L	TD	APD	H	TD base	APD base	prox	dis	TD	APD	TD	APD	TD	APD
BAT-1'04 E5-85 (r)	—	—	—	—	15.0	—	—	63.0	32.0	37.0	50.0	25.0	43.0	22.0
BAT-1'04 F6-150 (l)	356.0	45.1	80.3	100.0	20.9	76.6	60.8	68.2	31.7	36.3	29.5	55.4	—	—

Table S9			ace	
Pelvis	L	TDcol	H	APD
BAT-1'05 F5 w/n (l)	76.7	80.7	—	~ 230

Table S10			
Patella	TD	APD	H
BAT-1'04 F5-158	69.1	35.3	78.8
BAT-1'04 E5-9 (r)	68.4	32.3	78.7

Table S11						head		prox epi				dia					dis epi	
Femur	L	Ltroc-prox	Ltroc	Ltroc-dis		TD	APD	TD	APD	TD-cue	TD3t	TD	APD	R1	R2	TDtroc	TD	APD
BAT-1'04 F5-141 (l)	387.0	108.0	38.4	196.0		69.8	69.0	135.0	94.0	114.0	98.0	52.8	47.1	85.8	69.7	44.8	100.7	134.7
BAT-1'04 E5-69 (r)	—	102.0	37.7	—		68.9	69.0	118.0	85.5	127.0	95.8	—	—	—	—	—	—	—

Table S12			prox epi		dia		dis epi	
Tibia	L	LfFi	TD	APD	TD	APD	TD	APD
BAT-1'04 F5-58 (l)	297.0	256.0	—	—	41.0	40.3	82.3	59.1

Table S13		prox epi		dia		dis epi	
Fibula	L	TD	APD	TD	APD	TD	APD
BAT-1'04 F5-w/n	262.0	—	21.1	20.6	17.0	43.0	18.7

APPENDIX 2 (CONT.)

Measurements (mm) of the scaphoids (Table S14), lunates (Table S15), pyramidals (Table S16), magnums (Table S17), trapezoids (Table S18), trapeziums (Table S19), unciforms (Table S20), pisiforms (Table S21), astragali (Table S22), calcaneum (Table S23), navicular (Table S24), cuboid (table S25), ectocuneiform (Table S26), mesocuneiform (Table S27), and entocuneiform (Table S28) of *Aceratherium incisivum* from Batallones-1, 3 and 5 (Cerro de los Batallones, Madrid Province, Spain). Side is detailed as follows: l, left; r, right.

Table S14

	prox art			dis art					
Scaphoid	TD	APD	H	TD	APD	APD-fMa	APDfTz	APDfTr	TD	APD
BAT-1'04 E5-89 (r)	42.3	70.1	52.3	41.8	42.6	24.0	19.5	18.1	62.9	30.0
BAT-1'04 F6-151b (l)	45.8	74.0	53.9	41.9	45.2	27.5	19.3	21.9	28.0	65.3

Table S15

Semilunate	TD-prox	TDdist	TDpal	DAP	H	APD fUn	Hart
BAT-3'10 468 (l)	34.6	18.6	34.4	55.4	36.6	25.5	35.9
BAT-1'04 E5-81 (r)	36.8	26.1	26.4	63.8	42.2	21.2	37.8
BAT-1'04 F6-151c (l)	34.8	23.0	26.5	61.3	42.9	34.3	39.9

Table S16

Pyramidal	TD	H	APD	APD prox
BAT-1'04 E5-90 (r)	39.3	48.9	39.1	28.2
BAT-1'04 F6-151d (l)	34.1	47.8	46.9	28.5

Table S17

Magnum	TD	LfUn	LfSl	APD	H	Hdor	Hvproc	Hart
BAT-1'04 F6-151a (l)	41.9	27.4	21.0	76.1	55.5	31.4	31.5	30.5
BAT-1'04 E5-86 (r)	41.4	27.0	21.3	74.1	55.6	32.3	27.8	30.6

Table S18

Trapezoid	TD	APD	H	Hmin
BAT-1'04 F6-151b (l)	37.7	24.4	31.2	22.0
BAT-5'01 5 (r)	31.9	25.1	28.4	22.2
BAT-1'04 E5-88 (r)	39.6	25.1	32.1	21.3

Table S19

Trapezium	TD	H	Hmin
BAT-1'04 E5-91 (r)	30.6	21.5	14.8
BAT-1'04 F6-151g (l)	27.3	28.5	17.1

Table S20

Unciform	TD	H	APDan	APDab
BAT-1'04 E5-82 (r)	59.8	43.5	45.2	59.1
BAT-1'04 F6-151e (l)	58.7	46.5	49.2	62.5

Table S21

Pisiform	APD	DT	H	Hcol	Hart
BAT-1'04 E5-87 (r)	50.1	16.6	35.1	22.2	27.5
BAT-1'04 F6-151f (l)	50.6	19.7	36.9	21.9	29.4

Table S22

	(trochlea)									dis art		
Astragalus	TD	H	TDmd	DLinf	H1	Hmin	H2	L1	L2	DL	TD	APD	APD int
BAT-5'01 1 (r)	77.8	59.1	70.4	36.1	56.3	39.4	54.8	31.3	21.7	52.8	52.9	37.7	52.0
BAT-1'04 F5 w/n (l)	73.8	63.2	68.0	38.6	54.8	38.2	56.5	30.7	21.7	50.7	49.6	35.0	52.9

Table S23

		tuber				
Calcaneum	H	TD	APD	TDsus	APDbeak	TDdis
BAT-1 F5 w/n (l)	90.4	41.9	48.1	70.0	52.4	37.0

Table S24

					prox art	
Navicular	APD	TD	H	Hmin	TD	APD
BAT-1'04 F5 w/n (l)	42.4	54.3	22.3	19.8	42.2	38.4

Table S25

						prox art	
Cuboid	TD	APD	H	Hdor	Hvproc	TD	APD
BAT-1 F5 w/n (l)	36.0	53.5	39.4	32.2	30.5	32.8	41.7

Table S26

	prox art			
Ectocuneiform	TD	APD	H	Hmin
BAT-1 F5-w/n (l)	39.1	44.3	20.1	17.5

Table S27

Mesocuneiform	TD	APD	H	Hmin
BAT-1 F5 w/n (l)	22.3	32.3	13.7	10.0

Table S28

Entocuneiform	TD	APD	Hart	H
BAT-1 F5 w/n (l)	18.7	40.2	38.7	42.4

APPENDIX 2 (CONT.)

Measurements (mm) of the Mc II (Table S29), Mc III (Table S30), Mc IV (Table S31), Mc V (Table S32), Mt II (Table S33), Mt III (Table S34), and Mt IV (Table S35) of *Aceratherium incisivum* from Batallones-1 and 5 (Cerro de los Batallones, Madrid Province, Spain). Side is detailed as follows: l, left; r, right.

Table S29		prox epi		prox art		dia			dis art	
Mc II	**L**	**TD**	**APD**	**TD**	**APD**	**TD**	**APD**	**TDmd**	**TD**	**APD**
BAT-1'04 E5-78 (r)	122.5	39.0	31.7	25.8	32.7	28.9	14.6	31.3	28.4	32.0
BAT-1'04 F6-151i (l)	126.2	43.3	35.1	22.6	36.5	29.9	15.5	36.7	29.7	35.6
BAT-5'10 I13-80 (r)	117.1	24.3	29.2	20.5	28.1	28.5	13.5	29.4	27.9	31.0

Table S30		prox epi		prox art			dia			dis art	
Mc III	**L**	**TD**	**APD**	**TD**	**APD**	**HfUn**	**TD**	**APD**	**TDmd**	**TD**	**APD**
BAT-1'04 E5-79 (r)	132.9	55.9	~ 34	36.1	~ 34	19.1	39.1	~ 15	51.1	44.1	~ 27
BAT-1'04 F6-153 (l)	134.8	54.6	40.6	35.7	40.1	22.9	37.9	16.3	49.0	40.4	37.6

Table S31		prox epi		prox art		dia			dis art	
Mc IV	**L**	**TD**	**APD**	**TD**	**APD**	**TD**	**APD**	**TDmd**	**TD**	**APD**
BAT-1'04 E5-80 (r)	106.6	32.2	—	31.6	—	29.2	16.4	35.2	26.8	~ 32
BAT-1'04 F6-152 (l)	113.4	28.1	40.6	26.1	36.7	29.7	16.5	35.5	30.7	36.2

Table S32		prox epi		prox art		dia			dis art	
Mc V	**L**	**TD**	**APD**	**TD**	**APD**	**TD**	**APD**	**TDmd**	**TD**	**APD**
BAT-1'04 E5-91c (r)	71.1	~ 20	~ 25	~ 17	~ 25	~ 18	~ 11	~ 27	~ 24	~ 12
BAT-1'04 F6-152b (l)	70.0	22.8	23.3	18.5	20.1	26.5	11.9	25.8	20.5	19.2

Table S33		prox epi		prox art		dia			dis art	
Mt II	**L**	**TD**	**APD**	**TD**	**APD**	**TD**	**APD**	**TDmd**	**TD**	**APD**
BAT-1'05 F5 w/n (l)	108.9	33.2	25.0	31.9	17.4	26.5	18.1	30.8	28.9	32.6

Table S34		prox epi		prox art		dia			dis art	
Mt III	**L**	**TD**	**APD**	**TD**	**APD**	**TD**	**APD**	**TDmd**	**TD**	**APD**
BAT-1'05 F5 w/n (l)	118.5	41.8	35.5	40.9	37.0	34.1	17.0	47.9	38.5	34.0

Table S35		prox epi		prox art		dia			dis art	
Mt IV	**L**	**TD**	**APD**	**TD**	**APD**	**TD**	**APD**	**TDmd**	**TD**	**APD**
BAT-1'05 F5 w/n (l)	104.2	32.6	35.2	27.6	35.3	25.3	21.4	27.3	28.1	32.8
BAT-5'10 I14-51 (r)	104.5	34.5	—	26.3	—	20.1	18.0	27.1	25.7	29.6

APPENDIX 2 (CONT.)

Measurements (mm) of the first (Table S36), second (Table S37), and third (Table S38) phalanges of *Aceratherium incisivum* from Batallones-1 (Cerro de los Batallones, Madrid Province, Spain). Side is detailed as follows: l, left; r, right; ant., anterior; post, posterior.

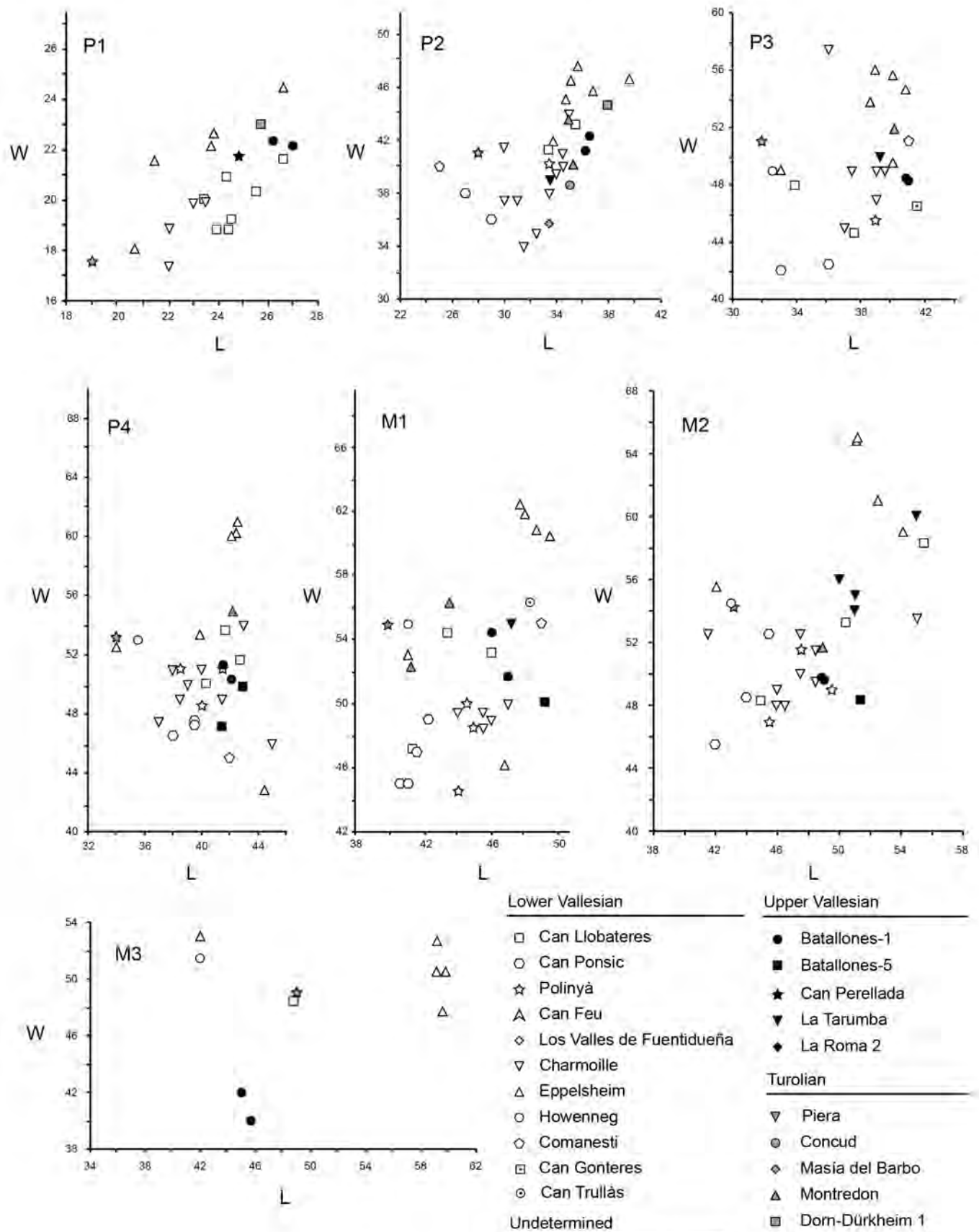
Table S36	finger	side					prox art		dis art	
First phalanges			TD	APD	H	Hprox	TD	APD	TD	APD
BAT-1'04 F6-162 (l)	II	ant	31.9	30.0	24.9	11.9	29.4	27.0	28.9	24.4
BAT-1'04 F6-157 (l)	III	ant	42.3	30.4	24.2	12.6	40.2	27.5	33.9	23.1
BAT-1'04 F6-154 (l)	IV	ant	31.9	33.6	27.5	11.7	29.5	31.2	29.1	23.3
BAT-1'04 F6-152c (l)	V	ant	31.4	31.8	25.5	11.7	27.5	27.6	29.1	23.7
BAT-1 F5 w/n (l)	II	post	28.3	30.6	27.4	10.8	27.1	26.8	25.1	24.6
BAT-1 F5 w/n (l)	III	post	30.2	30.2	27.3	11.6	27.4	25.9	27.0	24.0
BAT-1 F5 w/n (l)	IV	post	41.1	30.2	28.3	11.5	37.8	26.7	33.5	19.9

Table S37	finger	side					prox art		dis art	
Second phalanges			TD	APD	H	Hprox	TD	APD	TD	APD
BAT-1'04 F6-158 (l)	II	ant	41.6	24.0	18.3	7.5	37.5	20.5	35.4	23.6
BAT-1'04 F6-163 (l)	III	ant	30.7	23.7	19.2	7.3	26.6	24.0	25.2	27.9
BAT-1'04 F6-155 (l)	IV	ant	35.0	22.2	17.7	7.8	30.4	20.9	27.4	22.0
BAT-1'04 F6-152d (l)	V	ant	14.8	16.8	11.6	5.1	14.1	16.7	14.0	16.1
BAT-1 F5 w/n (l)	II	post	31.4	21.1	19.8	7.5	26.0	19.5	25.1	24.1
BAT-1 F5 w/n (l)	III	post	31.4	24.4	18.0	9.7	24.5	21.6	24.7	25.7
BAT-1 F5 w/n (l)	IV	post	38.5	24.3	20.1	7.4	33.6	19.6	35.1	21.7

Table S38	finger	side						art	
Third phalanges			TD	DAP	H	Ldor	Lpla	DT	H
BAT-1'04 F6-164 (l)	II	ant	681	262	204	248	254	406	196
BAT-1'04 F6-159 (l)	III	ant	565	280	223	272	258	350	193
BAT-1'04 E5-91g (r)	V	ant	220	133	122	122	122	188	116
BAT-1 F5 w/n (l)	II	post	558	245	171	260	233	294	158
BAT-1 F5 w/n (l)	III	post	554	289	207	266	261	313	191
BAT-1 F5 w/n (l)	IV	post	—	326	196	317	324	426	191

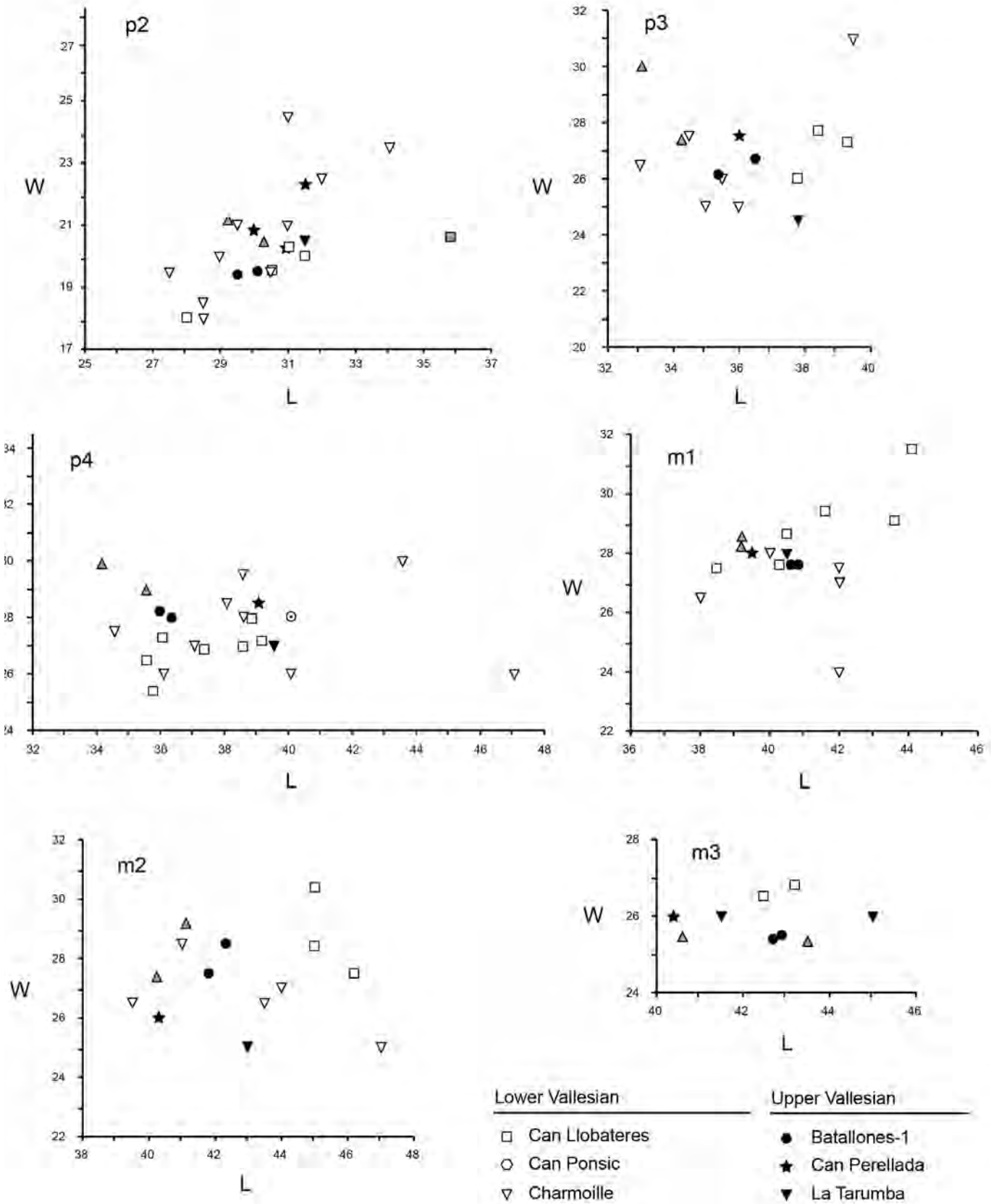
APPENDIX 3

Scatter diagram (in mm) of the upper dentition of *Aceratherium incisivum* from Cerro de los Batallones (Madrid Province, Spain; black circles and squares) compared with other European localities. Additional data obtained from Cerdeño (1989), Becker (2003) and Hunermann (1989).



APPENDIX 3 (CONT.)

Scatter diagram (in mm) of the lower dentition of *Aceratherium incisivum* from Batallones-1 (Cerro de los Batallones, Madrid Province, Spain; black circles) compared with other European localities. Additional data obtained from Cerdeño (1989), Becker (2003) and Hunermann (1989).



11. *Lartetotherium* sp. (Rhinocerotidae, Perissodactyla) from the Vallesian of Cerro de los Batallones area (Upper Miocene, Spain)

Oscar Sanisidro
María Teresa Alberdi
and Jorge Morales

Abstract. *Lartetotherium* is a genus of horned rhinoceros that appeared in Europe in the late Lower Miocene with the species *Lartetotherium sansaniense*. We describe a partial skeleton of an unnamed *Lartetotherium* species from the locality of Batallones-1, and additional remains from Batallones-2, Batallones-10, and Valdeinfierno (all of them dated as Late Vallesian; MN 10 Biozone and located in the Madrid Province, Spain). The material, which consists in two mandibles, one skull, anterior and posterior limb-bone elements, a hyoid, and some vertebrae, is the most complete known of this species. The available sample from Los Batallones area is compared to the type specimens from Sansan as well as to other Iberian specimens. Additionally, related Rhinocerotina genera like *Dihoplus* or *Gaindatherium* have been used for comparison. The discovery of the present skull provides novel cranial information for the variability of the genus. The form from Los Batallones Area has resemblances to *Lartetotherium* and more derived taxa such as *Dihoplus* and *Diceros*. The limb mediportal proportions together with isotopic results indicate that this particular *Lartetotherium* species had preferences for more open habitats if compared with sympatric aceratheriine species.

INTRODUCTION

Gray (1825) separated Rhinocerotina from the other ungulates like elephants, hippopotamuses, suids and tapirs, a Tribe conception roughly equivalent to the current Family level. Curiously, he grouped them all in Elephantidae. At that time rhinoceroses were restricted to the living forms and a couple of fossil species from the Pleistocene. An updated and more restrictive concept of Rhinocerotina is found in the last phylogenetic proposals (Antoine, 2003; Becker et al., 2013). Rhinocerotina includes all living rhinoceroses and several other species with big nasal horns as their most conspicuous weapons, a tridactyl manus and brachyodont dentition as plesiomorphic conditions. This clade is equivalent to Heissig's Rhinocerotini (Heissig, 1989). The first Rhinocerotina appeared in the earliest Miocene of Eurasia and Africa, but they did not flourish until the Pliocene. The Miocene European record of the Rhinocerotina starts with the species *Lartetotherium sansaniense* and the poorly-known *Lartetotherium montesi*. Three Rhinocerotina species have been cited in the Iberian Upper Miocene. These are *Lartetotherium sansaniense* and *Lartetotherium steinheimensis* in the Lower Vallesian and *Dihoplus schleiermacheri* from the Upper Vallesian to the Latest Turolian. The first two are primitive forms of small to medium size, one-horned, simple dentition and slender proportions. On the other hand, *D. schleiermacheri* is larger, more robust and bears two tandem-placed horns.

Cerro de los Batallones (Los Batallones butte, elevation 700 m; Figure 1) is located one kilometer west of the city of Valdemoro, Madrid Province. Mining activities have been exploiting the abundant sepiolite of the butte since 1974. In July 1991, mechanical diggers accidentally unearthed fossil remains from the first fossil site of the butte, named as Batallones-1. The systematic excavations of the in situ fossiliferous levels started in November of the same year by the researchers of the Museo Nacional de Ciencias Naturales of Madrid. These excavations conducted in Batallones-1 revealed an irregular cavity 12 m deep widened at its base. A pseudokarstic erosive process known as piping favored its formation. It was subsequently filled with greenish clay deposited during fast episodic floods together with slow sedimentary gaps in between (Domingo et al., 2011). This greenish clay is discordant with the three distinct stratigraphic units recognized through the butte. These are (from bottom to top): a lower level of magnesian lutite beds (Unit I), paleosols formed of sepiolite and opal named as Unit II, and siliciclastic, marlstone and carbonate beds (Unit III; Morales et al., 2008, Figure 1C). Once established, they acted as natural vertebrate traps, preventing fallen animals from escape through the slippery sepiolite walls when wet. Subsequently, dead animals attracted carnivores, which were trapped too (Figure 1E). The excavations carried out until 2014 have shown that the mammalian fauna of Batallones-1 site is vastly dominated by carnivore mammals (with a complex guild formed by up to 10 species; Salesa et al., 2012). As a result, the studies

of the carnivores found in the trap represent a paramount contribution to the evolution of the group, as they are rarely recorded in other European sites and are usually represented by fragmentary remains.

So far, nine fossiliferous sites have been located, named as Batallones-1 to Batallones-7 and Batallones-9 and 10. Their temporal datation indicates that an Upper Vallesian age (~ 9-10 Ma, MN 10) is plausible (Morales et al., 2008; Peigné et al., 2008; Salesa et al., 2005). Despite the rather homogeneous temporal background of the different sites of the butte, some minor time lags have been detected. The study of the micromammals found that Batallones-10 is slightly older than Batallones-1 and both are older respect to Batallones-3 (López-Antoñanzas et al., 2010). The temporary gap between Batallones-1 and 3 is also reflected in some differences between the proportions of some species (i.e. the smaller size of *Machairodus aphanistus* in Batallones-3) and the distinct carnivore assemblages of both sites (e.g. the presence of Thaumastocyon sp. in Batallones 3; Monescillo et al., 2014). Unfortunately, the relative stratigraphic position of the remaining fossil sites of the butte is unknown due to insufficient data. The formation processes described for the vertebrate trap of Batallones-1 are shared by other sites of the butte (i.e. Batallones-3 and the lower levels of Batallones-2). These sites, named as Lower level assemblages (LLA's; Domingo et al., 2012b) or cavity-type sites (Morales et al., 2008), have common stratigraphic, taxonomic, and taphonomic settings.

Upper level assemblages (ULA's; Domingo et al., 2011), so-called sinkhole-type sites (Morales et al., 2008), are more superficial, as only contact the Unit III of the butte. These sites show a well-defined stratification typical of a small pond or lacustrine area (Domingo et al., 2011). Other ULA's are Batallones-4, 5, 6, 7, and 10. Both types of assemblages (ULA's and LLA's) are not mutually exclusive. Indeed, they form a 'hourglass'-shaped complex which combined a lower 'pouch'-like vertebrate trap at the bottom (LLA) together with an inverted 'cone'-like, uppermost section of variable extension that acted as a ULA. They were connected through a sterile

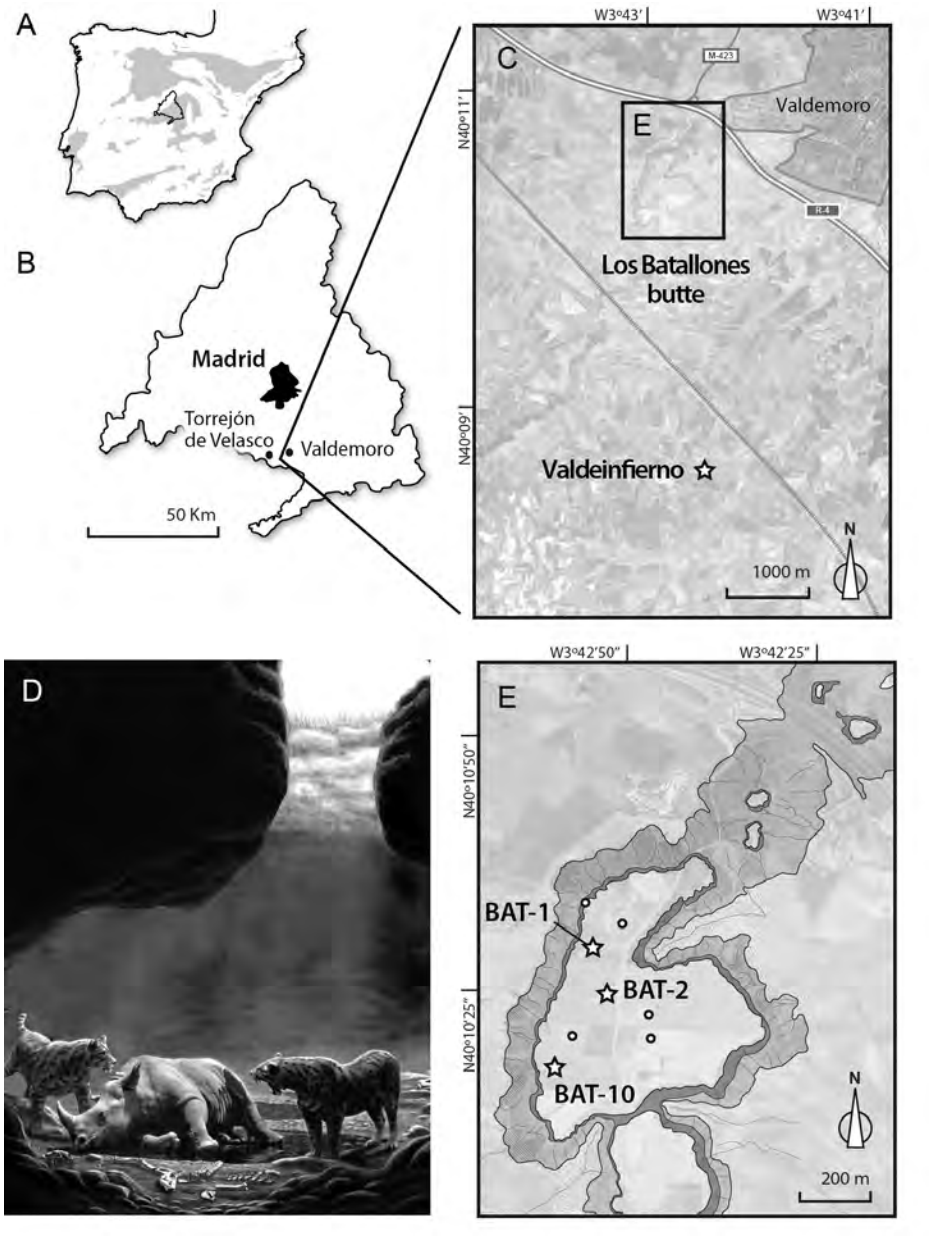


Fig. 1 A, simplified geographic map of the Iberian Peninsula with the Tertiary basins shaded and the Madrid Province outlined; B, detailed map of the Madrid Province with the situation of Batallones area; C, aerial photo showing the position of the Batallones butte fossil complex (represented by a square, detailed in E) and the fossil site of Valdeinfierno, represented as a star; D, reconstruction of the juvenile individual of ***Lartetotherium*** sp. found in the bottom of the trap of Batallones-1 being scavenged by two ***Machairodus aphanistus*** (illustration by Mauricio Antón); E, aerial photo showing the position of the areas of systematic excavations within the butte (indicated as empty circles). ***Lartetotherium*** sp. has been found in Batallones-1, 2, and 10 (represented as stars). Medium gray, dark gray and light gray shaded areas represent the outcrops of the Unit I, II and III respectively, whereas light gray lines represent current drain channels.

and narrow 'pipe'-like conduit, as found in Batallones-5 and 10 (Morales et al., 2008). Both upper and lower parts represent consecutive faunal concentration episodes differenced by changes in the physical conditions and cavity dimensions (Domingo et al., 2011).

Despite the predominance of carnivore fossils, herbivores are represented by a several individuals in the trap of Batallones-1. The presence of rhinoceros where originally noticed in Batallones-1 with the species *Aceratherium incisivum* (Morales et al., 1992). A complete mandible together with some isolated dental and postcranial remains were posteriorly ascribed to the same species (Cerdeño and Sánchez, 1998). However, most of these postcranial bones do not pertain to *A. incisivum* but a large rhinocerotina rhinoceros (Sanisidro et al., this volume), being re-described in the present work in the light of new data. The skeletal elements were scattered through a significant part of the trap, in contrast to the anatomically associated skeleton of *A. incisivum* (Sanisidro et al., this volume). Additionally, unpublished remains from Batallones-2, 5 and 10 (all of them within Cerro de los Batallones fossiliferous area) are also studied.

The fossil locality of Valdeinfierno is placed 2,25 km South of Cerro de los Batallones butte, in the so-called Batallones-Malcovadeso area (Figure 1C). In this case, the sedimentary deposits from Valdeinfierno are linked to an expansion of the regional lacustrine conditions during the Late Vallesian (Pozo et al., 2006). The only fossil remain found in the locality is a rhinoceros calcaneum towards the top of the level U5, formed by a 2 m thick layer of light-coloured limestone with siliceous nodules (the geologic context of Valdeinfierno is described in detail by Pozo et al., 2006). We have included it in the present work, ascribing it to the same large *Lartetotherium* species from Los Batallones butte.

MATERIAL AND METHODS

All the studied specimens from Cerro de los Batallones butte are stored in the Museo Nacional de Ciencias Naturales, Madrid. Measurements are given in millimeters with an accuracy of one decimal digit. Approximate measurements are given in parentheses. Measurements were made with a digital caliper and a measuring tape for elements larger than 150 mm. The terminology applied in the description of the anatomical characters generally follows Guérin (1980), but that used by other authors has also been taken into consideration (Antoine, 2002; Heissig, 1972, 1999). Hyoid nomenclature follows that of van der Made (2010).

Anatomical Abbreviations—ant, anterior; art, articulation; dia, diaphysis; dis, distal; int, interior; epi, epiphysis; max, maximum; Mc, metacarpal; min, minimum; Mt, metatarsal; prox, proximal; 3tr, third trochanter. I, M and P designate incisors, molar and premolar respectively. Lower-case letters designate teeth from lower jaws and upper-case letters teeth from upper jaws according to the terminology proposed by Van Valen (1966). A preceding 'D' or 'd' indicate decidual teeth (e.g., DP4 or dp2).

Measurements abbreviations—APD, antero-posterior diameter; DL, distal length; H, height; L, length; TD, transverse diameter.

Institutional abbreviations— **MNCN**, Museo Nacional de Ciencias Naturales-CSIC (Madrid, Spain); **AMNH**, American Museum of Natural History (New York, USA); **w/n**, without field number; **NMB**, Naturhistorisches museum Basel; **BSPG**, Bayerische Staatssammlung für Paläontologie und historische Geologie, (Munich, Germany); **FSL**, collections de l'Universite Claude-Bernard Lyon-I; **HLMD**, Darmstadt Hessisches Landesmuseum; **LGPUT**: Laboratory of Geology and Paleontology, University of Thessaloniki; **w/n**, without field number. '**B-**' refers to fossils extracted in Batallones-1 from 1991 to 2000. '**BAT-**' refers to the remaining fossils of *Lartetotherium* from the butte (extracted between 2001 and 2014, depending on the locality), which are labeled with the abbreviation of the fossil site (e.g. Batallones-10 is labeled as BAT-10) followed by the year of extraction, the grid code, and the field number (e.g. BAT-10'12 D6-8).

Referred material—See appendix 1.

CT-Scanning—The skull was scanned in coronal orientation on a Philips MX 4000 Dual at the Centro Militar de Veterinaria (CEMILVET), with the following parameters: slice thickness of 1 mm, inter-slice spacing of 0.5 mm, matrix size of 768 x 768 pixels. Scanner energy was 140 kV and 170mA.

SYSTEMATIC PALEONTOLOGY

Family Rhinocerotidae Owen, 1845

Subfamily Rhinocerotinae Owen, 1845

Tribe Rhinocerotini Owen, 1845

Subtribe Rhinocerotina Gray, 1825

Genus *Lartetotherium* Ginsburg, 1974

Type species— *Lartetotherium sansaniense* (Lartet in Laurillard, 1848)

Other species—Heissig (2012) cites *L. sansaniense* is the only species by monotypy. However, other Rhinocerotina species from Europe like *Lartetotherium montesi*, and *Lartetotherium steinheimensis* have been also ascribed to the genus.

Diagnosis—(Heissig, 2012) "Medium-sized one-horned rhinoceros with a skull of medium length with a strongly concave dorsal profile. Anterior dentition with two pairs of lower incisors in each hemimandible, the mesial ones being sometimes lost in older individuals. Jugal teeth unirradicular, with a deep groove along the root. Strong metacone fold on the premolar teeth, weaker but present in the molars. Limbs with the primitive characters of the Tribu".

Differential diagnosis—(modified from Ginsburg, 1974, p. 597) "Rhinocerotid close to *Dicerorhinus* but with a higher

occiput, pterigoidean crests posteriorly extended to almost the level of the paraoccipital apophysis, upper incisors more developed, retained lower p1 and shortened upper P2-M3, with narrow transversal valleys. Nearly straight postglenoid processes (curved in *D. sumatrensis*), posttympanic ones short and anteriorly oriented (long and curved in the extant species). The nasal bone is longer and wider".

Lartetotherium sp.

Holotype—juvenile skull BAT-1'05 E3-150

Hypodigm—All the referred material from Batallones-1 listed in material and methods. All of them pertain to a single, juvenile, individual.

Locus typicus—Batallones-1 (Madrid Province, Spain)

Stratum typicum—Late Miocene, Late Vallesian, Mammal Zone MN 10.

Stratigraphic and geographic distribution—restricted to the type locality.

Diagnosis—*Lartetotherium* species with larger size and raised occiput. The premaxilla is shortened and the lower anterior dentition reduced. The nasal bones are blunt and shortened. The dentiton discontinuous lingual cingula on both upper premolar and molar teeth and reduced anterior dentition. Long bones with widened (higher TD) epiphyses and shortened autopodium

Differential diagnosis—Differs from *L. sansaniense* species in its bigger size, more robust metapodials, reduced lower anterior dentition, presence of discontinuous lingual cingula on both upper premolar and molar teeth and reduced anterior dentition. All carpal bones are lower and have longer volar processes than the type species. The pisiform has a squared lateral contour. The Mc V is pointed and has a larger trapezoid-facet. The astragalus has a lower trochlea and a bigger distal area. The calcaneum has a rounder tuber calcis.

DESCRIPTION

Craniomandibular and Dental Morphology

Skull (Fig. 2 and Table S1)—BAT-1'05 E3-150 is a well-preserved, complete juvenile skull, with both P2-3, DP4 and M1-2 series. The P2 is unworn, the P3 is emerging, the DP4 has an advanced wear and the M1-2 are little worn. The M3 are not erupted and the P1 is missing. According to the age categories proposed by Anders (2011), BAT-1'05 E3-150 pertains to the IDAS 2, juvenile. The whole skull presents both dorsoventral and lateral shearing deformations. The premaxillary bones are at the level of the nasal tip. They are robust, ventrally slanted and their proximal ends are separated. The emerging I1 is peg-like and vertically oriented. The rostral tip of the nasal bones is pointed and ventrally bent. The internasal groove is deep and marked along the horn boss. The latter is strongly convex and presents a finely grooved horn insertion area, a feature observable in young individuals of extant species. The ventral surface of the nasals is flattened and present two inflated ridges parallel to the nasal suture. In lateral view, the nasal incision is U-shaped, has a straight lower rim, a concave upper one and extends backwards above the P2. There is a single large infraorbital foramen placed over the middle of the P2-3 boundary. The anterior rim of the orbit is at the level of the DP4's hypocone on the left side, and the M1-2 boundary on the right side. There is a strongly developed lachrymal process. The supraorbital apophyses are trapezoidal, wide, laterally projected, and individualized from the orbital margins. The gap between both is narrow and profound. There is no trace of postorbital process. The facial crest starts smoothly, where it protrudes distally above the molar series (DP4 on the left side). The zygomatic arch is robust, low and presents a straight border on its anterior half and a strong orientation change at its midpoint. The transversal profile of the articular area is flat. Even though there is an elevated region between the orbits, its surface is smooth and crushed due to the general skull deformation, so the presence of a developed frontal horn in such a young age is unlikely. The dorsal profile of the skull is bumpy due to its compression. Such dorso-ventrally crushed and, as a result, a big crack runs from the anterior rim of the orbit to the dorsal area of the infraorbital foramen. The same can be observed in the dorso-ventrally *A. incisivum* skull BAT-1'05 F5-157. The occiput is elevated at the level of the higher part of the zygomatic archs. As a result, the posterior half of the skull presents a concave dorsal profile. The frontoparietal crests are well separated by a flattened surface, running parallel through the saggital plane of the skull. The occipital face is backwards oriented. In posterior view, the nuchal tubercle the occipital foramen is oval. The occipital condyles are subtriangular and share a wide bastion. In ventral view, the posterior palate margin is placed just behind the level of the M2 protocone. Its anterior border is U-shaped, narrowed due to the lateral shearing deformation. The pterygoidean crests are short and crushed, with a rough and horizontal ventral margin. The postglenoid and posttympanic processes are short and stout. The postglenoid has an oval section and posteriorly projected flattened area. However, they lack their tips in both sides, preventing their description. The paraoccipital process is bumpy, very short and irregular. Their lateral side is connected to the posttympanic, a swollen area as a ventral extension of the nuchal plate. The lateral flanges of the postglenoid and posttympanic processes contact but remain unfused, forming the external auditory meatus. The condylar fossa is well delimited, and presents a foramen nervi hypoglossi placed in its middle part. The condylar fossa is divided by the sagittal crest of the basilar process. It begins at the posterior end of the pterygoidean crests as a bumpy area, sharpening posteriorly.

Mandible (Fig. 3 and Table S2)—BAT-1'07 F4-22 is a well-preserved mandible of a juvenile individual. It has both dp3-m1 series and an emerging right p3. A second juvenile individual has been found in Batallones-2 (BAT-2'00 31). It preserves the right dp1-dp4 and m1 and the left dp2-dp4 and m1. Only the right angular process and the top of the

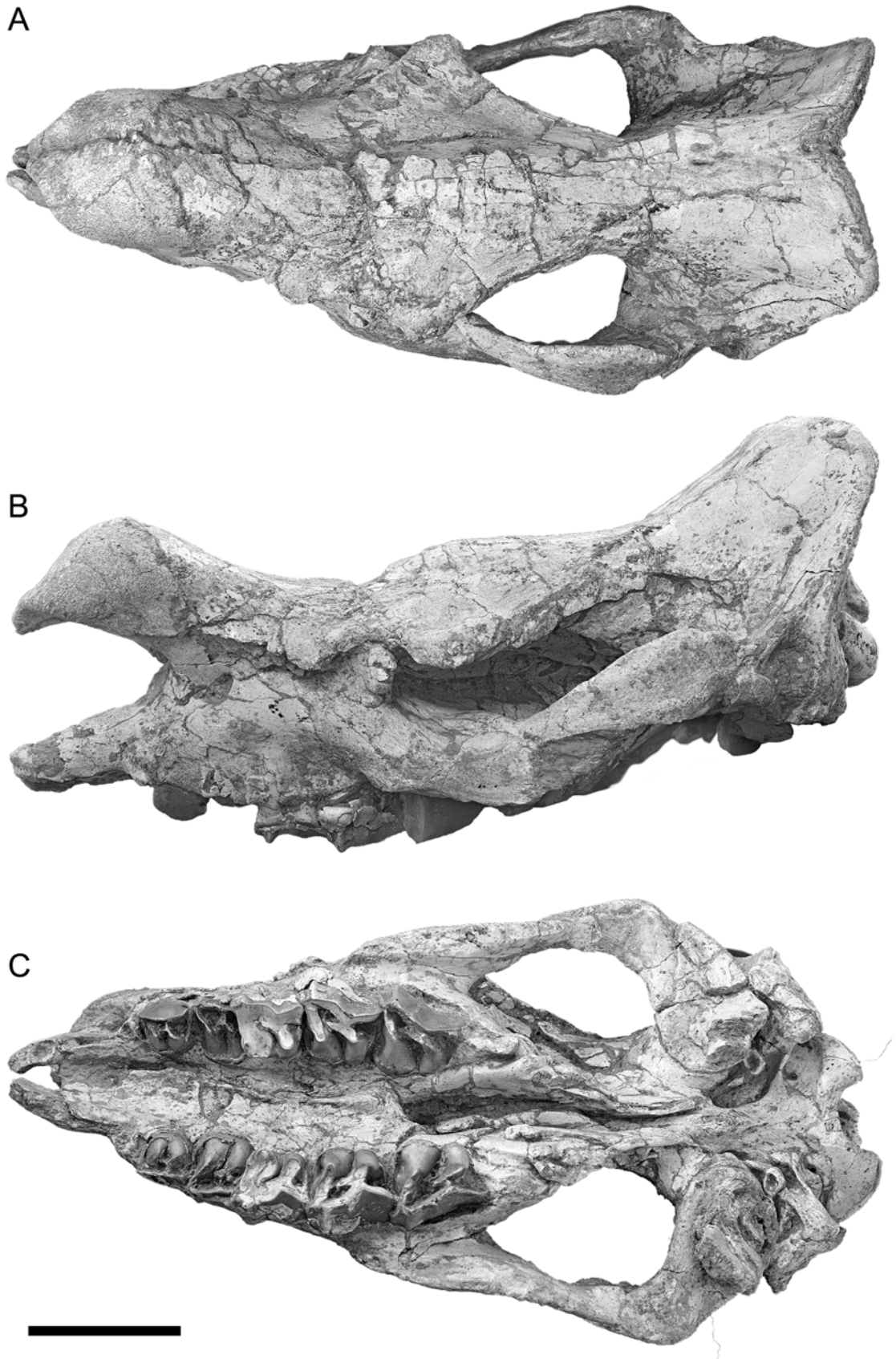


Fig. 2 Juvenile skull of *Lartetotherium* sp. BAT-1'05 E3-150 from Batallones-1 (Cerro de los Batallones, Madrid Province, Spain) in A, dorsal; B, left lateral, and C, ventral views. Scale bar equals 100 mm

coronoid process are missing and the left dp3 and the right dp1 are damaged. The horizontal ramus is long and slender. The lower margin of the mandible is gently convex from the m1 onwards. The angular process is very developed, semicircular and flanked by a strong insertion for the *m. masseter*. Its dorso-caudal extent reaches the midpoint of the vertical ramus. The vertical ramus is robust, low and wide. Its anterior border is concave, the posterior short, concave. Both have swollen rims, the caudal one strongly developed in BAT-1'07 F4-22 probably due to its older age. The coronoid process is short, thin, has a triangular outline and is slightly curved backwards. The mandibular foramen is placed below the level of the coronoid process in BAT-2'00 31, the only mandible with the medial area accessible. The condyle is rectangular, latero-medially curved in the left side of BAT-1'07 F4-22 due to ontogenetic distortion and laterally displaced on the right side. The symphisis is narrow. In lateral view, it has a straight to little concave border, changing gentle convex curvature of the ventral side of the horizontal ramus. It is separated from the dp1 by a short diastema (shorter in BAT-2'00 31). It is

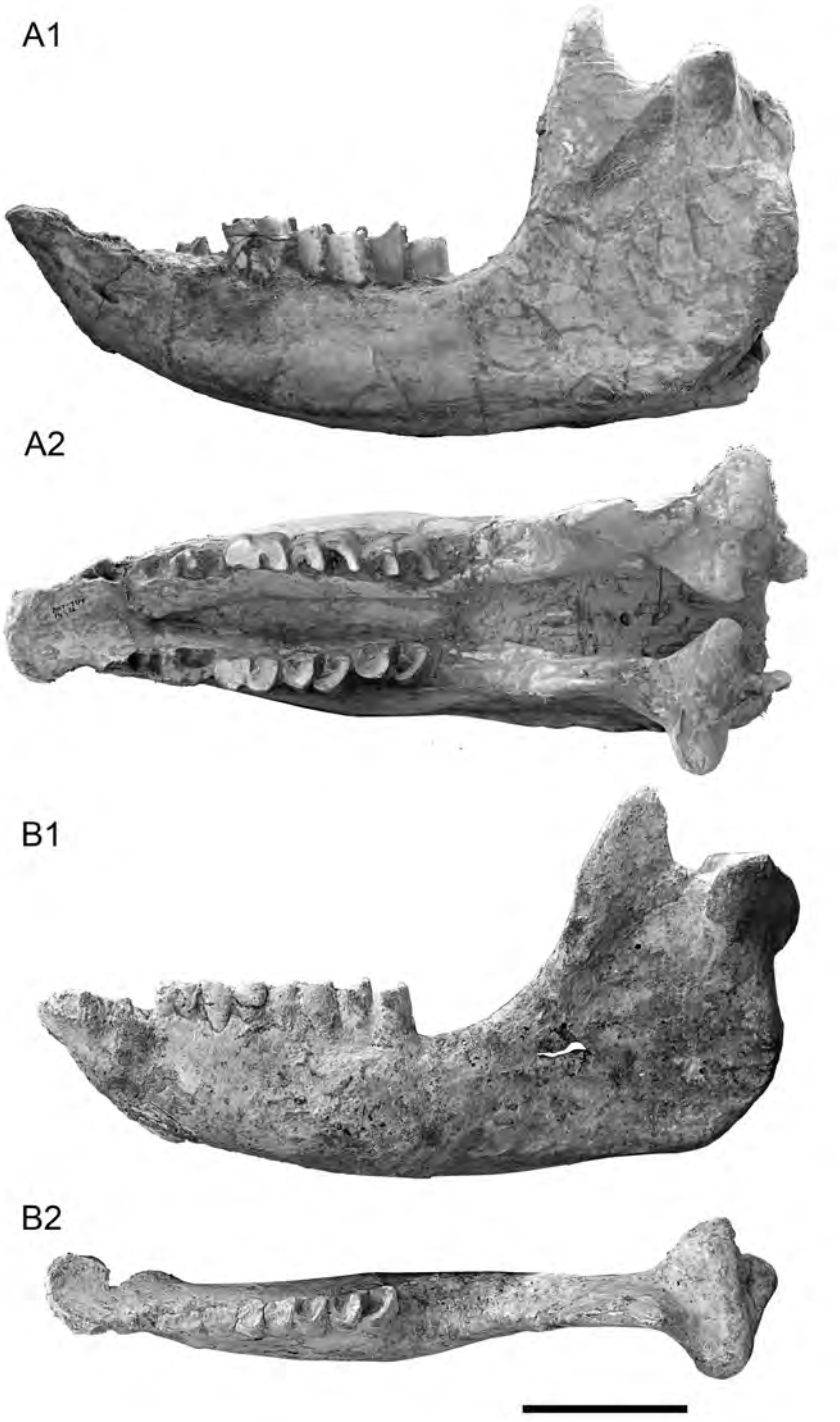


Fig. 3 Mandibles of *Lartetotherium* sp. from Cerro de los Batallones, (Madrid Province, Spain). A, mandible of BAT-1'07 F4-22 from Batallones-1 in A1, lateral left and A2, dorsal view; B, left hemimandible BAT-2'00 31 from Batallones-2 in B1, left lateral and B2, dorsal views. Scale bar represents 100 mm.

flanked by bilateral ridges along the margo interalveolaris and presents a median constriction, attaining a minimum width of 51 mm in BAT-1'07 F4-22. The posterior margin of the symphisis extends back to the level of the hypoconid of the dp2. Due to the lateral compression in BAT-1'07 F4-22 and the separation of the two hemimandibles in BAT-2'00 31, is difficult to reconstruct the original shape of the inner symphiseal border. The rostral margin of the mandible has a narrow irregular ridge. This area is slightly eroded, and no i2 alveoli can be observed.

Upper dentition (Fig. 4 and Table S3)—Deciduous teeth are represented in our sample by the dentition of the juvenile skull BAT-1'07 F4-22. The DP4 is wide. The ectoloph is undulated and presents a prominent and sharp metacone. The protocone is bigger than the hypocone, which has a more protruding lingual margin. The paracone style is well-delimited, favoring a well-marked, V-shaped paracone fold. The advanced wear leaves a narrow and sinusoid median valley. There is a wide but short crochet. The anterior cingulum is present as a short ridge contacting the protocone. The posterior one is very worn and limited to the space between metastyle and the posterior side of the hypocone. The tooth is void of lingual cingulum, possibly due to its advanced wear stage. An isolated P1 (BAT-1'02 D7-66) has been found. It has a wide, convex

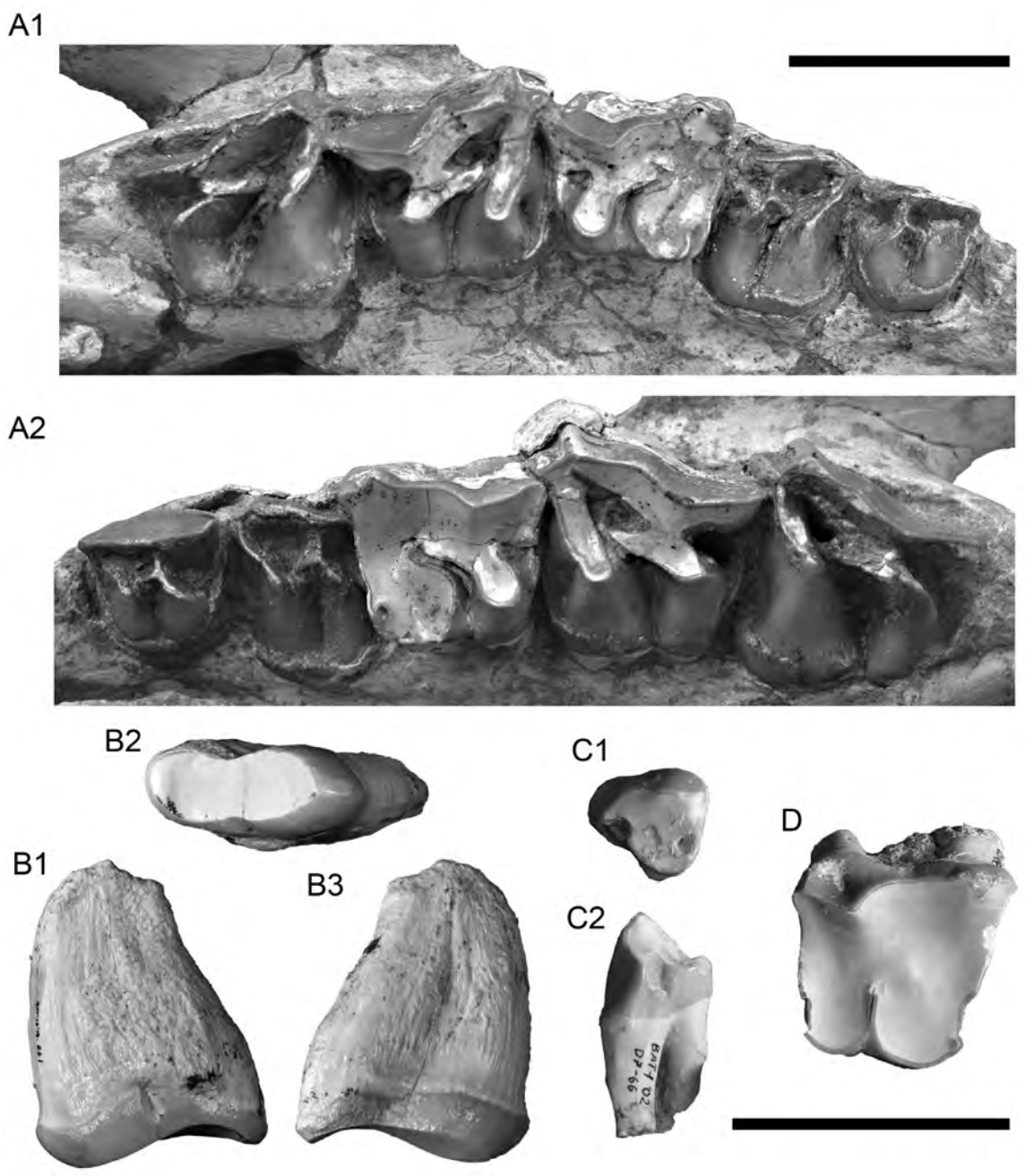


Fig. 4 Upper dentition of *Lartetotherium* sp. from Batallones-1 and 10 (Cerro de los Batallones, Madrid Province, Spain). A1, right and A2, left P2-3, DP4, and M1-2 series of the skull BAT-1'05 E3-150 in occlusal view; B, right I1 (possibly of *Lartetotherium* sp.) found in Batallones-10; C, left (D)P1 BAT-1-02 D7-66 in C1, occlusal, and C2, anterior views; D, right DP3 B-5261(2) in occlusal view. Scale bar for A placed on the bottom left, for B and C on the bottom right. Both scale bars equal 50 mm.

ectoloph, and a short, anterolingually-oriented triangular parastyle. Both protoloph and metaloph are constricted. Protocone and hypocone are fused as a single rounded labial ridge, around half as width as the ectoloph. A small anterior cingulum is present from the parastyle to the anterior side of the protocone, delimiting a squared-shaped valley. The posterior cingulum is well developed and encloses an oval postfossette between metastyle and hypocone. The P2 has a wide ectoloph. It has a continuous lingual cingulum. The P2 is as long as wide. The ectoloph is smoothly convex, with gentle undulations on the metacone rib, the mesostyle and the paracone style. The protoloph is separated from the ectoloph from a shallow valley. The metaloph is slightly longer and curved posteriorly. There is a continuous anterior and labial cingulum which encircles the protocone and walls the median valley, fading out on the anterior side of the hypocone. The posterior cingulum continues right after from the lingual side of the hypocone to the metastyle. The enclosed postfossette is semicircular and deep. There is no trace of labial cingulum. There is a thin crochet, but further internal folding is difficult to describe at this early stage of wear. The P3 is emerging. It has a flattened occlusal border of the ectoloph, parallel protoloph and metaloph (and about the same length), and a lingual cingulum that, as in the P2, fades out in the anterior side of the hypocone. Likewise as the P2, the P3 has a narrow crochet. The anterior and posterior cingula, if present, are not visible. The first two molars share a similar morphology. Both have a trapezoidal outline in occlusal view, but the M2 has a relatively smaller distal width. In labial view, the ectoloph has two sharp cusps at the paracone style and the metacone rib. The protoloph is weakly attached to the ectoloph, leaving a constriction between parastyle and the style of the paracone in unworn pieces as the M2. The metaloph is almost anteroposteriorly oriented and parallel to the ectoloph. This configuration leaves a triangular and wide medial valley together with a strong and long crochet. The paracone style is strong and sharp. The paracone fold is shallow and smooth in occlusal view. The anterior cingulum is low and extends as irregular bumps around the protocone. The posterior cingulum is low and regular, being restricted to the posterior side of the tooth. There is no trace of labial or lingual cingula.

Lower dentition (Fig. 5 and Table S4)—Cement is absent along the tooth row. The dp1 is present by a single and badly preserved tooth (BAT-2'00 31), so no description can be given. The dp2 has a short but partially eroded paralophid. The anterior valley is almost absent, the posterior is very narrow and deep. The labial groove is poorly marked and occupied by a faint labial cingulid at its base. The metaconid

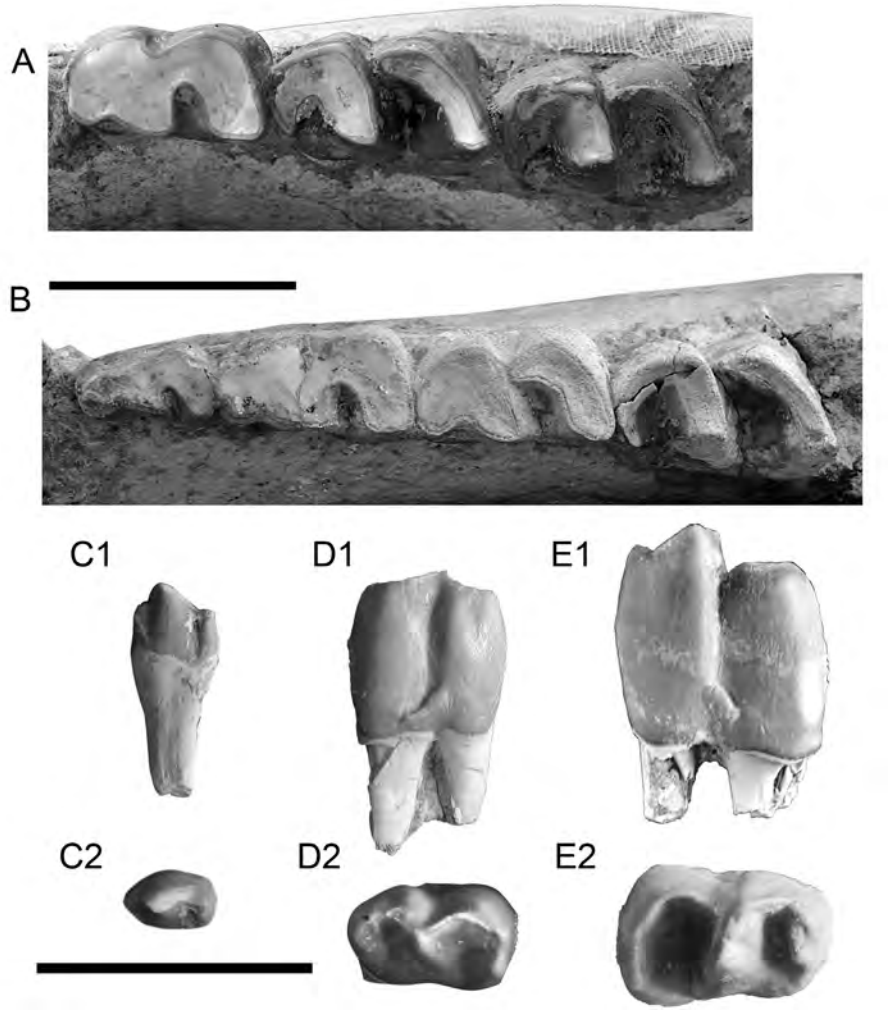


Fig. 5 Lower dentition of *Lartetotherium* sp. from Cerro de los Batallones, (Madrid Province, Spain). A1, right dp4, m1-2 series of BAT-1'07 F4-22 from Batallones-1; A2, left series of the same individual; B1, right dp2-4 and m1of BAT-2'00 31; B2, left series of the same individual; C, right (d?)p1 B-w/n in C1, lingual, and C2, occlusal views. Scale bar for A and B is placed on the lower right corner, scale bar for C on the upper right. Both scale bars equal 50 mm.

has a flattened lingual surface. The dp3 is considerably bigger than the former. The paralophid is double, leaving a small and triangular preanterior valley close to the anterior side of the tooth. The anterior valley is wide, smooth and very shallow. The posterior valley is triangular and deep. The protoconid is very low, due to a probable malocclusion with the upper row. Between the protoconid and paraconid there is a continuous fold along the labial wall. There is a short and faint posterior cingulid. The dp4 presents a shallow anterior valley and a profound and wide posterior one, 'V'-shaped in lingual view. Despite the advanced wear degree, hypoconid and protoconid remain independent. There is a low and faint rim at the basis of the labial groove, which is wide but well delimited. The posterior cingulid is present. The m1 has a profound 'U'-shaped anterior valley. The posterior is bigger, deeper and present a more acute transversal profile. On the labial side there is a tubercle at the basis of the labial groove and an intermittent rim of rugosities attached to the base of the tooth, more evident on the anterior and posterior extents. The posterior cingulid is present and stronger than in the decidual series. The m2 has a shorter hypolophid than the m1. Both anterior and posterior valleys are 'V'-shaped. The wear facets in the recently worn m2 of BAT-1'07 F4-22 are restricted over the hypolophid, the ectolophid and, to a lesser extent, the paralophid. They are nearly vertical and leave a sharp enamel ridge. There is an incipient and narrow occlusal facet on the ectolophid. The labial groove is marked and straight.

Postcranial skeleton

Hyoid (Fig. 6)—Rhinos' hyoids are rarely found in the osteological collections. Up to now, a single fossil specimen, probably pertaining to *Coelodonta antiquitatis*, has been described (van der Made, 2010). Additionally, the hyoid NNML 5738 of *Diceros bicornis* has been used for comparison. The hyoid BAT-1 w/n was found together with some carpal bones (pisiform, lunate and pyramidal) of *Lartetotherium* sp. Therefore, we tentatively assign it to the species. However, no hyoid bone was found associated with the sub-articulated skeleton of *A. incisivum* from Batallones-1, which was also found near and its belonging to the latter is not discarded. The lingual process is short (22 mm length) and subtriangular in section. It presents a short ridge on the ventral side. In *C. antiquitatis* this process is considerably longer and wider. The body of the basihyoid is 63.7 mm wide and 23 mm long. It is flattened on its dorsal side, rugous on the ventral. The tubercles for the articulation of the ceratohyoid are oval (TD = 18.5 mm wide; APD = 10.4 mm; left side) and flat (the right one has a deep fracture and is partially broken). Their anterior side is placed at the level of the base of the lingual process. In *C. antiquitatis* they are smaller, posteriorly placed, more separated, and slightly protruding from the basihyoid. The thyrohyoid bones are stout and rectangular in section. Unfortunately, their distal tips are broken and their total length is unknown.

Vertebral column

Several vertebrae were found scattered through the trap of Batallones-1. The juvenile age of this individual is reflected in most vertebrae, which lack the vertebral disks and do not have fully ossified dorsal borders of the neural spines.

C3 (Fig. 7)—A C3 has been recovered (BAT 1'05 E4 201). The main cranial facet is oval in cranial view (TD = 42 mm; H = 57 mm), symmetrical, and presents parallel lateral borders. The vertebral canal is subtriangular to rounded (TD = 30 mm; H = 34 mm). The dorsal spine is short, but lacks the tip. The anterior cranial articular process is semicircular in section, present a sharp cranial edge and a rounded outline in lateral view (APD ~ 35 mm). Its medial side is flat (left side) to slightly convex (right one). The caudal articular facets are oval (APD ~ 35 mm), flat and latero-distally oriented. The transverse foramen is 'kidney'-shaped (the only preserved is the right one). The ventral crest is very wide, as much as the total width of the bone at the level of the vertebral arches (TD = 75 mm). The transverse processes show two different parts with a smooth transition in between. The anterior one is



Fig. 6 Hyoid bone BAT-1 w/n of *Lartetotherium* sp. from Batallones-1 (Cerro de los Batallones, Madrid Province, Spain) in A, ventral, and B, dorsal views. Scale bar represents 50 mm.

rectangular, flat, and latero-dorsally oriented. Their posterior side is semicircular to 'sickle'-shaped, have a rounded caudal border and have a cranio-caudally slightly concave dorsal side. The main caudal facet is rounded, but asymmetrical (the maximum width, TD = 64 mm, is ventrally displaced).

C4 (Fig. 7)—The C4 (BAT 1'05 E4 202) is very similar to the C3. However, some differences can be distinguished. The main cranial facet is higher and narrower (TD = 40 mm; H = 60 mm), and present a more pointed distal border. The vertebral body is longer (~ 37 mm from the dorsal side of the main cranial facet to the dorsal notch of the main caudal facet in C3; ~ 50 mm in C4). The vertebral canal, the morphology of the base of dorsal spine (also broken in this bone) and the vertebral arch, and the angle formed by the spine with the transverse processes are homologous. One of the main differences relies in the transverse processes. These are clearly shorter (lower APD) and specially visible on its caudal side (APD of the horizontal caudo-lateral border = 18 mm in C3; 40 mm in C4). The caudal articular facets are larger (H = 41/35 mm), the main caudal facet is narrower (60 mm at its widest point) and has a more concave distal border in distal view, giving a vaguely 'heart'-shaped outline instead of circular. Such outline gives a more angular appearance to the distal border of the vertebral body in cranial view.

T5? (Fig. 7)—(1'06 D3-40) The fifth thoracic vertebrae stands out for its very long dorsal spine, triangular in section and has a very sharp cranial border (more salient towards the proximal side). The longitudinal concavity of the caudal side of the spine forks near the top, leaving a narrow bridge in the middle. The tip of the spine is widened (TD = 53 mm) and presents a rugous dorsal surface (due to its immature condition). The main cranial facet is not preserved but has a square rugous insertion (TD = 55 mm; H = 42 mm). The transverse processes are short (L from the anterior articular process = 33/36 mm). On their cranial side there is a small, blunt protuberance (the right one is badly preserved) separated from the cranial articular processes by a narrow channel. These processes are in turn laterally separated by another channel from the lateral costal facets. These are rounded to oval (H = 23/25 mm; TD = 22/23 mm), slightly concave and latero-distally oriented. The vertebral canal is trapezoidal (L = 31 mm; l = 13 mm; H = 20 mm; cranial side). The cranial articular processes are placed on both sides, defining its lateral borders. They are oval (H = ~28 mm), slightly convex, and cranio-dorsally oriented. The attachment place for the main caudal facet is rugous, rounded (TD ~ 55 mm; H = 52 mm) and laterally flanked by the two posterior costal facets. They are semicircular (H = 30/27 mm) and dorsally aligned with the upper border of the articular insertion.

L1? (Fig. 7)—(BAT 1 B2748) The dorsal spine is thin (~ 7 mm), rectangular (APD = 30 mm; H = 86 mm), and has a broken cranio-dorsal border. The cranial main articular facet is 'heart'-shaped (TD = 60 mm; H = 45 mm) and slightly convex. It presents a short ridge protruding from its ventral border. The vertebral canal is wide and subtriangular (TD = 35 mm; H = 19 mm; cranial side). The vertebral arch is robust. The cranial articular facets are rhomboidal (TD = 27/28 mm; H ~38/37 mm), have a laterally oriented ventral side and a flattened central area. A small gap (4 mm) separate them. Only the left cranial articular process is complete. It is a flat squared flange dorso-laterally protruding from the lateral borders of the cranial articular facets. The caudal articular facets are projected from the caudal side of the base of the dorsal spine. They are long, latero-caudally oriented, 'tear'-shaped (TD = 46/42 mm; H = 24/25 mm), and concave. They are separated by a concave grove 13 mm width. The transverse processes are badly preserved. The left one is missing, the right lacks its lateral tip. The main caudal facet is not ossified. Its insertion is also 'heart'-shaped and rugous, but bigger than the cranial one (TD ~ 80 mm; H = 53 mm).

T1 (Fig. 7)—The first thoracic vertebrae BAT 1'07 F4-40 1 lacks most of its dorsal spine. Both main cranial and caudal facets have lost the articular surface, showing irregular surfaces instead. The main cranial facet is convex and has aomewhat rounded outline (TD = 68 mm; H = 63 mm). The poor ossification makes distinguishing the cranial costal facets difficult. The rounded lateral prominences would be their place of insertion. The ventral crest is straight but not well-delimited. The vertebral canal is subtriangular and high (TD = 30 mm; H = 31 mm; cranial side). The cranial articular facets are dorso-medially oriented, flat, 'pear'-shaped (APD = 39/38 mm; TD = 24/36 mm) and placed dorsal to the transverse process. The pillar-like connection between these facets and the transverse process are strong and present a small tubercle each on is cranial border. A deep depression separates these pillars from main cranial facet. The lateral side of the transverse processes is curved (only preserved on the left side), leaving a large, deep and concave fossa on its ventral side, place of insertion for a huge lateral costal facet. The main caudal facet has the shape of an inverted pentagon (TD = 57 mm; H =55 mm). It is slightly concave. The boundaries with the caudal costal facets are not clear due to its immature condition. The latter seem to be semicircular and high, but the facet is missing. The caudal articular facets are 'tear'-like shaped (TD = 25 mm; H = 46 mm), flat and latero-caudally oriented.

T5? (Fig. 7)—(BAT-7'03 w/n) The main cranial facet is not preserved. Its rugous insertion is pentagonal (with the apex facing downwards; TD = 43 mm; H = 51 mm). On both sides of the main cranial facet there are two cranial costal facets. They are rounded (TD = mm; H= mm), concave and cranio-laterally oriented. The vertebral canal is triangular and low (TD = 40 mm; H = 21 mm; cranial side). It is flanked by the cranial articular facets. They are oval (TD = 19/18 mm; H = 34/33 mm), flat, and considerably dorsally oriented. On their lateral sides, there are two rounded, rough, and deep areas.The transverse processes are short (L from the anterior articular process = 35/- mm), robust, and present a spatulated outline in dorsal view. On their lateral sides there is one anterior costal facet (only the left one is preserved). It is latero-distally oriented, oval (APD = 29 mm; H = 22 mm) and has a slightly

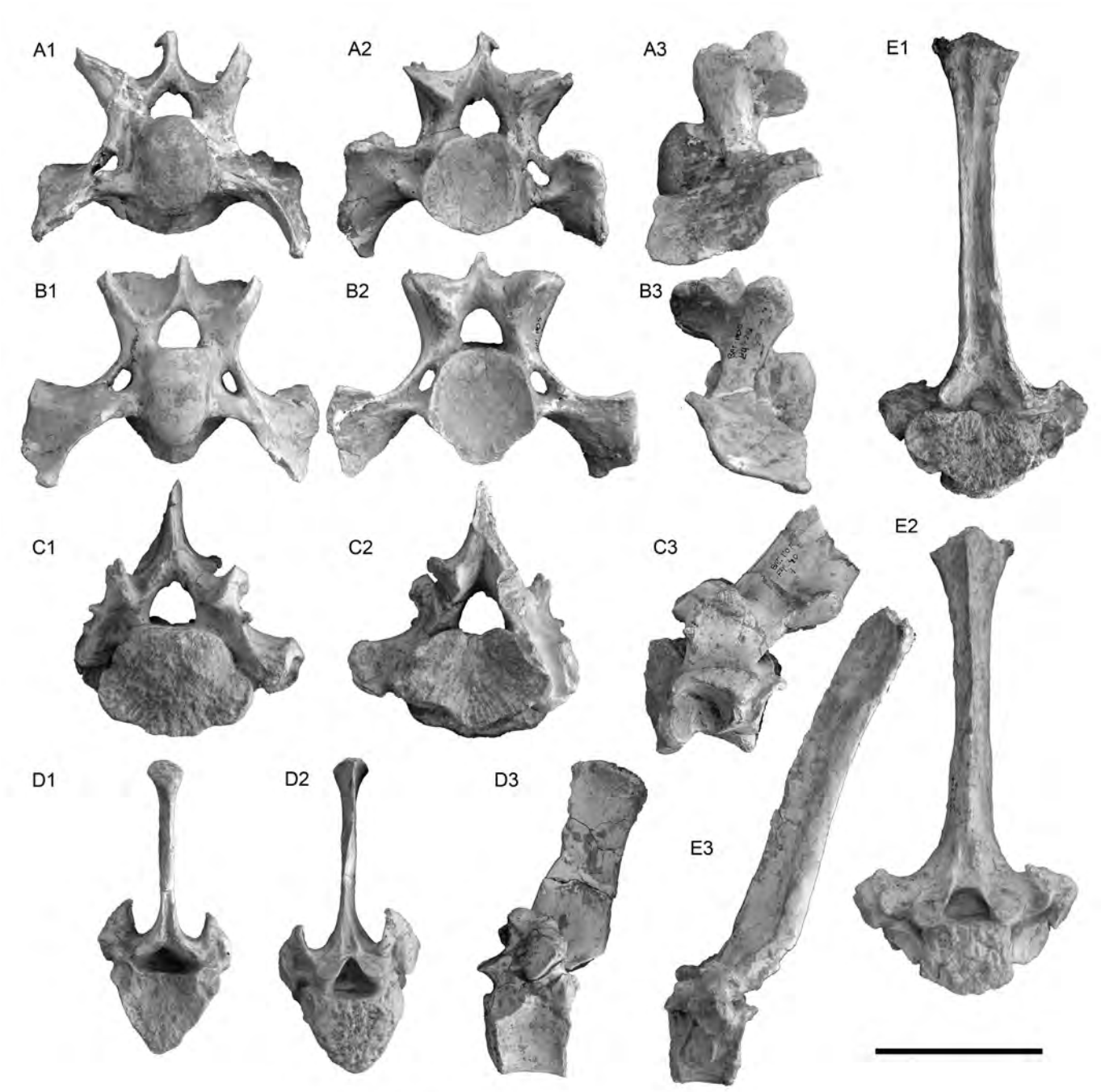


Fig. 7 Vertebrae of *Lartetotherium* sp. from Cerro de los Batallones (Madrid Province, Spain) A, C3 vertebra BAT-1'05 E4-201 in A1, cranial, A2, caudal, and A3, lateral left views; B, C2 vertebra BAT-1'05 E4-202 in B1, cranial, B2, caudal, and B3, lateral right views; C, T1? vertebra BAT-1'07 F4-40 1 in C1, cranial, C2, caudal, and C3, lateral left views; D, L1? vertebra B2748 in D1, caudal, D2, cranial, and D3, lateral left views; E, T5? vertebra BAT-1'06 D3-40 in E1, caudal, E2, cranial, and E3, lateral left views. Scale bar represents 50 mm.

concave surface.The main caudal facet is subsquare (TD = 56 mm; H = 51 mm). Of the couple of caudal costal facets, only the left one is preserved. It is rhomboidal (TD = 28 mm; H = 37 mm), concave and caudally oriented. Additionally, it presents a protruding dorsal edge. The caudal articular processes are placed on the caudal side of the base of the neural spine. Only the right one is preserved. It is oval (TD = 20 mm; H = 26 mm) and flat.

T8? (Fig. 7)—BAT-1'07 F4-61. The main cranial facet is rounded (TD = 58 mm) and present a rough surface, pointing to the loss of the vertebral disk. The neural spine is long (L = 214 mm; measured from the dorsal border of the vertebral canal) and topped by a widened area. Its caudal side is depressed. The vertebral canal is subtriangular (TD = 22 mm; H = 17 mm; cranial side). The cranial articular facets, placed on both sides of the canal, are oval (TD = 18/23 mm; APD = 19/29 mm), flat, and dorso-cranially oriented. The neural arch that separate them from the main cranial facet is very low (H = 9/12 mm). The transverse processes are robust but short and present a flattened dorsal surface. The lateral costal facets are flat, placed on the lateral borders of the transverse processes, are semicircular to oval (APD = 23/25 mm; TD =

24/22 mm), and cranio-laterally oriented. The left one has a small cranial expansion. The articular area of the main caudal facet is flattened and 'heart'-shaped (TD = 64 mm; APD = 55 mm). The dorsal border of the caudal costal facets is aligned with that of the main caudal facet. The first are oval (TD = 21/20 mm; H = 26/26), small and concave.

T10? (Fig. 7)—BAT-1'07 F4-60. Presents a rectangular dorsal spine (H = 125 mm; APD = 43 mm; measured from the dorsal border of the vertebral canal), thin along the shaft (TD = 9 mm), and with smoothed sides. The dorsal tip is rugous and widened. The insertion for the main cranial facet is 'heart'-shaped (TD = 49 mm; H = 48 mm), and rugous. Both vertebral disks are missing. Laterally to the main cranial facet, the cranial costal facets are placed at the level of the dorsal border of the main cranial facet. They are circular (TD = 19/18 mm), flat, cranio-laterally oriented, and do not protrude from the vertebral body in cranial view. The vertebral canal is triangular (TD = 26 mm; H = 23 mm; cranial side). The neural arches present a short (H = 14/16 mm) cranial side and supports the cranial articular facets. They are 'pear'-shaped (TD = 16/12 mm; APD = 22/22 mm), flat, and dorso-cranially oriented. The transverse processes are represented by two short and dorsally oriented lateral flanges. Each one shows a 'comma'-like robust ridge, with the cranial costal facet on the ventralmost side. These facets are long and oval (APD = 17/18 mm; H = 24/25 mm). The insertion of the caudal main facet is triangular (TD = 54 mm; H = 52 mm). The caudal costal facets are rounded (TD = 17/17 mm), flat and caudally oriented. They midpoint surpasses the dorsal border of the main caudal facet. The caudal articular facets are oval (APD = 27/26 mm; TD = 17/14 mm). A longitudinal ventral keel is marked along the ventral border of the vertebral body. B-150 is morphologically homologous and should be ascribed to a adjacent position in the column.

Apendicular skeleton

Scapula (Fig. 8 and Table S5)—The scapula has an triangular contour. Its cranial margin is straight, the dorsal one is convex, and the caudal is sigmoid. The supraspinous fossa is long and nearly rectangular (H ~ 305 mm; APD ~ 90 mm). It is concave and presents a medial bending of the cranial border. The infraspinous fossa is semicircular (H ~ 265 mm; APD ~ 120 mm), flat and presents a short rugous area on its postero-caudal border. The glenoid cavity is rounded, has a long (APD = 62 mm; TD = 15 mm) lateral attachment area. The neck of the acetabulum is well defined. The supraglenoidean tubercle is large, rounded and rugous. It presents a medial expansion close to the acetabulum separated by a shallow depressed area. Such expansion is thin, blunt and rugous. The spine of the scapula starts above the supraglenoidean tubercle. It is triangular (L ~ 275 mm; H ~ 93 mm) and topped with a blunt and rugous tip. The medial side of the bone is flattened. Its excellent preservation permits to describe some muscular insertions.

Humerus (Fig. 9A and Table S6)— Described in Cerdeño (1998). BAT-1'05 E4-224 is robust. The proximal epiphysis has a large (TD = 97 mm; APD = 85 mm) and flattened articular head. The smoothed boundaries of the articular area present a straight angle on its craniolateral side. The trochinter is sharp but not very elevated (~30 mm from the level of the

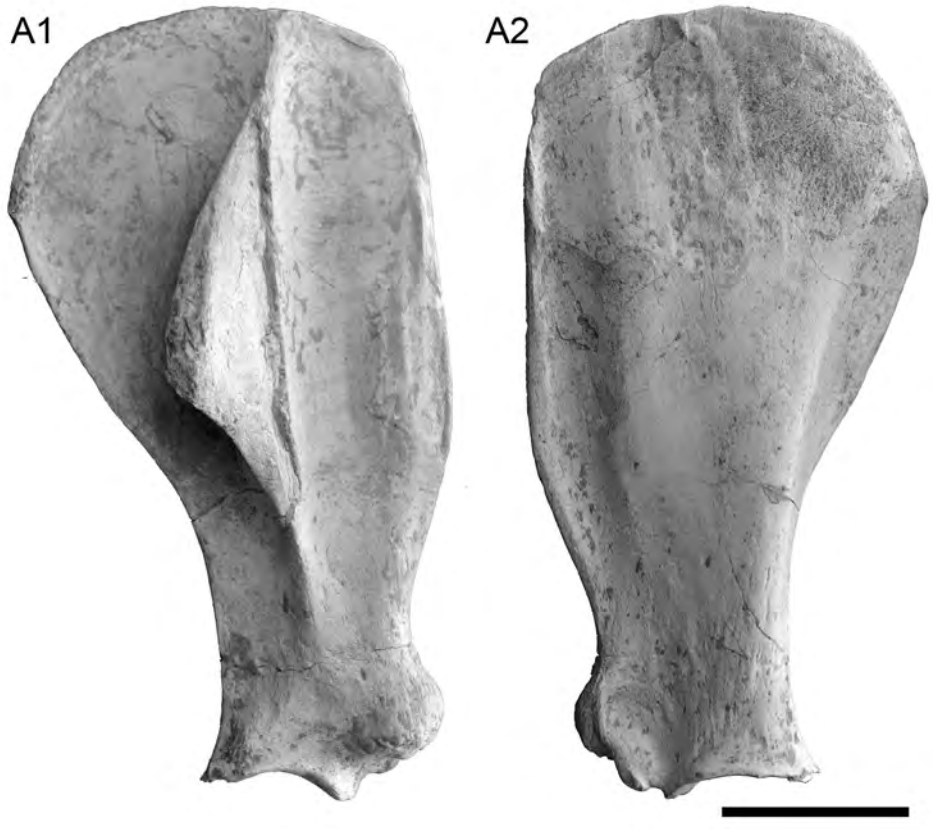


Fig. 8 Right scapula BAT-1'05 F6-241 of *Lartetotherium* sp. from Batallones-1 (Cerro de los Batallones, Madrid Province, Spain) in A, laterall, and B, medial views. Scale bar represents 100 mm.

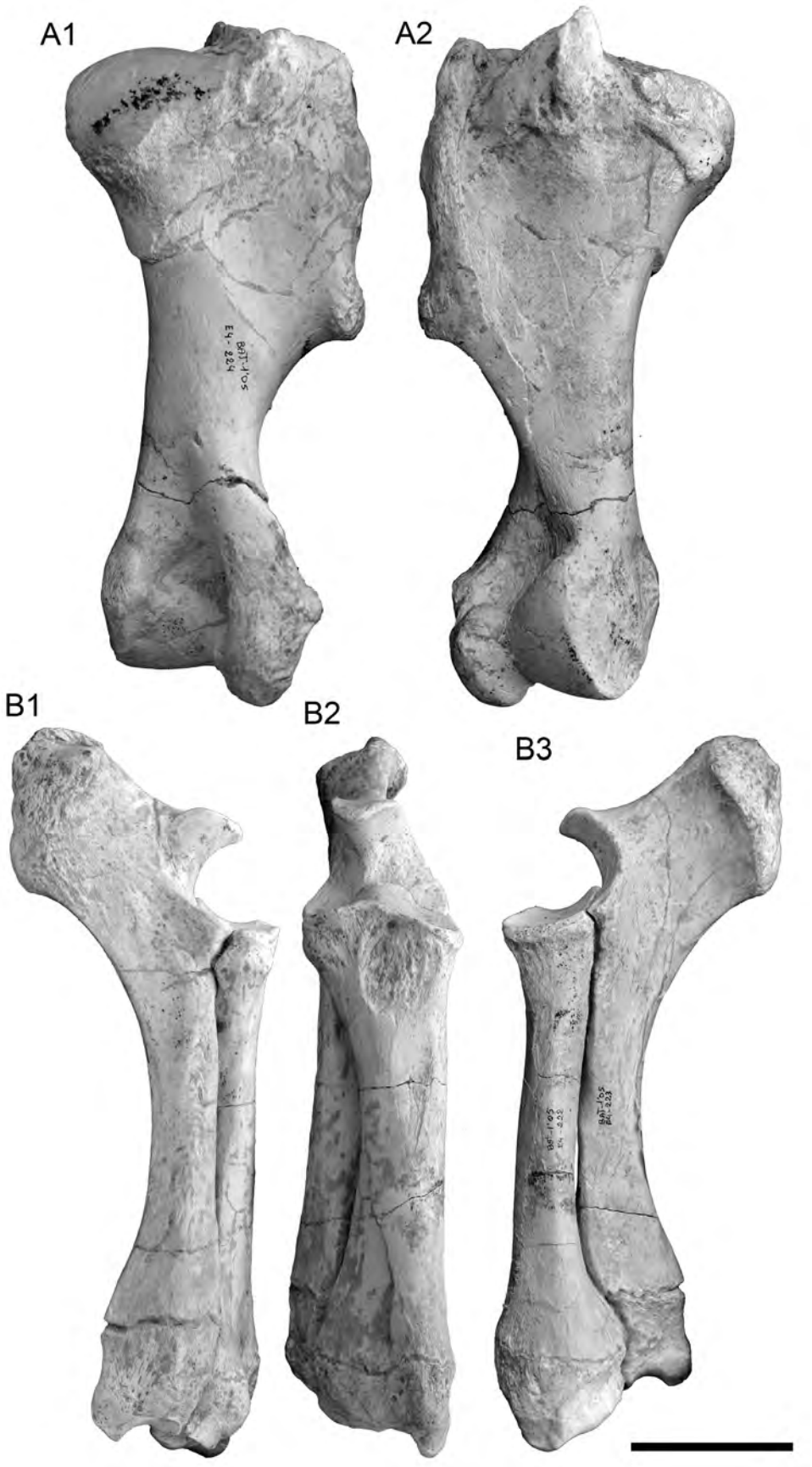


Fig. 9 Anterior limb bones of *Lartetotherium* sp. from Batallones-1 (Cerro de los Batallones, Madrid Province, Spain). A, right humerus BAT-1'05 E4-224 in A1 caudal and A2, cranial views; B, right radius (BAT-1'05 E4-222) and ulna (BAT-1'05 E4-223) in B1 lateral, B2 cranial, and B3 medial views. Scale bars equal 100 mm.

trochlea). The cranial side of the bone is flat and smooth, only interrupted by a big, irregular ridge attached to the border of the deltoid tuberosity (insertion for the m. teres minor). Such ridge extends along the lateral side up to the proximal epiphysis, where it continues as a long ridge (L = 220 mm, H ~20 mm) to the articular head, leaving a shallow, narrow and well-vascularized inner fossa. Both trochinter and the craniolateral extent of the lateral ridge correspond to the attachment of the m. supraspinatus. On the other hand, the posterior half of the lateral ridge serves for the attachment of the m. infraspinatus. The space left between them is wide (L = 60 mm) and shallow (~30 mm). The deltoid tuberosity has nearly straight and rugous lateral border. It ends in a rough protruding angle, place of insertion for the m. deltoideus. The distal end of the deltoid tuberosity is placed at about a half of the total length of the bone. The diaphysis is short and has a subtriangular to rounded section. The fossa olecrani is low and wide (TD = 47 mm). The trochlea is asymmetrical (H major lip = 91.2 mm; H minor side = 59.3 mm). The distal epicondyle hosts the attachment areas for the main flexor muscles of the forearm. The bone B-5981 (left humerus) pertains to the same individual.

Radius (Fig. 9B and Table S7)—The right radius BAT-1'05 E4-222 is slender. The surface of the proximal humeral articular area is biconcave. In proximal view, the medial humeral articular surface is 'D'-shaped, has a concave lateral and caudal borders and convex medial and cranial ones. The lateral humeral articular surface is also 'D'-shaped but smaller. Except for the caudal concave border, the rest of its contour is convex. The caudal ulnar facets of the proximal epiphysis are not accessible. The cranial insertion for the *m. biceps brachii* is coarse, superficial and rounded (TD = 43 mm; H = 53 mm). It is separated from the proximal articular surface by a narrow rim (H = 6 mm). The section of the diaphysis is oval up to its midshaft, 'tear'-shaped thereinafter. The suture of the distal epiphysis is 'V'-shaped in cranial view and placed well-below the ulnar one. The distal epiphysis is laterally wide (high TD) but cranio-caudally narrow (low APD). In dorsal view, the distal epiphysis presents a stout and well-defined bump (TD = 27 mm; H = 39 mm) placed closer to the lateral border. The caudal expansion of the scaphoid-facet is large and bilobed. The medial expansion is high (H = 28 mm) and rounded, the lateral is lower (H = 18 mm) and shows a straighter proximal border in medial view. The whole medial expansion protrudes from the medial surface. In distal view the distal articular surface is divided between the scaphoid and lunate-facets. In this view, the scaphoid-facet is trapezoidal. The lateral border (which contacts with the lunate-facet) is smooth and slightly curved. The cranial and lateral borders are straight, the medial one, boundary between the distal scaphoid-facet and its medial expansion is curved smooth and swollen. Its surface is 'saddle'-shaped cranio-caudally and transversally flat. The lunate-facet is nearly trapezoidal, has a convex lateral border, a convex cranial one, a straight caudal, and a sigmoid medial border (which form an obtuse angle). The surface is cranio-caudally concave and transversally flat. The medial expansion of this facet continues in the medial side with a flattened border that narrows cranially. The caudal pyramidal-facet is semicircular (TD = 14 mm; H = 13,5 mm), flat and does not contact the scaphoid-facets.

Ulna (Fig. 9B and Table S8)—The right ulna BAT-1'05 E4-223 is attached to the radius BAT-1'05 E4-222 through the area below the articular surface in the cranial side of the bone. It contacts the proximal epiphysis of the caudal side of the radius, reaching the distal boundary of the insertion for the m. biceps brachii. The distal contact area between these two bones is located just above the ulnar distal epiphysis suture (equivalent to the lateral border of the radius distal epiphysis). The olecranon is wide but short. The angle formed with the diaphysis is wide and outlines a concave caudal border in lateral view. Its proximal surface is faintly rugous on the lateral side and does not present any bony crest along its border, probably due to its juvenile status. On the other hand, there is a marked shelf along the medial side of the olecranon and a big and narrow bridge running along its proximal edge. In lateral view, the posterior margin of the rugous area of the olecranon is vertical, the proximal one obliquely oriented. The humeral articular surface presents the typical trilobed outline. The proximal lobe is stout and wide (TD = 44.3 mm). The medial one has a straight medial border. The lateral is larger and rounder. All three configure a transversally concave but cranio-caudally convex articular surface.. As in the radius, the cranial radial-facets are not accessible and cannot be described. The cranial angle of the distal articular surface is pointed and distally projected. The diaphysis is triangular near the proximal side, rounded in the midpoint and 'tear'-like towards the distal end of the shaft. In medial view, the distal epiphysis is sigmoid in shape. The pyramidal-facet is semicircular, cranio-caudally concave and transversally convex. It presents a large medial expansion over the caudal half of the epiphysis (H = 25 mm). A narrow lunate-facet runs along the cranial side of the distal articular surface. It is narrow (APD = 6 mm) and flat.

Scaphoid (Fig. 10A and Table S13)—The right scaphoid BAT-1 w/n is very low and rectangular in dorsal view. In proximal view, the radial articular surface is deep (high APD), vaguely rhomboidal, and presents a 'saddle'-shaped surface. The dorsal border is curved, both latero-palmar and medio-palmar somewhat concave and the caudal expansion has a nearly straight outline. Its dorsal surface is irregular and presents a notch above the magnum-facet. In distal view, the three articular surfaces form a semicircular articular area with a convex dorsal outline and a straight medial one (TD = 64.8/64.1 mm; APD = 34.8/36.6 mm). The trapezium-facet is semicircular (TD = 22/17.4 mm; APD = 22/20.7 mm), dorso-plantarly concave and transversally flat, the trapezoid-facet is rectangular (TD = 26.1/27.3 mm; APD = 32.1/31.7 mm), has a longer and curved dorsal border and a straight caudal one. Finally, the magnum-facet is trapezoidal (TD = 31.8/31.7 mm; APD = 29.4/28.8 mm), with parallel and straight lateral and medial borders (the latter longer). This facet is expanded

along the palmar side. The boundary between the magnum and trapezoid-facets is straight, the one between the trapezium and the trapezoid slightly curved. In plantar view, the three lunate-facets are unequally developed. The latero-distal facet is 'leaf'-shaped (APD = 20.1/20 mm; H = 10.5/12 mm), flat, obliquely oriented and placed on the lateral protuberance of the bone, which shows a straight lateral border and is plantarly bended. The latero-proximal facet is bigger, oval (TD = -/35.7 mm; APD = 12.6/12.3 mm), and flat. The third lunate-facet is placed more medially, along the lateral side of the edge of the plantar protuberance. It is long, 'comma'-like (H = -/22.2 mm; APD = -/8 mm), narrow, and flat. This plantar protuberance occupies the medial half of the plantar side, reaching the medial border of the bone. This protuberance is stout, blunt and does not overhangs from the plantar outline.

Magnum (Fig. 10F and Table S16)—The magnum BAT-1'05 E4-192 is long and has a high dorsal ridge in lateral view, with a concave anterior outline and a developed posterior ridge limiting a small, deeply concave space. In anterior view, the anterior side of the bone is wide and has a rounded distal border. The anterior outline of the semilunate-facet is considerably concave and medially projected, resulting in a blunt and protruding peak. The anterior border of the unciform-facet, smaller than the latter, is straight. On the medial side, the medial indentation is not only present but well developed. It is wide, profound and has a posterior straight border. The Mc II-facet is 'sickle'-shaped. The scaphoid-facet is trapezoidal. In distal view, the Mc III-facet is big, oval and presents convergent borders towards the posterior side. On the medial side of this facet, a small rounded salient is present close to the anterior side of the bone. On the lateral one, a more posteriorly-placed shallow rounded indentation is present. The volar process is well developed, horizontally implanted, oval in shape and separated by a basal constriction.

Semilunate (Fig. 10B and Table S14)—The anterior protuberance of BAT-10'09 F3-48 is triangular with keeled lateral borders. The distal border is straight in anterior view. The proximal radius-facet is wide and little expanded posteriorly. The ulnar-facet is present. It is wide and rectangular. On the lateral side, the pyramidal-facet is triangular and flat, with a smooth boundary with the ulnar-facet. The medial scaphoid-facet is oval, narrow and forms an acute angle with the medialmost side of the radial-facet. The unciform-facet is oval and transversally concave. Its posterior end is straight. The magnum-facet is semicircular, concave and presents a smooth boundary with the scaphoid-facet, not reaching the anterior side of the bone. The volar process is less wide than the radius-facet maximum width. The process is posteriorly oriented and laterally tilted.

Pyramidal (Fig. 10C and Table S15)—The pyramidals from Batallones-1 are robust. The dorsal side is smooth and finely vascularized. In proximal view, the proximal ulnar-facet is nearly rectangular. Both dorsal and medial borders are straight, the caudal is convex and the lateral side extends over the lateral side of the bone with a long and triangular expansion with a caudally oriented tip. In medial view, the bone has a straight dorsal border and a concave caudal one. The proximal lunate-facet of the medial side is semicircular (TD = 32.5 mm; H = 10.2 mm), symmetrical, and flat. The distal lunate-facet is narrow (H = 4 mm) except for its caudal expansion, which is well-delimited, large (APD = 15.3 mm; H = 16.1 mm), rounded, flat, and caudally inclined. In caudal view, the bone has a 'tear'-like facet for the pisiform (with a small indentation on its medial side; APD = 15.9 mm; H = 34.4 mm). It is slightly concave and attached to the triangular expansion of the ulnar-facet. The distal unciform-facet is 'fan'-shaped, latero-medially concave and transversally flat. The dorsal border is convex, the caudal and medial ones straight.

Pisiform (Fig. 10D and Table S19)—(BAT-1 w/n). The volar process is quadrangular, has a straight proximal and distal borders and a slightly curved plantar one. The proximal neck is very short in lateral view. A small salient is placed on the distal border next to the articular surface. The medial side is concave and smoothed. Some vascular foramina form an arch along the central side of the volar process. The medial tubercle is big and blunt. The articular surface is transversally swollen. The proximal ulnar-facet is semicircular, the distal pyramidal-facet is subtriangular. Both facets share a narrow contact close to the lateral border and form a straight angle in lateral view.

Trapezium (Fig. 10E and Table S18)—The outline of the left trapezium BAT-1'06 E3-44 is triangular in dorsal view. The dorsal trapezoid-facet is flat, has a straight proximal border and two distal and medial rounded expansions. Both have a shallow indentation between and a deep together with a distally-placed rounded fossa. In proximal view, the scaphoid-facet is semicircular (TD = 18.5 mm; APD = 17.3 mm), dorso-plantarly flat and transversally convex.

Trapezoid (Fig. 10G and Table S17)—A single trapezoid (BAT-10'13 F2-44) has been found. The bone is very robust. The proximal scaphoid-facet is dorso-plantarly concave and slightly convex transversally. Both lateral and medial borders are raised at the same height. The medial facet is loosely separated from the proximal one. The former is trapezoidal and flat. The medial notch is rounded and occupies the whole dorsal half. The notch is not very profound but very well-defined by sharp edges. The plantar side is rectangular and oblique. The lateral magnum-facet has a markedly concave dorsal side, flattening to the plantar one. The distal Mc II-facet is square, has a convex dorsal border, a rounded and expanded dorso-medial angle and a large and convex dorsal one.

Mc II (Fig. 10H and Table S27)—The bone BAT-1'06 F4-203 (right Mc II) is slender. The proximal trapezoid-facet is semicircular, dorso-palmarly concave, and transversally convex. All three dorsal, medial and caudal borders are rounded, the lateral sigmoid. There is a small incision in the medial side of the caudal expansion. In the lateral side of the proximal epiphysis bear two consecutive articular surfaces. The magnum-facet is long, 'tear'-like (APD = 40 mm; H = 13.6) and present two distinct surfaces: the dorsal one is 'sickle'-

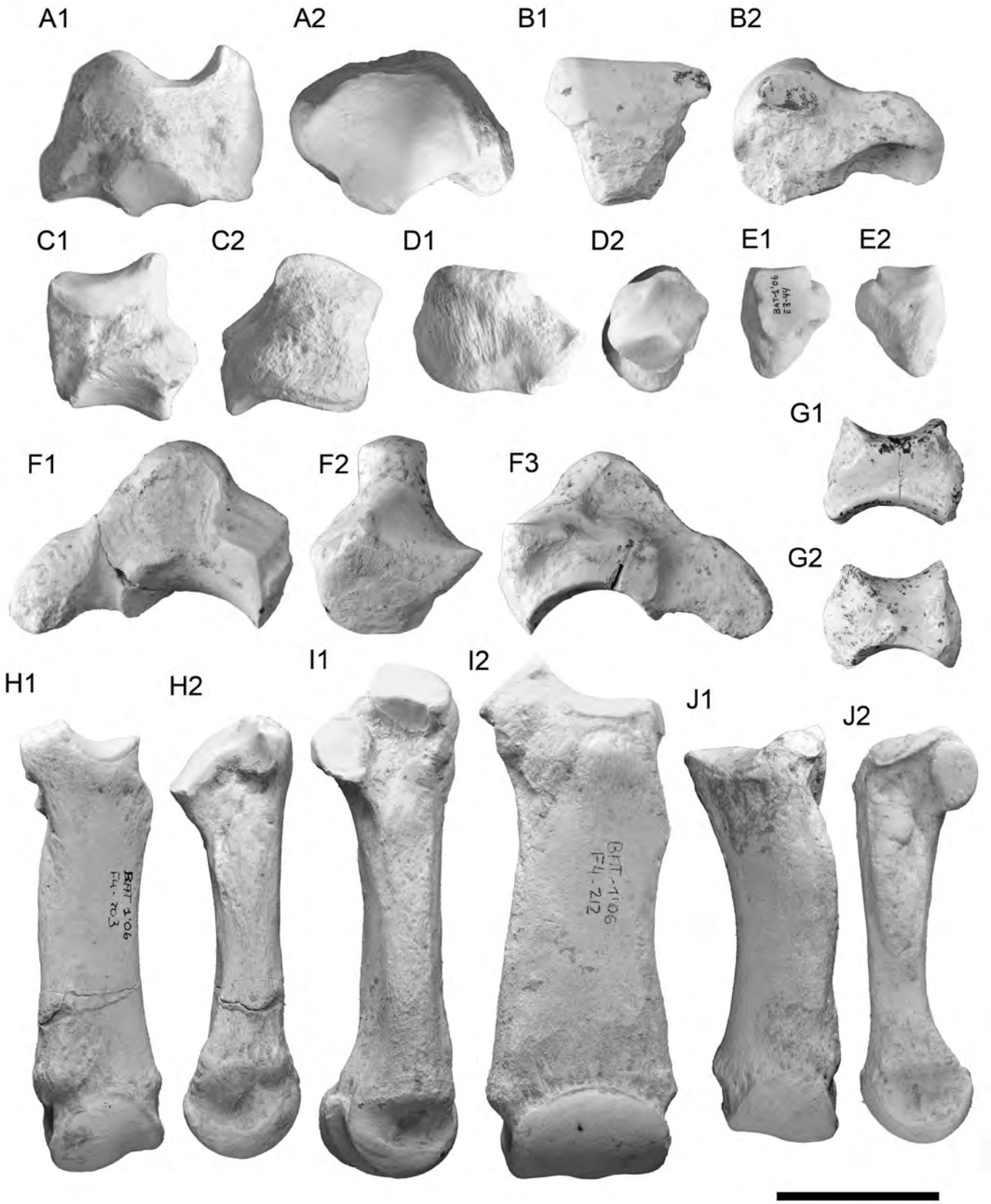


Fig. 10 Carpal and metacarpal bones of *Lartetotherium* sp. from Cerro de los Batallones (Madrid Province, Spain). A, right scaphoid B-w/n in A1, dorsal, and A2, proximal views; B, right lunate BAT-10'09 F3-48 in B1, dorsal and B2, medial views; C, right pyramidal B-w/n in C1, medial and C2, dorsal views; D, right pisiform B-w/n in D1, lateral and D2, dorsal views; E, left trapezium BAT-1'06 E3-44 in E1, dorsal and E2, palmar views; F, right magnum BAT-10'09 E1-21 in F1, lateral, F2, dorsal, and F3, medial views; G, right trapezoid BAT-10'13 E10-44 in G1, lateral and G2, medial views; H, right Mc II BAT-1'06 F4-203 in H1, dorsal and H2 lateral views; I, right Mc III BAT-1'06 F4-212 in I1, dorsal and I2, medial views; J, right Mc IV BAT-1'06 233-292 in J1, dorsal, and J2, medial views. B, C, F, and G are from Batallones-10, whereas A, D, H, I, and J come from Batallones-1. Scale bars equal 50 mm.

shaped and concave, the palmar is flat and 'tear'-like. The Mc III-facet runs distal to the former. It has a semicircular dorsal expansion (APD = 18.3 mm; H = 14 mm) caudally followed by a narrow (H = 4 mm) and flattened rim. Both parts of this facet form an obtuse angle with straight distal borders. The diaphysis has a concave medial border and a convex lateral one. The section is oval and slightly deeper on the lateral side of the bone. The reliefs for the *m. interosei* are smooth and more developed on the lateral side. On the contrary, the medial ones are more distally placed and weaker. The palmar reliefs of the distal epiphysis are shallow and restricted to two depressed longitudinal areas.

Mc III (Fig. 10I and Table S28)—The bone BAT-1'06 F4-212 (right Mc III) is large and robust. In proximal view, the proximal magnum-facet is 'tear'-shaped, has a dorso-plantarly concave and transversally convex surface. The dorsal border is convex and has a small notch on its lateral side, the l ateral border is straight, the medial concave, and the palmar border of the magnum-facet is triangular and palmarly expanded. In lateral view, the articular facets are separated by a shallow and small gap (APD = 6.4 mm). The dorsal facet is formed by the unciform (proximal) and the dorsal Mc IV-facet. Both form a straight angle and present a curved boundary. The unciform-facet is proximo-laterally oriented (with a faint orientation change in its palmar side), flat and semicircular (APD = 29.7 mm; H = 21 mm). The dorsal Mc IV-facet is smaller, narrow, flat, and has a 'tear'-shaped outline (APD = 25.7 mm; H = 11.4 mm). The palmar Mc IV-facet is attached to the proximal border, is somewhat oval to pentagonal (APD = 16.3 mm; H = 23 mm), and flat. It presents a very small, semicircular, extra facet attached to it in the palmar side. The space between both facets is shallow and widens distally. In medial view, the Mc II-facet is 'comma'-like (APD = 21.5 mm; H = 13.2 mm), flat, and has a plantar triangular expansion, distally oriented. This expansion continues as a narrow shelf along the palmar expansion of the proximal articular surface. In dorsal view the bone is smooth, only interrupted by a bumpy area next to the proximal epiphysis that extends to the dorsal side of the lateral protuberance for the unciform-facet. In plantar view, the area of insertion for the m. extensor carpalis are shallow and weak. The lateral is shorter than the medial one, with almost reaches the distal epiphysis. The diaphysis cross section is oval and both lateral and medial borders of the bone diverge distally. In the medial border, there is a small pointed area that marks the limits between the proximal epiphysis and diaphysis. The insertion for the m. interosei are weak and delimited in their distal side but not proximally.

Mc IV (Fig. 10J and Table S29)—The Mc IV BAT-10'10 F4-18 is stout, has an enlarged proximal epiphysis and presents very little distal bending. The proximal unciform-facet is trapezoidal and shows a convex anterior profile. Its surface is transversally concave and longitudinally convex. The Mc III-facets are independent. The proximal one is 'tear'-shaped and flat, the posterior one is bigger, rounded and nearly contacts the proximal articular surface. The Mc V-facet is long and shows a smooth boundary. The area of insertion for the medial m. interosei is coarse but no too swollen. The lateral one, more posteriorly placed, is well delimited by a sharp edge. The diaphysis is profound (has high APD values) and has a subtriangular section. The medial insertion for the m. extensor carpalis is pointed and very proximally placed. The lateral one is blunter and very weak. The distal epiphysis is smooth. The central keel is marked on the posterior side of the bone.

Pelvis (Fig. 11 and Table S9)—(B-2226) A single left hemipelvis including the articular facet of the acetabulum has been found in Batallones-1. The bone is incomplete, and part of the ischium and pubis are missing. The specimen is larger and more robust than that of A. incisivum from the same locality. However, the original morphology of the latter is faded by its proximo-distal flattened, making its comparison difficult. In proximal view, the border of the iliac blade has a rounded latero-cranial side and a shallow concavity on its cranial portion. The shaft of the illium has a triangular section (TD = 88.7 mm; H = 43.2 mm). The iliac blade has a semicircular outline (TD ~ 385 mm; APD = 205 mm from the base of the neck of the ilium). The cranial spinous process of the ilium (coxal tuber) is restricted to a triangular roughened area (53 mm thick) on the lateral angle of the blade. The tuber sacrale has a broken tip. It is wide and aligned with the medial side of the sacropelvic surface. In ventral view, the sacropelvic surface is flat and smoothed except for the sacroiliac joint, which is bumpy, rugous, and extends through an irregular oval surface on the medial side of the blade (93 x 55 mm). On the proximal border of the acetabular area, the ischiatic spine is laterally rugous (with three rugous and parallel oval notches preceding a shallow and rounded fossa). The acetabulum is oval (98.9 x 75.6 mm) and deep. The acetabular notch is 'D'-shaped (has a straight cranial border) and has a wide lateral entrance (13 mm long).

Femur (Fig. 12A and Table S11)—(B-221) The proximal half of the bone is considerably widened at its proximal side, resulting in a nearly triangular outline. The femoral head is oval. In anterior view, the neck of the femoral head is well-defined and rounded in anterior view. The greater trochanter is big, obliquely oriented and has a distal overhanging flange on its latero-distal side. The medial flange is obliquely oriented, running parallel to the greater trochanter, has a straight medial border in anterior view and fades out distally, reaching the distalmost level of the third trochanter. The third trochanter has a trapezoidal outline, is big and anteriorly projected. The anterior side of the distal epiphysis is inclined respect to the posterior side of the epiphysis. The patellar trochlea has a big intercondilar radius. It is centered on the anterior side between both epicondyles. The lateral epicondyle is large and rounded in anterior view, the medial has a pointed outline.

Patella (Fig. 12B and Table S10)—The patella (B-303) is high and has a big and rounded lateral flange. The proximal tip is triangular and rounded, slightly smaller than the lateral flange. The caudal and medial borders are rounded.

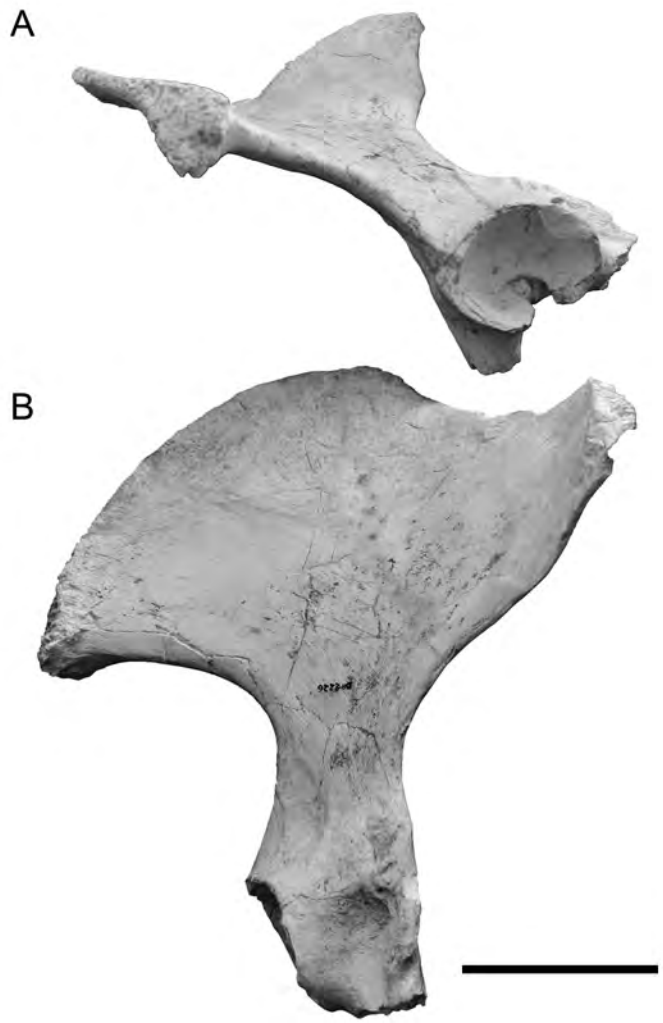


Fig. 11 Left iliac blade of the pelvis B266 of *Lartetotherium* sp. from Batallones-1 (Cerro de los Batallones, Madrid Province, Spain) in A, lateral left view and B, dorsal view. Scale bar equals 100 mm.

The femoral facets of the caudal side are very asymmetrical. The medial one is semicircular and concave, the lateral is rhomboidal, with a blunt proximal border. This facet is not expanded over the lateral flange.

Tibia (Fig. 12C and Table S12)—Described in Cerdeño (1998). B-186 (right tibia) is stout. The proximal articular surface is cranio-caudally collapsed. The proximal epiphysis is wide. The proximal fibular facet is not well-preserved, small (H = 38 mm; TD = 32 mm), and caudally oriented. The insertion for the m. popliteus is wide (TD = 53 mm), rugous, and very shallow. Both tibial spines are similarly developed. The lateral femoral-facet is 'pear'-shaped (APD = 48 mm; TD = 60 mm). Its cranial and caudal borders are straight and diverge towards the lateral border, which presents a straight angle. The surface is cranio-plantarly concave and transversally somewhat convex. The medial femoral facet is 'mushroom'-shaped (APD = approx 57 mm; TD = 56 mm), cranio-plantarly concave and transversally flat. In plantar view, the depression for the ligamentum collaterale mediale is wide (TD = 48 mm) and shallow. It continues through the cranial side of the bone with a shallow gutter (TD = 19 mm; H = 55 mm) which fades out in the diaphysis. The lateral condyle for the ligamentum patellare mediale is placed on the lateral side of the gutter. It is stout, rounded and placed lower than the medial protuberance that delimits the cranial gutter. The diaphysis is robust and presents a triangular section, with a sharp lateral border and rounder medial ones. The distal fibular-facet is triangular, high (H = 59 mm; TD = 48 mm), rugous, and more laterally oriented than the proximal one. A narrow (H = 3 mm; TD = 36 mm) lateral facet runs parallel to the latero-distal border. It presents a semicircular expansion (H = 13 mm) on its cranial side. The distal astragalar articulation is somewhat 'hourglass'-shaped. Both cranial and caudal borders are 'S'-shaped. The medial trochlea is deeper and has a straight medial profile. The lateral one is wider, semicircular, and shallower.

Calcaneum (Fig. 13B and Table S21)—The bone B-2513-2 is stout. The tuber is broad and short, with a marked neck topped with a protruding ridge on the medial side. The sustentaculum is very short and forms a straight angle. The lateral side of the bone is concave. The three astragalar facets are close to each other, being the second and third fused. The first astragalar-facet is big and concave-convex, with a pointed distal and a small and straight uppermost extent. The second one has a trapezoidal to rounded profile and a distally oriented medial border. The third one is a long and narrow surface extending through the distal border of the medial side of the bone. On the distal side, the cuboid-facet has an irregular posterolateral profile and a straight anteromedial one. Its surface is anteroposteriorly convex and leteromedially concave. The calcaneum (w/n; Figure 14) from Valdeinfierno is stouter than the sample from Batallones, probably as a result of the adult age of the individual. The rest of the bone is morphologically equivalent except for its distal side, which is deeper (higher APD).

Astragalus (Fig. 13A and Table S20)—The astragalus BAT-10'12 F2-18 is large and as high as wide. The trochlea is asymmetrical and shallow. The articular surface for the *malleolus medialis* is subvertical. Both lips show a nearly vertical orientation. The lateral one expands distally, leaving a short neck of 3 mm to the cuboid-facet. Except for this constricted far medial of the neck of the astragalus, the rest of the neck is wide and profound. Its trochlear relief fades out on its last medial third. The medial prominence is blunt and poorly developed. The first calcaneum-facet is concave-convex transversally. It is big roughly square and has appointed proximo-medial corner. The calcaneum-facets 2 and 3 fused through a feebly constricted link. The second one is oval and vertically oriented, with a proximal small expansion and a straight distal border. The third calcaneum-facet is elongated, has convex proximal and distal borders and a straight lateral one. The navicular-facet is wide and square and transversally convex. The cuboid-facet is elongated, has a sinusoid surface and is stopped by a very protruding posterior end.

Cuboid (Fig. 13F and Table S23)—The cuboid is large and robust. In anterior view, the cuboid is as wide as high and has

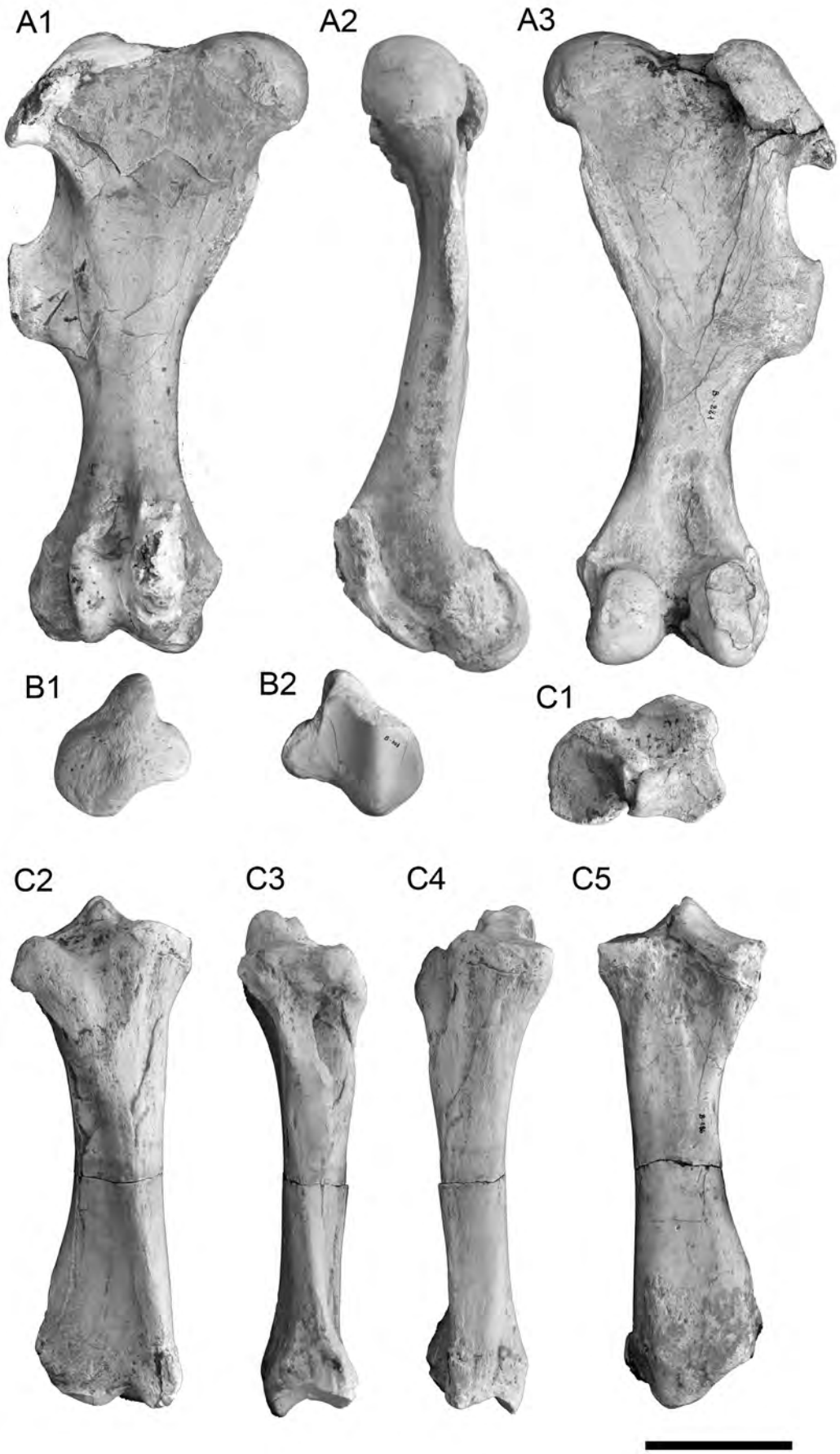


Fig. 12 Posterior limb bones of *Lartetotherium* sp. from Batallones-1 (Cerro de los Batallones, Madrid Province, Spain). A, right femur B-221 in A1, cranial, A2, medial, and A3, caudal views; B, right patella B-303 in B1, cranial, and B2, caudal views; C, left tibia B-186 in C1, proximal, C2, cranial, C3, lateral, C4, medial, C5, caudal views. Scale bars equal 100 mm.

a smooth surface. The volar process is inflated and is very vertically oriented in lateral view, with a distal end surpassing the distal Mt IV-facet. It is limited from the body of the cuboid by a profound and wide gutter. The proximal articular surface is wide, lateromedially convex and has a square outline, with rectangular calcaneum and astragalar facets. Both facets are slightly raised posteriorly. On the lateral side, the anterior navicular-facet is triangular and faint. The posterior navicular-facet is isolated from the anterior one, is oval to 'kidney'-shaped and presents a protruding distal border. The posterior ectocuneiform-facet is attached to the distal end of the posterior navicular-facet, is semicircular and flat. Their boundary is obliquely oriented. The distal Mt IV-facet is very wide, flattened and subtriangular.

Navicular (Fig. 13D and Table S22)—The proximal astragalar-facet of BAT-10'12 F2-36 is squared, has straight anterior and posterior borders, the anterior is convex and the posterior sinusoid. There is no trace of lateral notch. The articular surface is transversally concave and presents a projected and pointed anterolateral angle. On the lateral side, the posterior cuboid-facet is semicircular and has a proximal high trapezoidal expansion, attached to the proximal articular facet. The anterior cuboid-facet is long and semicircular. The distal ectocuneiform-facet is almost triangular, with a rounded and wide indentation on its lateral side, raised from the rest of the articular facet. The mesocuneiform-facet is rectangular, has rounded lateromedial borders and is transversally concave, spreading on the medial side of the bone. The boundary between both facets is rectilinear and presents two triangular lateromedial indentations. The entocuneiform-facet is oval and flat. A marked gutter surrounds the limit between the projection for the cuboid-facet and the mesocuneiform and entocuneiform facets.

Entocuneiform (Fig. 13E and Table S26)—The bone BAT-10'12 F2-32 is large and very wide. The anterior navicular-facet is wide and flat, has a rounded proximal border and an oval to subtriangular outline. The volar process is short, robust and medially curved. The body of the bone shows a medially inflated medial border. The distal mesocuneiform-facet is small and semicircular and is attached to the navicular-facet. The distal Mt II facet is rounded, medially projected and well separated from the mesocuneiform one. The entocuneiform B-791-6 is smaller, has an oval mesocuneiform-facet, a very narrow and faint mesocuneiform-facet and a more curved volar process.

Mesocuneiform (Table S25)—Two Rhinocerotina mesocuneiforms have been found in the butte of Cerro de los Batallones. They show some variation in both medio-lateral and proximo-distal facets while retaining similar proportions. In proximal view, BAT-1'06 F4-210 has a proximal subrectangular surface, a rounded lateral border and a pointed and raised medial tip. In dorsal view, the ectocuneiform facet is semicircular, long in BAT-1'06 F4-210 (TD = 18.5 mm; H = 4 mm) and flat. In BAT-10'13 F2-34 is triangular and higher (TD = 18 mm; H = 7.6 mm). Both are attached to the proximal border and slightly medially displaced. In plantar view, the entocuneiform-facets of these individuals run along the distal part of the proximal border of the plantar side. Both facets are semicircular (TD = 15 mm), flat, and long. In distal view they have flattened, 'kidney'-like distal articular surfaces for the Mt II. They show a rounded lateral border and a medial pointed tip (broken in BAT-1'06 F4-210).

Ectocuneiform (13C and Table S24)—The proximal navicular-facet of B-791-4 has a 'hearth'-shaped outline is flat except for the lateral borders, which are moderately raised. The anterior border is rounded, whereas the posterior one finishes in a blunt tip. In lateral view, the posterior pyramidal-facet is small and semicircular. Only its anterior border protrudes from the lateral side. The anterior pyramidal-facet is not well preserved and has a small size. Both are separated by the lateral incision. On the medial side, the mesocuneiform-facet is restricted to a small ridge on the proximal border. The anterior Mt II-facet is almost imperceptible, as a triangular and blurred area attached to the distal border. There is no trace of posterior Mt II-facet. The distal Mt III-facet is subtriangular, with a smooth and wide lateral incision.

Mt II (Fig. 13G and Table S30)—In proximal view, the bone BAT-10'12 G2-5 has a 'kidney'-shaped proximal facet, with a concave lateral border and a convex medial one. The surface is almost transversally concave and longitudinally flat. A small isolated bump plantarly protrudes from its plantar angle border. In lateral view, the Mt III-facets are about the same size and separated by a small gap (APD = 6 mm). Both facets are aligned in proximal view and laterally-oriented. The dorsal Mt III-facet is circular to pentagonal (H = 14 mm; APD = 15 mm in BAT-10'12 G2-5), flat and contacts the proximal border by a short and straight proximal border. The plantar Mt III-facet is 'tear'-shaped (APD = 14 mm; H = 15 mm), is flat, and does not contact the proximal articular surface (being separated by a very short rim 2 mm high). In plantar view, the entocuneiform-facet is rounded (BAT-10'12 G2-5; TD = 16 mm; H = 15 mm) to oval (B-791(1) and B-2657; TD = 10.6/11.9 mm; H = 15.4/17.3 mm), flat, and medio-plantarly oriented. The proximal lateral insertion for the *m. interossei* is weak but extends along the whole lateral border of the shaft, narrowing from the midpoint of the shaft towards the distal epiphysis as a faintly rugous lateral border. The diaphysis is stout, the proximal half has a 'D'-shaped section, becoming rounder distally. The insertions for the *m. extensor carpalis* are poorly developed, and are only noticeable on B-2657 and B-791 (1). They are represented by faint 'W'-shaped ridges. On the distal articular surface, the lateral lip is convex and the medial one is weakly concave and very reduced in anterior view. The space between the lateral lip and the medial keel is flattened, as in other species.

Mt III (Fig. 13H and Table S31)—the bone is of mediportal type. In proximal view, the proximal ectocuneiform-facet is 'D'-shaped. The dorsal border is convex, the medial one is straight (and forms a nearly straight angle with the former), the plantar border shows straight medial and lateral sides

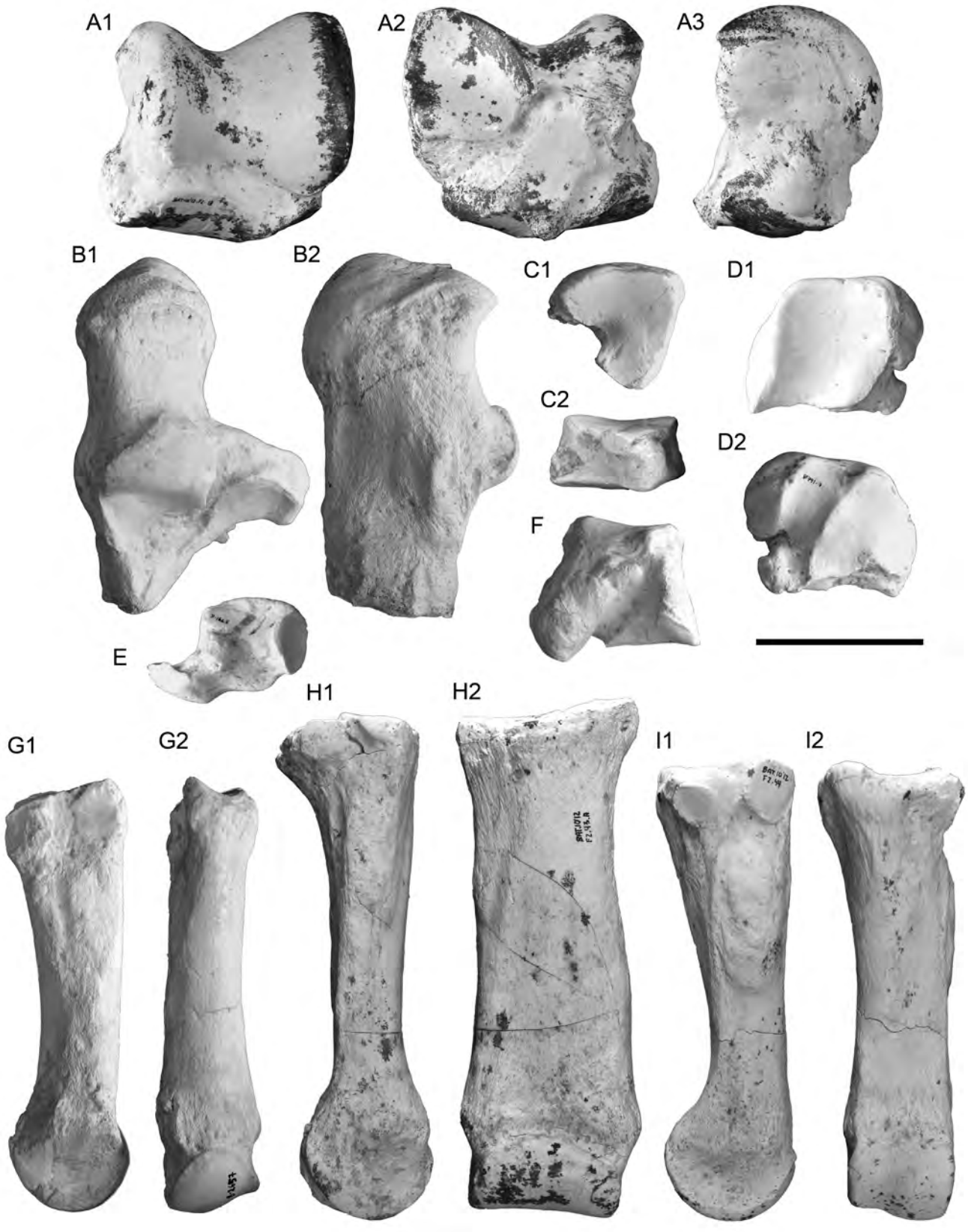


Fig. 13 Tarsal and metatarsal bones of *Lartetotherium* sp. from Cerro de los Batallones (Madrid Province, Spain). A, left astragalus BAT-10'12 F2-18 in A1, dorsal; A2, plantar, and A3, medial views; B, right calcaneum in B1, dorsal and B2, lateral views; C, left ectocuneiform B791-4 in C1, proximal and C2, plantar views; D, left navicular B791-7 in D1, proximal, and D2, distal views; E, left entocuneiform B791-6 in lateral view; F, right cuboid B-2727 in lateral view; G, right Mt II B2657 in G1, lateral, and G2, dorsal views; H, left Mt III BAT-10'12 F2-43A in H1, medial and H2, dorsal views; I, left Mt IV BAT-10'12 F2-44 in I1, medial and I2, dorsal views. A, H, and I are from Batallones-10; B, C, D, E, F, and G come from Batallones-1. Scale bars equal 50 mm.

interrupted by a short (TD = 19.3 mm) and slightly concave central stretch. The proximal articular surface is almost flattened, only showing a faint dorso-plantarly concavity. In medial view, the two Mt II-facets are closely attached to the proximal border, medially oriented, separated by a short gutter (APD = 5 mm) and aligned. Both facets are well-separated from the epiphysis by a short ridge. The dorsal Mt II-facet is rounded to 'D'-shaped (APD = 13 mm; H = 10 mm) and flat. The plantar Mt II-facet is 'fan'-shaped (APD = 13.6 mm; H = 11.9 mm), is flat, and its plantar and proximal borders configure a straight angle. In medial view, the bone presents the two Mt IV-facets attached to the proximal articular surface. They are independent, separated by a gutter 8 mm width and form an open obtuse angle. The anterior Mt IV-facet is rounded (with a straight proximal border; APD = 16.5 mm: H = 18.7 mm), flat and plantarly oriented. The plantar Mt IV-facet is damaged in B-2622 but well-preserved in BAT 10'12 G2-5. In dorsal view, both medial and lateral sides of the shaft are nearly parallel (B-2622) to slightly divergent. The shaft has an oval section. In the plantar side, the insertions for the m. interossei run parallel to the lateral and medial borders of the proximal half of the shaft. They are two long (H = 43 mm; TD = 15 mm), smoothed and carved areas (the lateral is deeper). The insertions for the *m. extensor carpalis* are modest, slightly protruding from the bone outline, and smooth. The distal epiphysis has a flattened distal border in dorsal view.

Mt IV (Fig. 13I and Table S32)—The bone is robust and shows a laterally expanded proximal half. The proximal epiphysis is latero-plantarly expanded. The cuboid-facet is oval, has straight medial and pantar borders and a convex dorsal one. It is transversally concave and longitudinally flattened. A blunt shelf encircles the medio-plantar angle of the facet, and a big tubercle protrudes proximo-plantarly from the latero-plantar side of the proximal facet. As a result, the latero-plantar border of the proximal facet is raised. On the medial side, both Mt III-facets are separated by a narrow gap (APD = 6.7 mm). The anterior Mt III-facet is rounded (APD = 19.2; H = 18.7), flat, bigger than the posterior one, and contacts the proximal articular surface. The posterior facet is oval (APD = 15.8 mm; H = 13.5 mm), flat, and clearly separated from the proximal articular surface by the medio-plantar shelf (H = 7 mm). A small bony crest flanks plantarly the posterior facet. The diaphys has a nearly straight medial border (except for the insertion for the *m. interossei*) and a slightly concave lateral one. It performs an oval section. The medial insertion for the *m. interossei* is nearly rectangular (H = 43.8 mm; APD = 15 mm) and smooth, protruding from the shaft towards its midpoint. The insertions for the *m. extensor carpalis* are poorly-developed as two 'W'-shaped faint ridges.

DISCUSSION

Systematic remarks

Comparison with Lartetotherium

The skull MNHN Sa 6478 from Sansan is cranio-caudally distorted. The diagnosis of *Lartetotherium* includes a strongly concave dorsal profile. Younger rhinoceros individuals show a straighter skull roof, a shorter braincase and an underdeveloped occipital crest. Despite the juvenile age of the skull BAT-1'05 E3-150 from Batallones-1 and its dorso-ventral compression, the occiput is raised and the dorsal profile of the skull concave. This feature, together with the relatively short orbitoaural length roots the skull from Batallones with *L. sansaniense* besides their noticeable difference in size.

The mandibles from Los Batallones Butte show a narrow symphyseal regions and a convex ventral profile. This feature is found in younger genera such as *Ceratotherium*, *Diceros*, or *Stephanorhinus* and is probably related with a loss of the anterior dentition. The anterior teeth of the mandibles found in the butte However, this feature also varies with ontogeny, and younger individuals show more curved ventral borders. Up to

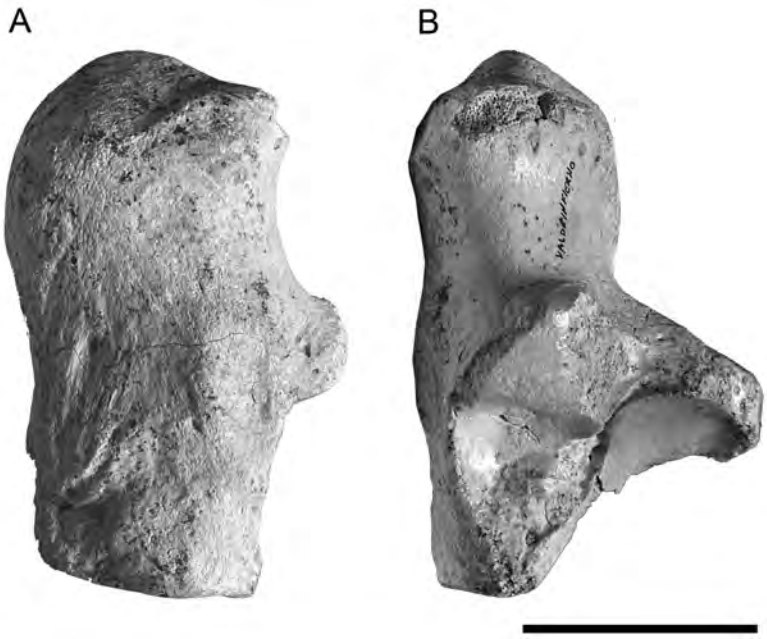


Fig. 14 Right calcaneum VI-w/n of *Lartetotherium* sp. from Valdeinfierno (Madrid Province, Spain) in A, lateral, and B, dorsal views. Scale bars equal 50 mm.

now, no anterior dentition has been found in the butte. The possibility of the presence of small *Lartetotherium*-like tusk-like i2 still encased in the mandible is unlikely, as the individual BAT-2'00 31 (which is broken through the symphyseal region) shows no trace of roots or enamel. In BAT-1'07 F4-22 there are two depressions in the rostral border of the symphisis. If they represent alveoli for the di2, these teeth would be small and short. A single I1 has been found in all the traps from Los Batallones butte. The specimen BAT-10'14 G3-1 has a low crown, its enamel presents a very light longitudinal wrinkling, the root is very robust and triangular in lateral view, has a rugous lateral side and a concave and striated medial one. The apex of the root is blunt and centered along the crown. There is a smoothed rim running along the gingival border of the medial side to the posterior half of the lateral one. The crown is short, presents a medial rounded indentation in occlusal view, and has a transversally concave surface. If compared with the premaxillary bones from the skull BAT-1'05 E3-150, the I1 BAT-10'14 G3-1 is too large for the alveoli and the general outline of the bone, so the belonging to a distinct rhino species not identified yet in the Butte is possible. The reduction and loss of all lower incisors is confined to the Rhinocerotina and some Elasmotheriina, and have been related to the grazing habits of these groups (Heissig, 1989). Regardless of the presence of reduced i2's or the total loss of them, this trait not only separates the Rhinocerotina from Los Batallones from *L. sansaniense* but from other later genera such as *Dihoplus*, placing it closer to *Diceros*.

The upper dentition of *L. sansaniense* from Sansan and Sandelzhausen shares with that from Batallones the rather simple transverse lophs and a lingually-tilted metacone. In contrast, both samples present distinct cingular patterns: in the dental series of BAT-1'05 E3-150 the lingual cingula reach the median valley (in the molar series they fade out from the midpoint of the protocone). The dental series from Sansan (MNHN Sa 6478) lack any cingula in both premolar and molar teeth (except for a small tubercle on the posterior side of the M3). Additionally, the lingual edges of their median valleys do not reach the base of the teeth (leaving a short, inflated neck). In contrary, the median valleys in BAT-1'05 E3-150 are sharper and deeper, reaching the base of the crown. The P2 from the holotype MNHN Sa 6478 has a rectangular outline, squared in Batallones. The DP4 from both samples are very similar as their principal difference, the less lingually expanded protocone than the hypocone in Sansan (MNHN Sa 6371), is probably the result of a broken lingual base of the protocone. Some lesser differences, like the nearly-straight protoloph of the M2 in Batallones can be explained by its earlier wear stage. The smooth anterior protocone fold at its base points to a slightly sinusoid trajectory in more advanced wear stages, more alike to that present in Sansan (MNHN Sa 6478). Another distinctive feature are the more transversally-oriented metaloph in the M1-2 from Batallones, different from the teeth from *L. sansaniense* and other early Rhinocerotina (i.e. *Gaindatherium*), which share parallel metaloph and protoloph and both, in turn, more perpendicular to the ectoloph. However, this character may be also affected at some point by wear.

The radii of the specimens from Batallones area show a more extensive attachement area for the m. biceps brachii, even if we take into account the immature age of the individual from Batallones-1. This surface is rough and carved into the cranial surface of the bone. On the other hand, the radii from *L. sansaniense* have a smaller attachment area. In BAT-1'05 E4-222, this attachment area seems to be divided into two vertically-oriented ovals which recall those found in CA2-46 from M-407 Rotonda (this volume) but with a greater development. If compared with the femora from Batallones, *L. sansaniense* has a more slender bone with a narrower proximal epiphysis, a more developed greater trochanter, and a narrower (but longer) third trochanter. On the other hand, the tibiae of *Lartetotherium* sp. are comparable with those from Sansan and Sandelzhausen. The only differences are a slightly higher robustness as a result of a shorter diaphysis. The astragali from Sandelzhausen (e.g. NB2/NBZ 20.8.1996) have a higher and more slender neck and a more laterally-projected trochlea. The plantar calcanear facets are similar. The calcanei from Sandelzhausen are somewhat distinct: in lateral view, the plantar border of the tuber calcis is smaller and restricted to the proximal side of the bone. In the specimens from Batallones, the tuber calcis is larger and its planto-distal limit is placed just above the level of the proximal border of the 'beak' in lateral view. In the same view, the 'beak' is poorly dorsally projected and the first astragalar facet forms a straight angle (not a smoothed convexity). Metapodials from Batallones are much more robust and have a proportionally wider proximal epiphysis. In the Mt III, while the lateral border of the shaft is also slightly concave, coinciding with *L. sansaniense*, the medial differs in its sinuous border (straight in *L. sansaniense*).

The rhinocerotid remains from Layna (Castilla and Leon Province, Spain) were separated into its own species, *Lartetotherium miquelcrusafonti* by Guérin (1978). Its adult dentition has a more developed secondary enamel folds in both premolars and molars. Some bones like the pyramidal, the ectocuneiform, or the cuboid are comparable in shape. However, others like the metapodials are easily distinguishable from those from Batallones: the overall proportions are more slender, have parallel shaft borders, the Mc III has a narrower unciform-facet, and proportionally narrower epiphyses. The Mt III of *L. miquelcrusafonti* is somewhat more similar, but still differs in the narrower proximal epiphysis and slender shaft. All these differences discards its inclusion to the species.

In summary, the Rhinocerotina skull from Los Batallones butte is larger than the type material of *L. sansaniense*. The differences with the *L. sansaniense* from Sansan and Sandelzhausen rely on the higher development of lingual cingula in both premolars and molars, and the higher robustness and distinct morphology of several postcranial bones. Contrariwise to the craniodental morphology, the postcranial bones, while not close at a specific level, shares a common morphology.

Comparison with other Rhinocerotina genera

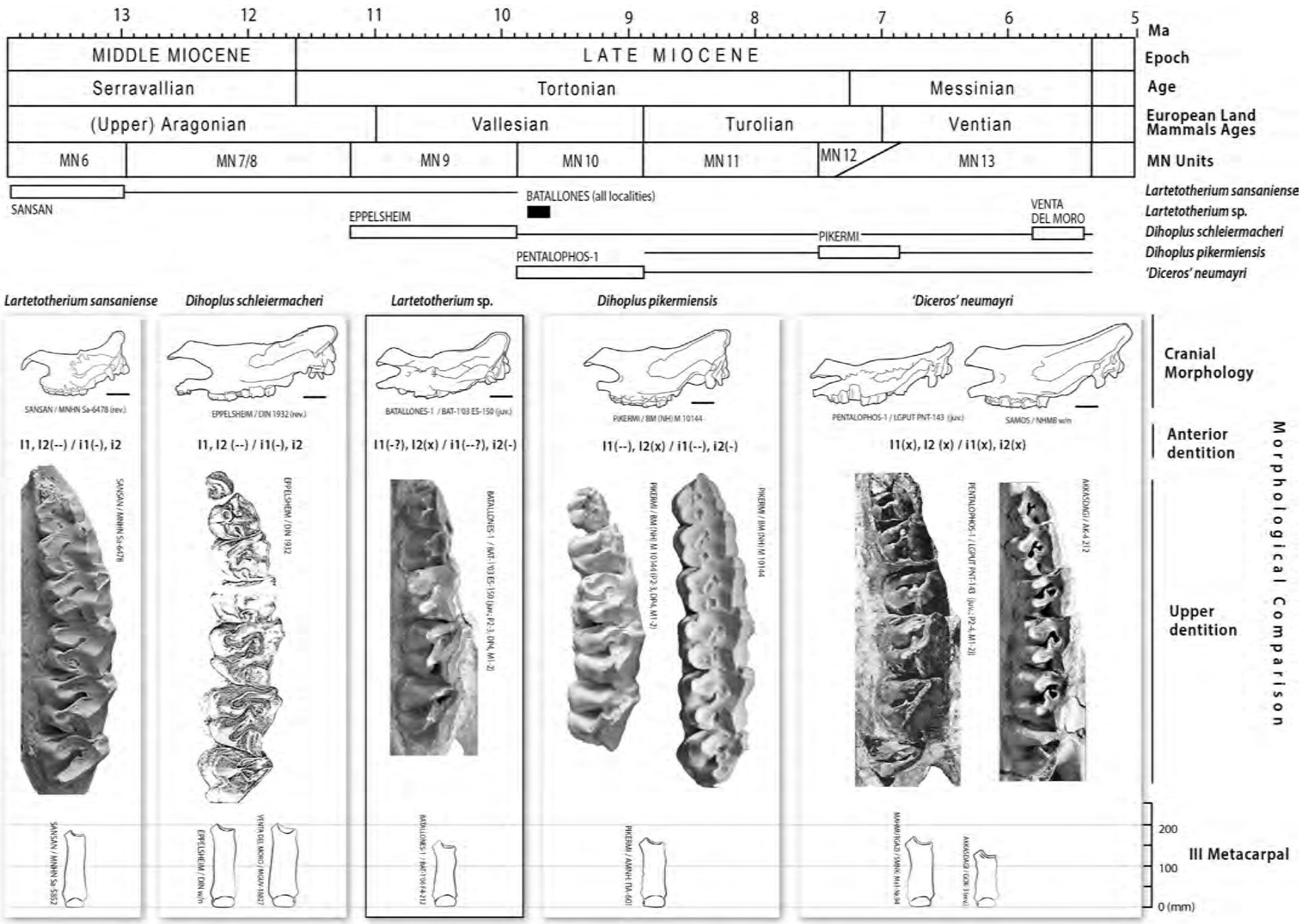
The rather complete view of this new *Lartetotherium* form permits to establish some comparisons with other rhinocerotina genera as *Gaindatherium*, *Dihoplus*, *Diceros*, or *Dicerorhinus*. Craniodental comparisons with some genera discussed in the text are summarized in the Figure 15.

Gaindatherium is one of the earliest Rhinocerotina recorded in the fossil record. If compared with Los Batallones skull BAT-1'05 E3-150, the palate is wider at the level of the P1 and the premaxillary bone shorter. The P1 of *Gaidatherium* lacks the protoloph and the remaining upper dentition differs in its much simpler structure, as it is void of lingual cingula (in BAT-1'05 E3-150 is rather developed in premolars, restricted to the protocone in molars) and the crista is poorly developed (if present). The metaloph of the M1-2 is closer to be parallel to the ectoloph (more parallel to the protoloph in Los Batallones butte). All these characters pose *Gaindatherium* as a more basal genus distinct from the remains from Los Batallones, as demonstrated by phylogenetic analyses (Antoine, 2002; Cerdeño, 1995). In the Iberian Peninsula the genus was cited in the Middle Miocene localities of the Lisbon Area (Antunes and Ginsburg, 1983). However, posterior works discarded its occurrence, in favor of the teleoceratine *Prosantorhinus* (Cerdeño, 1989). Despite little information is available about the postcranial skeleton of *Gaindatherium*, the cited craniodental differences permit to discard the ascription of the remains from Los Batallones Area.

The genus *Dihoplus* encompasses large Eurasian Rhinocerotina species from the Late Miocene and early Pliocene (e.g.: *Dihoplus schleiermacheri*, *Dihoplus pikermiensis* or *Dihoplus megarhinus*). *D. schleiermacheri* is a common representative of the Vallesian and Turolian faunas from Western and Central Europe. The species has been recorded in several localities from the Vallesian and Turolian of the Iberian Peninsula (Cerdeño, 1992). With the exception of *Acerorhinus alfambrense*, large postcranial remains from the Western European Late Miocene have been consistently assigned to *D. schleiermacheri*. The variation shown by these remains exceeds the specific limits and a profound review is indeed required. Given this systematic issue, most comparisons with *D. schleiermacheri* have been restricted to the type collection from Eppelsheim. Up to now, the only two skulls known for the species come from the type locality. A third skull from the locality of Cimişlia (Moldova) was attributed to *D. schleiermacheri* (figured and described in Simionescu, 1940; p. 18). However, the shorter orbitoaural length, the trapezoidal occipital plate, the flattened and high dorsal border of the skull, and the dental morphology point to *D. pikermiensis*. The holotype of *D. schleiermacheri* HLMD DIN1932 hosted in the Darmstadt Hessisches Landesmuseum show several differences with BAT-1'05 E3-150. Most of them are, however, variable with ontogeny. Among these, HLMD DIN1932 has a longer and wider nasal bones with a more pointed nasal tip and stronger horn insertion and a more cranially extended zygomatic crest of the maxilla. Others, though affected to some point by the late juvenile stage, seem reliable to outline the particularities of BAT-1'05 E3-150. These include the presence of a second frontal horn in HLMD DIN1932, the larger and raised occiput of BAT-1'05 E3-150 (nearly straight in *D. schleiermacheri*), the long rostrum of HLMD DIN 1932 or the different outline of the premaxilla in the latter. The type mandible of *D. schleiermacheri* from Eppelsheim (Kaup, 1832; 1834, pl. 11, fig. 8) shows two small but present i1 alveoli and short, but well-developed, tusk-like i2. Giaourtsakis et al. (2006) cites additional mandibles from the type locality that confirms the presence of the i1 alveoli. Both symphyseal regions found in Los Batallones butte (i.e. BAT-1'07 F4-22 and BAT-2'00 31) pertain to immature individuals and show eroded cranial borders. Their detailed examination shows that even though i2 alveoli are indeed visible, the presence i1 alveoli are, at best, questionable. The reduction of the lower anterior dentition takes place at some point between the Vallesian and Turolian. The cheek teeth of *D. schleiermacheri* (HLMD DIN 1932) show several differences respect to BAT-1'05 E3-150. The P1 lacks the oval protocone and protoloph of BAT-1'05 E3-150. The protoloph of the P2 of *D. schleiermacheri* is typically an isolated cusp (like that observed in HLMD DIN 1932). With advanced wear, a faint protoloph is found in some Iberian P2's (Cerdeño, 1989). Instead, in BAT-1'05 E3-150, a weak continuous protoloph is present from an early wear, similar to that observed in *L. sansaniense*. The main differences with the dentition of *D. schleiermacheri* rely on the much more complex secondary enamel folding (as exemplified by the thin crochets in both premolar and molar teeth), and the connection between protocone and hypocone through a lingual wall in P3-4. Moreover, the ectoloph on the premolars are undulated in DIN 1932, flattened in BAT-1'05 E3-150. The cingular configuration of DIN 1932 is similar in the molar teeth but differs on premolars (the lingual cingulum encircles the hypocone and not the protocone as in Los Batallones). Finally, the lingual cingula of the dentition of *D. schleiermacheri* is coincident in the premolars (nearly continuous), but less developed in the M1-2, which show weaker or no cingula encircling the anterior side of the protocone.

In contrast to the overall resemblances in their dentitions, the postcranial skeleton of *D. schleiermacheri* shows several particularities that set this taxa apart from the Rhinocerotina

Fig. 15 (next page) Morphological comparison of several Rhinocerotina species from Europe compared with the sample from Los Batallones Butte (Batallones-1 and 10). For a better comparison, equivalent teeth series to those from Batallones BAT-1'05 E5-150 have been figured apart from the adult ones when possible. Thick bars represent the statigraphic position of the studied localities mentioned in the text. Black lines below represent the biostratigraphic range of the studied species. Dentition of *Dihoplus schleiermacheri* obtained from Kaup (1832-34); dentition from '*Diceros*' *neumayri* from Pentalophos-1 follows Geraads and Koufos (1990); that from Akkasdagi is obtained from Antoine and Saraç (2005). Dentitions not to scale. Scale bar of the skulls equal 100 mm. Abbreviations: juv. : juvenile; rev.: reversed skull for compartive purposes. Anterior dentition abbreviations: I, upper incisors; i, lower incisors;"-", reduced; "--", very reduced, sometimes absent; "x", lost.


13
12
11
10
9
8
7
6
5
Ma
MIDDLE MIOCENE
LATE MIOCENE
Epoch
Serravallian
Tortonian
Messinian
Age
(Upper) Aragonian
Vallesian
Turolian
Ventian
European Land Mammals Ages
MN 6
MN 7/8
MN 9
MN 10
MN 11
MN 12
MN 13
MN Units
SANSAN
BATALLONES (all localities)
EPPELSHEIM
VENTA DEL MORO
PIKERMI
PENTALOPHOS-1
Lartetotherium sansaniense
Lartetotherium sp.
Dihoplus schleiermacheri
Dihoplus pikermiensis
'Diceros' neumayri
Lartetotherium sansaniense
Dihoplus schleiermacheri
Lartetotherium sp.
Dihoplus pikermiensis
'Diceros' neumayri
SANSAN / MNHN Sa-6478 (rev.)
EPPELSHEIM / DIN 1932 (rev.)
BATALLONES-1 / BAT-103 E5-150 (juv.)
PIKERMI / BM (NH) M 10144
PENTALOPHOS-1 / LGPUT PNT-143 (juv.)
SAMOS / NHMB w/n
I1, I2(--) / i1(-), i2
I1, I2 (--) / i1(-), i2
I1(-?), I2(x) / i1(--?), i2(-)
I1(--), I2(x) / i1(--), i2(-)
I1(x), I2 (x) / i1(x), i2(x)
Cranial Morphology
Anterior dentition
Upper dentition
Morphological Comparison
SANSAN / MNHN Sa-6478
EPPELSHEIM / DIN 1932
BATALLONES-1 / BAT-103 E5-150 (juv.; P2-3, DP4, M1-2)
PIKERMI / BM (NH) M 10144 (P2-3, DP4, M1-2)
PIKERMI / BM (NH) M 10144
PENTALOPHOS-1 / LGPUT PNT-143 (juv.; P2-4, M1-2)
AKKASDAGI / AK-4-212
SANSAN / MNHN Sa-5852
EPPELSHEIM / DIN w/n
VENTA DEL MORO / MGAV-10027
BATALLONES-1 / BAT-106 F4-212
PIKERMI / AMNH: TIA-601
MAMMUTOAZI / SNHM: M41-W-94
AKKASDAGI / GDK-3 (rev.)
III Metacarpal
200
100
0 (mm)

from Los Batallones Area. For example, the morphology of the semilunate of *D. schleiermacheri* is highly recognizable for its very high dorsal side and shortened (low APD) volar process (e.g. DIN-1363). In contrast, the sample from Los Batallones shows a short (low H) dorsal border and longer and wider volar process. The femur from Eppelsheim w/n is mostly similar to those from Batallones. Even though, the latter has a more robust proximal epiphysis, a more proximally-placed third trochanter and a more distally-hanging greater trochanter. Similarly, the humerus w/n from Eppelsheim also shows a slightly slender diaphysis and a larger proximal epiphysis. In the astragalus, the lateral lip of the trochlea is significantly larger in Batallones-1 and 10, smaller in the two astragali from Eppelsheim (DIN-1365 and DIN-1922). As a result, the lateral border of the neck of the astragali from Batallones is much lower. The particular shape of the rectangular second calcaneum-facet from Batallones is different from the more squared-shaped that from Eppelsheim. The calcaneum AMNH 98022 (cast) from Eppelsheim is very slender, the proximal side of the medial process is not distally oriented, and the tuber calcis has a characteristic notch dividing two blunt and protruding protuberances. These traits found in Eppelsheim are shared by other calcanei attributed to *D. schleiermacheri* like IPS TR-15585 from Piera (Santafé and Casanovas-Cladellas, 1982). On the other hand, the calcanei from los Batallones butte have a wider distal portion (higher APD), and lack the notch of the tuber calcis. Additionally, the beak is shorter (low APD) and the medial process distally oriented. Despite the overall coincident dental features, we can exclude the assignation of the Rhinocerotina from Batallones to *D. schleiermacheri* for the cited list of differences found in their postcranial skeletons.

D. pikermiensis is a *Dihoplus* species from the Turolian from Eastern Europe. Its anatomy is best known from the Greek locality of Pikermi. As in *D. schleiermacheri*, the skulls of *D. pikermiensis* have a well-developed frontal horn that forms a 'humbacked' dorsal profile of the skull in aged individuals (as that figured in Heissig, 1999; p. 184). As mentioned, this trait is probably absent in BAT-1'05 E3-150 from Los Batallones. Rhinocerotina experienced a hand in hand reduction of both anterior dentition and premaxilla in the Late Miocene-Early Pliocene transition. In this sense, *D. pikermiensis* is more derived if compared to *D. schleiermacheri* (i.e.: highly reduced i1, and reduced i2 and a more reduced premaxilla in the first). This, together with the presence of a unique sagittal crest and a less retracted orbit distinguish the skulls of *D. pikermiensis* from *D. schleiermacheri* (Geraads, 1988; Giaourtsakis et al., 2006). The dental series HLMD 28.1.2000 of *D. pikermiensis* from Pikermi (P2-3, DP4, and M1-2 of equivalent wear to BAT-1'05 E3-150; cast) is morphologically homologous to that from Batallones: the cingular pattern matches that of BAT-1'05 E3-150. The only observed difference is the more constricted hypocone on the DP4 from *D. pikermiensis*. Additional adult series of *D. pikermiensis* reveal an additional difference: the protoloph is often incomplete and does not reach the ectoloph (as in *D. schleiermacheri*). The mandibles of *D. pikermiensis* from Kerassia (Greece; Giaourtsakis et al., 2006) have a straighter ventral border smoothly bended from the m1 to the anterior side. The orientation change observed in the symphisis from Batallones is absent in Kerassia's mandible AMPG K4.387 (figured in Giaourtsakis et al., 2006) and the anterior border of the vertical ramus seem slightly backwards oriented in *D. pikermiensis*, more vertical in *Lartetotherium* sp. Despite the extensive number of fossils bones from *D. pikermiensis* stored in the Greek collections (up to 11 individuals only in the Mytilinii Basin), only a small part of the postcranial skeleton of the species has been figured. The length and proportions of the metapodials of *D. pikermiensis* are consistent with those found in Los Batallones. However, a closer look reveals some differences. The proximal ectocuneiform-facet of the Mt III of *D. pikermiensis* (Antoine and Saraç, 2005; Giaourtsakis et al., 2006) clearly differs from the *Lartetotherium* sp. from Batallones butte () and the proximal epiphysis is larger in the sample from Batallones Area. In proximal view, the dorsal border of the facet is deeply sinuous. Additionally, the cuboid-facets differ in shape and orientation between both species. The astragalus of *D. pikermiensis* has a bigger and rounder second calcanear-facet (narrow, rectangular and obliquely-placed in Los Batallones butte) and a higher neck. The dentition of *D. pikermiensis* has the strongest similarity to that from Los Batallones butte from the taxa used comparison in the present work. However, and as in *D. schleiermacheri*, the postcranial skeleton differs broadly.

D. megarhinus and *D. ringstroemi* are two of the more derived *Dihoplus* species. The premaxillary bones of *D. megarhinus* (finely preserved in the skull AC 2683 from Montpellier) are much longer (gently ventrally bended in AC 2683; straighter in FSL 40026) that of *Lartetotherium* sp. The nasal dome form the median nasal horn insertion is well-delimited (not preserved in AC 2683 but in the incomplete skull without USTL collection number also from Montpellier). The robust and straight nasal bones are also present in the Asian *Dihoplus ringstroemi* (BSPG 2000 I 56), clearly distinct from the shorter and convex nasals from BAT-1'05 E3-150. Besides, the size of the cranial, dental and postcranial bones exceeds by far those of Los Batallones.

The species *'Diceros' neumayri* has been alternatively included in the genera *Ceratotherium* (Geraads, 1988, 2010) and *Diceros* (Giaourtsakis et al., 2009), the same lineages of the extant African rhinos. *'D'. neumayri*, its remains are commonly found in the Turolian of Eastern Europe and Asia (Anatolian Peninsula and the Caucasus). Guérin (1980) reported the the species in the Spanish localities of Cenes de la vega and Los Hornillos. However, these remains were subsequently reassigned to *Dihoplus schleiermacheri* (Cerdeño, 1989). If compared with the adult skull AK4-212 from Akkaşdaği (Antoine and Saraç, 2005), the premaxillary bone is stronger in *Lartetotherium* sp., the occiput raised, the zygomatic arch stronger and the braincase proportionally

shorter. However, most (if not all) of these differences may be modified by their different ontogenetic stages (IDAS 2 of BAT-1'05 E3-150 and IDAS 3 of AK4-212). The subadult skull LGPUT PNT-143 from Pentalophos-1 (Geraads and Koufos, 1990) is equivalent in age with BAT-1'05 E3-150, serving as a reliable source of comparisons. Significantly, both skulls are similar, particularly in lateral view. *Lartetotherium* sp. has a more concave dorsal profile and raised occiput, a longer premaxilla, a less constricted basicranium behind the level of the glenoid articulations, and a trapezoidal occipital plate (not squared as in '*D*'. *neumayri*). Apart from the great resemblance of their skulls, the immature dentition from LGPUT PNT-143 closely matches that from Batallones-1 in practically every feature. However, observations on adult specimens from other localities reveal some differences, mostly related with higher secondary enamel folding (i.e. the presence of crista and long crochet in all premolar and molars, enclosing medifossetes at moderate to advanced wear stages). As far as their postcranial skeletons are concerned, *Lartetotherium* sp. has similar postcranial proportions on the metapodials but more slender carpal and tarsal bones.

The Rhinocerotina remains from Los Batallones Butte represent a new form of *Lartetotherium* species. Its morphology is quite puzzling in the sense that while the skull and dentition resembles the later *Dihoplus*, the postcranial skeleton retains a plesiomorphic morphology closer to *Lartetotherium*. Most features, mainly based on the postcranial skeleton, match that of the type species *L. sansaniense*. The derived characters include the presence of lingual cingula, the loose connection between protocone and ectoloph in the P2, robust long bones, and the reduction of the anterior dentition. The more striking feature, the limb shortening has been reported in other rhinocerotina genera during the Late Miocene. For example, '*D*'. *neumayri* experiences a gradual augment from Vallesian to Turolian (Antoine and Saraç, 2005; Fortelius et al., 2003; Heissig, 1975). In Aceratheriines like *Chilotherium* or *Acerorhinus* a trend towards shorter metapodials has been also reported (Fortelius et al., 2003). It should be added that the presence of a new horned form in the Late Miocene from Los Batallones Area widens the diversity of Rhinocerotina, precluding the taxic turnover that took place in the Mio-Pliocene transition, with the replacement of Aceratheriine and Elasmotheriine by Rhinocerotina species.

Paleoecology and anatomical reconstruction

The completeness of the individual from Batalllones-1 permits to reconstruct its overall life appearance. The result shows a shoulder height of approximately 160 cm, similar to the smaller individuals of white rhino. In living species, juveniles and subadults range between 2/3 and 3/4 of the adult's size (Bigalke et al., 1950; Hitchins, 1970; Schenkel and Schenkel-Hulliger, 1969). In consequence, the potential adult height of the specimen from Batallones-1 might be even higher, surpassing the 190 cm. The dentition of the Rhinocerotina from Batallones while still brachyodont, is closer to the genus *Dihoplus*, and to *D. pikermiensis* in particular. All share unspecialized dentitions typical of generalist browsers (Fig. 15). Among the living species, the closer analogous dentition is that from the Sumatran rhino (*Dicerorhinus sumatrensis*). However, the presence of lingual cingula, and stronger protocone folds may indicate a slightly wider dietary flexibility. Previous authors have linked this dentition with selective browsing on riverine woodlands and open forests, in a similar way to that found in some forest-adapted living *Diceros* subspecies (Giaourtsakis et al., 2009). This kind of specialized browsing on a variable set of environments has been previously proposed for other Rhinocerotina (Sanisidro et al., this work). Isotopic $\delta^{13}C$ (‰ VPDB) analyses from the trap of Batallones-1 were published by Domingo et al., 2012a. The resulting values of the two sympatric rhinos from Batallones-1, showed some small differences. The specimen of *A. incisivum* presents $\delta^{13}C$ (‰ VPDB) isotopic values ranging between -10,52 and -11.78 ‰, whereas the values of *Lartetotherium* sp. ranged between -9.42 and -11.41 ‰ (Domingo et al., 2012a). These results revealed a forested habitat patched with open areas and predominance of C_3 plants (Domingo et al., 2012a) and a similar woodland habitat for both species. The slightly lower values of *A. incisivum* may point to more forested preferences for *A. incisivum*. *Lartetotherium* sp. individual from Batallones-1 would have frequented primarily relatively open woodlands with scattered grasslands. This habitat is more similar to the living black rhino (*D. bicornis*) to the montane forests and closed environments of the Sumatran rhino (*D. sumatrensis*), coinciding to previous works (Giaourtsakis et al., 2009). A niche partition between sympatric acerathere and Rhinocerotina species has been recorded in the isotopic values of $\delta^{13}C$ (‰ VPDB) obtained from the acerathere species *Alicornops simorrense*, which showed more forested preferences than the sympatric *Lartetotherium sansaniense* (Sanisidro et al, this volume). However, only one individual of each taxa have been found in the trap of Batallones-1 thus limiting further isotopic comparisons.

Teeth enamel sampling took place prior to the preparation of most fossil bones from the butte, and follows the taxonomic assignations available at that time (listed in Cerdeño and Sánchez, 1998). The updated study of the sample from Batallones-1 has permitted to assign all the isolated dental remains to a single individual. The arranged isotopic data track a $\delta^{13}C$ depletion along the dental series of *Lartetotherium* sp. from the anterior to the posterior lower teeth (Figure 16). Previous isotopic analyses conducted in rhinoceros teeth show different results. Oxygen isotopes sampled in a mandible of *Diaceratherium douvillei* from Montréal-du-Gers (Béon 1; MN 4) featured a similar increase in heavy isotopes from the p2 to the m3. However, the values for the m1 are not consistent with this increase, being the lowest of the series (Bentaleb et al., 2006).

Adults of extant larger herbivores like rhinos, elephants or hippos, are only preyed opportunistically due to their body size (apart from a few exceptions like the Savuti

lions, which occasionally prey on elephants). Cerro de los Batallones area was populated by a numerous and complex carnivore guild. Among the potential apex predators of large herbivores like *Lartetotherium* sp. there are two sabertooth cats (*Promegantereon ogygia* and the larger *Machairodus aphanistus*) and a bear-dog (*Magericyon anceps*). Such predator-prey interactions were difficult to test among fossil ecosystems. Recent stable isotope analysis has proved to be a useful tool to evaluate the predation-prey relationships among fossil communities (Domingo et al., 2012b). Its results showed that megaherbivores were a minor diet source for these three taxa. However, sick, wounded or younger individuals, as well as carcasses would have been possible dietary resources for the largest carnivores of the butte and cannot be ruled out as occasional preys.

Significantly, most rhinoceros individuals from Cerro de los Batallones fossil complex are immature: one young adult (IDAS stage 3) and four juvenile (IDAS 2). In Batallones-1 two rhinoceros individuals have been found. The first, ascribed to a juvenile *Lartetotherium* sp. (and described in the present work), is associated with the lower ULA and upper LLA of Batallones-1. Its remains are far from being complete and show little weathering and no compactation or fragmentation (unlike most of LLA's; Domingo et al., 2013). Missing parts of this juvenile skeleton may be destroyed during the sepiolite quarrying of the butte. In contrast, the young adult *A. incisivum* individual from the LLA was found almost totally articulated, lying belly-up at the bottom of the trap. The only disarticulated part is the skull, the mandible and part of the neck (found in dorso-ventral orientation). In this case, the animal would have accidentally fallen into the trap. Herbivore trapping would have been a rare success

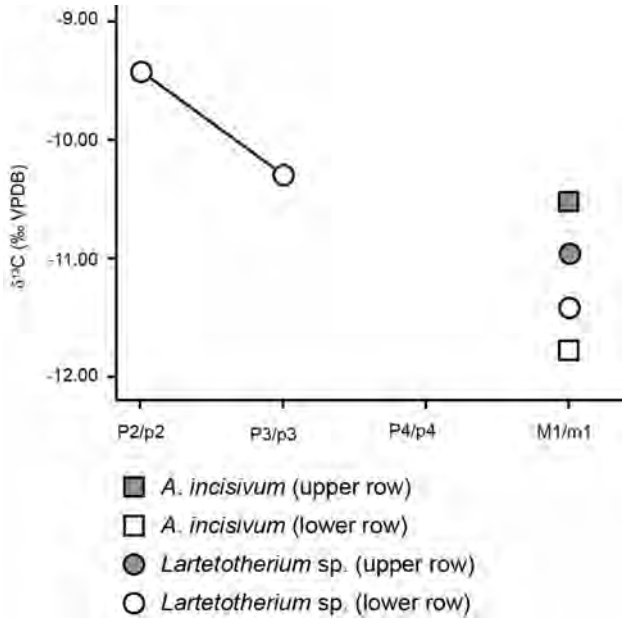


Fig. 16 Samples of $\delta^{13}C$ isotopic values (‰VPDB) from the rhinoceroses from Batallones-1 (Cerro de los Batallones, Madrid Province, Spain) according to Domingo et al.(2012b) ordered by species and dental position.

and the trapping of the *A. incisivum* individual may be an exceptional occurrence (Domingo et al., 2013). Subsequently, it possibly acted as bait that favored the entrance of posterior large carnivores. However, scavenging was somewhat limited, as the skeleton was found rather articulated and lacks large scavenging and/or predation marks. On the other hand, two individuals of *Lartetotherium* sp. and one Aceratheriina indet. have been unearthed from Batallones-10 (ULA), all juvenile. As mentioned, ULA's are associated with lacustrine or swampy habitats, where this rhino may have stuck and rapidly sunk. Young individuals would have been more prone to fall in the traps of the LLAs or stuck in the water bodies typical of the ULAs. In view of the prevalence of immature individuals in Batallones area two questions arise: is the mortality of rhinos higher on immature individuals? and, are the younger specimens more prone to accidental death?. Mortality profiles of living rhino populations vary little among species, and the mortality peaks are commonly centered in adult individuals. Relocated rhinos in Moremi Game Reserve (Botswana) demonstrated that mortality seems biased towards sub-adult males (Lettie Pitlagano, 2007). Black rhinos (*D. bicornis*) from Tsavo NP (Kenya) show a mortality peak around adults (adults; Foster, 1965). Similarly, the study of several wild populations of Sumatran rhino between 1984 and 1999 revealed that most deaths produced by natural causes were focused in adults (Foose, 1999). Demographic studies on the Great one-horned in Chitwan NP (Nepal) show that mortality is much higher in adult individuals, and the main causes of natural death are the old age and intraspecific fighting followed by tiger predation. Mud sink and floods (two of the possible death causes for the large mammals from ULA's like Batallones-1 and 10) are the last causes (12 and 5 % of the total respectively; Adhikari, 2015). On the other hand, studies linking age and causes of death are scarce. Black rhino mortality from Matusadona NP (Zimbabwe) show no link between age and accidental death (N = 18; time span of 11 year; Matipano, 2004).

During the CT-scanning of the skull of *Lartetotherium* sp., electrodense inclusions caused streaking interferences on the detector. In contrast with the density of the surrounding sediment, which provides an average of 878 Hounsfield Units (HUs; Max: 1994; Min: -161) and the type A inclusions, which present 1713 HUs (Max: 2404; Min: 837), the electrodense inclusions presented densities exceeding the maximum attenuation values of the scanner (3071 HUs; Fig. 17A and B). These latter deposits were divided into irregular inclusions (with a maximum diameter of 14.6 mm), small punctual ones (with a maximum diameter of 0.2 mm) or diffuse precipitations filling the fractures (Figure 17A). The results of the RX diffractogram show that the type A inclusions are formed by calcite and the electrodense ones by barite. The presence of authigenic minerals such as barite is not unexpected as it is commonly found associated with opal, frequent in the butte. Jennings et al. (2005) shown that barite formation is linked with shallow water of palustrine-lacustrine environments from poorly drained floodplains.

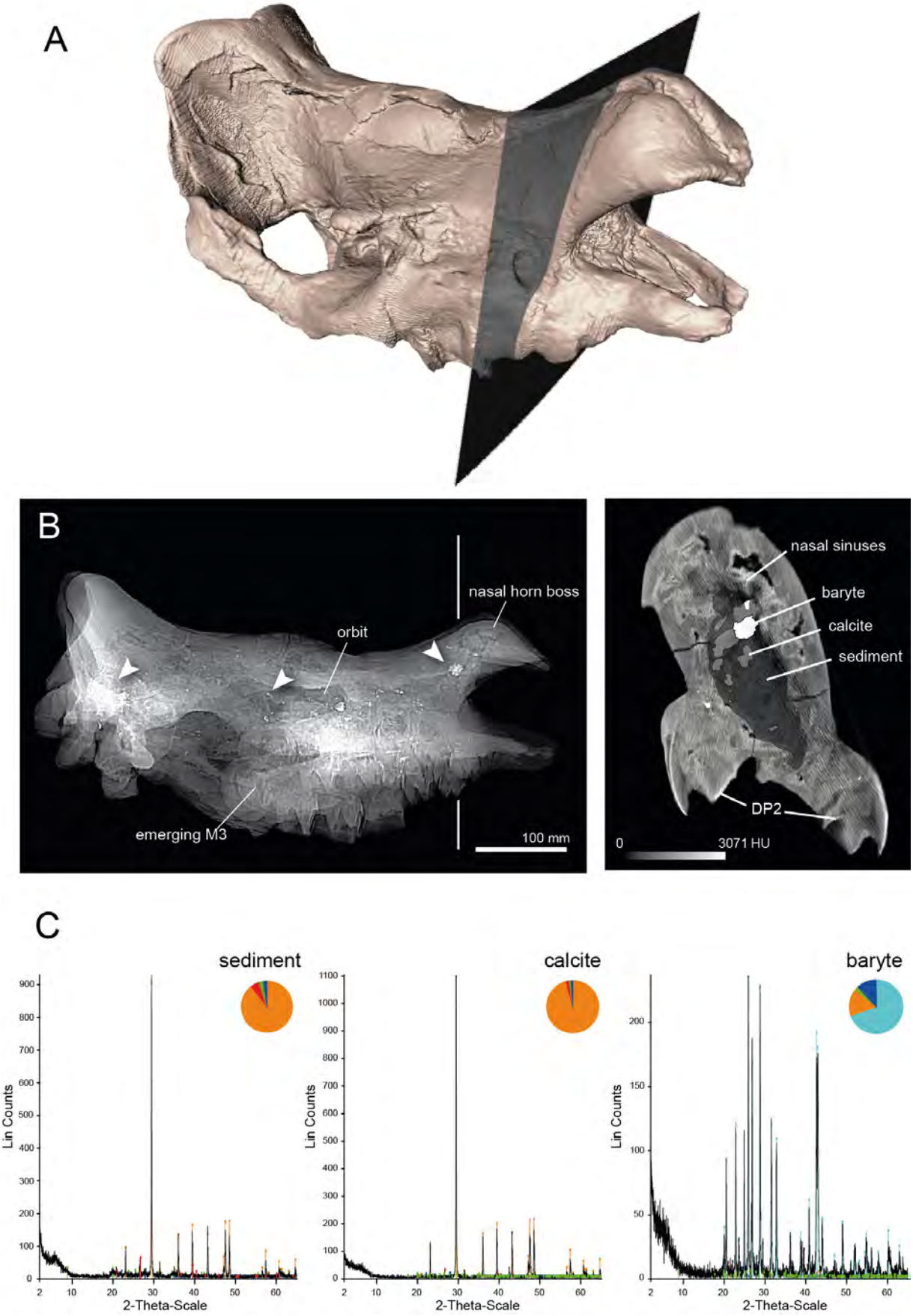


Fig. 17 A, voxel reconstruction of the skull of *Lartetotherium* sp. BAT-1'05 E3-150 from Batallones-1 (Cerro de los Batallones, Madrid Province, Spain) to simulate a lateral radiograph. Arrows indicate, from left to right respectively, the presence of diffuse fillings, punctual precipitations and amorphous concretions of baryte. B, CT-scan slice of the nasal opening at the DP2 level (indicated as a while line in figure A) showing the sampled areas: 1, surrounding sediment. 2, calcite nodule; 3, baryte nodule. C, RX diffractograms from the samples extracted in area detailed in figure B. Scale of figure A equals 100 mm; slice of the figure B (right side) not to scale.

However, the occurrence of barite in continental deposits is not only restricted with such permanent or semi-permanent subaquatic environments. Studies on post-mortem alterations of bones sampled from the savannah grasslands of Amboseli NP (Kenya) gives important clues about the barite formation in vertebrate remains from not-permanently immersed environments similar to those estimated for Los Batallones Area (Morales et al., 2008). In the bones from Amboseli, barite is a very common authigenic mineral (together with calcite, whose is commonly found associated). Barite is always found in void spaces (Trueman et al., 2004). Its development starts early after decaying is initiated as demonstrated by the considerable barite deposits reported in osteonal cavities from 1-2 years post mortem bones (Trueman et al., 2004). However, the described crystals from Amboseli are typically euhedral. In contrast, the observed crystals in Batallones-1 are larger, anhedral-subhedral, and not restricted to the inner bone cavities but to the surrounding space (as shown by the crystal lodged in the middle of the nasal notch).

In summary, the presence of a new form of *Lartetotherium* firstly reported in the present work increases the impoverished diversity of Late Miocene rhinoceros species from Western Europe. Its comparison with the type species *L. sansaniense* revealed several differences related with the dental anatomy and a more robust postcranial proportions. The new *Lartetotherium* has a mosaic of derived (e.g. dentition) and basal features (postcranial skeleton) in a very unique combination.

ACKNOWLEDGMENTS

We acknowledge P. Gutiérrez and B. Alonso for the specimen preparation and P. Pérez Dios (Museo Nacional de Ciencias Naturales de Madrid-CSIC), Dr. O. Sandrock and E. Milson (Darmstadt Hessisches Landesmuseum) for kindly helping with the specimens in her care. Thanks to the Centro Militar de Veterinaria (CEMILVET) and especially to the Vet. Cdr. M. Chamorro for their technical assistance with the CT-scanner and C. Morant for the photographic assistance. This study has been supported by the project CGL2008-05813-CO2-01 (Spanish Ministry of Education and Science).

LITERATURE CITED

Adhikari, K., 2015, Ecology, demography, conservation and management of greater one horned rhinoceros (*Rhinoceros unicornis*) in Chitwan National Park, Nepal [Doctor of Philosophy in Wildlife Science: Saurashtra University, 190 p.

Anders, U., Koenigswald, W. v., Ruf, I., and Smith, B. H., 2011, Generalized individual dental age stages for fossil and extant placental mammals: Paläontologische Zeitschrift, v. 85, p. 321-339.

Antoine, P. O., 2002, Phylogénie et évolution des Elasmotheriina: (Mammalia, Rhinocerotidae): Mémoires du Muséum National d'Histoire Naturelle, v. 188, p. 5-350.

Antoine, P. O., 2003, Middle Miocene elasmotheriine Rhinocerotidae from China and Mongolia: taxonomic revision and phylogenetic relationships: Zoologica Scripta, v. 32, no. 2, p. 95-118.

Antoine, P. O., and Saraç, G., 2005, Rhinocerotidae (Mammalia, Perissodactyla) from the late Miocene of Akkasdagi, Turkey: Geodiversitas, v. 27, no. 4, p. 601-632.

Antunes, M. T., and Ginsburg, L., 1983, Les Rhinocérotidés du Miocène de Lisbonne. Systématique, écologie, paléobiogéographie, valeur stratigraphique: Ciências da Terra (UNL), v. 7, p. 17-98.

Becker, D., Antoine, P. O., and Maridet, O., 2013, A new genus of Rhinocerotidae (Mammalia, Perissodactyla) from the Oligocene of Europe: Journal of Systematic Palaeontology.

Bentaleb, I., Langlois, C., Martin, C., Iacumin, P., Carré, M., Antoine, P.-O., Duranthon, F., Moussa, I., Jaeger, J.-J., Barrett, N., and Kandorp, R., 2006, Rhinocerotid tooth enamel 18O/16O variability between 23 and 12 Ma in southwestern France: Comptes Rendus Geosciences, v. 338, no. 3, p. 172-179.

Bigalke, R., Steyn, T., de Vos, D., and de Waard, K., 1950, Observations on a juvenile female square-lipped or white rhinoceros (*Ceratotherium simum simum* Burchell) in the national Zoological Gardens of South Africa: Proceedings of the Zoological Society of London, v. 120, p. 519-528.

Cerdeño, E., 1989, Revisión de la sistemática de los rinocerontes del Neógeno de EspañaPh.D. Dissertation]: Universidad Complutense de Madrid, 429 p.

-, 1992, Spanish Neogene Rhinoceroses: Palaeontology, v. 35, p. 297-308.

-, 1995, Cladistic analysis of the Family Rhinocerotidae (Perissodactyla): American Museum Novitates, v. 3143, p. 1-25.

Cerdeño, E., and Sánchez, B., 1998, *Aceratherium incisivum* (Rhinocerotidae) en el Mioceno superior de Cerro de los Batallones (Madrid): Revista Española de Paleontología, v. 13, no. 1, p. 51-60.

Domingo, L., Koch, P. L., Grimes, S. T., Morales, J., and López-Martínez, N., 2012a, Isotopic paleoecology of mammals and the Middle Miocene Cooling event in the Madrid Basin (Spain): Palaeogeography, Palaeoclimatology, Palaeoecology, v. 339-341, p. 98-113.

Domingo, M. S., Domingo, L., Badgley, C., Sanisidro, O., and Morales, J., 2012b, Resource partitioning among top predators in a Miocene food web: Proceedings of the Royal Society B.

Domingo, M. S., Domingo, L., Sánchez, I. M., Alberdi, M. T. A., B., and Morales, J., 2011, New insights on the taphonomy of the exceptional mammalian fossil sites of Cerro de los Batallones (Late Miocene, Spain) based on

rare earth element geochemistry: Palaios, v. 26, p. 55-65.

Domingo, M. S., M. Teresa Alberdi, Beatriz Azanza, Pablo G. Silva, and Morales, J., 2013, Origin of an Assemblage Massively Dominated by Carnivorans from the Miocene of Spain: Plos ONE, v. 8, no. 5, p. 1-14.

Foose, T. J., 1999, International studbook for Sumatran rhino (*Dicerorhinus sumatrensis*), Columbus.

Fortelius, M., Heissig, K., Saraç, G., and Sen, S., 2003, Rhinocerotidae (Perissodactyla), *in* Fortelius, M., Kappelman, J., Sen, S., and Bernor, R. L., eds., Geology and Paleontology of the Miocene Sinap Formation, Turkey: New York, Columbia University Press, p. 282-307.

Foster, J. B., 1965, Mortality and ageing of black rhinoceros in East Tsavo Park, Kenya: East African Wildlife Journal, v. 3, p. 118-119.

Geraads, D., 1988, Révision des Rhinocerotinae (Mammalia) du Turolien de Pikermi. Comparaison avec les espèces voisines: Annales de Paleontologie, v. 74, p. 13-41.

-, 2010, 34. Rhinocerotidae, *in* Werdelin, L., and Sanders, W. J., eds., Cenozoic Mammals of Africa, University of California Press, p. 669-683.

Geraads, D., and Koufos, G., 1990, Upper Miocene Rhinocerotidae (Mammalia) from Pentaloph-1, Macedonia, Greece: Palaeontographica Abteilung A, v. 210, p. 151-168.

Giaourtsakis, I., Phlevan, C., and Haile-Selassie, Y., 2009, 14. Rhinocerotidae, *in* Haile-Selassie, Y., and Woldegabriel, G., eds., *Ardipithecus kadabba*. Late Miocene Evidence from the Middle Awash, Ethiopia: Berkeley, Los Angeles, and London, University of California Press and University of California Press, Ltd., p. 429-472.

Giaourtsakis, I., Theodorou, G., Roussiakis, S., Athanassiou, A., and Iliopoulos, G., 2006, Late Miocene horned rhinoceroses (Rhinocerotinae, Mammlia) from Kerassia (Euboea, Greece): Neues Jahrbuch Fur Geologie Und Palaontologie-Abhandlungen, v. 239, no. 3, p. 367-398.

Ginsburg, L., 1974, Les Rhinocerotides du Miocene de Sansan (Gers): Compte Rendus des Seances de l'Academie des Sciences, Paris, v. 278, no. 5, p. 597-600.

Gray, J. E., 1825, An outline of an attempt at the disposition of Mammalia into tribes and families, with a list of the genera apparently appertaining to each tribe: Annals of Philosophy NS, v. 10, p. 337-344.

Guérin, C., 1980, Les rhinocéros (Mammalia, Perissodactyla) du Miocène terminal au Pléistocène supérieur en Europe occidentale : comparaison avec les espèces actuelles: Documents des Laboratoires de Géologie de Lyon, v. 79, p. 1-1184.

Guérin, C., and Santafé, J. V., 1978, *Dicerorhinus miguelcrusafonti* nov sp., une nouvelle espece de rhinoceros (Mammalia, Perissodactyla) du gisement pliocene superieur de Lagna (Soria, Espagne) et de la formation pliocene de Perpignan (Pyrenees-Orientales, France): Geobios, v. 11, no. 4, p. 457-491.

Heissig, K., 1972, Die obermiozäne Fossil-Lagerstätte Sandelzhausen. 5. Rhinocerotidae (Mammalia), Systematik und Okologie: Mitteilungen der Bayerischen Staatssammlung Paläontologie und historische Geologie, v. 14, p. 37.

-, 1975, Rhinocerotidae aus dem Jungtertiär Anatoliens: Geologisches Jahrbuch, v. B.15, p. 145-151.

-, 1989, The Rhinocerotidae, *in* Prothero, D., and Schoch, R. M., eds., The evolution of Perissodactyls, Oxford University Press, p. 399-417.

-, 1999, 16. Family Rhinocerotidae, *in* Rössner, G. E., and Heissig, K., eds., The Miocene Land Mammals of Europe: Pfeil, Munich, p. 175-188.

-, 2012, Les Rhinocerotidae (Perissodactyla) de Sansan, *in* Peigné, S., and Sen, S., eds., Mammifères de Sansan, Volume 203: Paris, Muséum national d'Histoire naturelle, p. 317-485.

Hitchins, P. M., 1970, Field criteria for ageing immature black rhinoceros, *Diceros bicornis* l.: Lammergeyer, v. 12, p. 48-55.

Jennings, D. S., 2005, A paleoenvironmental analysis of Morrison Formation deposits, Big Horn Basin, Wyoming: a multivariate approach [Masters Degree: University of Arkansas, 110 p.

Kaup, J. J., 1832, Über *Rhinoceros incisivus* Cuv. und eine neue Art *Rhinoceros schleiermacheri*: Isis, v. 8, no. 1832, p. 898-904.

-, 1834, Description d'ossements fossiles de Mammifères inconnues jusqu'à présent qui se trouvent au Muséum grand-ducal de Darmstadt, *in* Heyer, J. G., ed., cuaderno 3, p. 33-64.

Lettie Pitlagano, M., 2007, Movement patterns, home ranges and mortality of re-introduced White rhinoceros in the Moremi Game Reserve, Botswana [Master Degree in tropical Ecology and Natural resource Management: University of Life Sciences (UMB).

López-Antoñanzas, R., Peláez-Campomanes, P., Álvarez-Sierra, M. Á., and García-Paredes, I., 2010, New species of *Hispanomys* (Rodentia, Cricetodontinae) from the Upper Miocene of Batallones (Madrid, Spain): Zoological Journal of the Linnean Society, v. 160, p. 725-747.

Matipano, G., 2004, Black rhinoceros mortality in Matusadona National Park, Zimbabwe: 1992-2003: Pachyderm, v. 36, p. 109-112.

Monescillo, M. F. G., Salesa, M. J., Antón, M., Siliceo, G., and Morales, J., 2014, *Machairodus aphanistus* (Felidae, Machairodontinae, Homotherini) from the late Miocene (Vallesian, MN 10) site of Batallones-3 (Torrejón de Velasco, Madrid, Spain): Journal of Vertebrate Paleontology, v. 34, no. 3, p. 699-709.

Morales, J., Capitán, J., Calvo, J. P., and Sesé, C., 1992, Nuevo

yacimiento de vertebrados del Mioceno Superior al Sur de Madrid (Cerro Batallones, Torrejón de Velasco): Geogaceta, v. 12, p. 77-80.

Morales, J., Pozo, M., Silva, P. G., Domingo, M. S., López-Antoñanzas, R., Sierra, M. A. Á., Antón, M., Escorza, C. M., Quiralte, V., Salesa, M. J., Sánchez, I. M., Azanza, B., Calvo, J. P., Carrasco, P., García-Paredes, I., Knoll, F., Fernández, M. H., Ostende, L. v. d. H., Merino, L., Meulen, J. v. d., Montoya, P., Peigné, S., Peláez-Campomanes, P., Sánchez-Marco, Turner, A., Abella, J., Alcalde, G. M., Andrés, M., DeMiguel, D., Cantalapiedra, J. L., Fraile, S., Yelo, B. A. G., Cano, A. R. G., Guerrero, P. L., Pérez, A. O., and Siliceo, G., El sistema de yacimientos de mamíferos miocenos del Cerro de los Batallones, Cuenca de Madrid: estado actual y perspectivas, *in* Proceedings Paleontologica Nova (VI EJIP)2008, Volume 8, p. 41-117.

Peigné, S., Salesa, M. J., Antón, M., and Morales, J., 2008, A new amphicyonine (Carnivora: Amphicyonidae) from the Upper Miocene of Batallones-1, Madrid, Spain: Paleontology, v. 51, no. 4, p. 943-965.

Pozo, M., Casas, J., Medina, J. A., Calvo, J. P., and Silva, P. G., 2006, Caracterización de depósitos carbonáticos ligados a paleosurgencias en el sector de Batallones-Malcovadeso (Neógeno de la Cuenca de Madrid): Estudios Geológicos, v. 62, no. 1, p. 73-88.

Salesa, M. J., Antón, M., Morales, J., and Peigné, S., 2012, Systematics and phylogeny of the small felines (Carnivora, Felidae) from the Late Miocene of Europe: a new species of Felinae from the Vallesian of Batallones (MN 10, Madrid, Spain): Journal of Systematic Palaeontology, v. 10, no. 1, p. 87-102.

Salesa, M. J., Antón, M., Turner, A., and Morales, J., 2005, Aspects of the functional morphology in the cranial and cervical skeleton of the sabre-toothed cat *Paramachairodus ogygia* (Kaup, 1832) (Felidae, Machairodontinae) from the Late Miocene of Spain: implications for the origins of the machairodont killing bite: Zoological Journal of the Linnean Society, v. 144, p. 363-377.

Santafé, J. V., and Casanovas-Cladellas, M. L., 1982, Los Rinocerótidos (Mammalia, Perissodactyla) del Turoliense del Penedès (Piera, Barcelona): Bullt.Inf. Inst. Paleont. Sabadell, v. Any XIV, nº 1-2, p. 39-47.

Schenkel, R., and Schenkel-Hulliger, L., 1969, Ecology and Behaviour of the Black Rhinoceros (*Diceros bicornis*), a Field Study, Hamburg and Berlin, Mammalia Depicta.

Simionescu, I., 1940, Mamiferele Pliocene dela Cimislia (România) – IV. Rhinocerotidae: Academia Româna, Publicatiunile Fondului Vasile Adamachi, Monitorul Oficial si Imprimeriile Statului, Imprimeria Nationala, Bucuresti, v. IX, no. 3, p. 1-50.

Trueman, C. N., Behrensmeyer, A. K., Tuross, N., and Weiner, S., 2004, Mineralogical and compositional changes in bones exposed on soil surfaces in Amboseli National Park, Kenya: Diagenetic mechanisms and the role of sediment pore fluids: Journal of Archaeological Science, v. 31, no. 6, p. 721-739.

van der Made, J., 2010, The rhinos from the Middle Pleistocene of Neumark-Nord (Saxony-Anhalt), p. 463-527.

Van Valen, L., 1966, Deltatheridia, a new order of mammals: Bulletin of the American Museum of Natural History, v. 132, p. 1-126.

APPENDIX 1

Remains of *Dihoplus schleiermacheri* from los Batallones butte area (Madrid Province) and the surrounding area studied in the present work. Localities include Batallones-1, 2, 5, and 10, and Valdeinfierno.

Batallones-1

All the remains of *D. schleiermacheri* found in Batallones-1 pertain to a single juvenile individual. Unlike the other skeleton of *A. incisivum* (found in partial anatomic connection), bones were found scattered in the upper meters of the lower level assemblage of the trap.

BAT-1'05 E3-150, juvenile skull with both P2-3, DP4, and M1-2 series; BAT-1'02 D7-66, left P1; B-5261-2, right DP4; BAT-1'07 F4-22, juvenile mandible with both dp4 and m1-2 series; BAT-1'05 E4-202, C2 vertebra; BAT-1'05 E4-201, C3 vertebra; BAT-1'07 F4-40, T1? vertebra; B2748, L1? vertebra; BAT-1'06 D3-40, T5? vertebra; BAT-1 w/n, hyoid bone.

The following bones pertain to the left limb, scattered around Batallones-1 and mainly found in the earlier campaigns: B791bis, left scapula; B598-1, left humerus; B1530, left scaphoid; B-w/n left pyramidal; BAT-1'06 E3-44, left trapezium; B-w/n, left pisiform; B3219, left lunate; BAT-1'05 D3-34, left Mc II.

The right limb is represented by: BAT-1'05 F6-241, right scapula; BAT-1'05 E4-224, right humerus; BAT-1'05 E4-222, right radius; BAT-1'05 E4-223, right ulna; B-w/n, right pyramidal; B-w/n, right scaphoid; BAT-1'05 E4-192 right magnum; B-w/m, right lunate; B-w/n right pisiform; BAT-1'06 F4-203, right Mc II; BAT-1'06 F4-212, right Mc III; BAT-1'06 233-292, right Mc IV; BAT-1'06 F4-214, right first anterior phalanx III; BAT-1'06 233-292, right second anterior phalanx III; BAT-1'06 233-292, right third anterior phalanx III.

An iliac blade of a left hemipelvis (B-226) has been found in the trap. The correspondent left hindlimb is formed by the following bones: BAT-1'91 791, left femur; B-w/n, left patella; B2513(2), left calcaneum; B791-7, left navicular; B791-5, left cuboid; B791-5, left cuboid; B791-6, left entocuneiform; BAT-1'06 F4-210, left mesocuneiform; B791-4, left ectocuneiform; B791-1, left Mt II; B-791-8, left Mt IV; B791-2, left first posterior phalanx II; B791-9 left metacarpophalangeal sesamoid of the hindlimb.

The right hindlimb is formed by: B221, right femur; B303, right patella; B186, right tibia; B2658, right entocuneiform; B2727, right cuboid; B2513(1)bis, right astragalus; B2657, right Mt II; B2622, right Mt III; B2665, right Mt IV; B581, right first posterior phalanx III; B4887, right second posterior phalanx III.

Batallones-2

BAT-2'00 31, juvenile mandible with both independent ramus (with a dp1-4 and m1 series each); BAT-2 w/n, right second posterior phalanx III.

Batallones-5

BAT-5 w/n, left distal epiphysis of a humerus.

Batallones-10

Remains of *D. schleiermacheri* from Batallones-10 were found in a main cluster within the grids F2, F3, and F4. Additional isolated bones were scattered through the rest of the site.

BAT-10'14 G3-1, I1; BAT-10'09 F3-64, right ulna; BAT-10'09 F3-48, right lunate; BAT-10'13 F2-44, right trapezoid; BAT-10'09 E1-21, right magnum; BAT-10'13 F2-44, right trapezoid; BAT-10'13 F2-47, right Mc II; BAT-10'13 F4-18, right Mc IV; BAT-10 w/n, distal epiphysis of a right femur; BAT-10'12 F2-46, left tibia; BAT-10'12 F2-18, left astragalus; BAT-10'12 F2-18, left navicular; BAT-10'14 F2-9, right navicular; BAT-10'09 F3-27, left cuboid; BAT-10'14 F2-34, left mesocuneiform; BAT-10'12 F2-32, right entocuneiform; BAT-10'12 G2-5, left Mt II; BAT-10'12 F2-43, left Mt III; BAT-10'12 F2-44, left MtIV; BAT-10'13 F2-42, right first posterior phalanx III; BAT-10'13 F2-46, right second posterior phalanx III; BAT-10'12 F4-17, third posterior phalanx III.

Valdeinfierno

VI-w/n, right calcaneum

APPENDIX 2

Measurements (mm) of the skull (Table S1) and mandible (Table S2) of *Lartetotherium* sp. from Batallones-1 and 2 (Cerro de los Batallones, Madrid Province, Spain). Side is detailed as follows: l, left; r: right.

Table S1	BAT-1'05 E3-150
1. Distance between occipital condyle and premaxillary tip	567.0
2. Distance between occipital condyle and nasal tip	532.0
3. Distance between nasal tip and occipital crest	~ 180
4. Distance between the nasal tip and notch	102.0
5. Minimal width of braincase	81.0
6. Distance between occipital crest and postorbital process	311.0
7. Distance between occipital crest and supraorbital tubercle	294.0
8. Distance between occipital crest and lacrimal tubercle	290.0
9. Distance between nasal notch and orbit	150.0
13. Distance between occipital condyle and M3	—
14. Distance between the nasal tip and the orbit	262.0
15. Width of occipital crest	181.0
16. Width between mastoid processes	247.0
17. Minimal width between parietal crests	59.0
18. Width between postorbital processes	~ 190
19. Width between supraorbital tuberosities	~ 195
20. Width between lachrimal tubercles	~ 200
21. Maximal width between zygomatic arches	304.0
22. Width of nasal base	110.0
23. Height of occipital surface	142.0
25. Cranial height in front of P2	181.0
26. Cranial height in front of M1	~ 183
27. Cranial height in front of M3	~ 189
28. Width of the palate in front of P2	~ 62
29. Width of the palate in front of M1	~ 70
30. Width of the palate in front of M3	~ 59
31. Width of foramen magnum	58.0
32. Width between exterior borders of occipital condyles	128.0

Table S2	BAT-1'07 F4-22		BAT-2'00 31g	BAT-2'00 31a
	l	r	l	r
L	497.0	504.0	—	445.0
DAPdia	25.9	36.5	—	42.5
HP1	—	—	—	—
HP2	~ 62	~ 49	65.5	66.8
HP3	~ 64	~ 59	71.7	76.0
HP4	~ 67	~ 64	79.2	82.5
HM1	78.8	83.1	80.5	87.7
HM2	84.2	88.4	89.3	89.1
HM3a	82.3	89.2	—	85.6
HM3p	96.5	94.4	—	—
DAPdent	224.0	220.0	165.0	152.2
Lcor	199.0	198.0	—	—
Lart	214.0	214.0	218.0	259.0
Hcor	258.0	257.0	—	—
Hart	223.0	208.0	—	188.0
DAPhr	174.0	178.0	127.8	138.0
DAPproc	76.4	75.0	—	—
DAPcor	29.5	28.5	34.8	37.0
DAPart	26.4	25.3	24.7	26.7
DTia	—		—	—
DTip	57.8		—	—
Lsin	98.6		—	91.5
DTpx	~ 58		—	—
DTm3p	~ 52		—	—
DTcor-cor	~ 106		—	—
DTart-art	~ 107		—	—
DTart	~ 91	95.6	100.8	98.5

APPENDIX 2 (CONT.)

Measurements (mm) of the upper (Table S3) and lower (Table S4) dentition of *Lartetotherium* sp. from Batallones-1 and 2 (Cerro de los Batallones, Madrid Province, Spain). Side is detailed as follows: l, left; r: right. (D)/(d): decidual tooth.

Table S3		BAT-1'05 E3-150		BAT-1'02 D7-66	B-5261-2
Upper teeth		**l**	**r**	**l**	**r**
	L			(D) 19.7	
P1	W			(D) 20.5	
	H			(D) 20.3	
	L	34.2	33.5		
P2	W	33.9	34.5		
	H	28.1	29.3		
	L		40.1		(D) 40.4
P3	W		46.8		(D) 41.4
	H				(D) 12.7
	L	48.0	49.8		
DP4	W	40.4	42.3		
	H	23.5	22.9		
	L	56.6	53.7		
M1	W	54.0	56.2		
	H	49.0	43.4		
	L	58.6	59.7		
M2	W	55.2	56.4		
	H	—	—		

Table S4		BAT-1'07 F4-22a		BAT-2'00 31b		B-461	Bloque-1 (w/n)
Lower teeth		**l**	**r**	**l**	**r**	**r**	**l**
	L			(d) 16.8			
p1	W			—			
	H			(d) 13.7			
	L			(d) 25.5	(d) 25.6	30.1	
p2	W			(d) 16.7	(d) 16.5	19.5	
	H			(d) 17.7	(d) 15.4	30.4	
	L			(d) 37.2	(d) 37.4		39.1
p3	W			(d) 23.0	(d) 24.3		26.2
	H			(d) 14.7	(d) 13.8		39.7
	L	(d) 41.2	(d) 41.8	(d) 38.1	(d) 39.0		
p4	W	(d) 25.2	(d) 23.6	(d) 25.1	(d) 23.7		
	H	(d) 14.3	(d) 16.5	(d) 16.9	(d) 19.4		
	L	45.0	44.5	45.8	42.8		
m1	W	33.5	32.7	29.7	29.6		
	H	34.3	38.7	34.7	30.9		
	L	49.5	48.4				
m2	W	32.4	31.2				
	H	42.9	45.2				

APPENDIX 2 (CONT.)

Measurements (mm) of the scapulae (Table S5), humeri (Table S6), radius (Table S7), ulnae (Table S8), pelvis (Table S9), patellae (Table S10), femora (Table S11), and tibiae (Table S12) of *Lartetotherium* sp. from Batallones-1, 2, 5, and 10 (Cerro de los Batallones, Madrid Province, Spain). Side is detailed as follows: l, left; r: right.

Table S5			col			art	
Scapula	L	APD max	TD	APD	APD tuber	APD	TD
BAT-1'05 F6-241 (r)	415.0	226.0	30.9	105.7	122.2	84.9	74.9
B-791bis (l)	423.0	—	29.0	102.0	119.0	79.0	69.0

Table S6				prox epi		dia			dis epi					
Humerus	L	Lprox	TD tuber	TD	APD	TD	APD	Ldis	TD	TDtroc	R1	Rmin	R2	APD
B-598-1 (l)	365.0	171.0	132.0	176.0	107.0	67.0	56.0	92.0	150.0	99.0	91.0	45.0	59.0	99.0
BAT-5 w/n (l)	—	—	—	—	—	—	53.6	56.0	—	—	82.9	46.3	—	96.3
BAT-1'05 E4-224 (r)	365.0	167.0	129.0	170.0	128.0	61.0	59.0	75.0	135.0	95.0	89.0	47.0	59.0	109.0

Table S7			prox epi		prox art		dia		dis epi		dis art	
Radius	L	l	TD	APD	TD	APD	TD	APD	TD	APD	TD	APD
BAT-1'05 E4-222 (r)	345.0	325.0	93.0	58.0	93.0	58.0	51.0	43.0	86.0	63.0	81.0	45.0

Table S8		olec					TDtroc		dia		dis art		dis epi	
Ulna	L	TD	APD	H	TD base	APD base	prox	dis	TD	APD	TD	APD	TD	APD
BAT-10'09 F3-64 (r)	438.0	—	—	~ 144	~ 15	~ 96	116.5	84.0	51.3	37.0	—	—	—	—
BAT-1'05 E4-223 (r)	403.0	58.0	101.0	135.0	17.0	93.0	111.0	99.0	35.0	40.0	37.0	55.0	—	—

Table S9			ace	
Pelvis	L	TDcol	TD	APD
B-226 (l)	101.0	88.1	386.0	205.0

Table S10			
Patella	TD	APD	H
B-w/n	81.7	37.7	95.2
303	91.1	39.4	101.1

Table S11						head		prox epi				dia					dis epi	
Femur	L	Ltroc-prox	Ltroc	Ltroc-dis	TD	APD	TD	APD	TD-cue	TD3t	TD	APD	R1	R2	TDtroc	TD	APD
B-791 (l)	427.0	160.0	63.0	218.0	74.1	82.6	180.0	85.7	165.0	113.0	63.5	45.8	115.0	77.6	73.2	107.0	160.0
B-221 (r)	422.0	129.0	61.1	210.0	68.7	86.4	200.0	75.9	19.5	124.0	64.8	48.0	110.0	83.0	67.8	123.0	159.0
BAT-10 w/n (r)	—	—	—	—	—	—	—	—	—	—	—	—	—	80.5	88.7	—	~ 148

Table S12		prox epi		prox art		dia		dis epi	
Tibia	L	LfFi	TD	APD	TD	APD	TD	APD	TD	APD
B-186 (r)	352.0	280.0	58.9	58.3	84.8	114.0	62.0	43.0	93.0	57.0
BAT-10'12 F2-46 (l)	352.0	284.0	~ 62	~ 64	97.0	115.0	65.0	49.0	97.8	79.6

APPENDIX 2 (CONT.)

Measurements (mm) of the scaphoids (Table S13), lunates (Table S14), pyramidals (Table S15), magnums (Table S16), trapezoid (Table S17), trapezium (Table S18), pisiforms (Table S19), astragali (Table S20), calcanei (Table S21), naviculars (Table S22), cuboids (Table S23), ectocuneiform (Table S24), mesocuneiform (Table S25), and entocuneiform (Table S26) of *Lartetotherium* sp. from Batallones-1 and 10 (Cerro de los Batallones, Madrid Province, Spain) and Valdeinfierno. Side is detailed as follows: l, left; r: right.

Table S13

	prox art			dis art						
Scaphoid	TD	APD	H	TD	APD	APD-fMa	APDfTz	APDfTr	TD	APD
B-1530 (l)	44.7	70.0	~ 46	43.9	55.4	31.5	17.9	13.8	64.7	32.3
B w/n (r)	45.7	71.9	51.8	45.9	45.7	31.2	17.3	17.6	49.0	54.4

Table S14

Semilunate	TD-prox	TDdis	TDpal	DAP	H	APD fUn	Hart
BAT-10'09 F3-48 (r)	50.8	29.1	51.4	66.2	45.4	39.6	37.1
B-3219 (l)	50.3	35.3	35.8	65.0	44.8	35.8	21.6

Table S15

Pyramidal	TD	H	APD	APD prox
B-w/n (r)	43.4	52.1	44.7	34.6
B-w/n (l)	45.7	54.9	44.0	31.9

Table S16

Magnum	TD	LfUn	LfSl	APD	H	Hdor	Hvproc	Hart
BAT-1'05 E4-192 (r)	46.5	23.2	30.8	88.8	61.3	38.4	45.9	41.4
BAT-1'04 192 (r)	47.0	31.8	23.1	86.3	60.1	38.6	25.6	32.0
BAT-10'09 E1-21 (r)	48.8	37.1	20.3	88.0	57.2	35.8	30.4	31.4

Table S17

Trapezoid	TD	APD	H	Hmin
BAT-10'13 F2-44 (r)	42.1	27.4	32.1	21.7

Table S18

Trapezium	TD	APD	H
BAT-1'06 E3-44 (l)	36.9	28.7	—

Table S19

Pisiform	APD	DT	H	Hcol	Hart
B-w/n (l)	55.6	29.7	40.1	33.2	31.9
B-w/n (r)	56.3	29.7	40.0	31.4	41.1

Table S20

	(trochlea)										dis art		
Astragalus	TD	H	TDmd	DLinf	H1	Hmin	H2	L1	L2	DL	TD	APD	APD int
B-2513(1) bis (r)	92.8	74.6	69.6	45.5	68.3	45.4	62.5	41.0	24.4	63.0	61.3	42.9	59.4
BAT-10'12 F2-18 (l)	83.6	81.0	74.5	45.1	69.1	46.0	62.7	41.2	23.1	61.6	61.9	42.6	55.2

Table S21

		tuber				
Calcaneum	H	TD	APD	TDsus	APD-beak	TDdis
B-2513(2) (l)	121.5	48.8	65.9	71.1	63.2	42.6
Vl w/n (r)	120.0	48.0	62.0	70.0	69.0	35.0

Table S22

					prox art	
Navicular	APD	TD	H	Hmin	TD	APD
BAT-10'12 F2-36 (l)	64.6	47.0	32.0	22.9	45.5	42.6
B-791-7 (l)	47.4	54.1	29.2	21.2	44.7	43.9
BAT-10'14 F2-9 (r)	47.0	63.0	26.0	23.0	46.0	46.0

Table S23

						prox art	
Cuboid	TD	APD	H	Hdor	Hvproc	TD	APD
B-2727 (r)	42.6	58.5	42.0	40.2	33.4	42.4	42.3
BAT-10'09 F3-27 (l)	41.9	67.8	40.1	39.2	41.2	43.8	41.9

Table S24

	prox art			
Ectocuneiform	TD	APD	H	Hmin
B-791-4 (l)	45.5	41.4	24.9	22.8

Table S25

Mesocuneiform	TD	APD	H	Hmin
BAT-10'14 F2-34 (l)	17.3	36.0	24.0	18.2
BAT-1'06 F4-210 (l)	17.8	—	22.7	16.5

Table S26

Entocuneiform	TD	APD	Hart	H
B-2658 (r)	23.4	35.8	38.0	56.1
BAT-10'12 F2-32 (r)	29.3	59.5	31.2	27.3

APPENDIX 2 (CONT.)

Measurements (mm) of the Mc II (Table S27), Mc III (Table S28), Mc IV (Table S29), Mt II (Table S30), Mt III (Table S31), and Mt IV (Table S32) of *Lartetotherium* sp. from Batallones-1 and 10 (Cerro de los Batallones, Madrid Province, Spain). Side is detailed as follows: l, left; r: right.

Table S27		prox epi		prox art		dia			dis art	
Mc II	L	TD	APD	TD	APD	TD	APD	TDmd	TD	APD
BAT-1'05 D3-34 (l)	138.9	48.7	40.8	26.2	38.6	33.6	20.7	40.4	38.2	36.5
BAT-1'06 F4-203 (r)	141.8	45.0	40.1	29.9	39.5	33.9	20.9	42.9	37.0	37.1
BAT-10'13 F2-47 (r)	146.6	42.0	29.1	24.3	38.1	30.4	25.5	33.9	31.4	39.5

Table S28		prox epi		prox art			dia			dis art	
Mc III	L	TD	APD	TD	APD	HfUn	TD	APD	TDmd	TD	APD
BAT-1'06 F4-212 (r)	161.8	59.0	47.4	43.6	48.1	26.9	46.9	23.3	59.4	49.2	41.4

Table S29		prox epi		prox art		dia			dis art	
Mc IV	L	TD	APD	TD	APD	TD	APD	TDmd	TD	APD
BAT-1'06 233-292 (r)	132.0	43.2	40.0	37.2	36.5	32.5	20.1	40.7	36.5	36.8
BAT-10'10 F4-18 (r)	126.0	48.2	41.5	48.2	36.1	35.2	24.5	43.2	35.6	36.0

Table S30		prox epi		prox art		dia			dis art	
Mt II	L	TD	APD	TD	APD	TD	APD	TDmd	TD	APD
B-791-1 (l)	129.9	39.9	25.5	35.3	21.2	27.0	23.1	27.0	27.2	38.2
B-2657 (r)	131.6	38.2	27.4	35.5	19.5	24.8	22.9	31.8	28.7	37.4
BAT-10'12 G2-5 (l)	134.9	43.4	26.2	20.1	36.0	26.0	25.0	34.2	32.9	36.6

Table S31		prox epi		prox art		dia			dis art	
Mt III	L	TD	APD	TD	APD	TD	APD	TDmd	TD	APD
B-2622 (r)	152.0	48.7	—	46.0	39.7	42.0	23.0	51.1	45.0	39.8
BAT-10'12 F2-43 (l)	154.0	55.0	44.3	53.2	42.0	43.6	24.0	55.0	45.9	38.4

Table S32		prox epi		prox art		dia			dis art	
Mt IV	L	TD	APD	TD	APD	TD	APD	TDmd	TD	APD
B-791-8 (l)	131.5	44.4	37.6	38.6	32.6	25.8	24.3	27.7	27.0	36.5
B-2665 (r)	135.1	41.7	39.7	38.2	32.7	26.0	27.6	28.4	28.1	38.2
BAT-10'12 F2-44 (l)	138.0	47.9	38.8	44.4	31.2	31.2	23.7	33.7	32.0	39.5

12. Rhinocerotidae remains (Mammalia, Perissodactyla) from the Upper Miocene site of Corral de Lobato (Guadalajara, Spain)

Oscar Sanisidro
Patricia Pérez
and Jorge Morales

Abstract. It is the aim of this paper to describe the first rhinoceros remains from the Turolian site (MN12-13) of Corral de Lobato (Guadalajara, Spain) These remains belong to *Dihoplus* cf. *Dihoplus schleiermacheri*. This taxon is known from several Upper Miocene sites from Western and Central Europe but usually remains as a scarce species in the Iberian Peninsula. The likely *D. schleiermacheri* remains discussed here show some postcranial particularities respect the type collection from Eppelsheim as the shortened and robust Mc III and Mc IV.

INTRODUCTION

Corral de Lobato fossil site is situated on the slope of a butte about 2 Km East of the village of Molina de Aragón (40º50'N, 1º51'W, Guadalajara Province, Spain; Figure 1). The fossils are embedded in a sandy clay matrix together with quarzitic clasts (both rounded and subangulous). These fossiliferous sediments fill the spaces left by the erosion of the Raethian / Hettangian dolomitic basement of the hill. Topping the dolomitic materials of the butte, there is an upper layer of reworked materials used as crop fields. Fossils from the Late Miocene fauna from Corral de Lobato have been collected sporadically for more than 50 years. Systematic excavations conducted by the Museo Nacional de Ciencias Naturales-CSIC at the site of Corral de Lobato began in September 2013. Up

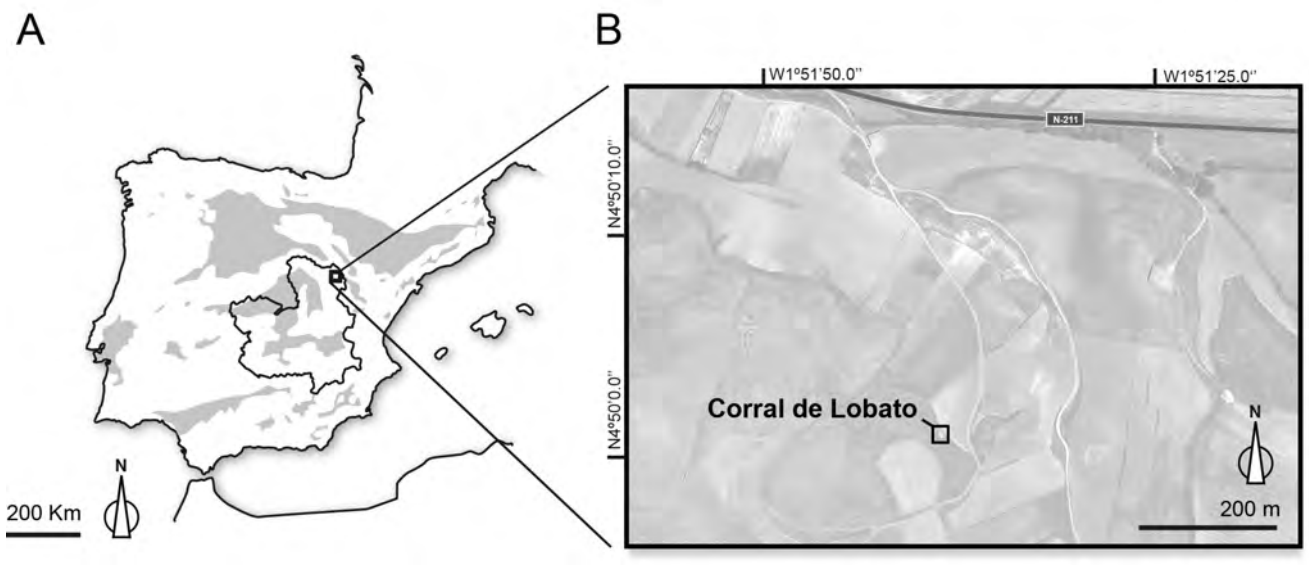


Fig. 12.1. A, Simplified general map of the Iberian Peninsula with the Tertiary basins represented as shaded outlines and B, a detail map showing the Castilla la Mancha Province with the location of Corral de Lobato.

to now, the fossil site has provided a rich faunistic association formed by the taxa: *Hipparion concudense*, *Gazella deperdita*, *Tragoportax gaudryi*, *Microstonyx erymanthius*, *Pliocervus* aff. *matheroni*, Sivatheriinae indet., *Amphimachairodus giganteus*, *Thalassictis hipparionum*, *Adcrocuta eximia*, and remains of an undetermined small carnivore species (Pérez et al., 2013). The faunal assemblage has been dated as Turolian, probably an early MN 13 biozone (Mein, 1999) based on the ocurrence of the cervid *Pliocervus* aff. *matheroni*. However, a late MN 12 cannot be excluded due to the persistence of *Microstonyx erymanthius*, *Hipparion concudense*, and the abundance of *Gazella deperdita*. The rhino from Corral de Lobato was originally determined as *Dihoplus* cf. *Dihoplus schleiermacheri*. *D. schleiermacheri* is one of the largest rhinoceros species from the Miocene. Its biostratigraphic distribution extends from the upper Vallesian (MN 9 Mein's Biozone) to the lowermost Pliocene (MN 14) of Alcoy-Mina, where it remained as relict taxa. Its holotype was described by Kaup (1832, 1834) on the basis of the type material from the German locality of Eppelsheim. Thereinafter, the species has been reported from 25 localities of Western Europe. Despite poorly represented in Corral de Lobato (the species comprises the 0,75% of the total recovered elements), a few European sites yield rather complete osteological samples. These are Eppeslheim, Mont Luberon, and La Roma-2. In the present paper we describe new material from Corral de Lobato (Upper Miocene) and compared them with other remains from Western Europe, providing new insights into the intraspecific variability of the species.

MATERIAL AND METHODS

All the studied specimens from Corral de Lobato are stored in the Museo Nacional de Ciencias Naturales, Madrid. Measurements are given in millimeters with an accuracy of one decimal digit. Approximate measurements are given in parentheses. Measurements were made with a digital caliper and a measuring tape for elements larger than 150 mm. The terminology applied in the description of the anatomical characters generally follows Guérin (1980), but that used by other authors has also been taken into consideration (Antoine, 2002; Heissig, 1972, 1999).

Anatomical Abbreviations—ant, anterior; art, articulation; dia, diaphysis; dis, distal; dor, dorsal; int, interior; epi, epiphysis; max, maximum; min, minimum; pal, palmar; prox, proximal. Capital letters are used for upper teeth (D, P, M; upper decidual, premolar and molar respectively), and lower case for lower teeth (d, p, m).

Measurements abbreviations—APD, antero-posterior diameter; H, height; L, length; TD, transverse diameter.

Institutional abbreviations—FSL, collections de l'Universite Claude-Bernard Lyon-I; HLMD, Darmstadt Hessisches Landesmuseum; MNCN, Museo Nacional de Ciencias Naturales - CSIC (Madrid, Spain).

Some postcranial associated bones of *D. schleiermacheri* ascribed to "Eppelsheim" were recovered. Among the available casts made from the type collection and stored in the AMNH, neither ectocuneiform nor Mc II are present. Additionally, we have used as a reference the remains of *D. schleiermacheri* from the localities of Venta del Moro, Crevillente-2, Alcoy-Mina (this volume), Concud, Puente Minero (Teruel, Spain), and Montredon (Hérault, France).

Referred material—CL'12-100, fragmentary DPx; CL'12-384, incomplete right DP1; CL'13-16, right P3; CL'12-101, left p3; CL'12-591, right p3; CL'13 A5-62, right p4; CL'14 A3-29, right px; CL'13 A5-46; CL'14 A3-24, m3?; CL'14 A4-98, left Mc III; CL'14 A5-removido, right Mc IV; CL'13-43, distal fragment of a tibia; CL'13-45, right ectocuneiform.

SISTEMATIC PALEONTOLOGY

Family Rhinocerotidae Gray, 1821

Subfamily Rhinocerotinae Gray, 1821

Genus *Dihoplus* Brandt 1878

Type species—*Dihoplus shcleiermacheri* Kaup, 1832

Other species—*Dihoplus pikermiensis* (Toula, 1906), *Dihoplus ringstroemi* (Ringstrom, 1924).

Dihoplus cf. *Dihoplus schleiermacheri* Kaup 1832

Holotype—Complete skull of an adult DIN 1932 with both P2-M3 (Text-fig 2) from Eppelsheim (MN9).

Type locality— Eppelsheim, Rheinhessen, Germany (probably MN 9, Early Vallesian)

Diagnosis—Guérin (1980) defines *D. schleiermacheri* according to the following diagnosis: "*Dicerorhinus* of a large size. Long skull with bulky nasal bones finishing in a downwards curved tip; a frontal convexity that corresponds to the insertion of the second horn; high occipital crest and occipital plate little backwards and upwards inclined; sagittal crest preset; open auditory meatus; posttympanic apophysis longer than postglenoid; long mandibular symphisis with a constant width forming a strong angle with the horizontal ramus; high ascending ramus with a concave-convex ventral border; strong angular process; developed anterior dentition (I1, small I2, and i2). Upper cheek teeth with undulated ectoloph, crista and crochet generally present and variable development, sometimes multiple; protoloph and metaloph of the upper premolars in contact from their bottom and forming a lingual wall with wear; usually absence of lingual nor labial cingula; protocone and, sometimes, hypocone isolated in little worn premolar teeth; lower cheek teeth frequently with 'V'-shaped valleys and a considerable unlevelling in their lingual cusps, usually without anterior or posterior cingulida; *Dicerorhinus*-like postcranial skeleton with elongation of the second and third limb segments".

Posteriorly, Geraads and Spassov (2009)completes the

previous diagnosis as follows: "nasal notch reaches only the anterior border of P2; temporal lines closely approaching; zygomatic arch robust; paroccipital process long. Upper I1 rather large and functional, I2 and i1 present, i2 very large".

DESCRIPTION

Dental remains

Upper dentition—The right P3 CL'13-16 has a deep and sinusoid median valley. Protoloph and metaloph run parallel. The protocone is slightly thicker than the ectoloph and finishes in a postero-lingually oriented flattened surface. The posterior protocone fold is only represented as a very smooth indentation at the posterior base of the protocone. The anterior fold is slightly more marked at the base level of the protocone. The hypocone is oval and bigger than the protocone. It is connects with the crochet and the ectoloph through a constricted stretch. Its posterior side contacts with a poorly-preserved posterior cingulum, enclosing an oval deep postfossette. There is no trace of anterior hypocone folding. A single rounded crochet is present. There are anterior, lingual and posterior cingula. The anterior one is very low but sharp and contacts the lingual one. The lingual cingulum is low and fades out at the lingual side of the hypocone, rising up to the occlusal level. The DP1 CL'12-384 lacks its posterior extent. The reliefs of the ectoloph are smoothed. An acute notch can be observed at its base. The anterior prefossete is triangular and shallow. The anterior cingulum is low and shows a shallow central valley. The protoloph is thin and curved, being isolated from the paracone through a small groove. The tooth CL'12-100 shows an isolated labial wall of an undetermined upper teeth, with a large part of the ectoloph preserved to the parastyle. The ectoloph is smoothly undulated, with the metacone and paracone cusps slightly protruding in labial view. The paracone is well individualized along the total height of the tooth, being delimited from the parastyle from a smooth paracone fold. The enamel thickness points to a decidual tooth.

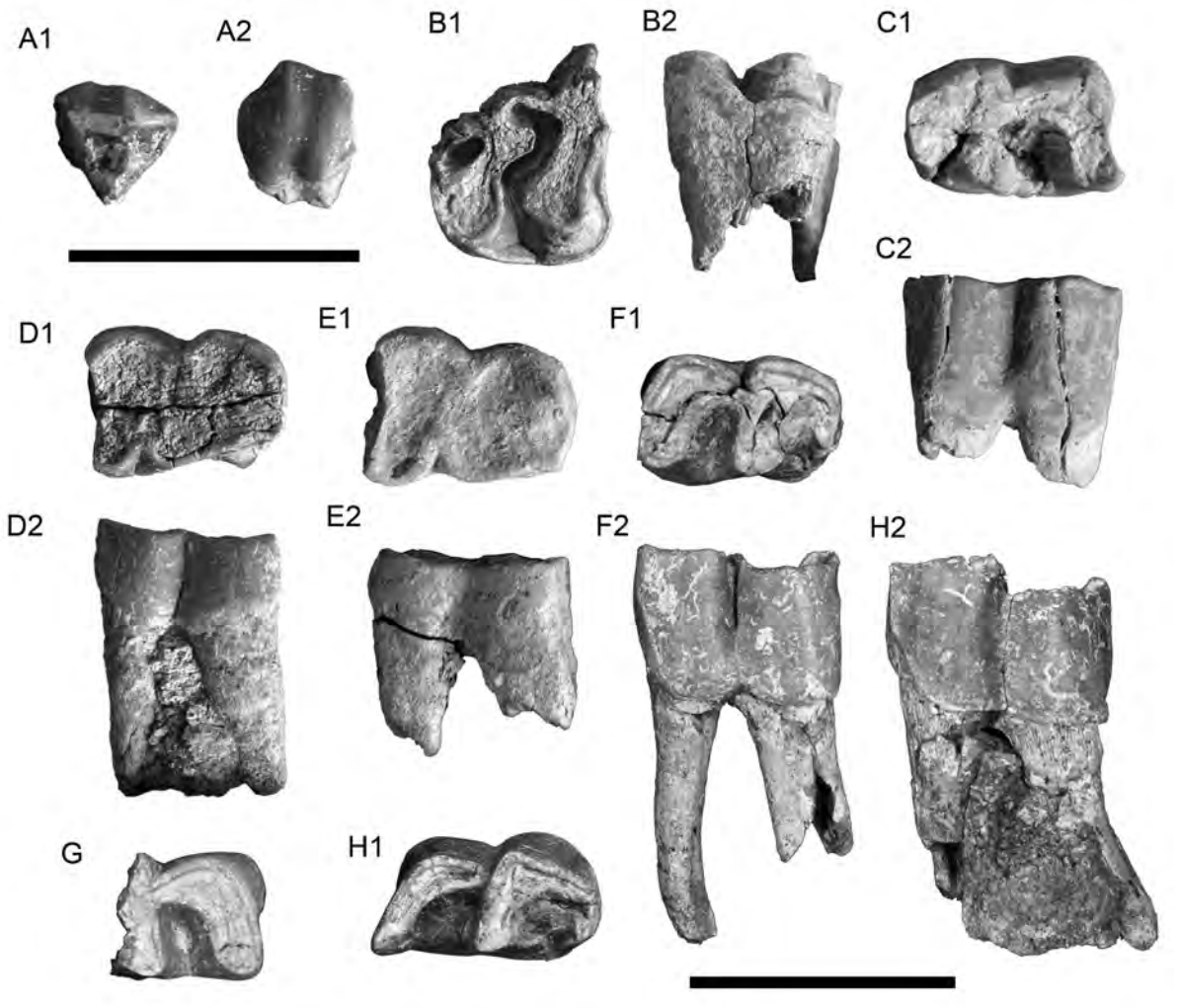


Fig. 12.3. Dental remains of *Dihoplus* cf. *Dihoplus schleiermacheri* from Corral de Lobato (Castilla la Mancha, Spain). A, right DP1 CL'12-384 in A1, occlusal and A2 labial views; B, right P4 CL'13 w/n in B1, occlusal and B2, lingual views; C, left p3 CL'12-101 in C1, occlusal and C2, labial views; D, right p4 CL'13 A5-62 in D1, occlusal and D2, labial views; E, right p3 CL'12-591 in E1, occlusal and E2, labial views; F, right px CL'14 A3-29 in F1, occlusal and F2 labial views; G, right px CL'14 A3-28 in occlusal view; H, left px in H1, occlusal and H2, labial views.Both scale bars represent 50 mm.

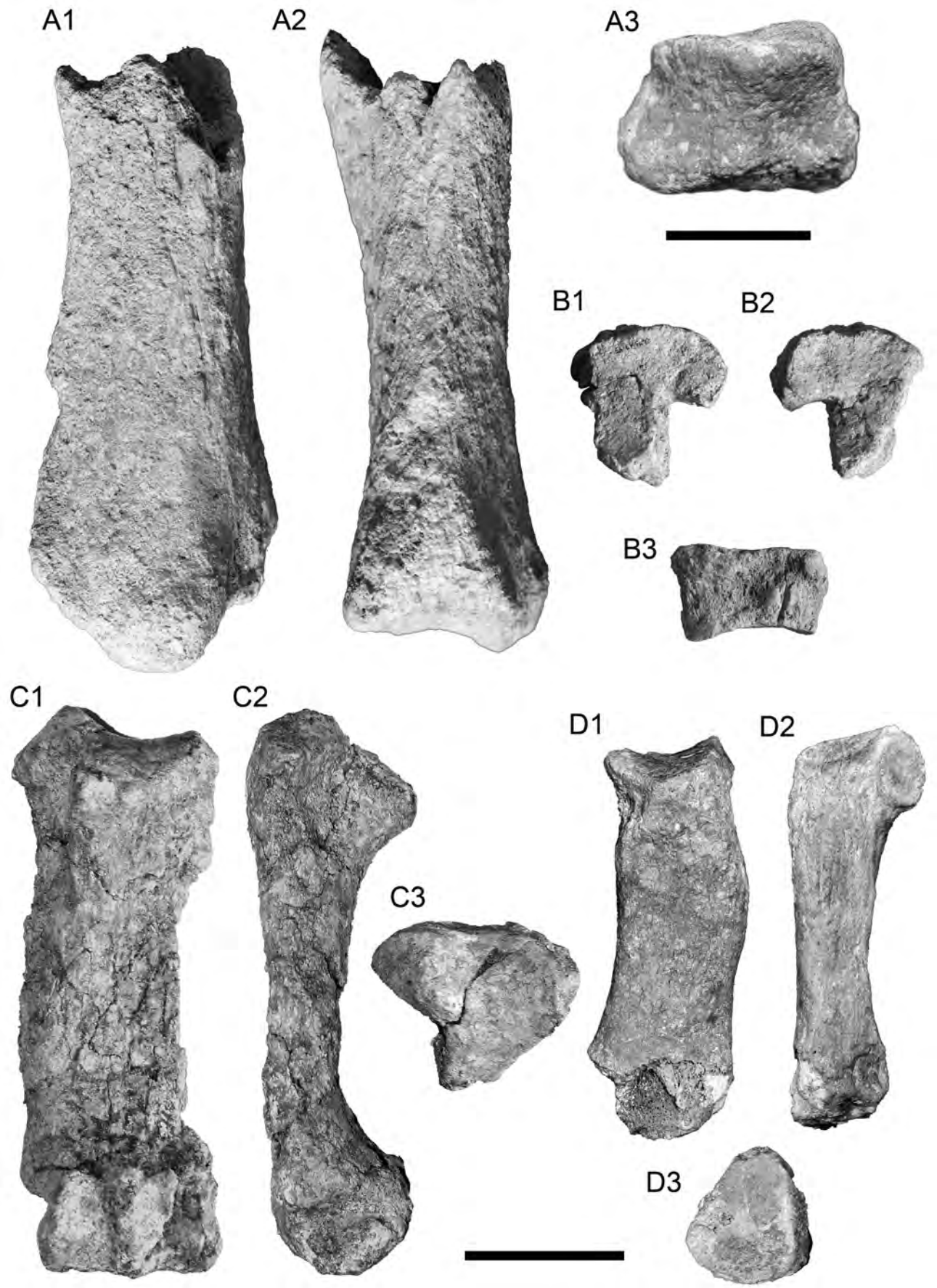


Fig. 12.2. Postcranial remains of *Dihoplus* cf. *Dihoplus schleiermacheri* from Corral de Lobato (Castilla la Mancha, Spain). A, distal fragment of a left tibia CL'13 A3-43 in A1, caudal, A2, lateral, and A3, distal views; B, right ectocuneiform CL'13 A3-45, in B1, distal, B2, proximal, and B3, dorsal views; C, left Mc III CL'14 A4-98 in C1, plantar, C2, lateral, and C3, proximal views; D, right Mc IV CL'14 A5-removido in D1, dorsal, D2, medial, and D3, proximal views. Scale for A placed on the top right, scale for B, C, and D on the bottom. Both bars represent 50 mm.

Lower dentition—The p3 has a short and poorly curved paralophid enclosing a small posterior valley, rounded in occlusal view. The tooth lacks anterior and posterior cingulid. There is a short flange attached to the posterior side of the paralophid. The posterior valley is 'V'-shaped but presents a rounded base. Metaconid and entoconid are rounded, protruding the occlusal surface. The labial groove is well-marked, dividing two flattened surfaces in the labial side. The enamel surface presents a horizontally banded texture. Both teeth have a slightly swollen band at the base of the labial side, flattening towards the occlusal surface. Other p3, CL'14 A3-28, has a thin ridge in the base of the labial groove (not preserved in CL'14 A3-29). Both anterior and posterior valleys are 'V'-shaped. A short cingulid is attached to the base of the paralophid. The p4 has a bigger posterior contact facet than the p3, a bigger anterior lobe than the posterior one and a greater overall length. The p4 CL'12-591 is highly worn (H=12 mm). The enamel thickness is considerable, with a mean value of 4 mm along the labial border (comparable to individuals from La Alberca or Venta del Moro). The posterior valley is narrow and 'V'-shaped. Due to its advanced wear stage, the anterior valley is represented as a small lingual scar. The only m1, CL'13 A5-46, is represented by a posterior half morphologically equivalent to CL'12-591 but with more acute labial groove (practically absent in CL'12-591) but slightly bigger. In the m3, the basal border of the tooth is not swollen and presents a very narrow rim. Both anterior and posterior valleys are 'V'-shaped. It also shares a short cingulid at the base of the paralophid. The trigonid is square-shaped. It presents a small and blunt cusp on the posterior side of the tooth.

Postcranial remains

Regarding the postcranial skeleton, only four bones have been found. As with the dentition, their surfaces are deteriorated and the edges smoothed and/or broken, pointing to some degree of transport.

Mc III—Apart from its extensively cracked surface, CL'14 A4-98 shows a damaged medial border of the diaphysis. The proximal articular surface for the magnum is subtriangular (DT = 44.5 mm; APD = 55.6 mm) in proximal view and 'saddle'-shaped (i.e. dorso-palmarly concave and transversally convex). The dorsal and planto-medial borders are roughly straight and the lateral one sigmoid. In medial view, the Mc II-facet is attached to the proximal articular surface. It is 'tear'-like (APD = 21 mm; H = 13.2 mm), flat, and proximo-medially oriented. On the lateral side, the unciform-facet is subtriangular (APD = 29.2 mm; H = 30.7 mm), has a convex palmar extent, and, in dorsal view, forms an approximately straight angle with the magnum-facet. The notch of the lateral border of the shaft distal to the unciform-facet is weak but long (approx. 60 mm) and shows no acute relief thereinafter). In medial view, the two Mc IV-facets are separated by a shallow groove 7.8 mm long. The dorsal Mc IV-facet is attached to the distal border of the unciform-facet. It is oval to semicircular (APD = 32 mm; H = approx. 11.7 mm) and flat. The plantar Mc IV-facet is in a lower position. It is 'tear'-shaped (APD = 16.8 mm; H = 23.9 mm), flat, and medially-oriented. The latero-distal protuberance for the m. extensor carpalis (the only preserved) is rounded, does not protrudes from the shaft but from the distal epiphysis. The distal articular surface is nearly symmetrical, with two equivalent halves and a faintly-protruding central keel.

Mc IV—The bone CL'14 A5-removido is very robust. The proximal unciform-facet is trapezoidal (TDdor = 21.2 mm, TDpal = 45.5 mm, APD = 36.6 mm), transversally concave, and dorso-palmarly flat. The dorsal and medial borders of this facet are straight and form an obtuse (near straight) angle. Both sides are separated by two rounded angles. In medial view, the Mc III-facets are flat, medially oriented (the dorsal slightly more dorso-medially) and separated by a narrow gutter 5.4 mm wide. The dorso-medial Mc III-facet is semicircular, flat, long (APD = 29.5 mm, H = 9.5 mm), medio-dorsally oriented, and is attached to the whole medial border of the proximal articular surface. The planto-medial Mc III-facet is oval (APD ~18 mm, H = 23.2 mm), flat and is placed just below the proximal articular surface (without contacting it). In dorsal view, there is a gap below the proximo-lateral protuberance of the proximal epiphysis. The dorsal surface of the shaft is wide, smooth and flattened. The diaphysis bends from the midshaft on and present a swollen first third. Its section is oval, with the medial side straight. The insertion for the m. extensor carpalis extends over more than a half of the medial side of the shaft. It is oval (APD = 25 mm; H = 57 mm) and rugous, but not very protruding from the medial border in dorsal view. The distal epiphysis is broken.

Tibia—The surface of this distal fragment (CL'13 A3-43) is corroded, fading out most of its morphology. The section of the diaphysis is subtriangular, with a rounder cranial angle. The distal articulation has a trapezoidal outline. The medio-distal groove is not visible. The fibular-facet is wide, triangular and poorly preserved. The medial malleolus is not preserved.

Ectocuneiform—The right ectocuneiform CL'13 A3-45 from Cerro de Lobato is robust and high. The proximal navicular-facet is 'L'-shaped and concave. The lateral incision forms a straight angle in proximal view, more acute in distal one. The anterior side is as thick as the posterior expansion and somewhat shorter (44.6 and 45.6 mm respectively). All lateral and medial facets are poorly preserved.

DISCUSSION

According to Cerdeño (1992), two rhinoceros species have been recorded in the Turolian (MN 11-13) of the Iberian Peninsula: *Aceratherium incisivum* and *D. schleiermacheri*. While *A. incisivum* is a hornless and medium-sized aceratherine species, *D. schleiermacheri* is a large tandem-horned rhinoceros that pertains to the Rhinocerotina (*sensu* Antoine, 2003). The greater size of the dental and postcranial

remains recovered from Corral de Lobato, the thicker enamel, the morphology of the upper DP1, the absence of labial cingulids in the lower premolars, and the absence of the lateral Mc V facet of the Mc IV points to a Rhinocerotini rhinoceros and discards the ascription to *A. incisivum*.

The DP1 CL'12-384 from Corral de Lobato has a reduced parastyle and a subtriangular to oval outline in occlusal view, similar to the DP1 from Eppelsheim (figured by Kaup, 1832; Plate XI, Fig. 4). In contrast, the hypocone of CL'12-384 continues labially through a thin and curved protoloph, a feature which contrasts with the DP1 from Eppelsheim, where the protoloph is straighter and more antero-posteriorly oriented. Both teeth differ from those of *Lartetotherium*, another Miocene Rhinocerotini genus from the Iberian Peninsula (see Sanisidro et al., this volume for a brief description). The P4 CL'13-16 closely matches the morphology (i.e. cingular configuration, protocone and hypocone folding, shape of the median valley and crochet and absence of crochet) and proportions (maximum width of the lingual side: 34,8 and 35,6 respectively) of the specimen FSL 210310 from Montredon. Despite the coincident cingular configuration of CL'13-16 and the P4 of the holotype skull DIN 1932, the later displays a strong lingual wall (i.e. connection of protocone and hipocone) at the entrance of the median valley and a long and narrow crista, both absent in Corral de Lobato and Montredon. The p3 CL'12-101 from Corral de Lobato is very long and relatively narrow if compared with other Iberian remains of *D. schleiermacheri*, being close to those of Crevillente. On the other hand, the p4 CL'12-591 is clearly wider, probably due to its advanced wear stage. All the studied lower teeth share a 'V'-shaped valley, a characteristic trait of the species (Guérin, 1980).

The left Mc III CL'14 A4-98 is short, barely reaching the minimum length values recorded for *D. schleiermacheri*. Additional differences are the broader shaft, the larger unciform-facet, and the more acute insertions for the m. interossei. *D. schleiermacheri* has a relatively slender Mc III and, even with an even size increase, the latest Ventian populations of the Eastern Iberian basins keeps relatively constant GI values (Sanisidro et al., this volume). The same GI can be outlined from *Dihoplus megarhinus*, a posterior *Dihoplus* species from Western Europe with more slender proportions than CL'14 A4-98 (e.g. FSL 40040 from Montpellier). The higher robustness can be linked to a larger and more heavy-built individual, maybe a dominant bull. Unfortunately, the intraspecific variability of the postcranial skeleton of *D. schleiermacheri* is obscured by the lack of large samples. If compared with other Rhinocerotini species, CL'14 A4-98 coincides with the mean length values of *Dihoplus pikermiensis*, a smaller *Dihoplus* species from the Turolian of Eastern Europe. The abundant sample of *D. pikermiensis* from the Greek localities of Samos and Pikermi poses this species a useful proxy for estimating the intraspecific variability in *D. schleiermacheri*. While most of the Mc III's of *D. pikermiensis* show moderate gracility indices, some specimens attain particularly higher values (e.g. NHMA: MYT-48 GI = ; (Giaourtsakis et al., 2009), similar to that of CL'14 A4-98. These large specimens would correspond to large bulls, as observed in extant rhino species (CITA). If compared with the *Lartetotherium* species from Cerro de los Batalones, the proximal unciform-facet is deeper (higher APD) in Corral de Lobato, has a rounder (and more palmarly displaced) lateral angle, and a rounder and more palmarly expanded posterior angle. Besides, the gap in the proximo-lateral protuberance of the proximal epiphysis is absent in *Lartetotherium*. Additionally, the individuals from Cerro de los Batallones have a distinct outline in the Mc II-facet, a less proximally-protruding lateral border of the unciform-facet, and a lower (lower H) plantar Mc IV-facet. The faint lateral protrusion of the unciform-facet and the roughly straight lateral border of the shaft discards the ascription to "*Diceros*" *neumayri*, another rhinoceros from the Turolian of Eastern Europe and Anatolia of similar proportions but higher maximum lenght. In the later, the unciform area is more projected and the shaft has a markedly concave lateral outline (Giaourtsakis et al., 2009).

In the Mc IV, the palmar shelf (of the proximal articular surface) is high (H = 20.3 mm) and swollen if compared with the narrow rim found in Cerro de los Batallones. In the lateral border of the proximal epiphysis there is a noticeably notch in Corral de Lobato (partially eroded but originally present in the bone), absent in Batallones sample. Finally, the insertion of the *m. extensor carpalis* is more developed in Corral de Lobato, not as much as in length (it barely surpass the length of the individuals from Batallones) but in dorso-palmar widening. In a similar way, the Mc IV of *Dihoplus megarhinus* FSL 40053 from Montpellier is more slender and presents a shorter (lower APD) proximal epiphysis.

The tibia CL'13 A3-43 from Corral de Lobato is large and robust. If compared with the adult fragmentary tibia from Venta del Moro (MGUV 11293), the medial side is much more deep (higher APD) and the distal fibular insertion is higher (H approx = 76 mm). Unfortunately, its surface is broadly corroded, fading out some details as the articular facets in the cranial and lateral sides of the distal epiphysis.

In summary, while overall similar to the species *D. schleiermacheri*, the observed disconformities in the dentition and postcranial proportions of the new rhinocerotid remains from the Turolian locality of Corral de Lobato has lead us to determine them as *Dihoplus* cf. *Dihoplus schleiermacheri*.

REFERENCES

Antoine, P. O., 2002, Phylogénie et évolution des Elasmotheriina: (Mammalia, Rhinocerotidae): Mémoires du Muséum National d'Histoire Naturelle, v. 188, p. 5-350.

Antoine, P. O., 2003, Middle Miocene elasmotheriine Rhinocerotidae from China and Mongolia: taxonomic revision and phylogenetic relationships: Zoologica Scripta, v. 32, no. 2, p. 95-118.

Cerdeño, E., 1989, Revisión de la sistemática de los rinocerontes del Neógeno de EspañaPh.D. Dissertation]: Universidad Complutense de Madrid, 429 p.

-, 1992, Spanish Neogene Rhinoceroses: Palaeontology, v. 35, p. 297-308.

Geraads, D., and Spassov, N., 2009, Rhinocerotidae (Mammalia) from the Late Miocene of Bulgaria: Palaeontographica A, v. 287, p. 99-122.

Giaourtsakis, I., Phlevan, C., and Haile-Selassie, Y., 2009, 14. Rhinocerotidae, *in* Haile-Selassie, Y., and Woldegabriel, G., eds., *Ardipithecus kadabba*. Late Miocene Evidence from the Middle Awash, Ethiopia: Berkeley, Los Angeles, and London, University of California Press and University of California Press, Ltd., p. 429-472.

Guérin, C., 1980, Les rhinocéros (Mammalia, Perissodactyla) du Miocène terminal au Pléistocène supérieur en Europe occidentale : comparaison avec les espèces actuelles: Documents des Laboratoires de Géologie de Lyon, v. 79, p. 1-1184.

Heissig, K., 1972, Die obermiozäne Fossil-Lagerstätte Sandelzhausen. 5. Rhinocerotidae (Mammalia), Systematik und Okologie: Mitteilungen der Bayerischen Staatssammlung Paläontologie und historische Geologie, v. 14, p. 37.

-, 1999, 16. Family Rhinocerotidae, *in* Rössner, G. E., and Heissig, K., eds., The Miocene Land Mammals of Europe: Pfeil, Munich, p. 175-188.

Kaup, J. J., 1832, Über *Rhinoceros incisivus* Cuv. und eine neue Art *Rhinoceros schleiermacheri*: Isis, v. 8, no. 1832, p. 898-904.

-, 1834, Description d'ossements fossiles de Mammifères inconnues jusqu'à présent qui se trouvent au Muséum grand-ducal de Darmstadt, *in* Heyer, J. G., ed., cuaderno 3, p. 33-64.

Mein, P., 1999, European Miocene mammal biochronology, *in* Rössner, G. E., and Hessig, K., eds., The Miocene Land Mammals of Europe: München, Verlag Dr. Friedrich Pfeil, p. 25-38.

Santafé, J. V., 1978, Revisión de los Rinocerótidos miocénicos del Vallès-Penedès: Acta Geologica Hispanica, v. 13, no. 2, p. 43-45.

APPENDIX 1

Measurements (mm) of the remains of *Dihoplus* cf. *Dihoplus schleiermacheri* from Corral de Lobato (Guadalajara Province, Spain).

Table S2	CL'14 A3-24 (l)	CL'14 A3-28 (l)	CL'13 A5-62 (l)	CL'12-591 (l)	CL'12-101 (r)
Lower teeth					
					38.7
p3					26.5
					29.4
			40.2	40.2	
p4			31.3	31.3	
			22.8	15.3	
		40.4			
m1		28.3			
		29.8			
	45.8				
m2	36.3				
	—				

Table S3			prox epi		dia		dis epi		dis. epi.	
Tibia	L	LfFi	TD	APD	TD	APD	TD	APD	TD	APD
CL'14 A3-43 (l)	—	—	—	—	—	—	67.9	67.6	92.5	62.7

Table S4	prox art			
Ectocuneiform	TD	APD	H	Hmin
CL'14 A3-45 (r)	44.9	51.5	28.2	23.5

Table S5		prox epi		prox art			dia			dis art	
Mc III	L	TD	APD	TD	APD	HfUn	TD	APD	TDmd	TD	APD
CL'14 A4-98 (l)	184.0	69.6	57.9	44.5	55.6	32.6	—	28.9	—	60.7	48.5

Table S6		prox epi		prox art		dia			dis art	
Mc IV	L	TD	APD	TD	APD	TD	APD	TDmd	TD	APD
CL'14 removido (r)	~ 137	44.5	48.2	36.3	43.5	42.7	24.9	50.6	—	—

13. New data on *Dihoplus schleiermacheri* (Rhinocerotidae, Perissodactyla) from the Turolian of Venta del Moro and Crevillente-2 (Comunidad Valenciana, Spain)

Oscar Sanisidro
Esperanza Cerdeño
and Plinio Montoya

Abstract. *Dihoplus schleiermacheri* is a large two tandem-horned rhinoceros from the Upper Miocene of Central and Western Europe. The species was described by Kaup in 1832 on the basis of the cranial, mandibular and postcranial remains from the German locality of Eppelsheim (probably MN 9; Early Vallesian). New rhinocerotid remains from the Turolian (Upper Miocene) sites of Venta del Moro, Crevillente-2 and Alcoy-Mina (Comunidad Valenciana, Spain) are recorded. They are compared with other known material of this taxon that characterizes the European upper Miocene. Numerous postcranial remains have been found in Venta del Moro site, one of the classical Spanish macrommals localities. On the other hand, Crevillente-2 and Alcoy-Mina provide an almost complete sample of *D. schleiermacheri* dentition. The new material has been compared with other Spanish and European localities, establishing a general view of the species and increasing the previous knowledge of the intraespecific variation of this big-sized rhinoceros.

INTRODUCTION

Dihoplus schleiermacheri is the largest rhinoceros of the Miocene of Western Europe. The species was named by J. J. Kaup after M. Schleiermacher, who unearthed the skull HLMD DIN1932 from the German locality of Eppelsheim. A second skull together with additional isolated mandibular, dental, and postcranial remains configured the type collection of the species. Georges Cuvier was the first to document and describe (but not figure) the skull HLMD DIN1932. By recognizing its rhinocerotini affinities, he compared it with the living Asian species and found enough differences to erect a new species (Cuvier, 1824, p. 502). Prior to the study of the Schleiermacher's skull, he examined an upper incisor found in Weisenau (Germany), naming it as "*Rhinoceros incisivus*" (Giaourtsakis and Heissig, 2004). When Cuvier observed some drawings of isolated upper incisors from Eppelsheim sent by M. Schleiermacher, he erroneously concluded that both skull HLMD DIN1932 and incisors pertained to the Weisenau's species "*R. incisivus*". To complicate the situation, years after the original description of "*R. incisivus*", Kaup ascribed to the species two small and hornless skulls from Eppelsheim (HLMD DIN1930 and HLMD DIN1927). The absence of frontal horn in these two rhinoceros skulls was so striking that attracted a considerable attention from the experts, and they rapidly became the reference for *Aceratherium incisivum* (formerly known as "*R. incisivus*"). However, these skulls lack the premaxillary bone (so the presence of upper incisors is, at best, uncertain) and is incorrect to link them with the upper incisors collected from Eppelsheim but with a third species, *Brachypotherium goldfussi*, which coincides with Weisenau's incisor (as posteriorly demonstrated by Giaourtsakis and Heissig, 2004). If the two smaller, hornless skulls HLMD DIN1930 and HLMD DIN1927 were assigned to *A. incisivum*, the large, horned skull HLMD DIN1932 clearly represented a completely new taxon. After a detailed examination of the cranial, dental and postcranial material, Kaup recognized its distinctiveness as a new species (Kaup, 1832). As no holotype was designated in the original publication, the skull HLMD DIN1932 currently stored in the Darmstadt Hessisches Landesmuseum is considered lectotype of *D. schleiermacheri*.

The classic locality of Eppelsheim, to which holotype of *D. schleiermacheri* pertains, is so far considered to date back from the Vallesian (~ 9.5 Ma, MN 9, Upper Miocene). However, some remarks of the biostratigraphic context of the area are worth to mention in order to contextualize and compare the type material of *D. schleiermacheri* within the European fossil record. In last decade, a renewed interest in the geological context of the Eppelsheim Formation (Mainz Basin) has partially untangled its complex regional stratigraphy. The so-called Dinotheriensande contains material from a considerable variety of sediments related with the development of the Rhine River south of the Rhenian Slate Mountains (summarized in Böhme et al., 2012). Their datation spans over a short period of time after the *Hipparion* datum (11.1 Ma; Grimm, 2011).

However, middle Miocene deposits have been also cited in the area (Böhme et al., 2012). Pickford and Pourabrishami (2013) estimated that the total period of time recorded in the area ranges from MN 4 (ca. 17 Ma) to MN 13 (ca 6 Ma). Most of the fossils from the classic collections labeled as collected from Eppelsheim (including the postcranial remains housed primarily in HLMD Darmstadt and partly in BMNH London), lack a precise stratigraphic context. A distinct origin within the Deinotheriensande for the skull HLMD DIN1932 of *D. schleiermacheri* and the skulls HLMD DIN1930 and HLMD DIN1927 of *A. incisivum* cannot be excluded, as they present a different preservation (brownish-coloured, evenly cracked surface in the skull of *D. schleiermacheri*, big cracks and light-coloured surface in those of *A. incisivum*). Future rare earth elements (REE) analyses can be a highly useful tool in characterizing the origin and provenance of the Eppelsheim rhino collection in order to confirm this point. Apart from its presence in the German type locality of Eppelsheim, the species is known from Gauweinheim (Germany; MN 9), Esselborn (Germany; MN 9), Soblay (France; MN 9), Mont Lebéron (France; MN 9), Dorn-Dürkheim 1 (Germany; MN 11), Slatino-2 (Bulgaria; Upper Miocene; Geraads and Spassov, 2009), Yulafli (Turkey, MN 11 or 12; Kaya and Heissig, 2001), and Baltavar (Hungary; MN 12; Giaourtsakis et al., 2009). Summarizing, the European stratigraphic range of *D. schleiermacheri* spans from the MN 9 to MN 12 (Giaourtsakis et al., 2009; Heissig, 1999)(Guérin, 1982), and is in the Iberian Peninsula where the species persists into the latest Turolian (MN 13).

The Iberian Peninsula yields an important number of records of *D. schleiermacheri* (Cerdeño, 1989, 1992; Guérin, 1980; Santafé, 1978)(van Dam et al., 2001; Aguirre et al., 1980; Alcalá et al., 1987). The species is best represented in the Teruel-Alfambra Region (Teruel Province), included in the Calatayud-Daroca Basin. It includes the localities of Masía del Barbo 2A (MN 10), Masía del Barbo 2B (MN 10), La Roma 2 (MN 10), Puente Minero (MN 11), Concud Barranco (MN 12), Concud Cerro de la Garita (= Cerro de la Garita; MN 12), El Arquillo 1 (= Arquillo de la Fontana or Rambla de Valdecebro; MN 13), and Las Casiones (MN 13). Among the Eastern Iberian basins, *D. schleiermacheri* has been cited in Crevillente 2 (Alicante; MN 11), Crevillente 15 (Alicante; MN 12), Alcoy (Alicante; MN 13), Venta del Moro (Valencia; MN 13), and La Alberca (Murcia; MN 13). Regarding the

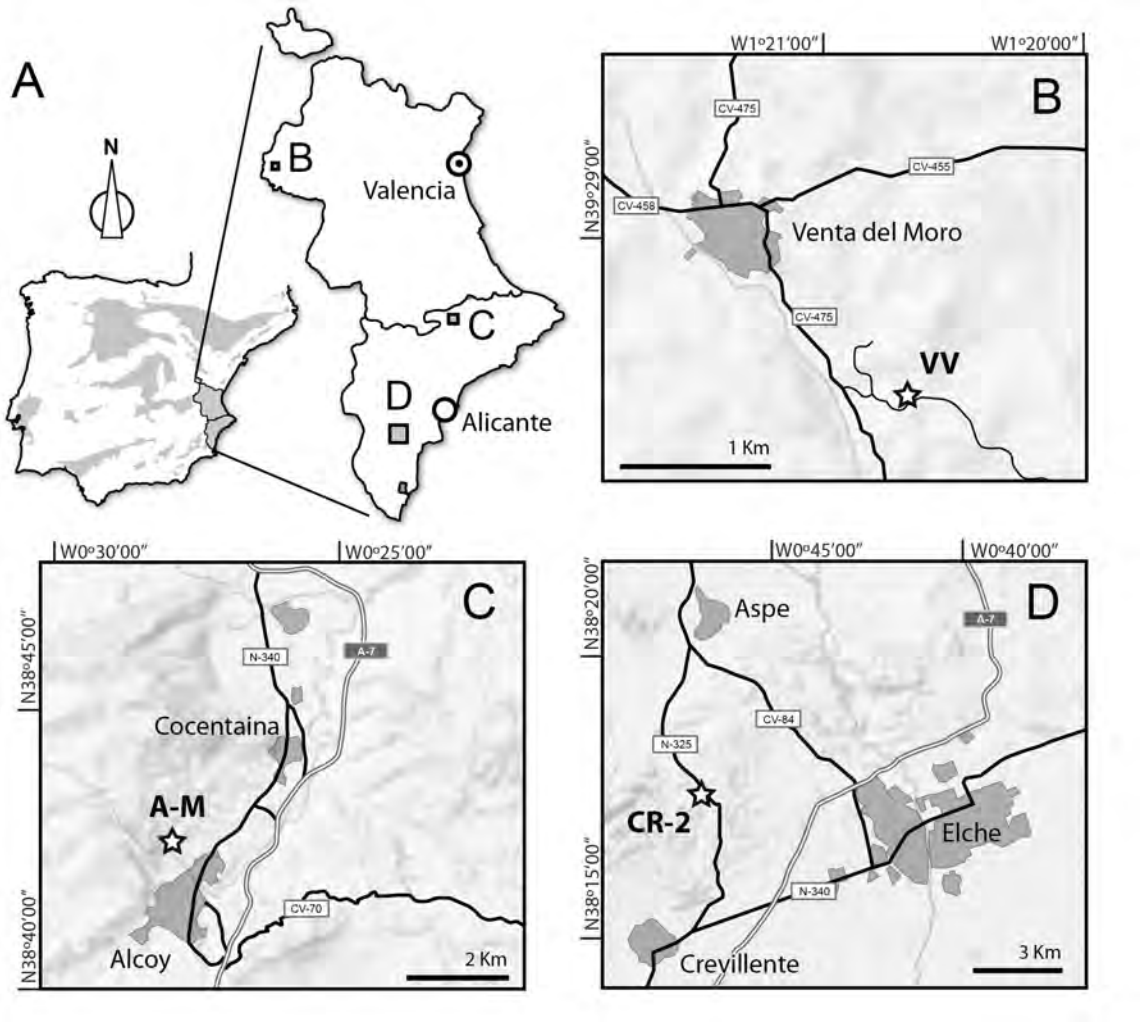


Fig. 1 A, simplified general map of the Iberian Peninsula with its Cenozoic basins represented as shaded contours. B, detailed map showing the location of Venta del Moro (VM), C, Alcoy-Mina (A-M) and D, Crevillente-2 sites (CR-2), all three represented as stars.

Betic basins, *D. schleiermacheri* is cited in Cenes de la Vega (= Lancha de Cenes, Granada; MN 13), El Fargue – Fábrica de Pólvora and El Fargue – Río Beiro (both considered as "*Dicerorhinus* cf. *schleiermacheri*" by Cerdeño, 1992; Granada; MN 13), Los Hornillos (Granada). The Vallès-Penedès Basin (Barcelona) is represented by the localities of Can Llobateres (MN 9), Subsuelo de Sabadell (MN 9), Can Jofresa (MN 10), Can Trullàs (MN 10), Piera (MN 11), and Can Perellada (MN 10). Finally, a single locality of the Ebro Basin, Cellórigo (Upper Miocene) has been cited.

The purpose of this paper is to report the new remains of *D. schleiermacheri* from Venta del Moro, Alcoy-Mina and Crevillente-2, localities from the Levantine basins of the Iberian Peninsula. All three have yielded a considerable amount of new data about the faunal and floristic terminal Miocene assemblages over the past 25 years of systematic excavations. The locality of Crevillente-2 has been designated as the reference locality for MN11 Biozone, included in the lower Turolian between 9 and 8 m.a. The site is located near Crevillente, close to the city of Alicante (Figure 1D). Venta del Moro site has been dated as upper Turolian, MN13 Biozone (Mein, 1975, 1990, 1999), between 5.5 and 5.8 m.a. (Opdyke et al., 1997; Opdyke et al., 1990). The locality is placed near Utiel, East from the city of Valencia (Figure 1B). At this time important transformations along the Mediterranean basin took place, which rebounded in a series of faunistic interchanges between Europe, Africa and Asia. Venta del Moro and Crevillente provide a relatively unbiased picture of the upper Miocene Mediterranean paleoecosystems, which includes charophytes, pollen, macrofloral remains, foraminiferans, freshwater and terrestrial molluscs, ostracods, fishes, amphibians, reptilians and micro and macromammals. The number and variety of recovered fossils constitute a composite paleogeographic framework that fills the scarcity of uppermost Miocene records among Western Mediterranean basins. Alcoy-Mina is another classic locality of the Iberian Miocene record. The site is placed close to the city of Alcoy, Alicante Province (Figure 1C) and has a controversial age, between the latest Miocene and the earlier Pliocene (Montoya et al., 2006a). More information about the geological setting of Venta del Moro, Crevillente and Alcoy-Mina can be found on Montoya et al. (2006b), Martín Suárez and Freudenthal (1998) and Pierson d'Autrey (1987) respectively.

MATERIAL AND METHODS

All the studied specimens from Cerro de los Batallones butte are stored in the Museo Nacional de Ciencias Naturales, Madrid. Measurements are given in millimeters with an accuracy of one decimal digit. Approximate measurements are given in parentheses. Measurements were made with a digital caliper and a measuring tape for elements larger than 150 mm. The terminology applied in the description of the anatomical characters generally follows Guérin (1980), but that used by other authors has also been taken into consideration (Antoine, 2002; Heissig, 1972, 1999). The larger rhinocerotini postcranial casts from Eppelsheim stored in the AMNH have been used as reference for the type collection of the species. Even though we are aware that the cast of the skull HLMD DIN1932 of *D. schleiermacheri* stored in the same institution is partially reconstructed (and should not be used for systematic comparisons in agreement with Giaourtsakis and Heissig, 2004), postcranial bones, though of variable quality and a "smoothed" appearance, can serve as a rough reference for the overall proportions of the species.

Anatomical Abbreviations—ant, anterior; art, articulation; dia, diaphysis; dis, distal; int, interior; epi, epiphysis; max, maximum; min, minimum; prox, proximal; 3tr, third trochanter. Capital letters are used for upper teeth (D, P, M; upper decidual, premolar and molar respectively), and lower case for lower teeth (d, p, m).

Measurements abbreviations—APD, antero-posterior diameter; DL, distal length; H, height; L, length; TD, transverse diameter.

Institutional abbreviations—AMNH, American Museum of Natural History; FSL, collections de l'Universite Claude-Bernard Lyon-I; HLMD, Darmstadt Hessisches Landesmuseum; MGUV, Museo de Geología de la Universidad de Valencia; MHMN, Museo de Historia Municipal de Novelda (Alicante, Spain); MNCN, Museo Nacional de Ciencias Naturales - CSIC (Madrid, Spain). Specimens figured in the present paper are housed in the. Prefixes VV, A-M, and CR-2 pertains to Venta del Moro, Alcoy-Mina, and Crevillente-2 sites respectively.

Referred material—See Appendix 1.

SYSTEMATIC PALEONTOLOGY

Family Rhinocerotidae Gray, 1821

Subfamily Rhinocerotinae Gray, 1821

Genus *Dihoplus* Brandt 1878

Type species—*Dihoplus shcleiermacheri* Kaup, 1832

Other species—*Dihoplus pikermiensis* (Toula, 1906), *Dihoplus ringstroemi* (Ringstrom, 1924).

Diagnosis—(Geraads and Spassov, 2009) A two-horned rhino; tooth row rather caudal, nasal notch above anterior premolars; cranial basis short, post-glenoid apophysis close to the paroccipital process; P1 absent; upper premolars primitive and submolariform; molars with vestigial antecrochet and weak cristae, missing on DP3-DP4; lower i2 present.

Dihoplus schleiermacheri Kaup 1832

Holotype—Complete skull of an adult with P1-M3 (Text-fig 2) from Eppelsheim (probably MN9).

Type locality— Eppelsheim, Rheinhessen, Germany (probably MN 9, Early Vallesian)

Updated diagnosis—(Geraads and Spassov, 2009) Nasal

notch reaches only the anterior border of P2; temporal lines closely approaching; zygomatic arch robust; paroccipital process long. Upper I1 rather large and functional, I2 and i1 present, i2 very large.

According to Guérin (1980), *D. schleiermacheri* is a rhinocerotine rhinoceros of great size. Skull long, with large, domed nasals, curved downward at the tip. Frontal convexity corresponding to a frontal horn. Occipital crest high, occipital face little inclined backward proximally. Sagittal crest present. Auditory channel ventrally open. Postimpanic apophysis longer than postglenoid one. Mandibular symphysis long and not enlarge anteriorly, forming a strong angle with the high horizontal ramus. Anterior dentition functional (I1, small I2, i2 well developed). Upper cheek teeth with undulated ectoloph; crista and crochet usually present, sometimes multiple; protoloph and metaloph in premolars fused with wear; usually without lingual or labial cingula; the protocone and sometimes the hypocone may appear isolated in unwear premolars. Lower cheek teeth with V-shaped valleys, at different level; without lateral cingula. Postcranial skeleton relatively slender.

Stratigraphic and geographic distribution—Upper Miocene (from the earliest Vallesian to the latest Turolian) of Central and Western Europe (Spain, France, Germany, and Austria).

DESCRIPTION

Mandibular and Dental Morphology

Mandible (Figure 2). MNCN-w/n is an incomplete mandible with the right p3-m3 and left p4-m3 which lacks the rostral part of the symphiseal region, both ascending rami. The horizontal ramus is approximately straight. The ventral profile is irregular: straight from the angular process to the level of the m2/3 boundary, convex from the m2/3 to the p4/m1 and straight again narrowing towards the rostral side.



Fig. 2 Mandible MNCN-110977 of *Dihoplus schleiermacheri* from the Upper Turolian of Venta del Moro (Valencia Province) in A, proximal and B, lateral right views. Scale bar equals 100 mm.

There are one alveoli for the p2 and no trace of alveoli for the p1. The symphisis constricts abruptly from the last alveoli onwards, pointing to a narrow rostral border. The symphiseal ridge, only preserved on the right side, is narrow. In proximal view, the symphiseal notch reaches the level of the p3's labial groove and is 'U'-shaped. In lateral right view, there are two aligned and rounded mental foramina. The anterior is placed at the level of the diastema, the lower with the anterior side of the p2 alveoli. The angular process has a rough, thickened border. Two main muscle attachment marks are clearly visible on the right ascending ramus.

Dentition (Figure 2; Tables 2 and 3). The right DP4 MGUV-11306 is an unworn teeth.

Dental remains have been found in all three localities. The

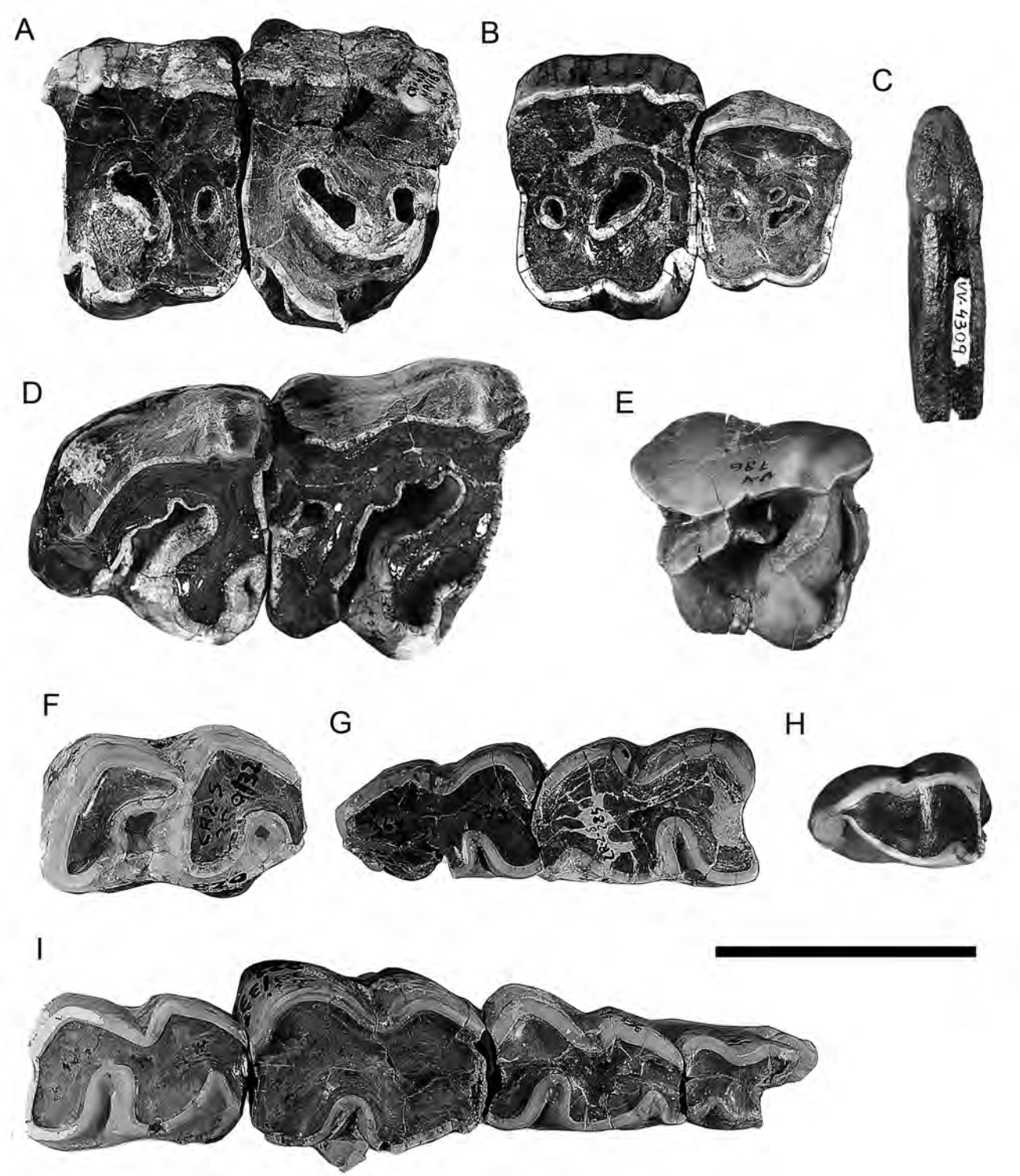


Fig. 3 Dentition of *Dihoplus schleiermacheri* from the Upper Turolian of Venta del Moro (Valencia Province; labelled as MGUV), and the Lower Turolian of Crevillente-2, Alicante (Alicante Province; labelled as CR2). A, left P3-P4 series (CR2-216; CR2-408); B, right P2-P3 series (CR2-95-S; CR2-150); C, left i2? (MGUV-11304, VV-4309); D, right M2-M3 (CR2-M237; CR2-S-106); E, right DP3 (MGUV-11306, VV-786). F, left m3 (CR2-S-359); G, right p3-p4 series (CR2-M260; CR2-M415) found in association with F; H, right p1 (MGUV-7825, VV-11305) and I, left p2-m1 series (CR2-S-346; CR2-S-349; CR2-S-348; CR2-S-353; CR2-S-359). All teeth represented in occlusal view. Scale bar equal 50 mm.

most abundant and characteristic teeth are the P2, recovered at Crevillente-2 (and other Iberian localities like La Roma 2, Masía del Barbo, Concud and Cellórigo). It is a rather squared tooth, with protoloph and metaloph lingually close from the base, being fused on the specimen from Crevillente (with advanced wear). Paracone and metacone folds are smoothly marked. The protocone is isolated, especially on the less worn P2 from Concud. On the P2 from Masía del Barbo, hardly worn, the hypocone is also isolated and the protocone unites to the ectoloph at a very low level. On the P2 from Cellórigo, both protocone and hypocone are isolated (on the P4 from this site the hypocone is isolated). The P2 have small crochet and crista, joined on the Crevillente specimen. Only the P2 from Cellórigo has lingual and labial cingula (Crusafont et al., 1966).

P3 and P4 are large teeth, rectangular in outline, with labial folds eroded due to the wear degree. Protocone and hypocone are fused by wear. The crochet is small; a large and rounded crista is present on the P3 CR2M306 from Crevillente, but it lacks on the other specimens. The P4 CR2408 has a swelling on the median valley that divides it into two parts; the postfossette is large and connects with the median valley.

Molars are large teeth, M1-2 with marked paracone fold and a smooth convexity corresponding to the mesostyle. The protocone is limited by an anterior groove, the posterior one is smooth. Crista and crochet vary among the specimens; the crista can be small and rounded or long; the crochet can be small and rounded, strong and pointed, multiple, with two or three folds. The M2 from Masía del Barbo has a small anticrochet and two short cristae. The curvature degree of the ectometaloph on the M3 is also variable.

Postcranial Skeleton

Venta del Moro site has provided numerous postcraneal



Fig. 4 Anterior long bones of *Dihoplus schleiermacheri* from the Upper Turolian of Venta del Moro (Valencia Province, Spain). A, right fragmentary humerus MGUV-11295 in caudal view; B, right humeral trochlea MGUV-15973 in distal view (probably from the same specimen as A); C, right ulna MGUV-14522 in C1, lateral, C2 cranial, and C3, medial views. Scale bar for A and B (left) equals 50 mm; scale bar for C (bottom right) equals 100 mm.

remains of anterior and posterior autopodiums, which complements the dental pieces from Alcoy-Mina and Crevillente-2. The best postcranial skeleton representation of *L. schleiermacheri* in the Iberian Peninsula has been found in La Roma-2 site (Cerdeño, 1989).

Humerus (Figures 5B and 5C)—Este elemento está representado por una mitad distal de diáfisis de húmero izquierdo con las epífisis no conservadas (MGUV-11295, VV-2020) y una epífisis distal (MGUV-15973) con tróclea y capitulum intactos. Toda la cara distal está ocupada por la tróclea articular distal. Ésta presenta una asimetría considerable entre los labios lateral y medial.

Radius (Figure 6A)—Este elemento está representado por un radio derecho completo (MGUV-s/n, VV-s/n). El ejemplar MGUV s/n pertenece al mismo individuo que la ulna MGUV 14522 con la que comparte una fuerte compresión lateromedial. The radius RO 293 from La Roma 2 has a very large proximal epiphysis, with the internal facet much shorter (in APD) than the external one. The diaphysis is narrow with respect to the epiphysis; its posterior face is slightlyt concave and the anterior one is regularly convex on the proximal half; its cross-section becomes more triangular on the distal half. A proximal fragment from Puente Minero, with an estimate APD of (63.5), is similar to La Roma 2 specimen (Table 4). The radius from Can Trullás (Santafé, 1978) has a slightly wider diaphysis (57).

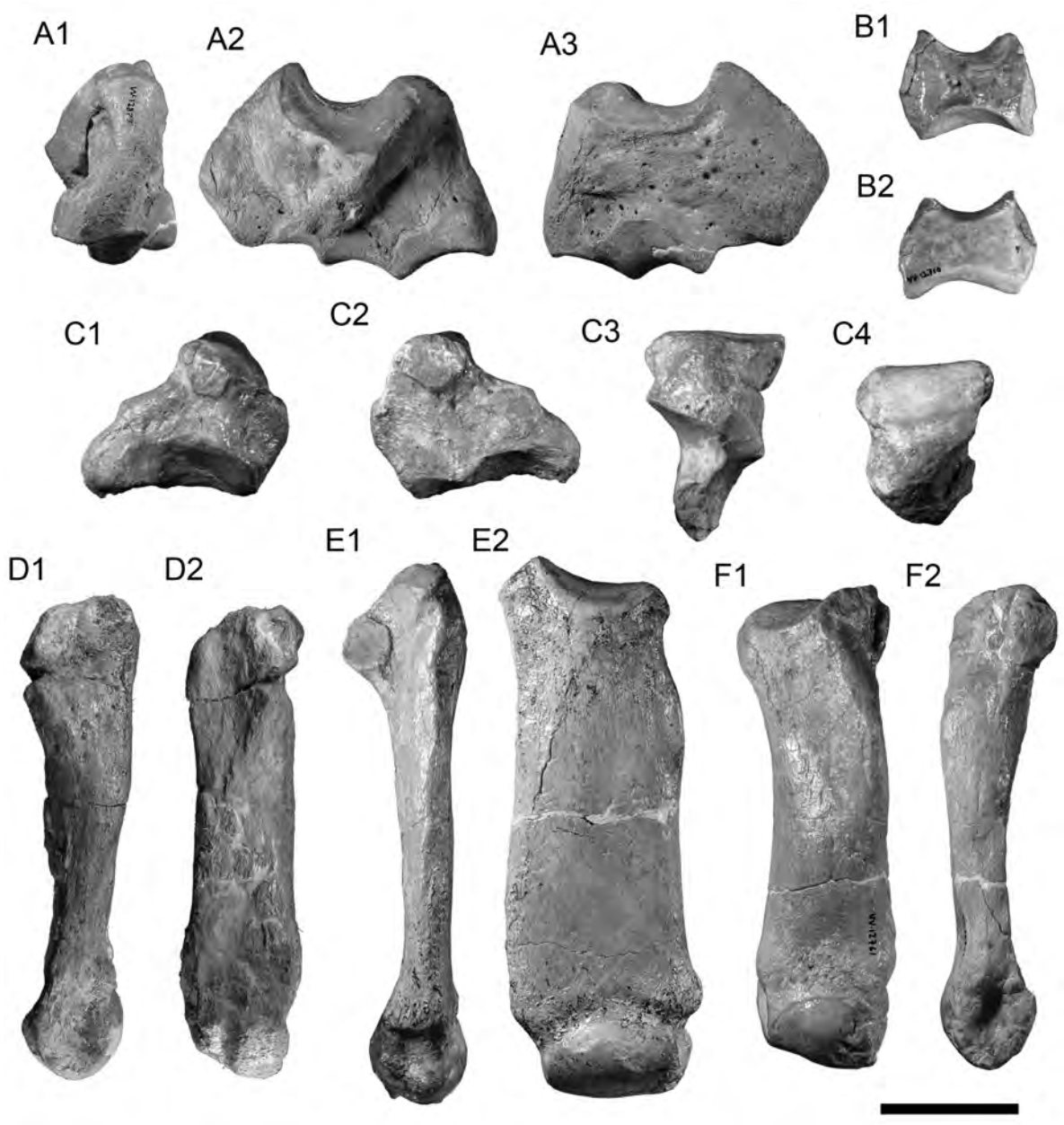


Fig. 5 Carpal and metacarpal bones of *Dihoplus schleiermacheri* from the Upper Turolian of Venta del Moro (Valencia Province, Spain). A, right scaphoid MGUV-18524 in A1, dorsal, A2 lateral and A3, medial views; B, right trapezoid MGUV-18521, VV-12710 in B1, palmar and B2, dorsal views; C, right semilunate MGUV-18523, VV-12872 in C1, lateral, C2, medial, C3, distal, and C4, dorsal views; D, right Mc II, MGUV-w/n in D1, lateral and D2, dorsal views; E right Mc III MGUV-12204, VV-12204 in E1, lateral and E2, dorsal views; F, right Mc IV MGUV-18522, VV-12761 in F1, dorsal and F2, medial views. Scale bars equals 50 mm.

Ulna (Figure 6B)—A complete, but very transversely crushed ulna has been recovered. The olecranon is short and narrow. The caudal border is straight and nearly vertical. The radius articular surface is typically trilobed.

Scaphoid (Figure 7A)—The right scaphoid MGUV-18524 is latero-medially pressed, resulting in very low TD values. The proximal radial facet is subtriangular to 'heart'-shaped in proximal view, has a typical concave-convex surface and a more elevated caudal ridge than the rounded dorsal bulge. The medial side of the bone is flattened and finely vascularized. Two shallow grooves runs along the proximal and distal articular surfaces. In lateral view, the dorsal side of the bone is almost straight and slightly dorso-laterally protruding from the body of the bone. The palmar flange of the bone is palmarly projected. It has a blunt angle dividing two straight dorsal and distal sides. The lateral tuberosity is triangular but not very laterally projected, partially due to its latero-medial compression. The dorso-distal lunate-facet is attached to the dorsal half of the lateral border of the magnum-facet through a very smooth boundary. The dorso-distal lunate facet is subtriangular, and flat. The dorso-proximal lunate-facet is attached to the dorsal side of the lateral tuberosity and is dorso-laterally oriented. Its outline is oval and its surface flat. In distal view, there are three successive facets forming a unique articular complex. The dorsal-most magnum-facet is semicircular and convex, spreading along the lateral side of the bone with a semicircular expansion. The trapezoid-facet has a squared outline, a 'saddle'-shaped surface and limits through two sharp ridges with the magnum (dorsal) and the trapezium (palmar) respectively. Finally, the palmar-facet is disto-palmarly oriented, is triangular in distal view, dorso-palmarly concave and transversally flat.

Lunate (Figure 7B)—The right lunate MGUV-18523 is well-preserved. The dorsal side is very high if compared with the palmar one. In dorsal view, the dorsal surface of the bone has a very protruding dorsal relief with steep latero-medial sides. The distal border of the lunate is flattened, the lateral curved, and the medial straight. In proximal view, the radial-facet is rectangular, strongly dorso-palmarly convex and transversally flat. The palmar expansion is limited to a small rectangular surface on the medial side. The articular surface of the radial-facet barely overhangs the body of the bone in dorsal view. In lateral view, there are two facets for the scaphoid. The proximal scaphoid-facet is oval and flat. The distal scaphoid-facet is semicircular and flat. In medial view, the three pyramidal-facets are aligned. The dorso-proximal

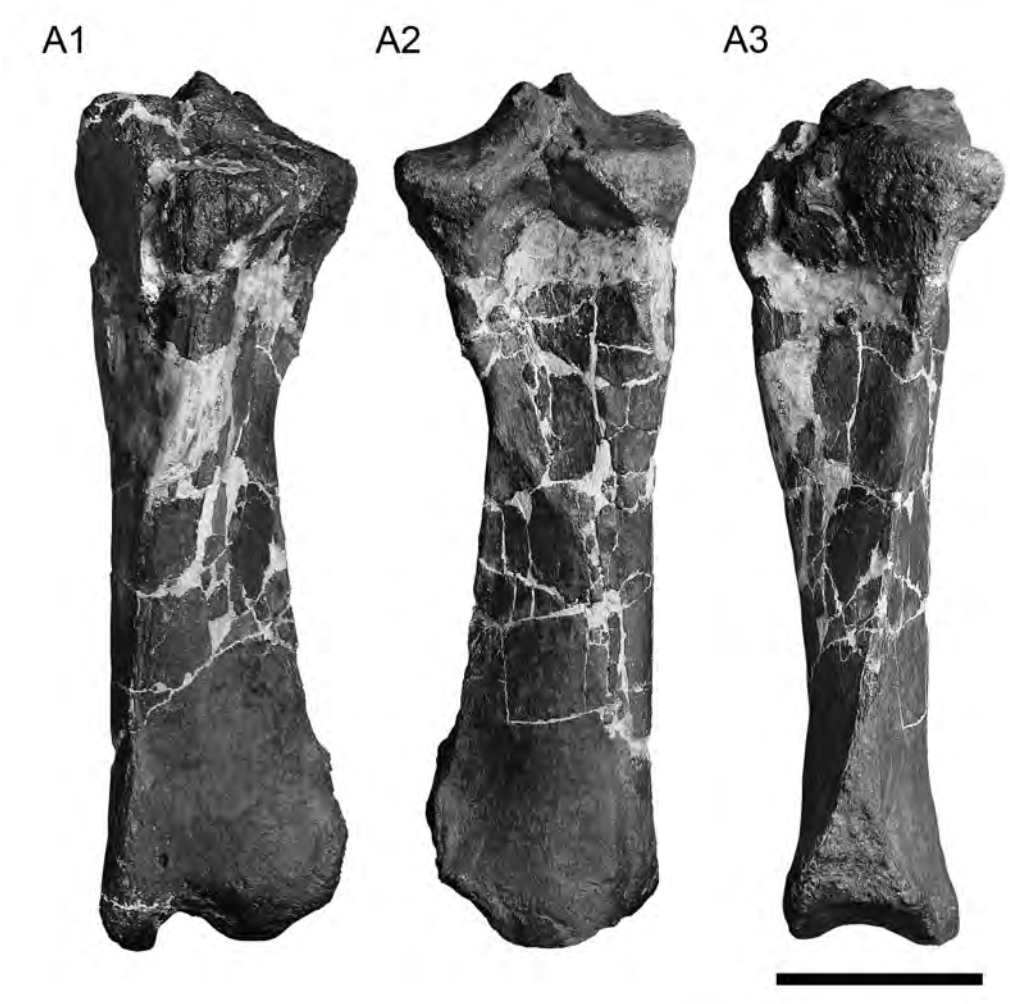


Fig. 6 Left tibia MGUV-11293 of *Dihoplus schleiermacheri* from the Upper Turolian of Venta del Moro (Valencia Province, Spain). Scale bar equals 100 mm.

pyramidal-facet is oval and flat. The dorso-distal pyramidal-facet is semicircular, flat, and palmarly topped by a protruding peak. On the other hand, the palmar pyramidal-facet is rounded and flat. There are two distinct facets carving the distal surface of the bone. The unciform-facet, which occupies the lateral side, is attached to the dorsal border. It is oval, strongly dorso-palmarly concave, and latero-distally oriented. The magnum-facet is placed on the medial side of the distal side of the bone. It is rectangular concave, and divided in two distinct areas, the dorsal dorsally oriented, the palmar more palmarly oriented. The volar process of MGUV-18523 is very short and remarkably narrowed transversally, resulting in a high and blunt palmar end. It is delimited from the body of the bone by a clear notch, visible in lateral view.

Trapezoid (Figure 7C)—The right trapezoid MGUV-18521 has a very concave proximal scaphoid-facet in lateral view. The proximal scaphoid-facet is rectangular and has a typical 'saddle'-shaped surface (i.e. latero-medially concave and dorso-palmarly convex). The lateral surface, place of contact with the magnum, is 'hourglass'-shaped), smooth, and flat. The dorsal indentation of the medial side is very small and shallow. The medial surface is occupied by the trapezium-facet. This facet is vaguely 'arrow'-like due to its strongly concave proximal side and which converge in a pointed angle on the disto-palmar angle of this side of the bone. The medial indentation is triangular and deep (reaching the midpoint of the bone) but shallow. The distal Mc II-facet has a similar configuration than the proximal one for the scaphoid. However, it is oval and less concave in lateral view.

Mc II (Figure 8B)—The right Mc II (MGUV w/n) is complete, but has a somewhat eroded surface and is dorso-plantarly pressed. The proximal epiphysis is deep (high APD). In proximal view, the proximal trapezoid-facet facet has a 'sickle'-like outline. It is dorso-plantarly convex and transversally flat. There is a blunt lateral ridge that starts below the level of the proximal articular surface running up to the on third of the shaft. In lateral view, the Mc III/magnum-articular complex is 'kidney'-like. The proximal border of the lateral side is occupied by the magnum-facet. It is long, rectangular, and flat. Attached to the dorsal and palmar sides of its distal border there are two flat and semicircular expansions which form an obtuse angle with the magnum-facet. Between them, there is a shallow and rounded notch. The section of the shaft is oval. The reliefs for the *m. interossei* are high and rounded. In dorsal view, the distal epiphysis has a straight distal edge with a also straight lateral condyle (both forming a wide obtuse angle).

Mc III (Figure 8C)—The right Mc III (MGUV-18827) is complete and, except for its dorso-palmar compression, very well-preserved. Its proximal magnum-facet is trapezoidal and has a 'saddle'-like surface, a long and convex dorsal border and a concave plantar one. Both are flanked by a sinusoid lateral, and a nearly straight medial one. In dorsal view, the unciform-facet is short and forms a straight angle in dorsal view with the latter. Its surface is semicircular and slightly convex. In lateral view, the lateral Mc IV-facets are separated by a shallow channel which widens towards both proximal and distal extents. The dorsal Mc IV-facet is subtriangular, attached to the plantar border of the unciform-facet, flat, and palmarly oriented. Alternatively, the plantar Mc IV-facet is rounded, flat, placed at a lower level than the dorsal one, and is latero-proximally oriented. It also flanks the lateral side of the magnum-facet plantar expansion. In medial view, the medial Mc II-facet is oval, flat, proximo-medially oriented, and attached to the medial border of the magnum-facet. The dorsal surface of the bone is flat and smooth. The shaft widens under the proximal epiphysis, giving the appearance of a short neck in the lateral border. Thereinafter both medial and lateral borders are nearly straight and parallel. Its section is oval and very narrow (low APD) due to the dorso-palmar distortion. The insertions for the *m. interossei* are rounded (the lateral is aligned with the lateral border of the shaft; the medial little protruding) and low. A shallow but continuous groove encircles the distal articulation, which is narrow (low TD) and bulbous.

Mc IV (Figure 8D)—Despite pertaining to the same individual than the Mc II and the Mc III, the right Mc IV (MGUV-18522) is finely preserved. In proximal view, the proximal unciform-facet is triangular and lacks the posterior shelf observed in the individuals CR1, M1 from Cervillente or RO 411 from La Roma (Cerdeño, 1989). In medial view, the Mc III-facets are separated by a space. The dorsal Mc III-facet is semicircular, dorso-medially oriented, and flat. The plantar Mc III-facet, better preserved, is circular, medially oriented, and flat. While the dorsal facet is attached to the proximal articular facet, this facet is separated through a short neck. There is no trace of Mc V-facet on the lateral side. In its place, the lateral border is inflated as a blunt proximal protuberance that narrows distally. The shaft of the Mc IV is not very laterally bended, especially if compared with other Upper Miocene species like *Aceratherium incisivum*. The medial border is straight and the lateral one slightly concave. On the other hand, in lateral view the shaft of the bone shows a thickened proximal half followed by a much narrower distal one (which also presents a change in orientation). The section of the diaphysis is rectangular at its midpoint. The insertions for the *m. interossei* are weak and are barely projected from the shaft.

Tibia (Figure 1D)—A single left tibia (MGUV-11293) has been found in the new campaigns in Venta del Moro. The whole proximal epiphysis is slightly laterally oriented. In proximal view, both femoral facets are oval, roughly similar in size, and flat except for the intercondylar eminence. The latter is high, has a more developed lateral lip, laterally twisted, and attached to the caudal border of the proximal side of the bone. The tibial tuberosity is damaged. The central intercondylar notch starts as a deep gutter an opens in a wide and shallow popliteal notch. This area is proximally enclosed by the medial and lateral condyles, and laterally flanked by the distal expansion of the proximal fibular-facet (which is rough and extends up to the midshaft). The medial side of the popliteal

notch is medially expanded, resulting in a convex first third of the medial border of the bone in caudal view. The proximal fibular-facet is triangular, cranio-caudally convex, and distally expanded along the lateral edge of the shaft. The section of the shaft is triangular, with a very sharp lateral border and more rounded medio-cranial and medio-caudal ones. Except for the first third of the diaphysis, the remaining shaft has straight borders that vaguely diverge. The distal fibular-facet is triangular, rough, and extends through a narrow ridge along the lateral border. The medial malleolus is blunt and rounded; the lateral is slightly more distally protruding and curved. In distal view, the distal articular surface has a sigmoid cranial border, a convex caudal one over the medial astragalar facet (straight along the medial one), and straight lateral and medial borders (nearly parallel). Both astragalar surfaces are concave, the medial bigger. The medial malleolus is semicircular in this

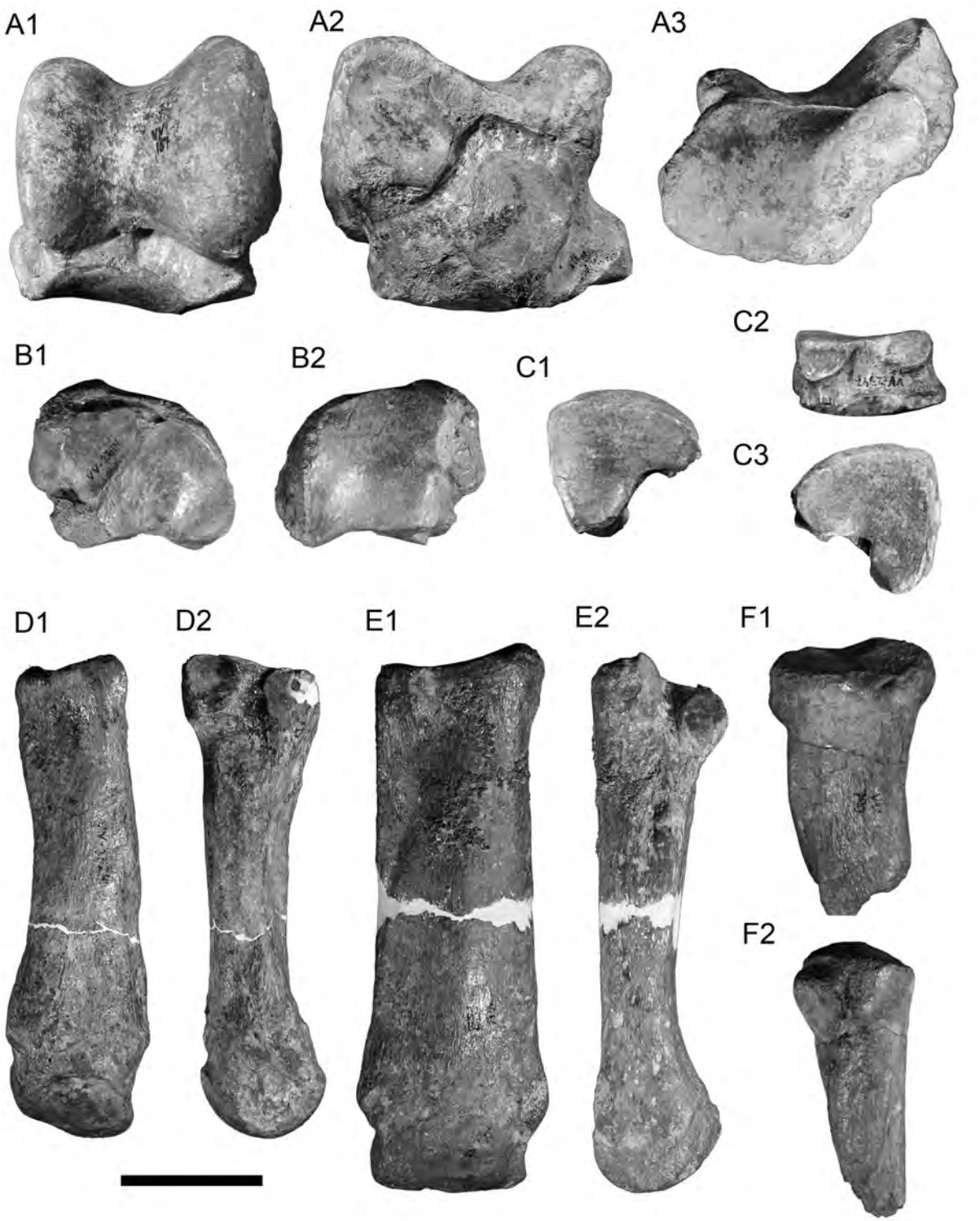


Fig. 7 Tarsal and metatarsal bones of *Dihoplus schleiermacheri* from the Upper Turolian of Venta del Moro (Valencia Province, Spain). A, left astragalus MGUV-11229 in A1, dorsal, A2, plantar, and A3, distal views; B, left navicular MGUV-11289 in B1, distal and B2, proximal views; C, right ectocuneiform MGUV-11233 in C1, distal, C2, medial, and C3 proximal views. Scale bar equals 50 mm.

view.

Astragalus (Figure 9A)—The astragali are represented by a left astragalus (MGUV-11229) and a fragmentary right one (MGUV-7050). The trochlea is wide, not very assymetrical. The lateral surface of the lateral lip is inflated and laterally projected. The neck of the astragalus is high, widens in the central part and narrows at the level of both lips (the medial of which does reaches the distal articular surface and forms a gutter. Also in dorsal view, the medial tubercle is blunt, low, and has a straight medial border. In plantar view, the first calcaneum-facet is roughly oval, lacks its distal side, and has a concave surface. The second calcaneum-facet is rounded, and flat. Both first and second facets are similar in size. The gutter that divides them is wide and has a constant width. The third calcaneum-facet is 'tear'-like and contacts the second by a narrow bridge. In distal view, the navicular-facet is 'tear'-like. While the dorsal and plantar borders are approximately straight and parallel, the medial one (the contact with the cuboid-facet) is convex and the lateral deeply sinuous. The whole surface of this facet is dorso-plantarly straight and transversally convex. The cuboid-facet has an oval to 'kidney'-shaped outline, a dorso-plantarly convex surface, and has a dorsally-projected dorsal border (not aligned with the dorsal border of the navicular-facet).

Navicular (Figure 9B)—The navicular sample from the Levantine basins (MGUV-11289 from Venta del Moro and CR-2 and CR-1045 from Crevillente-2) share a common morphology. In proximal view, the proximal astragalar-facet has a 'fan'-like contour: the lateral and plantar borders form a straight angle whereas the dorso-medial one is smoothly convex. Its surface is dorso-plantarly concave and transversally flat. In lateral view, the dorsal cuboid-facet is restricted to a triangular and flat area attached to the proximal border. The plantar cuboid-facet has a 'keylock'-like outline, with a rounded and big facet on the distal side proximally flanked by a flattened "T"-like expansion attached to the proximal border which contacts with the dorsal cuboid-facet. Its surface is slightly concave. In distal view, the dorsal ectocuneiform-facet is flattened and 'heart'-shaped with rounded dorso-lateral and planto-lateral expansions. The mesocuneiform-facet is subtriangular to oval and flat. Thirdly, the entocuneiform-facet, placed on the plantar border, is oval, flat, and slightly plantarly oriented. A narrow groove starts in the medial corner of the ectocuneiform-facet, running along the medial border of the mesocuneiform one. On the lateral border of the distal side of the bone, the lateral protuberance seems well-delimited but broken at its base.

E**ctocuneiform** (Figure 9C)—This bone is represented by a righ well-preserved ectocuneiform (MGUV-11233). In proximal view, the ectocuneiform has a big, flat, and 'L'-shaped navicular-facet which shows a rounded plantar expansion. The dorsal side of the bone is finely vascularized. In lateral view, the three lateral mesocuneiform-facets are divided into two semicircular facets of about the same size attached to the distal border and separated by a rounded gap, and a single proximal facet, semicircular and longer than the formers. In medial view, the dorso-distal cuboid-facet is semicircular, flat, and distally oriented. The proximo-plantar cuboid-facet is semicircular (but badly preserved) and flat. Both are separated by a gap. The distal Mt III-facet is more triangular and 'heart'-like shaped than the proximal one (due to its rounder expansions) and flat.

Mt II (Figure 10A)—As with the metacarpals, all three metatarsals pertain to a single individual. The left Mt II (MGUV-11290) is complete and well-preserved. In proximal view, the proximal mesocuneiform-facet is oval, has a sinuous medial border and a straight lateral one. Its surface is concave. There are two shelves attached to the lateral side of the bone (the dorsal more pointed and protruding), place of insertion for the lateral articular clusters. In lateral view, there are two aligned clusters of ectocuneiform/Mt III-facets separated by a gap. They are rounded and the dorsal more elevated. Each complex has a semicircular and flat ectocuneiform-facet and a semicircular, flat, and more distally oriented Mt III-facet. The boundary between both facets is oblique. The proximal insertion is inflated and starts as a rounded and rough area below the proximo-lateral facets. The lateral border of the diaphysis is straight, the medial concave. Its section is rectangular. The distal epiphysis is swollen and medially tilted. The insertions for the m. interossei are pointed, narrow, and well-separated from the distal articular surface. The distal articular surface is globous, has a rounded dorsal border in distal view and well-marked metacarpo-phalangeal sesamoid insertions in the plantar one.

Mt III (Figure 10B)—The left Mt III (MGUV-11291) is complete except for a fracture at its midpoint and dorso-plantarly pressed. In proximal view, the proximal ectocuneiform-facet is 'L'-shaped with rounded plantar and lateral extents and a sinusoid dorsal border. It is smoothly concave in dorsal view and transversally flattened. The lateral side is rounded and more elevated, the medial one blunt and forms a straight angle with the medial edge of the shaft. In medial view, a single Mt II-facet is placed on the medio-plantar angle of the proximal epiphysis and attached to the proximal articular surface. It is semicircular and flat. The dorsal Mt II-facet is not preserved. In lateral view, the lateral Mt IV-facets are rounded and separated by a well-delimited gutter. Both facets form an obtuse angle. The dorsal Mt IV-facet is more elevated, rounded, flat, and plantarly-oriented. The plantar Mt IV-facet is smaller, rounded, flat, laterally oriented, and placed in a short shelf latero-plantarly projected. The diaphysis has parallel and straight latero-medial borders, and a flattened dorsal surface. The lateral insertion covers three quarters of the lateral side of the bone. It is rough and narrows distally. The section is oval and shallow (low APD), mainly due to the dorso-plantar compression. The insertions for the *m. interossei* are rounded, weakly protruding from the latero-medial borders, and close to the distal articular surface. The latter is wide, narrow, and has a convex distal border.

Mt IV (Figure 10C)—The Mt IV is represented by a single

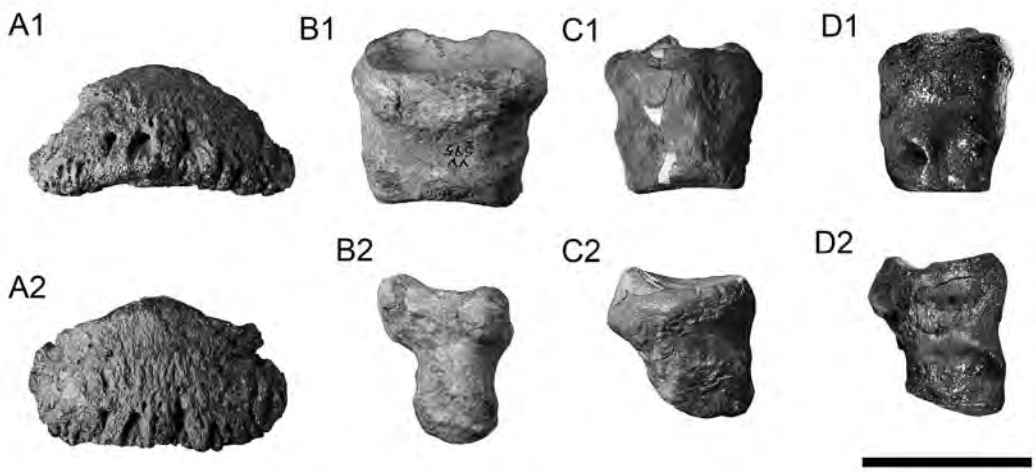


Fig. 8 Phalanges of *Dihoplus schleiermacheri* from the Upper Turolian of Venta del Moro (Valencia Province, Spain). A, third central phalanx MGUV-11230, VV-1594 in A1, dorsal and A2, proximal views; B, first central phalanx MGUV-11231, VV-595 in B1, dorsal, and B2, lateral/medial views; C, second lateral phalanx MGUV-11232, VV-794 in C1, dorsal and C2, lateral/medial views; D, second lateral phalanx MGUV-12817, VV-3220 in D1, dorsal and D2, lateral/medial views. Scale bar equals 50 mm.

proximal half of a left Mt IV (MGUV-11294). In proximal view, the cuboid-facet is trilobed and its surface concave. Its latero-medial borders are expanded. In the same view, the plantar expansion of the cuboid-facet has two shelves at both sides. In medial view, the two Mt III-facets are separated by a small gap. The dorsal Mt III-facet is roughly oval, but its plantar border is broken. The plantar Mt III-facet is placed on a small shelf. It is vertically-oriented, oval and flat. The preserved part of the diaphysis is laterally bended and flattened.

DISCUSSION

Only mandibular fragments from Venta del Moro and La Alberca are identified as *D. schleiermacheri* (Table 1). They differ in some characters: the horizontal ramus is higher in Venta del Moro, its height more constant along the ramus; the posterior symphyseal border reaches the level of the posterior half of the p2 (the specimen from La Alberca specimen lacks the symphiseal region). Comparing the mandible from Venta del Moro with the Eppelsheim mandibles of *D. schleiermacheri* and *A. incisivum*, it is observed that the former is comparable with that of *D. schleiermacheri*, since the horizontal rami are straighter, the toothrows are more parallel, and the symphysis is not so enlarged as in *A. incisivum*; besides, the posterior border of the symphysis reaches the level of the posterior half of p2, whereas it reaches the p3 in *A. incisivum*, where the mandible begins to enlarge. This is why we considered the mandible from Venta del Moro as *D. schleiermacheri* (Cerdeño, 1989) contrary to Guérin (1980) and Morales (1984) who considered it as *A. incisivum*. Compared with a mandible from Aubignas (Ardèche, France; MNHN, Paris) of *D. schleiermacheri* (Guérin, 1980), the mandible from Venta del Moro has narrower horizontal rami and smaller teeth, especially the molars. Mandibular dimensions of Venta del Moro and La Alberca specimens fall into the variation range provided by Guérin (1980) for *D. schleiermacheri*; the mandibular height on the Venta del Moro mandible closes the maximum values, whereas that on the La Alberca specimen closes the minimum; instead, the width of the former is even below the minimum. The toothrow length is also around the minimum values in both cases, exceeding the maximum of *A. incisivum*. The material from Venta del Moro shares with Alcoy-Mina site the oblique orientation from the medial part of the metalophid, which is generally oriented in a longitudinal way (Montoya et al., 2006a). The robustness of the turolian forms even exceed the type material from Eppelsheim. The fossils from Venta del Moro and Crevillente, despite being more graceful, they are closer to La Roma specimens than to the rest of the Iberian fossils.

Upper dental remains, especially P2, are perfectly comparable with those from the holotype figured by Kaup (183234, pl.11, fig.5), and the observed morphological variation (different folds development) coincides with Guérin's (1980) descriptions for *D. schleiermacheri*.

Permanent lower dentition is well represented at Crevillente. Cheek teeth are large, and there is a great difference between premolars and molars. There are no lateral cingula and the labial groove is well marked, especially on the p4. The anterior cingulum is slightly prolonged lingually on the m1 CR2S,353. Worn teeth show a massive metaconid (Crevillente, Venta del Moro, La Alberca). Dimensions are similar among different specimens, only the length of m2 and m3 is slightly lesser at Venta del Moro (Table 1). Isolated teeth such as those from Los Hornillos, determined as *Diceros pachygnathus* by Guérin (1980), are characterized by a strong unevennes between anterior and posterior valleys. The m3 is very similar to that from Concud. The labial groove is deep and the protoconid angle is stronger than on the m3 from Crevillente and La Alberca. In our opinion, the recognition of *Diceros pachygnathus* at Los Hornillos is not justified. This species was defined on material from Pikermi (Greece), later revised by Geraads (1988), who named it as *Ceratotherium neumayri*. Geraads explained the difficulties in separating the two species present at Pikermi (*C.*

neumayri and "*Dicerorhinus*" *pikermiensis*, formerly known as *Dihoplus pikermiensis*), based on dentition and postcranial skeleton. *Stephanorhinus pikermiensis* was originally related to *D. schleiermacheri*, and it seems natural to find similarities between the teeth from Los Hornillos and those from Pikermi.

The radius from Venta del Moro and La Roma 2 coincides with *D. schleiermacheri* (Guérin, 1980, p. 258) in the narrow proximal external facet, in the entering of the anterior border between both proximal facets, in the strong development of the lateral tuberosity, and in the projecting medial proximal border. Dimensions are very close (Guérin, 1980, t. 53). The scaphoid from Eppelsheim figured in Kaup (1832-34; cast number AMNH 98028) shows some differences with MGUV-18524 from Venta del Moro. The dorsal border is shorter in Eppelsheim's scaphoid,

Dimensions of the tibiae from Eppelsheim and Venta del Moro are very similar. However, the tibia from Venta del Moro is considerably robust (Ig = 17,6), which contrasts with the mean of 14,2 previously calculated for the species (Guérin, 1980). The tibial fragments from La Roma 2 show a great distal epiphysis and the diaphysis triangular in section, with the lateral border acute. The lateral distal facet is very little concave.

The described astragali are coincident with the Kaup's figure (183239, pl.13). The specimen from Eppelsheim directly studied as well as that from Dorn-Dürkheim 1 (Cerdeño, 1997) have similar dimensions (Table 6), although the Spanish specimens are slightly wider. The specimen from Eppelsheim has a wider connection between facets 2 and 3, the former being larger and more flattened. With respect to the variation range given by Guérin (1980, t. 68), the specimens from La Roma 2 and Puente Minero reach the maximum width value, whereas their height is around the average. The astragali of *D. pikermiensis* from Pikermi (e.g. PK 18) show an equivalent morphology than the Spanish specimens, but with facets-1 and 2 united. In contrast with the sample from Venta del Moro, in the astragalus from La Roma RO 275 (which is similar in size), the medial lip contacts the distal articular surface. A small salient between the navicular and cuboid-facets has been observed in the sample from La Roma (Cerdeño, 1989), but not recorded in MGUV-11229.

The naviculars from Venta del Moro and Crevillente-2 are among the bigger for the species. Other navicular cited in the Iberian Peninsula include one individual from Can Trullàs (Santafé, 1978) and four from Concud (Santafé y Casanovas, 1983-84).

Guérin (1980, p.324) states for the cuboid of *D. schleiermacheri* that the anterior face is slightly wider than high, being H 94.4% of W (in *A. incisivum* this proportion is 88.7%), but present data do not corroborate this statement. The Venta del Moro specimen is considerably wider than the average Iberian sample. Within La Roma 2 cuboids, it can be observed that proportions vary with age, and the adult specimen has a relatively wide anterior face, even more than the Venta del Moro specimen. The calculated rate is: Venta del Moro 80.7%, Concud 95.6% and La Roma 90.6% (adult) and 103% (juvenile). In absolute values, the TD tends to the maximum given by Guérin (op.cit., t. 70), surpassing it the cuboid from Venta del Moro; the APD on the contrary is below the minimum.

The ectocuneiforms are wider than the respective homologous from Montredon (Guérin, 1988). Two distinct ectocuneiform morphologies have been ascribed to *D. schleiermacheri*. The first type fits with that found in Venta del Moro. This type of ectocuneiforms are somewhat similar to those of the poorly known *Stephanorhinus miquelcrusafonti*

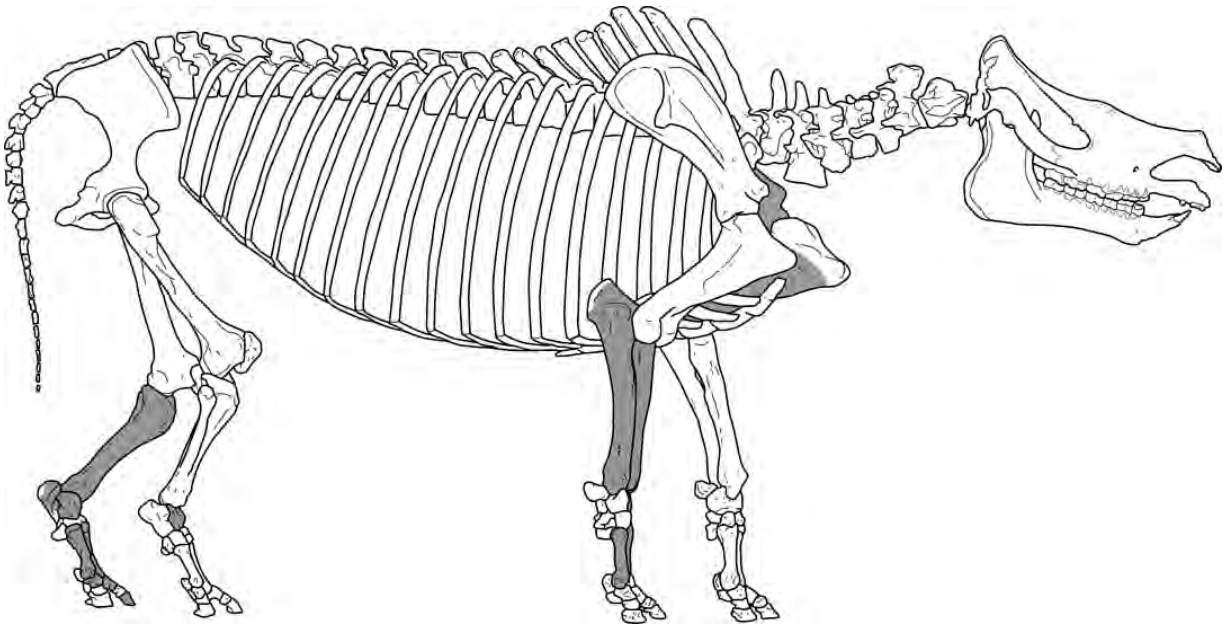


Fig. 9 Remains of *Dihoplus schleiermacheri* from Venta del Moro (depicted in grey). Not all recovered fossils pertain to the same specimen, so the proportions have been estimated. Non recovered parts have been represented following the Eppelsheim type series and the axial skeleton of a Sumatran rhino (Dicerorhinus sumatrensis).

described in the Pliocene site of Layna (Guérin, 1978). The second ectocuneiform morphology can be exemplified by the individual PM 620 from Puente Minero (Spain) and resembles the Pliocene species *Dihoplus megarhinus* (e.g. FSL 40042 from Montpellier, France). The Mt II-facets, separated in MGUV-11233, are fused in PM 620 from Puente Minero, only leaving a faint constriction in the proximal border of the bridge.

The morphology is comparable within the samples. Differences among compared metapodials mainly refer to the degree of gracility. Although variability in the degree of gracility in metapodials is not significative between species, it could represent a good indicator for comparisons inside a single species. One of the two Mc II from Dorn-Dürkheim (Cerdeño, 1997) has two lateral facets for the Mc III, while the other has only the most anterior one as in the Spanish specimens. This reduction of the Mc III facet is also observed in "*D. pachygnathus*" from Pikermi. The gracility index calculated are as follows (1, after Santafé, 1978; 2, from average values of *D. schleiermacheri* after Guérin, 1980):

- Mc II: Dorn-Dürkheim 25.5; La Roma 23.5; Venta del Moro 21,3.
- Mc III: Venta del Moro 31; La Roma 29.9; Concud (1) 29.5; Subsuelo de Sabadell (1) (25.6).
- Mc IV: Crevillente 24.7; Venta del Moro 24,5; Subsuelo de Sabadell (1) 20.9.
- Mt II: Venta del Moro: 22,8; La Roma 21.1, 20.2; El Fargue 19.0; Cenes de la Vega 17.6.
- Mt III: La Roma 30, 29.3, juv. 26; Venta del Moro 27,2; El Fargue 27.1.
- Mt IV: La Roma 21.8, 20.2, juv. 20.2; Cenes de la Vega 19.8; El Fargue 19.7.

Differences of gracility are not very marked. In La Roma 2, metapodials are slightly more robust than in the other Spanish sites.

Guérin (1982a) recognizes two (possibly three) "evolutionary stages" among the European populations of *D. schleiermacheri*, one for the Vallesian and other for the MN12-13 Mein's biozones.

Postcranial remains of *D. schleiermacheri* are scarce if compared with the overwhelming sample of its closest relative, *Dihoplus pikermiensis*, recovered from Pikermi. The presence of large aceratheres and *Lartetotherium*-like rhinocerotines in Cerro de los Batallones (Sanisidro et al., this volume) would complicate the picture. As a result, many Iberian sites with postcranial samples of small to moderate size attributed to *D. schleiermacheri* (particularly those from the Vallesian) should be reviewed on the light of the new findings.

In summary, samples from Crevillente and La Roma 2 show a more robust skeleton than other Spanish populations. About the type material from Eppelsheim, Kaup (183239) only provided the length of a Mc IV and a Mc III (178 and 204 mm, respectively), both longer than the Spanish specimens.

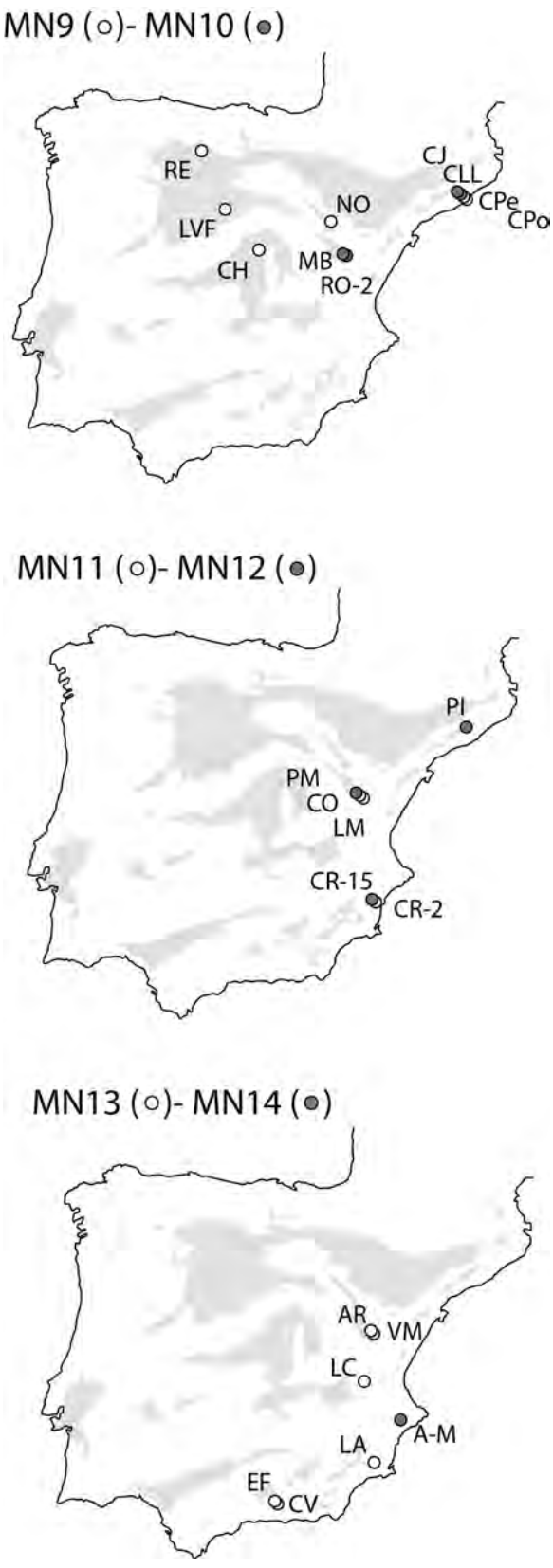


Fig. 10 Localities with presence of *Dihoplus schleiermacheri* in the Iberian Peninsula along the following intervals Vallesian (MN 9-10 Mein's biozone), early to middle Turolian (MN 11-12) and late Turolian-Ruscinian (MN13-14). A-M: Alcoy-Mina; CH: Chiloeches; CLl: Can Llobateres; CJ: Can Jofresa; CO: Concud; CPe: Can Perellada; CPo: Can Ponsic; CR-2: Crevillente-2; CR-15: Crevillente-15; EF: El Fargue, LA: La Alberca; LM: Los Mansuetos; MB: Masía del Barbo; PI: Piera; PM: Puente Minero; RE, Relea; RO-2: La Roma 2; VM: Venta del Moro.

Therefore, the new material presents a similar morphology than the type material of *D. schleiermacheri*, but with a slight difference in proportions.

Between samples from Venta del Moro-Crevillente and Teruel area there are no outstanding differences. In both cases, the skeleton is more robust (astragalus, metapodials) than in other Spanish localities and also than the European average. In the VallésPenedés basin, metapodials are longer and their gracility is slightly greater than in Concud, La Roma 2 and the European average. The general size is smaller (e.g., pyramidal from Can Llobateres, Table X, and metapodial diameters, Tables XX). La Roma 2, on the contrary, besides a greater robustness present in many cases a big general size, surpassing the maximum values established previously for *D. schleiermacheri*.

D. schleiermacheri enters to the Iberian Peninsula during lower Vallesian together with *Hipparion*, remaining until the lower Pliocene. As a whole, the studied material allows to notice some increase of robustness from the early Vallesian to the middle Turolian. In the late Turolian, different isolated remains indicate, on one hand, that the gracility increase maintaining a similar size (Cenes de la Vega, Corral de Lobato), whereas, on the other hand, the robustness is maintained while the general size increases (El Fargue). These remains from El Fargue are problematic for their differences with respect to the other samples, but the scarcity of remains does not provide data enough to consider them as a different species, and it is better to determine them as *Dihoplus* cf. *schleiermacheri*.

D. schleiermacheri had a wide biogeographic range. It was distributed along central and western Europe (Cerdeño, 1989; Guérin, 1980, 1982b). Classically is considered that the biostratigraphic range of *D. schleiermacheri* extended from the lower Vallesian, MN9 Mein Biozone to the upper Turolian, MN13 Mein Biozone (Guérin, 1982b; Heissig, 1999). The site of Alcoy-Mina (Alicante) is one of the first localities cited in Spain (Ezquerra de Bayo, 1850). Crusafont & Villalta (1955) dated it as lower Pliocene, describing several remains of *Rhinoceros* sp. (cf. *megarhinus*). Guérin (1980) indentified four molars, assigning them to (*D*). *schleiermacheri* and dating the site as Pikermian (MN13). Morales (1984) related Alcoy-Mina site with the European localities of Montpellier and Perpignan, placing it in the upper Miocene (Ventian MN13). Alcoy-Mina is currently considered to belong to the lower Pliocene (Ruscinian, MN14) (Montoya et al., 2006a), although the authors do not discard that the site could reflect the faunistic transitional moment between Miocene and Pliocene, founding typical faunas from both. If the Pliocene age of Alcoy-Mina is finally confirmed, the presence of *D. schleiermacheri* would demonstrate that the species was still present in some western European localities at the earlier Pliocene, probably as isolated populations. Thereafter new climatic conditions replaced this Miocene rhinoceros by the typical Plio-Pleistocene genus *Stephanorhinus* in Western Europe. Spanish localities where *D.schleiermacheri* has been found ordered by sedimentary basins) are represented in the figure 3.

ACKNOWLEDGMENTS

We acknowledge P. Pérez Dios (Museo Nacional de Ciencias Naturales de Madrid-CSIC), A. García Forner (Museo de Geología de la Universidad de Valencia), Dr. O. Sandrock, and E. Milson (Darmstadt Hessisches Landesmuseum) for kindly helping with the specimens in her care.

LITERATURE CITED

Antoine, P. O., 2002, Phylogénie et évolution des Elasmotheriina: (Mammalia, Rhinocerotidae): Mémoires du Muséum National d'Histoire Naturelle, v. 188, p. 5-350.

Böhme, M., Aiglstorfer, M., Uhl, D., and Kullmer, O., 2012, The antiquity of the Rhine River: stratigraphic coverage of the Dinotheriensande (Eppelsheim Formation) of the Mainz Basin (Germany). PloS ONE, v. 7, no. 5.

Cerdeño, E., 1989, Revisión de la sistemática de los rinocerontes del Neógeno de EspañaPh.D. Dissertation]: Universidad Complutense de Madrid, 429 p.

-, 1992, Spanish Neogene Rhinoceroses: Palaeontology, v. 35, p. 297-308.

Crusafont, M., and Villalta, J. F. d., 1955, Sur l'âge des mammifères d'Alcoy (Espagne): Comptes Rendus sommaires des Séances de la Société géologique de France, v. 12, p. 148.

Cuvier, G., 1824, Recherches sur les ossements fossiles., Paris.

Ezquerra de Bayo, J., 1850, Ensayo de una descripción general de la estructura geológica del terreno de España en la península: sección 3ª: Memorias de la Academia de Ciencias de Madrid, v. 1, p. 161-184.

Geraads, D., and Spassov, N., 2009, Rhinocerotidae (Mammalia) from the Late Miocene of Bulgaria: Palaeontographica A, v. 287, p. 99-122.

Giaourtsakis, I., Phlevan, C., and Haile-Selassie, Y., 2009, 14. Rhinocerotidae, *in* Haile-Selassie, Y., and Woldegabriel, G., eds., *Ardipithecus kadabba*. Late Miocene Evidence from the Middle Awash, Ethiopia: Berkeley, Los Angeles, and London, University of California Press and University of California Press, Ltd., p. 429-472.

Giaourtsakis, I. X., and Heissig, K., On the nomenclatural status of *Aceratherium incisivum* (Rhinocerotidae, Mammalia), *in* Proceedings 5th International Symposium on Eastern Mediterranean Geology, Thessaloniki, Greece, 14-20 April 2004 2004.

Grimm, K. I., 2011, Chronostratigraphie, Deutsche Stratigraphische Kommission: Stratigraphie von Deutschland IX Tertiär, Teil 1. , Volume 75: Hannover, Schriftenreihe der Deutschen Gesellschaft für Geowissenschaften, p. 42.

Guérin, C., 1980, Les rhinocéros (Mammalia, Perissodactyla) du Miocène terminal au Pléistocène supérieur en Europe occidentale : comparaison avec les espèces actuelles: Documents des Laboratoires de Géologie de Lyon, v. 79, p. 1-1184.

-, 1982a, Les Rhinocerotidae (Mammalia, Perissodactyla) du Miocène terminal au Pléistocène supérieur d'Europe occidentale comparés aux espèces actuelles: Tendances évolutives et relations phylétiques: Geobios, v. 15, p. 599-605.

-, 1982b, Première biozonation du Pléistocène européen, principal résultat biostratigraphique de l'étude des Rhinocerotidae (Mammalia, Perissodactyla) du Miocène terminal au Pléistocène supérieur d'Europe occidentale: Geobios, v. 15, p. 593-598.

Heissig, K., 1972, Die obermiozäne Fossil-Lagerstätte Sandelzhausen. 5. Rhinocerotidae (Mammalia), Systematik und Okologie: Mitteilungen der Bayerischen Staatssammlung Paläontologie und historische Geologie, v. 14, p. 37.

-, 1999, 16. Family Rhinocerotidae, *in* Rössner, G. E., and Heissig, K., eds., The Miocene Land Mammals of Europe: Pfeil, Munich, p. 175-188.

Kaup, J. J., 1832, Über *Rhinoceros incisivus* Cuv. und eine neue Art *Rhinoceros schleiermacheri*: Isis, v. 8, no. 1832, p. 898-904.

Kaya, T., and Heissig, K., 2001, Late Miocene rhinocerotids (Mammalia) from Yulafli (Corlu-Thrace, Turkey): Geobios, v. 34, p. 457-467.

Martín-Suarez, E., and Freudenthal, M., 1998, Biostratigraphy of the Continental Upper Miocene of Crevillente (Alicante, SE Spain) Geobios, v. 31, no. 6, p. 839-847.

Mein, P., 1975, Proposition de Biozonation du Neogène Mediterraneern à partir des Mammifères: Trabajos sobre Neógeno-Cuaternario, v. 4, p. 112-113.

-, 1990, Updating of MN zones, *in* Lindsay, E., Fahlbusch, V., and Mein, P., eds., European Neogene Mammal Chronology: New York, Plenum Press, p. 73-90.

-, 1999, European Miocene mammal biochronology, *in* Rössner, G. E., and Hessig, K., eds., The Miocene Land Mammals of Europe: München, Verlag Dr. Friedrich Pfeil, p. 25-38.

Montoya, P., Ginsburg, L., Alberdi, M. T., Van der Made, J., Morales, J., and Soria, M. D., 2006a, Fossil large mammals from the early Pliocene locality of Alcoy (Spain) and their importance in biostratigraphy: Geodiversitas, v. 28, no. 1, p. 137-173.

Montoya, P., Morales, J., Robles, F., Abella, J., Benavent, J. V., Marín, M. D., and Sánchez, F. J. R., 2006b, Las nuevas excavaciones (1995-2006) en el yacimiento del Mioceno final de Venta del Moro, Valencia: Estudios Geologicos, v. 62, no. 1, p. 313-326.

Morales, J., 1984, Venta del Moro: su macrofauna de mamíferos y biostratigrafía continental del Mioceno terminal mediterráneo: Editorial de la Universidad Complutense, 340 p.

Opdyke, N., Mein, P., Lindsay, E., Pérez-González, A., Moissenet, E., and Norton, V. L., 1997, Continental deposits, magnetostratigraphy and vertebrate paleontology, late Neogene of Eastern Spain: Palaeogeography, Palaeoclimatology, Palaeoecology, v. 133, p. 129-148.

Opdyke, N., Mein, P., Moissenet, E., Pérez-González, A., Lindsay, E., and Petko, M., 1990, The magnetic stratigraphy of the late Miocene sediments of the Cabriel Basin, Spain, *in* Lindsay, E., Fahlbusch, V., and Mein, P., eds., European Neogene Mammal Chronology: New York, Plenum Press, p. 507-514.

Pickford, M., and Pourabrishami, Z., 2013, Deciphering Dinotheriensande deinotheriid diversity: Palaeobiodiversity and Palaeoenvironments.

Pierson D'Autrey, L., 1987, Sédimentation et structuration synsédimentaire dans le bassin néogène d'Alcoy (Cordillères Bétiques externes Orientales Espagne): Université de Paris, 315 p.

Santafé, J. V., 1978, Rinocerótidos fósiles de EspañaPh.D. Dissertation]: Universidad de Barcelona, 488 p.

SUPPLEMENTARY DATA 1.

Referred material from the localities of Venta del Moro, Crevillente-2, and Alcoy-Mina included in the present study. The collection from Venta del Moro is stored in the Museo de Geología de la Universitat de València (MGUV) and the Museo Nacional de Ciencias Naturales – CSIC (MNCN).

Unpublished remains:

Venta del Moro: i2, MGUV-11304; P2, MGUV-11305; Dx, MGUV-11306; left fragmentary humerus, MGUV-11295; left humeral trochlea, MGUV-15973; radius, MGUV-w/n; left ulna, MGUV-14522; right scaphoid, MGUV-18524; lunate, MGUV-18523; trapezoid, MGUV-18521; Mc II, MGUV-w/n; Mc III, MGUV-18827; Mc IV, MGUV-18522; second lateral phalanx, MGUV-12817; tibiae MGUV-11293; astragali, MGUV-7050; MGUV-11229; calcanei, MGUV-11298; navicular MGUV-11289; ectocuneiform MGUV-11233; Mt II MGUV 11290; Mt III, MGUV-11291; Mt IV, MGUV-11294; first lateral phalanx, MGUV-11232; first central phalanx, MGUV-11231; third central phalanx, MGUV-11230. The remains include an anterior right autopodium and a posterior left autopodium; MNCN-11870, cuboid; MNCN-11872, fragmentary pyramidal; MNCN-11871, ectocuneiform; MNCN-11874 pyramidal; MNCN-11875, unciform; MNCN-11868, fragmentary diaphysis of a tibia; MNCN-11869, distal epiphysis of a lateral metapodial.

Re-described material:

Venta del Moro: MNCN-10977, mandible with both horizontal rami, right p3-m3 and left p4-m3; cuboid, MNCN w/n; ectocuneiform, MNCN w/n. The mandible was originally described in Morales (1984), being reviewed in Cerdeño (1989). The other two fossils have been cited and used for comparison in Cerdeño (1989).

Crevillente-2: The remains from Crevillente were originally studied by Montoya in this Master Thesis (Montoya, 1994) and posteriorly published in Montoya and Alberdi (1995) and cited in Cerdeño (1989). The list of remains is as follows: CR2-405, CR2-854: two upper incomplete deciduals; MHMN CR2-95-S, CR2-150: Right series P2-P3; MGUV CR2-216, CR2-408: Left series P3-P4; MGUV CR2-217: P2 fragment; MHMN CR2-M306: Right P3; MHMN CR2-M262: Right P4; MGUV CR2-245: Right P4; MHMN CR2-M286: Left P4 fragment; MGUV CR2-140: P4 fragment; MGUV CR2-185-397: M1 fragment; MPV CR2-M237: Right M2; MHMN CR2-S-106: Right M3; MHMN CR2-M261: Left M3; MGUV CR2-135: M3 fragment; MHMN CR2-S-346, CR2-S-349, CR2-S-348, CR2-S-353, CR2-S-359: Left series P2-M1 and M3; MHMN CR2-S-347, CR2-S-285: Right p3-p4; MHMN CR2-M260, CR2-M415: Right p3-p4; MHMN CR2-M2: Right incomplete Mc III; MHMN CR2-M1: Right Mc IV; MHMN CR2-140-S: Right navicular; MGUV CR15-30: Incomplete right M1; MGUV CR15-59: Mx fragment; MGUV CR15-1-S: First central phalanx; MGUV CR15-86: lateral phalanx.

Alcoy-Mina: The remains from Alcoy-Mina were described in detail in Montoya et al. (2006). The list of remains is as follows: MAA w/n, right P3; MAA w/n, left m2; 2118M, left lower molar; Alc 24, right p3; Alc 25, left p4; Alc 26, right m1; Alc 27, left m1; Alc 28, right m3; Alc 29, fragment of left m3.

LITERATURE CITED

Cerdeño, E., 1989, Revisión de la sistemática de los rinocerontes del Neógeno de EspañaPh.D. Dissertation]: Universidad Complutense de Madrid, 429 p.

Montoya, P., 1994, Los macromamíferos del Mioceno superior del área de Crevillente (Alicante) [Tesis doctoral: Universitat de València, 421 p.

Montoya, P., and Alberdi, M. T., 1995, Crevillente 15 y Crevillente 16, dos nuevos yacimientos con macromamíferos en el Mioceno superior de Alicante (España): Estudios Geológicos, v. 51, p. 159-182.

Montoya, P., Ginsburg, L., Alberdi, M. T., Van der Made, J., Morales, J., and Soria, M. D., 2006, Fossil large mammals from the early Pliocene locality of Alcoy (Spain) and their importance in biostratigraphy: Geodiversitas, v. 28, no. 1, p. 137-173.

Morales, J., 1984, Venta del Moro: su macrofauna de mamíferos y biostratigrafía continental del Mioceno terminal mediterráneo: Editorial de la Universidad Complutense, 340 p.

SUPPLEMENTARY DATA 2

TABLE S1. Measurements (mm) of the mandible (Table S1), upper (Table S2) and lower (Table S3) dentition of *Dihoplus schleiermacheri* from Venta del Moro and Crevillente-2 (Valencia and Alicante Provinces respectively, Spain).

Table S1	MNCN-w/n	
Mandible	l	r
L	—	—
DAPdia	—	—
HP1	—	—
HP2	—	—
HP3	—	—
HP4	—	—
HM1	—	—
HM2	—	—
HM3a	—	—
HM3p	—	—
DAPdent	—	—
Lcor	—	—
Lart	—	—
Hcor	—	—
Hart	—	—
DAPhr	—	—
DAPproc	—	—
DAPcor	—	—
DAPart	—	—
DTia	—	
DTip	—	
Lsin	—	
DTpx	—	
DTm3p	—	
DTcor-cor	—	
DTart-art	—	
DTart	—	—

Table S2					
Upper teeth		l	r	l	r
(D)P1	L				
	W				
	H				
P2	L				
	W				
	H				
P3	L				
	W				
	H				
DP4	L				
	W				
	H				
M1	L				
	W				
	H				
M2	L				
	W				
	H				

Table S3		MNCN-w/n			
Lower teeth		l	r	l	r
p1	L				
	W				
	H				
p2	L				
	W				
	H				
p3	L	39.0	36.0		
	W	28.6	26.3		
	H				
p4	L	42.8	39.0		
	W	30.5	29.3		
	H				
m1	L	45.6	42.0		
	W	32.0	31.8		
	H				
m2	L	47.5	46.0		
	W	29.0	33.0		
	H				
m3	L		47.0		
	W		29.8		
	H				

SUPPLEMENTARY DATA 2 (CONT.)

TABLE S1. Measurements (mm) of the postcranial bones of *Dihoplus schleiermacheri* from Venta del Moro (Valencia Province, Spain) including the humerus (Table S4), ulna (Table S5), tibia (Table S6), scaphoid (Table S7), semilunate (Table S8), trapezoid (Table S9), astragalus (Table S10), navicular (Table S11) and ectocuneiform (Table S12)

Table S4				prox. epi.		dia.			dis. epi.					
Humerus	L	Lprox	TDtub-delt	TD	APD	TD-min	APD	Ldist	TD	TD-art	R1	Rmin	R2	APD
MGUV-11295 (r)	—	—	—	—	—	—	—	—	—	—	—	—	—	—
MGUV-15973 (r)	—	—	—	—	—	—	—	—	—	—	—	—	—	—

Table S5		olecranon							TDart		APDart		dia.		dis. art.		dis. epi.	
Ulna	L	TD	APD	H	TDbase	APDbase	APDart1	DAP artinf	prox1	dist	med	lat	TD	APD	TD	APD	TD	APD
MGUV-14522 (r)	—	—	—	—	—	—	—	—	—	—	—	—	—	—	—	—	—	—

Table S6			prox. dia.		dis.. art.		dia.		dis. epi.	
Tibia	L	Lfib	TD	APD	TD	APD	TD	APD	TD	APD
MGUV-11293 (l)	—	—	—	—	—	—	—	—	—	—

Table S7				prox. art.		dis. art.				
Scaphoid	TD	APD	H	TD	APD	APD-fMa	APDfTz	APDfTr	TD	APD
MGUV-18524 (r)	~ 51	~ 100	64,0	~ 41	~ 54	—	—	—	~ 27	~ 72

Table S8							
Semilunate	TD-prox	TDdist	TDpal	DAP	H	APD fUn	Hart
MGUV-18523 (r)	48.2	—	—	72.9	56.5	—	47.7

Table S9				
Trapezoid	TD	APD	H	Hmin.
MGUV-18521 (r)	—	47.5	39.3	23.8

Table S10					art surface						art. dis.		
Astragalus	DT	H	DTmd	DLinf	H1	Hmin	H2	L1	L2	DL	DT	APD	APD int
MGUV-7050 (r)	—	—	—	—	—	—	—	—	—	—	—	—	—
MGUV-11229 (l)	—	—	—	—	—	—	—	—	—	—	—	—	—

Table S11					art. prox.	
Navicular	APD	TD	H	Hmin	TD	APD
MGUV-11289 (l)	—	—	—	—	—	—

Table S12	art. prox.			
Ectocuneiform	TD	APD	H	Hmin
MGUV-11233 (r)	—	—	—	—

SUPPLEMENTARY DATA 2 (CONT.)

TABLE S1. Measurements (mm) of the metapodials of *Dihoplus schleiermacheri* from Venta del Moro (Valencia Province, Spain). These include the Mc II (Table S13), Mc III (Table S14), Mc IV (Table S15), Mt II (Table S16), Mt III (Table S17) and Mt IV (Table S18).

Table S13		prox. epi.		prox. art.		dia.			dis. art.	
Mc II	L	TD	APD	TD	APD	TD	APD	TDmd	TD	APD
MGUV-w/n (r)	—	—	—	—	—	—	—	—	—	—

Table S14		prox. epi.		prox. art.			dia.			dis. art.	
Mc III	L	TD	APD	TD	APD	HfUn	TD	APD	TDmd	TD	APD
MGUV-18827 (r)	203.0	65.0	~ 49	46.0	~ 49	—	62.9	~ 18	74.0	51.6	32.5

Table S15		prox. epi.		prox. art.		dia.			dis. art.	
Mc IV	L	TD	APD	TD	APD	TD	APD	TDmd	TD	APD
MGUV-18522 (r)	—	—	—	—	—	—	—	—	—	—

Table S16		prox. epi.		prox. art.		dia.			dis. art.	
Mt II	L	TD	APD	TD	APD	TD	APD	TDmd	TD	APD
MGUV-11290 (l)	160.0	33.6	43.2	26.1	36.4	26.5	36.5	43.8	38.2	39.5

Table S17		prox. epi.		prox. art.		dia.			dis. art.	
Mt III	L	TD	APD	TD	APD	TD	APD	TDmd	TD	APD
MGUV-11291 (l)	—	—	—	—	—	—	—	—	—	—

Table S18		prox. epi.		prox. art.		dia.			dis. art.	
Mt IV	L	TD	APD	TD	APD	TD	APD	TDmd	TD	APD
MGUV-w/n (l)	—	—	—	—	—	—	—	—	—	—

Appendix: Rhinocerotidae Craniodental Morphology

INTRODUCTION

Fossil record of vertebrates typically consists of skeletal remains. Unfortunately, a variable amount of information is missing in fossil species. In order to make accurate descriptions and reliable comparisons, paleontologists require a consistent background of living species' anatomy. Therefore, living species are regularly used as analogues for the structures observed in fossil ones. This is expected to be particularly effective when both species (the model and the fossil one) are close phylogenetically and has several advantages: large samples of living taxa are stored in many vertebrate collections, vertebrate remains from extant animals are usually better preserved, and osteological features in living species can be traced back to the soft-tissue interacting with it. However, living rhinos attain large dimensions and, in contrast to horses, are highly-threatened animals (which difficults the access to specimens for dissections and their manipulation). Therefore, and in contrast to the horse, no monographic works of overall rhinoceros osteology have been published, not even for veterinary purposes. It is not surprising that the few attempts to describe it in a comprehensive way are related to Paleontological studies. In the exceptional "The extinct rhinoceroses", made by Osborn (1898), the author encompasses contemporary findings from an evolutionary view, including comparisons between certain traits like the skull or the dental patterns. The vast rhino fossil remains found in several quarries during the last decades of the XIX century in North America favored the publication of several works describing the osteology of newly discovered species (e.g. Peterson, 1920). All these publications largely relied on their own observations on comparative anatomy. In the second half of the XX century, several examples describing the muscular insertions and articular facets of particular fossil species were eventually published (Borsuk-Bialynicka, 1973; Cerdeño, 1982; Prothero, 2005). This Chapter is devoted to the overall description of the cranio-dental and vertebral anatomy in Rhinocerotidae. It is designed as a complement to the appendicular descriptions Figured in Chapter 4 (postcranial skeleton of *H. matritense*).

MATERIAL AND METHODS

Homologous muscular and tendinous insertions represented in this chapter have been recognized from the scarce rhino literature (Borsuk-Bialynicka, 1973; Goldfinger, 2004; Prothero, 2005). Soft-tissue nomenclature is taken from the Nomina Anatomica Veterinaria (-, 2005) as well as horse anatomical works (Budras et al., 2009; Goldfinger, 2004; Schaller, 2007). Figures of the dentition have been modified from Osborn's 1898 monography (Osborn, 1898). Figures of the skull pertain to the fossil species *Aceratherium incisivum* (Kaup, 1932) taking advantage of Hünnerman's (1989) richly illustrated monography. The completely known osteology of *A. incisivum* and mediportal proportions poses it as a useful generic model. Figures of the species *Stephanorhinus etruscus* and *Menoceras arikarense* obtained from Peterson (1920) and Loose (1975) have been used as well.

CRANIODENTAL MORPHOLOGY OF RHINOCEROTIDAE

Skull (Figs. 2-3)

If compared to extant tapirs or horses, living rhinoceros species show stout skulls, reduced premaxillary bones, a relatively enlarged postorbital part and a flat to concave skull roof. 24 bones compose the rhinoceros skull, these are: two maxilla, two ethmoids, two nasals, two lachrymals, two palatines, two parietals, two temporals, two zygomatics, two jugals, one vomer, one frontal, one palatine, one occipital, one ethmoid and one sphenoid.

To sketch an overall view of the cranial morphology in the Family Rhinocerotidae, an introductory analysis using geometric morphometrics and a wide skull sample has been performed (Figure 1; Supplementary Data 1). Primitive genera (e.g. *Hyracodon*) have a relatively short nasal, enlarged lachrymal region and a straight upper skull profile. Some species (e.g. *Trigonias*) have a relatively shorter nasal, larger tooth row and a forward oriented occiput, whereas others like *Iranotherium* have a relatively longer muzzle and a backward oriented occiput. Skull morphology in some Rhinocerotina species as *Ceratotherium simum* or *Coelodonta antiquitatis* shows a certain degree of convergence with that of the Subtribe Elasmotheriina, related to similar trophic requirements and horn development.

One of the most characteristic traits of the rhinoceros anatomy is the horn. Nearly all extant rhinoceros species develop horns when adults (except for some females of the Javan rhinoceros, *Rhinoceros sondaicus*). Rhino horns are conical epithelial structure made of hair-like filaments sur-

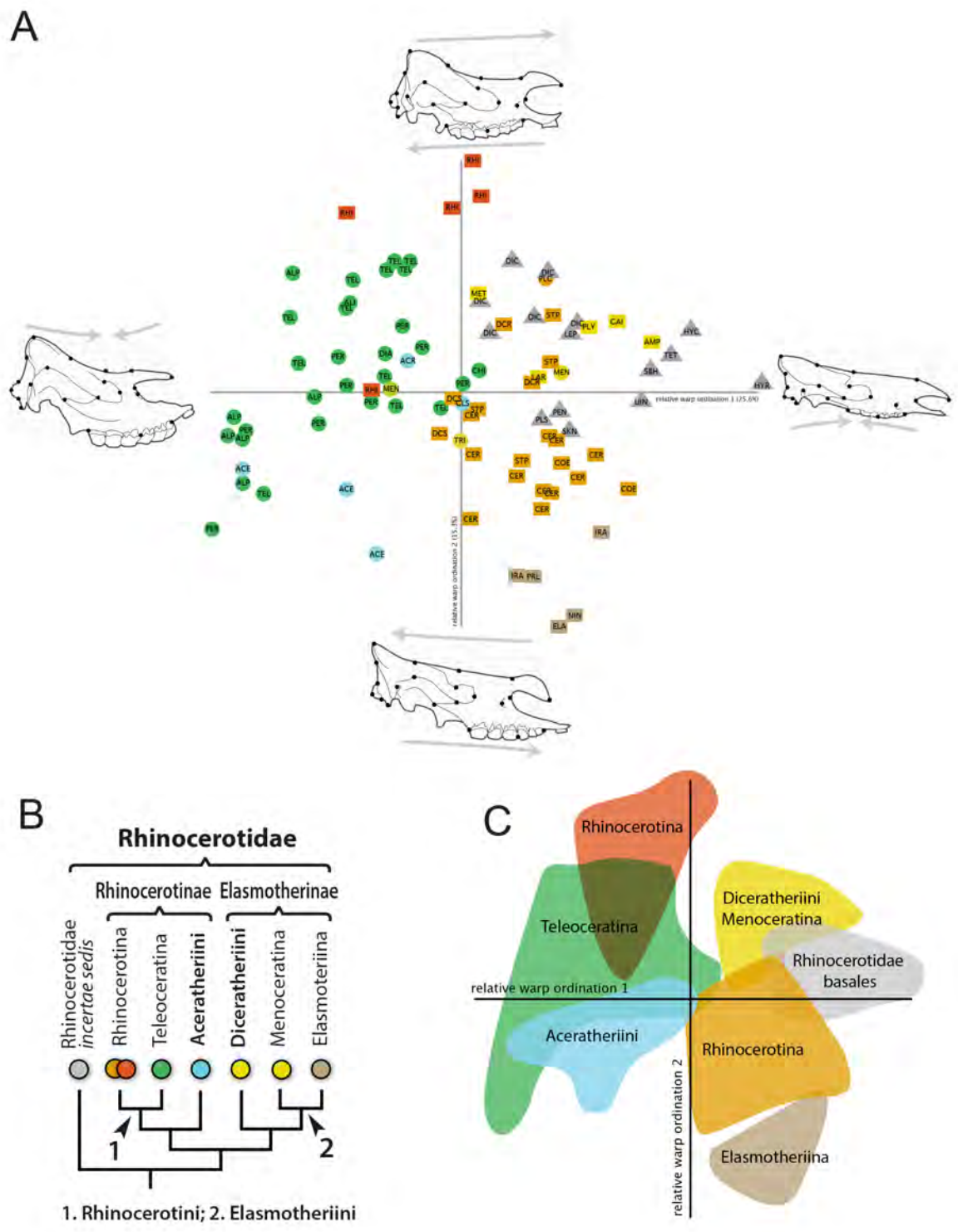


Fig. 1 A, scatter plot of relative warps 1 and 2 for shape changes in the skulls of 38 rhinoceros genera. The schematic drawings show morphological standards at the extreme of each axis (with deformations arbitrary magnied). Relative warps 1 and 2 summarizes 25.6% and 15.3%, respectively, of sample variation of the analysis. Colours represent the phylogenetic groups of gure 3.2. ACE, Aceratherium; ACR, Acerorhinus; ALI, Alicornops; AMP, Amphicaenopus; ALP, Alphelops; BRA, Brachypotherium; CER, Ceratotherium; CHI, Chilotherium; COE, Coelodonta; DIA, Diaceratherium; DIC, Diceratherium; DIS, Diceros; DCR, Dicerorhinus; ELA, Elasmotherium; GAI, Gaindatherium; GLS, Galushaceras; HIS, Hispanotherium; HYR, Hyrachyus; IRA, Iranotherium; LAR, Lartetotherium; LEP, Leptaceratherium; MEN, Menoceras; NIN, Ningxiatherium; PAR, Paraceratherium; PER, Peraceras; PEN, Penetrigonias; PLX, Pleuroceros; RHI, Rhinoceros; RAD, Radinskyia; SHA, Shanshirhinus; STP, Stephanorhinus; TET, Teletaceras; TEL, Teleoceras; TRI, Trigonias; SBH, Subhyracodon; UIN, Uintaceras.B, phylogenetic relationships among suprageneric groups in the family Rhinocerotidae (obtained from Antoine, 2002). Subfamily Rhinocerotinae include the subtribes Aceratheriini and Rhinocerotini. The later are divided in Rhinocerotina (rhinoceros with one or two nasal horns) and Teleoceratina (short-limbed robust rhinoceros with or without horn) in turn. On the other hand, the subfamily Elasmotheriinae are divided in Diceratheriini and Elasmotheriini. Elasmotheriini are splitted in Menoceratina, a mainly north-American basal group, and Elasmotheriina, a specialized group of hypsodont running rhinoceros. Hornless rhinoceros from Teleoceratina and Aceratheriini groups ll a specialized area of the morphospace characterized by morphologies with short muzzle, concave skull prole and elongated and convex tooth row. C, same scatter plot as A with the main suprageneric groups outlined. See Supplementary Data 1.

rounded by a keratinized and mineralized matrix. Each horn is attached to the nasal bone through extrinsic fibers from the reticular dermis (Hieronymus and Witmer, 2004). The partial mineralization of these fibers confers an irregular appearance to the attachment bony area. The fossil record shows a wide array of possibilities in number, size and placement, including many hornless species, as many basal genera and most Aceratherini. Within Rhinocerotina, two types of medial horn are considered depending on the bone where attached: the nasal and the frontal horns. The medial nasal horn is placed in the nasal bone. The extension of the nasal insertion is highly variable. Most Rhinocerotina species have domed nasal bones with wide rough areas, sometimes described as having a 'cauliflower' texture. The medial frontal horn of Rhinocerotina is attached to a slightly domed, rough area of the frontal bone over the orbits. Teleoceratine rhinoceros and the aceratherini *Aliconops* show a small wrinkled area (typically double), tandem-placed and slightly laterally-oriented on the distal end of their nasal tips. This is one of the multiple nasal horn morphologies restricted to the fossil record with no living representatives. The same occurs with other singular configurations as paired bumpy structures in the nasal bone recorded in the males of the genera *Menoceras* and *Diceratherium*. The males of *Diceratherium* present parallel ridges along the nasal bones whereas in *Menoceras* there are two blunt and rounded insertions. The basal Elasmotheriina are hornless, whereas the remaining species show two main morphologies: a single medial nasal horn (i.e. *Huaqingtherium*, *Victoriaceros*, *Iranotherium*, *Parelasmotherium* and *Ningxiatherium*) and a massive bony dome that served as attachment for a huge medial frontal horn in other like *Sinotherium* or *Elasmotherium*. Such massive frontal horn attachment may have originated as a fusion of a retracted nasal horn with the frontal one (Deng et al., 2013).

Apart from all the disparity observed among rhino horns, it is obvious that horns are functional structures with a major role in the cranial architecture. Here is a detailed list of horn functions cited in the literature:

Intraspecific competition. Males of African rhinos use their horns in intraspecific combat (Fortelius, 1983). The presence of tandem-placed paired structures in the males of genera like *Diceratherium* or*Menoceras* could be also related to male to male horn fights. Intraspecific interaction could lead some species to ritualized horn combats, preventing wounds and establishing easily recognizable dominance hierarchies (Fortelius, 1983). This situation has been hypothesized for *C. antiquitatis* which developed huge nasal horns (in addition to foraging facilitation; Fortelius, 1983). Another intraspecific role for the horns is that proposed for *Elasmotherium sibiricum*, which its nasal horn could be used as sexual display in addition to foraging facilitation (Mazza and Azzaroli, 1993).

Aggression against outsiders. Two possible mechanisms have been cited in defensive interaction in extant rhino species:horns and second tusk-like lower incisors. Horns are used regarding territorial conflicts and against their potential predators. For example, the females of African species charge against predators with their horns to protect young calves (Fortelius, 1983).

Displacement. The horn can be used as a wedge, thus facilitating the displacementthrough dense forested areas. This functionlead the horn to a considerable wear while clearing obstacles,asobserved in the extant Javan rhinoceros(Hoogerwerf, 1970).

Feeding. The flattened horns of Plio-Pleistocene rhinocerotines have been proposed to been used for digging and uncovering the forage as many extant ungulates do, especially those living in cold biomes (Fortelius, 1983; Mazza and Azzaroli, 1993).

A substantial proportion of fossil species have neither nasal nor frontal horns. Instead of the wide and well-developed nasal bones of the nasal-horned species, hornless ones use to bear slender and pointed nasal bones variable in length with a flattened dorsal surface. In these species, the lateral borders of the nasal bones can present two lateral apophysis on the lateral nasal borders (Antoine, 2002). These small protuberances are a plesiomorphic character also present in other Ceratomorpha, but no function has been cited.

The nasal septum is a bony wall in the middle of the nasal cavities. The maximum development of the septum causes the total closure of the nasal notch. The ossification of the nasal septum has appeared independently in Elasmotheriina and Rhinocerotina, being frequent in species of medium and high latitudes of the Plio-Pleistocene. Moreover, nasal septum ossification depends on the ontogeny: *C. antiquitatis* shows an ossification increase from the young condition, which is partially ossified, to the complete closure of the nasal notch in adults. Extant species are usually considered as lacking an ossified septum, and this is certainly the case of the white rhino (as observable in the CT-scanning of Kethla, a 42-year old white rhino; www.digimorph.com). In contrast, the skull AMNH 54763, a Sumatran rhino (*D. sumatrensis*) from Burma stored in the AMNH, show a small portion of the nasal septum fully ossified attached to the distal surface of the nasal bone. Curiously, an ossified nasal septum has been reported in the Javan rhino (Fraser, 1875), the living species with a feebler developed horn boss. Therefore, a stronger septum despite the horn development among Asian species may point to a different skull structure respect to the African ones. It is considered as a parallelism favored by mechanical constraints. The presence of nasal septum seems to be related with the extension of the horn insertion (Thenius, 1955).The insertion area is directly related with the horn size. A big, heavy horn produces a vertical strain towards the nasal bone that can be dispersed through the nasal septum. In contrast, Mazza and Azzaroli (1993) proposed that the septum is not related with the weight of the horn but influenced by a frequent and intense habit of lateral horn sweeping in Plio-Pleistocene species.

The premaxillary bones protrude anteriorly from the maxillary bone, sometimes contacting at their tip. The space left between them is called incisive foramina (Syn: palatal fissure).

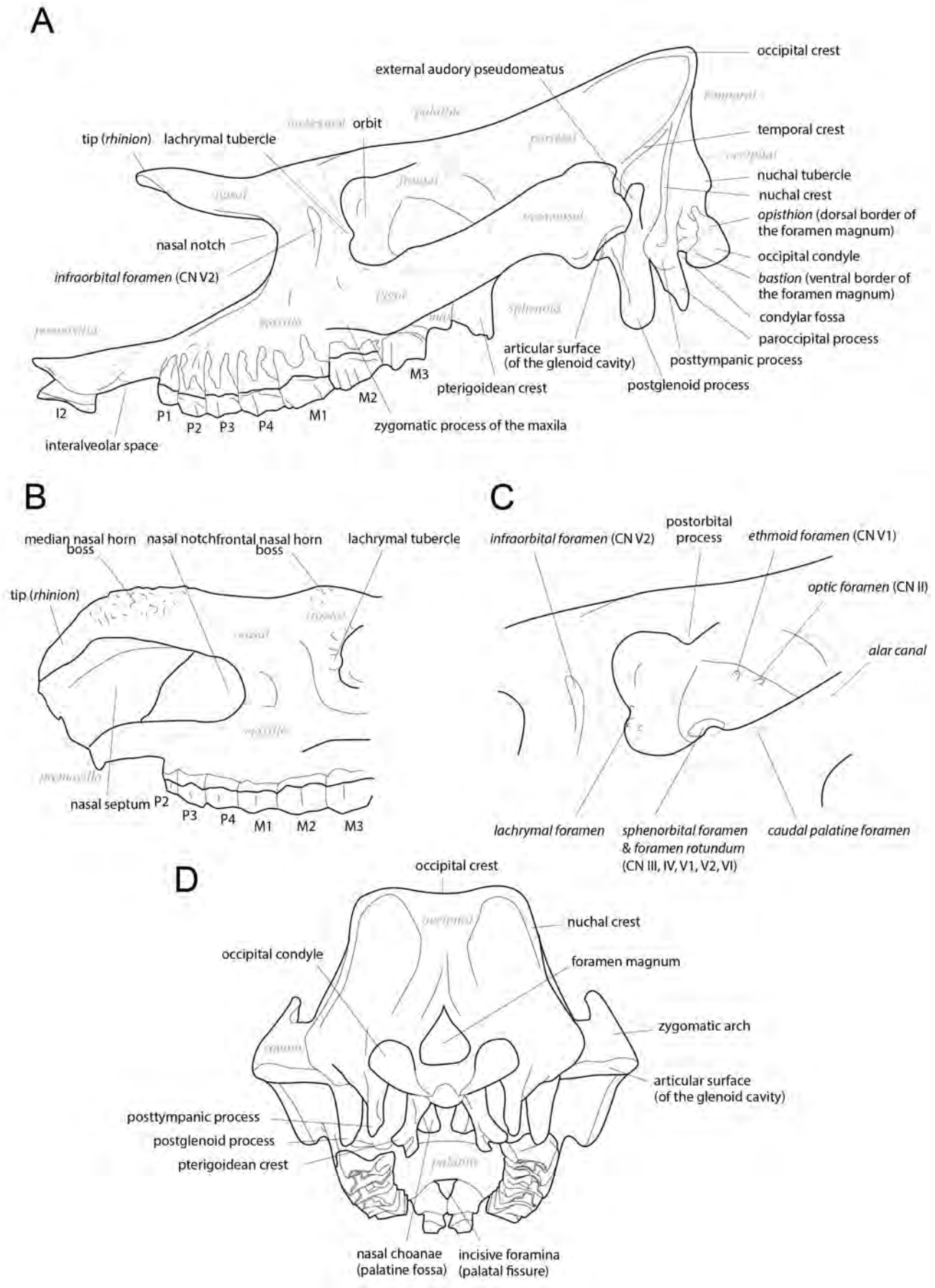


Fig. 2 Rhinocerotidae skull morphology. A, skull of A*ceratherium incisivum* in A and C, left lateral and D, caudal views. B, left lateral view of *Stephanorhinus etruscus*. Figures redrawn from Hünermann (1989) and Loose (1975).

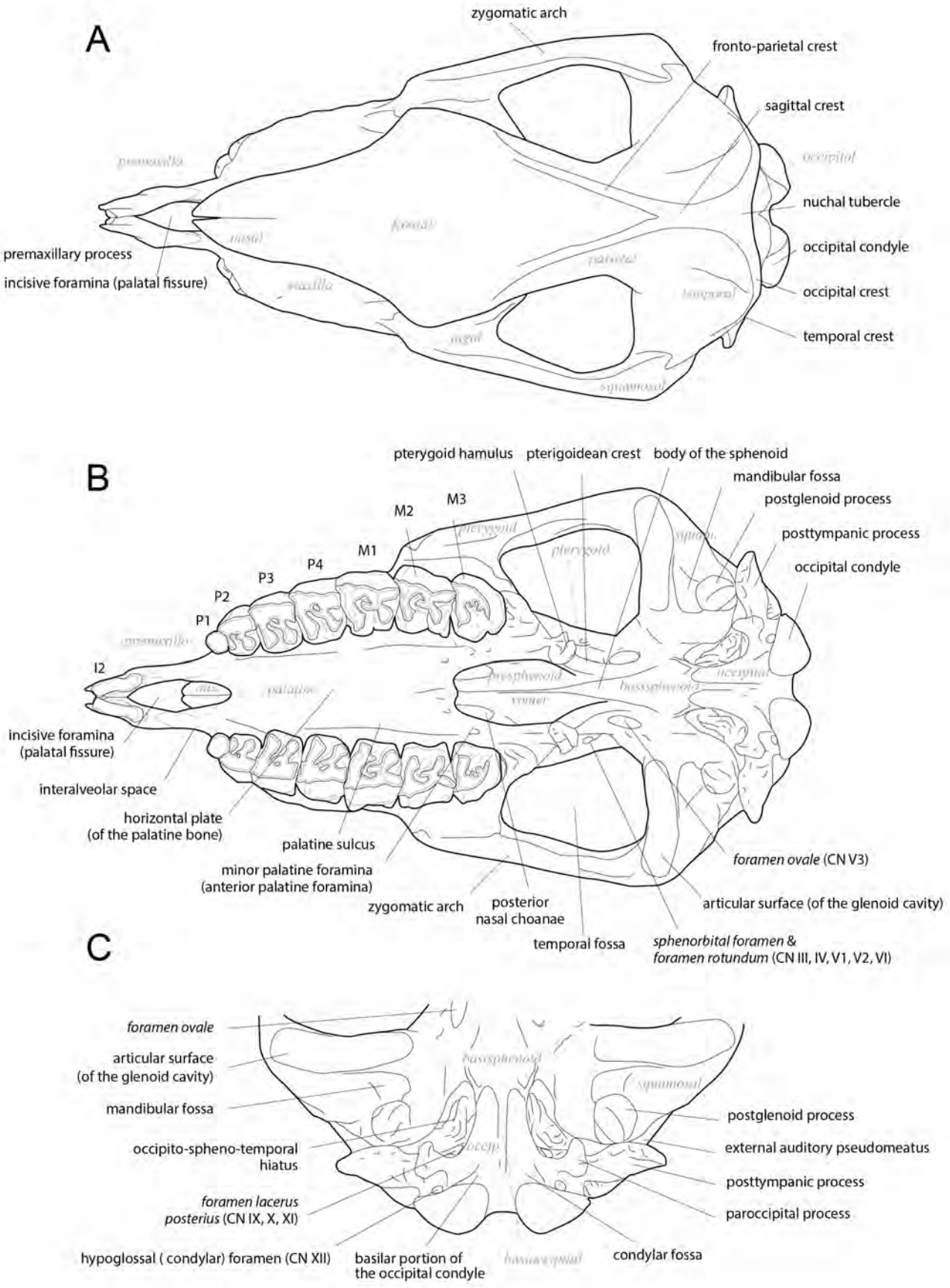


Fig. 3 Rhinocerotidae skull morphology. Skull of A*ceratherium incisivum* in A, dorsal and B-C, ventral views. Figures redrawn from Hünermann (1989).

The premaxillary bones house the alveoli for the upper incisors. The suture between premaxilla and maxilla is weak, and the premaxilla are lost in most in fossil specimens. The premaxillary reduction is coupled with the loss of upper anterior dentition observed through the family (Heissig, 1989). Some aceratheriine genera with huge tusk-like lower incisors present a premaxilla reduced to two tiny plates. In some Rhinocerotina (i.e. *Ceratotherium*), the premaxillary bone is highly reduced. The infraorbital foramen is placed in the maxillary bone, anterior to the orbital cavity. Primitive species have a posteriorly placed foramen whereas teleoceratine rhinoceros have an infraorbital foramen placed in the lateral walls of the nasal incision. It houses the passage for the infraorbital artery, infraorbital vein and the CN V_2 maxilar ramification of the trigeminal nerve, which enervates the rostral area. The rostrum is the place of insertion of most muscles of the facial expression, being some of them important to outline the muzzle morphology when reconstructing soft tissues of extinct species. Their reconstruction is usually based on compared anatomy with extant representatives, as these muscles do not use to leave any appreciable bony print.

The orbit is enclosed by the lachrymal and frontal bones. This cavity is rounded to oval, and is often surrounded by several irregular processes, more developed in the anterior and dorsal borders. In some species the entire orbit rim is laterally telescoped, a trait possibly linked with the development of the frontal horn insertion. The most anterior bony protuberance is the lachrymal process. It is a rough tubercle, simple or double, in the anterior border of the orbit. On the postero-dorsal side of the orbit, the frontal bone develops a triangular protuberance, the processus postorbitalis. This process, together with the processus postorbitalis of the zygomatic arch, is the point of insertion of the orbital ligament which encloses the rear part of the orbit. This closure is totally made of soft tissue, as all the Rhinocerotidae lack a postorbital bar. The processus postorbitalis of the frontal bone is absent in *C. antiquitatis* and the African extant rhinocerotines. Both advanced rhinocerotine and elasmotheriine species have backward placed orbits, being located behind the first upper molar (Antoine, 2002).

The zygomatic arch is formed by the jugal and the squamosal bones. Its anterior border can be directly placed over the tooth row or rose over it. A small processus postorbitalis can appear on the dorsal surface of one of these bones. The males of *Iranotherium morgani* show a hypertrophied hemispherical area on the top of each zygomatic arch. These may reflect the presence of callused structures for mating combat, display or an enlarged insertion area for the masseteric and temporal muscles (Deng, 2005). In ventral view, the posterior end of the zygomatic arch has the articular surface of the glenoid cavity (synonym: articular tubercle; Van der Made, 2010), a wide oval articulation for the mandible. On its posterior side, attached to the anterior surface of the postglenoid process, there is a smaller concavity, the mandibular fossa. The foramen sphenorbitale and the foramen rotundum of the sphenoid are fused in Rhinocerotidae in a single sphenorbital foramen placed behind the orbit and covered by the zygomatic arch.

The dorsal profile of the skull is defined by the frontal and parietal bones. Its shape can be flat to strongly concave. The fronto-parietal crests depart backwards as a ridge from the orbits, fusing with the nuchal crests in the posterior-most border. In some species, the fronto-parietal crests are fused, resulting into a single sagittal crest. This has been mentioned as a sexually dimorphic character in the genera *Hispanotherium* and *Menoceras*, with the males presenting a unique sagittal crest and the females two separated fronto-parietal crests. The temporal bone displays two converging crests, called temporal and nuchal crest. Between them there is a triangular space that can be flat to concave and has a wide groove for the external auditory pseudomeatus on its lower part. This groove can be totally closed by the postglenoid and posttympanic apophyses, leaving a closed gutter with an elevated opening: an auditory meatus (synonym: acoustic meatus; Van der Made, 2010).

Differences in the orientation of the nuchal area in the Family Rhinocerotidae were detected as early as the first studies in comparative anatomy (Cuvier, 1834). This orientation can describe the feeding habits when it deviates in both directions from the right angle formed between the occipital area and the tooth row (Heissig, 1989), enclosing important adaptations in the head articulation and the masticatory functions (Bales, 1996). The grazing white rhino (*C. simum*) has a very inclined backwards occipital side, translating into a greater posterior pull of the temporary muscle and a restricted rotational upward movement of the head. A lower position of the head during foraging permits the posterior part of the temporary muscle to act as an almost vertical vector, whereas the masseter one performs a strongly-biased horizontal force. On the other hand, the slightly forward-inclined occiput of the Indian rhino (*R. unicornis*) permits a wider rotational angle of the head and shorter posterior temporary muscle fibers. A plausible raised head during foraging in *R. unicornis*, with the muzzle over the orbits, produces a clear vertical component of the masseter muscle, while the posterior temporary muscle vector is similar to that of *C. simum*. The black rhino (*D. bicornis*), a browser species closely related to *C. simum*, has an intermediate orientation between *C. simum* and *R. unicornis*.

The horizontal plate of the palate is interrupted by the choanae (or palatine fossa), the posterior nasal apertures to the nasopharynx. They are divided by the vomer bone and each one possesses a sphenopalatine foramen at the bottom. The pterigoidean crests are to ridges hanging from both sides of the sphenoid bone, running parallel to the body of the sphenoid. In some species, as *Lartetotherium sansaniense*, these crests are well developed and anteriorly extended. In the posterior end of each pterigoidean crest there is a big foramen ovale (synonym: oval incisure; Van der Made, 2010). In rhinoceros, the foramen ovale is sometimes fused with the *foramen lacerum anterius*, being separated by connective tissue in some extant species(Cave, 1959). The resulting channel houses the cranial nerves III, IV, V_1, V_2 and VI. Three pairs of apophyses are placed on the basicranium of the rhinoceros skull. The first

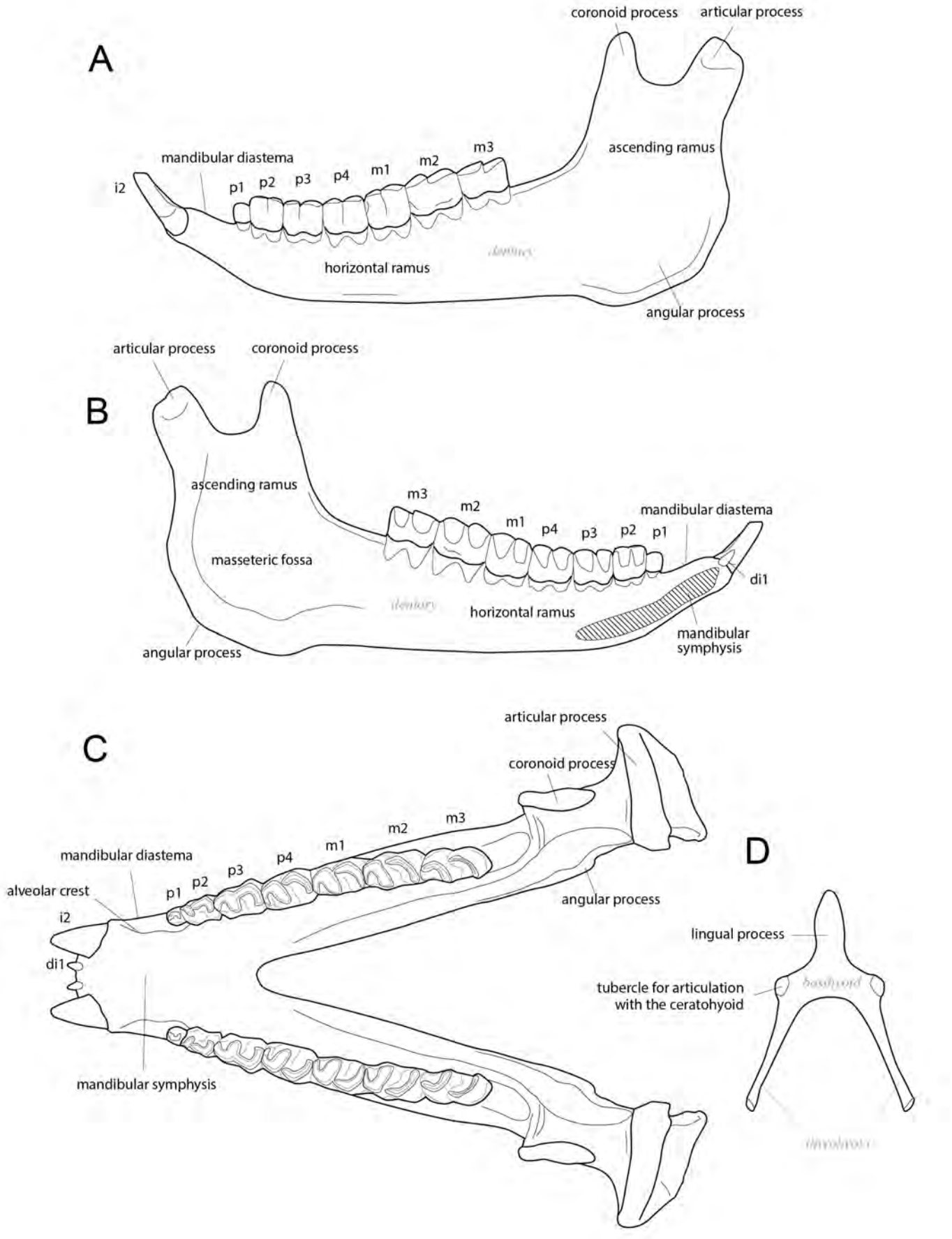


Fig. 4 morphology of the mandible and hyoid apparatus of Rhinocerotidae. A, left hemimandible of *Aceratherium incisivum* in left lateral view; B, same specimen in lateral right view; C, reconstructed hemimandibles in dorsal view; D, hyoid apparatus of *Lartetotherium* sp.

pair, called postglenoid processes (syn: retroarticular process; Van der Made, 2010), is placed behind the articular surfaces of the glenoid cavities for the mandible (syn.: articular tubercle; Van der Made, 2010).Each one is a blunt process, sometimes flattened and/or curved. The second apophyses are the post-tympanic processes (synonym: jugular process; Van der Made, 2010). They are a thick and small plates usually attached to third ones, the paroccipital processes, through their bases. The occipital bone articulates with the atlas through the occipital condyles. They are subtriangular articular facets surrounding the foramen magnum and surrounded by a shallow depression. On the both sides of the condylar area there are two small and rounded hypoglossal foramens for the XII cranial nerve (synonymies: condylar foramen).

Mandible (Fig. 4)

The mandible is composed by two symmetrical halves fused through their mandibular symphysis. Each hemimandible is formed from a single bone, the dentary. The coronoid process or ascending ramus is the place of insertion of the *m. masseter*. The articular process is a widened area that articulates the mandible with the articular facet of the glenoid cavity of the skull. The ventral notch for facial vessels (= *Incisura vasorum facialium*) separates the horizontal from the ascending rami and hosts the course of the A. facialis. This, in turn, irrigates the preorbital part of skull and mandible. The mandibular foramen (syn. foramen mentale Antoine, 2002) is placed in the ventral side of the ascending ramus, slightly closer to the cranial border. It hosts the inferior alveolar artery, the vein of the mandible, and the inferior alveolar nerve (which is a branch of the mandibular nerve). They continue rostrally following the horizontal ramus supplying innervations and irrigation for the lower jaw. Along the mandible, consecutive secondary vessels (*Rami dentales*) depart in parallel to the gingival region from the main artery (*A. mentalis*). The later, together with the rostral extent of the nerve exit from the mandible through the mental foramen up to the symphiseal region. The angular process hosts the insertion for the caudalmost extent of the *m. digastricus*.

Hyoid apparatus (Fig. 4)

The hyoid apparatus suspends the larynx from the base of the skull. It is divided into stylohyoid, connected to the base of the skull, ceratohyoid, which serves as mobile intermediate articulation, and thyrohyoid, attached to the rostral cornu of the thyroid cartilage. This bone is rarely present in fossil osteological collections, so little is known about its variation among rhinoceros. Among the described hyoid bones, some differences can be stressed. The hyoid from *Coelodonta antiquitatis* (van der Made, 2010) is .On the other hand, the hyoid of *Lartetotherium* sp. (this volume).

Dentition

Generalities

Rhinoceros dentition is typically composed by three premolars and three molars in both upper and lower series (P^1_1-P^4_4; M^1_1-M^3_3; p^1_1-p^4_4; m^1_1-m^3_3). Rhinoceros upper cheek teeth are generally square in occlusal view and have a characteristic 'π'-shaped configuration of lophs (except for the M3, which is typically triangular in most species because of the reduction of the metaloph). Lower cheek teeth are smaller, rectangular in occlusal view and have two adjacent, medially-oriented valleys, configuring a 'w'-shaped arrangement of lophs. The upper series form a continuous 'saw'-like ridge that overlaps with the zigzagging lower one.

From a histological point of view each tooth is divided into two main layers: a thick enamel outer wall and an inner dentine filling. The outer enamel layer can vary in thickness and shape, ranging from simple to extremely fold, as seen in some derived hypsodont species of the Subtribe Elasmotheriina. The enamel is a highly mineralized material, being the hardest mammalian tissue. This mechanical aspect is linked with the enamel microstructure. The enamel is formed by consecutive layers of enamel prisms made of organized hydroxyapatite cristallites. The different prism orientation of two adjacent enamel layers (usually about 90º in rhinoceros) or different symmetric arrangement produce an optical effect resulting in banded variations in light refraction. These bands, called Hunter-Schreger Bands (or HSB) are present in most large mammals, even though their disposition varies from one group to another. All rhinocerotids are characterized by bearing vertical HSB orientation in cheek teeth, a character shared with other rhinocerotoids as hyracodontids or amynodontids (Koenigswald et al., 2011). This orientation of the HSB is parallel to the occlusal plane, permitting to reduce the abrasion and thus increasing the teeth performance (Koenigswald et al., 2011)S. In rhinoceros teeth, HSB can be achieved at eyesight as light and dark bands along the enamel occlusal border. On the tooth walls, the enamel macroscopic appearance can attain different textures: wrinkled, ramified, corrugated and/or banded (or a combination of two or more types). The dentineis placed inside the enamel walls. Its bone-like matrix is full of dentinal tubules and odontoblasts. Due to alower mineralization, the dentine has a faster wear rate than the enamel, molding a concave surfaceand sharper occlusal edges. To confer an additional resistance to the enamel, some species can present cementum, a hard material that can be found on the median valley, filling the enamel foldings and coating the ectoloph wall.

From a morphologic point of view, rhinoceros teeth can be divided into brachyodont and hypsodont. Brachyodont teeth have lower crowns, absent or thin-layered cementum and smooth and thin enamel whereas hypsodont species have higher teeth crowns, thick cement and rough, thick enamel (Fortelius, 1982). Whereas basal rhinos are basically brachyodont, derived species of teleoceratines, aceratheriines, rhi-

nocerotines and, specially, elasmotheriines, show hypsodont representatives. The elasmotheriine species of the genus *Elasmotherium* constitute a unique case among Perissodactyla. These species have developed euhypsodonty *sensu* Mones (1982), an extreme case of sidewall hypsodonty were teeth have open roots and continuous growing, a highly specialized adaptation towards a very abrasive diet more common in other mammals Families as rodents or cetartiodactyls.

Dental replacement is a valuable trait to estimate the ontogenetic stage of fossil mammals. In rhinoceros, these are defined by the presence and wear degree of some key teeth. Nevertheless, only the African species seem to have focused the attention (Anderson, 1966; Bigalke et al., 1950; Foster, 1965; Hitchins, 1970, 1978; Roth and Child, 1968a; Schenkel and Schenker-Hulliger, 1969). Neonate rhinoceros of *D. bicornis* (younger than 1.5 years) have only decidual upper teeth. Juvenile ones (1.5-4 years) have a combination of decidual and permanent teeth, but always retaining the DP4. The replacement of the upper DP4 by the permanent tooth characterizes the sub-adult stage (4-6 years). By this time, the M3 has started to erupt. Finally, the wear of the M3 is the distinguishing feature of the adult ontogenetic stage (≥ 6 years). The erupting dental sequence in *D. bicornis* follows the next sequence: DP1; DP2; DP3; DP4; M1; M2; P2; P3; P4; M3. The lower series has the next one: dp2, dp3; dp1, dp4; m1; m2; p4; p1; p2, p3; m3. It is significant that most of the anomalous teeth cited in the literature have been upper P4, the last upper teeth to appear (Garutt, 1994; Garutt, 1990, 1992; Groiss et al., 1981; Vialli, 1955). For that reason, upper P4 may suffer from critical pressures in the masticatory mechanics when the rest of the dental series is fitting together and strains are concentred in less occlusal surface. Several age categories have been proposed according to the teeth eruption, age, and relative size in *D. bicornis* (being summarized in (Tong, 2001). Neonate rhinos have only milk teeth in use (Foster, 1965), are less than 1.5 year old (Anderson, 1966; Foster, 1965; Roth and Child, 1968b), and have a size of less than 2/5 of the adult (Bigalke et al., 1950; Hitchins, 1970; Schenkel and Schenkel-Hulliger, 1969). Juvenile ones not only retain the DP4 but have a one or two molar teeth erupted. Their age spans between 1.5 and 4 years and show a size between 2/3 and 3/4 of the adult. Subadult category is defined by the fully erupted M3, but not into use. They are between 4 and 6 years old and show a relative size between 3/4 to the full adult size. From the 6 years on, adult individuals have the M3 coming into use and have reached its maximum size. An alternative ordination is the individual dental age stages (IDAS) proposed by Anders and colleagues (2011) for placental mammals. Their six categories include:

- IDAS 0: prenatal stage of tooth development, rare among fossil samples.
- IDAS 1: infant, from the birth to the unfinished eruption of the M1/m1 (not included).
- IDAS 2: juvenile, spans from the first facets on the M1/m1 to the full eruption of the M3/m3 and the replacement of the DP4/dp4 by the P4/p4.
- IDAS 3, adult, spans from the total eruption during the use of the complete set of dentition as long as all the molars' characters are still visible.
- IDAS 4, late adult, covers the period from the loss of the inner profile of the M1 to the loss of the profile in the M2 (not included).
- Finally, IDAS 5, senile, denotes the period from the loss of the inner profile of the M2 to the breakdown by wear and/or tooth loss.

These stages do not match exactly those previously represented. Both classifications mix events related with first wear facets of teeth and first teeth eruption. However, while Foster's classification focus on earlier stages, IDAS remains useful for distinguishing between adult ones.

Anterior dentition

There is a general reduction of the premaxilla and the anterior dentition in Rhinocerotidae (Prothero et al., 1986). Therefore, the upper anterior dentition has been repeatedly used in rhinoceros phylogenies (Antoine, 2002; Cerdeño, 1995; Fortelius and Heissig, 1989; Groves, 1983; Prothero et al., 1986). Basal-most genera have three upper incisors, a condition shared with most perissodactyl families. The upper I1 is usually well developed and chisel-like shaped. Last phylogenetic hypotheses points that the upper I1 has been lost independently in the two major lineages, Rhinocerotina and Elasmotheriina (Antoine, 2002).The upper I2 is small and peg-like shaped. Only some primitive genera retain it (e.g. *Ronzotherium*, *Trigonias, Diceratherium*). The upper I3 has a similar appearance than the I2. It is only present in the basal most genera (e.g. *Trigonias*). The same occurs with the upper canines, a plesiomorphic trait typical of primitive genera (e.g. *Trigonias*, *Diceratherium*).

The lower anterior dentition is more developed in primitive rhinoceros than the upper one. The lower i1 is small and rounded, being lost several times during the evolution of the group. The lower i2 is lost in derived species of both Elasmotheriina and Rhinocerotina. When present, it is always tusk-like, one of the diagnostic features of Rhinocerotidae. The i2 is often sexually dimorphic in size and shape, being the i2 of the males bigger and sharper. In some species, the i2 can attain large dimensions, modifying the mandibular symphisis. The presence of lower i3 and lower canine are very primitive traits, as only basal rhinoceros, like *Teletaceras radinsky* or *Trigonias taylori*, bear them. Contrariwise, other non-rhinocerotid perissodactyls as tapirs present well developed i1-3 and tusk-like canines (instead of the tusk-like i2 found in rhinos).

Cheek teeth

Rhinoceros upper cheek teeth are formed by four main cusps or cones and four secondary ones. Between the four main cusps three main lophs are distinguished, giving the tooth its characteristic 'π'-shape appearance, as represented in the Fig-

ure 2. The main cusps are the paracone, metacone, protocone and hypocone. The main cusps act as primary growth centers for the secondary enamel folding. The secondary cusps are the parastyle, metastyle, paraconule and metaconule. Finally, the trhee main lophs are named ectoloph, protoloph and metaloph. More information about each structure can be found in following section. Radinsky (1969) restricted the meaning of protoloph and metaloph to the crest between the secondary cusps (protoconule and metaconule respectively) and the labial primary ones (protocone and hypocone). In Rhinocerotidae, paraconule can be displaced to almost contact the protocone, thus limiting the protoloph (sensu Radinsky, 1969) to a very short section. In the present work, we consider protoloph as the major loph between paracone and protocone and metaloph as the major loph between metacone and hypocone following most studies on fossil rhinoceros species.

Teeth parts

Main characters for upper teeth have been described and divided in the following main categories: major cusps, major lophs, secondary enamel folding and fossetes. Characters included in each category have been alphabetically ordered and main features remarked in bold face. Both upper and lower teeth parts have been represented in the Figure 3. Most definitions are modified after Osborn (1888), but other authors have been also taken into consideration (Fukuchi, 2003; Groves, 1972; Lydekker, 1884).

Upper teeth (Fig. 5)

Major cusps

Hypocone: Major posterolingual cusp on an upper cheek tooth.It can be constricted by an anterior and/or posterior enamel grooves, named as anterior and posterior **hypocone folds**.

Metacone: Major posterolabial cusp on an upper cheek tooth.

Paracone: Major anterolabial cusp on an upper cheek tooth. It can present a labial expansion limited by the parastyle fold. Synonymies: *parastylfurche* (Peter, 2002); fold of the paracone (Van der Made, 2010).

Protocone: Major anterolingual cusp on an upper cheek tooth. It can be constricted by an anterior and/or posterior grooves, named as anterior and posterior **protocone folds**. Synonymies:*hintere* and *vordere protoconusfurche* (Peter, 2002); protoconal constriction (Van der Made, 2010).

Major lophs

Ectoloph: Major loph that joins paracone and metacone, covering most of the labial side of the teeth. It may be flat or undulated by three main ribs (parastyle, mesostyle and/or metastyle). Synonymies: outer wall (Lydekker, 1884). **Ectometaloph**: continuous loph formed by the connection between paracone, metacone and hypocone onthe M3 withabstent or poorly-developed parastyle.

Metaloph: Major loph resulting of the connection between metacone, metaconule and hypocone. Synonymies: median collis (Lydekker, 1884).In the upper P3, the hypocone can join the crista instead of the metacone. In this case, this sigmoidal narrow ridge is named as **pseudometaloph**(Antoine, 2002). The character has been recorded in the elasmotheriines *Elasmotherium caucasicum* and *Sinotherium lagreli*.

Protoloph: Major loph resulting of the connection between paracone, paraconule and protocone. Synonymies: anterior collis (Lydekker, 1884).

Secondary enamel folding

Antecrochet: Posterior expansion of the protoloph oriented to the median valley delimited by the posterior fold of the protocone. The main antecrochet is originated by the paraconule secondary cone. Synonyms: anterocrochet;. **Secondary crochet**(s) can be present as small ridges, also protruding from the protoloph and median valley-oriented, but more labially-placed. Synonyms: crochet *gegenfalte* (Peter, 2002); ; anticrochet (Van der Made, 2010); *replis d'émail* (when they appear repeatedly along the posterior side of the protoloph; Antoine, 2002).

Cingulum: an enamel ridge encircling partially or totally the base of the upper teeth (Anderson et al., 2011). It can be placed on the **anterior**, **posterior**, **lingual** or **labial** side of the teeth. The height, extension and development are variables. Their extension ranges from a continuous ridge to some aligned clumps, including short ridges restricted to the major cusps or a single wall connecting the space between two adjacent major cusps. The labial half of the posterior cingulum can develop a high ridge, more evident in some specimens with advanced wear. We consider this structure as a very developed stage of the posterior cingulum and not an independent stylus (*hypostyl*; Peter, 2002).

Crista: a ridge resulting from folding the enamel on the lingual side of the paracone. It is generally postero-lingually oriented. It is considered a relatively variable structure (Guérin 1980: 58). Ringström (1924: 131, 139) differenced a second anterior crista, naming it as **cristella**. This structure has been observed in several derived Elasmotheriines as *Sinotherium lagrelii*, *Elasmotherium* spp. or *Iranotherium morgani*. The crista can display the role of the metaloph when the latter is absent (see metaloph; pseudometaloph). Syn: parastilidion (Altuna, 1979).

Crochet: enamel ridge projecting from the lingual side of the metaloph, sometimes generated as a result of an orientation change of the labial side of the metaloph (e.g. Rhinocerotini). Its number (simple or multiple), orientation and shape (smooth or pointed) are variable. Syn: stilidion (Altuna, 1979).

Mesostyle: Pillar of the ectoloph, placed between paracone and metacone folds (Guérin, 1980: 62). Synonymies: metacone style(van der Maarel, 1932); *pli du métacône*(Guérin,

1980), metacone rib (Cerdeño, 1995).

Metastyle: Secondary folding of the enamel posteriorly placed to the metacone. Synonym: postero-external angle (Lydekker, 1884).

Parastyle: Secondary folding of the enamel anteriorly placed to the paracone. Synonymies: second costa (Lydekker, 1884); antero-external pillar(Matthew, 1932), *parastyl anterior*(Peter, 2002); *pli du paracone* (Guérin, 1980), paracone rib (Qiu et al., 1987); parastyl (Van der Made, 2010).

Fossetes

Mediofossete is theenamel basinresulting from a closing of the median valleywhen crochet and crista contacts. In cement bearing species (many elasmotheriina and some rhinocerotina) is often filled. Synonymies: medisinus (Fortelius, 1982); medifossete (Hooijer, 1946; van der Maarel, 1932); accessory fossete (Lydekker, 1884). The whole median valley can be considered as a fossete when is closed on its lingualmost end by a lingual bridge connecting protocone and hypocone. In this case is named as **closed median valley** (Antoine, 2002). Synonymies: prefossete (in part)(de Blainville, 1844; Prothero et al., 1986) .If a well-developed crista is present, the two resulting median valleys have been named as prefossa and middle fossa respectively (Van der Made, 2010).

The **prefossete**is a narrow enamel basin delimited by the anterior cingulum and the protoloph(Antoine, 2002). As previously commented, some authors (de Blainville, 1844; Prothero et al., 1986)consider the prefossete as the antero-labialextent of the median valley when a crista is present. Nevertheless, if the specimen displays a cristella, anadditional intermediate fossete may appear, making the precedingdefinitionunclear. Therefore, I coincide with Antoine restricting the prefossete to the fossete anteriorly placed to the protoloph.

The **postfossete** is the enamel basin enclosed by metaloph (or pseudometaloph) and the posterior cingulum. Synonymies: posterior valley (Lydekker, 1884).

Lower teeth (Fig. 5)

Major cusps

Entoconid: Major posterolingual cusp of the talonid on a lower cheek tooth. It can be as wide as the hypolophid or preceded by a constriction.

Hypoconid: Major anterolabial cusp of the talonid on a lower cheek tooth.

Metaconid: Major posterolingual cusp of the trigonid on a lower cheek tooth, placed between the anterior and posterior valleys. It can be as wide as the metalophid or constricted.

Paraconid: Major anterolabial cusp of the trigonid on a lower cheek tooth.

Protoconid: Major posterolabial cusp of the trigonid on a lower cheek tooth placed between the paraconid and the hypoconid.

Major lophs

Hypolophid: Major loph of the talonid that joins hypoconid and entoconid, covering most of the posterolabial side of the teeth. See hypoconid.

Metalophid: Major loph of the trigonid that runs from the protoconid to the metaconid.

Paralophid: Major loph of the trigonid that extents along the anterior border of the teeth departing from the paraconid, covering most of the posterolabial side of the teeth.

Ectolophid: Major loph of the trigonid that joins protoconid and paraconid. Its caudal border is nearly perpendicular to the major axis of the tooth and separates it into two independent valleys. Syn: metalophid (Guérin, 1980).

Talonid: anterior portion of the tooth formed by paraconid protoconid, and metaconid and their correspondent contacting lophs.

Trigonid: posterior portion of the tooth formed by entoconid and hypoconid and their corresponding contacting lophs.

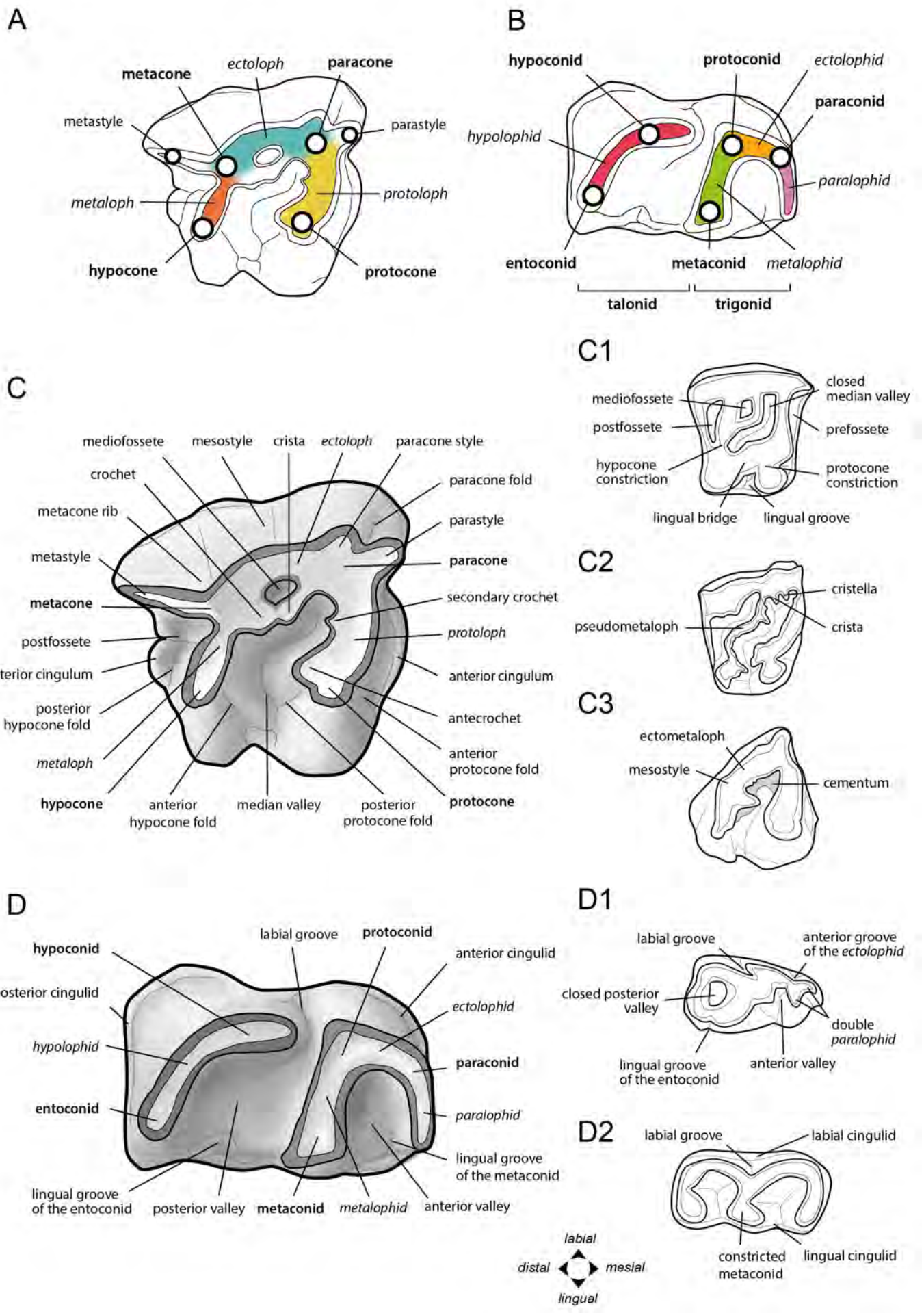
Secondary enamel folding

Cingulid: an enamel ridge encircling partially or totally the base of the lower teeth (Anderson et al., 2011). It can be placed on the **anterior**, **posterior**, **lingual** or **labial** side of the teeth. The height, extension and development are variables.

Labial groove: A vertical fold in the labial border of the enamel between protoconid and the beginning of the metalophid. Its development ranges from 'V'-shaped to practically absent. The labial groove can remain opened until the neck of the teeth or vanish at the neck. Synonymies: synclinal externe (Guérin, 1980); external syncline (van der Made, 2010); aubenfurche (Heissig, 1969).

Paralophid: Secondary folding of the enamel lingually placed to the paraconid extending the anterior loph of the lower teeth.

Fig. 5 diagram of a generic A, superior and B, inferior molar in occlusal view showing the major cones as growth centers for secondary folds. Primary cones are displayed in bold faces and lophs in cursive. Modified from Osborn (1898). C, superior and D, inferior generic molars showing main features described in the text. C1-C3 and D1-D3 represent additional characters not shown in the main Figures. Main cones are displayed in bold face and lophs in cursive. Teeth drawings are displayed in occlusal view and based on several authors (Antoine, 2002; Heissig, 1972).


A
metacone
ectoloph
paracone
metastyle
parastyle
protoloph
metaloph
hypocone
protocone
B
hypoconid
protoconid
ectolophid
paraconid
hypolophid
paralophid
entoconid
metaconid
metalophid
talonid
trigonid
C
mediofossete
mesostyle
crista
ectoloph
paracone style
crochet
paracone fold
metacone rib
parastyle
metastyle
paracone
metacone
secondary crochet
postfossete
protoloph
posterior cingulum
anterior cingulum
posterior hypocone fold
antecrochet
metaloph
anterior protocone fold
hypocone
anterior hypocone fold
median valley
posterior protocone fold
protocone
C1
mediofossete
closed median valley
postfossete
prefossete
hypocone constriction
protocone constriction
lingual bridge
lingual groove
C2
cristella
pseudometaloph
crista
C3
ectometaloph
mesostyle
cementum
D
hypoconid
labial groove
protoconid
anterior cingulid
posterior cingulid
ectolophid
hypolophid
paraconid
entoconid
paralophid
lingual groove of the metaconid
lingual groove of the entoconid
posterior valley
metaconid
metalophid
anterior valley
D1
labial groove
anterior groove of the ectolophid
closed posterior valley
double paralophid
lingual groove of the entoconid
anterior valley
D2
labial groove
labial cingulid
constricted metaconid
lingual cingulid
labial
distal
mesial
lingual

Fossetes

Median valley: central valley enclosed by proloph, ectoloph and metaloph (or ectometaloph in the case of the M3). Synonymies: lingual valley (Van der Made, 2010); talonidgrube (Peter, 2002).

Anterior valley: semicircular valley on the lingual side of the lower teeth delimited by the paralophid, anterior side of the metalophid and the lingual border of the teeth. Synonymies: trigonid basin (Fukuchi, 2003); metaflexid (Groves, 1972).

Posterior valley: semicircular valley on the lingual side of the lower teeth delimited by the hypolophid, posterior side of the metalophid and the lingual border of the teeth. The shapeof the posterior valley in lingual view can be 'U'-shaped or 'V'-shaped. In some cases the valley is very reduced, resulting in a short groove lingual groove of the entoconid (Figure C1).Synonymies: talonid basin (Fukuchi et al., 2009); entoflexid (Groves, 1972); postfossa (Van der Made, 2010).

REFERENCES

-, 2005, Nomina Anatomica Veterinaria, Editorial Comitee Hannover, Columbia, Gent, Sapporo, 190 p.:

Anders, U., Koenigswald, W. v., Ruf, I., and Smith, B. H., 2011, Generalized individual dental age stages for fossil and extant placental mammals: Paläontologische Zeitschrift, v. 85, p. 321-339.

Anderson, J. L., 1966, Tooth replacement and dentition of the black rhinoceros (Diceros bicornis Linn): Lammergeyer, v. 6, p. 41-46.

Anderson, P. S. L., Gill, P. P., and Rayfield, E. J., 2011, Modeling the Effects of Cingula Structure on Strain Patterns and Potential Fracture in Tooth Enamel: Journal of Morphology, v. 272, p. 50-65.

Antoine, P. O., 2002, Phylogénie et évolution des Elasmotheriina: (Mammalia, Rhinocerotidae): Mémoires du Muséum National d'Histoire Naturelle, v. 188, p. 5-350.

Bales, G. S., Thin-plate spline analysis of shape differences between a primitive and modern rhinoceros, *in* Proceedings Fifth North American paleontological convention, abstracts and program, Field Museum of Natural History. Chicago, June 28 - July 1, 1992 1992, Volume Special publication no. 6, The Paleontological Society.

Bales, G. S., 1993, A multivariate comparison of variation in fossil and living rhinoceros skulls.: Journal of Vertebrate Paleontology, v. 13, no. Suppl. To no. 3, p. 24A-25A.

-, 1994, Skull evolution in living and fossil rhinoceroses: morphometric analyses of within and between group variation: Journal of Morphology, v. 220, no. 3, p. 322-323.

-, 1995, A multivariate morphometric study of living and fossil rhinoceros skulls.: University of South California, 416 p.

-, 1996, Skull Evolution in the Rhinocerotidae (Mammalia, Perissodactyla): Cartesian Transformations and Functional Interpretations: Journal of Mammalian Evolution, v. 3, no. 3, p. 261-279.

-, 1998, Patterns of foramen magnum size and shape in Rhinocerotoidea (Ceratomorpha: Perissodactyla): Journal of Vertebrate Paleontology, v. 18, no. Suppl. To no. 3, p. 25A-26A.

-, 2001, A morphometric contribution to rhinoceros phylogeny. Canonical variate studies of extant and fossil skulls (Rhinocerotoidea: Perissodactyla): Journal of Vertebrate Paleontology, v. 21, no. Suppl. To no. 3, p. 31A.

Bigalke, R., Steyn, T., de Vos, D., and de Waard, K., 1950, Observations on a juvenile female square-lipped or white rhinoceros (*Ceratotherium simum simum* Burchell) in the national Zoological Gardens of South Africa: Proceedings of the Zoological Society of London, v. 120, p. 519-528.

Borsuk-Bialynicka, M., 1973, Studies on the Pleistocene Rhinoceros Coelodonta antiquitatis (Blumenbach): Acta Palaeontologica Polonica, v. 29, p. 1-97.

Budras, K.-D., Sack, W. O., and Röck, S., 2009, Anatomy of the Horse, Hannover, Schlütersche Verlagsgesellschaft mbH & Co.

Cave, A. J. E., The foramen ovale in the Rhinocerotidae, *in* Proceedings Proceedings of the 15th International Congress of Zoology1959, Volume Sect 5. Paper 20, p. 1-3.

Cerdeño, E., 1982, Estudio descriptivo del esqueleto postcraneal de *Hispanotherium matritense* del yacimiento de Torrijos (Toledo)Tesis de Licenciatura]: Universidad Complutense de Madrid, 117 p.

-, 1995, Cladistic analysis of the Family Rhinocerotidae (Perissodactyla): American Museum Novitates, v. 3143, p. 1-25.

Cuvier, G., 1834, Reserches sur les Ossemens Fossiles, París.

de Blainville, H. M. D., 1844, Ostéographie des mammifères, 3, atlas. Des rhinocéros, Paris, 232 p.:

Deng, T., 2005, New discovery of *Iranotherium morgani* (Perissodactyla, Rhinocerotidae) from the Late Miocene of the Linxia Basin in Gansu, China, and its sexual dimorphism: Journal of Vertebrate Paleontology, v. 25, no. 2, p. 442-450.

Deng, T., Wang, S., and Hou, S., 2013, A bizarre tandem-horned elasmothere rhino from the Late Miocene of northwestern China and origin of the true elasmothere: Chinese Science Bulletin, v. 15, p. 1811-1817.

Fortelius, M., 1982, Ecological Aspects of Dental Functional Morphology in the Plio-Pleistocene Rhinoceroses of Europe, *in* Kurtén, B., ed., Teeth: Form, Function and Evolution: New York, Columbia University Press, p. 163-181.

-, 1983, The morphology and paleobiological significance of the horns of *Coelodonta antiquitatis* (Mammalia: Rhinocerotidae): Journal of Vertebrate Paleontology, v. 3, p. 125-135.

Fortelius, M., and Heissig, K., 1989, The phylogenetic relationships of the Elasmotherini (Rhinocerotidae, Mamm.): Mitteilungen Bayerische Staatssammlung Paläontologische historische Geologie v. 29, p. 227-233.

Foster, J. B., 1965, Mortality and ageing of black rhinoceros in East Tsavo Park, Kenya: East African Wildlife Journal, v. 3, p. 118-119.

Fraser, O. L., 1875, Note on a partially ossified nasal septum in *Rhinoceros sondaicus*: Journal of the Asiatic Society of Bengal, v. 44, p. 10-12.

Fukuchi, A., 2003, A note on dental nomenclature in the Rhinocerotidae: Earth Science Reports, v. 10, no. 1, p. 33-37.

Fukuchi, A., Nakaya, H., Takai, M., and Ogino, S., 2009, A preliminary report on the Pliocene rhinoceros from Udunga, Transbaikalia, Russia: Asian Primatology, v. 5, p. 61-98.

Garutt, N., 1994, Dental ontogeny of the woolly rhinoceros *Coelodonta antiquitatis* (Blumenbach, 1799): Cranium, v. 11, no. 1, p. 37-48.

Garutt, N. V., 1990, Anomalii zubnoj sistemy scerstistogo nosoroga Coelodonta antiquitatis (Blum., 1799). Fauna mlekopit. i ptiz pozdn. plejstoz. i goloz. SSSR: Leningrad, Akad. Nauk SSSR, v. 212, p. 59-64.

-, 1992, Ontogenez zubnoj sistemy scerstistogo nosoroga *Coelodonta antiquitatis* (Blumenbach, 1799). Istorija krupnyh mlekopit. i ptiz severnoj Evrazii: Skt. Petersburg: Rossijsk. Akad. Nauk (Zool. Institut), v. 246, p. 81-102.

Goldfinger, E., 2004, Animal Anatomy for Artists, Oxford, New York, Oxford University Press.

Groiss, J., Guenther, A., and Keupp, H., 1981, Eine quartäre Spaltenfüllung im Steinbruchgebiet Wintershof bei Eichstätt, A. Paläontologische Untersuchungen (*C. antiquitatis* u. *D. kirchbergensis*), B. Zur Grabung, C. Zur geologischen situation: Geologische Blätter für Nordost-Bayern und Angrenzende Gebiete, v. 31, no. 1-4, p. 165-188.

Groves, C. P., 1972, *Ceratotherium simum*: Mammalian Species. The American Society of Mammalogists, v. 8, p. 1-6.

-, 1983, Phylogeny of the living species of Rhinoceros: Zeitschrift fur Zoologische Systematik und Evolutionsforschung, v. 21, no. 4, p. 293-313.

Guérin, C., 1980, Les rhinocéros (Mammalia, Perissodactyla) du Miocène terminal au Pléistocène supérieur en Europe occidentale : comparaison avec les espèces actuelles: Documents des Laboratoires de Géologie de Lyon, v. 79, p. 1-1184.

Heissig, K., 1969, Die Rhinocerotidae (Mammalia) aus der oberolizogänen Spaltenfüllung von Gaimersheim bei Ingolstadt in Bayern und ihre phylogenetische Stellung: Bayerische Akademie der Wissenschaften, Mathematisch-Naturwissenschaftliche Klasse, Abhandlungen, v. 138, p. 1-133.

-, 1972, Paläontologische und geologische Untersuchungen im Tertiär von Pakistan. 5. Rhinocerotidae (Mamm.) aus den unteren und mittleren Siwalik-Schichten.: Bayerische Akademie der Wisseschaften, Mathematisch-Naturwissenschaftliche Klasse Abhandlungen, v. 152, p. 1-112.

-, 1989, The Rhinocerotidae, *in* Prothero, D., and Schoch, R. M., eds., The evolution of Perissodactyls, Oxford University Press, p. 399-417.

Hieronymus, T. L., and Witmer, L. M., 2004, Rhinoceros horn attachment: anatomy and histology of a dermally influenced bone rugosity: Journal of Morphology, v. 260, no. 3, p. 298.

Hitchins, P. M., 1970, Field criteria for ageing immature black rhinoceros, *Diceros bicornis* l.: Lammergeyer, v. 12, p. 48-55.

-, 1978, Age determination of the black rhinoceros (Diceros bicornis Linn.) in Zululand: South African Journal of Wildlife Research, v. 8, p. 71-80.

Hoogerwerf, A., 1970, Udjung Kulon the Land of the Last Javan Rhinoceros, Brill Archive.

Hooijer, D. A., 1946, Prehistoric and Fossil Rhinoceroses from the Malay Archipelago and India: Zoologische Mededelingen, v. 26, no. 1, p. 1-138.

Hünnerman, K. A., 1989, Die Narshornskelette (*Aceratherium incisivum* Kaup 1832) aus dem Jungtertiär vom Höwennegg im Hegau (Südwestdeutschland): Andrias, v. 6, p. 117.

Koenigswald, W. v., Holbrook, L. T., and Rose, K. D., 2011, Diversity and evolution of Hunter-Schreger band configuration in tooth enamel of perissodactyls mammals: Acta Palaeontologica Polonica, v. 56, no. 1, p. 11-32.

Loose, H., 1975, Pleistocene Rhinocerotidae of W. Europe with reference to the recent two-horned species of Africa and S. E. Asia: Scripta Zoologica, v. 33, p. 1-59.

Lydekker, R., 1884, Additional Siwalik Perissodactyla & Proboscidea: Memoirs of the Geological Survey of India. Palaeontologia Indica Series 10, v. 3, no. 1, p. 1-34.

Matthew, W. D., 1932, A review of the rhinoceroses with a description of *Aphelops* material from the pliocene of Texas: University of California Publications in Geological Sciences, v. 20, no. 12, p. 411-480.

Mazza, P., and Azzaroli, A., 1993, Ethological inferences on Pleistocene rhinoceroses of Europe: Rendiconti Lincei, v. 4, no. 2, p. 127-137.

Osborn, H. F., 1888, The nomenclature of the mammalian molar cusps: American Naturalist, v. 22, no. 262, p. 926-928.

-, 1898, The Extinct Rhinoceroses: Memoirs of the American Museum of Natural History, v. 1, no. 3, p. 75-164.

Peter, K., 2002, Odontologie der Nashornverwandten (Rhinocerotidae) aus dem Miozän (MN 5) von Sandelzhausen (Bayern): Zitteliana. Abhandlungen der Bayerischen Staatssammlung für Paläontologie und Geologie, v. 22, p. 3-168.

Peterson, O. A., 1920, The American Diceratheres: Memoirs

of the Carneghie Museum, v. 7, no. 6, p. 399-477.

Prothero, D., 2005, The Evolution of North American Rhinoceroses, Cambridge, Cambridge University Press, 218 p.:

Prothero, D., Manning, E., and Hanson, C. B., 1986, The phylogeny of the Rhinocerotoidea (Mammalia, Perissodactyla): Zoological Journal of the Linnean Society, v. 87, p. 341-366.

Qiu, Z. X., Xie, J. Y., and Yan, D. F., 1987, A new chilothere skull from Hezheng, Gansu, China with special reference to the Chinese "*Diceratherium*": Scientia Sinica. Series B, v. 5, p. 545-552.

Radinsky, L. B., 1969, The Early Evolution of the Perissodactyla: Evolution, v. 23, no. 2, p. 308-328.

Ringström, T. J., 1924, Nashörner der Hipparion Fauna Nord-Chinas: Palaeontologia Sinica, Series C, v. 1, p. 1-156.

Roman, F., 1924, Contribution a l'Étude de la Faune de Mammifères des Littorinenkalk (Oligocène Supérieur) du Bassin de Mayence. Les Rhinocéros: Travaux du Laboratoire de Géologie de la Faculté des Sciences de Lyon, v. 7, no. 6.

Roth, H. H., and Child, G., 1968a, Distribution and population structure of black rhinoceros (Diceros bicornis L.) in the Lake Kariba basin: Zeitschrift für Säugetierkunde, v. 33, no. 4, p. 214-226.

-, 1968b, Distribution and population structure of black rhinoceros (Diceros bicornis L.) in the Lake Kariba basin: Zeitschrift fur Saugetierkunde, v. 33, no. 4, p. 214-226.

Sanisidro, O., Head shape evolution in Rhinocerotidae (Perissodactyla): an overview of its paleoecological implications, *in* Proceedings Journal of Vertebrate Paleontology, Pittsburgh, 2010.

Schaller, O., 2007, Illustrated Veterinary Anatomical Nomenclature, Sttutgart, Enke.

Schenkel, R., and Schenkel-Hulliger, L., 1969, Ecology and Behaviour of the Black Rhinoceros (*Diceros bicornis*), a Field Study, Hamburg and Berlin, Mammalia Depicta.

Schenkel, R., and Schenker-Hulliger, L., 1969, Ecology and Behaviour of the Black Rhinoceros (Diceros bicornis), a Field Study: 101, Hamburg & Berlin, Mammalia Depicta.

Thenius, V. E., 1955, Die Verknöcherung der Nasenscheidewand bei Rhinocerotiden und ihr systematischer Wert (Zum Geschlechtsdimorphismus fossilier Rhinocerotiden): Schweizt Paleontologische Abandhungen, v. 71, p. 1-17.

Tong, H., 2001, Age profiles of rhino fauna from the Middle Pleistocene Nanjing man site, south China - explained by the rhino specimens of living species: International Journal of Osteoarchaeology, v. 11, no. 3, p. 231-237.

van der Maarel, F. H., 1932, Contribution to the knowledge of the fossil mammalian fauna of Java: Wetenshapenlijke Mededeelingen, v. 4, no. 15, p. 58-81.

van der Made, J., 2010, The rhinos from the Middle Pleistocene of Neumark-Nord (Saxony-Anhalt), p. 463-527.

Vialli, V., 1955, Su una anomalia nella dentatura di un rinoceronte Africano: Natura, Milano, v. 46, p. 131-134.

SUPPLEMENTARY MATERIAL 1

Se han analizado un total de 93 individuos pertenecientes a 61 especies y 38 géneros de rinocerótidos actuales y fósiles (tabla A1 del Anexo). Han sido incluidas distintas especies dentro de cada género para conocer el rango morfométrico de la muestra. Por el mismo motivo, y cuando ha sido posible, se han incluido individuos machos y hembras, a pesar de las dificultades de diferenciación entre ambos en las especies fósiles (Prothero, 1996). Se han analizado tanto ilustraciones como fotografías tomadas de la bibliografía. En algunos casos ha sido necesario reflejar horizontalmente la imagen digitalizada, (quedando indicado en la tabla 1 del Anexo). Las fuentes de las imágenes de referencia son muy diversas, por lo que no es posible cuantificar el error de paralaje de la muestra. A pesar de ello, al observar puntos característicos pares y simétricos (p. ej. extremos distales de los huesos nasales), se han descartado aquellas fotografías en las que éste era evidente rechazando también cráneos deformados tangencialmente.

El análisis se ha realizado empleando los programas Morpheus (Slice, 1998) y MorphoJ (Klingenberg, 2008) y los pertenecientes a la serie tps: tpsUtil (2008c), tpsDig2 (Rohlf, 2008a), tpsRelw (Rohlf, 2008b), tpsSpline (Rohlf, 2004), tpsRegr (Rohlf, 2007) y tpsSuper (Rohlf, 2004).

En primer lugar fue creado un archivo con las imágenes de referencia mediante el programa tpsUtil (Rohlf, 2008c). A continuación se empleó el programa tpsDig2 (Rohlf, 2008a) para el emplazamiento de los landmarks. Se han escogido un total de 21 landmarks morfológicos y geométricos distribuidos de forma homogénea (figura 1 y tabla 1). De entre los 18 landmarks morfológicos, 8 de ellos son de tipo 1 y 10 de tipo 2. Se han concentrado la distribución de landmarks en la región occipital, ya que estudios previos (Bales, 1995) muestran su importancia desde un punto de vista trófico (figura 1). No se han concentrado landmarks en el hueso nasal, relacionado con la implantación de los cuernos nasales, ya que este carácter se muestra irrelevante desde un punto de vista filogenético, trófico y/o paleoecológico (muchos géneros han alcanzado el estado de desarrollo de cuernos de forma independiente). En los cráneos de Rhinocerotidae es complicado reconocer las suturas craneales debido a la hiperostosis del tejido óseo que las circunda. Esto disminuye drásticamente el número de landmarks de tipo 1 identificables. Se ha decidido evitar puntos característicos para el análisis ya que el problema se acentúa en los ejemplares fósiles. Entre los cráneos empleados existen muchos casos en los que se han figurado en conexión con las mandíbulas, imposibilitando la toma de datos de la porción basilar anterior del neurocráneo. Esto es más frecuente entre los ejemplares fósiles, por lo que esa zona ha sido obviada a la hora de emplazar los landmarks. La región anterior del hueso premaxilar también ha sido obviada en los análisis, ya que es su unión al maxilar se estrecha, siendo una parte que se pierde frecuentemente en ejemplares fósiles. A continuación se generó un archivo de líneas para una observación más clara de los resultados.

En primer lugar se han superpuesto todos los individuos mediante el Análisis Procrustes de Superposición o General Procrustes Analysis (GPA). Este análisis realiza una superposición mediante el algoritmo de mínimos cuadrados, minimizando la suma de las distancias entre los residuos de los diferentes individuos. Esto implica la rotación, traslación y escalado de cada conjunto de landmarks, pero no su deformación. Con esto se elimina el factor tamaño en la muestra y permite una exploración preliminar de los datos. La superposición procrustiana y visualización de los landmarks se realizó gracias al programa Morpheus (Slice, 1998).

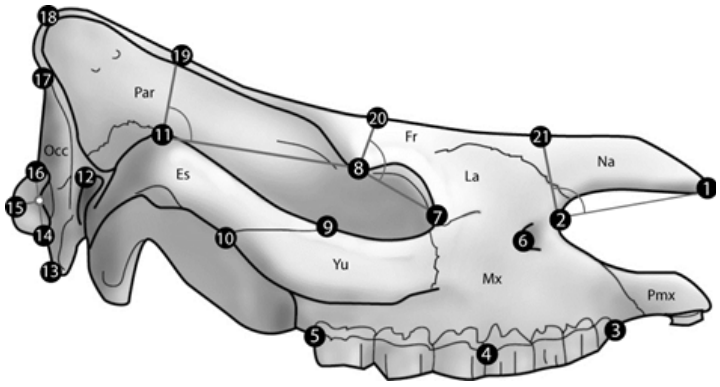


Figura SD1. Ilustración de un cráneo promedio en vista lateral derecha indicando la situación de los 21 landmarks empleados en el análisis. El cráneo promedio tomado como referencia ha sido generado gracias al programa tpsSuper (Rohlf, 2004). Definición de los landmarks: (1); Punto más anterior del hueso nasal. (2); Punto más posterior del entrante nasal. (3); Punto más anterior del contacto labial entre P1 y el hueso maxilar. (4); Punto más dorsal del contacto labial entre la base del esmalte de P4 y M1. (5); Punto más posterior del lado labial de la base del M3. (6); Punto medio del borde externo posterior del canal infraorbital. (7); Punto más anterior del borde orbital. (8); Punto más ventral del borde de la tuberosidad supraorbital. (9); Intersección entre la sutura entre los huesos yugal y escamoso y el borde dorsal del arco zigomático. (10); Intersección entre la sutura entre los huesos yugal y escamoso y el borde ventral del arco zigomático. (11); Punto más dorsal del borde dorsal del arco zigomático. (12); Punto más dorso-posterior del borde externo del canal auditivo. (13); Punto más ventral del proceso paraoccipital. (14); Punto más ventral del borde ventral del cóndilo occipital. (15); Intersección del borde lateral del cóndilo occipital con la máxima distancia de la proyección perpendicular de la línea entre los landmarks 16 y 18. (16); Punto más dorsal del cóndilo occipital. (17); Punto más dorsal del contacto entre la cara posterior del hueso occipital y la cresta occipital. (18); Punto más posterodorsal de la cresta occipital. (19); Intersección entre el borde dorsal del cráneo y la proyección del ángulo recto entre los landmarks 11 y 12. (20); Intersección entre el borde dorsal del cráneo y la proyección del ángulo recto entre los landmarks 2 y 9. (21); Intersección entre el borde dorsal del cráneo y la proyección del ángulo recto entre los landmarks 1 y 2. En gris se muestran las líneas de referencia entre landmarks. Pmx: premaxilar, Mx: maxilar, Na: nasal, La: lacrimal, Fr: frontal, Yu: yugal, Es: Escamoso, Par: parietal, Occ: occipital. Escala: 10 cm.

Tras realizar el GPA, se ha continuado minimizando la distancia de los residuos mediante la deformación de los residuos superpuestos a dos escalas de detalle: afín [A] y local [D]. Las variables de deformación obtenidas o Principal Warps A esto se le denomina GPLS.

Mediante tpsRelw (Rohlf, 2008b) se han obtenido 20 Partial warp scores y la variación de la forma para cada uno de ellos. El número de Partial warp es igual al número de landmarks menos uno. Por último se han calculado los Relative warps, cuantificando las variaciones en la forma de forma más precisa. Para detectar qué componentes han contribuido a la variación de la forma se ha empleado un análisis estadístico multivariable de componentes principales (PCA), forzando a las variables a proyectarse bidimensionalmente dos a dos. Gracias a esto se pueden interpretar gráficamente los componentes principales responsables de la dirección en la variación en la forma. Una vez llegado a este punto, el conjunto de modificaciones y deformaciones se pueden aislar como variable, lo que permite su comparación con otras variables como el tamaño (Centroid size).

Finalmente, para agrupar las diferentes morfologías se ha calculado un dendrograma de similitud para comprobar la relación morfológica entre los distintos géneros. Para ello se ha empleado el algoritmo de Ward, adecuado para este tipo de análisis (Hammer & Harper, 1999-2007). El análisis estadístico se ha realizado con el programa PAST (Hammer & Harper, 2006).

Los datos representados por el programa Morpheus muestran una nube de puntos y contornos. Tras el análisis GPA se puede analizar la variación de los distintos landmarks respecto de la media, observándose una mayor variación relativa en la región rostral.

La variación de la morfología craneal de Rhinocerotidae se encuentra distribuida entre más de diez variables (tabla 1). Este elevado número indica que existen numerosos factores interactuando a la vez en la muestra. Como se discutirá más adelante algunos de ellos, como el componente principal 3, pueden asociarse al error de muestreo. En la discusión se han tenido en cuenta los primeros cuatro componentes principales, ya que explican más del 7% de la varianza observada cada uno. En total explican un 60,19% de la muestra.

CONCLUSIONES GENERALES

En la presente Tesis Doctoral se ha estudiado el material fósil de rinocerontes del Mioceno de la Península Ibérica, donde se ha señalado la presencia de los géneros *Aceratherium, Alicornops, Diaceratherium, Dihoplus, Hispanotherium, Lartetotherium,* y '*Protaceratherium*'. En total se ha estudiado, descrito y medido más de 2,650 restos de dentición y esqueleto tanto craneal como postcraneal procedente de 21 yacimientos de las Cuencas del Tajo, Bierzo, las Cuencas Levantinas y la Cuenca del Vallès-Penedès. También se ha examinado el material disponible de especies próximas de diversas instituciones nacionales e internacionales, incluyendo aquellos restos pertenecientes a las colecciones tipo de las especies *Aceratherium incisivum, Alicornops simorrense, Dihoplus schleiermacheri* e *Hispanotherium matritense*. Esta información ha sido incluida en el análisis filogenético y en los estudios comparativos.

Implicaciones sistemáticas

- Nuevos restos fósiles (tanto craneales como postcraneales) de rinoceronte de las localidades de Mesegar-1 y Mesegar-2 han sido descritos y medidos. El análisis filogenético de los restos disponibles ha confirmado la presencia de un nuevo género y especie de rinoceronte presente en ambos yacimientos. Aunque los restos han sido provisionalmente incluidos en el género '*Protaceratherium*', el análisis filogenético de la nueva especie muestra que pertenece a un linaje independiente basal a Aceratheriina+Rhinocerotini que también incluye los restos de las localidades de Loranca y Valquemado, previamente asignados a *Protaceratherium minutum*. Del mismo modo se plantea la revisión del género *Plesiaceratherium*, al tratarse de un género potencialmente parafilético.

- Se ha estudiado el material de *Hispanotherium matritense* procedente de varios yacimientos del área de Madrid. Esta especie se cita por primera vez en los yacimientos de Príncipe Pío-2, Fábrica Mahou, Embajadores-R, La Peineta, Yunquera de Tajo y Fresno del Torote. La cantidad de material estudiado ha permitido realizar un estudio de la variabilidad intraespecífica. Dicho estudio ha permitido actualizar la diagnosis de la especie y revisar la sistemática del grupo, descartando la ascripción de diversos elasmoteriinos Euroasiáticos a *H. matritense*. Toda esta información se ha traducido en forma de una guía osteológica, la primera de este tipo para rinocerontes elasmoteriinos, que convierte *H. matritense* en uno de los elasmoterinos mejor conocidos.

- Se cita por primera vez la presencia de los rinocerontes *Alicornops simorrense* y *Lartetotherium* cf. *Lartetotherium sansaniense* en el yacimiento de M-407 Rotonda (Provincia de Madrid), lo cual amplía la variabilidad conocida para ambas especies.

- Se describe detalladamente la presencia de una nueva forma de *Lartetotherium* procedente de los yacimientos de Batallones-1, Batallones-2, Batallones-10 y Valdeinfierno (Provincia de Madrid). Los restos fueron previamente identificados como pertenecientes a *A. incisivum*. La comparación con la especie tipo *L. sansaniense* muestra una mayor robustez y diferencias morfológicas en la dentición y el esqueleto postcraneal.

- Se describen los restos de *Aceratherium incisivum* del Cerro de los Batallones (Batallones-1, 3, 5 and 6), incluido un esqueleto casi completo. La comparación con otros restos Europeos revelan un tamaño similar y algunas particularidades en el cráneo como y el esqueleto postcraneal.

- Se han descrito nuevos restos de *Dihoplus schleiermacheri* de las localidades de Venta del Moro y Corral de Lobato y se revisan los restos de la especie procedentes de Crevillente-2 y Alcoy-Mina.

Implicaciones estratigráficas y paleogeográficas

- El estudio paleobiogeográfico para los Elasmotheriina realizado a partir de la hipótesis filogenética obtenida para *H. matritense* permite establecer un patrón de migración Este-Oeste para los elasmoterinos europeos en la base del Aragoniense seguida de una radiación regional del grupo.

- Los restos de *Diaceratherium* sp. de la localidad de Santalla del Bierzo suponen los primeros restos de vertebrados encontrados en la Cuenca del Bierzo. Su presencia restringe el contexto bioestratigráfico de la Formación Santalla al Mioceno (probablemente inferior), confirmando estudios previos basados en correlaciones estratigráficas.

Implicaciones paleoecológicas y paleobiológicas

- El estudio sobre la evolución del grupo a escala general y continental ha identificado un máximo de diversidad en el Mioceno Medio seguido de otro en el Mioceno superior. Además, las tasas de diversificación muestran cuatro momentos de alta diversificación acompañados de tasas variables de reemplazo faunístico. Los análisis a escala continental muestran historias evolutivas distintas y diferenciadas entre sí.

- El análisis paleoecológico de *A. simorrense* y *L. sansaniense* muestra una segregación ecológica evidente para ambas especies. Los resultados, obtenidos a partir del análisis de isótopos de oxígeno / carbono y la comparación morfológica de la dentición y el esqueleto postcraneal, situan a *L. sansaniense* como un ramoneador de hábitats abiertos mientras, *A. simorrense* sería un habitante de ambientes más cerrados y dieta más abrasiva.

- Se ha realizado el primer estudio histológico en rinocerontes a partir del esqueleto apendicular de *H. matritense*. Los resultados indican una alta remodelación ósea en las primeras etapas del desarrollo y una madurez sexual en torno a los diez años de vida.

GENERAL CONCLUSIONS

This Thesis deals with the study of new remains of Rhinocerotidae from the Miocene of the Iberian Peninsula. The presence of the genera *Aceratherium, Alicornops, Diaceratherium, Dihoplus, Hispanotherium, Lartetotherium* and *'Protaceratherium* is reported. For this purpose, 2,650 dental, cranial, and postcranial remains from 21 localities of the Tagus, Bierzo, Levantine and Vallès-Penedès Basins have been studied, described, and measured. Additionally, the material of closely related species from several national and international institutions has been examined, including the type collections of the species *Aceratherium incisivum, Dihoplus schleiermacheri* e *Hispanotherium matritense.* This information has been included in the phylogenetic analysis and the comparative studies.

Systematic implications

- New rhinocerotid cranial, dental, and postcranial remains from the locality of Mesegar-2 are described and measured. These remains have been provisionally included as a new genus and species, provisionally assigned to '*Protaceratherium*'. New remains from Mesegar-2 clusters together with the localities of Loranca and Valquemado (previously assigned to *Protaceratherium minutum*), forming an endemic Iberian clade that roots with Aceratheriina+Rhinocerotini. Additionally, '*Plesiaceratherium*' appears as a probable paraphyletic genus.

- In the review of the postcranial skeleton of *Hispanotherium matritense*, the remains from several localities from the Madrid Area have been studied. The species is cited for the first time in the fossil sites of Príncipe Pío-2, Fábrica Mahou, Embajadores-R, Ventas, Yunquera de Tajo and Fresno del Torote. The new findings multiply the number of remains of the species, posing it as one of the best known elasmotheres. Additionally, an update of the species' dianogsis and the quantitative study of the intraspecific variability of the postcranial skeleton are proposed. As a result, the systematics of previously *H. matritense*-purported taxa has been reviewed, discarding their synonymy in agreement with previous works. Finally, an exploratory osteological guide of the postcranial skeleton in *H. matritense* has been performed.

- Remains from the species *Alicornops simorrense* and *Lartetotherium* cf. *Lartetotherium sansaniense* have been described from the locality of M-407 Rotonda (Madrid Province). Their study widens the known variability for both genera.

- A new lineage of a robust *Lartetotherium* species from the localities of Batallones-1, 2, 10, and Valdeinfierno (Madrid Province) is recognized. These remains, previously identified as *A. incisivum*, comprise a complete portrait of the species. Its comparison with the type species reveals a greater robustness and several dental and postcranial particularities.

- New remains of the species *Aceratherium incisivum* are described from Los Batallones Butte (localities of Batallones-1, 3, 5 and 6). These remains include a nearly complete skeleton, which completes the available information for the species. Their study revealed some differences in the cranial and postcranial skeleton.

- New remains from *Dihoplus schleiermacheri* from the localities of Corral de Lobato and Venta del Moro are described. Additionally, the remains from Crevillente-2 and Alcoy-Mina have been reviewed and compared with the remaining Iberian sites. The co-occurrence of *D. schleiermacheri* and *Dihoplus pikermiensis* during the European Turolian is confirmed.

Stratigraphical and paleogeographical implications

- A paleobiogeographic study has been performed for Elasmotheriina. The results show a Eastern-Western migration at the earliest Aragonian followed by a regional radiation of the group.

- The remains of *Diaceratherium* sp. in the locality of Santalla del Bierzo are the first vertebrate remains found in El Bierzo Basin. Their presence restricts the biostratigraphic context of the Santalla Formation to the (Lower) Miocene, confirming previous studies based on stratigraphic correlations.

Paleobiological and Paleoecological implications

- A large-scale study on the evolutionary patterns in Rhinocerotidae at both global and continental scales has been performed. The results revealed a maximum diversity peak in the Middle Miocene followed by a second one in the Late Miocene. Diversification rates show four peaks of high diversification accompanied by variable rates of specific turnover. The continental-scale analysis revealed particular evolutionary histories in agreement with previous studies.

- The results of the multiproxy paleoecological study of the species *A. simorrense* and *L. sansaniense* revealed different ecologic niches. The results, obtained by means of the analysis of carbon and oxygen isotopes extracted from teeth enamel together with morphological comparison, poses *L. sansaniense* as a flexible browser of more open environments. On the other hand, *A. simorrense* is a forest-dweller of higher attritional diet.

- The first histological study in rhinoceros has been performed using the appendicular skeleton of *H. matritense*. The results show a high bone remodeling early in development and a sexual maturity reached around ten years old.

mncn
museonacionaldecienciasnaturales

CSIC
Consejo Superior de Investigaciones Científicas

UAM
UNIVERSIDAD AUTONOMA
DE MADRID

